東京帝國大學

地震研究所彙報

第14號

昭和11年

BULLETIN

OF THE

EARTHQUAKE RESEARCH INSTITUTE

TOKYO IMPERIAL UNIVERSITY

Vol. XIV

1936

目　　次

第 14 號

第 1 冊 (昭 和 11 年 3 月)

			頁
1.	自由振動の持續性と共振の振幅との關係—海峽に於けるセイシの問題（英文）……	妹澤克惟 金井清	1
2.	局所的內力を種々の速さで變化する場合に生ずる彈性波（英文）……	妹澤克惟 金井清	10
3.	淺間火山の精密水準測量結果（邦文）……	高橋龍太郎	18
4.	小淺間及棒錄三角點に於ける緯度の測定（邦文）……	高橋龍太郎	26
5.	昭和8年3月3日の大地震—III. 大地震前後の三陸沖の地震活動及一般に大地震の餘震に就て（獨文）……	松澤武雄	38
6.	伊豆下田に於ける過去地震津浪の高さ（邦文）……	福富孝治	68
7.	中部關東平野の海成洪積層（摘要）（關東造盆地運動の一資料）（英文）……	大塚彌之助	75
8.	武藏野臺地の地質構造に就いて（佛文）……	今村學郎 矢島仁吉	83
9.	丹那隧道の地質斷面圖（英文）……	久野久	92
10.	高層建築の地震動による振動（邦文）……	齊田時太郎 鈴木正治	104
11.	三菱仲7號館別館，仲8號館別館，仲13號館の種々の狀態に於ける震動勢力の逸散性（英文）……	妹澤克惟 金井清	119
12.	6階建築に於ける震動勢力の逸散性. 共振と餘共振とが一致する問題（英文）……	妹澤克惟 金井清	134
13.	宮古—青森間水準檢測成果（邦文）……		146

第 2 冊 (昭 和 11 年 6 月)

14.	震源と震波との關係に就て（英文）……	妹澤克惟	149

15. 不連續層を通過する横波の性質（英文）…………………… 妹澤克惟 金井清 157

16. 構造物に於ける震動逸散理論の吟味（英文）…………… 妹澤克惟 金井清 164

17. 7階建築に於ける震動勢力の逸散性（英文）…………… 妹澤克惟 金井清 189

18. 昭和10年4月21日臺灣地震の走時曲線と地殼構造上の一問題（英文）…………………………………… 河角廣 本間正作 201

19. 最近の活動に伴へる淺間火山の高さの變化（英文）…… 水上武 222

20. 地震と雨雪量，氣壓，及氣溫との關係（補遺）（英文）… 山口生知 235

21. 出羽村及び濱松町における地震動卓越周期の觀測（邦文）…………………………………………… 石本巳四雄 240

22. 器械的記錄を行ふ微動計の製作（佛文）………………… 石本巳四雄 248

23. 南伊豆，下賀茂・蓮臺寺・下河津3溫泉の物理，化學的性質に就て（第1報）（英文）……………………… 福富孝治 259

24. 仙臺大年寺山の山崩（邦文）…………………………… 田山利三郎 271

25. 昭和11年2月21日河内大和强震調査報告（邦文）…… 那須信治 萩原尊禮 285

26. 大阪市内に於ける土地の固有振動の測定（邦文）……… 那須信治 萩原尊禮 290

27. 昭和11年2月21日河内大和强震に關する調査報告（邦文）…………………………………………… 宮部直巳 297

28. 昭和11年2月21日河内大和强震被害の地質及地形的考察（邦文）…………………………………… 齊田時太郎 307

第3册（昭和11年9月）

29. 地震計初動の理論的及實驗的研究並びに地震初動の定量的研究（其1）（英文）……………………………… 河角廣 319

30. 地震計初動の理論的及實驗的研究並びに地震初動の定量的研究（其2）（英文）……………………………… 河角廣 木下潤一 339

31. 斜のディスターバンスによつて生じた地表層の固有振動の減衰（英文）……………………………………… 妹澤克惟 金井清 354

32. 灣のセイシに伴ふ逸散波（英文）……………………… 妹澤克惟 金井清 360

33. 床の剛度が架構の水平振動に及ぼす影響（英文）……… 妹澤克惟 金井清 367

34. 改良せる理論から見た實在建物の震動勢力逸散性（英文）…… 妹澤克惟・金井清 377

35. 地殼變動の程度に就て（英文）…… 宮部直巳 387

36. 地震現象の統計的研究の成果に關する檢討（英文）…… 山口生知 399

37. 振動方程式を實驗的に解く一方法（英文）…… 淵田隆門 415

38. 關東地方に於ける震原の垂直分布（邦文）…… 永田武 420

39. 關東地方に於ける地震の發生（共1）（邦文）…… 那須信治・萩原尊禮・表俊一郎 427

40. 秋田縣由利郡地方の高瀬川綠色凝灰岩及び日本の下部新第三系の對比（英文）…… 大塚彌之助 438

41. 火山列島硫黄島の地質及岩石に就いて（英文）…… 津屋弘逵 453

42. 袋井—興津—小田原間及び興津—甲府間の一等水準檢測成果報告（邦文）…… 481

43. 湯河原町—城東村間の一等水準檢測成果報告（邦文）…… 486

第 4 册（昭和11年12月）

44. 平面源を有する彈性波勢力の偏り（英文）…… 妹澤克惟・金井清 489

45. 媒體の異同が地震初動の分布に及ぼす影響（英文）…… 妹澤克惟 506

46. 8 階建築に於ける震動勢力の地下逸散性（英文）…… 妹澤克惟・金井清 514

47. 五重塔の耐震性（英文）…… 妹澤克惟・金井清 525

48. 土の粘彈性と剪斷抵抗（邦文）…… 石本巳四雄・飯田汲事 534

49. 土のプラスティック變形に關する實驗（序報）（英文）…… 宮部直巳 543

50. 垂直荷重による砂層の變形（序報）（英文）…… 宮部直巳 553

51. 土壤層中に於ける人工地震波の傳播並に土壤の彈性に關する研究（共1）（邦文）…… 那須信治・萩原尊禮・表俊一郎 560

52. 發震機構に就いて（英文）…… 井上宇胤 582

53. 茨城縣大賓村及上大津村に於ける地震動卓越週期の觀測（邦文）…… 萩原尊禮 599

54. 有感地震の1日中の分布に就いて（英文）……………… 岸 上 冬 彦 604
55. 明治9年以降東京觀測各月地震回數統計（邦文）……… 石 本 巳 四 雄 610
56. 本邦に於ける火山活動の移動に就て（英文）…………… 寺 田 寅 彦 616
57. 更新世以後に於ける丹那斷層の運動に就いて（英文）… 久 野 久 619
58. 振動方法による土の彈性測定（英文）…………………… 石 本 巳 四 雄／飯 田 汲 事 632

Contents.

Vol. XIV.

Part 1.—March, 1936.

Page

1. K. SEZAWA and K. KANAI, Damped Free Oscillation and Amplitudes in Resonance, with Special Reference to Decay of Seiches in Straits. (in English). 1
2. K. SEZAWA and K. KANAI, Elastic Waves Formed by Local Stress Changes of Different Rapidities. (in English). 10
3. R. TAKAHASI, Precise Levelling at the Asama Volcano. (in Japanese). 18
4. R. TAKAHASI, Latitude Determination at the Koasama and the Boroku Triangulation Points. (in Japanese). 26
5. T. MATUZAWA, Seismometrische Untersuchungen des Erdbebens vom 2. März 1933. III. Erdbebentätigkeit vor und nach dem Grossbeben. Allgemeines über Nachbeben. (in deutsch). 38
6. T. FUKUTOMI, Heights of Tunamis at Simoda in Southern Idu Peninsula. (in Japanese). 68
7. Y. OTUKA, Marine Lower Pleistocene of the Central Kwanto Plain. (An evidence of basin forming force of the Kwanto plain). (in English). 75
8. G. IMAMURA et N. YAZIMA, Contributions à l'Etude Géologique du Plateau de Musasino, près de Tokyo. (en français)... 83
9. H. KUNO, The Geologic Section along the Tanna Tunnel. (in English). 92
10. T. SAITA and M. SUZUKI, Vibration of a Tall Building

Caused by Earthquake Shocks. (in Japanese). 104

11. K. SEZAWA and K. KANAI, Energy Dissipation in Seismic Vibrations of Actual Buildings of Unlike Structure. (in English). 119

12. K. SEZAWA and K. KANAI, Energy Dissipation in Seismic Vibrations of a Six-storied Structure. Coincidence of Resonance and Corresonance. (in English). 134

13. Precise Levelling along the Line from Miyako to Aomori. (in Japanese). 146

Part 2.—June, 1936.

14. K. SEZAWA, On the Relation betweenSeismic Origins and Radiated Waves. (in English). 149

15. K. SEZAWA and K. KANAI, The Nature of Transverse Waves transmitted through a Discontinuity Layer. (in English) ... 157

16. K. SEZAWA and K. KANAI, Improved Theory of Energy Dissipation in Seismic Vibration of a Structure. (in English)... 164

17. K. SEZAWA and K. KANAI, Energy Dissipation in Seismic Vibrations of a Seven-storied Structure. Nature of Corresonance. (in English). 189

18. H. KAWASUMI and S. HONMA, On a Problem Concerning the Internal Structure of the Earth as Discussed from the Time-distance Curve of the Formosa Earthquake of April 20, 1935. (in English). 201

19. T. MINAKAMI, Changes in the Heights of Volcano Asama caused by Eruptions in 1935. (in English). 222

20. S. YAMAGUTI, Relation between Earthquakes and Precipitation, Barometric Pressure, and Temperature. A Supplementary Note. (in English). 235

21. M. ISHIMOTO, Observation des périodes prédominantes dans les secousses séismiques à Dewa-mura et à Hamamatu-tyô. (en japonais). 240

22. M. ISHIMOTO, Construction d'un microséismographe mécanique. (en français). 248

23. T. FUKUTOMI, Physical and Chemical Properties of the Simogamo, Rendaizi and Simokawazu Thermal Springs in Southern Idu Peninsula. I. (in English). 259

24. R. TAYAMA, Landslide in Dainenzi Hill, Sendai. (in Japanese). 271

25. N. NASU and T. HAGIWARA, The Kawati-Yamato Earthquake of February 21st, 1936. (in Japanese). 285

26. N. NASU and T. HAGIWARA, Determination of the Proper Periods of the Ground in Osaka. (in Japanese). 290

27. N. MIYABE, Some Phenomena associated with the Kawati-Yamato Earthquake of Feb. 21, 1936. (in Japanese). 297

28. T. SAITA, Geological and Topographical Investigation of the Earthquake Damages on the Boundary between Osaka and Nara Prefecture on the 21st of February, 1936. (in Japanese). 307

Part 3.—September, 1936.

29. H. KAWASUMI, Theoretical and Experimental Study of Initial Motion of Seismographs and the Quantitative Study of First Impulsion of Earthquake. Part I. (in English). 319

30. H. KAWASUMI and Z. KINOSITA, Theoretical and Experimental Study of Initial Motion of Seismographs and the Quantitative Study of First Impulsion of Earthquake. Part II. (in English) 339

31. K. SEZAWA and K. KANAI, Damping in Seismic Vibrations of a Surface Layer due to an Obliquely Incident Disturbance. (in English). 354

32. K. SEZAWA and K. KANAI, Dissipation Waves Accompanying Forced Seiches in a Bay. (in English). 360

33. K. SEZAWA and K. KANAI, The Effect of Stiffness of Floors on the Horizontal Vibrations of a Framed Structure. (in

English). 367

34. K. SEZAWA and K. KANAI, Energy Dissipation in Seismic Vibrations of Actual Buildings Predicted by means of an Improved Theory. (in English). 377

35. N. MIYABE, On the Degree of Disturbance of the Earth's Crust. (in English). 387

36. S. YAMAGUTI, A Discussion on the Results of a Statistical Investigation of Earthquake Phenomena. (in English). 399

37. T. FUCHIDA, An Experimental Method to solve the Equation of Motion of the Seismograph. (in English). 415

38. T. NAGATA, Space Distribution of Earthquake Hypocentres in the Kwantô District. (in Japanese). 420

39. N. NASU, T. HAGIWARA and S. OMOTE, Studies on Earthquakes in the Kwantô District. Part I. (in Japanese). 427

40. Y. OTUKA, The Takasegawa Green Tuff beds of the Yuri district, Akita pref., Japan, and Correlation of the Lower Neogene in Japan. (in English). 438

41. H. TSUYA, Geology and Petrography of Io-sima (Sulphur Island), Volcano Islands Group. (in English). 453

42. Relative Vertical Displacements of Bench-marks along the Lines of Levels from Hukuroi to Okitu, from Okitu to Odawara, and from Okitu to Kôhu. (in Japanese). 481

43. Relative Vertical Displacements of Bench-marks along the Line of Levels from Yugawara to Zyôtô-mura, on the East Coast of the Idu Peninsula. (in Japanese). 486

Part 4.—December, 1936.

44. K. SEZAWA and K. KANAI, Polarization of Elastic Waves generated from a Plane Source. (in English). 489

45. K. SEZAWA, The Effect of Differences in the Media on the Distribution of Displacements in a Seismic Wave Front. (in English). 506

46. K. SEZAWA and K. KANAI, Energy Dissipation in Seismic Vibrations of an Eight-storied Structure. (in English). ... 514
47. K. SEZAWA and K. KANAI, On the Seismic Vibrations of a Gozyûnotô (Pagoda). (in English). ... 525
48. M. ISHIMOTO et K. IIDA, Experiences sur le sol. (in japonais). 534
49. N. MIYABE, Preliminary Notes on Experimental Studies on the Plastic Deformation of Soil. (in English). ... 543
50. N. MIYABE, Experimental Studies on the Deformation of Sand Masses due to Vertical Loads. I. (in English). ... 553
51. N. NASU, T. HAGIWARA and S. OMOTE, Studies on the Propagation of the Artificial Earthquake Waves through superficial Soil or Sand Layers and the Elasticity of Soil and Sand. (in Japanese). ... 560
52. W. INOUYE, Notes on the Origins of Earthquakes. (in English). ... 582
53. T. HAGIWARA, Observation of the Predominating Periods in the Earthquake Motions at Daihô-mura and Kamiôtu-mura, Ibaraki Prefecture. (in Japanese). ... 599
54. F. KISHINOUYE, On the Diurnal Periodicity of Felt Earthquakes. (in English). ... 604
55. M. ISHIMOTO, Etudes statistiques sur les séismes observés à Tôkyô depuis 1876. (en japonais). ... 610
56. T. TERADA, On the Slow Migratory Motion of the Volcanic Activity in Japan. (in English). ... 616
57. H. KUNO, On the Displacement of the Tanna Fault since the Pleistocene. (in English). ... 619
58. M. ISHIMOTO and K. IIDA, Determination of Elastic Constants of Soils by means of Vibration Methods. Part I. Young's Modulus. (in English). ... 632

1. *Damped Free Oscillation and Amplitudes in Resonance, with Special Reference to Decay of Seiches in Straits.*

By Katsutada SEZAWA and Kiyoshi KANAI,

Earthquake Research Institute.

(Read Nov. 19, 1935.—Received Dec. 20, 1935.)

Persistency of Free Oscillation and Amplitudes in Forced-Resonance Oscillation.

1. We discussed in a previous paper[1] the nature of the decay in an epicontinental sea, both in the amplitudes of forced seiches and in the damping of free seiches. The problem was discussed dynamically. It was found that, corresponding to incident waves of surface elevation,

$$w_1 = \cos f(\sqrt{g\xi}t + x), \tag{1}$$

the seiches excited in the epicontinental sea of surface elevation assume the form

$$w' = \frac{2\cos f'(x+l)\cos\{f'\sqrt{g\xi'}t - \tan^{-1}(a\tan f'l)\}}{a\sqrt{\cos^2 f'l + a^2\sin^2 f'l}}, \tag{2}$$

where $a = \sqrt{\xi'/\xi} = f'\xi'/f\xi$, ξ, ξ' being depths in the outer sea and epicontinental sea respectively. The decay factor, namely, the ratio of the successive amplitudes of the same phase of the free oscillation, was expressed by

$$\left(\frac{1-a}{1+a}\right)^2, \tag{3}$$

Equation (2) shows that, the greater the value of a, the larger the diminution in the amplitudes of seiches under resonance conditions, compared with those out of resonance, while equation (3) indicates the contingency that, the nearer the value of a is to unity, the more does the damping factor diminish. This means that, in the problem of dissipation, smallness of amplitudes in or almost in resonance condition is not sufficient index of high damping in the case of free oscillation.

1) K. SEZAWA, *Proc. Imp. Acad.*, **11** (1935), 177; *Bull. Earthq. Res. Inst.*, **13** (1935), 476~483.

We shall next consider the case of damped oscillation of a non-dissipative nature. Taking the case of a pendulum, and letting the displacement of the supporting point be

$$w_1 = \cos pt, \tag{4}$$

the solution of the oscillation is then expressed by

$$w' = Ae^{-kt}\cos(nt+\varphi) + \frac{p^2}{\sqrt{(n_0^2-p^2)^2+4k^2p^2}}\cos\left(pt - \tan^{-1}\frac{2kp}{n_0^2-p^2}\right), \tag{5}$$

where $n^2 = n_0^2 - k^2$, $2\pi/n_0$ = period of free oscillation. This equation shows that, the greater the damping of free oscillation, the smaller become the amplitudes of forced oscillation, in any case, under resonance conditions.

In almost all geophysical problems, the damping of oscillations is mainly due to the energy dissipation in the form of waves. If the oscillation of an apparently proper period be observed, it is possible to postulate two different conditions, namely, the one in which the quantity similar to α in the equations (2), (3) is very large and the other in which that quantity is very small. Let such a quantity be β; then a large β indicates the case in which the velocity of transmission of any disturbance in the prescribed limited region is large compared with its velocity outside of it, whereas a small β indicates the reverse case. Now, if β be very large, forced periodic oscillation is improbable, it being a free oscillation. If, on the other hand, β be very small, it is partly forced and partly free oscillation. In the case of an epicontinental sea, β (or α) being a certain fraction of unity, the forced oscillation of resonance type should also be of some pronounced amplitude, like the ones in free oscillation. The only possible way of identifying free oscillation in this case is to ascertain the particular type of damping. Since in the previous investigation, the type of such damping was rather regular, it was possible for us to determine the damping factor of the oscillation fairly accurately. In the case of a strait, the factor corresponding to β being rather greater than unity, the nature of free seiches is more clearly determined.

Persistency of Seiches in Straits.

2. A kind of seiche was found to appear in straits by Honda, Terada, Yoshida, and Isitani as the result of observation made along

the coasts of the Japanese islands.[2] Hidaka[3] studied mathematically the possible periods of free seiches in certain straits. From the physical point of view, the problem whether such seiches are likely to exist or not, is rather an important one.

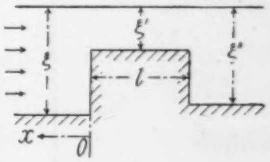

Fig. 1a.

We shall first deal with the forced oscillation of the straits. For simplicity, the straits and the two outer seas are assumed to have respectively uniform depths and breadths of values ξ', ξ, ξ'', η', η, η'', and we take the axis of x directed outwards with its origin at one end of the straits. The elementary solutions of incident waves (u_1, w_1) and reflected waves (u_2, w_2) in the first outer sea; the incident waves (u_1', w_1') and reflected waves (u_2', w_2') in the straits, and the transmitted waves (u'', w'') in the second outer sea are

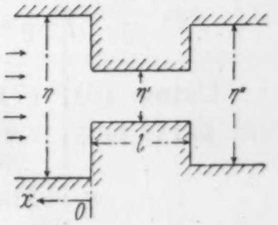

Fig. 1b.

$$\left.\begin{aligned} u_1 &= -ie^{i(\sigma t+fx)}, & w_1 &= f\xi e^{i(\sigma t+fx)}, \\ u_2 &= iAe^{i(\sigma t-fx)}, & w_2 &= f\xi Ae^{i(\sigma t-fx)}, \end{aligned}\right\} \tag{6}$$

$$\left.\begin{aligned} u_1' &= -iBe^{i(\sigma t+f'x)}, & w_1' &= f'\xi' Be^{i(\sigma t+f'x)}, \\ u_2' &= iCe^{i(\sigma t-f'x)}, & w_2' &= f'\xi' Ce^{i(\sigma t-f'x)}, \end{aligned}\right\} \tag{7}$$

$$u'' = -iDe^{i(\sigma t+f''x)}, \qquad w'' = f''\xi'' De^{i(\sigma t+f''x)}, \tag{8}$$

where u, w signify the horizontal displacements and surface elevations of waves; $2\pi/f$, $2\pi/f'$, $2\pi/f''$ are the lengths of the waves in the successive seas corresponding to the period $2\pi/f'$, so that $\sigma/f=\sqrt{g\xi}$, $\sigma/f'=\sqrt{g\xi'}$, $\sigma/f''=\sqrt{g\xi''}$.

The boundary conditions are such that

$$x=o: \qquad w_1+w_2=w_1'+w_2', \tag{9}$$

$$\xi\eta(u_1+u_2)=\xi'\eta'(u_1'+u_2'), \tag{10}$$

$$x=-l: \quad w_1'+w_2'=w'', \quad \xi'\eta'(u_1'+u_2')=\xi''\eta''u''. \qquad (11),\ (12)$$

Substituting (6), (7), (8) in these conditions, it is possible to determine A, B, C, D as follows:

---

2) K. Honda, T. Terada, Y. Yoshida, D. Isitani, *Publ. Earthq. Inv. Comm.*, No. 26 (1908); *Journ. Coll. Sci., Tokyo Imp. Univ.*, **24** (1908).

3) K. Hidaka, *Mem. Imp. Marine Obs.*, **5** (1935), 267~326, 327~358.

$$A\phi=(\alpha-\beta)(\alpha'+\beta')e^{i(f'-f'')}+(\alpha+\beta)(\alpha'-\beta')e^{-i(f'+f'')}, \tag{13}$$

$$B\phi=2(\alpha'+\beta')e^{i(f'-f'')}, \tag{14}$$

$$C\phi=2(\alpha'-\beta')e^{-i(f'+f'')}, \tag{15}$$

$$D\phi=4, \tag{16}$$

where

$$\phi=(\alpha+\beta)(\alpha'+\beta')e^{i(f'-f'')}+(\alpha-\beta)(\alpha'-\beta')e^{-i(f'+f'')}, \tag{17}$$

$$\alpha=\frac{f'\xi'}{f\xi}=\sqrt{\frac{\xi'}{\xi}},\quad \alpha'=\frac{f''\xi''}{f'\xi'}=\sqrt{\frac{\xi''}{\xi'}},\quad \beta=\frac{\xi'\eta'}{\xi\eta},\quad \beta'=\frac{\xi''\eta''}{\xi'\eta'}. \tag{18}$$

Using (6), (7), (8), (13), (14), (15), (16), (17) and taking the real parts only, we obtain, corresponding to the incident waves of type

$$u_1=\sin f(\sqrt{g\xi}t+x),\qquad w_1=f\xi\cos f(\sqrt{g\xi}t+x), \tag{19}$$

the expressions for the combined incident and reflected waves in the first sea, those for the seiches in the straits, and that for the transmitted waves as follows:

$$u=u_1+u_2$$

$$=\frac{2\sqrt{\{\alpha'(\alpha\cos f'l\sin fx+\beta\sin f'l\cos fx)\}^2+\{\beta'(\alpha\sin f'l\sin fx-\beta\cos f'l\cos fx)\}^2}}{\sqrt{\{(\alpha\beta'+\alpha'\beta)\sin f'l\}^2+\{(\alpha\alpha'+\beta\beta')\cos f'l\}^2}}$$

$$.\cos\Big\{\sigma t-\tan^{-1}\Big(\frac{\alpha\beta'+\alpha'\beta}{\alpha\alpha'+\beta\beta'}\tan f'l\Big)$$

$$+\tan^{-1}\Big(\frac{\beta'(\alpha\sin f'l\sin fx-\beta\cos f'l\cos fx)}{\alpha'(\alpha\cos f'l\sin fx+\beta\sin f'l\cos fx)}\Big)\Big\}, \tag{20}$$

$$w=w_1+w_2$$

$$=\frac{2f\xi\sqrt{\{\alpha'(\alpha\cos f'l\sin fx+\beta\sin f'l\cos fx)\}^2+\{\beta'(\alpha\sin f'l\sin fx-\beta\cos f'l\cos fx)\}^2}}{\sqrt{\{(\alpha\beta'+\alpha'\beta)\sin f'l\}^2+\{(\alpha\alpha'+\beta\beta')\cos f'l\}^2}}$$

$$.\cos\Big\{\sigma t+\tan^{-1}\Big(\frac{\alpha\beta'+\alpha'\beta}{\alpha\alpha'+\beta\beta'}\tan f'l\Big)$$

$$+\tan^{-1}\Big(\frac{\beta'(\alpha\sin f'l\sin fx-\beta\cos f'l\cos fx)}{\alpha'(\alpha\cos f'l\sin fx+\beta\sin f'l\cos fx)}\Big)\Big\}, \tag{21}$$

$$u'=u_1'+u_2'=\frac{2\sqrt{\{\alpha'\sin f'(x+l)\}^2+\{\beta'\cos f'(x+l)\}^2}}{\sqrt{\{(\alpha\alpha'+\beta\beta')\cos f'l\}^2+\{(\alpha\beta'+\alpha'\beta)\sin f'l\}^2}}$$

$$.\sin\Big\{\sigma t+\tan^{-1}\Big(\frac{\alpha\beta'+\alpha'\beta}{\alpha\alpha'+\beta\beta'}\tan f'l\Big)+\tan^{-1}\Big(\frac{\alpha'}{\beta'}\tan f'(x+l)\Big)\Big\}, \tag{22}$$

$$w' = w_1' + w_2' = \frac{2f'\xi' \sqrt{\{\alpha' \cos f'(x+l)\}^2 + \{\beta' \sin f'(x+l)\}^2}}{\sqrt{\{(\alpha\alpha' + \beta\beta')\cos f'l\}^2 + \{(\alpha\beta' + \alpha'\beta)\sin f'l\}^2}}$$

$$\cdot \cos\left\{\sigma t + \tan^{-1}\left(\frac{\alpha\beta' + \alpha'\beta}{\alpha\alpha' + \beta\beta'}\tan f'l\right) + \tan^{-1}\left(\frac{\beta'}{\alpha'}\tan f'(x+l)\right)\right\}, \quad (23)$$

$$u'' = \frac{2}{\sqrt{\{(\alpha\alpha' + \beta\beta')\cos f'l\}^2 + \{(\alpha\beta' + \alpha'\beta)\sin f'l\}^2}}$$

$$\cdot \sin\left\{\sigma t + f''(x+l) + \tan^{-1}\left(\frac{\alpha\beta' + \alpha'\beta}{\alpha\alpha' + \beta\beta'}\tan f'l\right)\right\}, \quad (24)$$

$$w'' = \frac{2f''\xi''}{\sqrt{\{(\alpha\alpha' + \beta\beta')\cos f'l\}^2 + \{(\alpha\beta' + \alpha'\beta)\sin f'l\}^2}}$$

$$\cdot \cos\left\{\sigma t + f''(x+l) + \tan^{-1}\left(\frac{\alpha\beta' + \alpha'\beta}{\alpha\alpha' + \beta\beta'}\tan f'l\right)\right\}. \quad (25)$$

These equations show that the maximum horizontal or vertical displacement of the seiches under resonance condition, $\cos f'l = 0$, in the usual sense, is $(\alpha\alpha' + \beta\beta')/(\alpha\beta' + \alpha'\beta)$ times that of the case in which the incident waves are exceedingly long. This is due to the energy

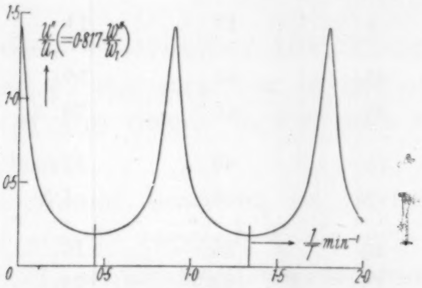

Fig. 2. Tugaru Straits.

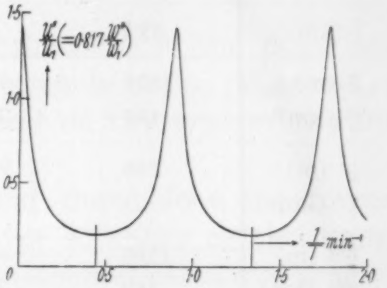

Fig. 3. Yura Straits.

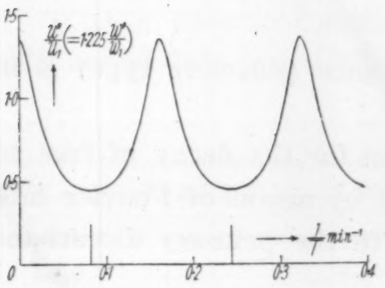

Fig. 4. Akasi Straits.

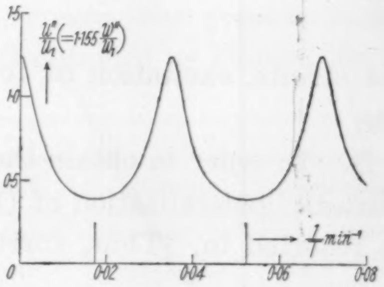

Fig. 5. Naruto Straits.

of seiches having dissipated into the two outer seas. The variation in

displacements at $x=-l$, with the differences in the period of disturbing waves for a few actual straits given below, were calculated, as shown in Figs. 2~6. The short vertical strips indicate cases corresponding to resonance conditions (we may call the condition, at which the curves assume maximum values just at the middles between successive resonance, by *corresonance*). The most probable values of l, ξ, η, ξ', η', ξ'', η'' were taken from the charts published by the Imperial Hydrographic Department, rough sketches of the coast lines being shown in Figs. 7~9. Since in all these straits the values of $(\alpha\alpha'+\beta\beta')/(\alpha\beta'+\alpha'\beta)$ are less than unity, the ratio of the displacement under resonance conditions to that at zero frequency is small in every example. It follows then that, in

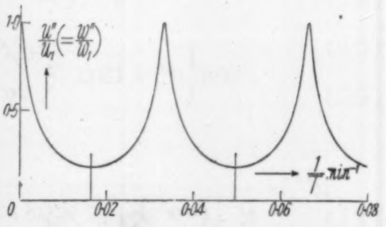

Fig. 6. Simonoseki Straits.

Table I.

Straits	Tugaru	Yura	Akasiseto	Naruto	Simonoseki
Station	Hakodate	Yura	Iwaya	Naruto	Simonoseki
l (km)	89·7	1	5	17	11
ξ (m)	1500	40	45	40	10
η (km)	140	25	25	40	20
ξ' (m)	200	90	75	40	15
η' (km)	23	3	3	6	1·5
ξ'' (m)	1500	60	30	30	10
η'' (km)	140	30	25	40	20
T (min)	140	2·0	12.5	51~59	54·3~57·6 64·8

these straits, excitation of forced resonance (selective type) is improbable.

3. In order to obtain the expression for the decay of free seiches in straits, generalization of (1), (2), (3) by means of Fourier integrals was resorted to. Thus, corresponding to the primary disturbance,

$$w_1=F(\sqrt{g\xi}t+x), \tag{21}$$

we obtain

$$w_2=\left(\frac{\alpha-\beta}{\alpha+\beta}\right)\sum_{m=0}^{\infty}(-1)^m\left\{\frac{(\alpha-\beta)(\alpha'-\beta')}{(\alpha+\beta)(\alpha'+\beta')}\right\}^m F(\sqrt{g\xi}t-2m\gamma l-x)$$

$$+\left(\frac{\alpha'-\beta'}{\alpha'+\beta'}\right)\sum_{m=0}^{\infty}(-1)^m\left\{\frac{(\alpha-\beta)(\alpha'-\beta')}{(\alpha+\beta)(\alpha'+\beta')}\right\}^m F(\sqrt{g\xi}t-\overline{2m+1}\gamma l-x), \quad (22)$$

$$w'=\left(\frac{2\alpha}{\alpha+\beta}\right)\sum_{m=0}^{\infty}(-1)^m\left\{\frac{(\alpha-\beta)(\alpha'-\beta')}{(\alpha+\beta)(\alpha'+\beta')}\right\}^m F\left\{\gamma(\sqrt{g\xi'}t-2ml+x)\right\}$$

$$+\frac{2\alpha(\alpha'-\beta')}{(\alpha+\beta)(\alpha'+\beta')}\sum_{m=0}^{\infty}(-1)^m\left\{\frac{(\alpha-\beta)(\alpha'-\beta')}{(\alpha+\beta)(\alpha'+\beta')}\right\}^m F\left\{\gamma\sqrt{g\xi'}t-\overline{2m+1}l-x)\right\}, \quad (23)$$

$$w''=\frac{4\alpha\alpha'}{(\alpha+\beta)(\alpha'+\beta')}\sum_{m=0}^{\infty}(-1)^m\left\{\frac{(\alpha-\beta)(\alpha'-\beta')}{(\alpha+\beta)(\alpha'+\beta')}\right\}^m$$

$$\cdot F\left\{\gamma\gamma'\left(\sqrt{g\xi''}t-\frac{1}{\gamma'}\overline{2m+1}l+l+x\right)\right\}, \quad (24)$$

where $\gamma=f'/f, \qquad \gamma'=f''/f'.$ (25)

The decay factor thus assumes the value

$$\left\{\frac{(\alpha-\beta)(\alpha'-\beta')}{(\alpha+\beta)(\alpha'+\beta')}\right\}^2, \quad (26)$$

regardless of whether the incident disturbance is in the outer sea at one end of the strait or in the other or even in both. Moreover, the form of the decay factor does not depend on the type of the initial disturbance.

It should however be borne in mind that, since the forms of actual straits towards their ends are never so sharp as those shown in Fig. 1, which form was assumed for mathematical convenience, the decay factors of seiches in the case of an actual straits should assume values much less than those calculated here.

4. With a view to comparing, at any rate, the present calculation with actual data, we studied the result obtained by Honda, Terada,

Table II.

Straits		Tugaru	Yura	Akasi	Naruto	Simonoseki
T (min)	cal.	135	2·25	12·3	57	61
	obs.	140	2·0	12·5	51～59	54·3～57·6 64·8
Decay factor	cal.	0·61	0·30	0·25	0·27	0·48
	obs.	0·50	0·30	0·25	0·25	0·40

etc.[4] The fact that the large wave oscillations in the straits were free from selective resonance is obvious from the explanation already given.

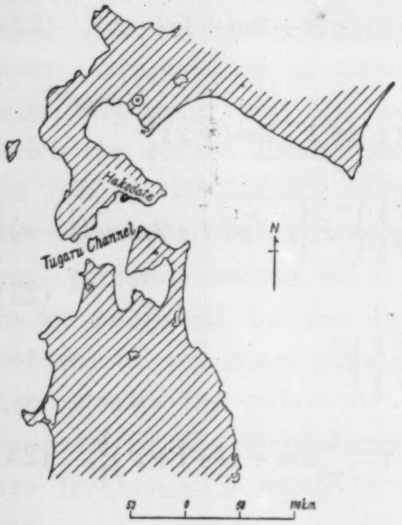

Fig. 7.

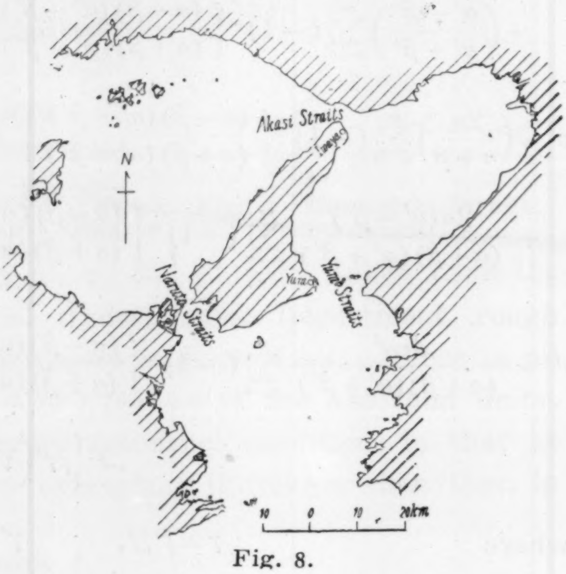

Fig. 8.

We compared the periods as well as the types of decay in order to ascertain the most probable free seiches, the result being shown in Table II.

This table shows that, although the observed decay factors are never larger than the calculated values, the factors are rather very close to the calculated ones, indicating that the phenomena of seiches in these straits are, though incidentally, very similar to those mathematically predicted.

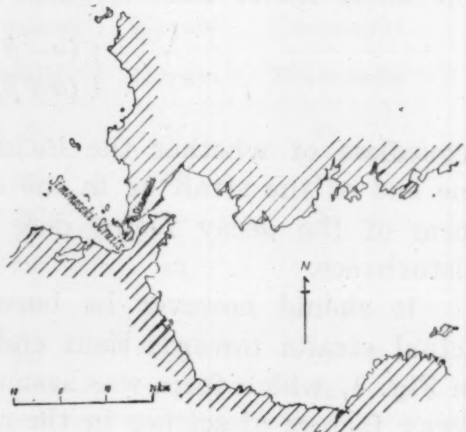

Fig. 9.

---

4) K. HONDA, T. TERADA, Y. YOSHIDA, D. ISITANI, *loc cit.*

1. 自由振動の持續性と共振の振幅との關係 海峽に於けるセイシの問題

地震研究所 妹澤克惟
金井清

振動體の振動勢力が摩擦共他により，即ち熱に變る機構によつて失はれる場合には，自由振動の減衰が多いもの程，共振に於ける振幅も小さいといふことがいはれる．然るに地球物理學の諸問題で振動振幅の減少するのは多くは振動勢力が波動の形として外部へ流れて行くため，即ち勢力逸散性に基くものである．

このやうな場合に，自由振動の減衰と共振の振幅とがやはり同じやうな關係になるかといふに必ずしもそうでないことがわかる．即ちこの場合には，自由振動をなす部分の現象の波動速度が外部のそれよりも速いときにはその部分の强制共振振動に於ける振幅が小さくなる傾向を取り，逆に自由振動をなす部分の現象の波動速度が外部のそれよりも遲いときにはその部分の强制共振振動に於ける振幅が大きくなる傾向がある．然るに自由振動の減衰性を見ると，考へてゐる部分に於ける速度と外部の速度とが等しいとき(但し斷面が等しいとき)，又は効果的の速度が等しいとき（但し斷面が異なる場合）にその自由振動が速く減衰することがわかる．即ち强制振動の振幅の小さいことが必ずしも自由振動の速く減衰する意味とはならないのである．

前に陸棚に於けるセイシを考へたのと同じやうにして理論を導き出し，その結果を，津輕，由良，明石，鳴門，下關等の海峽や瀨戸につき，本多博士，寺田博士等の觀測結果と比較してみたのである．週期は單に長波往復の速度を示すだけであるから勿論非常によく一致した．物理的に一層面白い減衰性を比較して見たところが，之も豫想以上によくあつたのである．理論は寧ろ餘り減衰しない極限の場合を示すのに過ぎないのに，比較結果は餘りに合ひ過ぎる位である．これは海峽の深さ，幅等の平均値に對する扱方が實際問題によく適合してゐる爲か，それともセイシの方が割合に理論通りに行はれる爲かも知れぬ．

尙，海峽の場合に選擇共振がないかとの危惧は，初め述べた關係により，寧ろ共振の振幅が非常に小さくなる場合に屬してゐることがわかるから，全然問題とならないものである．

2. *Elastic Waves Formed by Local Stress Changes of Different Rapidities.*

By Katsutada SEZAWA and Kiyoshi KANAI,

Earthquake Research Institute.

(Read Oct. 15, 1935.—Received Dec. 20, 1935.)

Criterion on Positive and Negative Change in Local Stress.

1. It was shown in a previous paper[1] that, if a stress is applied to a body or released from it, the energy transmitted to infinity depends on the rapidity with which the stress is applied or released. The greater the rapidity with which the stress is applied or released, the greater the energy that is transmitted to infinity, and at the same time the greater the energy that is required at the origin. If the stress were applied or released extremely slowly, no wave energy would be transmitted to infinity, whereas, if done with infinite rapidity, exactly half the energy given at the origin will be transmitted to infinity.

When the previous paper was read, the question arose as to whether the energy transmission due to the release of the stress at a certain rapidity would be equal to that due to the application of the same stress— a rather natural question, in view of the prevalent idea that the large energy of some earthquakes is due to sudden release of the strain energy that was stored in the focal region. Our opinion however is that, even should there be an inequality between two cases, the inequality would be due to an origin concerned with the theory of thermodynamics, namely the problem of compression and that of rarefaction differ entirely from each other, particularly in the nature of the supply and evolution of the heat energy, whence it is of pressing importance to explain first why the two cases, when it comes to the problem of elastic waves, are, from the dynamical point of view, equivalent to each other.

Since however we are here dealing merely with a pure elasticity problem, not involving any transfer of heat energy, we can assume that the change is adiabatic. Again, although there is essential

1) K. SEZAWA, "Elastic Waves Produced by Applying Statical Force to a Body or by Releasing it from a Body," *Bull. Earthq. Res. Inst.*, **13** (1935), 729~739.

difference between compression and rarefaction in the change in density of material arising from a force applied, the amount in actual cases is negligible.

2. Fourier's series and integrals, which play an important part in the solution of the present and similar problems, are used under the assumption that the difference between compression and rarefaction in stress, or that between push and pull in displacement, is concerned merely with the algebraic sign in tensor quantities, superposition or subtraction among these quantities being thus permissible in almost every case. The solution of the problem in which a stress is released from a stressed body, is the same as the one in which stress of the same amount but of opposite signs is added to the same body in a stressed condition, the initial stress being assumed to be statical and permanently induced in the body. Since, mathematically, permanent stress cannot be affected by a fresh disturbance, no energy transfer can ever be expected to occur from the addition of new stresses. This manner of treatment is resorted to in several branches of mathematical physics. Thus, the algebraic superposition of wave forms is not restricted to the case of sinusoidal curves, but generally applied to cases of other complex curve forms.

The most important restriction with respect to the problem under consideration is that the curves to be analysed should finally (not necessarily after a long interval of time or space) return to the same zero line as the one at the beginning of the problem. Symbolically, if u be the amplitude of a curve at the coordinate point x, the above condition may be written

$$\int_{-\infty}^{\infty} u' dx = 0\,, \tag{1}$$

or

$$\int_{-\infty}^{\infty} u dx = \text{a finite quantity}, \tag{1'}$$

where x may be used as the coordinate in space or in time.

3. The number of actual examples that could be given in proof of the conception just mentioned is endless. The simplest examples of it in mechanics are perhaps the longitudinal waves along a tense string and the sound waves in a deep sea. If the disturbance were of rarefactional type, it is possible for the initial stress in the transmission media to be neutralized, making the resulting stress zero in some extreme cases. Even in a case of this kind, the manner of transmission of the waves, or of their energy cannot be changed unless every law governing physical quantities, such as Young's modulus,

compressibility, etc., differ with differences in the amplitudes of the transmitted disturbances. There are a number of similar examples in wave phenomena in every branch of physics. It will be clear from these examples that superposition or subtraction of disturbances, or more generally, addition or removal of disturbances in a body, is related merely to the algebraic signs of the disturbances.

4. In order to obtain a clearer understanding of the problem with respect to the energy supply, which is also one of physical phenomena in wave or vibratory motion, let a stress P be removed from some point of a body, and let the velocity of the corresponding movement of the same point be $\dot{u}_1$. The work applied to the body is then expressed by

$$\int_{-\infty}^{\infty} P\dot{u}dt\,, \qquad (2)$$

where $P=P_0+P_1$, P_0 being the initial stress. This expression can be transformed to

$$\int_{-\infty}^{\infty} P\dot{u}dt=\int_{-\infty}^{\infty}(P_0+P_1)(\dot{u}_0+\dot{u}_1)dt$$
$$=P_0\int_{-\infty}^{\infty}\dot{u}dt+\int_{-\infty}^{\infty}P_1\dot{u}dt \qquad (2')$$

where $\dot{u}_0$ is zero and P_0 is independent of t. From (1) it is obvious that $\int_{-\infty}^{\infty}\dot{u}dt=0$, it being well known that $\int_{-\infty}^{\infty}P_1\dot{u}dt$ is always of positive sign, which shows that the work done to the body is the same whether a given stress is added to it or taken from it, provided the transfer of heat is not taken into account. It is to be remembered that in certain problems, the condition, $\int_{-\infty}^{\infty}udt=$ a finite quantity, may be used in lieu of $\int_{-\infty}^{\infty}\dot{u}dt=0$.

5. In the previous paper we treated a disturbance of the type

$$\left.\begin{aligned} &P=0, \quad (r=a,\ t<0) \\ &P=-P_0e^{-ct}(1-e^{-qt}), \quad (r=a,\ t>0,\ c\to 0) \end{aligned}\right\} (3)$$

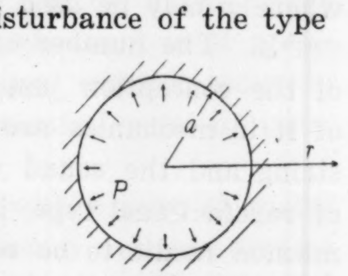

Fig. 1.

transmitted outwards with a velocity peculiar to elastic waves. This form of disturbance indicates that the expressions for disturbance satisfy the condition in (1). Even were we to take the more general state at any t or x, namely,

$$\left.\begin{aligned}\phi&=0,\quad (\tau<0)\\ \phi&=\frac{aP_0}{2\pi i\rho r}\left\{\int_{-\infty}^{\infty}\frac{e^{ip\tau}\,dp}{(p-ic)(p-\alpha)(p-\beta)}-\int_{-\infty}^{\infty}\frac{e^{ip\tau}\,dp}{(p-iq)(p-\alpha)(p-\beta)}\right\},\ (\tau>0)\end{aligned}\right\}(4)$$

in which $\tau=t-(r-a)/v$, condition (1) is also satisfied, representing the transmission of the disturbance outwards with velocity v. Since ϕ indicates the mere radial transmission of waves from the origin, the nature of ϕ would not be changed if there were any preexisting stress in the medium or even if another series of waves were travelling through that medium.

An alternative way of introducing c in the first term on the right-hand side of (4) for satisfying condition (1) is to use

$$\phi=\frac{aP_0}{2\pi i\rho r}\int_{-\infty}^{\infty}\frac{e^{ip\tau}-e^{ip\tau_1}}{p(p-\alpha)(p-\beta)}\,dp\,, \qquad (5)$$

where $\tau_1=t-(r-a)/v-t_1$. But, the nature of the problem with respect to the ineffectiveness of the preexisting stresses or displacements on the disturbance under consideration is the same as in case (4).

6. We shall show what an odd result would be obtained were the initial stress confused with that of a prescribed dynamical disturbance. It is well known that the energy of waves is proportional to the square of their amplitudes. Let the amplitudes of the initial stress be V and that of the prescribed dynamical stress U. Then, on the assumption that the initial stress also participates in wave energy, we would have the condition that the amount of the change in energy due to the disturbing motion is

$$(U+V)^2-V^2(=2UV+V^2),$$

which may be modified in any way by adjusting V for the initial stress. It follows then that, in the case of seismology, were longitudinal waves of compressional type propagated through a deep layer of the earthcrust, a very large energy would be transmitted, whereas, were the same waves of rarefactional type propagated also through a deep layer of the crust, very feeble or sometimes negative energy would be transmitted. It is an established fact in the classical theory of elasticity that the initial stress does not affect the new disturbing stress phenomena, excepting the action due to density change in the material caused by the initial stress.

Elastic Waves Formed by Local Stress Changes of Different Rapidities.

7. The nature of the initial stress, which is essential to the consideration of the elastic waves produced by releasing a stress from a body, has now been clearly ascertained. We shall next calculate the displacement of the medium as well as the amount of the transmitted energy, both at an infinite distance from the origin of the stress change.

We found in the previous paper the expressions for the displacement of the medium and the transmitted energy. The change in the pressure at $r=a$, namely

$$\left.\begin{aligned} &P=0\,, \quad (r=a, \quad t<0) \\ &P=P_0 e^{-ct}(1-e^{-qt}), \\ &\qquad\quad (r=a, \quad t>0) \end{aligned}\right\} \quad (3')$$

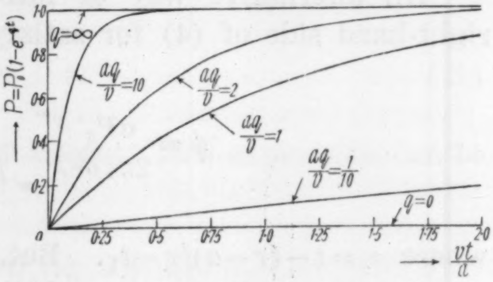

Fig. 2.

in which $c\to 0$ (as will be shown graphically in Fig. 2), and q indicates the rapidity of the stress change. The dispalcement at $r\to\infty$ can be determined from equation (13) of the previous paper, namely, from

$$u=\frac{a^3P_0}{4\mu}\left[\frac{1}{r^2}+\frac{\alpha\beta}{Q}\left(\frac{q}{vr}-\frac{1}{r^2}\right)e^{-q\tau}+\frac{\beta q}{(\alpha-\beta)(\alpha-iq)}\left(\frac{\alpha}{vr}-\frac{i}{r^2}\right)e^{i\alpha\tau}\right.$$
$$\left.-\frac{\alpha q}{(\alpha-\beta)(\beta-iq)}\left(\frac{\beta}{vr}-\frac{i}{r^2}\right)e^{i\beta\tau}\right],$$

writing in a more convenient form,

$$u=\frac{a^3P_0}{4\mu r^2}+\frac{\dfrac{a^3P_0}{4\mu r^2}}{\left\{4-4\left(\dfrac{aq}{v}\right)+\left(\dfrac{v}{\mathfrak{v}}\right)^2\left(\dfrac{aq}{v}\right)^2\right\}}\left\{\left[-4e^{-q\tau}+\left(\frac{aq}{v}\right)e^{-X\tau}\right.\right.$$
$$\left.\cdot\left\{4-\left(\frac{v}{\mathfrak{v}}\right)^2\left(\frac{aq}{v}\right)\cos Y\tau+\frac{\left(4-2\left(\dfrac{v}{\mathfrak{v}}\right)^2-\left(\dfrac{v}{\mathfrak{v}}\right)^2\left(\dfrac{aq}{v}\right)\right)}{\sqrt{\left(\dfrac{v}{\mathfrak{v}}\right)^2-1}}\sin Y\tau\right\}\right]$$
$$\left.+4\left(\frac{r}{a}\right)\left(\frac{aq}{v}\right)\left[e^{-q\tau}-e^{-X\tau}\left\{\cos Y\tau+\frac{\left(2-\left(\dfrac{v}{\mathfrak{v}}\right)^2\left(\dfrac{aq}{v}\right)\right)}{2\sqrt{\left(\dfrac{v}{\mathfrak{v}}\right)^2-1}}\sin Y\tau\right\}\right]\right\}, \quad (6)$$

where $$X = 2\frac{v}{a}\left(\frac{\mathfrak{v}}{v}\right)^2, \quad Y = 2\frac{\mathfrak{v}}{a}\sqrt{1-\left(\frac{\mathfrak{v}}{v}\right)^2}.$$

The final result for the displacement variation in t as well as in r (in the case $r \to \infty$) due to stress change at $r = a$ with different rapidities, is shown in Fig. 3.

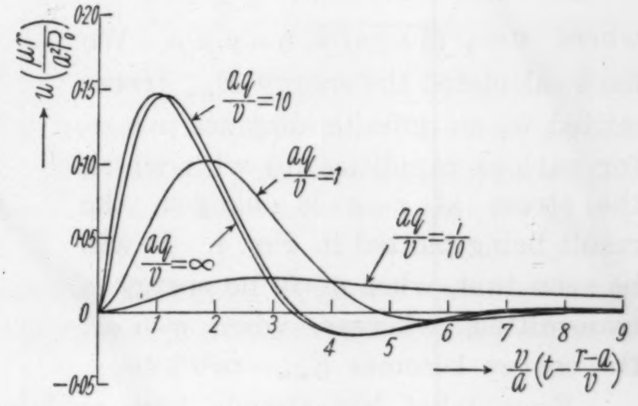

Fig. 3.

The transmission of energy is determined from equation (18) in the previous paper, namely

$$\begin{aligned}
E_{r\infty} = {} & \frac{\pi a^9 P_0^2}{\mu r^3} + \frac{\pi a^6 P_0^2}{2\mu\left(\frac{4\mu}{\rho a^2} - \frac{4\mu q}{\rho a v} + q^2\right)^2}\Bigg[-\left(\frac{4\mu}{\rho a^2}\right)^2\left(\frac{1}{r^3} - \frac{2q}{v r^2}\right) \\
& + \frac{1}{a^3}\left(q^2 + \frac{4\mu q}{\rho a v} + \frac{4\mu}{\rho a^2}\right)q^2 - \frac{1}{r^3}\left(q^2 - \frac{8\mu q}{\rho a v} + \left(\frac{4\mu}{\rho a v}\right)^2\right)q^2 \\
& - \frac{2}{r}\left(\frac{4\mu}{\rho a^2}\right)^2\left(\frac{1}{v^2} + \frac{1}{4\mathfrak{v}^2}\right)q^2 - \frac{8\mu}{\rho a^2 r^2 v}\left(-\frac{4\mu}{\rho a v} + q\right)q^2 \\
& - \frac{\frac{4\mu}{\rho a^2}q}{\left(\frac{4\mu}{\rho a^2} + \frac{4\mu q}{\rho a v} + q^2\right)}\Bigg\{\frac{\rho}{\mu v}\left[\left(\frac{4\mu}{\rho a^2}\right)^2 + \frac{4\mu q^2}{\rho a^2}\right]q^2 \\
& - \frac{2}{r}\left(\frac{1}{r^2} + \frac{1}{4\mathfrak{v}^2}\right)\left[\left(\frac{4\mu}{\rho a^2}\right)^2 + \frac{16\mu^2}{\rho^2 a^3 v}q + \frac{4\mu}{\rho a^2}q^2\right]q \\
& + \frac{2}{v r^2}\left[\left(\frac{4\mu}{\rho a^2}\right)^2 + \frac{32\mu^2}{\rho^2 a^3 v}q + \left(\frac{4\mu}{\rho a v}\right)^2 q^2 - q^4\right] \\
& + \frac{2}{r^3}\left[-\frac{16\mu^2}{\rho^2 a^3 v} + \left(\frac{16\mu^2}{a^2\rho^2 v^2} + \frac{4\mu}{\rho a^2}\right)q + q^3\right]\Bigg\}\Bigg].
\end{aligned}$$

We recently discovered that this equation can be transformed to a very simple form

$$E_{r\infty}=\frac{\pi a^6 P_0^2}{2\mu r^3}+\frac{\pi a^6 P_0^2}{2\mu a^3}\frac{\left(\frac{aq}{\mathfrak{v}}\right)^2}{\left\{4+4\frac{aq}{v}+\left(\frac{aq}{\mathfrak{v}}\right)^2\right\}}, \qquad (7)$$

where $v=\sqrt{(\lambda+2\mu)/\rho}$, $\mathfrak{v}=\sqrt{\mu/\rho}$. We have calculated the energy $E_{\infty\infty}$ transmitted to an infinite distance $r=\infty$ for various rapidities (q) with which the stress at $r=a$ is changed, the result being plotted in Fig. 4. It will be seen that, when $q=0$, no energy is transmitted, whereas, when $q\rightarrow\infty$, the energy becomes $E_{\infty\infty}=\pi a^3 P_0^2/2\mu$.

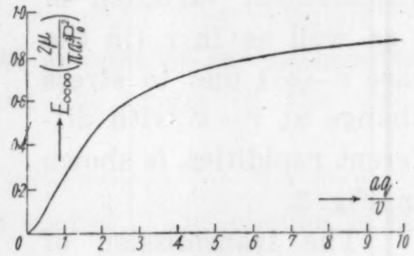

Fig. 4.

From what has already been explained, the result in Fig. 4 is the same whether a stress is applied at $r=a$ or removed from the same origin. It will also be known that, were the energy possible to evolve from the strained part with a certain volume through which elastic waves are transmitted, energy $E_{\infty\infty}$ would not assume zero value even when $q=0$.

Remarks on Compressional and Rarefactional Waves.

8. From the fact that wave phenomena are independent of the initial stress, it is now possible to conclude that the push and pull types of wave motion may be made to coincide respectively with the compressional and rarefactional types of waves.

It is obvious that, if a pressure were applied with some rapidity to a cavity as we have considered, waves of push type, namely, compressional waves, would be observed, whereas, if the pressure were released, waves of pull type, namely, rarefactional waves, would result.

We shall next consider the case in which a large volume of the earth's crust is uniformly compressed, and that a break in the form of a cavity (which actually is improbable) has occurred at some point in the crust. Waves of the pull type, namely, rarefactional waves will then be radiated from this cavity, notwithstanding that the crust is initially compressed. If, on the other hand, a large volume of the crust were pulled uniformly from all directions, the resulting break at any point within that volume would produce waves of the push type, namely, compressional waves, in spite of the fact that the crust is initially in a rarefied state.

2. 局所的內力を種々の速さで變化する場合に生ずる彈性波

地震研究所 {妹澤克惟
金井清

この前の論文で示したところの局所的內力を附加へたり，取除いたりする場合に生ずる彈性波の問題を，內力變化の符號的關係につき一層委しく說明し，次に種々の速さで變化したときに生ずる彈性波の波形，勢力の割合等を算出したのである．又前の論文で非常に複雜な形をなした公式を極く簡單な形に直した．

この研究から，地殼の靜力學的壓力卽ち普通の如く全體的壓力であらうと，又特に張力的狀態にあらうと，地震初動の押しと引きとは必ず壓縮性地震波と膨脹性地震波とに相當するものであるといふ說明を附加へて置いた．

3. 淺間火山の精密水準測量結果

地震研究所 高橋龍太郎

(昭和10年10月15日發表—昭和10年12月20日受理)

緒言

火山の活動に伴つて火山の山體のみならず火山の周圍に相當な廣範圍に亘つて隆起又は沈降等の地形變動を起した事は珍らしくない．否寧ろ火山の活動の消長は必ず火山山體及其附近の地域の地形變動を伴ふものであると考へ得るのである．其の最も著しい例は1914年櫻島の噴火である．此の噴火の後に行はれた水準測量によれば[1]此の噴火に伴つて火山周圍數十粁半徑の地域が火山を中心とした圓錐狀の沈下を爲したものと見做す事が出來る．其の中心附近に於ける最大沈下量は 220 cm に達してゐる．此の外に北海道駒ヶ岳の噴火の場合にも火山體周圍の沈降を伴つた事が噴火後の精密水準測量[2]によつて檢測されてゐる．尙此等の例の外に北海道有珠岳の場合には火山活動の消長に伴つて隆起，沈降を混有した複雜なる變化を爲した事が判明してゐる．[3]

此れに關聯して面白いのは火山に於ける地盤の傾斜變化である．昭和7年から行つてゐる淺間火山南麓小諸町に於ける觀測[4]によると，噴火の1～2ヶ月前より地盤の傾斜に大きな變化が現れ，噴火の終熄と共に舊位に復する．其の傾斜變化の方向は噴火前に山の南東麓が膨れ上る樣な向である．其後山の東麓峰の茶屋に竣工した淺間火山觀測所に据付けた傾斜計によつても，矢張噴火の前に山の東南麓が膨れ上ると考へれば說明出來る樣な向の地盤の傾斜運動が起る事が觀測されてゐる．[5] T. A. Jaggar[6] は Hawaii の Kilauea Volcano に於て此と類似の現象を觀測してゐる．

從つて火山の附近に於て精密水準測量を行つて，其れによつて噴火前に傾斜計に現れる地形變動が如何なる性質のものであり，如何なる分布を爲すものであるかを判明せしむる事は火山現象と火山の構造を簡明する上に甚だ有意義な事柄である．

淺間火山の中央火口丘が活動の消長と共に昇降する事は古來の記錄にも見え，又近

---

1) F. OMORI, *Bull. Imp. Earthq. Inv. Comm.*, **8** (1914), 1.
2) C. TSUBOI, *Bull. Earthq. Res. Inst.*, **8** (1930), 298; *Jap. Journ. Astro. Geophys.*, **10** (1933), 174.
3) F. OMORI, *Bull. Imp. Earthq. Inv. Comm.*, **5** (1911), 1.
4) R. TAKAHASI, *Bull. Earthq. Res. Inst.*, **11** (1933), 25.
5) T. MINAKAMI, *Bull. Earthq. Res. Inst.*, **13** (1935), 625.
6) T. A. JAGGER and R. H. FINCH, *Bull. Seis. Soc. Amer.*, **19** (1929), 38.

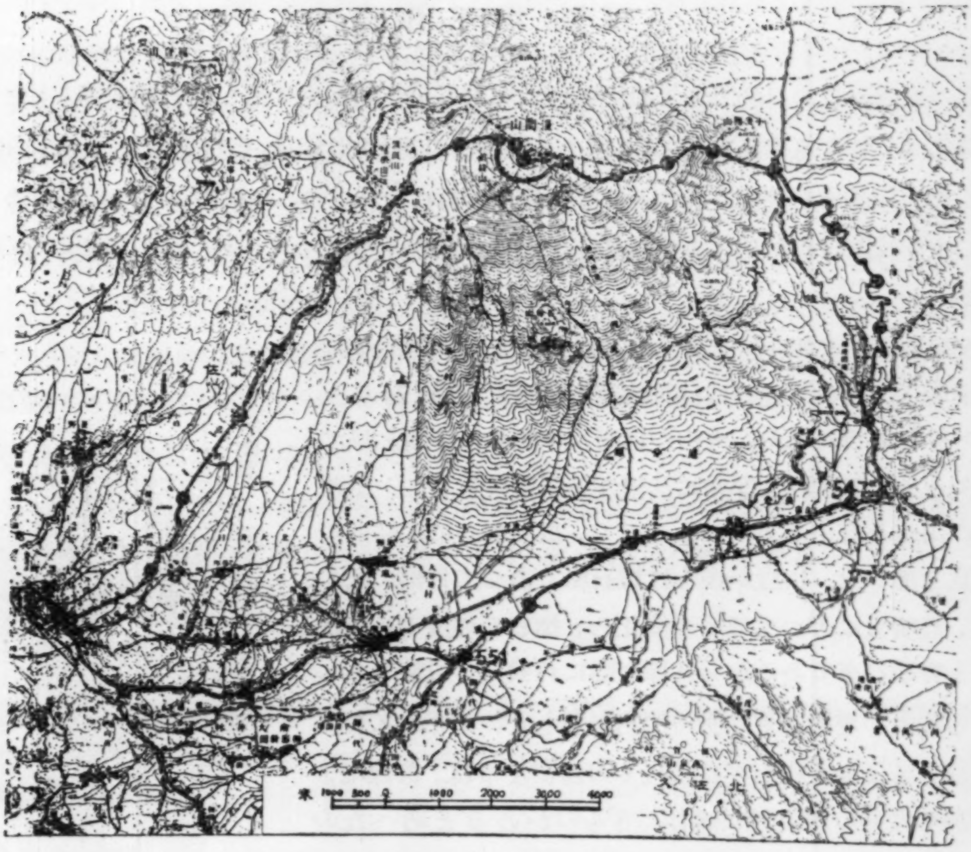

第1圖 淺間山近傍地形と新設水準線

The newly established levelling route.

年八木貞助氏は中央火口丘が外輪山前掛山に對して上昇した事を唱ふるものゝある事を述べて居る.[7] 又最近の水上氏[8]の測定に依れば中央火口丘は前掛山に對し 1912 年の測定に比し約 10 m の隆起を爲してゐる. 然し此等は何れも前掛山に對しての上昇であつて, 前掛山自體の高さの變化は全く不明である. 前掛山の高さを正確に求めるには山麓より精密水準測量を爲す事が最も確實である. 斯くする事によつて同時に山腹に標高の正確に判明してゐる水準點を數點設け得る事は將來此の火山に於て行はれんとする各種の測定, 研究に大いに役立つ事である. 淺間火山の精密水準測量は以上の樣な目的を以て其の施行を計畫されてゐたが, 幸にして學術振興會の補助を得たので, 陸地測量部に委囑し昨年 10~11 月に埋石を爲し, 約半年の Seasoning を經て本年 6~9 月に第一回の測定を完了したので其の結果を報告する.

7) 八木貞助 地學雜誌 **45** (1933), 552.
8) 水上武 地震研究所彙報 **13** (1935), 318.

撰點，埋石作業

此の水準測量の目的である以上各種の要求を可及的に充す爲，第一期計畫として第1圖に示す如き水準路を撰んだ．卽ち小諸町より御代田，追分，沓掛を通り，淺間山東麓なる火山觀測所を經由，其れより登山道を山頂に登り，次に小諸町へ下る經路である．此の水準線路は御代田より沓掛に至る間は既設の水準點 551～547 を利用するものである．

撰點は昭和9年10月22～23日陸地測量部浦野測量師と筆者とで行ひ，埋石は浦野測量師により10月24日～11月5日に行はれた．火山の精密水準測量は今回を以て嚆矢とし，且其れも非常に活潑なる活動性を有し，急傾斜の山腹を有する火山であるので，撰點埋石には特別の注意を拂つた．山腹が多くは燒石原であつて目標に乏しく，且噴火によつて地形の變化し，標石の埋沒する事は最も普通の事であるから其樣な際に再發見を可能ならしめる爲に，周圍顯著地物の測角を爲した．又平地に於て用ひらるゝ如き標石では根入りの僅少なる爲，砂礫地帶に於ては其の安定性に疑はしきものがあると考へたので，此の地帶に於ては特に第2圖に示す如き金屬製標識を用ひた．且埋石場所は噴灰砂礫に埋沒する事を極力防止する爲と雪害を避ける意味から，なる可く尾根筋に撰んだのである．

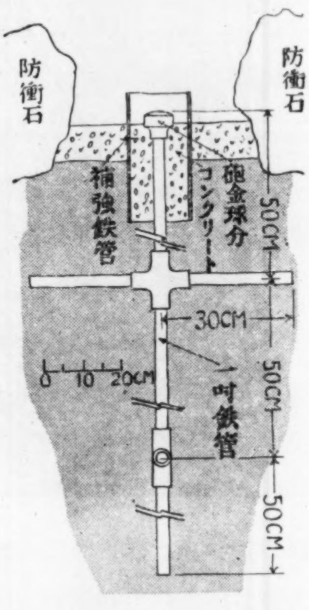

第2圖　金屬標識
The Metal B.M.

中央火口丘上の點は噴火に因る埋沒，火口內への崩落等の危險率多大なるを以て，特に個數を增して300 m 宛の間隔を置き3箇となし火口の西，南及東方に埋設した．

小諸町より火山館に至る間，沓掛より峯の茶屋に至る間の標石には運搬の便と經費の都合により陸地測量部規定の小型標石を用ひた．砂礫地帶に埋設した金屬標識は特に必要な場合には其上に更に鑄鐵製蓋を冠らせる事になつてゐる．

測量經過と測定の結果

埋石終了と同時に降雪期に入り測量不能となつたので，約半年の Seasoning を爲して標石を落付かせ，昭和10年5月頃より雪解後に測量を爲す計畫であつた．然る所，昭和 10 年1月頃より山は活動期に入り4月 20 日の大爆發以來屢々爆發を繰返して居り測量には甚だ危險を感じたが6月に至り活動やゝ衰へたので6月 15 日より測量

に着手した．測量は陸地測量部の浦野千代藏氏によつて爲されたが測量中屢々の爆發と此の年特に不良であつた天候とに禍されて6月中旬より9月上旬まで3ケ月の日月を費した．其の間爆發の危險と悪天候と戰つて遂に測量を成し遂げた浦野氏の努力は誠に感謝に堪えぬものである．

山頂に於ける金屬標識金5～金8は8月 17 日の爆發により埋沒し，其後爆發の連續せる爲捜査の機會なく，爲に8月 14 日片道測量を爲したるのみにて往復の測量を爲し得ず，水準路の閉塞に頗る苦心を爲し，遂に小諸口中央火口丘下より無間の谷（中央火口丘と前掛山及東前掛山間の火口原）を通つて東前掛山北端の鞍部にある金4に閉塞する新道路を開鑿して此を行つたのであつた．成果表中大丸石とあるは此の迂回路の略中央に設けた臨時水準點である．

水準點の所在，種類，水準點相互間の距離，觀測眞高及び觀測眞高を閉塞誤差に對して平均し且楕圓補正を施したる平均値は第1表に示した通りである．

結　　語

從來知られてゐる淺間山の高さ及形態は凡て三角水準測量と平板測量とに依るものであつて，今回の水準測量と同程度の精度を有するものでないから今回の水準測量の結果と比較して直ちに噴火に伴ふ山體の變形に言及する事は出來ない．此の爲には適當な時季に於て今一度同程度の精度を有する水準測量を行なはなければならない．唯二三の水準點の位置の元の標高は地形圖から 5 m 位の誤差で讀取る事が出來るから，此を今回の水準測量の結果に比較して見ると，此の位の範圍では一般に變化が認められない．即ち5 m 以上の隆起，沈降はない樣に見えるのである．唯火口の南椽にある金6水準點の原標高の地圖から讀取つた値は 2525 m であるが今回の測量では 2534 m であり，又火口東椽の金5水準點の原標高は地圖の最高點とは少しく離れてゐるから 2540 m 位であるのに，今回得た値は 2558 m である．即ち火口西椽では地形圖と比較して判明する程度の變化はないのに，火口南椽では約 8 m，火口東椽では約 18 m の隆起をしてゐる．換言すれば中央火口丘は傾斜し且隆起した樣に見える．然し此の隆起の一部分は噴出物の堆積による見掛上のものであつて，其の堆積が事實上東側に多い爲に東側が餘計に隆起する樣に見えるのである．

水上武氏の 1934 年 9～10 月の測定によれば，中央火口丘最高點は前掛山に對し 10 m の相對的隆起を爲してゐる事は前に既に述べた通りであるが，前掛山の高さは 1912 年以來變らないと考へて此を今回の測定値と比較すれば，中央火口丘は昨年 10 月以來約 8 m の隆起をした事になる．此れは水上氏の測定と殆んど同時に埋設した水準點

第 I 表

所在地							標石番號	距離	觀測の眞高
縣	國	郡	町村	大字	字	通稱			
長野	信濃	北佐久	御代田村	——	谷地澤		551	2082 m	828·3829 m
〃	〃	〃	小沼村	馬瀬口	北側	柵口神社参道	10827	2472	800·8103
〃	〃	〃	南大井村	平原	東居祖		10826	2453	748·8661
〃	〃	〃	北大井村	柏木	前原	四谷下	10825	2277	710·2932
〃	〃	〃	小諸町	——	町屋敷	八幡神社內	10824	1700	711·7181
〃	〃	〃	〃	——	中郷土		小 22	1745	835·0944
〃	〃	〃	〃	——	高峰		小 21	1587	970·3819
〃	〃	〃	〃	——	上天池	七尋石脇	小 20	1603	1110·8426
〃	〃	〃	〃	——	高峰		小 19	1926	1271·2098
〃	〃	〃	小沼村	鹽野	南ケ原	淺岳ホテル前	金 11	1550	1485·6375
〃	〃	〃	大里村	菱平	高峰	二ノ鳥居下	金 10	1609	1694·7530
〃	〃	〃	小沼村	鹽野	南ケ原	火山館前	小 18	1408	1983·4359
〃	〃	〃	〃	〃	〃	湯ノ平	金 9	862	2192·6361
〃	〃	〃	〃	〃	淺間山	前掛山北	金 8	1586	2429·6452
〃	〃	〃	輕井澤町	長倉	——	東前掛北	金 4	1044	2425·0376
〃	〃	〃	〃	〃	——	横道下	金 3	1219	2162·2519
〃	〃	〃	〃	〃	——	三ノ鳥居下	金 2	1060	1822·8774
〃	〃	〃	〃	〃	——	二ノ鳥居北	金 1	1224	1566·8660
〃	〃	〃	〃	〃	——	峰ノ茶屋	10823	2215	1405·8331
〃	〃	〃	〃	〃	——	見晴臺下	小 17	2219	1377·0635
〃	〃	〃	〃	〃	獅子岩	千ケ瀧	小 16	2212	1212·1580
〃	〃	〃	〃	〃	〃	千ケ瀧	小 15	2124	1073·2723
〃	〃	〃	〃	〃	芹ケ澤		小 14	2224	975·3406
〃	〃	〃	〃	〃	舟久保		547	1940	951·1005
〃	〃	〃	西長倉村	長倉ノ內借宿	東屋敷		548	2140	977·3107
〃	〃	〃	〃	追分	西町		549	2071	979·4106
〃	〃	〃	御代田村	——	大林		550	1610	906·2413
〃	〃	〃	〃	——	谷地澤		551		828·3902
長野	信濃	北佐久	小沼村	鹽野	淺間山	前掛山北	金 8	374	
〃	〃	〃	〃	〃	〃	小諸 下山口	金 7	340	
〃	〃	〃	西長倉村	追分	〃	御代田下山口	金 6	331	
〃	〃	〃	輕井澤町	長倉	——	沓掛下山口	金 5		
長野	信濃	北佐久	小沼村	鹽野	淺間山	前掛山北	金 8	690	
〃	〃	〃	〃	〃	〃	無間谷	大丸石	896	
〃	〃	〃	輕井澤町	長倉	——	東前掛北	金 4		

標石番號中"小"とあるは小型標石，"金"とあるは金屬標識なる事を示す．

Table I

平均値	備考
m 828·3829	既設水準點
800·8098	神社に向ひて參道の左側石門より 28 m，石燈籠より 3·5 m
748·8650	土屋榮一宅隣消防倉裏手，消防倉より 11 m
710·2915	小諸，岩村田道路分岐點
711·7159	拜殿鳥居の中間左側鳥居より 11 m, 拜殿より 22 m
835·0909	松井へ至る道路の分岐點の北 100 m
970·3770	關東道との交叉點より北 140 m
1110·8365	七尋石の北 102 m
1271·2025	山林境石 167 號の南 41 m
1485·6286	淺岳ホテル西側の大岩に固定
1694·7429	二ノ鳥居下に現れ居る岩盤に固定，鳥居より 7·6 m
1983·4245	登山路と天狗露路に至る小徑との分岐點
2192·6237	前掛山南西斜面登山道より 22 m 上方の大岩塊に固定
2429·6327	無間谷の入口，釜山と前掛山の鞍部の北端
2425·0250	東前掛と釜山との鞍部，横道を登り切りたる所
2162·2392	横道下稍々傾斜緩なる所 小淺間△一草水△＝29°23′24·″0　小淺間△一離山△＝5[illegible]°46′58·″0
1822·8646	三ノ鳥居下　小淺間△一離山△＝69°39′15·″5 小淺間△一觀測所旗竿＝27°11′21·″0，　小淺間△一草水△＝43°06′03·″8
1566·8530	小淺間と淺間山との鞍部の中央，二ノ鳥居より北 40 m
1405·8201	淺間火山觀測所前庭
1377·0514	箱根土地專用道路見晴臺より 100 m 下道路の南側
1212·1467	輕井澤に至る環狀線道路分岐點下 200 m
1073·2619	千ケ滝 900 番地平井宅向側
975·3311	星野溫泉入口の北 38 m, 變電所前
951·0919	以下 5 箇既設水準點　昭和 7 年檢測値　m 951·0695
977·3024	977·2831
979·4027	979·3931
906·2337	906·2272
828·3829	828·3829
2429·6327	無間谷入口
2535·3263	小諸下山口　火口線より 5 m 三角尖山一前掛南杭 91°40′55·″0 大火山彈の下側　前掛南杭一北杭 32°29′13·″8
2534·5906	御代田下山口　火口線より 14 m 三角尖山一前掛南杭 65°28′19·″8,　前掛南杭一北杭 36°01′30·″0
2557·9933	輕井澤下山口，火口線より 20 m，大正岩の東側 小淺間△一觀測所旗竿＝9°49′41·″7,　小淺間一草水＝18°39′44·″7, 小淺間一離山＝44°22′50·″2
2429·6327	釜山頂上に至る指導標より 60 m 無間の谷へ入る赤色の大火山彈
2463·7144	追分下山口の西 150 m 無間谷底の南 15 m
2425·0250	

水準線路全長　48159 m　　　閉塞誤差　7·5 mm

に準據してゐるのであるから噴出物の堆積を見てゐるのでない事は明かである．若し中央火口丘の隆起がなかつたものとすると，前掛山が昨年來 8 m 程の沈下をした事になるが，前述の種々の考察からして此の考へよりも中央火口丘が隆起したと考へた方が妥當の様に思はれる．

此れに關聯して注意すべきは前出八木貞助氏の述べて居られる越保氏等の測定値で，此れによると 1933 年の活動の末期には中央火口丘は前掛山に比し 41.2 m の隆起をした事になつてゐる．

以上の事柄から考へると中央火口丘は活動期には，極く簡單な測量によつても容易に發見出來る程の隆起を爲すものと思はれる．唯中央火口丘以外の山體の隆起沈降は今回施行の如き程度の精密測量に依らなければ容易に判明し難い様である．因に今回の水準測量と昭和 7 年に檢測された 547～551 水準點の標高とを比較すると沓掛の 547 水準點は 551 に對し 22.4 mm 上昇してゐる．昭和 7 年の水準測量と今回のとの間には昭和 7 年の活動と本年の活動とを含んで居る事，小諸及峯ノ茶屋に於て觀測される地盤の傾斜變化が活動と山の南東麓の隆起との關係を示す事等から考へて，此の變動は火山活動と密接な關係にあるのではないかと思はれる．尚此の線路の明治 21 年來の變動は第 3 圖の様になつてゐる．

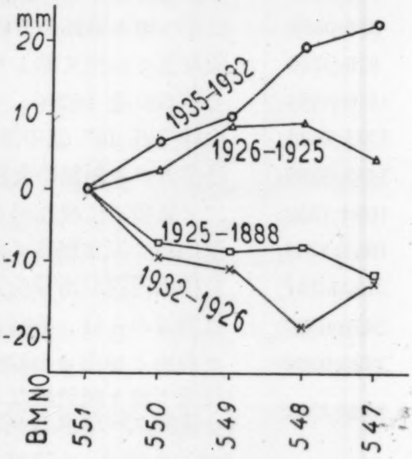

第 3 圖

今回の測量は凡て學術振興會の補助によつて施行されたものであつて，同會に對し深く感謝の意を表す．又陸地測量部並に陸地測量師浦野千代藏氏に對し深甚の謝意を表する次第である

3. *Precise Levelling at the Asama Volcano.*

By Ryûtarô TAKAHASI,

Earthquake Research Institute.

It is well known that the eruption of a volcano is often attended by the swelling and subsidence of the volcano itself as well as of the region surrounding it. In order to study both the spatial and time distribution of such crustal deformations related to eruptions, precise levelling was done this summer at volcano Asama, one of the most active in Japan.

The new line of levels, which is shown in Fig. 1, which begins from bench mark No. 551 previously established at Miyota, goes up the western slope of the volcano, and after passing arround the southern brink of the crater at the summit, descends the eastern slope down to the Asama Volcano Observatory, ending at bench mark No. 547 previously established at Kutukake, the whole forming a loop 48 km long.

The observations were made by Mr. Tiyozo Urano of the Japanese Land Survey. A Zeiss geodetic level was used. The observation conditions were extremely severe owing to the abnormal bad weather this summer, to the long and steep slopes of the mountain, and also to the frequent violent eruptions that occurred during the observations. Thanks to the ability of the observer, the closing error was surprisingly small.

The results are given in Table I. This being the first observation, naturally crustal deformations cannot yet be known, but upon comparing these results with the heights given in the topographic map of 1912, we may conclude that there has been no crustal deformations exceeding 5 m, except for the central cone, the eastern brink of the crater of which seems to have risen about 18 m. Undoubtedly, this elevation is partly due to the volcanic bombs and ashes that have accumulated since 1912, although there are evidences that true upheavals of the central cone take place during active periods of the volcano.

4. 小淺間及棒錄三角點に於ける緯度の測定

地震研究所 高 橋 龍 太 郎

(昭和10年10月15日發表——昭和10年12月20日受理)

緒 言

精密水準測量の結果の比較から地形の變動を云々する場合にはゼオイドの形狀の變らぬ事を假定してゐる．普通の地域に於ては此の假定は或ひは眞に近いであらうが，火山地方，殊に淺間山の如き活潑な活動を續けてゐる火山の近傍にあつては，地下の岩漿の狀態の變化によつてゼオイドの形に變化を起す疑は充分にあるのである．筆者は火山活動と關聯して如何なるゼオイドの變形が起るか，又淺間山頂を通つて實施される精密水準測量によつて將來檢出される地形の變動の幾部分がゼオイドの變形によるものであり，幾部分が眞の地殼の變形によるものであるかを推定する爲に，現在に於ける淺間山近傍のゼオイドの形を測定する必要を感じた．此處に記すものは其の一部として，今夏精密水準測量と同時に，淺間山東麓なる小淺間及び淺間山東南中腹にある棒錄三角點に於て行つた緯度の測定である．

測點及觀測器械

小淺間山頂に於ける測點は，小淺間3等三角點の東 4·93 m，北 0·90 m の地點で，標高 1655·1 m である．此處に混凝土の觀測臺を設置した．

棒錄に於ける測點は，棒錄3等三角點の東 4·10 m，北 2·38 m の地點で，標高は

第 I 表　測　點

三角點名	小淺間	棒錄
測地緯度	36° 24′ 24″·452	36° 22′ 55″·900
測地徑度	9h 14m 15s·684	9h 14m 14s·253
標高	1655m·07	1471m·64
歸心（緯度）	−0″·029	−0″·062
歸心（徑度）	−0s·013	−0s·011

1471·6 m，5 寸丸太を3本組合せ，根枷を打ち地表下へ 1·3 m 埋込み，地面より上は外函を作り，土砂を堅く詰め込みたる觀測臺を用ひた．三角點の測地經緯度，測點よ

り三角點への歸心修正値は第I表に示した通りである.

觀測に用ひた器械は Bamberg No. 11950 の子午儀で，焦點距離 67 cm，口經 70 mm, 90° 回轉出來る測微計の附屬したものである. 測微計1回轉の値は $78''.83$ で水準器の1分劃の値は Hanging が $1''.168$，Talcott の I が $1''.226$，II が $1''.233$ である.

時辰儀は Negus No. 1888 で，簡單な受信機によつて JJC の學用時報を受けた.

觀 測 し た 星 對

星は Boss の Preliminary General Catalogue に記載のものを用ひた. 小淺間と棒錄とは緯度の差が僅かに $1'.5$ 過ぎないので，撰んだ凡ての星對を兩方の測點で共通に用ふる事が出來た. 星對の重さとしては

$$p \backsim \frac{1}{\varepsilon_1^2+\varepsilon_2^2+\frac{4e^2}{n}}$$

を用ひた. 此處に ε_1，ε_2 は夫々星表に與へられてある數値から計算した南北兩星の位置の平分誤差，e は後に述べる1回の觀測に對する筆者の平分誤差，n は觀測回數である.

辻氏も既に言つて居らるゝ樣に[1]，現在では星表が古くなつて，星の位置の平分誤差が大きく，數回の觀測で星の位置の平分誤差と觀測の平分誤差とは同程度になるから，觀測回數を多くするよりも寧ろ星對の數を多く取る樣にした.

星對間の間隔の長い時を利用して方位星の經過を觀測した. 方位星としては 22 H Cam, μ Sgr, δ Del, ζ Cap, γ Gru, α Pisc, β Ceti, α UMi の中の數個を觀測した. 觀測時間に於ける晴曇の關係から南の星のみ觀測した場合もある. 特に小淺間に於ては最後の日に後に述べる樣な觀測を行つて方位角を精密に定めた.

觀 測 と 其 の 結 果

今回の觀測は非常な惡天候に禍されて，最初に計劃した通りの成績を擧げ得なかつた. 即ち棒錄三角點に於ては8月2日より8月9日迄の滯在中觀測爲し得たのは 6, 7, 8の3日間で然も 7, 8 兩日は明方1時間位晴れたるのみであつた. 余の日は毎日降雨乃至は夜に入りて濃霧となり，遂に豫定の觀測數を得ずして小淺間へ移轉するに到つた. 輕井澤，沓掛方面の霧多き事は有名であるが，殊に棒錄三角點は大窪澤と千

1) 辻光之助 東京天文臺報 2 (1934), 191.

第II表　星　對　表

星對番號	星表番號	光度	赤緯 (1935·0) ° ′	赤徑 (1935·0) h m s	重さ	星對番號	星表番號	光度	赤緯 (1935·0) ° ′	赤徑 (1935·0) h m s	重さ
9	4358	5·6	36 01	17 05 44	136	26	5865	3·0	29 53	22 39 57	190
	4381	3·2	36 53	17 12 47			5897	5·1	42 58	22 49 06	
13	4653	5·3	49 05	18 19 53	180	27	5957	5·6	46 02	23 04 41	229
	4683	6·0	23 49	18 26 54			5974	6·5	26 30	23 08 40	
14	4721	5·6	33 25	18 34 14	274	28	6006	6·0	30 04	23 17 38	278
	4749	4·6	39 33	18 42 14			6034	5·8	42 33	23 23 59	
16	4920	6·2	46 53	19 15 00	224	29	6080	4·3	43 58	23 37 12	265
	4942	5·2	26 08	19 20 11			6114	6·2	28 29	23 46 22	
17	4986	3·0	27 49	19 28 06	156	30	6172	6·0	26 44	23 58 46	208
	5048	2·8	44 58	19 42 57			19	5·2	45 43	0 06 56	
18	5085	6·0	47 46	19 50 12	171	31	52	6·1	43 26	0 15 16	290
	5134	5·5	24 45	19 59 16			89	5·3	29 24	0 26 41	
19	5193	6·0	33 32	20 12 52	177	32	123	4·4	33 22	0 33 24	280
	5220	6·5	39 12	20 17 54			138	5·5	39 06	0 37 35	
20	5265	5·1	48 44	20 28 03	129	33	223	6·1	41 00	0 59 15	255
	5303	5·1	23 53	20 35 42			248	6·4	31 40	1 04 25	
21	5373	4·8	26 51	20 49 21	134	34	281	4·7	24 14	1 10 13	272
	5414	5·5	45 54	20 58 55			346	6·4	48 23	1 32 28	
22	5433	5·5	38 26	21 03 59	178	35	379	5·7	34 55	1 38 18	260
	5471	4·4	34 37	21 15 15			402	6·3	37 38	1 44 49	
23	5567	5·4	42 59	21 37 38	206	36	489	6·4	38 44	2 06 56	342
	5617	5·3	29 52	21 46 58			514	5·1	33 56	2 13 05	
24	5669	5·7	44 20	22 00 19	112	37	536	6·1	41 06	2 18 47	286
	5730	6·2	28 17	22 10 40			555	5·9	31 31	2 23 36	
25	5764	4·6	46 13	22 18 20	226	38	619	5·7	44 01	2 39 51	225
	5798	6·0	26 26	22 26 07			634	4·8	28 59	2 44 02	

第 III 表　棒　錄　測　點

月日	星對番號	接眼鏡	測微計	水器準 I	水器準 II	緯度	重さ
1935 VIII						36° 22′	
6	17	W	9·9570	882	2896		
		E	11·4872	776	2772	57″·53	0·20
6	24	E	6·7498	924	2924		
		W	12·9570	805	2831	59·84	0·67
6	25	W	12·6760	892	2898		
		E	7·2185	841	2877	60·72	1·00
6	29	E	13·4372	672	2695		
		W	9·4822	944	2977	59·47	1·00
6	27	W	15·4095	817	2859		
		E	5·0550	819	2858	60·05	0·86
6	28	E	6·5458	708	2736		
		W	13·2252	819	2858	61·14	1·00
6	29	W	17·1152	774	2779		
		E	3·2228	805	2805	60·25	1·00
6	30	E	2·8892	940	2979		
		W	17·0510	904	2968	60·05	1·00
6	32	E	3·3818	790	2841		
		W	16.8222	690	2737	59·74	1·00
6	33	W	11·4240	877	2900		
		E	6·9618	861	2866	59·14	1·00
6	34	E	7·1362	707	2755		
		W	12·9632	632	2702	59·28	1·00
7	31	E	11·5768	689	2680		
		W	8·6735	827	2848	60·75	1·00
7	32	W	15·8515	856	2888		
		E	2·3335	745	2779	59·79	1·00
7	34	E	7·5322	787	2823		
		W	13·4088	795	2897	59·81	1·00
8	32	W	16·5820	784	2825		
		E	3·1748	979	2980	60·07	1·00
8	34	W	12·0968	917	2916		
		E	6·1918	763	2769	59·39	1·00

$\varphi = 36^\circ\ 22'\ 59''{\cdot}75 \pm 0''{\cdot}21 \qquad e = 0''{\cdot}234$

$R = 78''{\cdot}790 \pm 0''{\cdot}023$

小　淺　間　測　點

月日	星對番號	接眼鏡	測微計	水準器 I	水準器 II	緯度	重さ
1935 VIII						36° 24′	
17	34	E	5·6988	666	2699		
		W	13·9428	655	2660	36″·54	1·00

（次頁へ續く）

小　淺　間　測　點（續）

月日	星對番號	接眼鏡	測微計	水準器 I	水準器 II	緯度	重さ
1935 VIII						36°24′	
17	35	W E	16·2805 4·2580	714 848	2712 2845	″ 36·86	1·00
18	24	E W	5·9978 14·6008	833 797	2829 2785	36·92	1·00
18	25	W E	13·2255 5·5010	677 857	2682 2880	36·11	0·40
18	28	W E	13·7675 4·7862	795 784	2789 2785	36·97	1·00
18	30	W E	18·1860 1·6268	747 697	2762 2720	36·98	1·00
18	31	E W	10·0918 9·5438	795 850	2767 2823	37·52	1·00
18	32	E W	17·6610 1·7732	818 775	2804 2762	37·20	1·00
18	33	E W	6·0170 12·9192	701 878	2736 2901	36·07	0·33
18	34	W E	13·3400 5·1432	829 962	2781 2935	36·69	0·40
18	35	E W	3·3445 15·4960	840 1018	2838 2981	37·49	0·67
18	36	W E	13·4130 6·4893	731 824	2773 2872	37·24	1·00
18	37	E W	3·9192 13·0812	835 783	2888 2834	37·31	1·00
18	38	W E	5·7715 14·2778	931 883	2886 2845	35·38	1·00
19	13	E W	12·3012 7·8500	836 691	2859 2695	36·45	1·00
19	14	W E	6·4375 13·0438	692 718	2727 2760	35·74	0·67
19	18	W E	16·1800 2·7622	838 766	2865 2815	36·72	0·67
19	19	E W	7·7398 11·5598	720 837	2758 2871	37·14	1·00
19	20	W E	14·6312 5·9305	773 889	2806 2905	36·39	1·00
19	22	E W	15·8418 4·7540	734 668	2778 2689	36·29	1·00
19	23	W E	9·6912 11·4010	790 628	2839 2682	36·64	0·80
19	24	E W	5·7472 14·4378	677 897	2720 2928	36·78	1·00
19	25	W E	13·5795 5·7758	760 747	2799 2787	36·43	1·00
19	26	E W	11·2248 9·5200	739 742	2787 2793	36·22	1·00
19	27	W E	16·1220 3·4672	764 875	2816 2918	36·16	1·00

（次頁へ續く）

小 淺 間 測 點 (續)

月日	星對番號	接眼鏡	測微計	水準器 I	水準器 II	緯度	重さ
1935 VIII						36°24′	
19	28	E	5·3925	698	2778	″	
		W	14·3818	750	2838	36·83	1·00
19	29	W	18·3300	747	2834		
		E	2·1570	914	2978	35·87	1·00
19	30	E	1·5755	766	2838		
		W	18·1342	824	2885	37·13	1·00
19	31	W	9·8805	715	2764		
		E	10·4840	737	2803	36·85	1·00
19	32	E	1·7382	761	2834		
		W	17·5930	753	2815	37·00	1·00
19	33	W	13·1120	784	2880		
		E	6·2912	848	2910	36·43	1·00
19	34	E	6·1880	743	2824		
		W	14·4840	848	2920	37·04	1·00
19	35	W	3·6652	838	2888		
		E	15·7540	856	2886	37·62	1·00
19	36	E	6·7382	751	2836		
		W	13·7028	820	2905	36·47	1·00
19	37	W	14·3768	699	2774		
		E	5·2210	722	2809	36·84	1·00
19	38	E	14·2490	693	2796		
		W	5·7545	687	2781	36·90	1·00
20	13	W	7·7320	730	2706		
		E	12·1870	904	2878	36·81	0·60
20	14	E	13·4065	734	2743		
		W	6·9202	941	2945	37·11	1 00
20	16	W	5·7270	879	2863		
		E	14·8395	760	2758	36·31	1·00
20	17	E	9·1280	804	2831		
		W	9·9610	774	2815	36·34	1·00
20	18	W	16·2330	723	2736		
		E	2·9058	850	2884	36·48	1·00
20	19	W	11·5225	813	2820		
		E	7·7875	840	2860	36·42	0·67
20	22	W	3·9658	843	2859		
		E	15·0692	909	2901	35·63	0·80
20	25	E	5·8862	762	2812		
		W	13·7480	919	2963	36·88	1·00
20	26	W	8.3745	804	2816		
		E	10·0548	684	2698	35·74	0·50
20	27	E	4·1652	879	2906		
		W	16·8665	856	2904	36·84	0·67
20	28	W	14·1852	746	2749		
		E	5·2488	784	2794	36·52	1·00
20	29	E	1·5262	764	2819		
		W	17·8575	1000	3023	36·62	1·00
20	30	W	18·2252	738	2735		
		E	1·7525	870	2878	36·95	1·00

(次頁へ續く)

小淺間測點（續）

月日	星對番號	接眼鏡	測微計	水準器 I	水準器 II	緯度	重さ
1935 VIII						36°24′	
20	31	E	9·9318	700	2721	″	
		W	9·4110	913	2905	36·79	1·00
20	32	W	18·0380	840	2845		
		E	2·1652	799	2794	37·04	1·00
20	33	E	6·0648	779	2798		
		W	12·8838	728	2752	36·62	1·00
20	34	W	13·7815	704	2729		
		E	5·5188	659	2684	36·78	1·00
20	36	W	12·7648	730	2790		
		E	5·8072	700	2760	36·96	1·00
20	37	E	4·9738	750	2811		
		W	14·2148	920	2963	37·83	1·00
20	38	W	4·2770	717	2764		
		E	13·7938	763	2827	36·88	1·00
21	9	E	11·4728	843	2835		
		W	7·6442	899	2878	36·25	1·00
21	14	W	5·7400	905	2880		
		E	12·2857	828	2841	37·25	0·60
21	16	E	14·4735	774	2756		
		W	5·3540	883	2872	36·27	1·00
21	21	W	11·0462	797	2813		
		E	8·3978	745	2780	36·36	1·00
21	22	E	16·0042	782	2800		
		W	4·9010	732	2744	35·97	0·80
21	23	W	8·8710	721	2732		
		E	10·7048	781	2804	35·88	1·00
21	24	E	5·4980	737	2738		
		W	14·1418	870	2860	36·91	1·00
21	25	W	13·5848	712	2719		
		E	5·7782	646	2662	36·45	1·00

$$\varphi = 36^\circ 24' 36''.548 \pm 0''.052 \qquad \epsilon = 0''.263$$

$$R = 78''.792 \pm 0''.011$$

ケ瀧の澤との間に狹まれた低い山稜の突角にある爲に常に霧の往來が激しいのではないかと思はれる.

小淺間に移轉の後も天候依然として不良にして晴夜は全くなかつたが 18 日明方より天候回復して 21 日夜半迄に豫定の觀測を爲し得た. 21 日夜半より夜明までの時間に方位角，視準恆數及び經度の簡單な測定を爲した.

觀測の結果は第 III 表に示す如くである. 同表に於ては日附は Astyonomical Date で，E, W は接眼鏡の位置，測微計の値は星が視野を通る間に子午線に對稱に 4 回讀

んだ値の平均値で測微計の1廻轉を單位として揭げてある．水準器の値は星を Bisect する前及後に於ける氣泡兩端の讀みの和の和である．緯度は此等の値から

$$\varphi=\frac{1}{2}(\delta_N+\delta_S)+\frac{1}{2}R(M_W+M_E)+\frac{1}{16}d_I\left\{\sum L_{IE}-\sum L_{IW}\right\}$$

$$+\frac{1}{16}d_{II}\left\{\sum L_{IIE}-\sum L_{IIW}\right\}+\text{微分濛氣差}+\text{子午線への更正},$$

$$=\frac{1}{2}(\delta_N+\delta_S)+\frac{1}{2}R\left[\left\{M_W+\frac{d_I}{8R}(\sum L_{IE}-\sum L_{IW})\right.\right.$$

$$\left.\left.+\frac{d_{II}}{8R}(\sum L_{IIE}-\sum L_{IIW})\right\}-M_E\right]+\text{微分濛氣差}+\text{子午線への更正},$$

等々にて計算した．R は微測計1廻轉の値で $78''\!\cdot\!83$ と採つた．M 及 $\sum L$ は夫々前出の測微計及び水準器の値で，I, II, 及 E, W は夫々 I 及 II の水準器，及接眼鏡 E 及 W の場合に就ての値である事を示す．d_I 及 d_{II} は水準器1分劃の値，δ_N 及 δ_S は南北星の Apparent place で

$$\frac{1}{2}(\delta_N+\delta_S)=\frac{1}{2}(\delta_1+\delta_2)+\frac{1}{2}(\mu_1+\mu_2)t+g\cos\left(G+\frac{\alpha_1+\alpha_2}{2}\right)\cos\frac{\alpha_2-\alpha_1}{2}$$

$$+\frac{1}{2}\left\{h\cos(H_1+\alpha_1)\sin\delta_1+h\cos(H_2+\alpha_2)\sin\delta_2\right\}$$

$$+i\cos\frac{\delta_1+\delta_2}{2}\cos\frac{\delta_1\sim\delta_2}{2}+g'\cos\left(G'+\frac{\alpha_1+\alpha_2}{2}\right)$$

によつて計算する．δ, α は星の Mean place で，1，2 の suffix は一つの星對の先に來る星と，後に來る星とを表す．μ は固有運動である．特に固有運動の大きい星に就ては $\frac{1}{2}\Delta\mu t^2$ を計算に採り入れた．

上記の觀測の中，霧の往來の爲に，星が視野を通過する間に隱見して，完全に4回の Bisection の出來なかつた場合が度々あつた．此の樣な場合には此れを1回の觀測とせず

$$\frac{n_1n_2}{2(n_1+n_2)}$$

回の觀測として取扱かつた．但し n_1, n_2 は夫々一つの星對の南及北の星を Bisect した回數である．

上記の表に見られる通り一つの星對を2夜以上觀測してゐるのがあるから，これ等を前述の觀測回數を重さとして星對毎に平均すると，共の殘差から筆者の1回の觀測に對する平分誤差が次の如くに得られた．

$$e=0.6745\sqrt{\frac{[p\Delta\Delta]}{m-n}}=0''.263 \qquad \text{小淺間}$$

$$=0''.234 \qquad \text{棒鏃}$$

此の値の稍々大きいのは可動較合絲が少しく太すぎた事による．第 II 表の星對の重さは上記の e の値を採用して，小淺間と棒鏃と別々に計算してある．

測微計 1 廻轉の値を 78″83 として各星對毎に平均した緯度の値に星對の重さを入れて平均値を求め更に緯度と測微計の値の修正値を最小自乘法によつて求めて加へた結果は次の通りになつた．

$$\left.\begin{aligned}\varphi&=36^\circ\,24'\,36''.548\pm0''.052\\ R&=78''.792\pm0''.011\end{aligned}\right\}\text{小淺間測點}$$

$$\left.\begin{aligned}\varphi&=36^\circ\,22'\,59''.75\pm0''.21\\ R&=78''.790\pm0''.023\end{aligned}\right\}\text{棒鏃測點}$$

此等の値に第 1 節の歸心修正値を加へる時は三角點の値として

$$\varphi=36^\circ\,24'\,36''.519\pm0''.052 \qquad \text{小淺間三角點}$$

$$36^\circ\,22'\,59''.69\pm0''.21 \qquad \text{棒鏃三角點}$$

を得る．從つて此の兩三角點に於ける緯度の鉛直線偏倚 (A-G) は

$$+12''.07 \qquad \text{小淺間}$$

$$+3''.79 \qquad \text{棒鏃}$$

原點に於ける凡ての誤差を除外した時ので，三角點の測地的位置の誤差は 10cm の order のものであるから，上記偏倚の誤差は矢張 0″.1 の order であると考へられる．尤も淺間附近に於ける緯度の變化又は鉛直線偏倚の時間的變化を調べる場合には三角點の測地的位置の不確實さは問題とはならない．

此れに關聯して面白いのは 1921 年に松隈教授が棒鏃の略々眞南約 3 km の地點にある借宿三角點に於て測定された經緯度である．同氏の得た緯度の値は[2]

$$\varphi=36^\circ\,21'\,21''.04\pm0''.072$$

となつてゐて，緯度の鉛直線偏倚は +7″.28 となつてゐる．從つて小淺間を通る南北

2) 川畑幸夫「日本に適合する回轉橢圓體の近似的計算」地震研究所彙報 13 (1935), 58.

垂直面によるゼオイドの切口は借宿の値が昔と變らぬとすれば第1圖の如くになる．上記の如く相互に僅かに數粁を隔てるに過ぎない地點で此の様な複雑且大なるゼオイドの起伏のある事は火山の構造の複雑性を示すと共に，更に廣範圍に亙る測定の必要を感ぜしめるのである．

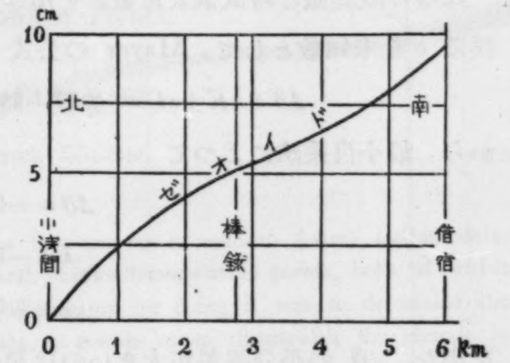

第1圖　ゼオイドの切斷面
The profile of geoid.

小淺間測點の經度

8 月 22 日午前1時から夜明までの時間を利用して數個の星の子午線經過を耳目法によつて測定し，共れから子午儀の方位の誤差，視準の誤差及經度の鉛直線偏倚を最小自乗法で求めた．星の撰擇が主に方位誤差を求めるに便なる様になつてゐたので，經度の誤差は非常に大きくなつた．

観測の結果は次表の様である．時辰儀の修正値は 11^h ，21^h の JJC 學用報時を取つた．

第 IV 表　經度測定

水準器1分劃値　$0^s.0778$
前夜午後9時の時辰儀修正値　-63.847
毎時歩分　-0.037

番號	星名	接眼鏡	經過時	水準器	赤徑	赤緯	時辰儀修正値	K	C
			h m s	s	h m s	° ′	s		
1	39*H* Cep	W	23 28 44·72	+ 0·276	23 27 57·25	+ 86 57	−64·007	−14·81	+18·79
2	ι Pis	W	23 37 44·50	+ 0·018	23 36 40·43	+ 5 17	−64·012	+ 0·52	+ 1·00
3	φ Peg	W	23 50 18·68	+ 0·019	23 49 14·70	+ 18 46	−64·020	+ 0·31	+ 1·06
4	ω Pis	W	23 57 06·56	+ 0·015	23 56 02·34	+ 6 31	−64·025	+ 0·49	+ 1·01
5	2 Cet	W	0 01 33·10	+ 0·010	0 00 28·85	− 17 41	−64·027	+ 0·84	+ 1·05
6	α And	E	0 06 10·16	+ 0·018	0 05 05·39	+ 28 44	−64·030	+ 0·16	+ 1·14
7	γ Peg	E	0 11 02·06	+ 0·008	0 09 57·11	+ 14 50	−64·033	+ 0·38	+ 1·04
8	6*B* UMi	E	0 15 15·75	0·000	0 14 14·17	+ 88 03	−64·036	+24·38	−29·54
9	12 Cet	E	0 27 52·22	− 0·007	0 26 47·22	− 4 19	−64·043	+ 0·65	+ 1·00
10	θ And	E	0 36 15·90	− 0·021	0 35 10·89	+ 28 58	−64·049	+ 0·14	+ 1·14
11	θ′ Cet	W	1 21 54·34	− 0·009	1 20 50·10	− 8 31	−64·077	+ 0·71	+ 1·01
12	υ Cet	E	1 58 04·86	− 0·009	1 56 59·92	− 21 23	−64·099	+ 0·89	+ 1·08

観測には普通の星に對しては I，V，VIII，XI，XV の較合絲經過の時を測定したが，極く近くの運動の遅い星に對しては VI，VII，VIII，IX，X の絲を用ひた表中の經過時は此等5箇の測定値を夫々の絲の赤道絲間隔によつて中央絲 VIII に直し，平均した値である．望遠鏡は観測の中央で反轉したのみで，一つの星の観測中に

反轉する事はしなかつた．水準器は觀測の初と終及び反轉の前と後とに讀んだ．

此等の觀測値と時辰儀更正値とを用ひ，經度の鉛直線偏倚 $\Delta\vartheta$，方位誤差 k，視準誤差 c を未知數として，Mayer の公式

$$\Delta\vartheta+kK\pm cC=\text{赤經}-\text{時辰修正}-\text{經過時}-\text{水準器更正}$$

から，最小自乘法によつて

$$\Delta\vartheta=-0\overset{s}{.}242\pm0\overset{s}{.}125,$$

$$k=-0\overset{s}{.}487\pm0{\cdot}006,$$

$$c=+0\overset{s}{.}493\pm0{\cdot}022 \quad (\text{接眼鏡 W のとき})$$

を得た．$\Delta\vartheta$ の平分誤差が大きいのは星の選擇が k 及 c を主としたからである．上記計算中に於ける時辰儀の修正値は便宜上三角點に對するものを用ひて居り，且時報發振の誤差を考へてないから $\Delta\vartheta$ の値は眞の鉛直線偏倚とは歸心修正と時報誤差丈違つてゐる．歸心修正値は $-0\overset{s}{.}013$ であり，觀測を挾む時報の發振誤差[3] の平均は $+0\overset{s}{.}005$ であるから，此を入れると鉛直線偏倚（A−G）は

$$-0\overset{s}{.}260\pm0\overset{s}{.}125$$

となり，小淺間三角點の經度として

$$L=9^{h}14^{m}15\overset{s}{.}424\pm0\overset{s}{.}125$$

を得る．

以上に述べた測定を綜合した結果は凡て淺間山の東南麓に過剩の質量が存在すると假定すれば說明し得る方向を持つてゐる．又ゼオイドには相當の起伏が存在してゐる樣に見える．火山活動，火山の構造等との關係に就ては，更に多くの測點に於ける觀測の結果に俟たねばならない．

終に臨み本測定も其の費用の一部を學術振興會の補助にあおいだもので，此處に同會に對し深甚の謝意を表す．又午子儀を貸與せられたる陸地測量部に對し，又種々助言を與へられたる辻光之助氏及川畑幸夫氏に對し感謝する次第である．

3）天文月報 28 (1935), 177.

4. Latitude Determination at the Koasama and the Boroku Triangulation Points.

By Ryûtarô TAKAHASI,

Earthquake Research Institute.

In connection with the precise levelling done this summer at volcano Asama, latitude determinations were made by the writer at Koasama and Boroku triangulation points, both of which are situated on the eastern slope of the volcano. The reason for doing it was to determine the present shape of the geoid, in order to obtain data to enable us to distinguish the change in shape of the geoid from true deformations of the volcano, when relevelling the mountain in the future.

The results of the observation are

$$36^\circ 24' 36''\cdot 519 \pm 0''\cdot 052, \quad \text{Koasama},$$
$$36\ \ 22\ \ 59\cdot 75 \pm 0\cdot 21, \quad \text{Boroku}.$$

Besides these observations, a rough estimate of the longitude was made at Koasama, giving

$$9^h\,14^m\,15^s\,424 \pm 0^s\,125.$$

These values give deviations of vertical (A−G) of the following magnitudes:

$$\text{Koasama:} \begin{cases} 12''07 & \text{in latitude;} \\ -X^s\,260 & \text{in longitude;} \end{cases}$$
$$\text{Boroku:} \quad 3''79 \quad \text{in latitude.}$$

5. *Seismometrische Untersuchungen des Erdbebens vom 2. März 1933.*

III. Erdbebentätigkeit vor und nach dem Grossbeben. Allgemeines über Nachbeben.

Von Takeo MATUZAWA,

Institut für Erdbebenforschung.

(Vorgelegt 19. Nov. 1935.—Eingegangen 20. Dez. 1935.)

1. Erdbebentätigkeit in einem gegebenen Erdgebiet in einem gegebenen Zeitraum kann einwandfrei mit der totalen Energiemenge definiert werden, die während des Zeitraums in elastische Schwingung umgesetzt worden ist. Ähnlich wird die Grösse eines Erdbebens eindeutig mit der in elastische Schwingung umgesetzten Energiemenge definiert. Aber im heutigen Zustand der Seismometrie ist es nicht immer möglich, die ausgestrahlte Energiemenge bei einem Erdbeben genau abzuschätzen. Darum wird gewöhnlich die Zahl der Erdbeben als Maß der Tätigkeit in einem Gebiet in einem Zeitraum genommen. Sehr oft ist die Zahl der Beben über einer bestimmten Grösse als Maß genommen worden. Das ist natürlich nur berechtigt, wenn die Tätigkeit der Beben in jeder Grössenstufe parallel geht.

Erst wird dieser Punkt untersucht. Nach 1926 sind alle möglich bestimmte Erdbeben in Japan in Kisyô-Yôran (Monatliche Meteorologische Berichte) gegeben worden. In der folgenden statistischen Untersuchungen sind fast alle Materialien von diesem Berichte genommen worden.

2. **Erdbebentätigkeit in Sanriku-Oki.** Hier bedeutet Sanriku-Oki ein Gebiet, welches ungefähr zwischen 145°E und 141°E, so wie 41°N und 38°N liegt. Das Großbeben vom 1933 liegt in $\varphi=39.°15$, $\lambda=144.°40$. Monatliche Zahl der Beben (je gefühlt und ungefühlt) in diesem Gebiet ist in den folgenden Tabellen (I, II) gezeigt.

Tabelle I.
Erdbebenhäufigkeit in Sanriku-Oki. (gefühlt)

Jahr / Monat	1926	1927	1928	1929	1930	1931	1932	1933	1934	Summe
Jan.	0	1	1	0	1	2	2	5	1	13
Feb.	1	1	1	0	0	0	0	0	1	4

(*Fortsetzung folgt.*)

Tabelle. I. (*Fortsetzung.*)

Monat \ Jahr	1926	1927	1928	1929	1930	1931	1932	1933	1934	Summe
März	0	3	0	7	2	3	1	32	1	49
April	2	3	0	2	0	2	2	12	2	25
Mai	0	2	9	1	0	3	0	1	1	17
Juni	2	1	11	0	2	2	4	5	0	27
Juli	3	0	2	0	0	0	1	5	3	14
Aug.	1	1	4	2	0	0	1	3	4	16
Sept.	5	1	1	1	0	0	3	4	2	17
Okt.	3	1	1	0	1	0	2	1	1	10
Nov.	2	2	0	0	1	0	0	1	0	6
Dez.	1	1	3	2	0	3	1	1	1	13
Summe	20	17	33	15	7	15	17	70	17	211

Tabelle II.

Erdbebenhäufigkeit in Sanriku-Oki (ungefühlt)

Monat \ Jahr	1926	1927	1928	1929	1930	1931	1932	1933	1934	Summe
Jan.	1	3	0	2	2	2	1	116	9	136
Feb.	4	2	2	0	8	0	3	10	11	40
März	1	2	0	5	9	5	3	1239	11	1275
April	0	5	1	1	1	1	8	218	4	237
Mai	7	4	57	12	4	2	2	95	5	188
Juni	6	0	48	7	1	3	1	40	0	106
Juli	10	0	2	6	0	0	2	35	5	60
Aug.	2	6	5	14	1	4	3	5	3	43
Sept.	8	4	8	7	1	1	3	24	8	64
Okt.	0	2	2	13	4	0	1	10	2	34
Nov.	6	2	4	5	0	3	3	13	9	45
Dez.	6	0	0	1	1	2	1	2	7	20
Summe	51	30	129	73	32	23	31	1807	74	2250

Aus diesen Tabellen kann man Korrelationsdiagramm der gefühlten und ungefühlten Erdbeben bilden, und dann Regressionskurven bekommen. (Tabelle III.)

Tabelle III.

Korrelationsdiagramm.
Nummer ohne Klammer, 1926~1932,
Nummer in Klammer, 1926~1934.

Ungefühlt \ Gefühlt	0	1	2	3	4	5	7	12	32	Mittel
0	7(8)	4	1	2						0·86(0·80)
1	8	1	6		1					1·06
2	2	7(9)	3	3						1·46(1·05)
3	3	3	1	1						1·0
4	3	3	1(2)		(1)					0·7 (1·2)
5	1	(1)		2(4)	1		1			3·4 (3·0)
6	1	2	2							1·2
7	1	2(3)								0·66(0·75)
8	1	1	1(2)			1				2·0 (2·0)
9	(1)	(1)	(1)							2·0 (1·0)
10	(1)	(1)		1						3·0 (1·3)
11		(2)								(1·0)
12		1								1
13	1	(1)								0 (0·08)
14			1							2
16						(1)				(5)
21					(1)					(4)
35						(1)				(5)
40						(1)				(5)
95		(1)								(1)
218								(1)		(12)
1239									(1)	(32)
Mittel	2·6 (2·9)	3·5 (7·3)	3·5 (3·8)	3·2 (3·5)	3·0 (8·5)	8·0 (24·7)	5	(·218)	(1239)	

Fig. 1 zeigt die Regressionskurven für Intervalle 1926~1932. Für kleine Bebenhäufigkeit sind die Kurven für 1926~1934 ziemlich ähnlich, aber wegen der zahlreichen Nachbeben des Großbebens vom 1933 sind sie für große Häufigkeit ganz anders. Für kleine Häufigkeit ist jede Kurve ungefähr parallel zur Koordinatenachse, d. h. es gibt keine Korrelation zwischen der Häufigkeit der gefühlten Beben und der ungefühlten wenigstens für kleine Häufigkeit in diesem Gebiet. Im

allgemeinen hat ein Großbeben zahlreiche kleine Nachbeben, aber starke Beben begleiten nicht immer einen Schwarm zahlreicher kleiner Beben.

3. **Periodizität der Bebenhäufigkeit.** F. Omori[1] zeigte einmal jahreszeitliche Schwankung der Bebenhäufigkeit in mehreren Gebieten. Beobachtungsmaterial ist heute erheblich verbessert als damals. Darum wird hier auch solche Untersuchung stattfinden. Für diesen Zweck ist Anwendung der Theorie[2] über zufällige Schwankungen am zweckmäßigsten.

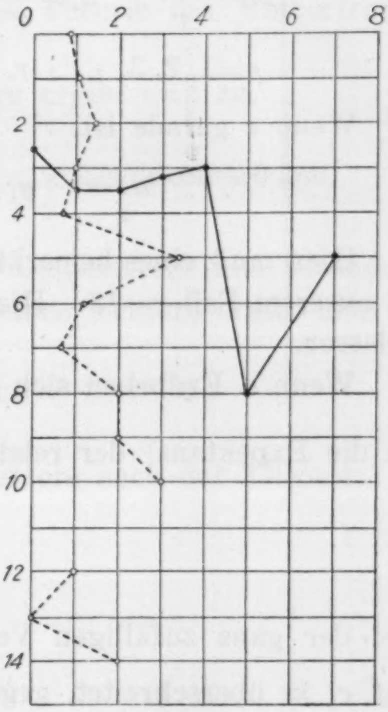

Fig. 1.

Abszissa: Zahl der gefühlten Beben
Ordinate: 〃 〃 ungefühlten 〃
Ausgezogene Kurve: Mittel der ungefühlten Beben.
Gestrichene Kurve: 〃 〃 gefühlten Beben.

Zu erst wird jahreszeitliche Schwankung der gefühlten Beben in Tabelle I untersucht. Wir haben 13 Beobachtungen in der angenommenen Periode nämlich von Januar zu Januar des nächsten Jahres. Wir können diese Beobachtung wie folgt harmonisch darstellen.

$$\phi_\kappa(x)=$$
$$a_0+(a_1\cos x+b_1\sin x)+(a_2\cos 2x+b_2\sin 2x)+\cdot\cdot\cdot+(a_\kappa\cos\kappa x+b_\kappa\sin\kappa x),$$

r: Zahl der Beobachtungen in der gegebenen Periode,

y_ρ: Beobachtung Nr. ρ,

$x_\rho=\rho\left(\frac{2\pi}{r}\right)$: Abscissa Nr. ρ.

Man kann $\phi_\kappa(x)$ so bestimmen, daß

$$\zeta_\kappa^2=\sum_\rho[y_\rho-\phi_\kappa(x_\rho)]^2/r,$$

minimum ist.

Dann bekommt man

1) F. Omori, *Rep. Earthq. Inv. Comm.*, **30** (1900); *Publ. Earthq. Inv. Comm.*, **8** (1902).

2) Z. B. sieh J. Bartels, *Terr. Magn. and Atm. Elect.*, **40** (1935), 1~60.

$$a_0 = \frac{\sum_\rho y_\rho}{r}, \quad a_\nu = \frac{2}{r}\sum_\rho y_\rho \cos\nu x_\rho, \quad b_\nu = \frac{2}{r}\sum_\rho y_\rho \sin\nu x_\rho,$$

$$\rho = 1, 2, 3, \cdots r. \quad \nu = 1, 2, 3, \cdots k. \quad 2k+1 \leqq r.$$

Wenn r gerade ist,

$$a_{\frac{r}{2}} = (-y_1 + y_2 - y_3 + \cdots + y_r)/r.$$

Hier muß eines bemerkt sein, daß a_ν, b_ν, unabhängig von k sind. In unserem Fall $r=13$. Hier werden die Glieder über $\nu=2$ außer acht gelassen.

Wenn n Erdbeben sich ganz zufällig in einem Jahr verteilen, dann ist die Expektanz[3] der relativen Amplitude $c_\nu = \frac{\sqrt{a_\nu^2 + b_\nu^2}}{a_0}$,

$$\varepsilon = \sqrt{\frac{\pi}{n}}.$$

Bei der ganz zufälligen Verteilung ist die Wahrscheinlichkeit $W(k)$, daß c_ν $k\varepsilon$ überschreitet, gegeben durch $W(k) = e^{-\frac{\pi}{4}k^2}$.

Das ganze Rechenverfahren ist in Tabelle IV gezeigt.

Tabelle IV.

Analyse der Jahresschwankung der Bebenhäufigkeit (gefühlt) in Sanriku-Oki.

Jahr	a_0	a_1	b_1	a_1/a_0	b_1/a_0	ε	c_1^2	c_1	c_1/ε	$W(x)$
1926	1·60	−·67	−1·01	−·42	−·63	·386	·576	·759	1·94	·047
27	1·38	·08	·55	·06	·40	·417	·162	·402	·97	·477
28	2·54	−2·39	1·37	−·94	·54	·308	1·174	1·08	3·51	·000
29	1·23	·54	·93	·44	·76	·443	·763	·874	1·97	·047
30	·69	·43	1·33	·62	·19	·590	·419	·647	1·10	·386
31	1·31	·75	1·03	·57	·79	·430	·948	·973	2·26	·018
32	1·69	·24	−·113	·14	−·07	·377	·024	·155	·41	·876
33	5·9	1·34	5·12	·23	·87	·249	·809	·900	3·61	·000
Summe				·698	2·84		4·875			
				$l=$·782,	$l_m=$·276,		$c_m=$·366,		$c_m/l_m=$1·33.	

In den Jahren mit kleiner Wahrscheinlichkeit für Zufall kamen die Erdbeben schwarmartig vor.

Um irgendeine jahreszeitliche Bevorzugung der Erdbebenentstehung zu entdecken, muß man wieder alle Vektoren im ganzen Zeitintervalle

3) Lord RAYLEIGH, *Phil. Mag.*, [v], 10 (1880). 73~78.

zusammen untersuchen und zwar im Licht der Wahrscheinlichkeitstheorie. Ganz zweckmäßig kann man die Theorie des Umherirrens (random walk) anwenden.

Der gemittelte Vektor für alle 8 Jahre ergibt sich zu,

$$\sum\frac{a_1}{a_0}\Big/ 8=0{\cdot}0872,\qquad \sum\frac{b_1}{a_0}\Big/ 8=0{\cdot}356,\qquad c_m=\text{Resultante}=0{\cdot}366.$$

Hier handelt es sich um die Theorie des Umherirrens mit veränderlichen Schritten. Die Expektanz des einzelnen Vektors ergibt sich zu

$$l=\sqrt{\frac{\sum c_1^2}{8}}=0{\cdot}782\,.$$

Also ist die Expektanz des gemittelten Vektors nach der Theorie

$$l_m=\frac{l}{\sqrt{8}}=0{\cdot}276\,.$$

Fig. 2 macht das Resultat ganz anschaulich.

Man bekommt hier $c_m/l_m=k=1{\cdot}33$. Die Wahrscheinlichkeit[4] für Überschreitung dieses Wertes ist ungefähr 0·175. Obwohl mehr Vektoren sich scheinbar in März und April sammeln, doch kann man mit dieser Wahrscheinlichkeit nichts über jahreszeitliche Schwankung schliessen.

Zu nächst wird Jahresschwankung der allen Erdbeben nämlich gefühlten und ungefühlten Beben zusammen in ganz ähnlicherweise untersucht. Das Rechenverfahren ist in Tabelle V zusammengestellt.

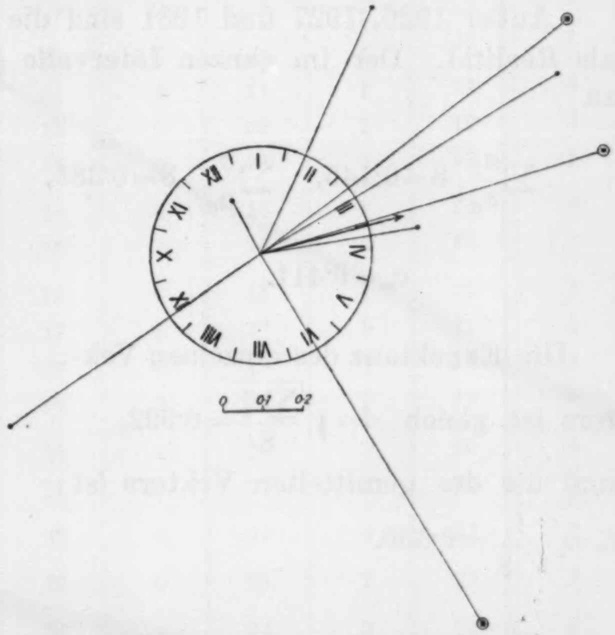

Fig. 2. Jahresschwankung der Erdbebenhäufigkeit (gefühlt) in Sanriku-Oki.
Ziffer zeigt die Monate.
Radius des Kreises zeigt die Expektanz des gemittelten Vektors. Vektor mit Pfeil ist der gemittelte Vektor.
Vektor mit Funkt im Kreis: über $\kappa=2{\cdot}2$.

4) $W'(k)=e^{-k^2}$.

Tabelle V.

Analyse der Jahresschwankung der Bebenhäufigkeit (gefühlt und ungefühlt zusammen) in Sanriku-Oki.

Jahr	a_0	a_1	b_1	a_1/a_0	b_1/a_0	ε	c_1^2	c_1	c_1/ε	$W(\kappa)$
1926	5·77	−1·95	−1·66	−·338	−·288	·204	·197	·44	2·17	·025
27	3·70	·83	·73	·022	·128	·256	·021	·15	·57	·77
28	12·60	−13·85	10·60	−1·10	·84	·138	1·91	1·38	10·0	·000
29	7·00	−3·12	−·85	−·446	−·123	·186	·214	·46	2·49	·008
30	3·15	1·92	1·81	·625	·574	·277	·719	·85	3·07	·0006
31	3·15	1·08	1·35	·343	·429	·277	·302	·55	1·99	·044
32	13·00	18·03	·83	1·38	·064	·136	1·908	1·38	10·2	·000
33	145·20	98·00	211·6	·675	1·46	·041	2·585	1·61	39·3	·000
Summe				1·161	3·084		7·856			
				$l=\cdot992$,	$l_m=\cdot350$,		$c_m=\cdot411$,		$c_m/l_m=1\cdot18$.	

Außer 1926, 1927 und 1931 sind die Vektoren für sich zweifellos als Realität. Der im ganzen Intervalle gemittelte Vektor ergibt sich zu

$$\sum\frac{a_1}{a_0}\Big/8=0\cdot145,\qquad \sum\frac{b_1}{a_0}\Big/8=0\cdot385,$$

$$c_m=0\cdot411.$$

Die Expektanz des einzelnen Vektors ist gleich $l=\sqrt{\frac{\sum c_1^2}{8}}=0\cdot992$, und die des gemittelten Vektors ist $l_m=\frac{l}{\sqrt{8}}=0\cdot350.$

$$k=\frac{c_m}{l_m}=1\cdot175,\quad W'(k)=0\cdot25.$$

Hier kann man wieder nichts über die jahreszeitliche Schwankung der Bebenhäufigkeit schliessen. Das ganze Verfahren ist in Fig. 3 anschaulich gemacht.

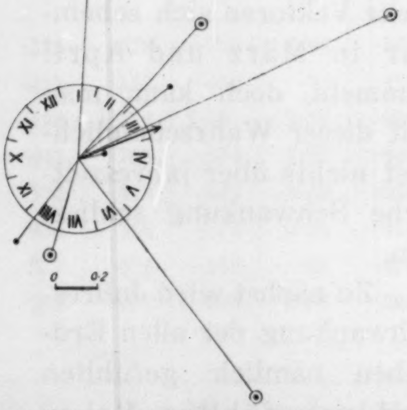

Fig. 3. Jahresschwankung der Bebenhäufigkeit (alle Beben) in Sanriku-Oki.
Ziffer: die Monate.
Radius des Kreises zeigt die Expektanz des Gemittelten Vektors.
Vektor mit Pfeil ist der gemittelte Vektor.
Vektor mit Punkt in Kreis: über $k=2\cdot49$

4. Zeitlicher Verlauf der Erdbebenhäufigkeit nach dem Großbeben. Tägliche Häufigkeit der Erdbeben in Sanriku-Oki nach dem Großbeben ist bis zum Juli in Tabelle VI gegeben.

Tabelle VI.

Tägliche Häufigkeit des Nachbebens. (Summe gefühlte Beben und ungefühlte.) Zahl in Klammer: gefühlte Beben. Datum. L. Z. 135°E.

Datum.	Häufigkeit	Datum.	Häufigkeit	Datum.	Häufigkeit	Datum.	Häufigkeit	Datum.	Häufigkeit
		IV 1	9 (3)	V 1	1	VI 1	0	VII 1	3
		2	12	2	8	2	0	2	3
III 3	426 (19)	3	8	3	6	3	0	3	3 (1)
4	195 (9)	4	7	4	4	4	1	4	0
5	119 (2)	5	2	5	6	5	1	5	3
6	98	6	5	6	1	6	0	6	2
7	76	7	5 (1)	7	1	7	2	7	1
8	79 (1)	8	11	8	1	8	0	8	1 (1)
9	30 (1)	9	56 (4)	9	2	9	2 (1)	9	1
10	42	10	37	10	6	10	1	10	1 (1)
11	19	11	12	11	4	11	1	11	0
12	22	12	7	12	5	12	2	12	0
13	11	13	2	13	0	13	9 (1)	13	1
14	19	14	6	14	0	14	1	14	0
15	14	15	5 (1)	15	1	15	0	15	2
16	14	16	5	16	0	16	1	16	3
17	4	17	6	17	4	17	0	17	0
18	8	18	2	18	0	18	3	18	3
19	17	19	2 (1)	19	2	19	5 (1)	19	0
20	13	20	8	20	4	20	2	20	1
21	8	21	9	21	24	21	1	21	2 (1)
22	6	22	3	22	8	22	0	22	2 (1)
23	13	23	16 (2)	23	6	23	2 (1)	23	3
24	13	24	2	24	1 (1)	24	2	24	0
25	1	25	4	25	1	25	3 (1)	25	1
26	7	26	2	26	0	26	1	26	0
27	5	27	2	27	2	27	3	27	1
28	8	28	0	28	0	28	0	28	1
29	1	29	2	29	0	29	0	29	0
30	2	30	1	30	0	30	1	30	1
31	1			31	0			31	0

Hyperbolische Abflutung der Nachbebenhäufigkeit ist bisher manchmal gemerkt worden.

Eine Formel $y=\frac{a}{b+t}$ annehmend, werden die Konstanten a, b ganz formal mit der Methoden der kleinsten Quadrat bestimmt, indem der 3. März als Anfangspunkt der Zeit genommen ist und die Berechnung bis zum Ende März erstreckt ist. Dann bekommt man folgende Formel.

$$y_1=\frac{177{\cdot}8}{{\cdot}0065+t}\,.$$

Wenn man die Zahl am Bebentag (dem 3. März L. Z.) ausnimmt, bekommt man

$$y_2=\frac{159}{t-0{\cdot}87}\,.$$

Die beobachtete tägliche Häufigkeit und diese Kurven sind in Fig. 4 gezeigt.

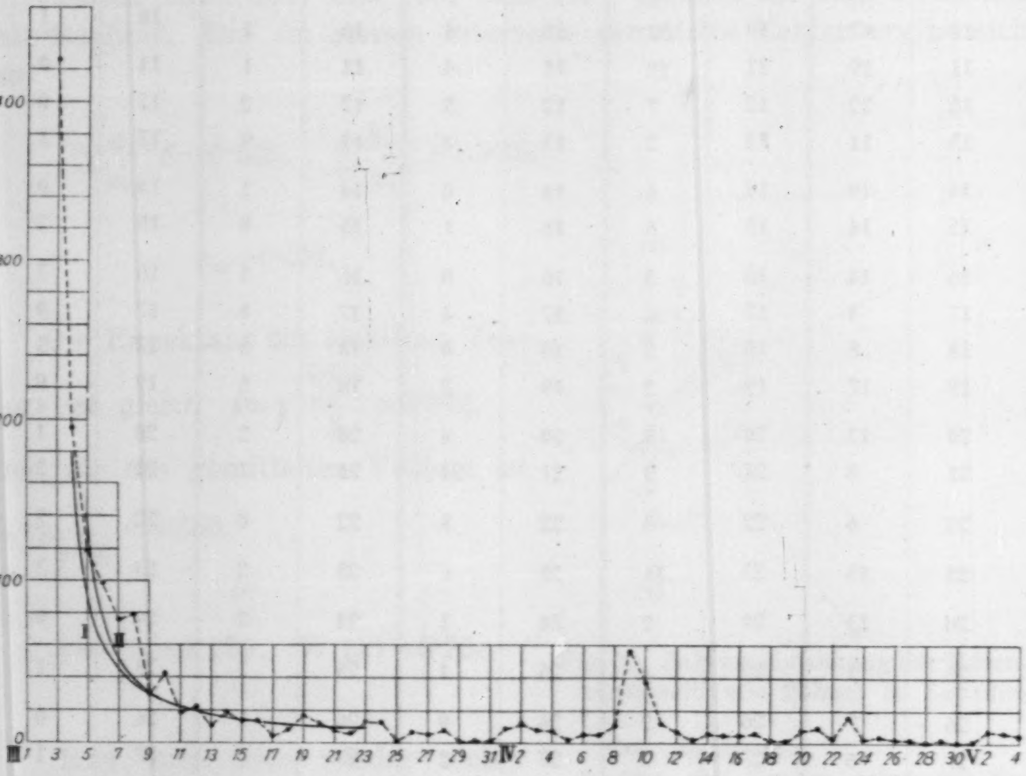

Fig. 4.

Kurve I, $y=\frac{177{\cdot}8}{{\cdot}0065+t}$. Kurve II, $y=\frac{159}{t-0{\cdot}87}$.

Die Bebenhäufigkeit flaute mit der Zeit schwankend ab, und zwar

im ersten Anblick ähnlich wie Hyperbelkurve. Aber die Abweichung von der Formel ist wie folgt (Tabelle VII).

Tabelle VII.

t	0	1	2	3	4	5	6	7	8	9	10	11	12
$y-y_1$	−27000	+17	+30	+33	31	43	1	17	−3	3	−7	3	−1
$y-y_2$		−1030	−23	+23	25	40	−1	16	−3	4	−6	3	0
y	426	195	119	98	76	79	30	42	19	22	11	19	14
t	13	14	15	16	17	18	19	20	21	22	23	24	25
$y-y_1$	0	−9	−4	6	3	−2	−3	4	5	−7	−1	−2	1
$y-y_2$	1	−8	−3	7	3	−1	−3	5	5	−7	0	−2	1
y	14	4	8	17	13	8	6	13	13	1	7	5	8

Die Abweichung ist immer groß in der Nähe vom Hauptbeben. Lange nach dem Hauptbeben scheint es doch natürlich, daß die Abweichung immer kleiner wird, weil die Asymptote der Hyperbel parallel zur Zeitachse ist. Als ein Physikalisches Gesetz mag die Hypelbelformel zu grop sein. Das gilt auch von exponentiellen Formeln.

5. **Untersuchungen über tägliche Schwankung des Nachbebens.**[5] Die Häufigkeit der Nachbeben ist stundenweise in Tabelle VIII zusammengestellt.

Tabelle VIII.
Stündliche Häufigkeit des Nachbebens.

Datum / Uhr	III 3	4	5	6	7	8	9	10	11	12	13	14	15	16	17	18	19	20	21	22	23	24	25	26	27	28
0~1		13	3	1	4	4	1	1	0	0	0	1	0	0	0	0	0	0	1	0	1	0	0	0	0	1
1~2		7	6	4	1	4	0	5	1	2	2	2	2	0	0	0	0	0	0	0	3	1	0	0	0	0
2~3	4	12	7	8	6	4	0	2	0	1	1	1	1	1	0	0	0	1	0	1	1	0	0	0	0	0
3~4	29	8	3	3	4	4	0	1	0	0	0	1	0	1	0	0	0	0	0	0	0	0	0	0	1	0
4~5	39	9	5	8	3	2	1	2	1	0	0	0	0	0	0	2	1	0	0	0	0	1	0	1	0	0
5~6	31	6	4	5	0	2	3	2	0	1	0	0	0	0	1	0	0	1	0	0	0	0	0	0	0	0
6~7	32	5	5	2	4	1	2	0	1	1	0	1	0	0	0	0	3	1	0	1	2	0	0	1	0	1

(Fortsetzung folgt.)

5) Definition des Nachbebens. Wenn in einem beschränkten Teil der Erde Erdbeben mit übernormaler Häufigkeit vorkommen, so ist die ganze Menge von allen diesen Erdbeben ein Bebenschwarm genannt. Die Beschränktheit des Gebietes zeichnet sich burch Dichtigkeit der Raumverteilung der Hypozetren aus. Das allergrösste Erdbeben in dem Erdbebenschwarm ein Hauptbeben genannt. Alle Erdbeben in diesem Schwarm, welche nach dem Hauptbeben entstehen, sind Nachbeben. Vorfall von mehreren sekundären Häufigkeitsmaxima wird nicht ausgeschlossen.

Tabelle VIII. (*Fortsetzung.*)

Datum / Uhr	III 3	4	5	6	7	8	9	10	11	12	13	14	15	16	17	18	19	20	21	22	23	24	25	26	27	28
7~8	21	9	8	4	1	4	1	1	4	1	1	0	0	1	1	0	4	1	1	0	0	1	0	0	1	0
8~9	19	7	4	6	3	4	3	1	0	1	0	2	2	0	0	0	1	0	0	2	0	1	0	0	0	1
9~10	19	11	6	1	2	1	1	1	1	1	1	0	2	0	0	1	0	0	0	0	1	1	0	0	0	0
10~11	17	4	2	5	3	2	1	2	0	2	0	1	3	0	0	0	2	0	0	1	0	0	0	0	0	2
11~12	16	6	10	3	1	3	1	5	0	2	0	0	1	0	0	1	2	0	0	0	0	0	0	0	0	0
12~13	22	8	2	4	3	2	1	1	0	2	0	0	1	0	0	0	1	1	0	0	0	0	0	0	0	0
13~14	20	7	5	6	6	3	1	0	2	1	0	3	0	0	9	0	1	0	1	0	1	0	0	0	0	0
14~15	17	6	8	3	4	2	2	3	0	4	0	1	0	0	0	0	0	2	0	0	0	2	0	0	0	0
15~16	17	9	7	5	3	3	1	2	0	0	1	0	1	1	0	1	0	0	0	0	0	2	0	0	0	0
16~17	12	9	5	2	8	2	2	3	1	0	0	2	0	0	0	0	0	0	2	0	0	1	0	0	1	0
17~18	18	6	7	8	2	3	1	2	1	1	0	0	1	2	0	0	0	1	0	0	0	1	0	0	0	1
18~19	18	10	3	5	3	3	1	2	1	0	1	0	0	2	0	2	1	0	0	3	2	0	0	0	0	0
19~20	22	8	5	3	7	2	4	0	0	0	0	0	0	1	1	0	0	3	0	1	1	0	0	1	0	0
20~21	9	8	5	3	4	6	0	2	2	0	2	0	0	2	1	1	0	0	1	0	0	0	0	0	0	1
21~22	13	5	3	4	2	5	1	1	0	0	1	2	0	1	0	0	1	2	1	0	1	1	1	1	1	0
22~23	5	8	1	3	1	8	0	1	1	1	0	1	0	1	0	0	0	0	1	0	0	1	0	2	0	1
23~24	7	5	3	2	1	4	1	2	3	1	1	1	0	1	0	0	0	6	0	0	0	0	0	1	1	0

Diese Beobachtung ist in ganz ähnlicherweise wie im 3. Abschnitt untersucht. Das Rechenverfahren ist in Tabelle IX dargestellt.

Merkwürdigerweise hat jede tägliche Schwankung der Häufigkeit außer der vom 19. März beträchtliche Wahrscheinlichkeit als Zufall. In Bezug auf die halbtägige Schwankung scheinen sie alle zufällige Verteilung der Entstehung zu haben.

Die Verhältnis der gemittelten Amplitude der Schwankung zu der Expektanz ist auch klein. Also kann man hier auch nichts über tägliche Schwebung der Häufigkeit

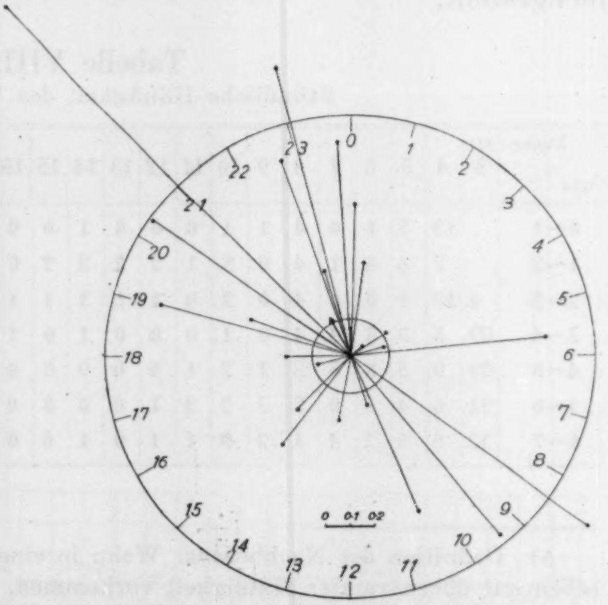

Fig. 5. Eintägige Schwebung der Nachbeben des Großsanrikubebens im 1933.
Vektor mit Pfeil: der gemittelte Vektor.
Radius des inneren Kreises: Expektanz des gemittelten Vektors.

Tabelle IX.

Analyse der täglichen Schwankung der Bebenhäufigkeit in Sanriku-Oki nach dem Großbeben vom 1933.

Datum	a_0	a_1	b_1	a_2	b_2	a_1/a_0	b_1/a_0	c_1^2	c_1	a_2/a_0	b_2/a_0	c_2^2	c_2	ε	c_1/ε	c_2/ε
III 5	4·80	−·97	·32	−·23	·79	−·20	·07	·045	·21	−·05	·17	·029	·17	·162	1·30	1·01
6	4·08	·15	·20	−·19	·96	·04	·05	·004	·06	−·05	·24	·057	·24	·173	·35	1·39
7	3·20	−·01	−·84	·09	·89	−·00	−·26	·069	·26	·03	·28	·078	·28	·198	1·31	1·41
8	3·16	1·10	−·35	·57	−·72	·35	−·11	·134	·37	·18	−·23	·085	·29	·199	1·86	1·46
9	1·20	−·32	−·06	−·62	−·09	−·27	−·05	·073	·27	−·51	−·08	·269	·52	·323	·84	1·61
10	1·68	−·06	−·22	·48	·40	−·04	−·13	·019	·14	·29	−·24	·139	·37	·273	·51	1·35
11	·76	·07	·11	−·21	−·27	·10	·14	·029	·17	−·28	−·35	·201	·46	·406	·42	1·13
12	·88	−·56	·25	·58	·03	−·63	·28	·477	·69	·66	·03	·430	·66	·378	1·83	1·75
13	·48	·39	−·14	·10	·15	·80	−·29	·725	·85	·20	·31	·138	·37	·511	1·66	·72
14	·76	·09	−·00	·42	·08	·12	−·00	·014	·12	·55	·11	·309	·56	·406	·30	1·38
15	·56	−·41	·34	·30	·14	−·74	·61	·911	·96	·53	·25	·344	·59	·473	2·03	1·25
16	·56	·31	−·45	−·37	−·10	·56	−·81	·960	·98	−·66	−·18	·462	·68	·473	2·07	1·44
17	·16	·06	·01	−·25	−·11	·38	·05	·147	·38	1·55	−·69	2·87	1·70	·885	·44	1·92
18	·32	−·07	−·07	−·21	·03	−·22	−·22	·096	·31	−·66	·09	·443	·67	·625	·50	1·07
19	·68	−·48	·65	−·31	−·42	−·70	·96	1·410	1·19	−·46	−·62	·585	·77	·430	2·77	1·79
20	·56	−·09	−·23	−·22	−·03	·15	−·41	·186	·43	−·39	−·06	·152	·39	·473	·91	·82
21	·32	·07	−·25	0	−·08	·21	−·77	·640	·80	0	−·25	·063	·25	·627	1·27	·40
22	·28	·02	·22	−·07	−·18	·07	·79	·633	·80	−·25	−·64	·463	·68	·670	1·19	1·01
23	·52	·33	·00	·01	·03	·63	·01	·390	·63	·02	·06	·003	·06	·491	1·28	·12
24	·52	−·19	−·14	−·07	·18	−·37	−·28	·212	·46	−·13	·34	·135	·37	·491	·94	·75
25	·04	·06	−·06	0	·08	1·42	−1·42	4·04	2·01	0	2·00	4·00	2·00	1·77	1·14	1·13
26	-28	·33	−·09	−·04	−·23	1·19	−·30	1·51	1·23	−·14	·82	·690	·88	·670	1·84	1·24
27	·24	·21	−·01	·04	−·01	·88	−·05	·768	·88	·17	·04	·030	·17	·723	1·22	·24
28	·32	−·01	−·04	−·03	−·35	·03	·13	·019	·14	−·09	−1·08	1·173	1·08	·626	·22	1·43
Σ						3·76	−2·01	13·51		·51	·80	13·15				
Mittel						·16	−·08			·02	·03					

$l_1 = \cdot 752$, $l_{1m} = \cdot 153$, $c_{1m} = \cdot 18$, $\frac{c_{1m}}{l_{1m}} = 1\cdot 17$. $l_2 = \cdot 74$, $l_{2m} = \cdot 151$, $c_{2m} = \cdot 04$, $\frac{c_{2m}}{l_{2m}} = \cdot 27$.

schliessen. Expektanz der Schwankung für jede Periode (eintägig und halbtägig) ist fast gleich mit einander, was im Falle der zufällige Entstehung natürlich als Prinzip der Gleichverteilung der Schwankung (Equipartition of variance) erwartet wird. Das ganze Rechenverfahren ist in Fig. 5 ersichtlich.

6. **Raumverteilung der Epizentren im Sanriku-Oki Gebiet im 1933.** Raum- und Zeitkoordinaten der Beben sind in Tabelle X zusammengestellt, insofern sie gegeben worden sind.

Tabelle X.

M. Merkwürdig (Kentyo): über 300 Km gefühlt.
Z. M. Ziemlich Merkwürdig (Yaya Kentyo): bis 300~200 Km gefühlt.
K. Klein: innerhelb 200 Km gefühlt.

Datum					λ	φ	Bemerkung	
		d	h	m	°	°		
1933	I	4	0	27	144·0	40·4	Z. M.	
		7	13	07	144·0	40·3	M.	
		7	"	54	143·4	40·3	Z. M.	
		7	1	00	141·0	38·0	K.	
		7	15	24	143·7	40·3	K.	
		7	18	15	144·0	40·4	K.	
	III	3	2	31	144·4	39·15	M.	Das Hauptbeben.
		3	2	40	144·2	40·1	M.	
		3	2	57	144	39	M.	
		3	3	26	144	39	M.	
		3	3	44	143	40	Z. M.	
		3	3	48	144·2	40.5	Z. M.	
		3	4	42	143·2	39·4	M.	
		3	5	07	143	40·6	M.	
		3	5	42	144·6	39·3	M.	
		3	6	48	143	39·2	K.	
		3	7	35	143·7	39·6	Z. M.	
		3	8	58	142·8	39·4	K.	
		3	9	43	142·4	39·8	K.	
		3	13	38	143·6	39	Z. M.	
		3	18	13	143	39	M.	
		3	18	39	143	39	M.	
		3	19	04	144	39	M.	
		3	19	32	143	39·7	M.	
		3	20	57	145	38·2	M.	
		4	0	02	144·4	39	M.	
		4	0	08	144	39·4	M.	

(Fortsetzung folgt.)

Tabelle X. (*Fortsetzung.*)

Datum				λ	φ	Bemerkung
	d	h	m	°	°	
III	4	0	51	143·7	39	M.
	4	1	12	145·1	39·1	Z. M.
	4	3	47	143·8	38·8	Z. M.
	4	4	08	144·4	39	M.
	4	4	51	143·5	39·3	Z. M.
	4	5	20	143·5	39·5	Z. M.
	4	21	40	144·8	39·2	M.
	5	5	28	144·7	39·3	M.
	5	10	26	143·5	39·4	Z. M.
	8	10	36	144	39·6	M.
	9	18	55	143·4	39·6	K.
IV	2	0	59	143·5	39·5	M.
	2	7	41	144·8	38·6	M.
	2	19	11	144·0	39·4	M.
	7	0	12	144·3	39·7	M.
	9	11	47	144·0	39·2	M.
	9	11	57	144·0	39·3	Z. M.
	9	15	28	144·0	39·4	Z. M.
	9	19	30	144·2	39·2	M.
	15	20	09	144·2	40·5	Z. M.
	19	11	55	144·5	39·6	M.
	23	16	14	143·6	39·7	M.
	23	16	26	143·3	39·4	K.
V	24	8	34	143·9	39·5	M.
VI	9	3	11	144·0	40·2	M.
	13	6	08	141·7	38·8	M.
	19	6	37	142·8	38·5	M.
	25	10	48	143·4	39·4	K.
VII	3	1	48	142·8	40·1	Z. M.
	10	9	22	144·8	38·9	M.
	21	8	14	144·8	38·5	M.
VIII	7	9	42	144·7	39·4	M.
IX	21	18	48	143·0	39·3	Z. M.
	12	14	05	143·6	39·6	K.
	21	22	42	143·3	39·4	K.
	25	1	06	143·0	39·3	K.
XI	28	04	14	143·2	39·7	Z. M.

Fig. 6 zeigt die Raumverteilung der Beben, die in Tabelle X gegeben sind.

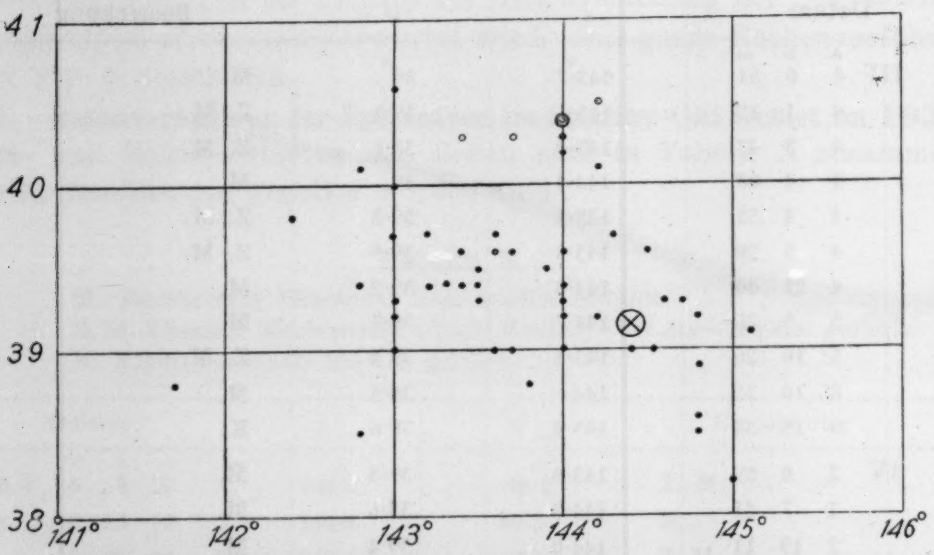

Fig. 6. Verteilung der Nachbeben des Großbebens vom 1933.
Kreuz im Kreis: Hauptbeben.
Punkt: Nachbeben.
Kreis: Bebenschwarm im Januar.

Ganz merkwürdigerweise liegt das Hauptbeben ziemlich seitlich im Bebengebiet. Diese merkwürdige Tatsache wird nachher auch in anderen Fällen verifiziert und diskutiert.

7. **Über die Folge der Entstehung.** Bei Untersuchungen der Nachbeben ist manchmal vermutet, daß es irgendeine räumliche Persistenz der hintereinander folgenden Nachbeben gäbe. Hier werden zu diesem Zwecke Vektoren von der folgenden Bedeutung gebildet.

$$\Lambda_\mu = \lambda_{\mu+1} - \lambda_\mu \,,$$

$$\Phi_\mu = \varphi_{\mu+1} - \varphi_\mu \,,$$

wo $\lambda_1 = 144{\cdot}40°\mathrm{E}\,, \quad \varphi_1 = 39{\cdot}15°\mathrm{N}\,,$

λ_μ, φ_μ, Koordinaten des vom Hauptbeben μ ten Bebens in Tabelle X. Zu diesen Vektoren kann man hier auch zweckmäßig die Theorie des Umherirrens anwenden. Diese Vektoren sind in Fig. 7 gezeigt.

Expektanz von Λ, Φ heißt $l = \sqrt{\dfrac{\sum(\Lambda_\mu^2 + \Phi_\mu^2)}{57}} = 1{\cdot}11$, und $l_m = 0{\cdot}15$.

$$\textstyle\sum \Lambda_\mu / 57 = -0{\cdot}02\,, \quad \sum \Phi_\mu / 57 = 0{\cdot}007\,. \quad C_m / l_m = 0{\cdot}14\,.$$

Also als ganzes hat es keine Persistenz.

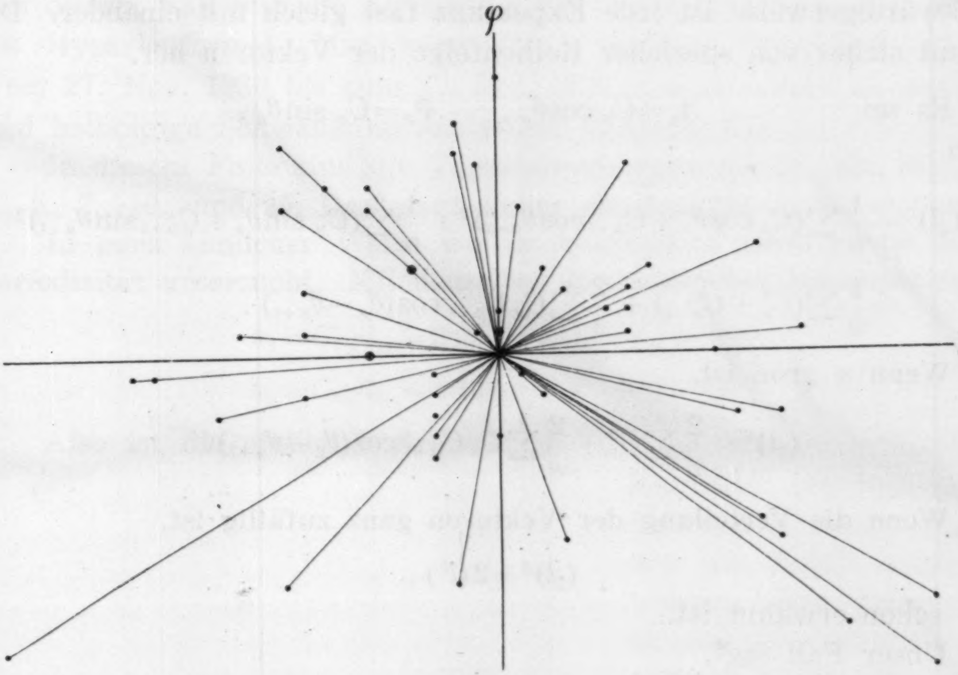

Fig. 7.

Zunächst bilde man folgende Vektoren;

$$\begin{cases} {}_2\Lambda_\mu = \Lambda_\mu + \Lambda_{\mu+1}\,, \\ {}_2\Phi_\mu = \Phi_\mu + \Phi_{\mu+1}\,, \end{cases}$$

$$\begin{cases} {}_3\Lambda_\mu = \Lambda_\mu + \Lambda_{\mu+1} + \Lambda_{\mu+2}\,, \\ {}_3\Phi_\mu = \Phi_\mu + \Phi_{\mu+1} + \Phi_{\mu+2}\,, \end{cases}$$

. . . .

und $({}_2l)$, $({}_3l)$, . . . Expektanz des einzelnen Vektors. Bei der zufälligen Verteilung ist nach Wahrscheinlichkeitstheorie

$$l = \frac{({}_2l)}{\sqrt{2}} = \frac{({}_3l)}{\sqrt{3}} = \cdot\cdot\cdot\cdot\cdot\cdot\cdot,$$

bei der vollständigen Persistenz

$$l = \frac{({}_2l)}{2} = \frac{({}_3l)}{3} = \cdot\cdot\cdot\cdot\cdot\cdot\cdot,$$

und bei Quasi-persistenz

$$l < \sqrt{2}\,({}_2l) < \sqrt{3}\,({}_3l) < \cdot\cdot\cdot\cdot\cdot\cdot\cdot$$

In diesem Falle bekommt man

$$l = 0{\cdot}15\,, \quad {}_2l = 0{\cdot}154\,, \quad {}_3l = 0{\cdot}150\,. \;\cdot\cdot\cdot\cdot\cdot$$

Merkwürdigerweise ist jede Expektanz fast gleich mit einander. Das kommt sicher von spezieller Reihenfolge der Vektoren her.

Es sei $\Lambda_\mu = C_\mu \cos\theta_\mu\,, \qquad \Phi_\mu = C_\mu \sin\theta_\mu\,,$

dann

$$({}_2l)^2 = \frac{1}{n}\sum^n (C_\mu \cos\theta_\mu + C_{\mu+1}\cos\theta_{\mu+1})^2 + \frac{1}{n}\sum^n (C_\mu \sin\theta_\mu + C_{\mu+1}\sin\theta_{\mu+1})^2$$

$$= \frac{1}{n}\sum^n (C_\mu^2 + C_{\mu+1}^2) + \frac{2}{n}\sum^n C_\mu C_{\mu+1}\cos(\theta_\mu - \theta_{\mu+1})\,.$$

Wenn n groß ist,

$$({}_2l)^2 = \frac{2}{n}\sum^n C_\mu^2 + \frac{2}{n}\sum^n C_\mu C_{\mu+1}\cos(\theta_\mu - \theta_{\mu+1}).$$

Wenn die Verteilung der Vektoren ganz zufällig ist,

$$({}_2l)^2 = 2(l^2)\,,$$

was schon erwähnt ist.

Unser Fall sagt,

$$({}_2l)^2 \doteq (l)^2\,,$$

nämlich,

$$\frac{2}{n}\sum^n C_\mu C_{\mu+1}\cos(\theta_\mu - \theta_{\mu+1}) = -\frac{1}{n}\sum^n c_\mu^2\,.$$

Bei zufälliger Verteilung von C_μ bekommt man diese Folge, wenn

$$\cos(\theta_\mu - \theta_{\mu+1}) = -\frac{1}{2}\,,\quad \text{nämlich}\quad \theta_\mu - \theta_{\mu+1} = \pm 120°,$$

was leicht bewiesen wird. Wenn diese Bedingung erfüllt ist, dann ist wieder $({}_3l)^2 = (l)^2$ u. s. w. In solchem Fall kann man höheren Wert von k erwarten, wenn man jeden hintereinander folgenden vierten Vektor $(\lambda_\mu, \varphi_\mu)$, $(\lambda_{\mu+3}, \varphi_{\mu+3})$ u. s. w. auswählt.

Z. B. vom λ_1, φ_1 anfangend, ergibt sich zu

$$(l_m)_4 = 0{\cdot}26\,, \qquad (C_m)_4 = 0{\cdot}362\,.$$

Also $(C_m)_4/(l_m)_4 = 1{\cdot}4$, was wirklich größer ist als $\dfrac{C_m}{l_m} = 0{\cdot}14$.

Aber dieser Wert $k = 1{\cdot}4$ lässt natürlich noch keine Persistenz mehr als Zufälligkeit schliessen.

8. **Zeitverlauf der Häufigkeit der Nachbeben vom Nord-Idu-Grossbeben vom 26. Nov. 1930.** Stündliche Häufigkeit der Nachbeben ist von S. Sagisaka[6] gegeben.

6) S. SAGISAKA, *Kensin-Zihō* (Erdbebenberichte), 5 (1931), 136~137; Tabelle III.

Bei diesem Fall war die Abflautung der Bebenhäufigkeit ganz anders als Hyperbelformel. Man kann sie in mehrere Schwärme einteilen. Vom 27. Nov. 1930 bis zum 27. Dez. 1930 sind sie wieder in eintägige und halbtägige Schwankung analysiert. (Tabelle XI)

In diesem Falle sind die Tagesschwebungen am 27., 28., 30. Nov., 2., 5., 7., 10., und 25. Dez. ganz sicher als Realität.

In ganz ähnlicher Weise wie in Abschnitt 3 wird wieder Tagesperiodizität untersucht. Mit denselben Rechenzeichen bekommt man

$$k_1 = C_{1m}/l_{1m} = 2{\cdot}25\,, \qquad W'(k_1) = {\cdot}006,$$

$$k_2 = C_{2m}/l_{2m} = 1{\cdot}14\,, \qquad W'(k_2) = {\cdot}27.$$

Also ist die eintägige Schwebung ziemlich wahrscheinlich als Realität. Die halbtägige Schwebung muß dagegen nur als Zufall angesehen werden. Das ganze Verfahren für eintägige Schwebung ist in Fig. 8 gezeigt.

Die Summe der eintägigen Schwankungen ist in Fig. 9 ersichtlich, was sehr merkwürdig ist.

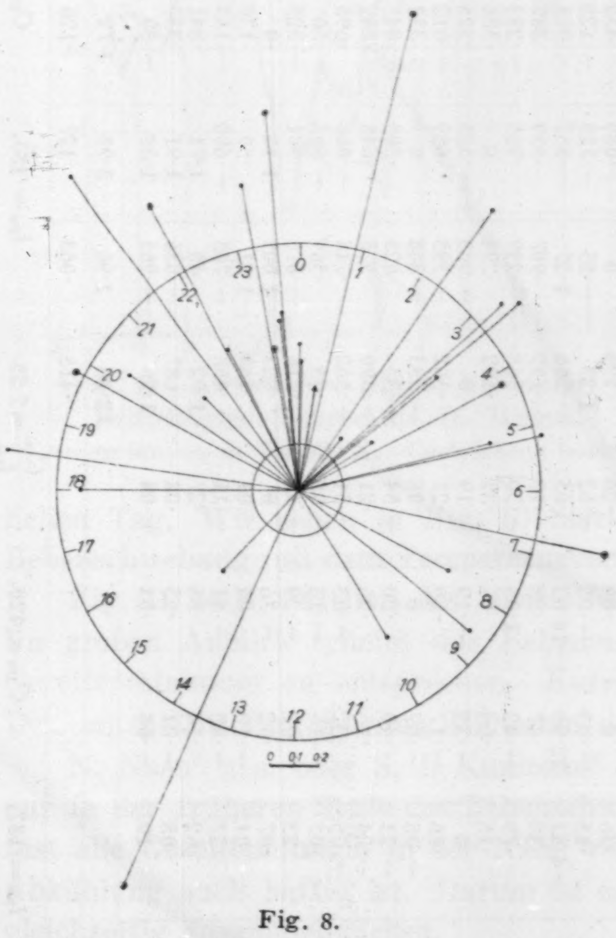

Fig. 8.
Punkt im Kreis: Vektor mit großer Wahrscheinlichkeit.
Vektor mit Pfeil: der gemittelte Vektor.
Der innere Kreis: mit Radius von Expektanz.

Fig. 9. Summe der eintägigen Schwebungen der Nachbeben des Groß-Nord-Idu-Bebens im 1930.

In Fig. 8 oder in Fig. 9 sieht man den Summenvektor zwischen

Tabelle XI.

Analyse der täglichen Schwankung der Bebenhäufigkeit in Nord-Idu nach dem Großbeben vom 1930.

Datum	a_0	a_1	b_1	a_2	b_2	$\frac{a_1}{a_0}$	$\frac{b_1}{a_0}$	$\frac{a_2}{a_0}$	$\frac{b_2}{a_0}$	$\sqrt{\frac{\pi}{n}}$	c_1^2	c_1	c_2^2	c_2
XI 27	4·44	2·54	−·45	·04	·42	·572	−·101	·010	·095	·168	·337	·581	·009	·095
28	3·48	1·47	2·91	−1·79	·30	·423	·837	−·515	·085	·190	·879	·938	·272	·522
29	1·40	·73	·01	−·07	·24	·520	·008	−·050	·169	·299	·270	·520	·031	·716
30	1·32	·62	−1·22	−·79	−·31	·468	−·925	−·600	−·233	·308	1·075	1·04	·414	·644
XII 1	·76	·15	·23	−·05	.19	·193	·304	−·066	·249	·406	·130	·360	·066	·258
2	4·56	7·00	−·70	3·59	−2·94	1·53	−·154	·788	−·623	·166	2·37	1·54	1·009	1·004
3	9·08	10·39	7·19	4·12	9·00	1·14	·792	·458	·99	1·17	1·927	1·338	1·19	1·09
4	1·16	·25	·20	·26	·72	·211	·175	·225	·622	·329	·075	·274	·438	·661
5	1·52	1·75	−·96	·39	−·80	1·15	−·632	·256	−·524	·287	1·72	1·31	·340	·583
6	·60	·45	·50	−·20	·36	·75	·833	−·33	·597	·457	1·256	1·121	·465	·682
7	8·28	−13·09	−5·80	9·41	8·90	−1·58	−·70	1·14	1·07	·123	2·986	1·728	2·245	1·498
8	·60	·36	0	·05	·26	·594	0	·080	·432	·457	·353	·594	·193	·439
9	·12	·15	−·03	−·02	−·02	1·23	−·25	−·125	−·125	1·02	1·575	1·255	·0312	·177
10	18·05	−4·81	22·90	−10·02	·05	−·266	1·27	−·557	·003	·083	1·684	1·293	·310	·557
11	·52	·39	·47	·28	·15	·752	·907	·539	·287	·490	1·388	1·178	·373	·611
12	1·40	·79	−·42	1·35	−·30	·565	−·299	·965	−·213	·299	·409	·639	·977	·988
13	·80	·15	·64	0	·31	·192	·794	0	·386	·396	·667	·817	·149	·386
14	·36	0	−·32	−·19	·19	0	−·903	−·525	·525	·590	·816	·903	·551	·742
15	·44	·16	−·17	·29	−·27	·362	−·395	·659	−·612	·533	·287	·536	·809	·899
16	·24	−·08	−·07	0	·08	−·333	−·308	0	·333	·723	·206	·454	·111	·333
17	·64	−·21	·40	·20	−·54	−·33	·628	·308	−·843	·443	·503	·710	·806	·898
18	·40	−·24	·15	·26	·21	−·590	·378	·648	·562	·560	·491	·701	·736	·858
19	·44	−·25	·32	−·03	·31	−·562	·718	−·066	·698	·533	·831	·912	·492	·701
20	·16	·07	·16	−·14	−·08	·45	·569	−·863	−·50	·885	·526	·726	·995	·997
21	·32	·23	−·02	−·29	−·12	·716	−·075	−·901	−·325	·625	·518	·720	·917	·958
22	·32	·07	·32	−·36	0	·223	1·005	−1·12	·0	·625	1·060	1·030	1·254	1·12
23	·08	·01	−·10	·04	·01	·160	−1·21	·50	·130	1·25	1·490	1·221	·267	·517
24	·60	·27	−·42	−·41	−·11	·458	−·705	−·680	−·183	·457	·702	·438	·496	·704
25	·32	·62	·14	·55	·27	1·92	·45	1·71	·841	·625	3·89	1·972	·363	1·91
26	·12	·08	−·01	·23	·04	·687	−·086	1·91	·333	1·02	·479	·692	2·76	1·66
27	·08	·10	−·08	·01	−·04	1·26	−·965	1·30	−·50	1·25	2·52	1·59	·267	·517
Σ						12·86	1·96	3·93	3·72		33·42		22·6	
Mittel						·415	·063	·127	·120					

$l_{1m}=\cdot187,\quad C_{1m}=\cdot420,\quad \frac{C_{1m}}{l_{1m}}=2\cdot25.\quad l_{2m}=\cdot153,\quad C_{2m}=\cdot175,\quad \frac{C_{2m}}{l_{2m}}=1\cdot14.$

24^h und 1^h Mitternacht liegen. In Fig. 8 ist auch auffällig, daß sich mehrere Vektoren in der Nacht als am Tage sammeln. Das erinnert uns an irgendeine Korrelation mit Temperaturverlauf, was E. Tams[7] auch bei der vogtländischen Erdbebenschwärmen bemerkt hatte.

Fig. 10 zeigt den Barometerverlauf, die dritteltägige (6^h, 14^h, 22^h) Temperatur, c_1 und a_0. Temperatur um 6^h und 14^h entspricht im allgemeinen respektiv dem Minimum und Maximum am gewöhn-

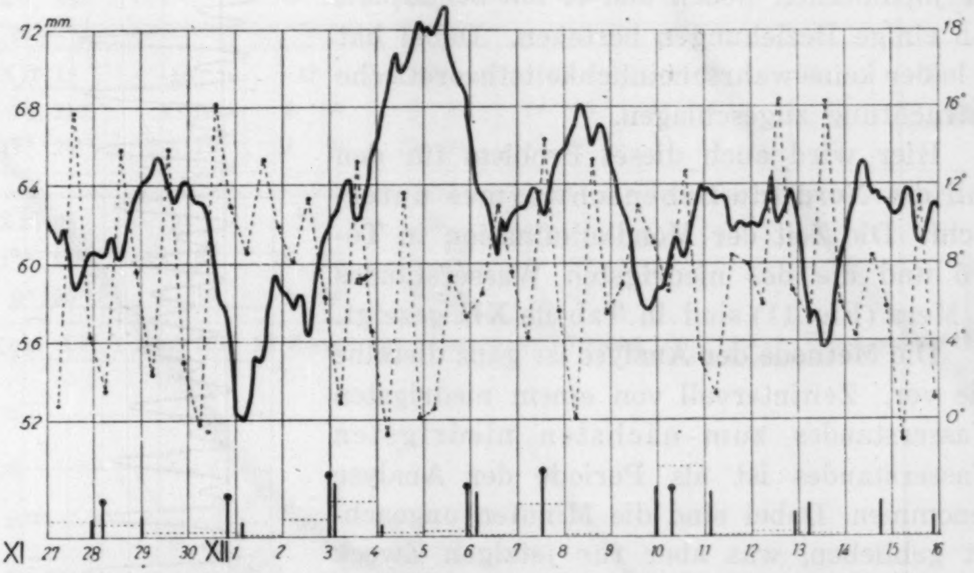

Fig. 10. Ausgezogene Kurve: Barometer. Gestrichene Linie mit Punkt: Dritteltägige Temperatur in Misima. Ausgezogene Ordinate ganz unten: c_1 in Tabelle X. Gestrichene horizontale Linie: a_0 in Tabelle X.

lichen Tag. Wir sehen in Fig. 10 merkwürdige Zusammenhang der Bebenschwebung mit dem Temperaturverlauf mit wenigen Ausnahmen.

Fig. 11 zeigt Gezeiten des Meeres in Mera und Bebenschwebung. Im groben Anblick scheint das Bebenmaximum im allgemeinen dem Gezeitenminimum zu entsprechen. Korrelationsausnahme z. B. am 7. Dez. entspricht dem zweiten Minimum der Gezeiten.

N. Nasu[8] u. a. oder S. I. Kunitomi[9] bemerkten solche Korrelation nur in der früheren Stufe des Bebenschwarmes. In diesem Falle fielen fast alle Gezeitenminima in der Nähe von Mitternacht, wo nächtliche Abkühlung auch heftig ist. Darum ist es möglich, daß beide Faktoren gleichzeitig zusammenwirken.

---

7) E. Tams, *Z. f. Angw. Geophys.*, **1** (1925), 193~213.

8) N. Nasu, F. Kishinouye und T. Kodaira, *Bull. Earthq. Res. Inst.*, **9** (1931), 22~35.

9) S. I. Kunitomi, *The Geophys. Mag. Cent. Met. Obs. Tôkyô*, **4** (1931), 79~80.

9. Gezeiten des Meeres und Erdbebenhäufigkeit. Die Erdbebenhäufigkeit in ihren Beziehungen zu den Gezeiten des Meeres oder zu den der festen Erde ist ein ziemlich veraltetes Problem. Doch ist es immer wieder untersucht und disktiert.[10]

S. Yamaguti[11] untersuchte manche Fälle der japanischen Beben und er hat behauptet, daß einige Beziehungen bestehen. Dabei hat er leider keine wahrscheinlichkeitstheoretische Betrachtung zugeschlagen.

Hier wird auch dieses Problem für den Fall des Nord-Idu-Bebenschwarmes untersucht. Die Zeit der Mondkulmination in Tôkyô und die des niedrigsten Wasserstandes in Mera (Fig. 11) sind in Tabelle XII gezeigt.

Die Methode der Analyse ist ganz dieselbe wie vor. Zeitintervall von einem niedrigsten Wasserstandes zum nächsten niedrigsten Wasserstandes ist als Periode der Analyse genommen. Dabei sind die Minuten ungeachtet geblieben, was aber für jetzigen Zweck belanglos sein soll. Darum ist das Intervall manchmal in 24 Stunden und manchmal in 25 Stunden eingeteilt. Das ganze Rechenverfahren ist in Tabelle XIII zusammengestellt und in Fig. 12, Fig. 13 graphisch dargestellt.

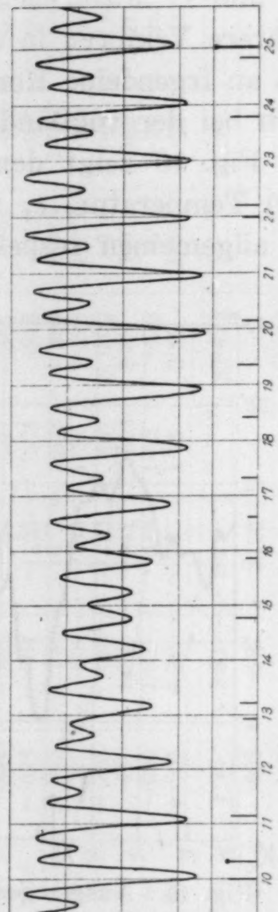

Fig. 11. Dicke Kurve, Gezeiten des Meeres in Mera. Dicke Ordinate, C_1 in Tabelle X.

Tabelle XII.

Zeit der Mondkulmination in Tokyo.
Zeit des niedrigsten Wasserstandes in Mera.

Datum	XI 27	28
Mondkulmination	17^h 12^m	17 54
der niedrigste Wasserstand	2^h 15^m	3 15

(Fortsetzung folgt.)

10) Sieh z. B. V. CONRAD, „die zeitliche Folge der Erdbeben und bebenauslösende Ursachen," *Handb. d. Geophys.*, 4 (1932), Lieferung 4.

11) S. YAMAGUTI, *Bull. Earthq. Res. Inst.*, 8 (1930), 393~408.

Tabelle XII. (*Fortsetzung.*)

XI 29	30	XII 1	2	3	4	5	6 ○
18^h 34^m	19 14	19 54	20 36	21 21	22 11	23 05	
4^h 20^m	5 10	20 00	20 15	21 05	21 40	22 10	22 55
XII 7	8	9	10	11	12	13 ☾	14
0^h 04^m	1 09	2 09	3 10	4 06	4 58	5 47	6 34
23^h 35^m		0 20	1 10	1 50	2 35	3 40	4 50
XII 15	16	17	18	19	20 ●	21	22
7^h 21^m	8 08	8 58	9 50	10 45	11 41	12 36	13 29
19^h 20^m	20 15	21 00	21 45	2 15	22 55	23 25	
XII 23	24	25	26	27 ☽			
14^h 19^m	15 06	15 49	16 30	17 09			
0^h 00^m	1 50	1 20	1 50	2 25			

(am XII 1 und XII 15 findet der Phasensprung des niedrigsten Wassers statt.)

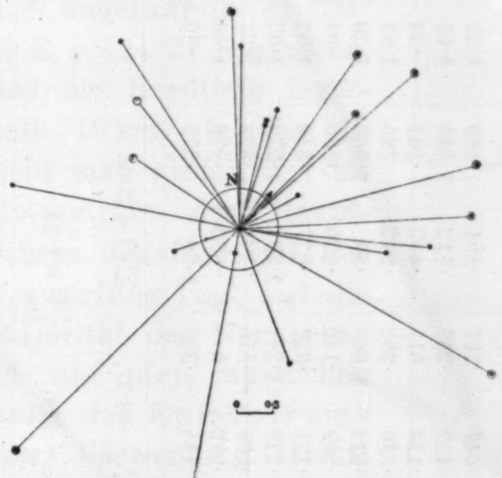

Fig. 12. Gezeiten und Erdbebenhäufigkeit. (Ein periodisch)
N, Phase des niedrigsten Wassers.
Vektor mit Pfeil, der gemittelte Vektor.
Kreis mit Radius der Expektanz.
Punkt im Kreis, Vektor mit *k* über 2·2.

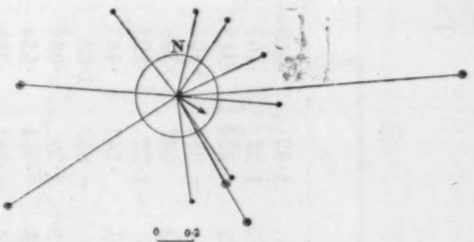

Fig. 13. Gezeiten und Erdbebenhäufigkeit. (halbperiodisch)
N, Phase des niedrigsten Wasserstandes.
Vektor mit Pfeil, der gemittelte Vektor.
Kreis, mit Radius der Expektanz.
Punkt in Kreis, Vektor mit *k* über 3.

Für $k_1 = \frac{C_{1m}}{l_{1m}} = 1{\cdot}24$ und $k_2 = \frac{C_{2m}}{l_{2m}} = 0{\cdot}80$ bekommt man respektiv $W'(k_1) = 0{\cdot}214$ und $W'(k_2) = 0.527$.

Mit solchen kleinen Werten von k ist die Beziehung zwischen den Gezeiten des Meeres und der Erdbebenhäufigkeit von kleiner Bedeutung.

10. **Großbeben und räumliche Verteilung der Nachbeben.** Über

Tabelle XIII.

Datum	a_0	a_1	b_1	$\frac{a_1}{a_0}$	$\frac{b_1}{a_0}$	ε	c_1	κ_1	a_2	b_2	$\frac{a_2}{a_0}$	$\frac{b_2}{a_0}$	c_2	κ_2
XII 1~2	1·24	−·963	1·76	−·78	1·42	·318	1·62	5·09	−·755	−1·15	−·608	−·928	1·11	3·49
2~3	11·35	3·99	14·90	·352	1·31	·103	1·35	13·1	−7·80	4·51	−·688	·398	·795	7·72
3~4	1·28	·233	·414	·182	·324	·313	·372	1·19	−·563	·397	−·440	·310	·538	1·72
4~5	1·31	1·55	−·071	1·18	−·054	·304	1·18	3·88	·593	−·480	·453	−·367	·569	1·87
5~6	1·04	·981	·673	·943	·647	·348	1·26	3·62	·469	·098	·451	·094	·461	1·32
6~7	7·93	−9·05	−9·71	−1·20	−1·22	·123	1·55	12·6	1·035	12·57	·130	1·58	1·59	13·0
7~8	·615	·360	·088	·585	·143	·443	·854	1·93	−·024	·346	−·039	·562	·563	1·27
9	·115	·117	−·077	1·02	−·667	1·02	1·30	1·27	−·067	·01	−·58	·087	·587	·576
10~11	18·10	1·36	23·4	·075	1·29	·084	1·31	15·6	−8·68	5·06	−·479	·280	·555	6·7
11~12	·423	·357	·408	·843	·964	·534	1·34	2·52	·175	·113	·413	·267	·492	·92
12~13	1·54	·592	−·898	·384	−·583	·280	·98	3·50	·086	−1·34	·056	−·870	·872	3·11
13~14	·654	·406	·419	·620	·641	·430	1·13	2·62	·151	·309	·231	·473	·527	1·23
15~16	·385	·249	·080	·647	·207	·561	·680	1·21						
16~17	·480	−·730	−·124	−·152	−·259	·512	1·540	3·01						
17~18	·50	−·067	−·007	−·134	− 015	·492	·141	·29						
18~19	·462	−·337	·135	−·730	·292	·512	·786	1·53						
19~20	·160	−·015	·170	−·094	1·06	·89	1·065	1·20						
20~21	·308	·175	·043	·569	·140	·626	·586	·94						
21~22	·320	−·0386	·262	−·121	·820	·627	·830	1·32						
22~23	·077	·0184	−·097	·239	−1·26	1·25	1·279	1·02						
24~25	·770	·530	−·444	·688	−·576	·396	·898	2·27						
25~26	·360	·555	0	·990	0	·670	·990	1·48						
26~27	·077	−·009	·028	−·115	−·357	1·25	·375	·30						

$\sum \frac{a_1}{a_0} = 4{\cdot}62$, $\sum \frac{b_1}{a_0} = 4{\cdot}27$, $\sum c_1^2 = 25{\cdot}86$

$l_{1m} = {\cdot}220$, $c_{1m} = {\cdot}274$, $\frac{c_{1m}}{l_{1m}} = 1{\cdot}24$

$\sum \frac{a_2}{a_0} = -1{\cdot}10$, $\sum \frac{b_2}{a_0} = 1{\cdot}89$, $\sum c_2^2 = 7{\cdot}47$

$l_{2m} = {\cdot}228$, $c_{2m} = {\cdot}182$, $\frac{c_{2m}}{l_{2m}} = {\cdot}80$

die Raumverteilung der Nachbeben des Großbebens vom 2. März 1933 ist schon in Abschnitt 6 (Fig. 6) einiges bemerkt. Hier werden mehrere andre Fälle gezeigt.

(1) Das Großbeben vom 26. Nov. 1930 in Nord-Idu. Vom Zeitverlauf dieses Bebens ist schon im vorigen Abschnitt die Rede gewesen. Die Raumverteilung ist in Fig. 14 ersichtlich.

Das Epizentrum des Hauptbebens war von A. Imamura[12] in $\lambda=139{\cdot}0°$E, $\varphi=35{\cdot}2°$N und von H. Honda[13] in $\lambda=138°59'$E, $\varphi=35°03'$N gegeben. Der kleine Unterschied ist in dieser Diskussion unwesentlich. Es ist ungefähr auf der Bodenverwerfung orientiert, und fast alle Nachbeben sind ganz westlich derselben zerstreut. Materialschäden durch das Hauptbeben waren auch an dieser Seite ganz merkwürdiger als an der anderen Seite.

(2) Das Großbeben vom 21. April 1935 in Taiwan (Formosa.) Fig. 15.

Seismometrisch ist das Epizentrum von H. Honda[14] ungefähr in $\lambda=120°49'$E, $\varphi=24°21'$N gegeben, und die Herdtiefe innerhalb 10 km. In Fig. 15 sieht man wieder, daß das Epizentrum des Hauptbebens ungefähr auf der Verwerfung liegt und die Majorität der Nachbeben ist auf der westlichen Seite des Epizentrums bzw. Verwerfung orientiert. Obgleich die genauigkeit der Herdbestimmung der Nachbeben nicht sehr hoch sein sollte, doch kann man innerhalb der Genauigkeit sagen, daß diese merkwürdige Erscheinung Realität sei.

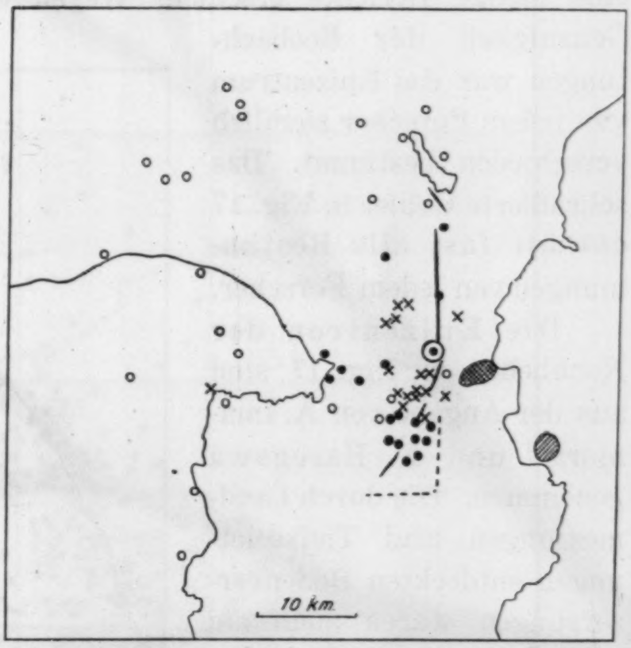

Fig. 14. Punkt im Kreis: Hauptbeben. Das einmal schraffierte Gebiet: Bebenschwarm vom Feb. bis zum Mai 1930. Das zweimal schraffierte Gebiet: Bebenschwarm im Nov. 1930. Kreuz: Vorbeben nach K. Hayata. Kreis: Nachbeben nach K. Hayata. Punkt: Nachbeben nach N. Nasu u. a. Dicke Linie: Beim Beben erzeugte Bodenverwerfungen.

(3) Das Großbeben vom 7. März 1927 in Nord-Tango und dessen

12) A. Imamura, *Bull. Earthq. Res. Inst.*, **9** (1931), 36~49.
13) H. Honda, *Kensin-Zihô*, **5** (1531), 94.
14) H. Honda, *Kensin-Zihô*, **9** (1935), 1.

Nachbeben. (Fig. 16)

Die Nachbeben vom 12. März 1927 bis zum 31. Aug. 1928 dieses Erdbebens waren von N. Nasu[15] untersucht worden. Fig. 16, welche die Raumverteilung der Nachbeben zeigt, ist die Zusammenfassung der N. Nasu'schen Beobachtungen. Das Epizentrum des Hauptbebens ist auch von mehreren Forschern seismometrisch untersucht worden. Im Durchschnitt ist es in Fig. 16 mit Punkt im Kreis gegeben. Es liegt wieder ungefähr auf den Ketten der Verwerfungen. Die Nachbeben verteilen sich meistens westlich von den Ketten der Verwerfungen bzw. vom Epizentrum. Nur kleines Prozent davon zerstreut sich auf der anderen Seite.

(4) Das Großbeben vom 1. Sept. 1923 in Kwantô und dessen Nachbeben.

Dieses Erdbeben wurde von sehr vielen Forschern untersucht und eine Menge Berichte erschien. Wegen des damaligen Mangels der Genauigkeit der Beobachtungen war das Epizentrum von jedem Forscher ziemlich verschieden bestimmt. Das schraffierte Gebiet in Fig. 17 enthält fast alle Bestimmungen von jedem Forscher.

Die Epizentren der Nachbeben in Fig. 17 sind aus der Angabe von A. Imamura[16] und K. Hasegawa genommen. Die durch Landmessungen und Tiefseelotungen entdeckten Bodenverzerrungen waren auch am merkwürdigsten in der Nähe vom Epizentralgebiet des Hauptbebens. Es ist wieder ganz merkwürdig, daß die große Mehrzahl der Nachbeben ganz ostlich davon entstand.

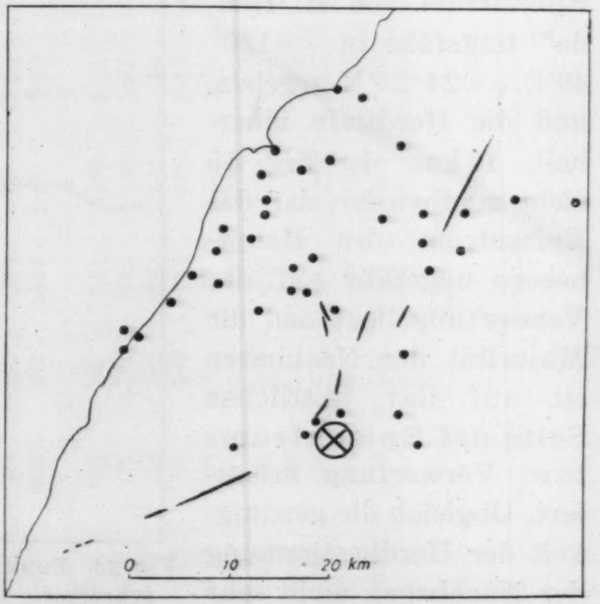

Fig. 15. Verteilung der Nachbeben des Bebens von 1935 in Taiwan. (nach T. Isikawa) Kreuz im Kreis: Hauptbeben. Punkt: Nachbeben vom 21. April bis zum 30. April 1935. Dicke Line: Bodenverwerfungen beim Hauptbeben.

15) N. NASU, *Jour. Fac. Sci. Tôkyô Imp. Univ.*, [ii], **3** (1929), 29~129; *Bull. Earthq. Res. Inst.*, **13** (1935), 335~399.

16) A. IMAMURA und K. HASEGAWA, *Bull. Imp. Earthq. Inv. Com.*, **11** (1928), 64~92.

11. Die allen oben erwähnten fünf Fälle zusammenfassend kann man die folgenden wichtigen Eigenschaften sehen;

(i) Das seismometrisch bestimmte Epizentrum eines Großbebens liegt ganz seitlich im von Nachbeben geregten Gebiet.

(ii) Es hat immer irgendeinen Platz auf den Ketten der beim Erdbeben erschienenen Bodenverwerfungen genommen, wenigstens in so fern sie sichtbar erschienen sind.

Diese Erscheinungen werden einen wichtigen Anhaltspunkt zur Theorie der Entstehung des Großbebens geben. Ein seismometrisch zubestimmender Herd bedeutet den Entstehungspunkt der Erdbebenwellen oder dessen Äquivalent. Die Tatsache (ii) lässt uns vermuten, daß die erste wichtige Welle plötzliche Umwandlung der Verzerrungsenergie in die Wellenenergie gleichzeitig mit der Formation neuer Diskontinuität im Boden bedeutet.

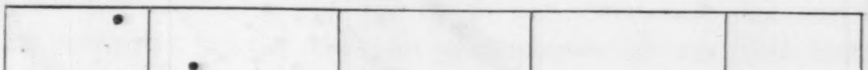

Fig. 16. Verteilung der Nachbeben des Großtangobebens in 1927. Punkt im Kreis: Hauptbeben. Punkt: Nachbeben vom 12. März bis zum 31. Aug. 1927. Dicke Kurve: Verwerfungen beim Hauptbeben.

Im großen und ganzen kann die Erde als eine Wärmemaschine oder deren Kombination angesehen werden, weil sie Wärmereservoirs und auch Arbeitsmittel hat. Man denke sich einen Teil Erdkruste. Der

erste Hauptsatz der Thermodynamik sagt in Bezug auf diesen Teil,

$$\Delta U \equiv U_b - U_a = Q + A ,$$

wo U_b, U_a, innere Energie des Zustandes (b) bzw. (a) bedeuten, Q, die während der Zustandsänderung in den Teil zugeführte Wärmemenge ist, und A, die Zugeführte Arbeit ist.

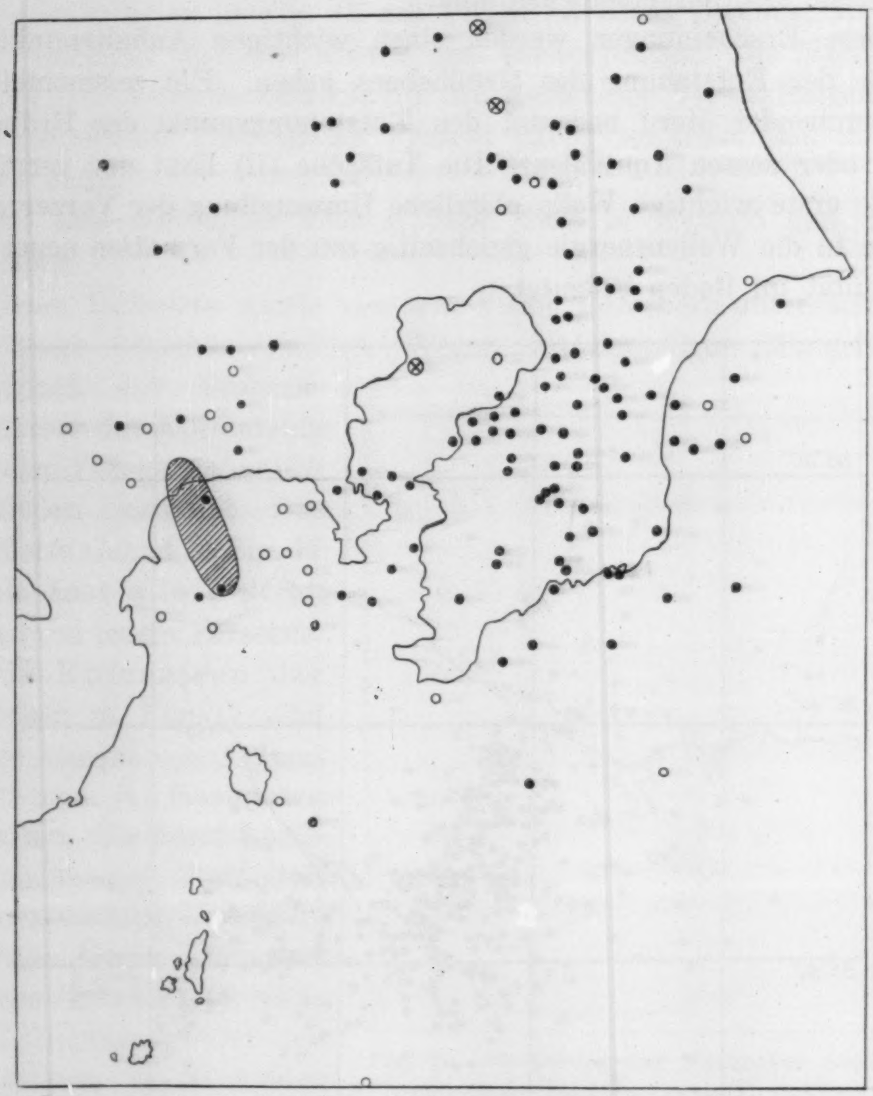

Eig. 17. Verteilung der Nachbeben des Groß-kwantô-bebens in 1923. Punkt: kleine Nachbeben im Sept. 1923. Kreis: Wichtige Nachbeben. bis zum 18. Sept. 1924. Kreuz im Kreis: Erdbeben vom 3. Aug. 1926 bis zum 12. Feb. 1928. Das schraffierte Gebiet enthält das Epizentrum des Hauptbebens von allen Forschern, die dieses Erdbeben untersuchten.

Die Zustandsänderung des Bodenteilchens vor einem Erdbeben wird als quasistatischer Vorgang angesehen.

Die innere Energie ΔU wird hier bequemlichkeitshalber in vier Teile eingeteilt, nämlich Gestaltänderungsenergie $\delta\Omega$, Volumenänderungsenergie δL im Sinne von A. Nadai,[17] durch Formänderung verursachte Gravitationspotentielleenergie δV und andere Art Energie δM. Also

$$\Delta U \equiv \delta\Omega + \delta L + \delta V + \delta M .$$

Nach der Theorie von R. v. Mises und von H. Hencky kommt Störung des elastischen Äquilibriums vor, wenn die Gestaltänderungsenergie in einem Einheitsvolumen einen bestimmten Wert erreicht.

$$\tau_1^2 + \tau_2^2 + \tau_3^2 = 2k^2 ,$$

wo τ_1, τ_2, τ_3, Hauptschubspannungen sind, $2k$ die Fliessgrenze bei der reinen Zugbeanspruchung ist. Dieser Vorgang kann natürlich auch ohne Energiezufuhr (oder Abzug) von außen ($Q=0$, $A=0$) vorkommen, z. B. durch Umwandlung von δM in $\delta\Omega$ etc., was z. B. bei der Radioaktivität vermutet wird. Aber im allgemeinen ist ein Teil Erdkruste nicht ein abgeschlossenes System. Darum ist Energiezufuhr (oder Abzug) von außen unvermeidlich. Bei Erdbebenentstehung handelt es sich nur um Zuwachs von $\delta\Omega$.[18] Das kann auch bei Abzug der Wärme $-|Q|$ stattfinden, z. B. Druckerhöhung in bestimmten magmatischen Vorgängen bei Wärmeabzug, oder Bodenverzerrung bei der Abkühlung der Erdrinde.

Wann und wie $\delta\Omega$ zuwächst, hängt von dem mechanischen Zusammenhang und dem thermodynamischen Zustand des betreffenden Erdteils ab.

Bei dem Erdbeben selbst mag der Vorgang fast adiabatisch vor sich gehen. Sehr wahrscheinlich werden neue Diskontinuitäten erzeugt. Dabei wird nur ein Teil Formänderungsenergie als Wellenenergie nach außen ausgesandt, was einen Teil von $-|A|$ bildet. Wesentliche Abspannung soll im allgemeinen nur in der Nähe von Diskontinuität stattfinden. Anderer Teil Formänderungsenergie wird in andere Arten Energie übergehen, z.B. in Reibungswärme, Grenzflächenenergie, u.s.w. Es ist sehr wahrscheinlich, daß je mehr Diskontinuitäten erzeugt werden, desto leichter Erreichung von $2k^2$ der Gestaltänderungsenergie stattfinden kann, weil effektive Querschnitte für Aushaltung der den betreffenden Teil beanspruchenden Kraft immer kleiner werden. Von dieser Betrachtung ist die Möglichkeit der sogenannten sympathetischen

---

17) A. Nadai, Der bildsame Zustand der Werkstoffe, Julius Springer, (1929), 49.

18) Hier sind die Ishimoto Theorie des Stoßes von Magma oder die Galitzin Theorie über das Pamirbeben von 1911 ausser acht gelassen, die beide Umwandlung von kinetischer Energie in Wellenenergie behaupten.

Erdbebenaktivität von weit entfernten Gebieten nicht ausgeschlossen, weil jeder Teil der Erde mehr oder weniger mechanisch gekoppelt sein muß. Die ungeheure Menge Nachbeben eines Großbebens wird in dieser Weise erklärt. Die Abflautung der Nachbeben bedeutet Abnahme von $\frac{d\Omega}{dt}$, bis nur vorläufiges mechanisches Äquilibrium des ganzen betreffenden Systems erreicht wird. Darum kann der Typus des Zeitverlaufes der Nachbebenhäufigkeit mannigfaltig sein gemäß des mechanischen Zusammenhanges und des thermodynamischen Zustandes.

Die Tatsache (i) lehrt uns etwas detailliertes Bild der Großbebenentstehung. Dazu ist die Untersuchung der Nachbeben des Tangobebens von N. Nasu[19] sehr lehrreich. Dabei gab es ein prismatisches Stück Erdkruste in der Nähe von Erdoberfläche, in dem fast keine Nachbeben vorkamen, indem außerhalb dessen Mehrzahl der Beben entstand. Die Bodenverwerfungen bzw. das Epizentrum des Hauptbebens sollten als oberflächliche Spur der Grenze dieses Stückes angesehen werden. Das prismatische Stück wurde wahrscheinlich schüppenartig von der Erdkruste getrennt und war fast unabhängiges System geworden, in so fern es den Verlauf von $\delta\Omega$ in demselben anbetrifft.

Bei stark beanspruchten Werkstoffen ist in der Regel erwartet, daß ein prismatisches Stückchen in der Nähe von Oberfläche keilförmig abgetrennt wird. In der Nähe von beanspruchter Erdoberfläche kann auch solches vorkommen. In der Nähe von Keilgrenze wird der mechanische Zustand günstiger zur Erreichung von $2k^2$ der Gestaltänderungsenergie als vorher. Dann werden als natürliche Folge die Tatsachen (i) und (ii) erwartet.

---

19) N. Nasu, *l. c.*

5. 昭和8年3月3日の大地震

III. 大地震前後の三陸沖の地震活動及一般に大地震の餘震に就て

地震研究所 松澤武雄

1. 三陸沖及北伊豆地方の地震の回數に就て統計的の研究を試みた. 多くの場合は時間的に見て偶然な分布とえらぶ所がない. 北伊豆大地震の餘震の場合は夜中に多く起つてゐてもし偶然な出來事としてみるとその確率は ·006 位に過ぎない.

潮との關係は潮の最底から$\frac{1}{8}$週期位おくれた所に多いが偶然な出來事としてみても 0·214 位の確率はある.

2. 地震波の觀測から定まる大地震の震央は其餘震の多く起る區域の片端にある場合の多いことを注意する. そしてまた地上に現れた地變の上に位する. したがつて地變の體係はまた餘震區域の端の界になつてゐる. 斯樣なことは張合ひを受けた地殼の壞れ方から見れば寧ろ當然なことに思はれる.

6. 伊豆下田に於ける過去地震津浪の高さ

三井地球物理研究所　福　富　孝　治

(昭和10年11月19日發表—昭和10年12月20日受理)

伊豆下田は古來津浪の害を蒙つた事が少くない．南伊豆の古記錄に殘つて居る津浪の中，人命財產に可成りの被害を及ぼしたものとして以下に述べる7の地震津浪，2の風津浪を擧げる事が出來るが，古記錄の中には津浪の高さに就て幾分の手掛りとなるものがあるので，夫等に就て求めた元祿，寳永，安政年度の三地震津浪の大體の高さと，大正12年關東大地震の際の津浪は未だ12年を經たに過ぎないので町家の壁に其跡の殘つて居る處も多く，今春水準測量に依つて之等の津浪の高さを測定して，其分布を略々知り得たので其結果に就て簡單に御報告申上げる次第である．

先づ下田附近に於ける過去地震津浪に就て見るに今より500年以前足利時代以前に就いては古記錄の見るべきものに乏しく津浪に就ても知る術が無い．足利時代以後の津浪に就ては以下に述べる通りであつて之を年代順に揭げると，

1. 明應7年8月25日（西曆1498年9月20日）の地震津浪

南伊豆仁科佐波神社の沿革慶長10年の上梁文の裏書に「是より先116年戊午歲（註，明應7年に當る）の海嘯には波頭寺川の大堰に到る」と（註，寺川の大堰は海岸を去る15～16町の一部落なり）又豆陽舊跡記に本社の沿革に就て「400年前は鴨ケ池の傍に在りしが海嘯のため今の地（澤田）に流寄りしを以て卽ち其地に遷祀す」とあり，相當に津浪の害を蒙つた事が判る．

2. 慶長9年12月16日（西曆1605年2月3日）の地震津浪

「慶長9年甲辰12月16日仁科鄕海溢れて陸地を浸す事凡そ十二，三町」と豆州志稿にある．

3. 寛永20年（西曆1643年）より數年前の風津浪

寛永20年起工，正保2年完成の下田防波堤に關し，正保3年建立の起工碑の碑面に「頃年大風浪打碎西崖之巖碧洪潮浸來低下田之民家故往返旅舡不能泊于下田津，積

歳漁民枕籍以患焉云々」とある.

4. 元禄16年11月23日（西暦1703年12月31日）の地震津浪

當時の津浪の模様を記した古記錄も少くないが，下田町役場藏下田年中行事に依れば「元祿 16 年癸未 11 月 22 日丑の刻に至り，大地震津浪打寄，家數 492 軒流亡，內 332 軒流失，160 軒半潰，船大小 81 艘破船痛船し，溺死男女 37 人，又 20 人あり，此時月二つ現ると云ふ．怪異前代未曾有の事也．此時浪先寶福寺大門迄，浸來と此寺の記錄に見るなり云々」とある．當時の寶福寺大門附近の高さを水準測量に依り求めた結果，中等海水面上 240 糎であつて津浪の高さは此處では約 2·5 米であつた事となるが，これは後述する大正 12 年關東大地震の津浪の高さと同程度であつて，大正年度の津浪の際には殆ど被害が無かつたのに元祿年度の津浪の際には上記の如き被害があつた事から考へると此津浪の高さは小に失し，此大門の位置の傳承に對して疑をもつのである．

5. 寶永4年10月4日（西曆1707年10月28日）の地震津浪

一例を擧ぐれば上記の下田年中行事中に「寶永 4 年丁亥 10 月 4 日未の刻，亦大地震津浪打寄，家數 912 軒流亡，857 軒流失，55 軒半潰，船大小 93 艘破船痛船し，此時波先寶福寺中後園竹林の際に至ると云，云々」とある．寶福寺の竹林は殆ど當時の儘にて現在もあるので，その際附近の高さを求めると中等海水面上 360 糎にて津浪の高さも大體此程度であつた事が判る．

6. 安政1年11月4日（西曆1854年12月23日）の地震津浪

この時の津浪の様子を最も詳細に知り得るのは大日本地震史料[1] 記載の憂北生，伊豆下田よりの書狀であつてその大要を揭ぐれば「扨當月 4 日朝五つ 2 分 5 厘許の頃，下田湊大地震，土藏等は壁落ち，土地少々割れ申候，泥少々出候位之事に御座候，市中大騷動仕居候處 1 刻許も過候間に，大勢又々騷立候間出火と存じ表に出申候處煙も不見候間，是は定而異人共亂妨仕候事と存じ，我も內に脇差を取に入出候處，早市中に大波參り申候，大工町川岸（註，下田町中南部，第 4 圖中彌治川と稻生澤川との合流點附近）に大船之帆柱搖動致し，あたまの上倒れ候許に相成候間，漸く津浪なる事をしりて，先づ山際へ上り，旅宿本覺寺へ行んと存候に，市中一面津浪に而，中々渡

1）大日本地震史料　震災豫防調査會報告　46 B (1905), 440.

りがたく候間，早々了仙寺と申寺の山へ上り見申候處，早1の潮は其の節引去り申候に，其波の中を渡りて，市人並諸役人等皆山に上り申候，扨然るに，又煙草 1，2 服許も呑候間に2の潮來り候やと人々騒ぎ候得共，一向其様子も無之，大工町邊りに煙立上り出火出火と騒ぎに，寺鐘を撞かけ候に又阿治川（註，了仙寺附近より東流する小川）邊に出火燃立候間に，2 の潮柿崎濱へ突かけ，浪除土手を越て，下田湊へ参り候に，其浪にて2ケ所の出火消え900軒の人家一時に將棋倒しに相成，青海原と相成候800石以上の船 13 艘程下田町を打越岡方村，本郷村の畑中又村中へ上り，其時異國船（註，露國軍艦 Diana）は若の浦と申處に繋ぎ有之候處早纜切れて犬走島の上の方鴎島の下の方に漂ひ來りしに，早三段にかけし檣，壹段と致し，大ゆれに成りて流れ來りしが，其2の潮の引につけて，元の邊へ戻りたり．扨又しばし有て3の汐，柿崎へつきかけ候に此汐にて百餘軒の柿崎村，一時に碎かれ，皆流れ又其邊に繋ぎし大船凡17,18艘（此船皆 500~800 石なり）村中に打上げ碎かれ流れたり，其潮下田の方へ廻り來りたれども最早1軒の家も無く青海原の事なれば其潮，本郷村，岡方村の邊一面にさし込みて，山際まで打かけたり．（中略）4の潮5の潮6の潮も最早追々干潟にも成る時節につき追々輕く相成候．（中略）纔一時半許の間，1000 軒の下田，150 軒の岡方村漸く殘る所は坂下町と申に 18 軒有之候事に御座候，其餘山際に立候寺は半潰れ位に相成候其寺に御止宿に御座候，伊澤美作守様御宿寺稻田寺半流に相成候，床の上泥水つき申候，村垣様御宿長樂寺無難少々のいたみ，筒井様御旅宿海禪寺皆流れ，應接所福泉寺（註，稻田寺の少し北方）流申候，川路様御宿泰平寺皆流，松平様御宿本覺寺皆流れ，魯西亞人小休息所了仙寺半流れ，（中略）其夜 3 度程地震仕候，云々」とある．下田港の靜振に就ては本多，寺田兩博士の研究[2] があつて，15~ 18 分周期の靜振が優越する事が知られて居るが，上記の古記錄中にも大振幅の靜振特に第 2 回目の靜振が大であつた事等がよく示されて居る．傳承に依れば津浪は八幡神社境内石段の 3~4 段目迄來た．又寶福寺本堂唐紙にも第1圖に示す様な此津浪の跡が殘つて居る．水準測量結果に依れば津浪の高さは夫々，中等海水面上 430糎，467糎であつた．第3圖は此津浪の浸水區域を示す．

7. 安政1年11月5日（西暦1854年12月24日）の地震津浪

前地震の翌日，土佐沖に起れる地震であるが，前述の憂北生の手紙に「5 日又九ツ頃大津浪來り候由，誰いふとなく風聞致し候，我々本覺寺山より本郷村江引移止宿仕候處，夕六ツ半頃又津浪來り申候，下田．岡方村江上り候得共，最早流れ候人家無故

---

2) K. Honda and T. Terada, *Publ. Earthq. Inv. Comm.*, **26** (1908), 1.

にさして騒ぎ不申候，2 の潮も凡 10 町許の方まで上り申候」とある．

第 3 圖 安政元年 11 月 4 日地震津浪の浸水區域

8. 安政 3 年 8 月 25 日（西曆 1856 年 9 月 25 日）の風津浪

柿崎玉泉寺藏名主濱田與平治日記に依れば，此大風大時化にて下田港の廻船 25 艘破船したりと云ふ．

9. 大正 12 年 9 月 1 日（西曆 1923 年）の地震津浪

津浪は大地震後約 10 分後に引潮にて初まつたと云ふ．前述の通り關東大地震後未だ 12 年を經たに過ぎないので，當時の津浪跡の壁等に殘つた家も多く，叉跡はなくても津浪の目擊者に依つて聞いた各家内の浸水狀態は 20 糎以上の誤差は先づ無いと考へられるので，これら 26 ケ所の津浪の高さを下田八幡神社内の水準點に準據して "Y" レベルと標尺とを用ひて水準測量を行ひ測定した．第 4 圖中黑丸は津浪の高さの測られた場所，數字は中等海水面上の津浪の高さ（單位糎）括弧内の數字は土地の中等海水面上の高さ（單位糎）である．斜線を施した太い黑線は浸水區域，黑線は津浪

の中等海水面上の等高線，破線は土地の等高線である．即ち津浪は下田港より稲生澤川に入つて突當つた附近に最も高く3米以上に達し，それより川を上るにつれて低くなつて居る．又津浪の最高個所から一部は彌治川に沿つて上り了仙寺北西方の田にも浸水したと云ふ．浸水の模樣は上記の通りであるが幸にして，被害は輕微で下田町役場の調査に依れば，全町1379戸中床上浸水190戸，全潰2，半潰5，人命の損失は皆無であつた．此處に全潰，半潰を出した部分が標高1.5米以下の土地であつたのは注意に値する。

以上に伊豆下田附近に於ける過去津浪の主なるものを擧げたのであるが，極く小な

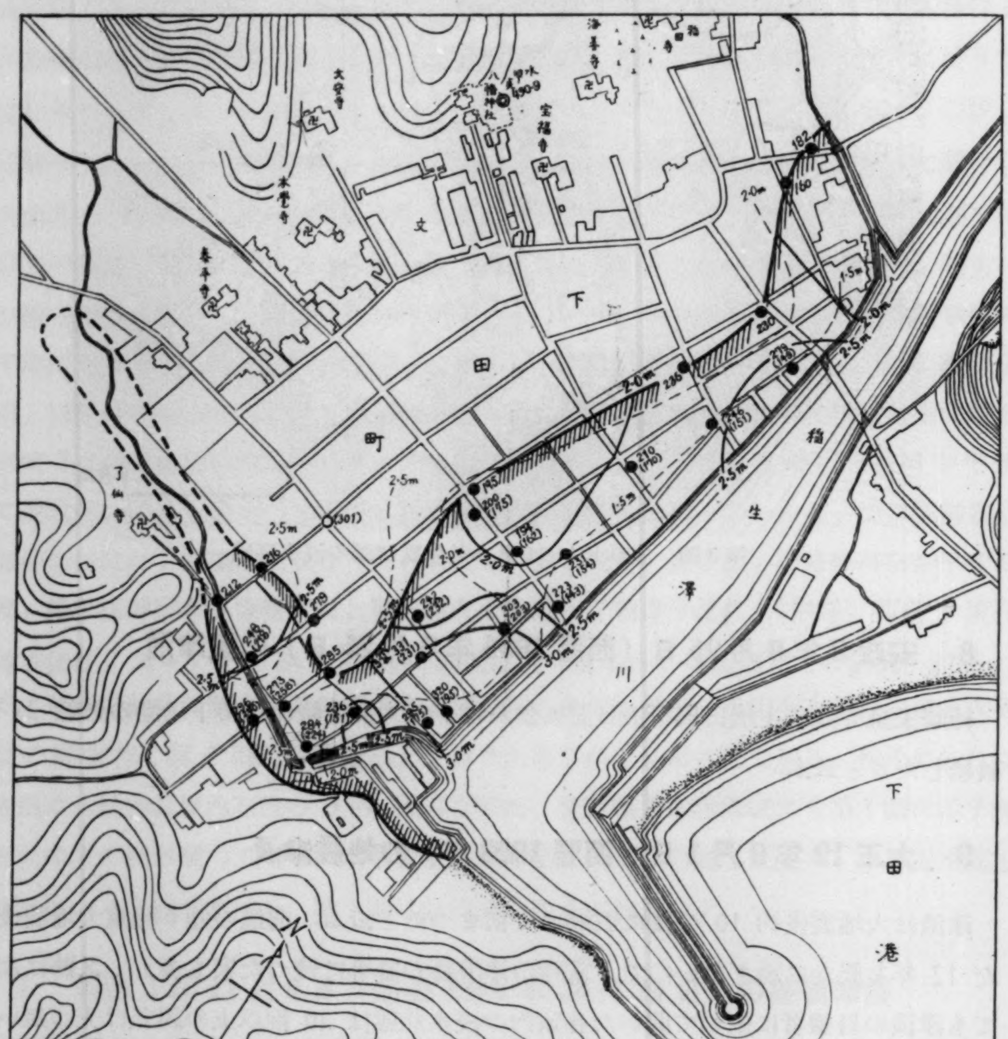

第4圖　伊豆下田に於ける大正12年關東地震津浪の高さの分布．
黒丸は津浪の高さの測られた場所；數字は平均海水面上津浪の高さ（單位糎）；
括弧内の數字は土地の高さ；太き實線は津浪の高さの平均海水面上の等高線；
破線は土地の等高線．

る津浪は享保 14 年已酉2月9日の地震津浪，寳暦年中及び安永4年の風津浪等少くない．

次に以上の津浪を起した地震の震央[3] の分布を見るに第5圖に示す如く房總半島の南沖から四國沖に到る廣範圍に渉つて居る事が判る．

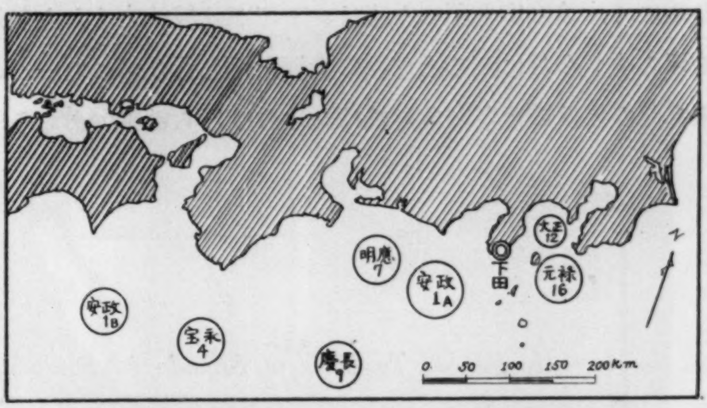

第5圖　下田附近に害を及ぼした地震津浪の震央　但し（安政1A）とあるは安政元年 11 月 4 日，（安政 1 B）は 11 月 5 日の地震震央なり．

今上記地震津浪の中，津浪の高さの推定された，元祿，寳永，安政，大正年度の4地震津浪に就て其被害並に津浪の高さを要約表記すれば第I表の如くである．

第I表　元祿，寳永，安政，大正地震津浪の比較

津　浪	浸水家數	流　失	半　潰	流　死	破　船	津浪の高さ(平均海面上)
元祿 16 年	492	332	160	27	大小 81	250 糎(?)
寳永 4 年	912(全町)	857	55	11	93	360 糎
安政 1 年(11月4日)	984(全町)	937 (172土藏)	43 (15土藏)	122	大 36	平均 450 糎
大正 12 年	190 (1379の中)	2	5	0	——	平均 246 糎

次に下田附近は過去に 1·5 米に及ぶ比較的急な土地隆起[4] のあつた事が知られて居るが，此土地隆起が元祿 16 年の關東地震の際に起つた地殼變動である事は既に南伊豆の地殼變動を論じた際に注意した所であつて，此場合に於て，上表の各津浪の高さは大體眞の津浪高を示すものと考へて差支へあるまいと思ふ．

次に一言したい事は，下田防波堤に就てである．これに就て寛永 20 年風津浪の項に述べた通り，津浪の害を憂ひ，時の下田奉行今村傳四郎正長が私俸を拋ち造らしめたものにて寛永 20 年起工，正保2年8月に完成したものである．堤は其後寳永2年，

3) A. IMAMURA, *Jap. Jour. Astro. Geophys.*, **6** (1928), 119.
4) 福富孝治　地震　**6** (1934), 351.
T. FUKUTOMI, *Jap. Journ. Astro. Geophys.*, **12** (1935), 279.

文化5年，文化 13 年に修築されたが，安政1年の津浪の爲めに大破したが，更に築造されて今日に及んで居る.

下田附近が上述の如く今日迄凡そ450年間に9回，換言すれば平均凡そ 50 年1回の割にて津浪の害を蒙つた事は，下田が比較的古くから交通文化の開けた町であつたに係らず，今日に到るも左程の發展を爲し得なかつた一つの主要な原因であつて，將來も此の點は愼重な考慮を拂はなければならぬ事であらう.

---

6. *Heights of Tunamis at Simoda in Southern Idu Peninsula.*

By Takaharu FUKUTOMI,

Mitsui Geophysical Observatory.

During 450 years from the middle years of the Asikaga era up to present, Town Simoda in southern Idu Peninsula was frequently submerged under the waters and lost many lives by 7 tunamis caused by marine earthquakes and 2 kazetunamis caused by typhoon. This is one of the most powerful reasons for her gradual decline, in spite of her prosperity in the later years of Tokugawa era.

The writer picked up some suggestive facts about the heights of the tunamis from the old records of these calamities and required the heights of the tunamis from the present mean sea-level by levelling method. And get 2·5 m, 3·6 m and 4·5 m for the tunamis in 1703, 1707 and 1854. The heights of the tunamis which were caused by the great Kwantô earthquake of 1923 could be told by the indisputable traces left on the walls of the houses at Simoda even nearly 12 years after that. Thus, the heights of 26 points from the mean sea-level were determined with a "Y" level as shown in Fig. 4. The numerals near the small black circles are the reduced heights of the water in cm, while the numerals in bracket are the heights of the ground. The boundaries of the inundated areas are shown with hatchings, and the full and broken lines are contour lines of the heights of the tunamis and geographical features respectively.

It is very noticeable that the epicentres of the earthquakes which caused the above-mentioned tunamis at Simoda are distributed in far great areas in the outer zone of Japan Arc extending from off Bôsô Peninsula to off the coast of Sikoku.

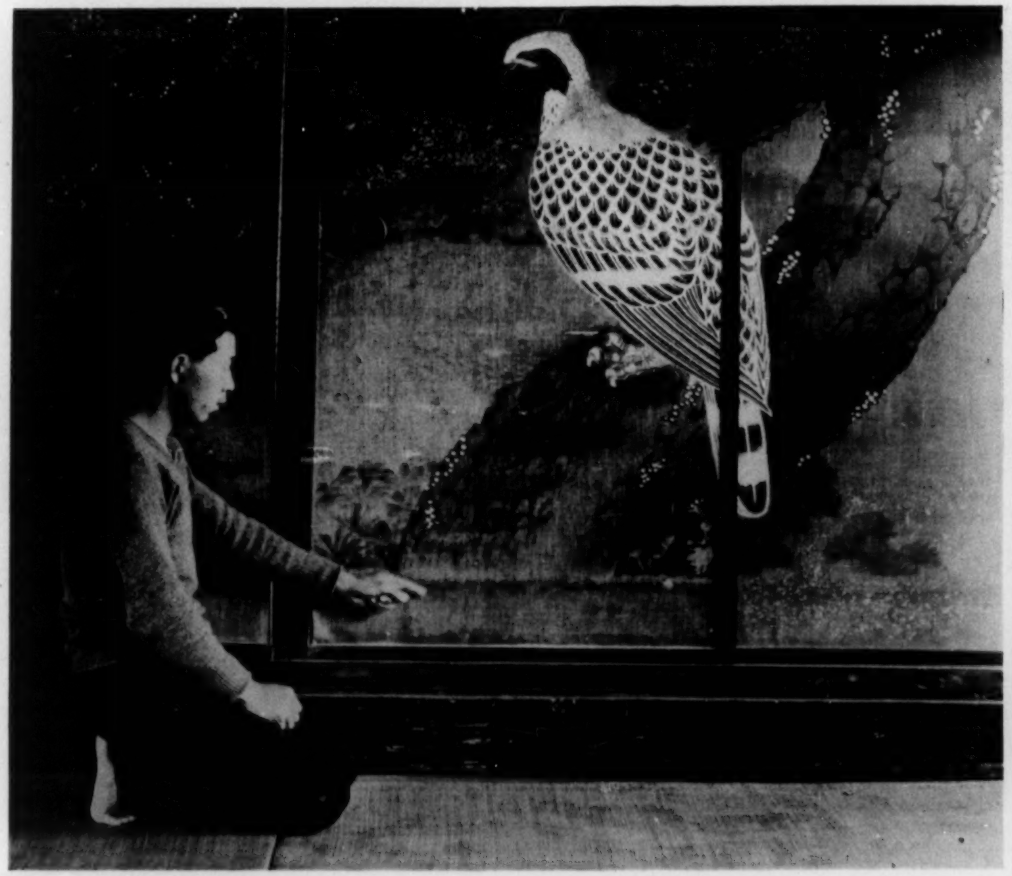

第1圖　下田町寶福寺本堂唐紙に殘れる安政元年 11 月 4 日の地震津浪の跡（平均海水面上 4 米67 糎高）

第2圖　當時の外人休息所了仙寺玄關柱に殘れる安政地震津浪の爲陸上に揚りたる大なる廻船の衝突して出來たと云ふ傷跡

7. *Marine Lower Pleistocene of the Central Kwanto Plain.*

(*An evidence of basin forming force of the Kwanto plain.*)

By Yanosuke OTUKA,

Earthquake Research Institute.

(Read Dec. 17, 1935.—Received Dec. 20, 1935.)

It is regrettable that our knowledge regarding the distribution of the marine Lower Pleistocene in the Central Kwanto plain is so meagre. Recently the writer through the courtesy of the Nippon Sakusen Company, had occasion to examine some boring cores from Hudooka-mati, near Kazo-mati, Saitama pref.

The boring was made in the grounds of the Katakura Seisi Boseki Company situated at the east end of Hudooka-mati, near Kazo-mati, in Saitama prefecture, as shown in Fig. 1. Fig. 2 is a columnar section, showing the underground formation. In the columnar section, the sandy clay between the 106~116 m depths and the gravels of pumice between the 128~141 m depths below the ground surface are interesting.

The former contains many fossil mollusca and foraminifera, as listed below:

List I.

	Geologic occurrence nr. Tokyo		
	Pliocene	Pleistocene	Recent
Arca (Scapharca) inflata REEVE	Naganuma	Tokyo	Tokyo Bay
Meretrix meretrix (LINNÉ)	Omma series	Tokyo	Tokyo Bay
Dosinia (Phacosoma) japonica (REEVE)	Naganuma	Tokyo	Tokyo Bay
Cadulus sp.	*unknown*	*unknown*	*unknown*
Dentalium (Dentalium) hexagonum GOULD	Naganuma?	Tokyo	Tokyo Bay
Menestho nishiana (YOKOYAMA)	*unknown*	Tokyo	*unknown*
Odostomia sublimpida YOKOYAMA	Miyata?	Tokyo	*unknown*
Turbonilla edoensis YOKOYAMA	*unknown*	Tokyo	Turumi
Turbonilla keiskeana YOKOYAMA	*unknown*	Tokyo	*unknown*
Turbonilla (Mormula?) sp.	*unknown*	*unknown*	*unknown*
Pyramidella (Tiberia) ebarana YOKOYAMA	*unknown*	Tokyo	*unknown*
Polynices sagamiensis PILSBRY	Low. Kakegawa	Noto	Tokyo Bay
Natica (Tectonatica) janthostoma DESHAYES	Low. Musasino	Tokyo	Tokyo Bay
Nassarius (Hinia) muroii OTUKA n. sp.	*unknown*	Tokyo	Tokyo Bay
Clavatula consimilis (SMITH)	Naganuma	Tokyo	Tokyo Bay

(*to be continued.*)

List I. (*continued.*)

Suavodrillia declivus (MARTENS)	*unknown*	Simosa	Matusima Bay
Mangelia aff. *deshayesii* DUNKER	Low. Musasino	Tokyo	Matusima Bay
Mangelia gracilenta (REEVE) var.	*unknown*	Tokyo	Tokyo Bay?
Mangelia makiyamai OTUKA	*unknown*	Noto	*unknown*
Etrema fortilirata (SMITH)	*unknown*	Tokyo	C. W. Jap.
Terebra (*Strioterebrum*) *bathyraphe* SMITH	*unknown*	Tokyo	Tokyo Bay
Ringicula (*Ringiculella*) *yokoyamai* TAKEYAMA	Naganuma	Simosa	*unknown*
Rotalia sp.			
Echinoderm spines			

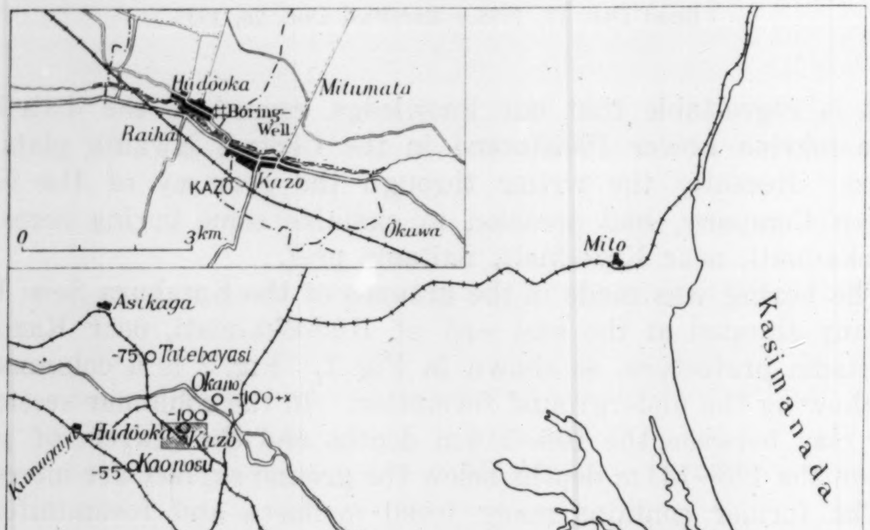

Fig. 1. Index map. Circles (○) show the localities of marine Lower Pleistocene. Numeral near the locality shows the height or depth of the marine Lower Pleistocene referred to the mean sea-level.

In the above list, 77 percent (17 out of 22 sp.) of mollusca are common to the marine Lower Pleistocene nr. Tokyo, in which a Lower Pleistocene mammal, *Elephas namadicus naumanni* MAKIYAMA,[1] is associated. Of these 17 sp., 4 sp. have been described by YOKOYAMA[2] as new from the Lower Pleistocene just mentioned.

"The gravels of pumice", which consists of andesite tuff is a characteristic bed. Similar beds are widely distributed below the marine Lower Pleistocene in Saitama and Tokyo prefectures; the borings at Urawa and Oomiya in Saitama prefecture, Akabane and Hongo in Tokyo prefecture having yielded pumice gravels below the marine Lower Pleistocene. From all this the writer concludes that the fauna of the shell bearing sandy clay between depths 106~116 m below the land surface at Hudooka-mati is probably contemporaneous with the marine Lower Pleistocene of Tokyo. Owing to this occurrence of marine fauna, the Lower Pleistocene shore line (dl II) in the writer's figure[3] on page 1591 in the Proc. 5th Pacific Sci. Congr., Canada, has to be extended to the northern corner of Saitama prefecture.

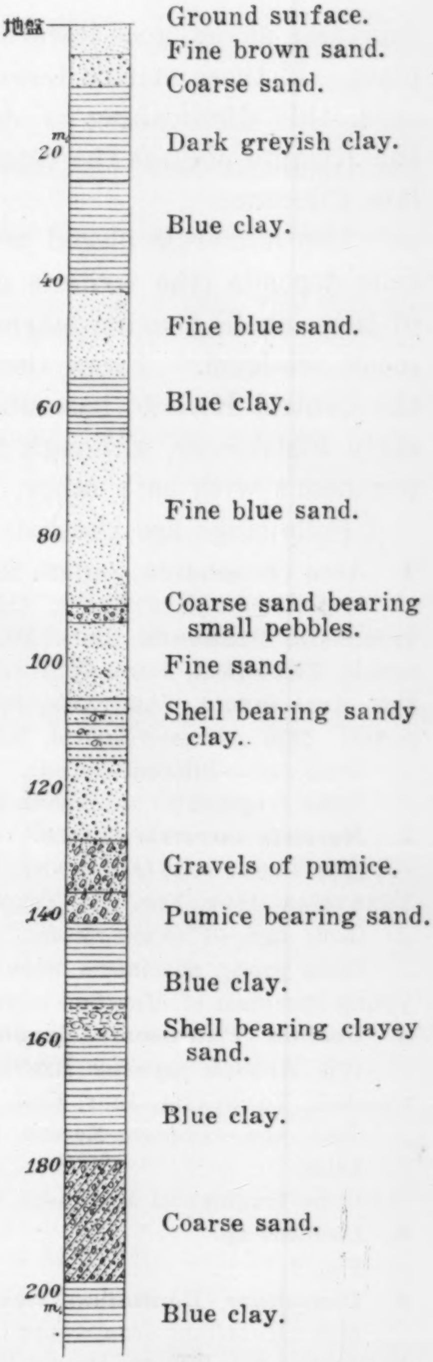

Fig. 2. Columnar section of bore well in the grounds of the Katakura Seisi Boseki Company, Hudooka mati, Kitasaitama-gori, Saitama-pref.

As the land surface of Hudooka-mati is about 10 m above sea level, the shell bearing sandy clay is situated at about 100 m below sea-level, while the depth of the Lower Pleistocene shell bearing bed at Tatebayasi, Koonosu, Oomiya, Akabane, Hongoo, Kanagawa and Tiba prefecture gradually

1) S. TOKUNAGA, *Jour. Coll. Sci. Imp. Univ. Tokyo*, **21** (1906), 72~75.
J. MAKIYAMA, *Mem. Coll. Sci. Kyoto Imp. Univ.*, [B], **1** (1924), 255~264.
2) M. YOKOYAMA, *Jour. Fac. Sci. Imp. Univ. Tokyo*, [2], **1** (1927), 391~457.
3) Y. OTUKA, *Proc. 5th Pacific Sci. Congr.*, (1933), 1591.

decreases as one goes toward the south and west margin of the Kwanto plain. If these marine Lower Pleistocene beds are all almost the same ones, this diminishing of depth may support R. Aoki's[4] opinion that the Kwanto plain is the result of basin forming forces operating since late Pliocene.

The numerals placed near the localities of marine Lower Pleistocene deposits (the writer's dl II) in fig. 1 show the heights or depths of these shells bearing marine Lower Pleistocene beds referred to recent mean sea-level. From these numerical values, it may be seen that the Central Kwanto has subsided relatively to the south and west since early Pleistocene, although these marine beds are not strictly contemporaneous with eath other.

Followings are the list and the description of the fossils.

1. *Arca (Scapharca) inflata* REEVE

1844 *Arca inflata* REEVE, Conch. Icon. *Arca*, Pl. 25, fig. 30; 1859-67 *Arca broughtoni* SCHRENCK, Reis. Amurl. Zool., Moll.p. 578, Pl. 24, fig. 1~3; 1906 *Arca tenuis*, TOKUNAGA, Jour. Coll. Sci. Imp. Univ. Tokyo, Jap. **21**, 2, p. 53, Pl. 4, fig. 1; 1927 *Arca inflata*, YOKOYAMA, Jour. Fac. Sci. Imp. Univ. Tokyo, (2), **1**, 10, p. 403, p. 446; 1930 *Anadara inflata*, KURODA, Venus, **2**, 1, Appendix p. 32.

Geol. age.—Pliocene-Recent. Geogr. distr.-Around Honsyu, Hokkaido, Kyusyu.

Some fragmental specimens were collected. Rg. No. 2542, Coll. E. R. I.*

2. *Meretrix meretrix* (LINNÉ)

1758 *Venus meretrix* LINNÉ, Syst. Nat. ed. **10**, p. 686; 1927 *Meretrix gordonis* YOKOYAMA, Jour. Fac. Sci. Tokyo Imp. Univ. (2), **1**, p. 429.

Geol. age.—Pliocene-Recent. Geogr. distr.—Around Honsyu, Kyusyu.

Some young specimens were collected. *Meretrix gordonis* YOKOYAMA may be young specimen of *Meretrix meretrix* (LINNÉ).

3. *Dosinia (Phacosoma) japonica* (REEVE)

1850 *Artemis japonica* REEVE, Conch. Icon., *Artemis*, Pl. 3, fig. 17; 1920 *Dosinia troscheli*, YOKOYAMA, Jour. Coll. Sci. Tokyo Imp. Univ., **39**, 6, p. 119, Pl. 8, fig. 5, 6.

Geol. age.—Pliocene-Recent. Geogr. distr.—Central and Western Japan, Hokkaido.

Some fragmental specimens were collected.

4. *Cadulus* sp.

Fig. 7.

5. *Dentalium (Dentalium) hexagonum* GOULD

1859 *Dentalium hexagonum* GOULD, Proc. Bost. Soc. Nat. Hist., **7**, p. 166.

Geol. age.—Pliocene-Recent. Geogr. distr.—Kyusyu, Honsyu, Sikoku.

8 fragmental specimens were collected.

6. *Menestho nishiana* (YOKOYAMA)

1927 *Odostomia (Menestho) nishiana* YOKOYAMA, Jour. Fac. Sci. Imp. Univ. Tokyo, (2), **1**, 10. p. 421~2, Pl. 47, fig. 14.

Geol. age.—Lower Pleistocene.

One fragmental specimen was collected.

7. *Odostomia sublimpida* YOKOYAMA

4) R. AOKI, *Jour. Geol. Soc. Tokyo.*, **37**, (1930), 255~258.

* Coll. E. R. I.=Collection of Earthquake Research Institute.

1920 *Odostomia (Odostomia) sublimpida* YOKOYAMA, Jour. Coll. Sci. Tokyo Imp. Univ., **39**, 6, p. 82, Pl. 5, fig. 13.

Geol. age.—Pliocene-Lower Pleistocene. Geogr. distr.—Central Japan.

8. *Turbonilla edoensis* YOKOYAMA

1927 *Turbonilla (Chemnitzia) edoensis* YOKOYAMA, Jour. Fac. Sci. Imp. Univ. Tokyo, (2), **1**, 10, p. 424, Pl. 47, fig. 24.

Geol. age.—Lower Pleistocene-Recent (Turumi?) Geogr. distr.—Kwanto. Rg. No. 2543. Coll. E. R. I.

Specimens from Oogisima, nr. Turumi have more distinct axial ribs than the fossil specimens. Hudooka specimens are quite identical with the type specimens from Kurumatyo near Sinagawa in Tokyo.

9. *Turbonilla keiskeana* YOKOYAMA

1927 *Turbonilla (Chemnitzia) keiskeana*, YOKOYAMA, Jour. Fac. Sci. Imp. Univ. Tokyo, (2), **1**, 10, p. 424, Pl. 47, fig. 19.

Geol. age.—Lower Pleistocene. Geogr. distr.—Tokyo.

Specimen from Hudooka is a fragmental shell. Rg. No. 2594, Coll. E. R. I.

10. *Turbonilla* sp.

This species closely allied to *Turbonilla (Mormula) semicolorata* YOKOYAMA[5] in its outline, but the former differs from the latter in having no spiral sculpture in interspaces between axial ribs. Rg. No. 2596, Coll. E. R. I.

11. *Pyramidella (Tiberia) ebarana* YOKOYAMA

Pyramidella (Tiberia) ebarana YOKOYAMA, Jour. Fac. Sci. Imp. Univ. Tokyo, (2), **1**, 10, p. 418, Pl. 47, fig. 6.

Geol. age.—Pleistocene. Geogr. distr.—Central Japan.

4 specimens were collected. Rg. No. 2544, Coll. E. R. I.

12. *Polynices sagamiensis* PILSBRY

1904 *Polinices sagamiensis* PILSBRY, Proc. Acad, Nat. Sci. Philadelphia, **56**, p. 23, Pl. 4, figs. 37, 37 a; 1935 *Polynices sagamiensis*, OTUKA, Bull. Earthq. Res. Inst., **13**, 4, p. 866, Pl. 53, fig. 36.

One fragmental specimen was collected.

13. *Natica janthostoma* DESHAYES

Natica janthostoma DESHAYES, Revue d. Zool. p. 361.

One specimen was collected.

14. *Nassarius (Hinia) muroii* OTUKA n. sp.

Fig. 8, 9.

Shell ovate-turreted, solid and thick. Sculpture of strong rounded longitudinal folds as wide as their intervals, 12∼16 in number on last whorl, last one much larger, forming a prominent, rounded swollen varix behind lip, usually preceeded by a small rib. Varix usually visible on last 2 whorls. Over folds and intervals coarsely run fine and large spiral cords, rounded or flattened, as wide as their intervals or narrower. On last whorl, there are 1∼3 fine in subsutural area, and 9∼10 large cords on surface except subsutural area. Whorls about 7·5∼7; 2·5 of which smooth embryonal. Aperture ovate; outer lip with 7∼10 equal teeth within; columella calloused, well defined, white, with one small tooth near posterior corner.

(Holotype)	Length 10·4 mm	diam. 6·7 mm,	largest diam. of aperture 4·6 mm.
(Paratype)	〃 8·7 mm	〃 4·6 mm,	〃 〃 〃 4·0. mm.

This form may be a variety of *Nassarius semiplicatus hiradoensis* PILSBRY (Proc. Acad. Nat. Sci. Philad. **56** (1904), pp. 20∼21, Pl. 4, fig. 35), but the former has fine

5) M. YOKOYAMA, *Jour. Fac. Sci. Imp. Univ. Tokyo*, [ii], **1** (1927), 424, Pl. 47, fig. 22.

subsutural spiral cords, almost equal teeth on the inner side of outer lip, and well defined callous with one tooth on the posterior corner of columella.

Nassarius fraterculus (DUNKER)[6] has a higher shell with finer sculptures.

Nassarius (*Hinia*) *dominulus* (TAPPARONE-CANEFRI)[7] is another allied species. But this sp. has a shell sculptured with 16 axial ribs. Inner side of outer lip of this shell is toothed irregularly.

Holotype and Paratype: No. 2593, in E. R. I.

15. *Clavatula consimilis* (SMITH)

1879 *Pleurotoma consimilis* SMITH, Proc. Zool. Soc. London, p. 188, Pl. 19, fig. 11.
1935 *Clavatula consimilis*, OTUKA, Bull. Earthq. Res. Inst. Imp. Univ. Tokyo, **13**, 4, p. 172, Pl. 54, figs. 103, a, b, c.

Geol. age.—Pliocene-Recent. Geogr. distr.—Isikawa pref. Tokyo, Kanagawa, Matusima bay, Hukui pref. Rg. No. 2590, Coll. E. R. I.

16. *Suavodrilla declivus* (MARTENS)

Pleurotoma declivus MARTENS, Conchol. Mittheil., p. 39, Pl. 9, fig. 2.

Geol. age.—Pliocene-Recent. Geogr. distr.—Northern Japan, Tokyo, Tiba, Ibaraki. Rg. No. 2591, Coll. E. R. I.

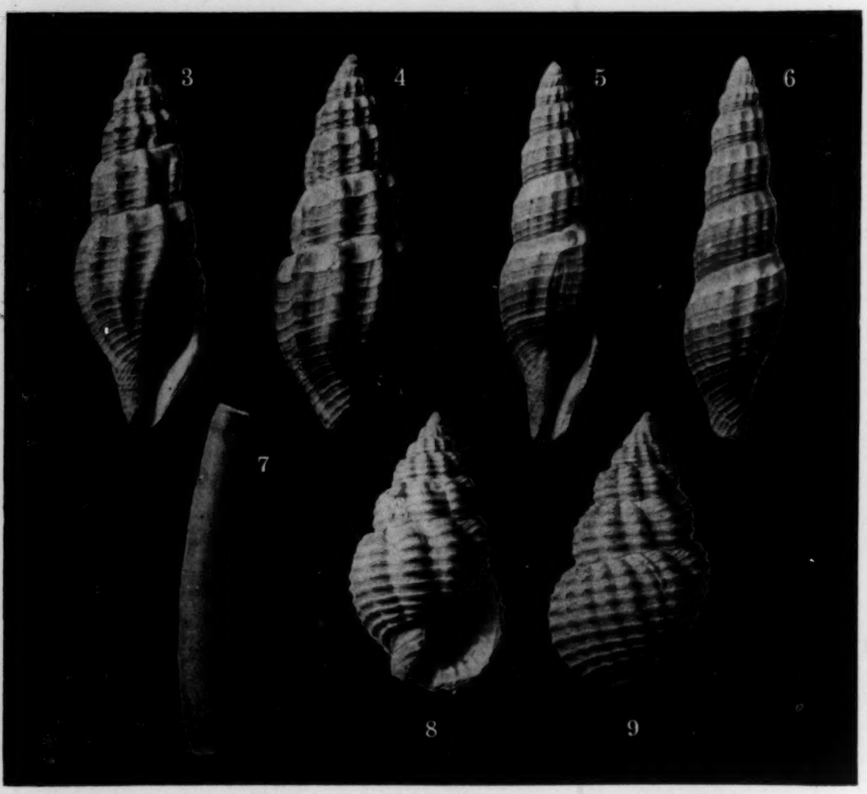

Fig. 3, 4. *Mangelia deshayesi* DUNKER. Fig. 5, 6. *Mangelia gracilenta* var. Fig. 7. *Cadulus* sp. Fig. 8, 9. *Nassarius muroii* n. sp.

17. *Mangelia deshayesii* DUNKER

Fig. 3, 4.

6) DUNKER, *in malakoz. Bl.* 1860, p. 380.

7) (TAPPARONE-CANEFRI, *Zool. del Viaggio intorno al globo della Regia fregata Magenta durante gli Anni* 1865~68, *Malacologia*, 1874, p. 19, Pl. 1, fig. 17.)

1860 *Mangilia (Pleurotoma) deshayesii* DUNKER, in malakoz. Bl., **6**, p. 228; 1920 *Mangilia deshayesii*, YOKOYAMA, Jour. Coll. Sci, Tokyo Imp. Univ., **39**, 6, p. 41, Pl. 1, fig. 24.

Shell very small, fusiform; spire terraced; whorls about 7~8, apical 3 of which nuclear. First and second nuclear whorls smooth, third ornamented with spiral sculpture which sometimes worned. Postnuclear whorl sculptured with slightly curved, obliquely longitudinal ribs and unequal spiral threads. Axial ribs prominent, angled near preceding suture. Body whorl sculptured with 8~9 axial ribs which are crossed by about more than 13 spaced spiral threads, with 5~8 smaller threads between them. On penultimate whorl 9~11 axial ribs, 4~5 large spiral threads, and 5~7 fine intercalaries exist. Broad sloped subsutural area sculptured with fine spiral threads (about 16), and bounded by blunt shoulder angle on which uppermost large spiral thread located. Aperture oblong; columellar margin concave slightly above the middle. Outer lip thick, with a moderately deep rounded sinus above; smooth within. Varix visible on last three whorls.

Length 8·7 mm	Diam. 3·0 mm	Largest diam. of aperture 4·1 mm.
〃 7·2 mm	〃 2·8 mm	〃 〃 〃 3·4 mm.

Hypotype: No. 2546, Coll. E. R. I.

This species corresponds fairly well with *Mangelia kamakurana* PILSBRY[8] in its sculpture. It differs from the latter species in having higher shell.

Cythara tabatensis (TOKUNAGA)[9] differs from *Mangelia deshayesii* DUNKER in its sculpture.

Mangelia makiyamai OTUKA[9] has a lower spire than DUNKER's species.

Mangelia semicarinata PILSBRY[10] has 16 axial ribs.

18. *Mangelia gracilenta* (REEVE) var.

Fig. 5, 6.

This specimen colsely identical with *Mangelia gracilenta* (REEVE),[11] but the former has longer shell. Rg. No. 2592, Coll. E. R. I.

19. *Mangelia makiyamai* OTUKA

1935 *Mangelia makiyamai* OTUKA, Bull. Earthq. Res. Inst. Imp. Univ. Tokyo, **13**, 4, p. 874, Pl. 54, fig. 94.

Geol. age.—Lower Pleistocene. Geogr. distr.—Noto, Saitama. Homoeotype: Rg. No. 2545, Coll. E. R. I.

20. *Etrema fortilirata* (SMITH)

1879 *Drillia fortilirata* SMITH, Proc. Zool. Soc., p. 195, Pl. 19, fig. 22; 1927 *Drillia fortilirata*, YOKOYAMA, Jour. Fac. Sci. Imp. Univ. Tokyo, (2), **1**, 10, p. 410, Pl. 46, fig. 20.

7 specimens were collected. Rg. No. 2587, Coll. E. R. I.

21. *Terebra (Strioterebrum) bathyraphe* SMITH

1875 *Terebra bathyraphe* SMITH, Ann. Mag. Nat. Hist., (4), **15**, p. 415; 1927 *Terebra edoensis* YOKOYAMA, Jour. Fac. Sci. Imp. Univ. Tokyo, (2), **1**, 10, p. 409, Pl. 46, fig. 8.

---

8) PILSBRY, *Proc. Acad. Nat. Sci. Philad.*, **56**, (1904), p. 10, Pl. 2, fig. 11.

9) TOKUNAGA, *Jour. Coll. Sci. Tokyo Imp. Univ.*, **21** (1906), p. 15, Pl. 1, fig. 27.

10) OTUKA, *Bull. Earthq. Res. Inst. Imp. Univ. Tokyo*, **13** (1935), p. 874, Pl. 54, fig. 94.

11) PILSBRY, *Proc. Acad. Nat. Sci. Philad.*, **56**, (1904), p. 9, Pl. 2, fig. 16.

12) *M. gracilenta*, YOKOYAMA, *Jour. Fac. Sci. Imp. Univ. Tokyo.*, [2], **1**, (1927), p. 411, Pl. 46, fig. 13.

2 specimens were collected. Rg. No. 2590, Coll. E. R. I.

22. *Ringicula (Ringiculella) yokoyamai* TAKEYAMA

1922 *Ringicula musashinoensis*, YOKOYAMA, Jour. Coll. Sci. Tokyo Imp. Univ., **44**. 1, p. 30, fig. 16, 17 (not of YOKOYAMA 1920); 1935 *Ringicula yokoyamai* TAKEYAMA, Venus, **5**, 2, 3, p. 74~78, Pl. 5, figs. 19~20, Pl. 6, figs. 21~25.

Geol. age.—Lower Pliocene-Pleistocene. Geogr. distr.—Central Japan.

17 specimens were collected. Rg. No. 2589, Coll. E. R. I.

23. *Rotalia* sp.

---

7. 中部關東平野の海成洪積層(摘要)

(關東造盆地運動の一資料)

地震研究所 大塚彌之助

日本鑿泉株式會社の好意により埼玉縣北埼玉郡不動岡町の地下地質系統の性質を知り得た．地表下 106~116 米の間にある含貝化石砂質粘土は多くの貝化石を含み，第1表の如き種を含み，東京層の動物群に比べられる．同貝層下の輕石層（地表下 128~141 米）は東京府，埼玉縣の地下に廣く見られるものと類似し，上記の貝層が東京層たるを知るよき手懸りとなつた．東京層の地上・地下の海拔高度を記すと第1圖の如くになり，嘗て青木廉二郎學士が述べた關東造盆地運動を證明する一資料となろう．最後に採集貝化石の表と二，三の種の簡單な記載がしてある．

---

8. *Contributions à l'Etude Géologique du Plateau de Musasino, près de Tokyo*[*]

par

Gakurô IMAMURA et Nikiti YAZIMA.

L'Institut de Géographie, Université de Littérature et Science, Tokyo.

(Lu le 17 Septembre 1935, reçu le 18 Novembre 1935)

Méthode d'investigation

Les constructions géologiques de Musasino ne peuvent pas encore être bien étudiées, parce que l'érosion de la surface du plateau n'est pas avancée et qu'on doit se contenter de la connaissance de la périphérie. Sans doute, les sondages nous indiquent la section géologique jusque dans les profondeurs, mais leur nombre est très réduit pour la grande plaine de Musasino et ils ne suffisent pas pour nous renseigner.

Heureusement, des puits existent en grand nombre sur la surface de Musasino et ils peuvent nous révéler des affleurements un peu différents des affleurements ordinaires: nous croyons qu'ils nous fournissent ainsi une méthode d'enquête. Après avoir creusé le limon et la couche caillouteuse caractéristiques des puits, on atteint la couche argileuse et on rencontre l'eau souterraine. Généralement, le fond du puits correspond à la surface de la couche argileuse. Celle-ci a à peine un mêtre d'épaisseur; on le constate si l'on creuse davantage. Donc, quand la hauteur du fond du puits indique une distribution régulière, nous pouvons en déduire la direction et l'inclinaison de la couche caillouteuse.

Nous avons mesuré la distance verticale de la surface du sol jusqu'au fond du puits et la hauteur au dessus du niveau de la mer de l'endroit où l'on se trouve. La première mesure peut s'obtenir exactement avec une corde de coton et un poids, mais la deuxième est incertaine même si on emploie la ligne de contour de la carte topographique au 1:50,000. On doit absolument employer la carte au 1:25,000. D'autre part, il faut faire attention à la condition météorologique, mais nous avons obtenu les meilleurs résultats, en utilisant la hauteur

---

* Communiqué par M. Ishimoto.

exacte des points de triangle et des cotes indépendantes et en trouvant la différence de hauteur, au moyen d'un anéroïde sensitif[1] (Fabrication de Short & Mason). Cependant, si on emploie la carte topographique, on aura les erreurs de dessous:

1) de dessiner la ligne de contour par l'interpolation,

2) d'être à l'endroit où il y a des puits plus haut ou plus bas,

3) de faire une erreur quant à la situation que le niveau indique sur la carte,

4) de ne pas remarquer la différence existant dans les détails, entre la configuration du sol actuel et la carte topographique.

A l'aide des procédés indiqués, nous trouvons h, c'est-à-dire la

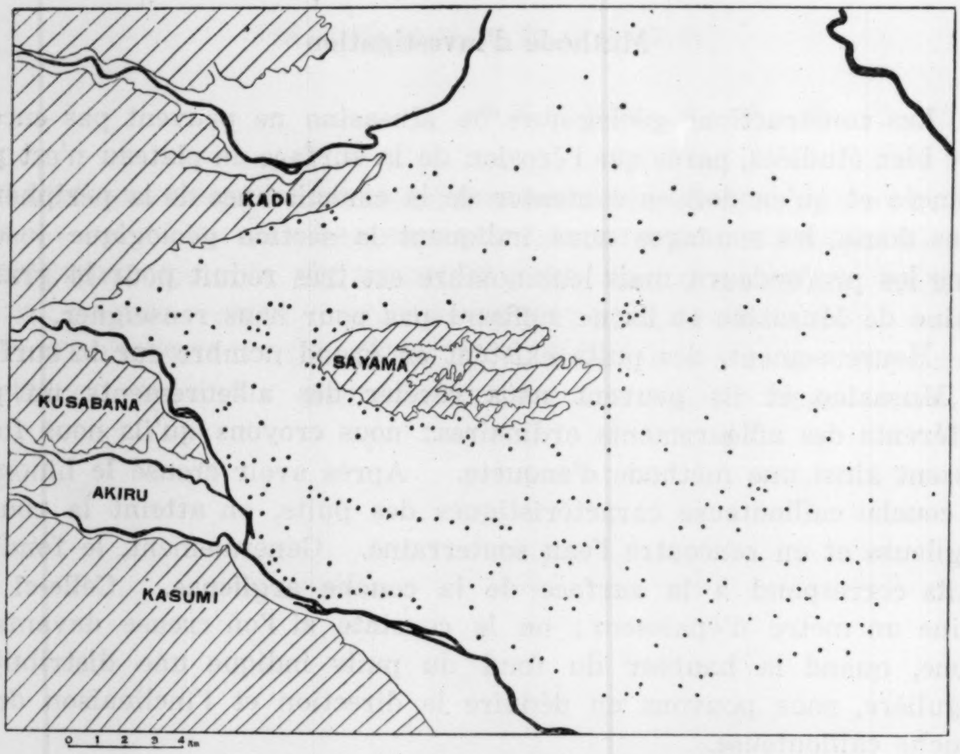

Fig. 1. Distribution des puits examinés.

hauteur du fond de puits au dessus du niveau de la mer. La distribution des puits examinés, est représentée dans la première figure.

Résultats des investigations

La différence de la hauteur au dessus du niveau de la mer de chaque puits est assez grande, car la surface du plateau dessine une

1) Comme il faut noter cette différence le plus tôt possible, nous avons utilisé une automobile pour obtenir les meilleurs résultats.

pente relativement rapide, en partant des alentours de la colline Sayama vers l'Est où il y a une rangée de lacs — Inokasira, Zempukuzi, Sanbôzi et Myôsyôzi. Par conséquent, les erreurs possibles dans la mesure susdite sont sans importance. Cependant, l'inclinaison de la surface du plateau devient moins forte, en poursuivant vers l'Est, que dans la rangée des lacs, donc l'importance de l'erreur grandit en comparaison de la différence de hauteur des puits, même au moyen de l'anéroïde; on est incapable de connaître précisément la distribution de h. Nous n'obtiendrons pas de bons résultats, si nous n'employons pas quelque autre moyen de mesurer la hauteur jusqu'à un ordre de plus de précision. La distribution des h est donnée dans la figure 2.

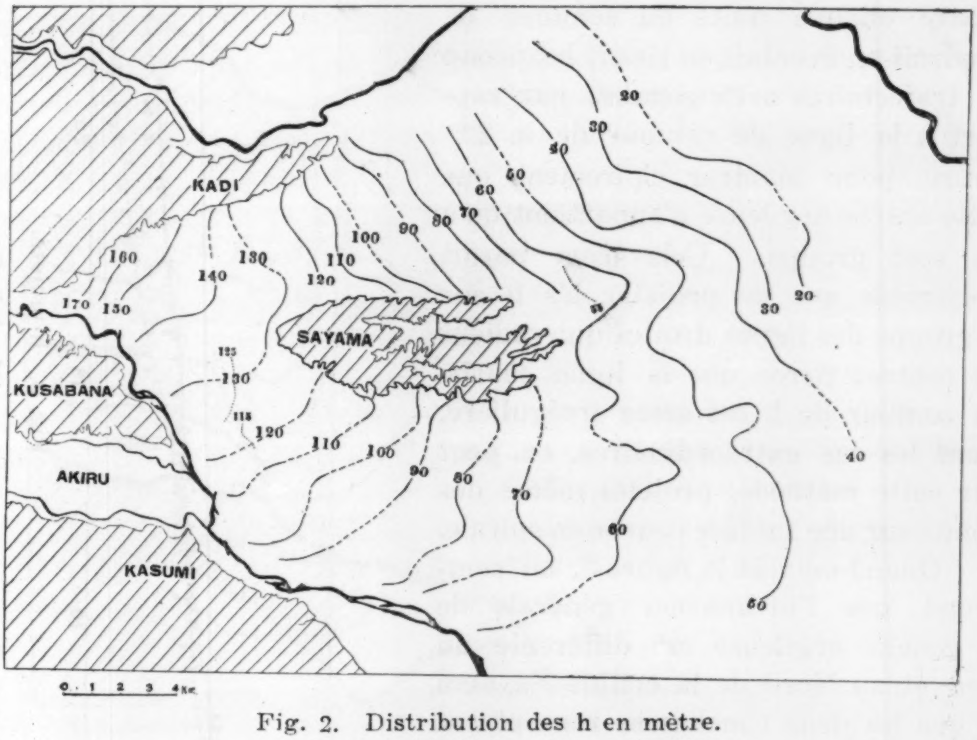

Fig. 2. Distribution des h en mètre.
h de couche inférieure, en pointillé.

Grâce à un anéroïde sensitif, nous avons pu indiquer la couche argileuse très lente par de simples lignes courbes horizontales, tandis que nous aurions fini par avoir une ligne de contour de h plus compliquée, si nous avions employé la carte topographique au 1:50,000.

La couche argileuse imperméable de Musasino est ainsi continue ou au moins, il y existe un groupe de couches argileuses. En outre, il est possible de prouver suffisamment que cette couche argileuse porte la même couche d'eau souterraine par la distribution de pH, la déviation de température de l'eau, et la distribution de l, c'est-à-dire

l'épaisseur de l'eau. Cependant il y a deux endroits où l'on a creusé profondément jusqu'à atteindre une couche différente: l'un est dans la ville de Tokorozawa et l'autre est au Sud de Hakone-ga-saki. Ces deux endroits ont une couche imperméable plus profonde et sont différents quant à la direction et à l'inclinaison de la couche supérieure et quant au caractère de l'eau.

Dans la figure 3, nous indiquons le rapport entre h et la distance qui sépare chaque puits du sommet de l'endroit en éventail, en tirant beaucoup de trajectoires orthogonales, par rapport à la ligne de contour de la 2ème figure, pour montrer clairement que cette couche argileuse n'appartient qu'à un seul groupe. Cela nous paraît préférable que de projeter les h sur le groupe des lignes droites qui radient du centre; parce que la ligne courbe du contour de h est assez irrégulière. Dans les cas extraordinaires, on peut par cette méthode, projeter même des points sur une surface courbe en spirale.

Quand on voit la figure 3, on comprend que l'inclinaison générale de la couche argileuse est différente au Sud et au Nord de la colline Sayama et que les deux couches se rencontrent en formant un petit angle. On peut reconnaître que toutes les deux sont des couches continues ou, au moins, en groupe. On ne peut pas parler avec précision, de couche argileuse profonde, à cause de sa distribution étroite; mais les deux endroits ci-dessus montreront peut-être la communication des couches.

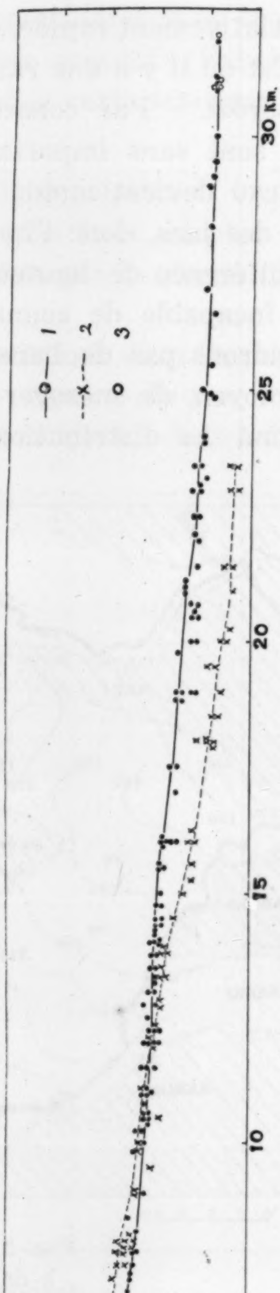

Fig. 3. h projeté.
1 — au Sud de Sayama 2 — au Nord de Sayama 3 — rangée des lacs

Surface de dépôts de Musasino

D'après les études faites jusqu'à présent[2], on a trouvé que la surface de Musasino est une *terrasse* et que la distribution des *terrasses* corrélatives est extrêmement grande[3]. Cette surface terrestre est-elle formée par un dépôt ou est-elle la conséquence d'une érosion, cela n'est pas mentionné clairement. Il nous semble qu'elle est regardée comme une surface d'érosion. En tout cas, nous pouvons déclarer que le mot *terrasse* ne convient pas pour représenter cette topographie.

Nous obtenons la figure 4, si nous faisons une carte du niveau des crêtes. Il est dangereux de tirer des conclusions trop détaillées d'une

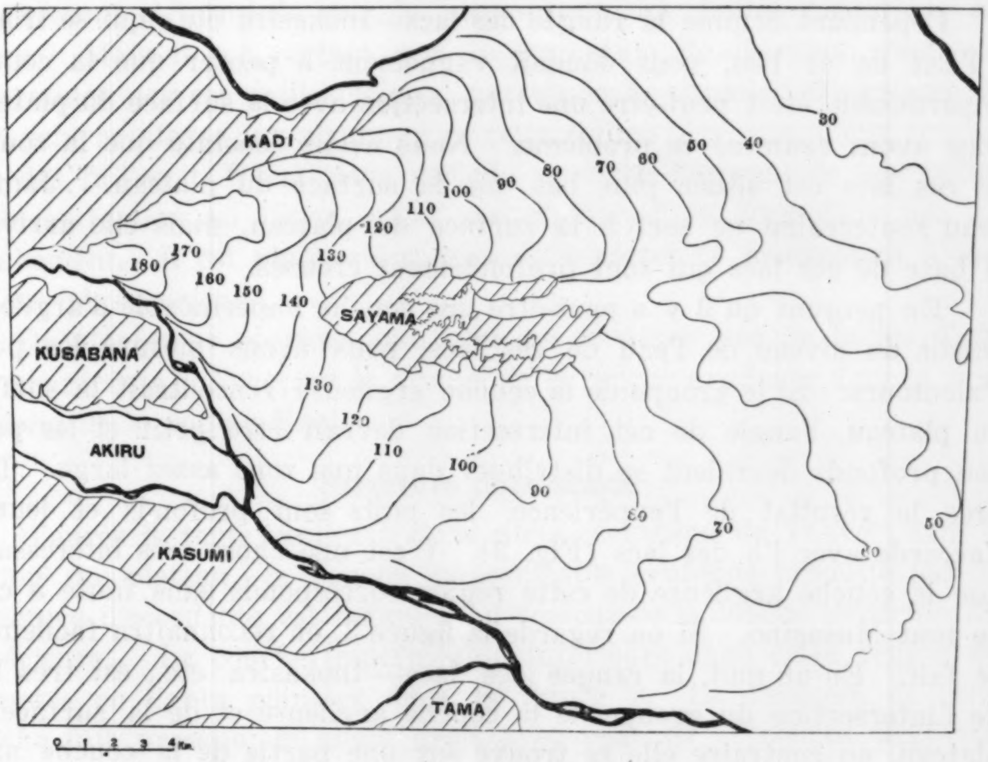

Fig. 4. Carte du niveau des crêtes en mètre.

carte du niveau des crêtes, car celui-ci change facilement la forme suivant les procédés employés. Cependant nous voyons immédiatement, en comparant la figure 2 et la figure 4: la ligne de contour des deux figures tracée dans la région occidentale, la ligne droite allant de l'Est à l'Ouest comme un axe symétrique, tandis qu'elle devient asymétrique dans la partie orientale. Ainsi, nous pouvons dire que les deux sont

2) H. YABE et R. AOKI, *Geogr. Rev. Japan*, **3** (1927), 79~87, (en japonais).
R. AOKI et R. TAYAMA, *Sci. Rep. Saitô Hôonkai*, [viii] (1930).

3) H. YABE, *Proc. Imp. Acad.*, **5** (1929), 430~433.

bien parallèles surtout pour les surfaces courbes qui sont si lentes; nous concluons donc que la surface de Musasino n'est pas une surface d'érosion mais, une surface de dépôt. Nombreux sont les endroits où ce caractère se présente en détail. Il ne nous semble pas exact de dire que les deux sont nécessairement parallèles, puisque la profondeur des puits se maintient dans une certaine limite. Dans les livres d'hydrogéologie[4], il y a beaucoup d'exemples montrant que parfois les couches et la surface du sol sont loin d'être parallèles et présentent même de grands écarts dans des endroits plus étroits que celui-ci. Il est plutôt difficile de trouver un exemple montrant un parallélisme aussi complet que dans le cas de Musasino. Donc, la surface de Musasino est un bon exemple de surface de dépôts.

Cependant comme la rangée des lacs—Inokasira etc., qui se trouve à l'Est de ce lieu, nous donnait vaguement à penser que la couche imperméable était peut-être une intersection avec la surface du plateau, nous avons examiné ce problème. Nous avons constaté que la source de ces lacs est située plus bas que la surface du plateau. Jamais l'eau souterraine ne sort à la surface du plateau, mais elle arrive à la base de ces lacs qui sont profondément creusés.

En pensant qu'il y a peut-être une couche imperméable d'argile au dessus du niveau de l'eau de ces lacs, nous avons mesuré les puits d'alentours. Si le groupe de la couche argileuse rencontrait la surface du plateau, l'angle de cet intersection devrait être petit et les puits peu profonds devraient se distribuer dans une zone assez large. D'après le résultat de l'expérience, les puits sont profonds et leur h s'accorde avec l'h des lacs (Fig. 3). C'est une chose très intéressante que la couche argileuse de cette région corresponde sans faute à celle de tout Musasino. Si on regarde la figure 3, on reconnaîtra facilement ce fait. En un mot, la rangée des lacs — Inokasira etc., est très loin de l'intersection du groupe de la couche argileuse et de la surface du plateau, au contraire elle se trouve sur une partie de la couche argileuse qui s'étend dans tout Musasino. Dans cette couche, les lacs ont été creusés en rang par une cause quelconque. Le résultat de l'examen de cette rangée prouve que la surface des dépôts s'étend jusqu'à cet endroit.

Cette surface de dépôts de Musasino est une zone en éventail, d'après la substance des constructions et la topographie, mais elle n'a pas une forme conforme à l'opinion de Murata[5]. Que cette surface ait été déformée par un bombement ou par une autre raison, on ne

---

4) Par exemple: E. IMBEAUX, Essai d'Hydrogéologie. (Paris, 1930).
5) T. MURATA, *Geogr. Rev. Japan*, 7 (1931), 560~586, (en japonais).
T. MURATA, *Geogr. Rev. Japan*, 7 (1931), 649~663, (en japonais).

pourra pas le décider sans prouver stratigraphiquement le mouvement de l'écorce terrestre. Tant qu'il n'y a pas de preuve solide, cette question appartient au domaine de l'hypothèse. Otuka[6] qui a expliqué la formation du groupe de la surface d'érosion dans tout le Japon comme "Piedmonttreppen", a déclaré: "On ne peut pas donner une explication meilleure que la mienne." Cependant sa théorie ne peut pas s'appliquer à Musasino. Il faut bien noter que la surface de Musasino devient comme critérium, si nous établissons la corrélation des surfaces M dans les différentes régions.

Failles

Huzimoto[7] a écrit: "la topographie de la colline de Sayama est entièrement déterminée par le mouvement des failles postérieur au limon." Mais il est certain que la formation de Sayama n'est pas déterminée par ces failles jeunes, parce que la situation du groupe de la couche argileuse aux alentours de cette colline n'indique aucun trouble par des failles. Il est donc difficile de fixer l'époque de ces failles postérieurement au limon, ainsi que d'affirmer sa formation par un bombement. Il est plutôt nécessaire de reporter ce mouvement à une époque plus ancienne.

De plus, nous ajoutons que nous ne trouvons pas de failles d'une époque récente qui coupent le groupe de la couche argileuse dans la zone au long de la colline Kazi.

Structure discordante

D'après le texte explicatif de la carte géologique de Tokyo[8], dans la région du plateau, la couche imperméable profonde produite par la structure discordante est indiquée au dessous de la couche imperméable supérieure. La couche imperméable inférieure dans cette région est marquée en lignes pointées dans la figure 2. La direction de cette couche fait presque un angle droit avec celle de la couche argileuse supérieure comme l'indique le texte explicatif. La direction et l'inclinaison de la couche basse sont déterminées, en mesurant ses hauteurs dans une large étendue; ce procédé est plus sûr que de mesurer les hauteurs par clinomètre dans cette couche même.

Enfin nous obtenons la figure 5, si nous faisons une carte de distribution de la profondeur totale des puits. A mesure que la couche argileuse approche de la colline des alentours, elle devient tout à coup

6) Y. OTUKA, *Jour. Géol. Soc. Japan*, **37** (1930), 175~178, (en japonais).

7) H. HUZIMOTO, *Pub. Geogr. Soc. Ôtuka*, **1** (1933), 222~235, (en japonais),

8) N. KIYONO, Expl. Text Geol. Map Japan, 1:75,000. TOKYO, zone 24, col. V, sheet 112, (1935).

moins profonde et révèle une structure discordante. Par cette figure,

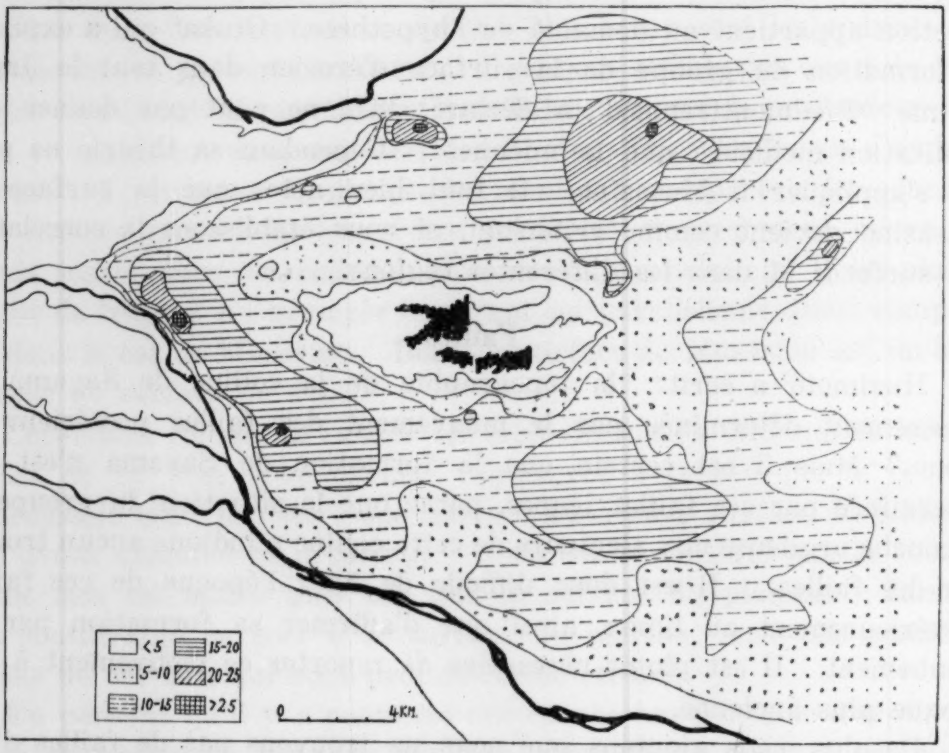

Fig. 5. Distribution de la profondeur totale des puits en mètre.

nous pouvons savoir que les alentours de la colline ne présentent aucune faille. Ces faits nous permettent de supposer que la surface de toutes collines sont des surfaces d'érosion et qu'elle rencontre par discordante les dépôts d'alentours plus jeunes qu'elle. La surface discordante, nous semblet-il, s'étend assez loin sous le plateau.

Conclusions

1) Un groupe de la couche argileuse s'étend abondamment à Musasino et presque parallèlement à la surface du plateau.

2) Par conséquent, Musasino est une surface de dépôts et a été couverte de limon postérieurement.

3) Dans les alentours de Sayama et de la colline Kazi, il n'existe aucune faille plus jeune que le limon.

4) C'est la structure discordante qu'on prenait jusqu'à présent pour la faille et la surface discordante s'étend certainement sous le plateau.

8. 武藏野臺地の地質構造に就いて

東京文理科大學 地理學教室 今村學郎 矢島仁吉

井戸といふ一風變つた露頭を多數調査することによつて

1) 西武藏野臺地面は堆積面であり

2) 四圍の丘陵との境はローム後といふやうな新期斷層ではなく

3) 在來の斷層は不整合であり，この不整合面は臺地下に延長されて居る

等の事を證明し得た．

9. *The Geologic Section along the Tanna Tunnel.**

By Hisashi KUNO,

Geological Institute, Tokyo Imperial University.

(Read Feb. 19, 1935.—Received Dec. 18, 1935.)

Introduction.

This paper embodies that part of the geological work of Idu district now in progress at the auspice of the Earthquake Research Institute, which is concerned particularly to the Tanna tunnel.

Along the east coast of the northern part of Idu peninsula, there extends a mountainous land, built up of thick piles of Tertiary and Quaternary volcanic rocks, forming the main divide of the district. The Tanna fault line, famous among seismologists for its behaviour at the time of the great Idu earthquake of November 26, 1930, runs meridionally on the western slope of the mountainous land. The district is also of geological interest, and many problems, as for example that of the origin of Tanna basin, a circular depression about 1 km across, situated on the Tanna fault, were much debated by geologists.

In 1934, the excavation of a railway tunnel traversing the abovementioned mountainous land in west-north-west direction, was completed; and the underground geological structure of the Tanna district, especially that beneath the Tanna basin, was brought into sight. The tunnel connects two towns Atami and Misima, and has total length of 25,603 feet or 7,804 meters.

The present paper contains the description of the geologic section along the eastern half of the Tanna tunnel, based on the observation along the tunnel wall, and the examination of rock specimens there collected, as well as on the general geological survey in the district.

The late Dr. Takeshi HIRABAYASHI described in 1925 the geology of those parts of the tunnel which were accessible at that time when the tunnelling from the both entrances was not much advanced.[1] When I examined the tunnel, the lining of the wall of the tunnel had been completed for most of these parts, so that my observation upon

---

* Communicated by S. TSUBOI.

1) T. HIRABAYASHI, On the geology of the Tanna basin. (Published from the Railway Department in 1925).

the actual exposures on the wall was confined only to the central part of its whole length, that is, between the points about 10,000 feet and 15,300 feet from the eastern entrance. Fortunately, however, complete series of rock specimens collected from the floor of the tunnel for the distance of 10,335 feet from the eastern entrance, were available to me. This ennabled me to determine exactly the distribution of different rock types, although the relations between them could be only inferred on the basis of my knowledge of the geology of the district. From these data, the geologic section given in Fig. 1 was constructed, which differs from HIRABAYASHI's in some essential points.

In the following descriptions, the numbers of feet indicating the position of each point in the tunnel refer to its distance from the eastern entrance.

Acknowledgement.

I wish to express my thanks to the Director and other members of the staff of the Earthquake Research Institute for many respects during the present work, and especially to Professor Dr. Seitarô TSUBOI for his kindness in reviewing this paper in manuscript.

Thanks are also due to Messrs. Hirosi ARIMA and Kyûgo ISIKAWA, the engineers in the Government Railway Department, as well as to Mr. Kôiti HIROTA, the geologist in the same Department, who kindly gave facilities for my geological survey in the tunnel.

Description of the Geologic Section along the Tanna Tunnel. (See Fig. 1)

***From 0 to 2,600 feet*:**

Compact andesitic lavas of the Ainohara beds (lower Pliocene?).

The Ainohara beds, composed of an alternation of dark green compact lavas of two-pyroxene-andesites and thin beds of tuffs or loose slaggy parts of the lavas, are spread to the north and west of Atami-mati.[2)]

Along the tunnel wall, are exposed the lavas of this formation. They are massive, dark green, and very compact, between 0 and 1,900 feet, and massive greyish, between 2,112 and 2,600 feet. The latter is separated from the former by an intercalating thin bed of greyish white, pumiceous tuff (between 1,900 and 2,112 feet), indicating the two probably to represent separate flows.

These rocks are intensely altered along cracks or joints to a greyish blue or whitish clayey masses by the action of solfataric gases

2) Y. ÔTUKA and H. KUNO, *Bull. Earthq. Res. Inst.*, **10** (1932), 473.

or of hot-spring solutions. These clayey masses are frequently met with in other portions of the tunnel wall as well as in surface outcrops in the vicinity of Atami-mati. They will be referred to in the present paper as "solfataric clay".

Along the valley of Ainohara (see Fig. 1) runs a fault in the NW-SE direction, the southwestern side of which is uplifted relatively to the northeastern. This fault crosses the tunnel at the 1,050 ft point, where much solfataric clay is developed in the wall rock. The direction of inclination of the fault plane is unknown.

On the ground surface, the Ainohara beds are represented, in most places, by lavas, resting unconformably upon the Nonaka beds to be referred to later, but occasionally, by thin dikes cutting the latter. In the tunnel section Fig. 1, they are provisionally shown as lavas resting upon the Nonaka beds. According to HIRABAYASHI, the boundary plane between the two formations now in question as seen on the tunnel wall has a steep inclination toward the south.

Under the microscope, the lavas of the Ainohara beds occurring in the tunnel belong to a single type of two-pyroxene-andesite. It contains phenocrysts of plagioclase, augite, hypersthene, and magnetite, in a fine-grained compact groundmass. The rocks are in most instances altered to a considerable degree, with secondary chlorite filling the interstices between the primary crystals or replacing hypersthene phenocrysts. To this process the rocks owe their dark green colour and compactness.

The rocks occurring between 2,112 and 2,600 feet are, however, rather fresh in appearance, with distinctly visible phenocrysts of pyroxene in greyish matrices. Under the microscope, they are poor in secondary chlorite.

As shown in Fig. 1, the Ainohara beds are covered by the Tensyô-zan beds (a complex of basaltic lavas and agglomerates) which occur on the slope to the west of Atami-mati, but not inside the tunnel.

***From 2,600 to 3,950 feet*:**

Dacitic tuffs and mudstones of the Nonaka beds (upper Miocene or lower Pliocene).

The Nonaka beds consist of an alternation of beds of tuffs of two-pyroxene-dacite and those of mudstones, and outcrop along the margin of Atami-mati.[3)]

Along the tunnel wall, they consist of an alternation of beds of

3) Y. ÔTUKA and H. KUNO, *op. cit.*, 473.

pale greyish mudstones, whitish or pale green pumiceous tuffs, and whitish tuff-breccias. According to HIRABAYASHI, they occasionally contain wood fragments, and show bedding planes, str. N 50° E, dip SE 6∼12°.

From the general resemblance of their constituent volcanic materials, and from their stratigraphic relations, the Nonaka beds are correlated to the Hayakawa beds, which the latter form the base of the Hakone volcano and contain molluscan fossils of upper Miocene or lower Pliocene age.[4]

Under the microscope, the tuffs of the Nonaka beds occurring in the tunnel consist mainly of fragments of pumice containing phenocrysts of plagioclase, hypersthene, augite, and quartz, in a groundmass of colourless vesicular glass.

***From 3,950 to 4,250 feet*:**

Lavas of the Basalts of the Hudô tunnel (Miocene).

They are, on the tunnel wall, massive, dark grey or black, and compact. Their petrographic characters are essentially the same as those of the type basalts occurring in the Hudô and Minakuti tunnels (Itô Railway Line), south of Atami-mati. In the last-mentioned tunnel, the basalts are covered unconformably by the Nonaka beds. In constructing the section of Fig. 1, the just-mentioned relation is assumed, because the actual relation at this particular point is unknown.

***From 4,250 to 5,700 feet*:**

Altered andesitic lavas, tuff-breccias, and agglomerates of the Hirogawara beds[5] *(lower Miocene).*

In the eastern part, the lavas predominate, while in the western, the tuff-breccias and agglomerates. These rocks are in much altered condition, being penetrated by veinlets of calcite or zeolites. In this and other respects, these rocks resemble to some rocks of the Hirogawara beds, especially to those occurring at Sogayama, south of Atami-mati.

The Hirogawara beds are the oldest known formation in the north Idu district, and are correlated to the Yugasima series (lower Miocene) of the south Idu district.[6]

The lavas occurring in the tunnel show quite similar appearance to each other in hand specimen, carrying sporadic phenocrysts of

4) Y. ÔTUKA, *Jour. Geol. Soc. Tokyo*, **41** (1934), 564.
5) Corresponding to the Sogayama beds in the earlier paper: Y. ÔTUKA and H. KUNO, *op. cit.*, 472.
6) R. TAYAMA and H. NIINO, *Report of Saitô Hôonkai*, **13** (1931).

cloudy plagioclase and black augite in a black compact matrix. Augite usually shows a good crystal outline. Under the microscope, these rocks belong to a single type of olivine-pyroxene-andesite with a glassy groundmass. Augite is the only mineral that is free from alteration.

In this part of the tunnel now under consideration, more fresh basaltic rocks are also met with at three separate places. They have the same characters as those of the Basalts of the Hudô tunnel characterized in the above. In Fig. 1, these basalts are shown provisionally as resting upon the undulating surface of the Hirogawara beds. But it is as well possible that, at these particular points, they are separated from the Hirogawara beds by sets of closely-spaced faults.

***From 5,700 to 6,500 feet*:**

Lavas of the Basalts of the Hudô tunnel (Miocene).

Massive, dark grey, compact basalts quite similar in character to the Basalts of the Hudô tunnel appear again in this part of the tunnel.

The Basalts of the Hudô tunnel occurring between 3,950 and 6,500 feet are somewhat variable in petrographic characters. In hand specimen, they are compact and dark grey or black in colour, often with indistinctly visible phenocrysts of plagioclase and pyroxene. Under the microscope, they are mostly hypersthene-basalts carrying phenocrysts of calcic plagioclase and hypersthene, rarely with those of augite. But some of the rocks are olivine-basalts carrying phenocrysts of calcic plagioclase and olivine. The groundmasses are typically basaltic in texture, ranging in granularity from fine-grained to coarse-grained types. They consist of plagioclase, monoclinic pyroxene, magnetite, cristobalite, and pale brown glass. The rocks are often more or less altered, with carbonate mineral completely replacing olivine, and chlorite filling the interstices between the primary crystals.

***From 6,500 to 8,000 feet*:**

Basaltic lavas and scoriae of the Hata beds (upper Pliocene?).

In this part of the tunnel, a few compact lavas occur among thick piles of purplish red scoriae or scoriaceous lavas. The rocks are quite free from any kind of alteration. In this and other petrographic features, the present lavas resemble to the rocks of the Hata beds to be described later.

Inferred from the quite unaltered condition of the rocks, the Hata beds may be probably younger than the Basalts of the Hudô tunnel occurring immediately adjacent to the east, and than the Acid Andesites occurring immediately adjacent to the west. However, it is not im-

possible that these formations are bounded by faults on the tunnel wall. But this is rather improbable, because no fault has been observed by HIRABAYASHI at the boundary points.

From 8,000 to 9,050 feet:

Lavas of the Acid Andesites (Miocene or lower Pliocene?).

They are massive, more or less compact, and accompany subordinate scoriaceous parts. They are intensely altered to the solfataric clay already mentioned, especially between 8,200 and 9,000 feet.

The present formation is not correlated to any of the formations that appear on the ground surface. But from the highly altered condition of the rocks, it is inferred to be of rather old age (Miocene or lower Pliocene), at least older than the Hata beds, though younger than the Hirogawara beds. The above-mentioned alteration of the rocks of the present formation to the solfataric clay may have probably taken place prior to the formation of the Hata beds, since the rocks of the latter beds are entirely unaffected by this action.

The rocks of the Acid Andesites are clearly separated by a fault at the 9,050 ft point from those of the Hata beds occurring immediately to the west. This fault corresponds to the fault indicated by the unusual topography on the main divide at the point just above the tunnel, where the road from Atami-mati to the Tanna basin crosses the divide. This fault strikes N 45° W, and dips about 70° or more toward the southwest. The direction of the displacement along this fault is unknown. At the time of the great north Idu earthquake of November 26th, 1930, the concrete wall of the tunnel was cracked in N 45° W direction at the 9,050 ft point, the point where the fault in question crosses the tunnel.

Another fault was observed by HIRABAYASHI at the 8,218 ft point.

The rocks of the Acid Andesites are, in hand specimen, usually light grey in colour, showing sporadic phenocrysts of plagioclase. Under the microscope, they belong to a single type of two-pyroxene-andesite containing phenocrysts of plagioclase, hypersthene, augite, and magnetite, in a fine-grained groundmass consisting of plagioclase, monoclinic pyroxene, magnetite, and cristobalite, either with or without glass base.

From 9,050 to 12,900 feet:

Basaltic lavas and scoriae of the Hata beds (upper Pliocene?).

The name Hata beds is given to a thick complex of basaltic lavas, scoriae, and tuffs, which outcrops on the lower part of the steep slope

rising from the eastern margin of the Tanna basin. At Simotanna, west of the Tanna basin, one of the lavas of this formation is covered unconformably by pumiceous mudstones of the Simotanna beds which are considered by Y. ÔTUKA as of lower Pleistocene age.[7] From this stratigraphic relation, as well as from the quite unaltered condition of the rocks, the age of the Hata beds may be inferred as upper Pliocene.

On the tunnel wall, the present formation consists of a complicated alternation of compact lavas (usually less than several meters in thickness) and fragmental materials such as scoriae, tuffs, tuff-breccias, and agglomerates, the latter predominating the former greatly in amount. Dikes are rather rare. The abundance of purplish red scoriae and beautiful yellowish tuff-breccias is a characteristic feature of this formation. Spindle-shaped bombs attaining to 2 feet in length are occasionally found in the scoria beds. Such bombs are also found occasionally from the surface outcrops of the Hata beds along the eastern margin of the Tanna basin. This occurrence of bombs was once taken erroneously by some previous authors as an evidence of the crater origin of the Tanna basin. The rocks of the Hata beds occurring in the tunnel are almost free from any kind of alteration.

Besides the above-mentioned fault at the 9,050 ft point, two remarkable faults are also seen, namely, at 11,200 and 11,500 ft points.

The fault at the 11,200 ft. point corresponds probably to the meridional fault which is indicated by a slicken-side at the foot of the steep scarp along the eastern margin of the Tanna basin.

The fault at the 11,500 ft point appears on the tunnel wall with a slicken-side. It strikes north-north-west and dips steeply toward the west. On the ground surface, this fault plane is concealed beneath a thick talus that fringes the foot of the above-mentioned steep scarp. It has been reported[8] however that, at the time of the great north Idu earthquake, a meridional earthquake fissure appeared upon this talus slope. The position of this fissure corresponds exactly to the upward prolongation of the fault plane observed in the tunnel.

Besides the above-mentioned faults, there may be found several less significant ones between 9,050 and 11,500 feet. But it is rather striking that, except a few quite insignificant ones, no fault has been detected between 11,500 feet and 13,850 feet, the latter being the point where the famous Tanna fault crosses the tunnel.

Between 9,050 and 11,500 feet, layers of lavas and fragmental

7) Y. ÔTUKA, *Bull. Earthq. Res. Inst.*, **11** (1933), 547.
8) Y. ÔTUKA, *Bull. Earthq. Res. Inst.*, **11** (1933), Pl. XXVI.

materials of the Hata beds show moderately steep (up to 40°) inclinations toward the north or northwest. These inclinations agree well with those of the same formation as seen in the surface outcrops along the eastern margin of the Tanna basin, that is, just above this part of the tunnel now under consideration.

But on the west side of the fault at the 11,500 ft point, these layers show a westward inclination, with angles ranging from 40° in the immediate west of the above-mentioned fault, to 10° in the further west. They are then abruptly folded at the 12,711 ft point, and assume a renewed inclination toward the southeast with an angle of 50°. At the 12,900 ft point, these folded layers are truncated clearly by a plane of unconformity, which inclines toward the west and is overlain by stratified tuffs and agglomerates of the Taga volcano to be mentioned later. The rocks of the Hata beds occurring immediately below this plane of unconformity scarcely show signs of decomposition due to weathering. The relations as above mentioned are shown in Fig. 2.

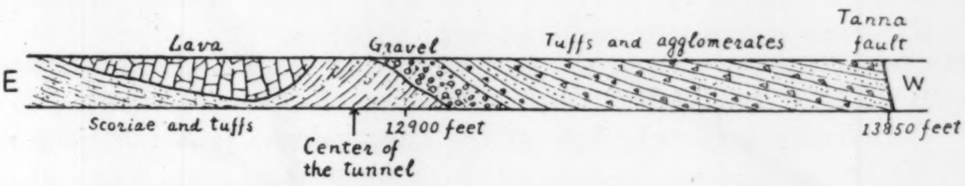

Fig. 2. A sketch of the exposure along the tunnel wall between 12,200 and 13,850 feet.

The compact lavas of the Hata beds that occur in the tunnel between 6,500 and 12,900 feet, are quite variable in petrographic characters. In hand specimen, they are dark grey or black in colour, and either compact or slightly vesicular. Sometimes they carry abundant visible phenocrysts, but sometimes they are almost non-porphyritic. In the porphyritic representatives, beautiful crystals (up to 5 mm in length) of clear white plagioclase, clear yellow olivine, and dark green augite are usually seen.

Under the microscope, these rocks vary in type from more basic olivine-basalts to less basic augite-hypersthene-basalts. Phenocrysts of calcic plagioclase are always present. Those of pale green augite are usually present, being especially abundant in the rocks of intermediate basicity, and sometimes absent in the most basic ones. Phenocrysts of olivine and those of hypersthene occur with a reciprocal relation to each other in amount. The former is abundant in the more basic rocks, while its place is often taken by the latter in the less basic

ones. Phenocrysts of magnetite are seen only in some of the less basic rocks in which those of olivine are usually absent.[9]

In texture, the groundmass varies from fine-grained compact type, through medium-grained intergranular type, to coarse-grained doleritic type. The constituent minerals of the groundmass are plagioclase, monoclinic pyroxene, magnetite, and cristobalite, either with or without pale brown glass.

Some of the olivine-basalts of the Hata beds may be probably the most melanocratic representatives of the common volcanic rocks of Japan.

It is interesting to note that the less basic types (augite-hypersthene-basalts) tend to occur toward the eastern part of the tunnel, while the more basic types (olivine-basalts) toward the western part of the tunnel and in the surface outcrops of the formation. In other words, the lavas of the present formation become more basic in composition toward the upper horizon of the series.

The only example of alteration is seen in a specimen collected at a point very close to the fault at the 9,050 ft point, where phenocrysts of olivine are completely replaced with chlorite.

***From 12,900 to 15,000 feet*:**

Andesitic lavas and tuffs of the Taga volcano (lower Pleistocene).

The Taga volcano consists of thick piles of basaltic and andesitic lavas interbedded with tuffs and agglomerates. It extends from the south of Aziro (5 km south of Atami-mati) to Atami pass (4 km northwest of Atami-mati). At Simotanna, west of the Tanna basin, some of the lavas of this volcano is seen to cover the pumiceous mudstones of the Simotanna beds (lower Pleistocene). From this and other facts, the age of the present volcano is inferred to be lower Pleistocene.

The lavas and the fragmental materials appearing in the Tanna tunnel are those representing only the intermediate stage of the history of the volcano now under consideration. In the section Fig. 1 is also shown another group of lavas underlying the lavas of the intermediate stage, which will be referred to as the lavas of Wada type (olivine-two-pyroxene-andesites). However, the lavas of Wada type do not appear on the tunnel wall.

On the tunnel wall, only a few sheets of lavas of the Taga volcano

9) Such a tendency of the association of the porphyritic minerals in rocks of different basicity is a general feature of many suits of volcanic rocks in the north Idu district.

are intercalated between thick beds of yellowish tuffs and agglomerates. These rocks are entirely free from any kinds of alteration.

As has been already mentioned, the present formation is separated from the easterly lying Hata beds by a thin gravel bed that rests directly upon the plane of unconformity truncating the latter formation. The pebbles of this gravel bed are derived mostly from the rocks of the underlying Hata beds, and are subangular in form.

The tuffs and agglomerates of the Taga volcano show distinct stratification planes dipping toward the west, with angles ranging from 40° at the immediate west of the above-mentioned gravel bed to 10° at the east of the Tanna fault. These relations are shown in Fig. 2.

Although no sheet of lava appears on the tunnel wall between the Tanna fault and the junction point of the Taga volcano with the easterly lying Hata beds, a boring at the Tanna basin carried out by the Railway Department (Boring D in Fig. 1) revealed the existence of three sheets of compact lavas lying immediately above the beds of tuffs and agglomerates occurring in the tunnel. It must be noted that one of the lavas detected by the boring is entirely the same in petrographic characters as that occurring at the summit of Takidiyama (672·2 meters), 1 km north of the highest point in the section Fig. 1. They belong probably to one and the same flow.

At the junction of the Taga volcano with the westerly lying Hata beds, a sheet of somewhat scoriaceous lava is seen to lie upon the former, dipping gently toward the east.

The famous Tanna fault, which runs meridionally through the center of the Tanna basin, crosses the tunnel at the 13,850 ft point with a remarkable development of fault breccia. At the time of the great north Idu earthquake, this fault caused a remarkable deformation upon the ground surface as well as upon the tunnel wall. It has been reported that a new slicken-side appeared crossing the tunnel, along which the western block was shifted southward horizontally for a distance of about 8 feet relatively to the eastern. It is interesting to note that this slicken-side had a northwest strike in spite of the general meridional trend of the earthquake fault appeared on the ground surface. It follows then that the actual underground displacement, at least in the neighbourhood of the Tanna tunnel, took place along a series of parallel gliding planes arranged *en echélon*.

By comparing the position of the earthquake fault appeared on the ground surface with that of the slicken-side appeared in the tunnel, it may be inferred that the plane of the Tanna fault inclines

steeply toward the west, or is nearly vertical.

The lavas of the Taga volcano occurring in the tunnel and detected by the boring are, in hand specimen, usually compact and dark grey in colour, carrying visible phenocrysts of abundant plagioclase and a few pyroxenes.

Under the microscope, they are usually basic two-pyroxene-andesites almost transitional to basalts in mineral composition. Olivine-bearing type is also found.

***From 15,000 to 15,300 feet*:**

Basaltic lavas and scoriae of the Hata beds (upper Pliocene?).

The lavas have gentle inclinations toward the east.

It is certain that the rocks of the present formation extend further to the west of the point 15,300 feet.

The rocks are fresh olivine-basalts differring in no respect from those of the same formation already described.

The lacustrine deposits of the Tanna basin.

The result of the borings in the Tanna basin, carried out by the Railway Department, has shown that the surface of the basin in question is covered by beds of sandy muds and gravels of about 50 meters in thickness.[10] They are probably lacustrine and fluviatile deposits.

On the Geologic Structure of the Tanna Basin.

Two remarkable features regarding the geologic structure of the basin are to be noticed from the above descriptions and also from the section Fig. 1: –

1) The layers of the lavas and the fragmental meterials of the Hata beds and of the Taga volcano, as well as the plane of unconformity between these two, incline toward the center of the basin. Probably they form a syncline or a basin structure.

2) Relative vertical displacement of the blocks on both sides of the Tanna fault is apparently slight. (See the symmetrical disposition of the rocks of the two formations, the Hata beds and the Taga volcano, on both sides of the Tanna fault in Fig 1).

These features show that the Tanna basin is not a mere "Graben" nor was originated simply through a sort of kettle depression, as has been suggested by some earlier authors, but was originated mainly through the down-warping of the layers of the lavas and the fragmental materials of the Taga volcano which formed primarily the land

10) T. WATANABE, On the geology of the Tanna basin. (Published from the Railway Department in 1925.)

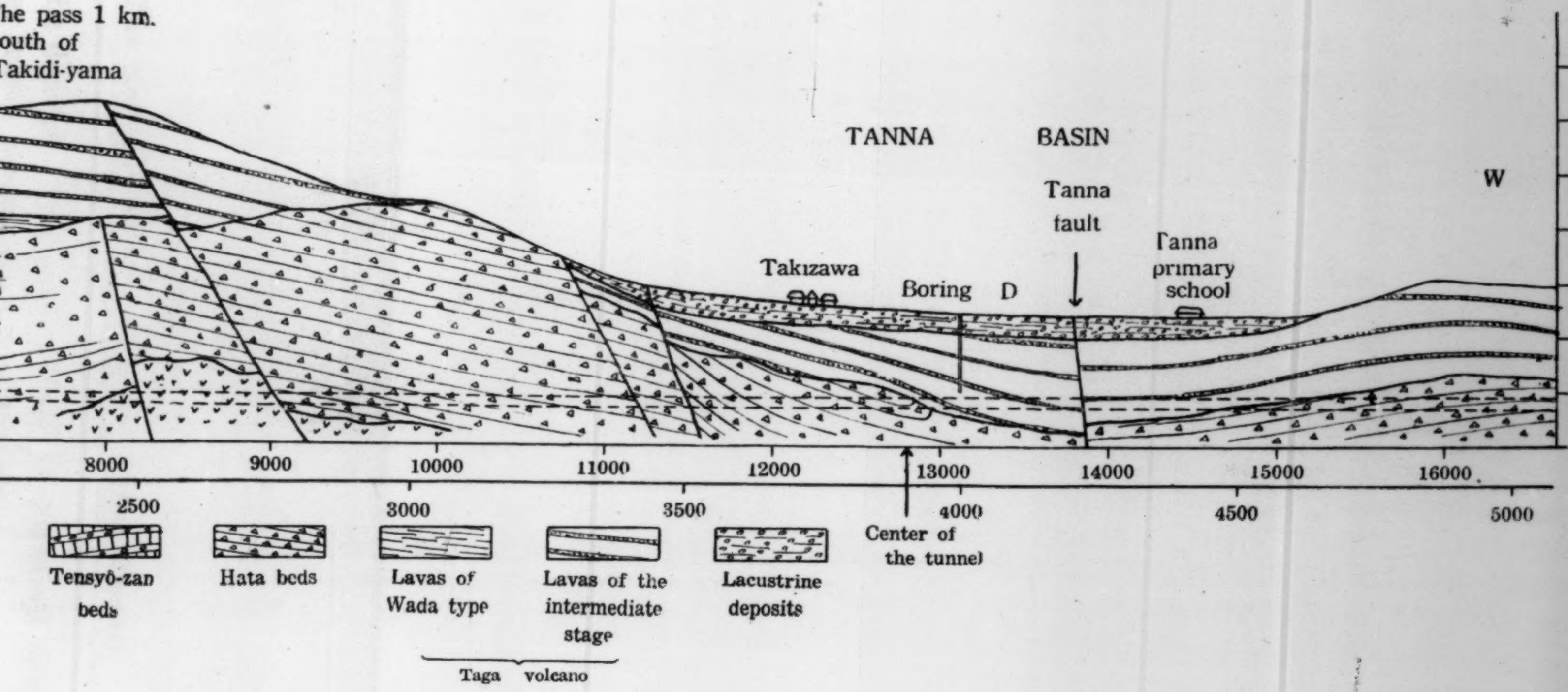

g the eastern half of the Tanna tunnel.

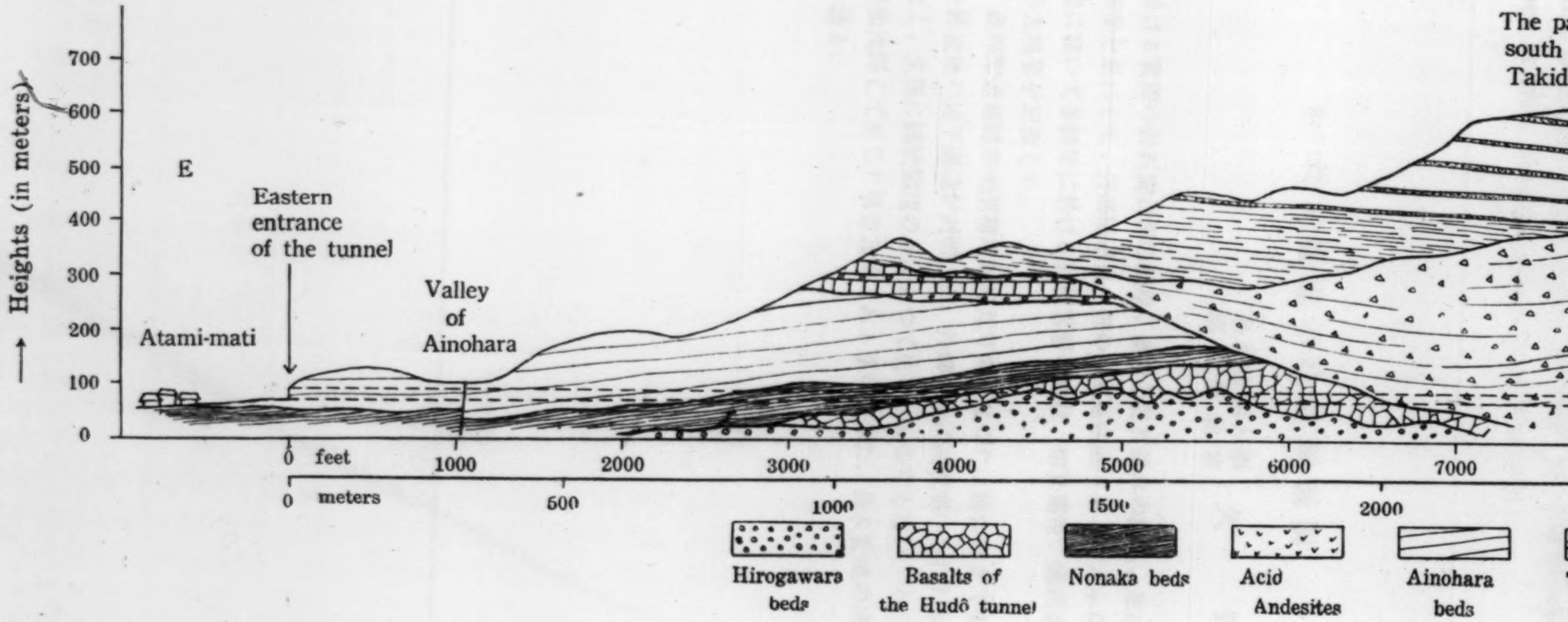

Fig. 1. The geologic section along the

surface of the district. This problem will be discussed more fully in another paper which is now under preparation.

---

9. 丹那隧道の地質斷面圖

東京帝國大學
地質學教室 久野 久

丹那隧道內に於ける實際の岩石露出面の觀察，多數の岩石標本の採集，並びに隧道附近地表面の地質調查等の結果を基にして，丹那隧道東半部の地質斷面圖（第1圖）を作製した．本論文にては，此の斷面圖に就いて各部分に於ける諸種岩層の產狀，相互關係，構造並びにその構成物質の岩石學的性質の大略等を記載した．

本研究の結果，此の附近地域の地質構造が可なり明になつた．特に今まで多數の學者によつて議論されて來た丹那盆地の地下構造が判明した．丹那盆地は從來唱へられた如く火口跡でもなく單なる地溝でもなく，又單に鍋狀陷沒のみによつて生じたものでもない．それは多賀火山の噴出物層が主として撓曲沈降して生じた構造盆地である事が分つた．尙本盆地の成因に關する詳しい議論は他の機會に讓る．

---

10. 高層建築の地震動による振動

地震研究所 齋田時太郎 鈴木正治

（昭和10年3月19日發表——昭和10年12月20日受理）

內　容

本文は高さ略々100尺の高層建築の地下室，第2階，第4階，及屋上の4箇所に加速度地震計を据ゑて，地震動による建物の振動を觀測して知り得た，若干の性質について述べてあるが，次の三つが重要なものと認められる．

（1） 地震動により誘發される建物の振動週期には，卓越週期が存在し且共振曲線の極大値と略々一致することより，建物の固有週期の存在と其値とが明かに認められる．

（2） 第4階と屋上とでは卓越週期が一致し，其値は建物の固有週期を現はし，何れの地震にても變らざるも，第2階と地下室との卓越週期は一致するも，其値は地震によつて異なる．このことは第3階附近を界として，上下で振動の性質の異なることを示す．

（3） 觀測せる程度の强さの地震に於て，屋上の加速度は地下室の略々6倍にも達することがあつた．

目　次

1. 序　言…………………… 104
2. 地　盤…………………… 104
3. 建物の構造概要………………… 105
4. 觀測方法…………………… 106
5. 卓越振動週期………………… 106
6. 颱風による卓越振動週期…… 110
7. 共振曲線…………………… 110
8. 主要動の初期中期及終期に於ける卓越振動週期……… 111
9. 各階に於ける加速度………… 114
10. 結　語…………………… 117

1. 序言　本文は高層建築物が地震動により如何なる振動をなすかを調査する目的で，昭和9年6月より昭和10年3月に亘り，東京市京橋區南傳馬町三丁目に在る第一生命保險相互會社の建物內に加速度地震計を据ゑつけて觀測し，其結果として得られた，若干の事項に關する報告である．

2. 地盤　第一生命保險相互會社所在地附近の地盤は東京下町に屬し，洪積地層（復興局の第三紀層）を沖積地層の軟弱なるものが覆ふてゐる．この建築地域の沖積層の厚さを知る資料を有せざるにより，復興局施行の鑿井のうちこの地域に最も近きものを周圍に求めてみると次の表の如くなる．

鑿井番號	位置	海抜高距 (m)	地層の厚さ(m)		第一相互館よりの距離 (m)
			盛土埋土	沖積層	
M 27	京橋區南鞘町二五	4·09	1·4	2·2	200
m 26	京橋區南槇町南愼町小學校	4·37	4·6	9·0	350
m 28	京橋區銀座一丁目二九	3·20	3·2	7·7	200
L 28	京橋區五郎兵衛町三	4·30	4·6	1·5	210

これ等の數値より推察すると，この建築地域の沖積層盛土埋土總計の厚さは 8 m 位あると思はれる.

3. 建築物の構造概要　この建物は大正 4 年 5 月基礎工事に着手し，同 9 年竣工せるもので建坪 512 坪，延坪 3278 坪，建物の高さは地上 6 階小壁迄 92 尺，7 階小壁迄 102 尺，塔家軒蛇腹迄 120 尺，同最高部迄 150 尺あり，外部は地上 3 階窓臺迄常陸產御影石積，6 階軒蛇腹迄化粧煉瓦張付，7 階以上は人造石塗仕上げとなつてゐる. 基礎は根伐深 9 尺，杭木松 3 間及 3 間半末口 6 寸のものを打ち，基礎鐵骨 12 吋乃至 9 吋の I 字形梁を組合せ，鋼柱取付のボールトを埋込む. 軸部鐵骨は英國ドロマンロング會社及米國カーネギー會社等の匚，乚等の鋼材を以て柱梁胴差となして，建物の軸部を構成してある. 壁體は外部 3 階迄花崗石裏積煉瓦，6 階屋根迄煉瓦 2 枚厚，それ以上は鐵筋コンクリートとし間內柱防火壁は鐵筋コンクリート，其他仕切壁は鐵骨メタルラス張となつてゐる. 地下室床は地下 7 尺で四周及底部はアスファルト厚 5 分，燒付トラスコンモルタル塗で 1 階以上各階床及階段は全部鐵筋コンクリート床に電線其他埋設のため，シンダーコンクリートを施し煉革床リグノイド等にて仕上げてある. 屋根全部はアスファルトマルソイド防水層を施し，更に薄き洗ひ出し小砂利コンクリートを以て之を被覆し，塔家其他は銅板及亞鉛鍍金鐵板葺としてある. この建物に要した主要材料の數量を擧ぐれば下の如くである.

第 1 圖　第一相互館

杭木	1,950本	木材挽立材尺貫	340本
鐵骨材	800噸	鐵筋材	120噸
セメント	9,000樽	コンクリート材	610立坪
煉瓦	950,000本	花崗石	10,000立方尺
化粧煉瓦	130,000枚	大理石	4,520平方尺
硝子	18,000平方尺	漆喰壁	7,700面坪
リクノイド及煉革床	1,800面坪		

なほこの建物は大正大地震にて震害を免れたことを特記しておく．

4. 觀測方法 石本式加速度地震計3基を最初屋上，第4階及地下室に据えつけ，向は建物の間口及奥行の方向（A，Bとす）と各一致せしめ，10秒毎に時刻を記入するやう3基を電氣的に連絡し絶えず記象紙を廻轉し，1日1回取換ることゝした．數回の地震觀測の結果屋上と第4階とは卓越週期に於て全く一致することが解つたので，屋上の器械を第2階に移し第4階及地下室とで前と同様に觀測を續けた．使用せし加速度地震計の性能については，石本博士の論著* に譲りこゝには次の事項を記するに止む．

幾何倍率	213	
振子の振動週期	0·115秒	
制振器	ピストン型空氣制振器	
記象同轉速度	約1分間に6 cm	
記象同轉原動機	同調電動機	
地震計感度	1 mmの振れに對する加速度	
	B成分	A成分
地下室	1·63 gal	1·63 gal
第4階	1·59 gal	1·96 gal
屋上（第8階）及第2階	1·55 gal	1·60 gal

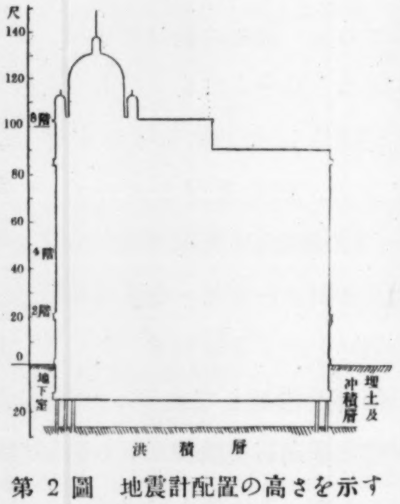

第2圖 地震計配置の高さを示す

制振器は空氣制振器なる故に溫度に對する補正を行ふ必要はないが，振子が臨界振動にあるやう常に注意をはらつた．

5. 卓越振動週期 各階に於て得た記象を寫眞により約3·85倍に引延ばし，各波の週期を逐次0·1 mm（0·026秒に相當する）迄讀んで，各0·1 mm毎に相當する波數を求め，更に得たる數の相隣れる數を平均して，卓越振動週期を決定した．其結果は第4圖に示してある．

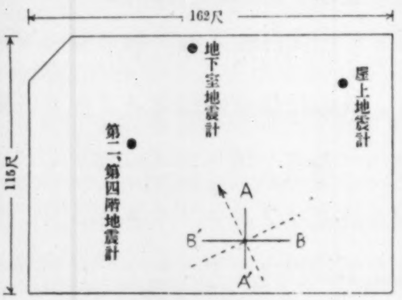

第3圖 地震計の位置を示す

圖より直に解ることは地下室の卓越振動週期は

* 石本巳四雄「加速度地震計及び其の記象」地震研究所彙報，9 (1931)，316.
同 上「地震とその研究」，(昭和10年2月，古今書院)，31〜32.

地震により異るも，第4階は何れの地震に於ても不變で恰も誤差曲線の如く見られる．屋上（第8階）のものも第4階についで單純な形を示すが，卓越振動周期が何れの地震にても不變なることは，第4階と同樣であるが，屋上に於て A 及 B の成分に分けて曲線を作ると，其の形が第4階に比して單純でない原因が解るやうである．即ち點線で示した B 成分の 2 倍と第 4 階と比較すれば全く同樣な形を得ることからして，屋上に於ては A 成分に建物の構造或は他の原因による局部的振動が誘發されるらしく考へられる．第2階に於ては地下室と第4階とを混合せるやうに現はれてゐる．このことは或は次の如く考へるが妥當である．即ち第2階以上の卓越振動週期は何れの地震にても變りはないが，地下室の卓越振動週期は地震によつて變り且地下室の振動が第2階或はそれ以上の階にも及び，其限度は高々第4階にあるらしい．しかしこれ等のことは觀測せし程度の强さの地震に對しての解釋であるのは當然である．これを要するに第3階附近を界として其の上下にて振動の性質が著しく異ることが解つた．

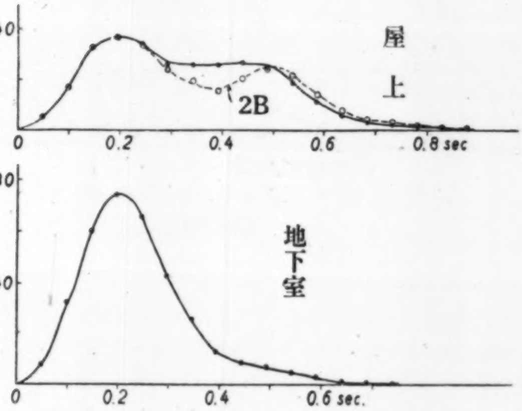

第 4 圖（a） 昭和9年7月16日多摩川溝の口附近地震
震動加速度周期頻度曲線，横軸は周期，縱軸は波數を示す

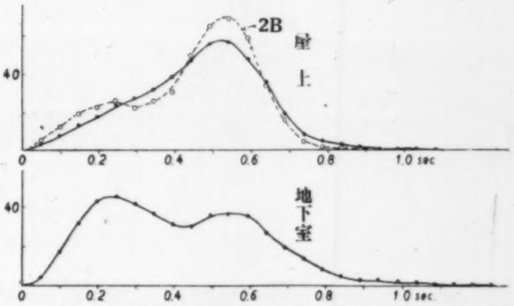

第 4 圖（b） 昭和9年7月20日霞ケ浦東南端地震

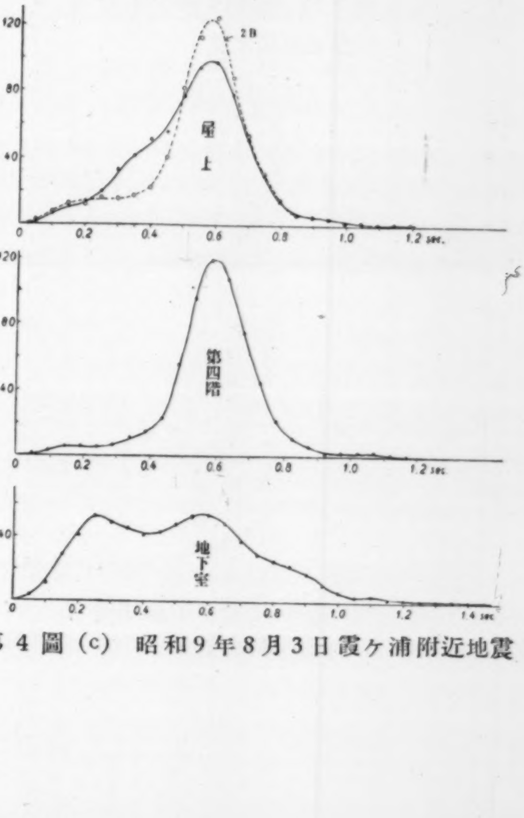

第 4 圖（c） 昭和9年8月3日霞ケ浦附近地震

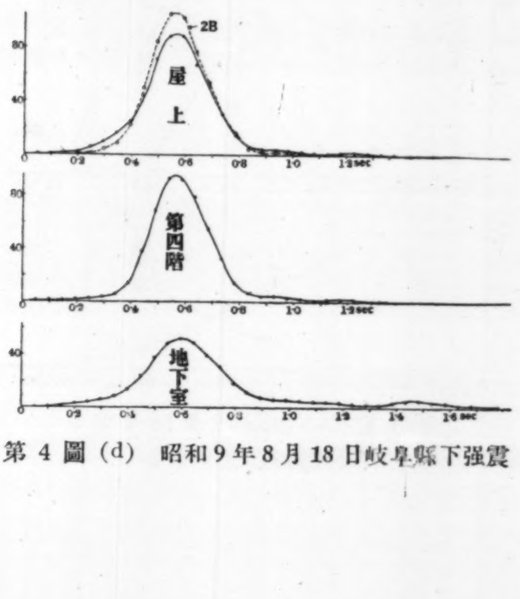

第 4 圖（d） 昭和9年8月18日岐阜縣下强震

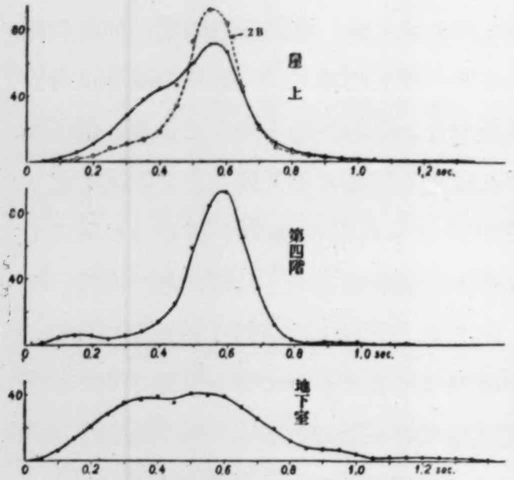

第 4 圖 (e) 昭和 9 年 9 月 24 日
山中湖附近地震

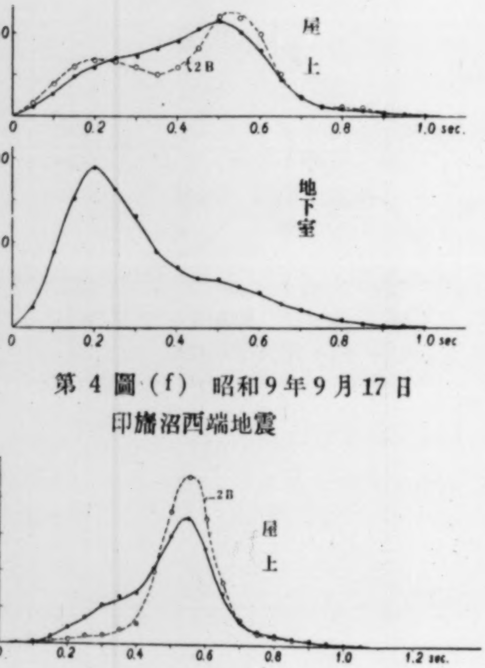

第 4 圖 (f) 昭和 9 年 9 月 17 日
印旛沼西端地震

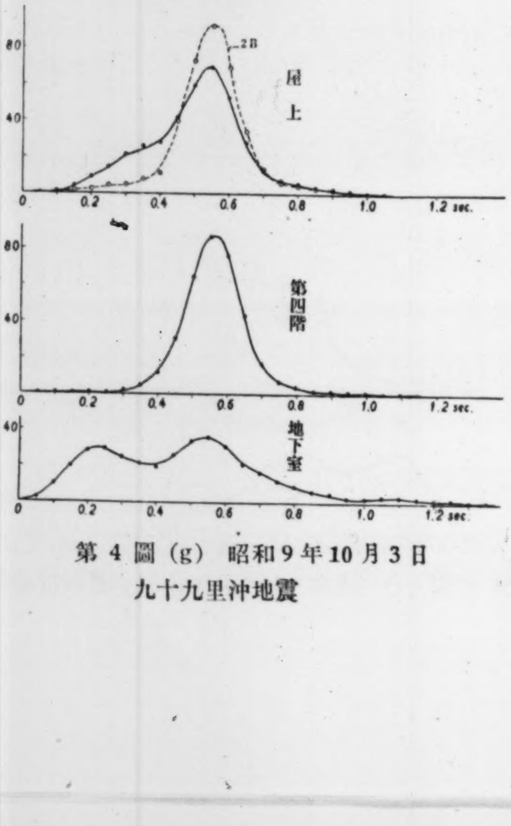

第 4 圖 (g) 昭和 9 年 10 月 3 日
九十九里沖地震

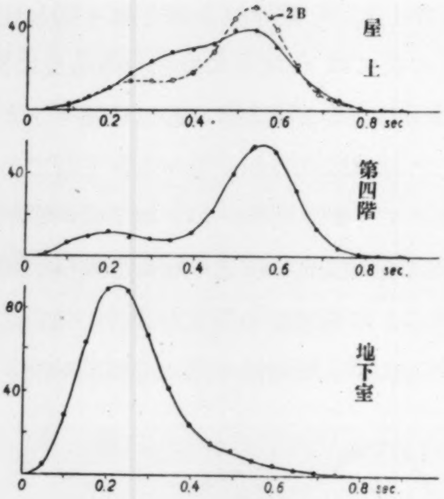

第 4 圖 (h) 昭和 9 年 11 月 26 日
武州松山地震

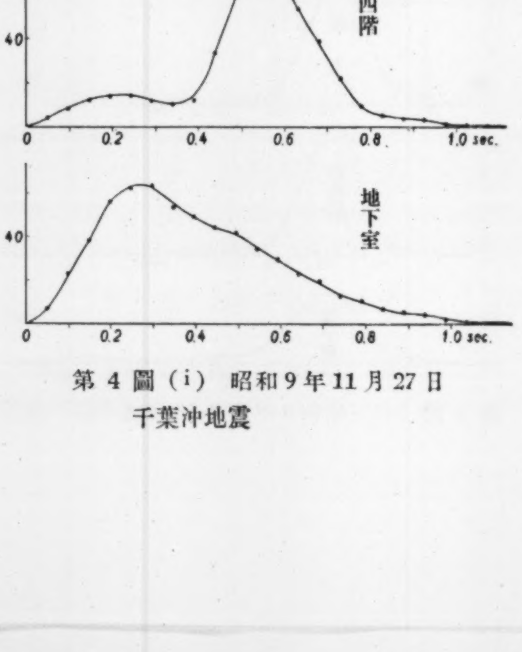

第 4 圖 (i) 昭和 9 年 11 月 27 日
千葉沖地震

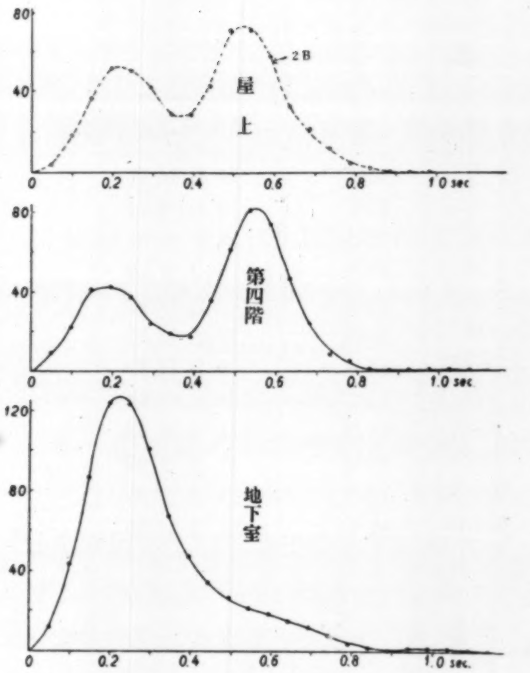

第 4 圖 (j) 昭和 9 年 11 月 28 日
水海道地震

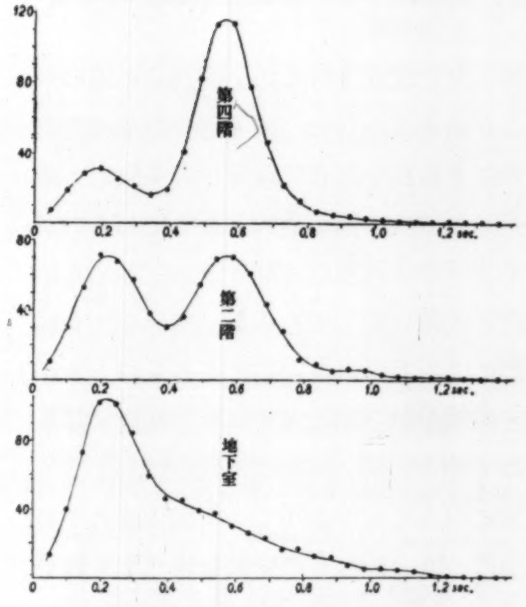

第 4 圖 (k) 昭和 10 年 1 月 19 日
多摩川溝の口地震

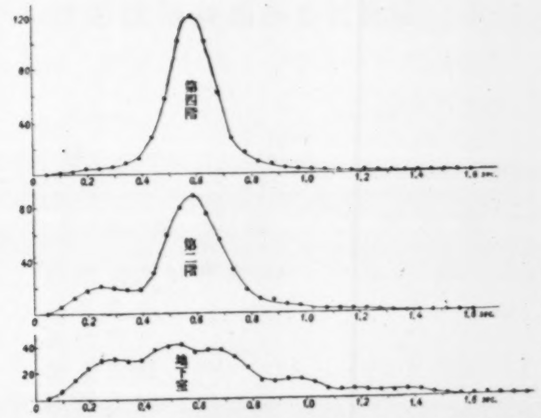

第 4 圖 (l) 昭和 10 年 2 月 20 日九十九里沖地震

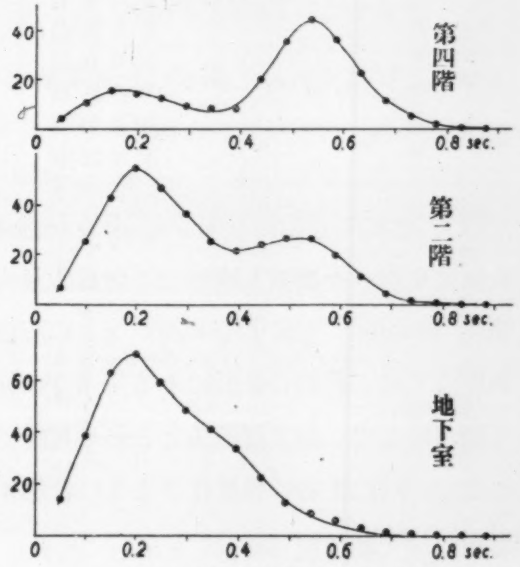

第 4 圖 (m) 昭和 10 年 3 月 7 日
三浦半島沖地震

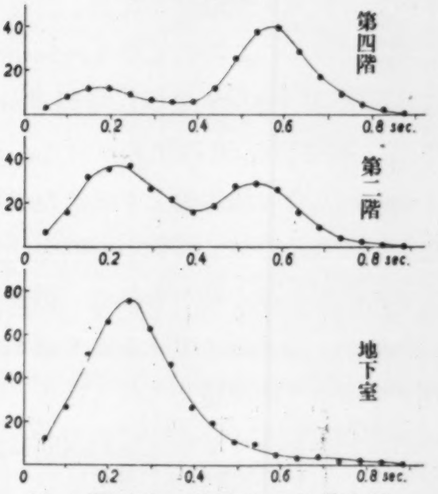

第 4 圖 (n) 昭和 10 年 3 月 2 日
手賀沼北部地震

6. 颱風による卓越振動週期　今回の觀測中大なる風壓を建物に與へるやうな暴風は中央氣象臺に於ける觀測を氣象要覽より摘出すれば12回ある．卽ち第 I 表の如くである．

第 I 表

測候所名	暴風觀測日	最大風速度 (米/秒)		最大風速度觀測時
東　京	昭和9年6月20日	S	11·6	20日16時
〃	9月9日	S	10·7	9日18時
〃	9月21日	S	22·3	21日11時40分
〃	10月8日	N	11·5	8日8時
〃	11月2日	S	10·2	2日15時
〃	11月28日	N	10·6	28日11時
〃	昭和10年2月6日	NNE	10·0	6日16時
〃	2月23日	N	12·7	23日16時
〃	3月10日	SSW	11·2	10日6時
〃	3月17日	NNW	12·4	17日2時
〃	3月25日	WNW	13·3	25日13時
〃	3月26日	WNW	12·1	26日11時

以上12回の中昭和9年9月21日の關西に大被害を與へた颱風を除けば，何れも最大風速度 10 m/sec 乃至 13·3 m/sec でこの程度の風速にては，建物の振動による加速度は極めて微弱にして，始ど認めることが不可能であつたが，9月21日の颱風によるものは第4階に於て最大加速度 0·6 gal を示してゐた．屋上（第8階床）のものは當然これ以上の値を示したと想像されるが，觀測室に雨の飛沫浸入し記象を損傷せるため，共値を知ることが出來なかつた．第4階の記象は寫眞に示してある．これによると何れの部分も大差なき振動をなしてゐるが，東京にて最大風速度 22·3 m/sec を示した11時40分頃が共の加速度振幅が最大となつてゐるのが解る．該時刻の60秒間をとつて，既記の如き方法で卓越振動週期を求めてみると第5圖の如くなり地震動より求めた卓越振動週期と大體一致してゐるが，幾分小さき値となつてゐるのは，建物の振動變位振幅が風壓によるものが地震動によるものより小さきためであると考へられる．震度大なるほど卓越振動週期は大きくなる傾向が認められるが，第4圖にて見らるゝ通り共値は極めて小さいが，共れは建物の變形を全く許さざるやうに構造せられてゐるこの種の建築に限ることであつて，次回に報告する木造家屋にありては卓越振動週期は震度の大小により，かなりの變動を現はすものである．

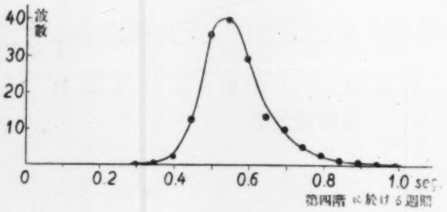

第 5 圖　颱風による卓越振動周期を示す昭和9年9月21日の颱風による頻度曲線

7. 共振曲線　地震動及風壓による建物の卓越振動週期が明かに存在し，共値が

略々0·6 秒であることは既に記述せる通りで，これを以てこの建物の固有振動週期とするも差支へないと考へられるが，第6圖に示す如き共振曲線を畫くことができ，しかも其極大値が上記の卓越振動週期と一致するので，固有振動週期の存在し其値が略々0·6秒であることは確かなことゝなつた．なほこの圖によれば，屋上(第8階床)の加速度は地下室の6倍にも達することがあるのが認められる．しかしそれは主要動の中期以後に多く現はれる地震動加速度の大して大きくない時期であつて，地震動加速度の大きい主要部の初期にありては3倍程度と考へられる．

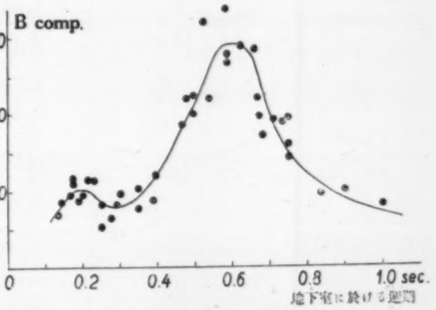

第 6 圖　共振曲線，縱軸は屋上に於ける加速度を地下室に於ける加速度にて除したる數を示す

8. 主要動の初期中期及終期に於ける卓越振動週期　各地震動について各階の卓越振動週期が時の經過と共に如何に變化するかを調らべてみると，次の第7圖に示す如くなる．時間は便宜上30秒づゝに區劃してある．これによると地下室に於ける卓越週期は時間の經過と共に變化するも，第4階及屋上（第8階）に於ては始終一定の狀態にあることが認められる．

第 7 圖 (a)　主要動の初期，中期及終期に於ける卓越周期の變化を示す．
昭和9年8月3日霞ケ浦附近の地震

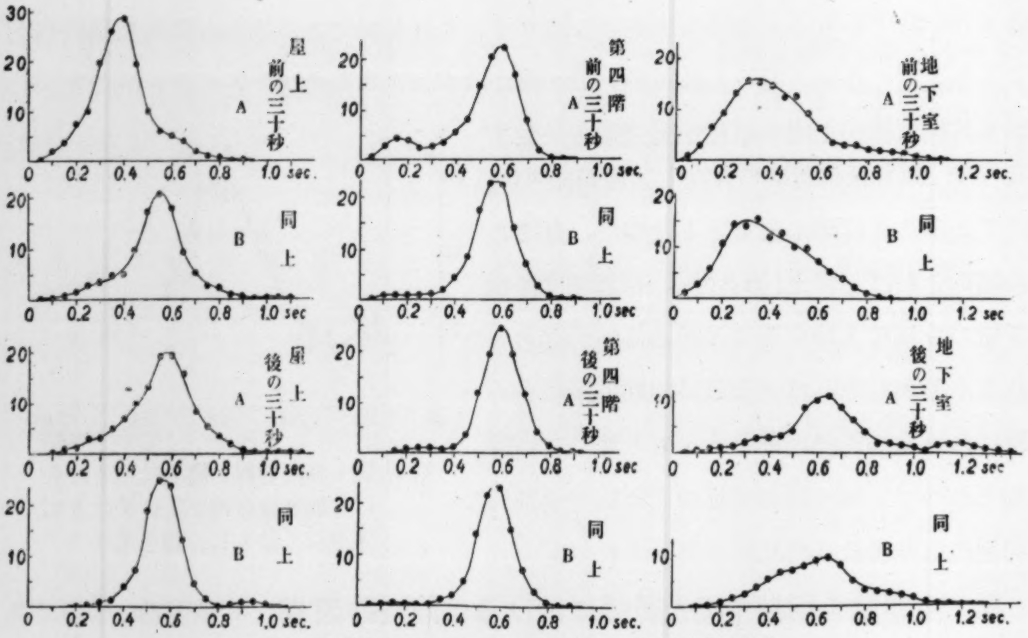

第 7 圖 (b) 昭和 9 年 9 月 24 日山中湖附近地震

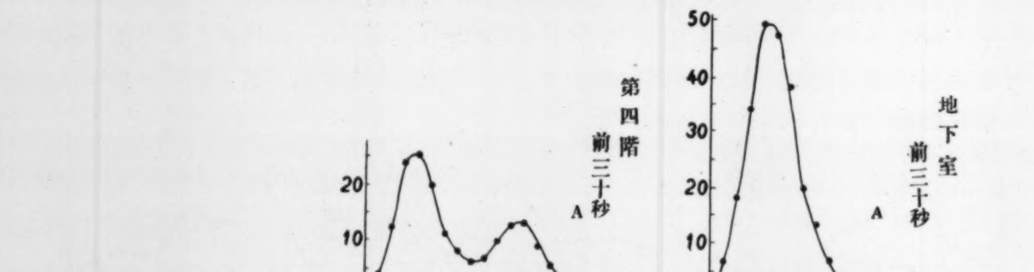

第 7 圖 (c) 昭和 9 年 11 月 28 日水海道地震

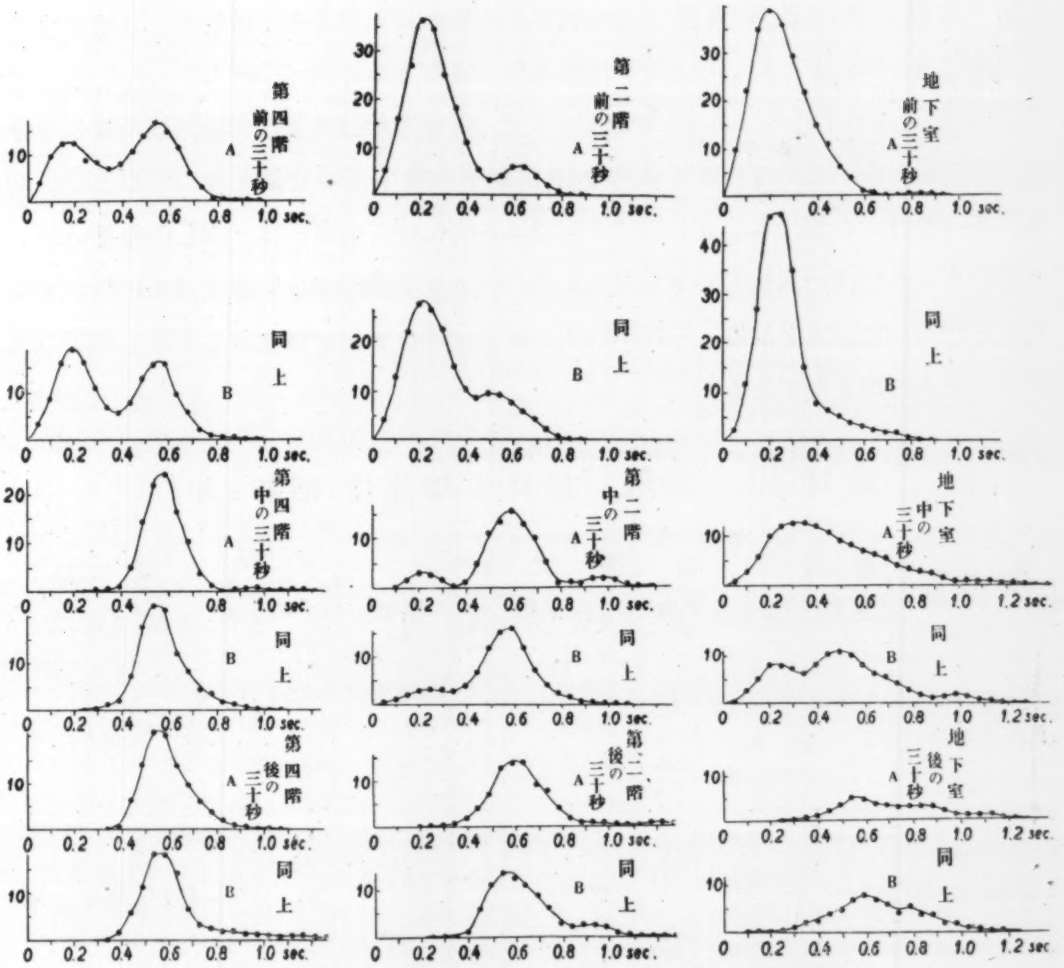

第 7 圖 (d)　昭和10年1月19日多摩川溝の口附近地震

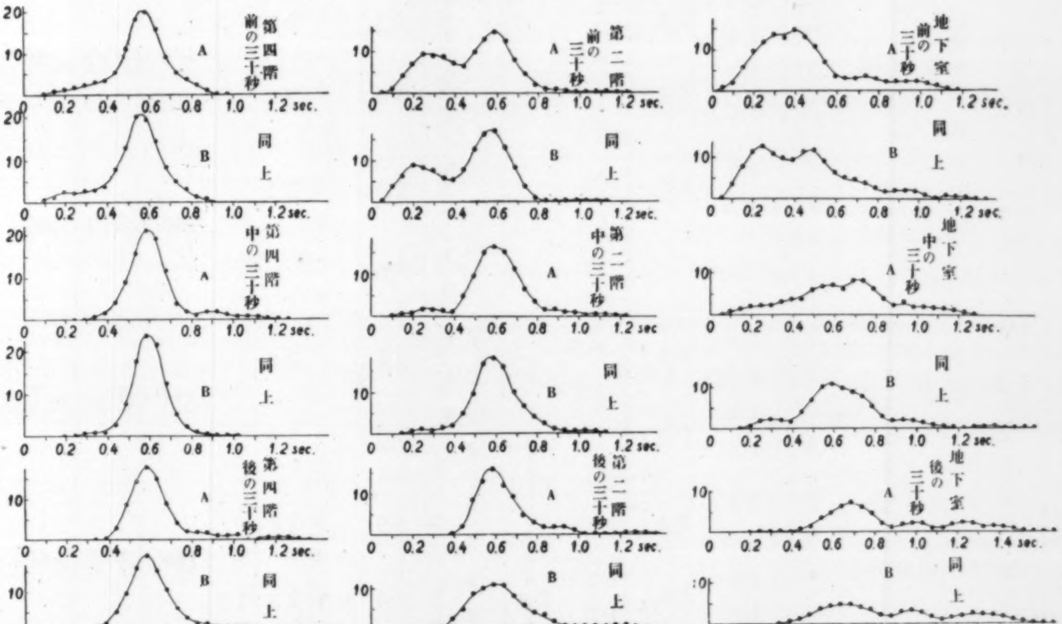

第 7 圖 (e)　昭和10年2月20日九十九里沖地震

9. 各階に於ける加速度 各地震毎に各階の最大加速度を讀取り，且地下室の最大加速度を單位として，其上階が何倍になつてゐるかを調べてみると，次の第II表及び第III表に示す通りである．これによると，震央距離近きものは短週期の波を多分に含む關係から，上階に於ける最大加速度が寧ろ地下室の分數となつてゐるのが見られる．なほこの最大加速度を現はす時刻は各階に於て嚴密には一致してゐないが，大體のところでは一致してゐると見られる．次に主要動の初より遂次 2·5 秒間づゝに於ける平均の加速度を求め，それが時間の經過に伴ひ如何に變化するかを，各階の比にて示せるが第8圖である．

第 II 表　各階に於ける加速度（昭和9年）

發震時	震度	方向	加速度 (gal) 地下室	平均 α_0	第4階	平均 α_4	屋上	平均 α_8	$\frac{\alpha_4}{\alpha_0}$	$\frac{\alpha_8}{\alpha_0}$	$\frac{\alpha_8}{\alpha_4}$	震央 東經	北緯	深さ
月 日 時 分												(°)	(°)	(km)
6 21 8 59	I	B	1·1	1·2			3·4	3·3		2·7		139·8	36·1	30
		B′	1·3				3·1							
		A′	0·8	0·9			2·4	2·3		2·6				
		A	1·0				2·2							
7 16 5 06	I	B	2·6	2·5			3·4	3·7		1·5		139·6	35 6	30
		B′	2·3				3·9							
		A′	2·3	2·2			3·7	3·5		1·6				
		A	2·0				3·2							
7 20 22 39	I	B	2·3	2·0			3·9	4·3		2·2		140·6	35·9	40
		B′	1·6				4·7							
		A′	1·1	1·4			4·0	3·4		2·4				
		A	1·6				2·8							
7 24 19 12	I	B	1·1	1·2			2·3	2·5		2·1		140·2	35·1	40
		B′	1·2				2·6							
		A′					2·4	2·4						
		A					2·4							
7 28 21 13	I	B	1·6	1·4			3·1	2·8		2·0		141·4	37·7	?
		B′	1·2				2·5							
		A′	1·1	1·2			2·4	3·3		2·8				
		A	1·3				4·2							
8 2 17 07	I	B	2·3	2·4			4·7	3·9		1·6		140·1	36·0	60
		B′	2·4				3·1							
		A′	1·6	1·5	2·2	2·0	3·2	3·4	1·3	2·3	1·7			
		A	1·3		1·7		3·5							

（次頁へ續く）

發震時	震度	方向	加速度 (gal) 地下室	平均 a_0	第4階	平均 a_4	屋上	平均 a_8	$\frac{a_4}{a_0}$	$\frac{a_8}{a_0}$	$\frac{a_8}{a_4}$	震央 東經	北緯	深さ
月 日 時 分 8 3 21 24	III	B	13·4	12·0	29·4	29·1	37·5	37·8	2·4	3·2	1·3	140·2	36·1	60
		B′	10·6		28·7		38·0							
		A′	13·0	13·4	32·0	29·5	28·0	27·3	2·2	2·1	0·9			
		A	13·8		27·0		26·5							
8 5 17 43	I	B	1·0	0·9	1·1	1·1	2·3	2·3	1·2	2·6	1·9	140·2	35·6	60
		B′	0·8		1·1		2·3							
		A′	1·1	1·1	0.8	0·8	3·0	2·9	0·7	2·6	3·6			
		A	1·0		0·8		2·8							
8 18 11 39	I	B	1·2	1·2	3·2	3·1	4·3	4·3	2·6	3·6	1·4	137·1	35·8	淺
		B′	1·2		3·0		4·2							
		A′	1·1	1·2	3·4	3·3	2·8	3·0	2·8	2·5	0·9			
		A	1·2		3·2		3·2							
9 1 20 17	II	B	17·1	15·1	15·9	16·8	30·2	32·1	1·1	2·1	1·9	139·9	36·1	50
		B′	13·0		17·6		34·0							
		A′	13·0	13·0	18·6	17·8	30·4	32·0	1·4	2·5	1·8			
		A	13·0		16·9		33·6							
9 17 9 30	II	B	4·1	4·9			7·7	7·7		1·6		140·1	35·8	30
		B′	5·7				7·6							
		A′	4·9	4·5			11·2	10·4		2·3				
		A	4·1				9·6							
9 24 13 53	II	B	2·4	2·0	2·7	2·8	4·7	3·9	1·4	2·0	1·4	138·9	35·4	20
		B′	1·6		2·9		3·1							
		A′	1·0	1·3	3·8	4·1	5·8	5·7	3·1	4·4	1·4			
		A	1·6		4·4		5·5							
11 26 12 38	I	B	2·6	2·5	2·4	2·4	4·7	4·9	1·0	2·0	2·0	139·4	35·9	40
		B′	2·3		2·4		5·1							
		A′	2·9	2·9	2·2	2·2	4·5	4·7	0·8	1·6	2·1			
		A	2·8		2·2		4·8							
11 27 14 50	I	B	3·6	3·5	6·4	6·4	10·5	10·1	1·6	2·9	1·6	140·6	35·5	40
		B′	3·3		6·4		9·6							
		A′	2·4	2·0	3·4	3·4				1·7				
		A	1·6		3·4									
11 28 0 56	II	B	5·7	6·1	5·1	4·8	10·1	10·9	0·8	1·8	2·3	140·0	36·1	40
		B′	6·5		4·5		11·7							
		A′	5·7	5·2	8·8	8·7				1·7				
		A	4·6		8·5									

第III表　各階に於ける加速度（昭和10年）

發震時	震度	方向	加速度 (gal) 地下室	平均 a_0	第2階	平均 a_2	第4階	平均 a_4	$\frac{a_2}{a_0}$	$\frac{a_4}{a_0}$	$\frac{a_4}{a_2}$	震央 東經	北緯	深さ
												(°)	(°)	(km)
月 日 時 分 1 3 23 55	III	B	40·0	35·7	29·0	25·4	18·0	18·7	0·7	0·52	0·7	139·9	35·5	60
		B′	31·4		21·7		19·4							
		A′			34·0	34·3	28·7	29·6			0·8			
		A			34·5		30·4							
1 19 7 43	II	B	4·9	4·6	7·3	6·6	6·5	7·1	1·4	1·5	1·1	139·6	35·6	30
		B′	4·2		5·9		7·6							
		A′	3·9	4.5	7·2	6·8	5·9	5·9	1·5	1·3	0·9			
		A	5·1		6·4		5·9							
2 12 2 20	I	B	1·6	1·6	2·5	2·5	2·7	2·3	1·6	1·4	0·9	139·7	36·1	40
		B′	1·6		2·5		1·9							
		A′	1·6	2·2	2·6	3·0	3·9	3·9	1·4	1·8	1·3			
		A	2·8		3·4		3·9							
2 20 5 10	II	B	5·5	5·4	6·7	5·9	7·8	7·3	1·1	1·4	1·3	140·5	35·4	30
		B′	5·2		5·1		6·8							
		A′	4·1	4·4	7·7	7·6	7·8	8·1	1·7	1·8	1·1			
		A	4·6		7·5		8·3							
3 2 3 45	II	B	2·9	2·9	3·7	3·8	3·3	3·5	1·3	1·2	0·9	140·1	35·9	50
		B′	2·8		3·9		3·7							
		A′	3·1	2·7	3·4	3·3	3·7	3·7	1·2	1·4	1·1			
		A	2·3		3·2		3·7							
3 7 17 53	I	B	2·1	2·7	4·0	4·2	5·1	5·0	1·6	1·9	1·2	139·6	35·1	40
		B′	3·3		4·3		4·8							
		A′	2·0	2·7	2·4	3·0	2·9	3·6	1·1	1·3	1·2			
		A	3·4		3·5		4·2							
3 9 1 8	I	B	1·5	1·7	1·9	2·1	1·4	1·3	1·2	0·8	0·6	141·7	36·5	40
		B′	1·8		2·3		1·1							
		A′	1·0	0·9	1·3	1·2	1·4	1·4	1·3	1·6	1·2			
		A	0·8		1·1		1·4							
3 14 23 16	I	B	2·9	2·2	2·9	2·8	2·2	2·3	1·3	1·0	0·8	139·2	35·2	?
		B′	1·5		2·6		2·4							
		A′	2·4	2·0	3·0	2·9	2·5	3·0	1·5	1·5	1·0			
		A	1·6		2·7		3·4							
3 26 18 2	I	B	4·9	4·9	4·7	4·3	3·3	4·2	0·9	0·9	1·0	139·9	35·7	35
		B′	4·9		3·9		5·1							
		A′	2·4	3·0	3·2	2·7	4·2	4·0	0·9	1·3	1·5			
		A	3·6		2·1		3·7							
3 31 6 20	II	B	5·2	5·1	5·9	6·9	8·8	8·6	1·4	1·7	1·2	141·8	31·2	?
		B′	4·9		7·8		8·3							
		A′	4·1	4·4	6·9	6·8	10·5	10·4	1·5	2·4	1·5			
		A	4·7		5·6		10·2							

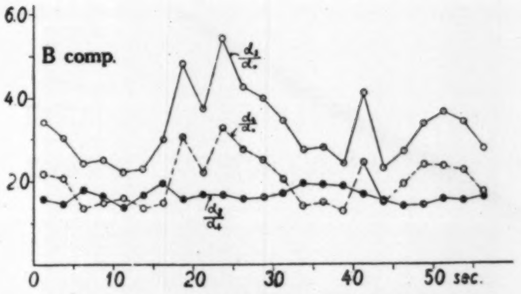

第 8 圖 (a)　各階加速度比の時間の經過に伴ふ變化を示す
昭和9年8月3日の地震

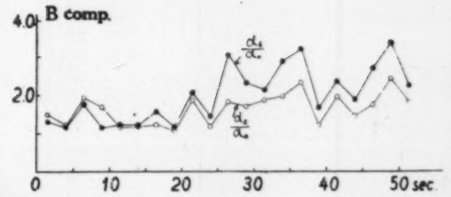

第 8 圖 (c)　昭和10年1月19日の地震

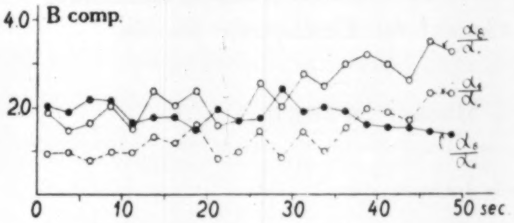

第 8 圖 (b)　昭和9年11月28日の地震

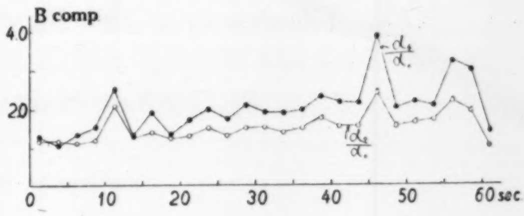

第 8 圖 (d)　昭和10年2月20日の地震

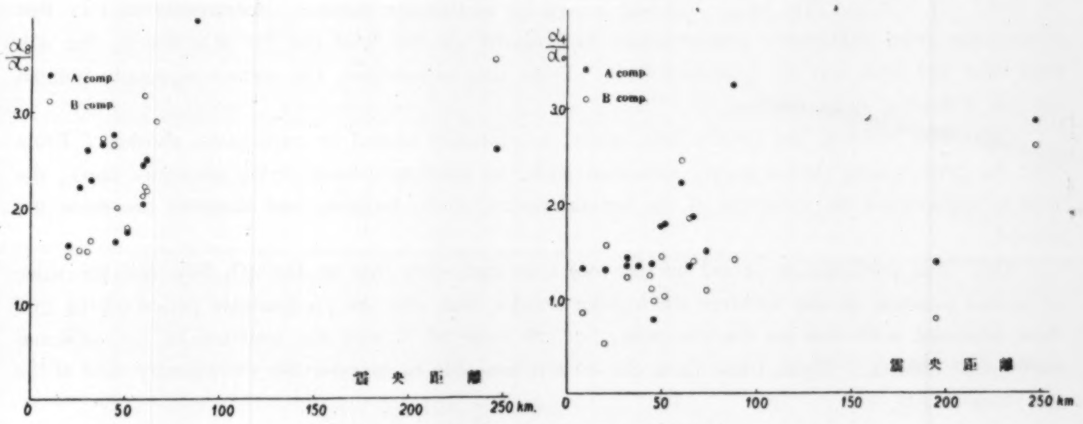

第 9 圖　震央距離と加速度との關係を示す

屋上（第8階）と第4階との比は始終略々一定であるが，屋上と地下室及第4階と地下室との比は中期部に於て著しく增大することが認められるが，それは既に記述せる如く地下室に於ける卓越振動週期が中期部に於て建物の固有振動週期に接近する傾向あることによるもので，所謂共振の狀態を現はすものと考へられる．震央距離と建物に生ずる振動加速度との關係を調べて見ると，第9圖に示す如くである．これによると 50～100 km の中距離の地震によるものに振動加速度の大なるものを生ずる傾向が見える．

10.　結語　これ迄說述せるは，主として地震動記象より容易に求めらるゝ事項に關するもののみで，未だ重要なる事項の硏究調査が殘されてゐることは筆者等のよく

知るところであるが，この方面の調査資料の乏しき現今の狀勢に於ては，尙ほ資料としての價値を有するものと信ずる．

筆を擱くにあたり今回の觀測に際し受けし學術振興會の補助と觀測のための諸設備其他を負擔せられた第一生命保險相互會社の御好意とに深く謝意を表する次第である．

---

10. *Vibration of a Tall Building Caused by Earthquake Shocks.*

By Tokitaro SAITA and Masazi SUZUKI,

Earthquake Research Institute.

The object of the following article is to explain the results of observation which was executed on about one hundred feet heigh building caused by earthquake shocks. Instruments used in this observation were Ishimoto's accelerometer and placed on the roof (or the 8th floor), the 4th floor, the 2nd floor and the basement floor. From this observation the writers especially pointed out the following three matters.

(a) The building has predominate period in vibration caused by earthquake shocks. From that the predominate period nearly coincided with the maximum value of the resonance curve, the writers appreciated the existence of the natural period of the building and observed the value 0·6 second.

(b) The predominate period on the roof coincided with that on the 4th floor and the value of it was constant in any different earthquake shocks, and also the predominate period on the 2nd floor coincided with that on the basement, but the value of it was not constant in any different earthquake shocks. From these facts the writers are able to suppose the vibrationary node at the 3rd floor nearly.

(c) The acceleration on the roof in some cases came up to six from three times of that on the basement floor.

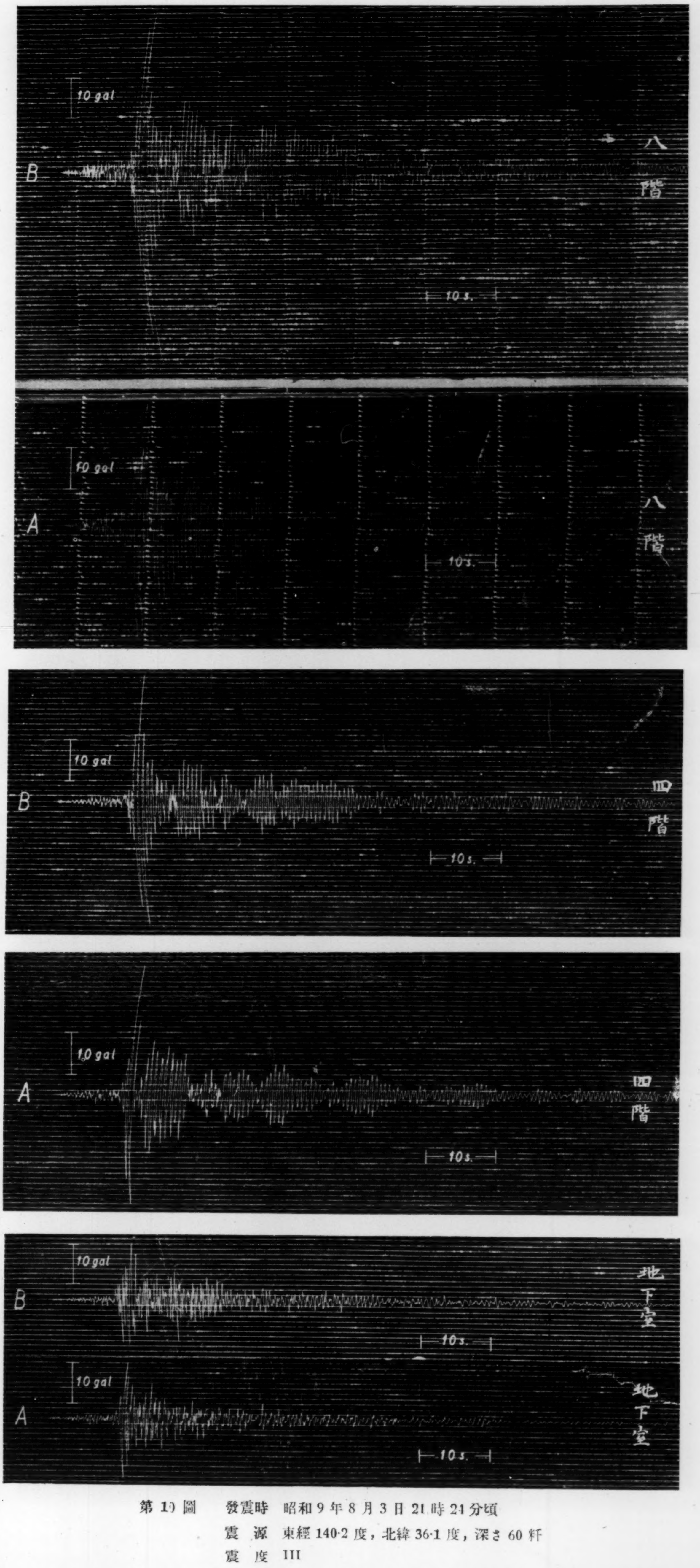

第10圖 發震時 昭和9年8月3日21時21分頃
震 源 東經140·2度，北緯36·1度，深さ60粁
震 度 III

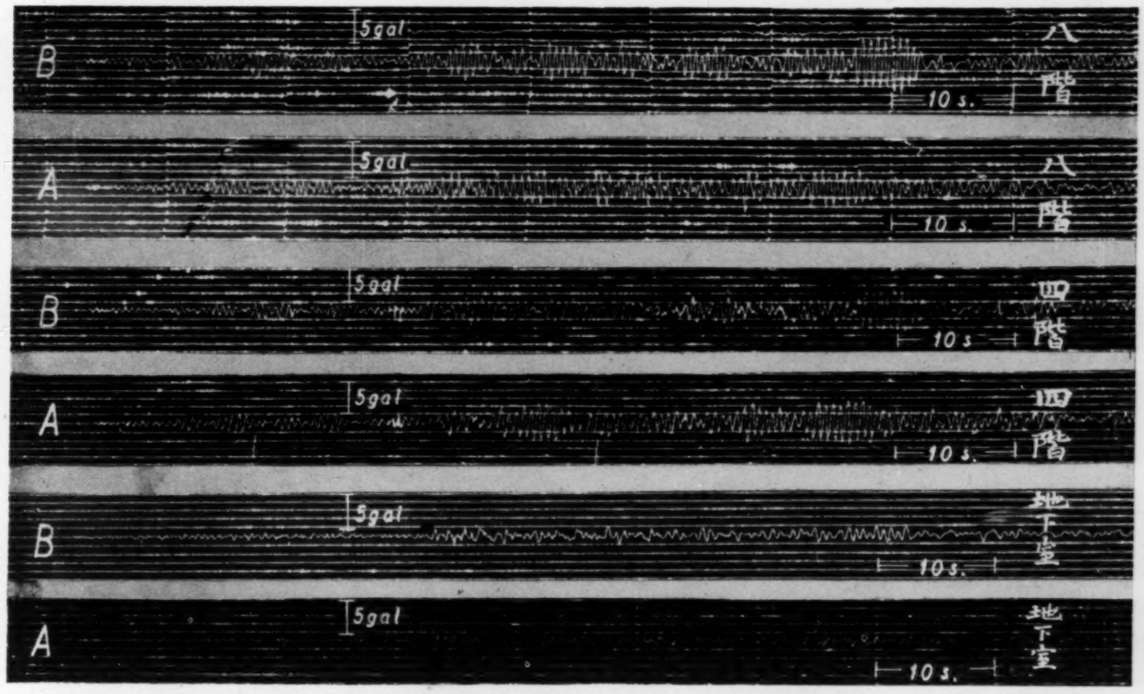

第 11 圖 發震時 昭和 9 年 8 月 18 日 11 時 39 分頃
震　源 東經 137·1 度，北緯 35·8 度，深さ 15 粁
震　度 I

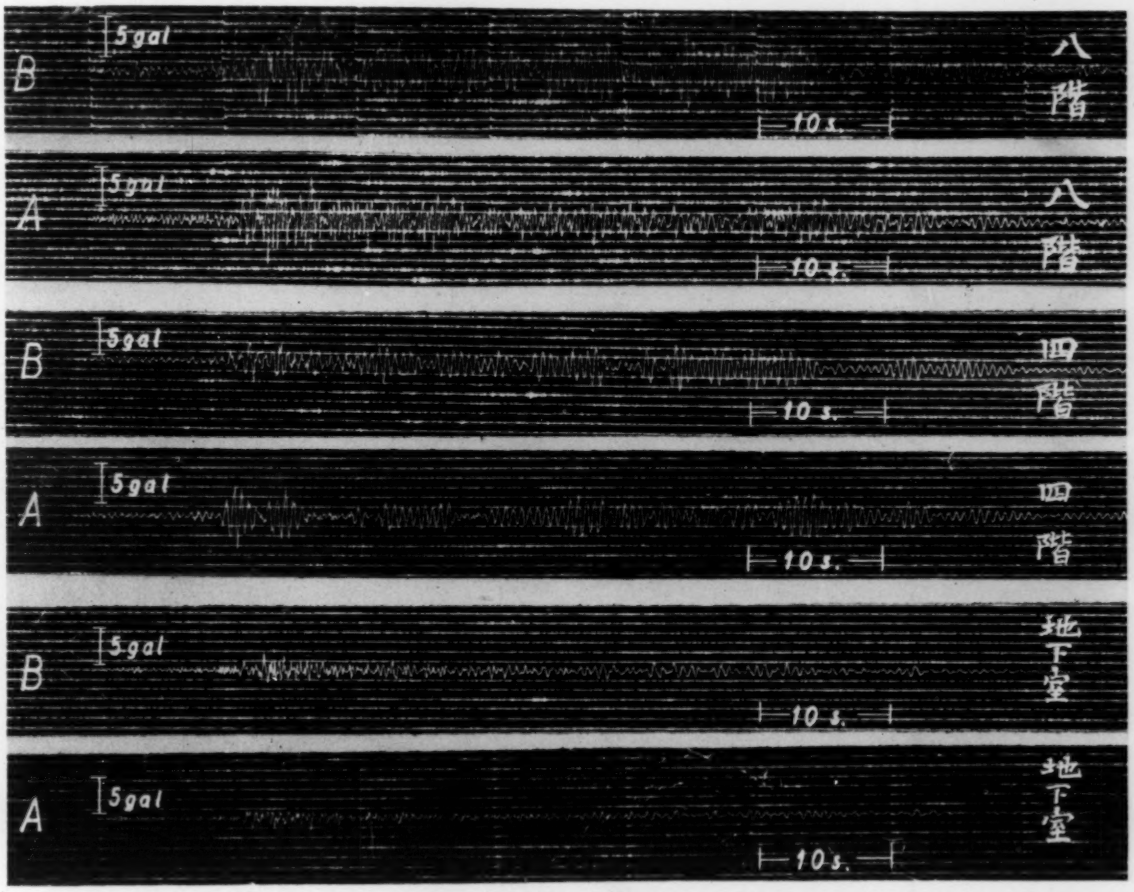

第 12 圖 發震時 昭和 9 年 9 月 24 日 13 時 53 分頃
震　源 東經 138·9 度，北緯 35·4 度，深さ 20 粁
震　度 II

(震研彙報 第十四號 圖版 齊田・鈴木)

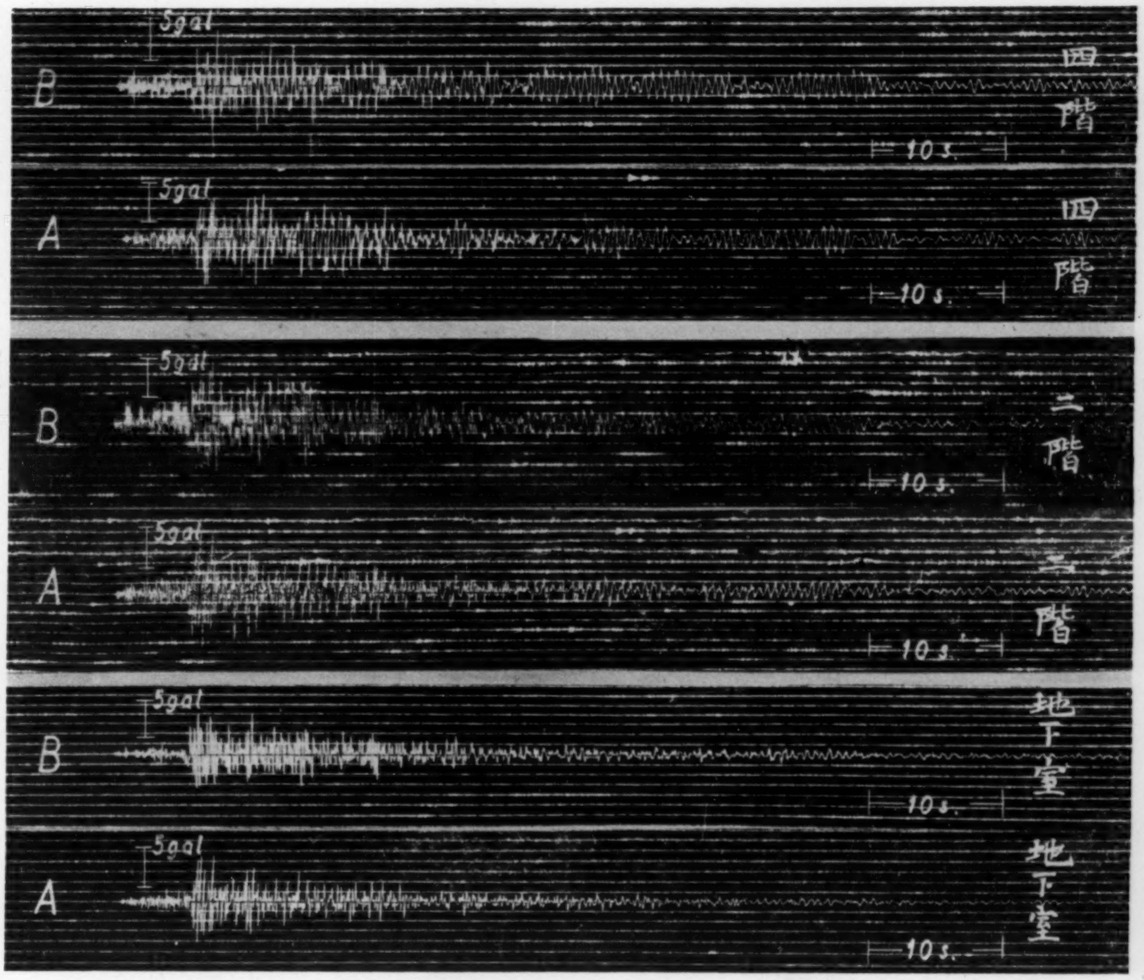

第 13 圖　發震時　昭和 10 年 1 月 19 日 7 時 43 分頃
震　源　東經 139·6 度，北緯 35·6 度，深さ 30 粁
震　度　II

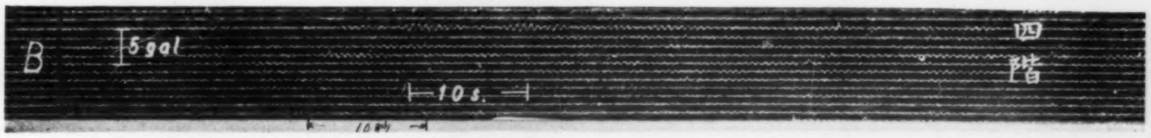

第 14 圖　昭和 9 年 9 月 21 日京・阪・神地方に多大なる被害を與へたる颱風による振動（第 4 階にて觀測せるもの）

（震研彙報 第十四號 圖版 齊田・鈴木）

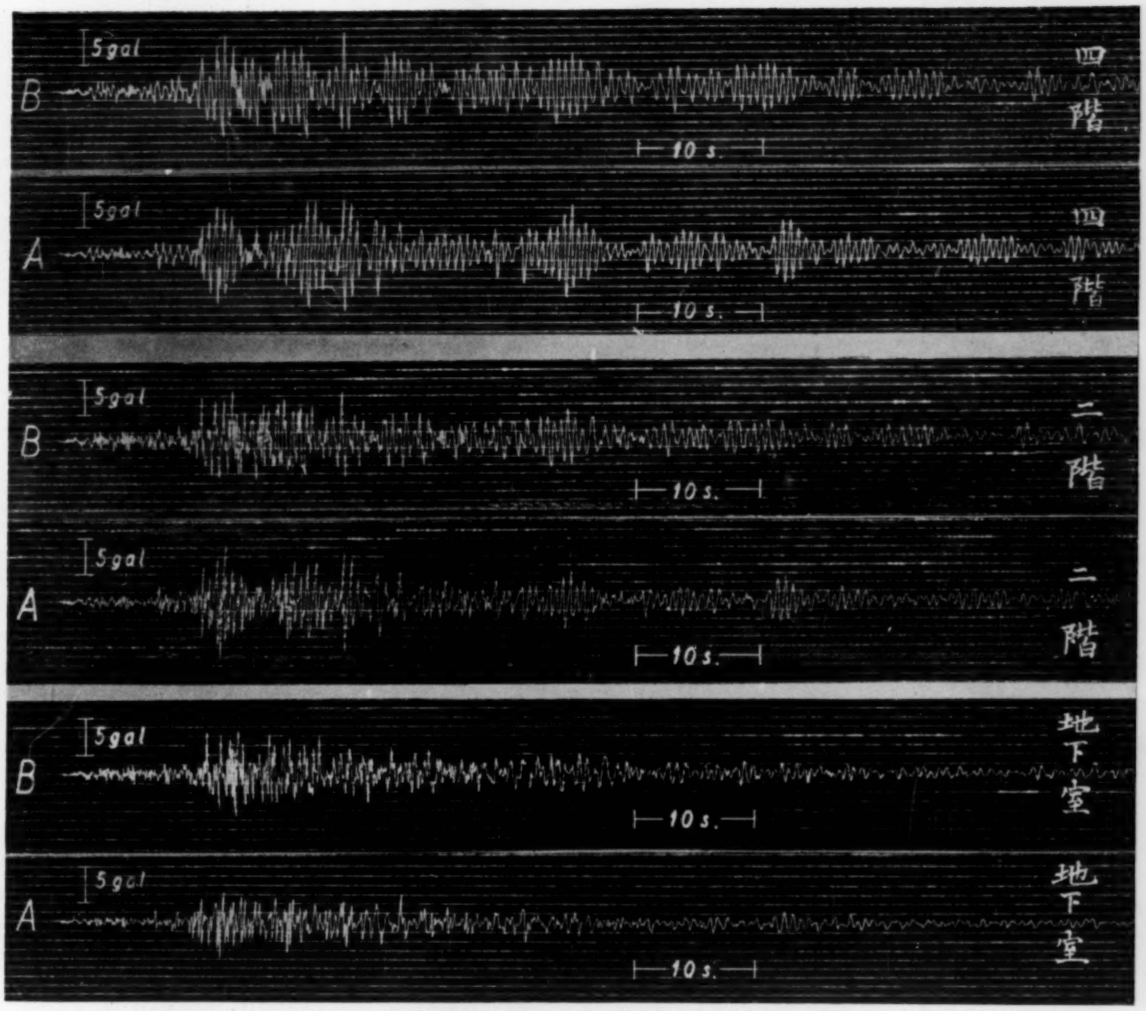

第 15 圖　發震時　昭和 10 年 2 月 20 日 5 時 10 分頃
震　源　東經 140·5 度，北緯 35·4 度，深さ 30 粁
震　度　II

11. *Energy Dissipation in Seismic Vibrations of Actual Buildings of Unlike Structure.*

By Katsutada SEZAWA and Kiyoshi KANAI,

Earthquake Research Institute.

(Read Oct. 15, 1935.—Received Dec. 20, 1935.)

1. In our last paper[1] we discussed the nature of decay in the seismic vibrations of three actual buildings of different stories, namely, 3–, 4–, and 5–, storied reinforced concrete structures, all owned by the Mitsubishi Co. The assumption in the problem regarding the condition of the floors was that the beams, etc., forming the members of the floors, are of such rigid construction that the inclination of columns at both their ends always remains vertical even in seismic vibrations[2]. It may appear improbable that exactly such conditions could exist in an actual building, and although the inclination under consideration in vibratory condition would differ somewhat, it would be very slight, compared with the undisturbed condition. It follows then that, although the nature of decay in seismic vibrations differs very little with conditions, the period of free oscillations of the building differs appreciably from that of the case in which the floor is extremely rigid.

With a view to ascertaining thoroughly the nature of the condition just mentioned, we investigated the vibration problem of three structures (one of which was studied in the previous case) under different assumptions regarding the condition of the structual connection between the vertical members and the floors. The two possible extreme conditions are a structure in which the floors are so infinitely rigid that they cannot bend and one in which the floors are so flexible that they are unable to impart any elastic resistance to horizontal oscillations. The buildings now under discussion were restricted to 3-storied reinforced concrete structures, the details of whose costruction were kindly supplied by the Mitsubishi Co., the owner of these buildings. One of these called the annexe of the Middle 7 th House

1) K. SEZAWA and K. KANAI, "Energy Dissipation in Seismic Vibrations of Actual Buildings", *Bull. Earthq. Res. Inst.*, **13** (1935), 925~941,

2) Appropriateness of such a condition in actual buildings will be seen from our paper, *Bull. Earthq. Res. Inst.*, **12** (1934), 804~822.

(Naka 7 gô-kan Bekkan) and constructed in March 1925, has no basement; that called the annexe of the middle 8 th House (Naka 8 gô-kan Bekkan) built on July 1926 has a basement; while the remaining one numbered Middle 13 th House (Naka 13 gô-kan) which was described in the last paper[3], completed in April 1915, also has a basement. The first two are let for restaurants (now "Tikuyôtei" and "Tokiwa-ya" respectively) and the last for business offices.

The methods of calculation were shown in a preceding paper[4]. As to the correction due to the effect of the basement, we calculated on the assumption mentioned in the last paper[5].

As will presently be seen, notwithstanding the exceedingly long periods of vibration of the structure having extremely flexible floors, it is still possible for the vibrational energy to dissipate into the ground at such a rate (though in somewhat less degree) that the amplitudes under resonance conditions are not very marked.

2. *Annexe of Middle 7th House* (Naka 7 gô-kan Bekkan).

The general plan of all the floors being virtually the same, we have given a sketch of only the first floor (Nikai), besides a photograph of a profile of the building. Neither construction plans of the different parts of the building nor details of our calculation will be given here owing to the difficulty of presenting them in simple form. The total areas and moments of inertia of cross section of the vertical members, and the total mass concentrated on every floor (the mass of the columns and walls are concentrated on the floor next above them) are shown in Table I. In this table, it is assumed that $E=2\cdot1.10^9\ \mathrm{kg}/m^2=2\cdot1.10^9.9\cdot8$ kg mass m/s²/m², $\rho=2.10^3$ kg mass/m³, $\mu=8.10^7$ kg mass/ms² (corresponding to $\sqrt{\mu/\rho}=200$ m/s). Here again, it is possible to put $I_1=I_2=\cdots\cdots=I$, $m_1=m_2=\cdots\cdots=m$, $l_1=l_2=\cdots\cdots=l$, where I, m, l are the mean values of the respective quantities.

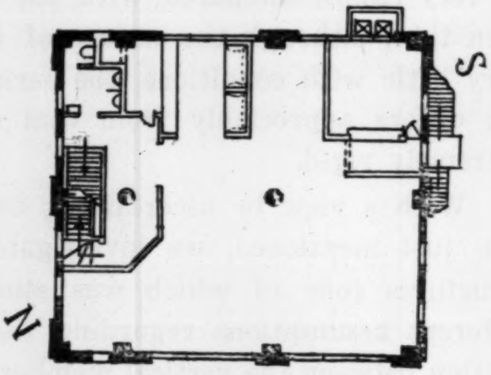

Fig. 2. Naka 7 gô-kan Bekkan. Scale 1/300.

3) K. SEZAWA and K. KANAI, *loc. cit.*, 1).

4) K. SEZAWA and K. KANAI, "Energy Dissipation in Seismic Vibrations of a Framed Structure", *Bull. Earthq. Res. Inst.*, **13** (1935) 698~714.

5) K. SEZAWA and K. KANAI, *ibid.*, 3).

Table I. Annexe of Middle 7th House.
(Naka 7 gô-kan Bekkan)

Floor		1 st	2 nd	Roof	Mean
Height of floor below	l (m)	4·397	3·484	3·789	3·890
Sect. area of columns and walls	a (m²)	9·500	6·648	5·840	7·329
Mt. inertia of columns and walls	I (m⁴)	0·807	0·396	0·390	0·531
Sect. area of columns	a (m²)	7·090	3·420	2·414	4·308
Mt. inertia of columns	I (m⁴)	0·6709	0·0811	0·0382	0·263
Beams volume	(m³)	15·21	15·21	13·29	14·57
Beams weight	(kg)	$0{\cdot}365.10^5$	$0{\cdot}365.10^5$	$0{\cdot}319.10^5$	$0{\cdot}350.10^5$
Floors volume	(m³)	9·83	9·83	9·14	9·60
Floors weight	(kg)	$0{\cdot}236.10^5$	$0{\cdot}236.10^5$	$0{\cdot}219.10^5$	$0{\cdot}230.10^5$
Columns volume	(m³)	26·03	9·54	7·33	14·30
Columns weight	(kg)	$0{\cdot}625.10^5$	$0{\cdot}229.10^5$	$0{\cdot}176.10^5$	$0{\cdot}343.10^5$
Walls volume	(m³)	10·61	11·59	13·20	11·80
Walls weight	(kg)	$0{\cdot}255.10^5$	$0{\cdot}278.10^5$	$0{\cdot}317.10^5$	$0{\cdot}283.10^5$
Total weight	(kg)	$1{\cdot}481.10^5$	$1{\cdot}108.10^5$	$1{\cdot}031.10^5$	$1{\cdot}207.10^5$
Area of floor	(m²)	145·5	145·5	145·5	145·5
$\frac{1}{a}\sqrt{\frac{mEI}{l^3\rho\mu}}$ Columns+walls		1·532[6]	1·535[6]	1·730[6]	1·615
$\frac{1}{a}\sqrt{\frac{mEI}{l^3\rho\mu}}$ Columns		1·878[6]	1·355[6]	1·318[6]	1·935

The periods of the free oscillation in the case without dissipation are determined from

$$\sqrt{\gamma}=\frac{2\pi}{T}\sqrt{\frac{ml^3}{EI}},$$

where $\gamma=2{\cdot}3765$, $18{\cdot}6630$, $38{\cdot}9605$ for the case in which the floors and beams are extremely rigid, and $\gamma=0{\cdot}08555$, $3{\cdot}6676$, $26{\cdot}4776$ for the case in which the floors and beams are extremely flexible. The periods (in sec) of free oscillations of the movement in NS-direction in different conditions of loading and resistance of the vertical members are shown in Table II. This table indicates that, although the periods of free vibrations corresponding to the case of extremely rigid floors are somewhat less than those actually observed in similar structures, the periods of vibrations corresponding to the case of extremely flexible floors are too long to be accepted as being their near values.

6) The respective mean values for l and m were used.

Table II. Period in sec.

Floor condition		Rigid	Flexible
Vertical member =columns+walls	Without live load	0·104, 0·037, 0·0257	0·547, 0·0837, 0·0311
	With live load	0·125, 0·0446, 0·0309	0·659, 0·101, 0·0374
Vertical members =columns alone	Without live load	0·147, 0·0525, 0·0364	0·776, 0·119, 0·0441
	With live load	0·177, 0·0633, 0·0439	0·935, 0·143, 0·0531

The maximum values of bending moments $M=E_sI_s(d^2y_s/dx_s^2)$ at each end of the columns corresponding to the maximum of the acceleration $(2\partial^2u/\partial t^2)$ of the ground (on which no structurs is standing and in which $\lambda=14\mu$) were determined from the equations shown in the preceding paper[7], namely,

(i) The floors rigid, and $E_1=E_2=E_3$, $I_1=I_2=I_3$, $l_1=l_2=l_3$, $m_1=m_2=m_3$,

$$y_1=\frac{\left(7\sqrt{\frac{\lambda}{\mu}+2}-4\right)}{4\sqrt{P^2+Q^2}}\left[(\gamma^3-60\gamma^2+864\gamma-1728)\right.$$

$$\left.-\gamma(12-\gamma)(36-\gamma)\left\{3\left(\frac{x_1}{l}\right)^2+2\left(\frac{x_1}{l}\right)^3\right\}\right]\cos\left(pt-\tan^{-1}\frac{P}{Q}\right),$$

$$y_2=\frac{3\left(7\sqrt{\frac{\lambda}{\mu}+2}-4\right)}{\sqrt{P^2+Q^2}}\left[-(\gamma^2-36\gamma+144)\right.$$

$$\left.-\gamma(24-\gamma)\left\{3\left(\frac{x_2}{l}\right)^2+2\left(\frac{x_2}{l}\right)^3\right\}\right]\cos\left(pt-\tan^{-1}\frac{P}{Q}\right),$$

$$y_3=\frac{-36\left(7\sqrt{\frac{\lambda}{\mu}+2}-4\right)}{\sqrt{P^2+Q^2}}\left[(12-\gamma)\right.$$

$$\left.+\gamma\left\{3\left(\frac{x_3}{l}\right)^2+2\left(\frac{x_3}{l}\right)^3\right\}\right]\cos\left(pt-\tan^{-1}\frac{P}{Q}\right),$$

7) K. SEZAWA and K. KANAI, *Bull. Earthq. Res. Inst.*, **18** (1935), 698~714.

where

$$P=-9\sqrt{\frac{\lambda}{\mu}+2}\left(\frac{Ej^2}{\mu kl^3}\right)\gamma(12-\gamma)(36-\gamma),$$

$$Q=\left(\sqrt{\frac{\lambda}{\mu}+2}-1\right)(\gamma^3-60\gamma^2+864\gamma-1728),$$

(ii) The floors flexible, and $E_1=E_2=E_3$, $I_1=I_2=I_3$, $l_1=l_2=l_3$, $m_1=m_2=m_3$,

$$y_1=\frac{\left(7\sqrt{\frac{\lambda}{\mu}+2}-4\right)}{2\sqrt{P^2+Q^2}}\left\{2(13\gamma^3-393\gamma^2+1296\gamma-108)\right.$$

$$+3\gamma(-19\gamma^2+294\gamma-216)\left(\frac{x_1}{l}\right)^2$$

$$\left.+\gamma(-31\gamma^2+372\gamma-108)\left(\frac{x_1}{l}\right)^3\right\}\cos\left(pt-\tan^{-1}\frac{P}{Q}\right),$$

$$y_2=\frac{3\left(7\sqrt{\frac{\lambda}{\mu}+2}-4\right)}{2\sqrt{P^2+Q^2}}\left\{4(-23\gamma^2+171\gamma-18)\right.$$

$$+\gamma(7\gamma^2-216\gamma+324)\left(\frac{x_2}{l}\right)+6\gamma(2\gamma^2-13\gamma-18)\left(\frac{x_2}{l}\right)^2$$

$$\left.+\gamma(5\gamma^2+10\gamma-24)\left(\frac{x_2}{l}\right)^3\right\}\cos\left(pt-\tan^{-1}\frac{P}{Q}\right),$$

$$y_3=\frac{3\left(7\sqrt{\frac{\lambda}{\mu}+2}-4\right)}{2\sqrt{P^2+Q^2}}\left[12(3\gamma^2+23\gamma-6)+2\gamma(-\gamma^2-15\gamma+234)\left(\frac{x_3}{l}\right)\right.$$

$$\left.-\gamma(\gamma^2+36\gamma+12)\left\{3\left(\frac{x_3}{l}\right)^2+\left(\frac{x_3}{l}\right)^3\right\}\right]\cos\left(pt-\tan^{-1}\frac{P}{Q}\right),$$

where

$$P=9\sqrt{\frac{\lambda}{\mu}+2}\left(\frac{Ej^2}{\mu kl^3}\right)\gamma(-31\gamma^2+372\gamma-108),$$

$$Q=4\left(\sqrt{\frac{\lambda}{\mu}+2}-1\right)(13\gamma^3-393\gamma^2+1296\gamma-108).$$

The calculated bending moments due to vibrations in NS-direction of the case in which, the floor being extremely rigid, the resistance

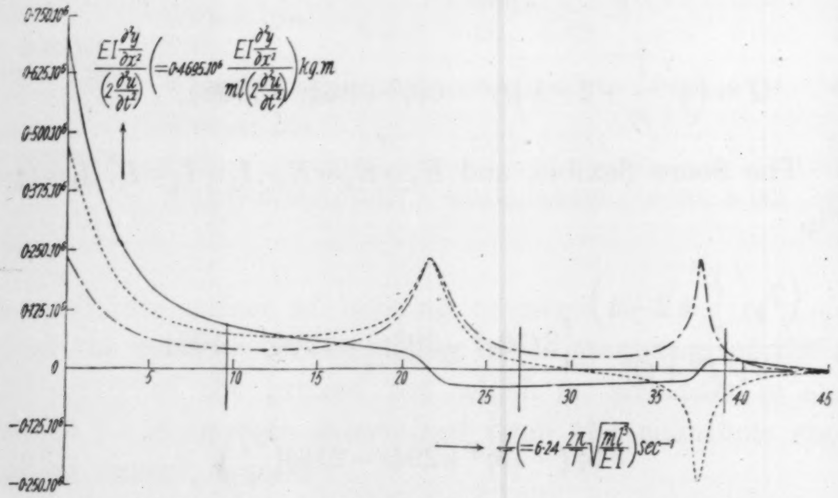

Fig. 3 Naka 7 gô-kan Bekkan. NS-movement (with extremely rigid floors), walls being attached to columns. Full, broken, and chain lines represent moments in columns of ground, first, and second floors respectively.

to bending of columns as well as walls, are shown in Fig. 3, whereas similar moments of the case in which, the floor being extremely flexible, the bending is resisted by the columns alone, is shown in Fig. 4. In both these cases, there is no live load on any floor, and it is to be

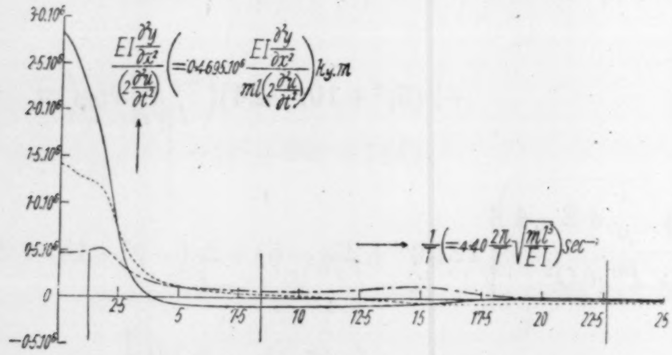

Fig. 4. Naka 7 gô-kan Bekkan. NS-movement (with extremely flexible floors), columns alone being resisting members. Full, broken, and chain lines represent moments in columns of ground, first, and second floors respectively.

remembered that the dimensions of E should be taken in kg mass $m/s^2/m^2$ and that of $2(\partial^2 u/\partial t^2)$ in m/s^2. The vertical strips in these figures represent cases corresponding to resonance conditions in the case without any dissipation.

These figures show that the bending moments of the columns, etc., even under resonance, are not very marked, provided the values of the acceleration at any period are the same. The moments under resonance in the case of extremely rigid floors are rather less than those at periods out of resonance, whereas the moments under resonance in the case of extremely flexible floors indicate a somewhat different aspect, namely, the moments under resonance are not necessarily smaller than those at periods out of resonance. Upon comparing these two cases it will be seen that making the floors as rigid as possible diminishes the bending moments especially the vertical members in periods approaching resonance. It used to be held that rigid connection of floors with the vertical members diminishes the moments in the case of zero frequency of vibrations, but the present investigation shows that such rigid connection is more advantageous in decreasing the moments under resonance conditions.

It is also a remarkable fact that the bending moments in the columns below the first floor, particularly in the case in which the floors are extremely rigid, become very small at frequencies beyond the first (principal) resonance condition.

If, in order to ascertain the extent to which stress is induced in the structure, we assume that the acceleration of the ground is $2(\partial^2 u/\partial t^2) = g/10$, then, in the former case, namely in the case in which the floors are extremely rigid,

maximum stress in wall $= 15{\cdot}07$ kg/cm^2,

do. in column $= 8{\cdot}24$ kg/cm^2,

while, in the latter case, namely in the case in which floors are extremely flexible,

maximum stress in column $= 66{\cdot}4$ kg/cm^2.

These values are possible only in vibrations of zero frequency.

3. *Annexe* of *Middle 8th House* (Naka 8 gô-kan Bekkan).

For the same reason as in the preceding case, we show a photographic view as well as the general plan of the first floor. While no details of the numerical calculation will be given here, the total areas and moments of inertia of the vertical members and the total mass concentrated on every floor etc., are shown in Table III.

To arrive at the mean height of the floors, we added 1/3 of the part of the basement height to the actual mean between floor height from the ground to the second floors. The assumptions regarding the values of E, ρ, μ are the same as in the preceding case. The periods of free vibrations in NS-direction under different conditions of loading and resistance of the vertical members are shown in Table IV.

This table shows that the periods of vibrations corresponding to the extremely flexible floors are too long to be expected in the case of ordinary buildings.

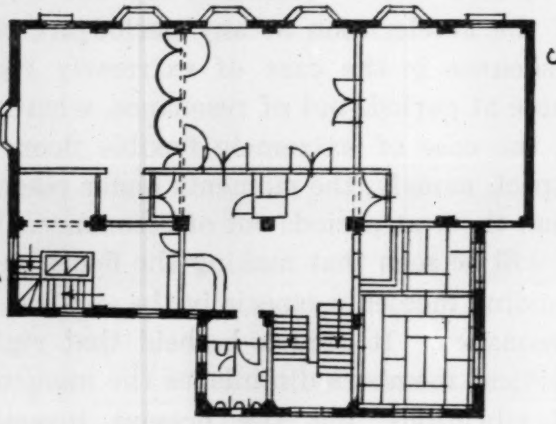

Fig. 6. Naka 8gô-kan Bekkan.
Scale 1/300.

The maximum bending moments due to vibrations in NS-direction were calculated by using the same equations as shown in the last section. Fig. 7 represents the case in which both columns and walls are taken as resisting members, the floors being assumed to be infinitely rigid, and Fig. 8 the case in which the columns

Table III. Annexe of Middle 8 th House.
(Naka 8 gô-kan Bekkan)

Floor		1 st	2 nd	Roof	Mean
Height of floor below	l (m)	3·635	3·332	3·795	3·587+0·252
{ Sect. area of columns and walls	a (m²)	13·59	12·42	11·16	12·39
{ Mt. inertia of columns and walls	I (m⁴)	1·171	1·354	1·312	1·279
{ Sect. area of columns	a (m²)	8·992	7·301	5·412	7·235
{ Mt. inertia of columns	I (m⁴)	0·245	0·178	0·105	0·176
Beams { volume	(m³)	15·57	14·62	10·04	13·41
Beams { weight	(kg)	$0·374.10^5$	$0·351.10^5$	$0·241.10^5$	$0·322.10^5$
Floors { volume	(m³)	20·90	20·92	19·17	20·33
Floors { weight	(kg)	$0·502.10^5$	$0·503.10^5$	$0·460.10^5$	$0·488.10^5$
Columns { volume	(m³)	26·83	20·13	16·91	21·29
Columns { weight	(kg)	$0·645.10^5$	$0·483.10^5$	$0·406.10^5$	$0·511.10^5$
Walls { volume	(m³)	28·39	29·56	33·34	30·43
Walls { weight	(kg)	$0·653.10^5$	$0·680.10^5$	$0·768.10^5$	$0·700.10^5$
Total weight	(kg)	$2·174.15^5$	$2·017.10^5$	$1·875.10^5$	$2·022.10^5$
Area of floor	(m²)	234·3	234·3	234·3	234·3
$\frac{1}{a}\sqrt{\frac{mEI}{l^3\rho\mu}}$ { Columns+walls		1·705[8)]	2·004[8)]	2·200[8)]	1·959
$\frac{1}{a}\sqrt{\frac{mEI}{l^3\rho\mu}}$ { Columns		1·184[8)]	1·240[8)]	1·285[8)]	1·245

8) The values of l and m were taken similarly as in the last example.

Table IV. Periods in sec.

Floor condition		Rigid	Flexible
Vertical members =columns+walls	Without live load	0·085, 0·0303, 0·021	0·448, 0·0685, 0·0255
	With live load	0·102, 0·0363, 0·0251	0·535, 0·0819, 0·0304
Vertical members =columns alone	Without live load	0·229, 0·0817, 0·0566	1·208, 0·185, 0·0686
	With live load	0·274, 0·0977, 0·0677	1·442, 0·221, 0·0820

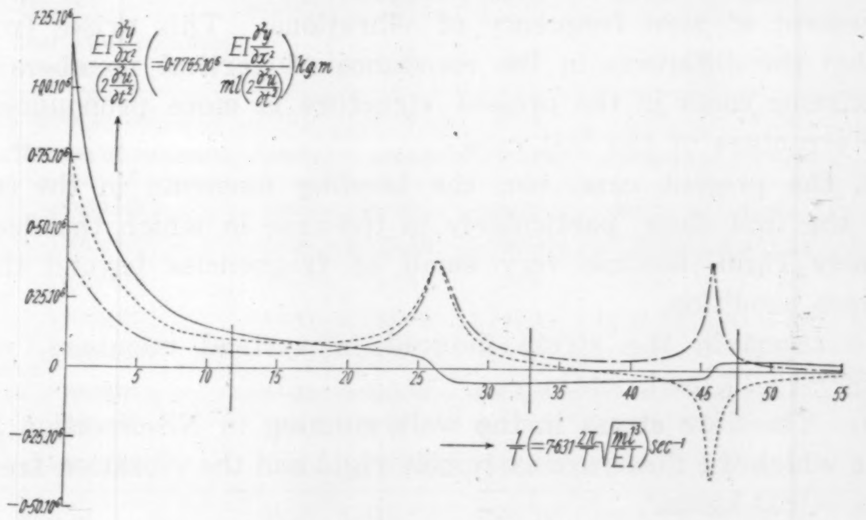

Fig. 7. Naka 8 gô-kan Bekkan. NS-movement (with extremely rigid floors), walls being attached to columns. Full, broken, and chain lines represent moments in columns of ground, first, and second floors respectively.

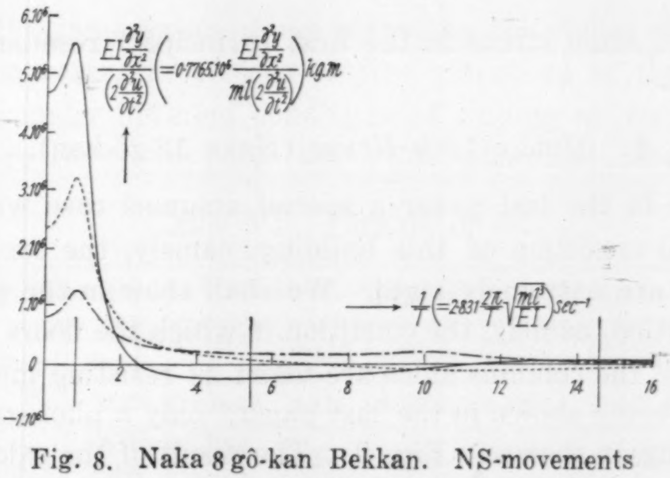

Fig. 8. Naka 8 gô-kan Bekkan. NS-movements (with extremely flexible floors), columns alone being resisting members. Full, broken, and chain lines represent moments in columns of ground, first, a⁻d second floors respectively.

alone resist vibrations, the floors being assumed to be extremely flexible. The difference in the feature of the bending moment curves for the present structure with the assumed difference in its structural conditions, namely the difference between the case in which the floor is extremely rigid and the one in which the floor is extremely flexible, is almost similar to that in the case of the Annexe of the Middle 7th House. But, in the present case, if the floors be extremely flexible and the columns alone be resisting members, the bending moment in the first (principal) resonance condition would be rather larger than the moment at zero frequency of vibrations. This arises from the fact that the difference in the resistance of vertical members of the two extreme cases in the present structure is more pronounced than in the structure of the last case.

In the present case, too, the bending moments in the columns below the first floor, particularly in the case in which the floors are extremely rigid, become very small at frequencies beyond the first resonance condition.

To ascertain the stress induced in vertical members, we put $2(\partial^2 u/\partial t^2)=g/10$, and obtain

(i) The fibre stress in the walls running in NS-direction for the case in which the floors are extremely rigid and the vibration frequency is zero $=9{\cdot}31$ kg/cm^2,

(ii) The fibre stress in the columns attached to the walls in the same case as (i) at zero frequency of vibrations $=2{\cdot}756$ kg/cm^2,

(iii) The fibre stress in the columns for the case in which the floors are extremely flexible and the vibration frequency is zero $=80{\cdot}3$ kg/cm^2,

(iv) The same stress in the first (principal) resonance condition $=94{\cdot}5$ kg/cm^2.

4. *Middle 13th House* (Naka 13 gô-kan).

We gave in the last paper a special assumed case with regard to the structural condition of this building, namely, the condition where in the floors are extremely rigid. We shall show in the present paper another condition, namely, the condition in which the floors are extremely flexible and the columns alone are taken as resisting members. The general plan being shown in the last paper,[9] only a photographic profile of the building is shown in Fig. 9. The result of the calculation with respect to the important elements is shown in Table V, although some of the elements were partly described in the last paper. The method

9) K. SEZAWA and K. KANAI, *loc. cit.*, 1).

of making the correction to be made for intermediate floor heights due to presence of the basement is the same as in the preceding case.

Table V. Middle 13th House (Naka 13 gô-kan).

Floor			Ground	1 st	2 nd	Rcof	Mean
Height of floor below		l (m)	2·58	3·82	3·52	3·52	3·62+0·32
Sect. area of columns and walls		a (m²)	33·83	31·34	31·34	22·66	28·45
Mt. inertia of columns and walls		I (m⁴)	11·23	2·54	2·54	2·54	2·54
Sect. area of columns		a (m²)	10·98	10·98	8·25	8·25	9·16
Mt. inertia of columns		I (m⁴)	0·1043	0·1043	0·0748	0·0743	0·0846
Beams	volume	(m³)	46·75	46·19	46·75	47·02	46·65
	weight	(kg)	$1{\cdot}123.10^5$	$1{\cdot}109.10^5$	$1{\cdot}123.10^5$	$1{\cdot}129.10^5$	$1{\cdot}120.10^5$
Foors	volume	(m³)	72·54	72·54	72·54	72·54	72·54
	weight	(kg)	$1{\cdot}741.10^5$	$1{\cdot}741.10^5$	$1{\cdot}741.10^5$	$1{\cdot}741.10^5$	$1{\cdot}741.10^5$
Columns	volume	(m³)	18·85	27·97	25·32	25·32	26·20
	weight	(kg)	$0{\cdot}453.10^5$	$0{\cdot}672.10^5$	$0{\cdot}608.10^5$	$0{\cdot}608.10^5$	$0{\cdot}629.10^5$
Walls	volume	(m³)	87·3	110·50	101·75	71·27	94·51
	weight	(kg)	$2{\cdot}095.10^5$	$2{\cdot}653.10^5$	$2{\cdot}442.10^5$	$1{\cdot}711.10^5$	$2{\cdot}269.10^5$
Total weight		(kg)	$5{\cdot}412.10^5$	$6{\cdot}106.10^5$	$5{\cdot}845.10^5$	$5{\cdot}120.10^5$	$5{\cdot}690.10^5$
Area of floor		(m²)	600	600	600	600	600
$\frac{1}{a}\sqrt{\frac{mEI}{l^3\rho\mu}}$	Columns+walls		1·670[10]	1·854[10]	1·854[10]	2·625[10]	1·939
	Columns		1·018[10]	1·018[10]	1·144[10]	1·144[10]	1·100

Under the same assumptions regarding the values of E, ρ, μ as in the preceding cases, the periods of free vibrations of the structure in NS-direction under different conditions of loading as well as of elastic resistance, are shown in Table VI. The abnormal largeness of the

Table VI. Periods in sec.

Floor condition		Rigid	Flexible
Vertical members =columns+walls	Without live load	0·110, 0·0375, 0·0260	0·554, 0·0846, 0·0314
	With live load	0·118, 0·0421, 0·0291	0·621, 0·095, 0·0353
Vertical members =columns alone	Without live load	0·577, 0·206, 0·142	3·035, 0·464, 0·173
	With live load	0·647, 0·231, 0·160	3·405, 0·521, 0·194

10) The values of l and m were taken similarly as in the last two cases.

periods arising from the conditions that the floors are extremely flexible and that the columns alone are resisting members, is particularly pronounced in the present case.

The maximum values of the bending moments at each end of the columns, when the floors are assumed extremely flexible and the columns alone are the resisting members, are shown in Fig. 10. In this case, the moments under resonance conditions are very marked.

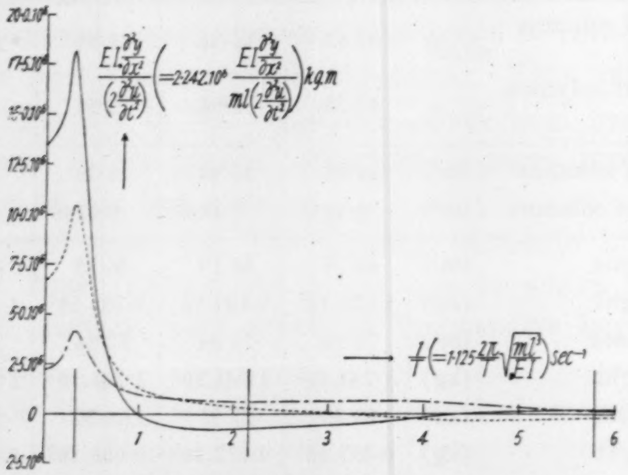

Fig. 10. Naka 13 gô-kan. NS-movement (with extremely flexible floors), columns alone being resisting members. Full, broken, and chain lines represent moments in columns of ground, first, and second floors respectively.

The bending stresses at zero frequency of vibrations, as well as under the first (principal) resonance condition, are shown below.

(i) Fibre stress in columns at zero frequency $=361\ \mathrm{kg/cm^2}$,

(ii) Same under resonance $=473\ \mathrm{kg/cm^2}$.

These stresses are induced in the columns below the first floor. It will be seen how large stresses would be induced in the columns were the condition of the problem so adjusted that the bending moments under resonance condition assume large values.

5. *Comparison of results and conclusion.*

We have now obtained the periods of free oscillations of three 3-storied structures as well as the bending moments induced in the vertical members of these structures due to a prescribed acceleration of the ground. The bending moment curves present somewhat different features according as the periods of the respective structures themselves differ. If (a) denote the case in which the floors are infinitely rigid and the columns and walls are resisting members, and (b) the case in which the floors are extremely flexible and the columns alone are

resisting members, then the ratio of the period of fundamental free vibrations (principal period) in case (b) to that in case (a); the ratio of the bending moment under resonance to that at zero frequency of vibration for case (a); and the same ratio for case (b) are all shown in Table VI.

Table VII.

Name of structure	Fnnd. T in (b) / Fund. T in (a)	Mt. in (a) at reson. / Mt. in (a) at zero freq.			Mt. in (b) at reson. / Mt. in (b) at zero freq.		
		Ground col.	1st col.	2nd col.	Ground col.	1st col.	2nd col.
Annexe of Mid. 7. Ho.	7·47	0·133	0·160	0·180	0·741	0·875	1·050
Annexe of Mid. 8. Ho.	14·2	0·110	0·132	0·140	0·14	1·37	1·60
Mid. 13. Ho.	27·6	0·109	0·128	0·139	0·30	1·55	1·85

This table shows that, whereas the ratio of the bending moment under resonance to that at zero frequency in case (b) increases with increase in the ratio of the period in (b) to that in (a), the same ratio of the bending moments in (a) diminishes somewhat with increase in the period ratio under consideration. The fact that the ratio of the bending moments in question in case (b) is much greater than that in case (a), is too obvious to need further comment.

From the experimetal data due to observers who have studied other buildings, it appears that the actual vibration periods of the structures are somewhat longer than those calculated by assuming infinitely rigid floors,[11] but much shorter than those calculated by assuming extremely flexible floors. This suggests that the conditions of the floors and beams differ slightly from an extremely rigid one. Even if the floors were not extremely rigid the moment ratios already mentioned would not go outside the two limiting values, as shown in Table VII, namely cases (b) and (a) as upper and lower critical limits. It is thus possible to ascertain both of these critical limits in the nature of the dissipation of vibrational energy into the ground.

Even if the floor were assumed extremely flexible, which could never be the case in actual structures, the bending moments under resonance conditions would not differ much from those in the case of

11) It is obvious from our preceding paper (*loc. cit.*, 2)) that, if the floors be infinitely rigid, the vibration period of a structure is proportional to its height. From SAITA'S study by means of results of observations, which were shown in papers, K. SUYEHIRO, *Proc. American Soc. Civ. Eng.*, **58** (1932), No. 4, as well as P. BYERLY, J. HESTER, & K. MARSHALL, *Bull. Seism. Soc. America*, **21** (1931), 268~278, the condition of such proportionality seems nearly satisfied in actual buildings.

zero frequency, both under the same acceleration of the ground, in which no structure is standing. This conclusion however seems to be valid only in the case of buildings of moderate height. In the case of high buildings, the bending moments under resonance conditions would not assume such small values were the floors extremely flexible; in other words, dissipation of the vibrational energy in such a condition would not be very large.

The most important fact related to condition (b) is that the peaks in the bending moment curves (namely, the peaks between successive resonance frequencies) are not so marked as those in the bending moment curves of case (a). Thus, the curves in case (b) gradually die away with increase in vibration frequency. Another fact to which attention is called is that, notwithstanding their largeness in zero frequency, the bending moments in the columns below the first floor, particularly in case (a), become very small at frequencies beyond the first resonance condition. The fact as observed, that damage to a building in a great earthquake occurs in the vertical members on the 1st or 2nd floor rather than in those on the ground floor, seems thus to ascertain that the floors is nearly extremely rigid. This, together with the remarks given in footnote 11) on the vibration periods of actual buildings, gives us the confirmation on the conditions of floors in actual buildings.

In conclusion, we take this opportunity of expressing our thanks to the members of the staff of the Mitsubishi Co, through whose courtesy valuable data were obtained for the present study, and also to the Council of the Foundation for the Promotion of Scientific and Industrial Research of Japan, for aid that greatly assisted our work.

Fig. 1. Naka 7 gô-kan Bekkan.

Fig. 2. Naka 8 gô-kan Bekkan.

Fig. 9. Naka 13 gô-kan.

11. 三菱仲7號館別館，仲8號館別館，仲13號館の種々の狀態に於ける震動勢力の逸散性

地震研究所 ｛妹澤克惟
金井清

前の論文で實在の3階4階5階の建物の震動逸散性を述べた場合には，床の固定狀態が極端に剛いといふ條件のもとに震動を取扱つたけれども，その固定狀態が多少違つてゐるときには固有振動週期は別として勢力逸散性に非常な影響があるかどうかを見る爲にこの研究を試みたものである．今回も三菱地所課の御好意によつて題名の如き3種の建物（何れも地上3階鐵筋コンクリート造）を選んで研究することができた．狀態の變化といふのは(a)床が極端に剛い場合と(b)床が極端に軟く從て水平動に對して何等の彈性的抵抗を與へぬ場合とである．尙附加へて構造壁が抵抗を及ぼさぬ場合をも考へて見たのである．

(a)の場合の固有週期は他の建物の觀測から推定されるものよりも稍短く算出されるけれども，(b)の場合の固有週期は如何に考へてもありそうもない程長くなるものである．さて，震動勢力が地中へ逸散するために，種々の地震動週期による建物の屈曲モーメントが如何なる値を取るかをしらべて見ると，(b)の場合と雖も3階建の場合には逸散性がそれ程少くはならぬやうに思はれる．しかし共振附近のモーメントが零の frequency の場合と同じ位かそれよりも稍大きい位のものである．

(a)の場合に1階にある柱や壁に起る屈曲モーメントは，zero frequency では最も大きいのに拘らず第1次共振以上の frequency では非常に小さくなる．(b)の場合には何れの床の柱と壁に起る屈曲モーメントも frequency の増加と共に漸次同じやうに小さくなるから，1階だけが屈曲モーメントが小さくなるとはいはれない．この事柄は地震動で4階や3階に被害が多い事に照して面白い現象と思はれ，同時に床を相當に剛い狀態にあるものと假定する方が實際に近いことがわかるのである．別に，齊田理學士が種々の建物の固有週期を比較して見たところが，その週期が大體に於て建物の高さに正比例することがわかつた．これは我々が彙報第12號に於て述べたやうに床が極端に剛い場合にのみ取り得る週期の割合であるから，齊田理學士の比較は結局建物の床が非常に剛いことを證明するのに他ならぬ譯である．卽ち，逸散性を考へたときに地震動のための被害と，固有週期の比較とから同時に床の剛さの程度がわかつた譯である．

たとひ床の狀態が極端に剛くないとしても，共振の場合の振幅が，床の極端に軟い場合以上には出ないことがわかるのである．又，(b)の狀態に於ける固有週期と(a)の狀態に於ける固有週期との比が大きな建物では，(b)の共振に於ける屈曲モーメントと(b)の零の frequency に於ける屈曲モーメントとの比が大きな値を取る．然るにその場合(a)の共振に於ける屈曲モーメントと(a)の零の frequency に於ける屈曲モーメントとの比は小さな値を取るものである．

ここに注意すべきことは，只今の研究では3階の場合だけを比較したのであつて高層建築の場合はどうなるかわからない．高層建築の場合には床を極端に軟くすると，恐らく逸散性が非常に減じ，共振の振幅が比較的に大きくなるもののやうに思はれる．

この論文では床や壁の種々の場合を態と論じたけれども，實際の建物がその樣な種々の狀態を取る譯ではなく，寧ろ床が極端に剛い場合の狀態，卽ち共振に於ける屈曲モーメントが非常に小さくなる場合が事實に最も近いのであつて，この論文の目的もそれを確めることにあつたのである．

12. *Energy Dissipation in Seismic Vibrations of a Six-storied Structure. Coincidence of Resonance and Corresonance.*

By Katsutada SEZAWA and Kiyoshi KANAI,

Earthquake Research Institute.

(Read Dec.17, 1935.—Received Dec. 20, 1935.)

1. Introduction.

After a protracted investigation we have at last succeeded in ascertaining the nature of energy dissipation, etc., in the seismic vibrations of a framed multistoried structure, but not exceeding 5-stories.[1)~6)] With this reservation in the number of stories, various problems in seismic vibrations, namely, the periods of free vibrations, the nature of forced vibrations both with and without energy dissipation, the same problems as applied to actual buildings, and the effect of structural conditions on the energy dissipation, etc., have been solved. For actual examples, the following buildings, owned by the Mitsubishi Co. are here discussed, namely, the annexe of the Middle 7th House, Annexe of the Middle 8th House, and the Middle 13th House for the case of a 3-storied structure; No. 6 of the Middle 12th Lot of Houses for that of a 4-storied structure, and the Annexe of the East 7th House for that of a 5-storied one. Mathematical formulae for treatment of the problem in the case of buildings of less than five stories have also been worked out to our satisfaction.

But we had not yet formulated a theory of dissipation for the

---

1) K. SEZAWA and K. KANAI, "Some New Problems of Free Vibrations of a Structure", *Bull. Earthq. Res. Inst.*, **12** (1934), 804~822.

2) Ditto, "Some New Problems of Forced Vibrations of a Structure", *ibid.*, **12** (1934), 823~853.

3) Ditto, "Decay in Seismic Vibrations of a Simple or Tall Structure by Dissipation of their Energy into the Ground", *ibid.*, **13** (1935), 681~697.

4) Ditto, "Energy Dissipation in Seismic Vibrations of a Framed Structure", *ibid.*, **13** (1935), 698~714.

5) Ditto, "Energy Dissipation in Seismic Vibrations of Actual Buildings.," *ibid.*, **13** (1935), 921~941.

6) Ditto, "Energy Dissipation in Seismic Vibrations of Actual Buildings in Different Structural Conditions," *ibid.*, **14** (1936), 110–120.

case of actual buildings higher than six stories. Through the courtesy of the Mitsubishi co., we had access to data regarding their Middle 28th House, and these enabled us to proceed with the problem for a 6-storied structure, the important mathematical formulae having been worked out specially for the purpose.

2. Mathematical Formulae for a 6-storied Structure with Rigid Floors and Clamped Base.

We have already given in a previous paper the general formula for an n-storied structure with rigid floors and clamped base[7]. Using equations (13)$\sim$(20) from that paper, it is possible to obtain A_1, B_1, C_1, D_1, ..., A_6, B_6, C_6, D_6 as follows. In these equations, $\gamma_s = m_s p^2 l_s^3 / E_s I_s$, and m_s is the mass concentrated on the s th floor.

$$
\left.\begin{aligned}
A_1\Phi &= \eta_4\{\eta_5(\gamma_5-12)(\gamma_6-12)-12\gamma_6\}\Big\{\eta_3(\gamma_4-12)\Big[\eta_2(\gamma_3\\
&\quad -12)\{\eta_1(\gamma_1-12)(\gamma_2-12)-12\gamma_2\}-12\gamma_3\{\eta_1(\gamma_1-12)-12\}\Big]\\
&\quad -12\gamma_4\Big[\eta_2\{\eta_1(\gamma_1-12)(\gamma_2-12)-12\gamma_2\}-12\{\eta_1(\gamma_1-12)-12\}\Big]\Big\}\\
&\quad -12\{\eta_5\gamma_5(\gamma_6-12)-12\gamma_6\}\Big\{\eta_3\Big[\eta_2(\gamma_3-12)\{\eta_1(\gamma_1-12)(\gamma_2-12)\\
&\quad -12\gamma_2\}-12\gamma_3\{\eta_1(\gamma_1-12)-12\}\Big]-12\Big[\eta_2\{\eta_1(\gamma_1-12)(\gamma_2-12)\\
&\qquad\qquad -12\gamma_2\}-12\{\eta_1(\gamma_1-12)-12\}\Big]\Big\},\\
D_1 l_1^3\Phi &= -2\Big[\eta_4\{\eta_5(\gamma_5-12)(\gamma_6-12)-12\gamma_6\}\Big\{\eta_3(\gamma_4\\
&\quad -12)\Big[\eta_2(\gamma_3-12)\{\eta_1\gamma_1(\gamma_2-12)-12\gamma_2\}-12\gamma_3(\eta_1\gamma_1-12)\Big]\\
&\quad -12\gamma_4\Big[\eta_2\{\eta_1\gamma_1(\gamma_2-12)-12\gamma_2\}-12(\eta_1\gamma_1-12)\Big]\Big\}-12\{\eta_5\gamma_5(\gamma_6\\
&\quad -12)-12\gamma_6\}\Big\{\eta_3\Big[\eta_2(\gamma_3-12)\{\eta_1\gamma_1(\gamma_2-12)-12\gamma_2\}-12\gamma_3(\eta_1\gamma_1\\
&\quad -12)\Big]-12\Big[\eta_2\{\eta_1\gamma_1(\gamma_2-12)-12\gamma_2\}-12(\eta_1\gamma_1-12)\Big]\Big\}\Big],
\end{aligned}\right\}\quad (1)
$$

7) K. SEZAWA and K. KANAI, *loc. cit.* 5).

$$
\left.
\begin{aligned}
A_2\Phi = & -12\eta_1\Big\{\eta_4\{\eta_5(\gamma_5-12)(\gamma_6-12) \\
& -12\gamma_6\}\Big[\eta_3(\gamma_4-12)\{\eta_2(\gamma_2-12)(\gamma_3-12)-12\gamma_3\} \\
& -12\gamma_4\{\eta_2(\gamma_2-12)-12\}\Big]-12\{\eta_5\gamma_5(\gamma_6-12) \\
& -12\gamma_6\}\Big[\eta_3\{\eta_2(\gamma_2-12)(\gamma_3-12)-12\gamma_3\} \\
& \qquad -12\{\eta_2(\gamma_2-12)-12\}\Big]\Big\}, \\
D_2l_2^3\Phi = & \, 2.12\eta_1\Big\{\eta_4\{\eta_5(\gamma_5-12)(\gamma_6-12)-12\gamma_6\}\Big[\eta_3(\gamma_4 \\
& -12)\{\eta_2\gamma_2(\gamma_3-12)-12\gamma_3\}-12\gamma_4(\eta_2\gamma_2-12)\Big] \\
& -12\{\eta_5\gamma_5(\gamma_6-12)-12\gamma_6\}\Big[\eta_3\{\eta_2\gamma_2(\gamma_3-12) \\
& \qquad -12\gamma_3\}-12(\eta_2\gamma_2-12)\Big]\Big\},
\end{aligned}
\right\} \quad (2)
$$

$$
\left.
\begin{aligned}
A_3\Phi = & \, 12^2\eta_1\eta_2\Big[\eta_4\{\eta_3(\gamma_3-12)(\gamma_4-12) \\
& -12\gamma_4\}\{\eta_5(\gamma_5-12)(\gamma_6-12)-12\gamma_6\} \\
& \qquad -12\{\eta_3(\gamma_3-12)-12\}\{\eta_5\gamma_5(\gamma_6-12)-12\gamma_6\}\Big], \\
D_3l_3^3\Phi = & -2.12^2\eta_1\eta_2\Big[\eta_4\{\eta_3\gamma_3(\gamma_4-12) \\
& -12\gamma_4\}\{\eta_5(\gamma_5-12)(\gamma_6-12)-12\gamma_6\} \\
& \qquad -12(\eta_3\gamma_3-12)\{\eta_5\gamma_5(\gamma_6-12)-12\gamma_6\}\Big],
\end{aligned}
\right\} \quad (3)
$$

$$
\left.
\begin{aligned}
A_4\Phi = & -12^3\eta_1\eta_2\eta_3\Big[\eta_4(\gamma_4-12)\{\eta_5(\gamma_5-12)(\gamma_6-12)-12\gamma_6\} \\
& \qquad -12\{\eta_5\gamma_5(\gamma_6-12)-12\gamma_6\}\Big], \\
D_4l_4^3\Phi = & \, 2.12^3\eta_1\eta_2\eta_3\Big[\eta_4\gamma_4\{\eta_5(\gamma_5-12)(\gamma_6-12)-12\gamma_6\} \\
& \qquad -12\{\eta_5\gamma_5(\gamma_6-12)-12\gamma_6\}\Big],
\end{aligned}
\right\} \quad (4)
$$

$$\left.\begin{aligned} &A_5\Phi=12^4\eta_1\eta_2\eta_3\eta_4\{\eta_5(\gamma_5-12)(\gamma_6-12)-12\gamma_6\}\,, \\ &D_5l_5^3\Phi=-2.12^4\eta_1\eta_2\eta_3\eta_4\{\eta_5\gamma_5(\gamma_6-12)-12\gamma_6\}\,, \end{aligned}\right\} \quad (5)$$

$$\left.\begin{aligned} &A_6\Phi=-12^5\eta_1\eta_2\eta_3\eta_4\eta_5(\gamma_6-12)\,, \\ &D_6l_6^3\Phi=2.12^5\eta_1\eta_2\eta_3\eta_4\eta_5\gamma_6\,, \end{aligned}\right\} \quad (6)$$

$$B_S=0\,, \qquad C_S=\frac{3}{2}\,l_SD_S\,, \qquad (S=1\,,2\,,\ldots,6) \qquad (7)$$

$$\begin{aligned} \Phi(Q+3ik\varepsilon P)=Q\Big[\,&\eta_4\{\eta_5(\gamma_5-12)(\gamma_6-12)-12\gamma_6\}\Big\{\eta_3(\gamma_4 \\ &-12)\Big[\eta_2(\gamma_3-12)\{\eta_1(\gamma_1-12)(\gamma_2-12)-12\gamma_2\} \\ &-12\gamma_3\{\eta_1(\gamma_1-12)-12\}\Big]-12\gamma_4\Big[\eta_2\{\eta_1(\gamma_1-12)(\gamma_2-12) \\ &-12\gamma_2\}-12\{\eta_1(\gamma_1-12)-12\}\Big]\Big\}-12\{\eta_5\gamma_5(\gamma_6-12) \\ &-12\gamma_6\}\Big\{\eta_3\Big[\eta_2(\gamma_3-12)\{\eta_1(\gamma_1-12)(\gamma_2-12)-12\gamma_2\} \\ &-12\gamma_3\{\eta_1(\gamma_1-12)-12\}\Big]-12\Big[\eta_2\{\eta_1(\gamma_1-12)(\gamma_2-12) \\ &-12\gamma_2\}-12\{\eta_1(\gamma_1-12)-12\}\Big]\Big\}\Big] \\ +\frac{36E_1\varepsilon j_1^2}{\mu l_1^3}P\Big[\,&\eta_4\{\eta_5(\gamma_5-12)(\gamma_6-12)-12\gamma_6\}\Big\{\eta_3(\gamma_4 \\ &-12)\Big[\eta_2(\gamma_3-12)\{\eta_1\gamma_1(\gamma_2-12)-12\gamma_2\}-12\gamma_3(\eta_1\gamma_1-12)\Big] \\ &-12\gamma_4\Big[\eta_2\{\eta_1\gamma_1(\gamma_2-12)-12\gamma_2\}-12(\eta_1\gamma_1-12)\Big]\Big\} \\ &-12\{\eta_5\gamma_5(\gamma_6-12)-12\gamma_6\}\Big\{\eta_3\Big[\eta_2(\gamma_3-12)\{\eta_1\gamma_1(\gamma_2-12)-12\gamma_2\} \\ &-12\gamma_3(\eta_1\gamma_1-12)\Big]-12\Big[\eta_2\{\eta_1\gamma_1(\gamma_2-12)-12\gamma_2\}-12(\eta_1\gamma_1-12)\Big]\Big\}\Big]\,, \end{aligned} \qquad (8)$$

$$\left.\begin{aligned} P&=(h\varepsilon k\varepsilon+4)-i(h^2\varepsilon^2k\varepsilon+2h\varepsilon+2k\varepsilon),\\ Q&=2\left[\left\{\frac{\lambda}{\mu}h^2\varepsilon^2(h\varepsilon k\varepsilon+4)-2(k\varepsilon-h\varepsilon)(h^2\varepsilon^2k\varepsilon+2h\varepsilon+4k\varepsilon)\right\}\right.\\ &\qquad\left.+2i(k\varepsilon-h\varepsilon)\left(\frac{\lambda}{\mu}h^2\varepsilon^2+2h^2\varepsilon^2+4\right)\right]. \end{aligned}\right\} \quad (9)$$

By putting $E_1=\ldots=E_6=E,\ \ I_1=\ldots=I_6=I,\ \ l_1=\ldots=l_6=l,$ $m_1=\ldots=m_6=m,\ \ h\varepsilon\to 0,\ \ k\varepsilon\to 0,$ we obtain

$$\left.\begin{aligned} A_1\Phi&=\{\gamma(\gamma-24)^2-12(\gamma-12)^2\}^2-12\gamma(\gamma-12)^2(\gamma-36)^2,\\ D_1l^3\Phi&=-2\gamma(\gamma-12)(\gamma-24)(\gamma-36)\{(\gamma-12)^2-24\gamma\}, \end{aligned}\right\} \quad (10)$$

$$\left.\begin{aligned} A_2\Phi&=-12\Big\{(\gamma-12)\{(\gamma-12)^2-12\gamma\}^2\\ &\qquad-12\gamma(\gamma-24)\Big[\{(\gamma-12)^2-12\gamma\}+(\gamma-12)(\gamma-36)\Big]\Big\},\\ D_2l^3\Phi&=2.12\gamma\Big[\{(\gamma-12)^2-12\gamma\}^2-24(\gamma-24)\{(\gamma-12)^2-12\gamma\}\Big], \end{aligned}\right\} \quad (11)$$

$$\left.\begin{aligned} A_3\Phi&=12^2\Big[\{(\gamma-12)^2-12\gamma\}^2-12\gamma(\gamma-24)^2\Big],\\ D_3l^3\Phi&=-2.12^2\gamma(\gamma-24)\Big[\{(\gamma-12)^2-12\gamma\}-12(\gamma-12)\Big], \end{aligned}\right\} \quad (12)$$

$$\left.\begin{aligned} A_4\Phi&=-12^3\Big[(\gamma-12)\{(\gamma-12)^2-12\gamma\}-12\gamma(\gamma-24)\Big],\\ D_4l^3\Phi&=2.12^3\gamma(\gamma-12)(\gamma-36), \end{aligned}\right\} \quad (13)$$

$$A_5\Phi=12^4\{(\gamma-12)^2-12\gamma\},\qquad D_5l^3\Phi=-2.12^4\gamma(\gamma-24), \quad (14)$$

$$A_6\Phi=-12^5(\gamma-12),\qquad D_6l^3\Phi=2.12^5\gamma, \quad (15)$$

$$B_S=0,\qquad C_S=\frac{3}{2}l_SD_S,\qquad (S=1,\ 2,\ \ldots\ldots,\ 6) \quad (16)$$

$$\left.\begin{aligned} \Phi&=4\left\{\left(\sqrt{\frac{\lambda+2\mu}{\mu}}-1\right)M-9i\sqrt{\frac{\lambda+2\mu}{\mu}}\frac{Ej^2}{\mu kl^3}N\right\}\left(7\sqrt{\frac{\lambda+2\mu}{\mu}}-4\right)^{-1},\\ M&=\{\gamma(\gamma-24)^2-12(\gamma-12)^2\}^2-12\gamma(\gamma-12)^2(\gamma-36)^2,\\ N&=\gamma(\gamma-12)(\gamma-24)(\gamma-36)\{(\gamma-12)^2-24\gamma\}, \end{aligned}\right\} \quad (17)$$

In the same special case of a 6-storied structure, the ratio of the bending moment in the columns on each floor to the product of ml by the acceleration of the ground (on which no structure stands) is expressed by equations of the forms

$$\left.\begin{aligned}
&EI\frac{\partial^2 y_1}{\partial x_1^2}\Big/ ml\left(2\frac{\partial^2 u_0}{\partial t^2}\right)=\frac{-6}{\sqrt{\mathfrak{A}^2+\mathfrak{B}^2}}\\
&\qquad\qquad .(\gamma-12)(\gamma-24)(\gamma-36)\{(\gamma-24)^2-432\},\\
&EI\frac{\partial^2 y_2}{\partial x_2^2}\Big/ ml\left(2\frac{\partial^2 u_0}{\partial t^2}\right)=\frac{6.12}{\sqrt{\mathfrak{A}^2+\mathfrak{B}^2}}\\
&\qquad\qquad .\{(\gamma-18)^2-180\}\{(\gamma-30)^2-180\},\\
&EI\frac{\partial^2 y_3}{\partial x_3^2}\Big/ ml\left(2\frac{\partial^2 u_0}{\partial t^2}\right)=\frac{-6.12^2}{\sqrt{\mathfrak{A}^2+\mathfrak{B}^2}}\\
&\qquad\qquad .(\gamma-24)\{(\gamma-24)^2-288\},\\
&EI\frac{\partial^2 y_4}{\partial x_4^2}\Big/ ml\left(2\frac{\partial^2 u_0}{\partial t^2}\right)=\frac{6.12^3}{\sqrt{\mathfrak{A}^2+\mathfrak{B}^2}}(\gamma-12)(\gamma-36)\\
&EI\frac{\partial^2 y_5}{\partial x_5^2}\Big/ ml\left(2\frac{\partial^2 u_0}{\partial t^2}\right)=\frac{-6.12^4}{\sqrt{\mathfrak{A}^2+\mathfrak{B}^2}}(\gamma-24),\\
&EI\frac{\partial^2 y_6}{\partial x_6^2}\Big/ ml\left(2\frac{\partial^2 u_0}{\partial t^2}\right)=\frac{6.12^5}{\sqrt{\mathfrak{A}^2+\mathfrak{B}^2}},
\end{aligned}\right\}\quad(18)$$

where

$$\left.\begin{aligned}
&\mathfrak{A}=\{\gamma(\gamma-24)^2-12(\gamma-12)^2\}^2-12\gamma(\gamma-12)^2(\gamma-36)^2,\\
&\mathfrak{B}=12\left(\frac{1}{a}\sqrt{\frac{mEI}{l^3\rho\mu}}\right)\sqrt{\gamma}(\gamma-12)(\gamma-24)(\gamma-36)\{(\gamma-24)^2-432\}.
\end{aligned}\right\}\quad(19)$$

The form of displacement of the ground surface, on which no structure is standing, is

$$u_0=2\cos pt.$$

Since $\mathfrak{A}=0$ gives the frequency equation of the free vibrations of the structure, it follows that, when $\gamma=mp^2l^3/EI$ satisfies this equation, $\mathfrak{A}=0$, namely, $\gamma=0{\cdot}7005$, $6{\cdot}038$, $15{\cdot}49$, $26{\cdot}9$, $37{\cdot}63$, $45{\cdot}25$, we have the

resonance condition of the vibrations in the usual sense. It is possible to consider the condition, $\mathfrak{B}=0$. We shall call the case in which $\gamma=mp^2l^3/EI$ satisfies the equation, $\mathfrak{B}=0$, as *corresonance.*

If γ were to satisfy the conditions, $\mathfrak{A}=0, \mathfrak{B}=0$, then the amplitudes of vibrations or bending moments in the columns would assume infinitely large values. At certain vibration frequencies in the present problem, such conditions are almost, but not entirely, satisfied.

3. Middle 28 th House (*Naka* 28 *gô-kan*).

This is a six-storied reinforced concrete structure that was built in January 1926, a photographic view of the profile and the general plan of the first floor being shown in Figs. 1, 2. The basement being

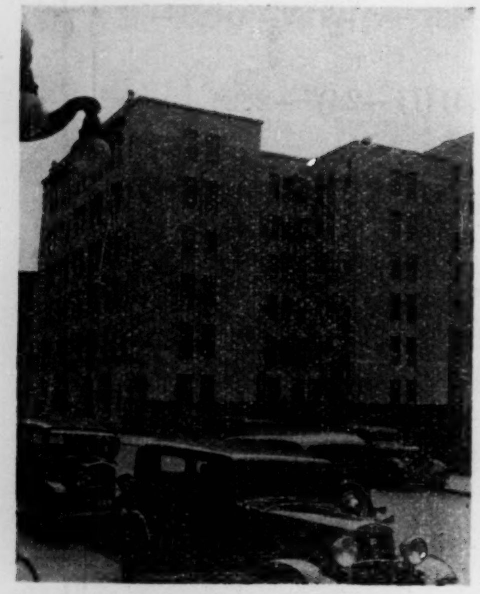

Fig. 1. Naka 28 gô-kan.

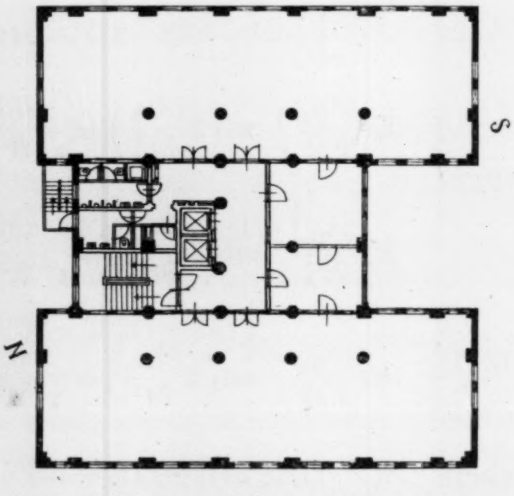

Fig. 2. Naka 28 gô-kan. Scale 1/500.

of very strong construction and its floor height much less than those of the other floors, we applied a correction by adding 1/6 of the basement height to the actual mean between floor height from the ground floor to the fifth floor. It was also assumed that all floors, including the roof, have live loads of intensity 370 kg/m^2 of the floor area, or a live load of $2 \cdot 442.10^5$ kg on every floor. The calculated results of the important elements are given in Table I.

Table I. Middle 28 th House (Naka–28 gô–kan).

Floor		1 st	2 nd	3 rd	4 th	5 th	Roof	Mean
Height of floor below l (m)		4·015	3·483	3·483	3·483	3·483	3·787	3·622 +0·518
Area of vertical members a (m²)		38·461	38·461	31·702	27·201	24·873	24·004	30.784
Mt. inertia of vertical members I (m⁴)		2·641	2·641	1·934	1·562	1·450	1·429	1·943
Beams	volume (m³)	75·40	60·45	60.45	60·45	60·45	60·35	62·93
	weight (kg)	$1{\cdot}81.10^5$	$1{\cdot}45.10^5$	$1{\cdot}45.10^5$	$1{\cdot}45.10^5$	$1{\cdot}45.10^5$	$1{\cdot}449.10^5$	$1{\cdot}510.10^5$
Floors	volume (m³)	50	50	50	50	50	50	50
	weight (kg)	$1{\cdot}2.10^5$	$1{\cdot}2.10^5$	$1{\cdot}2.10^5$	$1{\cdot}2.10^5$	$1{\cdot}2.10^5$	$1{\cdot}2.10^5$	$1{\cdot}2.10^5$
Columns	volume (m³)	74·32	46·00	39·55	32·22	26·23	23·37	40·28
	weight (kg)	$1{\cdot}783.10^5$	$1{\cdot}104.10^5$	$0{\cdot}950.10^5$	$0{\cdot}774.10^5$	$0{\cdot}630.10^5$	$0{\cdot}561.10^5$	$0{\cdot}967.10^5$
Walls	volume (m³)	68·40	59·32	49·45	49·45	49·45	53·70	54·96
	weight (kg)	$1{\cdot}641.10^5$	$1{\cdot}423.10^5$	$1{\cdot}187.10^5$	$1{\cdot}187.10^5$	$1{\cdot}187.10^5$	$1{\cdot}289.10^5$	$1{\cdot}319.10^5$
Total mass (kg)		$6{\cdot}434.10^5$	$5{\cdot}177.10^5$	$4{\cdot}787.10^5$	$4{\cdot}611.10^5$	$4{\cdot}467.10^5$	$4{\cdot}499.10^5$	$4{\cdot}996.10^5$
Area of floor (m²)		660·7	660·7	660·7	660·7	660·7	660·7	660·7
$\frac{1}{a}\sqrt{\frac{mEI}{l^3\rho\mu}}$		1·436	1·436	1·492	1·563	1·648	1·693	1·540

The periods of free vibrations are determined by the equation, $\mathfrak{A}=0$, namely

$$\{\gamma(\gamma-24)^2-12(\gamma-12)^2\}^2-12\gamma(\gamma-12)^2(\gamma-36)^2=0, \tag{20}$$

where $\gamma=mp^2l^3/EI$. This equation gives us

$$\gamma=0{\cdot}7005,\quad 6{\cdot}038,\quad 15{\cdot}49,\quad 26{\cdot}90,\quad 37{\cdot}63,\quad 45{\cdot}25,$$

from which we obtain the periods

$$T(\text{sec})=0{\cdot}295,\quad 0{\cdot}1004,\quad 0{\cdot}0627,\quad 0{\cdot}0475,\quad 0{\cdot}0402,\quad 0{\cdot}0367,$$

$E=2{\cdot}1.10^9$ kg/m² $=2{\cdot}1.10^9.9{\cdot}8$ kg mass m/s²/m² being used in Table I as well as in the determination of T. These periods are somewhat longer than what they actually would be. The values of the present case come from the assumption that the floors are extremely rigid.

Although such smallness of the periods may be inconvenient for investigators aiming only at finding the periods of natural vibrations, which however are rather meaningless in our present investigation, the nature of the energy dissipation in seismic vibrations is not greatly affected by such changes in periods.

The maximum values of the bending moments $M=E_S I_S(d^2y_S/dx_S^2)$ at each end of the columns corresponding to the maximum values of the acceleration of the ground (on which no structure is standing and in which $\lambda=14\mu$) due to the movement in NS-direction, were determined from equation (18), the results being shown in Figs. 3 a, 3 b. Since resonance conditions exist at the periods indicated by the vertical strips, we may conclude that the bending moments

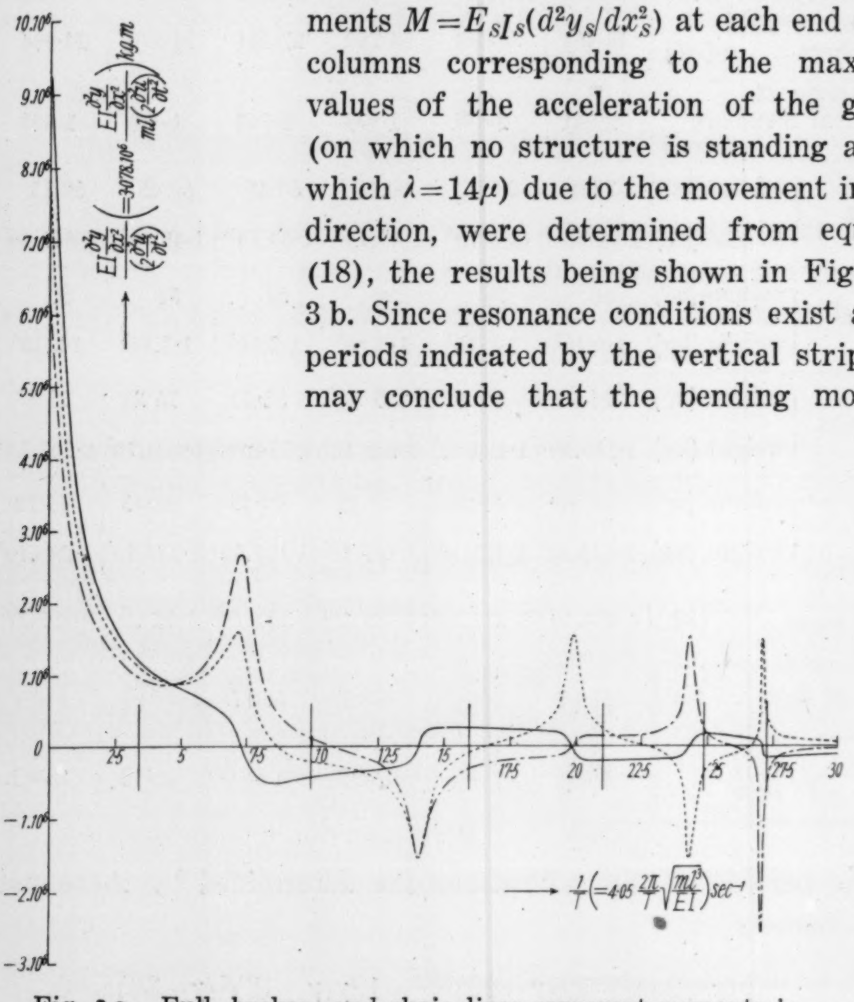

Fig. 3 a. Full, broken, and chain lines represent moments in columns of ground, first, and second floors respectively.

under resonance conditions are rather less than those at periods out of resonance. It is also an important fact that the bending moments in the columns below the first floor are generally very small for any vibration period of the disturbance, excepting those near where the vibration period is very long, namely, near zero frequency of vibrations. Another remarkable fact is that, at the highest natural frequency, resonance and corresonance virtually coincide, tending to cause each of the denominators in (17) to vanish. This will be referred to again in the next section.

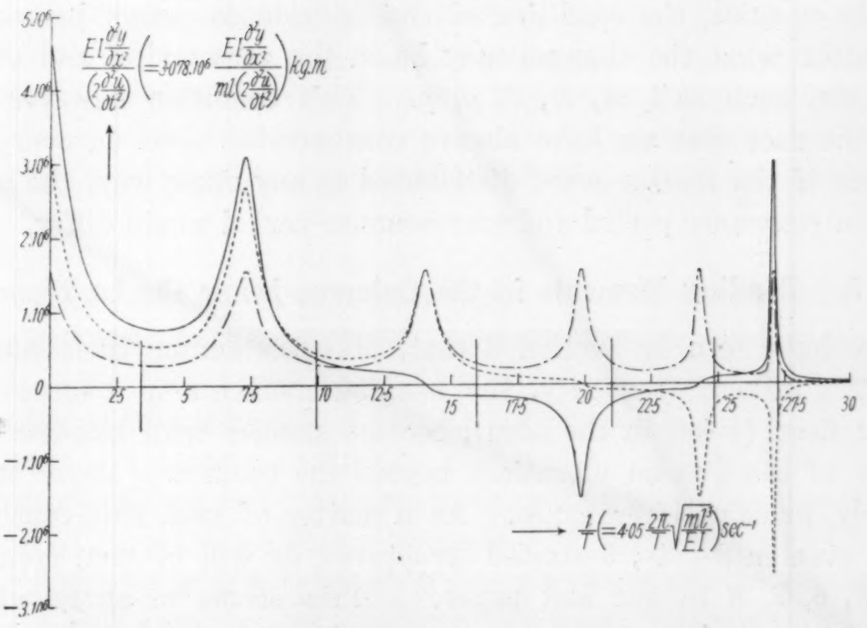

Fig. 3 b. Full, broken, and chain lines represent moments in columns of third, fourth, and fifth floors respectively.

Finally, the induced stresses in the columns and walls will be calculated. Assuming that the acceleration of the ground, (on which no structure is standing), is $g/10$, the stresses in the lowest columns at zero frequency become

maximum stress in walls running in NS-direction $=36.0$ kg/cm^2,
maximum stress in columns attached the same walls $=27{\cdot}4$ kg/cm^2.

4. Coincidence of Resonance and Corresonance.

It was said in the last section that, since at period, 0·0367 sec, resonance and corresonance approximately coincide, the bending moments in the columns below the 3 rd, 4 th, and 5 th floors (namely those between 3 gai and 5 kai in the plan), assume fairly large values. If resonance and corresonance were to coincide exactly, which, in the present problem, is mathematically impossible, infinitely large vibrations would result. Nevertheless, at such a short vibration period as 0·0367 sec, the material itself damping as in solid viscosity,[8] etc., plays an important part in energy dissipation, as the term is generally understood, actual large vibrations being thus improbable from the physical point of view.

The manner in which the period for resonance approaches that for corresonance at the period corresponding to the sixth natural frequency never changes provided the number of stories, in the present

case six, is stipulated. Thus, even if resonance and corresonance were to coincide, the condition of the coincidence cannot be modified, no matter what the changes may be in the geometrical and physical constants, such as l, m, E, I, μ, ρ. This condition however arises from the fact that we have always concentrated mass on every floor, whereas if the masses were distributed in any other way, the relation between resonance period and corresonance period would differ.

5. Bending Moments in the Columns below the 1st Floor.

we have seen in Section 3 that, notwithstanding their abnormal largeness in zero frequency, the bending moments in columns below the 1st floor (1–kai in the plan), become smaller with increase in frequency of the ground vibrations beyond the frequency above the first (namely, principal) resonance. As a matter of fact, this contingency exists even in 3–, 4–, 5–storied structures, as will be seen from Figs. 2, 3, 5, 6, 7, 8 in our last paper.[9] This seems to agree with the fact as observed that damage to a building in a great earthquake occurs in the vertical members on the 1st or 2nd floor rather than in those on the ground floor. Without invoking the theory of dissipation (for instance, considering the structure with hinged base), it would be very difficult[10] to explain this apparent anomaly.

In conclusion we wish to express our sincere thanks to the members of the staff of the Mitsubishi Co., for having supplied us with valuable data for the present investigation, and also to the Council of the Foundation for the Promotion of Scientific and Industrial Research of Japan, with whose aid the work was begun.

Added Note *to Vol. 13, Paper 54,* (*pp. 681～697*) *Equation*(*2′*).

The form of Δ was approximate from the reason of its mathematical simplicity and also of its practical unimportance in such engineering problem. We forgot to remark this fact in that paper. The accurate formulae will be seen in foot note (4) in the same paper.

---

8) K. SEZAWA, The part, "Waves propagated in Beam...", which was appended at the end of the paper, "On the Decay of Waves in Visco-elastic Solid Bodies", *Bull. Earthq. Res. Inst.*, **3** (1927), 50, etc.

9) K. SEZAWA and K. KANAI, *loc. cit.* 5).

10) Ditto, *loc. cit.* 2).

12. 6階建築に於ける震動勢力の逸散性・共振と餘共振とが一致する問題

地震研究所 妹澤克惟
金井清

これまでの研究によつて5階までの高さの建物の地震による振動勢力の逸散性その他の性質がわかつた．何れの場合にも三菱地所課の御好意によつて實際の建物にあてはめて見ることができたのである．しかし6階以上の場合までやつてなかつたので，ここにあらためてその計算を試み，更に三菱仲28號館の場合を借用してそれと比較研究をやつてみた．

大體の性質はこれまでの場合やつた研究と似たものであるから，この抄錄に於て委しく述べるのを省くけれども，特に注意したいことは1階の柱や壁に於ける屈曲モーメントが zero frequency では非常に大きいのに拘らず，第1次共振以上では frequency とともに非常に小さくなることである．このことは建物の大地震に於ける被害が1階よりも2階3階に多いといふことと一致してゐる．このやうな建物も風壓等に對してはやはり1階の方が被害の多いことが豫期されるから，震動逸散性を用ひることなく，單に床が剛く建物脚部が鉸脚になつてゐるやうな場合を考へても，この問題の說明がむづかしいやうに思はれる．末廣博士が考へられたやうに建物の rocking motion のやうなことを導入してこの事實を說明しやうとする行方もあるけれども，（rocking motion の面白さは別として）地震の上下動の成分までも適當に入れなければならぬ上に，問題それ自體に種々の難點（殊に高層建築では）がある．しかし，rocking motion を入れたからといつて，この問題の性質には殆ど變化がなく，それに相當して再び別個の震動逸散性が增加するのみである．

6階建築の問題に於て特に著しい現象は第6次の共振が餘共振（corresonance）と略一致することである．若し完全に一致するものであるとするとその場合に無限大の屈曲モーメントが得られる譯であるけれども，理論的にそのやうにはならぬ．共振と餘共振とが略一致する事柄は，質量を各床に集め且つ6階といふことから生ずるのであつて，質量を別の方法で分布すると違つた結果になる．又，この一致することは建物の彈性，質量，階高，土地の性質などに何等關係がないものである．但し注意すべきことは，たとひ，共振と餘共振とが一致するにしても，frequency の非常に高い所であるから，物質に關係する粘性抵抗などがよく働き，實際問題としては恐れるに足らぬといふことである．

13. 宮古一青森間水準檢測成果

昭和 10 年度に於いて，帝國學士院より本所々員寺田寅彥教授に對して與へられたる學術研究資金を以て，陸地測量部に委囑し，宮古一青森間の水準測量を施行せり．この測量の結果を前回の測量の結果と比較して得たる各水準點の垂直變動量は，別圖に示したる所の如し．

測量の結果に關する要領は下記の如し．

(1) 測量期	前回：	宮　古一淺田村間は	1900,
		淺田村一野邊地間は	1897,
		野邊地一青 森 間 は	1902.
	今回：	全　部	1935.

(2) 水準點の垂直變動は凡て，上揭の期間に於ける垂直變動量 $-72{\cdot}4$ mm を算したる宮古町所在の水準點 6885 號に準據して算出せられたるものなり．

昭和 11 年2月　　　　地 震 研 究 所

13. Precise Levelling along the Line from Miyako to Aomori.

By the aid of the research fund granted to Prof. T. Terada, one of the chief staffs of members of our Institute, from the Council of the Imperial Academy, a precise levelling was revised in 1935 along the line from Miyako (Iwate Prefecture) to Aomori.

The relative vertical displacements of bench-marks obtained by comparing the results of the recent measurements with the earlier ones are shown in the plate.

The dates of the field works are as follows:

Earlier survey:	1900	for the section of the line Miyako-Asadamura
	1897	for the section of the line Asadamura-Nohedi
	1902	for the section of the line Nohedi-Aomori.
Later survey:	1935.	

The vertical displacements deduced and shown in the plate are referred to B. M. 6885, the height of which is regarded as have changed by -72.4 mm during the period of successive surveys mentioned above.

Feb., 1936.　　　　The Earthquake Research Institute.

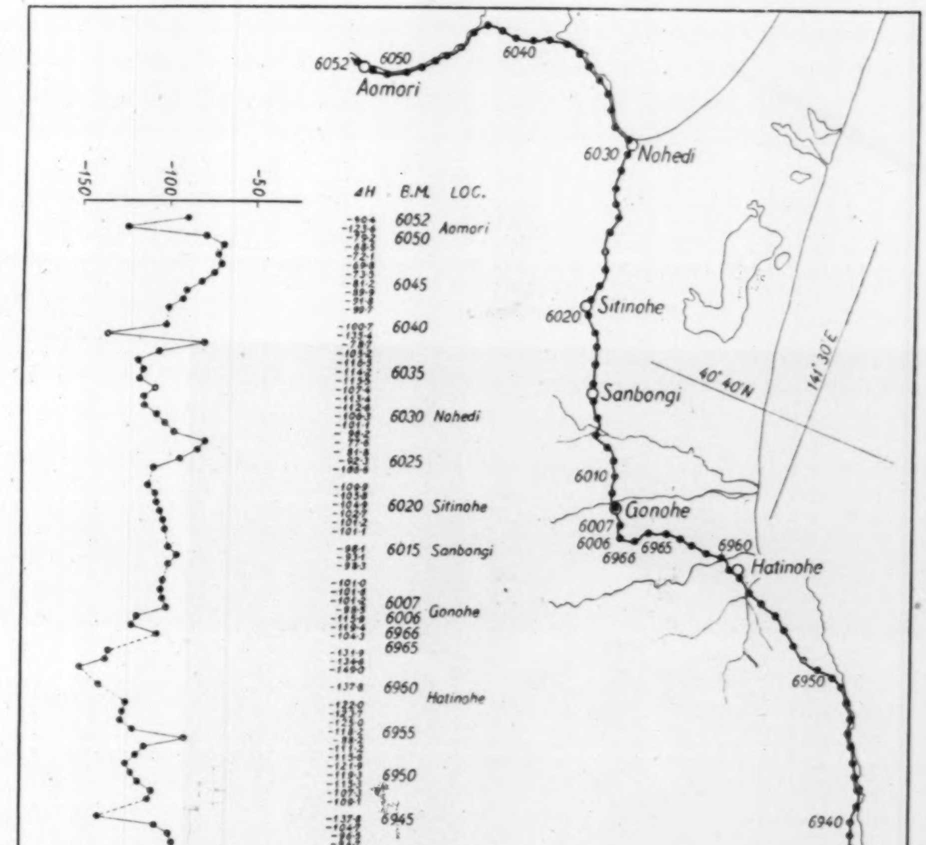
Aomori
Nohedi
Sitinohe
Sanbongi
Gonohe
Hatinohe
Kuzi
Miyako
40°40'N
141°30'E
ΔH B.M. LOC.
-150 -100 -50
LINE OF LEVELS
SCALE FOR MAP
0 5 10KM.

寺田寅彦

14. *On the Relation between Seismic Origins and Radiated Waves.*

By Katsutada SEZAWA,

Earthquake Research Institute.

(Read Feb. 18 and March 17, 1936.—Received March 20, 1936.)

1. Several attempts have been made mathematically and experimentally with a view to ascertaining the mechanism of a seismic origin from the nature of the waves radiated therefrom. But, the shock-generating deformation of the earth's crust differs somewhat from the one assumed from the theory of elasticity, while the prevalent ideas on the nature of radiated waves from the same origin, even under the theory of elasticity, can not yet be said to be satisfactory. It is therefore of pressing importance to investigate the problem in the most rational manner possible, notwithstanding that a number of inherent ambiguities exist in the problem.

In a previous paper[1] we arrived at the conclusion that wave phenomena are independent of initial stress, and that the total wave energy is radiated from the origin itself at which a shock or stress is applied.

The absolute amount of wave energy is the same whether a given stress is applied at the origin or released from it. It was also shown that a given additive statical energy is also radiated (in the form of waves) from the same origin in both conditions of the problem. The same conclusion may also be obtained from the discussion in Love's text book[2], a brief summary of which is shown in the next section.

2. In the first place, the correspondence of the movement at the origin and the radiated waves will be discussed. The work done by the surface force at the origin, namely the applied surface energy, is

$$\int dt \iint \left(X_\nu \frac{\partial u}{\partial t} + Y_\nu \frac{\partial v}{\partial t} + Z_\nu \frac{\partial w}{\partial t} \right) dS, \tag{1}$$

where X_ν, Y_ν, Z_ν, u, v, w are components of force and displacement

1) K. SEZAWA and K. KANAI, *Bull. Earthq. Res. Inst.*, **14** (1936), 10~17.
2) A. E. H. LOVE, *Mathematical Theory of Elasticity*, §§ 61~62.

at the surface in x, y, z directions respectively. Using the relations

$$X_\nu = X_x \cos(x, \nu) + X_y \cos(y, \nu) + X_z \cos(z, \nu), \quad \cdots\cdots,$$
$$Y_z = Z_y, \quad \cdots\cdots\cdots\cdots\cdots\cdots\cdots\cdots\cdots\cdots\cdots\cdots,$$

and applying Green's theorem on the solid bounded by the surface at the origin and one at a sufficiently large distance from that origin, the integral (1) reduces to

$$\int dt \left\{ \iiint \left(\frac{\partial X_x}{\partial x} + \frac{\partial X_y}{\partial y} + \frac{\partial X_z}{\partial z} \right) \frac{\partial u}{\partial t} + \left(\frac{\partial X_y}{\partial x} + \frac{\partial Y_y}{\partial y} + \frac{\partial Y_z}{\partial z} \right) \frac{\partial v}{\partial t} + \left(\frac{\partial Z_x}{\partial x} + \frac{\partial Y_z}{\partial y} + \frac{\partial Z_z}{\partial z} \right) \frac{\partial w}{\partial t} \right\} dxdydz$$
$$+ \iiiint \left[X_x \frac{\partial e_{xx}}{\partial t} + \cdots + \cdots + Y_z \frac{\partial e_{yz}}{\partial t} + \cdots + \cdots \right] dxdydz \qquad (2)$$

The increase of kinetic energy in the body is roughly

$$\int dt \iiint \rho \left(\frac{\partial^2 u}{\partial t^2} \frac{\partial u}{\partial t} + \frac{\partial^2 v}{\partial t^2} \frac{\partial v}{\partial t} + \frac{\partial^2 w}{\partial t^2} \frac{\partial w}{\partial t} \right) dxdydz . \qquad (3)$$

When the differential equations of wave motion are used, (3) can be replaced by

$$\int dt \iiint \left[\left(\frac{\partial X_x}{\partial x} + \frac{\partial X_y}{\partial y} + \frac{\partial X_z}{\partial z} \right) \frac{\partial u}{\partial t} + \cdots + \cdots \right] dxdydz . \qquad (4)$$

Thus, from (2) and (4) it is possible to express the excess work done by the surface force beyond the increase of the kinetic energy as follows.

$$\int dt \iiint \left[X_x \frac{\partial e_{xx}}{\partial t} + Y_{yy} \frac{\partial e_{yy}}{\partial t} + Z_z \frac{\partial e_{zz}}{\partial t} + Y_z \frac{\partial e_{yz}}{\partial t} + X_z \frac{\partial e_{xz}}{\partial t} + X_y \frac{\partial e_{xy}}{\partial t} \right] dxdydz ,$$

or

$$\int dt \iiint [X_x \delta e_{xx} + \cdots + \cdots + Y_z \delta e_{yz} + \cdots +]\, dxdydz , \qquad (5)$$

which is possible for any change of stress conditions, $\delta e_{xx}, \cdots\cdots$ being increments of strain components in δt.

Let δT_1 and δU be the respective increments of kinetic energy and the intrinsic energy, both in δt per unit volume. Again, let δW_1 and δQ be the work done by the surface force and the mechanical value

of heat supplied in ∂t. Then, the first law of thermodynamics gives

$$\int_t \iiint (\partial T_1 + \partial U)\, dxdydz = \int_t (\partial W_1 + \partial Q). \tag{6}$$

By means of (5) we have

$$\int_t \partial W_1 - \int_t \iiint \partial T_1 dxdydz$$

$$= \int_t \iiint (X_x \partial e_{xx} + \cdots + \cdots + Y_z \partial e_{yz} + \cdots + \cdots) dxdydz\,. \tag{7}$$

Thus

$$\int_t \iiint \partial U dxdydz = \int_t \partial Q + \int_t \iiint (X_x \partial e_{xx} + \cdots + \cdots)\, dxdydz\,. \tag{8}$$

In the shock problem, which belongs to adiabatic phenomena, it is possible to put

$$\partial Q = 0\,.$$

Hence

$$\partial U = X_x \partial e_{xx} + \cdots + \cdots\,.$$

Since the right-hand side is an exact differential, it is possible to replace U by the potential energy function W showing the energy stored per unit volume of the body by the strain, so that

$$X_x = \frac{\partial W}{\partial e_{xx}}\,,\ \cdots\cdots,\ Y_z = \frac{\partial W}{\partial e_{yz}}\,,\ \cdots\cdots \tag{9}$$

It will be seen from (8) and (9) that our previous conclusions[3] with respect to the energy of elastic waves as well as that of the statical strain is valid.

Since, as shown in the foregoing and in our paper cited there, the wave phenomena are independent of the initial stress, namely they are reckoned from the standard state of a body, it is possible to conclude that, even if a large volume of the earth's crust were uniformly compressed by earth pressure, the type of the radiated waves will always correspond with that of deformation at the origin merely during wave generation without being under any influence of the initial stress. Thus, for longitudinal waves, the rarefactional waves and the compressional waves correspond respectively with waves of pull type and of push type. A similar conclusion naturally holds for transverse waves.

---

3) K. SEZAWA, *Bull. Earthq. Res. Inst.*, **13** (1935), 729~739; K. SEZAWA and K. KANAI, *Bull. Earthq. Res. Inst.*, **14** (1936), 10~17.

3. The simplest possible mechanism of radiation of seismic waves will next be dealt with. It has already been shown that the surface stress at the origin forms an important link in the evolution of seismic waves, so that postulation of the phenomena of break of materials obviously becomes necessary.

We have quite a number of theories on the break or failure of materials, among which the plastic theories due to Mohr, Mises, etc., may be accepted as reliable. From investigations made by Bridgman[4] and Taylor[5], Mises's theory and a few others in the same field appear most adapted to experimental results, but, owing to the simplicity in the form of its expression and to the fact that there is but little difference in their essential characters, Mohr's maximum shear stress theory may temporarily be used. The earth's pressure

$$p_0 = \frac{1}{2}\rho_0 g \frac{a^2 - r^2}{r}, \tag{10}$$

where a, ρ_0 are radius and mean density of the Earth, may be transformed to

$$p_0 = \rho g z \tag{11}$$

in the case $r \to a$, where ρ is mean density of the earth in the vicinity of the Earth's surface and z the depth from the same surface. Thus, the vertical component of stress in the earth's crust is

$$Z_z = \rho g z . \tag{12}$$

If we use the parameters of elastic deformation (which may not be valid in the actual case but which's may be used for approximately determining its nature), the transverse components of stress are expressed by

$$X_x = Y_y = \frac{\lambda}{\lambda + 2\mu}\rho g z . \tag{13}$$

This relation exists under the conception that no displacement is possible in horizontal directions in the earth's crust, whence it follows that from Mohr's theory, for instance, a maximum shear stress of amount

$$\tau_{\max} = \frac{Z_z - X_x}{2} = \frac{Z_z - Y_y}{2} = \frac{2\mu}{\lambda + 2\mu}\rho g z \tag{14}$$

4) P. W. BRIDGMAN, *Proc. Amer. Acad.*, **58** (1927). 166; etc.
5) G. I. TAYLOR, *Proc. Roy. Soc.*, **145** (1934), 1~17.

acts in a direction 45–degrees to the horizontal plane. From this expression it will be seen that for a great depth, τ_{max} is exceptionally large.

It is however obscure whether or not the earth's crust at a great depth is subjected to such a large shearing stress. My idea at present is that large shear stress in the crust at such a depth under usual conditions is rather improbable. One reason for it is that μ should be very small compared with λ under high pressure, particularly for statical deformation, with the result that τ_{max} is not too large at a great depth. This explanation however may not be convincing, seeing that for μ to be so very small compared with λ is virtually outside the scope of usual experiments. An alternative explanation is that, since the earth's crust at great depth is not liable to slide or to displace, such plastic deformation as is usually known cannot occur.

As a matter of fact nearly every authority on plastic deformation assumes that displacements of material points are permissible even under high hydrostatic pressure, so that the stresses are always accompanied by deformation (or deformation velocity) of material points. Break of materials may rather be accounted for as the result of relative displacements of its configuration points as will be recognized from the experiments under high hydrostatic pressure due to Bridgman, etc. Thus, even should a material, after subjection to hydrostatic pressure without relative displacements of points in it, be released from that pressure, the material would not experience the state of break. It follows then that, since the sliding or displacement of the crust at a great depth is not likely to happen, any actual break of materials under the assumed τ_{max} seems improbable.

In order that τ_{max} which is assumed from the theory of plasticity, may be active in the break of materials in the case of the earth's crust, the crust should become deformable. For that purpose the neighbourhood of the crust under consideration should be semi-fluid or should have faults. The faults themselves therefore do not radiate seismic energy unless they have a certain form of friction, but they are important in the sense that the crustal part in the neighbourhood of fault regions make the shearing stress τ_{max} active. It is evident from the explanation in Section 2 that the relative movements of the crust at a frictionless fault[6] contribute very little to radiation of the seismic energy.

The activity of earth blocks in seismology would be almost mean-

6) Fault having large friction partake somewhat of the nature of a continuous medium.

ingless were the condition already cited to be disregarded. Thus, if an earth block were completely surrounded by frictionless faults as well as by the land surface, any movement of the block merely with respect to the faults under consideration, would be incapable of radiating sensible seismic energy. If, on the other hand, the block were bounded by faults at some part of its boundary, and were continuous elastically or plastically with outer medium at the remaining part of that boundary, the latter part is liable to be in the actual stressed condition owing to easy deformation of the crust, thus evolving a large amount of seismic energy in the case of break or sliding. It should be borne in mind that local fusion of the earth's crust in the case without faults, has the same effect as that in the case of partly existing faults. Although the mechanism of deep-seated earthquakes may be of this nature, I shall not discuss at present the problem in relation to that matter. My explanation here, at any rate, may appear to differ but little from the prevalent belief. But, the fact that the radiation of seismic waves requires stress change at the origin, is a totally different matter that was arrived at through my theoretical investigations.

It should be borne in mind that, since plastic theories due to Mises, etc., fairly conventionally take volume integrals, the belief, that critical plastic energy is radiated directly from the volume of the body, is liable to be accepted. Actually, however, stresses concentrated locally in the body due to critical plastic deformation cause break of the body at some surfaces (internally) and the surface energy or work given at these surfaces is then radiated in forms of seismic waves, etc. Thus, it is by no means necessary to apply pressure at a free surface to get surface energy or work.

The present study shows that the mechanism of seismic origin is probably of the nature of plastic deformation as the result of a relatively sudden movement and mainly of shearing type. The radiated waves would then be mainly distortional. In the usual earthquakes of relatively shallow origins, transverse waves are predominant rather than the longitudinal. My result seems then to be more in line with Jeffreys's particular conclusion[7] that P waves are merely generated from S waves by reflection at discontinuity surfaces than with other theories.

---

7) *Publ. Bureau Centr. Séis., Int.*, A, No. 11 (1935).

14. 震源と震波との關係に就て

地震研究所 妹澤克惟

1. 震源と震波との關係といふやうな大きな問題は一朝一夕に決定出來るものではないけれども，少くとも種々の權威ある力學的研究に基づく機構を作つて見てそれと抵觸しなければ，これが一つの Particular solution と考へても差支がないであらう．地震現象そのものを一種の力學的實驗と見てそれから結論を出すことはむしろ望ましいのであるけれども，それは單に Boundary surface の問題とも考へられるから，假りにそれが事實を決定するとしても，科學的價値は少いものといはればならぬ．

2. 最初に，地震波動の勢力が如何なる場所から出るものであるかを調べる爲に，Love の教科書にある關係と我々が前に提出した論文とから次の如き結論に達した．地震波の勢力は固體中のある面に應力の或る速さの變化（正負の符號に關係せず）とそれに伴ふ變位が起るときにその面から發生する．從て單に固體中全體から勢力が出ることはなく，强ひて固體全體を震源とする爲には固體中全體に Disturbances を加へるか取去るかしなければならぬ．固體の一部に Disturbance を作用せしめた結果固體中から勢力が出ると考へるのは誤りであつて，それは波動が一度傳播してからの結果に過ぎないのである．上の結論の結果を具體的に考へると，地震の發生には應力變化を伴ふ斷層のやうなものが必要となる譯である．從て，斷層面に於て破壞力や固體摩擦が何等働かぬやうな場合は地震發生に殆ど貢獻しない譯になる．多くの人の研究によると，かくの如き斷層もあるらしく思はれるけれども，斯る斷層は震波を大して發散しないものと考へられる．尙序でに附加へたいことは，地殼に如何に壓力が加はつてをつても，地震縱波の押しと引きとは夫々密波と粗波とに相當することである．これは震源の面に力を加へることゝ力を取除くことゝは單に應力の符號の問題に過ぎぬといふ理論と密接の關係がある．

3. 次に如何にして震源に應力變化が起り得るかといふ問題を吟味して見る．これには種々の事柄が考へられるけれども，前述の如く力學上に根據のない說明法では問題の決定性が少い．たとひ地球化學の考へを用ひても，地震波の出る直接の機構には一度尤もらしい力學を通さなければ，彈性波の如き地震波の勢力が作られないのは明かである．最も容易に不衡力及び應力變化を考へ易いのはプラスチック性の理論（粘性液體の問題と混同せざる）である．これには種々有名な人の研究があり，現在ではその解き得る極限に達した感があるが，ともかくそれによることにする．しかしこれ等の理論は物質點が互に距離の變化をなし得る場合についてゞある．然るに一方には高氣壓に於けるプラスチック性の實驗がある．之等の結果を綜合して見ると，地殼內のある面で適當の速度の應力變化とそれに從て起る勢力發散には，物質の變位性が必要になるのである．この爲には地殼の一部に既存の斷層があり，その附近の地殼が破壞（主としてプラスチックに）すればよいのである．しかしその置換として地殼の一部が熱の關係で熔ければ物質の變位性が可能になり得る譯である．但しそれには熱力學及物性論から多少の難點が存在する．只今のところでは斷層のみを考へて置くことにして，さて地殼のブロックの一部分が既存斷層に境され，殘りの部分が外部と固體的に續いてゐるとすれば，斯るブロックは，外と連つてゐる部分の破壞に依つて大きな震波勢力を發散し得ることになる．しかしそのブロックが斷層により完全に外部と境されてをれば，斯る斷層が大した勢力を出し得ないのは明かである．筆者は七八年前に一里四方もある豆腐の如き剛性の物體が方形のまゝ傾く爲には，その周圍の固體摩擦だけにしても如

何に小さいかといふことを以て他の人のブロック理論（筆者のブロック理論は關東地震の翌年に出してある）を吟味したことがあるが，上述の既存斷層とは斯る極端なるブロックを形成する斷層を指すのである．

玆に注意したいことは，Mises 等のプラスチック論で，或容積内のプラスチック的の勢力が一定値に達したときに，プラスチックの辷りが起る形となつてゐる爲に，この辷りが起る場合に上述の容積中の勢力がその儘で彈性波として送られるものと誤解されることである．Mises 等の容積積分形が既に相當に Conventional のものであるから問題にならぬことは明であるが，たとひ之が本當に容積積分であるとしても，波動の起るのは，實際はプラスチックの或極限に達したときに，固體に大なる剪力ができ，その結果特定の場所に應力の集中を生じ，こゝが破壞を起すのである．而して波の勢力はこの破壞面（理想的にいへば）から發散するのである．Surface energy 又は Surface work とはこの事であつて，何も自由面を壓力で押す必要はないのである．

以上述べた考方は，所謂 Elements を取つたものであつて，このやうな Elements を數多く結合して所謂 Coupled action となすことは複雜なだけであつて考方としては容易である．そのやうにしても特に新しい事柄がわかるとは考へられないから，こゝでは Elements だけを取扱つておいた次第である．

尙，地震波に橫波及び同種の波の多いことはプラスチック性の說明に一層好都合な譯である．深發地震についてはその說明に多少困難な點もあるやうであるが，その問題には餘り觸れないことゝして置いた．

終りに附加へたいことは，この論文では地震波の出る機構が固體の破壞の如く固體の中の面に關係することを力說してあるけれども，彈性波が固體の破壞のみに原因するといふ說ではないことである．波動が出る爲には必ず物質の慣性力が直接又は間接に誘起しなければならぬことは力學の敎へる所である．その爲には或容積が急にふくれるとか，物が衝突するとか，固體面に急に力が加はるとかいふことがあればよい．しかし地殼の場合に最も考へ易いのは固體の破壞又は類似の事，卽ち固體の中の面に應力の急變化が起るといふことである．そのやうな意味に於て破壞といふ言葉を委しい說明もなく用ひたのである．

15. *The Nature of Transverse Waves transmitted through a Discontinuity Layer.*

By Katsutada SEZAWA and Kiyoshi KANAI,

Earthquake Research Institute.

(Read March 17, 1936.—Received March 20, 1936.)

1. Although from some need in discussing the vibratory feature of seismic vibrations, we once studied the problem of multiple reflection of bodily waves transmitted through discontinuity layers,[1] the problem however was connected merely with the case for normal incidence of primary disturbances. With regard to the case of oblique incidence no theoretical investigation other than Knott's problem,[2] namely the one for oblique transmission through a discontinuity plane between two media, has been undertaken, the theoretical information with respect to the similar transmission through a discontinuity layer being yet very scanty. Although our aim was to discuss all cases of such a problem, the one which we particularly deal with in this paper, is limited to transverse waves with displacements orientated parallel to the plane of the discontinuity layer, owing to the reason that, notwithstanding its comparative simplicity the solution still seems to show the general character of the problem.

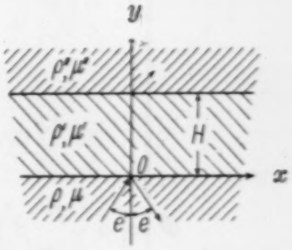

Fig. 1.

2. Let u, u', u'' be displacements in the first, second (layer), and third media respectively. Let again x-axis be parallel to the layer, and y axis perpendicular to that layer with its origin at the boundary between the first and second (layer) media, its positive direction being towards the third medium. The expressions of u, u', u'' then are denoted by

$$\left.\begin{aligned} u=u_1+u_2=e^{if(x+\alpha y-nt)}+Ae^{if(x-\alpha y-nt)}, \\ u'=Be^{if(x+\beta y-nt)}+Ce^{if(x-\beta y-nt)}, \\ u''=De^{if(x+\gamma y-nt)}, \end{aligned}\right\} \tag{1}$$

1) K. SEZAWA and K. KANAI, "Possibility of Free Oscillations of Strata excited by Seismic Waves. Part III", *Bull. Earthq. Res. Inst.*, **10** (1932), 1~18.
2) C. G. KNOTT, *Phil. Mag.*, [5], **48** (1899), 64~97.

corresponding to the incident waves

$$u_1=e^{if(x+\alpha y-nt)}. \tag{2}$$

Since these solutions satisfy

$$\rho\frac{\partial^2 u}{\partial t^2}=\mu\nabla^2 u,\qquad \rho'\frac{\partial^2 u'}{\partial t^2}=\mu'\nabla^2 u',\qquad \rho''\frac{\partial^2 u''}{\partial t^2}=\mu''\nabla^2 u'', \tag{3}$$

where ρ, ρ', ρ'', μ, μ', μ'' are densities and rigidities of respective media, we have

$$n^2=\frac{\mu}{\rho}(1+\alpha^2)=\frac{\mu'}{\rho'}(1+\beta^2)=\frac{\mu''}{\rho''}(1+\gamma^2). \tag{4}$$

The boundary conditions are evidently such that

$$\left.\begin{array}{lll} y=0; & u=u', & \mu\partial u/\partial y=\mu'\partial u'\partial y,\\ y=H; & u'=u'', & \mu'\partial u'/\partial y=\mu''\partial u''/\partial y, \end{array}\right\} \tag{5}$$

in which H is thickness of the layer. Substituting (1) in (5) we finally obtain

$$\left.\begin{array}{l} A\Phi=\left(\alpha+\frac{\mu'}{\mu}\beta\right)\left(\beta-\frac{\mu''}{\mu'}\gamma\right)e^{if\beta H}+\left(\alpha-\frac{\mu'}{\mu}\beta\right)\left(\beta+\frac{\mu''}{\mu'}\gamma\right)e^{-if\beta H},\\ B\Phi=2\alpha\left(\beta+\frac{\mu''}{\mu'}\gamma\right)e^{-if\beta H},\\ C\Phi=2\alpha\left(\beta-\frac{\mu''}{\mu'}\gamma\right)e^{if\beta H},\\ D\Phi=4\alpha\beta e^{-if\gamma H},\\ \Phi=\left(\alpha-\frac{\mu'}{\mu}\beta\right)\left(\beta-\frac{\mu''}{\mu'}\gamma\right)e^{if\beta H}+\left(\alpha+\frac{\mu'}{\mu}\beta\right)\left(\beta+\frac{\mu''}{\mu'}\gamma\right)e^{-if\beta H}. \end{array}\right\} \tag{6}$$

3. Now, we divide the problem in four cases, namely (i) $\beta^2>0$, $\gamma^2>0$, (ii) $\beta^2>0$, $\gamma^2<0$, (iii) $\beta^2<0$, $\gamma^2>0$, (iv) $\beta^2<0$, $\gamma^2<0$. (i) is the case where there is no any total reflection; (ii) the case where a total reflection takes place at the boundary between the second and third media, but not at the boundary between the first and second media; (iii) the case where the total reflection takes place at the boundary between the first and second media, but not at the boundary between the second and third media; and finally (iv) the case where the total reflection takes place at both the boundaries under consideration.

(i) $\beta^2>0,\ \gamma^2>0.$

$$u_1=\cos f(x+\alpha y-nt),$$

$$u_2=\sqrt{\frac{\left\{\beta\left(\alpha-\frac{\mu''}{\mu}\gamma\right)\cos\beta fH\right\}^2+\left\{\left(\frac{\mu'}{\mu}\beta^2-\frac{\mu''}{\mu'}\alpha\gamma\right)\sin\beta fH\right\}^2}{\left\{\beta\left(\alpha+\frac{\mu''}{\mu'}\gamma\right)\cos\beta fH\right\}^2+\left\{\left(\frac{\mu'}{\mu}\beta^2+\frac{\mu''}{\mu'}\alpha\gamma\right)\sin\beta fH\right\}^2}}$$

$$\cdot\cos\left[f(x-\alpha y-nt)+\tan^{-1}\left\{\frac{\left(\frac{\mu'}{\mu}\beta^2-\frac{\mu''}{\mu'}\alpha\gamma\right)}{\beta\left(\alpha-\frac{\mu''}{\mu}\gamma\right)}\tan\beta fH\right\}\right.$$

$$\left.+\tan^{-1}\left\{\frac{\left(\frac{\mu'}{\mu}\beta^2+\frac{\mu''}{\mu'}\alpha\gamma\right)}{\beta\left(\alpha+\frac{\mu''}{\mu}\gamma\right)}\tan\beta fH\right\}\right], \quad (7)$$

$$u'_{y=0}=2\alpha\sqrt{\frac{(\beta\cos\beta fH)^2+\left(\frac{\mu''}{\mu}\gamma\sin\beta fH\right)^2}{\left\{\beta\left(\alpha+\frac{\mu''}{\mu}\gamma\right)\cos\beta fH\right\}^2+\left\{\left(\frac{\mu'}{\mu}\beta^2+\frac{\mu''}{\mu'}\alpha\gamma\right)\sin\beta fH\right\}^2}}$$

$$\cdot\cos\left[f(x-nt)-\tan^{-1}\left(\frac{\mu''\gamma}{\mu'\beta}\tan\beta fH\right)+\tan^{-1}\left\{\frac{\left(\frac{\mu'}{\mu}\beta^2+\frac{\mu''}{\mu'}\alpha\gamma\right)}{\beta\left(\alpha+\frac{\mu''}{\mu}\gamma\right)}\tan\beta fH\right\}\right], \quad (8)$$

$$u''=\frac{2\alpha\beta}{\sqrt{\left\{\beta\left(\alpha+\frac{\mu''}{\mu}\gamma\right)\cos\beta fH\right\}^2+\left\{\left(\frac{\mu'}{\mu}\beta^2+\frac{\mu''}{\mu'}\alpha\gamma\right)\sin\beta fH\right\}^2}}$$

$$\cdot\cos\left[f\{x+\gamma(y-H)-nt\}+\tan^{-1}\left\{\frac{\left(\frac{\mu'}{\mu}\beta^2+\frac{\mu''}{\mu'}\alpha\gamma\right)}{\beta\left(\alpha+\frac{\mu''}{\mu}\gamma\right)}\tan\beta fH\right\}\right]. \quad (9)$$

(ii) $\beta^2>0,\ \gamma^2<0\ \ (\gamma=i\gamma').$

$$u_1=\cos f(x+\alpha y-nt),$$

$$u_2=\cos\left[f(x-\alpha y-nt)-2\tan^{-1}\left\{\frac{\mu'\beta\left(\frac{\mu''}{\mu'}\gamma'-\beta\tan\beta fH\right)}{\mu\alpha\left(\beta+\frac{\mu''}{\mu'}\gamma'\tan\beta fH\right)}\right\}\right], \quad (10)$$

$$u'_{y=0}=\frac{2\alpha\left(\beta+\frac{\mu''}{\mu'}\gamma'\tan\beta fH\right)}{\sqrt{\left\{\alpha\left(\beta+\frac{\mu''}{\mu'}\gamma'\tan\beta fH\right)\right\}^2+\left\{\frac{\mu'}{\mu}\beta\left(\frac{\mu''}{\mu'}\gamma'-\beta\tan\beta fH\right)\right\}^2}}$$

$$\cdot\cos\left[f(x-nt)-\tan^{-1}\left\{\frac{\mu'\beta\left(\frac{\mu''}{\mu'}\gamma'-\beta\tan\beta fH\right)}{\mu\alpha\left(\beta+\frac{\mu''}{\mu'}\gamma'\tan\beta fH\right)}\right\}\right], \qquad (11)$$

$$u''=\frac{2\alpha\beta e^{\gamma'(H-y)}}{\sqrt{\left\{\alpha\left(\beta+\frac{\mu''}{\mu'}\gamma'\tan\beta fH\right)\right\}^2+\left\{\frac{\mu'}{\mu}\beta\left(\frac{\mu''}{\mu'}\gamma'-\beta\tan\beta fH\right)\right\}^2}}$$

$$\cdot\cos\left[f(x-nt)-\tan^{-1}\left\{\frac{\mu'\beta\left(\frac{\mu''}{\mu'}\gamma'-\beta\tan\beta fH\right)}{\mu\alpha\left(\beta+\frac{\mu''}{\mu'}\gamma'\tan\beta fH\right)}\right\}\right]. \qquad (12)$$

(iii) $\beta^2<0,\quad \gamma^2>0\quad (\beta=i\beta')$

$$u_1=\cos f(x+\alpha y-nt),$$

$$u_2=\sqrt{\frac{\left\{\beta'\left(\alpha-\frac{\mu''}{\mu}\gamma\right)\right\}^2+\left\{\left(\frac{\mu''}{\mu'}\alpha\gamma+\frac{\mu'}{\mu}\beta'^2\right)\tanh\beta' fH\right\}^2}{\left\{\beta'\left(\alpha+\frac{\mu''}{\mu}\gamma\right)\right\}^2+\left\{\left(\frac{\mu''}{\mu'}\alpha\gamma-\frac{\mu'}{\mu}\beta'^2\right)\tanh\beta' fH\right\}^2}}$$

$$\cdot\cos\left[f(x-\alpha y-nt)-\tan^{-1}\left\{\frac{\left(\frac{\mu''}{\mu'}\alpha\gamma+\frac{\mu'}{\mu}\beta'^2\right)}{\beta'\left(\alpha-\frac{\mu''}{\mu}\gamma\right)}\tanh\beta' fH\right\}\right.$$

$$\left.+\tan^{-1}\left\{\frac{\left(\frac{\mu''}{\mu'}\alpha\gamma-\frac{\mu'}{\mu}\beta'^2\right)}{\beta'\left(\alpha+\frac{\mu''}{\mu}\gamma\right)}\tanh\beta' fH\right\}\right], \qquad (13)$$

$$u'_{y=0}=2\alpha\sqrt{\frac{\beta'^2+\left(\frac{\mu''}{\mu'}\gamma\tanh\beta' fH\right)^2}{\left\{\beta'\left(\alpha+\frac{\mu''}{\mu}\gamma\right)\right\}^2+\left\{\left(\frac{\mu''}{\mu'}\alpha\gamma-\frac{\mu'}{\mu}\beta'^2\right)\tanh\beta' fH\right\}^2}}$$

$$\cdot\cos\left[f(x-nt)-\tan^{-1}\left(\frac{\mu''\gamma}{\mu'\beta'}\tanh\beta' fH\right)+\tan^{-1}\left\{\frac{\left(\frac{\mu''}{\mu}\alpha\gamma-\frac{\mu'}{\mu}\beta'^2\right)}{\beta'\left(\alpha+\frac{\mu''}{\mu}\gamma\right)}\tanh\beta' fH\right\}\right], \qquad (14)$$

$$u''=\frac{2\alpha\beta'}{\cosh\beta' fH\sqrt{\left\{\beta'\left(\alpha+\frac{\mu''}{\mu}\gamma\right)\right\}^2+\left\{\left(\frac{\mu''}{\mu'}\alpha\gamma-\frac{\mu'}{\mu}\beta'^2\right)\tanh\beta' fH\right\}^2}}$$

$$.\cos\left[f\{x+\gamma(y-H)-nt\}+\tan^{-1}\left\{\frac{\left(\frac{\mu''}{\mu'}\alpha\gamma-\frac{\mu'}{\mu}\beta'^2\right)}{\beta'\left(\alpha+\frac{\mu''}{\mu}\gamma\right)}\tanh\beta' fH\right\}\right].\quad(15)$$

(iv) $\beta^2<0$, $\gamma^2<0$ ($\beta=i\beta'$, $\gamma=i\gamma'$).

$$u_1=\cos f(x+\alpha y-nt),$$

$$u_2=-\cos\left[f(x-\alpha y-nt)+2\tan^{-1}\left\{\frac{\mu\alpha\left(\beta'+\frac{\mu''}{\mu'}\gamma'\tanh\beta' fH\right)}{\mu'\beta'\left(\frac{\mu''}{\mu'}\gamma'+\beta'\tanh\beta' fH\right)}\right\}\right],\quad(16)$$

$$u_{y=0}=\frac{2\alpha\left(\beta'+\frac{\mu''}{\mu'}\gamma'\tanh\beta' fH\right)}{\sqrt{\left\{\alpha\left(\beta'+\frac{\mu''}{\mu'}\gamma'\tanh\beta' fH\right)\right\}^2+\left\{\frac{\mu'}{\mu}\beta'\left(\frac{\mu''}{\mu'}\gamma'+\beta'\tanh\beta' fH\right)\right\}^2}}$$

$$.\cos\left[f(x-nt)-\tan^{-1}\left\{\frac{\mu'\beta'\left(\frac{\mu''}{\mu'}\gamma'+\beta'\tanh\beta' fH\right)}{\mu\alpha\left(\beta'+\frac{\mu''}{\mu'}\gamma'\tanh\beta' fH\right)}\right\}\right],\quad(17)$$

$$u''=\frac{2\alpha\beta' e^{\gamma'(H-y)}}{\cosh\beta' fH\sqrt{\left\{\alpha\left(\beta'+\frac{\mu''}{\mu'}\gamma'\tanh\beta' fH\right)\right\}^2+\left\{\frac{\mu'}{\mu}\beta'\left(\frac{\mu''}{\mu'}\gamma'+\beta'\tanh\beta' fH\right)\right\}^2}}$$

$$.\cos\left[f(x-nt)-\tan^{-1}\left\{\frac{\mu'\beta'\left(\frac{\mu''}{\mu'}\gamma'+\beta'\tanh\beta' fH\right)}{\mu\alpha\left(\beta'+\frac{\mu''}{\mu'}\gamma'\tanh\beta' fH\right)}\right\}\right].\quad(18)$$

4. We shall now consider in what conditions among μ/ρ, μ'/ρ', and μ''/ρ'', the four cases can be obtained.

(a) If $\mu/\rho>\mu'/\rho'>\mu''/\rho''$, (i) only exists.

(b) If $\mu''/\rho''>\mu'/\rho'>\mu/\rho$, (i), (ii), (iv) exist. Beyond the critical incidence angle at the first boundary, (ii) should be applied, and beyond the critical at the second boundary (iv) holds.

(c) If $\mu'/\rho'>\mu/\rho>\mu''/\rho''$, (i), (iii) exist. Beyond the critical incidence angle at the first boundary, (iii) should be applied.

(d) If $\mu/\rho>\mu''/\rho''>\mu'/\rho'$, (i), (ii) exist. Beyond the critical in-

cidence angle at the second boundary (ii) should be applied.

(e) If $\mu'/\rho' > \mu''/\rho'' > \mu/\rho$, the cases are the same as in (c).

(f) If $\mu''/\rho'' > \mu/\rho > \mu'/\rho'$, the cases are the same as in (d).

The most particular and interesting conditions are those in (c) and (e), where μ'/ρ' (belonging to the layer) is greater than either of μ/ρ or μ''/ρ''. In such a condition, notwithstanding that the waves are apparently totally reflected at the first boundary plane beyond a certain critical angle, the waves are however transmitted outwards with a certain velocity component in y direction. They belong to the case (iii). Thus, waves are not totally reflected at the layer in an actual meaning.

Another important fact is that, if $\mu'/\rho' \to \infty$ in (c) or (e), or if $\mu'/\rho' \to 0$ in (d) or (f), no waves can be transmitted in the third medium as will be seen from the expressions of u'' in (9), (12), (15), (18). Thus the word "total reflection" may rather be used for the meaning of these cases.

5. Amplitudes of transmitted waves differ not only with the difference in incidence angle but also with the difference in the ratio of length of incident waves to the thickness of the layer. We have calculated the cases (a) $\rho=\rho'=\rho''$, $\mu'/\mu=1/2$, $\mu''/\mu'=1/2$, (b) $\rho=\rho'=\rho''$, $\mu'/\mu=2$, $\mu''/\mu'=2$, the result being shown in Figs. 2, 3. In these figures $2\pi/f$ is the length of the incident waves whose amplitude is unity, and e the angle between the direction of wave propagation and the normal to the layer. In the condition (a), the amplitudes become larger and larger as the incidence angle tends to zero, whereas in the condition (b) the reverse is the case. In both two cases the amplitudes change periodically with the change of fH, the periods assuming smaller values for smaller e. In the case (b) of the present example, $\cot e=2$ gives the approximate critical of

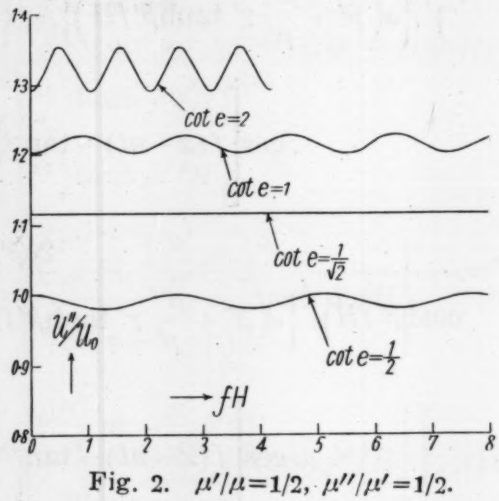

Fig. 2. $\mu'/\mu=1/2$, $\mu''/\mu'=1/2$.

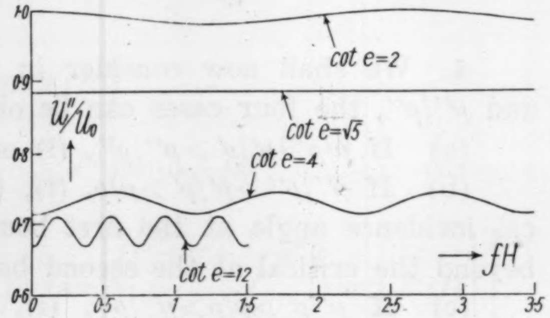

Fig. 3. $\mu'/\mu=2$, $\mu''/\mu'=2$.

the incidence angle at the second boundary. It may be a remarkable fact that the amplitudes of transverse waves in this condition of (b) is the same as the ones in such condition of (a) as specified by cot $e=1/2$, namely in the condition that the complementary relation between the incidence angles for both cases exists.

---

15. 不連續層を通過する横波の性質

地震研究所 {妹澤克惟
金井清

前に不連續層を通過する地震波について述べたことがあるけれども，それはその層に直角に波が通過する場合であつた．斜に通過する場合は Knott の問題の如く不連續面を通過する場合しかやつてないやうである．しかし不連續層を通過する波の全反射を議論する爲に，問題を簡單にして橫波が通過する場合を研究して見たのである．

この研究で種々のことがわかつたが，特に著しいことは，波動か斜にやつて來て，不連續層の前面で一度所謂全反射した積りのものが，不連續層後面からは或條件さへかなへば，波動がどんどん出て行くことである．この意味に於て所謂全反射といふ言葉は餘り適當しないやうに考へられる．

ほんとうに全反射となるのは不連續層の彈性又は密度が外部のそれと著しく異なる場合であることも知られるのである．

---

16. *Improved Theory of Energy Dissipation in Seismic Vibrations of a Structure.*

By Katsutada SEZAWA and Kiyoshi KANAI,

Earthquake Research Institute.

(Read March 17, 1936.—Received March 20, 1936.)

1. *Introduction.*

After several investigations since last year we h[illegible] ascertained the nature of energy dissipation in se[illegible] a structure. Since in spite of its importance on [illegible] construction the problem hardly received the att[illegible] until recently and furthermore the treatment of [illegible] too easy, we took a somewhat approximate met[illegible] cularly in the form of dissipating waves, wit[illegible] qualitative results as simply as possible. As [illegible] scattered waves that dissipate from the structur[illegible] longitudinal as well as transverse waves, associated [illegible] the consideration of all kinds of dissipating waves [illegible] being therefore practically impossible. We made conse[illegible] rough approximation with respect to the form of scattered long[illegible] waves as taking $\Delta = a\cos\theta \exp.i(pt-hr)/r$ instead of its more accurate form $\Delta = a\cos\theta \exp.i(pt-hr)\{1/r+1/i\,hr^2\}$, under the assumed condition that the surface waves are temporarily omitted. The next step was to use a rather general case, $y_{x=0} = u_{0x=0} + u_{r=\varepsilon,\,\theta=0}$ and $\partial u_0/\partial x_{x=0} = a$ *finite*, in lieu of its more convenient condition, $y_{x=0} = u_{0\,x=0} + u'_{0x=0} + u_{r=\varepsilon,\,\theta=0}$ and $\partial(u_0+u'_0)/\partial x_{x=0} = 0$, where u'_0 is the displacement of normally reflected waves. Another important assumption was to put $\lambda = 14\mu$ in place of taking arbitrary λ and μ. Furthermore, we neglected higher orders of such apparently small quantities as ε, the result of which is sometimes contradictory to the assumed condition of the problem. Generally speaking, however, these assumptions are not likely to affect the main charater of the problem resulting from its solution, owing probably to the reason that the assumed conditions deviate little, physically, from the actual ones.[1] Since, on the other hand, our study is being

1) K. SEZAWA and K. KANAI, *Bull. Earthq. Res. Inst.*, **13** (1935), 682~683, 687, 690; 918~919.

understood more or less by many investigators quite recently and the assumptions above cited are liable to be criticized by them, we are now in position to improve the problem in a stricter way. Our new study attempted from this intention, shows that the calculation under the improved assumptions is not too much difficult and furthermore gives rise to such new results as incapable of being found in the previous study. The theoretical part of the improved problem will be shown in this paper.

2. *A simplest structure subjected to incident longitudinal waves.*[2)]

Let the incident and reflected longitudinal waves with their displacements orientated vertically be

$$u_0 = e^{i(pt+hx)}, \qquad u_0' = e^{i(pt-hx)}, \tag{1}$$

where $h^2 = \rho p^2/(\lambda+2\mu)$. The scattered longitudinal as well as transverse waves and the vibration of the structure are expressed by

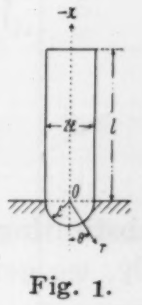

Fig. 1.

$$\left.\begin{aligned} \Delta &= \alpha\cos\theta\, e^{i(pt-hr)}\left(\frac{1}{r}+\frac{1}{ihr^2}\right), \\ \varpi &= -\beta\sin\theta\, e^{i(pt-kr)}\left(\frac{1}{r}+\frac{1}{ikr^2}\right), \end{aligned}\right\} \tag{2}$$

$$\left.\begin{aligned} u_1 &= -\frac{\alpha}{h^2}\cos\theta\frac{d}{dr}e^{i(pt-hr)}\left(\frac{1}{r}+\frac{1}{ihr^2}\right), \\ v_1 &= \frac{\alpha}{h^2}\sin\theta\frac{1}{r}e^{i(pt-hr)}\left(\frac{1}{r}+\frac{1}{ihr^2}\right), \end{aligned}\right\} \tag{3}$$

$$\left.\begin{aligned} u_2 &= -\frac{4\beta}{k^2}\cos\theta\frac{1}{r}e^{i(pt-kr)}\left(\frac{1}{r}+\frac{1}{ikr^2}\right), \\ v_2 &= \frac{2\beta}{k^2}\sin\theta\frac{1}{r}\frac{d}{dr}e^{i(pt-kr)}\left(1+\frac{1}{ikr}\right), \end{aligned}\right\} \tag{4}$$

$$u' = Be^{i(pt+h'x)} + Ce^{i(pt-h'x)}, \tag{5}$$

$$h^2 = \frac{\rho p^2}{\lambda+2\mu}, \qquad k^2 = \frac{\rho p^2}{\mu}, \qquad h'^2 = \frac{\rho' p^2}{E}, \tag{6}$$

where u_1, v_1 and u_2, v_2 satisfy accurately the equations of motion for both longitudinal and transverse bodily waves and u' that for the vibration of the structure; ρ, λ, μ; ρ', E being densities and elastic con-

2) *Bull. Earthq. Res. Inst.*, **13** (1935), 682.

16. *Improved Theory of Energy Dissipation in Seismic Vibrations of a Structure.*

By Katsutada SEZAWA and Kiyoshi KANAI,

Earthquake Research Institute.

(Read March 17, 1936.—Received March 20, 1936.)

1. *Introduction.*

After several investigations since last year we have qualitatively ascertained the nature of energy dissipation in seismic vibrations of a structure. Since in spite of its importance on the earthquake-proof construction the problem hardly received the attention of investigators until recently and furthermore the treatment of the problem was not too easy, we took a somewhat approximate method of solution, particularly in the form of dissipating waves, with a view to obtaining qualitative results as simply as possible. As a matter of fact, the scattered waves that dissipate from the structure into the ground are longitudinal as well as transverse waves, associated with surface waves, the consideration of all kinds of dissipating waves in an exact way being therefore practically impossible. We made consequently such a rough approximation with respect to the form of scattered longitudinal waves as taking $\Delta = a\cos\theta\ \exp. i(pt-hr)/r$ instead of its more accurate form $\Delta = a\cos\theta\ \exp. i(pt-hr)\{1/r+1/i\,hr^2\}$, under the assumed condition that the surface waves are temporarily omitted. The next step was to use a rather general case, $y_{x=0}=u_{0x=0}+u_{r=\varepsilon,\,\theta=0}$ and $\partial u_0/\partial x_{x=0}=a$ *finite*, in lieu of its more convenient condition, $y_{x=0}=u_{0\,x=0}+u'_{0\,x=0}+u_{r=\varepsilon,\,\theta=0}$ and $\partial(u_0+u'_0)/\partial x_{x=0}=0$, where u'_0 is the displacement of normally reflected waves. Another important assumption was to put $\lambda=14\mu$ in place of taking arbitrary λ and μ. Furthermore, we neglected higher orders of such apparently small quantities as ε, the result of which is sometimes contradictory to the assumed condition of the problem. Generally speaking, however, these assumptions are not likely to affect the main charater of the problem resulting from its solution, owing probably to the reason that the assumed conditions deviate little, physically, from the actual ones.[1] Since, on the other hand, our study is being

1) K. SEZAWA and K. KANAI, *Bull. Earthq. Res. Inst.*, **13** (1935), 682~683, 687, 690; 918~919.

understood more or less by many investigators quite recently and the assumptions above cited are liable to be criticized by them, we are now in position to improve the problem in a stricter way. Our new study attempted from this intention, shows that the calculation under the improved assumptions is not too much difficult and furthermore gives rise to such new results as incapable of being found in the previous study. The theoretical part of the improved problem will be shown in this paper.

2. *A simplest structure subjected to incident longitudinal waves.*[2)]

Let the incident and reflected longitudinal waves with their displacements orientated vertically be

$$u_0 = e^{i(pt+hx)}, \qquad u_0' = e^{i(pt-hx)}, \tag{1}$$

where $h^2 = \rho p^2/(\lambda+2\mu)$. The scattered longitudinal as well as transverse waves and the vibration of the structure are expressed by

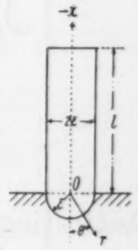

Fig. 1.

$$\left.\begin{aligned} \Delta &= a\cos\theta\, e^{i(pt-hr)}\left(\frac{1}{r}+\frac{1}{ihr^2}\right), \\ \varpi &= -\beta\sin\theta\, e^{i(pt-kr)}\left(\frac{1}{r}+\frac{1}{ikr^2}\right), \end{aligned}\right\} \tag{2}$$

$$\left.\begin{aligned} u_1 &= -\frac{a}{h^2}\cos\theta\frac{d}{dr}e^{i(pt-hr)}\left(\frac{1}{r}+\frac{1}{ihr^2}\right), \\ v_1 &= \frac{a}{h^2}\sin\theta\frac{1}{r}e^{i(pt-hr)}\left(\frac{1}{r}+\frac{1}{ihr^2}\right), \end{aligned}\right\} \tag{3}$$

$$\left.\begin{aligned} u_2 &= -\frac{4\beta}{k^2}\cos\theta\frac{1}{r}e^{i(pt-kr)}\left(\frac{1}{r}+\frac{1}{ikr^2}\right), \\ v_2 &= \frac{2\beta}{k^2}\sin\theta\frac{1}{r}\frac{d}{dr}e^{i(pt-kr)}\left(1+\frac{1}{ikr}\right), \end{aligned}\right\} \tag{4}$$

$$u' = Be^{i(pt+h'x)} + Ce^{i(pt-h'x)}, \tag{5}$$

$$h^2 = \frac{\rho p^2}{\lambda+2\mu}, \qquad k^2 = \frac{\rho p^2}{\mu}, \qquad h'^2 = \frac{\rho' p^2}{E}, \tag{6}$$

where u_1, v_1 and u_2, v_2 satisfy accurately the equations of motion for both longitudinal and transverse bodily waves and u' that for the vibration of the structure; ρ, λ, μ; ρ', E being densities and elastic con-

2) *Bull. Earthq. Res. Inst.*, **13** (1935), 682.

stants of the earth and the structure respectively.

Let us assume that the structure is a uniform circular cylinder of radius ε and of length l, then the boundary conditions are such that, at the upper end of the structure, $x=-l$,

$$\frac{\partial u'}{\partial x}=0\,; \tag{7}$$

and at its lower end, $x=0$, $r\to\varepsilon$,

$$(u_1+u_2)_{\max.}=-(v_1+v_2)_{\max.}\,, \tag{8}$$

$$u'=u_0+u_0'+(u_1+u_2)_{\theta=0}\,, \tag{9}$$

$$E\pi\varepsilon^2\frac{\partial u'}{\partial x}=\int_{\varphi=0}^{\varphi=2\pi}\int_{\theta=0}^{\theta=\frac{\pi}{2}}\mu\left\{\frac{\partial(v_1+v_2)}{\partial r}-\frac{v_1+v_2}{r}+\frac{1}{r}\frac{\partial(u_1+u_2)}{\partial\theta}\right\}r_2\sin^2\theta\, d\varphi d\theta\,,$$

$$+\int_{\varphi=0}^{\varphi=2\pi}\int_{\theta=0}^{\theta=\frac{\pi}{2}}\left\{\lambda\Delta+2\mu\frac{\partial(u_1+u_2)}{\partial r}\right\}r^2\sin\theta\cos\theta\, d\varphi d\theta\,. \tag{10}$$

Substituting the solutions in these conditions and taking the real part only, we get

$$u_0=\cos(pt+hx)\,, \tag{1'}$$

$$u'=4\sqrt{\frac{\Gamma_1^2+\Gamma_2^2}{P^2+Q^2}}\cosh'(x+l)\cos\left(pt+\tan^{-1}\frac{\Gamma_2}{\Gamma_1}-\tan^{-1}\frac{Q}{P}\right), \tag{11}$$

where

$$\left.\begin{aligned}
P&=2\Gamma_1\cos h'l+\frac{3E\varepsilon}{\mu l}\Lambda_1 h'l\sinh'l\,,\\
Q&=2\Gamma_2\cos h'l+\frac{3E\varepsilon}{\mu l}\Lambda_2 h'l\sinh'l\,,\\
\Gamma_1&=3+\nu(h'l)^2\left(\frac{\lambda}{\mu}-3\sqrt{\frac{\lambda}{\mu}+2}\right),\\
\Gamma_2&=\sqrt{\nu}\,(h'l)\left\{3\left(\sqrt{\frac{\lambda}{\mu}+2}+1\right)+\nu(h'l)^2\left(\frac{\lambda}{\mu}+2-2\sqrt{\frac{\lambda}{\mu}+2}\right)\right\},\\
\Lambda_1&=\frac{\mu}{\lambda+2\mu}+2-\nu(h'l)^2\,,\\
\Lambda_2&=\sqrt{\nu}\,(h'l)\left(\sqrt{\frac{\mu}{\lambda+2\mu}}+2\right),\\
\nu&=\frac{\rho E\varepsilon^2}{\rho'(\lambda+2\mu)l^2}\,.
\end{aligned}\right\} \tag{12}$$

The right-hand term under the root sign of the denominator of (11) represents the effect of the dissipation of energy scattered as seismic waves. The larger the absolute value of the term under consideration, the larger will be the decrease in the amplitudes of vibration at the period corresponding to the resonance condition, $2\Gamma_1 \cosh h'l + (3E\varepsilon/\mu l)\cdot A_1 h'l \sinh h'l = 0$, of the case without dissipation of energy. It should be remembered that the equation showing the resonance condition in the present accurate calculation is somewhat modified from the previous one. Numerical examples of the result of the present as well as following sections will be left to next occasion.

3. *A tall structure with rigid floors subjected to incident transverse waves.*[3)]

Let ρ, λ, μ; $\rho' (=m/al_1)$, $G(=12{\cdot}4Ej^2/l_1^2)$ be the density and elastic constants of the earth, and the effective density and the effective rigidity of the structure, where E, j, l_1, a are Young's modulus, radius of gyration of section, length and total sum of the sectional areas of the columns between two adjacent floors respectively. Provided the incident transverse waves in the earth are transmitted vertically upwards, the solutions of the incidednt as well as reflected waves, and those of the structural vibrations are as follows:

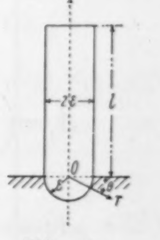

Fig. 2.

$$u_0 = e^{i(pt+kx)}, \qquad u_0' = e^{i(pt-kx)}, \tag{13}$$

$$u' = Be^{i(pt+k'x)} + Ce^{i(pt-k'x)}, \tag{14}$$

where $k^2 = \rho p^2/\mu$, $k'^2 = \rho' p^2/G$, the forms of scattered waves being the same as those in (3), (4). The boundary conditions are expressed by

$$\frac{\partial u'}{\partial x} = 0 \tag{15}$$

at $x = -l$, and

$$(u_1 + u_2)_{\max.} = -(v_1 + v_2)_{\max.}, \tag{16}$$

$$u' = u_0 + u_0' + (u_1 + u_2)_{\theta=0}, \tag{17}$$

$$G\pi\varepsilon^2 \frac{\partial u'}{\partial x} = \int_{\varphi=0}^{\varphi=\pi}\int_{\theta=0}^{\theta=\pi} \mu\left\{\frac{\partial(v_1+v_2)}{\partial r} - \frac{v_1+v_2}{r} + \frac{1}{r}\frac{\partial(u_1+u_2)}{\partial\theta}\right\} r^2 \sin^2\theta \, d\varphi \, d\theta$$

$$+ \int_{\varphi=0}^{\varphi=\pi}\int_{\theta=0}^{\theta=\pi} \left\{\lambda\Delta + 2\mu \frac{\partial(u_1+u_2)}{\partial r}\right\} r^2 \sin\theta \cos\theta \, d\varphi \, d\theta, \tag{18}$$

3) *Bull. Earthq. Res. Inst.*, **13** (1935), 687.

at $x=0$, $r=\varepsilon$. Substituting the solutions in these conditions and taking real parts, we obtain

$$u_0=\cos(pt+kx), \tag{13'}$$

$$u'=4\sqrt{\frac{\Gamma_1^2+\Gamma_2^2}{P^2+Q^2}}\cos k'(x+l)\cos\left(pt+\tan^{-1}\frac{\Gamma_2}{\Gamma_1}-\tan^{-1}\frac{Q}{P}\right), \tag{19}$$

where

$$\left.\begin{aligned}
P&=2\Gamma_1\cos k'l+\frac{3G\varepsilon}{\mu l}\Lambda_1 k'l\sin k'l,\\
Q&=2\Gamma_2\cos k'l+\frac{3G\varepsilon}{\mu l}\Lambda_2 k'l\sin k'l,\\
\Gamma_1&=3\left(\frac{\lambda}{\mu}+2\right)+\nu(k'l)^2\left(\frac{\lambda}{\mu}-3\sqrt{\frac{\lambda}{\mu}+2}\right),\\
\Gamma_2&=\sqrt{\nu}\,(k'l)\left\{3\left(\frac{\lambda}{\mu}+2+\sqrt{\frac{\lambda}{\mu}+2}\right)+\nu(k'l)^2\left(\sqrt{\frac{\lambda}{\mu}+2}-2\right)\right\},\\
\Lambda_1&=\left(\frac{2\lambda}{\mu}+5\right)-\nu(k'l)^2,\\
\Lambda_2&=\sqrt{\nu}\,(k'l)\left(2\sqrt{\frac{\lambda}{\mu}+2}+1\right),\\
\nu&=\frac{\rho G\varepsilon^2}{\rho'\mu l^2}.
\end{aligned}\right\} \tag{20}$$

The solutions show certain features of vibrations similar to those in the previous case.

4. *A tall structure with flexible floors subjected to incident transverse waves.*[4]

Let ρ, λ, μ; $\rho'(=m/al_1)$, j be the density and elastic constants of the earth, the effective density of the structure and the radius of gyration of a section of a column, where m, l_1, a are mass concentrated on every floor, and the length and total sum of the sectional areas of columns between two adjacent floors respectively. From the equation of motion of the structure

$$\frac{\partial^2 y}{\partial t^2}+\frac{Ej^2}{\rho'}\frac{\partial^4 y}{\partial x^4}=0, \tag{21}$$

4) *Bull. Earthq. Res. Inst.*, **13** (1935), 690.

we find

$$y=e^{ipt}\left[Ae^{i\sqrt{p}cx}+Be^{-i\sqrt{p}cx}+Ce^{\sqrt{p}cx}+De^{-\sqrt{p}cx}\right], \tag{22}$$

in which $c=(\rho'/Ej^2)^{\frac{1}{4}}$. The forms of incident waves, u_0, plane reflected waves u_0', and scattered waves, u_1, v_1; u_2, v_2 are respectively the same as those in (13), (3), (4). Using the same figure as Fig. 2, the boundary conditions are such that, at $x=-l$,

$$\frac{\partial^2 y}{\partial x^2}=0, \qquad \frac{\partial^3 y}{\partial x^3}=0; \tag{23), (24}$$

and, at $x=0$, $r=\varepsilon$,

$$(u_1+u_2)_{\text{max.}}=-(v_1+v_2)_{\text{max.}}, \tag{25}$$

$$y=u_0+u_0'+(u_1+u_2)_{\theta=0}, \tag{26}$$

$$\frac{\partial y}{\partial x}=0, \tag{27}$$

$$-E\pi\varepsilon^2 j^2\frac{\partial^3 y}{\partial x^3}=\int_{\varphi=0}^{\varphi=\pi}\int_{\theta=0}^{\theta=\pi}\mu\left\{\frac{\partial(v_1+v_2)}{\partial r}-\frac{(v_1+v_2)}{r}+\frac{1}{r}\frac{\partial(u_1+u_2)}{\partial\theta}\right\}r^2\sin^2\theta d\varphi d\theta$$
$$+\int_{\varphi=0}^{\varphi=\pi}\int_{\theta=0}^{\theta=\pi}\left\{\lambda\Delta+2\mu\frac{\partial(u_1+u_2)}{\partial r}\right\}r^2\sin\theta\cos\theta\, d\varphi d\theta. \tag{28}$$

The final solutions in real forms are as follows:

$$u_0=\cos(pt+kx), \tag{13''}$$

$$y=M\sqrt{\frac{\Gamma_1^2+\Gamma_2^2}{P^2+Q^2}}\cos\left\{pt+\tan^{-1}\frac{\Gamma_2}{\Gamma_1}-\tan^{-1}\frac{Q}{P}\right\}, \tag{29}$$

where

$$\left.\begin{aligned}
M=&\cos\sqrt{p}\,cl\cosh\sqrt{p}\,c(x+l)+\cosh\sqrt{p}\,cl\cos\sqrt{p}\,c(x+l)\\
&+\sin\sqrt{p}\,cl\sinh\sqrt{p}\,c(x+l)-\sinh\sqrt{p}\,cl\sin\sqrt{p}\,c(x+l)\\
&+\cos\sqrt{p}\,cx+\cosh\sqrt{p}\,cx,\\
P=&2(\cos\sqrt{p}\,cl\cosh\sqrt{p}\,cl+1)\Gamma_1+\frac{3E\varepsilon j^2}{\mu l^3}(\sqrt{p}\,cl)^3\\
&.(\cos\sqrt{p}\,cl\sinh\sqrt{p}\,cl+\sin\sqrt{p}\,cl\cosh\sqrt{p}\,cl)\Delta_1,\\
Q=&2(\cos\sqrt{p}\,cl\cosh\sqrt{p}\,cl+1)\Gamma_2+\frac{3E\varepsilon j^2}{\mu l^3}(\sqrt{p}\,cl)^3\\
&.(\cos\sqrt{p}\,cl\sinh\sqrt{p}\,cl+\sin\sqrt{p}\,cl\cosh\sqrt{p}\,cl)\Delta_2,
\end{aligned}\right\} \tag{30}$$

$$
\left.\begin{aligned}
\Gamma_1&=3\left(\frac{\lambda}{\mu}+2\right)+\nu(\sqrt{p}\,cl)^4\left(\frac{\lambda}{\mu}-3\sqrt{\frac{\lambda}{\mu}+2}\right),\\
\Gamma_2&=\sqrt{\nu}\,(\sqrt{p}\,cl)^2\left\{3\left(\frac{\lambda}{\mu}+2+\sqrt{\frac{\lambda}{\mu}+2}\right)+\nu(\sqrt{p}\,cl)^4\left(\sqrt{\frac{\lambda}{\mu}+2}-2\right),\right.\\
\Lambda_1&=\left(\frac{2\lambda}{\mu}+5\right)-\nu(\sqrt{p}\,cl)^4,\\
\Lambda_2&=\sqrt{\nu}\,(\sqrt{p}\,cl)^2\left(2\sqrt{\frac{\lambda}{\mu}+2}+1\right),\\
\nu&=\frac{\rho Ej^2\varepsilon^2}{\rho'\mu l^4}.
\end{aligned}\right\} \tag{31}
$$

The resonance condition is specified by $P=0$, the displacement of the structure then assuming the form

$$y=\frac{M\sqrt{\Gamma_1^2+\Gamma_2^2}}{Q}\cos\left\{pt+\tan^{-1}\frac{\Gamma_2}{\Gamma_1}\pm\frac{\pi}{2}\right\}.$$

5. *General theory in the case of a framed structure.*

Incident, reflected, and scattered waves are assumed to have the same forms as those in the preceding two sections. The solution of the vibratory motion of columns between $(s-1)$th and sth floors is determined from the differential equation of the type, $\partial^4 y_s/\partial x_s^4=0$, as follows:

$$y_s=(A_s+B_sx_s+C_sx_s^2+D_sx_s^3)e^{ipt} \qquad (s=1,\ 2,\ \cdots,\ n), \tag{32}$$

where x_s is the coordinate of a point of the columns measured negatively from their respective lower ends, y_s the horizontal deflection of point x_s. Let l_s, E_s, I_s be the length, Young's modulus, and the sum of the moments of inertia of cross sections of all the columns between $(s-1)$th and the sth floors, and m_s mass concentrated at sth floor. Then, imagining a figure similar to Fig. 2, the boundary conditions are as follows.

$$x_n=-l_n; \qquad E_nI_n\frac{\partial^3 y_n}{\partial x_n^3}+m_n\frac{\partial^2 y_n}{\partial t^2}=0, \tag{33}$$

$$\frac{\partial y_n}{\partial x_n}=0 \text{ (rigid floors), or } \frac{\partial^2 y_n}{\partial x_n^2}=0 \text{ (flexible floors)}, \tag{34}$$

$$x_s=-l_s,\ x_{s+1}=0;\ E_{s+1}I_{s+1}\frac{\partial^3 y_{s+1}}{\partial x_{s+1}^3}=E_sI_s\frac{\partial^3 y_s}{\partial x_s^3}+m_s\frac{\partial^2 y_s}{\partial t^2}, \tag{35}$$

$$y_s = y_{s+1}, \tag{36}$$

$$\frac{\partial y_s}{\partial x_s} = 0, \quad \frac{\partial y_{s+1}}{\partial x_{s+1}} = 0 \text{ (rigid floors)},$$

$$\text{or } \frac{\partial y_s}{\partial x_s} = \frac{\partial y_{s+1}}{\partial x_{s+1}}, \quad E_{s+1} I_{s+1} \frac{\partial^2 y_{s+1}}{\partial x_{s+1}^2} = E_s I_s \frac{\partial^2 y_s}{\partial x_s^2} \text{ (flexible floors)}, \tag{37}$$

$$(s = 1, 2, \cdots, n-1)$$

$$x_1 = 0, \quad r = \varepsilon; \quad (u_1 + u_2)_{\text{max.}} = -(v_1 + v_2)_{\text{max.}}, \tag{38}$$

$$y_1 = u_0 + u_0' + (u_1 + u_2)_{r=\varepsilon,\ \theta=0}, \tag{39}$$

$$\frac{\partial y_1}{\partial x_1} = 0 \text{ (clamped base)}, \text{ or } \frac{\partial^2 y_1}{\partial x_1^2} = 0 \text{ (hinged base)}, \tag{40}$$

$$-E\pi\varepsilon^2 j^2 \frac{\partial^3 y_1}{\partial x_1^3} = \int_{\varphi=0}^{\varphi=\pi} \int_{\theta=0}^{\theta=\pi} \mu \left\{ \frac{\partial (v_1 + v_2)}{\partial r} - \frac{(v_1 + v_2)}{r} + \frac{1}{r} \frac{\partial (u_1 + u_2)}{\partial \theta} \right\} r^2 \sin^2\theta \, d\varphi \, d\theta$$

$$+ \int_{\varphi=0}^{\varphi=\pi} \int_{\theta=0}^{\theta=\pi} \left\{ \lambda \Delta + 2\mu \frac{\partial (u_1 + u_2)}{\partial r} \right\} r^2 \sin\theta \cos\theta \, d\varphi \, d\theta. \tag{41}$$

Substituting the solutions for incident, reflected, and scattered waves, as well as for the vibratory motion of all the columns in these boundary conditions in respective cases it is possible to obtain the deflections or bending moments of columns.

From the relations (38), (39), (41), which are connected with the nature of dissipation, we obtain

$$\Gamma A_1 + \frac{9E_1 j_1^2 \varepsilon}{\mu} \Lambda D_1 = 2\Gamma, \tag{42}$$

where

$$\left.\begin{aligned}
&\Gamma = \Gamma_1 + i\Gamma_2, \quad \Lambda = \Lambda_1 + i\Lambda_2, \\
&\Gamma_1 = \frac{3(\lambda + 2\mu)}{\mu} + \nu\gamma_1 \left(\frac{\lambda}{\mu} - 3\sqrt{\frac{\lambda + 2\mu}{\mu}} \right), \\
&\Gamma_2 = \sqrt{\nu\gamma_1} \left\{ 3\left(\frac{\lambda + 2\mu}{\mu} + \sqrt{\frac{\lambda + 2\mu}{\mu}} \right) + \nu\gamma_1 \left(\sqrt{\frac{\lambda + 2\mu}{\mu}} - 2 \right) \right\}, \\
&\Lambda_1 = \frac{2\lambda + 5\mu}{\mu} - \nu\gamma_1, \\
&\Lambda_2 = \sqrt{\nu\gamma_1} \left(2\sqrt{\frac{\lambda + 2\mu}{\mu}} + 1 \right), \\
&\nu = \frac{E_1 \rho I_1 \varepsilon^2}{\mu m_1 l_1^3}.
\end{aligned}\right\} \tag{43}$$

These relations hold in any case of a framed structure irrespective of the conditions of columns at the floors as well as at the base. It should be borne in mind that the symbols

$$\left.\begin{aligned} \gamma_s=\frac{m_s p^2 l_s^3}{E_s I_s}\ (s=1,2,\cdots,n)\,,\quad \eta_s=\frac{E_{s+1}I_{s+1}l_s^3}{E_s I_s l_{s+1}^3}\,, \\ \xi_s=\frac{l_{s+1}}{l_s}\ (s=1,2,\cdots,n-1) \end{aligned}\right\} \tag{44}$$

are commonly used in (43) and in treatments which will appear hereafter. Again, in the subsequent sections, we shall mainly show the general expressions of A_s, B_s, C_s, D_s, by means of which it is possible to write the formulae for the deflections (or bending moments) of columns. The expressions of bending moments will also be added, though for simplest cases, with a view to getting a quick application of the result.

6. *A structure with rigid floors and clamped base.*[5]

From (33), (34), (35), (36), (37), (39) we find the relations such that[6]

$$\left.\begin{aligned} &B_s=0\,,\quad C_s=\frac{3}{2}l_s D_s\,,\quad (s=1,2,3,\cdots,n) \\ &A_{s+1}=\frac{1}{2}(2A_s+l_s^3 D_s),\ (s=1,2,3,\cdots,n-1) \\ &D_{s+1}=\frac{E_s I_s}{12E_{s+1}I_{s+1}l_s^3}\Big\{-2\gamma_s A_s+(12-\gamma_s)l_s^3 D_s\Big\}\,, \\ &\qquad\qquad (s=1,2,3,\cdots,n-1) \\ &A_n=\frac{12-\gamma_n}{2\gamma_n}l_n^3 D_n\,. \end{aligned}\right\} \tag{45}$$

By means of these relations and (42), we obtain the absolute values of A_s, B_s, C_s, D_s, the final result being shown below. The incident waves are assumed to be of the type $e^{i(pt+kx)}$ in determining the coefficients under consideration, whereas they should take the form $\cos(pt+kx)$ in the solution of bending moments described here.

(i) $n=1$;

$$\left.\begin{aligned} &A_1=\frac{2(12-\gamma_1)\Gamma}{\Phi}\,,\quad B_1=0\,,\quad D_1=\frac{4\gamma_1\Gamma}{\Phi l_1^3}\,,\quad C_1=\frac{3}{2}l_1 D_1\,, \\ &\Phi=(12-\gamma_1)\Gamma+\frac{18E_1 j_1^2\varepsilon}{\mu l_1^3}\gamma_1\Lambda\,, \end{aligned}\right\} \tag{46}$$

5) *Bull. Earthq. Res. Inst.*, **13** (1935), 700.
6) *Ditto*, 919.

$$EI\frac{\partial^2 y}{\partial x^2}\Big/ 2\,p^2 ml = \frac{6\sqrt{\Gamma_1^2+\Gamma_2^2}}{\sqrt{P^2+Q^2}}\left(1+\frac{2x}{l}\right)\cos\left(pt+\tan^{-1}\frac{\Gamma_2}{\Gamma_1}-\tan^{-1}\frac{Q}{P}\right), \quad (47)$$

where $E=E_1$, $I=I_1$, $m=m_1$, $l=l_1$, and

$$\left.\begin{aligned} P&=(12-\gamma)\,\Gamma_1+\frac{18Ej^2\varepsilon}{\mu l^3}\gamma\Lambda_1\,,\\ Q&=(12-\gamma)\,\Gamma_2+\frac{18Ej^2\varepsilon}{\mu l^3}\gamma\Lambda_2\,.\end{aligned}\right\} \quad (48)$$

(ii) $n=2$;

$$\left.\begin{aligned} A_1&=2\Big\{12\gamma_2\eta_1-(12-\gamma_1)(12-\gamma_2)\Big\}\frac{\Gamma}{\Phi}\,,\\ D_1&=-4\Big\{12\gamma_2\eta_1+\gamma_1(12-\gamma_2)\Big\}\frac{\Gamma}{l_1^3\Phi}\,,\\ A_2&=-2.12(12-\gamma_2)\frac{\Gamma}{\Phi}\,,\quad D_2=-4.12\gamma_2\frac{\Gamma}{l_2^3\Phi}\,,\\ B_1&=B_2=0\,,\quad C_1=\frac{3}{2}l_1D_1\,,\quad C_2=\frac{3}{2}l_2D_2\,,\\ \Phi&=\Big\{12\gamma_2\eta_1-(12-\gamma_1)(12-\gamma_2)\Big\}\Gamma-\frac{18E_1j_1^2\varepsilon}{\mu l_1^3}\Big\{12\gamma_2\eta_1+\gamma_1(12-\gamma_2)\Big\}\Lambda\,.\end{aligned}\right\} \quad (49)$$

$$\left.\begin{aligned} EI\frac{\partial^2 y_1}{\partial x_1^2}\Big/ 2\,p^2ml&=6(\gamma-24)\sqrt{\frac{\Gamma_1^2+\Gamma_2^2}{P^2+Q^2}}\left(1+\frac{2x_1}{l}\right)\\ &\qquad .\cos\left(pt+\tan^{-1}\frac{\Gamma_2}{\Gamma_1}-\tan^{-1}\frac{Q}{P}\right),\\ EI\frac{\partial^2 y_2}{\partial x_2^2}\Big/ 2\,p^2ml&=6.12\sqrt{\frac{\Gamma_1^2+\Gamma_2^2}{P^2+Q^2}}\left(1+\frac{2x_2}{l}\right)\\ &\qquad .\cos\left(pt+\tan^{-1}\frac{\Gamma_2}{\Gamma_1}-\tan^{-1}\frac{Q}{P}\right),\end{aligned}\right\} \quad (50)$$

in which $E=E_1=E_2$, $I=I_1=I_2$, $m=m_1=m_2$, $l=l_1=l_2$, and

$$\left.\begin{aligned} P&=\Big\{(12-\gamma)^2-12\gamma\Big\}\Gamma_1+\frac{18Ej^2\varepsilon}{\mu l^3}\gamma(24-\gamma)\Lambda_1\,,\\ Q&=\Big\{(12-\gamma)^2-12\gamma\Big\}\Gamma_2+\frac{18Ej^2\varepsilon}{\mu l^3}\gamma(24-\gamma)\Lambda_2\,.\end{aligned}\right\} \quad (51)$$

(iii) $n=3$;

$$
\left.
\begin{aligned}
A_1&=2\Big[12\eta_2\gamma_3\Big\{12\eta_1+(12-\gamma_1)\Big\} \\
&\qquad\qquad +(12-\gamma_3)\Big\{12\eta_1\gamma_2-(12-\gamma_1)(12-\gamma_2)\Big\}\Big]\frac{\Gamma}{\Phi}, \\
D_1&=-4\Big[12\eta_2\gamma_3(12\eta_1-\gamma_1)+(12-\gamma_3)\Big\{12\eta_1\gamma_2+\gamma_1(12-\gamma_2)\Big\}\Big]\frac{\Gamma}{l_1^3\Phi}, \\
A_2&=2.12\Big\{12\eta_2\gamma_3-(12-\gamma_2)(12-\gamma_3)\Big\}\frac{\Gamma}{\Phi}, \\
D_2&=-4.12\Big\{12\eta_2\gamma_3+\gamma_2(12-\gamma_3)\Big\}\frac{\Gamma}{l_2^3\Phi}, \\
A_3&=-2.12^2(12-\gamma_3)\frac{\Gamma}{\Phi}, \qquad D_3=-4.12^2\gamma_3\frac{\Gamma}{\Phi}, \\
B_1&=B_2=B_3=0\,, \quad C_1=\frac{3}{2}l_1D_1\,, \quad C_2=\frac{3}{2}l_2D_2\,, \quad C_3=\frac{3}{2}l_3D_3\,,
\end{aligned}
\right\} \tag{52}
$$

$$
\begin{aligned}
\Phi=&\Big[12\eta_2\gamma_3\Big\{12\gamma_1+(12-\gamma_1)\Big\}+(12-\gamma_3)\Big\{12\eta_1\gamma_2-(12-\gamma_1)(12-\gamma_2)\Big\}\Big]\Gamma \\
&-\frac{18E_1j_1^2\varepsilon}{\mu l_1^3}\Big[12\eta_2\gamma_3(12\eta_1-\gamma_1)+(12-\gamma_3)\Big\{12\eta_1\gamma_2+\gamma_1(12-\gamma_2)\Big\}\Big]\Lambda.
\end{aligned} \tag{53}
$$

$$
\left.
\begin{aligned}
EI\frac{\partial^2 y_1}{\partial x_1^2}\Big/2p^2ml&=6(12-\gamma)(36-\gamma)\sqrt{\frac{{\Gamma_1}^2+{\Gamma_2}^2}{P^2+Q^2}}\Big(1+\frac{2x_1}{l}\Big) \\
&\qquad .\cos\Big(pt+\tan^{-1}\frac{\Gamma_2}{\Gamma_1}-\tan^{-1}\frac{Q}{P}\Big), \\
EI\frac{\partial^2 y_2}{\partial x_2^2}\Big/2p^2ml&=6.12(24-\gamma)\sqrt{\frac{{\Gamma_1}^2+{\Gamma_2}^2}{P^2+Q^2}}\Big(1+\frac{2x_2}{l}\Big) \\
&\qquad .\cos\Big(pt+\tan^{-1}\frac{\Gamma_2}{\Gamma_1}-\tan^{-1}\frac{Q}{P}\Big), \\
EI\frac{\partial^2 y_3}{\partial x_3^2}\Big/2p^2ml&=6.12^2\sqrt{\frac{{\Gamma_1}^2+{\Gamma_2}^2}{P^2+Q^2}}\Big(1+\frac{2x_3}{l}\Big) \\
&\qquad .\cos\Big(pt+\tan^{-1}\frac{\Gamma_2}{\Gamma_1}-\tan^{-1}\frac{Q}{P}\Big),
\end{aligned}
\right\} \tag{54}
$$

in which $E=E_1=E_2=E_3$, $I=I_1=I_2=I_3$, $m=m_1=m_2=m_3$, $l=l_1=l_2=l_3$, and

$$\left.\begin{aligned} P&=(1728-864\gamma+60\gamma^2-\gamma^3)\Gamma_1+\frac{18Ej^2\varepsilon}{\mu l^3}\gamma(12-\gamma)(36-\gamma)\Delta_1\,, \\ Q&=(1728-864\gamma+60\gamma^2-\gamma^3)\Gamma_2+\frac{18Ej^2\varepsilon}{\mu l^3}\gamma(12-\gamma)(36-\gamma)\Delta_2\,. \end{aligned}\right\} \quad (55)$$

(iv) The cases, for which n is greater than 4, will be dealt with separately.

7. *A structure with flexible floors and clamped base.*[7)]

In this case too we assume the incident waves, $e^{i(pt+kx)}$, in the determination of A_s, B_s, C_s, D_s, and the ones, $\cos(pt+kx)$, in the solution of bending moments.

(i) $n=1$;

$$\left.\begin{aligned} &A_1=4(3-\gamma_1)\frac{\Gamma}{\Phi}\,, \quad D_1=2\gamma_1\frac{\Gamma}{l_1^3\Phi}\,, \quad B_1=0\,, \quad C_1=3l_1D_1\,, \\ &\qquad \Phi=2(3-\gamma_1)\Gamma+\frac{9E_1j_1^2\varepsilon}{\mu l_1^3}\gamma_1\Delta\,. \end{aligned}\right\} \quad (56)$$

$$EI\frac{\partial^2 y}{\partial x^2}\bigg/ 2\,p^2ml=6\left(1+\frac{x}{l}\right)\sqrt{\frac{\Gamma_1^2+\Gamma_2^2}{P^2+Q^2}}\cos\left(pt+\tan^{-1}\frac{\Gamma_2}{\Gamma_1}-\tan^{-1}\frac{Q}{P}\right), \quad (57)$$

where $E=E_1$, $I=I_1$, $\cdots$, and

$$\left.\begin{aligned} P&=2(3-\gamma)\Gamma_1+\frac{9Ej^2\varepsilon}{\mu l^3}\gamma\Delta_1\,, \\ Q&=2(3-\gamma)\Gamma_2+\frac{9Ej^2\varepsilon}{\mu l^3}\gamma\Delta_2\,. \end{aligned}\right\} \quad (58)$$

(ii) $n=2$;

$$\left.\begin{aligned} &A_1=2\left[3\gamma_1\gamma_2\left\{\xi^2(12-\gamma_1)+4(1+3\xi)\right\}-4(3-\gamma_1)(3-\gamma_2)\right]\frac{\Gamma}{\Phi}\,, \\ &\qquad B_1=0\,, \\ &C_1=-6\left\{3\eta\gamma_2(2+2\xi-\xi^2\gamma_1)+2\gamma_1(3-\gamma_2)\right\}\frac{\Gamma}{l_1^2\Phi}\,, \\ &D_1=-4\left\{3\eta\gamma_2(1-\xi^2\gamma_1)+\gamma_1(3-\gamma_2)\right\}\frac{\Gamma}{l_1^3\Phi}\,, \\ &A_2=12\left\{3\xi\eta\gamma_2(1+2\xi)-2(3-\gamma_2)\right\}\frac{\Gamma}{\Phi}\,, \\ &B_2=12\xi\left\{3\eta\gamma_2(1+2\xi)+\gamma_1(3-\gamma_2)\right\}\frac{\Gamma}{l_2\Phi}\,, \\ &C_2=-18\gamma_2(2+\xi\gamma_1)\frac{\Gamma}{l_2^2\Phi}\,, \qquad D_2=-6\gamma_2(2+\xi\gamma_1)\frac{\Gamma}{l_2^3\Phi}\,, \end{aligned}\right\} \quad (59)$$

---

7) *Bull. Earthq. Res. Inst.*, **13** (1935), 704.

$$\Phi=\Big[3\eta\gamma_2\Big\{\xi^2(12-\gamma_1)+4(1+3\xi)\Big\}-4(3-\gamma_1)(3-\gamma_2)\Big]\Gamma$$
$$-\frac{18E_1j_1^{2\epsilon}}{\mu l_1^3}\Big\{3\eta\gamma_2(1-\xi^2\gamma_1)+\gamma_1(3-\gamma_2)\Big\}\Lambda, \tag{60}$$

where $\xi=\xi_1$, $\eta=\eta_1$,

$$\left.\begin{aligned}
&EI\frac{\partial^2 y_1}{\partial x_1^2}\Big/2\,p^2ml=6\Big\{(18-5\gamma)+4(3-2\gamma)\frac{x_1}{l}\Big\}\sqrt{\frac{\Gamma_1{}^2+\Gamma_2{}^2}{P^2+Q^2}}\\
&\qquad\qquad\cdot\cos\Big(pt+\tan^{-1}\frac{\Gamma_2}{\Gamma_1}-\tan^{-1}\frac{Q}{P}\Big),\\
&EI\frac{\partial^2 y_2}{\partial x_2^2}\Big/2\,p^2ml=18(2+\gamma)\Big(1+\frac{x_2}{l}\Big)\sqrt{\frac{\Gamma_1{}^2+\Gamma_2{}^2}{P^2+Q^2}}\\
&\qquad\qquad\cdot\cos\Big(pt+\tan^{-1}\frac{\Gamma_2}{\Gamma_1}-\tan^{-1}\frac{Q}{P}\Big),
\end{aligned}\right\} \tag{61}$$

in which $E=E_1=E_2$, $I=I_1=I_2$, ... ,

$$\left.\begin{aligned}
&P=(36-108\gamma+7\gamma^2)\Gamma_1+\frac{36Ej^{2\epsilon}}{\mu l^3}(3-2\gamma)\Lambda_1,\\
&Q=(36-108\gamma+7\gamma^2)\Gamma_2+\frac{36Ej^{2\epsilon}}{\mu l^3}(3-2\gamma)\Lambda_2.
\end{aligned}\right\} \tag{62}$$

(iii) $n=3$; the general case being omitted, it is assumed that $E=E_1=E_2=E_3$, $I=I_1=I_2=I_3$, ... ,

$$\left.\begin{aligned}
&A_1=4(108-1296\gamma+393\gamma^2-13\gamma^3)\frac{\Gamma}{\Phi}, && B_1=0,\\
&C_1=6\gamma(216-294\gamma+19\gamma^2)\frac{\Gamma}{l^2\Phi}, && D_1=2\gamma(108-372\gamma+31\gamma^2)\frac{\Gamma}{l^3\Phi},\\
&A_2=24(18-171\gamma+23\gamma^2)\frac{\Gamma}{\Phi}, && B_2=-6\gamma(324-216\gamma+7\gamma^2)\frac{\Gamma}{l\Phi},\\
&C_2=36\gamma(18+13\gamma-2\gamma^2)\frac{\Gamma}{l^2\Phi}, && D_2=6\gamma(24-10\gamma-5\gamma^2)\frac{\Gamma}{l^3\Phi},\\
&A_3=72(6-23\gamma-3\gamma^2)\frac{\Gamma}{\Phi}, && B_3=-12\gamma(234-15\gamma-\gamma^2)\frac{\Gamma}{l\Phi},\\
&C_3=18\gamma(12+36\gamma+\gamma^2)\frac{\Gamma}{l^2\Phi}, && D_3=6\gamma(12+36\gamma+\gamma^2)\frac{\Gamma}{l^3\Phi},
\end{aligned}\right\} \tag{63}$$

$$\Phi=2(108-1296\gamma+393\gamma^2-13\gamma^3)\Gamma+\frac{9Ej^{2\epsilon}}{\mu l^3}\gamma(108-372\gamma+31\gamma^2)\Lambda, \tag{63}$$

$$
\left.\begin{aligned}
EI\frac{\partial^2 y_1}{\partial x_1^2}\Big/2\,p^2ml &= 6\left\{(216-294\gamma+19\gamma^2)+(108-372\gamma+31\gamma^2)\frac{x_1}{l}\right\} \\
&\quad\cdot\sqrt{\frac{\Gamma_1^2+\Gamma_2^2}{P^2+Q^2}}\cos\left(pt+\tan^{-1}\frac{\Gamma_2}{\Gamma_1}-\tan^{-1}\frac{Q}{P}\right), \\
EI\frac{\partial^2 y_2}{\partial x_2^2}\Big/2\,p^2ml &= 18\left\{2(18+13\gamma-2\gamma^2)+(24-10\gamma-5\gamma^2)\frac{x_2}{l}\right\} \\
&\quad\cdot\sqrt{\frac{\Gamma_1^2+\Gamma_2^2}{P^2+Q^2}}\cos\left(pt+\tan^{-1}\frac{\Gamma_2}{\Gamma_1}-\tan^{-1}\frac{Q}{P}\right), \\
EI\frac{\partial^2 y_3}{\partial x_3^2}\Big/2\,p^2ml &= 18(12+36\gamma+\gamma^2)\left(1+\frac{x_3}{l}\right) \\
&\quad\cdot\sqrt{\frac{\Gamma_1^2+\Gamma_2^2}{P^2+Q^2}}\cos\left(pt+\tan^{-1}\frac{\Gamma_2}{\Gamma_1}-\tan^{-1}\frac{Q}{P}\right),
\end{aligned}\right\}\quad(65)
$$

where

$$
\left.\begin{aligned}
P &= 2(108-1296\gamma+393\gamma^2-13\gamma^3)\Gamma_1+\frac{9Ej^2\varepsilon}{\mu l^3}\gamma(108-372\gamma+31\gamma^2)\Lambda_1, \\
Q &= 2(108-1296\gamma+393\gamma^2-13\gamma^3)\Gamma_2+\frac{9Ej^2\varepsilon}{\mu l^3}\gamma(108-372\gamma+31\gamma^2)\Lambda_2.
\end{aligned}\right\}\quad(66)
$$

8. ***A structure with rigid floors and hinged base.***[8)]

The assumptions with respect to the form of incident waves are the same as those in the preceding two sections.

(i) $n=1$;

$$
\left.\begin{aligned}
&A_1=4(3-\gamma_1)\frac{\Gamma}{\Phi},\quad B_1=-6\gamma_1\frac{\Gamma}{l_1\Phi},\quad C_1=0,\quad D_1=2\gamma_1\frac{\Gamma}{l_1^3\Phi}, \\
&\qquad\Phi=2(3-\gamma_1)\Gamma+\frac{9E_1j_1^2\varepsilon}{\mu l_1^3}\gamma_1\Lambda.
\end{aligned}\right\}\quad(67)
$$

$$
EI\frac{\partial^2 y}{\partial x^2}\Big/2\,p^2ml=\frac{6x}{l}\sqrt{\frac{\Gamma_1^2+\Gamma_2^2}{P^2+Q^2}}\cos\left(pt+\tan^{-1}\frac{\Gamma_2}{\Gamma_1}-\tan^{-1}\frac{Q}{P}\right),\quad(68)
$$

where $E=E_1$, $I=I_1$, $\cdots$, and

$$
\left.\begin{aligned}
P &= 2(3-\gamma)\Gamma_1+\frac{9Ej^2\varepsilon}{\mu l^3}\gamma\Lambda_1, \\
Q &= 2(3-\gamma)\Gamma_2+\frac{9Ej^2\varepsilon}{\mu l^3}\gamma\Lambda_2,
\end{aligned}\right\}\quad(69)
$$

8) *Bull. Earthq. Res. Inst.*, **13** (1935), 708.

(ii) $n=2$;

$$\left.\begin{aligned} A_1&=4\left\{12\eta\gamma_2-(3-\gamma_1)(12-\gamma_2)\right\}\frac{\Gamma}{\Phi}, \quad B_1=6\left\{12\eta\gamma_2+\gamma_1(12-\gamma_2)\right\}\frac{\Gamma}{l_1\Phi}, \\ C_1&=0, \qquad\qquad D_1=-2\left\{12\eta\gamma_2+\gamma_1(12-\gamma_2)\right\}\frac{\Gamma}{l_1^3\Phi}, \\ A_2&=-12(12-\gamma_2)\frac{\Gamma}{\Phi}, \qquad B_2=0, \\ C_2&=-36\gamma_2\frac{\Gamma}{l_2^2\Phi}, \qquad D_2=-24\gamma_2\frac{\Gamma}{l_2^3\Phi}, \end{aligned}\right\} \quad (70)$$

$$\Phi=2\left\{12\eta\gamma_2-(3-\gamma_1)(12-\gamma_2)\right\}\Gamma-\frac{9E_1j_1^2\varepsilon}{\mu l_1^3}\left\{12\eta\gamma_2+\gamma_1(12-\gamma_2)\right\}\Lambda, \quad (71)$$

where $\eta=\eta_1$;

$$\left.\begin{aligned} EI\frac{\partial^2 y_1}{\partial x_1^2}\Big/ 2\,p^2ml&=6(24-\gamma)\frac{x_1}{l}\sqrt{\frac{\Gamma_1^2+\Gamma_2^2}{P^2+Q^2}} \\ &\quad\cdot\cos\left(pt+\tan^{-1}\frac{\Gamma_2}{\Gamma_1}-\tan^{-1}\frac{Q}{P}\right), \\ EI\frac{\partial^2 y_2}{\partial x_2^2}\Big/ 2\,p^2ml&=36\left(1+\frac{2x_2}{l}\right)\sqrt{\frac{\Gamma_1^2+\Gamma_2^2}{P^2+Q^2}} \\ &\quad\cdot\cos\left(pt+\tan^{-1}\frac{\Gamma_2}{\Gamma_1}-\tan^{-1}\frac{Q}{P}\right), \end{aligned}\right\} \quad (72)$$

where $E=E_1=E_2, \cdots$, and

$$\left.\begin{aligned} P&=2(36-27\gamma+\gamma^2)\Gamma_1+\frac{9Ej^2\varepsilon}{\mu l^3}\gamma(24-\gamma)\Lambda_1, \\ Q&=2(36-27\gamma+\gamma^2)\Gamma_2+\frac{9Ej^2\varepsilon}{\mu l^3}\gamma(24-\gamma)\Lambda_2. \end{aligned}\right\} \quad (76)$$

(iii) $n=3$;

$$\begin{aligned} A_1&=4\Big[12\eta_1\left\{12\eta_2\gamma_3+\gamma_2(12-\gamma_3)\right\} \\ &\qquad+(3-\gamma_1)\left\{12\eta_2\gamma_3-(12-\gamma_2)(12-\gamma_3)\right\}\Big]\frac{\Gamma}{\Phi}, \\ B_1&=6\Big[12\eta_1\left\{12\eta_2\gamma_3+\gamma_2(12-\gamma_3)\right\} \\ &\qquad-\gamma_1\left\{12\eta_2\gamma_3-(12-\gamma_2)(12-\gamma_3)\right\}\Big]\frac{\Gamma}{l_1\Phi}, \\ C_1&=0, \end{aligned}$$

$$\left.\begin{aligned}
D_1&=-2\Big[12\eta_1\Big\{12\eta_2\gamma_3+\gamma_2(12-\gamma_3)\Big\}\\
&\qquad-\gamma_1\Big\{12\eta_2\gamma_3-(12-\gamma_2)(12-\gamma_3)\Big\}\Big]\frac{\Gamma}{l_1^3\Phi},\\
A_2&=12\Big\{12\eta_2\gamma_3-(12-\gamma_2)(12-\gamma_3)\Big\}\frac{\Gamma}{\Phi},\qquad B_2=0,\\
C_2&=-36\Big\{12\eta_2\gamma_3+\gamma_2(12-\gamma_3)\Big\}\frac{\Gamma}{l_2^2\Phi},\\
D_2&=-24\Big\{12\eta_2\gamma_3+\gamma_2(12-\gamma_3)\Big\}\frac{\Gamma}{l_2^3\Phi},\\
A_3&=-144(12-\gamma_3)\frac{\Gamma}{\Phi},\qquad B_3=0,\\
C_3&=-432\gamma_3\frac{\Gamma}{l_3^2\Phi},\qquad D_3=-288\gamma_3\frac{\Gamma}{l_3^3\Phi},
\end{aligned}\right\}\tag{74}$$

$$\begin{aligned}
\Phi&=2\Big[12\eta_1\Big\{12\eta_2\gamma_3+\gamma_2(12-\gamma_3)\Big\}+(3-\gamma_1)\Big\{12\eta_2\gamma_3-(12-\gamma_2)(12-\gamma_3)\Big\}\Big]\Gamma\\
&-\frac{9E_1j_1^2\varepsilon}{\mu l_1^3}\Big[12\eta_1\Big\{12\eta_2\gamma_3+\gamma_2(12-\gamma_3)\Big\}-\gamma_1\Big\{12\eta_2\gamma_3-(12-\gamma_2)(12-\gamma_3)\Big\}\Big]\Lambda.
\end{aligned}\tag{75}$$

$$\left.\begin{aligned}
EI\frac{\partial^2y_1}{\partial x_1^2}\Big/2p^2ml&=6(12-\gamma)(36-\gamma)\frac{x_1}{l}\sqrt{\frac{\Gamma_1^2+\Gamma_2^2}{P^2+Q^2}}\\
&\quad.\cos\Big(pt+\tan^{-1}\frac{\Gamma_2}{\Gamma_1}-\tan^{-1}\frac{Q}{P}\Big),\\
EI\frac{\partial^2y_2}{\partial x_2^2}\Big/2p^2ml&=36(24-\gamma)\Big(1+\frac{2x_2}{l}\Big)\sqrt{\frac{\Gamma_1^2+\Gamma_2^2}{P^2+Q^2}}\\
&\quad.\cos\Big(pt+\tan^{-1}\frac{\Gamma_2}{\Gamma_1}-\tan^{-1}\frac{Q}{P}\Big),\\
EI\frac{\partial^2y_3}{\partial x_3^2}\Big/2p^2ml&=432\Big(1+\frac{2x_3}{l}\Big)\sqrt{\frac{\Gamma_1^2+\Gamma_2^2}{P^2+Q^2}}\\
&\quad.\cos\Big(pt+\tan^{-1}\frac{\Gamma_2}{\Gamma_1}-\tan^{-1}\frac{Q}{P}\Big),
\end{aligned}\right\}\tag{76}$$

in which $E=E_1=E_2=E_3$, $\cdots\cdots$, and

$$\left.\begin{aligned}
P&=2(432-540\gamma+51\gamma^2-\gamma^3)\Gamma_1+\frac{9Ej^2\varepsilon}{\mu l^3}\gamma(12-\gamma)(36-\gamma)\Lambda_1,\\
Q&=2(432-540\gamma+51\gamma^2-\gamma^3)\Gamma_2+\frac{9Ej^2\varepsilon}{\mu l^3}\gamma(12-\gamma)(36-\gamma)\Lambda_2.
\end{aligned}\right\}\tag{77}$$

9. *A four-storied structure with rigid floors and clamped base.*[9]

$$
\left.\begin{aligned}
A_1&=2\Big[-12\eta_2\Big\{12\eta_1+(12-\gamma_1)\Big\}\Big\{12\eta_3\gamma_4+\gamma_3(12-\gamma_4)\Big\}\\
&\quad+\Big\{-12\eta_3\gamma_4+(12-\gamma_3)(12-\gamma_4)\Big\}\Big\{-12\eta_1\gamma_2+(12-\gamma_1)(12-\gamma_2)\Big\}\Big]\frac{\Gamma}{\Phi},\\
D_1&=4\Big[12\eta_2(12\eta_1-\gamma_1)\Big\{12\eta_3\gamma_4+\gamma_3(12-\gamma_4)\Big\}\\
&\quad+\Big\{-12\eta_3\gamma_4+(12-\gamma_3)(12-\gamma_4)\Big\}\Big\{12\eta_1\gamma_2+\gamma_1(12-\gamma_2)\Big\}\Big]\frac{\Gamma}{l_1^3\Phi},\\
A_2&=2.12\Big[-12\eta_2\Big\{12\eta_3\gamma_4+\gamma_3(12-\gamma_4)\Big\}\\
&\quad+(12-\gamma_2)\Big\{-12\eta_3\gamma_4+(12-\gamma_3)(12-\gamma_4)\Big\}\Big]\frac{\Gamma}{\Phi},\\
D_2&=4.12\Big[12\eta_2\Big\{12\eta_3\gamma_4+\gamma_3(12-\gamma_4)\Big\}\\
&\quad+\gamma_2\Big\{-12\eta_3\gamma_4+(12-\gamma_3)(12-\gamma_4)\Big\}\Big]\frac{\Gamma}{l_2^3\Phi},\\
A_3&=2.12^2\Big\{-12\eta_3\gamma_4+(12-\gamma_3)(12-\gamma_4)\Big\}\frac{\Gamma}{\Phi},\\
D_3&=4.12^2\Big\{12\eta_3\gamma_4+\gamma_3(12-\gamma_4)\Big\}\frac{\Gamma}{l_3^3\Phi},\\
A_4&=2.12^3(12-\gamma_4)\frac{\Gamma}{\Phi},\qquad D_4=4.12^3\gamma_4\frac{\Gamma}{l_4^3\Phi},\\
B_s&=0,\qquad C_s=\frac{3}{2}l_sD_s.\quad (s=1,\ 2,\ 3,\ 4)
\end{aligned}\right\}\tag{78}
$$

$$
\begin{aligned}
\Phi=\Gamma\Big[&-12\eta_2\Big\{12\eta_1+(12-\gamma_1)\Big\}\Big\{12\eta_3\gamma_4+\gamma_3(12-\gamma_4)\Big\}\\
&+\Big\{-12\eta_3\gamma_4+(12-\gamma_3)(12-\gamma_4)\Big\}\Big\{-12\eta_1\gamma_2+(12-\gamma_1)(12-\gamma_2)\Big\}\Big]\\
&+\frac{18E_1J_1^2\varepsilon}{\mu l_1^3}\Delta\Big[12\eta_2(12\eta_1-\gamma_1)\Big\{12\eta_3\gamma_4+\gamma_3(12-\gamma_4)\Big\}\\
&\qquad+\Big\{-12\eta_3\gamma_4+(12-\gamma_3)(12-\gamma_4)\Big\}\Big\{12\eta_1\gamma_2+\gamma_1(12-\gamma_2)\Big\}\Big].
\end{aligned}\tag{79}
$$

9) *Bull. Earthq. Res. Inst.*, **13** (1935), 919.

$$\left.\begin{aligned}
&EI\frac{\partial^2 y_1}{\partial x_1^2}\bigg/ 2\,p^2 ml = 6(24-\gamma)\left\{24(6-\gamma)+(12-\gamma)^2\right\}\left(1+\frac{2x_1}{l}\right)M\,,\\
&EI\frac{\partial^2 y_2}{\partial x_2^2}\bigg/ 2\,p^2 ml = 6.12(12-\gamma)(36-\gamma)\left(1+\frac{2x_2}{l}\right)M\,,\\
&EI\frac{\partial^2 y_3}{\partial x_3^2}\bigg/ 2\,p^2 ml = 6.12^2(24-\gamma)\left(1+\frac{2x_3}{l}\right)M\,,\\
&EI\frac{\partial^2 y_4}{\partial x_4^2}\bigg/ 2\,p^2 ml = 6.12^3\left(1+\frac{2x_4}{l}\right)M\,,
\end{aligned}\right\}\qquad(80)$$

where $E=E_1=E_2=E_3=E_4, \cdots$, and

$$\left.\begin{aligned}
&M=\sqrt{\frac{\Gamma_1^2+\Gamma_2^2}{P^2+Q^2}}\cos\left(pt+\tan^{-1}\frac{\Gamma_2}{\Gamma_1}-\tan^{-1}\frac{Q}{P}\right),\\
&P=\phi\Gamma_1+\frac{18Ej^2\varepsilon}{\mu l^3}\psi\Lambda_1\,,\quad Q=\phi\Gamma_2+\frac{18Ej^2\varepsilon}{\mu l^3}\psi\Lambda_2\,,\\
&\phi=-12\gamma(24-\gamma)^2+\left\{-12\gamma+(12-\gamma)^2\right\}^2,\\
&\psi=\gamma(24-\gamma)\left\{24(6-\gamma)+(12-\gamma)^2\right\}.
\end{aligned}\right\}\qquad(81)$$

10. ***A five-storied structure with rigid floors and clamped base.***[10]

$$\begin{aligned}
A_1=2\Big\{&12\eta_3\left\{12\eta_4\gamma_5+\gamma_4(12-\gamma_5)\right\}\Big[12\eta_2\left\{12\eta_1+(12-\gamma_1)\right\}+\Big\{-12\eta_1\gamma_2\\
&+(12-\gamma_1)(12-\gamma_2)\Big\}\Big]-\left\{-12\eta_4\gamma_5+(12-\gamma_4)(12-\gamma_5)\right\}\Big[-12\eta_2\gamma_3\Big\{12\eta_1\\
&+(12-\gamma_1)\Big\}+(12-\gamma_3)\left\{-12\eta_1\gamma_2+(12-\gamma_1)(12-\gamma_2)\right\}\Big]\Big\}\frac{\Gamma}{\Phi}\,,
\end{aligned}$$

$$\begin{aligned}
D_1=-4\Big\{&12\eta_3\left\{12\eta_4\gamma_5+\gamma_4(12-\gamma_5)\right\}\Big[12\eta_2(12\eta_1-\gamma_1)-\Big\{12\eta_1\gamma_2\\
&+\gamma_1(12-\gamma_2)\Big\}\Big]+\left\{-12\eta_4\gamma_5+(12-\gamma_4)(12-\gamma_5)\right\}\Big[12\eta_2\gamma_3(12\eta_1-\gamma_1)\\
&+(12-\gamma_3)\left\{12\eta_1\gamma_2+\gamma_1(12-\gamma_2)\right\}\Big]\Big\}\frac{\Gamma}{l_1^3\Phi}\,,
\end{aligned}$$

10) *Bull. Earthq. Res. Inst.*, **13** (1935), 920.

$$A_2=2.12\Big[12\eta_3\Big\{12\eta_4\gamma_5+\gamma_4(12-\gamma_5)\Big\}\Big\{12\eta_2+(12-\gamma_2)\Big\}$$
$$-\Big\{-12\eta_4\gamma_5+(12-\gamma_4)(12-\gamma_5)\Big\}\Big\{-12\eta_2\gamma_3+(12-\gamma_2)(12-\gamma_3)\Big\}\Big]\frac{\Gamma}{\Phi},$$

$$D_2=-4.12\Big[12\eta_3\Big\{12\eta_4\gamma_5+\gamma_4(12-\gamma_5)\Big\}(12\eta_2-\gamma_2)$$
$$+\Big\{-12\eta_4\gamma_5+(12-\gamma_4)(12-\gamma_5)\Big\}\Big\{12\eta_2\gamma_3+\gamma_2(12-\gamma_3)\Big\}\Big]\frac{\Gamma}{l_2^3\Phi},$$

$$A_3=2.12^2\Big[12\eta_3\Big\{12\eta_4\gamma_5+\gamma_4(12-\gamma_5)\Big\}$$
$$-(12-\gamma_3)\Big\{-12\eta_4\gamma_5+(12-\gamma_4)(12-\gamma_5)\Big\}\Big]\frac{\Gamma}{\Phi},$$

$$D_3=-4.12^2\Big[12\eta_3\Big\{12\eta_4\gamma_5+\gamma_4(12-\gamma_5)\Big\}$$
$$+\gamma_3\Big\{-12\eta_4\gamma_5+(12-\gamma_4)(12-\gamma_5)\Big\}\Big]\frac{\Gamma}{l_3^3\Phi},$$

$$A_4=-2.12^3\Big\{-12\eta_4\gamma_5+(12-\gamma_4)(12-\gamma_5)\Big\}\frac{\Gamma}{\Phi},$$

$$D_4=-4.12^3\Big\{12\eta_4\gamma_5+\gamma_4(12-\gamma_5)\Big\}\frac{\Gamma}{l_4^3\Phi},$$

$$A_5=-2.12^4(12-\gamma_5)\frac{\Gamma}{\Phi},\qquad D_5=-4.12^4\gamma_5\frac{\Gamma}{l_5^3\Phi},$$

$$B_s=0,\qquad C_s=\frac{3}{2}l_sD_s,\quad (s=1,\ 2,\ \cdots,\ 5) \tag{82}$$

$$\Phi=\Gamma\Bigg\{12\eta_3\Big\{12\eta_4\gamma_5+\gamma_4(12-\gamma_5)\Big\}\Big[12\eta_2\Big\{12\eta_1+(12-\gamma_1)\Big\}+\Big\{-12\eta_1\gamma_2+(12$$
$$-\gamma_1)(12-\gamma_2)\Big\}\Big]-\Big\{-12\eta_4\gamma_5+(12-\gamma_4)(12-\gamma_5)\Big\}\Big[-12\eta_2\gamma_3\Big\{12\eta_1$$
$$+(12-\gamma_1)\Big\}+(12-\gamma_3)\Big\{-12\eta_1\gamma_2+(12-\gamma_1)(12-\gamma_2)\Big\}\Big]\Bigg\}$$
$$-\frac{18E_1\bar{\gamma}_1^2\varepsilon}{\mu l_1^3}\Lambda\Bigg\{12\eta_3\Big\{12\eta_4\gamma_5+\gamma_4(12-\gamma_5)\Big\}\Big[12\eta_2(12\eta_1-\gamma_1)-\Big\{12\eta_1\gamma_2$$
$$+\gamma_1(12-\gamma_2)\Big\}\Big]+\Big\{-12\eta_4\gamma_5+(12-\gamma_4)(12-\gamma_5)\Big\}\Big[12\eta_2\gamma_3(12\eta_1$$
$$-\gamma_1)+(12-\gamma_3)\Big\{12\eta_1\gamma_2+\gamma_1(12-\gamma_2)\Big\}\Big]\Bigg\}. \tag{83}$$

$$\left.\begin{aligned}
&EI\frac{\partial^2 y_1}{\partial x_1^2}\Big/2\,p^2ml=6\Big\{(12-\gamma)^2-12\gamma\Big\}\\
&\qquad\qquad\cdot\Big\{(12-\gamma)(48-\gamma)+144\Big\}\Big(1+\frac{2x_1}{l}\Big)M\,,\\
&EI\frac{\partial^2 y_2}{\partial x_2^2}\Big/2\,p^2ml=6.12(24-\gamma)\Big\{(12-\gamma)(24-\gamma)-12\gamma\Big\}\Big(1+\frac{2x_2}{l}\Big)M\,,\\
&EI\frac{\partial^2 y_3}{\partial x_3^2}\Big/2\,p^2ml=6.12^2(12-\gamma)(36-\gamma)\Big(1+\frac{2x_3}{l}\Big)M\,,\\
&EI\frac{\partial^2 y_4}{\partial x_4^2}\Big/2\,p^2ml=6.12^3(24-\gamma)\Big(1+\frac{2x_4}{l}\Big)M\,,\\
&EI\frac{\partial^2 y_5}{\partial x_5^2}\Big/2\,p^2ml=6.12^4\Big(1+\frac{2x_5}{l}\Big)M\,,
\end{aligned}\right\}\quad(84)$$

in which $E=E_1=E_2=\cdots,\ \cdots,$ and

$$\left.\begin{aligned}
&M=\sqrt{\frac{\Gamma_1^2+\Gamma_2^2}{P^2+Q^2}}\cos\Big(pt+\tan^{-1}\frac{\Gamma_2}{\Gamma_1}-\tan^{-1}\frac{Q}{P}\Big),\\
&P=\phi\Gamma_1+\frac{18Ej^2\varepsilon}{\mu l^3}\psi\Lambda_1\,,\qquad Q=\phi\Gamma_2+\frac{18Ej^2\varepsilon}{\mu l^3}\psi\Lambda_2\,,\\
&\phi=-12\gamma(12-\gamma)(24-\gamma)(36-\gamma)\\
&\qquad+\Big\{(12-\gamma)^2-12\gamma\Big\}\Big[(12-\gamma)\Big\{(12-\gamma)^2-24\gamma\Big\}-144\gamma\Big],\\
&\psi=\gamma\Big\{(12-\gamma)^2-12\gamma\Big\}\Big\{(12-\gamma)(48-\gamma)+144\Big\}\,.
\end{aligned}\right\}\quad(85)$$

11. *A six-storied structure with rigid floors and clamped base.*[11]

$$\begin{aligned}
A_1=2\Bigg[&R\Bigg\{-12\eta_3\gamma_4\Big[12\eta_2\Big\{12\eta_1+(12-\gamma_1)\Big\}+\Big\{-12\eta_1\gamma_2+(12-\gamma_1)(12-\gamma_2)\Big\}\Big]\\
&+(12-\gamma_4)\Big[-12\eta_2\gamma_3\Big\{12\eta_1+(12-\gamma_1)\Big\}+(12-\gamma_3)\Big\{-12\eta_1\gamma_2\\
&+(12-\gamma_1)(12-\gamma_2)\Big\}\Big]\Bigg\}+12S\eta_4\Bigg\{12\eta_3\Big[12\eta_2\Big\{12\eta_1+(12-\gamma_1)\Big\}\\
&+\Big\{-12\eta_1\gamma_2+(12-\gamma_1)(12-\gamma_2)\Big\}\Big]+\Big[-12\eta_2\gamma_3\Big\{12\eta_1+(12-\gamma_1)\Big\}\\
&\qquad+(12-\gamma_3)\Big\{-12\eta_1\gamma_2+(12-\gamma_1)(12-\gamma_2)\Big\}\Big]\Bigg\}\Bigg]\frac{\Gamma}{\Phi}\,,
\end{aligned}$$

---

11) *Bull. Earthq. Res. Inst.*, **14** (1936),

$$D_1=-4\Bigg[-R\Bigg\{12\eta_3\gamma_4\Big[12\eta_2(12\eta_1-\gamma_1)-\Big\{12\eta_1\gamma_2+\gamma_1(12-\gamma_2)\Big\}\Big]$$

$$+(12-\gamma_4)\Big[12\eta_2\gamma_3(12\eta_1-\gamma_1)+(12-\gamma_3)\Big\{12\eta_1\gamma_2+\gamma_1(12-\gamma_2)\Big\}\Big]\Bigg\}$$

$$+12S\eta_4\Bigg\{12\eta_3\Big[12\eta_2(12\eta_1-\gamma_1)-\Big\{12\eta_1\gamma_2+\gamma_1(12-\gamma_2)\Big\}\Big]$$

$$-\Big[12\eta_2\gamma_3(12\eta_1-\gamma_1)+(12-\gamma_3)\Big\{12\eta_1\gamma_2+\gamma_1(12-\gamma_2)\Big\}\Big]\Bigg\}\Bigg]\frac{\Gamma}{l_1^3\Phi},$$

$$A_2=2.12\Bigg\{R\Big[-12\eta_3\gamma_4\Big\{12\eta_2+(12-\gamma_2)\Big\}+(12-\gamma_4)\Big\{-12\eta_2\gamma_3$$

$$+(12-\gamma_2)(12-\gamma_3)\Big\}\Big]+12S\eta_4\Big[12\eta_3\Big\{12\eta_2+(12-\gamma_2)\Big\}$$

$$+\Big\{-12\eta_2\gamma_3+(12-\gamma_2)(12-\gamma_3)\Big\}\Big]\Bigg\}\frac{\Gamma}{\Phi},$$

$$D_2=4.12\Bigg\{R\Big[12\eta_3\gamma_4(12\eta_2-\gamma_2)+(12-\gamma_4)\Big\{12\eta_2\gamma_3+\gamma_2(12-\gamma_3)\Big\}\Big]$$

$$+12S\eta_4\Big[-12\eta_3(12\eta_2-\gamma_2)+\Big\{12\eta_2\gamma_3+\gamma_2(12-\gamma_3)\Big\}\Big]\Bigg\}\frac{\Gamma}{l_2^3\Phi},$$

$$A_3=2.12^2\Big[R\Big\{-12\eta_3\gamma_4+(12-\gamma_3)(12-\gamma_4)\Big\}+12S\eta_4\Big\{12\eta_3+(12-\gamma_3)\Big\}\Big]\frac{\Gamma}{\Phi},$$

$$D_3=4.12^2\Big[R\Big\{12\eta_3\gamma_4+\gamma_3(12-\gamma_4)\Big\}+12S\eta_4(-12\eta_3+\gamma_3)\Big]\frac{\Gamma}{l_3^3\Phi},$$

$$A_4=2.12^3\Big\{R(12-\gamma_4)+12S\eta_4\Big\}\frac{\Gamma}{\Phi},\qquad D_4=4.12^3(R\gamma_4-12S\eta_4)\frac{\Gamma}{l_4^3\Phi},$$

$$A_5=2.12^4R\frac{\Gamma}{\Phi},\qquad D_5=-4.12^4S\frac{\Gamma}{l_5^3\Phi},$$

$$A_6=-2.12^5(12-\gamma_6)\frac{\Gamma}{\Phi},\qquad D_6=-4.12^5\gamma_6\frac{\Gamma}{l_6^3\Phi},$$

$$B_s=0,\qquad C_s=\frac{3}{2}l_sD_s,\quad (s=1,\ 2,\ \cdots,\ 6) \tag{86}$$

$$\Phi=\Gamma\Bigg[R\Bigg\{-12\eta_3\gamma_4\Big[12\eta_2\Big\{12\eta_1+(12-\gamma_1)\Big\}+\Big\{-12\eta_1\gamma_2+(12-\gamma_1)(12-\gamma_2)\Big\}\Big]$$

$$+(12-\gamma_4)\Big[-12\eta_2\gamma_3\Big\{12\eta_1+(12-\gamma_1)\Big\}+(12-\gamma_3)\Big\{-12\eta_1\gamma_2$$

$$+(12-\gamma_1)(12-\gamma_2)\Big\}\Big]\Big\}+12S\eta_4\Big\{12\eta_3\Big[12\eta_2\Big\{12\eta_1+(12-\gamma_1)\Big\}$$

$$+\Big\{-12\eta_1\gamma_2+(12-\gamma_1)(12-\gamma_2)\Big\}\Big]+\Big[-12\eta_2\gamma_3\Big\{12\eta_1+(12-\gamma_1)\Big\}$$

$$+(12-\gamma_3)\Big\{-12\eta_1\gamma_2+(12-\gamma_1)(12-\gamma_2)\Big\}\Big]\Big\}\Big]$$

$$-\frac{18E_1 j_1^2 \varepsilon}{\mu l_1^3}\Lambda\Big[-R\Big\{12\eta_3\gamma_4\Big[12\eta_2(12\eta_1-\gamma_1)-\Big\{12\eta_1\gamma_2+\gamma_1(12-\gamma_2)\Big\}\Big]$$

$$+(12-\gamma_4)\Big[12\eta_2\gamma_3(12\eta_1-\gamma_1)+(12-\gamma_3)\Big\{12\eta_1\gamma_2+\gamma_1(12-\gamma_2)\Big\}\Big]\Big\}$$

$$+12S\eta_4\Big\{12\eta_3\Big[12\eta_2(12\eta_1-\gamma_1)-\Big\{12\eta_1\gamma_2+\gamma_1(12-\gamma_2)\Big\}\Big]$$

$$-\Big[12\eta_2\gamma_3(12\eta_1-\gamma_1)+(12-\gamma_3)\Big\{12\eta_1\gamma_2+\gamma_1(12-\gamma_2)\Big\}\Big]\Big\}\Big],$$

$$R=12\eta_5\gamma_6-(12-\gamma_5)(12-\gamma_6), \qquad S=12\eta_5\gamma_6-\gamma_5(12-\gamma_6). \tag{87}$$

$$\left.\begin{aligned}
&EI\frac{\partial^2 y_1}{\partial x_1^2}\Big/ 2p^2ml=6(12-\gamma)(24-\gamma)(36-\gamma)\\
&\qquad\qquad\cdot\Big\{(24-\gamma)^2-432\Big\}\Big(1+\frac{2x_1}{l}\Big)M,\\
&EI\frac{\partial^2 y_2}{\partial x_2^2}\Big/ 2p^2ml=6.12\Big\{(18-\gamma)^2-180\Big\}\Big\{(30-\gamma)^2-180\Big\}\Big(1+\frac{2x_2}{l}\Big)M,\\
&EI\frac{\partial^2 y_3}{\partial x_3^2}\Big/ 2p^2ml=6.12^2(24-\gamma)\Big\{(24-\gamma)^2-288\Big\}\Big(1+\frac{2x_3}{l}\Big)M,\\
&EI\frac{\partial^2 y_4}{\partial x_4^2}\Big/ 2p^2ml=6.12^3(12-\gamma)(36-\gamma)\Big(1+\frac{2x_4}{l}\Big)M,\\
&EI\frac{\partial^2 y_5}{\partial x_5^2}\Big/ 2p^2ml=6.12^4(24-\gamma)\Big(1+\frac{2x_5}{l}\Big)M,\\
&EI\frac{\partial^2 y_6}{\partial x_6^2}\Big/ 2p^2ml=6.12^5\Big(1+\frac{2x_6}{l}\Big)M,\\
&\text{in which } E=E_1=E_2=\cdots,\ \cdots,\ \text{and}
\end{aligned}\right\} \tag{88}$$

$$\left.\begin{aligned} &M=\sqrt{\frac{\Gamma_1^2+\Gamma_2^2}{P^2+Q^2}}\cos\left(pt+\tan^{-1}\frac{\Gamma_2}{\Gamma_1}-\tan^{-1}\frac{Q}{P}\right),\\ &P=\phi\Gamma_1+\frac{18Ej^2\varepsilon}{\mu l^3}\psi\Lambda_1, \qquad Q=\phi\Gamma_2+\frac{18Ej^2\varepsilon}{\mu l^3}\psi\Lambda_2,\\ &\phi=\left\{\gamma(24-\gamma)^2-12(12-\gamma)^2\right\}^2-12\gamma(12-\gamma)^2(36-\gamma)^2,\\ &\psi=\gamma(12-\gamma)(24-\gamma)(36-\gamma)\left\{(24-\gamma)^2-432\right\}. \end{aligned}\right\} \tag{89}$$

12. *General law in and comparison of the results of the present as well as the original problems.*

The deflections, y, or bending moments, $EI(\partial^2y/\partial x^2)$ of columns of the structure in any case have the types:

$$y=f_1(x)M, \qquad EI\frac{\partial^2y}{\partial x^2}=f_2(x)M, \tag{90}$$

where

$$M=\sqrt{\frac{\Gamma_1^2+\Gamma_2^2}{P^2+Q^2}}\cos\left(pt+\tan^{-1}\frac{\Gamma_2}{\Gamma_1}-\tan^{-1}\frac{Q}{P}\right), \tag{91}$$

$$P=\phi\Gamma_1+\frac{18Ej^2\varepsilon}{\mu l^3}\psi\Lambda_1, \quad Q=\phi\Gamma_2+\frac{18Ej^2\varepsilon}{\mu l^3}\psi\Lambda_2, \text{ (or similar forms)} \tag{92}$$

and Γ_1, Γ_2, Λ_1, Λ_2 are functions of λ, μ, $m_1p^2l_1^3/E_1I_1$, $E_1\rho I_1\varepsilon^2/\mu m_1l_1^3$, but independent of the number of stories and the conditions with respect to the stiffness of floors, etc.; whereas ϕ, ψ, which were shown in the respective preceding sections, are functions of the structural conditions, but not affected by the dissipation nature of the ground. $\phi=0$ gives the resonance condition of a structure in the case that the ground, on which the structure is standing, is so rigid as does not participate in dissipation, whereas $\psi=0$ indicates the corresonance condition under the criterion shown in our foregoing papers. Actually, $\psi=0$ is the resonance condition of the structure in the case that the ground is so soft as does not partake in dissipation. $f_1(x)$, $f_2(x)$ are quite of the same forms as those also shown in the same papers.

If there were such a condition as $Ej^2\varepsilon/\mu l^3=0$, y or $EI(\partial^2y/\partial x^2)$ would have ϕ as its denominator. The phenomena of perfect resonance of the structural vibration — in usual sense — would then result in the condition under consideration.

It may seem that our present and original theories are different each other particularly with respect to the forms of P as well as Q.

In our original theory P and Q had the terms similar to $\phi\Gamma_1$ and $(18Ej^2\varepsilon/\mu l^3)\psi\Lambda_2$ respectively, and the terms corresponding to the second one in P and the first one in Q in (92) did not exist. If however the higher orders in $h\varepsilon$ and $k\varepsilon$ were not neglected in the original theory, M would be of the form

$$M=\sqrt{\frac{(\Gamma_1-3\sqrt{(\lambda+2\mu)/\mu}\,\Lambda_2)^2+(\Gamma_2+3\sqrt{(\lambda+2\mu)/\mu}\,\Lambda_1)^2}{P^2+Q^2}}$$

$$\cdot\cos\left\{pt+\tan^{-1}\frac{\Gamma_2+3\sqrt{(\lambda+2\mu)/\mu}\,\Lambda_1}{\Gamma_1-3\sqrt{(\lambda+2\mu)/\mu}\,\Lambda_2}-\tan^{-1}\frac{Q}{P}\right\}, \tag{93}$$

$$\left.\begin{aligned}
P&=\phi\Gamma_1+\frac{36}{a}\sqrt{\frac{\lambda+2\mu}{\mu}}\sqrt{\frac{m_1E_1I_1}{\rho\mu l_1^3}}\frac{1}{\sqrt{\gamma_1}}\psi\Lambda_1,\\
Q&=\phi\Gamma_2+\frac{36}{a}\sqrt{\frac{\lambda+2\mu}{\mu}}\sqrt{\frac{m_1E_1I_1}{\rho\mu l_1^3}}\frac{1}{\sqrt{\gamma_1}}\psi\Lambda_2,\\
\Gamma_1&=2\sqrt{\gamma_1\nu}\left[4\left\{\sqrt{\frac{(\lambda+\mu)^2}{(\lambda+2\mu)\mu}}+1-2\sqrt{\frac{\lambda+2\mu}{\mu}}\right\}+\gamma_1\nu\left(1-2\sqrt{\frac{\mu}{\lambda+2\mu}}\right)\right],\\
\Gamma_2&=4\left(1-\sqrt{\frac{\lambda+2\mu}{\mu}}\right)(\gamma_1\nu+4),\\
\Lambda_1&=-\left(4+\sqrt{\frac{\mu}{\lambda+2\mu}}\gamma_1\nu\right),\quad \Lambda_2=\sqrt{\gamma_1\nu}\left\{2\left(\sqrt{\frac{\mu}{\lambda+2\mu}}+1\right)+\frac{\mu}{\lambda+2\mu}\gamma_1\nu\right\},\\
\nu&=\frac{E_1\rho I_1\varepsilon^2}{\mu m_1 l_1^3}.
\end{aligned}\right\} \tag{94}$$

When $h\varepsilon\to 0$, $k\varepsilon\to 0$, M assumes the form

$$M=\frac{1}{\sqrt{\phi^2+\left\{\frac{12}{a}\sqrt{\frac{m_1E_1I_1}{\rho\mu l_1^3}}\frac{\psi}{\sqrt{\gamma_1}}\right\}^2}}\cos\left(pt+\tan^{-1}\frac{12E_1j_1^2\psi}{\mu l_1^3 k\phi}\right). \tag{95}$$

It will therefore be seen that the old and new theories are not essentially different with each other in their qualitative natures.

13. *The forms of $f_1(x)$, $f_2(x)$.*

As already stated, $f_1(x)$ and $f_2(x)$ shown in (90) are quite of the same forms for the present as well as for the original theories. It is somewhat difficult at present to describe the nature of $f_1(x)$, whereas $f_2(x)$'s of various cases are in obedience with a very simple law such that

$f_2(x_s)$ for columns between sth and $(s-1)$th floors of an n-storied structure
$=12f_2(x_{s-1})$ for columns between $(s-1)$th and $(s-2)$th floors of an $(n-1)$-storied structure
$=12^2f_2(x_{s-2})$ for columns between $(s-2)$th and $(s-3)$th floors of an $(n-2)$-storied structure
$= \ldots\ldots\ldots\ldots\ldots\ldots\ldots\ldots\ldots\ldots\ldots\ldots\ldots\ldots$ (96)

These relations hold only for the structure with extremely rigid floors and clamped base.

In conclusion we wish to express our thanks to the Council of the Foundation for the Promotion of Scientific and Industrial Research of Japan, with whose aid the study of present series was begun.

---

16. 構造物に於ける震動逸散理論の吟味

地震研究所 妹澤克惟 金井清

これまで種々の場合について論じた構造物震動の逸散問題では，計算を容易にする爲に二三の點を簡單化してあつたが，問題が最近多くの人に眞實に注意される傾向さなつて來たから，問題のできるだけ嚴格な取扱をなすことにして，今迄の理論全體を吟味して見たのである．その結果は數理の點に於て部分的に所々變つて來たが，全體としては大した變化がないことがわかつた．又，計算結果による逸散の性質も大體に於て同じであるばかりでなく，今迄多少都合の惡かつた點は寧ろ除外されるやうになつたのである．例へば，建物が極端に小さい場合に逸散が少いことや，建物の層數によつて最大屈曲モーメントの起る柱の違ひなどが數理的によくわかるやうになるのである．但し何れにしても計算が如何にも複雜であつて，實際問題に應用する場合に多大の困難を感じる次第である．しかしこの應用も只今着々として進行中である．

17. *Energy Dissipation in Seismic Vibrations of a Seven-storied Structure. Nature of Corresonance.*

By Katsutada SEZAWA and Kiyoshi KANAI,

Earthquake Research Institute.

(Read Feb. 18 and March 17, 1936—Received March 20, 1936.)

1. *Introduction.*

The problem of energy dissipation in seismic vibration of a framed structure not exceeding 6-stories has already been discussed. We are now intending to examine the same problem with respect to the case of a 7-storied framed structure. Mathematical formulae were determined in both two ways, namely the one corresponding to our original theory and the other corresponding to our new improved theory[1]. In applying the formulae, particularly those corresponding to our original theory, the Old Kaizyô Building, the data of which were kindly supplied by Tokyo Kaizyô Kasai Hoken Kaisha (Tokyo Marine and Fire Insurance Co.), the owner of the building, was carefully studied. Notwithstanding the comparative easiness of numerical application, our original theory still appears to indicate the qualitative nature of dissipation of the building under consideration. The application of our improved theory to the actual case, though it is excessively difficult matter, will appear in a near future.

2. *Mathematical formulae for a 7-storied structure with rigid floors and clamped base.*

The solutions and boundary conditions of the problem were shown in (32)—(41) of the preceding papar[2]. When $E_1=E_2=\cdots$, $m_1=m_2=\cdots$, the constants belonging to the expressions of deflections of columns are as follows:

$$A_1=(12-\gamma)\Big\{(12-\gamma)(24-\gamma)-144\Big\}\Big[-36\gamma(24-\gamma)(36-\gamma) + \Big\{(12-\gamma)(24-\gamma)-144\Big\}^2\Big]\frac{\Xi}{\Phi},$$

1) K. SEZAWA and K. KANAI, "Improved Theory of Energy Dissipation in Seismic Vibrations of a Structure", *Bull. Earthq. Res. Inst.*, **14** (1936).

2) *ibid.* 1).

$$D_1=2\gamma\Big\{(12-\gamma)^2(36-\gamma)-144(24-\gamma)\Big\}\Big\{(12-\gamma)(36-\gamma)^2-144(24-\gamma)\Big\}\frac{\Xi}{l^3\Phi},$$

$$A_2=12\Big[\Big\{\gamma(24-\gamma)^2-12(12-\gamma)^2\Big\}^2-12\gamma(12-\gamma)^2(36-\gamma)^2\Big]\frac{\Xi}{\Phi},$$

$$D_2=2.12\gamma(12-\gamma)(24-\gamma)(36-\gamma)\Big\{(24-\gamma)^2-432\Big\}\frac{\Xi}{l^3\Phi},$$

$$A^3=12^2\Big[(12-\gamma)\Big\{(12-\gamma)(24-\gamma)-144\Big\}^2 -24\gamma(24-\gamma)\Big\{(12-\gamma)(30-\gamma)-72\Big\}\Big]\frac{\Xi}{\Phi},$$

$$D_3=2.12^2\gamma\Big\{(12-\gamma)(24-\gamma)-144\Big\}\Big\{(24-\gamma)(36-\gamma)-144\Big\}\frac{\Xi}{l^3\Phi},$$

$$A_4=12^3\Big[\Big\{(12-\gamma)(24-\gamma)-144\Big\}^2-12\gamma(24-\gamma)^2\Big]\frac{\Xi}{\Phi},$$

$$D_4=2.12^3\gamma(24-\gamma)\Big\{(12-\gamma)(36-\gamma)-144\Big\}\frac{\Xi}{l^3\Phi},$$

$$A_5=12^4\Big[(12-\gamma)\Big\{(12-\gamma)(24-\gamma)-144\Big\}-12\gamma(24-\gamma)\Big]\frac{\Xi}{\Phi},$$

$$D_5=2.12^4\gamma(12-\gamma)(36-\gamma)\frac{\Xi}{l^3\Phi},$$

$$A_6=12^5\Big\{(12-\gamma)(24-\gamma)-144\Big\}\frac{\Xi}{\Phi},\qquad D_6=2.12^5\gamma(24-\gamma)\frac{\Xi}{l^3\Phi},$$

$$A_7=12^6(12-\gamma)\frac{\Xi}{\Phi},\qquad D_7=2.12^6\gamma\frac{\Xi}{l^3\Phi},$$

$$B_S=0,\qquad C_S=\frac{3}{2}l_SD_S,\qquad \Big[S=1,\,2,\,\cdots\cdots,\,7\Big] \tag{1}$$

where

$$\Phi=(12-\gamma)\Big\{(12-\gamma)(24-\gamma)-144\Big\}\Big[-36\gamma(24-\gamma)(36-\gamma) +\Big\{(12-\gamma)(24-\gamma)-144\Big\}^2\Big]\Gamma+\frac{18E_1\varepsilon j_1^2}{\mu l_1^3}\gamma\Big\{(12-\gamma)^2(36-\gamma) -144(24-\gamma)\Big\}\Big\{(12-\gamma)(36-\gamma)^2-144(24-\gamma)\Big\}\Lambda, \tag{2}$$

and $\gamma=mp^2l^3/EI$.

The ratio of bending moment in columns on each floor to the product of ml by the acceleration of the ground (on which no structure stands) is expressed by equations of the forms:

$$EI\frac{\partial^2 y_1}{\partial x_1^2}\Big/ 2p^2ml = 3\left\{(12-\gamma)^2(36-\gamma)-144(24-\gamma)\right\}\left\{(12-\gamma)(36-\gamma)^2 -144(24-\gamma)\right\}\left(1+\frac{2x_1}{l}\right)M,$$

$$EI\frac{\partial^2 y_2}{\partial x_2^2}\Big/ 2p^2ml = 3.12(12-\gamma)(24-\gamma)(36-\gamma)\left\{(24-\gamma)^2-432\right\}\left(1+\frac{2x_2}{l}\right)M,$$

$$EI\frac{\partial^2 y_3}{\partial x_3^2}\Big/ 2p^2ml = 3.12^2\left\{(12-\gamma)(24-\gamma)-144\right\}\left\{(24-\gamma)(36-\gamma) -144\right\}\left(1+\frac{2x_3}{l}\right)M,$$

$$EI\frac{\partial^2 y_4}{\partial x_4^2}\Big/ 2p^2ml = 3.12^3(24-\gamma)\left\{(12-\gamma)(36-\gamma)-144\right\}\left(1+\frac{2x_4}{l}\right)M,$$

$$EI\frac{\partial^2 y_5}{\partial x_5^2}\Big/ 2p^2ml = 3.12^4(12-\gamma)(36-\gamma)\left(1+\frac{2x_5}{l}\right)M,$$

$$EI\frac{\partial^2 y_6}{\partial x_6^2}\Big/ 2p^2ml = 3.12^5(24-\gamma)\left(1+\frac{2x_6}{l}\right)M,$$

$$EI\frac{\partial^2 y_7}{\partial x_7^2}\Big/ 2p^2ml = 3.12^6\left(1+\frac{2x_7}{l}\right)M. \tag{3}$$

The form of M differs in accordance with the difference in theory used (between the original and improved theories).

Case I. **In the Original thory,**

$$\Xi = \Gamma + 3i\sqrt{\frac{\lambda+2\mu}{\mu}}\Lambda, \tag{4}$$

$$M = \sqrt{\frac{\left(\Gamma_1 - 3\sqrt{\frac{\lambda+2\mu}{\mu}}\Lambda_2\right)^2 + \left(\Gamma_2 + 3\sqrt{\frac{\lambda+2\mu}{\mu}}\Lambda_1\right)^2}{P^2+Q^2}}$$

$$\cdot\cos\left\{pt + \tan^{-1}\left(\frac{\Gamma_2 + 3\sqrt{\frac{\lambda+2\mu}{\mu}}\Lambda_1}{\Gamma_1 - 3\sqrt{\frac{\lambda+2\mu}{\mu}}\Lambda_2}\right) - \tan^{-1}\frac{Q}{P}\right\}. \tag{5}$$

$$P = \phi\Gamma_1 + 36\sqrt{\frac{\lambda+2\mu}{\mu}}\left(\frac{1}{a}\sqrt{\frac{mEI}{\rho\mu l^3}}\right)\frac{\psi}{\sqrt{\gamma_1}}\Lambda_1,$$

$$\left.\begin{aligned} Q&=\phi\Gamma_2+36\sqrt{\frac{\lambda+2\mu}{\mu}}\left(\frac{1}{a}\sqrt{\frac{mEI}{\rho\mu l_3}}\right)\frac{\psi}{\sqrt{\gamma_1}}\Lambda_2\,,\\ \Gamma_1&=2\sqrt{\gamma_1\nu}\left\{4\left(1+\sqrt{\frac{(\lambda+\mu)^2}{\mu(\lambda+2\mu)}}-2\sqrt{\frac{\lambda+2\mu}{\mu}}\right)+\gamma_1\nu\left(1-2\sqrt{\frac{\mu}{\lambda+2\mu}}\right)\right\},\\ \Gamma_2&=4\left(1-\sqrt{\frac{\lambda+2\mu}{\mu}}\right)(4+\gamma_1\nu)\,,\\ \Lambda_1&=-\left(4+\sqrt{\frac{\mu}{\lambda+2\mu}}\gamma_1\nu\right),\\ \Lambda_2&=\sqrt{\gamma_1\nu}\left\{2\left(1+\sqrt{\frac{\mu}{\lambda+2\mu}}\right)+\left(\frac{\mu}{\lambda+2\mu}\right)\gamma_1\nu\right\}, \end{aligned}\right\}\quad(6)$$

$$\left.\begin{aligned} &\Gamma=\Gamma_1+i\Gamma_2\,,\qquad \Lambda=\Lambda_1+i\Lambda_2\,,\qquad \nu=\frac{E_1\rho I_1\varepsilon^2}{\mu m_1 l_1^{\,3}}\,,\\ &\phi=(12-\gamma)\Big\{(12-\gamma)(24-\gamma)-144\Big\}\Big[-36\gamma(24-\gamma)(36-\gamma)\\ &\qquad\qquad\qquad\qquad+\Big\{(12-\gamma)(24-\gamma)-144\Big\}^2\Big],\\ &\psi=\gamma\Big\{(12-\gamma)^2(36-\gamma)-144(24-\gamma)\Big\}\Big\{(12-\gamma)(36-\gamma)^2-144(24-\gamma)\Big\}. \end{aligned}\right\}\quad(7)$$

When $k\varepsilon\to 0$, $\lambda=14\mu$, M takes the form:

$$M=\frac{2}{\sqrt{\phi^2+\left\{\dfrac{12}{a}\sqrt{\dfrac{mEI}{\rho\mu l^3\gamma}}\psi\right\}^2}}\cos\left\{pt+\tan^{-1}\left(\frac{12}{a}\sqrt{\frac{mEI}{\rho\mu l^3\gamma}}\frac{\psi}{\phi}\right)\right\}. \qquad (8)$$

Case II. In the improved theory,

$$\Xi=2\Gamma, \qquad (9)$$

$$M=2\sqrt{\frac{\Gamma_1^2+\Gamma_2^2}{P^2+Q^2}}\cos\left(pt+\tan^{-1}\frac{\Gamma_2}{\Gamma_1}-\tan^{-1}\frac{Q}{P}\right), \qquad (10)$$

$$\left.\begin{aligned} &P=\phi\Gamma_1+\frac{18E\varepsilon j^2}{\mu l^3}\psi\Lambda_1\,,\qquad Q=\phi\Gamma_2+\frac{18E\varepsilon j^2}{\mu l^3}\psi\Lambda_2\,,\\ &\Gamma_1=3\left(\frac{\lambda+2\mu}{\mu}\right)+\gamma_1\nu\left(\frac{\lambda}{\mu}-3\sqrt{\frac{\lambda+2\mu}{\mu}}\right),\\ &\Gamma_2=\sqrt{\gamma_1\nu}\left\{3\sqrt{\frac{\lambda+2\mu}{\mu}}\left(1+\sqrt{\frac{\lambda+2\mu}{\mu}}\right)+\gamma_1\nu\left(\sqrt{\frac{\lambda+2\mu}{\mu}}-2\right)\right\},\\ &\Lambda_1=\frac{2\lambda+5\mu}{\mu}-\gamma_1\nu\,,\qquad \Lambda_2=\sqrt{\gamma_1\nu}\left(1+2\sqrt{\frac{\lambda+2\mu}{\mu}}\right), \end{aligned}\right\}\quad(11)$$

in which the expressions of ϕ, ψ, ν and the meanings of Γ, Λ are the same as those in (7).

Fig. 1.

The form of displacement of the ground surface, on which no structure stands, is

$$u_0 = 2 \cos pt. \tag{12}$$

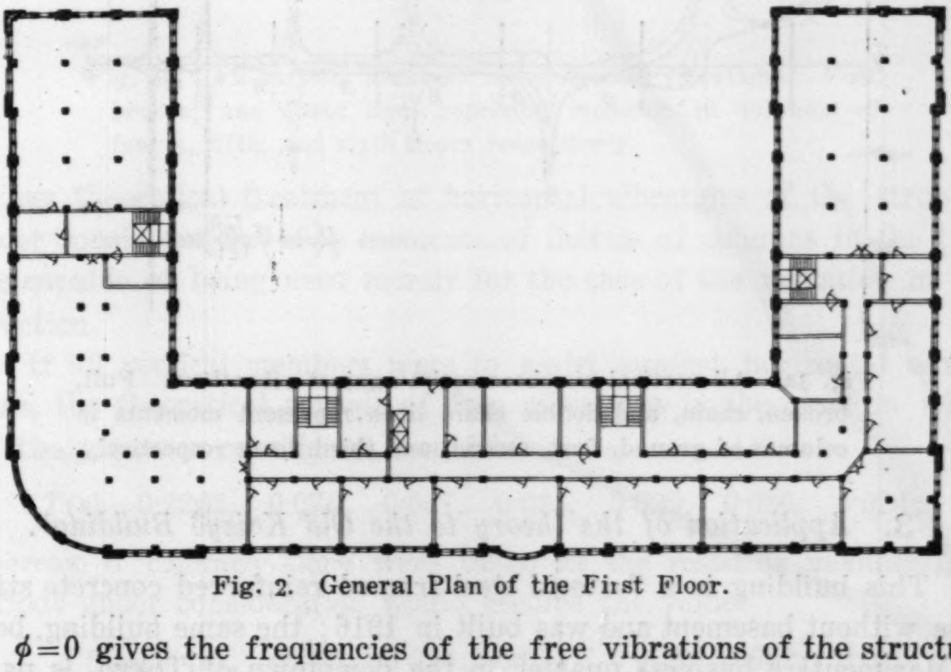

Fig. 2. General Plan of the First Floor.

$\phi = 0$ gives the frequencies of the free vibrations of the structure in usual sense, namely in the case that the ground is infinitely rigid. γ satisfies the equation $\phi = 0$, when

$$\gamma = 0{\cdot}525,\quad 4{\cdot}584,\quad 12,\quad 21{\cdot}49,\quad 31{\cdot}42,\quad 40{\cdot}03,\quad 45{\cdot}95,$$

or when

$$\sqrt{\gamma} = 0{\cdot}7246, \quad 2{\cdot}142, \quad 3{\cdot}464, \quad 4{\cdot}637, \quad 5{\cdot}607, \quad 6{\cdot}330, \quad 6{\cdot}777.$$

In the original theory, $\psi=0$ gives the condition of corresonance. γ satisfies $\psi=0$, when

$$\gamma = 2{\cdot}37, \quad 9{\cdot}04, \quad 18{\cdot}66, \quad 29{\cdot}35, \quad 38{\cdot}99, \quad 45{\cdot}60,$$

or when

$$\sqrt{\gamma} = 1{\cdot}540, \ 3{\cdot}007, \ 4{\cdot}320, \ 5{\cdot}418, \ 6{\cdot}243, \ 6{\cdot}754.$$

The bending moments of columns between the ground and first floors vanish at the conditions of corresonance.

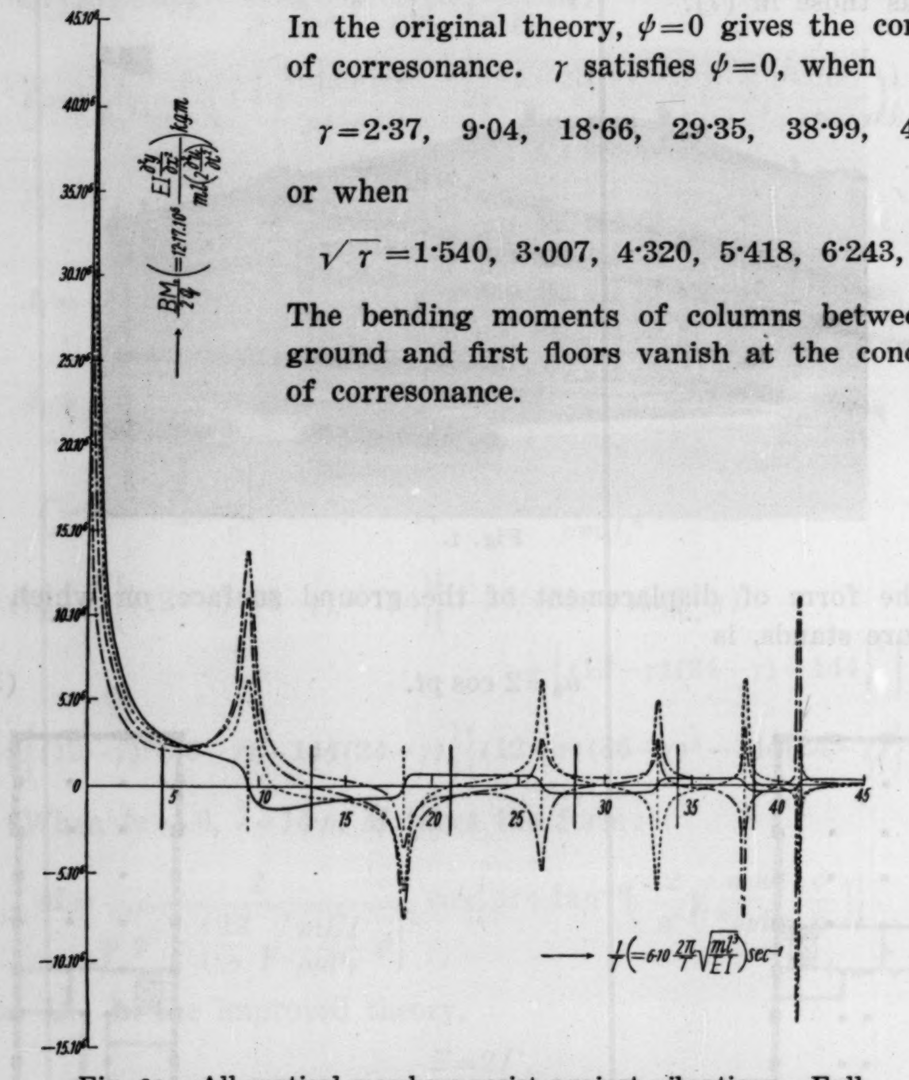

Fig. 3a. All vertical members resist against vibrations. Full, broken, chain, and double chain lines represent moments in columns of ground, first, second, and third floors respectively.

3. *Application of the theory to the Old Kaizyô Building*[3].

This building is a 7-storid steel-framed reinforced concrete structure without basement and was built in 1916; the same building, being in Marunouti, a business quarter in the downtown of Tokyo, is partly used by the owner and partly let for other business offices. A photographic view and the general plan of the first floor are shown in

3) The owner has another building which is just behind and larger than the present one.

Figs. 1, 2.

It was assumed in numerical calculation that $E = 1{\cdot}8.10^9\ \text{kg/m}^2 = 1{\cdot}8.10^9.9{\cdot}8\ \text{kg mass m/s}^2/\text{m}^2$ and the floors are so rigid that the ends of columns remain always vertical. The calculated results of the important elements are given in Table I, which however may be used almost

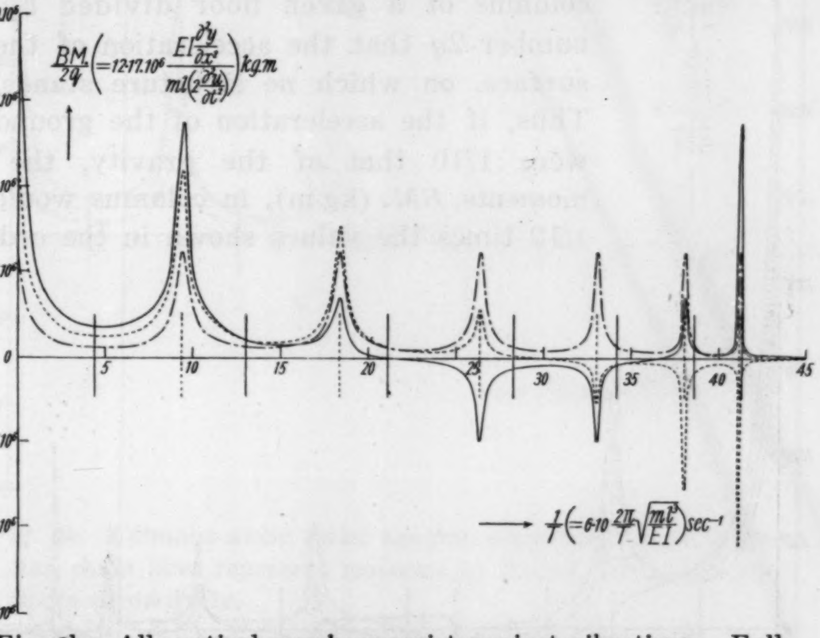

Fig. 3b. All vertical members resist against vibrations. Full, broken, and chain lines represent moments in columns of fourth, fifth, and sixth floors respectively.

in any theoretical treatment of horizontal vibrations of the structure under consideration. The moments of inertia of columns in the table are capable of being used merely for the case of the vibration in NS-direction.

If all vertical members were to resist against horizontal oscillations, the theoretical periods of free vibrations in the case, in which no dissipation is considered, would be

$$T(s) = 0{\cdot}2262,\quad 0{\cdot}076,\quad 0{\cdot}047,\quad 0{\cdot}035,\quad 0{\cdot}029,\quad 0{\cdot}026,\quad 0{\cdot}024;$$

whereas, if columns alone were taken as the resisting members, the periods under consideration would assume the values

$$T(s) = 0{\cdot}457,\quad 0{\cdot}155,\quad 0{\cdot}096,\quad 0{\cdot}071,\quad 0{\cdot}059,\quad 0{\cdot}052,\quad 0{\cdot}049.$$

The maximum values of the bending moments, $BM. = E_S I_S (d^2 y_S / dx_S^2)$, under the assumption that $\rho = 2.10^3$ kg mass/m³, $\sqrt{\mu/\rho} = 200$ m/s (which is somewhat too large), were calculated by means of our original theory. The results for two cases, namely the one in which all vertical mem-

bers partake in the resistance against oscillation and the other in which columns alone resist against the same oscillation, are shown in Figs. 3a, 3b and Figs. 4a, 4b respectively. The ordinates of these figures indicate the bending moments, *BM.* (kg m), in columns of a given floor divided by such a number $2q$ that the acceleration of the ground surface, on which no structure stands, is $2qg$. Thus, if the acceleration of the ground surface were 1/10 that of the gravity, the bending moments, *BM.* (kg m), in columns would then be 1/10 times the values shown in the ordinates.

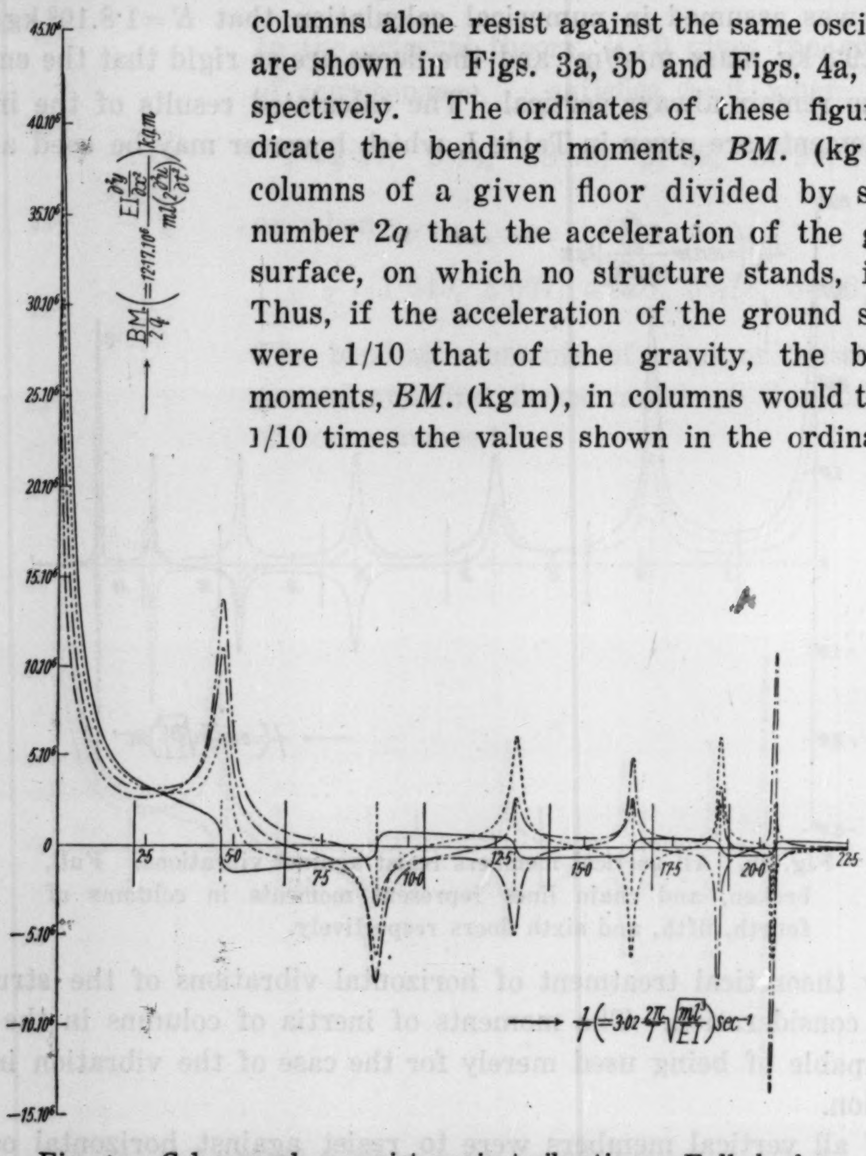

Fig. 4a. Columns alone resist against vibrations. Full, broken, chain and double chain lines represent moments in columns of ground, first, second, and third floors respectively.

In the present method of calculation the bending moments under resonance conditions, as indicated by the vertical strips of full line type in these figures, assume rather too small values. Were however the calculation made by the method in the line of the improved theory, the values of the moments under such resonance conditions would assume somewhat larger values, though not too large,—larger than the moments under corresonance conditions as indicated by the vertical strips of broken line type. The frequency for resonance under the improved theory would intermediate between the ones for resonance

and corresonance under the present theory.

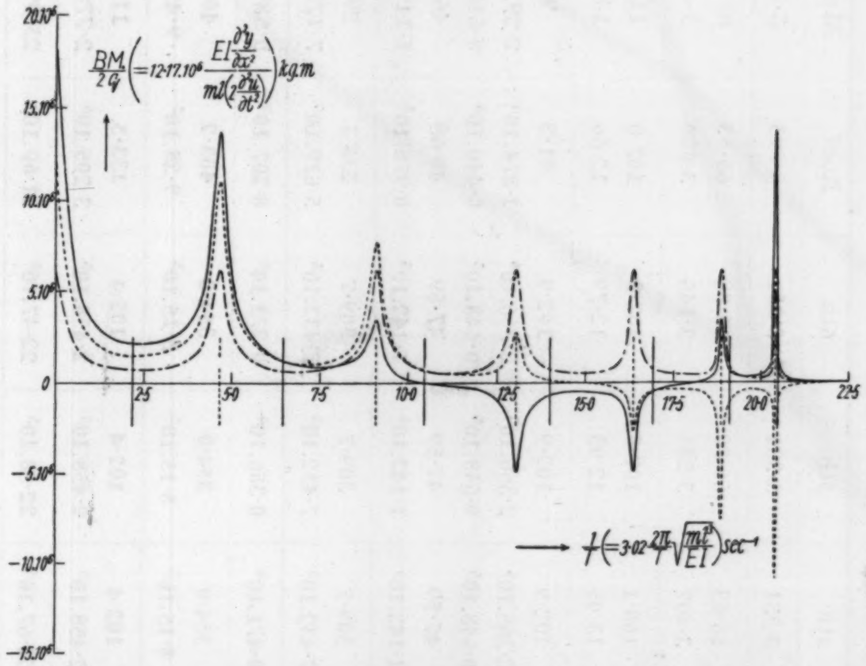

Fig. 4b. Columns alone resist against vibrations. Full, broken, and chain lines represent moments in fourth, fifth, and sixth floors respectively.

4. *The nature of corresonance, etc.*

The bending moments of columns on every floor under the conditions of corresonance will now be shown in dimensionless forms, namely in the forms of $\{EI(\partial^2 y/\partial x^2)\}/\{ml\,2(\partial^2 u/\partial t^2)\}$.

Let BM_0, BM_1, $BM_2, \cdots\cdots$, BM_6 represent the bending moments of columns on the ground, 1st, 2nd, $\cdots\cdots$, 6th floors respectively; then this table shows that the moments (absolute values) under consideration obey a law such that

(i) $BM_0 = 0$ under every corresonance,

(ii) $BM_1 = BM_6$, $\quad BM_2 = BM_5$, $\quad BM_3 = BM_4$

under every corresonance,

(iii) BM_S under 1st corresonance $= BM_S$ under 6th corresonance,
BM_S under 2nd corresonance $= BM_S$ under 5th corresonance,
BM_S under 3rd corresonance $= BM_S$ under 4th corresonance,

in columns of any floor (sth floor).

Another important fact is that BM_0, BM_1, $BM_2, \cdots$, BM_6 vanish 6–, 5–, 4–, $\cdots\cdots$, 1–times respectively and, when any of BM_0, BM_1, BM , $\cdots\cdots$, BM_6 vanishes, the remaining ones obey a law such that

Table I. Calculated Result for Every Element.

Floor			1st	2nd	3rd	4th	5th	6th	Roof	Mean
Height of floor below l (m)			4·695	3·786	3·786	3·331	3·331	3·331	3·793	3·722
Columns		a (m²)	70·65	67·59	67·22	66·63	66·30	65·88	65·53	67·11
		I (m⁴)	4·203	3·584	3·515	3·407	3·283	3·146	3·020	3·451
All vertical members		a (m²)	130·0	109·1	108·7	108·1	107·8	107·3	107·0	111·1
		I (m⁴)	20·34	13·23	13·16	13·05	12·93	12·79	12·66	14·02
Girders	Concrete	(m³)	102·9	102·9	102·9	102·9	102·9	102·9	81·5	99·8
	〃	(kg)	$2·366.10^5$	$2·366.10^5$	$2·366.10^5$	$2·366.10^5$	$2·366.10^5$	$2·366.10^5$	$1·874.10^5$	$2·295.10^5$
	Steel frame	(kg)	$0·648.10^5$	$0·648.10^5$	$0·648.10^5$	$0·648.10^5$	$0·648.10^5$	$0·648.10^5$	$0·440.10^5$	$0·618.10^5$
Beams	Volume	(m³)	47·59	47·59	47·59	47·59	47·59	47·59	40·68	46·61
	Weight	(kg)	$1·142.10^5$	$1·142.10^5$	$1·142.10^5$	$1·142.10^5$	$1·142.10^5$	$1·142.10^5$	$0·976.10^5$	$1·119.10^5$
Floors	Volume	(m³)	309·7	309·7	309·7	309·7	309·7	309·7	234·1	298·9
	Weight	(kg)	$7·432.10^5$	$7·432.10^5$	$7·432.10^5$	$7·432.10^5$	$7·432.10^5$	$7·432.10^5$	$5·619.10^5$	$7·173.10^5$
Steel frames in columns (kg)			$1·254.10^5$	$0·821.10^5$	$0·711.10^5$	$0·471.10^5$	$0·386.10^5$	$0·273.10^5$	$0·207.10^5$	$0·589.10^5$
All vertical members		(m³)	594·6	402·5	402·5	354·0	354·0	354·0	403·2	409·3
		(kg)	$13·67.10^5$	$9·26.10^5$	$9·26.10^5$	$8·15.10^5$	$8·15.10^5$	$8·15.10^5$	$9·28.10^5$	$9·42.10^5$
Entrance and window arches, etc.		(m³)	106·3	129·8	133·1	102·4	102·4	102·4	133·5	115·7
		(kg)	$2·552.10^5$	$3·116.10^5$	$3·196.10^5$	$2·458.10^5$	$2·458.10^5$	$2·458.10^5$	$3·205.10^5$	$2·778.10^5$
Total mass		(kg)	$29·06.10^5$	$24·79.10^5$	$24·76.10^5$	$22·67.10^5$	$22·58.10^5$	$22·47.10^5$	$21·60.10^5$	$23·99.10^5$
Area of floor		(m²)	235·3	235·3	235·3	235·3	235·3	235·3	235·9	235·4

Table II. $\{EI\partial^2 y/\partial x^2\}/\{ml2(\partial^2 u/\partial t^2)\}$ under corresonance.

Floor / $\sqrt{\gamma}$	Ground	1st	2nd	3rd	4th	5th	6th
1·540	0	0·5	0·899	1·122	1·122	0·899	0·5
3·007	0	−0·5	−0·624	−0·278	0·278	0·624	0·5
4·320	0	0·5	0 223	−0·401	−0·401	0·223	0·5
5·418	0	−0·5	0·223	0·401	−0·401	−0·223	0·5
6·243	0	0·5	−0 624	0·278	0·278	−0·624	0·5
6·754	0	−0·5	0·899	−1·122	1·122	−0·899	0·5

(i) For 6 cases of $BM_0=0$ (corresonance conditions),

$$BM_1=BM_6, \quad BM_2=BM_5, \quad BM_3=BM_4,$$

(ii) For 2 cases of $BM_1=0$,

$$BM_0=BM_2=BM_6, \quad BM_3=BM_5,$$

For 2 cases of $BM_1=0$,

$$BM_0=BM_2=BM_3=BM_5=BM_6, \quad BM_4=0,$$

For a case of $BM_1=0$,

$$BM_0=BM_2=BM_3=BM_4=BM_6, \quad BM_5=0,$$

(iii) For 4 cases of $BM_2=0$,

$$BM_0=BM_4=BM_5, \quad BM_1=BM_3=BM_6,$$

(iv) For 2 cases of $BM_3=0$,

$$BM_0=BM_2=BM_4=BM_6, \quad BM_1=BM_5,$$

For a case of $BM_3=0$,

$$BM_0=BM_2=BM_4=BM_6, \quad BM_1=BM_5=0,$$

(v) For 2 cases of $BM_4=0$,

$$BM_0=BM_2=BM_3=BM_4=BM_5=BM_6, \quad BM_1=0,$$

(vi) For a case of $BM_5=0$,

$$BM_0=BM_2\ \ BM_4=BM_6, \quad BM_1=BM_3=0.$$

Similar laws naturally hold for a structure having any different number of stories, the explanation of which will appear in a future occasion.

In conclusion we wish to express our thanks to the members of the Tokyo Marine and Fire Insurance Co., through whose courtesy we obtained the access to much valuable data for the investigation and

also to the Council of the Foundation for the Promotion of Scientific and Industrial Research of Japan, with whose aid the study of the present series is being continued.

---

17. 7階建築に於ける震動勢力の逸散性

地震研究所 { 妹澤克惟
金井　清

7階建築について以前の方法と新しい方法とを以て震動逸散の理論を作つた．東京海上火災保險會社の御好意によつて供給された構造圖を利用して同社の海上ビルデイングに上述の理論を應用して見たのである．但し應用した理論は以前の方卽ち簡單な方である．新しい方は非常に複雜であるが，目下計算中でありその結果は次の報告に發表できる積りである．しかしもつと低い建物の場合に照して，逸散の性質にそれ程違ひはないと思はれる．研究の結果，屈曲モーメント其他の性質は他の建物の場合と大體に於て似てをり，一々説明することを省略するけれども，第1階の柱に起る屈曲モーメントが第一次共振以上の振動數に於て依然として小さいことは注目に値する．又，餘共振に於ける各層の柱に起る屈曲モーメントの値に種々面白い規則があることもわかつたが，之等は本文に委しく説明してある．

18. *On a Problem Concerning the Internal Structure of the Earth as Discussed from the Time-distance Curve of the Formosa Earthquake of April 20, 1935.*

By Hirosi KAWASUMI and Syôsaku HONMA,

Earthquake Research Institute.

(Read Dec. 16, 1935.—Received March 20, 1936.)

The genuine discontinuity or so called first order discontinuity in the velocity distribution of seismic waves within the earth which is now under discussion is that supposed at the depth of 300 or 400 km from the earth's surface. The well known discontinuities near the earth's surface and at the boundary of the inner core are beyond the scope of present study. If we leave the earliest qualitative suggestions of Milne,[1] Omori,[2] Imamura,[3] Laska,[4] Benndorf[5] and Knott[7] out of account, the first qualitative discussion was that of S. Mohorovičić,[7] who remarked in 1916 that the velocity may suddenly decrease at the depth of about 400 km. On the other hand Byerly[8] showed in 1926 that the time-distance curve of the Montana earthquake showed abrupt change of slope at about $\Delta=20°$, which might correspond to sudden increase of velocity at the depth of 400 km. In a study of a deep-focus earthquake one[9] of the writers also considered the existence of such discontinuous increase of velocity at about 450 km. In 1931 Jeffreys[10] noticed from the statistical investigation of time-distance curves that the time curves show abrupt bending at about 20° from the epicentre, and worked out the discontinuity of velocity of about 25% at the depth of 273 km. Reviewing again Jeffreys data one of the writers reached to the conclusion that the negligence of the discontinuity is permissible so long as the observational accuracy at that time is concerned.

1) J. MILNE, *Brit. Assoc. Rep.*, 1902.
2) F. OMORI, *Publ. Earthq. Inv. Comm.*, **5** (1901), **13** (1903), **21** (1905).
3) A. IMAMURA, *Publ. Earthq. Inv. Comm.*, **16** (1904), 1~117.
4) W. LASKA, *Mitt. Erdbebenkomm., Wien.* [N.F.], **23** (1904).
5) H. BENNDORF, *do.*, **29** (1905); **31** (1904).
6) C. G. KNOTT, *Proc. Roy. Soc. Ed.* **28** (1908), 217~230.
7) S. MOHOROVIČIĆ, *Gerlands Beitr. z. Geophys.*, **14** (1916), 187.
8) P. BYERLY, *Bll. Seis. Soc. Amer.*, **16** (1626), 209.
9) H. KAWASUMI, *Journ. Met. Soc. Japan*, [ii], **5** (1927), 232~240.
10) H. JEFFREYS, *M. N. R. A. S., Geophys. Suppl.*, **2** (1931), 329~348.
11) H. KAWASUMI, *Jap. Journ. Astro. Geophys.*, **9** (1931), 15~22.

And Jeffreys[12] himself withdrew his statement in a later investigations, and Gutenberg and Richter[13] also presented negative opinion.

But recently the problem regained eminent supporters as Neumann[14] Byerly,[15] Lehmann[16] and Jeffreys and Bullen[17]. These authorities investigated independently time-distance curves, and found abrupt bending of P- and S-curves at the epicentral distance of about 16° or 19°. Moreover Lehmann presented conspicuous seismograms which show the appearence of late P- and S-phases beyond the epicentral distance of about 20°, and this will decide whether the time-distance curves in this region are double or merely simple curves with strong curvature, provided the appearance of the first smaller P- and S-phases at these distances is independent to the mechanism of the earthquake occurrence. The depths of the discontinuity surface estimated by Neumann, Byerly, Lehmann and Jeffreys and Bullen were 270, 216~315, and about 400 km respectively.

On the other hand, Matuzawa[18] also found strong bend in the P-curve of the Sanriku Earthquake of March 2, 1933, at $\Delta=21°$, but he stated that the change of the slope seems to be gradual.

Thus special studies of this important problem with any available data are urgent task of present seismology. The disastrous Formosa Earthquake of April 20, 1935 provided us with a good opportunity for this purpose, having numerous observations in the range of epicentral distances in question. And Sagisaka and Miura[19] have already elucidated upon this data a discontinuity surface of the second order at the depth of about 300 km from the earth's surface. But we independently took the opportunity to examine quantitative basis of these opinions by the analysis of the time-distance curve of this earthquake to throw some light on this problem.

But as the earthquake was not strong enough to be distinctly observed at the stations in Kwantô and Tôhoku districts which lie in the ranges of epicentral distances concerned, that is in the vicinity of $\Delta=20°$, where microseisms were prevailing at that time. And the time observation alone does not afford conclusive results, but closer

12) H. JEFFREYS, *M. N. R. A. S. Geophys. Suppl.*, **2** (1931), 399~407.

13) B. GUTENBERG and C. F. RICHTER, *Bull. Seism. Soc. Amer.*, **21** (1931) 216.

14) F. NEUMANN, *Trans. Amer. Geophys. Union*, (1933), 329.

15) P. BYERLY, *Bull. Seism. Soc. Amer.*, **24** (1934), 81~99.

16) I. LEHMANN, *Meddelelse Geod. Inst.*, **5** (1934), 1~45.

17) H. JEFFREYS and K. E. BULLEN, *Publ. du Bureau Centr. Seismol. Int.* (A), **11** (1935).

18) T. MATUZAWA, *Bull. Earthq. Res. Inst.*, **13** (1935), 171~193.

19) K. SAGISAKA and T. MIURA, *Kensin Zihô*, **9** (1935), 37~42.

re-examinations of seismograms, which on the writers' request are now in progress by the members of the Central Meteorological Observatory, will give some clue on this problem[20].

1. Determination of the Epicentre.

For such quantitative study as mentioned above we must determine the position of the epicentre as accurately as possible. We, therefore, gathered all the available data from Kisyô Yôran and bulletins of foreign observatories. Following Jeffreys[21] and Matuzawa[22] we assumed cubic equation for the time-distance curve ($t=t_0+\alpha\Delta-\beta\Delta^3$) and analysed the time of arrival of P-phase to determine the position of epicentre (φ_0, λ_0) and constants of time distance curve (t_0, α and β). In this analysis, we first adopted the position determined by the Central Meteorological Observatory[23]

$$\varphi_0 = 24°\,21'\ \mathrm{N},$$

$$\lambda_0 = 120°49'\ \mathrm{E},$$

as the primary epicentre, and the distance to each station was calculated by using geocentric latitude. Borrowing then the cubic equation

$$t_{\mathrm{cal}} = 1{\cdot}6 + 14{\cdot}55\Delta - 0{\cdot}0022\Delta^3\,,$$

determined by Matuzawa from the Sanriku Earthquake, the travel time t_{cal} was calculated. The correction δt_r for the difference of distance from the centre of the earth due to the ellipticity was calculated by the simple formula $\delta t_r = (r-r_0)/10$ sec.

Table I.

Station	Δ	P	δt_r	ε_1	$\delta\Delta$	δt	ε_2
	° ′	h m s	s	s	′	s	s
Taityû	0 07	7 2, 03·8	0·0	0·0	42	18·1	0·0
Arisan	48	2, 14·0	0·0	+0·1	42	18·1	+0·8
Kwarenkô	58	2, 14·8	0·0	−1·3	42	18·0	−0·7
Taihoku	1 03	2, 16·8	0·0	−0·8	42	18·0	−1·5

(*to be continued.*)

20) After the present paper has been written, the writers received detailed discussion of Gutenberg and Richter on this problem, which confirms their previous opinion. *Gerlands Beitr. z. Geophys.*, **45** (1935), 280~360.

21) H. JEFFREYS, *M. N. R. A. S Geophys. Suppl.*, **1** (1928), 500~521, etc..

22) T. MATUZAWA, *loc. cit.*, 17.

23) "Report of the Severe Formosa Earthquake", *Kensin Zihô*, **9** (1935), 1~63.

Table I. (*continue'.*)

Station	Δ	P	δt_r	ε_1	$\delta\Delta$	δt	ε_2
	° ′	h m s	s	s	′	s	s
Tainan	1 22	7 2, 20·0	0·0	−1·9	42	18·0	−1·6
Hôkotô	33	2, 22·0	0·0	−2·6	42	18·0	−1·8
Taitô	38	2, 26·3	+0·1	+0·4	42	18·0	+1·2
Takao	43	2, 31·9	+0·1	+4·6	42	18·0	+5·6
Kôsyun	2 18	2, 36·5	+0·1	+0·8	41	17·9	+2·1
Isigakizima	3 14	2, 49·6	0·0	+0·9	41	17·8	+1·9
Hongkong	6 36	3, 30	+0·1	−1·6	40	17·5	−3
Naha	6 37	3, 42·5	0·0	+6·3	40	17·5	+7·0
Zikawei	6 53	3, 37	−0·2	−3·0	40	17·5	−2
Naze	8 56	4, 08·9	−0·1	−0·1	39	17·3	+0·6
Manila	9 46	4, 19	−0·2	−0·7	38	17·1	0
Tomie	10 00	4, 37·3	−0·4	+9·3	38	17·1	+14·8
Kagosima	11 22	4, 45·9	−0·2	+1·8	37	16·8	+2·2
Nagasaki	38	4, 45·7	−0·3	+0·2	38	17·1	+0·5
Unzendake	52	4, 51·5	−0·3	+2·9	36	16·7	+3·2
Miyasaki	12 11	4, 54·0	−0 2	+1·3	36	16·6	+1·4
Kumamoto	12	4, 54·4	−0·3	+1·7	36	16·6	+1·9
Saga	17	4, 59·9	−0·3	+6·0	36	16·6	+5·5
Ituhara	24	5, 50·5	−0 3	+55·1	36	16·6	+55·7
Hukuoka	35	4, 57·7	−0·3	−0·5	36	16·6	−0·3
Husan	59	5, 14·5	−0·3	+11·0	35	16·5	+11·0
Ooita	13 05	5, 01·9	−0·3	+0·6	35	16·5	−0·0
Simonoseki	09	5, 16·0	−0·3	+10·2	35	16·5	+10·2
Taikyû	24	5, 12·5	−0·4	+3·3	35	16·4	+3·5
Uwazima	42	5, 24·9	−0·3	+11·7	34	16·3	+11·6
Simidu	43	5, 12·6	−0·3	−0·8	34	16·3	−0·9
Phulien	44	5, 10	+0·1	+0·8	34	16·3	−4·7
Zinsen	14 06	5, 18·1	−0·4	+0·0	34	16·2	+12·5
Matuyama	11	5, 19·8	−0·3	+0·6	34	16·2	+0·1
Keizyô	17	5, 20·5	−0·4	−0·2	34	16·2	−0·4
Kure	20	5, 51·4	−0·3	+30·1	34	16·1	+2·0
Hiroshima	22	5, 10·0	−0·3	−12·0	34	16·1	−12·1
Hamada	29	5, 21·5	−0·3	−1·8	34	16·1	−2·1
Kôti	33	5, 20·0	−0·3	−4·3	33	16·1	−4·7
Dairen	34	5, 34·1	−0·5	+9·8	33	16·1	+9·4
Muroto	50	5, 35·8	−0·3	+7·7	33	16·0	+7·4
Tadotu	15 08	5, 44·4	−0·3	−7·4	33	16·0	+12·2
Heizyô	16	5, 36·0	−0·5	+2·7	33	16·0	+2·0
Okoyama	29	5, 32·0	−0·3	−4·5	33	16·0	−2·7
Sakai	37	5, 44·8	−0·4	+6·1	32	15·7	+6·0

(*to be continued.*)

Table I. (*continued.*)

Station	Δ	P	δt_r	ε_1	$\delta\Delta$	δt	ε_2
	° ′	h m s	s	s	′	s	s
Tokusima		7 5, 32·9	−0·4				
Sumoto	15 43	5, 41·0	−0·3	+1·7	32	15·9	+0·7
Wakayama	16 04	5, 41·0	−0·3	−2·6	32	15·8	−3·8
Siomisaki	04	5, 44·0	−0·3	+0·3	32	15·8	−1·9
Kôbe	20	5, 47·6	−0·3	+0·5	32	15·7	−0·7
Eikô	21	5, 46·5	−0·5	−0·4	32	15·7	−1·8
Oosaka	33	5, 47·0	−0·3	−2·7	32	15·7	−4·1
Toyooka	36	5, 51·0	−0·4	+0·7	32	15·7	−0·7
Yagi	39	5, 51·6	−0·3	+0·6	32	15·7	−3·1
Miyadu	50	5, 47·6	−0·4	−5·4	31	15·7	−7·4
Kyôto	54	5, 54·2	−0·3	+0·1	32	15·7	−1·8
Kameyama	17 16	5, 59·5	−0·3	+0·4	31	15·6	−1·1
Tu	16	6, 04·3	−0·3	+5·5	31	15·6	−3·7
Hikone	23	6, 01·7	−0·4	−0·3	31	15·5	−0·2
Ibukisan	34	6, 02·9	−0·4	−1·4	31	15·5	−3·7
Gihu	48	6, 06·1	−0·4	+0·8	31	15·4	−0·8
Nagoya	49	6, 08·1	−0·3	+2·5	31	15·4	+0·5
Hukui	51	5, 56·2	−0·4	−9·9	31	15·4	−11·7
Hamamatu	18 06	6, 04·8	−0·3	−4·3	30	15·4	+3·3
Kanazawa	23	5, 20·0	−0·4	+7·1	30	15·3	+5·7
Omaesaki	24	5, 20·7	−0·3	+7·6	30	15·3	+5·2
Takayama	32	6, 57·5	−0·4	+42·8	30	15·3	+40·6
Husiki	47	6, 20·7	−0·4	+2·9	30	15·3	+0·2
Toyama	49	6, 18·3	−0·4	+0·2	30	15·2	−2·1
Hatidyôzima	19 02	6, 20·4	−0·3	−0·3	29	15·2	−3·1
Iida	05	6, 19·0	−0·4	−2·1	29	15·2	−5·1
Matumoto	05	6, 30·9	−0·4	+9·8	29	15·2	+6·9
Numadu	06	6, 21·9	−0·3	+0·7	29	15·2	−3·9
Kôhu	10	6, 25·9	−0·4	+4·0	29	15·2	+0·8
Misima	11	6, 19·4	−0·3	+0·8	29	15·2	−6·0
Hunatu	14	6, 21·1	−0·4	−1·5	29	15·2	−5·0
Nagano	28	6, 36·2	−0·4	+10·6	29	15·1	+7·5
Oiwake	31	6, 32·0	−0·4	+5·7	29	15·1	+3·0
Titizima	37	6, 23·7	−0·1	−3·7	29	15·1	−13·4
Tomisaki	43	6, 32·0	−0·3	+3·4	28	14·9	−1·9
Yokosuka	45	6, 55·8	−0·3	+26·7	29	15·1	+23·0
Yokohama	50	6, 36·0	−0·4	+6·1	28	15·0	+2·3
Maebasi	55	6, 32·0	−0·4	+1·2	28	15·0	−2·7
Kumagaya	20 00	6, 38·8	−0·4	+6·9	28	15·0	+3·1
Tôkyô	02	6. 38·8	−0·4	+4·6	28	15·0	+2·7

(*to be continued.*)

Table I. (*continued.*)

Station	Δ	P	δt_r	ε_1	$\delta\Delta$	δt	ε_2
	° ′	h m s	s	s	′	s	s
Wazima	20 32	7 6, 23·1	−0·4	−15·0	28	14·9	−19·2
Tukubasan	32	6, 32·0	−0·4	−6·1	28	14·9	−10·4
Utunomiya	34	6, 44·8	−0·4	+6·4	28	14·9	+2·0
Kakioka	36	6, 45·0	−0·4	+6·1	28	14·9	+1·8
Niigata	46	6, 24·5	−0·5	−15·3	27	14·9	−25·1
Tyôsi	51	6, 56·9	−0·4	+15·1	27	14·8	+10·4
Vladivostock		6, 41	−0·6				
Mito	52	6, 55·0	−0·4	+13·0	26	14·7	+8·2
Aidu	21 14	7, 06·6	−0·4	+20·4	27	14·8	+15·3
Hukusima	44	6, 49·1	−0·5	−2·4	26	14·7	−8·6
Yamagata	46	7, 07·8	−0·5	+15·6	26	14·7	+9·9
Sendai	22 09	7. 24·5	−0·5	+28·1	26	14·6	+22·4
Midusawa	47	6, 58·0	−0·5	−5·5	26	14·5	−12·3
Morioka	23 04	7, 07·7	−0·5	+1·1	25	14·5	+47·3

Using the formula

$$t_{ob}-t_{cal}=\delta t_0+\frac{\partial t}{\partial\varphi_0}\delta\varphi_0+\frac{\partial t}{\partial\lambda_0}\delta\lambda_0+\delta a\Delta+\Delta\beta\Delta^3\,, \tag{1}$$

the corrections to the assumed values (δt_0, $\delta\varphi_0$, $\delta\lambda_0$, δa and $\delta\beta$) were determined by the method of least squares.[24] Discarding the observations subjected to distinct errors, 46 stations in the range $\Delta=0{\cdot}8°$ and 18° were used in the analysis.

The results were

$$\delta t_0=0\overset{s}{\cdot}86\pm0\overset{s}{\cdot}91 \text{ (P. E.)},$$
$$\delta\varphi_0=-1'\!\cdot4\pm2'\!\cdot5\,,$$
$$\delta\lambda_0=-11'\!\cdot4\pm2'\!\cdot6\,,$$
$$\delta a=-0{\cdot}21\pm0{\cdot}13\,,$$
$$\delta\beta=0{\cdot}00003\pm0{\cdot}00033.$$

24) As is usually the case with large earthquake causing damage, the hypocentral depth of this earthquake seems to be about 10 km from the examination of the P-curve near the epicentre. This depth was worked out by Y. Oka ("Preliminary Report of the Severe Middle Formosa Earthquake", published by the Taihoku Observatory) as well as by members of the Central Meteorological Observatory (*Kensin Zihô*, **9** (1935), 8). This is also confirmed by the examination of reflected waves. And we can well neglect the consideration of the effect of this depth in the present analysis.

$$\therefore \quad \left.\begin{aligned} \varphi_0 &= 24^\circ\ 19'\!\cdot\!6 \pm 2'\!\cdot\!5\ \text{N}\,, \\ \lambda_0 &= 120^\circ\ 37'\!\cdot\!6 \pm 2'\!\cdot\!6\ \text{E}\,, \end{aligned}\right\} \qquad (2)$$

and

$$\left.\begin{aligned} t &= 7^{\text{h}}\ 2^{\text{m}}\ 2^{\text{s}}\!\cdot\!5 + 14\cdot337\Delta - 0\cdot00217\Delta^3, \\ &\quad\ \pm 0\cdot9 \quad \pm 0\cdot13 \quad\ \pm 0\cdot00033\,. \end{aligned}\right\} \qquad (3)$$

The probable error of individual observation were $\rho = 1\cdot5$ sec ($\sigma = 2\cdot2$ sec). The residue ε_1 of each observation were tabulated in Table I. The epicentre determined lies near the River Taikwo-kei in the southern vicinity of a town called Taikwo.

2. Examination of the Assumption of the Second Order Discontinuity.

Now that the epicentre and the time distance curve up to $\Delta = 18^\circ$ have been determined, we have only to examine the fitness of the curve with the observations above that distance. But as we have already stated, the observations show such a considerable scatter that we cannot get definite conclusion from the sole examination of these data. We are therefore compelled to compare it with the existing time-distance curves. The comparisons were made with two curves, the one was that of Jeffreys-Bullen table[25] of 1935 and the other was the mean[26] of the P-curve of the Sanriku Earthquake and reduced P curve of the deep focus earthquake of Feb. 20, 1932. (Table II.)

Table II. Mean P-curve (M) and its derivative.

Δ	20°	21°	22°	23°	24°	25°	26°	27°	28°	29°	30°
t (M) sec	278·6	288·9	299·3	309·3	319·4	329·3	339·0	348·5	357·9	367·2	376·3
$\frac{dt}{d\Delta}$ sec/degree	10·53	10·34	10·20	10·03	10·025	9·80	9·59	9·44	9·36	9·175	9·20

25) H. JEFFREYS and K. E. BULLEN, *Publ. Bur. Centr. Seismol. Int.*, (A), **11** (1935).

26) It was derived by the present writers by the revision of the data of the Sanriku Earthquake through the kindness of Prof. Matuzawa, and making use of the data in a paper by H. Kawasumi and R. Yosiyama (*Disin*, **6** (1934), 415). On comparing the two component curves we obtained that the delay in starting defined by Jeffreys was 7·9 sec, which is exactly the same with the value obtained by Jeffreys and Bullen. And this value was subtracted from the mean value in the above comparison. The analysis of the mean curve will be reported in near future.

In each case the extrapolated time curve of the Formosa Earthquake becomes nearly continuous with the time curve compared at about $\Delta = 20°$, though the slope suddenly increases by about 10% in passing the joint.

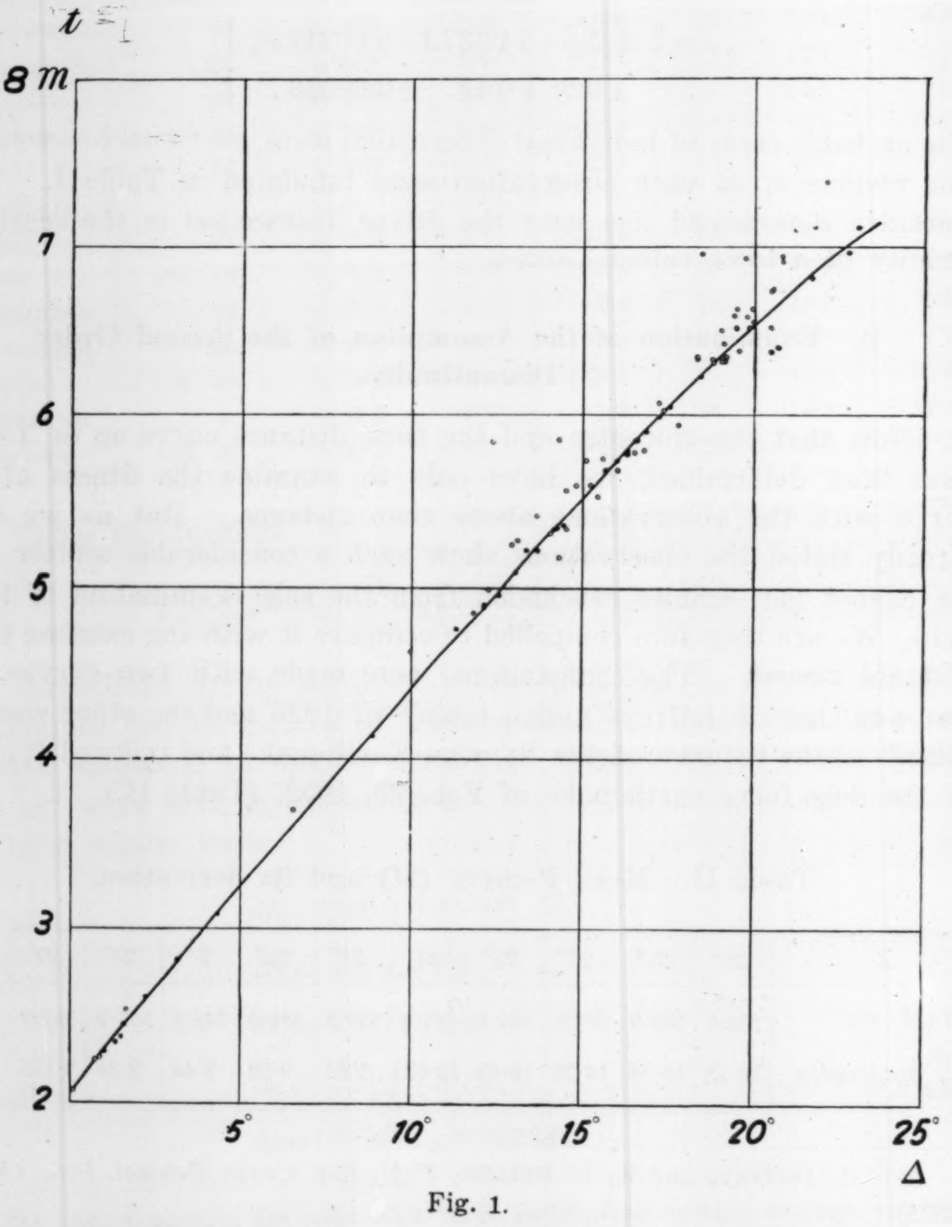

Fig. 1.

If we were to smooth these discontinuities, the necessary corrections derived, for example, by Comrie's method are, as we see in the raws of $-\frac{3}{35}\Delta_4$ in Table III, amount only to small fractions of a second. And such correction may be quite permissible from the present observational accuracy. But if this is actually the case, the consequence

contradicts to Lehmann's discovery of the sudden decrease of amplitude at the epicentral distance here concerned. Moreover the scatter of the observational points of the time-distance curve of the present earthquake at the very distances seems also disadvantageous to the above consequence. (See Fig. 1.)

Table III. Smoothed P-curves and the Correction applied by Comrie's method.

Δ	17	18	19	20	21	22	23	24	25	26	27	28
J. B.	233·1	245·4	257·6	269·8	280·4	290·6	300·6	310·4	319·8	329·1	338·2	347·2
M	233·1	245·4	257·5	269·5	280·8	291·5	301·5	311·5	321·4	331·1	340·6	350·0
$-\frac{3}{35}\Delta_4$(J.B)	−0·03	−0·01	+0·14	−0·21	+0·08	0	+0·02	0	−0·05	+0·07	−0·03	0
$-\frac{3}{35}\Delta_4$(M)	−0·03	+0·01	+0·01	0·07	−0·15	0·06	+0·02	0·01	−0·01	−0·01	+0·01	+0·02

Though the time observation of the present earthquake is insufficient to be decisive without support of the amplitude observations, there is an investigation by Sagisaka and Miura on the present as-

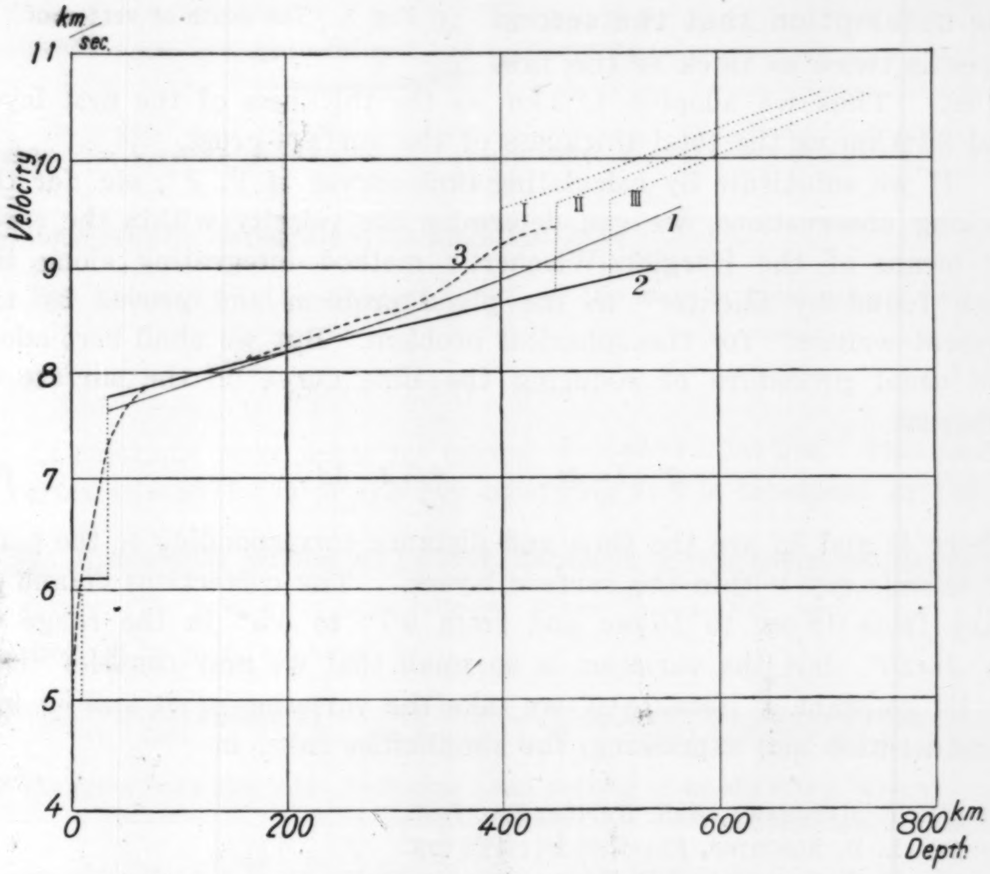

Fig. 2. Velocity distribution of P-wave. 1: The result of chapter 2. 2 (I, II, III): The results of chapter 3. 3: The results of Sagisaka and Miura.

sumption, so we shall here cite their results (curve 3 in Figs. 2 and 3.) and abstain from the detailed discussion. We shall only give here the analysis of the P-curve expressed as cubic equation of Δ, to see the accuracy of the present determination of velocity and path of seismic waves.

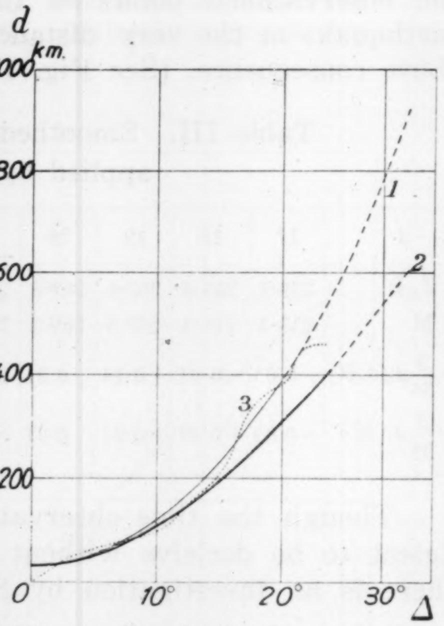

Fig. 3. The depth of vertex of sciomic ray.

For this purpose we must know the structure of the surface layers. But having no data to determine it from the observations, we have, for the present, assumed the two surface layers with the velocities of P-waves 5·0 and 6·1 km/sec respectively as determined by Matuzawa,[27] and determined the thickness of these layers so as the delay in starting becomes 7·9 sec under the assumption that the second layer is twice as thick as the first layer. Thus we adopted 11·3 km as the thickness of the first layer and 33·9 km as the total thickness of the surface crust.

If we substitute by calculating time curves of $\overline{P}$, P*, etc. for the lacking observations, we can determine the velocity within the earth by means of the Herglotz-Wiechert's method integrating along the path found by Slichter[28] in the plane problem and proved by the present writers[29] for the spherical problem. But we shall here adopt the usual procedure of reducing the time curve on the surface of subcrust.

$$T = t - \delta t\,, \qquad \theta = \Delta - \delta\Delta\,, \tag{4}$$

where δt and $\delta\Delta$ are the time and distance corresponding to the parts of seismic ray within the surface layers. The corrections δt and $\delta\Delta$ vary from 18 sec to 15 sec and from 0·7° to 0·5° in the range up to $\Delta=20°$, but the variation is so small that we may consider them to be constant. Because if we take the variation of δt and $\delta\Delta$ into consideration and expressing, for simplicities sake, in

27) T. MATUZAWA, *Bull. Earthq. Res. Inst.*

28) L. B. SLICHTER, *Physics.*, **3** (1932), 273.

29) H. KAWASUMI and S. HONMA, Read at the meeting of the Earthquake Research Institute on Sept. 17, 1935, and will be published shortly.

$$\delta t=\left(18-\frac{3}{20}\Delta\right)\sec\,,\qquad \delta\Delta=\left(0{\cdot}7-\frac{0{\cdot}2}{20}\Delta\right),\tag{5}$$

and carry out the transformation into

$$t-18=\alpha(\Delta-0{\cdot}7)-\beta(\Delta-0{\cdot}7)^3-\left(\frac{3}{20}-\frac{0{\cdot}2}{20}\alpha\right)\Delta-3\times\frac{0{\cdot}2}{20}\beta\Delta(\Delta-0{\cdot}7)^2\,,\tag{6}$$

the last two terms are almost negligible from the accuracy of the present determination of the coefficient of time-distance curve. We can therefore use, for the P-curve on the level of subcrust

$$T=\alpha\theta-\beta\theta^3\,,\tag{7}$$

where α and β are the same as those of P-curve on the earth's surface.

Then the Herglotz-Wiechert's formula

$$\log\frac{R}{r}=\frac{1}{180}\int_0^{\theta_1}\cosh^{-1}u\,d\theta\,,\qquad \text{where } u=\frac{dt}{d\theta}\Big/\frac{dT}{d\theta_1}\tag{8}$$

reduces to

$$\log\frac{R}{r}=\frac{1}{90}\sqrt{\frac{2}{\gamma}}\frac{K-E}{\sqrt{1-k^2}}\,,\tag{9}$$

[30)]

where $\gamma=\dfrac{3\beta}{\alpha}$, and $K=\displaystyle\int_0^{\frac{\pi}{2}}\frac{d\varphi}{\sqrt{1-k^2\sin^2\varphi}}$ and $E=\displaystyle\int_0^{\frac{\pi}{2}}\sqrt{1-k^2\sin^2\varphi}\,d\varphi$ are complete elliptic integrals with modulus $k^2=\dfrac{\gamma\theta_1^2}{2-\gamma\theta_1^2}$.

The velocity at the deepest point of the ray is then given by

$$v=\frac{\pi}{180}\frac{r}{(\alpha-3\beta\theta_1^2)}=\frac{\pi}{180\alpha}\frac{1+k^2}{1\quad k^2}r\,.\tag{10}$$

Calculations were made by taking $R=(6371-34)$ km. The depth of vertex ($d=6371-r$) of the ray emerging at θ is tabulated in Table

---

29) Examination problem set by Prof. Matuzawa in 1934, and solved by one of the writers. The brief proof is as follows. Since $\dfrac{dT}{d\theta}=\alpha-3\beta\theta^2$, $u=\dfrac{1-\gamma\theta^2}{1-\gamma\theta_1^2}$. Integrating (8) by parts, we have

$$\log\frac{R}{r}=\frac{1}{180}\Big[\theta\cosh^{-1}u\Big]_0^{\theta_1}-\frac{1}{180}\int_0^{\theta_1}\frac{\theta}{\sqrt{u^2-1}}\frac{du}{d\theta}d\theta=\frac{2\gamma}{180(1-\gamma\theta_1^2)}\int_0^{\theta_1}\frac{\theta}{\sqrt{u^2-1}}d\theta\,,$$

and changing variables into $\theta=\theta_1\sin\varphi$ and putting k^2 as above we have

$$\log\frac{R}{r}=\frac{1}{90}\sqrt{\frac{2-\gamma\theta_1^2}{\gamma}}\int_0^{\frac{\pi}{2}}\frac{k^2\sin^2\varphi}{\sqrt{1-k^2\sin^2\varphi}}d\varphi\,,$$

which reduces to (9).

II. The values corresponding to θ beyond 20° might be meaningless, but we have calculated for the sake of comparison with the following cases discussed in the next chapter.

Table IV. The depth (d) and velocity (v) at the vertex of a seismic ray emerging at epicentral distance θ.

θ	0°	4°	8°	12°	16°	20°	24°	28°
d km	33·9	46·9	88·3	157·8	257·9	392·0	568·6	787·4
v km/sec	7·56	7·69	7·82	8·04	8·38	8·87	9·57	10·61

Next we have to examine the accuracy of the values here determined. From the value of the coefficient of Δ in the P-curve we have

$$v_0 = 7{\cdot}65 \pm 0{\cdot}07 \text{ km/sec},$$

where v_0 is the velocity at 34 km level. The probable error of v will increase with the increasing depth of vertex of seismic ray. So we will examine it with the ray emerging at $\theta = 20°$. For this purpose we have calculated four cases answering to the four combinations of signs of errors of α and β. The errors of α and β obtained above from this earthquake are smaller than those obtained by Matuzawa, and nearly equal to those of Jeffreys and Bullen. So we have also calculated the cases corresponding to Matuzawa's values.

Table V. Examination of accuracies of determination of v and d corresponding to the errors of determination of time-distance curve, in cases of I, the Formosa earthquake ($\delta\alpha = \pm 0{\cdot}13$, $\delta\beta = \pm 0{\cdot}00033$) and II, the Sanriku earthquake ($\delta a = \pm 0{\cdot}35$, $\delta b = \pm 0{\cdot}0015$) for the ray emerging at $\theta = 20°$.

	I				II			
	1 (++)	2 (+−)	3 (−+)	4 (−−)	1 (++)	2 (+−)	3 (−+)	4 (−−)
v km/sec	9·03	8·54	9·24	8·71	9·86	7·70	10·59	10·46
d km	420·2	359·2	424·3	362·5	513·9	227·6	534·6	630·1

Comparing these values with those in Table II the accuracies of the present determination are $v = (8{\cdot}87 \pm 0{\cdot}33)$ km/sec, $d = (392 \pm 33)$ km in case I, while the ranges of v and d in case II are $(-1{\cdot}17 \sim +1{\cdot}59)$ km/sec and $(-154 \sim +238)$ km respectively. Thus the determination of the discontinuity of velocity, if any, cannot attain higher accuracies.

The values obtained are shown in Figs. 2 and 3 (curve 1) in which the results of Sagisaka and Miura are also indicated (curve 3) for comparison.

3. Examination of the Assumption of the Discontinuity of First Order.

As we have already stated the observations beyond $\Delta=20°$ seem to be subjected to large errors to draw definite conclusion, but the writers were struck by the fact that when they first draw the time-distance curve using the primary epicentral distance, smooth curve tentatively drawn was nearly coincident to the usual P-curves up to $\Delta=20°$ca. which suddenly deviate beyond that distance. This is easily explained by considering the branch as the late P-phase found by Lehmann, the first phase being missed owing to the smallness of amplitude.

We shall therefore proceed upon this assumption to test the existence of first order discontinuity. Then we shall be able to examine the depth and amount of discontinuity as well as the form of the time distance curve.

As the assumption itself is in question and the observational accuracy is not so good as we have seen in the preceding chapter, we shall be contented with the simple procedure on the assumption that the seismic ray is circular, and consequently the velocity distribution in the subcrust and time distance curve are given by

$$v=a-br^2\,, \tag{11}$$

and

$$T=\frac{1}{\sqrt{ab}}\sinh^{-1}\frac{\sqrt{ab}\;2\sin\frac{1}{2}\theta}{a-b} \tag{12}$$

[31]

respectively.

Selecting 42 stations including Kôhu, Oiwake, Toyama, Yokahama, Tokyo, Kumagaya, Utunomiya and Kakioka on the branch beyond $\Delta=18°$, we have determined T_0, a and b by the method of least squares. The formula used was

$$T_{ob}-T_{cal}-T_0=\delta T_0+\frac{\partial T}{\partial(a-b)}\partial(a-b)+\frac{\partial T}{\partial\sqrt{ab}}\delta\sqrt{ab}\,, \tag{13}$$

in which T and θ is reduced value on the 34 km level. And primary values adopted were $a-b=0{\cdot}001207$ and $\sqrt{ab}=0{\cdot}002338$ which was

31) H. KAWASUMI, *Bull. Earthq. Res. Inst.*, **10** (1032), 94~129; *Jap. Journ. Astro. Geophys.*, **9** (1931), 15~22.

determined by using the cotangent constant $\frac{a+b}{a-b}=\cot i \cot\frac{1}{2}\theta=4$.

The results were

$$\left.\begin{aligned} a-b&=0{\cdot}001227\pm0{\cdot}000008 \text{ (P. E.)},\\ \sqrt{ab}&=0{\cdot}001750\pm0{\cdot}000103,\\ T_0&=22\text{ h } 1\text{ m } 53{\cdot}7\pm0{\cdot}6\text{ s},\end{aligned}\right\} \qquad (14)$$

the probable errors of individual observation being $\rho=1{\cdot}3$ sec and consequently

$$\left.\begin{aligned} a&=0{\cdot}0024678\pm0{\cdot}000018,\\ b&=0{\cdot}0012409\pm0{\cdot}000018.\end{aligned}\right\} \qquad (15)$$

The velocity distribution $v=a-br^2$ and the depth of the vertex of the seismic ray emerging at θ or $\Delta=\theta+\delta\Delta$ are shown in Table VI, Fig. 2 and Fig. 3.

Table VI. v and d.

θ	4°	6°	8°	10°	12°	14°	16°	18°	20°	22°	24°	26°	28°
d km.	45	62	80	106	137	175	212	257	306	357	412	473	540
v km/sec	7·81	7·85	7·89	7·95	8·03	8·12	8·21	8·32	8·43	8·56	8·69	8·83	8·98

The residues ε_2 of all the observations calculated from the above values of T_0, a and b are tabulated in the last column of Table I. The residues beyond 18° are of course very large, and some of these may be explained by the hypothetical three branches (Fig. 4) of time-distance curve, the individual, reflected waves and the transmitted wave partly through the lower layer. We shall now proceed to determine these three branches of time-distance curve in order to have some clue on the discontinuity of velocity. Since we know the velocity distribution outside the hypothetical discontinuity surface, we can calculate two branches, i. e. the individual and reflected waves, provided we know the depth of discontinuity surface, by the formula (11) and

$$T=\frac{1}{\sqrt{ab}}\sinh^{-1}\frac{\sqrt{ab}\,d}{V}, \qquad (16)$$ [32]

where $V=\sqrt{(a-b)\{a-b(1-h)^2\}}$ and $d=\sqrt{h^2+4h\sin^2\frac{1}{2}\theta}$,

32) H. KAWASUMI, *loc. cit.*, 30).

in which h denotes the depth of the discontinuity surface measured in fraction of the earth's radius.

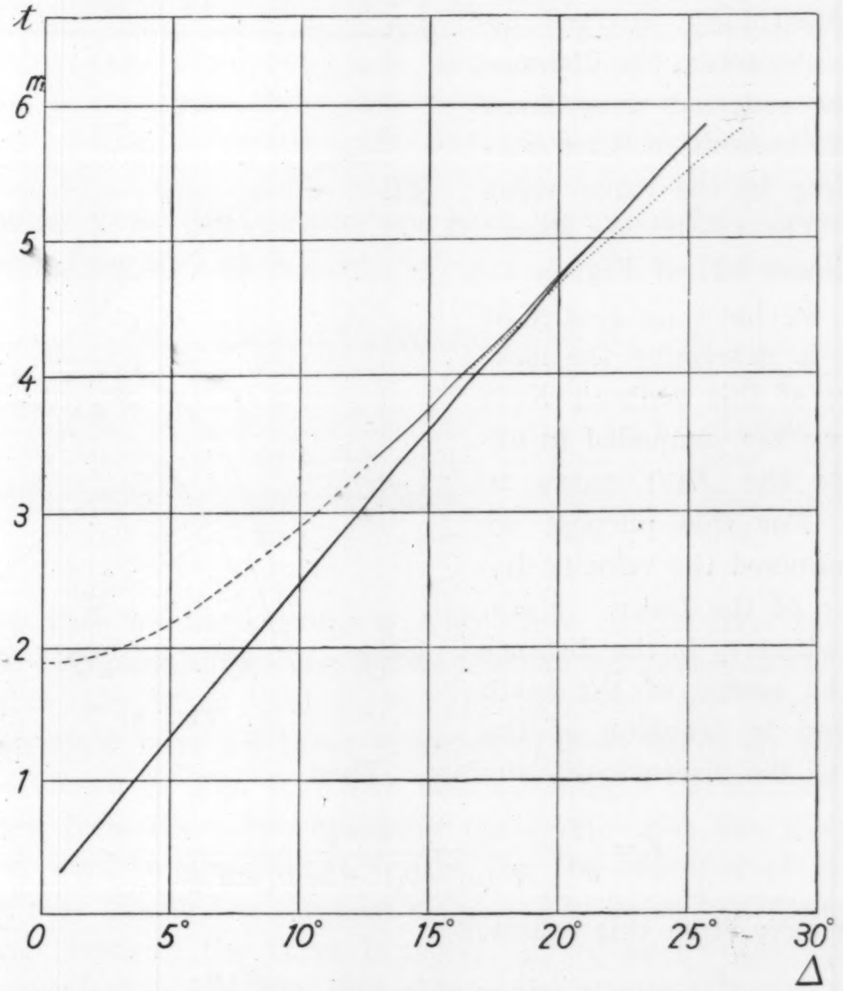

Fig. 4. Calculated three branches of P-waves using the velocity determined upon the assumption (II) that the first order discontinuity is at the depth of 450 km.

Assuming three values 400, 450, and 500 km as the thickness of the discontinuity surface we have first calculated the constant K of the seismic ray defined by

$$K=\frac{r}{v}\sin i=\frac{dT}{d\theta} \qquad (\theta \text{ in radian}) \qquad (17)$$

for each of these branches. (Fig. 5.) As we were not able to determine the branch of the transmitted wave from the observations of the present earthquake, the mean P-curve deduced from the Sanriku earthquake and the deep-focus earthquake of Feb. 20, 1931 was substituted in this place. (Table II.) The branch in the lower part and beyond

$\theta=20°$ denotes the value obtained from the mean P-curve.

We can now take off the effect due to the upper part of the discontinuity surface by simply subtracting the distance θ_r of the reflected wave from θ_t of the tansmitted wave corresponding to the same value of K. The results are shown in the lower left of Fig. 5.

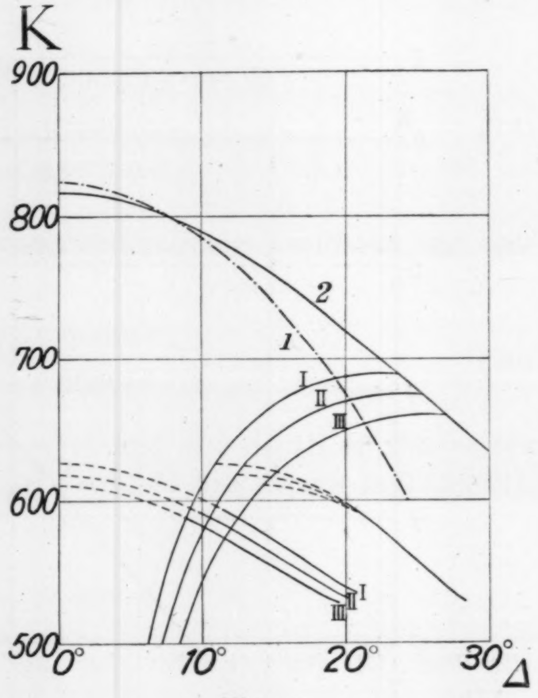

Fig. 5.

As we have no means at present to determine the lacking part of this reduced $K(\theta)$ curve, we are compelled to extrapolate the $K(\theta)$ curve to $\theta=0°$. For this purpose we again assumed the velocity distribution of the form $v_1=a_1-b_1r_1^2$ where r_1 is the distance from the centre of the earth measured in fraction of the radius of the discontinuity surface. Then

$$K=\frac{dT}{d\theta}=\frac{\cos\frac{1}{2}\theta}{\sqrt{(a_1-b_1)^2+4a_1b_1\sin^2\frac{1}{2}\theta}} \tag{18}$$

and we have from this equation

$$(a_1-b_1)^2+4a_1b_1\sin^2\tfrac{1}{2}\theta=\frac{\cos^2\frac{1}{2}\theta}{K^2}. \tag{19}$$

Since we know K as a function of θ we can determine $(a_1-b_1)^2$ and $4a_1b_1$ by means of this formula. Least square solutions using 9 values for the above three cases were obtained. The results are tabulated in Table VII.

Table VII. Constants of velocity formula for the inside of discontinuity surface.

d (km)	I 400	II 450	III 500
$(a_1-b_1)^2\times10^6$	26·162	27·912	30·814
$4ab\times10^6$	25·49	26·18	26·83
$a\times10^3$	3·477	3·572	3·713
$b\times10^3$	1·881	1·954	2·075

Table VIII. Velocity distribution within the discontinuity surface. (km/sec)

d	400	450	500	550	600	650	700	750	800	850
I	9.53	9·72	9·91	10·09	10·27	10·45	10·63	10·81	10·99	11·16
II		9·58	9·78	9·97	10·16	10·35	10·54	10·72	10·91	11·09
III			9·62	9·82	10·03	10·23	10·43	10·63	10·83	11·03

The values thus extrapolated are given in Table IX, and indicated by broken lines in Fig. 5.

Table IX. Extrapolated *K*.

θ	0	2	4	6	8	10
I	626·4	625·3	622·1	616·9	609·8	601·0
II	618·0	616·9	613·6	608·3	601·1	592·1
III	610·5	609·3	605·9	600·3	592·6	583·2

Now that we have complete $K(\theta)$ curve on the level surface of assumed discontinuity, we can deduce them to the values on the earth's surface or any other level surface by reversing the above process. Thus we could have all three branches of $K(\theta)$ curve on the 34 km level as shown in Fig. 5. The corresponding P-curves can also be calculated from the values we have obtained. But the $K(\theta)$ curve offers in itself a conspicuous means for the selection of the most suitable case among the assumed cases. The epicentral distances of the three joints of the three branches, if we have observation, are very convenient. We can also obtain the P-curves by integrating this $K(\theta)$ curve along the three branches.

Table X. Calculated 3 branches of P-curve for case II, d=450 km.

Individual wave	θ	0° 43′	2° 42′	4° 41′	6° 40′	8° 39′	10° 38′	12° 37′	14° 36′	16° 34′	18° 33′	20° 32′	22° 31′	24° 29′	26° 28′
	t	18·2 s	46·2	74·5	102·6	130·3	157·8	184·9	211·5	237·6	263·2	287·3	312·9	336·9	360·2
Reflected wave	θ	0°	2° 42′	4° 41′	6° 40′	8° 39′	10°·38′	12° 37′	14° 36′	16° 34′	18° 33′	20° 32′	22° 31′	24° 29′	26° 28′
	t	112·5 s	46·2	74·6	102·8	124·6	160·0	186·6	214·6	242·2	268·6	297·0	324·2	351·1	377·9

Transmited wave	θ	12° 46′	14° 41′	16° 25′	18° 04′	19° 34′	21° 03′	22° 31′	23° 56′	25° 23′	26° 52′
	t	202·8 s	223·5	242·3	259·4	275·7	291·0	305·8	320·0	334·5	348·5

The three branches of P-curve for the case II ($d=450$ km) indicated in Table X and Fig. 5 are calculated rigorously from the values of velocity, while the curves for cases I and III were deduced by the integration of $K(\theta)$ curves. The branch of the transmitted wave thus obtained is nearly conformal with the observed mean curve above used. The point of intersection of this branch with the curve of the individual wave and the constant difference between the observed and calculated curve for each case are as follows:

d (km)	I 400	II 450	III 500
Δ t_0-t_c	$17\overset{\circ}{\cdot}5$ $\overset{s}{2\cdot2}$	$19\overset{\circ}{\cdot}3$ $\overset{s}{-1\cdot4}$	$20\overset{\circ}{\cdot}4$ $\overset{s}{-3\cdot6}$

It seems from the value of t_0-t_c that the case II is nearest to the observed value. Moreover the epicentral distance of the point of intersection for this case is nearly coincident with the value 19° which was found by Neumann, Lehmann, Jeffreys and Bullen. If interpolation is permissible we have from the value of t_0-t_c the depth of the discontinuity surface of about 430 km from the earth's surface.

It is also to be noted that a number of points excluded in the preceeding analysis can be explained by the three branches calculated (Fig. 5), and especially the correspondence of the late observations from 13° to 18° with the late P-phase (probably the reflected wave) is worthy of some further examination even if it were mere coincidence.

The amounts of discontinuity of velocity thus worked out are

	I	II	III
v_0 (km/sec) v_i (km/sec) v_0-v_i (km/sec)	8·66 9·53 0·87	8·78 9·58 0·80	8·89 9·62 0·73

all within 1 km/sec, while the ranges of triplication of P- curve are

$$\text{I. } \Delta=11\overset{\circ}{\cdot}3-23\overset{\circ}{\cdot}9,\quad \text{II. } \Delta=12\overset{\circ}{\cdot}6-25\overset{\circ}{\cdot}6 \text{ and III. } \Delta=14\overset{\circ}{\cdot}6-27\overset{\circ}{\cdot}3$$

respectively.

These values are the results of our assumption that the six stations beyond 18° observed late P-phase. It also depends on the adopted travel time curve beyond 20°. But if we were to take the velocity determined in chapter II, the amount of velocity discontinuity and the

range of triplication of P-curve would be smaller, while the depth of discontinuity would be still larger.

The amount of discontinuity and range of triplication are thus unexpectedly smaller than the values anticipated by various authorities.

Another word to be added is on the amplitude variation of early P-phases near the joint at about 19°. Since the transmitted wave passes twice the discontinuity surface, the amplitude must diminish as the effect of refraction. Now the angles of emergence at the discontinuity surface of the waves emerging at $\Delta = 20°$, $22°$, and $24°$ are 13°, 19° and 23° respectively (for the case II, $d=450$ km), considerable decrease of amplitude of initial motion is to be expected in passing the joint at abouts=19°, but the increase of amplitude with increase of the angle of emergence is so large in the range concerned, that the amplitude will increase rapidly with increasing distance.

The variation of amplitude due to the variation of $\frac{dt}{d\theta}$ is also to be considered[33]. But we see from Fig. 4 that the $K(\theta)$ curves of the individual and transmitted waves are nearly parallel, the effect will be almost negligible. And if we were to use the P-curve used in Chapter II, the decrease of amplitude from this effect is only about $1/\sqrt{1{\cdot}5}$ at about 20°. The larger the variation of $\frac{dt}{d\theta}$ of the individual wave, or the smaller the variation of $\frac{dt}{d\theta}$ of the transmitted wave, the more decrease of amplitude is to be expected.

Thus we see, as already discussed by Lehmann and Gutenberg, essential difference of the consequences of the two assumptions of the discontinuity of the first and second order. But we must take care, in the examination of initial motion, of the fact that the appearance of smaller transmitted wave is restricted to very small range, which may be subjected to more complication by the superposition of late P-phases.

Concluding Remark.

We have discussed the problem on the existence of discontinuity surface in the mantle of the earth from the examination of P-curve due to the Formosa earthquake of April 20, 1935.

33) K. Zöppritz, *Nachr. d. Kgl. Geo. d. Wiss. zu Göttingen*, Math.-phys. Kl. (1912), 123~143.
E. Wiechert, *ibid.* foot note on page 127.
L. Geiger and B. Gutenberg, *do*, 144~206.
H. Jeffreys, *M. N. R. A. S. Geophys. Suppl.*, **1** (1926), 334~348.
H. Kawasumi, *Bull. Earthq. Res. Inst.*, **10** (1933), 403~453.

The epicentre determined by the method of least squares came out at

$$\varphi_0 = 24^\circ\, 19'.6 \pm 2'.5 \text{ N},$$

$$\lambda_0 = 120^\circ\, 37'.6 \pm 2'.6 \text{ E}.$$

And velocity distribution within the earth as well as the depth of vertex of the seismic ray emerging at any epicentral distance up to about 20 or so are determined, upon the two assumptions of the existence of the velocity discontinuity of first and second order.

The quantitative basis of these results are examined specially, and could see that discontinuity of second order may be adopted if correction amounting only to two tenths of a second is applied to the time distance curves used. While the assumption of the first order discontinuity seems in some respects more favourable, the amount of discontinuity may be smaller than 1 km/sec, which is much smaller than expected. The depth of discontinuity surface, if any, is about 430 km from the earth's surface. There may exist some correlation with the fact that the deep focus earthquake occurs outside this surface.

The range of triplication of P-curve was discussed, but other possibility of this cause of triplications than the first order discontinuity is not considered in this paper. The difference of triplication due to the existence or nonexistence of the first order discontinuity is to be examined by the change of sense of motion in the reflexion in the former case. The examination of the reflected wave at shorter epicentral distance may also be used for this purpose, though it will be difficult owing to the smallness of amplitude.

In conclusion the writers wish to acknowledge their cordial thanks to Prof. T. Matuzawa for the generosity in placing the data of the Sanriku Earthquake at our disposal.

18. 昭和10年4月21日臺灣地震の走時曲線と地殼構造上の一問題

地震研究所 河角廣
本間正作

上記の地震 P-波走時曲線を吟味して地下約 400 粁にありと云はれて居る不連續面を吟味した. 此の爲に最少二乘法により發震時を用ひて震央及び走時曲線を定めた.

$$\text{卽}\quad \varphi_0 = 24^{\circ}\ 19'{\cdot}6 \pm 2'{\cdot}5\ \text{N}$$

$$\lambda_0 = 120\ 37{\cdot}6 \pm 2{\cdot}6\ \text{E}$$

$$t = 20^{d}\ 22^{h}\ 2^{m}\ 2^{s}{\cdot}5 + 14^{s}{\cdot}337\Delta - 0^{s}{\cdot}00217\Delta^3$$

$$\pm 0{\cdot}9\quad \pm 0{\cdot}13\quad \pm 0{\cdot}00033.$$

此の震央は大甲街の南大甲溪岸に當る.

地球內部に於ける第2種及び第1種の不連續面の存在を假定し, 各の場合に於ける速度分布及び震波線最深點の深さ等を計算した. 特に其等數値の誤差の程度に注意し. 各假定の適否は現在尙走時のみよりは決定不可能なりしも, 其等の數量的根據を明にした.

卽速度分布に有限な不連續のないと云ふ假定に合はせるには走時曲線に僅か 2/10 秒の補正を加へれば十分であるが, 若し有限の不連續がありと假定しても其の不連續の分量は 0·8 粁の程度に過ぎず. 從來考へられたものより著しく小いものであり, 其の不連續面の深さは地下約 430 粁の程度である.

尙第1種の不連續面でなくても速度分布の狀態によつては走時曲線が3重になる事があり得るが此の點は其の觀測がないので吟味出來なかつた. 此れは初動の方向を吟味すれば直ちに解る問題である. 卽第1種の不連續面がある場合には反射波は 180° の位相の變化を受けるからである.

第1種の不連續面か, 第2種の不連續面かの區別は走時曲線の形だけでなく初動の大きさの吟味によつて完全に決定される筈であるが, 其の際極めて細心の注意を要する事を知つた.

19. Changes in the Heights of Volcano Asama caused by Eruptions in 1935.

by Takeshi MINAKAMI,

Earthquake Research Institute.

(Read Jan. 18, 1936.—Received March 20, 1936.)

1. Introduction.

Geophysicists and geologists have pointed out certain characteristic topographies near volcanoes from various points of view, especially on the fact that the presence of a number of lakes or regions of depression on the skirts of a volcano is due to topographic deformations that follow volcanic activities whether in recent or in geological times.

The results moreover of precise levellings and triangulations that were carried out around some volcanoes both before and after activities, helped to make clear the depressions and elevations of the ground, particularly those in the large provinces. At the time of the explosions of Sakura-zima[1] in 1914, the meaning of a depression of 2 m in the vicinity of the volcano and of those of several centimetres even at a distance of 100 km from it, became clear not only from precise levellings but from triangulations as well as. In the explosions of volcano Usu[2] in 1910, on the other hand, an upheaval of the volcano was reported. In the case of the eruption of Komagadaké[3] in Hokkaidô in 1929, the depression of elliptic form resembled what happened in the case of the eruptions of Sakura-zima above described, but the former deformations were on a smaller scale compared with the latter ones.

From triangulations carried out by the Land Survey Department, the height of the central cone of volcano Asama was determined as being 2542 m above sea level. In 1935, in the midst of volcanic activities, precise levellings were executed by experts of Land Survey Department. The present line of levels runs along the southern foot, the east and west-south slopes of the volcano and the southern margin of the crater. From the results of these surveys, it was found that the

1) F. ÔMORI, *Bull. Imp. Earthq. Inv. Comm.*, **8** (1914~1922), 158.
2) F. ÔMORI, *Bull. Imp. Earthq. Inv. Comm.*, **5** (1911), 101.
3) C. TSUBOI, *Bull. Earthq. Res. Inst.*, **8** (1930), 298.
J. UEDA, "Reports on the Eruption of Komagadaké", (1932), (in Japanese).

volcano increased about 18 m in height during an interval of 23 years. Dr. R. Takahasi[4] has reported in detail the results of present precise levellings in the same bulletin.

2. Observations of Zenith Distance at Asama in 1934 and 1935.

Most of the studies concerned with topographic deformations accompanied with volcanic activities, were made from comparisons of these surveys that were made a number of years before and after the volcanic activities. Consequently, the topographic deformations determined from the results of these surveys usually include chronic changes, so that they cannot be regarded as having been produced suddenly on the occasion of an eruption. Besides, we have not as a rule the means of distinguishing the chronic changes from the obtained results. Thus, in order to ascertain the topographic deformation directly due to the volcanic activities, free from chronic changes, the writer at Asama has

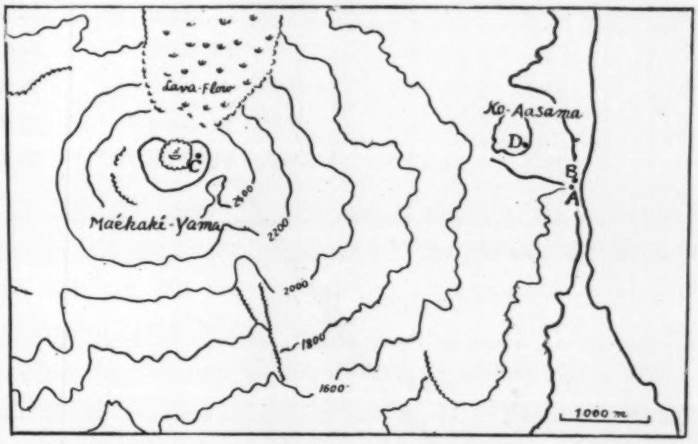

Fig. 1. Topographic map of volcano Asama and its vicinity.

successively carried out trigonometric levellings; that is, the observation of zenith distance, during the calm period of the volcano in 1934 and it's active period in 1935. For triangulation point (C) on the central cone, the writer utilized the upper edge of a large volcanic bomb, "Taisio-Iwa", which is 3·5 m in diameter and at a distance of about 20 m east from the margin of the crater (Fig. 1). For point (D), he adopted the top of the parasitic volcano, "Ko-Asama", which is about 1 km N-W from our observatory. The later triangulation point is a concrete pile 1·5 m in length. Thus, from a fixed stand (B) in our observatory, the observations of zenith distance were collimated with

4) R. Takahasi, *Bull. Earthq. Res. Inst.*, **14** (1936), 18~25.

Wild's theodolite for the two triangulation points above described. The observation which was begun July, 1934, is being continued (1936). Naturally, in cloudy weather, or when there is huge emission of vapour from the crater, it is impossible to carry out these measurements.

In the following Table I (a) (b), are given the complementary angles of zenith distance between triangulation point C and observation-stand B, during 1934 and 1935.

Table I. (a)

date	θ	$\Delta\theta$	date	θ	$\Delta\theta$
1934 h	15° 28′ ″	″	1934 h	15° 28′ ″	″
July 9, 12·8	37·2	+ 9·7	Aug. 19, 14·5	20·2	− 6·3
〃 19, 13·5	28·0	+ 1·5	〃 20, 11·0	21·2	− 5·3
Aug. 3, 6·0	33·8	+ 7·3	Sept. 11, 15·0	12·6	−12·9
〃 〃 16·0	23.8	− 2·7	〃 12, 11·5	23·1	− 3·4
〃 4, 10·0	22·8	− 3·7	〃 〃 13·5	38·7	+12·2
〃 〃 11·0	27·0	+ 0.5	Oct. 14, 10·0	15·6	− 9·9
〃 5, 16·7	12·2	−14·3	〃 20, 15·0	34·2	+ 7·7
〃 6, 11·0	23·2	− 3·3	〃 〃 13·0	28·8	+ 2·3
〃 〃 13 0	27·0	+ 0.5	〃 30, 14·4	20·2	− 6·3
〃 〃 14·0	39·8	+13·3	Nov. 13, 12·0	30·8	+ 4·3
〃 〃 15.0	36·2	+ 9·7			

Mean $\theta = 15° 28' 26{\cdot}5'' \pm 5.4''$

Table I. (b)

date	θ'	$\Delta\theta'$	date	θ'	$\Delta\theta'$
1935 h	15° 28′ ″	″	1935 h	15° 28′ ″	″
April. 21, 14·0	8·0	− 0·5	May 17, 14·0	7·9	− 0·6
〃 24, 11·5	4·8	− 3·7	〃 24, 13·0	15·0	+ 6·5
May 9, 10·0	3·0	− 5·5	〃 30, 12·0	7·0	− 1·5
〃 〃 14·0	14·0	+ 5·5	July 29, 14·0	7·9	− 0·6

Mean $\theta' = 15° 28' 8{\cdot}5'' \pm 2{\cdot}8''$

In Table I (a) (b), θ, θ' are average values of three direct and reverse measurements by Wild's theodolite, while $\Delta\theta$, $\Delta\theta'$ are residues for each observed value. Naturally, θ, θ' must involve errors due to the daily and seasonal refractions. Upon reviewing the residues, it will be found that those observed before 10 h and after 14 h are unusually large compared with the others. They will be regarded mostly as errors due to abnormal refraction and to errors of observation

due to difficulties of collimating with exactitude. Consequently, in the following discussion, observations carried out before 10 h and after 14 h will be excluded.

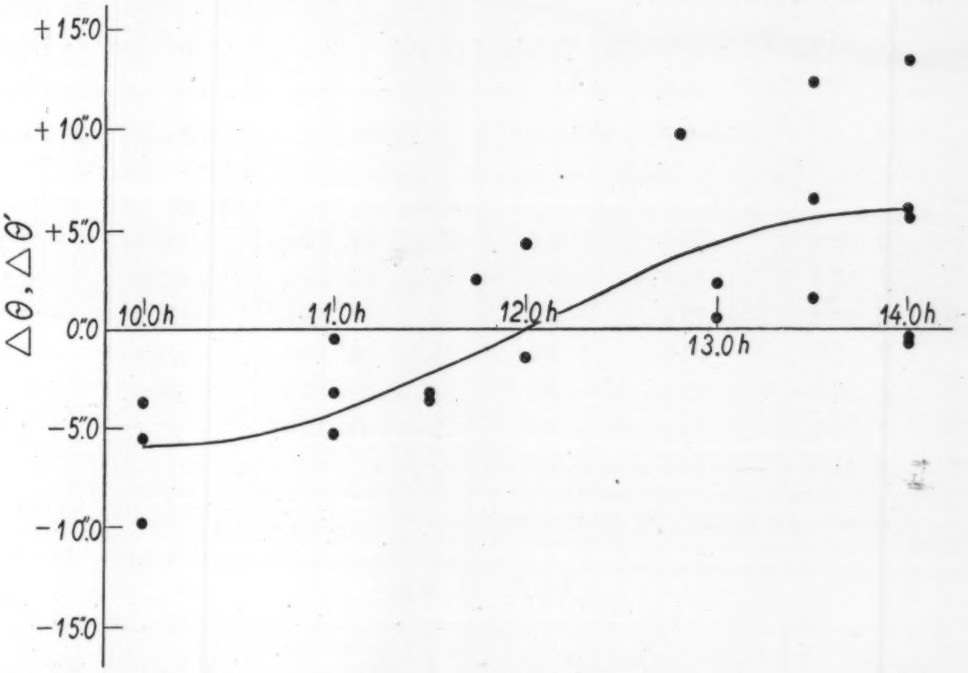

Fig. 2.

In Fig. 2, $\Delta\theta$, $\Delta\theta'$ are plotted as abscissa in taking the time in which the observations were executed. A glance at this Fig. 2, shows these residues $\Delta\theta$, $\Delta\theta'$ to be evidently systematic with respect to the time these observations were carried out. Though they somewhat fluctuate, roughly speaking, these residues observed from 10 h to 12 h are generally negative, while in contrast to them, those observed from 12 h to 14 h are generally positive. In addition, they vary somewhat linealy or in sine form with the time of observations. In consideration of the tendency illustrated in Fig. 2, we shall assume that these residues connected with observation-time are due to the daily refraction, which varies with sine form. On the other hand, it will be not far from the fact that other refractions, seasonal and annual, are considered approximately constant. For convenience, we shall consider the total refraction α to be composed of the daily one α_1 and the seasonal one α_2.

$$\alpha = \alpha_1 + \alpha_2 , \tag{1}$$

$$\alpha_1 = k \sin \frac{2\pi}{4} (h-12) , \tag{2}$$

$$\alpha_2 = \text{const.}. \tag{3}$$

Thus, by means of the method of least-squares, k in (2) is determined as $6{\cdot}0''$. As results, the observed values θ, θ' are corrected for daily refraction. In Table II, (a) (b) are given the corrected values for the daily refraction.

Table II. (a)

date	$\theta+\alpha_1$	$\Delta(\theta+\alpha_1)$	date	$\theta+\alpha_1$	$\Delta(\theta+\alpha_1)$
1934 h	15° 28′		1934 h	15° 28′	
July 9, 12·8	34·0″	+ 4·9″	Aug. 20, 11·0	26·9″	− 2·2″
〃 〃 13·5	24·0	− 5·1	Sept. 12, 11·5	27·0	− 2·1
Aug. 4, 10·0	29·8	+ 0·7	〃 〃 13·5	34·3	+ 5·2
〃 〃 11·0	32·3	+ 3·2	Oct. 14, 10·0	24·3	− 4·8
〃 6, 11·0	28·4	− 0·7	〃 20, 13·0	26·0	− 3·1
〃 〃 13·0	24·3	− 4·8	Nov. 13, 12·0	32·1	+ 3·0
〃 6, 14·0	34·6	+ 5·5			

Mean $\theta+\alpha_1=15°\ 28'\ 29{\cdot}1''\pm2{\cdot}7''$

Table II. (b)

date	$\theta'+\alpha'_1$	$\Delta(\theta'+\alpha'_1)$	date	$\theta'+\alpha'_1$	$\Delta(\theta'+\alpha'_1)$
1935 h	15° 28′		1935	15° 28′	
April 21, 14·0	2·0″	− 3·7″	May 17, 14·0	1·9″	− 3·8″
〃 24, 11·5	7·1	+ 1·4	〃 24, 13·0	11·0	+ 5·3
May 9, 10·0	7·0	+ 1·3	〃 30, 12·0	7·0	+ 1·3
〃 〃 14·0	8·0	+ 2·3	July 29, 14·0	1·9	− 3·8

Mean $\theta'+\alpha'_1=15°\ 28'\ 5{\cdot}7''\pm2{\cdot}2''$

At the same time, the observations for a triangulation point D on the parasitic cone "Ko-Asama" were carried out by the same method. In the following Table III (a) (b), the complementary angles of zenith distance φ, φ' in 1934 and 1935 are given with the date and time for observation executed. In the same Table, $\Delta\varphi$, $\Delta\varphi'$, $\Delta\varphi_s$, $\Delta\varphi'_s$ are residues from the average value of total observations and of selected observations carried out from 10 h to 14 h.

As will be seen from Table III, there do not appear any conspicuos changes of zenith distance for "Ko-Asama" caused by the present activities.

On the other hand, in the zenith distance for the triangulation point C, a remarkable change was produced at the interval between December, 1934, and April, 1935. While, as has already been reported in the previous paper, the violent explosion occurred on April 20, 1935.

Table III. (a)

date			φ	$\Delta\varphi$	$\Delta\varphi_s$
1934		h	16° 50′		
July	28,	10·5	37″·6	− 7″·7	− 8″·8
Aug.	1,	14·0	42·1	− 3·2	− 4·3
〃	2,	8·0	37·0	− 8·0	
〃	3,	16·3	31·4	−13·9	
〃	4,	10·0	48·4	+ 3·1	+ 2·0
〃	〃	11·0	44·6	− 0·7	− 1·8
〃	6,	11·0	45·0	− 0·3	− 1·4
〃	〃	13·0	40·8	− 4·5	− 5·6
〃	〃	15·0	57·0	+11·7	
〃	9,	10·0	46·8	+ 1·5	+ 0·4
〃	12,	8·0	57·2	+11·9	
〃	〃	11·0	54·6	+ 9·3	+ 8·2
〃	13,	14·0	49·2	+ 3·9	+ 2·8
〃	14,	16·0	41·2	− 4·1	
〃	19,	14·0	40·8	− 4·5	− 5·6
〃	20,	11·0	45·2	− 0·1	− 1·2
Sept.	12,	8·0	32·4	−12·9	
〃	〃	13·5	49·6	+ 4·3	+ 3·2
〃	〃	16·5	33·8	−11·5	
〃	27,	10·5	42·2	− 3·1	− 4·2
Oct.	14,	10·0	55·8	+10·5	+ 9·4
〃	20,	10·0	54·2	+ 8·9	+ 7·8
〃	13,	12·0	55·0	+ 9·7	+ 8·6

Mean $\varphi = 16° \ 50' \ 45{\cdot}3''$

Mean $\varphi_s = 16° \ 50' \ 46{\cdot}4'' \pm 3{\cdot}9''$

Table III. (b)

date			φ'	$\Delta\varphi'$	$\Delta\varphi'_s$
1935		h	16° 50′		
April	21,	15·6	36″·0	− 7″·3	
〃	24.	10·5	49·0	+ 5·7	+ 3″·2
May	4,	10·0	49·6	+ 6·3	+ 3·8
〃	9,	10·0	45·5	− 2·3	− 0·2
〃	17,	13·0	42·0	− 1·3	− 3·8
〃	24,	12·6	42·6	− 0·7	− 3·2
〃	30,	16·0	38·6	− 4·7	

Mean $\varphi' = 16° \ 50' \ 43{\cdot}3''$

Mean $\varphi'_s = 16° \ 50' \ 45{\cdot}8'' \pm 2{\cdot}4''$

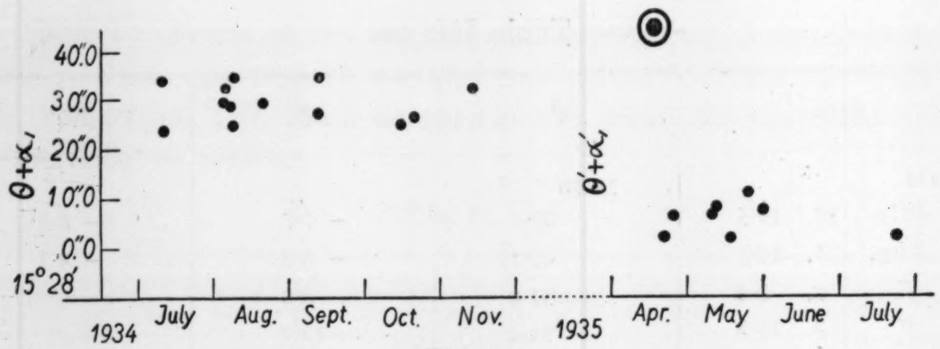

Fig. 3.

⊙; The explosion on April 20, 1935.

$\theta+\alpha_1=15°\ 28'\ 29{\cdot}1''\pm2{\cdot}7''$; mean value of complementary angle (B-C) of zenith distance before explosion.

$\theta'+\alpha_1'=15°\ 28'\ 5{\cdot}7''\pm2{\cdot}2''$; the one after explosion.

$\varphi_s=16°\ 50'\ 46{\cdot}4''\pm3{\cdot}9''$; mean value of complementary angle (B-D) of zenith distance before explosion.

$\varphi_s'=16°\ 50'\ 45{\cdot}8''\pm2{\cdot}4''$; the one after explosion.

$(\theta'+\alpha_1')-(\theta+\alpha_1)=-23{\cdot}4''\pm3{\cdot}5''$; change caused by explosion.

As the result, the changes of zenith distance for the triangulation point C were observed, which were accompanied directly with the present volcanic activities.

3. Distance between the Triangulation Point on central Cone and the fixed Point at our Observatory

If the distance between these two points — the one C on the central cone and the other B at our observatory — is known, it will give the variation in the zenith distance as the unit of length.

For the present purpose, we can utilize the results of precise levellings carried out in 1935. That is, the height of two bench-marks from the geoid, one on the central cone which coincides with triangulation point C above described, the other A at our observatory which differs from the fixed point B. First, in order to know the distance between B and C, we will determin the distance between two bench-marks A and C.

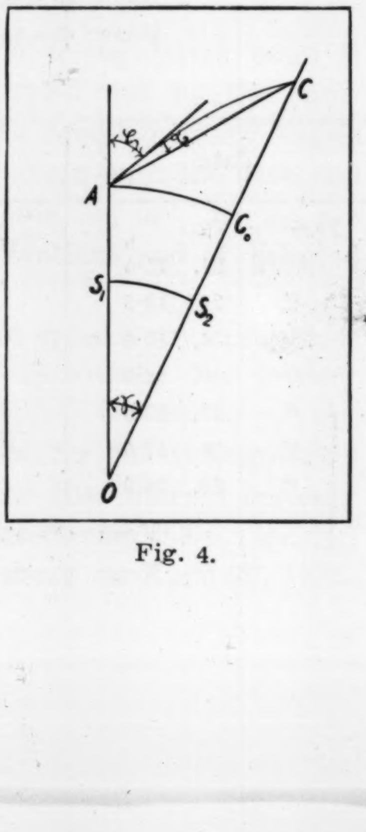

Fig. 4.

From a triangle ACC_0 in Fig. 4, we can obtain the following formula:

$$AC_0 = (h_2 - h_1 - H)\frac{\sin\left[\zeta - \left(\frac{1}{2}m\right)\gamma\right]}{\cos\left[\zeta - (1-m)\gamma\right]},$$

AS_1O, CS_2O; normals on the geoide S_1S_2,

$\angle AOC = \gamma$

$AS_1 = h_1 = 1405{\cdot}820$ m,

$CS_2 = h_2 = 2557{\cdot}993$ m,

$H = 1{\cdot}633$ m; height from the bench-mark A to the telescope of theodolite,

$$m = \frac{a_2}{\gamma} = 0{\cdot}06564;\ m \text{ refraction coefficient},$$

$$\delta = \frac{\pi}{2} - \zeta.$$

Table IV.

$\zeta = \frac{1}{2}(\pi \pm \delta)$		δ
97° 41′ 37·2″	weighted mean	
〃 〃 34·5″	97° 41′ 36·7″	15° 28′ 25·7″
〃 〃 36·8″		
82° 13′ 14·5″		
〃 〃 11·0″	82° 13′ 11·0″	
〃 〃 9·4″		

As the result, we obtain the horizontal distance between A and C,

$$AC_0 = \overline{AC} = 4146{\cdot}600 \text{ m}.$$

Thus, we can obtain the horizontal distance between B and C by making use of the above result. In Fig. 5, angle B is very small, so that the horizontal distance B-C is given by a simple correction to the horizontal distance A-C.

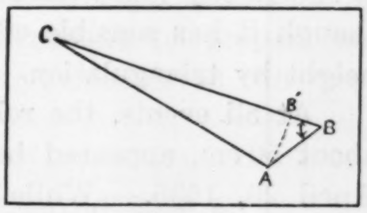

Fig. 5.

$$BC = BB' + B'C = AC + AB \tan B$$
$$= 4151{\cdot}397 \text{ m},$$

where $AB = 29{\cdot}475$ m,

$\angle B = 80°\ 38'\ 18''$.

Thus finally, the horizontal distance between two points B and C is determined.

Here, we will return to the problem of topographical deformation in the present volcanic activities. According to Fig. 6 the difference of height between the triangulation point C and the fixed point B is indicated in the following:

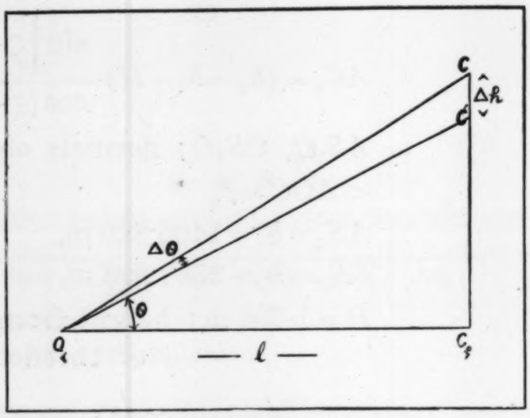

Fig. 6.

$C\,C_0 = h = l \tan(\theta + \alpha_1 + \alpha_2) + H$; height before explosion.

$C'C_0 = h' = l' \tan(\theta' + \alpha_1' + \alpha_2') + H'$; height after explosion.

We can put

$l = l' = 4151{\cdot}397$ m ; horizontal distance B–C,

$\alpha_1 = \alpha_1'$; angle caused by daily refraction,

$\alpha_2 = \alpha_2'$; angle caused by seasonal and other refractions,

$H = H'$; height of telescope of theodolite.

If we denote

$$\theta' - \theta = \Delta\theta = -23{\cdot}4'' \pm 3{\cdot}5'',$$
$$h' - h = \Delta h$$

as the topographical change, we get

$$\Delta h = l.\Delta\theta.\frac{1}{\cos^2(\theta + \alpha_1 + \alpha_2)} = -50{\cdot}7 \text{ cm} \pm 7{\cdot}5 \text{ cm}.$$

The amount of topographical change determined by this method is sufficiently independent of the error due to the refraction of light, though it has sensible effects in the case of determination of absolute height by triangulation.

At all events, the relative subsidence of the central cone which is about 50 cm, appeared before or soon after the violent explosion of April 20, 1935. While the relative change to the parasitic volcano "Ko-Asama" was not observed through the present volcanic activity.

4. Discussion of the Result.

Regarding the occurrence of topographical deformation in the present activities, it may be possible to explain it from various points of view.

For instance, decrease of vapour pressure owing to the explosion

may produce depression in the central cone and in the vicinity of crater.

Besides, large ejection of lava as volcanic bombs and volcanic ash from the crater at the occasion of an explosion, may cause depression of ground near the crater.

On the other hand, from the observations of volcano Kilauea and Mauna Loa, in Hawaii, T. A. Jagger[5] reported that the elevations and depressions in the vicinity of these volcanoes clarified by the precise levellings coincided with the direction of tilting observed by the horizontal pendulums. However, from the observations of tilting of ground by a pair of Ishimoto's clinograph in our observatory, as discussed in the previous paper,[6] tilting in the direction of crater lasted from April 13 to May 1, 1935 and amounted to about 10″. It means, therefore, that the direction of tilting coincided with the region of depression. Moreover, if tilting of ground between the central cone and our observatory be the same amount as the one observed at our observatory, about half the amount of depression of central cone will be explained by this tilting motion.

On the other hand, as an explanation of the depression of ground accompanied by the violent explosion of Sakura-zima, 1914, Dr. N. Miyabe[7] remarked that the huge accumulations of lava ejected in the circumference of volcano would produce an elastic deformation of the crust. Naturally, in the present case of Asama, the elastic deformation caused by load of ejecta may be possible, but increase of ejecta accumulated on the central cone in many eruptions did not coincide with that of depression. In consequence, it will be more plausible that, instead of load deformation, the elevation which had been produced before the explosion, recovered by the decrease of vapour pressure after the violent explosion on April 20, 1935.

Thus, there seems to be various alternative explanations to account for this phenomenon. It will be premature to propcse any definite conclusion on this point, unless other evidences on this question come to light.

5. Relative Changes in Height of central Cone in Comparison with Maékaké-yama.

In his previous paper[8], the writer reported the amount of ejecta

5) T. A. JAGGER and R. H. FINCH, *Bull. Seis. Soc. Amer.*, **19** (1929), 38.
6) T. MINAKAMI, *Bull. Earthq. Res. Inst.*, **13** (1935), 629.
7) N. MIYABE, *Bull. Earthq. Res. Inst.*, **12** (1934), 471.
8) T. MINAKAMI, *Bull. Earthq. Res. Inst.*, **13** (1935), 790.

accumulated on the central cone on May 31, 1935. As the result of frequent explosions since that day, the ejecta accumulated near the crater gradually increased its amount. According to the investigation of the depth of ejecta on October 23 of the same year, it amounted to about 3 m in maximum depth. In Fig. 7, the depth of ejecta measured along the east direction on an central cone from the crater edge is illustrated with the date of abservation.

In Fig. 7, C represents the large bomb of 3·5 m in diameter, which was used as the triangulation point in the observation of zenith distance. As the result, the large bomb C shows only its edge of about 0·4 m in the later part of November, 1935, through accumulation of ejecta.

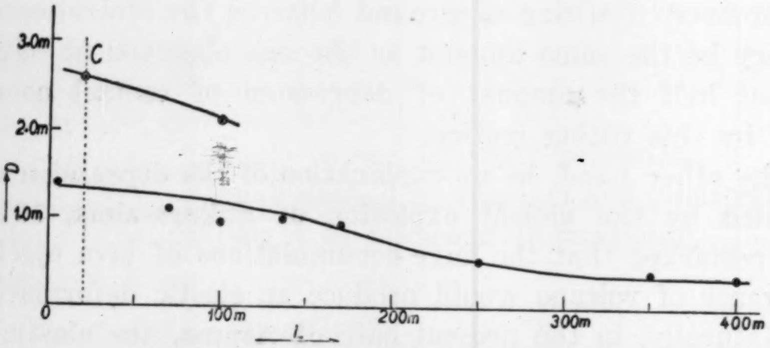

Fig. 7. Depth of ejecta accumulated on the central cone.
•; measurement on 31 May, 1935.
◉; measurement on 23 October, 1935.

On the other hand, the writer sometimes carried out observations of the relative height of two points, one the highest point on the central cone, the other on Maékaké-yama (ancient central cone). The survey was applied to the triangulation in taking the base line of 40 m on the central cone. Because of destruction of triangulation points on the central cone, it is impossible strictly to make clear the topographic changes which would be produced before and after the present volcanic activities. But, by determing the new triangulation point which approximately agrees with the old one, the writer carried out the survey after the explosion. The values obtained are given in Table V, with the date on which they were observed.

As will be seen in Table V, the height of the central cone relating to Maékaké-yama increased by 1·0 m on May 31 and 2·5 m on October 23, 1935 in comparison with the one of October, 1934. These changes of height correspond to the accumulation of ejecta. At any rate, the central cone increased its height by 2 m in comparison with

the one before the present volcanic activity, though the central cone itself depressed by 50 cm as described in the foregoing page.

Table V.

date	θ	$h=l \tan \theta$	Δh
Sept. 7, 1935	2° 31′ 28·0″	31·20 m	
″ 28, ″	2° 31′ 38·0″	31·26 ″	+0·06 m
Oct. 13, ″	2° 31′ 9·6″	31·22 ″	−0·04 ″
″ 26, ″	2° 31′ 46·2″	31·30 ″	+0·08 ″
May 31, 19 6	2° 39′ 46·0″	32·05 ″	+1·05 ″
Oct. 23, ″	2° 44′ 41·0″	33·50 ″	+1·45 ″

$l=722{\cdot}19$ m,
l; horizontal distance between two points.

In consideration of these facts, it may be plausible that the elevation of about 18 m which was made clear by the precise levellings carried out in 1935, is explained by the accumulation of ejecta, and that the volcano itself sometimes elevates and sometimes depresses within smaller ranges with the volcanic activities.

6. Résumé.

The writer carried out the triangulation in order to make clear the topographic deformation of volcano Asama. The observations have been continued since July, 1934, while, the volcano frequently repeated its explosive eruptions since April 20, 1935. From the result of triangulation, a depression of 50 cm of the central cone was observed through the present activities. Explanation of the present depression is possible from various stand-points, for instance, tilting of ground, deformation caused by decrease of vapour pressure.

On the other hand, the accumulation of ejecta amounted to 3 m in depth on the central cone, which was measured on October 23, 1935. After all, volcano Asama increased its height by about 2·5 m after the explosions of 1935, in spite of the depression of the central cone itself.

In conclusion, the writer wishes to express his thanks to Professor Mishio Ishimoto and Doctor Ryûtarô Takahasi for their interest, and encouragements given to the writer in the course of this research.

19. 最近の活動に伴へる淺間火山の高さの變化

地震研究所 水 上 武

I. 大正3年の櫻島大噴火並に昭和4年の北海道駒ヶ嶽の活動に伴ひ，同火山近傍に著しい土地の沈降が現れた．又明治 43 年の有珠火山の活動には土地の隆起が伴つた事が報告されて居る．然し，是等の地形變動は，火山活動の數年前或は數十年前の水準測量又は三角測量と火山活動後に施行された測量との比較から求められた變化である．從つて直接火山活動に伴つたものと慢性的のものとを含むものである．

II. 筆者は淺間火山に關して，火山活動に直接隨伴する地形變動を明かにするため，昭和9年7月より天頂角の測定を繼續して行つた．

その結果昭和9年7月より 11 月迄の中央火口丘の高さに比し，昭和 10 年4月 20 日の爆發後に於いては約 50 糎の相對的沈降が觀測された．この沈降に對しては種々の解釋が出來るが觀測點が少いので，今回の活動に伴つた同火山の地形變動の全般に亘つて論する事は，やゝ危險の樣に思はれる．從つて，こゝでは相對的沈下の事實の指摘に止める事にした．

III. 昭和 10 年4月以來の數十回の噴火の爲に中央火口丘上に堆積する噴出物は極めて多量に達し，同年 10 月 23 日の測定に依ると，厚さ3米に達する處がある．從つて 50 糎の相對的沈降は山體自身の沈下に依るとしても，淺間山の高さは，噴火前に比して2米以上も增した事になる．

今回の噴出物の堆積狀態を考慮すると，大正6年と昭和10年の測量の比較から判明した 18 米の淺間山の高さの增加は，噴火に伴つて噴出した火山彈，火山灰の堆積が主要な原因の樣に思はれる．

20. *Relation between Earthquakes and Precipitation, Barometric Pressure, and Temperature. A Supplementary Note.*

By Seiti YAMAGUTI,

Earthquake Research Institute.

(Read Feb. 18, 1936.—Received March 20, 1936.)

Introduction.

This investigation was made with the intention of ascertaining whether or not the results obtained in a previous paper[1] might have any real physical significance beyond the fact that they may by mere chance serve as the meteorological elements on these two sides of the country, namely on the Japan Sea side and on the Pacific side.

For this purpose, meteorological elements in other regions on the Pacific side were taken for argument. First, we took the precipitations, barometric pressure, and temperature, summed over each season and three meteorological stations, Mito, Isinomaki, and Miyako, the three being denoted by Q′, B′, and T′, respectively. Second, we took the same meteorological elements at three stations, Numadu, Hamamatu, and Nagoya, denoted by Q″, B″, and T″, respectively.

The data of earthquakes, that occurred in the Kwantô Districts,

Fig. 1. Number of "felt" earthquakes in Tokyo and Bôsô Hantô, and the differential precipitation in winter.
J: Japan Sea side.
P: Pacific side.

Fig. 2. Number of "felt" earthquakes in Tokyo and Bôsô Hantô, and the differential barometric height in winter.

1) S. YAMAGUTI, *Bull. Earthq. Res. Inst.*, 13 (1935), 569~575.

and which are to be compared with the meteorological elements, are the same as those given in a previous paper. The correlation coefficients between the frequencies of earthquakes and the new meteorological elements were calculated in the same way as before. Three representative diagrams which show the correlations, already cited in a previous paper, are given in Figs. 1, 2, and 3.

The results, which are shown in Table I, II, and III, may, to a certain extent, be considered as verifying the results given in a previous paper.

On the other hand, the probable error corresponding to the correlation coefficient with a value of about 0·5, was calculated and estimated to be 0·10.

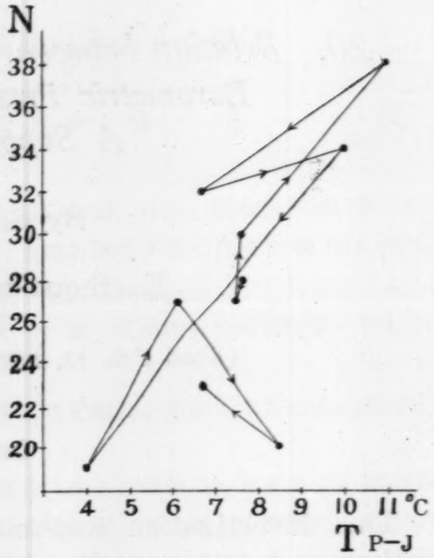

Fig. 3. Number of "felt" earthquakes in Kinugawa, Tonegawa, and Kasumigaura, and the temperature difference in winter.

Table I. Correlation Coefficients between the Precipitations (in 100 mm), and the Earthquakes in Kwantô Districts.

Earthquake regions / Season		"Felt" earthquakes.					"Conspicuous and rather conspicuous".	
		Iwaki Oki Kasima Nada	Tyôsi Oki Sagami Nada	Kinugawa Tonegawa Kasumigaura	Tokyo Bôsô Hantô	Sagami (land) Idu Hantô	Land	Marine
Spring	Q′	**−0·41**	0·33	0·12	0·07	−0·37	**−0·42**	0·09
	Q″	**0·59**	0·34	**0·50**	−0·04	0·05	−0·20	0·29
	Q′-Q″	**−0·75**	0·08	−0·21	0·09	−0·37	−0·25	−0·10
Summer	Q′	**−0·63**	−0·04	0·23	−0·21	0·17	**−0·42**	−0·09
	Q″	−0·32	−0·17	**−0·40**	−0·23	−0·17	**−0·42**	**−0·48**
	Q′-Q″	−0·03	0·18	**0·63**	0·13	−0·10	0·23	**0·52**
Autumn	Q′	**−0·43**	**−0·43**	0·27	0·36	0·14	0·14	−0·12
	Q″	−0·17	−0·26	0·12	0·32	−0·05	0·06	−0·26
	Q′-Q″	−0·21	0·01	0·09	−0·23	0·32	0·06	**0·43**
Winter	Q′	−0·32	−0·30	0·13	0·37	−0·35	0·04	−0·28
	Q″	**−0·40**	−0·05	0·12	0·18	−0·06	−0·07	−0·06
	Q′-Q″	0·16	−0·20	−0·02	0·11	**−0·23**	0·10	−0·17

Table II. Correlation Coefficients between the Barometric pressure (in mm. Hg), and the Earthquakes in Kwantô Districts.

Season \ Earthquake regions		"Felt" earthquakes.					"Conspicuous and rather conspicuous."	
		Iwaki Oki Kasima Nada	Tyôsi Oki Sagami Nada	Kinugawa Tonegawa Kasumigaura	Tokyo Bôsô Hantô	Sagami (land) Idu Hantô	Land	Marine
Spring	B′	**0·47**	**0·46**	0·06	0·05	−0·09	−0·13	**0·48**
	B″	0·33	**0·46**	−0·16	0·07	−0·11	−0·18	**0·57**
	B′-B″	**0·54**	**0·41**	0·27	0·02	−0·05	−0·06	**0·45**
Summer	B′	−0·04	−0·06	−0·27	**0·44**	0·12	0·25	0·23
	B″	0·19	0·01	−0·03	**0·47**	0·02	0·38	**0·43**
	B′-B″	−0·29	−0·08	−0·25	−0·02	0·11	−0·12	−0·20
Autumn	B′	0·13	0·27	−0·32	0·16	0·14	−0·11	−0·31
	B″	0·09	**0·45**	−0·27	0·22	0·17	−0·07	0·01
	B′-B″	0·17	−0·12	−0·29	0·01	0·04	−0·14	**−0·52**
Winter	B′	−0·05	0·39	−0·01	**0·67**	0·35	−0·16	**−0·54**
	B″	0·04	0·27	0·08	**0·64**	0·22	−0·16	**−0·48**
	B′-B″	−0·16	**0·46**	−0·10	**0·57**	**0·43**	−0·13	**−0·49**

Table III. Correlation Coeffiicents between the Temperature (in °C), and the Earthquakes in Kwantô Districts.

Season \ Earthquake regions		"Felt" earthquakes.					"Conspicuous and rather conspicuous".	
		Iwaki Oki Kasima Nada	Tyôsi Oki Sagami Nada	Kinugawa Tonegawa Kasumigaura	Tokyo Bôsô Hantô	Sagami (land) Idu Hantô	Land	Marine
Spring	T′	0·28	**0·64**	0·22	0·09	−0·03	−0·39	0·38
	T″	**0·62**	**0·64**	0·23	−0·16	−0·08	**−0·45**	**0·6[illegible]**
	T″-T′	**0·52**	0·05	0·03	−0·37	−0·07	−0·11	0·35
Summer	T′	0·18	0·34	0·24	−0·07	**−0·43**	−0·10	0·29
	T″	**0·43**	**0·47**	0·20	−0·09	**−0·55**	−0·02	0·13
	T″-T′	0·30	0·04	−0·18	−0·01	0·02	0·18	−0·36
Autumn	T′	0·06	0·21	−0·37	−0·03	−0·33	−0·33	−0·29
	T″	0·30	0·39	**−0·68**	0·03	**−0·51**	−0·36	−0·05
	T″-T′	0·32	0·22	−0·39	−0·04	−0·22	0·01	0·[illegible]8
Winter	T′	0·15	0·22	0·18	**0·44**	−0·32	−0·14	**−0·60**
	T″	0·12	**0·47**	0·19	**0·63**	−0·15	−0·18	**−0·72**
	T″-T′	−0·08	0·39	−0·01	0·25	**0·58**	−0·36	−0·11

Results and Discussions.

The results of the present study are summarized as follows:

1. For the precipitations.
   (*a*). The precipitations on the preceding regions, as cited in a previous paper, were most effective upon occurrence of the earthqakes *in winter*, while those on the present regions, are most effective for the same purpose *in spring and summer*.
   (*b*). The former precipitations were most effective on "felt" earthquakes in Tyôsi Oki and Sagami Nada, and the latter most effective on "felt" earthquakes in Iwaki Oki and Kasima Nada.
2. For the barometric pressure.
   (*a*). The barometric pressure on the former regions as well as on the present regions are in closer relations *in winter and spring*, with the occurrence of the earthquakes.
   (*b*). The barometric pressures in all regions in common are closely related to the occurrence of the "conspicuous and rather conspicuous" earthquakes in *marine* and not in *land* areas. They are also related, in common, to the occurrences of "felt" earthquakes in Tyôsi Oki and Sagami Nada as well as in Tokyo and Bôsô Hantô.
3. For the temperature.
   (*a*). The temperatures in the previous regions were effective in *autumn and winter* upon the occurrence of earthquakes, while those in the present regions are effective in *winter and spring*.
   (*b*). The temperatures in the present regions are effective upon the "felt" earthquakes in Tyôsi Oki and Sagami Nada, as well as in Sagami (land) and Idu Hantô, in which respects it is quite similar to that in the previous study.
4. The values of the correlation coefficients vary with the earthquake regions. It is interesting to find the existence of certain definite earthquake regions that have comparatively great correlation coefficients in their meteorological elements.
5. Precipitation, barometric pressure, and temperature govern the occurrence of earthquakes in different ways according to season and with regard to the particular earthquake region. They are by no means so simple as may be expected to exist some parallelism among the above three meteorological elements.
6. The result of the investigation on "Earthquakes and Rainfall"

made by Mr. J. F. Brennan[2] in Jamaica, has shown the correlation between them to be negative, with the results of my investigations, in the case of the correlation between the "felt" earthquakes in Kwantô Districts and the winter precipitation on the Japan Sea side, showing fair agreement with his, although the methods of the two investigators differ.

---

20. 地震と雨雪量，氣壓，及氣溫との關係（補遺）

地震研究所 山口生知

此の研究は前の研究の結果が，實際の物理的意味を有するか，或は偶然起り得るものかどうかを確かめる目的でなされた．

此の爲に先づ水戸，石巻，及宮古に於ける雨雪量，氣壓，及氣溫を採り，次いで沼津，濱松，及名古屋に於ける同樣の氣象要素を採り，之等と關東地方に起つた地震との間の相關係數を，前論文と全く同樣の方法で計算して見た．

其の結果は第 I 表，第 II 表，及第 III 表に示される通りであつて，前論文の結果を或る程度まで證明するものと考へられる．

卽ち之を綜合すれば，次の通りである．

1. 前論文に揭げられて居る地方の雨雪量は關東地方の地震と冬季に於いて，最も關係が深かつたが今回の地方に於けるものは春及夏に於いて最も關係が深い樣に見受けられる．又前回の雨雪量は銚子沖及相模灣の有感地震に最も影響があつたが，今回の雨雪量は磐城沖及鹿島灘の有感地震に影響が多い．
2. 氣壓は前回も今回も同樣に冬及春に於いて關東地方の地震と最も密接な關係がある．又凡ての地方に於ける氣壓は，關東地方の海底に起る顯著及稍々顯著地震と最も密接な關係があるが之に反して陸上に起る同上の地震とは餘り密接な關係が無い．
3. 前回の地方の氣溫は秋及冬關東地方の地震發生に影響を及ぼして居るが，今回の地方に於けるものは冬及春に於いて影響が多い．前回も今回も全く同樣に銚子沖及相模灘竝に相模及伊豆半島の地震に影響が多い．
4. 相關係數の値は，地震の起る地方別に依つて變化して居る，而して大なる相關係數を有する或る特定の地震地方が存在すると云ふことは面白いことゝ思ふ．
5. 雨雪量，氣壓，及氣溫の三つの間には密接な關係があつて，其の中の一つと地震との間の關係を研究すればそれで足ると考へられる向もあるが，實際問題としては決して左樣に簡單では無い．
6. 大森先生や寺田先生方の古い時代の研究の結果に於いても，雨雪量と地震との間には可成密接な關係があると云ふことになつて居り，又 J. F. Brennan 氏が中米の Jamaica に於いて研究された結果に於いても，負の相關々係があると云ふことを報告して居る（私の研究に於いて，日本海方面の冬季の雨雪量と關東地方の有感地震との間の關係に相當する．）ことは雨雪量と地震との間の相關々係存在の意味を強めるものと思はれる．

---

2) J. F. Brennan, *Earthq. Notes, East. Sect. Seis. Soc. America*, **7** (1935), 25～26.

21. 出羽村及び濱松町における地震動卓越周期の觀測

地震研究所　石本巳四雄

(昭和11年4月21日發表――昭和11年3月20日受理)

地震動中に卓越する加速度の大なる波動の周期は各地に於て一定ならず其の地盤の良否と密接な關係を有する事は既に數回報告[1]したものであるが，今回は特に地盤の悪いと考へられる埼玉縣出羽村と東京市芝區濱崎町とにおける觀測結果とを述べ，表面層の厚さと卓越振動周期との關係に就て言及し度いと思ふ．

出羽村に於ける觀測

埼玉縣南埼玉郡出羽村は關東地方に相當の地震が發生する場合常に家屋の被害を見る地方であつて，明治20年以來3回も倒壞家屋を出した．即ち明治27年6月20日の地震，大正12年9月1日の關東地震，昭和6年9月21日の埼玉地震によつて災害が齎らされたのである．なほ以上の3地震の震央は何れも此の地方を離れて相當の距離にあつたにも拘らず災害は此の附近に著しかつた事實を思へば，此の地方の地盤の震動の中には何か特種のものゝあり得べき事を想起せしめるのである．斯様の理由を以て，水平動二成分の加速度地震計を出羽村字越巻，菊池福太郎氏方に設置して觀測を繼續した次第である．

此の地震計の要素は次の如くである．

振子の重錘	15 kg.
振子の周期	0·1 秒．
幾何倍率	208 倍．
感度	(兩成分とも) 1 mm が 1·7 gal に當る．
制振器	空氣振制器にて振子は臨界減衰狀況．
起動機	毎分300回轉同期電動機．
圓筒回轉速度	10分に1回轉，1 mm は約1秒に當る．

觀測は昭和9年11月29日より開始されたが當地方には晝間送電なく，止むを得ず夜間のみ觀測を行つた．從つて相當な地震の發生があつても，晝間のものは全部記

1) 石本巳四雄　地震研究所彙報 10 (1932), 171; 12 (1934), 234; 13 (1935), 592.

錄し得なかつた事は遺憾に屬する．昭和 11 年3月迄約1ヶ年と 4ヶ月の間に記錄し得た主なる地震は次の通りである．

	昭和10年	震央	卓越周期(秒)
A	1月 3日 23時 55分頃	江戸川河口	0·29 0·72 1·04
B	2月 20日 5時 11分頃	九十九里濱	0·40 0·8 1·05 1·7
C	4月 19日 1時 31分頃	水海道附近	0·30 0·81 1·01
D	6月 21日 4時 30分頃	下妻附近	0·23 0·99 1·27
E	9月 17日 5時 52分頃	取手附近	0·25 0·42 0·67 0·9
F	9月 22日 23時 40分頃	熊谷附近	0·21 0·67

以上の地震の卓越周期は從來の方法によつて見出されたが，其れは第1圖に示してある．第1圖の示す如く此の地方の卓越周期は震央の遠近によつて異るが，震央の遠い場合には 1·0 秒程度のもの多く，1·7 秒も現はれる事がある．震央の近い場合には 0·2～0·3 秒であつて，從來の觀測から判斷すれば此の地方は地盤不良の例に屬する．なほEの地震は震央が近いが出羽村以外の觀測點に於ても近い地震の特性を示さぬのは恐らく地震發生の機巧に異るものがあるかも知れない．又F地震の震央は熊谷附近で震源は 100 粁程度の深さであるが，相當小周期の波動が現はれて居る．なほ比較的小周期の卓越周期と比較的大周期の卓越周期との間に簡單な比は見えない．從つて若し進んで議論を行ふ場合には東京丸ノ内で齊田學士の行つた如き觀測[2]をなす必要があらう．震央距離の近

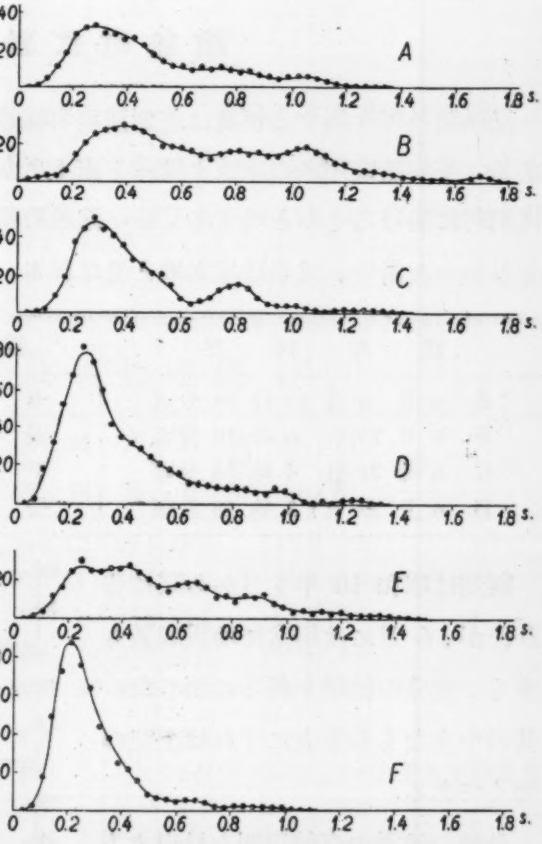

第1圖　埼玉縣出羽村に於て觀測せられた地震動卓越周期(縱軸は波數，橫軸は振動周期)

A	昭和10年	1月 3日地震
B	〃	2月 20日 〃
C	〃	4月 19日 〃
D	〃	6月 21日 〃
E	〃	9月 17日 〃
F	〃	9月 22日 〃

2)　齊田時太郎·鈴木正治　地震研究所彙報 12 (1934)，517.

い地震波の中には恐らく 0·3 秒程度の周期のものが多分に含有されて居る故に，表面層も此れによつて激勵されると思はれる．遠い所から來る地震波の中には小周期の波は消失して 1 秒程度の波動が大部分を占める爲め，此の程度の卓越周期が現はれると考へられる．大地震の場合にも單に距離の問題よりも，表面層中に起される比較的大周期の波動の加速度如何と云ふ事が問題となるであらう．

此の地方が特に地震に對して不適當であると云ふ事はないが，1 秒以上の卓越周期の現はれる所は東京附近でも餘り多くなく，濱松町或ひは横濱公園の例があるのみである．斯樣に大なる周期を生ずる原因としては，表面層の厚さが大であるのと，其れを形成する土質の剛性率が大ならざる事に歸納し得るであらう．

濱松町に於ける觀測

通稱濱松町と稱するが實は芝區濱崎町鐵道大臣官房研究所内に於て行はれた觀測である．平家造家屋内のコンクリート床上に加速度地震計が設置されたが，其の要素は出羽村に於けるものと殆ど等しい．濱松町附近は大正 12 年關東地震の際相當被害の著しかつた所で，元來は埋立地と思はれる．

	昭和 10 年	震央	卓越周期(秒)
A	6 月 8 日 13 時 58 分頃	土浦附近	0·35　0·78　1·03　1·7
B	6 月 15 日 6 時 10 分頃	安房沖	0·35　0·88　1·08　1·27
C	6 月 21 日 4 時 30 分頃	下妻附近	0·35　0·9　1·08
D	6 月 29 日 3 時 58 分頃	安房沖	0·95

觀測は昭和 10 年 5 月から開始されたが，6 月には相當に地震回數も多く，充分の結果を得るに至つた．其の中主なものを表にすれば上記の如くである．

此等の地震の卓越周期を見出す方法は從來と同じき方法によつたが，此の場合原記錄の寫眞引延しを 5·2 倍となし，0·1 mm 迄讀取つた．而して此等を從來の如き間隔に配分した關係上，波動周期の分布狀況には影響は無い．

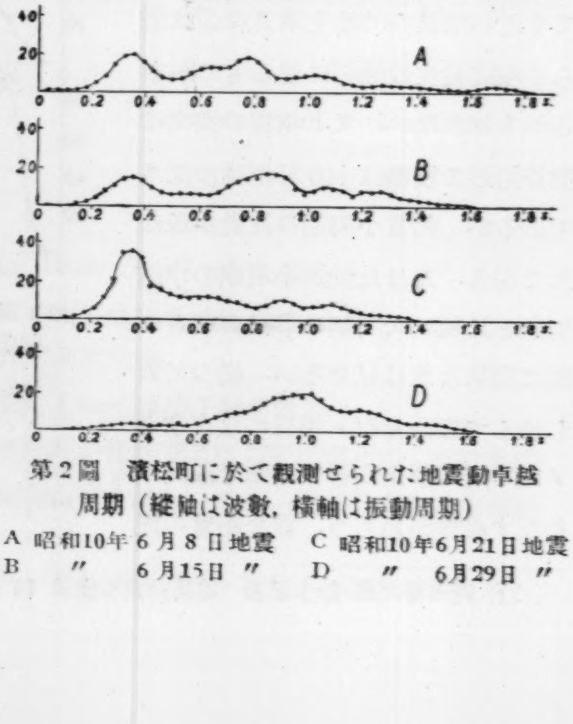

第 2 圖　濱松町に於て觀測せられた地震動卓越周期（縱軸は波數，橫軸は振動周期）
A 昭和10年 6 月 8 日地震　C 昭和10年6月21日地震
B 〃 6月15日 〃　D 〃 6月29日 〃

第2圖に見る如く震央の近い地震に對しては卓越周期も小で 0·35 秒が卓越し，震央の遠い地震に對しては 1·08 秒が卓越して居る．此れは大體3倍になつて居ると云ふ理由で基本振動周期と共の第三次振動と考へる事が出來やう．然し乍らDの地震に見る如く比較的遠い地震の場合でも 0·95 秒程度のみが激勵される事もある．

東京山手に於ける地震動の卓越周期に關しては震央距離の遠近に從つて多少の變化はあつても常に 0·3 秒程度に止まり，下町に見る樣な三倍程度の振動が誘導される事はない．此の現象の說明に就ては恐らく下町における表面層が基盤とは充分に異つた彈性を有すると云ふ事で充分であらうと思ふ．此の問題は將來の議論として殘して置き度い．

各地卓越周期の比較

次に同一地震に就て各地の卓越周期を比較して見やう．斯樣の研究は既に數回に亙つて報告を行つたものであるが，出羽村，濱松町の觀測も加はつた次第であるから，今一度繰返して見たのである．昭和 10 年は經費の關係上以前にあつた觀測所の中廢止を行つた所もあつて其の數は多くない．各所で多く記錄し得た地震の最大加速度，震央等は次の通りである．

第I表　各地最大加速度　gal

地震番號	月	日	時	分	震度		出羽村	本郷	駒場	丸ノ内	神田	向島	赤羽	濱松町	野毛山	高島町	震央
						S	24·0	14·0		34·0	12·7	60·8	15·7		65·4	9·3	
3	1	3	23^{h}	55^{m}	III	N	30·9	14·7		32·9	11·6	49·6	20·5		52·2	11·9	江戸川河口
						W	16·5	18·4	25·7	27·5	7·3	23·4	32·4		55·1	14·5	
						E	20·9	15·4	31·8	26·4	7·1	23·5	31·0		61·4	8·6	
						平均	**23·1**	**15·6**	**28·8**	**30·2**	**9·7**	**39·3**	**24·9**		**58·5**	**11·1**	
						S		3·9		9·2			6·1			3·8	
15	2	20	5^{h}	11^{m}	II	N		4·6		8·1			5·2			3·6	九十九里濱北部
						W	7·7	4·6		8·1			5·4			5·4	
						E	9·8	5·8		7·6			5·0			4·5	
						平均	**8·8**	**4·7**		**8·3**			**5·4**			**4·3**	
						S		10·3		14·9			12·6	6·4		5·2	
42	6	21	4^{h}	30^{m}	II	N		9·6		14·5			10·3	8·2		7·2	下妻附近
						W	17·0	9·3	21·2	13·0			14·0	6·6		5·6	
						E	20·8	7·6	21·4	17·0			9·7	6·3		4·5	
						平均	**18·9**	**9·2**	**21·3**	**14·9**			**11·7**	**6·9**		**5·6**	

卓越周期を決定する爲めに製作した曲線は第3圖～第5圖に示してある．從來研究

の行はれた地點のものは今回も全く同様の特性を示して居る．此れは各地に殆ど一定の固有振動周期—卓越振動周期—の存在する事實を益々證明する事となる．本郷，駒場等における東京山手においては 0·3 秒程度の卓越周期が現はれるに反し，下町にては相當長い周期のものも誘發される．

昭和 10 年 1 月 3 日の地震は横濱野毛山の加速度が大で 58·5 gal の最大加速度を與へて居る．下町においては一般に加速度は小であるが，向島は 39·3 gal が最大である．横濱高島町は野毛山と接近して居るが，其の約 5 分の 1 の　11·1 gal　を與へるに過ぎない．一般に山手の震動は 0·3 秒附近に總ての波動が密集して居る事が注意される．

2 月 20 日の地震は震央が九十九里濱にあつた關係上，稍遠い地震である．從つて

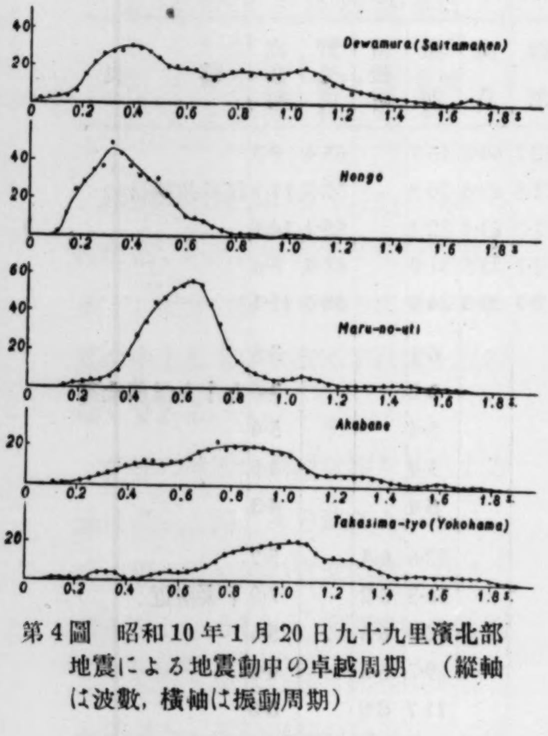

第 4 圖　昭和 10 年 1 月 20 日九十九里濱北部地震による地震動中の卓越周期　（縦軸は波數，横軸は振動周期）

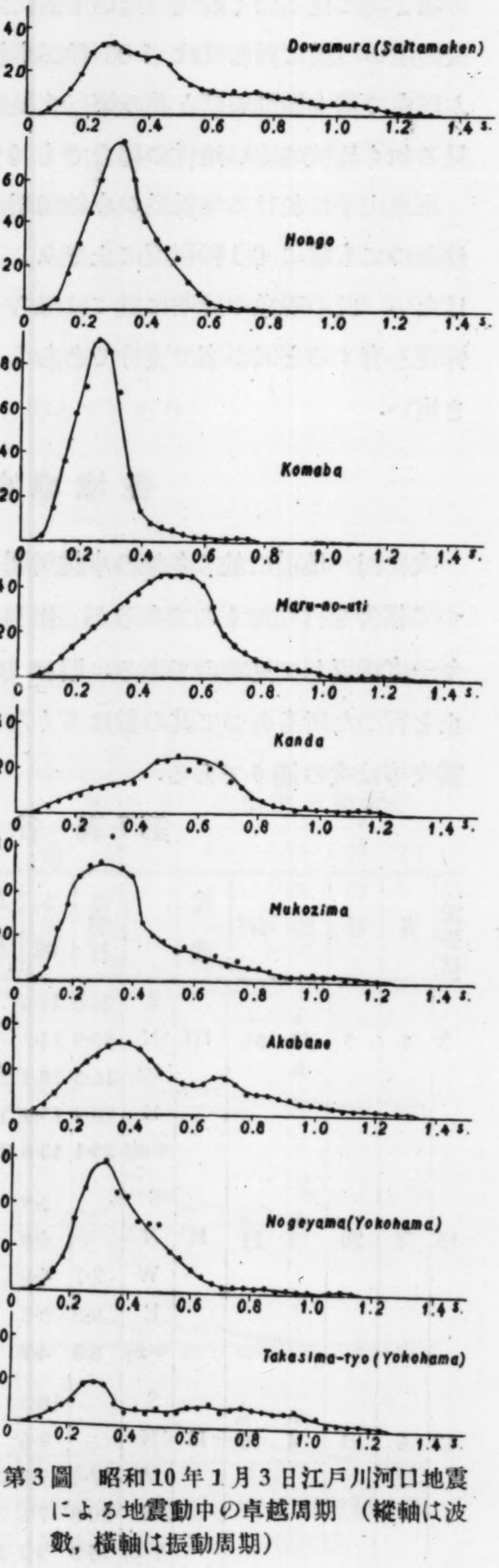

第 3 圖　昭和 10 年 1 月 3 日江戸川河口地震による地震動中の卓越周期（縦軸は波數，横軸は振動周期）

下町における卓越周期の中には比較的大なるものが見出し得る．即ち出羽村で 1·1 秒，

赤羽で 0·9 秒，高島町で 1·1 秒である．出羽村と高島町とは相當似通つた所がある様に見える．

6 月 21 日の地震の震央は寧ろ近い方である．殊に出羽村に最も近いものである．從つて出羽村に於ては 0·3 秒程度の卓越周期が明瞭に現はれた．本郷，駒場等の山手におけるものは同様の特性を示すが，赤羽，濱松町，高島町も亦別の類似の曲線を示して居る．此の事實は地盤の良否が同様ならば地震動も常に同様の特性を示すと云ふ事が云へるであらう．丸ノ内東京驛前に於ては卓越周期として0·6 秒程度であり，此れは比較的常に一定のものである．

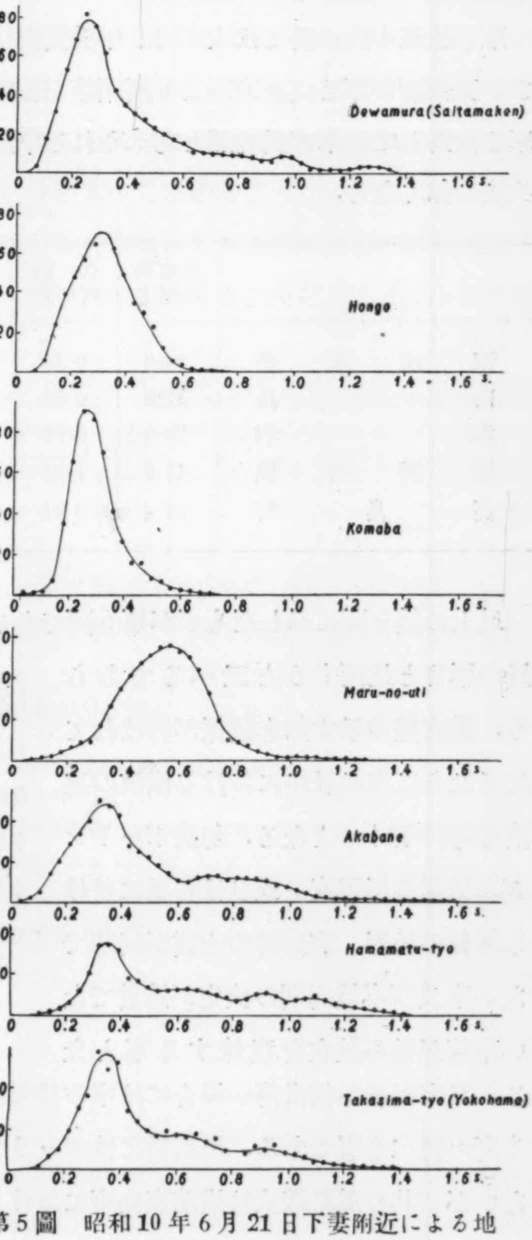

第 5 圖　昭和 10 年 6 月 21 日下妻附近による地震動中の卓越周期（縦軸は波數）

卓越周期と表面層の厚さ

地震動中に見出される振動周期の分布は山手と下町とにて其の特性の異る事は明かであるが，今山手におけるものは考へず下町におけるもののみを問題として見やう．下町における地震動，特に大なる加速度を與へる震動は大部分表面層の振動である事は充分信じ得べき事である．然も此の振動は表面層の剪斷振動による自己振動であると考へるならば其の周期 T は

$$T = \frac{4l}{1+2s}\sqrt{\frac{\rho}{\mu}}, \quad s = 0, 1, 2, 3 \cdots$$

但し l は表面層の厚さ，ρ は層を形成する物質の密度及び μ は其の物質の剛性率である．又此の物質内を傳播する横波の速度を V_s とすれば

$$V_s = \sqrt{\frac{\mu}{\rho}}$$

となる．從つて若し何處にても V_s が一定ならば，各地固有振動周期は單に表面層の厚さに正比例するものとなる．

東京橫濱市内に於ては大正 12 年震災直後，復興局において數多のボーリングを行ひ，表面層の厚さ（地表面より所謂第三紀層に至る距離）が決定されて居る．今此の厚さに對して基本振動周期と考へられる卓越周期が如何に變化するかを調べて見るに次表の如くなる．

	表面層の厚さ	卓越周期		表面層の厚さ	卓越周期
深川木場	34·8 m	0·88 s	濱松町	24·7 m	0·95 s
向島	32·8	0·80	丸ノ内(第一相互會社)	19·6	0·75
赤羽	20·0(?)	0·75	東京驛前	17·5	0·60
橫濱公園	41·0	1·23	神田電機學校	17·4	0·67
高島町	27·4	0·94	小石川柳町	8·5	0·51

以上の値を圖に示したものが第 6 圖である．此の圖に見る如く卓越周期は先づ表面層の厚さと比例すると云へるであらう．點直線の示す如き關係が行はれて居るならば表面層中における橫波の速度は每秒 134 m となる．勿論ボーリングの結果の信用度，或ひは各地に於ける基盤の地形，表面層の土質が同等でない事及び卓越周期の決定が適當でない事等が點の散在を意味する事となる．又表面層が相當薄い場合には寧ろ基盤における卓越周期が其のまゝ觀測される事も考へ得べき事である．出羽村にはボーリングの結果なく，表面層の厚さを知るに由ないが，其の震動樣式は橫濱高島町におけるものとよく似る事を以て，恐らく表面層の厚さは 30 米附近のものかと思はれる．

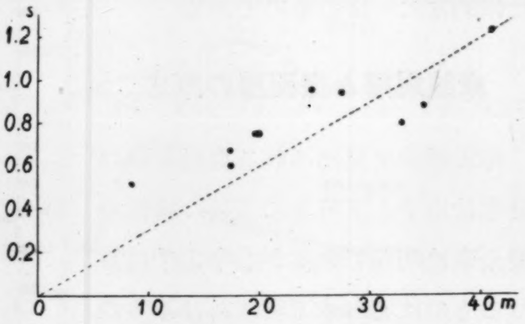

第　6　圖

結　　語

要するに地震動中加速度の大なる波動の周期は各地固有のものにて，此れは表面層の剪斷固有振動と考へられる．而して震央の遠近に從ひ其の一次或ひは三次の振動が誘發されるものと想像出來る．又大地震においても恐らく振動周期には變化ないものと思はれる．其の理由の一つは從來の大地震による災害を見るに，以上の考へを以て

すれば解釋が與へられるからである．但し加速度の値は寧ろ山手は下町に比較して大である．

從來地盤の良否が地震被害，特に木造家屋被害と關係づけて問題とされたが，此れは主として表面層の彈性と共の厚さとに關係した問題として取扱ふ事が出來るのである．卽ち木造家屋は卓越振動周期の比較的大なる地方においては，假令共の加速度は小であつても倒壞が實現される可能性が充分あるからである．

最後に此の研究を遂行するに當つては服部報公會竝に日本學術振興會の援助補助を得た事を明記して謝意を表すると同時に，各觀測點における直接觀測に從事された諸氏に對して共の勞を多とするものである．

---

21. *Observation des périodes prédominantes dans les secousses séismiques à Dewa-mura et à Hamamatu-tyô*

par Mishio ISHIMOTO,

Institut de Recherches sur les Tremblements de terre.

Nous avons installé deux séismographes accélérométriques à Dewa-mura et à Hamamatu-tyô et réussi à enregistrer certain nombre de séismes apparus surtout dans la région de Kantô. Il y a toujours les périodes prédominantes dans les secousses qui ont un rapport serré avec l'épaisseur du boue superficiel au desur la croûte comparativ ment solide.

---

22. *Construction d'un microséismographe mécanique*

par

Mishio ISHIMOTO,

Institut de Recherches sur les Tremblements de terre.

(Lu le 18 fev, 1936—reçu le 20 mars 1936.)

1. Introduction.

Il y a un certain nombre d'appareils qui sont employés pour enregistrer des secousses de petite amplitude: mais on adopte, presque sans exception, le procédé d'enregistrement optique. Nous savons que ce procédé d'enregistrement a beaucoup d'avantages surtout à cause de la facilité d'amplification des secousses. Mais, par ailleurs, nous pouvons énumérer les défauts de ce procédé: 1° nous ne pouvons pas regarder directement l'inscription pendant son observation; 2° largeur de la courbe inscrite est généralement trop grand; 3° nous sommes obligés, en effet, de donner une certaine vitesse au papier photographique enroulé sur un tambour tournant surtout pour distinger les oscillations de petite période: cette méthode d'observation est donc très onéreuse. Basant sur ces considérations, nous avons adopté définitivement le procédé mécanique et construit un microséismographe: appareil qui enregistre les secousses sur un papier recouvert de noir de fumée. Naturellement, il n'est pas nécessaire d'avoir un rapport d'amplification aussi grand que celui de l'amplification optique: c'est parce que le séismographe mécanique inscrit des courbes très fines. Il est possible d'agrandi plusieurs fois par le procédé photographique les secousses inscrites: nous voulons avoir simplement la portion enregistrée des secousses et il n'est pas nécessaire de tenir toujours le séismographe en condition de grande amplification: ce n'est qu'une grande perte de papier photographique. Le défaut du séismographe mécanique en général est le frottement solide au point de contact de la plume sur le papier recouvert de noir de fumée.

Certainement, le frottement solide empêche plus ou moin le déplacement du pendule: mais nous pouvons réduire cette influence avec l'augmentation de la masse du pendule ainsi qu'avec l'emploi d'une plume très légère. Nous discuterons cette condition plus loin.

En tous cas, nous avons r ussi à réaliser un microséismographe

de composante horizontale avec enregistrement mécanique et maintenant il nous sert pour exécuter les observations des secousses séismiques.

2. Dimensions.

Pour construire un séismographe, nous sommes obligés, tout d'abord, de déterminer la masse du pendule ainsi que le rapport d'amplification. Evidemment, il nous semble préférable d'avoir la masse plus grande possible: mais il n'est pas nécessaire d'accroitre cette masse au dela du point où nos buts seront atteints. Nous déterminerons ces deux éléments par des expériences et des calculs.

Quant au rapport d'amplification, il faut connaitre premièrement les valeurs d'inertie qui existent *a priori* dans tout levier, ainsi que les valeurs du frottement solide à la pointe de la plume. Mieux nous réussirons à réduire ces constantes, plus nous pourrons augmenter le rapport d'amplification.

Nous avons employé un pendule inversé pour le pendule principal du séismographe. L'aspect général de ce séismographe est montré schématiquement dans la Fig. 1a et sa photographie dans la Fig. 1b. La

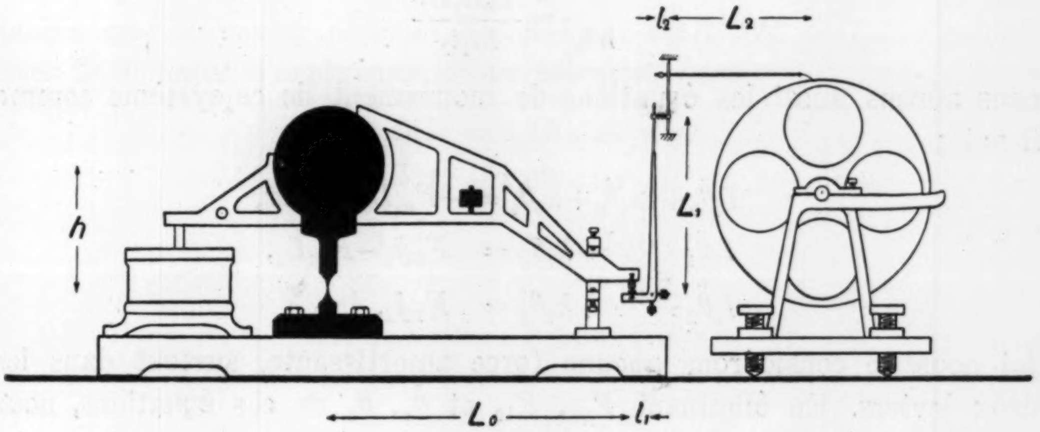

Fig. 1a. Aspect général du microséismographe représenté schématiquement.

masse prend la forme d'un cylindre (longueur 40 cm; diamètre 10 cm.) tenu par deux ressorts laminés d'acier. Nous donnons une certaine période propre d'oscillation en réduisant petit à petit les parties minces des ressorts.

Le déplacement du pendule relativement au sol sera amplifié par deux étages de leviers et, à la fin, la plume attachée à l'extrémité du dernière levier, inscrit les oscillations sur la surface d'un papier recouvert de noir de fumée, enroulé sur un tambour tournant.

Désignons, alors, les constantes des leviers dans le tableau suivant:

	Moment d'inertie	Angle de rotation	Bras sup.	Bras inf.
Pendule	I_0	θ_0	L_0	h
1er levier	I_1	θ_1	L_1	l_1
2me levier	I_2	θ_2	L_2	l_2

où h correspond à la distance entre l'axe de rotation du pendule et son centre de gravité. Désignons encore par F_{01} et F_{12} les forces de réaction existant entre les deux leviers consécutifs. Nous obtenons des conditions telles que les leviers consécutifs en contact entre eux, seront représentés par,

$$\begin{aligned} L_0\theta_0 &= l_1\theta_1, \\ L_1\theta_1 &= l_2\theta_2, \\ \xi &= L_2\theta_2, \end{aligned}$$

où ξ est le déplacement de la pointe de la plume. Nous pouvons, donc, tirer tout de suite le rapport géométrique d'amplification[1]

$$\frac{\xi}{h\theta_0} = \frac{L_0L_1L_2}{hl_1l_2}$$

nous aurons aussi les équations de mouvement de ce système comme il suit:

$$\begin{aligned} I_0\ddot{\theta}_0 + 2\varepsilon_0\dot{\theta}_0 + k_0\theta_0 &= -F_{01}L_0 - Mh\ddot{x}, \\ I_1\ddot{\theta}_1 \qquad\quad + k_1\theta_1 &= F_{01}l_1 - F_{12}L_1, \\ I_2\ddot{\theta}_2 \qquad\quad + k_2\theta_2 &= F_{12}l_2. \end{aligned}$$

Ici nous ne considérons aucune force amortissante, surtout dans les deux leviers. En éliminant F_{01}, F_{12} et θ_1, θ_2 de ces équations, nous aurons:

$$I\ddot{\theta}_0 + 2\varepsilon_0\dot{\theta}_0 + k\theta_0 = -Mh\ddot{x},$$

où
$$I = I_0 + I_1\frac{L_0^2}{l_1^2} + I_2\frac{L_0^2L_1^2}{l_1^2l_2^2},$$

$$k = k_0 + k_1\frac{L_0^2}{l_1^2} + k_2\frac{L_0^2L_1^2}{l_1^2l_2^2},$$

1) Il y a un cas où le mot "amplification géométrique" est employé avec un sens différent; mais ici nous adoptons ce mot comme représentant le rapport d'amplification du levier.

et nous trouvons la période propre de ce système représentée par:

$$T = 2\pi\sqrt{\frac{I}{k}}.$$

Nous voulons avoir I assez petit en comparaison de Mh^2. Si I devient plus grand, le rapport oscillant d'amplification diminuera proportionellement. Voici les constantes obtenues par les expériences:

$$\begin{aligned}
I_0 &= 4{,}63 \times 10^6 \text{ c. g. s.,} \\
I_1 &= 243 \quad '' \\
I_2 &= 1{,}5 \quad '' \\
h &= 11{,}0 \text{ cm}, \quad L_0 = 29{,}3 \text{ cm}, \\
l_1 &= 2{,}0 \quad '' \quad L_1 = 15{,}3 \quad '' \\
l_2 &= 0{,}54 \quad '' \quad L_2 = 10{,}0 \quad '' \\
M &= 33{,}9 \text{ kg.}
\end{aligned}$$

Avec ces constantes, nous pouvons calculer le rapport géométrique d'amplification V_g comme:

$$V_g = \frac{L_0 L_1 L_2}{h l_1 l_2} = 371$$

tandis que la valeur obtenue directement était 374 ce qui s'accorde avec le domaine d'expérience. Nous calculons aussi:

$$\begin{aligned}
Mh^2 &= 4{,}10 \times 10^6 \text{ c.g.s.,} \\
I_0 &= 4{,}63 \times 10^6 \quad '' \\
I_1 \frac{L_0^2}{l_1^2} &= 0{,}0522 \times 10^6 \quad '' \\
I_2 \frac{L_0^2 L_1^2}{l_1^2 l_2^2} &= 0{,}248 \times 10^6 \quad '' \\
\therefore \qquad I &= 4{,}93 \times 10^6 \quad '' \; .
\end{aligned}$$

Nous aprenons, alors, que $\frac{Mh^2}{I}$ deviend 83% approximativement et le rapport oscillant d'amplification vaut 310 environ.[2)]

3. Etalonnage.

a) *Période propre d'oscillation.*

Nous avons déterminé la période propre d'oscillation du pendule

---

2) Ces calculs ont déjà faits dans notre mémoire sur la construction d'un séismographe accélérométrique: ce Bulletin: **9** (1931), 316.

seul ainsi que celle du système du pendule avec un puis avec deux leviers. Grâce à ces déterminations, nous avons pu savoir l'effet du moment d'inertie de chaque levier ainsi que l'effet du ressort à boudin qui sert à réunit les leviers consécutifs. Nous avons, en tout cas, mesuré plusieurs périodes en différentes conditions:

Pendule seul	0,99 sec.
Pendule avec le bras	1,00 ″
Pendule, bras et amortisseur	1,006 ″
dito avec le premier levier	1,00 ″
dito avec le deuxième levier	1,00 ″

Naturellement, quand nous ajoutons le levier, la période propre de ce système doit augmenter: mais les réessorts runissant les deux leviers consécutifs donnent des forces restitutives qui au contraire, jouent un rôle pour diminuer la période. Dans les cas que nous avons observés avec notre appareil, ces deux effets se compensent sensiblement. Si nous employons des ressorts impropres, chaque état du système tend à diminuer sa période d'oscillation. Nous sommes obligés, donc, d'apporter beaucoup de soins dans le choix de ces ressorts.

b) *Rapport géométrique d'amplification.*

Pour mesurer le rapport géometrique d'amplification des leviers nous avons employé un micromètre à cadran, dont la plus petite division correspond à un centième de millimètre. Naturellement, nous avons déterminé la relation entre le déplacement du centre de gravité du pendule et la déviation de la plume (ξ) inscrite sur le papier recouvert de noir de fumée: les résultats des mesures sont donnés dans la Fig. 2. Nous obtenons, donc, le rapport géométrique d'amplification comme 374, ce qui concorde bien avec le résultat des calculs déjà décrits.

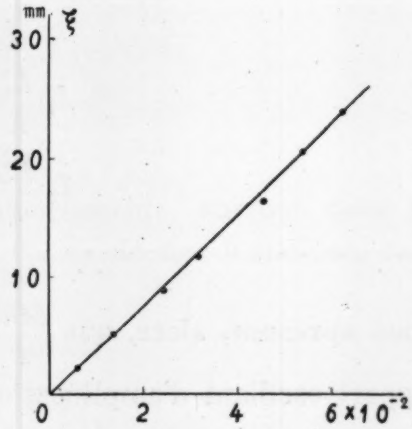

Fig. 2. Relation entre le déplacement du pendule et celui de la pointe de la plume.

c) *Déviation due à l'inclinaison.*

Quand nous inclinons le séismographe, la plume fait une déviation proportionelle à l'importance de l'inclinaison. Ce procédé d'étalonnage nous permet constater la sensibilité de l'appareil sous l'action d'accélération dans la composante horizontale.

Nous avons mesuré l'angle d'inclinaison du séismographe au moyen d'un niveau d'alcool déjà étalonné. La relation entre l'inclinaison (ψ) et le déplacement de la plume (ξ) est montré dans la Fig. 3.

D'un autre côté, nous avons l'équation théorique[3] suivante:

$$\xi = \frac{T'^2}{4\pi^2} \times g\psi \times V_g,$$

où ξ: le déplacement de la pointe de la plume.
T': la période propre du pendule en supposont que la masse est concentrée au centre de gravité.
g: l'accélération due à la gravité.
ψ: l'angle d'inclinaison.
V_g: le rapport géométrique d'amplification.

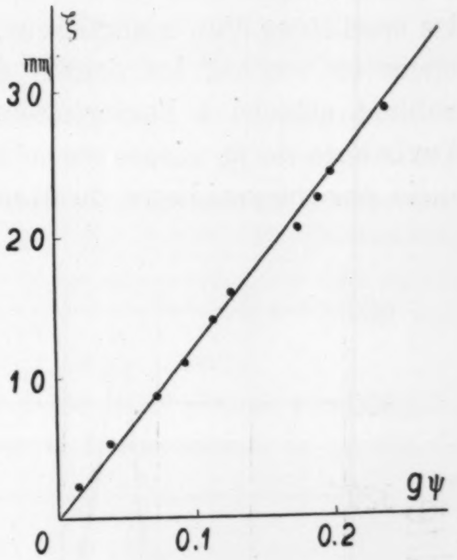

Fig. 3. Relation entre l'angle d'inclinaison et le déplacement de la pointe de la plume.

D'après la Fig. 3, nous tirons la relation que 1 mm de déviation de la plume correspond à $8{,}24 \times 10^{-3}$ gal. Evidemment, ce séismographe joue le rôle d'un accéléromètre, quand la période des secousses s'élève à plus d'une seconde et il a une sensibilité considérable; c'est-à-dire que ce séismographe a une sensibilité 200 fois plus grande que celle du séismographe accélérométrique que nous employons toujours pour observer les secousses séismiques perceptibles par les hommes. Cet ordre de sensibilité nous renseigne surtout sur la limite d'inscription des secousses de séismes éloignés, ainsi que sur les des secousses pulsatoires: c'est parce que leurs périodes d'oscillation sont beaucoup plus grandes que celles du séismographe. Naturellement, nous sommes obligés de tenir comte de l'effet du frottement solide existant à la pointe de la plume qui réduit le mouvement du pendule. Nous discuterons ce frottement plus loin.

d) *Expérience avec un fil de caoutchouc.*

Cette sorte d'expérience est très commode pour étudier l'effet de la force périodique sur le système du pendule. Nous avons attaché une des deux extrémités du fil au pendule et l'autre extrémité à un objet faisant une oscillation d'une amplitude constante et de diverses périodes. L'élongement du fil transmet la force au pendule, comme nous

3) *loc. cit.*

avons déjà appliqué dans le cas d'étalonnage d'un séismographe accélérométrique. Cet étalonnage joue un rôle important pour connaitre les conditions d'un amortisseur. Nous avons exécuté une série d'expériences en variant les degrés d'échappement de l'air, au moyen d'un robinet attaché à l'amortisseur. En tout cas, nous voulons constater l'existence de la résonance, s'il y en a, avec la force oscillante appliquée par intermédiaire du fil de caoutchouc. Les résultats obtenus sont

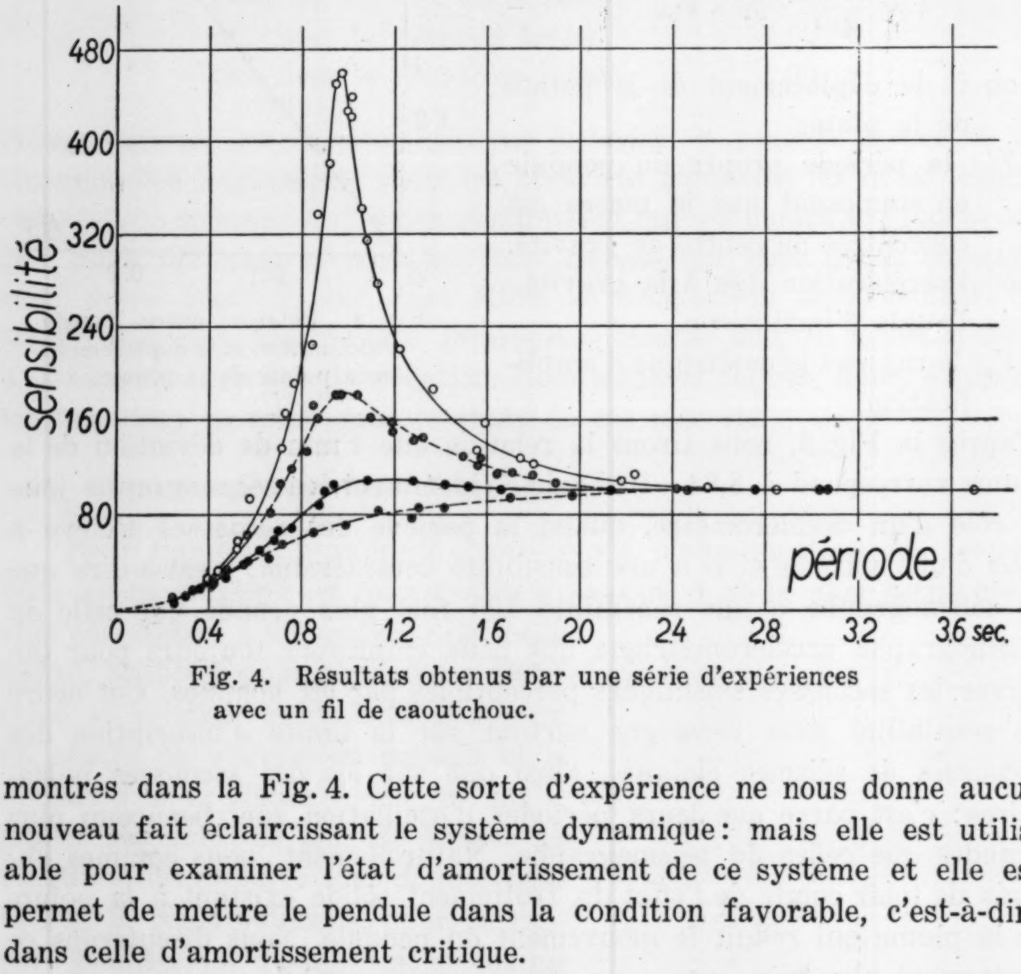

Fig. 4. Résultats obtenus par une série d'expériences avec un fil de caoutchouc.

montrés dans la Fig. 4. Cette sorte d'expérience ne nous donne aucun nouveau fait éclaircissant le système dynamique: mais elle est utilisable pour examiner l'état d'amortissement de ce système et elle est permet de mettre le pendule dans la condition favorable, c'est-à-dire dans celle d'amortissement critique.

Comme le microséismographe possède grande amplification, il nous semble qu'il est presque impossible d'avoir l'étalonnage exécuté sur une plate-forme oscillant artificiellement. Il nous semble, en tout cas, que cette expérience ne sera pas nécessaire tant que nous exécutons les autres étalonnages.

e) *Frottement solide à la pointe de la plume.*

Vraiment le frottement solide à la pointe de la plume, ainsi qu'au pivot de rotation du levier sont inévitables. Mais nous voulons réduire

ce frottement au minimum.

Quand on compare l'effet du frottement solide à la pointe de la plume à celui du frottement au pivot, on constate que le premier est un obstacle plus important au mouvement du pendule. Le frottement solide à la pointe de la plume depend entièrement de la pesanteur de la plume même: nous sommes obligés de la tendre la plus légère possible. D'un autre côté, la plume doit inscrire des secousses un produisant une rigole sur le papier, recouvert de noir de fumée. Naturellement, ce noir de fumée est assez mince pour nous permettre de distingeur la trace des secousses. Notre préoccupation est toujours de ne pas augmenter le frottement solide à la pointe de la plume.

Cette fois-ci, nous avons réussi à faire une plume très légère. Nous devons nous efforcer de distinguer le frottement à la pointe de la plume du frottement aux pivots. La Fig. 5a montre un des exemples de l'inscription d'après l'oscillation propre de pendule: certainement le frottement solide et le frottement liquide y sont confondus. Pour obtenir séparement la valeur de ces deux sortes de frottement, nous sommes obligés de faire l'analyse. Prenons $A_n - A_{n+2}$ de la courbe comme l'ordonnée et A_{n+1} comme l'abscisse.

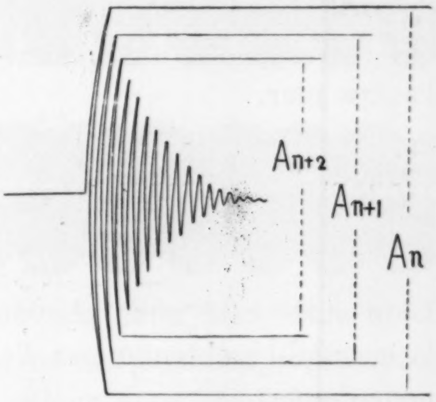

Fig. 5a. Un des exemples de l'oscillation amortissante.

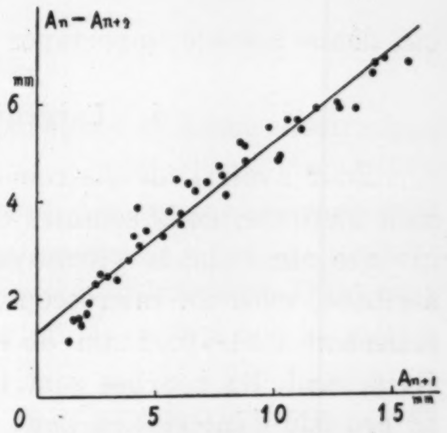

Fig. 5b. Procédé pour savoir la valeur du frottement solide.

Les points obtenus ainsi seront représentés par une ligne droite: généralement elle ne passe pas à l'origine. Le point d'intersection de cette ligne avec l'axe de l'ordonnée donnera la mesure du frottement solide: désignons cette valeur par y_0.

L'équation du mouvement d'un pendule avec le frottement solide ainsi qu'avec le frottement liquide sera représentée par

$$\ddot{y} + 2\lambda\dot{y} + n^2(y \pm \rho) = 0 \,.$$

Pour notre cas, cependant, $\rho = \frac{1}{16} y_0$: car nous avons pris $A_n - A_{n+2}$ pour l'ordonnée. Pour calculer la force du frottement solide, nous supposons qu'il existe entièrement à la pointe:

nous avons donc

$$F = \frac{n^2 M \rho}{V_g},$$

où F: force à la masse par le frottement solide.

$f = F/V_g$: force à la pointe de la plume.

$V_g = 374$

$n = \frac{2\pi}{T} = 6,28$

$M = 33,9\,\text{kg}$

$\rho = \frac{0,13}{16}\,\text{cm}$

$\therefore \; f = 0,078\,\text{dyne}$

Le frottement solide à la pointe de la plume vaut seulement 0,1 dyne qui correspond à un dixième de la valeur que nous avons déterminée l'autre jour.

La condition où le mouvement de la plume se réalise est dans le domaine: $f \times V_g < Ma$, où a représente l'accélération du mouvement du sol.

$$a > 8,6 \times 10^{-4}\,\text{gal}.$$

D'un autre côté nous pouvons appliquer cette limite d'accélération à la sensibilité obtenue par l'expérience au moyen de l'inclinaison. Cela nous donne:

$$\rho \times \text{sensibilité} = \frac{1,3}{16} \times 8,24 \times 10^{-3} = 6,7 \times 10^{-4}\,\text{gal}$$

qui donne aucune importance en pratique.

4. Largeur de la courbe inscrite.

Pour avoir l'enregistrement des secousses séismiques en condition bien distincte, nous sommes obligés de discuter la largeur de la courbe inscrite ainsi que la vitesse superficielle du tambour. Quand nous examinons, avec un microscope, la courbe inscrite, nous obtenons généralement 0,01∼0,02 mm de largeur; rarement elle arrive à 0,05 mm. Evidement, les courbes sont inscrites au moyen d'une pointe d'acier et ce procédé d'inscription peut être comparé à la trace de courbes avec une canne sur le sol couvert de gélée blanche. Il y a le cas, où l'excès de gélée blanche qu'il faut rejeter hors de la courbe, exagère la courbe même ce qui nous permet de remarquer assez d'irrégularités. Pour obvier à un inconvénient du même genre, il nous semble qu'il n'y aucun

autre moyen que de diminuer l'épaisseur du noir de fumée le plus mince possible.

D'un autre côté, plus nous faisons mince la largeur de la courbe, plus nous pouvons diminuer la vitesse superficielle du tambour. Nous considérons en effet un critérium sur la limite de la vitesse superficielle avec la longuer d'onde d'une courbe sinusoïdale. Supposons que la pointe possède une aire circulaire dont le rayon soit r. Considérons, en suite, le mouvement sinusoïdal de cette pointe. La vitesse superficielle du tambour (v) désigne la longeur d'onde (λ) et nous allons, en effet, étudier la relation entre r et λ. Nous posons, en tout cas, un critérium que la vitesse du tambour ne doit pas être inférieure à

$$r = \frac{\lambda}{4} \text{ où} = \frac{vT}{4}.$$

Cette condition est montrée graphiquement dans la Fig. 6.

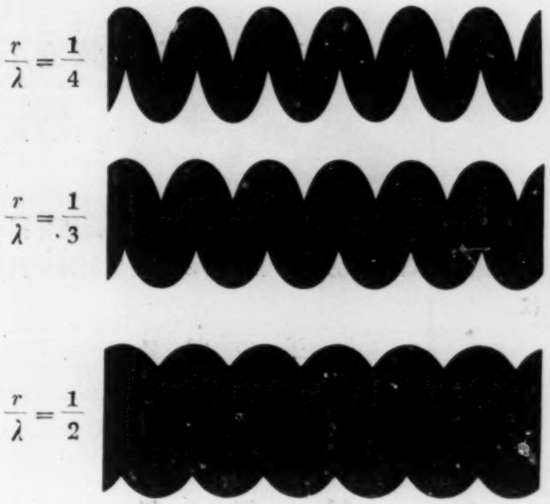

Fig. 6. Critérium entre λ et r.

Quant à la période d'oscillation, nous considérons les secousses séismiques dans la nature. La limite des secousses séismiques observée à Tôkyô est représentée par $T = 0{,}2$ sec. Nous introduisons cette valeur dans l'équation précédente. Nous avons, ainsi, $v = 0{,}2$ mm/sec: cette vitesse correspond à un cinquième de la vitesse que nous employons maintenant.

5. Inscription.

Nous avons installé deux microséismographes de même construction dans une cave de notre institut et réussi à avoir deux inscriptions séparées pour un certain nombre de séismes. Un des exemples obtenus est montré dans la Fig. 7. L'intensité des secousses n'a pas été grande: elles sont arrivées juste au seuil de la perception humaine. D'un coup d'oeil on comprendra que ces paires d'inscriptions ne sont que les mêmes secousses.

Même dans une journée tranquille, ce microséismographe inscrit toujours de petites amplitudes d'oscillation dont la période demeure 0,3 sec. Comme ce type d'oscillation est spécialement perceptible pendant la journée, nous le considérons comme dû à l'influence des camions, voitures, tramways, etc. qui passent dans la rue.

Nous constatons aussi l'existance d'oscillations du type de pulsations, surtout dans les moments de vent: elles ont une période de 8 sec. environ.

Nous nous proposons de rapporter dans les prochaines occasions les autres études que nous aurons pu faire avec cet appareil.

---

22. 器械的記錄を行ふ微動計の製作

地震研究所 石本巳四雄

多くの微動計は寫眞方法により地動の記錄を行ふが，一面に不便の所があるので，此の水平成分微動計は器械的方法により何の程度迄記錄が得られるか研究したものである．而して其の要素は

振子の質量	33·9 kg
擴大裝置	槓桿 2 段
幾何倍率	371 倍
振動倍率	310 倍（計算）
制振器	ピストン型空氣制振器
自己振動周期	1 秒
針先の固體摩擦	0·08 dyne

なほ感度試驗としては次の5種類のものが行はれた．

a) 各階段における自己振動周期
b) 幾何倍率
c) 傾斜による試驗
d) ゴム糸による試驗
e) 針先其他における固體摩擦の決定

同型の微動計2臺を製作し，同一地震を記錄せしめた所殆ど同一の記象を得た．

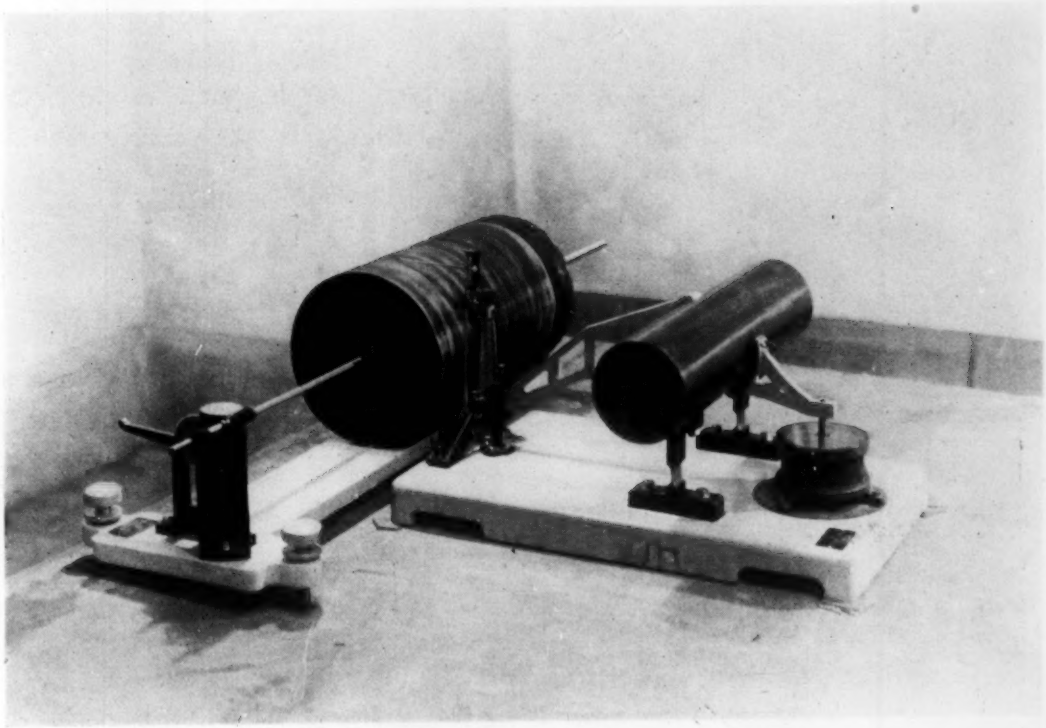

Fig. 1b. Aspect général du microséismographe.

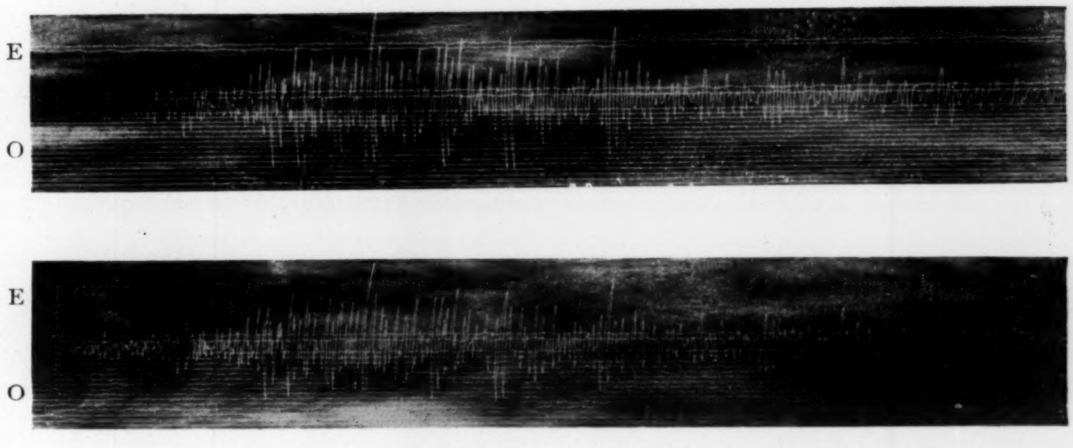

Fig. 7. Mêmes secousses inscrites séparément par deux microséismographes pour le séisme du 11 décembre 1935.

（震研彙報 第十四號 圖版 石本）

23. *Physical and Chemical Properties of the Simogamo, Rendaizi and Simokawazu Thermal Springs in Southern Idu Peninsula. I.*

By Takaharu FUKUTOMI,

Mitsui Geophysical Observatory.

(Read Feb. 18, 1936.—Received Mar. 20, 1936.)

The writer recently had an opportunity of observing the orifice temperatures besides analysing some of the chief chemical constituents of the water of a number of springs in the Simogamo, Rendaizi, and Simokawazu thermal regions in southern Idu peninsula. The results, in conjunction with the known physical properties of these springs, give some clue to constructions of the springs in the respective locality.

The results of this investigation are briefly described as follows:

I. Relation between the orifice temperature of a hot spring and the air temperature.

In a previous communication[1] the writer pointed out the close relation apparently existing between the orifice temperature of a certain hot spring at Rendaizi, records of which were taken continuously at about 2 metres below the ground, and those of the air temperature in the place as shown in Fig. 1.

For an explanation of the phenomena, the writer considered first the effect of loss of heat on the air and on the surrounding earth near the surface, and obtained as a relational formulae between the orifice temperature θ and air temperature θ_0 the following equation as first approximation:—

$$\left.\begin{aligned}\theta&=\frac{\theta_1}{1+\lambda}+\frac{\lambda}{1+\lambda}\theta_0,\\ \lambda&=\frac{KS}{Vc\rho},\end{aligned}\right\}\qquad(1)$$

where θ_1 is the underground temperature of the hot spring, V the volume output, ρ the density of water, c the specific heat, S the effective area for heat loss, and K the proportional constant.

1) T. FUKUTOMI and M. NAKADA, *Bull. Earthq. Res. Inst.*, **13** (1935), 616.

But, the fact that the amplitude of the diurnal change of the orifice temperature 2 metres below the surface was one half of that of the

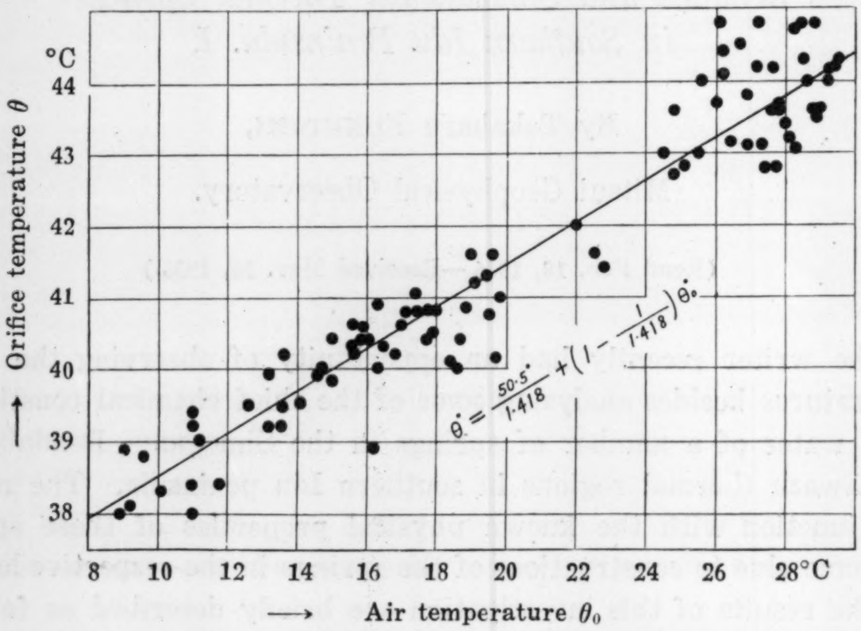

Fig. 1. Relation between the daily mean of orifice temperature in a Rendaizi hot spring and that of air temperature.

air temperature contradicts our common knowledge that the range of the diurnal change of underground temperature is very small in depth of 1 metre in general. This apparent contradiction suggests there is another effect to explain this phenomenon.

It is well next to consider the effect of mixing underground water that has nearly the temperature of air with the original hot spring in underground passages. The writer here uses "underground water" to mean, not the so-called underground water that flows at the slow speed of 1∼10 m/day, but streams that flow in the underground fissures of rocks at moderately speed. According to the results[2)] of recent observations of the water-heads of hot spring that flowed from the fissure of rock in the underground gallery of the Kawazu mine at Rendaizi, mixing of such underground water was distinctly traced in the shallow layer of the ground.

We shall consider a hot spring of temperature θ_1 mixed in a shallow layer of the ground with cold underground water of temperature θ_2 in volume proportion of $\mathfrak{v} : v = 1/R$, and flows out at the orifice in temperature θ.

2) T. FUKUTOMI, Read. Sept. 17th, 1935, at the meeting of the Earthquake Reserch Institute, Tokyo Imperial University.

We then get,

$$\theta = \frac{\theta_1}{1+\frac{c_u}{c_h}\frac{\rho_u}{\rho_h}R} + \frac{\frac{c_u}{c_h}\frac{\rho_u}{\rho_h}R}{1+\frac{c_u}{c_h}\frac{\rho_u}{\rho_h}R}\theta_2, \tag{2}$$

where c_h, c_u is the specific heat of the original hot spring and the underground water, ρ_h, ρ_u the density of these waters. Appoximately we can assume $c_h=c_u$, $\rho_h=\rho_u$, $\theta_2=k\theta_0$, and therefore obtain

$$\left.\begin{aligned} \theta &= \frac{\theta_1}{1+R} + \frac{R}{1+R}k\theta_0, \\ R &= \frac{v}{\mathfrak{v}}. \end{aligned}\right\} \tag{3}$$

If volume proportion R between the underground water and the original hot spring is constant, and k is nearly equal to 1, formulae (3) for the relation between orifice temperature and air temperature is exactly the same form as that of (1).

If the assumption[3] that the original hot spring, which was subjected first to the effect of mixing with the cold underground water as shown in equation (3), suffered through heat loss as shown in equation (1) is taken into consideration, then we get

$$\theta = \frac{\theta_1}{(1+\lambda)(1+R)} + \left[1 - \frac{k}{(1+\lambda)(1+R)} + \frac{k-1}{1+\lambda}\right]\theta_0. \tag{4}$$

If θ_1, R be constant, and also the output of spring V is constant or moderately large, we can express θ as a simple linear function of θ_0 as shown in equation (4). The linear relation between θ and θ_0 shown in Fig. 1 may represent this relation.

II. Relation between orifice temperature and the amount of chemical substances of a number of spring in a locality.

The simple relation between orifice temperatures of springs and the amounts of mineral substances dissolved in the water of springs was not known with for springs scattered over a very wide region, though it was frequently noticed in the case of springs within a narrow range

3) In another combination of these two effects, we obtained a different equation

$$\theta = \frac{\theta_1}{(1+\lambda)(1+R)} + \theta_0\left[k - \frac{1}{(1+\lambda)(1+R)} + \frac{1-k}{1+R}\right]$$

to equation (4).

of locality. According to Mr. Yoshimura's investigation[4] with respect to the Kamisuwa thermal springs in Nagano Prefecture, a linear relation exists between the amount of Cl-compounds in water of many springs and the corresponding orifice temperatures.

Similar relations were ascertained in the cases of Simogamo, Rendaizi, and Simokawazu thermal springs connection with the Cl- and Ca-compounds. Water taken from many of these thermal springs contained 4·5∼12·5 g/l, 0·10∼0·17 g/l, 0·02∼1·21 g/l of Cl respectively. These relations are shown in diagrams (Figs. 2∼4) in which the abscissa represents the orifice temperature, and the ordinate, the Cl-contents of the springs in their respective localities.

In explanation of this phenomena, a theory that first occurred in our minds is that

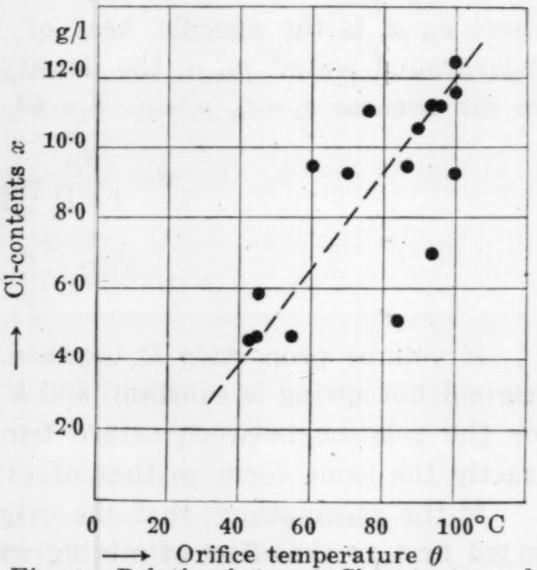

Fig. 2. Relation between Cl-contents and orifice temperatures in Simogamo thermal springs.

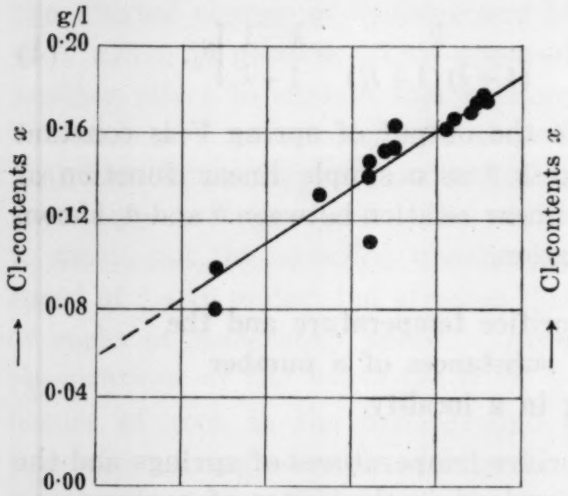

Fig. 3. Relation between Cl-contents and orifice temperatures in Rendaizi thermal springs.

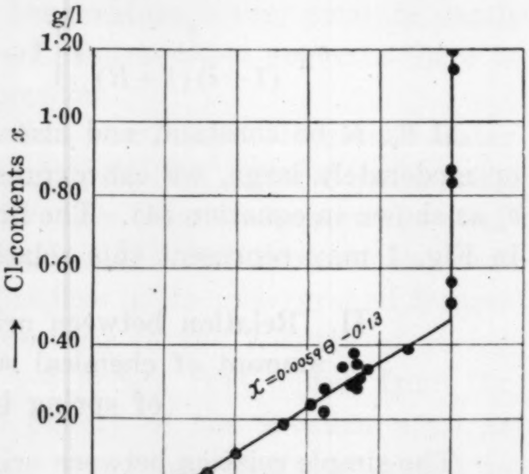

Fig. 4. Relation between Cl-contents and orifice temperatures in Simokawazu thermal springs.

though there are some exceptions, as $CaSO_4$, Na_2SO_3 etc., the solubility

4) S. YOSHIMURA, *Geograph. Rev., Jap.*, 8 (1932), 482.

of many materials in water, generally, was large in the case where the temperature of water was high in the extent of temperature in question, so that the amounts of the mineral constituents contained in springs of high temperature may be larger than those contained in springs of low temperature, so far as springs of equal output and non-saturated materials are concerned. Although this theory may be reasonable to a certain extent, we can not accept it in this case as a suitable explanation of the phenomena, first, because in above thermal and mineral springs regions, the temperatures and the amounts of the chemical constituent differed markedly, notwithstanding the short distance of only 20∼30 m between their sites, an example being the Simogamo springs the temperatures and Cl-contents of which change over the range 30∼100°C and 4∼12 5 g/l. If the above mentioned idea were justified in this case, we should unreasonably recognize the existence of many springs of different temperatures and of different chemical constituents that flow out independently from the deep in a narrow area.

Second the relations between the amounts of these chemical constituents and the corresponding orifice temperature in the Simogamo springs in which NaCl, $CaCl_2$ were its chief chemical constituents, with $Mg(HCO_3)_2$, etc., also in small amount, show positive linear relations with respect to the Cl- and Ca-compounds, but show negative linear relation with respect to the CO_3-compound, notwithstanding that $Mg(HCO_3)_2$ is similar to NaCl and $CaCl_2$, both of which are unsaturated in the temperature in question, and is more soluble in water of high temperature than in that of low. This facts can not be explained by the foregoing theory.

To explain these phenomena, the above quoted theory that the cold underground water mixies with the original hot spring in the superficial crust layer is most acceptable–(assuming that the chemical change or deposition of the materials do not taken place accompanied mixing).

If we now put N g/l (gram per litre) as the amount of a chemical constituent dissolved in the original hot spring, n g/l as that in the underground water, x g/l as that in the hot spring after mixing, and $R=\frac{v}{\mathfrak{v}}$ as the volume ratio of mixture of the underground water to the original hot spring, we then get

$$x=\frac{N}{1+R}+\frac{R}{1+R}n. \tag{5}$$

Eliminating R between (4) and (5), we obtain,

$$x=\frac{(N-n)(1+\lambda)}{(\theta_1-k\theta_0)}\theta+\left[n-\frac{(N-n)(1+\lambda)\theta_0}{(\theta_1-k\theta_0)}\left\{1+\frac{k-1}{1+\lambda}\right\}\right] \tag{6}$$

This is relational equation between the amount of the chemical constituents of the spring x and orifice temperature θ. If we take N, n, θ_1, $k\theta_0$, θ_0 as constant, and V also as constants, or so large, so that λ is so small in comparison with 1, as to be neglected, we can see that the relation between x and θ is linear, as shown in equation (6), and also recognize that whether the linear relation be positive or not is determined by the sigh of $(N-n)$. Since the relations between the Cl-contents and orifice temperatures in the above-mentioned three springs are all positive, as shown in Figs. 2～4, we concluded that Cl-compounds are largely contained in the original hot springs in this case.

III. A note on the relation between the Cl-contents and the orifice temperatures of the Simokawazu springs.

The relation between the Cl-contents and the orifice temperatures of a number of springs in Simokawazu is shown in Fig. 4. As to springs, the Cl-contents of which are less than 0·50 g/l, a positive linear relation exists between the Cl-contents and the orifice temperatures as just mentioned. As to springs, the Cl-contents of which are more than 0·50 g/l, the orifice temperatures are always constant at about 100°C displaying the phenomenon of a "Boiling spring".

This may be attributed to the loss of the excess heat of water of high temperature, which is less than that of boiling point under high pressure at depth as latent heat of evaporation due to lowering of pressure at the earth's surface. Before the phenomena of boiling occurs at depth, we may assume that the linear relation $x=A\theta+B$, as shown in Fig. 4, must be satisfied between the Cl-contents and the temperatures. Let θ' be the temperature of a spring before boiling, x g/l the amount of a chemical constituent in the spring before boiling, m g/l the amount of the same material in water at the orifice, V the volume output at the orifice, y the volume of the water that is evaporated, and l the latent heat of evaporation. We then get approximately

$$\left.\begin{aligned}(V+y)\rho c\theta' &= V\rho c\cdot 100+ly\rho\,,\\ (V+y)x &= Vm\,.\end{aligned}\right\} \tag{7}$$

Eliminating y from these equations, we obtain

$$m=\frac{x}{1-\dfrac{c}{l}\dfrac{(\theta'-100)}{1-\dfrac{c}{l}100}}\,. \tag{8}$$

Now put $x=A\theta+B\cdots(6)'$, ($A=0{\cdot}0059$ g/l degree $B=-0{\cdot}13$ g/l), then we get

$$\theta'=\frac{m-B(1-\frac{c}{l}100)}{m\frac{c}{l}+A(1-\frac{c}{l}100)}. \tag{9}$$

Assuming for example that $c=1{\cdot}007$, $l=539{\cdot}1$ cal., we then have $\theta'=120°C$ or $185°C$ for $m=0{\cdot}60$ g/l or $1{\cdot}20$ g/l respectively. Thus we can estimate the approximate temperature of the original hot spring of Simokawazu at depth as more than 185°C.

IV. Relation between two chemical constituents of a number of springs in a locality.

If the questions discussed in II are generally applicable, we can deduce a relational equation between two chemical constituents contained in water of one or more springs in a locality. Let N_a, N_b be the amounts of chemical constituents A, B in the original hot spring, n_a, n_b of those in the cold underground water, and x_a, x_b of those in the thermal spring after mixing. Then eliminating R from the two equations of (5) with respect to A and B, we have

$$x_b=\frac{N_b-n_b}{N_a-n_a}x_a+\frac{N_an_b-N_bn_a}{N_a-n_a}. \tag{10}$$

If we take x_b in the ordinate and x_a in the abscissa, equation (10) is an equation of a straight line joining the two points (N_a, N_b), (n_a, n_b). We can also see that the relation between the amounts of two chemical constituents is linear and that whether the relation is positive or not depends on the sign of $\frac{N_b-n_b}{N_a-n_a}$.

According to the result of analysis[5] of a certain hot spring in Simogamo, NaCl and $CaCl_2$ were its chief chemical constituents, the amounts of other chemical constituents being negligible compared with those of NaCl and $CaCl_2$. From the total amounts of Cl and Ca that were obtained by our chemical analysis[6], we calculated, therefore, the residual amounts of Cl in every spring of Simogamo subtracting the the amounts of Cl that combine with Ca to form $CaCl_2$. The relation between the residual amounts of Cl that correspond to the amounts of NaCl, and the amounts of Ca that correspond to the amounts of $CaCl_2$

5) Pan-Siduoka thermal spring association, "Onsen no Idu."

6) See Table I in the second report.

are shown in Fig. 5, from which it is well be seen that a simple linear relation exists between the amounts of NaCl and those of $CaCl_2$. Other example of such a relation are also shown in Fig. 6 with regard to CO_3-compounds and Cl-compounds. These results are in fair agreement with the expectation from the equation (10). Thus, we come to the conclusion that NaCl and $CaCl_2$ are the chemical components of the original hot spring, where as the CO_3-compounds, on the contrary, are those of the cold underground water.

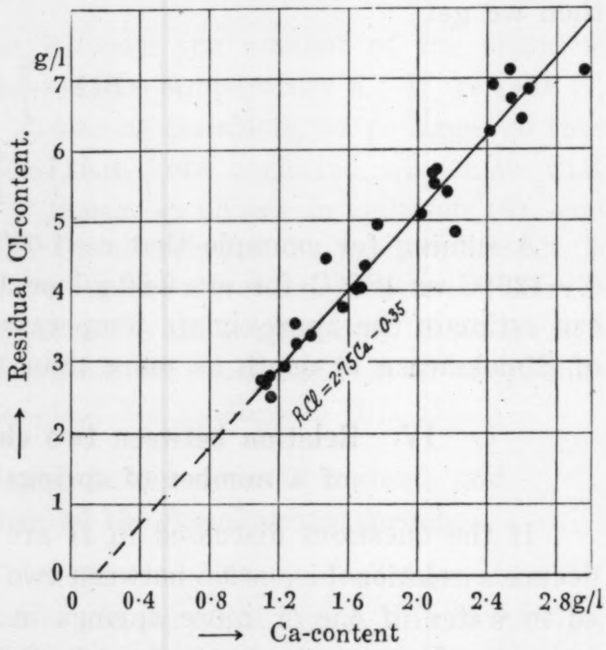

Fig. 5. Relation between residual amounts of Cl which correspound to the amounts of NaCl and amounts of Ca which correspond to the amounts of $CaCl_2$ in Simogamo thermal spring.

V. Relation between orifice temperature and volume output of spring.

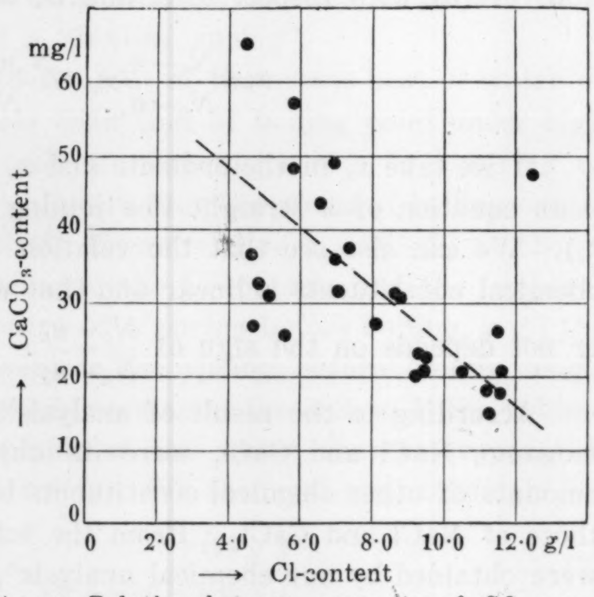

Fig. 6. Relation between amounts of CO_3-compounds and amounts of Cl-compounds contained is Simogamo thermal springs.

It is a well-known fact that the temperature of some ordinary hot springs rises with increase in volume output of the springs, neumerous cases[7] are also recorded of changes in the same sense in the output and temperature of hot springs accompanied by earthquakes. The mechanism of these phenomena is, however, not yet sufficiently understood. According to recent observations made by Mr. K. Maeda[8] in an Asamusi hot spring, the relation between change of orifice temperature and volume output of a spring is well

7) For example, see N. MIYABE, *Disin*, **5** (1933), 21.
8) K. MAEDA, *Disin*, **8** (1936), 1.

indicated by the following equation

$$\left.\begin{aligned} \theta &= \theta_1 - \frac{\lambda'(\theta_1-\theta_0)}{V+\lambda'}, \\ \lambda' &= \frac{KS}{c\rho}, \end{aligned}\right\} \tag{11}$$

which is another expression of equation (1).

Considering now the effect of mixing of the underground water, we change the form of equation (4), and get

$$\theta = \theta_0 + \left(\frac{\theta_1-\theta_2}{1+R} + \theta_2 - \theta_0\right)\frac{V}{\dfrac{KS}{c\rho}+V}. \tag{12}$$

When the temperature of the underground water is equal to air temperature, it takes the form

$$\theta = \theta_0 + \frac{\theta_1-\theta_0}{1+R}\,\frac{V}{\dfrac{KS}{c\rho}+V}, \tag{13}$$

$$\text{or} \quad \theta = \theta_0 + \frac{\theta_1-\theta_0}{1+R} - \frac{\theta_1-\theta_0}{1+R}\cdot\frac{\dfrac{KS}{c\rho}}{\dfrac{KS}{c\rho}+V}, \tag{13$'$}$$

and relation between orifice temperature θ and output V is *esteris paribus* hyperbolic relation, and the asymptotic value of temperature was $\theta_2 + \dfrac{\theta_1-\theta_2}{1+R}$ or $\theta_0 + \dfrac{\theta_1-\theta_0}{1+R}$ for (12) or (13) on the other hand that was θ_1 for the case of (11).

The points plotted in Fig. 7 give the relation between the orifice temperatures of several springs at Rendaizi and the corresponding outputs, the full lines being the graphic expression of equation (13) for $\theta_1=56°C$, $\theta_0=20°C$, $KS/\rho c=0{\cdot}66$. The relation is

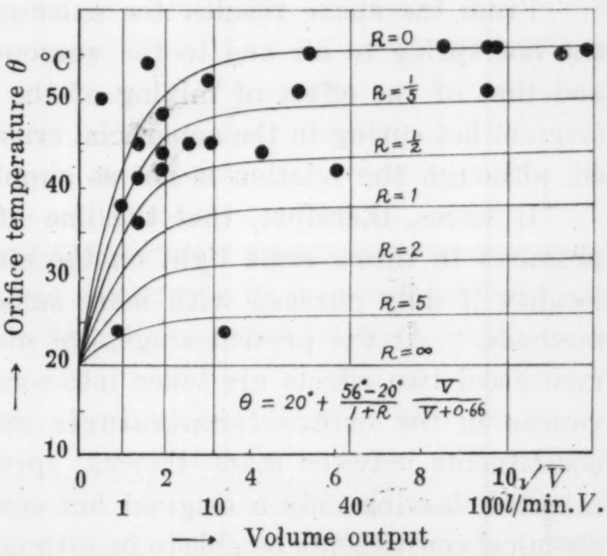

Fig. 7. Relation between orifice temperature of many springs in Rendaizi and the corresponding output. (Points are plotted by the normal scale θ in the oridinate, but by the functional scale $\sqrt{V}$ in the abscissa.)

not so simple as that in a spring. This may be attributed to the fact that the values of R were moderately different for respective springs in a locality, on the contrary that was fairly constant in regard to a spring. It seems, therefore, that the distinguishing phenomena with respect to the positive relation between change in the orifice temperature of a spring and that of volume output may be attributed to the constancy of R.

There are however some exceptions to this phenomena, examples of which are the Kageyu spring[9] in Nagano Prefecture, Unzen-digoku spring[10] in Nagasaki Prefecture, Sakurazima spring[11] in Kagosima Prefecture, the orifice temperatures of which sink after rain-fall. There are also cases in which fall of orifice temperature and increase in the output of hot springs are accompanied by earthquakes as in the Tazawa and Kutukake springs[12] in Nagano Prefecture at the time of the Kwantô earthquake of 1923.

It seems that in such a case the mixing ratio R between the underground water and the original hot spring is moderately variable and becomes temporarily large after rain-fall, or becomes temporarily or permanently large as the result of earthquake motion or crustal deformation accompanied by earthquakes.

VI. Conclusive remarks.

From the above results, the existence of the effect of heat loss of the hot spring to air and to the surrounding earth near the surface and that of the effect of mixing of the underground water with the original hot spring in the superficial crust layer is scarcely to be doubted, although the relation is not so simple as cited above.

It seems, therefore, that the line of investigation here taken up promises to throw some light on the studies of thermal springs in a locality if duly pursued with more sufficient data and more elaborate methods. At the present stage, we may conclude that if the above-mentioned two effects are taken into consideration, the apparent differences in the orifice temperatures and amounts of the chemical constituents between many thermal springs in a locality may be eliminated, leaving only a original hot spring of which temperature and chemical constituents be able to be estimated approximately as following

9) S. KATAOKA, *Glove*, **10** (1923), 179.
10) T. SIGA, "*Umi to Sora*", **5** (1925), 51.
11) S. ATA, *Journal of Geography*, **43** (1931), 504.
12) S. KATAOKA, *lcc. cit.*

for Simogamo; 130°C(?) $>\theta_1>$ 100°C, 16 g/l > Cl-content > 12·5 g/l,
3·5 g/l > Ca-content > 3·0 g/l,
for Rendaizi; $\theta_1=58$°C, Cl-content = 0 18 g/l,
for Simokawazu; $\theta_1>185$°C, Cl-content > 1·20 g/l.

It seems also highly desirable to investigate in future the differences in temperature and chemical properties between these three original hot springs in southern Idu peninsula, distance the distance separating them being only about 10 km.

---

23. 南伊豆，下賀茂・蓮臺寺・下河津３溫泉の物理，化學的性質に就て（第１報）

三井地球物理研究所 福 富 孝 治

最近南伊豆，下賀茂，蓮臺寺，下河津３溫泉の多くの溫泉穿井の採水，測溫を行ひ，主要なる化學成分の分析を行つた．之等の結果と從來研究して來た物理的性質とを簡單に纏めた研究の第１報である．

其概括を述べれば次の樣である．

1. 溫泉湧出溫度 θ は通常氣溫 θ_0 と正の相關 (Fig. 1) を示し，夏は高溫冬は低溫を示す．此關係の説明として湧出口附近に於て空中や地中へ逃去る熱の影響と，地殼の極めて淺所に於て氣溫に近き溫度の地下水が溫泉に混入すると云ふ影響とが考へられたが，夫等の關係は近似的に (4) 式の如く表された．
2. 次に上記３溫泉の各々に就き主要化學成分含有量と湧出溫度との關係を吟味したのに，近似的には直線的關係が認められた (Figs. 2～4)．此の關係の説明として (a) 物質の水に對する溶解度は槪して溶媒の溫度が高い程大であるから湧出量の略々等しい溫泉では，高溫な湧出溫度のもの程未だ飽和に達しない物質の含有成分量は大であると云ふ考と (b) 上に述べた地下水混入の影響とが考へられたが，此場合には (a) の影響は問題にならず，大部分 (b) の影響であるらしい事が判つた．然して其含有量 x と湧出溫度 θ との關係は (6) 式で近似的に表はされた．
3. 下河津溫泉に於ける Cl 含有量と溫度との關係は Cl 含有量 0·50 g/l 以下の溫泉では上に述べた如く直線的關係を示したが，夫より大なる含有量の溫泉では湧出溫度は 100°C 附近に一定し水蒸氣を噴出して所謂沸騰泉の現象を呈す．之等の溫泉の湧出口で採水された Cl 含有量から沸騰直前の溫度が推定されたのに下河津源泉は 185°C 以上の高溫を有すべき事が判つた．
4. 次に下賀茂溫泉に於ては NaCl と $CaCl_2$ とが其の主成分であるが，分析の結果から，之等の含有量の間には極めて簡單な正の相關關係 (Fig. 5) の存在すること，又 CO_3 化合物と Cl 化合物との間には負の相關關係 (Fig. 6) が存在する事が判つた．然して之等の關係は地下水の混入を考へて導かれた (7) 式とよく符號し，NaCl, $CaCl_2$ の如きは地下源溫泉中に含有され，CO_3 化合物等は地下水中に含有される事が確められた．

5. 上記の影響を考慮して溫泉の湧出溫度 θ と湧出量 V との關係を求めたのに (12) 式又は (13) 式が得られた．之と蓮臺寺溫泉の多くの溫泉の溫度，湧出量の測定結果と比較したが (Fig. 7)，地下水と溫泉との混入比 R が溫泉毎に可成り異つて居るので，あまり明瞭な關係を示さない．然して一溫泉に就ては可成り規則正しく變化する事が知られて居て，雨後湧出量の增加に伴つて湧出溫度が上る事はよく知られて居る．又地震時の溫泉變化に於ても湧出量，溫度變化に正の相關のある事は屢々注意されて居る．之は一溫泉に於ては混入比 R が略々一定である事に依るらしい．之等には稀に例外のある事に就ても一言した．

以上に述べた地表附近での熱の逃避の影響と，地下水混入の影響とを考慮すると，一地方の溫泉の湧出溫度や，化學性質の可成りの喰ひ違ひも大體消え去つて，上記の3溫泉に於て各々只一つづゝの源溫泉が得られる．

第2報以下に於ては之等の尙精密な調査と他の物理的性質に就て吟味を行ひ度い．

---

24. 仙臺大年寺山の山崩*

東北帝國大學地質學古生物學教室　田　山　利　三　郎

(昭和11年2月18日發表—昭和11年3月20日受理)

1. 緒　言 (第1圖)

曩日伊達伯爵家の家令豊島氏が本教室を訪れ同家の墓地大年寺山に異樣の山崩が最近に起つた事を知らして來たので筆者は直ちに同氏の案內で昭和 10 年 11 月 22 日にその調査に赴いた. その後再三該地に赴き又その四近をも步き調査に從事した. その結果を錄して將來の參考に資したいと思ふ.

仙臺近傍に於いて山崩の頻出する區域としては古來仙臺梯形臺地と鄕六盆地との間の廣瀨川峽谷地帶 (第1圖斜線區域) が有名であり有史以來山崩を反復し現在に及んでゐる. この地帶は筆者[1] の三瀧撓曲線に沿ふものであり地質時代より地盤運動の激しい地帶である. この區域以外に於いては仙臺近傍には餘り山崩の記錄が無かつた. 從つて今度の山崩の報告は筆者にとつて珍しいものであつた.

大年寺山は仙臺市街地の北西に位置する丘陵であり所謂宮城野撓曲線に沿ふものである. 筆者は嘗て宮城野撓曲は活撓曲であると稱した事がある. それで豊島氏より大年寺山の山崩の報告を受けた時直ちに頭に來たのはこの撓曲運動の活動の一つの表現では無いかとの疑であつた.

2. 地　形 (第2圖)

大年寺丘陵の地形を一瞥するに同丘陵は宮城野海岸平野に面する北東～西南方向の丘陵であり, 上面は3段になつてゐる. 第1段は南部に偏在して 110 m の平均高度を有し, この面上には矩形の塚あり, 標高 120·6 m の三角點が置かれてある. 嘗てこの塚には觀音像があり, その側には開山堂なる寺があつたとのことである. 第1段面は現在も館と呼ばれてゐる處であり, 粟野大膳の茂ケ崎城のあつた處と聞いてゐる. 多くの堤防, 水濠の跡が現存しその當時を偲ばしめるものがある. 第2段は第1段の北東に接して發達し大年寺丘陵上面の大半を占める處である. 第1段, 第2段間の斜

---

*　矢部所員紹介

1)　田山利三郎 「仙臺近傍最近地質時代の地盤運動に就て」 地震研究所彙報 12 (1934), 77～95.

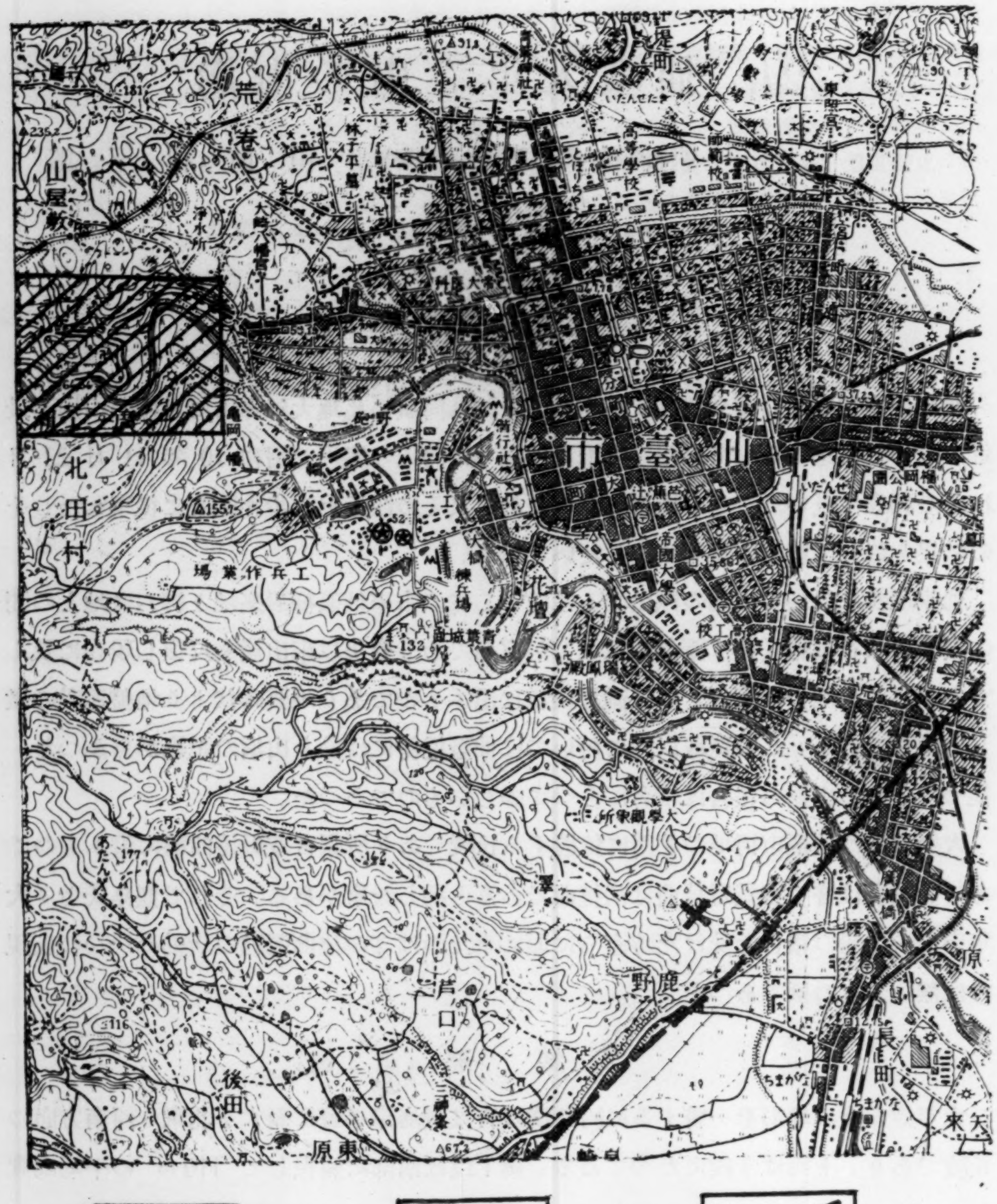

第1圖 (5萬分の1地形圖仙臺の一部)

面は現在竹林として利用され，その下に書扇園がある．第2段面は嘗ては大伽藍大年寺の境内であつた處であるが，明治初年に寺は壊され，今は一部は書扇園，小笠原園の苺園として利用され，一部は建築途中の大年寺の敷地となつてゐる．而してこの面

の北端に近く伊達家十三代の墓地がある．平均高距 100 m.

第3段は大年寺の北西斜面（現在一部は青葉園の苺園として利用されてゐる）と南部の八幡神社のある面であり，90 m の平均高距を有す．

A—愛宕丘陵
B—108·3 m 丘陵
D—大年寺丘陵
M—向山丘陵
K—經ケ峰
1—三角點(120·6m)
2—畫扇園
3—小笠原園
4—大年寺
5—伊達家墓地
6—青葉園
7—八幡社
8—大久保堤
9—愛宕神社
10—名殘川
11—米磨澤
12—黒門下
13—向山療養所
14—宗禪寺
15—愛宕橋
16—富澤橋
17—根岸大竹園
18—門前町
19—福聚院
20—鹿野
21—二ッ澤
22—東洋館
23—鹿落
24—越路
)(—切割
斜線區域—基岩の傾斜せる區域
點區域—山崩

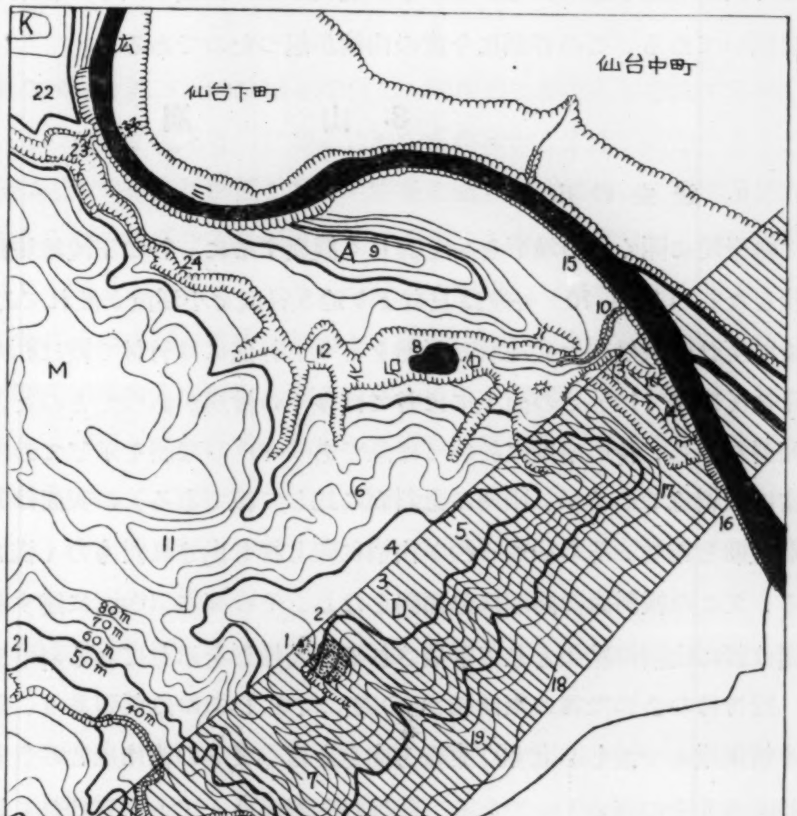

第　2　圖

大年寺丘陵の北斜面は越路の化石谷を距てゝ貫通丘陵なる愛宕丘陵に對してゐる．大年寺，愛宕兩丘陵間の低地帶には廣瀬川本支流の河岸段丘が數段發達し，化石谷底の大久保堤に發源する貧弱なる名殘川はその最下段丘を刻下してゐる．西斜面は平面形に於いてL字狀をなす米磨澤の下流部（南北向の部分）に面し，唯南西部の一部に於いてのみ急斜面を距てゝ向山丘陵に續いてゐる．南斜面は二ツ澤より鹿野に至る廣濶なる谷に面し，これを距てゝ標高 108·8 m の丘陵に對してゐる．東斜面は宮城野原に面し，兩者の接する處に緩斜面あり，一部に於いて扇狀地の如き形を示し，一部に

於いては段丘狀の地形を示してゐる．この緩斜面と海岸平野との境界の處に門前町の聚落があり，此處から第2段面上の大年寺まで石の階段が設けられてある．この階段の北に接して1個，南に3個の必從谷が發達し，何れも横斷面形は V 字狀をなし，深く斜面を刻下してゐる．この中の最大のものは書扇閣下に谷頭を有し福聚院の墓地に開いてゐる．この谷頭に今度の山崩が起つたのである．

3. 山崩

a. 過去の山崩

福聚院に開く谷の地形を少し詳しく觀察するに，谷の下流地域は前述の如く V 字狀をなし（寫眞 10）谷壁は左右より迫り谷底を小溪流が流れてゐる．然るに上流地域に至れば俄然開け盆地狀の形態をとり，谷底には竹林で被はれた舌狀の緩斜面地を見る（寫眞 11）．この面上には嘗ては多くの僧房があつたとのことである．谷壁は急傾斜を示し，特に南壁に於いては急であり 40° の傾斜を示してゐる．舌狀緩斜面（相當に傾斜急であるが，兩側の急斜面に比して緩である）の表面は非常に不規則であり階段狀をなし，その一つ一つが山崩に際し押し出されたものゝ様な外觀を呈してゐる．又この緩斜面の前端は急傾斜をなし，その高さ 10 m に達する．斯の如くこの谷頭は既に山崩の結果として形成される様な地形を示してゐるのである．

觀音像のあつた塚の東側 6 m の處に高さ 1 m の急斜面あり，その方向全く後述する新斷崖と一致し，北 40° 東の方向をとる．又その南にはこの急斜面を切る孤狀の急斜面ありその高さ 1 m である．此等の急斜面は人工とも思はれる節があるが，過去の山崩の崩崖と見るのが妥當である．尚，この谷頭の南斜面には地形圖上に大山崩の跡あり，現在雜木に被覆されてゐるが，一部には新鮮な山崩を見ることが出來る．

尚，大年寺丘陵四近に於ける山崩の個所を地形圖により又實地踏査により檢するに大體次の如きものである．最大のものは大年寺丘陵の北斜面にあり，地形圖では大崩崖を示してゐるが，現在は大部分針葉樹の被覆する處となつてゐる．併しその一部には依然として小規模の山崩あり，岩肌を裸出してゐる．又この東方向山療養所，粟野大膳の墓地，宗禪寺のある丘陵に對する處には數個の山崩が見られ，東端なる大竹園（茶園）側のものは最大である．西斜面に於いては米磨澤の一支谷の谷頭に見られ，東斜面に於いては根岸に一山崩が見られる．又この四近を刻む谷の斜面に多くの山崩の存在してゐることは論を俟たない．

b. 大正 13 年の山崩

豐島氏，八島氏並に伊達家墓地の監理者宮澤氏の語る處によれば關東大地震の翌年

即ち大正 13 年の梅雨の頃書扇園下の前記谷頭に於いて山崩が起つた．併しその時にはその地域が竹林であり人畜に被害無く，民有地（八島氏所有地）であつた爲め，世人の注意を引かなかつた．然るに今度のは伊達家の所有地に起り，且つ仙臺市の風致林になつてゐる處であつたので，伊達家の舊家臣，市當局者の注意を引くに至つたものである．

大正 13 年の山崩の狀態を前三氏の談話を綜合し，現地形を參照して推測するに，大體次の樣である．この山崩が起るまでは標高 120·6 m の塚から東南に突出する小山脚があり，この部分は芝生で被はれ眺望よく，V 字谷を通して宮城野，太平洋を見た姿は書いた扇の樣であるので書扇なる名が出たと言ふ事である（寫眞 10）．小學校兒童の遠足の時此處に足を運ぶもの多く，又外人の好んで散策した處であると聞く．處が大正 13 年の梅雨時にその山脚の大半が崩落し，崖高 6 m の垂直崖が生起した．併しこの大斷崖は一時に出來たものでなく數次の落下によつて完成された事は，始めの間は子供がこの崖から轉落しても怪我が無かつた樣な程度のものであつた等の宮澤氏の談話から推定される．

この時の崩崖は現存し崖面は傾斜を示してゐるが，崩落の當時は殆ど垂直であり，その表面もコンクリートで固めた樣であつたとのことである．現在崖面に接して 1 本の松樹あり，これが伊達家所有地から八島氏所有地に落下して入つて來たものであり，未だに殿樣のものであるとして保存されてをり，當時を偲ぶに好都合である．

崖線は屈曲し，その方向西南部の 2/3 は北 40° 東であり，北東部の 1/3 は東西である．その長さ 40 m，崖面は西南面し，崖高は中央屈曲點に於いて最高 6 m を示し，兩端に行くに從つて減少し單なる割目に移化してゐる．

この時の山崩の特長は垂直移動量より水平移動量の著しく大であつた事である．前記舌狀緩斜面はこの山崩の起る前に既に存在してゐたものであり，その末端は杉の森林により被はれてゐた．然るに山崩の結果として押出した土地は丁度この末端の處に達し，杉木を倒しこれを埋めたとのことである．杉木はその後伐採されたがその切株は殘つてゐる．而してこの押出したのは緩斜面の西南半のみであり，東北半には異狀が無かつた．又崩崖の西南延長上に於いては土地が凹み，山の際の處では反對に膨れ上り押しかぶされる樣になつたとのことである．從つて以上のことから滑動した地域の長さは西南部崖面から緩斜面の末端までの距離で 80 m と算定され，幅は北東部崖面から西南谷壁の際までの距離で測定され 50 m である．而して實際移動した量は山脚の麓に並べてあつた墓碑が，緩斜面の中央部まで移動した事實から 30 m と算定される．この滑動の結果として緩斜面にあつた泉（大年寺の僧侶達は常にこの水を使用

してゐたとのことである）が埋もり，その代り到る處に水が涌出した．併し前の様に良質でなく鐵分を含んでゐたと（現在は1個所，緩斜面の末端に於いてのみ小量涌出してゐる）．この滑動に際しては餘り多く龜裂を生ぜず，墓碑の如きものも倒れずにその儘移動したとのことである．併し少しは生じたのであり，八島氏は人夫を使役してこれを埋めしめたのである．この時龜裂は下底に行くに從つて大きくなつて行くのが看取されたとのことであるが，注意すべき事柄である．

尙，亀裂は既に 20 年前にも生じてをり，L字狀のもの2個あり，それを埋めるのに相當苦心したとのことである．尙，この亀裂の方向も北40°東であり，前記崩崖の方向と一致してゐるのは注意に値する．

c. 昭和 10 年 10 月の山崩（第3圖）

問題の山崩は昭和 10 年 10 月9日の夜，雨後に始まつた．大正 13 年に出來た崩崖の背後 17 m の處，觀音像の塚の緣から 13 m の處に一大裂罅を生じた，その方向は前記過去の崩崖を暗示する急斜面の方向と全く一致してゐるのは注意に値する．又

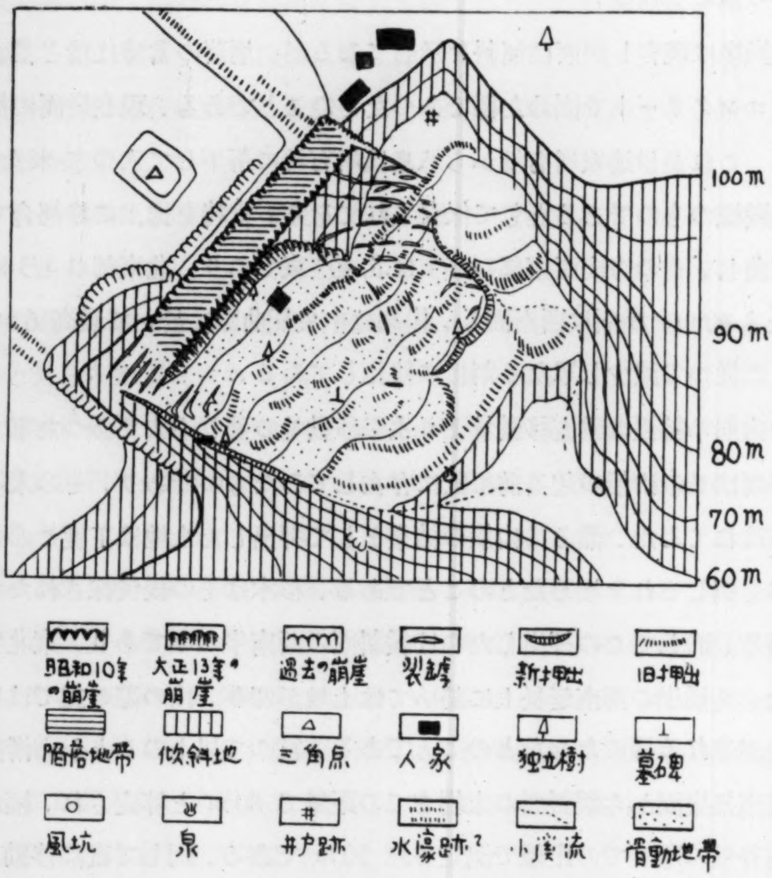

第　3　圖

大正13年の山崩の際に殘つた山脚を今度は完全に横斷してゐることも注意に値する．

この裂罅を生じた爲め大正 13 年の崩崖面は前進し，その結果として崖面から礫を崩落せしめた．この崩崖下 10 m の距離に住んでゐた竹林の番人遠藤氏は危險を感じ逸早く竹林中の安全地帶に避難を餘儀なくされた．この裂罅は日一日と開き，始めは容易に跨ぐことが出來たのが，遂に跨ぐこと不可能になつた位まで開きを增大して行つたとのことである．續いて 10 月 27 日夜，大雨の後に大音響と共に大正 13 年の崩崖の背後から大裂罅との間の地帶が陷沒し，此處に大斷崖を形成するに至つた．

斷崖 — 陷落地帶の西北壁に大斷崖が生じた（寫眞1，2）．これは前の裂罅の一面であり，從つてその方向北 40° 東であることは勿論である．斷崖の長さ 80 m，斷崖は山脚を切斷してゐるので崖面は弧狀をなし，從つて最高崖高は中央部にあり 9 m を示す．崖面は垂直，その中央部に波狀の境界線あり上部は礫層がその儘露出してゐるが，下部は礫層が泥で被覆され，その泥には垂直の無數の條線を見る．これ上半部は 10 月 9 日に出來たもので，その後の雨の爲めに崖面は洗はれたに對し，下半部は 10 月 27 日に生じて未だ十分雨に洗はれてゐない爲めであらう．礫層の礫は或は切斷され，或はその表面に垂直の平行條線を鮮に印じてゐる．寫眞 8，9 に示したのはその一例で，礫は安山岩礫である．斷崖は西南端に於いては崖高を減じ，遂に單なる裂罅に移化してゐる．東北端は過去の崩崖を思はしめる樣な書扇園下の急斜面地に終つてゐる．

陷落地帶の東南壁の崖は西北壁に比し長さに於いて相異ないが，高さに於いて著しく相異し崖高は最大 3 m であり，中央より北に偏在してゐる．この崖と大正 13 年の崩崖とは非常に接近し，而もその崖面の向を反對にしてゐる．西南半に於いては傾いた舊崩崖の中部を切斷してゐるため，上半部は背後に落下して下半部を並列し（寫眞 3），下半部は叉劍の刃の樣になるに至つた（寫眞 4）．北東半にあつては兩崖線は交錯する樣な形になるので，兩者の間に三角錐狀の山脚の殘片を挾む樣な形になつた．

陷落地域 — 前記 2 條の平行崖線間の地帶は陷落して小地溝帶を形成してゐる．中央部は西南崖の崖高小なる爲め地溝形態不鮮明であるが，兩側に於いては鮮明である．地溝帶の幅は中央に於て最も廣く兩側に稍々狹い．最廣 20 m，長さ 80 m．地溝帶內を觀察するに（第 4 圖參照）全地域は多くの小地塊に寸斷されて，多くの裂罅の生じてゐるのを見る．これを少しく注意して觀察すると，この間に何等かの系統のあるのが窺れる．即ち（1）小地塊は大體縱に 3 列に配列してゐる．（2）各小地塊は傾動地塊の形を取つてゐる（寫眞 3）．（3）中央部を橫斷する一弱線あり，その方向は大正 13 年の崖線の北半の方向と全く一致してゐる．この線上の大

斷崖直下の裂罅は崩落當時は容易に跨ぐこと出來たが，我等が最初に調査に行つたときは辛じて跨がれ，更に本年1月に行つたときは全々不可能になる位にまでに開

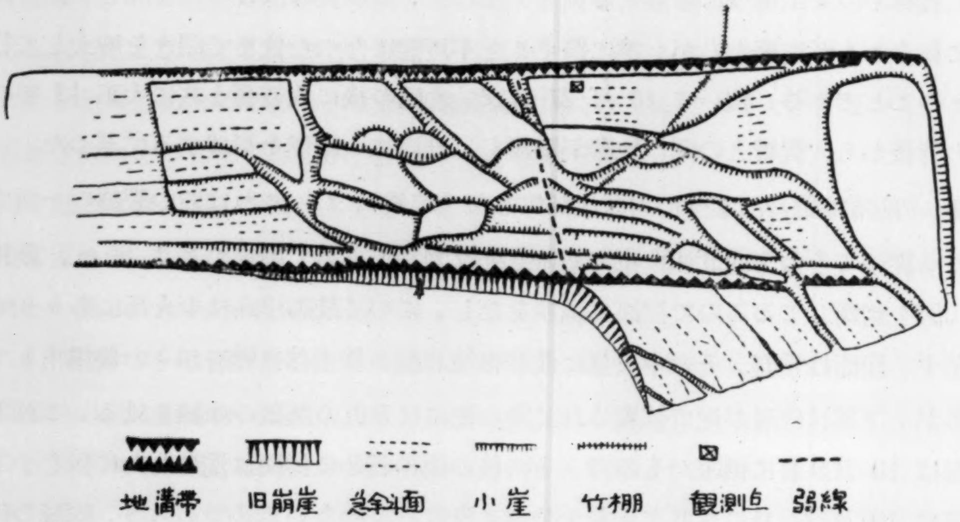

第 4 圖

き，現在も尙擴がる傾向を示してゐる．（4）この弱線を境して傾動地塊の傾きの方向を異にしてゐる．卽ち西側にあるものは東方傾下，東側にあるものは西方傾下を示してゐる．（5）弱線を挾んで高所あり兩側に向つて低下してゐる．卽ち全體として表面はアーチ狀をなすものであるが，この表面が必しも落下前の表面その儘で無いことは大斷崖上の平坦面と比較すれば直ちに了解されることである．

地溝帶に接する大正 13 年の崩崖は宮澤氏の語る處によれば，今度の山崩にあたり大體2間（3 m）前方に進出したとのことである．この事は書扇園の苺畑の畦の移動からも推定される．

滑動地域 — 山崩に際し舌狀緩斜面の大半は滑動を開始した．その範圍は大正 13 年の際の滑動地域に比しその長さに於いて稍々劣るが幅に於いて大である．滑動地域の西北限は大斷崖で示されることは勿論であり，西南限は山麓線を流れる小溪流の位置で示される．東南限は大正 13 年の際の押出の末端を內方に去る 20 m の處，北東限は書扇園下の舊普門院跡から發源する小溪谷で示される．この幅は大斷崖下で最廣を示し 100 m を算し，末端に行くに從つて狹くなつてゐる．長さ卽ち滑り出した方への距離は 75 m と算定される．

實際滑動した量は大正 13 年の場合に比し問題で無く小であり，陷落地帶にて 3 m と推定され，末端に於いては僅に最大1 m と測定されるに過ぎない．特に滑動の著しかつたのは北半の地域であり，大正 13 年の時動かなかつた部分に相當する．

この地帶の末端にあつては地表が盛り上り，階段狀をなし，その高さ 1m に達す (寫眞 7). 此處は山崩の前までは一續きの斜面であり，自由に登り得たものであつたとのことである．この末端部の竹は總て前方に傾き或は倒れ，又地表を蔽ふ芝生は疊み重り，或はそれが破れて表土を崩落してゐる．小溪谷に向つては押被せの形をとり，一部に於いては 1m 前出してゐる．

西南壁の小溪谷の處に於いても押被せの形をとり，これに沿ふ竹，樅は皆山の方に向つて傾いてゐる．併しその程度は前記末端部の如きもので無い．

大正 13 年に生じた崩崖の東延長線上，即ち今度最も多く滑動した地帶の南限にあたり多少の隆起を示した．この事はこの線上に倒れて安定してあつた圓柱狀墓碑が北方に轉落して行つた事實と八島氏の談話から推定される．

裂罅は滑動の甚しかつた北半地帶に多數生じその方向は大斷崖に直角の方向，即ち滑動方向に平行なものであり，雁行配列をなしてゐる．特に普門院跡の平坦地に於いて甚しく平行裂罅 5 條生じ北のものほど大であり，南側が僅に落下してゐる．(寫眞 6). この裂罅は更に三角錐狀の前記切斷山脚に達してをり，山脚の崩壊の遠からざるを示してゐる．この 5 條の主裂罅よりは 2~3 條の副裂罅を雁行的に派生してゐる．

第二に裂罅の多い處は西南隅であり，地溝帶の延長上に於いて北 40° 東の平行裂罅が生じ，その南に接してはL字狀の裂罅が生じてゐる．その方向は大斷崖線と西南壁の小溪谷に平行である．以上の二地域を除いては裂罅は少なく又微小である．

滑動は餘り急激のものでなかつたらしく，この地域中にある墓碑は一基も倒れたものが無く，番小屋も倒れず亀裂も入らず，僅に戸障子が立たなくなつた程度のものであつた．

4. 地　　質

山崩の原因を考察する前に，この四近の地質を一應吟味するのが順序である．仙臺近傍の地質に關しては，東北帝國大學地質學古生物學教室の職員學生により調査され明にされた處であるが，それを最近尾崎博學士が纏めてゐる．以下述べる處のものは同氏の調査とその後の筆者の觀察の結果の概要である．

仙臺近傍の層序は新期層より下記の如きものであり，大年寺丘陵四近に發達するものはその上位層群，即ち中部埋木層以上のものに局限されてゐる．

(1) 吉田段丘礫層(宮城野礫層)
(2) 廣 瀬—名取段丘礫層
(3) 七北田—王城寺段丘礫層
(4) 青葉山段丘礫層
(第四紀)

(5) 上部埋木層
(6) 中部埋木層
(7) 龍 口 層
(8) 下部埋木層
(9) 三瀧安山岩質玄武岩
(10) 佐保山層
(11) 名取川安山岩
(第三紀)

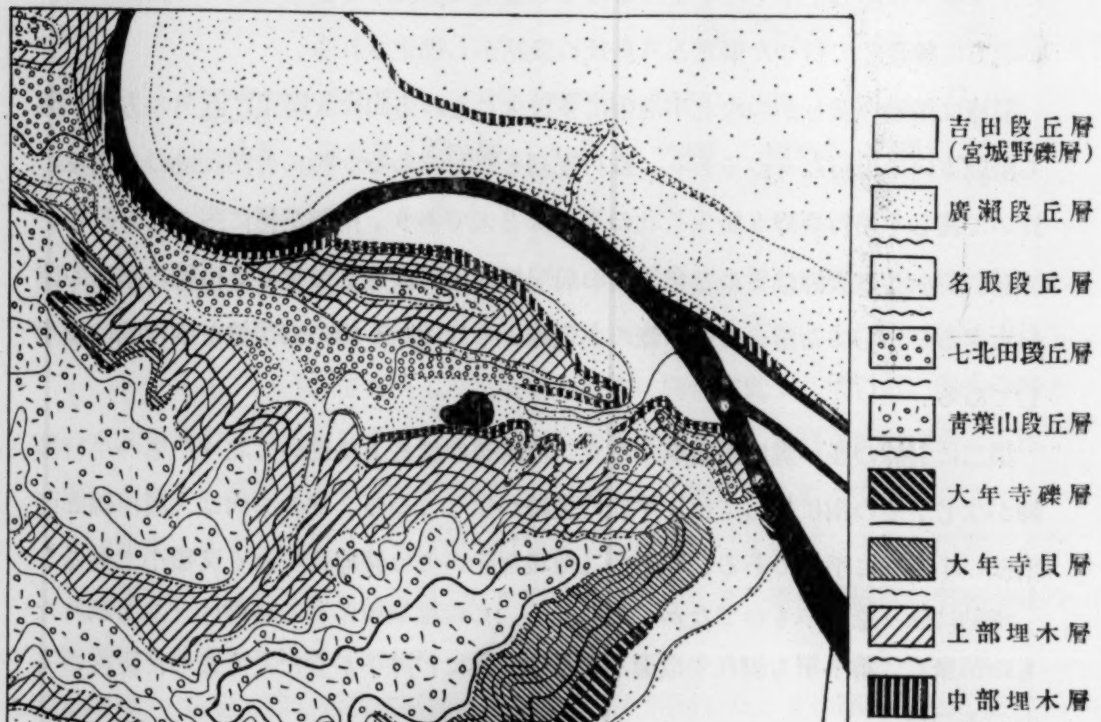

第 5 圖

中部埋木層の最上層に僞層に富む砂層であり，その下に所謂**廣瀬川凝灰岩**が來る．下層は埋木（褐炭）を夾在する砂，頁岩の互層である．本層群は愛宕山丘陵東端並に宗禪寺のある丘陵の切割に良好なる露出を示し，前者にあつては略々水平に近いが，後者にあつては東南に向つて 30° の傾斜を示してゐる（寫眞 12）．

上部埋木層の上層は大年寺礫層，中層は大年寺貝層，下層は埋木層本體（夾炭層）である．**埋木層本體**は最も廣く發達し大年寺丘陵の大半を占める處のものである．本層は埋木（褐炭）を挾む砂，頁岩の互層であり，宗禪寺の處に於いては 20° 東南に向つて傾斜を示すが，大年寺丘陵の西半愛宕丘陵にあつては略々水平である．

大年寺貝層は下部は青黝色，無層理の砂質頁岩であり，貝化石に富んでゐる．一部に於いては外觀龍口貝層と非常な類似を示してゐるが，生物相を異にしてゐる．上部は黄色の砂層であり，僅に化石を含む．本層は大年寺丘陵の前面卽ち東南斜面にのみ知られ東南に 20° の傾斜を示してゐる．又 108·3 m 丘陵の北東端鹿野の處に於ては寫眞 13 に見る如く大年寺貝層は東南に向つて傾斜し，又小斷層を伴つてゐるのが見られる．

大年寺礫層は大年寺丘陵東南斜面の一部を構成するものである．無層理であるが，この中に介在する砂のレンズにより大年寺貝層同樣東南に向つて 20° の傾斜を示してゐることが分る．本層の厚さはその上限が宮城野平原下に沒してゐる故，不明であるが少なくも 30 m を超えてゐる樣である．

青葉山段丘礫層は岩質に於いて大年寺礫層と區別すること困難であり，礫を主體とし砂のレンズを挾む．從來大年寺礫層と青葉山段丘礫層とは同一物と見做され，青葉山礫層なる名稱が與へられてゐたのである．同層は大年寺丘陵より向山丘陵に續く平坦面を被覆し，これが大年寺丘陵の端に於いて撓曲してゐると見られて來たものである．その後尾崎氏の調査により同層には新舊の 2 層あり，古期層は大年寺貝層に常に伴ひ，兩者は親密なる關係にあることが明になり，それに對し大年寺礫層なる名稱が與へられ，又一方新期層は臺地面を廣く蔽ふてゐるのが撓曲してゐないことが明になり，これに對し青葉山段丘礫層なる名稱が與へられた．同層は大年寺丘陵の北部に於いて見るに，一部に於いては大年寺貝層上に載り，一部に於いては上部埋木層本體に直接載つてゐる．

青葉山段丘礫層より新期の段丘礫層も大年寺丘陵四近に發達するが，山崩に直接の關係無い故記載を省く．併し讀者は地質圖によりその分布を知ることが出來るであらう．

大年寺礫層以下の第三紀層は大年寺丘陵の處に於いて撓曲してゐる．撓曲軸の方向

は北40°東であり，大年寺丘陵下の山麓線の方向と一致する．水平層が傾斜層に移化せんとする境界線の位置は，向山療養所より120.6 m の三角點を通り108.3 m 丘陵の頂の稍々東を通過してゐる．この境線より東南部は卽ち撓曲前面に相當するものである．(第2圖斜線部)．

5. 山崩の誘因

山崩を惹起した原因は單一で無いと思ふ．多くの遠因，近因があり，其等の共同の結果が山崩なる一現象を惹起したと見るべきである．今，山崩を誘發せしめたと思はれる諸因を列記して見る．

a. 地形的條件

山崩の地點は向山丘陵より續く一連の丘陵の末端にあり，宮城野海岸平野に急斜面を以て望んでゐる地帶にある．從つて侵蝕の最も效果的に作用する位置にある．

b. 地質的條件

山崩の地點の地質を見るに，舌狀緩斜面下の谷底には上部埋木層本體なる砂と頁岩の互層が露出してをり，走向北60°東，傾斜東に10°を示しこの上に石英粒のみよ

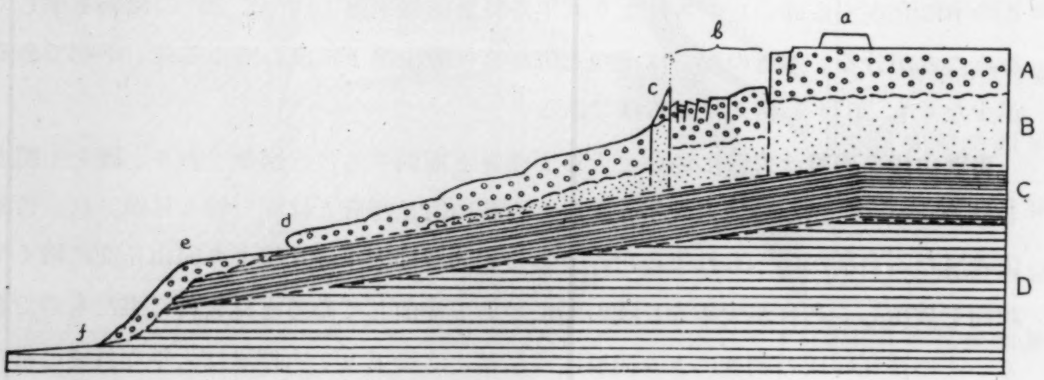

A-礫　B-砂　C-砂質頁岩　D-砂と頁岩の互層　a-塚　b-地溝帶　c-大正 13 年の崖崩　d-滑動地帶の末端　e-大正 13 年の押出の末端　f-谷底

第6圖　想像斷面圖

り成る砂岩が見られ，更にその上に大年寺貝層なる砂質頁岩と黃色砂層とが載つてゐる．最上層は水平なる靑葉山段丘礫層である．山崩の結果出來た斷崖を見るに斷崖の殆ど全部はこの地層より構成され，基底に僅に大年寺貝層の黃色砂層が露出してゐる．又，滑動地帶の東北端小溪谷の處では化石に富む黃色の砂質頁岩が見られる．靑葉山段丘層と大年寺貝層中の黃色砂層は透水層であり，大年寺貝層中の砂質頁岩は不透水層である．而もこの層は10°前後東南に向つて傾斜を示してゐる．こ

の上の地層が滑動するには最も好條件の下にある.

c. **構造的條件**

前述の如く山崩の地點は,撓曲軸に沿ふてゐる.而もこの撓曲運動が今尚,活動してゐるであらうとの暗示を與へる事實は,仙臺市內連場小路の鐵道線路に於いて觀察される.又,宮澤橋畔の石垣のみが崩壞してゐるのは,この運動を暗示するものか.斯の如き構造上不安定の位置にあることは,特に注意の必要がある.

d. **人爲的條件**

山崩の地點下は上部埋木層本體の廣く占有してゐる處であり,數枚の埋木層が夾在し,これは米磨澤と二ツ澤と,門前町の方よりの三方より坑道を掘り採掘され來つた處のものである.舌状緩斜面下の風坑は,此等3坑の共同の風取坑であるのである.山崩の地點下では3坑は連結してゐるので,此處で地盤が緩んで陷落し,今度の山崩を起したと普通人に考へられて來たものである.世人が餘り喧しいので,山崩後坑道に入つて見たが別狀が無かつたと埋木採集業者は言つてゐる.併し證明者が無いのであるから,直ちに信用することは出來ないが,恐らく坑道の存在は直接に山崩に關係無い樣である.

e. **歴史的條件**

今度の山崩に先立つて何回もの山崩がこの地域に起つてゐたことは,地形に又口碑に明であり,從つてこの際に受けた創傷は未だに癒えずにゐたと見られべきである.

f. **氣候的條件**

昭和 10 年は例年に比し,雨量多く特に 8,9 月の候は例外的に多く,全國的に水害の悲慘事を起した事は,記憶の新な處である.10 月に入り雨量は減じたが,東北帝國大學の向山觀測所での記錄を見るに

11〜12 日	33 mm	11〜18 日	17·5 〃	21〜22 日	2·0 〃
13〜14 日	0·4 〃	18〜19 日	1 7 〃	26〜27 日	7·0 〃
15〜16 日	2·6 〃	20〜21 日	0·8 mm	27〜28 日	85·7 〃

となつてをり 27〜28 日に非常に多く雨が降つてゐる.最初に割目が出來,番人が逃げ出したのは 10 月9日で雨の日であると言つてゐるが,觀測所の記錄には無雨となつてゐる.又陷落の起つたのは 10 月 24 日で矢張り雨の日と言つてゐるが,記錄には同樣無雨となつてゐる.併し後者は誰にきいても雨のひどかつた日と言つてゐるから,10 月 27 日の記憶違ひと判定したわけである.

雨量の増大は當然地下水の増大を來たさしめ,不透水層上の透水層は飽和狀態と

なり，岩石の凝集力を減退せしめることゝなり，その結果黄色砂層は相當に多く，湧水と共に流出したことゝ思はれる．又一方不透水層とその上の透水層との間の磨擦力を減退せしめ，滑動に好條件を與へた事と思はれる．

5. 結　言

大年寺の山崩は脇水博士，渡邊貫技師の分類に依れば，山滑（山辷）(Landslip) に屬するものであり，地形的，地質的，構造的，人爲的，歴史的，氣候的諸條件が何れも山崩を誘發するに好狀態にあつた．何れを主とし何れを從とするか，輕々しく決定することは出來ないが，地質的，氣候的條件が主であることは間違の無い處であらう．構造的の條件は花火の點火の役目を演じたものでは無からうか．故寺田博士と宮部學士の研究によれば，山崩は地質構造線上に多く分布してゐるとのことであるが，大年寺の山崩もその一例であることは否定出來ない．

尙，東北帝國大學物理學教室の加藤愛雄理學士は斷崖下に機械を裝置し，地盤の垂直，並に水平運動を觀測中であるから，何れその中發表されることゝ思ふ．

最後に助言を承つた東北帝國大學地質學教室の矢部教授以下の職員諸氏並に調査上便宜を與へられた伊達家の豊島氏，宮澤氏及び八島氏に感謝の意を表す．

(附記) この原稿の締切後又々第3回目の山崩が第2回目と同樣の形式に於いて起つた．これに就いては他日記載する機會があるであらう．

---

24. *Landslide in Dainenzi Hill, Sendai.*

By Risaburô TAYAMA,

Faculty of Science, Tohoku Imperial University.

On October 27, 1935, a landslide, uncommon in this district, took place at a valley-head of the eastern slope of Dainenzi Hill, south of Sendai. A block of earth about 90 m long and 20 m wide sank at the valley head to the maximum depth of 9 m, and another block in front of it, 90 m by 100 m, moved forward about 1 m. The following items may be taken into consideration as suggestive to the probable cause of this landslide.

(1) Meteorological condition.

We had an exceptionally heavy precipitation during September, 1935, and, 85·7 mm rainfall, on the day the landslide took place.

(2) Geological condition.

The upper layer of the ground of this district consists of pervious rocks, sand and gravel, and beneath there is a layer of impervious sandy shale with a dip of 10 degrees to the east.

(3) Tectonic condition.

This district rests on the so called "Miyagino Flexure" which seems to be still active.

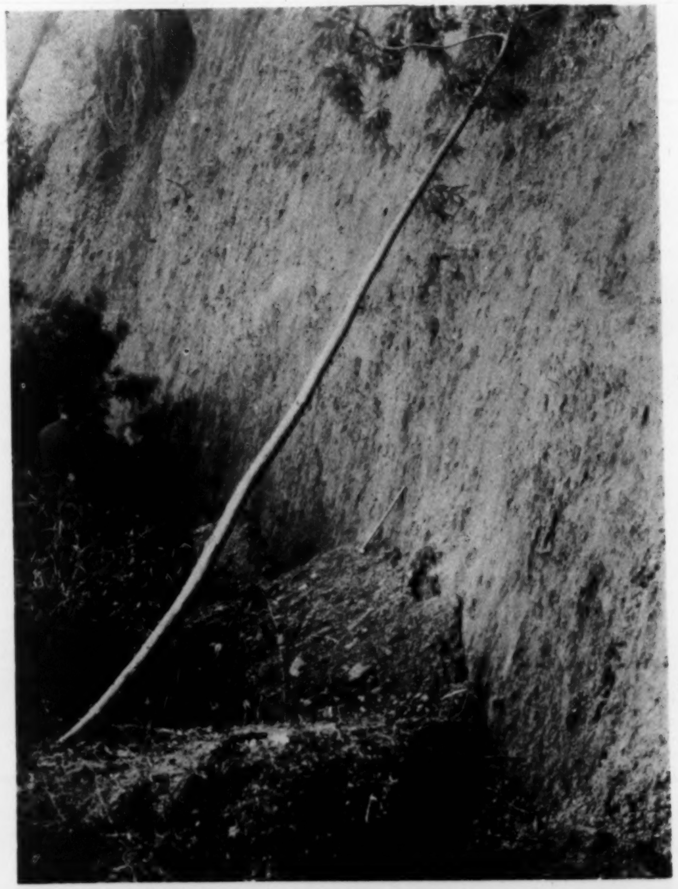

第 7 圖　寫眞 1（崖崩）

第 8 圖　寫眞 2（崖崩）

第 9 圖　寫眞 3 (前には a, b は同一面)

第 10 圖　寫眞 4 (a は大正 13 年の崖崩, b は今度の崩崖)

第 11 圖 寫眞 5 (普門院跡の裂罅)

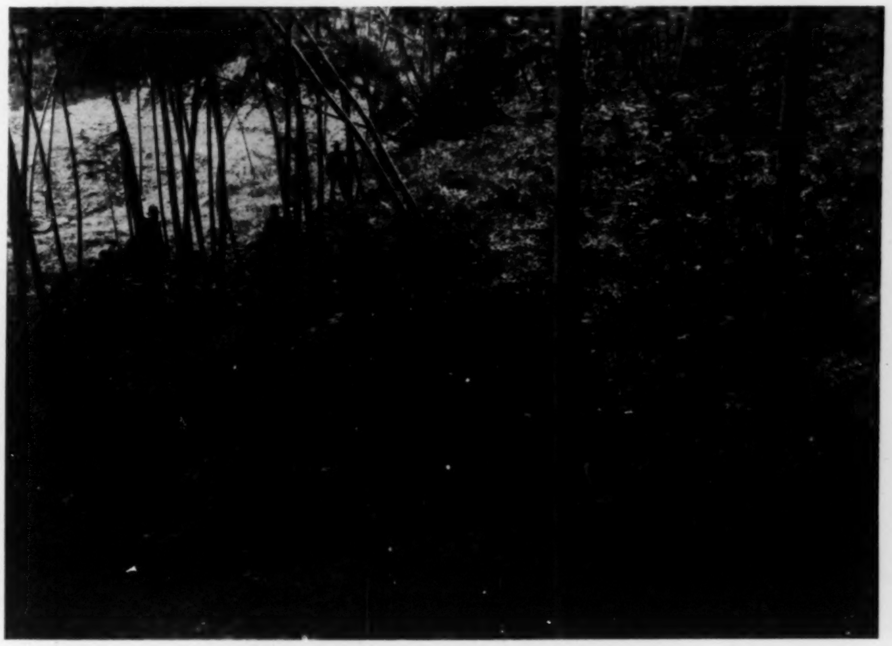

第 12 圖 寫眞 6 (滑動地帶の末端)

第 13 圖 寫眞 7

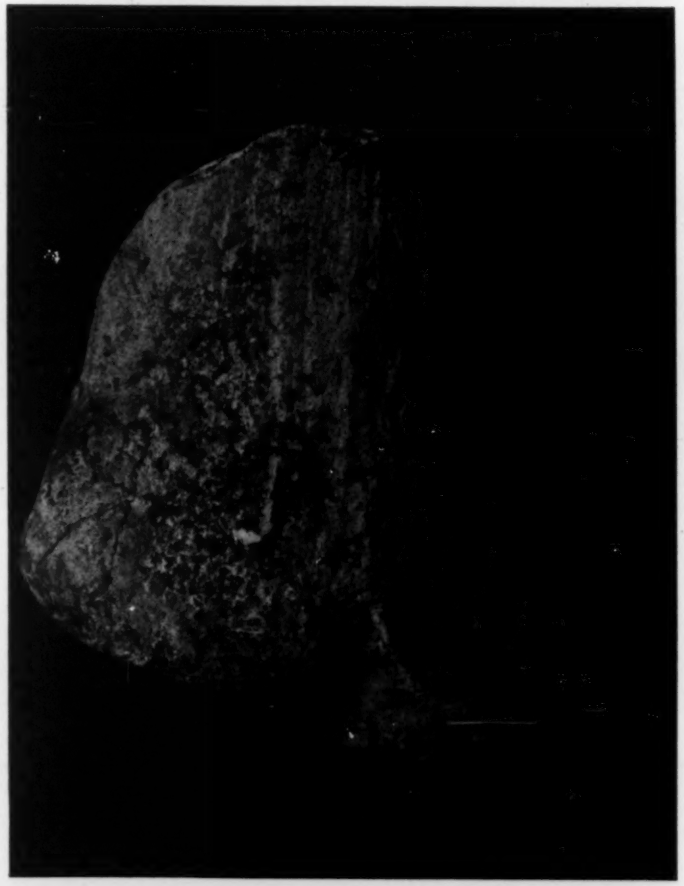

第 14 圖 寫眞 8

第 15 圖 寫眞 9 (V 字谷, a-舌狀緩斜面の末端, b-風坑)

第 16 圖 寫眞 10 (舌狀緩斜面 a は寫眞 10 の a と同一場所)

(震研彙報 第十四號 圖版 田山)

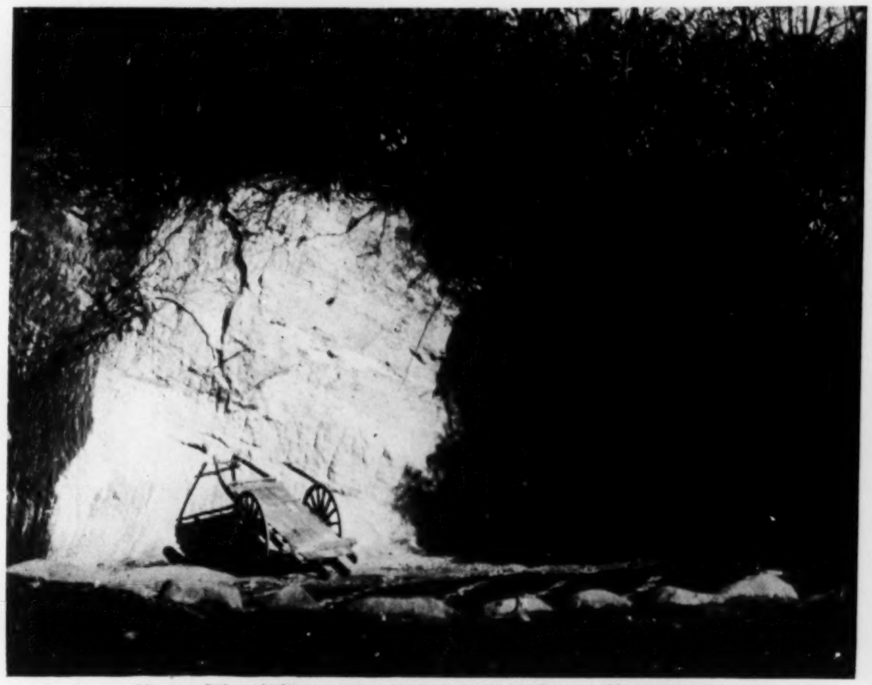

第 17 圖　寫眞 11（上部埋木層の撓曲—療養所裏切割）

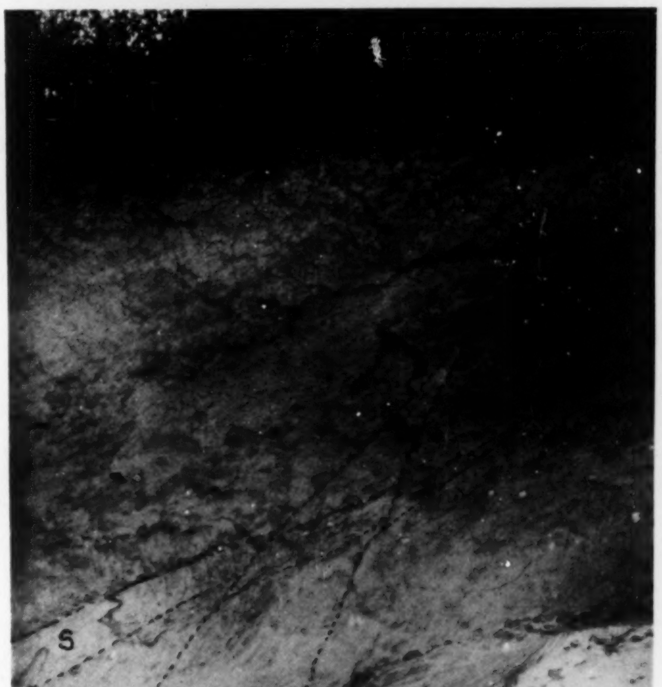

第 18 圖　寫眞 12（大年寺層の撓曲—斷層を伴ふ—鹿野の切割）
s–砂層のレンズ，f–斷層

25. 昭和11年2月21日河内大和強震調査報告

地震研究所 {那須信治
萩原尊禮}

(昭和11年3月17日發表—昭和11年3月20日受理)

緒言 昭和11年2月21日午前10時9分頃近畿地方に於ては稀らしい強震が起つた．大阪市では彼の昭和2年3月7日の丹後地震以來の強い地震であつたため，其後數日間市民を恐怖せしめた．此の地震の震央は中央氣象臺の調査によると東經135°40′，北緯34°30′卽ち二上山南麓であつて震源の深さは約10粁と推定されてゐる．

東京に於ては地震計には記錄されたが人體には何等の感覺を與へなかつた位であるから決して大地震といふ程の地震ではなく震央附近に於ても震度階のV（强震）に相當する强さであつたらう．

强震後直ちに出張を命ぜられ餘震觀測を行つた．又その餘暇を利用して震害の踏査をも行つた．踏査は被害の程度及分布狀態の全般を知るに止めておいた．以下これ等の結果に就いて記す．

震害 震害の外觀に表はるゝものは土塀の崩壞，煉瓦積煙突の龜裂或は上部損傷，堤防の龜裂，壁の龜裂剝落，石燈籠墓石の顚倒等が主である．人命に關するものでは，關西線大和川鐵橋北側王寺町字藤井で石材採掘中の人夫十數名は山崩れのため負傷し內1名は死亡した．又大阪市西淀川區大和田に於て煙突修繕中の工夫3名は地震のため振落されて死亡した．大阪市內に於ては壁に僅か龜裂を生ずる程度で震度はIV（强震弱き方）に相當すると思はれるが奈良盆地の西部及び大阪府の東部に於て震央に近いところに主として上述の如き被害が見られた．

震度分布 震度階のVに相當する地震，卽ち强震の際生ずる被害には壁の龜裂，石碑石燈籠の顚倒，煙突の破損等が普通に擧げられてゐる（例へば大日本氣象學會編纂の氣象常用表を見よ）．此の震度に相當する地震の强さであつた範圍を求めて見ると次の樣である．

（a） 强震區域の東北部は少くも郡山町の東端に達してゐる．郡山町に於ては東奈良口の石垣（高さ約2米，30×20×20 糎位の石を築いたもの）の崩壞あり，神社の

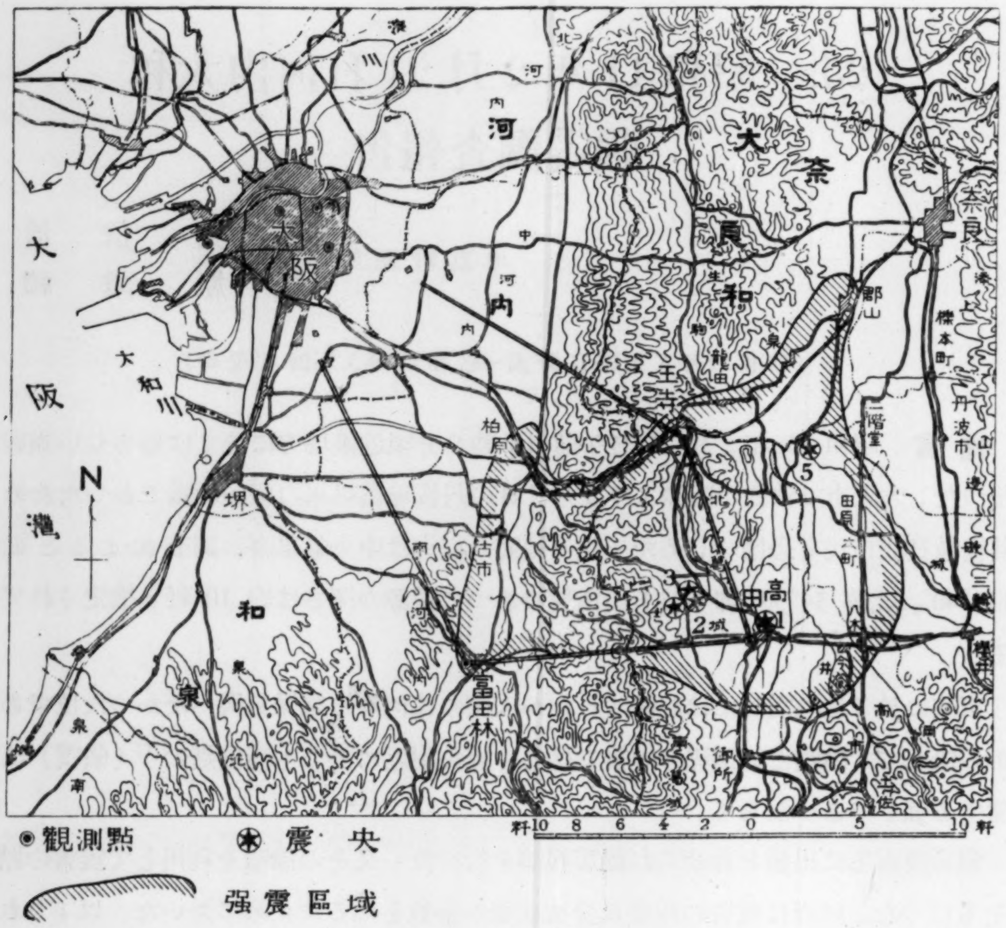

第 1 圖

石燈籠の顚倒，家屋の壁には可成りの破損を生じてゐる．

（b） 東部に於ては二階堂村附近に達してゐるであらう．二階堂村の西方約2粁川西村字梅戸に於ては膠工場の煉瓦積煙突（高さ 20 米，基部の徑約 2·5 米）の上部は震動のため振落されて缺損してゐる．

（c） 東南部に於ては八木町附近までは此の震度に相當する强さであつた．八木測候所に於ては扉の板が剝れたが櫻井町に於てはこれ程の被害はなかつた．

（d） 南部に於ては御所町附近迄であらう．同町附近の葛城川堤防には諸所に龜裂，又家屋には僅かに龜裂を生ずる程度で高田町に比較すると震動は遙に弱かつたことがわかる．

（e） 大阪府側に於ては柏原，古市，富田林に亘る範圍に於ては强震（V）に相當する．柏原に於ては土藏，壁等の損傷，大和川に沿ふアスフアルト道路の龜裂及び家屋半壞程度等の被害があり，大阪府側に於て被害の最も著しいところである．又古市に於ては壁の龜裂，石燈籠の顚倒，鳥居の破損等の被害があり，附近の譽田では小學

校の土塀の崩壊，八幡宮境内の土塀倒壊等の被害があつた．富田林に於て最も目立つ被害は工場の煉瓦煙突の上部缺損落下したものである．

（f） 北部に於ては大和川までゞあつたらう，こゝには前述の石材採掘場の被害があつたが昭和7年に地ごりのあつた峠部落には今回は何等見るべき異變はない．

以上の様な被害は何れも震度 V に擧げられるものであるから，これに對する分布を求めて見ると大體第1圖に示す通りになる．

餘震觀測　今回の地震の餘震は八木測候所の調査によると强震後 24 時間內に有感無感のものを合して 77 回，内 22 回は有感であつた．それから以後は急激に減少した．此の程度の回數は他の地震の場合に比較して決して多いとは言ひ得られない．今回筆者等によつて行はれた觀測の結果震源の決定されたものは僅かに5箇に過ぎなかつたのも一つは餘震が少なかつたためである．

2月 22 日午前2時より大阪市內船場（東區備後町五丁目二十五番地）に携帶加速度地震計を設置して觀測を開始し，同日午後には府下富田林高等女學校內に携帶變位地震計，23 日には奈良縣王寺小學校，24 日には同高田高等女學校內に，夫れ夫れ變位地震計を設置して觀測を行つた．

今回の地震觀測では大阪市內の土地の固有振動を測定する計畫もあつたので加速度地震計2臺を1箇所1臺宛として上記船場の外大手前，高津，市岡，野田へも逐次設置した．

震源の測定　これには從來と同樣初期微動繼續時間を用ひた．そして4點觀測が可能であつた場合には，公式，$D = kt$，の距離係數 k を求めた．玆に D は震源距離（粁），t は初期微動繼續時間（秒）である．

今回の觀測では3回の地震に就いて k の値を求めることが出來た．而して k の値は何れも 6·15 に極めて近く平均 6·15 となつた（第Ⅰ表A）．それ故に3點觀測によつて震源を求める場合には

$$D = 6{\cdot}15\,t$$

の公式を用ひることゝした．

餘震の分布　餘震の震源決定されたものが僅か5箇であるために立體分布を議論するには不十分であるがこれ等の地震は第Ⅰ表に示してある樣に何れも 10 粁以內の淺いところに起つてゐる（第Ⅰ表A）．震央の分布を見るに二上山附近に3箇，高田町附近に1箇，奈良盆地の略中央に1箇あることがわかる．而して諸種の情報を綜合して推察するに，强震後に起つた數十回の餘震は多くは二上山附近に震央を有するものであつたらう．その後餘震の活動範圍は二上山附近を中心として稍廣くなつたらし

く，高田町附近及び奈良盆地中央の餘震も誘發的に起されたものであらうと考へられるが此等の點を明かにすることの出來ないのは遺憾である．

終りに臨み今回の出張觀測に多大の便宜と援助を與へられた方々に謝意を表す．

第 I 表 河内大和强震餘震觀測表

(A)

番號	發震時	初期微動繼續時間								震源の深さ	*k*
		船津	大手前	市岡	野田	高津	王寺	高田	富田林		
	月 日 時 分	秒	秒	秒	秒	秒	秒	秒	秒	粁	
1	2 24 2 06	4·90					1·80		2·50	6·2	
2	〃 25 3 34		4·25				1·75		2·16	7·8	
3	〃 26 18 58		4·20	4·65			1·73	1·45	2·16	8·0	6·16
4	〃 27 12 10		4·26	4·65			1·90	1·54	2·15	8·5	6·14
5	3 3 3 07				4·90	4·05	1·40	1·80		6·4	6·15

(B)

番號	發震時	最大加速度					最大振幅		
		船場	大手前	市岡	野田	高津	王寺	高田	富田林
	月 日 時 分	gal	gal	gal	gal	gal	μ	μ	μ
1	2 24 2 06	2·75					56		154
2	〃 25 3 34		0·05				47		20
3	〃 26 18 58		2·60	0·46			12	37	27
4	〃 27 12 10		4·70	1·15			58	108	80
5	3 3 3 07				3·00	9·35	284	418	

25. *The Kawati-Yamato Earthquake of February 21st, 1936.*

By Nobuji NASU and Takahiro HAGIWARA,

Earthquake Research Institute.

The earthquake which shook Osaka and the surrounding country on Feb. 21st, 1936, has, from the point of view of the damage caused thereby, to be accounted the severest earthquake which has visited the central Japan since the destructive Tango earthquake of 1927. Although the intensity of the shock was not so great within the epicentral area it caused great panic among the citizen of Osaka. It is clear that the shock did not reach an intensity comparable to that experienced in some of the earthquakes that have affected Japan, notably the Kwantō, Tango, Idu earthquakes. The intensity has been estimated to be V on the intensity scale generally used in Japan, the second figure on that scale. In Fig. 1 the area over which the shock reached this intensity is shown by shaded boundary.

It is reported that 77 aftershocks were recorded during the first 24 hours after the earthquake, of which 22 were sensible. But, the aftershocks rapidly decreased in number from the next 24 hours.

The observations of the aftershocks were begun on Feb. 22 at 2 A. M. Three portable seismographs and two acceleration seismographs were installed at the stations as shown in Fig. 1. In Osaka the acceleration seismographs were installed at two places for the purpose of the simultaneous observation. After one or two earthquakes were recorded at these stations the instruments were installed at other places. In doing so the observations were made at five stations.

In five aftershocks which occurred in two weeks following the big earthquake, the positions of the seismic foci could be determined Fig. 1. The focal depths of these shocks were less than 10 km. The constant factor, k, in the formula, $D=kt$, which is used in computing the focal distance, D (in km), by means of the duration of the preliminary tremors, t (in sec.), has been determined with result that it takes a value 6·15 in the case of the present earthquakes.

26.　大阪市内に於ける土地の固有振動の測定

地震研究所　那須信治
　　　　　　萩原尊禮

(昭和11年3月17日發表――昭和11年3月17日受理)

緒　言

昭和 11 年2月 21 日河内大和强震は大阪市にとつては稀らしく大きな地震であつた．この强震の後數日間は市内に於ても日々數回の地震を感じた．今回此等の餘震の震源決定のため觀測網を張るに際し，大阪市内に觀測點の1點を設置して震源の決定にも又市内に於ける土地の固有振動の測定にも資せんと試みた．言ふまでもなく大阪は大都市であるから，震害對策上にも今回の如き土地の固有振動の測定が有意義であることは疑はない．從來大阪市内に於ける土地の震動習性に關する文獻の甚だ少いことを遺憾に思つてゐた矢先に今回の如き餘震が連續發生したので，此の機會に測定を行へば效果的であると考へたのである．然るに餘震は別記[1]報告中に述べてある樣に甚だ回數が少く從つて十分なる測定結果を擧げることが出來なかつた．それ故に此の報告は將來の研究に對する Preliminary Report に止めておく．

今回使用せる加速度地震計

今回大阪市内に於ける地震觀測に使用せる加速度地震計は概略の構造に於ては石本博士の加速度地震計[2]と大差は無いが特

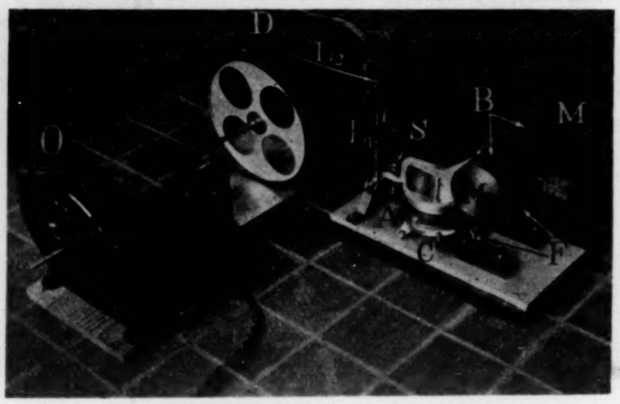

第1圖　携帶用加速度地震計
Portable acceleration seismograph.
M bob of pendulum, F flat spring, B metallic band, A air damper, C cock, S cramp, L_1, L_2 magnifying lever, D drum, O synchronous motor.

1) 那須・萩原「昭和11年2月21日河内大和强震調査報告」地震研究所彙報 14 (1936), 285.
2) 石本巳四雄「加速度地震計及び其の記象」地震研究所彙報 9 (1931), 316.

に出張觀測を目的とし，携帶に簡便なることを主眼として設計せられたことを特徵としてゐる．第1圖に示す如く振子は二つの板バネ（F）に依り逆立し，其の固有振動週期は約0.1秒である．Aはアルミニューム製ピストン型制振器であつて，ピストンの間隙は約0.1mmであるが，別にコック(C)を有し之を加減することに依り振子に加はる制振力を適宜な値に調節することが出來る．振子の運動は二つの槓杆(L_1，L_2)に依り擴大せられ幾何倍率は約100である．ドラム(D)は直徑20cm，100Vシンクロナスモートル（O）に依り廻轉せられる．モートルの廻轉はウオームギヤに依り2段に遞下され，交流の周波數60に對してドラムは8分20秒に1回轉する樣になつてゐる．從つて記錄紙の進行速度は每秒約1.25mmとなる．運搬に際しては螺子（R）に依り振子をクランプし，眞鍮製の帶(B)をゆるめて重錘(M)を振子から分離することが出來る．從つて器械それ自身は極めて輕量となるから携帶にも容易であるし，器械の調整に變化を來たす憂もない．第2圖は運搬に際して器械を取纏めたところを示す．尙今回使用せる加速度地震計は都合2臺であるが，其の固有週期及び感度は次に示す通りである．

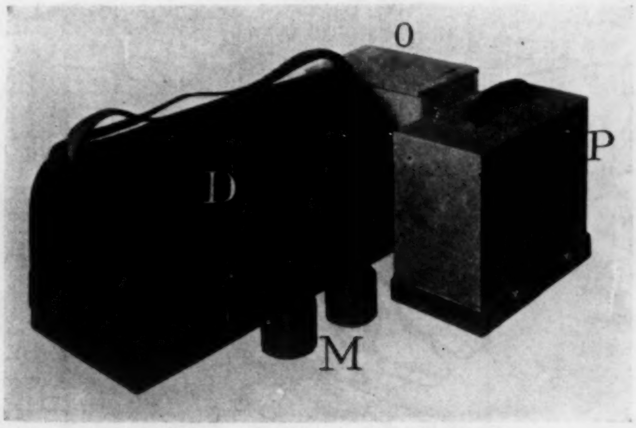

第2圖　同上（運搬に際し取纏めた所）
Portable acceleration seismograph kept in cases.
P seismograph, M bob of pendulum,
D drum, O syrchronous moter.

	固有週期	感度（記錄紙上1mmの振れに相當する加速度）
No. 1	0·13 sec.	2·2 gal
No. 2	0·14 sec.	2·6 gal

振子の制振狀態は何れも極限制振に近い狀態に置いた．

觀測結果

今回大阪市內に於て觀測を行つた場所は高津（高津中學校），大手前（大手前高等女學校），船場(東區備後町5丁目)，市岡（市岡高等女學校），及び野田(長谷川鐵工場)の合計5ヶ所である（第3圖參照）．第5圖に是等の觀測點で得られた加速度地震記象の代表的のものを掲げてある．

第3圖 大阪市地形圖
Map of Osaka.

是等の地震記象より地震動の卓越週期を決定したのであるが，其の方法は從來卓越週期決定に屢々行はれて來た方法を採つたのであつて，記象を寫眞に依り實物の約10倍に引伸したものから振動の週期を一つ一つ讀取り橫軸に週期を，縱軸に其の週期の頻度を記入し，頻度の極大を示す週期を以て卓越週期と定めたのである．週期の讀取方法は記象上に零線を假定し，之を振動の曲線が同一方向に過る點を求め，相隣る此の如き點の間の時間を以て其の時の週期とした．週期の讀取は主要動の始めから開始して尾部に至る約 10 秒乃至 20 秒で讀取れるだけは讀取る方針とした．第4圖は此の樣にして求められた市內5ケ所の地震動週期の頻度曲線を示す．之を見るに上町と呼ばれてゐる大阪の高臺を代表する大手前，高津に於ては何れも週期 0·15 秒附近に

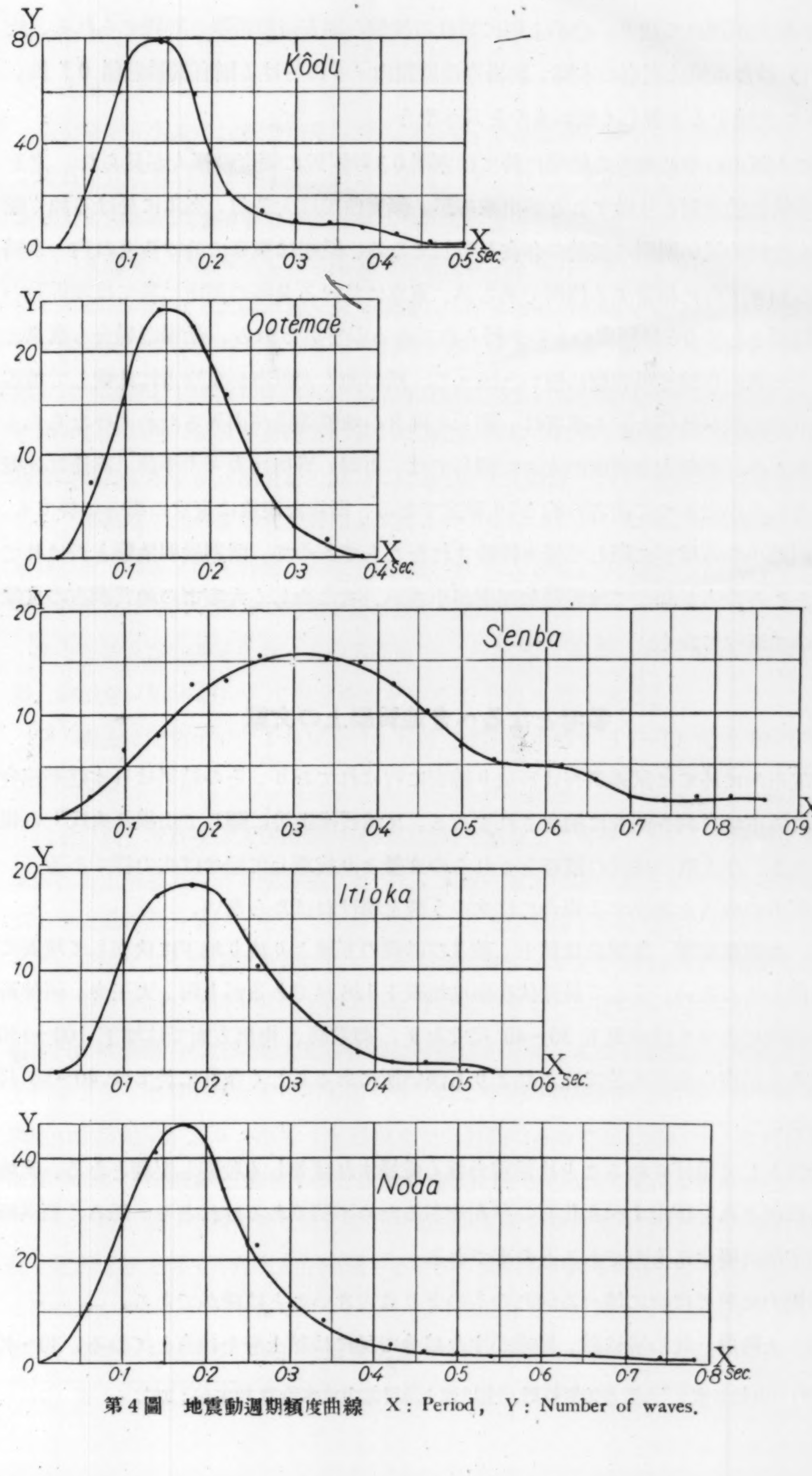

第4圖　地震動週期頻度曲線　X : Period,　Y : Number of waves.

頻度の極大が現れて居り，之が上町に於ける地盤の固有振動週期と解釋せられる．此の 0·15 秒なる値は東京の本郷，駒場等の所謂山ノ手に於ける固有振動週期 0·3 秒，0·2 秒に比較すると著しく短いものと云へやう．

次に大阪市の中心地たる船場に於ては週期 0·3 秒附近に頻度の極大が見られ　之を以て卓越振動週期と見做すことが出來るが，頻度曲線は大手前，高津に於ける如く鋭くなく比較的長い週期の振動の存在を示してゐる．船場は東京に於ける丸の内，京橋方面の如き下町に相當する箇所であるが，東京に於ける是等の箇所に於ては地震動の卓越週期として 0·6 秒程度のものが得られてゐるのであるから，船場の場合も東京と對比して其の卓越振動週期は短いと云へる．斯の如く大阪市が東京市に比較して地震動の卓越週期が短いと云ふ事實は，概して兩者の地盤構造が相異るために外ならぬものであらう．尚最大加速度の大さに關しては，市岡，野田は夫々大手前，高津に比較して著しく小であつて前者の約 3/10 程度である．斯様な現象は東京の場合に於ても，震源距離小なる地震に際して屢々經驗されたことであつて，所謂軟弱地盤と云はれてゐるところの方が却つて地震動加速度が小さい．次に少しく大阪市の地質調査の文獻に就いて述べておく．

参考となるべき地質學上の文獻

大阪市内に於ては試錐調査は可成り綿密に行はれており，その結果は日本建築協會發行大阪市地質調査圖表に網羅されてゐる．又地質構造等に關して山根新次氏[3] の報告がある．今大阪の地質の概略をこれらの文獻より抜萃して記せば次の様である．

大阪市の地質を考察する場合には次の5層を擧げねばならない．

1） **大阪基盤層**　基盤層は粘土，砂及び砂礫の互層より成り地下に伏在して地表には露出してゐない．そして最深伏在面は地表下 128 尺であるが上町，天王寺，阿部野等の臺地にあつては地表下 30~40 尺であり，御堂筋，梅田方面では地下 100~130 尺であるが市の南部に於てはこれよりも淺い所にあるらしく今宮に於ては 40~58 尺である．

性質として擧げられることは粘着力強く乾燥すれば著しく收縮し堅硬となる．又地質年代はこれを確定すべき化石の存在せざるため不明であるけれども，恐らく舊洪積層の下部に屬するものであるとの事である．

耐壓力に於ては次に述べる何れのものよりは大きいことは確かである．

2） **上町層**　此の層は砂，砂礫が主な成分で稀には粘土層を挾有してゐる．30~40

3） 山根新次「大阪市地質概觀」小川博士還暦記念地學論叢 (1930); 187.

尺の層厚を有して直接大阪基盤層を覆ふ．而して此の層は上町より天王寺，阿部野に亘る臺地に分布してゐる．

上町層と基盤層の比較の結果は詳かではないが基盤層の優ることは明かである．

地質年代は舊洪積層の下部に相當するとの事であり，又海棲生物遺殼がこの層內に缺如してゐるため陸成層であると考へられてゐる．

3）**天滿層**　平地區域に於て基盤層を直接覆ふ層は此の層である．然し地表面に露出してゐる所はなく天滿に於て最も發達して厚さ 92 尺に達してゐる．上町層に比較して後期に生成されたものであつて上町方面にはなく天滿，船場，島の內，難波，木津に亘つて著しく木津川以西に於ては厚さは減少す．此の層は砂及び砂礫層で粘土層を挾有しその內の砂及び砂礫層に就いて基盤層中のそれ等と耐壓力の比較をすると略同等の結果を示すが，粘土層に就いては基盤層：天滿層＝2：1 で此の層は軟弱である．

4）**梅田層**　此の層は天滿層の上位にあつて最厚 81 尺，梅田より木津東岸に亘る地帶の西方地域に於て發達して厚さは 64～81 尺である．又天滿，御堂筋より今宮方面での厚さは 30 尺內外で沖積新層に屬してゐる．

層中の砂及び砂礫層に就いての天滿層中のそれ等と耐壓力比較試驗の結果は天滿層：梅田層＝1·5～2·0：1 で粘土層に就いては 1·5：1 位である．

5）**表土**は同市に於て 1 尺以上 10 尺位で埋立地に於て 3.5～13 尺で 19 尺を最厚としてゐる．

以上の如き地質構造及び耐壓力試驗の結果を綜合して考察するに，高津及び大手前は何れも上町層上にある觀測點であつて，大阪に於て地盤の最良といはれる地域にあつて地震動週期も短い．そしてこの 2 地點に於ては略同じ卓越週期が存在してゐる．これに比較すると船場は上部に於ては所謂梅田層があり又その下には天滿層もある．そして上町方面と比較すれば上部の地層は軟弱であることは明かであるが，これ等の地層內には耐壓力の比較的大なる砂或は砂礫層が介在してゐる關係上，所によつては上町層よりも地盤堅硬なところもあらう．但し今回の觀測點たる船場に於ては 0·3 秒程度の卓越週期があり，而も 1·0 秒位までの波動のあることを認めた．これは東京，橫濱等に於ける經驗[4]と對照すると稍軟弱地盤に於て見られる型式である．

されど野田及び市岡に於ては比較的卓越週期が短いのは案外であつた．これ等は何れも軟弱地盤と考へられてゐた地域であるが，表面層中にも耐壓力が相當大なる砂或は砂礫層が所々介在してゐるとすれば，假令基盤層までは深くても基盤層が淺い場合と同じ結果にもならう．又此の觀測によつて得られた 0·2 秒程度の震動が表面層の第

4）石本巳四雄「東京橫濱市內10個所における地震動加速度觀測」震研彙報 **13**(1935), 592.

三次振動であり，基本振動は06秒程度のものであるとする考へ方もあらうが，それにしては06秒程度の波動が豫期以上に少い.

要するに地盤振動と地質との關係を論ずる場合には，層の彈性及び厚さが問題となり地質の年代等はさ程考慮すべきではなく，前にも述べた耐壓力試驗等を各層の各部に於て施行した後でなければ，判然たる關係を見出すことは不可能である．それ故に現在に於ては何等明かな關係は見出されない．この點は將來の研究に委ねる.

終りに臨み此の測定に對し援助を與へられたる方々に厚く謝意を表す.

---

26. Determination of the Proper Periods of the Ground in Osaka.

By Nobuji NASU and Takahiro HAGIWARA.

Earthquake Research Institute.

During a period of about two weeks following the strong earthquake of Feb. 21st, 1936, the aftershocks were observed at five temporary stations in Osaka for the purpose of determining the proper period of the ground. In this work two portable acceleration seismographs were used (Figs. 1, 2).

The most frequent period at Kôdu and Ootemae, stations in the upper town, was 0·15 sec., while at Itioka and Noda, stations lying in the lower town, it was about 0·2 sec. At the centre of the city, i.e., at Senba the proper period of the ground was 0 3 sec. Frequency curves of the period at these stations are shown in Fig. 4.

In interpreting the results, geological structure of the city has been taken into consideration.

 [Bull. Earthq. Res. Inst., Vol. XIV, Pl. XV.]

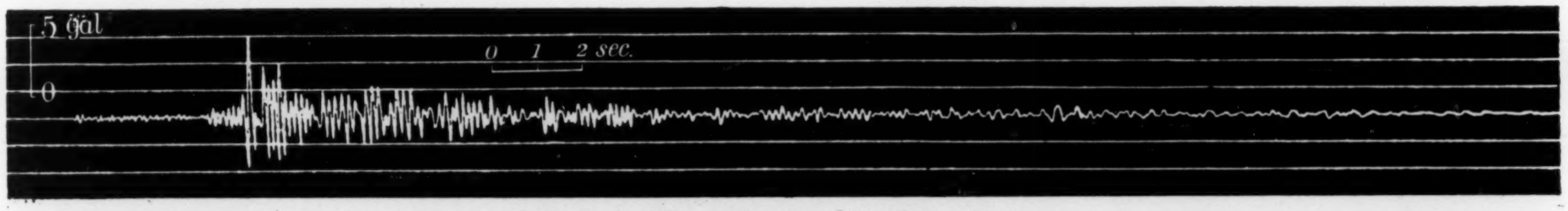

高津 Kôdu (The earthquake of March 3, 1936).

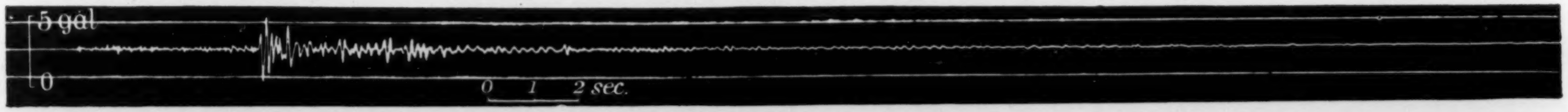

大手前 Ootemae (The earthquake of February 27, 1936).

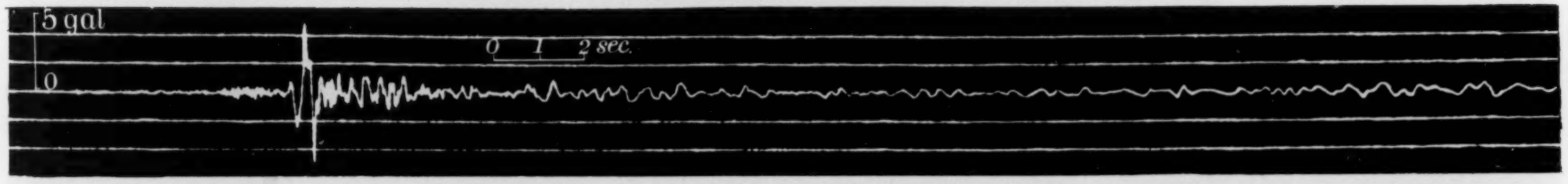

船場 Senba (The earthquake of February 24, 1936).

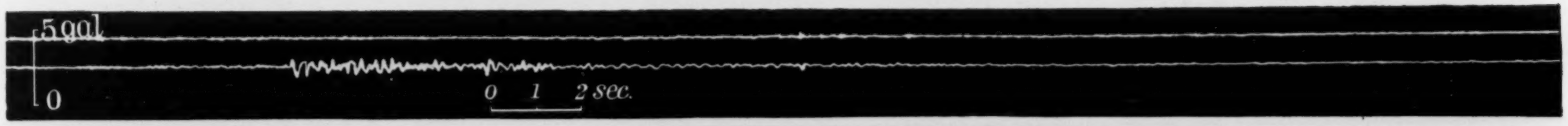

市岡 Itioka (The earthquake of February 27, 1936).

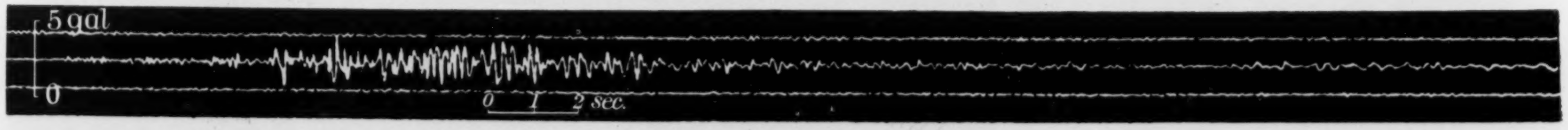

野田 Noda (The earthquake of March 3, 1936).

第 5 圖 加速度地震記象

Acceleration seismograms.

(震研彙報 第十四號 圖版 那須・萩原)

27. 昭和11年2月21日河内大和強震に關する調査報告

地震研究所　宮　部　直　巳

（昭和11年3月17日發表――昭和11年3月20日受理）

昭和11年2月21日，大阪府と奈良縣との境界上の二上山附近に震央を有する強震が起つて，大阪，奈良の兩府縣下に幾分かの被害を與へた．

この地震に伴つて氣付かれた 2～3 の現象に就いて，踏査，及び各地に問合せて得た所の回答によつて調査した結果を述べたい．

この地震に限らず多くの場合地震に伴つて認められる現象であるけれどもこの地震に於いても

（1） 地震に伴つた音響

（2） 井水位の變化

（3） 發光現象

等が認められてゐる．

以下是等の項目に就いて稍々詳細に敍述したいと思ふ．

1. 地震に伴つた音響

地震に伴ふ音響は，地震動の直前に聞えるものである．この音響の繼續時間に就いて，1～2 秒といふ報告があるが，地震時の心理狀態を考慮すれば必ずしも信ずべきものであるか否か幾分疑問を持たざるを得ない．

音響の種類も亦雜多である．而して，其等の音響の中には，所謂地震に伴へる音響ではなく，地震の爲に家具等が踊り或は振動して種々雜多の音を生じ，其等の音が重り合つて一種の騷音として聞えたと思はれるやうなものもある．併し是等の音は除いたとしても，地鳴と稱すべきものゝ各地で聞えた事は事實であるらしく，音の種類も大體に於いて2種類に分けられるやうである．

その1は，「ドーン」といふ音，「大砲を擊つた時のやうな音」，「大太鼓を打つたやうな音」といふやうな言葉で言ひ表はされ報告されてゐる所の單一な打擊性の音である．この種の音は多くの場合，唯1發で，後に直に急激な地震動が續いてゐる．例外

と思はれる1例は，大阪府南河内郡古市町譽田八幡に於いて聞かれた音で，ドーン，ドーン，ドーン，と，大太鼓を打ちならす様な音が 3~4 發聞えて後地震動を感じたと言はれてゐる．この事實は，若し記憶違ひ，又は聽覺えが驚きと畏れの爲に亂された時に聞かれる幻聽的のものではなかつたとすれば，稍々深く追究してよいことではないかと思はれる．

その2は，「ゴー」といふ音，「ドロドロ」又は「ドー」といふ音，トラツクの通過する時のやうな音，といふやうな言葉で報告される音である．

地震の時に聞かれる地鳴が，震源で發せられて空氣中を傳はつて來たものではない事は，其等の地鳴が，地震動に先驅して聞えるといふ事實から明白であらう．それ故地殼の中を傳播して來た比較的短周期の彈性波が地鳴を聞いた場所の附近に達した時にその震動を空氣に傳へ，それが音波として耳に入るものと考へられる．さうすると，その音波の Amplitude（强さ）に相當する Pressure は[1]

$$P=6{\cdot}6\times\frac{A}{f}$$

で與へられる．A，f，は地震動の Amplitude 及び Frequency である．それ故，震源の近くで，地震動の振幅の大なる地域では，比較的高い音も聞え易くなる筈である．「ドーン」といふ音と，「ゴー」といふ音と比較して，何れが高い（Pitch の高い）音であるかは容易に認定し難いので聞えた音の種類に關する議論は出來ないけれども，「ドーン」といふ音は，比較的震央に近い地域に於いて聞えてゐる傾向がある．併し又，一方に於いて，地盤の比較的堅固であると言はれる場所に於いては，短周期の震動が優越し，而も，その震動の加速度が，軟弱なる地盤の地域に比して大であるといふやうな事實も認められて居るから[2]，高い地鳴の聞える地域が單なる震央距離の函數であるとも言へないのである．

第1圖には，地鳴の音の種類とその聞えて來た方向とを，點線及び實線の矢で示してある．點線の矢は「ドーン」といふ音，實線の矢は「ゴー」又は「ドー」といふ音及び之に類すると思はれる音の聞えた場所である．この矢の分布について，次のことが氣付かれるのである．

（i）「ドーン」といふ音は，奈良縣の方面に於いて比較的廣い範圍に聞えてゐるが，大阪府内では，震源に近い僅少の區域に於てのみ聞えてゐる．

（ii）震源に近い地域に於いては，音響が，震源の方から聞えてきたと稱する者が

1) T. Hagiwara, *Bull. Earthq. Res. Inst.*, **12** (1934), 222~232.
2) 那須信治・萩原尊禮　地震研究所彙報 **14** (1936), 290.

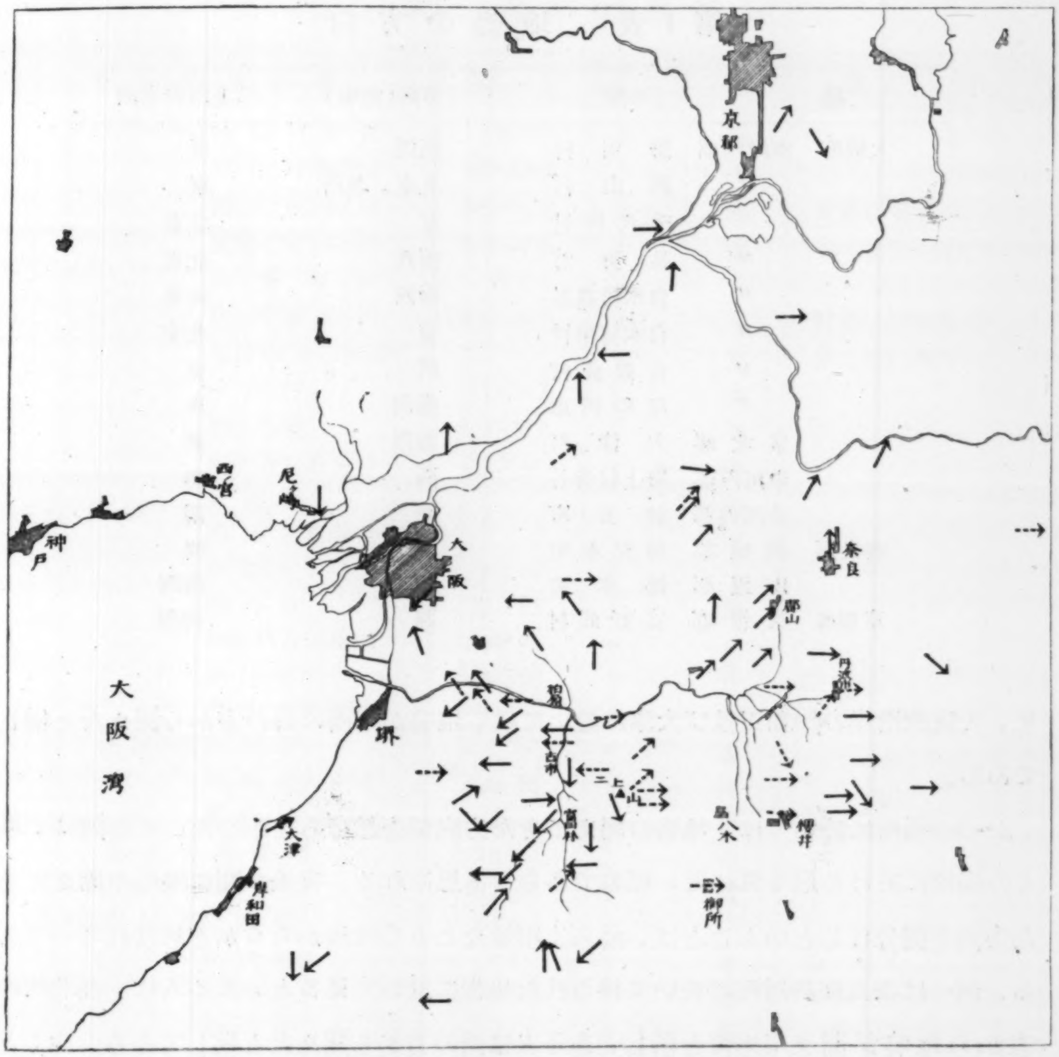

第1圖　地鳴傳播の方向分布圖

多數である様に思はれる．併し，この事は，震源が二上山であるといふことを知つて後に聞いた報告であるから，潜在的に震源の方向を知つてゐて，音の聞えて來た方向を震源の方向に歸する心理的傾向の結果も無視出來ないやうであるから，その結果に對しても幾分の疑をもつて見ねばならないかもしれない．その他の場所では一見無秩序の如くである．

（iii）前述の如く，多くの場所に於ける，地鳴の聞えてきた方向は一見無秩序ではあるが，その中に，仔細に見れば，幾分か規則的な傾向もみられる．その1は，震源の方位如何に拘らず近くの山の方から聞えたと認められる場合の多いことである．卽ち，次の場所に於けるものはその例である．（第I表）

第I表　地鳴の方向

場		所	方向(地鳴)	二上山の方向
大阪府	南河內郡	野田村	南西	東
	〃	狹山村	北東，北西	東
	〃	千代田村	東	北東
	〃	長野町	南西	北東
	〃	白木村森屋	南西	北東
	〃	白木村中村	東	北東
	〃	日置莊村	西	東
	〃	岸和田市	南西	東
	泉北郡	大津町	南西	東
	中河內郡	堅上村青谷	西	南
	北河內郡	枚方町	東	南
奈良縣	磯城郡	田原本町	北西	西
	山邊郡	櫟本町	西	南西
京都府	久世郡	富野莊村	西	南西

又，大阪灣沿岸の岸和田及び大津に於いては，地鳴が南西の海の方から聞えたと稱してゐる.

2～3の場所に於いては，地鳴の聞えてきた方向が全然分らなかつた. この例は，多くの場所に於ける最も眞に近い經驗であらうと思はれる. 突差の間に地鳴の聞えてきた方向を聞分けるといふことは，恐らく困難なことでは無からうかと思はれるのである. 例へば奈良縣御所町に於いて得られた報告に就いて見ると，ある人は，北北西の方から地鳴が聞えて來たと稱し，ある人は西の方から聞えたと稱してゐる. 少くとも，地鳴の聞えてきた方向にこの程度の喰違のある場合もあるのである.

2. 地下水位の異常並に之に關聯せる現象

地下水位の異常が地震に伴つて認められた事は從來も幾多の例があり，この地震に於いても多少の例を認めることが出來る. 併し，その異常現象を量的に表現することは容易でない.

先づ井戸に就いて水位の增減及び清濁の生じたものを調べてみると，現在までに得た結果は，第 II 表に揭げてある通りである.

第II表　井水の異常

井戸の所在地	深さ	井水の增(+)減(-)	濁	備考
大阪府南河内郡埴生村伊賀	5 m	+	濁	
川上村小學校	10〜15尺	+−	濁	
川上村大井	0·5〜6 m	+−	濁	井底は岩磐
道明寺村大井	1·5〜4 m	+−	濁	
長野町原	30尺	−	−	
山田村山田	2·5〜4 m	+	−	乾田に湧水あり
富田林(中學校調)		+−	濁	多く淺い井戸
千早村	6 m	−	濁	
駒ケ谷村	18尺	+−	濁	
駒ケ谷村通法寺	12尺位	−	濁	
古市町		−	濁	
西浦村東阪田		−	濁	
高鷲村	5·6 m	+	−	
磯長村	12尺餘	+	濁	
磯長村大字葉室	30尺位	+	−	
狹山村	40尺位	−	−	
白木村南加納	4 m	+	濁	
中河内郡三宅村		−	濁	
天美村大字堀	3 m 位	+	濁	
惠我村若林		+	濁	
泉北郡大津町	18尺	−	濁	
大阪市外大鐵沿線矢田	20尺位	−	濁	
奈良縣生駒郡椎鳩村	24尺	−		
北倭村上	17尺	−	濁	淺い井戸
片桐村	3〜5 m	+−	濁	
矢田村		+−	濁	一般に淺い井戸
都跡村小學校	12〜18尺	+	濁	
郡山町	3·5 m	+−	濁	
奈頁縣山邊郡丹波市町	4 m	+	濁	
高市郡越智岡村	3 m	+	濁	井底より泡が出た
南葛城郡忍海村西辻	3 m	−		
奈良市今小路町27	10 m	+	濁	
京都府綴喜郡八幡町		+	濁	
久世郡富野莊村		+	濁	
京都市伏見區		−		
兵庫縣伊丹町(高女)		+	濁	

この中，井水が溷濁したといふことは，地震動によつて，井戸の內壁に附着若しくは吸着してゐた微小塵が水の中に混入した結果生ずるものと思はれるので，比較的目立ち易い事ではあるけれども，地震の隨伴現象としては甚だしく興味のあるといふ程

のものではないと思はれる．それで，水位の増減のあつた井戸の所在だけを地圖上に記入してみると，第2圖の樣になる．この圖で一寸注意されることは，二上山の西側傾斜面に増水した井戸が比較的多く分布して居ることである．

この中，a と符號を附した場所は井戸ではなく，乾田中から水の湧出を生じた場所である．この場所は，大阪府南河內郡山田村畑地內で山田村から平岩部落へ通ずる道路の西側にある．最初，溫泉が湧出したと傳へられたものであるが，現在湧出せる水の溫度は，15°C で，氣溫及び地表の水に比して約 10°C 高い．溫度の點から考へて，この湧水は地表に近接せる帶水層からのものではなく，地表下 10 m 內外の帶水層から湧出するものではないかと思はれる．又，湧出量も地震直後は更に大であつたかもしれないが，3 月 2 日現在でも，每秒 100 c.c. 近くの割合で湧出してゐるやうに推定された．

第2圖　各地に於ける井水の增減

▲；增水した井戸の所在
△；減水した井戸の所在　を示す．

從來の地震に於けると同樣に冲積層地域，卽ち，平野や，谷に於ける井戸の水位の變化も著しかつた．併し，斯樣な地域に於ける井水の增減の分布狀況は極めて複雜してゐると言ふことが出來る．例へば，道明寺（第2圖の b の附近）では，2 月 21 日の午前中，水位が約 60 cm 位上昇したと認められる井戸が數個あるが，其處から 100 m 餘位しか離れてゐないと思はれる大鐵道明寺驛構內の井戸は地震直後一時水の湧出が止つて水が涸れたといふことである．又，第3圖には御所附近に於て異常に認められた井戸の分布を示してあるが，葛城川を隔てゝ存する2個の井戸の1方が增水し，他方が減水してゐる．斯樣な例は，他にも屢々見られることは，第II表の備考欄から知れるであらう．

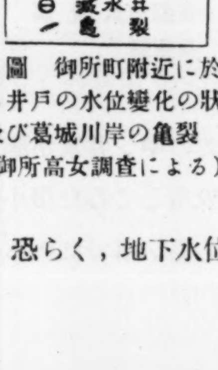

第3圖　御所町附近に於ける井戸の水位變化の狀況及び葛城川岸の龜裂
（御所高女調査による）

次に注意されることは，乾田中の噴砂の現象で，この現象は，恐らく，地下水位の

上昇と關聯する場合があるのではないかと思はれる．

噴砂現象の最も著しかつたと思はれるのは第4圖の寫眞に示した大阪府下古市町譽田附近のものである．南北に走る大鐵線路の西側に於いて，之と約45°角をなして西北へ，約10m位の間隔をおいて，1個又は數個の噴砂孔が直線上に列んでゐる．この噴砂孔列は約200m位はつゞいてゐる．同樣の噴砂孔の群は，道明寺附近の畑中(第5圖參照)にも認められ，駒ケ谷村，大軌沿線の關附近にもあるといふ事である．更に又，堺の大濱海岸における埋立地中にも認められた．噴出された砂は，何れも青味を帶びた粘土交りの細砂であつて，譽田，道明寺附近のものは5~6尺乃至10尺位地表より下に存在するものであり，堺の噴砂は，地下約30尺のところに在つたものであると言はれてゐる．

この噴砂現象の生ずることは，故寺田博士によつて指摘されたコロイドのthixotropy の應用でその解說の可能性がある[3]．噴砂の成分からみて，その砂が地下に於いて充分の水分を含む時，thixotropy的性質を具備するであらうことは容易に想像される．道明寺附近での話によれば，地震直前に地下水位は殆ど地表とすれすれに到達してゐたらしく思はれるし，堺の場合などでは海に面してゐること故，地下數米における水分は充分であつたことであらう．そこに，地震動若しくは地震に伴つて地殼の何等かの變動があつたとすれば（地下水位の昇降も同じ地殼變動に因ると考へられる），それによつて流動性を持つに至つた砂交り粘土のコロイドが，地表に噴出される道程は左程難しいことではないであらうと想像される．

噴砂現象の說明方法はこれだけではなく，他にもあることゝ思ふが，こゝでは現象の記載を主とする意味で止めておく．

これに關聯して考へられることは堺の三寶海岸において構築中の堤防が一部沈下したことであるが，これも以上の樣な考へから，地下の砂層のコロイドが流動性を持つに至つた爲に，所謂flowの現象が生じ，それが，地表の一部沈下を生ずるに至つたのではないかと考へられるのである．

以上に擧げた所の井水の變化とそれに關聯した現象の有樣から考へて，所謂地殼變動も幾分伴つたのではないかといふことが想像され，精密測量による變動の計測が望ましく思はれるのである．

3. 發光現象に就て

この地震に伴つて發光現象も亦觀察されたといふ報告が少くない．今，其等の報告

3) T. Terada, *Bull. Earthq. Res. Inst.*, **13** (1935), 562～568.

を表に纒めてみると次の様になる.

第III表 發光現象

觀察場所	時刻	色	形	方向	備考
大阪府南河内郡川上村	午後7時頃	?	直線的	?	
山田村山田	夜	黄青色	?	?	上下數十米帶の如し
古市町	21日夜	薄青	太き火柱	二上山の方	
大伴村大字別井	20日午後10時30分	輝紅黄	帶狀	二上山の方	二上山より南へ走れり
高鷲村	21日午後8時	?	?	?	電車のスパークの如し
駒ヶ谷村大字通法寺	?	?	?	東方より	弱い電車のスパークの如し
富田林中學校	22日午前4時	赤+青	棒狀	二上山北	下から上へ
中河内郡八尾町	?	赤	棒狀	藤井寺方面	
三宅村	23日午前9時頃	灰紫色	?	二上山南側	
惠我村若林	21日午後12時	?	?	金剛山方面	雷の如し
奈良縣磯城郡田原本町	?	赤味	?	二上山稍北方	イナヅマ樣
生駒郡片桐村	21日午後11時	黄青	長	?	
郡山町	夜3時	青白	柱形	西方	
山邊郡丹波市町	午後1時	黄	電光形	西山空	

以上の表の中，大阪府中河内部三宅村及び奈良縣丹波市町に於いて發光現象の觀察された時刻は夫々午後1時及び午前9時（23日）である．その日が丁度曇天であつたとしても晝間見えたといふ光は餘程强い光であつたと思はれる．

其の他光についても地震當日の頃の天候如何によつては，雷電を見たものかもしれないといふ疑もある[4)]．實際に雷電の如き光り方をしたものを見たといふ者もある程である．又二上附近には，大軌及び大鐵の電車線路が2條も通過してゐて，しかも，其等の交通は地震當時の僅少な時間だけが不通となつたに過ぎないのであるから，「二上山方面に見えたスパーク狀又は青白色，黄青色等の光」は實は電車のスパークであり得る可能性が充分にある．發光現象を認めたといふ日時の區々であるといふ事實も亦この疑を濃くする1資料ともなり得るであらう．

更に，同樣な發光現象が，特に地震の時だけに限られたものであるか，或は又，平常でも時々は表はれるのであるけれども，其等は氣付かないか無視されてゐるかの何

4) 氣象要覽によれば2月21日には雷雨がなかつた：氣象要覽 (1936, Feb.).

れかであるか，といふ點になると，矢張り，明確な回答を得難いものゝ如くに思はれるのである．

要するに今回の地震に際して，發光現象を認めた例は少くないのであるけれども，從來の多くの場合と同じく之を地震に隨伴せる現象であると考へるには餘りに疑問があり過ぎるやうに思はれるのである．

唯一つ，山田村春日（二上山西側）において上の太子（大鐵驛）方面に認められた發光現象に相應して，上の太子の北側の山に多少の山崩れがあつたといふことであるが，これが眞實とすれば地震現象と關聯せる發光現象として最も注意さるべきものではないかと思はれるのである．

4. そ の 他

その他，地震に關聯して注意すべき被害狀況としては，河岸の道路の龜裂（柏原附近，御所町附近，〔第3圖參照〕等），貯水池の堤防の龜裂（山田村東條〔第6圖參照〕）等があるけれども大したことはない．墓石は顚倒せるものは少なく，回轉せるものが多數であつた．墓石の回轉，顚倒に就いては，別に詳細なる調査報告がある筈である[6]．

譽田神社（大阪府古市町）の被害も多少注意に價するかもしれない．此處では土塀の倒壞（第7圖參照）が著しいが近所の住家には被害は殆ど皆無である．同社々掌の談によると，應神天皇御陵の濠が現在は一重であるが古圖によると三重になつて居り，その外濠に當る場所に現在の譽田神社があるといふことであるから，所謂地盤の惡い場所に相當するのではないかといふことである．土塀の倒壞といふ點からいへば從來の經驗とは反對なる現象であるが，或は他に理由があつて，上述の樣なことも考へられるかもしれない．

最後に，本調査に當り，報告を寄せられた，大阪，奈良，京都，兵庫各府縣下の中學校，女學校，及び小學校の校長，職員諸氏並にその他の諸氏に對して，厚く御禮を申上げる．

5） 武者金吉，「地震に伴ふ發光現象の研究及び資料」．(1932).
6） 吉山良一 地震 8 (1936), 105.

27. *Some Phenomena associated with the Kawati-Yamato Earthquake of Feb. 21, 1936.*

By Naomi MIYABE,

Earthquake Research Institute.

A strong earthquake occurred on Feb. 21, 1936, the epicentre of which is located in the neighbourhood of Mt. Hutagami, situated on the boundary of the prefectures of Osaka and Nara. In association with this earthquake, various phenomena were noticed, among which those described in the present report are somewhat remarkable.

(i) Earthsounds were heard in many places in the prefectures of Osaka, Nara, Kyôto and Hyôgo. It may be noticeable that the directions of the propagation of the earthsound felt at respective places were not always from the epicentre, but, in most cases, it was felt as had been propagated from the nearest mountain.

(ii) In several places in the neighbourhood of the epicentre, the level of the underground water was elevated, while, in several other places, it was found to have been depressed, as shown by the changes in level of the water of the shallow wells. It was also noticed that, in some fields, considerable amount of clayey sands was emitted from 1∼2 m below the surface, as shown in the photographs (Figs. 3∼4), which may probably be connected with the change in the depth of the level of the underground water.

(iii) Lights were also observed by several peoples as have been accompanying the earthquake. But, in the case of this earthquake, it may be a question that the appearance of the light was really related to the occurrence of the earthquake.

第4圖　乾　田　の　噴　砂
(大阪府古市町譽田附近)

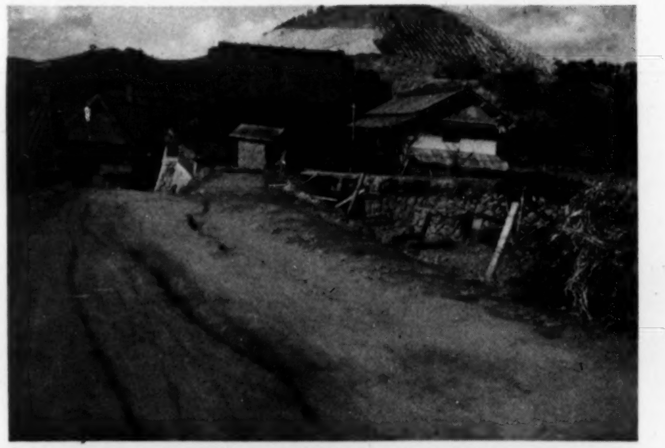

第6圖　貯水池堤防上の亀裂
(大阪府山田村東條)

第5圖　乾　田　の　噴　砂
(大阪府道明寺附近)

第7圖　譽田神社土塀の被害

28. 昭和11年2月21日河内，大和强震被害の地質及地形的考察

地震研究所　齊田時太郎

(昭和11年3月17日發表—昭和11年3月20日受理)

この地震は昭和11年2月21日午前10時8分頃起つたもので，被害程度よりすれば强震と言ふべき局部性地震であつた．其の被害の比較的著しく現はれたところは，大阪府と奈良縣との境界附近の大和川の本支兩流域及兩府縣界をなす葛城山脈中の二上山麓であつた．筆者は地震直後數日に亙り被害各地を調査した．しかし被害輕微なりし故，復舊速かにして建物，墓石，燈籠等の震害の實相を見るのに不便な場合もあつた．これより各地の被害情況を述べ，更に被害と地質及地形との關係について，若干の考察を下して見たい．

1. 各地の被害情況

被害地域の家屋は平家或は2階建にして，屋根は瓦葺きのもの多く草葺きのものは少い方であつた．軸部構造は特に異なると思はるゝ點はないが，壁體は小舞の兩面に壁土を塗りたるもので，其の厚さは關東地方のものゝ2倍以上もある．從て家の質量は關東地方のものゝ2倍にも達するであらう．軸部の仕口は舊來の手法になるもので，かなり粗惡なものも見受けられた．土臺を置いた家は寧ろ少い位であつた．農家には周圍に土塀をめぐらすもの多く，共の厚さは50糎，高さ2米位のもの，或は柱を立て小舞をかき土を塗りつけ漆喰仕上をなせるもの等，家の內外に土を使用せることの多いのが特に注目された．土壁は年月の經過と共に容易に龜裂剝落をなすもの故其の地震被害によるものか自然の損傷によるものかを注意して觀察するを要した．かゝる構造になる住家，非住家以外に若干の工場があつた．特に大阪府下に多くあつたが，これ等の工場建築は鐵筋コンクリート造，或は鐵骨亞鉛引鐵板張のものであつた．なほ奈良縣下の被害地域には法隆寺を初めとして，建築文化史上極めて貴重なる建造物が存在してゐた．

大　阪　府

大阪市　被害は輕微なりしが屋根瓦の滑落，ガラス窓の破損，土壁の龜裂等は市內

各所に生じた．府警務課の調査によれば市內に８箇所の水道鐵管の破損を生ぜしが，何れも下町沖積層の地盤にして昭和２年の丹後地震にて著しき被害を出現せしところと一致するのは注目すべきである．高層ビルディングの震動狀態を知るため，心齋橋の十合ビルディングにて當時の情況を尋ねてみた．この建物は地上100尺，地下３階にして我國にて既存の建物中最も深層建物であるが，この地震の人體感度は地下３階にては，地震動は感ぜしも何等恐怖の念起らざりしに，最上階の８階にては動搖甚しく，避難せんとして何れも陳列臺下に逃げ込みしほどであつた．被害としては第６階にて陳列用のガラス板と，レヂスターが滑落せるほか，建物には何等異狀はなかつた．第６階のかゝる被害は，何れも其据置に不利な點ありしために生ぜしもので，高層ビルディングの振動様式と關係あるものとは信ぜられざるも，參考までに書いておく．

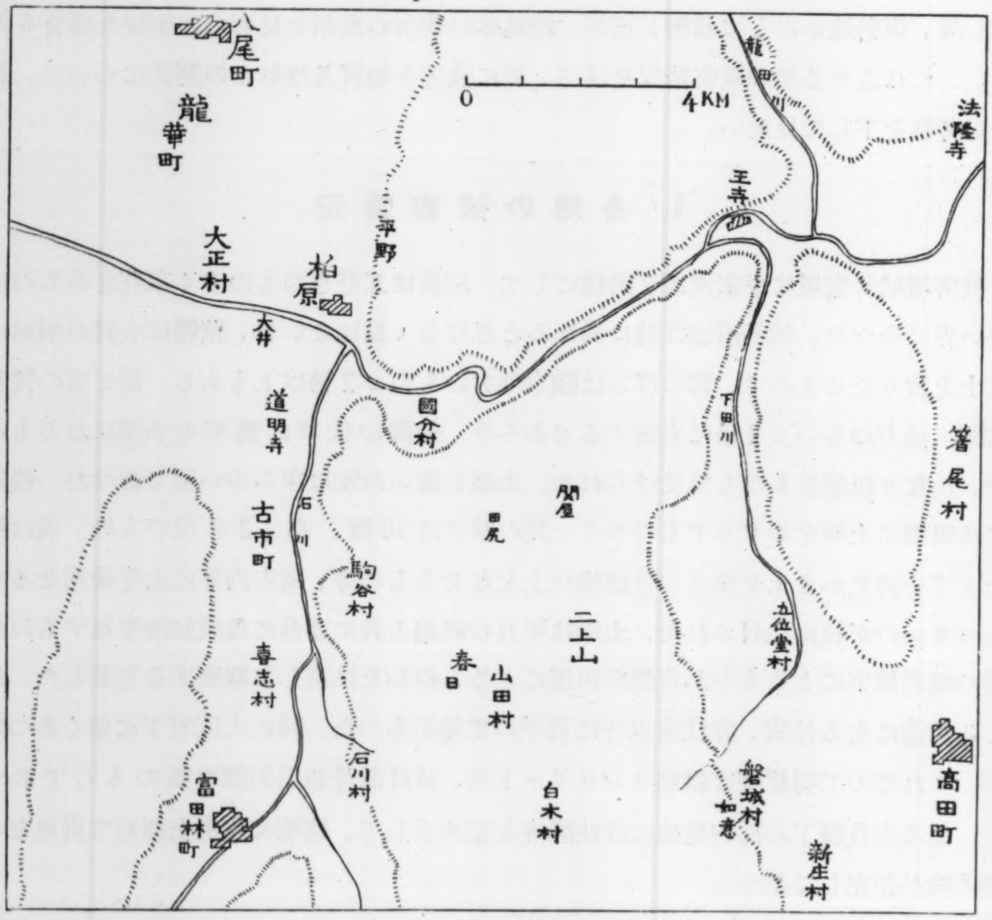

第１圖　震害地域の略圖

平野鄉町，久寶寺村，八尾村等は何れも被害輕微であるが，關西本線八尾驛の倉庫

の一部倒潰せるがあつた，この附近は石燈籠の倒れしものも極めて少く，屋根瓦は幾分移動せるものもあつたが，此の倉庫の倒潰は震力による軸部の直接の損傷に起因するものでなく，倉庫内に積んであつた．豆粕の崩潰による側壓に起因するものと思はれた．**龍華町**，**大正村**，**志紀村等**も上記の町村と大差なかりしも，龍華町に1棟の倉庫が下屋を破壊せられてあるのを見たが，其仕口甚だしく腐蝕し，且石垣の上に建てられたものであつた．**柏原町**は稍被害の度を高めてゐるが，被害箇所には變りがない．柏原町の東北方の鷹巣山々麓にて，冲積層平野と山地とに跨る**法善寺**及**平野**等の部落について，冲積層の厚さ及地盤の堅軟による被害の差異の有無を調べたが，全く差異なきを知つた．大和川左岸に沿ふ**大井**は柏原町よりも被害の度は高い．こゝで1棟の住家の大破せるを引き起し修築せるものを見たが，其の周圍の住家と比較すると最も古い建物であつた．**國分村**にも2棟の被害著しく修築の見込なき程度のものがあつたが，何れも其の周圍の建物と比較すると最も古い建物であつた．大井より**道明寺村**の臺地へ進むに從ひ被害は輕微となるが，允恭天皇御陵附近にて障子紙の破れてゐるのがあつた．道明寺入口の 27糎×51糎，高さ2·5米の花崗岩の石柱が轉倒せずにあつた．**古市町**にては譽田八幡宮が著しき被害を受けてゐる．石燈籠は倒れ，土塀，築地は大破してゐた．譽田小學校の土塀も倒潰を免れなかつた．古市町臥龍橋北方の火葬場煙突高さ10米位のものが中央にて折れ，上部は西方へ約10糎ほど移動し，底部は反時計式に廻轉し5糎の食ひ違ひを生じてゐた．古市町郵便局附近に一棟大破し取片づけてあるのを見た．古市町より南下し**喜志村**，**富田林**町に至れば住家の被害は順次輕微となるも，富田林驛附近の某工場の煉瓦煙突は大小無數の亀裂を生じ，其の頂部は墜落し，工場の一部を破壊せるが著しく注意された．二上山麓の**玉手村**及**圓明**は住家の被害は左程でないが，土塀の被害が著しく注目される．**駒谷村**は住家，非住家，土塀の被害は何れも其度著しくて玉手村，圓明の比ではない．駒谷より竹内街道を上り**飛鳥**，**春日**，**山田**に至れは被害は幾分甚しくなつたかの如く感ぜられる．春日西方の厩戸皇子御墓所の石燈籠は何れも倒れ，其方向は各異り一定せる方向を示さなかつた．山田村の推古天皇御陵の附近に火葬場あり．高さ約6米位の煉瓦煙突があつたが異狀はなかつた．山田村の西南の**石川村**及略南方の**白木村**は被害極めて輕微であつた．

奈　良　縣

奈良市　住家の被害は大阪市より遙かに輕いが，二月堂の燈籠若干が倒れた．奈良盆地一帶は略一様な震度であるが，**高田町**，**新庄村**，**五位堂村**が比較的被害を受け，**瀬南村**，**百濟村**，**箸尾町**，**田原本町**がこれ等につぐ被害を受けてゐた．高田町にては

屋根瓦は落ち，土壁に亀裂を生じ，ガラス窓は破損し，燈籠は倒れ，小學校の煉瓦塀は倒壊した．田原本町，箸尾町の被害は少く，土塀の倒潰せるが少しあつた．新庄村は土壁の剝落し，變電所の煉瓦造切妻の一端に亀裂を生じてゐた．五位堂村も新庄村と大差がなかつた．二上山の東南麓の**磐城村**は被害著しく，特に**如意**が代表的であつた．こゝの寺院である蓮生院は山の斜面を利用して建築せるものであるが，障子は破れ土塀は損傷をうけ，浴室は大破するなど相當の被害を見せてゐた．なほ同院裏手の墓石の多くは東南方へ轉倒してゐた．この寺院に隣接する西川氏の住家は，この附近に稀な入念の建築であるが，土塀，煉瓦塀が損傷し，障子紙が破れるなど著しい被害であつた．二上山麓を北方へ進み**當麻村**，**二上村**の部落を見るも被害は極めて輕微である．二上村の**關屋**，**田尻**に於ては更に被害らしきものを見なかつた．**王寺町**にては住家の土壁に亀裂の生ぜしもの多く，驛の石炭置場の煉瓦支柱の損傷し，陸橋の筋違の下端の切斷せるなどの被害があつた．**法隆寺**は築地の所々破損し，中門東側の一柱が僅か2分ほどずれたが，中門に接續する廻廊の柱列は地震にて箇々別々に運動し，恰も波動の傳播する如くに見へたと言ふことを，略柱列線上に園して目擊せる受付の人が筆者に語つた．奈良盆地の東方は奈良市と被害の程度大差なく，**丹波市町**にては假驛のガラス數枚破損し，住家の壁に亀裂が入り，石燈籠の頂部のみ落下せるを見た．

今回の被害は兩府縣下とも以上說述せる如く，特に注目すべき構造物の被害もなく極めて輕微のもので，昨年7月11日の靜岡地震に於ける有度山西麓の各部落の如き甚大なる震害はなく，又建物の基礎より滑動せるものも全く見ることができなかつた．

2. 被害の地質的考察

地盤の善し惡しは地盤固有のものでなく，地盤と其の上の構造物の性質とで規定されるものであることは，筆者[1]が關東大震災に於ける東京下町及山手の木造普通家屋と土藏，石造との著しき相異を指摘してより，昭和6年9月21日の北部武藏の强震及昭和10年4月21日の臺灣中部地震に於ても，全く同樣な現象が出現してゐることが認められた．今回の大阪府，奈良縣下の强震に於ても，かゝる現象が認められる．木造住家，非住家の被害は大阪府下にありては大和川本支流附近の沖積層地盤及奈良盆地の高田町附近に多く現はれ，土塀，土藏等の被害が二上山をめぐる山地に多く現はれてゐる．特に前述の磐城村字如意の蓮生院及西川氏宅の如き入念の施工になる堅固なる建物に被害多く現はれ，これ等の建物に隣接する粗末な農家に被害殆どなきこと

1)　齊田時太郎「耐震及び耐風家屋」防災科學（地震）岩波書店．
　　同　上　「臺灣に於ける震害と地盤に就て」地震研究所彙報別册 3 (1936), 96.

は，冲積層平地と堅固なる山地とにて地震動の性質の全く異なることを示すよき例證となる．地震動の性質は冲積層平野と山地とで全く別に考へなければならぬ．震央附近の山地にては地震動の加速度が冲積層平野より寧ろ大きいが，加速度の週期は反對に山地に於て小さく，平地に於て大きい．地震動の加速度の大小を簡單に震度なる語を以て表はすのが常であるが，上に述べた如く加速度週期は平地と山地とで相反してゐるから，建物の構造様式によつて建物を振ふ力卽ち振力は地震動の震度とは必ずしも相平行せず，寧ろ相反することがあるから，構造物の被害を見て地震動の震度を推定することは大に謹むべきことである．震度は其の地盤と構造とを併せ考へて定むべきで振力と混同せぬやう注意すべきである．

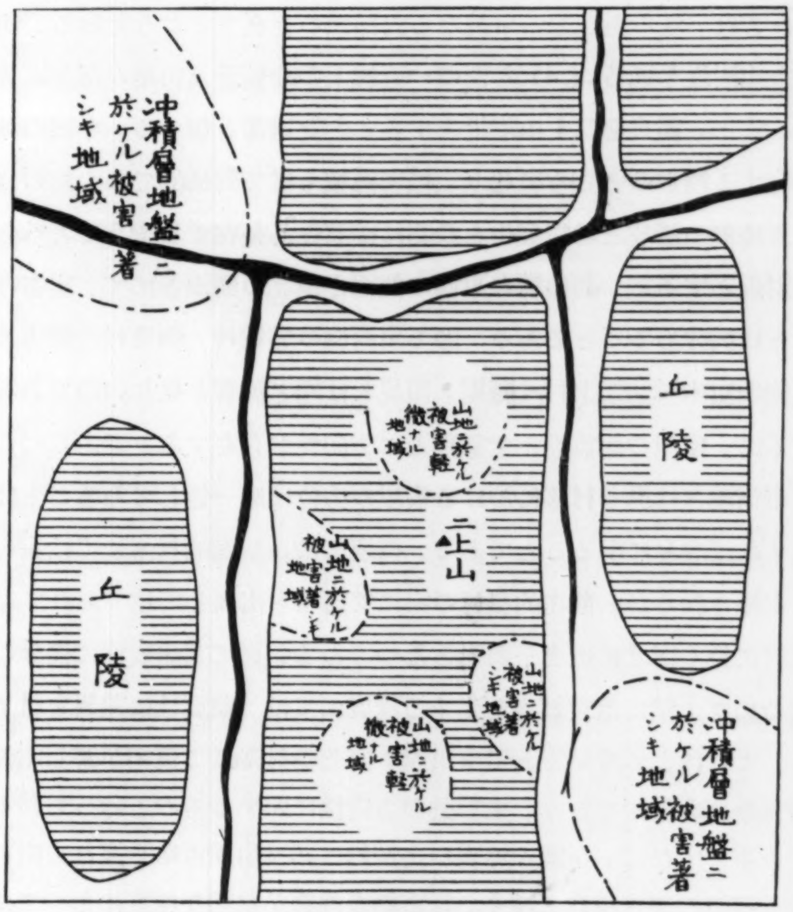

第2圖　震害地域と地形概觀

3. 被害の地形的考察

被害の地形による例證としてよく斷崖或は河岸の縁邊にて著しいことが知られてゐる．これは地表層の震動が特に自由端と考へられる場所にて大なることに起因する．筆者がこれより述べんとするものは，震源に於ける波動射出の機構が被害の地形的考

察により想像せられることで，主震動が單純なるものにあつては被害の輕重，物體の轉倒方向が地域的に異なるものにあらずやとの疑問が，昨年7月の靜岡地震の被害調査をなせるとき以來考へてゐた．今回の河内・大和强震の震央は二上山附近とされてゐるが地盤と被害分布とを併せ考へるときは，其の震央の位置は適當と考へられる．被害は地盤の性質に支配せられるものであるから，震央と被害地とは著しく異なることがあるが，今回の被害地の地形を見るに葛城山脈は南北にはしり，大和川がこの山脈を横斷するにあたり其の西麓に柏原町附近より山脈に平行に南下する支流石川あり，其の東麓に王寺附近より山脈に平行に南北2支流下田川，龍田川あり，又石川の西方及下田川の東方に各一つづゝ丘陵がある．從て略々二上山を中心とし東西南北の2線をひくときは，地形上二つの單純なる對稱性の存在することを知る．而して今回の被害が二上山附近を通る北45度西の一直線上の冲積層及山地の部落に著しくあつたことを考へると，震央を二上山附近とすることを適當と信ずる．今回の地震がかゝる對稱性を有する地形のところに起り，被害區域も從て對稱的であつたのは興味を覺える．かゝる地形の構成と地震發生との間に必然性が存在するやうに考へられる．震央を二上山附近とすると，其山麓の東西の側面と南北の側面とにて，震害の著しき差異を示すことは興味あることである．即ち東西側の磐城村，駒谷村の被害著しきに對して，南北側の白木村，二上村（關屋，田尻）は殆ど被害を見ないのである．この現象を說明するに，家屋の耐震性と主震動とに方向性が存在すると言ふ二つのことが考へられる．市街地とは異り村落に於ける家屋の方位は略一定してゐることは，少し注意して觀察すれば容易に解ることである．街道に沿ふ集團的村落にては家の方位が街道の方向に支配されるが，散在的農村の家にては殆ど南面して建てられてゐるから，通常家は東西に長く南北に短き平面形となつてゐる．從て其耐震性に幾分の差異はあるが，今回の如き土壁に亀裂剝落を生ずる程度にては，耐震性に差異を付することは妥當でない．これによつて見ると二上山麓，南北の村落にて被害が著しく輕微であるのは家の耐震性にあるのでなく，主震動の方向性に歸するものと考へられる．もしこれが眞實であるとすれば，今回の地震の主震動は葛城山脈に略垂直な方向にあつたと考へられる．震源の深さ極めて淺く，且震動の性質が單調な地震にあつては，主震動の發生機構が被害の上に現はるゝであらうと容易に想像される．今回の地震が既に述べた如く，特種な地形地質のところに發生し，其被害の上に筆者の上述の想像が全く架空なものでなく實在性の有ることを示した．なほ筆者はこの思想の正否を既往の震災誌及今後の震害調査に於て檢定するつもりである．もし，そこで確實なる實證を得て，初動方向並に精密測量による地震後の地盤の移動との間に何等かの關係を摑み，發震機構を窺ふことができるならば愉快なことである．

(附錄) 參考資料被害狀況

大阪府下地震被害狀況

(2月22日午前10時現在警務課調)

署名	死者	負傷者		建物倒壞			水道鐵管破裂	土地の狀況				出火
		重傷	輕傷	全壞	半壞	煙突		亀裂	山崩	低下	崩壞	
木津川水上署							鐵管破損 2					
新町署			1									
川口署					6		鐵管破損 1					
築港署			5									小火 1
泉尾署			1				鐵管破損 3					
天王寺署					1							
難波署							鐵管破損 1					
蘆原署		2	2									
天滿署							鐵管破損 1	1				
福島署			1									
今宮署												小火 1
今福署		2				1						
中津署			1									
十三橋署			1									
大和田署	3					1						
堺署		1						1		2	1	
福田署			1	1	1							
富田林署	2		6	1	6			20				
長野署								4				
古市署	1		2	1	2				1	1		
黑山署								1				
柏原署	2	6	11	2	15			諸所	1			
八尾署			2	3	4							
三宅署			1					1				
南高安署			1		6			5				
津田署								1				
茨木署								1				
合計	8	11	36	8	41	2	8	35	2	3	1	2

[備考] 瓦，窓硝子等の如き輕微なる被害は揭上せず

地震被害各警察署別調 (昭和11年2月21日)

署名	被害內容
木津川水上	(1) 署通用門上部壁約一坪落下 (2) 千代崎橋及岩崎橋添架水道鐵管損傷上水噴出
玉造	(1) 電柱倒壞 1, (2) 家根破壞 1, (3) 土塀倒壞 1, (4) 陳列臺破損 1, (5) ガラス破損 10
新町	(1) 西區阿波堀4丁目14西村運方店員安田常一當21年二階より飛降り輕傷す
川口	(1) 倉庫半壞 6 { イ, 港區富島町80田淵海運店倉庫; ロ, 西區江戸堀下通1丁目62日本電線株式會社倉庫; ハ, 西區勒北通2丁目8荒川權吾倉庫; ニ, 江戸堀南通1丁目54山本良久倉庫; ホ, 北區中之島3丁目5東神車庫; ヘ, 其他 1. } (2) 西區肥後橋上水道破裂 1.
築港	(1) 小火 港區八幡屋元町2丁目210賣藥商芳屋愛三佛壇燈明より; (2) 輕傷 五氏名不詳; (3) 家屋の傾斜 3; (4) 窓硝子破損 13.
泉尾	(1) 輕傷 1, 氏名不詳; (2) 水道管破裂 3.
島之內	(1) 赤玉カフエー頂上壁脫落約一坪; (2) 電線切斷 1.
天王寺	(1) 土塀崩壞上ノ宮町69佐々木顯誠方; (2) 寺の屋根半壞 1.
難波	(1) 浪速區元町2丁目97地先地下水道管破損.
天滿	(1) 道路亀裂北區堂ビル北入口前幅2分長5尺; (2) 北區天滿橋4丁目70麵類商加藤忠六方家約1寸傾斜; (3) 署道場天井全部1糎の亀裂.
蘆原	(1) 倉庫側壁損傷 1, (2) 重傷者西成區梅通大工岸岡幾三郎屋根修理中梯子より墜落右膝關節挫折治療2ヶ月, 住吉區朝日町2丁目76田中春吉方手傳鮮人木下一郎當29年作業中墻塀上より飛降り右足骨折治療8週間. (2) 輕傷者旭區赤川町1丁目1024地野々村義雄方店員高橋醜當26年自轉車にて疾走中顚倒右手首に治療10日間の傷害, 浪速區櫻川2丁目1097武田商會方雇人金泰文當22年二階より飛降り左足關節捻挫治療2週間, 其他氏名不詳の負傷者1名あり
曾根崎	(1) 地下鐵梅田驛の壁一部亀裂; (2) 北區天神橋筋4丁目街路鈴蘭燈十數ヶ落下
福島	(1) 大日本製藥株式會社職工1名輕傷; (2) 宇治川北通3丁目大同電力變電所蒸汽パイプ破裂及壁亀裂.
網島	(1) 北區東野田町1丁目78岸八衞門方煉瓦塀長さ半町に亘り亀裂.
今宮	(1) 小火西成區中開町3丁目8大阪金屬株式會社揮發油より引火す.
住吉	(1) 共同火藥庫隧道長さ5間, 幅4尺, 高1尺5寸より2尺隆起.
平野	住吉區中野町中井神社鳥居上部崩落.
今福	(1) 煙突倒壞 1; (2) 重傷者西淀川區海老江町上2丁目123山際林吉方煙突職片山正見當29年, 同野里町247栗山幸四郎方煙突職武田榮當32年.
中津	(1) 輕傷 氏名不詳 1名.
十三橋	(1) 久保田鐵工所職工1名輕傷; (2) 十三東之町商會ウインドガラス破壞.

(次頁へ續く)

地震被害各警察署別調（昭和11年2月21日）

署名	被害内容
大和田	(1) 死者　イ，西淀川區出來島町388東洋製薬貿易株式會社工場煙突頂上より墜落し西淀川區野里町135北村三十四當29年；ロ，同117矢原春夫當35年；ハ，此花區玉川町4丁目67北野秀夫方菊地政治郎當33年.
茨木	三島郡玉串村澤良宜茨木川右岸堤防亀裂（長さ 400米，幅2分）
堺	(1) 重傷 堺市龍神橋通2丁目日本製氷會社 南野安松當41年；(2) 三寶町海岸堤防低下約三四尺，長さ約75間；(3) 七道東之町大和川堤防長さ40間，幅2寸亀裂；(4) 大濱海岸埋立地諸所に亀裂；(5) 吾妻橋通1丁目13土井川岸長2間，幅4尺陷落；(6) 土井川岸陷落に因り吾妻橋派出所用地沈下し建物傾斜し使用不能
福田	(1) 家屋半壞 1；(2) 納家全壞 1.
富田林	(1) 死者2名（土塀崩壞のため遊戯中の幼兒壓死）南河内郡磯長村太子山本清次郎の二女よし江當7年及三女つれ子當5年；(2) 輕傷男1名，女5名；(3) 家屋全壞 2，半壞 6；(4) 土塀崩壞20ヶ所；(5) 石垣崩壞2ヶ所；(6) 道路亀裂2ヶ所.
長野	亀裂 {(1) 三日市村村道長5間；(2) 天美小學校々庭2間； (2) 千代田村村道長30間；(4) 天野村金剛寺境内.
古市	(1) 死者 山崩の爲壓死，南河内郡駒ヶ谷村駒ヶ谷番外の9近藤信次當35年；(2) 山崩のため輕傷者2名；(3) 住家倒壞駒ヶ谷村1；(4) 非住家倒壞西浦村 1，藤井寺町 1；(5) 非住家半壞，古市警察署食堂及埴生村 1；(6) 古市町水源地低下；(7) 大鐵石川橋沈下電車一時不通
黒山	(1) 狹山池堤防幅2寸，長3間及幅1寸，長30間の亀裂； (2) 南海高野線（野田，狹山間）西桶川鐵橋亀裂不通となりしも直に復舊； (3) 狹山一半田間長さ4間のガード兩端低下折返運轉せしも22日朝より復舊.
柏原	(1) 死者2名山崩のため壓死，中河内郡堅上村峠土工宮内松太郎當53年，同李又吉當32年；(2) 重傷者 6名；(3) 輕傷者11名；(4) 全壞家屋10戸；(5) 半壞家屋15戸；(6) 大鐵線柏原一道明寺間ガード石垣約2間崩壞不通となりしも夕刻復舊；(7) 柏原町古町方面道路亀裂諸所に生ず.
八尾	(1) 輕傷者2名；(2) 全壞家屋一龍華町 2，久寶寺村 1；半壞家屋一龍華町 1，曉川村 2，大正村 1.
三宅	(1) 輕傷中河内郡矢田村小學校高等科2年山岡千鶴子階段より辷り落ち負傷；(2) 土塀倒壞（中河内郡天美村小學校土塀）；(3) 堤防亀裂（中河内郡瓜割村西向割大和川北堤防長さ 200米，幅10糎.
額田	(1) 孔舍衛村にて土塀倒壞2ヶ所.
南高安	(1) 輕傷者 1；(2) 半壞家屋 6；(3) 土塀崩壞 7；(4) 道路亀裂幅2寸以下5分以上五ヶ所.
津田	(1) 北河内郡岩船村私市道路幅1寸長2丁亀裂；(2) 板塀約8間倒壞.

奈良縣下地震被害狀況

種別 / 市町村別	人				世帶			家屋(棟數) 住家			家屋(棟數) 非住家		
	死	傷	行衛不明	計	全壞	半壞	計	全壞	半壞	計	全壞	半壞	計
北葛郡城高田町	1	1		2	3		3					3	3
〃 五位堂村											2		2
〃 磐城村						4	4		4	4	1		1
〃 瀨南村											5	20	25
〃 百濟村						3	3		3	3	1	1	2
〃 箸尾町											1	15	16
磯城郡田原本町		3		3									
〃 平野村		1		1									
高市郡畝傍町		2		2								2	2
生駒郡三鄉村								1					
合計	1	7		8	3	7	10	1	7	8	10	41	51

區別 / 市町村別	堤防 決潰		堤防 破損		道路 埋沒		道路 龜裂		溜池	
	箇所數	延長	箇所數	延長	箇所數	延長	箇所數	延長	損壞箇所數	延長
北葛城郡磐城村									1	50間
〃 王寺村			1	10間						
〃 當麻村									2	22間
〃 二上村							1	83間		
北葛城郡御所町							3	5間		
高市郡八木町							1	30間		
〃 越智岡村							3	12間		
生駒郡生駒町							3	3間		
〃 北倭町									1	60間
宇陀郡神戸村									1	(幅3間) 長さ70間
添上郡櫟本町									1	3間半
合計			1	10間			11	133間	6	205間半

傾斜家屋

1. 生駒郡郡山町北郡山巡査駐在所.

2. 同郡平城村秋篠に於て土藏 1.

3. 同縣龍田警察署廳舍は約四五度東南へ傾斜せり.

第 3 圖　譽田八幡宮築地塀

第 4 圖　王子驛前駐在所の被害

第 5 圖　磐城村如意，蓮生院土塀の被害

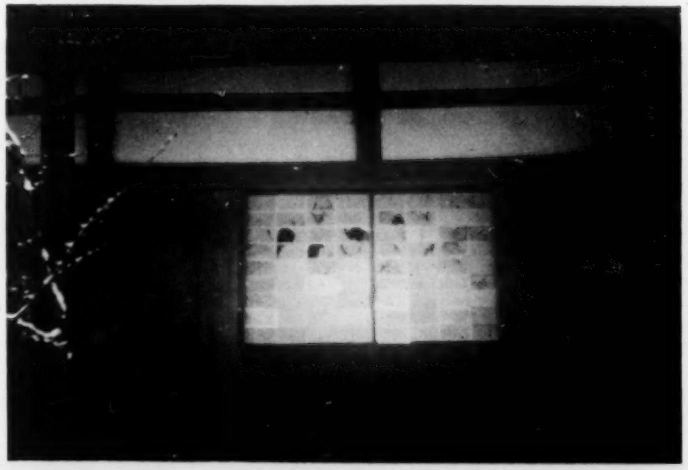

第 6 圖　磐城村如意，蓮生院本堂障子紙の被害

（震研彙報　第十四號　圖版　齊田）

第 7 圖　譽田小學校土塀の被害

第 8 圖　譽田八幡宮境内小祠の被害

第 9 圖　譽田小學校塀の被害

第 10 圖　道明寺村字大井，住家の被害

第 11 圖　國分村，住家の被害

第 12 圖　駒谷村，住家の被害

第 13 圖　龍華町，倉庫の被害

（震研彙報　第十四號　圖版　齊田）

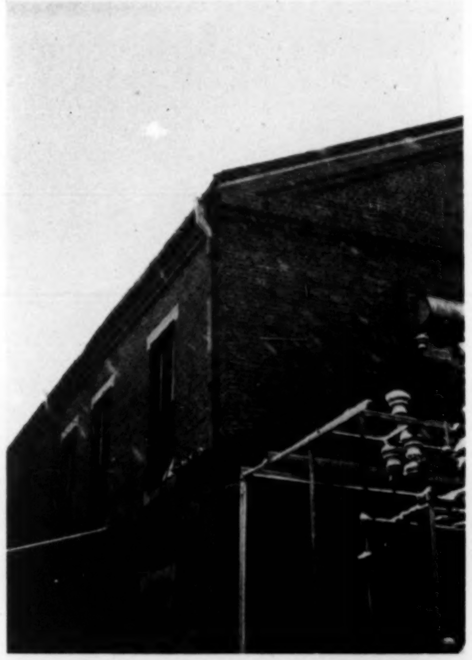

第 14 圖　新庄村，變電所の被害
切妻の左端に亀裂を生ず

第 15 圖　古市町火葬場煙突の
被害（上部）

第 16 圖　古市町火葬場煙突の被害（下部）

第 17 圖　富田林町某工場の被害

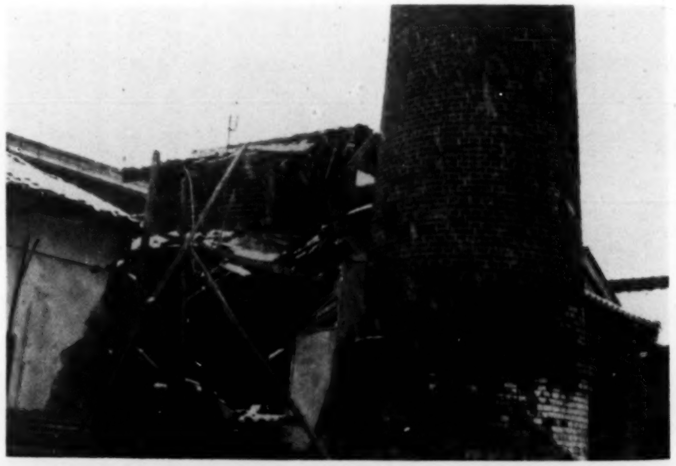

第 18 圖　富田林町某工場の被害

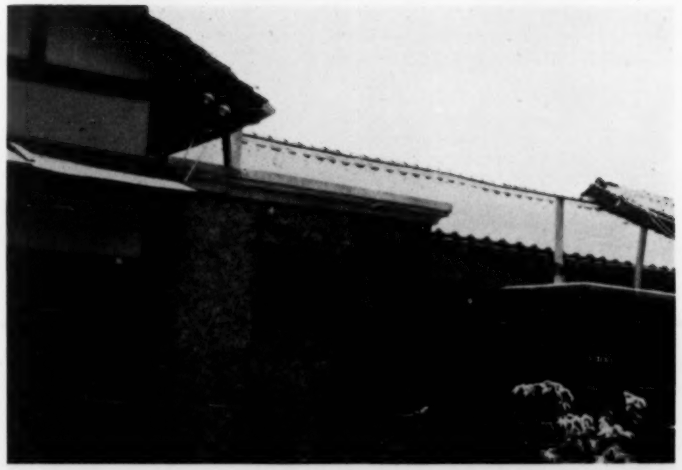

第 19 圖　新庄村，住家の被害

28. *Geological and Topographical Investigation of the Earthquake Damages on the Boundary between Osaka and Nara Prefecture on the 21st of February, 1936.*

By Tokitaro SAITA,

Earthquake Research Institute.

A strong earthquake shock was felt on the boundary between Osaka and Nara prefecture at 10h 8m, on the 21st of February. Railway, telephone and other communication services were crippled for a time, while many buildings were damaged and a number of landslips reported. There were also same who were crushed to death under landslips and collapsed heavy walls.

In this paper the writer remarked the following two interesting matters:

(i) Damages to building are divided into two kinds, namely: in hard ground, heavy buildings were collapsed seriously, while in soft ground, old or loose buildings damaged. These facts already were pointed out by this writer in the great Kwanto earthquake, 1923, in the earthquake of north Musasi, 1931, and in the several earthquakes of Taiwan (Formosa).

(ii) The topography in the district injured by this earthquake are simple and symmetrical. There are strictly contrast of the earthquake damages in orthogonal directions through the epicentre. From above these affairs, the writer proposed that the contrast of damages suggest the line of discharge of earthquake energy, especially in the such case of shallow hypocentre and of monotonous disturbances as this earthquake.

29. *Theoretical and Experimental Study of Initial Motion of Seismographs and the Quantitative Study of First Impulsion of Earthquake.*

Part I.—Initial Motion of Seismographs caused by Ground Motion of Shock Type, with Special Reference to a Simple Method of Reducing the First Impulsion of Earthquake Motion.

By Hirosi KAWASUMI,

Earthquake Research Institute.

(Read May 19, 1936.—Received June 20, 1936.)

Thirty years have elapsed since Omori[1] discovered that the initial motion of earthquake is directed toward or away from the epicentre, and that the geographical distribution of its direction as well as different types of seismograms may be correlated with the mechanism of earthquake occurrence. When Galitzin[2] pointed out that the azimuth of the epicentre of a distant earthquake could be derived from the direction of the first impulsion of P, he was careful enough to work out a method of reducing the amplitude of the first ground motion, though he assumed it to be of sinusoidal form with a sudden beginning. But as his treatment was restricted to the case of his own seismograph with electromagnetic recording, H. Benndorf[3] invented another method of reduction though his result was vitiated by certain unfortunate errors. While Galitzin[4] was endeavouring to investigate the earth's internal structure from the emergence angle deduced from the observed magnitude of the first impulsion of P, a new field was opened by T. Shida, who showed that it is possible to infer the mechanism of earthquake occurrence from a study of the geographical distribution of initial dilatational or compressional waves. The prob-

1) F. OMORI, *Publ. Earthq. Invest. Commit.*, **21** (1905), esp. 58~61. *Bull. Earthq. Invest. Comm.*, **1** (1907), 145~154; *Report Earthq. Invest. Comm.*, **68** A (1910), 3~19.

2) B. GALITZIN, *Bull. d. Acad. Imp. d. Sci. St. Petersbourg*, (1909), or *Verhandl. d. Int. Seismol. Assoc. Zermatt*, (1909), 132~141, and *Vorlesungen über Seismometrie*, (1914).

3) H. BENNDORF, *Mitt. d. Erdbeben Komm. Wien*, N. F., **46** (1913). 122~169.

4) B. GALITZIN, *Comptes Rendus Comm. Sis. Perm. Petrograd*, **7** (1919), 185~334. (His posthumous work.)

lem was extended by S. T. Nakamura, T. Matuzawa, K. Suda, and others to near earthquakes, and by E. Gherzi, O. Somville, P. Byerly and others to distant earthquakes. The more recent advances made on the same lines in its quantitative study scarcely need comment[5].

But since for such quantitative studies suitable corrections to the recorded magnitude of initial motion are indispensable, Berlage[6], Nakamura[7], Matuzawa[8] and Meisser[9] took these effect into consideration, and worked out methods of reducing the first ground impulsion. There still remained however persons who questioned the validity of the initial conditions for the solution of the equation of motion of seismometers, $\ddot{a}+2\varepsilon\dot{a}+n^2a=-V\ddot{\sigma}$. Though Wiechert[10], Galitzin[11], and Nakamura rightly put $a_0=0$ and $\dot{a}_0=-V\dot{\sigma}_0$ at $t=0$ when the ground begins to move from rest, S. Kusakabe[12] and O. Meisser put $a_0=\dot{a}_0=0$, notwithstanding that $\sigma_0\neq 0$. The present writer[13], who took up the problem in 1931, justified the first condition and also were able to confirm the applicability of the harmonic factor with tolerable accuracy to ground motion with a continuously varying period and amplitude after about one cycle from the beginning.

For reduction of the transient part the writer suggested the use of the reduction introduced by Galitzin and Nakamura. Then, by comparing records obtained from an ordinary displacement-seismograph and an Ishimoto acceleration-seimograph, T. Suzuki[14] found the existence of a ground motion of shock type that began gradually and enumerated the motions of some specified seismographs under the influence of ground motion of the type e^{-ct^2}, while C. Tsuboi[15] fully investigated the transient motion of a pendulum caused by an external vibration that began either suddenly or gradually, ($\sin pt$ or $2\sin pt-\sin 2pt$). But later ground motions of approximately one

5) For a fuller account of this problem, the reader is referred to the writer's paper in the *Bull. Earthq. Res. Inst.*, **11** (1933), 403~453; **12** (1934), 43~705, and his "A Historical Review of the Problem of the Initial Motion of an Earthquake" which will be published in the near future.

6) H. P. BERLAGE, *Doktordissertation, Buchdrukerei, J. Waltman, Delft*, (1934).

7) S. T. NAKAMURA, *Proc. Imp. Acad*, **3** (1927), 32.

8) T. MATUZAWA, *Proc. Imp. Acad.*, **3** (1927), 68~71.

9) O. MEISSER, *Veröff. Reichsanstalt f. Erdbebenforschung, Jena*, **9** (1929).

10) E. WIECHERT, *Abhandl. K. Ges. Göttingen, Math.-Phy. Kl.*, N.F., **2** (1903), 1~125.

11) B. GALITZIN, *for ex. Vorlesungen über Seismometrie*, (1914).

12) S. KUSAKABE, *General Seismology*, (1927), 90, (Japanese).

13) H. KAWASUMI, *Disin*, **4** (1931), 71~94, and 167~169.

14) T. SUZUKI, *Bull. Earthq. Res. Inst.*, **12** (1934), 15~18, and 155~162.

15) C. TSUBOI, *Bull. Earthq. Res. Inst.*, **12** (1934), 426~445.

sided impulsion were found on several occasions[16], with the result that studies[17] on the motion of seismographs caused by certain specified ground motions have also been published. But there are no studies covering instruments with so wide a range of constants as in the cases investigated by Tsuboi, neither has any inquiry been made relating to the selection of the appropriate ground motion in a practical study nor any examination into the suitabiltiy of each assumption when applied to other cases. In order to construct a complete table of reducing ground motions of shock type referred to above, the writer in 1934 intended to calculate as an exercise in seismometry at the Seismological Institute the case for ground motion of the type $3\sin pt - \sin 3pt$ in the time interval $0 \leqq pt \leqq \pi$ only, the motion being a symmetrical one sided impulsion easy to calculate. He was greatly encouraged by the generous loan of Dr. Tsuboi of the results of his calcutations of the sinusoidal ground motion ($\sin pt$) during $0 \leqq pt \leqq 300°$. The table was completed with the colaboration of R. Satô and the kind assistance of students, S. Kunori, T. Yamamura, Y. Hattori, S. Hukunaga, K. Kimura and K. Satô, after about a year's interruption, although a part of the results was read on April 3, 1935, at the annual meeting of the Physico-mathematical Society of Japan. A case exactly the same has also been treated by H. Martin[18] of Jena, both theoretically and experimentally, but not in so complete a manner as we would have wished. He has again erred in putting $a_0 = \dot{a}_0 = 0$ as the initial condition for the acceleration-seismographs in opposition to Tsuboi.

In the meanwhile, M. Ishimoto, the director of the Earthquake Research Institute proposed in an unofficial circular letter to include the magnitudes and directions of the first motions P as well as other important phases in the bulletins of all seismological stations. In view of the encouraging response that met Ishimoto's proposal, the Subcommittee on Seismology of the National Research Council of Japan proposed to the forthcomming International Congress to be held at Edinburgh, that Seismological bulletins published by all seismological stations shall contain

1) The components of amplitude of first impulsion of P as well as its period in addition to the usual data on its direction as hitherto

16) K. Wadati, *Kensin Zihô*, **8** (1934), 21~31.
H. Kawasumi, *Read at the meeting of Phys.-math. Soc. Japan*, on April 3, 1935.
J. A. Sharpe, *Bull. Seismol. Soc. Amer.*, **25** (1935), 199~222.

17) M. Kizima, *Kensid Zihô*, **7** (1935), 97~107.
G. Nishimura and T. Takayama, *Disin*, **7** (1935), 100~117.

18) H. Martin, *Veröff. Reichsanstalt f. Erdbebenforschuag, Jena*, **26** (1935).

given by certain stations.

2) Similar data relating to the first impulsion of any other particular phase whenever it is clearly recognised.

It is explained in the proposal that the components of amplitude shall be seismographic readings divided by their respective magnifications. The magnification for the present purpose should not, from the ideal point of view, be the constant instrumental magnification, nor the usual one for the harmonic motion in stationary condition, but should be some variable magnification for the transient state of the beginning of the respective ground motion. To put this proposal into rigorous practice necessitates the use of numerical integration, which would be very laborious. Moreover there is the uncertainty as to which of the various methods just described of dealing with the proposal could be used satisfactorily. These were the main points of the objection raised by some to Ishimoto's proposal. To obtain the approval of the International Congress, some simple and convenient method should be offered, or an examination made the accuracy of the methods now in use and the result made known.

For this purpose the results of our calculation for the case of single ground impulsion will be described below and compared with other cases with the view of finding a simple but workable method of obtaining the first ground impulsion.

We shall now deduce the motion of a pendulum caused by a sinusoidal ground motion of finite length using the proof given in the writer's previous paper, with certain generalisations in favour of the initial condition $a_0=0$ and $\dot{a}_0=-V\dot{\sigma}_0$.

The elementary solution of the equation of motion

$$\ddot{a}+2\varepsilon\dot{a}+n^2a=-V\ddot{\sigma} \tag{1}$$

corresponding to $\sigma=Ae^{i\omega t}+Be^{-i\omega t}$ is

$$a=A\frac{V\omega^2}{n^2-\omega^2+2\varepsilon\omega i}e^{i\omega t}+B\frac{V\omega^2}{n^2-\omega^2-2\varepsilon\omega i}e^{-i\omega t}.$$

If we put $A=f(\omega)d\omega$, $B=g(\omega)d\omega$ and integrate from 0 to ∞, the result

$$a=\int_0^\infty\frac{V\omega^2 f(\omega)}{n^2-\omega^2+2\varepsilon\omega i}e^{i\omega t}d\omega+\int_0^\infty\frac{V\omega^2 g(\omega)}{n^2-\omega^2-2\varepsilon\omega i}e^{-i\omega t}d\omega$$

is also the solution of (1) corresponding to

$$\sigma(t)=\int_0^\infty f(\omega)\,e^{i\omega t}d\omega+\int_0^\infty g(\omega)\,e^{i\omega t}d\omega\,,$$

so long as $f(\omega)$ and $g(\omega)$ are independent of time.

Comparing it with Fourier's double integral theorem

$$\sigma(t)=\frac{1}{2\pi}\int_0^\infty d\omega\int_{-\infty}^\infty \sigma(\lambda)\, e^{i\omega(t-\lambda)}d\lambda+\frac{1}{2\pi}\int_0^\infty d\omega\int_{-\infty}^\infty \sigma(\lambda)e^{-i\omega(t-\lambda)}d\lambda\,, \tag{2}$$

we have the general solution

$$a=\frac{V}{2\pi}\int_{-\infty}^\infty \frac{\omega^2 d\omega}{n^2-\omega^2+2\varepsilon\omega i}\int_{-\infty}^\infty \sigma(\lambda)\, e^{i\omega(t-\lambda)}d\lambda\,, \tag{3}$$

corresponding to the arbitrary ground motion $\sigma(t)$.

In the special case

$$\sigma(t)=\begin{cases} 0 & \\ \sin pt & \text{for} \\ 0 & \end{cases} \quad \begin{matrix} t<0\,, \\ 0\leqq t\leqq t_1\,, \\ t_1<t\,, \end{matrix} \tag{4}$$

with which we are concerned, we have

$$a=\frac{V}{2\pi}\int_{-\infty}^\infty \frac{\omega^2 d\omega}{n^2-\omega^2+2\omega\varepsilon i}\int_0^{t_1} \sin p\lambda\, \sigma^{i\omega(t-\lambda)}d\lambda$$

$$=\frac{V}{4\pi}\Bigg[\left\{\int_{-\infty}^\infty \frac{\omega^2 e^{i\omega t}d\omega}{(\omega-\alpha)(\omega-\beta)(\omega-p)}-\int_{-\infty}^\infty \frac{\omega^2 e^{i\omega t}d\omega}{(\omega-\alpha)(\omega-\beta)(\omega+p)}\right\}$$

$$-\left\{e^{ipt_1}\int_{-\infty}^\infty \frac{\omega^2 e^{i\omega(t-t_1)}d\omega}{(\omega-\alpha)(\omega-\beta)(\omega-p)}-e^{-ipt_1}\int_{-\infty}^\infty \frac{\omega^2 e^{i\omega(t-t_1)}d\omega}{(\omega-\alpha)(\omega-\beta)(\omega+p)}\right\}\Bigg], \tag{5}$$

where α and β are the roots of $\omega^2-2\varepsilon\omega i-n^2=0$,

$$\alpha=\sqrt{n^2-\varepsilon^2}+\varepsilon i\,, \qquad \beta=-\sqrt{n^2-\varepsilon^2}+\varepsilon i\,. \tag{6}$$

The infinite integral

$$I_\pm=\int_{-\infty}^\infty \frac{\omega^2 e^{i\omega\tau}d\omega}{(\omega-\alpha)(\omega-\beta)(\omega\pm p)} \tag{7}$$

is easily evaluated by contour integral along the real axis with a small indentation at $\omega=-p$ or $+p$ and infinite semi-circle on the upper or lower half of the complex plane according as τ is positive or negative. The result is

$$I_{\pm}=\left\{\begin{array}{ll} -\pi i\dfrac{p^2}{p^2+(\alpha+\beta)p+\alpha\beta}e^{\mp ip\tau}, & \text{for } \tau<0, \\ \pi i\dfrac{p^2}{p^2\pm(\alpha+\beta)p+\alpha\beta}e^{\mp ip\tau}+\dfrac{2\pi i}{\alpha-\beta}\left\{\dfrac{\alpha^2e^{i\alpha\tau}}{\alpha\pm p}-\dfrac{\beta^2e^{i\beta\tau}}{\beta\pm p}\right\}, & \text{for } \tau>0. \end{array}\right\} \quad (8)$$

and a little arithmetic shows that

(i) for $t<0$, $t-t_1<0$,

$$a=0,$$

(ii) for $0\leqq t\leqq t_1$,

$$a=\frac{V\sigma_m i}{2}\left[p^2\left\{\frac{e^{-ipt}}{p^2+(\alpha+\beta)p+\alpha\beta}-\frac{e^{ipt}}{p^2-(\alpha+\beta)p+\alpha\beta}\right\}\right.$$
$$\left.+\frac{2p}{(\alpha-\beta)}\left\{\frac{\alpha^2e^{i\alpha t}}{\alpha^2-p^2}-\frac{\beta^2e^{i\beta t}}{\beta^2-p^2}\right\}\right]\cdot$$

$$=\frac{V\sigma_m}{\sqrt{(1-u^2)^2+4h^2u^2}}\left\{\sin(pt-\Delta)-\frac{u}{\mu}e^{-\varepsilon t}\sin(\gamma t-\delta)\right\}, \quad (9)$$

where $u=n/p$, $\gamma=\sqrt{n^2-\varepsilon^2}=n\mu$,

$$\tan\Delta=\frac{2hu}{u^2-1} \quad \text{and} \quad \tan\delta=\frac{2h\mu}{u^2-1+2h^2},$$

(iii) for $t_1<t$,

$$a=\frac{V\sigma_m i}{2(\alpha-\beta)}\left[2p\left\{\frac{\alpha^2e^{i\alpha t}}{\alpha^2-p^2}-\frac{\beta^2e^{i\beta\tau}}{\beta^2-p^2}\right\}\right.$$
$$\left.-e^{ipt_1}\left\{\frac{\alpha^2e^{i\alpha(t-t_1)}}{\alpha-p}-\frac{\beta^2e^{i\beta(t-t_1)}}{\beta-p}\right\}+e^{-ipt_1}\left\{\frac{\alpha^2e^{i\alpha(t-t_1)}}{\alpha+\beta}-\frac{\beta^2e^{i\beta(t-t_1)}}{\beta+p}\right\}\right], \quad (10)$$

and in the special case with which we are concerned, $pt=(2k+1)\pi$, k being an integer, it reduces to

$$=\frac{-V\sigma_m}{\sqrt{(1-u^2)^2+4h^2u^2}}\frac{u}{\mu}\left\{e^{-\varepsilon t}\sin(\gamma t-\delta)+e^{-\varepsilon(t-t_1)}\sin\gamma(t-t_1-\delta)\right\}. \quad (11)$$

From the above solution we can see that the pendulum begins to move at $t=0$ with initial velocity $\dot{a}_0=-Vp\sigma_m=-V\dot{\sigma}_0$, while at $t=t_1$ the forced oscillations with frequency p come to an end, generating anew the proper oscillation of the pendulum, besides the one generated at $t=0$. In the case $pt=(2k+1)\pi$, the proper motion there generated is exactly equal to that generated at the beginning. The result is evident from the law of superposition characteristic of the linear differential equation.

By means of the above solution the motion of the pendulum caused by

$$\sigma(t)=\begin{cases} 0\,, & t<0\,, \\ 3\sin pt-\sin 3pt\,, & 0<pt<\pi\,, \\ 0\,, & \pi<pt\,, \end{cases} \qquad (12)$$

was obtained with the aid of Dr. Tsuboi's calculations. The results are shown in the following figures and tables. The instrumental magnification V is assumed to be unity.

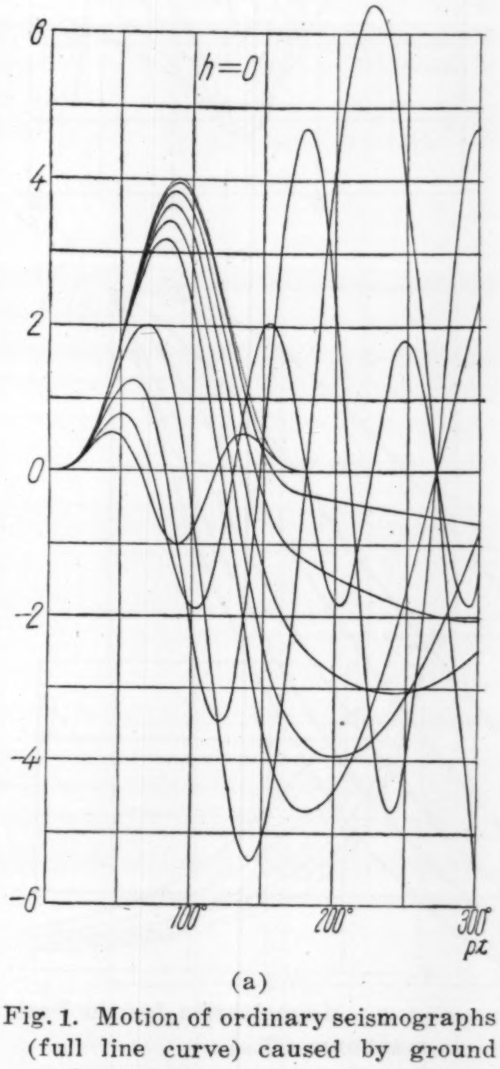

(a)

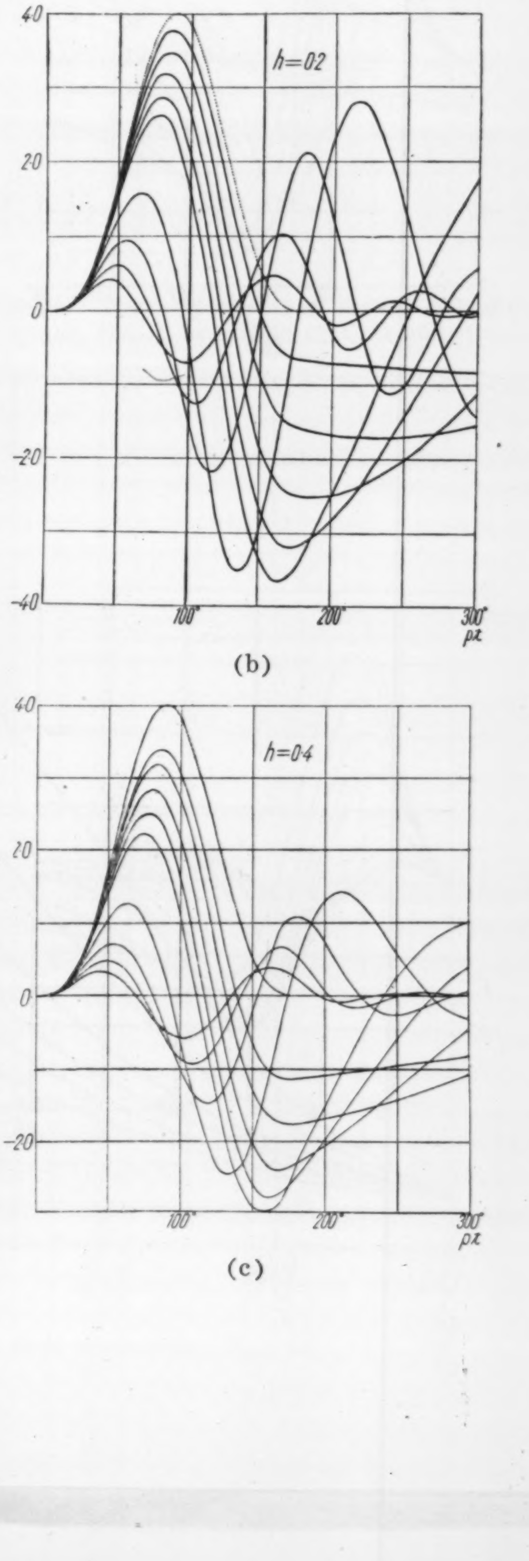

(b)

(c)

Fig. 1. Motion of ordinary seismographs (full line curve) caused by ground motion $\sigma=3\sin pt-\sin 3pt$ (dotted line). Respective curves correspond to $u=n/p=0{\cdot}2$, $0{\cdot}4$, $0{\cdot}6$, $0{\cdot}8$, $1{\cdot}0$, $2{\cdot}0$, $3{\cdot}0$, $4{\cdot}0$ and $5{\cdot}0$.

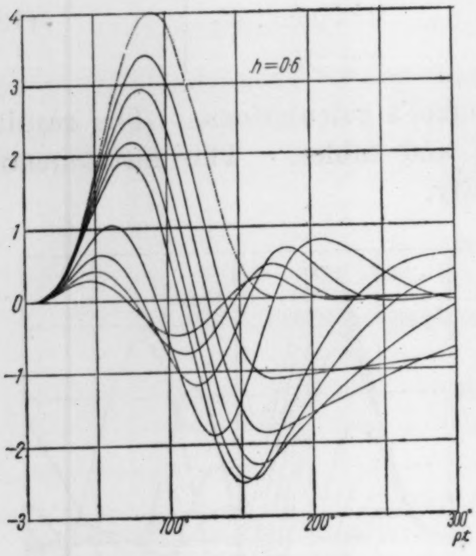

(d)

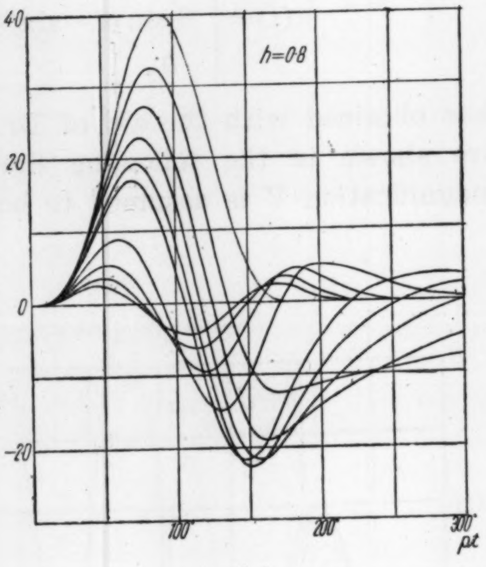

(e)

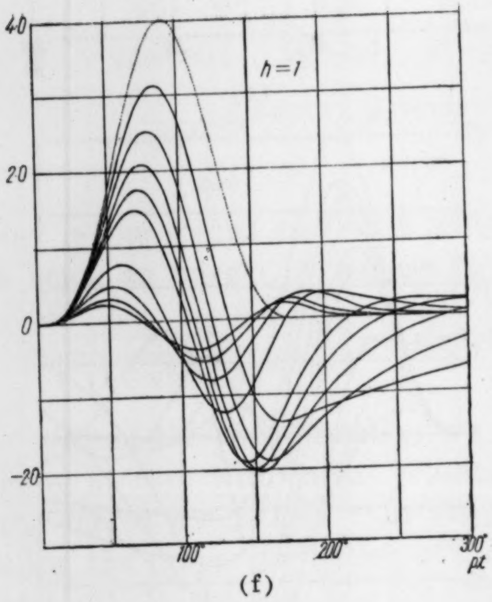

(f)

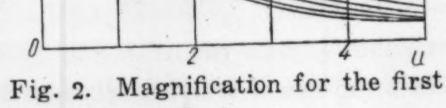

Fig. 2. Magnification for the first maximum ($\mathfrak{V}_{1m}$).

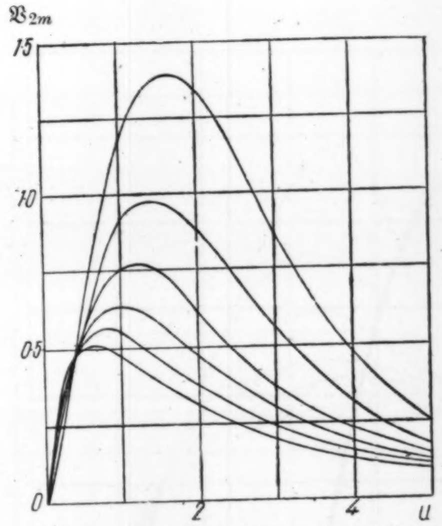

Fig. 3. Magnification for the second maximum.

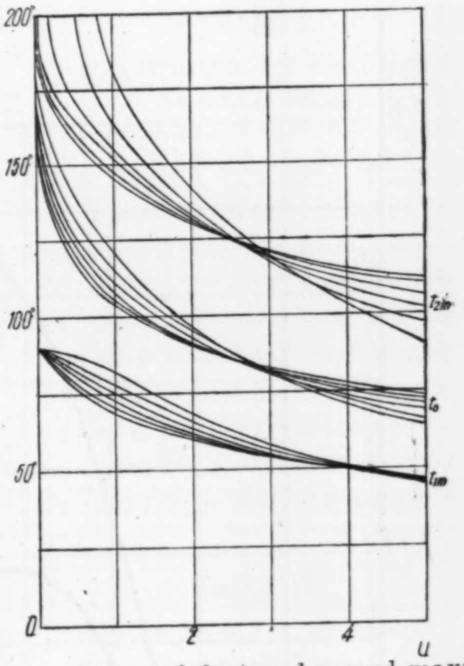

Fig. 4. Times of first and second maxima (pt_{1m}), (pt_{2m}), and time of first zero (pt_0).

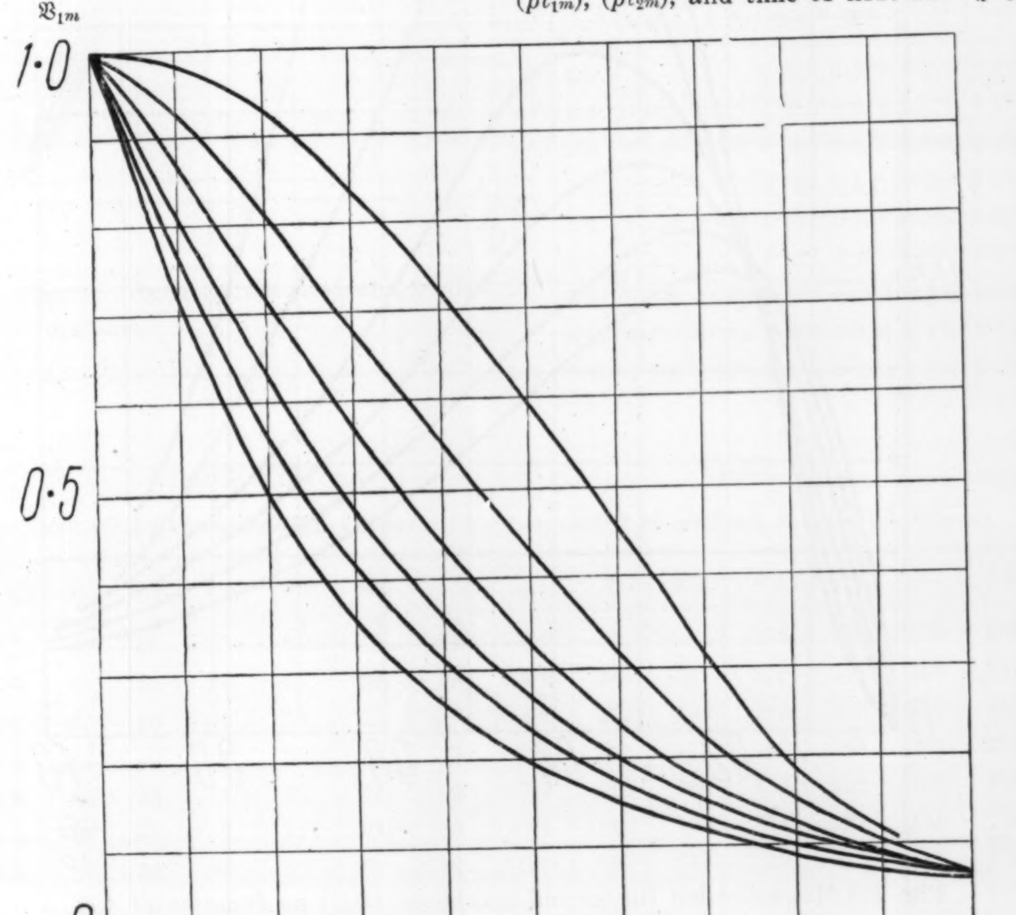

Fig. 5. Magnification for the first maximum ($\mathfrak{V}_{1m}$) as function of t_0/T_0.

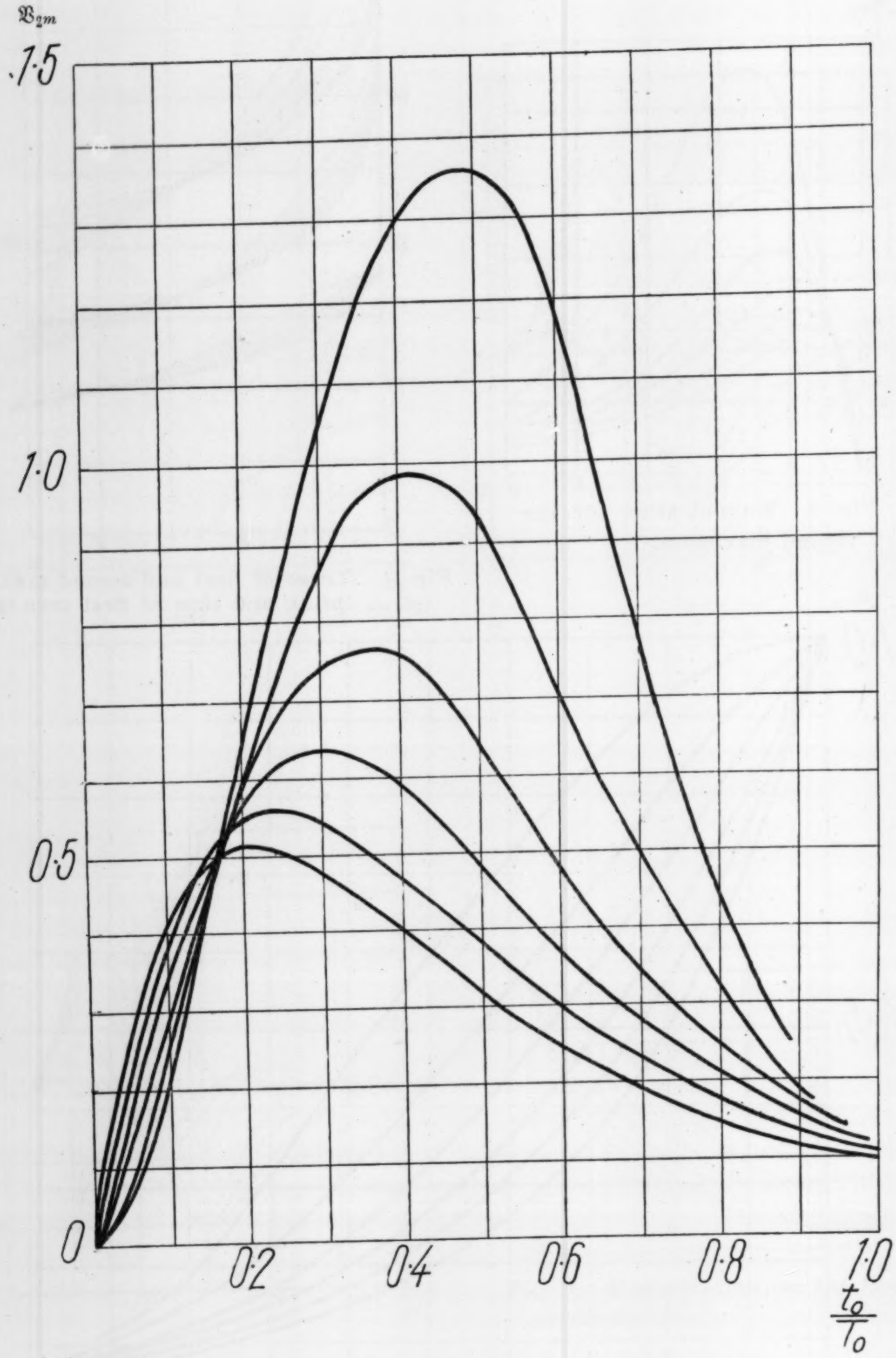

Fig. 6. Magnification for second maximum ($\mathfrak{B}_{2m}$) as function of t_0/T_0.

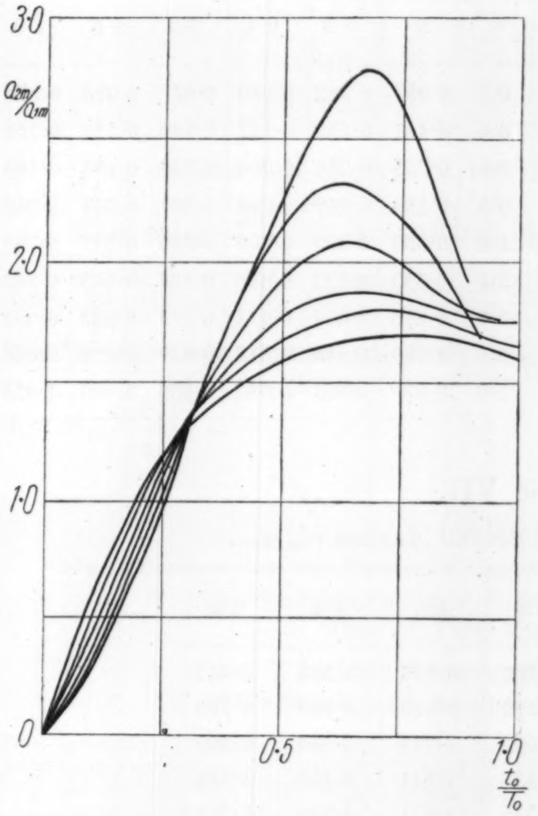

Fig. 7. Ratio of the first and second maxima.

Table I.

Magnification for the First Maximum ($\mathfrak{B}_{1m}$).

u \ h	0	0·2	0·4	0·6	0·8	1·0
0·2	0·988	0·943	0·896	0·850	0·813	0·783
0·4	0·960	0·866	0·796	0·731	0·678	0·630
0·6	0·915	0·795	0·705	0·634	0·570	0·520
0·8	0·860	0·715	0·623	0·545	0·478	0·435
1·0	0·798	0·656	0·551	0·475	0·420	0·370
2·0	0·530	0·395	0·314	0·263	0·223	0·195
3·0	0·313	0·233	0·179	0·158	0·133	0·118
4·0	0·195	0·152	0·123	0·104	0·090	0·078
5·0	0·130	0·104	0·083	0·070	0·065	0·060

Table II.

Magnification for the Second Maximum ($\mathfrak{B}_{2m}$).

u \ h	0	0·2	0·4	0·6	0·8	1·0
0·2			0·225	0·279	0·315	0·345
0·4	0·465	0·429	0·470	0·465	0·475	0·475
0·6	0·765	0·630	0·603	0·575	0·540	0·510
0·8	0·985	0·799	0·704	0·621	0·566	0·503
1·0	1·178	0·918	0·750	0·635	0·553	0·475
2·0	1·343	0·881	0·615	0·470	0·375	0·310
3·0	0·868	0·533	0·370	0·295	0·239	0·198
4·0	0·475	0·311	0·231	0·188	0·156	0·130
5·0	0·250	0·175	0·145	0·123	0·108	0·095

Table III.

Time of First Maximum (pt_{1m}).

u \ h	0	0·2	0·4	0·6	0·8	1·0
0.2	89°	88°	87°	86°	85°	84°
0·4	88	85	84	83	80	79
0·6	87	83	81	79	77	75
0·8	84	80	78	76	74	72
1·0	82	78	75	72	71	70
2·0	69	66	64	63	61	60
3 0	58	56	54	55	55	54
4·0	51	51	50	50	51	51
5·0	45	45	44	46	46	46

Table IV.

Time of Second Maximum (pt_{2m}).

u \ h	0	0·2	0·4	0·6	0·8	1·0
0·2			175°	175°	170°	170°
0·4	295°	237°	176	169	164	161
0·6	242	188	168	162	159	155
0·8	202	172	162	158	152	150
1·0	181	164	157	152	148	145
2·0	142	136	133	132	131	130
3·0	119	118	119	119	120	121
4·0	103	105	108	112	115	115
5·0	90	97	102	106	110	111

Table V.

Time of First Zero (pt_0).

u \ h	0	0·2	0·4	0·6	0·8	1·0
0·2	156·5°	148°	143°	139°	136°	133°
0·4	144·5	137	131	127·5	124·5	121·5
0·6	135	128	122·5	120	116·5	114
0·8	127·5	121	116·5	113	110	108
1·0	120·5	115	111	108	106	104
2·0	96	94	92·5	91·5	90·5	90
3·0	81	81	80·5	81·5	82	83
4·0	71	72·5	73·5	75·5	76·5	77·5
5·0	64	66·5	68·5	71	72·5	73·5

Table VI.

Time of First Zero Measured in Fraction of Proper Period of Pendulum (t_0/T_0).

u \ h	0	0·2	0·4	0·6	0·8	1·0
0·2	0·087	0·082	0·080	0·077	0·076	0·074
0·4	0·161	0·152	0·147	0·142	0·139	0·135
0·6	0·225	0·214	0·204	0·200	0·195	0·190
0·8	0·284	0·269	0·259	0·251	0.244	0·240
1·0	0·335	0·320	0·309	0·300	0·295	0·289
2·0	0·533	0·522	0·513	0·508	0·503	0·500
3·0	0·675	0·674	0·671	0·679	0·683	0·691
4·0	0·789	0·806	0·817	0·839	0·850	0·861
5·0	0·889	0·923	0·952	0·986	1·008	1·020

Table VII.

Ratio of the First and Second Maxima a_{1m}/a_{2m}.

u \ h	0	0·2	0·4	0·6	0·8	1·0
0.2			0·251	0·328	0·388	0·442
0·4	0·485	0·495	0·590	0·635	0·702	0·753
0·6	0·835	0·793	0·852	0·909	0·950	0·980
0·8	1·148	1·120	1·135	1·141	1·185	1·156
1·0	1·480	1·400	1·355	1·331	1·317	1·286
2·0	2·440	2·230	1·962	1·790	1·682	1·590
3·0	2·780	2·280	2·070	1·875	1·800	1·685
4·0	2·439	2·050	1·885	1·809	1·740	1·681
5·0	1·925	1·680	1·762	1·754	1·652	1·581

We next calculated the motion of the Galitzin seismograph ($T_0=T_1$, $\mu=0$) caused by

(i) $\sin pt$ for $0\leqq t$,

(ii) $3\sin pt-\sin 3pt$ for $0\leqq pt\leqq\pi$,

(iii) $2\sin pt-\sin 2pt$ for $0\leqq t$,

by mean of Galitzin's own solution

$$a_1=\frac{kA_1T_0\sigma_m}{\pi l}u\left\{e^{-u\xi}\left[a_0+a_1\xi+a_2\xi^2+a_3\xi^3\right]+g\cos\xi+h\sin\xi\right\}, \qquad (13)$$

where $\xi=pt$ and

$$a_0=\frac{1-6u^2+u^4}{(1+u^2)^4}\,, \qquad a_3=-\frac{1}{6}\frac{u^3}{1+u^2}\,,$$

$$a_1=\frac{u(3-u^2)}{(1+u^2)^3}\,, \qquad g=-a_0\,,$$

$$a_2=\frac{1}{2}\frac{u^2(3+u^2)}{(1+u^2)^2}\,, \qquad h=\frac{4u(1-u^2)}{(1+u^2)^4}\,.$$

The results are shown in the following table and figures.

The fator $\frac{kA_1T_0}{\pi l}$ is omitted in the following calculation. Therefore to obtain the first ground impulsion we have to divide the recorded first maximum (a_{1m}) by $\mathfrak{V}_{1m}\frac{kA_1T_0}{\pi l}$ or second maximum (a_{2m}) by $\mathfrak{V}_{2m}\frac{kA_1T_0}{\pi l}$.

Table VIII.

Magnification for the First and Second Maxima ($\mathfrak{V}_{1m}$, $\mathfrak{V}_{2m}$), and their Raito ($\mathfrak{V}_{2m}/\mathfrak{V}_{1m}=a_{2m}/a_{1m}$) and Epochs ($pt_{1m}$, pt_{2m}), as well as Time of First Zero pt_0, and t_0/T_0.

Galitzin Seismograph ($T_0=T_1$, $\mu=0$).

(i) $\sigma(t)=\sin pt$, (ii) $3\sin pt-\sin 3pt$, (iii) $2\sin pt-\sin 2pt$.

(i)

u	$\mathfrak{V}_{1m}$	$\mathfrak{V}_{2m}$	a_{2m}/a_{1m}	pt_{1m}	pt_{2m}	pt_0	t_0/T_0
0·2	0·150	0·235	1·57	127°	294°	207	0·115
0·4	0·154	0·308	2·00	99	268	165	0·183
0·6	0·137	0·284	2·07	83	233	140	0·233
0·8	0·121	0·239	1·98	72	210	121	0·269
1·0	0·105	0·196	1·87	58	191	107	0·297
1·5	0·077	0·122	1·58	45	152	84	0·350
2·0	0·060	0·079	1·32	35	125	69	0·384
3·0	0·044	0·039	0·84	25	100	54	0·450
4·0	0·033	0·017	0·52	21	75	45	0·500
5·0							

(ii)

u	$\mathfrak{V}_{1m}$	$\mathfrak{V}_{2m}$	a_{2m}/a_{1m}	pt_{1m}	pt_{2m}	pt_0	t_0/T_0
0·2	0·131	0·063	0·48	121		214	0·119
0·4	0·153	0·121	0·79	105	233	159	0·177
0·6	0·148	0·164	1·11	95	193	139	0·232

(to be continued.)

(ii) (*continued.*)

u	$\mathfrak{B}_{1m}$	$\mathfrak{B}_{2m}$	a_{2m}/a_{1m}	pt_{1m}	pt_{2m}	pt_0	t_0/T_0
0·8	0·136	0·188	1·38	89°	174°	127°	0·254
1·0	0·121	0·195	1·61	82·5	163·5	117	0·328
1·5	0·091	0·176	1·93	71·5	145	102·5	0·428
2·0	0·066	0·140	2·13	65	133	92·5	0·513
3·0	0·041	0·088	2·15	53·5	119	80	0·667
4·0	0·028	0·051	1·34	46	108	75·5	0·839
5·0	0·022	0·033	1·53	41	102	69	0·958

(iii)

u	$\mathfrak{B}_{1m}$	$\mathfrak{B}_{2m}$	a_{2m}/a_{1m}	pt_{1m}	pt_{2m}	pt_0	t_0/T_0
0·2							
0·4	0·151	0·296	1·96	133°	257°	184°	0·204
0·6							
0·8	0·117	0·300	2·56	111	221	153	0·340
1·0	0·102	0·273	2·67	102	219	142	0·394
1·5							
2·0	0·045	0·126	2·80	78	173	112	0·622
3·0	0·027	0·068	2·49	93	152	96	0·801
4·0	0·019	0·037	1·92	55	140	90	1·000
5·0							

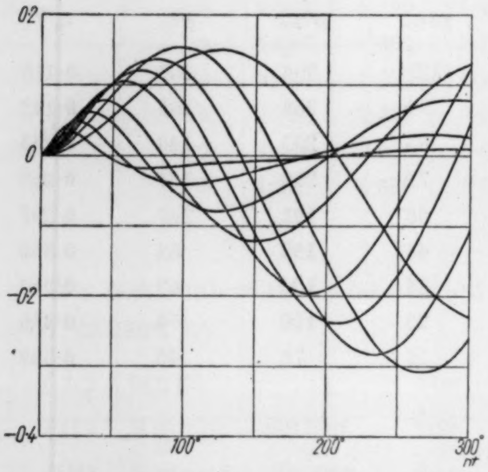

Fig. 8. Motion of the galvanometer of Galitzin seismograph caused by $\sigma=\sin pt$. Respective curves correspond to $u=n/p$ $=0{\cdot}2$, 0·4, 0·6, 0·8, 1·0, 1·5, 2·0, 3·0 and 4·0.

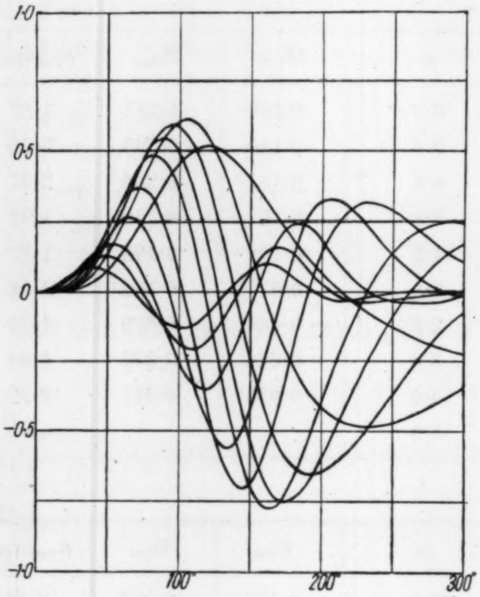

Fig. 9. Motion of the galvanometer of Galitzin seismograph caused by $\sigma=3\sin pt-\sin 3pt$. $0\leqq pt\leqq\pi$. Respective curves correspond to $u=n/p=$ 0·2, 0·4, 0·6, 0·8, 1·0, 1·5, 2·0, 3·0, 4·0 and 5·0.

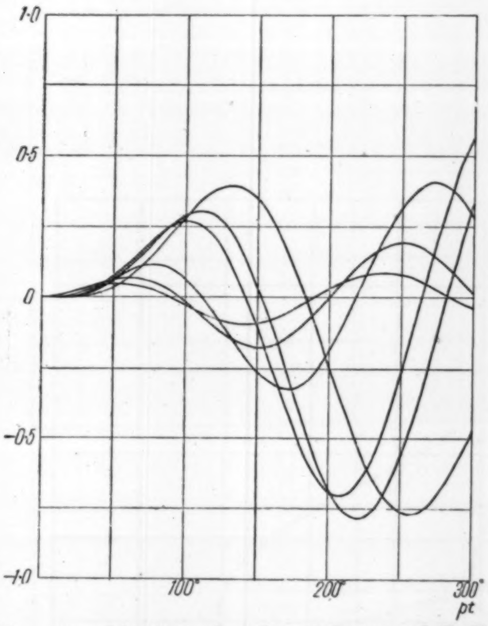

Fig. 10. Motion of galvanometer of Galitzin seismograph caused by $\sigma=2\sin pt-\sin 2pt$, $0\leqq pt$. Respective curves correspond to $u=n/p=0{\cdot}4$, $0{\cdot}8$, $1{\cdot}0$, $2{\cdot}0$ and $4{\cdot}0$.

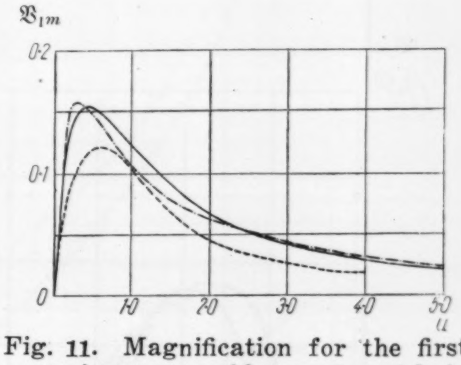

Fig. 11. Magnification for the first maximum caused by $\sigma=\sin pt$ (chain line), $3\sin pt-\sin 3pt$ (full line), or $2\sin pt-\sin 2pt$ (broken line). (Galitzin seismograph.)

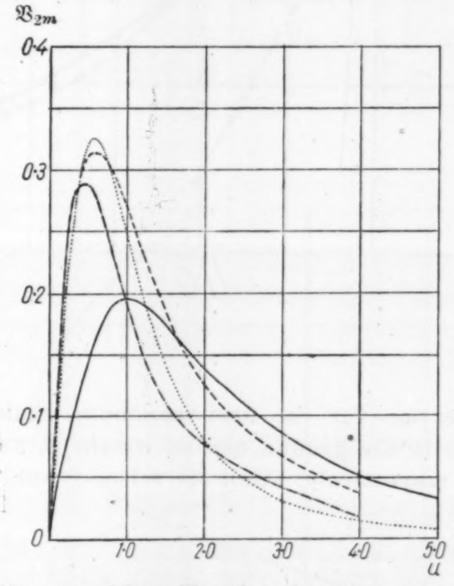

Fig. 12. Magnification for the second maximum. Broken, full and chain line correspond to the same as in Fig. 11. Dotted line represent the magnification for $\sin pt$ in stationary state. (Galitzin seismograph.)

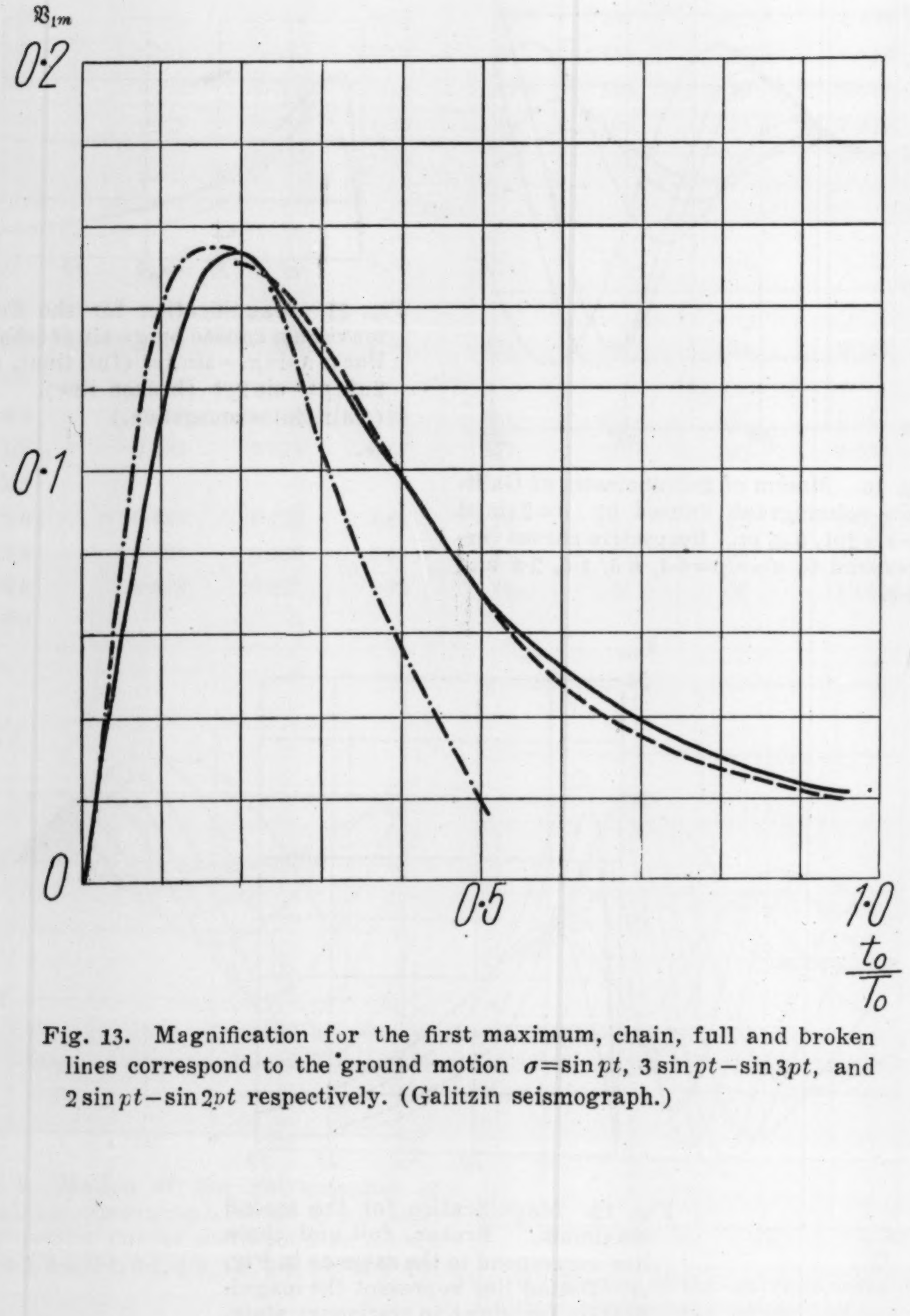

Fig. 13. Magnification for the first maximum, chain, full and broken lines correspond to the ground motion $\sigma=\sin pt$, $3\sin pt-\sin 3pt$, and $2\sin pt-\sin 2pt$ respectively. (Galitzin seismograph.)

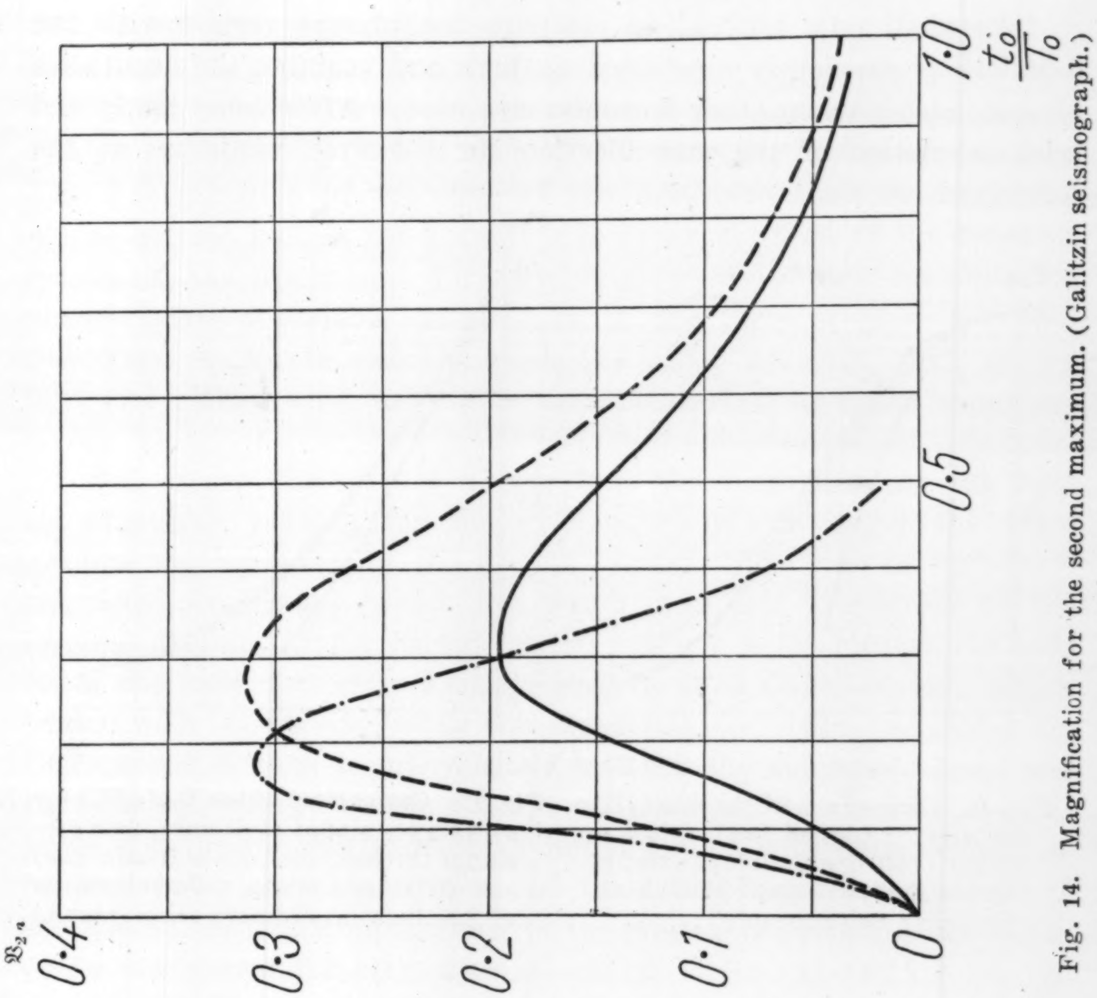

Fig. 14. Magnification for the second maximum. (Galitzin seismograph.)

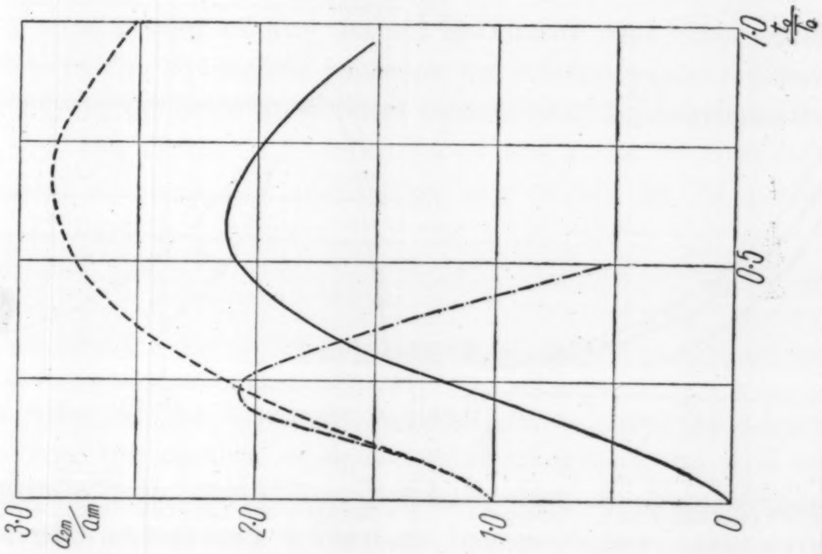

Fig. 15. Ratio of first and second maxima. (Galitzin seismograph.)

We shall now proceed to compare the present results with the calculations previously mentioned authors and examine the accuracies of each result when other formulae are used. After some study and trial, tabulation of the magnification for the first maximum as the

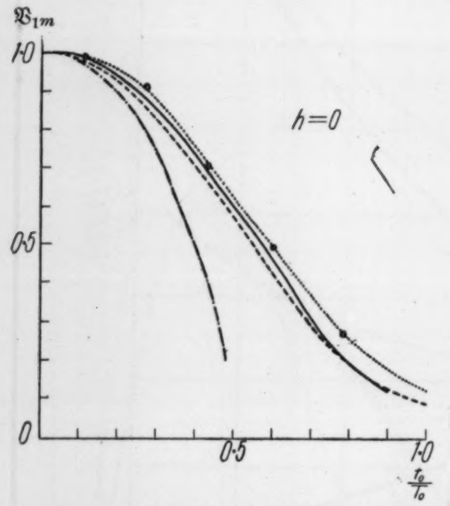

Fig. 16. Comparison of the $\mathfrak{V}_{1m}(t_0/T_0)$ for $\sigma=e^{-ct^2}$ (dotted line), $3\sin pt-\sin 3pt$ (full line), $2\sin pt-\sin 2pt$ (broken line), and $\sin pt$ (chain line). (Ordinary Seismograph.)

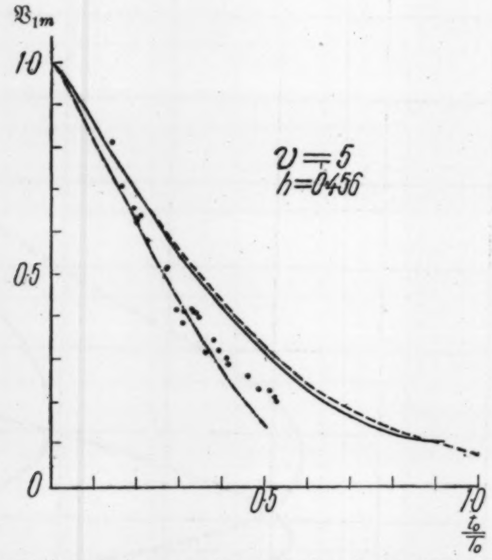

Fig. 17. Comparison of the $\mathfrak{V}_{1m}(t_0/T_0)$ for $\sigma=3\sin pt-\sin 3pt$ (full line), $2\sin pt-\sin 2pt$ (broken line), $\sin pt$ (chain line) and $te^{\beta t}\sin pt$ (points, different values of β inclusive). (Ordinary seismograph.)

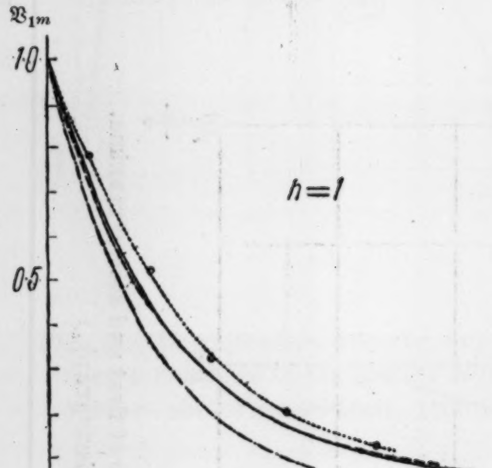

Fig. 18. Comparison of the $\mathfrak{V}_{1m}(t_0/T_0)$ for $\sigma=e^{-ct^2}$ (dotted line), $3\sin pt-\sin 3pt$ (full line), $2\sin pt-\sin 2pt$ (broken line) and $\sin pt$ (chain line). (Ordinary seismograph.)

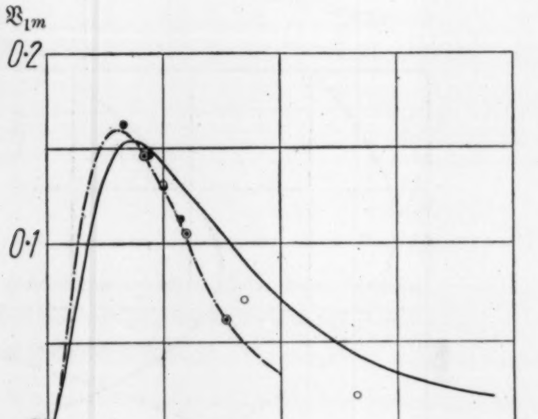

Fig. 19. Comparison of the $\mathfrak{V}_{1m}(t_0/T_0)$ for $\sigma=3\sin pt-\sin 3pt$ (full line), $\sin pt$ (chain line) and $e^{\beta t}\sin pt$ (points, different kind of points correspond to different value of β). (Galitzin seismograph.)

function of the time of first zero from the beginning measured in fractions of the proper period of the pendulum t_0/T_0, was found very convenient in practice for the reduction of the first impulsion, as already anticipated by Tsuboi although he used $2t_0/T_0$ instead of t_0/T_0. The determination of the time of the first zero from the beginning of the ground motion far surpasses in accuracy those of the times of maximum and minimum. The magnification of the first maximum is almost fairly invariable irrespective of the form of ground motion (see Figs. 16, 17, 18 and 19), while the other intervals, such as the first and second zero, are liable to be disturbed by other waves arriving later.

But closer examination shows that the magnitude of the first seismographic reading for the given t_0/T_0 is the larger the more gradual the beginning of the ground motion. The case of $\sigma(t)=e^{-ct^2}$ calculated dy Suzuki (which the writer was able to examine on the original diagams kindly loaned by the author) is the largest, the next being the case for $\sigma(t)=2\sin pt-\sin 2pt$, or $3\sin pt-\sin 3pt$, which begins with $\dot{\sigma}_0=\ddot{\sigma}_0=0$, while the case $\sigma(t)=te^{at}\sin pt$ calculated by Berlage and Kizima is intermediate between the above two cases and that for $\sigma(t)=\sin pt$ or the $e^{\beta t}\sin pt$ of J. Rybner[19]. Besides the improbability of the existence of an initial motion with finite velocity as believed in by some authorities, and the actual frequent appearance of the almost one-sided impulsion with the gradual beginning of an earthquake, the curves for $\sigma(t)=2\sin pt-\sin 2pt$ or $3\sin pt-\sin 3pt$ may be used in practice as the intermediate one. Yet still higher accuracy could be obtained if we could judge the ground motion more accurately by a comparison of the second maximum and other quantities by referring to the respective cases or by interpolation. Discrimination of the particular type of ground motion may be conveniently made by comparing the ratios of amplitudes of the recorded first with that of the second maxima. A still better way would be to install seismographs of various constants, like the acceleration- and velocity-seismometers.

Concluding Remarks.

In view of the frequent appearance of first impulsions of the shock type, the motion of ordinary seismographs as well as those of the Galitzin type caused by ground motion $\sigma=3\sin pt-\sin 3pt$ were theoretically calculated. Then as to actual application, the fair ac-

---

19) J. RYBNER, *Gerlands Bertr. z. Geophys.*, **31** (1931), 259~281.

curacy of this assumption though applied to other forms of ground motions was examined, and a simple method of reducing the first impulsion of earthquake with tolerable accuracy was pointed out. That is by reducing by means of magnification of the first maximum for the ground motion $2\sin pt - \sin 2pt$ or $3\sin pt - \sin 3pt$, taking the time of first zero from the beginning measured in fractions of the proper period of the pendulum as parameter.

In conclusion the writer offers his heartiest thanks to Prof. Ishimoto for his kind encouragement and to Dr. C. Tsuboi for the generous loan of his results of calculation. Thanks are due also to R. Satô and others who assisted him in the numerical computations. He also wish to express his thanks to the Council of the Foundation for the Promotion of Scientific and Industrial Research of Japan, whose aid greatly assisted the preparation of this paper.

---

29. 地震計初動の理論的及實驗的研究並びに地震初動の定量的研究

（其の1）衝動性地動による各種地震計の運動及び地震初動を求むる簡便法に就て

地震研究所　河　角　　廣

地震初動の定量的研究の國際的協力に關する日本學術研究會議地震分科會よりの萬國測地學地球物理學協會の國際會議への提案に關聯して，筆者は實際地震の際に屢々觀測される衝擊性地動に對する各種地震計の運動を計算し，これと他の地動に對する場合と比較し，地震記象上に於ける初動の倍率 $\mathfrak{V}_{1m}$ を t_0/T_0（t_0 は動き始めから最初の零點までの時間，T_0 は地震計の週期）の函數と見る時は $\mathfrak{V}_{1m}(t_0/T_0)$ 曲線はかなり種々の地動に對し實用上差支へない程度しか各の間で違がない事を知つた．然も坪井氏の計算した地動 $\sigma=2\sin pt-\sin 2pt$ 或は本論文に用ひた $\sigma=3\sin pt-\sin 3pt$ に對する $\mathfrak{V}_{1m}(t_0/T_0)$ 曲線は殆んど一致するものであるが今迄考へられて居る地動の形に對する倍率曲線 $\mathfrak{V}_{1m}(t_0/T_0)$ のほぼ中庸の値を示す故，兩者の中何れかを用ふれば現在必要とする程度に於て十分な程度に地震初動の大きさを知る事が出來る．

尙本研究に際し計算の勞を分たれた佐藤柳造氏及び地震學科學生，九里尙一，山村常正，服部保正，早川正已，福永三郎，木村耕三，佐藤光之助の諸氏に厚く感謝の意を表し，不斷の激勵を賜つた石本先生に深謝すると共に，本研究に對する補助に對し日本學術振興會に感謝する次第である．

---

30. *Theoretical and Experimental Study of Initial Motion of Seismographs and the Quantitative Study of First Impulsion of Earthquake.*

Part II.—An Experimental Study of the Initial Motion of Seismographs caused by Motions of Short Duration.

By Hirosi KAWASUMI and Zyun'iti KINOSITA,

Earthquake Research Institute.

(Read May 19, 1936.—Received June 20, 1936.)

A proposal was made by the Subcommittee on Seismology of the National Research Council of Japan to the forthcoming Congress of the International Union of Geodesy and Geophysics at Edinburgh in view of the unofficial circular letter of Prof. M. Ishimoto addressed to seismological stations throughout the world for the international co-operation with respect to quantitative studies of the initial motion of earthquakes. With the object of supporting the idea, Prof. Ishimoto advised us to study experimentally the initial motion of seismographs. At the same time one[1] of the authors showed that simple method, first suggested by Dr. Tsuboi[2], of reducing the first ground impulsion by observing the magnitude of the initial deflection and time of first zero from the beginning of motion on seismograms, may be applied with tolerable accuracy regardless of the form of the ground motion. This conclusion was derived by comparing the results of theoretical calculations for some types of ground motion of regular mathematical form. But the result of our present shaking table experiments proved the applicability of the above simple method to cases of somewhat irregular motions imparted to the shaking table by the unaided hand irrespective of the type of external motion. It also proved the applicability of the usual equation of motion

$$\ddot{a} + 2\varepsilon\dot{a} + n^2 a = -V(\ddot{\sigma} - gi) \qquad (1)$$

either in the statical or dynamical state including the beginning of motion.

---

1) H. KAWASUMI, Part I of the present study, *Bull. Earthq. Res. Inst.*, **14** (1936), 319~338.

2) C. TSUBOI, *Bull. Earthq. Res. Inst.*, **12** (1934), 426~445.

The seismographs used were an acceleration-seismograph designed by Prof. Ishimoto and the velocity- and displacement-seismographs designed by Mr. T. Hagiwara. All the seismographs are of the inverted pendulum type with air damper and mechanical recording, the construction details and the results of applications of which as well as comparative studies of them have already been reported by the respective designers on a number of occasions.[3]

1. Standardisation of Instruments, I.

As it behove us to know all the instrumental constants exactly in each experiment, special calibration were made as far as possible.

(i) *Geometrical Magnifications.*

Geometrical magnification V_G as defined by Prof. Ishimoto[4] is the

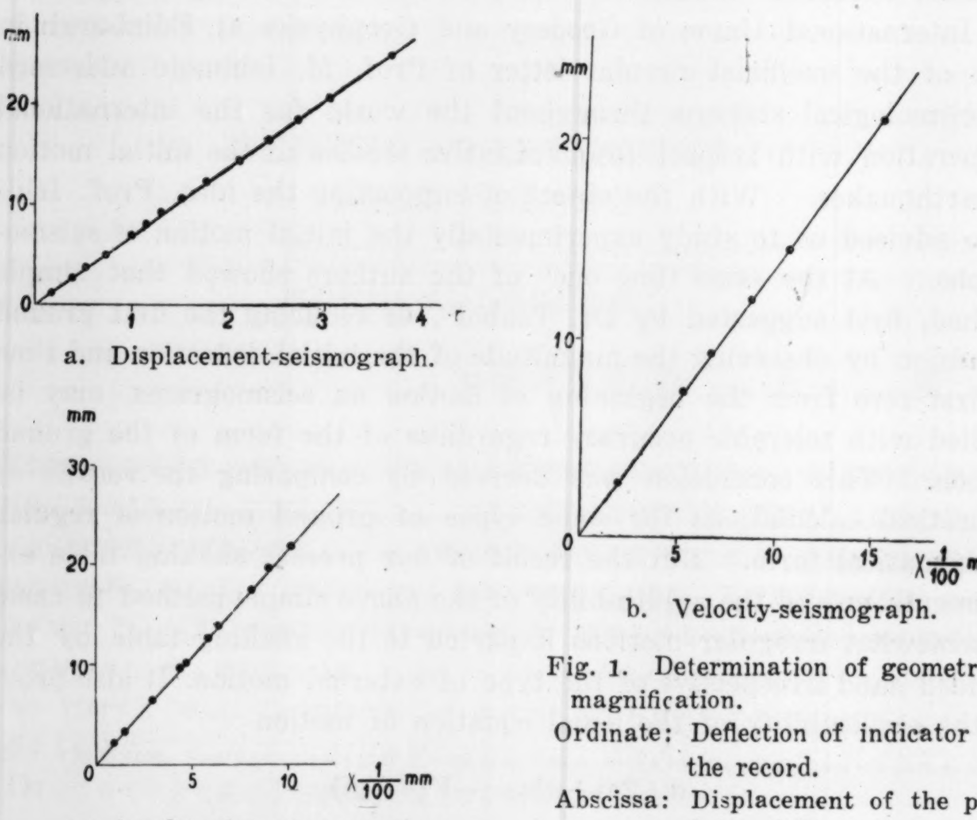

a. Displacement-seismograph.

b. Velocity-seismograph.

c. Acceleration-seismograph.

Fig. 1. Determination of geometrical magnification.
Ordinate: Deflection of indicator on the record.
Abscissa: Displacement of the pendulum bob.

3) M. ISHIMOTO, *Bull. Earthq. Res. Inst.*, **9** (1931), 316~332, 473~484; **10** (1932), 171~187; **12** (1934), 234~248; **13** (1935), 592~607; **14** (1936) 240~247. T. HAGIWARA, *Bull. Earthq. Res. Inst.*, **12** (1934), 776~787; **13** (1935), 138~145.

4) See M. Ishimoto, *loc. cit.* 3) and "Vibration Experiments and their Measurements", (Japanese.), *Kyôritusya Experimental Engineering Tracts*, Tokyo (1934).

magnification on the record of the displacement of the centre of gravity of the pendulum bob, and differs from the dynamical magnification for the infinitely rapid vibration V.

The difference between V_G and V increases with magnification, the number of magnifying levers, and their moments of inertia.

V_G was obtained by comparing the deflection of the indicator and the displacement of the centre of gravity of the bob as measured by means of a dial guage. (See Fig. 1, a, b, and c.)

From these diagrams we have, V_G=(a) 6·99 for the displacement-seismograph, which however was reduced in all the later experiments to 6/16·7 of this value, that is, 2·51. The values for the velocity- and acceleration seismographs are (b) 139 and (c) 214 respectively. A fairly linear relation between the deflection of the indicator and the displacement of the bob is noticable.

(ii) *Proper Periods of Free Oscillations and Soild Frictions.*

For determining these quantities the damping was minimised, and the free oscillations were recorded on a quick revolving drum by synchronous motor (9·3 mm per sec). The periods thus determined were (a) 6·87, (b) 0·502 and (c) 0·120 sec for the displacement-, velocity- and acceleration-seismogaphs respectively. And the width of solid friction ρ were obtained from the relation[5]

$$w_{k+1} = v w_k + \frac{\rho}{2(1+v)}\,, \tag{2}$$

where w_k is the k-th double amplitude and v is the damping ratio. By the graphical method (Fig. 2, a, b, c), we obtaine (a) 0·02, (b) 0·04 and (c) 0·04 mm as being at the most for the displacement-, velocity-, and acceleration-seismographs respectively. These small quantities are altogether negligible even in the present study. As will also be seen from the figures the damping ratios v are (a) 1·3, (b) 1·06 and (c) 1·02, so that the period above obtained may be adopted as T_0 without any corrections.

(iii) *Dynamical Magnification and Sensibility as determined from Statical Inclination Experiments.*

The equation of motion of seismograph (1) reduces for the present statical case to

$$n^2 a = Vgi\,,$$

5) B. GALITZIN, *Comptes Rendus, Comm. Sis. Perm.*, St., Petersburg, **5** (1912), 35~83, or Vorlesungen über Seismometrie, (1914), 491.

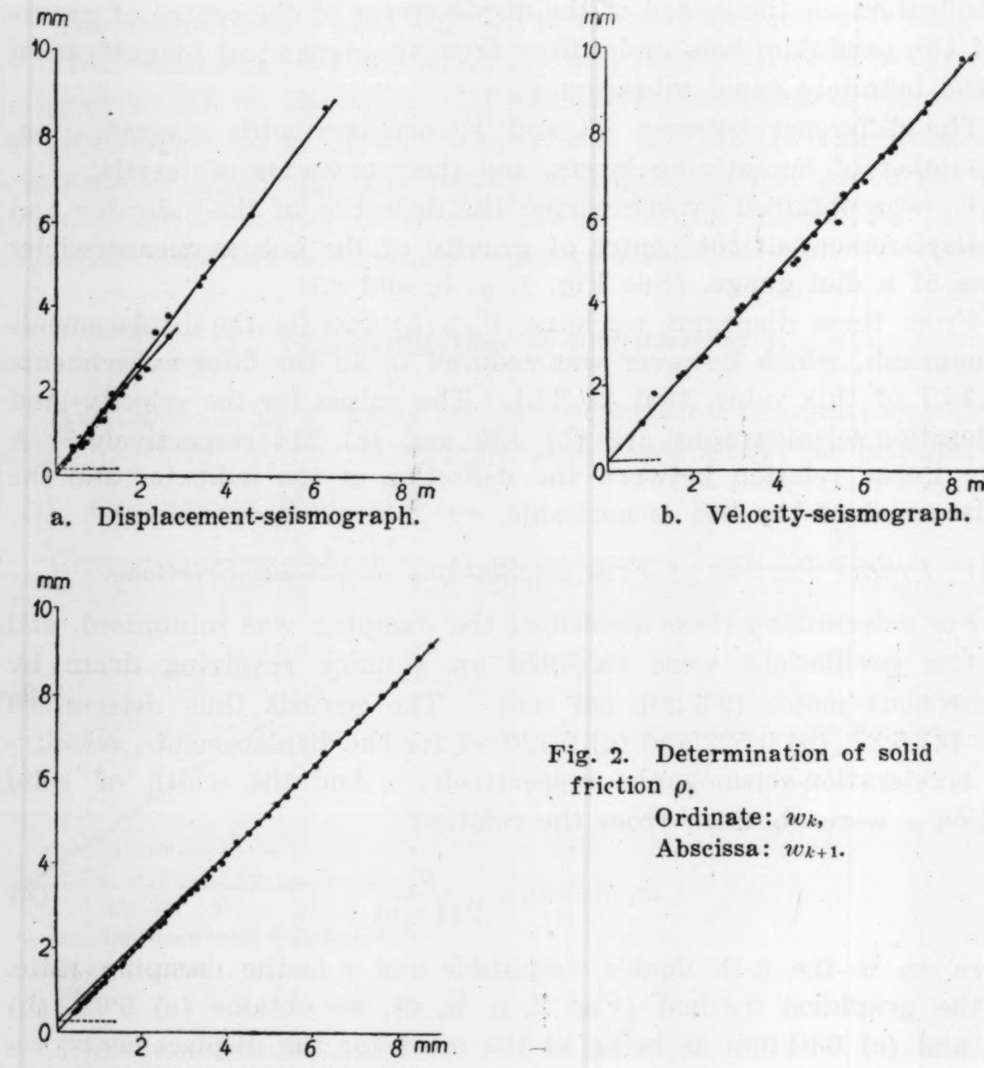

a. Displacement-seismograph.

b. Velocity-seismograph.

c. Acceleration-seismograph.

Fig. 2. Determination of solid friction ρ.
Ordinate: w_k,
Abscissa: w_{k+1}.

from which we have

$$V = \frac{n^2}{g}\frac{a}{i} = \frac{n^2}{g}\frac{da}{di}\,, \tag{3}$$

and we also have as the sensibility of the acceleration seismograph

$$S_c = \frac{V}{n^2} = \frac{a}{gi} = \frac{1}{g}\frac{da}{di}\,. \tag{4}$$

The values of $\frac{da}{di}$ were determined on an experimental platform whose inclination was measured by telescope and scale, or on the platform designed for an Ishimoto tiltometer, in which minute change

in level may be made by means of a tangent screw.

$$\frac{da}{di}=\text{(a) } 3020, \text{ (b) } 624, \text{ (c) } 55{\cdot}6 \text{ in cm/radian,}$$

whence we have

$$V=\text{(a) } 2{\cdot}58, \quad \text{(b) } 100, \quad \text{(c) } 156,$$

respectively, while the sensibility of the acceleration-seismograph works out to $S_c=0{\cdot}57$ mm/gal.

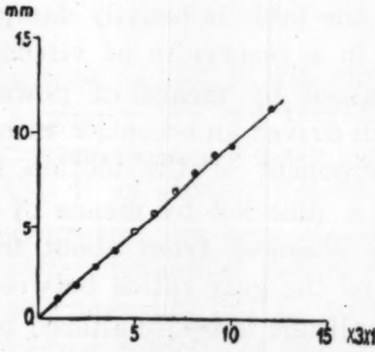

a. Displacement-seismograph.

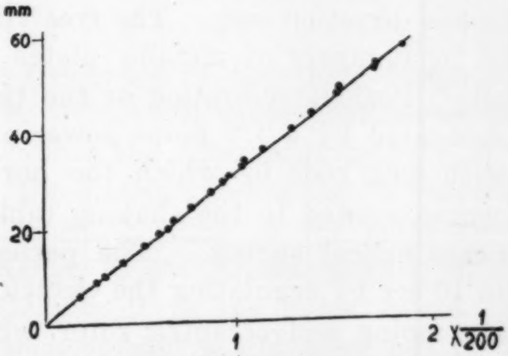

b. Velocity seismograph.

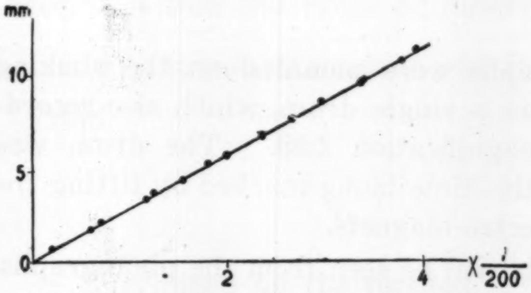

c. Acceleration-seismograph.

Fig. 3. Determination of *da/di*. Ordinate: *a*, deflection of indicator on the record. Abscissa: *i*, inclination of experimental table in radian.

2. Standardisation of the Instruments, II.

Althogh we have already determined some almost invariable instrumental constants, we have still to determine the damping factors as well as the dynamical magnifications under actual working conditions, since the former is liable to change with atmospheric conditions, etc., while the latter is subjected to certain factors that differ according as to whether it is in the dynamical state or in the statical, for example the effect of bending of the magnifying lever.

We therefore determined, as far as possible dynamically, the instrumental constants in the working state in each shaking table ex-

periment. This was conveniently done by using the shaking table constructed by Prof. Ishimoto, full details of which were described by him in his paper[6] "Détermination de la limite perceptible des secousses" in the Bulletin of this Institute.

(i) *Shaking Table.*

The shaking table, which is made of wood of dimensions 200 cm × 93 cm, is suspended by four ropes from hooks in the ceiling. The ropes are crossed obliquely so that the motion of the table is confined to one direction only. The free vibration of the table is heavily damped by dampers of metallic plates immersed in a reservoirs of viscous oil. Periodic vibration of the table is attained by means of power generated by a 1/2 horse power motor, which drives an eccentric rotor with long rods by which the horizontal component of the motion is communicated to the shaking table through a junction by means of a brass helical spring. The period is easily changed from about 0·1 to 10 sec by regulating the electric current and the gear ratios between the motor and eccentric rotor, while the amplitude is easily altered by changing the eccentricities of the rotors, or by chaing the leverage at the connecting device of the horizontal rods as well as altering the stiffness of the helical spring.

The foregoing three seismographs were mounted on the shaking table and their motions recorded on a single drum, which also recorded the motion of the table with magnification 2·38. The drum was rotated by a synchronous motor, the time being marked by lifting the indicating pointer by means of electro-magnets.

The experimental arrangements will be seen from the photographs, Fig. 4 and 5, Plate XXII. The instrumental constants were determined by observing resonance curves, that is the actual magnification curves for harmonic motions in the stationary state obtained by comparing the recorded table motions with the seismographic records. By means of the formula

$$\mathfrak{V}=\frac{Vp^2}{\sqrt{(n^2-p^2)^2+4n^2\varepsilon^2}}=\frac{V}{\sqrt{(1-u^2)^2+4h^2u^2}}, \qquad u=\frac{n}{p}, \tag{5}$$

we can generally determine V, $T_0=\frac{2\pi}{n}$, and ε or $h=\frac{\varepsilon}{n}$, from observations of $\mathfrak{V}$ and p.

6) M. ISHIMOTO et M. OTUKA, *Bull. Earthq, Res. Inst.*, **11** (1933), 113~121.

(ii) *Dynamical Magnification for Infinitely Rapid Vibration V.*

The value of V was estimated by the magnifications for motions with shortest periods[7] in the case of the displacement- and velocity-seismographs, while that in the case of acceleration-seismographs was determined by examining the sensibility for long periods, which is actually constant for motions with periods above 0·2 sec, namely,

$$V= \text{a) } 1{\cdot}90, \qquad \text{b) } 110,$$

$$S_c=\frac{a}{\sigma_m p^2}=0{\cdot}60\,\text{mm/gal}, \tag{6}$$

where σ_m and p are amplitude and frequency of the table motin $\sigma=\sigma_m\,sinpt$. We can therefore have the dynamical magnification by the formula (4). We are not certain whether the differences in the S_c or in the V as already determined from the statical inclination experiment from the one here obtained is due to the bending of the arms or to other dynamical causes or to a change in the proper period of the seismograph, but if we were to attribute it to the latter cause, the proper period for the acceleration-seismograph would work out to $T_0=0{\cdot}117$ sec, which, compared with the former determination $T_0=0{\cdot}120$ sec, is within the range of observational accuracy.

(iii) *Damping Constant and Proper Period.*

From

$$\left(\frac{\sigma_m}{a_m}\right)^2\left(\frac{V}{\mathfrak{B}}\right)^2=(1-u^2)^2+4h^2u^2 \quad U^2 \tag{7}$$

we determined by the method of least squares the proper period T_0 and the damping constant h by the formula

$$U^2-U_0^2=\frac{\partial U_0^2}{\partial T_0}\delta T_0+\frac{\partial U_0^2}{\partial h_0}\delta h_0 \tag{8}$$

for the displacement-seismograph, but for the velocity- and acceleration-seismographs we determind h only, because our observations of $\frac{\sigma_m}{a_m}$ for short period vibrations were not sufficient. The results as determined from tests at each initial motion experiments were

7) Since quick vibrations, such as would cause resonance of the indicator arms were of course avoided, magnification for the accelaration-seismograph could not be determined in this way.

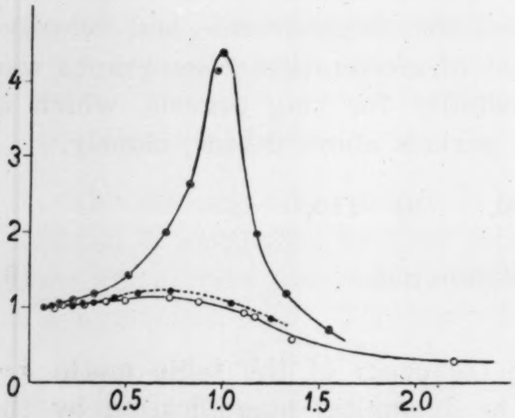

Fig. 6 a. Resonance curves of displacement-seismograph.

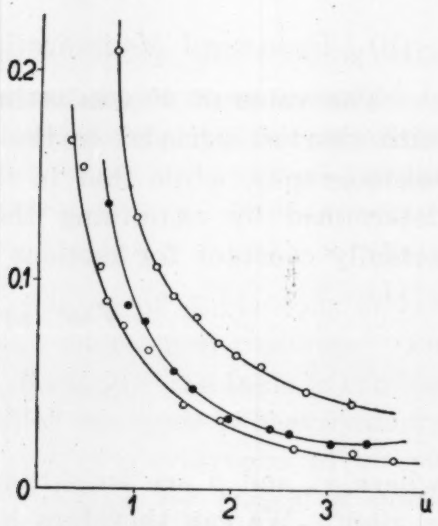

Fig. 6 b. Resonance curves of velocity-seismograph.

Fig. 6 c. Resonance curves (below) and sensibility curves (above) of acceleration-seismograph.

(a)(1) $T_0 = 6{\cdot}56$ sec, $h = 0{\cdot}513$,
(2) $T_0 = 6{\cdot}57$, $h = 0{\cdot}134$,
(3) $T_0 = (6{\cdot}22)$, $h = 0{\cdot}490$.
(b)(1) $h = 7{\cdot}99$,
(2) $h = 6{\cdot}25$,
(3) $h = 3{\cdot}69$.
(c)(1) $h = 0{\cdot}555$,
(2) $h = 0{\cdot}599$,
(3) $h = 0{\cdot}301$.

The mean sensibility of the velocity-seismograph was also determined, namely,

$$S_b = \frac{a_m}{\sigma_m p} = 12{\cdot}7 \text{ cm/kin.} \qquad (9)$$

Having now obtained all the necessary instrumental constants, we shall summaries them here in tabular form.

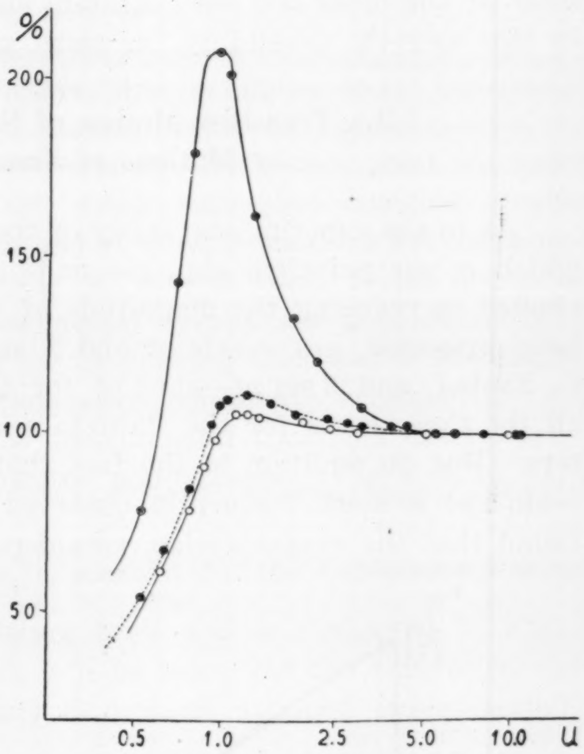

Fig. 7. Sensibility curves of acceleration-seismographs.

The sensibility variation with period for the acceleration-seismograph was also examined by applying a periodic force by means of an elastic rubber string connected to a small hook at the bob of the pendulum at one end and pulled periodically by an eccentric

Table I.
Instrumental constans for the seismographs used.

	Displacement-seismograph	Velocity-seismograph	Acceleration-seimograph
Weight of bob (kg)	6	15	15
V_G	2·51	139	214
V (stat.)	2·58	100	164
V (dyn.)	1·90	110	164
V (intial motion)	1·83	112	15
T_0 (sec)	6·565	0·502	0·118
h	0·513	7·99	0·555
	0·134	6·25	0·599
	0·490	3·69	0·301
ρ (mm)	0·02	0·04	0·04
S		12·7 cm/kin	0·60 mm/gal

rotor at the other end with constant amplitude and variable frequency. In this way the sensibility for short period was found (Fig. 7).

3. Transient Motion of Seismographs caused by Motions of Short Duration.

As to the experimental study of the initial motion of seismographs, which is our principal aim, the motions, for which the curve to be applied in reducing the magnitude of the first given impulsion have been prepared, are $\sigma = \sin pt$ and $2 \sin pt - \sin 2pt$, both due to Dr. C. Tsuboi, and $3 \sin pt - \sin 3pt$ for the ordinary seismographs and all the three cases for the Galitzin seismographs by one of the writers. But, in addition to the fact that motion of type e^{-ct^2} or $3 \sin pt - \sin 3pt$ is most frequently observed in actual earthquakes, it was found that the magnification, considered as a function of the time of

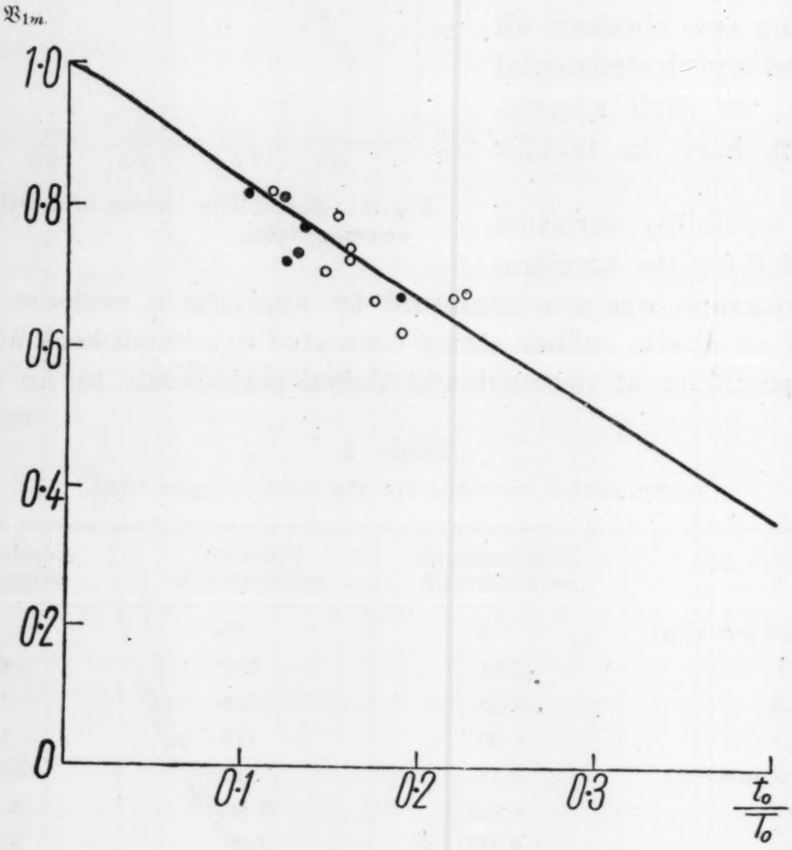

Fig. 13. Comparison of the magnification for the first maximum experimentally observed ($h=0{\cdot}51$ and $0{\cdot}49$ inclusive) with the theoretical curve for $h=0{\cdot}5$.
○ for table motion of nearly one-sided impulsion,
● for single vibration,
◎ for one and a half vibration.

first zero from the beginning measured in fractions of the proper period of seismograph for $\sigma=2\sin pt-\sin 2pt$ or $3\sin pt-\sin 3pt$, which is nearly equal to each other, may be applied as an intermediate magnification for reducing the various forms of ground motion with tolerable accuracy. We shall therefore verify this point by experiments with the shaking table, using somewhat irregular motions generated by the anaided hands and of types resembling the mathematical forms considered theoretically, as well as other forms not so considered. A part of the experimental results are reproduced in the annexed plates. The motions of the shaking table and of the displacement-, velocity- and acceleration-seismographs are arranged from the top in each photograph. The instrumental constants determined at the same time are given below the photographs. (Fig. 8, 9, 10, 11, 12, in Plate XXIII~XXVI.)

The measured $\mathfrak{V}_{1m}$, $\mathfrak{V}_{2m}$, $\dfrac{t_0}{T_0}$, and $\dfrac{a_{1m}}{a_{2m}}$ for the displacement-seismograph are given in the follwing table and is compared in Fig. 13 with the theoretical curve. It will be seen that the theoretical curve is applicable with fair accuracy to motions attained experimentally.

Table II.

The measured $\mathfrak{V}_{1m}$, $\mathfrak{V}_{2m}$, t_0/T_0 and a_{1m}/a_{2m}. (Displacement-seismograph), for table motion of nearly one-sided impulsion (○), of single vibration ● and of one and a half vibration (⊙).

h	$\mathfrak{V}_{1m}$	$\mathfrak{V}_{2m}$	t_0/T_0	type of σ
	0·77	1·09	0·13	●
0·490	0·68	0·57	0·23	○
	0·74	0·49	0·16	○
	0·83	0·84	0·25	●
0·134	0·88	0.44	0.15	○
	0·62	0.38	0.19	○
	0·82	1·08	0·10	●
	0·73	0·48	0·16	○
	0·67	0·60	0·22	○
	0·81	1·36	0.12	⊙
	0·53	0.24	0·17	○
0·513	0·58	0·55	0·12	○
	0·54	0.85	0·19	●
	0·57	0·41	0·15	○
	0·66	0·33	0·12	○
	0·59	0·96	0·13	⊙

We shall next examine the theoretical basis on which some authors may ask whether the simple equation of motion of the seismograph is applicable or not to such a transient state as the beginning of a motion. On the other hand we shall at the same time examine the applicability of Poincaré-Lippmann's[8] method of integrating term by term of

$$a+2\varepsilon\int_0^t a dt+n^2\int_0^t dt\int_0^t a dt=-V\sigma. \tag{10}$$

Readings of a were made from enlarged photographs, and corrections applied for the arcual movements of the indicator. Althogh the amplitude correction to reduce $a=L\sin\theta$ or $L\tan\theta$ to $L\theta$ was not necessary in the present cases, the correction for time $L(1\text{-}\cos\theta)$, where L is the length of the last indicator arm, was effective even in amplitudes of about 1 cm in the casc of $L=13$ or 15 cm. The motions were plotted on section paper, and the first and second integrals obtained by means of Coradi's intergraph. For the kind loan of this instrument the writers take this opportunity of offering their thanks to Prof. Takahasi of the Institute of Naval Architecture of this University. The resulting displacements thus worked out after applying whenever necessary little corrections for the zero line assuming the form $\alpha+\beta t+\gamma t^2$ are compared with the table motion in Fig. 14, (a), (b), (c). To prevent confusion, we have indicated the resulting $V\sigma$ curve

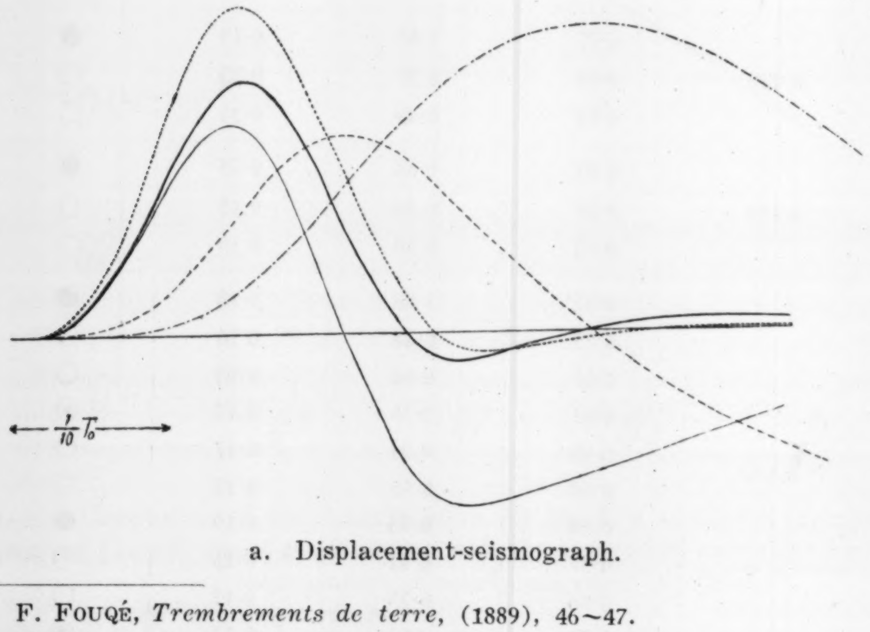

a. Displacement-seismograph.

8) F. FOUQÉ, *Trembrements de terre*, (1889), 46~47.
G. LIPPMANN, *Comptes Rendus*, **110** (1890), 440~446.

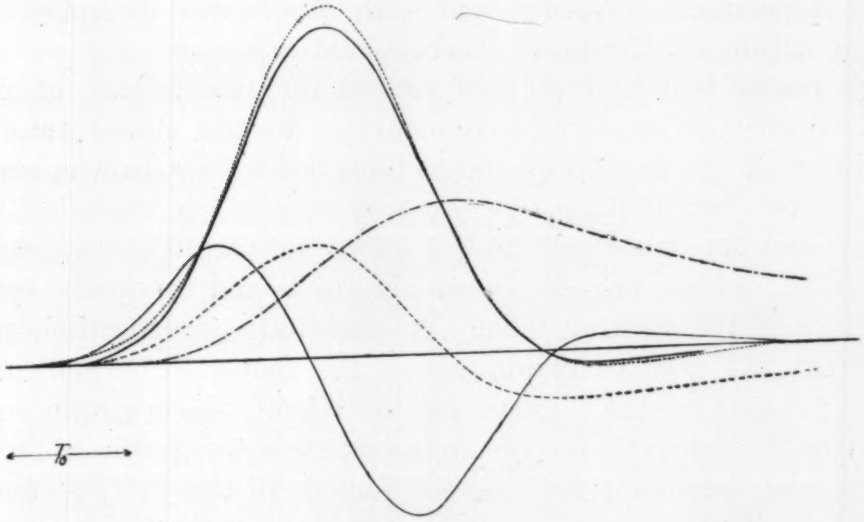

b. Velocity-seismograph.

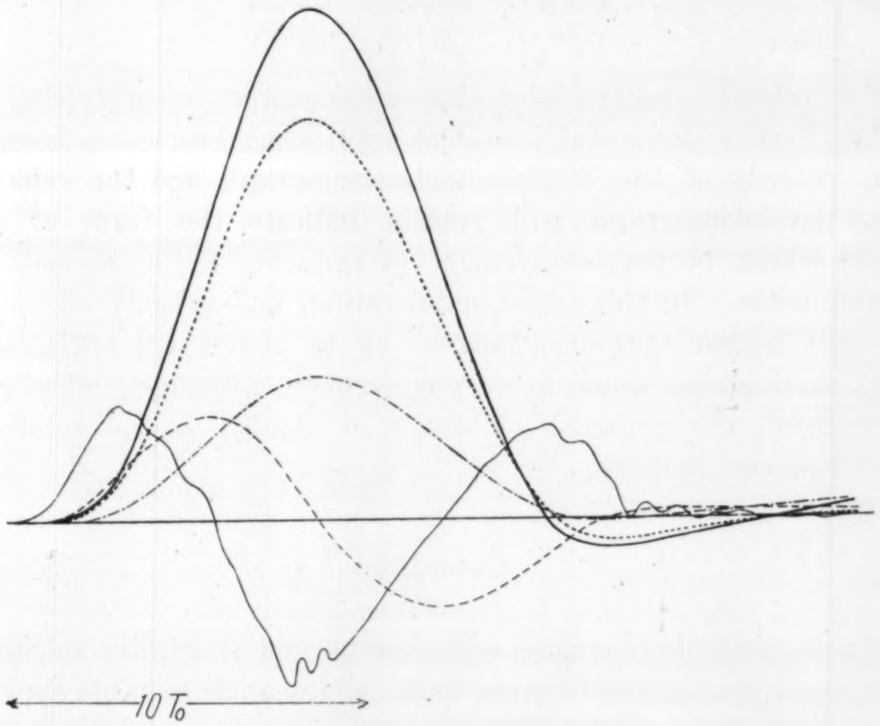

c. Acceleration-seismograph.

Fig. 14. Reduction of table motion by Poincaré-Lippmann's method. Thin full line: seismographic record a, broken line: $\int a dt$, chain line: $\int dt \int a dt$, thick full line: $V\sigma$ and dotted line: table motion σ.

on a smaller scale instead of σ itself. This proves the correctness of the usual equation of motion, as well as the accuracy of the instrumental constants n and ε that we determined as mentioned above. The magnifications V worked out in this way, are (a) 1·84, (b) 113 and

(c) 153 respectively, agreeing well with the former dynamical determination within the limits of observational accuracy.

The reader will have already noticed the resemblance of records of the velocity- or acceleration-seimograph to the actual velocity or acceleration of the motion of the shaking table σ. This is also confirmed by the fact that the first integral of a due to the velocity seismograph and the double integral of the same due to the acceleration-seismograph, which are shown in Fig. 14 b and c, closely resemble the motion of the shaking table. A quantitative verification will be made from the relative magnitude of the factor to be multiplied to the first integral of the a curve for the velocity-seismograph and that to the double integral for the acceleration-seismograph in order to obtain $V\sigma$ by formula (10), i. e., the factors to the first, second, and third terms of (10) are

(b)	1,	115·68,	52·41,
(c)	1,	21·12,	361·90,

for the velocity- and acceleration-seismographs respectively. This fact has a very important practical application because a comparison of the records of the displacement-seismograph and the velocity- or acceleration-seismograph will readily indicate the form of ground motion, which is very convenient in reducing the magnitude of the first impulsion. In this sense, acceleration- and velocity-seismographs with still higher magnifications so as to enable the registration of distant earthquakes would be very convenient, although, unless carefully examined, the presence of waves of smaller period totally mask those of slower motions.

Conclusion.

An Ishimoto acceleration-seismograph and Hagiwara velocity- and displacement-seismographs were used for the shaking table experiment.

(i) The instrumental constants were determined as far as possible by statical as well as dynamical methods. The results are summarised in Table I.

(ii) The transient motion of seismographs caused by some types of somewhat irregular motions, resembling the forms already investigated theoretically as well as other types of motions, were studied experimentally, and the applicability of the simple method of reduction of the first ground impulsion described in Part I of the present paper was verified. The applicability of the usual equation of motion was

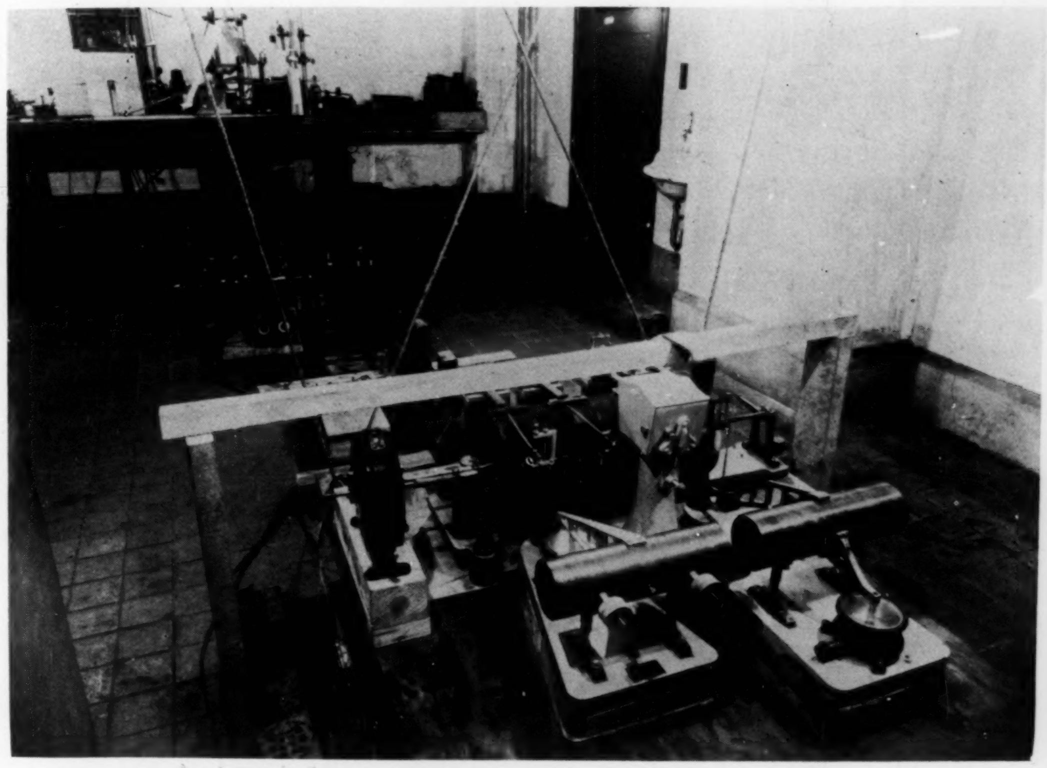

Fig. 4. Experimental arrangement of shaking table.

Fig. 5. Connection between motor and shaking table.

（震研彙報 第十四號 圖版 河角・木下）

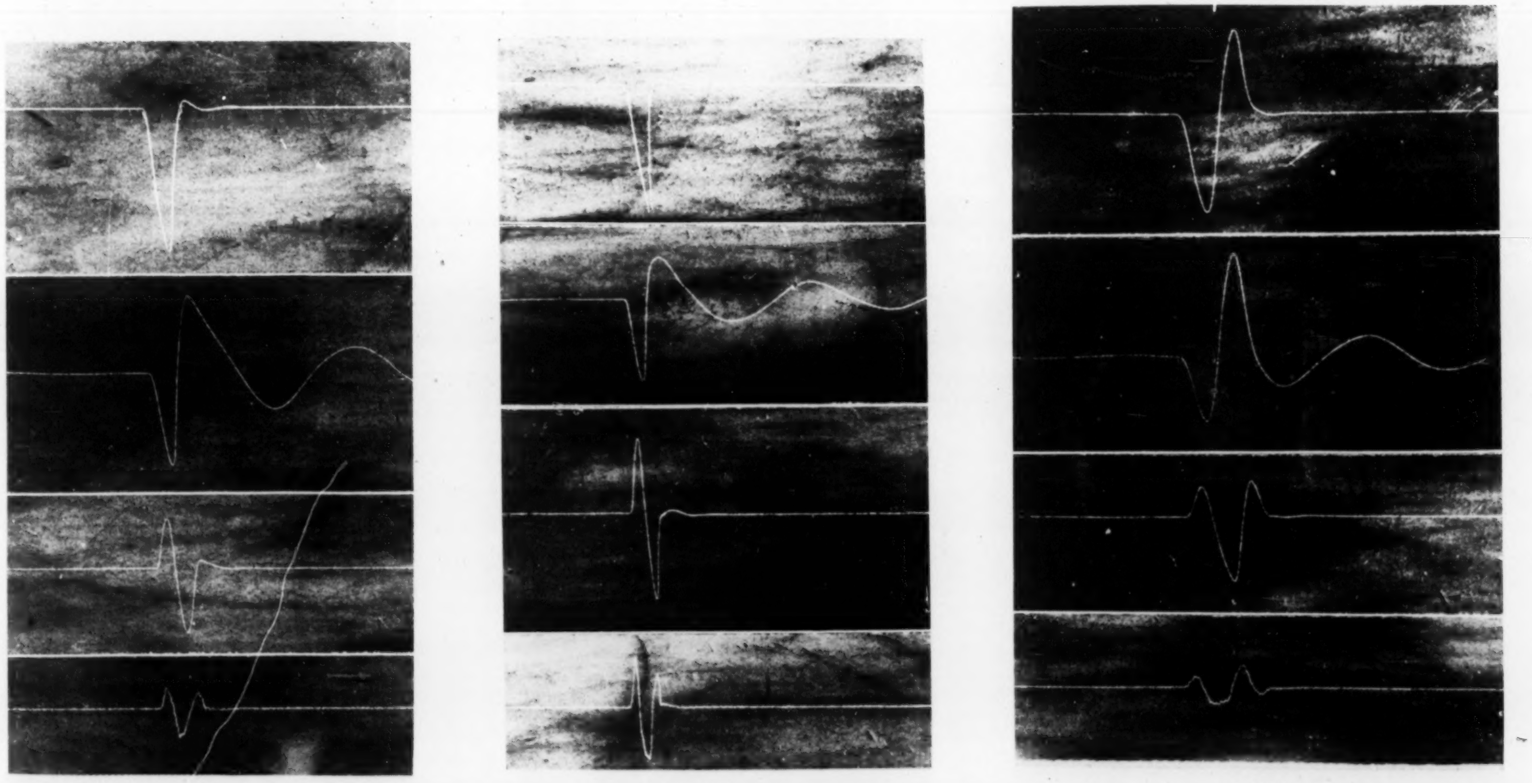

(i) (ii) (iii)

Fig. 8. Comparison of the motion of shaking table with those of displacement-, velocity- and acceleration-seismographs (from the top to below).
(a) $h=0{\cdot}134$, (b) $h=7{\cdot}99$, (c) $h=0{\cdot}555$.

(震研彙報 第十四號 圖版 河角・木下)

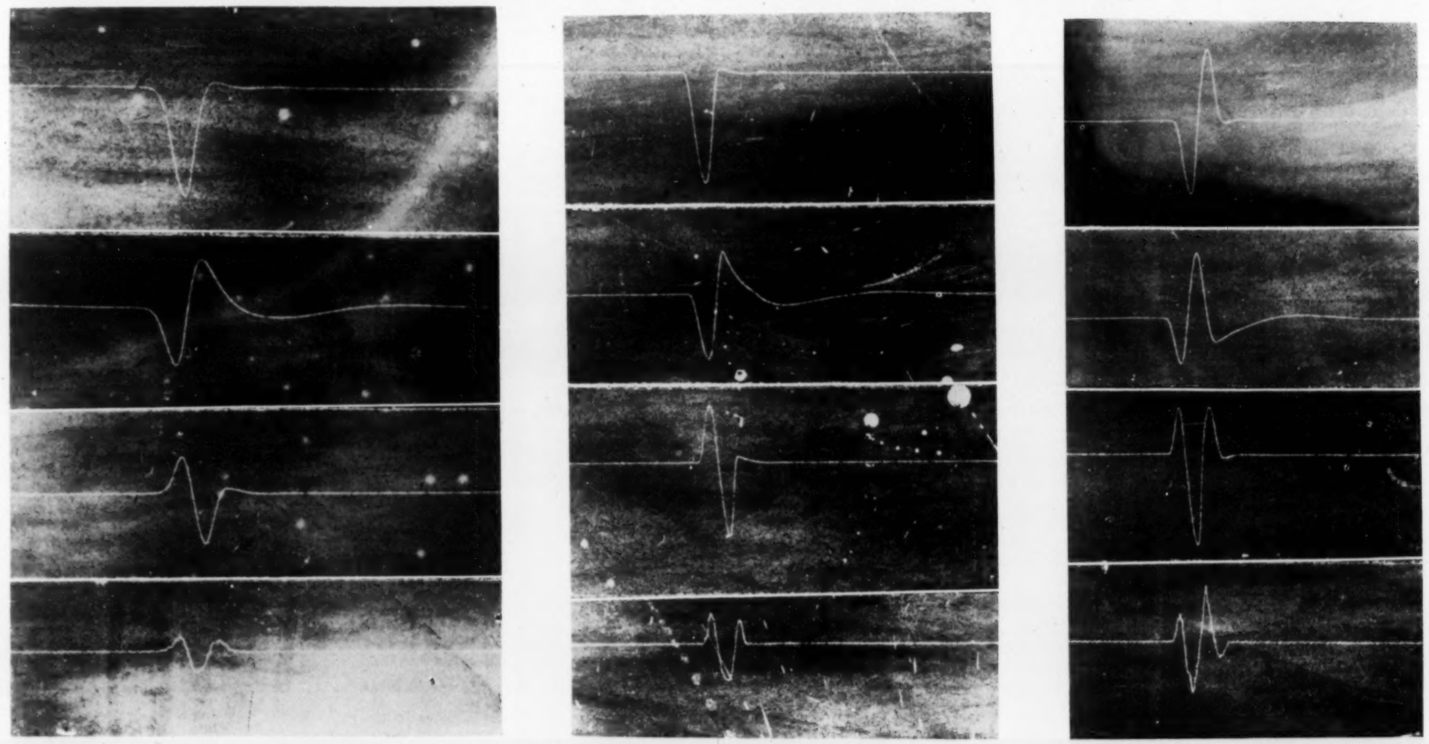

(i) (ii) (iii)

Fig. 9.

(a) $h=0{\cdot}489$, (b) $h=7{\cdot}99$, (c) $h=0{\cdot}555$.

VOL.6

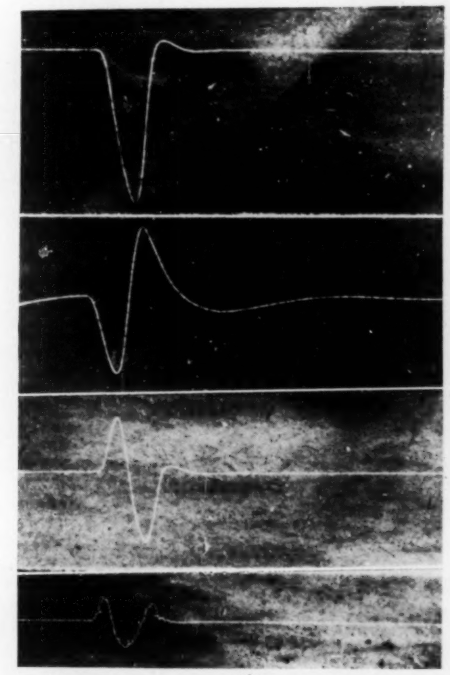

(i)

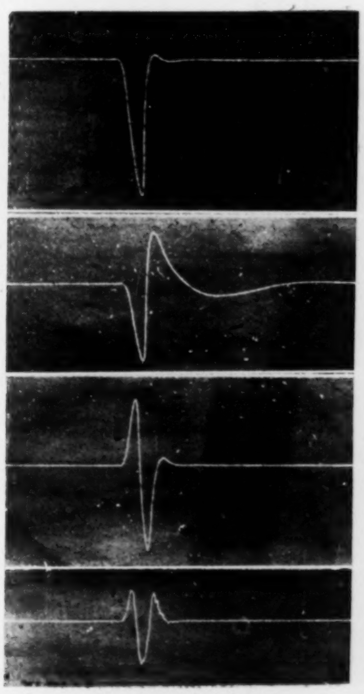

(ii)

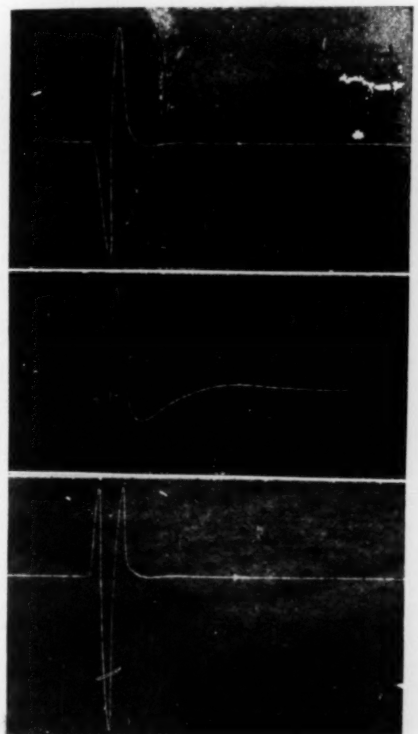

(iii)

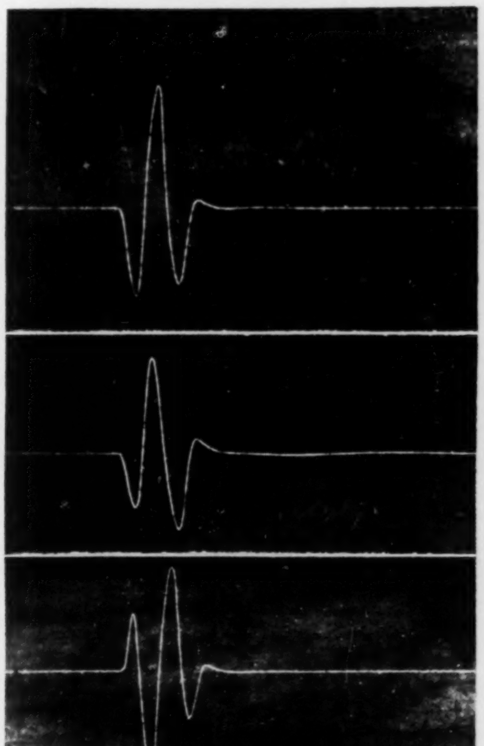

(iv)

Fig. 10.

(a) $h=0{\cdot}513$, (b) $h=7{\cdot}99$, (c) $h=0{\cdot}555$.

VOL.6

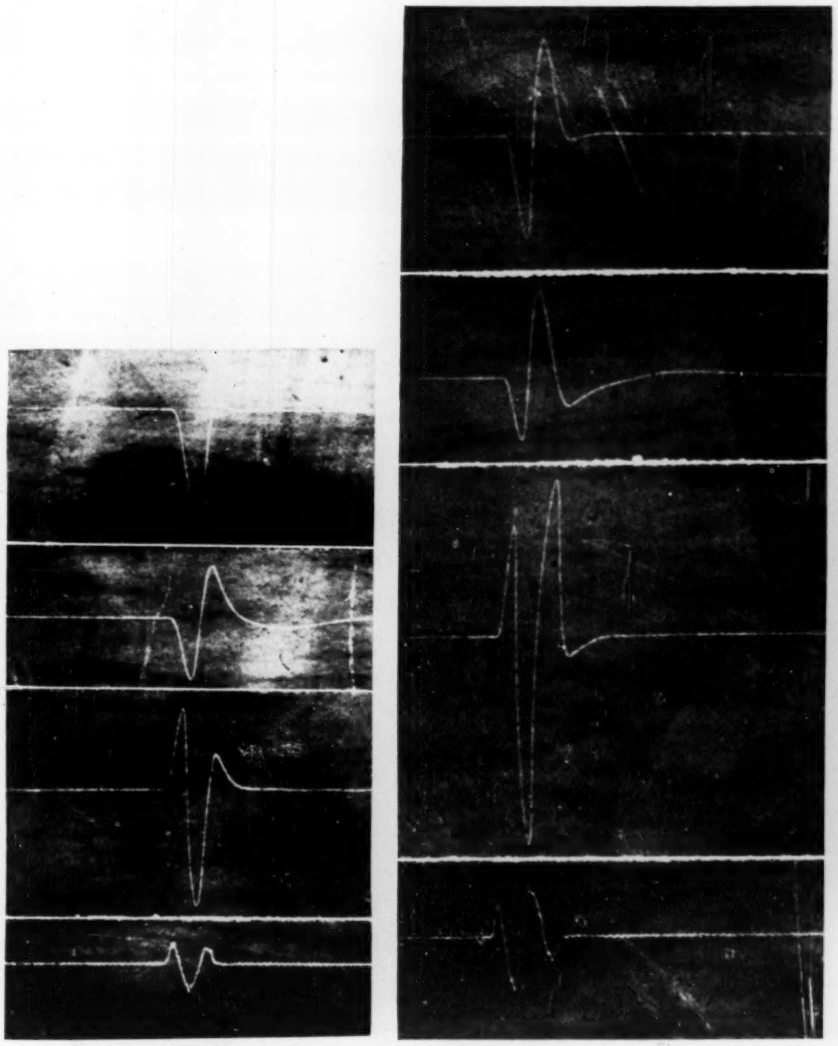

(i) (ii)

Fig. 11.

(a) $h=0{\cdot}513$, (b) $h=3{\cdot}69$, (c) $h=0{\cdot}301$.

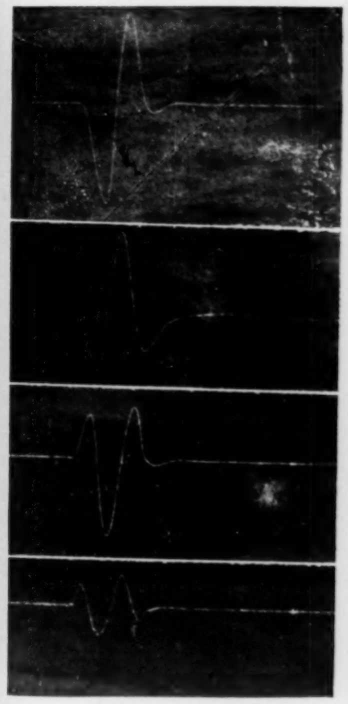

(i)

Fig. 12.

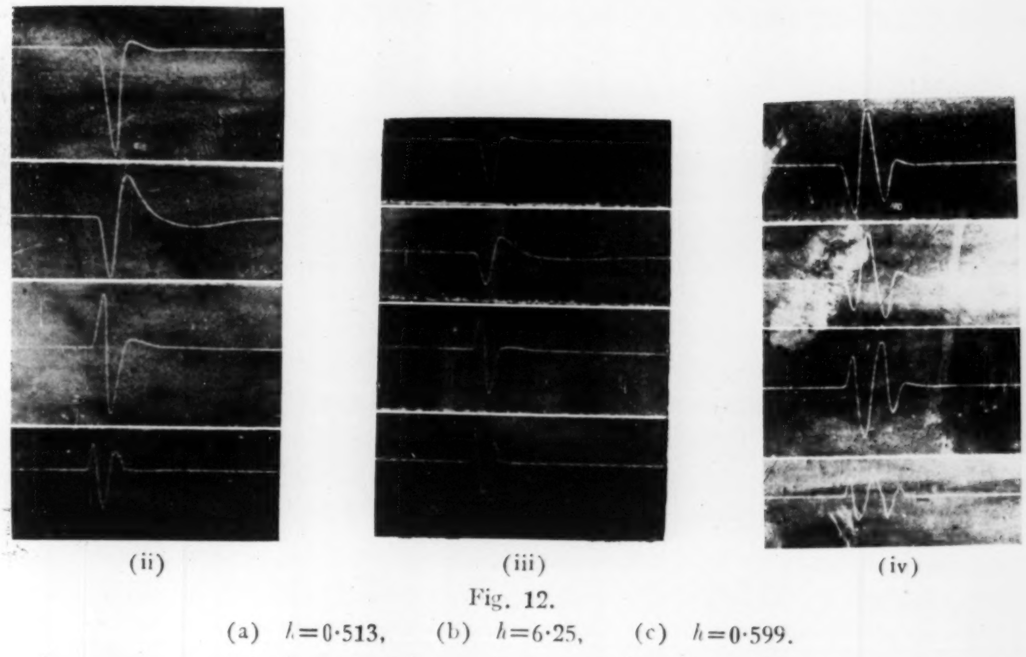

(ii) (iii) (iv)

Fig. 12.

(a) $h=0{\cdot}513$, (b) $h=6{\cdot}25$, (c) $h=0{\cdot}599$.

(震研彙報 第十四號 圖版 河角・木下)

also proved even for the start of motion of the pendulum with air damper so powerful that the damping constant h was 7·99. The accuracy of the method of integrating term by term due to Poincaré and Lippmann was also examined.

In conclusion, the writers wish to acknowledge their heartiest thanks to Prof. Ishimoto for his kind advice and encouragement throughout the course of our present study. They also wish to express their thanks to the Council of the Foundation for the Promotion of Scientific and Industrial Research of Japan, whose aid greatly assisted the progress of our work.

---

30. 地震計初動の理論的及び實驗的研究並びに地震初動の定量的研究

（其の2）地震計初動の實驗的研究

地震研究所 河角廣・木下潤一

本論文第1部に於て得たる所を確める爲に振動臺を用ひて地震計の初動實驗を行つた．此れに用ひた地震計は石本式加速度地震計，萩原式速度及び變位地震計である．靜力學的，動力學的方法により出來るだけ器械常數を測定し，各實驗毎に動力學的檢定を行つた．其の結果理論的に研究されて居る樣な形に近い運動を手にて振動臺に與へた場合にも，又其の他の運動をさせた場合にも第1部に於て得た第1動に對する倍率曲線 $\mathfrak{V}_{1m}\ (t_0/T_0)$ が相當な精度に於て利用出來る事を確め，更に項別積分の方法により各種地震計よりその運動を求め極めて滿足なる結果が得られた．かくて地震計の運動方程式

$$\ddot{a}+2\varepsilon\dot{a}+n^2a=-V(\ddot{\sigma}-gi)$$

が靜力學的にも動力學的にも，こゝに初動の場合にもあてはまる事を知つた．

尙本研究に對する不斷の敎示，激勵に對し石本先生に深甚の感謝の意を表し，合はせて本研究に對し補助を與へられた日本學術振興會に對し感謝する次第である．

---

31. *Damping in Seismic Vibrations of a Surface Layer due to an Obliquely Incident Disturbance.*

By Katsutada SEZAWA and Kiyoshi KANAI,
Earthquake Research Institute.

(Read May 19, 1936.—Received June 20, 1936)

1. It is rather odd that there should be a few seismologists, who although well aware of the nature of the propagation of seismic disturbances in the earth's crust, are disinclined to doubt the existence of such strong free oscillations of a layer as shall contradict the law of transmission and refraction of waves through the boundary of that layer. Some investigators, nevertheless, appear to treat the vibration problem of a layer from the same view point as ours,[1), 2)] namely, the view that the vibration of a surface layer, whether free or forced, should be of such damping type as shall depend on the ratios of both density and elasticity of the layer to those of the neighbouring medium. Köhler[3)] seems to be the first to have accepted our idea, having used it in an analysis of the ground vibration caused by artificial shock. Strictly speaking, our result applies only to that case in which the propagation of the primary shock is directed vertically. Since, on the other hand, the direction of propagation in an actual case is practically normal to the surface layer, the result of Köhler's investigation, wherin our formula was straightway used, appears fairly satisfactory, the agreement between calculation and experimental data rather surpassing that for determining the thickness of a layer by means of a seismic method.

As a matter of fact, however, it seems to have hardly been realized until now that, from the standpoint of accuracy, the period as well as the damping factor in the free vibration of a layer should change with the direction of the propagation of the disturbance, owing probably to the fact that such a conception clashes with the classical

1) K. SEZAWA and K. KANAI, "Decay Constants of Seismic Vibrations of a Surface Layer", *Bull. Earthq. Res. Inst.*, **13** (1935), 251~265.

2) *Ditto*, "The Rate of Damping in Seismic Vibrations of a Surface Layer of Varying Density or Elasticity", *Bull. Earthq. Res. Inst.*, **13** (1935), 484~495.

3) R. KÖHLER, "Dispersion und Resonanzerscheinungen im Baugrund", *Z. f. techn. Phys* , **17** (1935), 579~600.

idea of self-maintained natural vibrations. It may be asked whether the apparent anomaly resulting from our case would be of the nature of an echo. This question can be answered by taking into considera- tion the well known principle that the stationary oscillation of a deformable body is in essence nothing more than the result of superposition of the original disturbances and their repeated echoes.

Although the cases where the primary disturbance consists of dilatational waves or that where the distortional waves have a vertical component of displacement are practical ones, we restricted the calculation in the present paper to the case of distortional waves with displacement orientated horizontally in order to avoid the complexity of the problem. Investigation of even a restricted case as this one appears to indicate the essential feature of the problem. It should however be borne in mind that the initial disturbance, particularly in the case of artificial shock, does not have a plane wave front. Since, however, our aim is rather to show how closely the obliquely incident waves might be equivalent to the vertically incident ones, the curvature of the wave front in the case of artificial shock has no importance in the present problem.

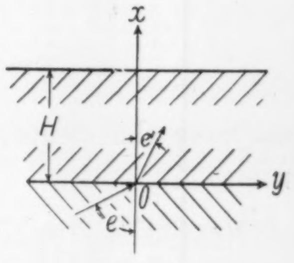

Fig. 1.

2. Let the axes of x and y be drawn vertically and horizontally from a point at the lower boundary of the surface layer, and let u, u', ρ, ρ', μ, μ' be the displacements, densities, and elastic constants of the subjacent medium and the surface layer respectively, H being the thickness of that layer. Let again e, e' be the angle of incidence of the primary waves and that of refraction of the waves in the upper layer. Then, putting

$$\alpha=\cot e, \qquad \beta=\cot e', \tag{1}$$

we get

$$\left.\begin{aligned} u&=u_1+u_2=e^{if(x+\alpha y-nt)}+Ae^{if(x-\alpha y-nt)},\\ u'&=Be^{if(x+\beta y-nt)}+Ce^{if(x-\beta y-nt)}, \end{aligned}\right\} \tag{2}$$

corresponding to the incident waves

$$u_1=e^{if(x+\alpha y-nt)}. \tag{3}$$

Since these solutions satisfy

$$\rho\frac{\partial^2 u}{\partial t^2}=\mu\nabla^2 u, \qquad \rho'\frac{\partial^2 u'}{\partial t^2}=\mu'\nabla^2 u', \tag{4}$$

we have

$$n^2 = \frac{\mu}{\rho}(1+\alpha^2) = \frac{\mu'}{\rho'}(1+\beta^2). \tag{5}$$

The boundary conditions are evidently such that

$$y=0; \quad u=u', \quad \mu\frac{\partial u}{\partial x} = \mu'\frac{\partial u'}{\partial x}; \quad y=H; \quad \frac{\partial u'}{\partial x}=0. \tag{6}$$

Substituting (2) in (6) we finally get

$$\left.\begin{aligned} A\Phi &= \left(\alpha+\frac{\mu'}{\mu}\beta\right)e^{if\beta H} + \left(\alpha-\frac{\mu'}{\mu}\beta\right)e^{-if\beta H}, \\ B\Phi &= 2\alpha e^{-if\beta H}, \qquad C\Phi = 2\alpha e^{if\beta H}, \\ \Phi &= \left(\alpha-\frac{\mu'}{\mu}\beta\right)e^{if\beta H} + \left(\alpha+\frac{\mu'}{\mu}\beta\right)e^{-if\beta H}. \end{aligned}\right\} \tag{7}$$

Writing

$$\nu = \frac{\mu'\beta}{\mu\alpha}\left(=\sqrt{\frac{\rho'\mu'}{\rho\mu}}\frac{\cos e'}{\cos e}\right), \tag{8}$$

we have the elementary solutions of u and u' such that

$$u = e^{if(x+\alpha y-nt)} + \sum_{m=0}^{\infty}(-1)^m\left(\frac{1-\nu}{1+\nu}\right)^{m+1} e^{if(x-\alpha y-nt)}e^{-2imf\beta H}$$

$$+\sum_{m=0}^{\infty}(-1)^m\left(\frac{1-\nu}{1+\nu}\right)^m e^{if(x-\alpha y-nt)}e^{-2i(m+1)f\beta H}, \tag{9}$$

$$u' = \frac{2}{1+\nu}\sum_{m=0}^{\infty}(-1)^m\left(\frac{1-\nu}{1+\nu}\right)^m\left\{e^{if(x+\beta y-nt)-2if(m+1)\beta H} + e^{if(x-\beta y-nt)-2ifm\beta H}\right\}. \tag{10}$$

3. Fourier's integral for a two-dimensional case is

$$\chi(x,y) = \frac{1}{4\pi^2}\int_{-\infty}^{\infty}df\int_{-\infty}^{\infty}dg\int_{-\infty}^{\infty}d\xi\int_{-\infty}^{\infty}\chi(\xi,\eta)\,e^{if(x-\xi)+ig(y-\eta)}d\eta. \tag{11}$$

Putting $g=f\alpha$ and using (11) we get

$$u_1 = F(x+\alpha y-nt), \tag{12}$$

$$u_2 = \sum_{m=0}^{\infty}(-1)^m\left(\frac{1-\nu}{1+\nu}\right)^{m+1}F(x-\alpha y+2m\beta H-nt)$$

$$+\sum_{m=0}^{\infty}(-1)^m\left(\frac{1-\nu}{1+\nu}\right)^m F(x-\alpha y+2\overline{m+1}\beta H-nt), \tag{13}$$

$$u' = \frac{2}{1+\nu}\sum_{m=0}^{\infty}(-1)^m\left(\frac{1-\nu}{1+\nu}\right)^m\Big\{F(x+\beta y+\overline{2m+1}\beta H-nt)$$
$$+F(x-\beta y+2m\beta H-nt)\Big\}. \qquad (14)$$

From the expressions in (13), (14) it will be seen that, were the primary disturbance $F(x+\alpha y-nt)$ to have a certain sharpness in its general or partial form, then the vibration of the surface layer, u', as well as that of the reflected waves, u_2, would be of the periodic and damping type. The period of oscillation is

$$\left.\begin{aligned} T&=\frac{4\beta H}{n}=\frac{4H}{V_2}\cos e', \qquad (\nu<1)\\ T&=\frac{2\beta H}{n}=\frac{2H}{V_2}\cos e', \qquad (\nu>1)\end{aligned}\right\} \qquad (15)$$

V_2 being the velocity of the transverse waves in the layer, whereas the ratio of the vibration amplitudes of the successive similar phases, namely the decay factor, K, is constant and expressed by

$$K=\left(\frac{1-\nu}{1+\nu}\right)^2 \quad \text{or} \quad K=\left|\frac{1-\nu}{1+\nu}\right| \qquad (16)$$

according as $\nu<1$ or $\nu>1$. Thus, putting $e^{-kT}=K$, we obtain the logarithmic decrement of the vibration of the form

$$k=\frac{V_2}{2H\cos e'}\log_e\left|\frac{1+\nu}{1-\nu}\right|, \qquad \left(\nu=\sqrt{\frac{\rho'\mu'}{\rho\mu}}\,\frac{\cos e'}{\cos e}\right) \qquad (17)$$

regardless of whether ν is greater or less than unity.

In Fig. 2 the periods of oscillation of the surface layer for three cases (i) $\mu'/\mu=1/20$, (ii) $\mu'/\mu=1/2$, (iii) $\mu'/\mu=2(\rho=\rho')$ are plotted. Since the ratio of μ'/μ that is liable to be present in an actual case, is rather very small, say $\mu'/\mu=1/20$, the period of the free vibration is approximately constant for any angle of incidence. Even in the case, $e=90°$, the change in period is merely 2 or 3 percent. Generally speaking, the larger the incidence angle, the more will the period of free vibrations of the surface layer diminish.

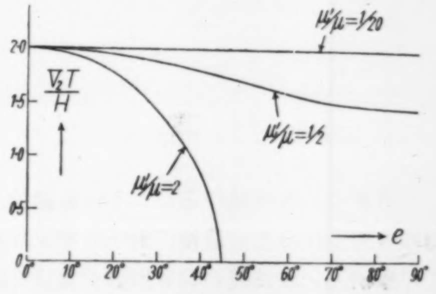

Fig. 2.

The nature of the decay factor K is somewhat complex. We shall

take the case of $\cos e' > \cos e$, namely the most probable case in an actual ground. If

$$\nu = \sqrt{\rho'\mu'/\rho\mu}\,(\cos e'/\cos e) = 1, \tag{18}$$

then K is zero, indicating that the initial disturbance dies away without repeated oscillation. Whether the value of ν be increased or decreased from the one specified in (18), the value of K would increase more and more, particularly for a greater value of e, showing the increasingly marked appearance of a type of repeated oscillations. Since, however, $\cos e'$, and accordingly $\cos e$ do not assume widely different values almost in any bodily wave transmitted through a long distance or even in shock waves applied artificially, it virtually appears to be possible to assume the same damping factor for any angle of incidence, the reliability of Köhler's result being thus confirmed.

Another question that might be raised is whether or not the solution (14) that corresponds to the vibratory motion of the layer could assume any other form, namely, a form showing pure stationary vibration rather than superposition of two wave systems propagated opposite to each other. Close examination of (12), (13), (14) will enable us to understand, however, that in the present case a solution other than (14) is scarcely possible unless another initial disturbance of a certain form transmitted in direction opposite to that of u_1 is assumed.

---

31. 斜のディスターバンスによつて生じた地表層の固有振動の減衰

地震研究所 { 妹澤克惟
金井清

地表層の固有振動の週期とその振動勢力が逸散するための振動減衰の割合とは，必しも一定不變のものではなく，最初に與へたディスターバンスの方向によつて少しく變り得るものである．この事柄は，彈性體の固有振動が實はそれ程固有のものでなく，適當の反響性波動を適當に組合せた所謂定常振動の特別の場合に過ぎないといふ意味を示すものである．この意味から地表層に於ける實際の振動は，反響性波動をあまり適當に組合し得ないだけそれだけ，定常性振動としては多少不完全なものに過ぎないことが想像されるであらう．

以前の論文に示したところの地表層の固有振動とその減衰係數は最初のディスターバンスが鉛

直方向に傳播するか又は同等な性質のある場合であつたのである．この論文ではそれが斜の方向をもち且つそれが水平變位を有する横波の性質のものである場合を考へることにした．その入射方向が鉛直線と e なる角をなすとき，地表層の中での振動波面の法線は屈折のために e' なる角をなすことになる．$\nu=\sqrt{\rho'\mu'/\rho\mu}(\cos e'/\cos e)$ と書けば振動週期は

$$\left.\begin{aligned} T&=\frac{4H}{V_2}\cos e', &&(\nu<1)\\ T&=\frac{2H}{V_2}\cos e' &&(\nu>1)\end{aligned}\right\}$$

となる．但し H は層の厚さ，V_2 は層中での波動速度である．

振動減衰の曲線が自然函數の曲線をなすことは以前の場合と同じであるが，その對數的減率は如何なる ν の場合でも

$$k=\frac{V_2}{2H\cos e'}\log_e\left|\frac{1+\nu}{1-\nu}\right|$$

の形を取るものである．

之等の結果から，ディスターバンスが斜の方向から來れば來る程，振動週期は短くなるし，對數的減率は $\nu<1$ の間は増加し $\nu>1$ の間は減少することがわかるのである．

實際問題としては $\cos e'=1$ に近い狀態の場合の方が多いと考へて差支がない．從てディスターバンスが鉛直に來たのと同じ結果を與へる場合の方が寧ろ多いやうに考へられる．卽ち地表層の固有振動もその減衰率も殆ど固有のものと假定しても大した誤がないやうである．

32. *Dissipation Waves Accompanying Forced Seiches in a Bay.*

By Katsutada SEZAWA and Kiyoshi KANAI,

Earthquake Research Institute.

(Read June 16, 1936.—Received June 20, 1936.)

1. In the preceding papers[1,2] we studied the problem of the decay of seiches in an epicontinental sea as well as in straits. Although the same problem in the case of a bay is of more practical importance, it was not possible for us to solve that problem until now owing to certain difficulties in mathematical calculation. As however the determination of the decay factor of seiches still remains a difficulty, we shall now merely ascertain the nature of the waves dissipated from a bay under the condition of forced seiches.

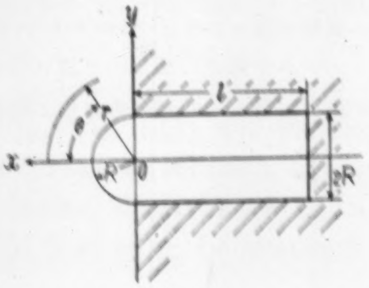

Fig. 1.

2. We shall suppose for simplicity that the bay is of rectangular shape and uniform depth, its breadth, length, and depth being $2R$, l, ξ respectively. The outer sea is also assumed to be of uniform depth ξ, while we shall take the axis of x directed outward with its origin at the mouth of the bay.

The incident waves (u_1, w_1) and the reflected waves (u_2, w_2) in the outer sea are

$$\left.\begin{aligned} u_1 &= ie^{i(\sigma t+fx)}, \qquad & w_1 &= -f\xi e^{i(\sigma t+fx)}, \\ u_2 &= -iAe^{i(\sigma t-fx)}, \qquad & w_2 &= -f\xi Ae^{i(\sigma t-fx)}, \end{aligned}\right\} \tag{1}$$

where u, w signify the horizontal displacements and the surface elevations of waves, and $2\pi/f$ is the wave length corresponding to the period $2\pi/\sigma$.

1) K. SEZAWA, "Growth and Decay of Seiches in an Epicontinental Sea," *Bull. Earthq. Res. Inst.*, **13** (1935), 476~483.

2) K. SEZAWA and K. KANAI, "Damped Free Osillation and Amplitudes in Resonance, with Special Reference to Decay of Seiches in Straits," *Bull. Earthq. Res. Inst.*, **14** (1936), 1~9.

The boundary condition at $x=0$ corresponding to the coast line is $u_1+u_2=0$, so that $A=1$. Thus we get

$$\left.\begin{aligned} u_1+u_2&=-2e^{i\sigma t}\sin fx,\\ w_1+w_2&=-2f\xi e^{i\sigma t}\cos fx. \end{aligned}\right\} \qquad (1')$$

This condition is approximate in the sense that the general reflection of the disturbance at the coast line is not affected by the existence of the bay.

The forms of the forced seiches in the bay are written $(u_1'+u_2', w_1'+w_2')$, where

$$\left.\begin{aligned} u_1'&=iCe^{i(\sigma t+fx)}, & w_1'&=-f\xi Ce^{i(\sigma t+fx)},\\ u_2'&=-iBe^{i(\sigma t-fx)}, & w_2'&=-f\xi Be^{i(\sigma t-fx)}. \end{aligned}\right\} \qquad (2)$$

At the end of the bay, namely at $x=-l$, we have $u_1'+u_2'=0$, so that

$$C=Be^{2ifl}, \qquad (3)$$

the expressions for forced seiches then being

$$\left.\begin{aligned} u_1'+u_2'&=-2Be^{ifl}\sin f(l+x)e^{i\sigma t},\\ w_1'+w_2'&=-2f\xi Be^{ifl}\cos f(l+x)e^{i\sigma t}. \end{aligned}\right\} \qquad (4)$$

The expressions for the dissipation waves in the outer sea, which are radiated from the mouth of the bay, may be put in the forms

$$\left.\begin{aligned} U_2&=-\sum_{n=0}^{\infty}a_n\frac{\partial H_n^{(2)}(fr)}{\partial(fr)}\cos n\theta e^{i\sigma t},\\ W_2&=-f\xi\sum_{n=0}^{\infty}a_nH_n^{(2)}(fr)\cos n\theta e^{i\sigma t},\\ V_2&=\frac{1}{fr}\sum_{n=0}^{\infty}a_n nH_n^{(2)}(fr)\sin n\theta e^{i\sigma t}. \end{aligned}\right\} \qquad (5)$$

where U_2, W_2, V_2 are the radial, vertical, and transverse components of displacement.

We now write

$$\left.\begin{aligned} U_1&=(u_1+u_2)\cos\theta, & U'&=(u_1'+u_2')\cos\theta,\\ W_1&=w_1+w_2, & W'&=w_1'+w_2',\\ V_1&=(u_1+u_2)\sin\theta, & V'&=(u_1'+u_2')\sin\theta. \end{aligned}\right\} \qquad (6)$$

Were the length of the bay relatively long compared with its breadth,

the boundary conditions at the mouth of the bay would be put approximately

$$\left.\begin{aligned} &[W_1+W_2]_{r=R,\ y=y}=[W']_{x=0,\ y=y}, \\ &\left[\int_{\theta=-\pi/2}^{\theta=\pi/2} U_2 R d\theta\right]_{r=R}=\left[\int_{y=-R}^{y=R} U' dy\right]_{x=0}. \end{aligned}\right\} \tag{7}$$

In these conditions the conception that the vertical elevation of the water at $r=R$ is the same as that at $x=0$ corresponding to the same value of y, and that the instantaneous mean flux of water through the boundary $r=R$ is the same as that at the mouth $x=0$, is implied. It should be borne in mind that, while U_2 takes important part in the flux of water, V_2 hardly contributes to the same flux.

Substituting from (5), (6) in (7), we obtain

$$2\cos fx-B\{e^{-ifx}+e^{2ifl+ifx}\}+\sum_{n=0}^{\infty}a_n H_n^{(2)}(fr)\cos n\theta=0, \qquad (x=0,\quad r=R) \tag{8}$$

$$B\left\{\sin 2f'l+i(1-\cos 2f'l)\right\}=\left[-\sum_{n=-}^{\infty}a_n\frac{\sin\frac{n\pi}{2}}{n}\frac{\partial H_n^{(2)}(fr)}{\partial(fr)}\right]. \quad (r=R) \tag{9}$$

It is well known that

$$\left.\begin{aligned} e^{ifx}&=J_0(fr)+2iJ_1(fr)\cos\theta+\cdots+2i^nJ_n(fr)\cos n\theta+\cdots, \\ e^{-ifx}&=J_0(fr)-2iJ_1(fr)\cos\theta+\cdots+(-1)^n 2i^nJ_n(fr)\cos n\theta+\cdots. \end{aligned}\right\} \tag{10}$$

Thus (8) is replaced by[3)]

$$2e^{ifl}B\left\{J_0(fR)\cos fl+2\sum_{n=1}^{\infty}J_n(fR)\cos n\theta\cos\left(\frac{n\pi}{2}+fl\right)\right\}$$
$$-\sum_{n=0}^{\infty}a_nH_n^{(2)}(fR)\cos n\theta-2\left\{J_0(fR)+2\sum_{n=1}^{\infty}(-1)^nJ_{2n}(fR)\cos 2n\theta\right\}=0. \tag{8'}$$

Equating the coefficient of each $\cos m\theta$ in (8′) to zero, we obtain

3) We used a similar method of treatment in the problem of seismic waves. K. SEZAWA, "Scattering of Elastic Waves and Some Allied Problems," *Bull. Earthq. Res. Inst.*, **3** (1927), 19~41; *ditto*, "The Reflection of Elastic Waves generated from an Internal Point of a Sphere", *ibid.*, **4** (1928), 123~130; T. MATUZAWA also used such a treatment in his recent paper, "Über Schattenwellen und Kernwellen", *ibid.*, **13** (1935), 18~38.

$$\left.\begin{aligned} a_0 &= \frac{2J_0(fR)(Be^{ifl}\cos fl-1)}{H_0^{(2)}(fR)}, \\ a_{2n+1} &= \frac{-4(-1)^n Be^{ifl}J_{2n+1}(fR)\sin fl}{H_{2n+1}^{(2)}(fR)}, \\ a_{2n+2} &= \frac{-(-1)^n J_{2n+2}(fR)(4Be^{ifl}\cos fl-1)}{H_{2n+2}^{(2)}(fR)}. \end{aligned}\right\} \quad (11)$$

Substituting (11) in (8′) it is possible to determine B. When the values of B thus determined are again substituted in (11), we obtain the values of a_0, a_1, a_2, $\cdots$, a_{2n+1}, a_{2n+2}, $\cdots$. We have calculated two cases, namely (i) $fR=1$, $fl=3$; (ii) $fR=24$, $fl=72$.[4]

3. In the case $fR=1$, $fl=3$; B, C, a_0, $\cdots$, a_{2n+1}, $\cdots$ assume values such that

$$\left.\begin{aligned} &B=0{\cdot}950-i0{\cdot}1421, && C=0{\cdot}8728-i0{\cdot}4019, \\ &a_0=-0{\cdot}1135-i0{\cdot}1016, && a_1=0{\cdot}059-i0{\cdot}2597, \\ &a_2=0{\cdot}06268+i0{\cdot}1890, && a_3=0{\cdot}000515+i0{\cdot}001748, \\ &a_4=0{\cdot}0000812+i0{\cdot}0003466, && \cdots\cdots\cdots, \end{aligned}\right\} \quad (12)$$

so that the equations for the dissipated waves are obtained by substituting these constants in (5), whereas the expression of the forced seiches is as follows.

$$W'=-2f\xi e^{3i}(0{\cdot}950-i0{\cdot}1421)\cos 3\left(1+\frac{x}{l}\right)e^{i\sigma t}. \quad (13)$$

The distribution of $W_2/f\xi$ for $fr=40$ and the different values of θ is shown in Fig. 2. Since, from the nature of the problem, resonance of the seiches is defined by $fl=\pi/2$, $3\pi/2$, $\cdots$ and corresonance of the same seiches by $fl=\pi$, 2π, $\cdots$, it is possible to assume that the present condition of the problem, namely $\cos fl=-0{\cdot}99$, is very close to first corresonance.

The maximum vertical elevations of the seiches at $x=-l$ as well as at $x=0$ assume the values

$$W'_{x=-l}=1{\cdot}921 f\xi, \qquad W'_{x=0}=1{\cdot}900 f\xi \quad (14)$$

respectively.

4. In the case of $fR=24$, $fl=72$; B, C, a_0, $\cdots$, a_{2n+1}, $\cdots$ assume values such that

---

4) There are a number of bays in Japan that have the dimensional ratio of $l/R=3$. Turuga, Oohunato, Hutami, and Hakodate are the bays, that may be mentioned as examples of the present case.

$$
\left.\begin{aligned}
&B=0{\cdot}079+i0{\cdot}2913, && C=0{\cdot}2119+i0{\cdot}2151,\\
&a_0=-0{\cdot}3675-i0{\cdot}4934, && a_1=0{\cdot}2187+i0{\cdot}1903,\\
&a_2=0{\cdot}2895+i0{\cdot}0350, && a_3=-0{\cdot}1918-i0{\cdot}2342,\\
&a_4=-0{\cdot}01916-i0{\cdot}00746, && a_5=0{\cdot}10413+i0{\cdot}2843,\\
&a_6=-0{\cdot}3010-i0{\cdot}3050, && a_7=0{\cdot}03658-i0{\cdot}2365,\\
&a_8=0{\cdot}1711+i0{\cdot}9029, && a_9=-0{\cdot}04892+i0{\cdot}04454,\\
&a_{10}=0{\cdot}5909-i0{\cdot}9015, && a_{11}=-0{\cdot}1818-i0{\cdot}02189,\\
&a_{12}=-0{\cdot}4567+i0{\cdot}0182, && a_{13}=0{\cdot}1201+i0{\cdot}2802,\\
&a_{14}=-0{\cdot}3226-i0{\cdot}6390, && a_{15}=0{\cdot}04784-i0{\cdot}04301,\\
&a_{16}=-0{\cdot}7467+i0{\cdot}6170, && a_{17}=0{\cdot}2179+i0{\cdot}1921,\\
&a_{18}=-0{\cdot}3277-i0{\cdot}3933, && a_{19}=0{\cdot}04777-i0{\cdot}0429,\\
&a_{20}=-0{\cdot}7356+i0{\cdot}3574, && a_{21}=0{\cdot}10464+i0{\cdot}2838,\\
&a_{22}=0{\cdot}0759-i1{\cdot}0402, && a_{23}=-0{\cdot}2177-i0{\cdot}07372,\\
&a_{24}=0{\cdot}3353+i0{\cdot}4378, && a_{25}=0{\cdot}08646-i0{\cdot}02003,\\
&a_{26}=-0{\cdot}1350-i0{\cdot}0797, && a_{27}=-0{\cdot}01618+i0{\cdot}00806,\\
&a_{28}=0{\cdot}02111+i0{\cdot}00914, && a_{29}=0{\cdot}001726-i0{\cdot}0009759,\\
&a_{30}=-0{\cdot}001772-i0{\cdot}000731, && a_{31}=-0{\cdot}0001113+i0.0000639,\\
&a_{32}=0{\cdot}0000914+i0{\cdot}00003753, && \cdots\cdots\cdots\cdots\cdots\cdots
\end{aligned}\right\}\qquad(15)
$$

While the equations for the dissipated waves are obtained by substituting these constants in (5) the expression of the forced seiches is written by

$$W'=-2f\xi e^{72i}(0{\cdot}079+i0{\cdot}2913)\cos 72\left(1+\frac{x}{l}\right)e^{i\sigma t}. \qquad (16)$$

The distribution of $W_\xi/f\xi$ for $fr=960$, that is for the same r as in the preceding case, and the different values of θ is also plotted in Fig. 2. Since, in the present case, $\cos fr=-0{\cdot}96726$, the condition of the problem is again very close to corresonance. It appears then that, from the results of the present as well as previous sections, the difference in dissipation waves with the difference in the frequency of disturbing waves is confirmable owing to the fact that the condition of the problem for both cases is capable of being assumed as corresonance.

The maximum vertical elevations of the seiches at $x=-l$ as well as at $x=0$ assume the values

$$W'_{x=-l}=0{\cdot}604f\xi, \qquad W'_{x=0}=0{\cdot}584f\xi. \qquad (17)$$

5. Comparison of the results of the two cases, namely (i) $fR=1$, $fl=3$, (ii) $fR=24$, $fl=72$, shows that, the higher the frequency of incident waves, the more is the energy of the dissipation waves in the outer sea polarised in the neighbourhood of the azimuth parallel to the lengthwise direction of the bay. The ratio of the vetical elevation of the dissipation waves at the radial distance $r/2R=20$ to that of incident waves is shown below.

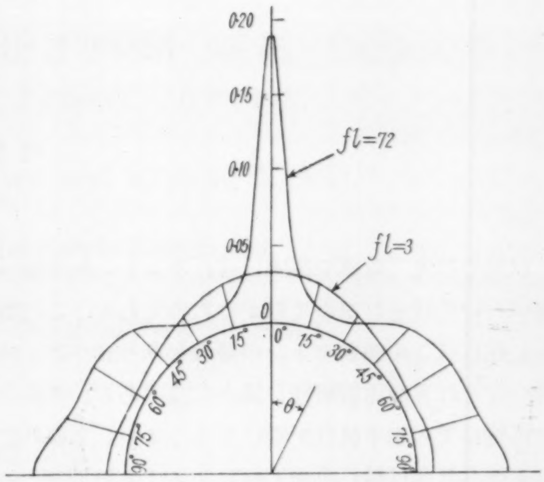

Fig. 2.

θ	0°	5°	15°	30°	45°	60°	80°	90°
$fR=1$	0·0312	——	0·0284	0·0209	0·01151	0·00645	0·01101	0·01279
$fR=24$	0·1899	0·0580	0·01547	0·01424	0·0346	0·0416	——	0·0627

These values are also assumed by the similar ratio for the horizontal displacements.

Another imporatant fact is that, while the total energy of the dissipation waves for the case of longer incident waves is much less than the one for the case of shorter incident waves as will be seen from the above table, the general amplitudes of the seiches in the bay for the former case is much greater than those for the latter as shown by (14) and (17). This is because of the energy of seiches more dissipated for higher frequency disturbance.

Although in the present paper the nature of the difference of the dissipation waves resulting from different vibrational condition of the bay, say, resonance or corresonance or intermediate condition, has not been studied, it appears however that the difference under consideration is very similar to the one in the case of the epicontinental sea or of the straits. For examples, in the condition close to resonance the vertical elevation at the mouth of the bay is very small, whereas in the condition close to corresonance the horizontal displacement at the same mouth is very small. The equation (4) in the present paper also suggests this fact.

32. 灣のセイシに伴ふ逸散性

地震研究所 {妹澤克惟
金井清

以前の研究で陸棚や海峡に現れるセイシが外海への逸散波のために減衰する狀態を考へたが，灣についてはまだ試みてなかつたのである．この問題を一般的に取扱ふことは相當困難であるから，玆にはこの强制セイシの場合を取り且つディスターバンスの週期が遲いものと速いものとを考へてそれらの比較研究を試みた譯である．共振のときに灣口での波高が零になり，餘共振のときに灣口での水平流れが零になることや，その外之等の場合の振幅比などの問題は大體わかつてゐるから只今は特に吟味しないことにした．

ディスターバンスの波長が長い場合と極く短い場合とでは逸散波やセイシの性質に著しい相異がある．波長が長い場合には，外海のすべての方向へ餘り極端な差異がなく逸散波が傳播するけれども，極く短くなると，灣口の向きの方向のみへ大きな勢力の逸散波が傳播し，所謂勢力傳播の方向性が現れるものである．

今一つ大切なことは，波長の長いときと短いときを比較して見ると，短いときの方が，逸散波の全勢力が遙かに大きくなり，セイシの振幅は逆に小さくなることである．振動勢力逸散の根本的性質であるとはいへ，セイシの場合にもよく現れてをるのは面白いともいひ得る．

33. *The Effect of Stiffness of Floors on the Horizontal Vibrations of a Framed Structure.*

By Katsutada SEZAWA and Kiyoshi KANAI,

Earthquake Research Institute.

(Read May 19, 1936.—Received June 20, 1936.)

1. *Introduction.*

In our investigation[1] on energy dissipation in the seismic vibrations of a framed structure, which appeared in a number of papers since last year, it was assumed in most cases that the floors of said structure are extremely rigid, and to meet a particular need, extremely flexible. Extremely rigid floors, besides relieving us from the difficulties of calculations to a certain extent, also appears to be a condition that is actually present in any structure. Our intentions now are to examine and ascertain to what extent the assumption under consideration would be reasonable.

Although the dynamical treatment of a problem of this kind is not difficult, no systematic solution has yet been found owing probably to the complexity of the mathematical calculation.[2]

In the present paper we have solved the case of a multi-spanned framed structure by our dynamical method as well as by the slope-deflection method, showing that by whichever way the problem is solved, the result would be the same. In any method it is assumed that the partial masses are suitably affixed to the respective panel points instead of being distributed in all the vertical as well as horizontal structural members. It has already been shown that, were the problem of a multi-spanned structure to be solved under such an assumption as that the number of spans is endless, the effect of the extreme spans would not be appreciable even were the number of spans only two.[3]

---

1) K. SEZAWA and K. KANAI, *Bull. Earthq. Res. Inst.*, **12** (1934), 804~822, 823~853; **13** (1935), 698~714, 931~941; **14** (1936), 119~133, 134~145, 189~200.

2) A. MIZUHARA, using the slope-deflection method, found equations for the vibrations of a high framed structure of single span, but he did not obtain systematic numerical solutions, excepting a few examples. *Journ. Arch., Japan*, **41** (1927), **43** (1929), **44** (1930).

3) K. SEZAWA and K. KANAI, *Bull. Earthq. Res. Inst.*, **10** (1932), 789.

2. *Dynamical equations of free oscillations for an n-storied structure.*

Take the two-dimensional problem and let the time factor be e^{ipt}; the solution of the vibratory motion of the columns between $s-1$th and the sth floors is then

$$u_s = A_s + B_s x_s + C_s x_s^2 + D_s x_s^3, \qquad (1)$$

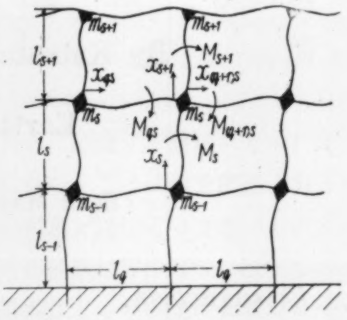

Fig. 1.

where x_s is the coordinate of a point of the same column measured from its lower end and u_s the horizontal deflection of the same point. The solution of the vibratory motion of the sth floor at the qth span is

$$u_{qs} = A_{qs} + B_{qs} x_{qs} + C_{qs} x_{qs}^2 + D_{qs} x_{qs}^3, \qquad (2)$$

where x_{qs}, u_{qs} are the coordinate of a point and the deflection of the same point. Let l_s, l_q, E_s, E_{qs}, I_s, I_{qs} be the length, Young's modulus, and the moment of inertia of a cross section of a column between the s—1th and sth floors; and similar particulars of the sth floor, m_s being the mass concentrated at any panel point of the sth floor. Then the boundary conditions are such that

$$x_1 = 0; \qquad u_1 = 0, \qquad \frac{du_1}{dx_1} = 0, \qquad (3), (4)$$

$$x_s = l_s, \ x_{s+1} = 0, \ x_{qs} = l_q, \ x_{(q+1)s} = 0;$$

$$u_s = u_{s+1}, \ u_{qs} = 0, \ u_{(q+1)s} = 0, \ \frac{du_s}{dx_s} = \frac{du_{s+1}}{dx_{s+1}} = \frac{du_{qs}}{dx_{qs}} = \frac{du_{(q+1)s}}{dx_{(q+1)s}},$$

$$(5), (6), (7), (8), (9), (10)$$

$$E_{s+1} I_{s+1} \frac{d^3 u_{s+1}}{dx_{s+1}^3} - E_s I_s \frac{d^3 u_s}{dx_s^3} = m_s p^2 u_s, \qquad (11)$$

$$M_s - M_{s+1} + M_{qs} - M_{(q+1)s} = 0, \qquad (12)$$

$$x_n = l_n, \ x_{qn} = l_{qn}, \ x_{(q+1)n} = 0;$$

$$u_{qn} = 0, \ u_{(q+1)n} = 0, \ \frac{du_n}{dx_n} = \frac{du_{qn}}{dx_{qn}} = \frac{du_{(q+1)n}}{dx_{(q+1)n}}, \qquad (13), (14), (15), (16)$$

$$-E_n I_n \frac{d^3 u_n}{dx_n^3} = m_n p^2 u_n, \ M_n + M_{qn} - M_{(q+1)n} = 0, \qquad (17), (18)$$

where M_s, M_{qs}... are, for example, of form such that

$$M_s = -E_s I_s \frac{d^2 u_s}{dx_s^2}. \tag{19}$$

By substituting the expressions of types (1), (2) in (3)~(19), we obtained the frequency equations for the cases from a one- to a four-storied structure.

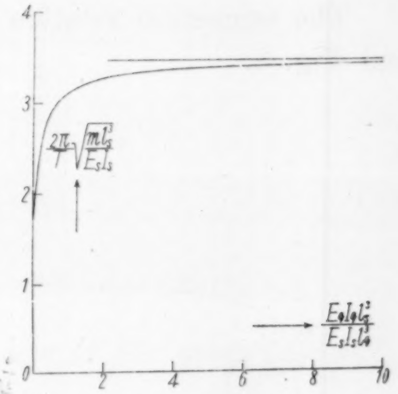

Fig. 2. 1-storied structure.

3. *A one-storied structure.*

The final solution is such that

$$3(\gamma-12)\eta+(\gamma-3)=0, \tag{20}$$

or

$$\gamma=\frac{3(1+12\eta)}{1+3\eta}, \tag{20'}$$

where $\gamma=\dfrac{m_1 p^2 l_1^3}{E_1 I_1}$, $\eta=\dfrac{E_{q1} I_{q1} l_1}{E_1 I_1 l_q}$, the result of the numerical calculation being shown in Table I and Fig. 2.

Table I.

η	0	0·2	0·5	1	1·5	2	5	7	10	∞
$\sqrt{\gamma}$	1·732	2 525	2·899	3·122	3·219	3·274	3·384	3·407	3·423	3·464

4. *A two-storied structure.*

The final solution in this case is

$$36\left\{(\gamma_1-12)(\gamma_2-12)-12\nu\xi^2\gamma_2\right\}\eta_1\eta_2+12\left\{(\gamma_1-12)(\gamma_2-3)-3\nu\xi^3\gamma_2\right\}\eta_1$$
$$+6\Big[3\gamma_2\left\{\gamma_1(\nu\xi+2)-2(\nu^2\xi^4+4\nu\xi^3+6\nu\xi^2+6\nu\xi+3)\right\}$$
$$-(\gamma_2+6)\left\{\gamma_1(\nu\xi+4)-12(\nu\xi+1)\right\}\Big]\eta_2$$
$$+\Big[4(\gamma_1-3)(\gamma_2-3)+3\nu\xi\gamma_2\left\{(\gamma_1-12)-4\xi(\xi+3)\right\}\Big]=0, \tag{21}$$

where $\gamma_1=\dfrac{m_1 p^2 l_1^3}{E_1 I_1}$, $\gamma_2=\dfrac{m_2 p^2 l_2^3}{E_2 I_2}$, $\eta_1=\dfrac{E_{q1} I_{q1} l_1}{E_1 I_1 l_q}$, $\eta_2=\dfrac{E_{q2} I_{q2} l_2}{E_2 I_2 l_q}$, $\nu=\dfrac{E_2 I_2}{E_1 I_1}$, $\xi=\dfrac{l_1}{l_2}$.

In the case $E_1 I_1=E_2 I_2(=EI)$, $E_{q1} I_{q1}(=E_q I_q)$, $l_1=l_2(=l)$, $m_1=m_2$ $(=m)$, it is possible to write $\eta_1=\eta_2(=\eta)$, $\gamma_1=\gamma_2(=\gamma)$, the solution thus being

$$36(\gamma^2-36\gamma+144)\eta^2+36(\gamma^2-27\gamma+36)\eta+(7\gamma^2-108\gamma+36)=0. \tag{22}$$

The numerical relation between η and $\sqrt{\gamma}$ are shown in Table II and Fig. 3.

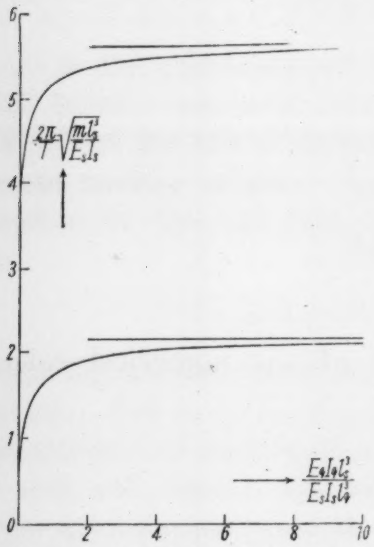

Fig. 3. 2-storied structure.

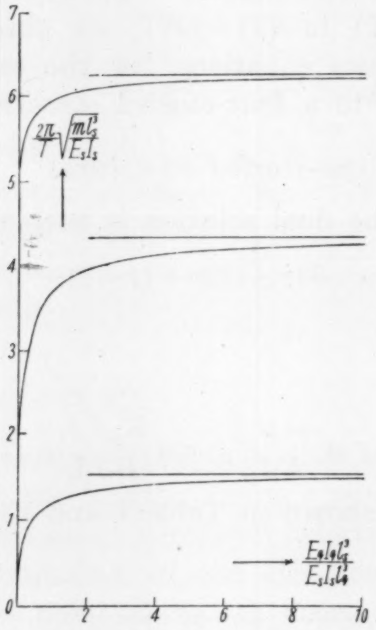

Fig. 4. 3-storied structure.

Table II.

η	0	0·2	0·5	1	1·5	2	2·5	5	7	10	∞
$\sqrt{\gamma}$	0·584 3·884	1·233 4·598	1·538 4·963	1·747 5·200	1·849 5·306	1·906 5·366	1·950 5·410	2·036 5·500	2·063 5·530	2·085 5·546	2·142 5·606

5. *A three-storied structure.*

We obtained the solution for the simple case $E_1I_1=E_2I_2=E_3I_3$ $(=EI)$, $E_{\eta1}I_{\eta1}=E_{\eta2}I_{\eta2}=E_{\eta3}I_{\eta3}(=E_\eta I_\eta)$, $l_1=l_2=l_3(=l)$, $m_1=m_2=m_3(=m)$, so that $\eta_1=\eta_2=\eta_3(=\eta)$, $\gamma_1=\gamma_2=\gamma_3(=\gamma)$, the result being

$$108\eta^3(\gamma^3-60\gamma^2+864\gamma-1728)+180\eta^2(\gamma^3-51\gamma^2+540\gamma-432)$$

$$+18\eta(5\gamma^3-204\gamma^2+1332\gamma-432)+(13\gamma^3-393\gamma^2+1296\gamma-108)=0, \quad (23)$$

where $\eta=\dfrac{E_\eta I_\eta l}{EIl_\eta}$, $\gamma=\dfrac{mp^2l^3}{EI}$.

The numerical relation between η and $\sqrt{\gamma}$ are shown in Table III and Fig. 4.

Table III.

η	0	0·2	0·5	1	2	5	10	∞
	0·2926	0·8019	1·035	1·204	1·337	1·448	1·493	1·542
$\sqrt{\gamma}$	1·915	2·843	3·344	3·688	3·950	4·155	4·234	4·320
	5·147	5·552	5·796	5·950	6·067	6·165	6·196	6·242

6. *A four-storied structure.*

Taking a special case similar to the one in the preceding section, the frequency equation becomes such that

$$\begin{aligned}1296(\gamma^4-84\gamma^3+2160\gamma^2-17280\gamma+20736)\eta^4&\\ +432(7\gamma^4-525\gamma^3+11340\gamma^2-66528\gamma+36288)\eta^3&\\ +108(23\gamma^4-1500\gamma^3+25812\gamma^2-98064\gamma+25920)\eta^2&\\ +12(70\gamma^4-3846\gamma^3+49464\gamma^2-112536\gamma+12960)\eta&\\ +(97\gamma^4-4332\gamma^3+38340\gamma^2-43200\gamma+1296)=0,&\quad(24)\end{aligned}$$

where $\eta=\dfrac{E_qI_ql}{EIl_q}$, $\gamma=\dfrac{mp^2l^3}{EI}$.

The numerical relations between η and $\sqrt{\gamma}$ are shown in Table V and Fig. 5.

Table V.

η	0	0·2	0·5	1	2	5	10	∞
	0·1757	0·5907	0·779	0·916	1·0285	1·1225	1·1602	1·2032
	1·1315	2·006	2·475	2·807	3·069	3·280	3·370	3·464
$\sqrt{\gamma}$	3·197	3·958	4·418	4·718	4·970	5·170	5·220	5·306
	5·757	6·030	6·190	6·306	6·392	6·460	6·486	6·510

7. *Application of the slope-deflection method.*

An alternative method is to apply the slope-deflection method. Although this method finds great favour among structural engineers, it is virtually the same as the one shown in Section 2. The principle underlying the method is as follows: Let the deflections and slopes of both ends A, B of a bar, which is free of transverse force between these two ends be u_A, u_B, θ_A, θ_B. The bending moments, M_A, M_B, and shearing forces, F_A, F_B, at these ends are then such that

$$
\left.\begin{aligned}
M_A&=\frac{2EI}{l}\left\{2\theta_A+\theta_B+\frac{3(u_A-u_B)}{l}\right\},\\
M_B&=\frac{2EI}{l}\left\{\theta_A+2\theta_B+\frac{3(u_A-u_B)}{l}\right\},\\
-F_A=F_B&=-\frac{6EI}{l^2}\left\{\theta_A+\theta_B+\frac{2(u_A-u_B)}{l}\right\},
\end{aligned}\right\} \tag{25}
$$

where E, I, l have the same meanings as those of the preceding sections, and the signs of M_A, M_B, F_A, F_B are so determined that the ends A, B should be reference points for M_A, F_A and for M_B, F_B respectively. The necessary equations for determining the problem are such that

$$\sum M=0, \qquad \sum F=P \qquad (26), (27)$$

vectorially at every panel point, where P is a vectorial force acting at that panel point. The special feature of the method is to write θ_A, θ_B, u_A, u_B, $\cdots$ in lieu of using A_s, B_s, C_s, D_s, $\cdots$ as shown in (1), (2) and to formulate M_A, M_B, F_A, F_B, $\cdots$ directly by means of such parameters. But, the actual difficulty in the problem of a high-storied structure lies in the solution of the simultaneous equations that come up after the preliminary treatment is ended. We believe that our dynamical method involves less uncertainties because of the fact that all the quantities are derived from the same parameters A_s, B_s, C_s, D_s, $\cdots$.

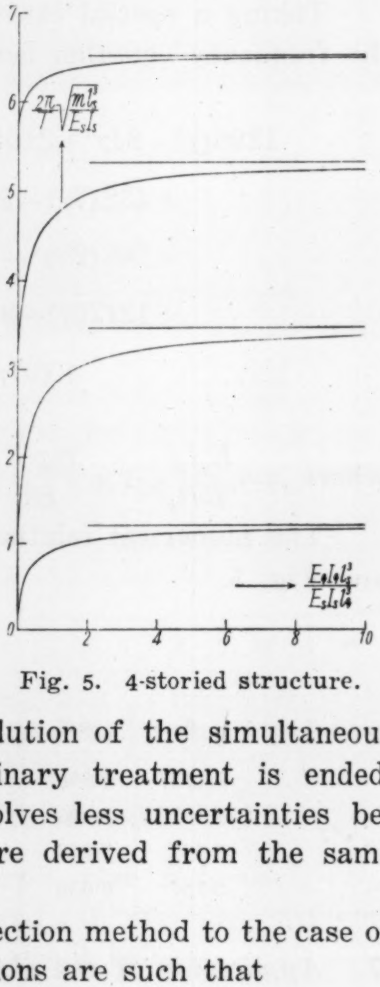

Fig. 5. 4-storied structure.

At all events, if we apply the slope-deflection method to the case of a one storied structure, the resulting equations are such that

$$
\left.\begin{aligned}
M_1&=\frac{2E_1I_1}{l_1}\left(2\theta_1-\frac{3u_1}{l_1}\right), & M_{q1}&=M_{(q+1)1}=\frac{6E_qI_q}{l_q}\theta_1,\\
-F_1&=-\frac{6E_1I_1}{l^2}\left(\theta_1-\frac{2u_1}{l_1}\right), & P&=-m_1p^2u_1.
\end{aligned}\right\} \tag{28}
$$

Solving these and using (26), (27), we obtain

$$3(\gamma-12)\eta+(\gamma-3)=0, \tag{29}$$

which is the same as that in (20).

In the case of a two-storied structure we have the equations

$$M_1=\frac{2E_1I_1}{l_1}\left(2\theta_1-\frac{3u_1}{l_1}\right),\quad M_{q1}=M_{(q+1)1}=\frac{6E_{q1}I_{q1}}{l_1}\theta_1,$$

$$M_2=\frac{2E_2I_2}{l_2}\left\{2\theta_1+\theta_2+\frac{3(u_1-u_2)}{l_2}\right\},$$

$$M_2'=\frac{2E_2I_2}{l_2}\left\{\theta_1+2\theta_2+\frac{3(u_1-u_2)}{l_2}\right\},$$

$$M_{q2}=M_{(q+1)2}=\frac{6E_{q2}I_{q2}}{l_2}\theta_2,$$

$$F_1=-\frac{6E_1I_1}{l_1^2}\left(\theta_1-\frac{2u_1}{l_1}\right),$$

$$-F_2'=-\frac{6E_2I_2}{l_2^2}\left\{\theta_1+\theta_2+\frac{2(u_1-u_2)}{l_2}\right\},$$

$$F_2=-\frac{6E_2I_2}{l_2^2}\left\{\theta_1+\theta_2+\frac{2(u_1-u_2)}{l_2}\right\},$$

$$P_1=-m_1p^2u_1,\qquad P_2=-m_2p^2u_2. \tag{30}$$

Substituting these in (26), (27), and solving the resulting simultaneous equations for the particular case $E_1I_1=E_2I_2$, $E_{q1}I_{q1}=E_{q2}I_{q2}$, $l_1=l_2$, $m_1=m_2$, we get

$$36(\gamma^2-36\gamma+144)\eta^2+36(\gamma^2-27\gamma+36)\eta+(7\gamma^2-108\gamma+36)=0. \tag{31}$$

This is the same as that in (22).

It is possible to obtain solutions for any number of stories in the same manner.

8. *Mathematical empirical formulae for the principal vibration frequencies for any number of stories.*

The mathematical solutions for the vibration frequencies of a high-storied structure, even when the stories are fewer than four, are not simple. Thus, using the exact solutions of four cases, namely cases for structures between one- and four-storied, we have obtained simple formulae that could be extrapolated to the case of any number of stories. Since the solution thus formulated is applicable with fair

accuracy to the case of an endless number of stories, the validity of the formulae is apparent. The type of the empirical formulae is such that

$$\frac{1}{\sqrt{\gamma}} = (An+B)^{\alpha} + C, \tag{32}$$

where n is the number of stories of a structure and A, B, C, α are constants to be determined, using the mathematical results for the cases $n=1$, 2, 3, 4. Similar method was already used successfully in the cases of $\eta=0$ as well as $\eta=\infty$.[4] The present result is as follows:

$$\eta=0\ ;\quad \frac{1}{\sqrt{\gamma}} = (0{\cdot}5342n + 0{\cdot}2615)^{2} - 0{\cdot}056,$$

$$\eta=0{\cdot}2\ ;\quad \frac{1}{\sqrt{\gamma}} = (0{\cdot}3925n + 0{\cdot}0923)^{1{\cdot}100} - 0{\cdot}055,$$

$$\eta=0{\cdot}5\ ;\quad \frac{1}{\sqrt{\gamma}} = (0{\cdot}2969n + 0{\cdot}1250)^{1{\cdot}0675} - 0{\cdot}053,$$

$$\eta=1\ ;\quad \frac{1}{\sqrt{\gamma}} = (0{\cdot}2483n + 0{\cdot}1367)^{1{\cdot}056} - 0{\cdot}045,$$

$$\eta=5\ ;\quad \frac{1}{\sqrt{\gamma}} = (0{\cdot}1945n + 0{\cdot}1554)^{1{\cdot}040} - 0{\cdot}04,$$

$$\eta=\infty\ ;\quad \frac{1}{\sqrt{\gamma}} (0{\cdot}1777n + 0{\cdot}1548)^{1{\cdot}039} - 0{\cdot}03.$$

In these expressions the parts of α and A are what are important, whereas the terms of B and C can be adjusted so as to satisfy the mathematical result. The result is also plotted in Fig. 6.

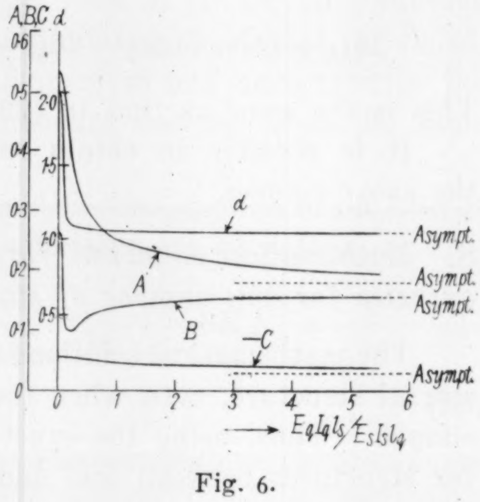

Fig. 6.

Our investigation made in 1934 for the case $\eta=0$ and ∞ gave apparently different forms, namely,

$$\eta=0\ ;\quad \frac{1}{\sqrt{\gamma}} = 0{\cdot}288n^2 + 0{\cdot}266n + 0{\cdot}025,$$

$$\eta=\infty\ ;\quad \frac{1}{\sqrt{\gamma}} = 0{\cdot}181n + 0{\cdot}106,$$

4) K. SEZAWA and K. KANAI, *Bull. Earthq. Res. Inst.*, **12** (1934), 816~819.

although the numerical difference is inappreciable.

9. *Interpretation of the result.*

The present series of investigations shows that the vibration frequencies of such a structure that η is almost greater than unity are roughly equal to that in which $\eta=\infty$, and furthermore that the linear relation between the principal natural period and the number of stories in different storied structures holds even for the case of very small η, say 0·2, the coefficient of the linear relation differing as the value of η differs. The coefficient under consideration in the case of $\eta=0{\cdot}2$ is about $3{\cdot}6(\simeq 0{\cdot}6379/0{\cdot}1777)$ times that of the case $\eta=\infty$.

In the case of an actual building the observed natural period is about twice that of the period calculated under the assumption that $\eta=\infty$. This suggests that the effective rigidity of the floors is very small, say, $\eta=0{\cdot}5$, which fact is equivalent to reducing the value of $\sqrt{EI/ml^3}$ to nearly one half the original value in the case where the formula for the case $\eta=\infty$ is used. It is possible to use such a convenient assumption because α does not change much for a large range of η.

In conclusion, we wish to express our thanks to the Council of the Foundation for the Promotion of Scientific and Industrial Research in Japan, with whose aid the present series of investigations is being continued.

---

33. 床の剛度が架構の水平振動に及ぼす影響

地震研究所 妹澤克惟
金井清

これまで述べた構造物の振動勢力の地下逸散の研究に於て，多くの場合に床の剛度を極端に剛く考へ，又特別の目的のために極端に柔く考へたけれども，たとひ極端に剛いとしてもそれが如何なる程度に剛いかといふことを見極めて置く必要がある．このやうな問題の研究はこれまでも多少試みた人もあるけれども，特別の場合だけであつて只今の目的には殆ど役に立たぬし，又問題それ自身にも少しく漠然としたところがないでもなかつたやうである．只今の研究では，純力學的方法と構造學者が用ひる撓角撓度法との兩方法を用ひて多張間架構の4層建までを嚴格に取扱ひ，その結果から數理的實驗式を作成して之を多層架構へ延長させたのである．その可能性はよく確めて置いたのである．

今，床の構造が層番によつて變らぬ場合その剛度を E_qI_q さし，柱のそれを EI さする．柱長さ張間徑間さを l, l_q さし，節點質量を m，振動數を p さすれば，構造物の主要振動數は

$$\frac{1}{\sqrt{\gamma}}=(An+B)^{\alpha}+C$$

て表される．玆に $\gamma=(mp^2l^3)/(EI)$，n=層數，α，A，B，C は $\eta=(E_qI_ql)/(EIl_q)$ の函數で示される常数である．この實驗式中，α さ A さが重要であつて，A は η によつて少しづゝ變化するけれども α は $\eta=\infty$ から $\eta=0{\cdot}2$ 位の間殆ど1に近い數であるこさが知られるのである．

この結果さ實際の建物の振動數さを比較して見るさ，實際の建物は $\eta=0{\cdot}5$ の近所に近いものであるこさが想像される．しかしそれにしても α は殆ど1であるから，構造物の床が極端に剛いさして問題を取扱つても，EI の値を適當に小さく見積つて置きさへすれば，大して誤りがないこさがわかる．

34. *Energy Dissipation in Seismic Vibrations of Actual Buildings Predicted by means of an Improved Theory.*

By Katsutada SEZAWA and Kiyoshi KANAI,

Earthquake Research Institute.

(Read April 21, 1936.—Received June 20, 1936.)

1. *Formulae for the problem.*

In the previous paper[1] we obtained improved formulae for the energy dissipation in seismic vibrations of a structure as the result of more accurate treatment of the points that had been somewhat approximate in the original problem. As suggested in that paper, the improved theory, when applied to actual structures, gives rise to new results that cannot be found in the original study.

The solution of the vibratory motion of the columns between the $s-1$th and sth floors is

$$y_s=(A_s+B_sx_s+C_sx_s^2+D_sx_s^3)e^{ipt}. \quad (s=1,\ 2,\cdots\cdots,\ n) \tag{1}$$

The boundary conditions in the case of a clamped base and extremely rigid floors are as follows.

$$x_n=-l_n; \qquad E_nI_n\frac{\partial^3 y_n}{\partial x_n^3}+m_n\frac{\partial^2 y_n}{\partial t^2}=0, \qquad \frac{\partial y_n}{\partial x_n}=0, \qquad (2),\ (3)$$

$$x_s=-l_s, \quad x_{s+1}=0; \quad E_{s+1}I_{s+1}\frac{\partial^3 y_{s+1}}{\partial x_{s+1}^3}=E_sI_s\frac{\partial^3 y_s}{\partial x_s^3}+m_s\frac{\partial^2 y_s}{\partial t^2}, \qquad (4)$$

$$\frac{\partial y_s}{\partial x_s}=0, \quad \frac{\partial y_{s+1}}{\partial x_{s+1}}=0, \quad y_s=y_{s+1}, \quad (s=1,\ 2,\cdots\cdots,\ n-1) \quad (5),\ (6),\ (7)$$

$$x_1=0, \quad r=\varepsilon; \qquad (u_1+u_2)_{max.}=-(v_1+v_2)_{max.}, \qquad (8)$$

$$\frac{\partial y_1}{\partial x_1}=0, \quad y_1=u_0+u_0'+(u_1+u_2)_{r=\varepsilon,\ \theta=0}, \qquad (9),\ (10)$$

1) K. SEZAWA and K. KANAI, "Improved Theory of Energy Dissipation in Seismic Vibrations of a Structure", *Bull. Earthq. Res. Inst.*, **14** (1936), 164~188. The significance of each symbol used in the present paper is shown in the preceding paper under consideration.

$$-E\pi\varepsilon^2 j^2 \frac{\partial^3 y_1}{\partial x_1^3} = \int_{\varphi=0}^{\pi}\int_{\theta=0}^{\pi}\Big[\mu\Big\{\frac{\partial(v_1+v_2)}{\partial r} - \frac{v_1+v_2}{r} + \frac{1}{r}\frac{\partial(u_1+u_2)}{\partial\theta}\Big\}\sin^2\theta$$

$$+\Big\{\lambda\Delta + 2\mu\frac{\partial(u_1+u_2)}{\partial r}\Big\}\sin\theta\cos\theta\Big]r^2 d\varphi d\theta. \tag{11}$$

In the present paper the cases of a 3-storied and 7-storied structures will be studied. Since the solution of a 3-storied structure has been formulated in pp. 174～175 in one[2] of our previous papers, and that of a 7-storied structure in pp. 189～192 of another paper,[3] details of the mathematical expressions ascertained by means of the improved theory will not be given. It is however rather important to note that the deflections as well as the bending moments on columns for any case have a common factor of type such that

$$M = \sqrt{\frac{\Gamma_1^2 + \Gamma_2^2}{P^2+Q^2}}\cos\Big(pt + \tan^{-1}\frac{\Gamma_2}{\Gamma_1} - \tan^{-1}\frac{Q}{P}\Big), \tag{12}$$

where

$$\left.\begin{aligned}
&P = \phi\Gamma_1 + \frac{18Ej^2\varepsilon}{\mu l^3}\psi\Lambda_1, \quad Q = \phi\Gamma_2 + \frac{18Ej^2\varepsilon}{\mu l^3}\psi\Lambda_2,\\
&\Gamma_1 = \frac{3(\lambda+2\mu)}{\mu} + \nu\gamma_1\Big(\frac{\lambda}{\mu} - 3\sqrt{\frac{\lambda+2\mu}{\mu}}\Big),\\
&\Gamma_2 = \sqrt{\nu\gamma_1}\Big\{3\sqrt{\frac{\lambda+2\mu}{\mu}}\Big(1+\sqrt{\frac{\lambda+2\mu}{\mu}}\Big) + \nu\gamma_1\Big(\sqrt{\frac{\lambda+2\mu}{\mu}} - 2\Big)\Big\},\\
&\Lambda_1 = \frac{2\lambda+5\mu}{\mu} - \nu\gamma_1, \quad \Lambda_2 = \sqrt{\nu\gamma_1}\Big(2\sqrt{\frac{\lambda+2\mu}{\mu}} - 1\Big),\\
&\nu = \frac{E_1\rho I_1\varepsilon^2}{\mu m_1 l_1^3},
\end{aligned}\right\} \tag{13}$$

in which

$$\left.\begin{aligned}
&\phi = 1728 - 864\gamma + 60\gamma^2 - \gamma^3,\\
&\psi = \gamma(12-\gamma)(36-\gamma)
\end{aligned}\right\} \tag{14}$$

in the case $n=3$; and

2) *loc. cit.* 1).

3) K. SEZAWA and K. KANAI, "Energy Dissipation in Seismic Vibrations of a Seven-storied Structure. Nature of Corresonance", *Bull. Earthq. Res. Inst.*, **14** (1936), 189～200.

$$
\left.
\begin{aligned}
\phi &= (12-\gamma)\Big\{(12-\gamma)(24-\gamma)-144\Big\}\Big[-36\gamma(24-\gamma)(36-\gamma) \\
&\qquad\qquad\qquad\qquad + \{(12-\gamma)(24-\gamma)-144\}^2\Big]. \\
\psi &= \gamma\Big\{(12-\gamma)^2(36-\gamma)-144(24-\gamma)\Big\}\Big\{(12-\gamma)(36-\gamma)^2-144(24-\gamma)\Big\}
\end{aligned}
\right\} \quad (15)
$$

in the case $n=7$.

If $(Ej^2\varepsilon)/(\mu l^3)=0$, the denominator of M has a factor ϕ, so that, were γ to satisfy $\phi=0$, M would assume an infinitely large value. If, on the other hand, $(Ej^2\varepsilon)/(\mu l^3)=\infty$, the denominator of M has a factor ψ, so that, were γ to satisfy $\psi=0$, M would again assume an infinitely large value. $\phi=0$, $\psi=0$ correspond respectively to the resonance and corresonance conditions in our previous conception That the two conditions $(Ej^2\varepsilon)/(\mu l^3)=0$ and $(Ej^2\varepsilon)/(\mu l^3)=\infty$ indicate critical cases in both of which there is very little dissipation, appears probable even from the ordinary physical standpoint.

In the case where $(Ej^2\varepsilon)/(\mu l^3)$ is neither zero nor infinity, the value of M becomes maximum within every range, the lower and the upper criticals of which are conditioned by every root of $\phi=0$ and that of $\psi=0$. Generally speaking, the value of γ that gives each of the maximum bending moments, increases from a value satisfying $\phi=0$ to that satisfying $\psi=0$ in accordance with increase in $(Ej^2\varepsilon)/(\mu l^3)$ from 0 to ∞.

2. *A three-storied structure.*

In the case of a 3-storied structure γ satisfies $\phi=0$ when

$$\gamma=2{\cdot}3765, \qquad 18{\cdot}6630, \qquad 38{\cdot}9605;$$

and γ satisfies $\psi=0$ when

$$\gamma=12, \qquad 36.$$

Thus, the two maxima of the bending moments in the resonance curves lie successively between $\gamma=2{\cdot}3765$ and 12, and between 18·6630 and 36.

The greatest value of the maximum bending moment is usually that in the range between $\gamma=2{\cdot}3765$ and 12 in the resonance curves. If the greatest bending moment were to be at γ near $\gamma=2{\cdot}3765$, that moment would be induced in the columns below the first floor, whereas, if the greatest moment were to be at γ near $\gamma=12$, that moment would be induced in the columns between the first floor and the roof, the

greatest moments in the columns of both two floors then being the same. If, on the other hand, the greatest bending moment were to arise at an intermediate γ in the range under consideration, that moment in the columns between the first and the second floors would be the greatest.

The calculated result for the case of Mitsubishi Naka-13 gô-kan is shown in Figs. 1, 2. The data of structure for the calculation are the same as those in an earlier paper[4] of ours, whereas E and ρ being $E=2\cdot1.10^9$ kg/m², $\rho=2\cdot0.10^3$ kg *mass*/*m*³, the value of $\mu(\lambda=\mu)$ is assumed to be (i) $\mu=8.10^7$ kg *mass*/*ms*² (corresponding to $\sqrt{\mu/\rho}=200$m/s), and (ii) $\mu=2.10^7$ kg *mass*/*ms*² (corresponding to $\sqrt{\mu/\rho}=100$ *m*/*s*), the two cases belonging to Figs. 1, 2 respectively. The vertical strips of full and broken lines represent the conditions $\phi=0$, $\psi=0$ respectively.

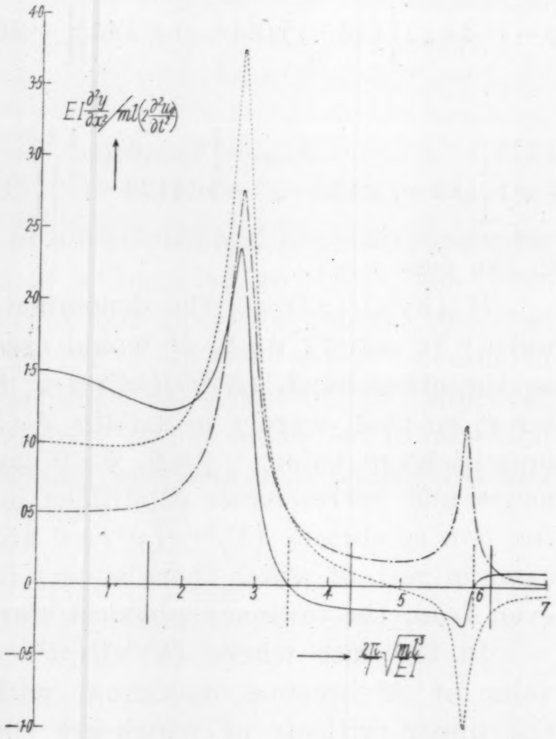

Fig. 1. Mitsubishi Naka-13gô-kan. $\sqrt{\mu/\rho}=200$ m/sec. Full, broken, and chain lines represent moments in columns of ground, first, and second floors respectively.

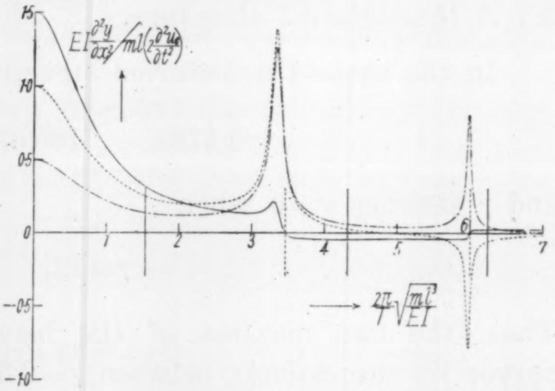

Fig. 2. Mitsubishi Naka-13gô-kan. $\sqrt{\mu/\rho}=100$m/sec. Full, broken, and chain lines represent moments in columns of ground, first, and second floors respectively.

Upon comparing the results in Figs. 1, 2 it will be seen that dissipation is more pronounced in the case of soft ground than in rigid ground.

The greatest bending moment in the present case lies between $\gamma=2\cdot3765$ and 12, namely $\sqrt{\gamma}=2\cdot78$ in the first case, $\sqrt{\mu/\rho}=200\,m/s$, and $\sqrt{\gamma}=3\cdot34$ in the second, $\sqrt{\mu/\rho}=100\,m/s$, in

4) K. SEZAWA and K. KANAI, *Bull. Earthq. Res. Inst.*, **13** (1935), 930.

both of which the greatest moments are induced in columns between the first and the second floors.

With a view to getting the solution of a problem such that the calculated natural frequency would coincide with the actual probable one (0·2 sec), we assume a rather small value of EI instead of calculating for the case in which the floor is sensibly flexible.[5] If we were to take 1/4 of the value of EI just mentioned so as to obtain a principal natural period of about 0·2 sec, it would be necessary to assume $\sqrt{\mu/\rho}=100\ m/s$ and $50\ m/s$ respectively to make the result in Figs. 1, 2 available. Since such conditions as that $I=I'/4$ (I' being the calculated value) and $\sqrt{\mu/\rho}=200\ m/s\sim100\ m/s$ are rather probable ones in the present structure, it seems that the results in Figs. 1, 2 are likely to represent dissipation somewhat in excess of what we should expect in the same structure.

3. *A seven-storied structure.*

In the case of a 7-storied structure, γ satisfies $\phi=0$ when

$$\gamma=0{\cdot}525,\quad 4{\cdot}584,\quad 12,\quad 21{\cdot}49,\quad 31{\cdot}42,\quad 40{\cdot}03,\quad 45{\cdot}95;$$

and γ satisfies $\psi=0$ when

$$\gamma=2{\cdot}37,\quad 9{\cdot}04,\quad 18{\cdot}66,\quad 29{\cdot}35,\quad 38{\cdot}99,\quad 45{\cdot}60.$$

The maxima of the bending moments in the resonance curves lie successively between $\gamma=0{\cdot}525\sim2{\cdot}37$, $4{\cdot}584\sim9{\cdot}04$, $12\sim18{\cdot}66$, $21{\cdot}49\sim29{\cdot}35$, $31{\cdot}42\sim38{\cdot}99$, $40{\cdot}03\sim45{\cdot}60$. The position of every maximum moment changes from the lowest critical to the upper in each of the above ranges in accordance with changes in $(Ej^2\varepsilon)/(\mu l^3)$ from 0 to ∞.

The greatest value of the maximum bending moments is usually that in the range $\gamma=0{\cdot}525\sim2{\cdot}37$. If the greatest bending moment were to be near $\gamma=0{\cdot}525$ in the resonance curves, that moment would be induced in the columns below the first floor, whereas, if the greatest bending moment were to be near $\gamma=2{\cdot}37$, that moment would be induced in columns between the 3rd and 5th floors, the greatest moment in the columns of the two floors then being the same. In accordance with the change in the position of the greatest bending moment in the resonance curves, namely from $\gamma=0{\cdot}525$ to $2{\cdot}37$, the greatest bending moment is induced in columns of different stories, namely from

5) K. SEZAWA and K. KANAI, "The Effect of the Stiffness of Floors on the Horizontal Vibrations of a Framed Structure", *Bull, Earthq. Res. Inst.*, **14** (1936), 367~376.

the columns below the first floor to those between the 3rd and 4th floors.

Finally, it will be seen that the gaps between the successive ranges, within which the resonance frequencies lie, become narrower, excepting the lowest gap, with increase in the order of resonance. In the present case the values of the gaps under consideration are such that 2·21, 2·96, 2·83, 2·07, 1·04, 0·35. It should be remembered that the final value of γ for which $\phi=0$ is not the critical of any range.

The calculation as applied to the case of the Old Kaizyô Building is shown in Figs. 3, 4. The value of I in the calculation is the same as that for the columns only in Table I in one of our papers,[6] whereas E, ρ, λ, μ being the same as those in the preceding section, cases $\sqrt{\mu/\rho}=200\ m/s$ and $\sqrt{\mu/\rho}=100\ m/s$ correspond to those in Figs. 3, 4.

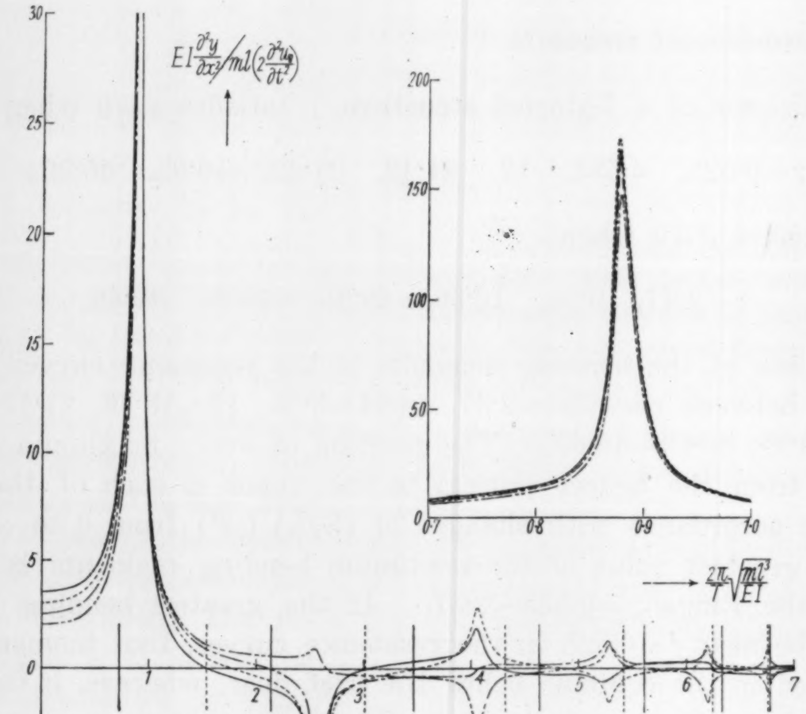

Fig. 3a. Old Kaizyô Building, $\sqrt{\mu/\rho}=200$ m/sec. Full, broken, chain, and double chain lines represent moments in columns of ground, first, second, and third floors respectively.

6) K. SEZAWA and K. KANAI, *loc. cit.* 3).

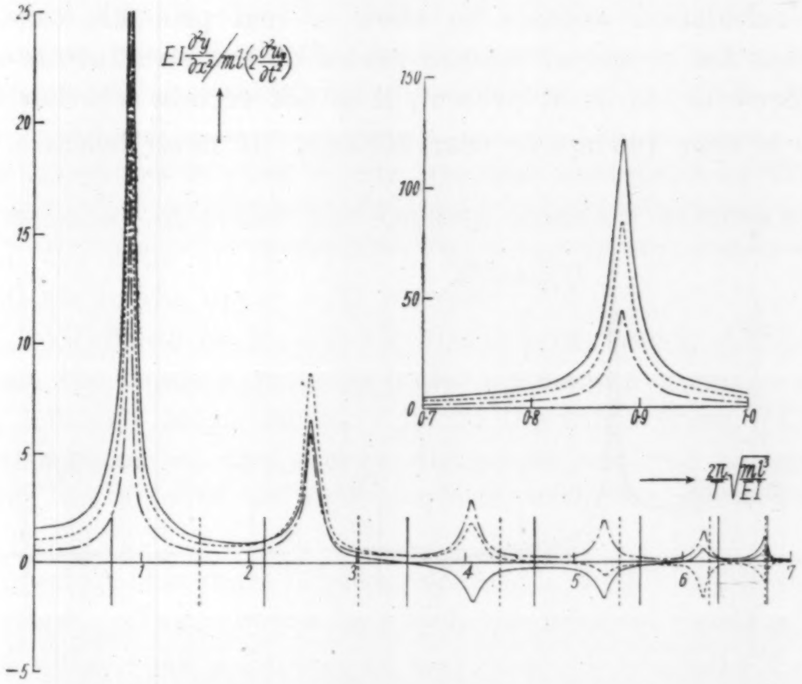

Fig. 3b. Old Kaizyô Building. $\sqrt{\mu/\rho}=200$ m/sec. Full, broken, and chain lines represent moments in columns of fourth, fifth, and sixth floors respectively.

The vertical strips of full and broken line types again represent the conditions $\phi=0$, $\psi=0$ respectively.

The effect of rigidity of ground on dissipation is more marked in the present case than in the preceding one. In the case of $\sqrt{\mu/\rho}=$ 200 m/s, dissipation is extremely small.[7]

The greatest bending moment in the present case lies in the range between 0·525 and 2·37, namely $\sqrt{\gamma}=0{\cdot}884$ in the first case, $\sqrt{\mu/\rho}=$ 200 m/s, and $\sqrt{\gamma}=1{\cdot}30$ in the second, $\sqrt{\mu/\rho}=100$ m/s. While the greatest moment in the first case is induced in columns between the first and second floors, the same moment in the second case is induced in columns between the third and fourth floors.

Since the value of I just mentioned is incidentally the same as one quarter of the moments of inertia of all the vertical members shown in the same table, the value of I here adopted may alternatively be interpreted as its value that has been modified in lieu of calculating the case in which the floor is sensibly flexible. As a matter of fact the

7) The effect of such a deeply piled foundation as in this building is rather to greatly increase the dissipation owing to the enormously increased area of contact surface between the piles and the ground. But, we are here discussing the problem of a pileless structure wherein the dissipation is not very marked.

present calculation appears to show a real probable case, for the reason that the principal natural period of the structure is about 0·46 sec.. However, to us at present, it is not certain whether the value of $\sqrt{\mu/\rho}$ is near 100 m/s or near 200 m/s. If nevertheless $\sqrt{\mu/\rho}$ were

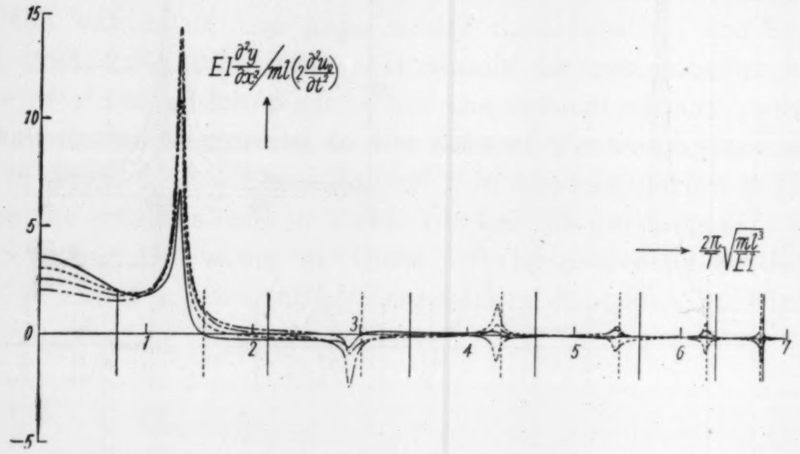

Fig. 4a. Old Kaizyô Building. $\sqrt{\mu/\rho}=100$ m/sec. Full, broken, chain, and double chain lines represent moments in columns of ground, first, second, and third floors respectively.

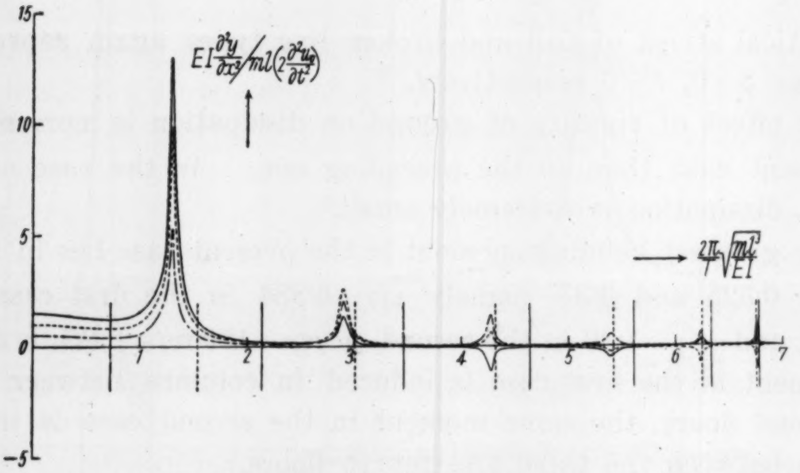

Fig. 4b. Old Kaizyô Building. $\sqrt{\mu/\rho}=100$ m/sec. Full, broken, and chain lines represent moments in columns of fourth, fifth, and sixth floors respectively.

to be near 100 m/s, it would be possible to conclude that the damping of the seismic vibration is mainly due to dissipation of the vibrational energy into the ground, in the present case at all events.

4. *Concluding remarks.*

Every maximum of the bending moments induced in the columns

lies within a certain specified range of resonance curves, the lower and the upper criticals of the range under consideration indicating the resonance of cases satisfying the condition $(Ej^2\varepsilon)/(\mu l^3)=0$ and the condition $(Ej^2\varepsilon)/(\mu l^3)=\infty$ respectively, namely the resonance and cor-resonance conditions implied in our previous conception. The vibrational frequencies at which the bending moments become maximum depend on the ratio of $(Ej^2\varepsilon)/(\mu l^3)$, their values increasing from the lower criticals to the upper with increase in $(Ej^2\varepsilon)/(\mu l^3)$ from 0 to ∞. When $(Ej^2\varepsilon)/(\mu l^3)=0$ or ∞, the vibration energy hardly dissipates into the ground, the bending moments under resonances in such a condition assuming infinitely large values. If, on the other hand, $(Ej^2\varepsilon)/(\mu l^3)$ were neither 0 or ∞, the energy dissipated into the ground would be of such an amount as shall conform with the difference in the value of $(Ej^2\varepsilon)/(\mu l^3)$.

The greatest maximum bending moment is within the lowest range just described. The columns in which the greatest bending moment is induced differ with difference in the value of $(Ej^2\varepsilon)/(\mu l^3)$. When $(Ej^2\varepsilon)/(\mu l^3)=0$, the columns in which the greatest bending moment is induced are those below the first floor. The larger the value of $(Ej^2\varepsilon)/(\mu l^3)$, the more the columns of floors still further up partake of the greatest bending moment. In the limiting case where $(Ej^2\varepsilon)/(\mu l^3)=\infty$, the floor under consideration is that which is immediately below the roof or that a few floors below the roof. The fact that the columns that were damaged most in the case of great earthquakes were those on floors a few stories above the ground floor, appears now to be well explained by the present study on the dissipation of vibrational energy.

In conclusion we wish to express our thanks to the Council of the Foundation for the Promotion of Scientific and Industrial Research in Japan, with whose aid the present series of investigations was begun, and also to the members of the staff of the Mitsubishi Co. and those of the Tokyo Fire and Marine Insurance Co., who kindly allowed us the use of their valuable data on these structures.

34. 改良せる理論から見た實在建物の震動勢力逸散性

地震研究所 {妹澤克惟 / 金井清

前回の論文で震動逸散の問題をできるだけ嚴格に取扱つて理想的結果を出して置いたが，この論文ではその理論を應用して，三菱仲十三號館（3階）と海上ビルデイング（7階）の場合の震動逸散性とを推定して見たのである．その結果から之等の建物の震動逸散性が一層よくわかつたのみでなく，今迄どうしてもはつきりしなかつた構造物の震動の性質が明瞭になつたのである．

何れの場合にも床の變位と柱の屈曲モーメントとは，強制振動がある振動數（1個でなく順次高次のものがある）で極大値を取る．この振動數は土地の剛度が極端に剛い場合の建物の各次の固有振動數と土地の剛度が極端に柔い場合のその各次の固有振動數との間の値であり，その値は建物の剛度と土地の剛度との比，卽ち $(Ej^2\varepsilon)/(\mu l^3)$ の如き數によつて定まるものである．且つ又，$(Ej^2\varepsilon)/(\mu l^3)=0$ の場合と $(Ej^2\varepsilon)/(\mu l^3)=\infty$ の場合とには，上記の變位や屈曲モーメントが無限大となり逸散性が無くなるけれども，その中間の場合には何れも有限値となつて逸散性のあることがわかる．換言すれば前の論文で示したところの共振と餘共振との間の振動數で現れ，且つその振動數は $(Ej^2\varepsilon)/(\mu l^3)$ の値によつて變化することが知られるのである．

柱の屈曲モーメントは上記の極大値中で最低次に相當するものが最大となるが，その場合に何れの床の柱のモーメントが一番大きくなるかといふと，その極大値を取るべき振動數の値，いひ換へれば $(Ej^2\varepsilon)/(\mu l^3)$ の値によつて變るものである．$(Ej^2\varepsilon)/(\mu l^3)=0$ の場合には最下階の柱の屈曲モーメントが最も大きくなり，$(Ej^2\varepsilon)/(\mu l^3)$ の增加とともに少しづつ上の層の柱の屈曲モーメントが最大値を取るやうになる．極論な場合卽ち $(Ej^2\varepsilon)/(\mu l^3)=\infty$ になると屋根から1階か2階下の柱の屈曲モーメントが最大になるものである．このやうな性質は土地の震動數が公平にあらゆる値を取る場合についていはれるから非常に都合がよいものといふことができる．大地震の時に高層建物で地上數階目かに建物の被害が多かつたといはれてゐるが，只今の逸散理論を應用すれば簡單に說明がつくのである．關東地震直後に筆者や其他の先輩學者方が建物の自己振動を添附したり，高次の共振を入れたり，或は他の種類の振動型を入れたりして，無理に說明を試みようとしたことなどもあるけれども，何れの場合にもディスターバンスの種々のもの、機會均等性を考へると不都合な點から免れ得なかつたものである．

35. *On the Degree of Disturbance of the Earth's Crust.*

By Naomi MIYABE,

Earthquake Research Institute.

(Read, May 19, 1936.—Received June 20, 1936.)

1. In the preceding paper, the frequency distribution of values of $\left[\frac{\partial}{\partial t}\left(\frac{\partial w}{\partial s}\right)\right]$ was studied with regard to several sections of lines of levels. As the result of these studies, it was shown that the frequency distribution of $\frac{\partial}{\partial t}\left(\frac{\partial w}{\partial s}\right)$ is of the type of a curve of error distributions for the time when the earth's crust was not much disturbed by earthquakes, whereas when the earth's crust is greatly disturbed, as was the case of the Kwantô districts[1], It diverges considerably from the curve of error distributions.

In order to express the degree of disturbance of the earth's crust, in the preceding paper[2], the absolute values of the vertical displacements of triangulation points was averaged over each unit area. This method of investigation however is not applicable to the present one, for, as the vertical displacements of bench-marks or triangulation points are measured with reference to some point the height of which is assumed not to have changed, the degree of disturbance thus calculated contains some parameters related to displacements of the assumed zero-points and its values therefore differ with periods.

In the present study, therefore, the mean values of $\left[\frac{\partial}{\partial t}\left(\frac{\partial w}{\partial s}\right)\right]^2$ are calculated over the sections of levels, as a measure representing the degree of disturbance in the earth's crust in the region under consideration.

2. The sections of lines of levels over which the degrees of disturbance were calculated are

(a) Hudisawa–Atami
(b) Tu–Atuta, I, II
(c) Tango district (Ebara–Miyadu)
(d) Eastern coast of the Idu peninsula

1) N. MIYABE, *Bull. Earthq. Res. Inst.*, **11** (1933), 639.
2) N. MIYABE, *ibid.*, **9** (1931), 1.

(e) In the neighbourhood of the Kagosima-wan

(f) Kasiwabara-Kanô.

To calculate $\sqrt{\Delta^2}$ is very simple; that is, if w_n and w_{n+1} are the vertical displacements of successive bench-marks, τ is the time interval during which vertical displacement w_n occurred, and the values of $\sqrt{\Delta^2}$ are calculated over the line in which N bench-marks are situated, as follows:

$$\sqrt{\Delta^2}=\left[\frac{\partial}{\partial t}\left(\frac{\partial w}{\partial s}\right)\right]^2=\sqrt{\frac{1}{N}\sum_{n=1}^{N-1}\left[\frac{w_{n+1}-w_n}{\tau}\right]^2}.$$

In calculating such a quantity, we sometimes meet with a special case in which the rates of changes in gradients between intervals of three bench-marks, $\frac{w_{n+1}-w_n}{\tau}$ and $\frac{w_n-w_{n-1}}{\tau}$, although too large, are almost equal in absolute values, whereas their signs are reversed, which means that the n-th bench-mark was much disturbed locally as shown in Fig. 1[3]. The existence of such a pair of values of Δ's contributes to the value of $\sqrt{\Delta^2}$ as given in the Table I.

Table I.

Section	Hudisawa-Atami	Tu-Kuwana	Kasiwabara-Kanô	
Period	1924~1925	1888~1894	1899~1916	1916~1928
$\sqrt{\Delta^2}$	11·97	2·21	2·09	4·41
$\sqrt{\Delta^2}$ (corrected)	7·89	1·32	0·74	0·97

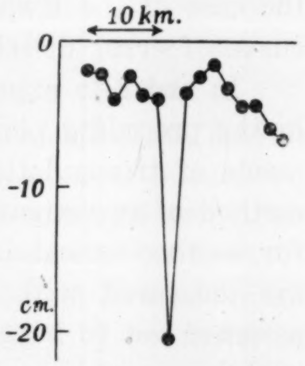

Fig. 1. An example showing a local remarkable subsidence of a bench-mark.

Such a pair of values of Δ's as just mentioned is excluded in calculating the degree of disturbance, $\sqrt{\Delta^2}$, so that we avoid errors due to disturbances from artificial causes.

The variations in the values of $\sqrt{\Delta^2}$ for various regions obtained from the foregoing calculations are as follows.

(a) *Hudisawa—Atami.*

This region forms the northern coast of Sagami-wan (Bay), in which the epicentre of the Kwantô earthquake of 1923, as determined seismometrically, is located. With this line of levels, surveys were

3) Such remarkable local disturbance as shown in Fig. 1 may generally be due to artificial causes rather than to disturbances of any geophysical significance.

made in 1895, 1924, 1925 and 1930. The vertical displacements measured in 1924 therefore consist of the slow crustal deformations that accumulated during the period 1895~1924, together with an acute deformation that occurred at the time of the 1923 earthquake. The distribution of bench-marks and the variations in the values of $\sqrt{\Delta^2}$ in this region are shown in Figs. 2 and 3 respectively.

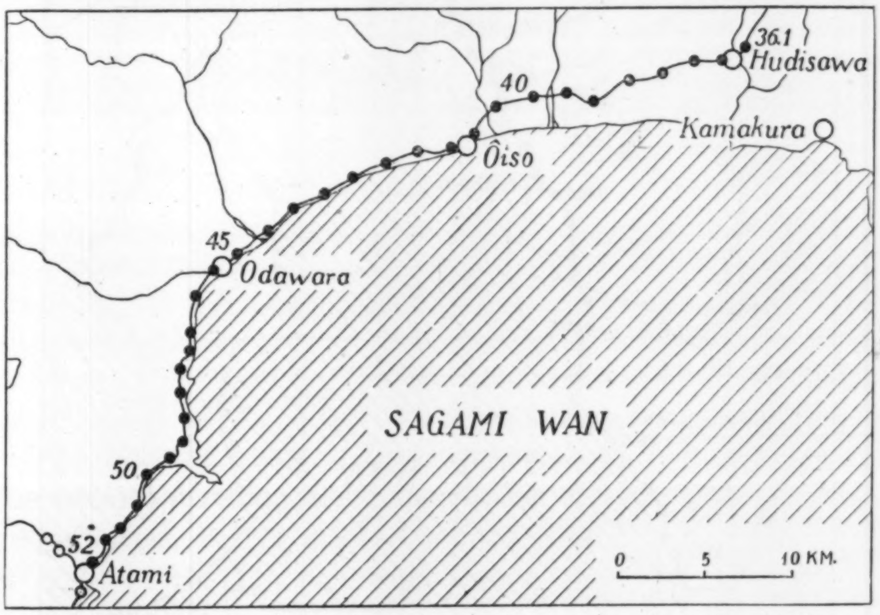

Fig. 2. Distribution of bench-marks in the region between Hudisawa and Atami. (Black circles are bench-marks under consideration.)

(b) *Tu—Atuta*

In beginning our study of variations in $\sqrt{\Delta^2}$ in this region, the line of levels is divided for convenience into two sections; that is, I, from Tu to Kuwana (B. M. 1445~1467), and II, from Kuwana to Atuta (B. M. 1468~1480, 174·1). The trend of the former section of the line of levels extends in a S–N direction, the levelling of which section of the line was done in 1888, 1894, 1929, and 1931, whereas that of the latter section is in a W–E direction, this section of the line having been levelled in 1888, 1894, 1916, 1929, and 1931.

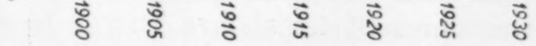

Fig. 3. Variation in values of $\sqrt{\Delta^2}$ in the region between Hudisawa and Atami.

Of the regions under consideration, that in which bench-marks of section II are distributed was greatly disturbed by the acute crustal deformation in connection with the Nôbi earthquake of 1891, while the

region of section I was not then much disturbed.

The geographical distribution of bench-marks and the variations in $\sqrt{\Delta^2}$ in this region are shown in Figs. 4 and 5 a, b.

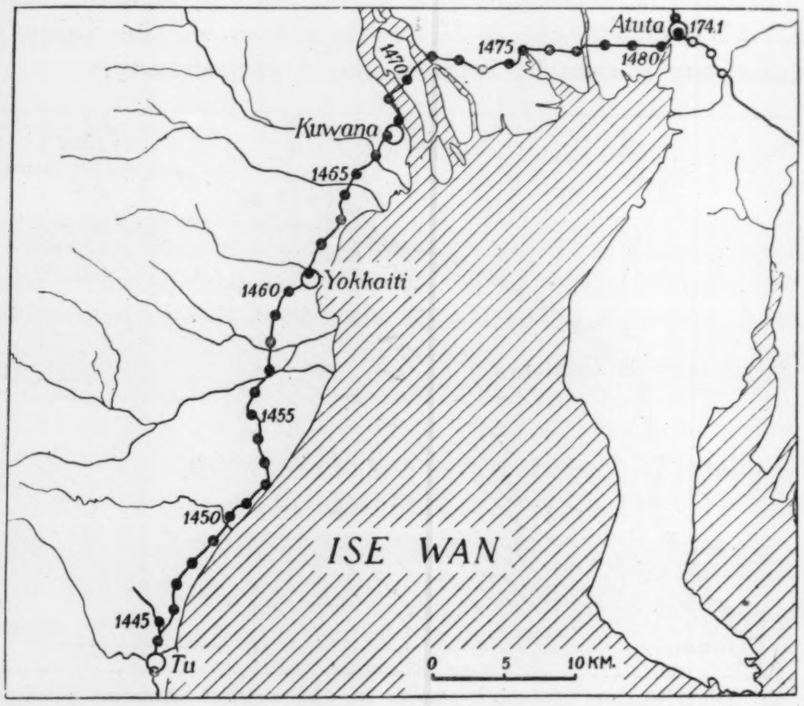

Fig. 4. Distribution of bench-marks in the region between Tu, Kuwana and Atuta. (Black circles are bench-marks under consideration.)

(c) *Tango District.*

In the Tango district, the line of levels from Ebara to Miyadu, by way of Toyooka, Kumihama and Mineyama, shown in Fig. 6, was relevelled five times since the Tango earthquake of 1927, the dates of which are

I. April～May, 1927
II. June～July, 1927
III. March～April, 1928
IV. August～September, 1929
V. July, August～September, 1930.

The variations in $\sqrt{\Delta^2}$ are shown in Fig. 7.

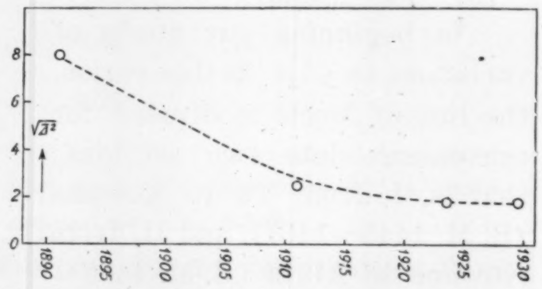

Fig. 5 a. Variation in values of $\sqrt{\Delta^2}$ in the region between Tu and Kuwana.

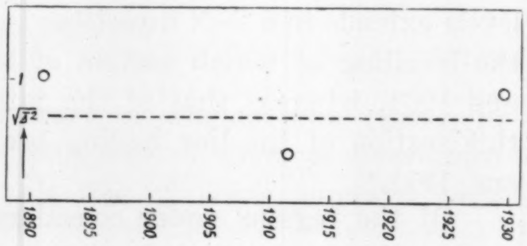

Fig. 5 b. Variation in values of $\sqrt{\Delta^2}$ in the region between Kuwana and Atuta.

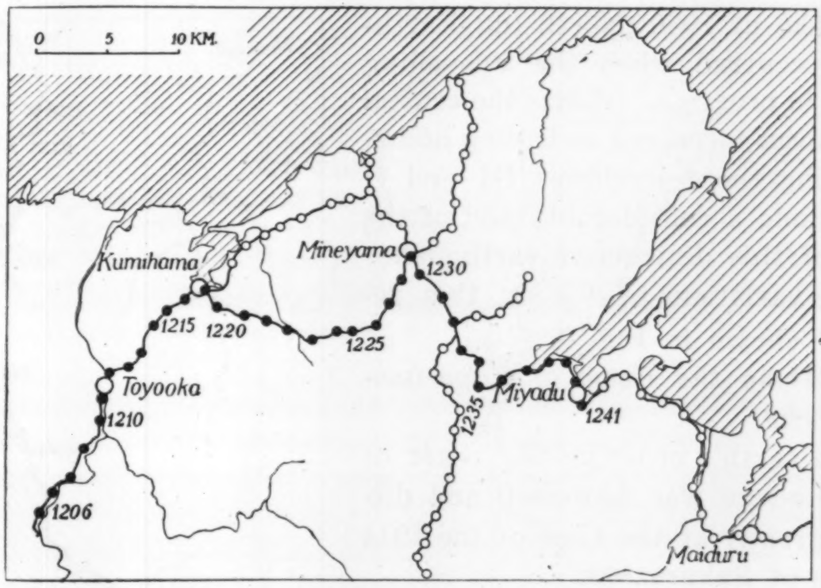

Fig. 6. Distribution of bench-marks in Tango district. (Black circles are bench-marks under consideration.)

(d) *The Eastern Coast of Idu Peninsula.*

The precise levelling along the section of the line of levels, B.M.'s 9328∼9342, on the eastern coast of the Idu peninsula shown in Fig. 8, was revised in

I. 1924∼1924
II. March 15–April 14, 1930
III. November 19–December 3, 1930
IV. December 19, 1930–January 16, 1931
V. 1933
VI. 1936.

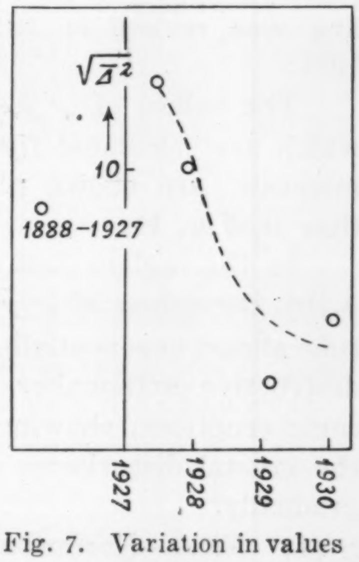

Fig. 7. Variation in values of $\sqrt{\Delta^2}$ in Tango district.

The crustal deformations deduced from these relevellings may be connected with the earthquake swarms that occurred in the neighbourhood of Itô (the epicentres of these earthquake swarms are concentrated in a region denoted by a dotted circle in Fig. 8); that occurred during Feb. ∼April and May of 1930, and the earthquake swarms that occurred in the neighbourhood of Aziro (epicentres of which are located in a region denoted by a dotted ellipse in Fig. 8) during Oct.∼ Nov., 1930.

These earthquake swarms may have contributed in some measure to the crustal disturbance measured as having occurred during the period of relevellings III and II. It is also notable that the destructive

earthquake of 1930 (North Idu Earthquake) occurred when the relevelling III was in progress. Hence the crustal disturbances measured as having occurred during the relevellings III and II may include a considerable part of the effects of this destructive earthquake.

Fig. 8. Distribution of bench-marks in the neighbourhood of Ito. (Black circles are bench-marcks under consideration.)

The variations in $\sqrt{\Delta^2}$ in this region are shown in Fig. 9.

(e) *Along the Coast of Kagosima-wan.*

The earth's crust on the coast of Kagosima-wan was depressed and disturbed greatly at the time of the 1914 eruption of Sakurazima.

Along the line of levels of this region, shown in Fig. 10, precise levelling was revised in 1915, 1919, and 1931.

The values of $\sqrt{\Delta^2}$ of this region which are calculated for various time intervals, are shown plotted against time in Fig. 11.

In the regions just mentioned, (a) ~ (b), the values of $\sqrt{\Delta^2}$ decrease with time almost exponentially after destructive earthquakes or volcanic eruptions, showing that the crustal disturbance ceases gradually.

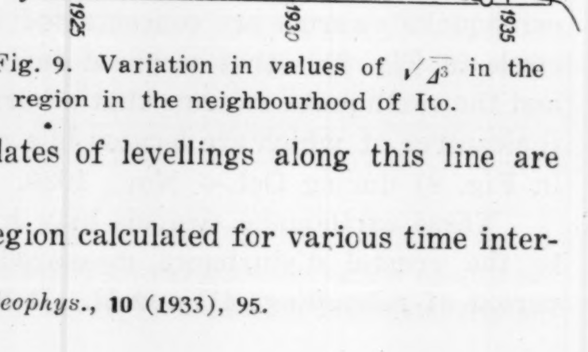

Fig. 9. Variation in values of $\sqrt{\Delta^2}$ in the region in the neighbourhood of Ito.

(f) *Kanô—Kasiwabara.*

In this region, the line of levels extends in an E-W direction as shown in Fig. 12, approximately parallel to the trend of the section of the line from Kuwana to Atuta. The dates of levellings along this line are 1895, 1899, 1917, and 1928.

The values of $\sqrt{\Delta^2}$ in this region calculated for various time inter-

4) C. Tsuboi, *Jap. Journ. Astr. Geophys.*, **10** (1933), 95.

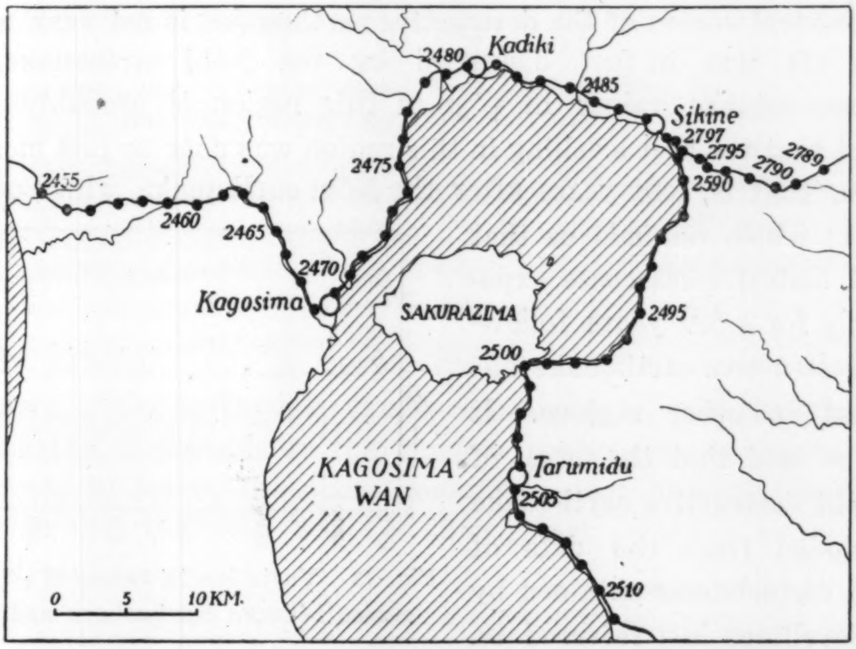

Fig. 10. Distribution of bench-marks in the region along the coast of Kagosima-wan. (Black circles are bench-marks under consideration.)

vals are shown protted against time in Fig. 13.

Since the values of $\sqrt{\Delta^2}$ in this region and those in region between Tu and Kuwana referred to in (b) are approximately constant from the time of the first relevelling up to the present, it may therefore be supposed that the effect of destructive earthquakes on crustal disturbances in regions sufficiently far from

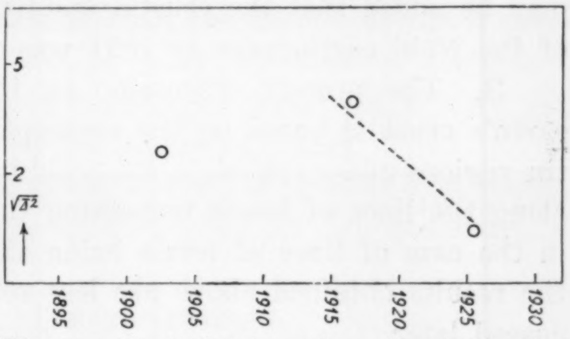

Fig. 11. Variation in values of $\sqrt{\Delta^2}$ in the region along the coast of Kagosima-wan.

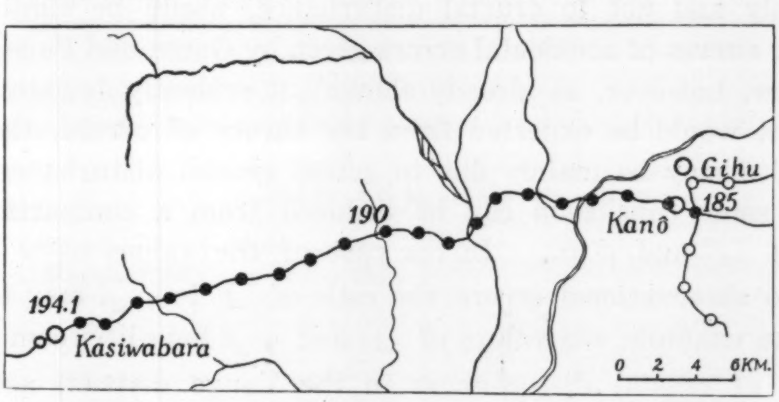

Fig. 12. Distribution of bench-marks in the region between Kasiwabara and Kanô. (Black circles are the bench-marks under consideration.)

the epicentral region of the destructive earthquake, is not very marked. Region (f) was in fact disturbed by the Nôbi earthquake. The smallness of the values in $\sqrt{\overline{\Delta^2}}$ in this region is probably due to the fact that the first levelling in this region was done as just mentioned in 1895, that is, four years after the Nôbi earthquake, which occurred in 1891; which reminds us that crustal disturbances cease exponentially for a few years following a destructive earthquake has occurred in other regions. It may be said that the effect of the Nôbi destructive earthquake is excluded from the data of crustal disturbances obtained by the relevellings just referred to.

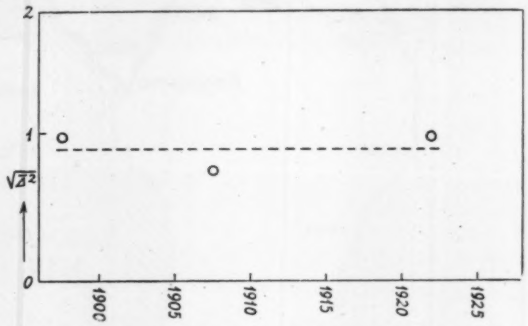

Fig. 13. Variation in values of $\sqrt{\overline{\Delta^2}}$ in the region between Kasiwabara and Kanô.

As for the smallness of the value of $\sqrt{\overline{\Delta^2}}$ in region I of (b), it may be added that the crustal disturbance in this region at the time of the Nôbi earthquake of 1891 was not so marked as in region II.

3. The present discussion on the degree of disturbance of the earth's crust is based on the assumption that crustal disturbances in the regions under consideration could be represented by the disturbances along the lines of levels traversing the regions, whence it follows that in the case of lines of levels being situated in the corner of a region, the results obtained above are less reliable. This point will be discussed later.

The frequency distribution of Δ, if it were due to observational errors only and not to crustal disturbance, would be similar to the frequency curves of accidental errors given by Gauss and Poisson. In an actual case, however, as already shown[5)], it evidently deviates from the curve that would be expected from the theory of errors, that is, the values of Δ may be mainly due to actual crustal disturbance.

The same conclusion can be deduced from a comparison of the values of $\overline{|\Delta|}$ and $\sqrt{\overline{\Delta^2}}$. In the case of the values of Δ being due mainly to observational errors, the ratio of $\overline{|\Delta|}$ to $\sqrt{\overline{\Delta^2}}$ may tend to 1.

As an example, the values of $\overline{|\Delta|}$ and $\sqrt{\overline{\Delta^2}}$ have been compared with the data of crustal disturbances in the Tango district, as given in the Table II.

5) N. MIYABE, *Bull. Earthq. Res. Inst.*, **11** (1933), 639.

Table II. (Tango District).

Period	1888~Apr., May 1927	Apr., May~ June, July, 1927	June, July, 1927~ March, Apr., 1928	1928~1929	1929~1930
$\overline{\lvert\Delta\rvert}$	3·84	10·70	4·28	1·78	3·41
$\sqrt{\overline{\Delta^2}}$	7·18	13·21	6·93	2·44	4·62
$\overline{\lvert\Delta\rvert}/\sqrt{\overline{\Delta^2}}$	0.53	0·81	0·70	0.73	0·74

The ratio of $\overline{|\Delta|}/\sqrt{\overline{\Delta^2}}$ during the period of time near that of the occurrence of the earthquake closely approaches 1. On the other hand, as fluctuation Δ depends on the random movements of crustal blocks as referred to below, the above mentioned fact may not lead to the conclusion that the value of $\sqrt{\overline{\Delta^2}}$ during that period is mainly due to observational errors.

Since the earth's crust has been shown to be composed of crustal blocks, the horizontal dimensions of which are some 10 km or less[6], we may say that the fluctuation in Δ is probably due to block movements.

If the fluctuation in Δ is, as just said, the results of block movements, the values of $\sqrt{\overline{\Delta^2}}$ calculated by using the data of changes in the differences of heights of every alternate bench-mark may give results similar to that obtained in the preceding pages.

This was, in fact, proved almost true for the crustal disturbances in the Tango district and on the eastern coast of Idu peninsula, as shown in Table III.

Table III a. (Tango District).

Period	1888~Apr., March, 1927	Apr., May~ June, July, 1927	June, July, 1927~ March, Apr., 1923	1924~1929	1929~1930
$\sqrt{\overline{\Delta^2}}$ (2km)	7·18	13·21	6·03	2·44	4·62
$\sqrt{\overline{\Delta^2}}$ (4km)	{ 6·25 6·42	13·50 12·90	8.23 7·37	2·17 2·54	4·98 5·18

Table III b. (Ito).

Period	1923, 4~ March, 1930	March~ Nov., 1930	1930~1931	1931~1933	1933~1936
$\sqrt{\overline{\Delta^2}}$ (2km)	2·56	30·0	87·3	9·10	1·20
$\sqrt{\overline{\Delta^2}}$ (4km)	{ 3·52 3·43	42·7 38·0	108·9 68·2	12·02 12·57	1·45 1·57

6) C. Tsuboi, *Jap. Journ. Astr. Geophys.*, loc. cit.
N. Miyabe, *Bull. Earthq. Res. Inst.*, loc. cit.

We may therefore conclude that the value of $\sqrt{\overline{\Delta^2}}$ may represent in the main the degree of disterbance of the earth's crust.

As already pointed out, the present discussion is based on the assumption that the values of $\sqrt{\overline{\Delta^2}}$ along the lines of levels represent the degree of disturbance in the regions where the lines of levels under consideration is located.

If, in a region under consideration, the directions and amounts of tilts, and the mean vertical displacements of crustal blocks are at random, and the line of levels in question traverses a number of these crustal blocks, the degree of disturbance is given by

$$\sqrt{\overline{\Delta^2}}=\sqrt{\frac{1}{N}\left\{\sum_n\left[\phi_{0n}\cos\theta_n\right]^2+\sum_n\left[\frac{\delta W_n}{L_n}\right]^2\right\}},$$

neglecting the term due to observational errors, where ϕ_{0n} is the amount of tilt of the n-th block, θ_n is the difference between the azimuth of the trend of the line and that of the tilt of the n-th block, δW_n is the difference in mean vertical displacements of adjacent block, L_n is the horizontal linear dimensions of the crustal blocks, and N is the number of blocks traversed by the line of levels in question.

The summation of terms in the square root of the above expression may be calculated theoretically from the statistical point of view, based on some very probable assumptions.

4. The values of $\sqrt{\overline{\Delta^2}}$ discussed above may, on the other hand, be regarded as some measure of the resultant of the force applied to disturb the earth's crust and the mobility of the earth's crust or crustal blocks.

The fact that the earth's crust is greatly disturbed when a destructive earthquake occurs may mean that the applied force at the time of a destructive earthquake was great enough to cause such an acute and conspicuous disturbance.

Since the earth's crust seems always in motion of some sort, although very slowly, it may be suspected that some force is constantly being applied to it, so that the fact that the value of $\sqrt{\overline{\Delta^2}}$ ceases exponentially after an earthquake may be taken to mean that the mobility of the crustal blocks may have been lessening during that period.

This tendency of the crustal disturbance to cease is also parallel to certain other geophysical phenomena, for instance, changes in the difference in heights of two bench-marks situated on opposite sides of active faults that appeared at the time of destructive shocks, as in the cases of the Tango and the North Idu earthquakes[7].

7) C. TSUBOI, *Jap. Journ. Astr. Geophys., loc. cit.*

5. Summary. In this paper, the writer has calculated the values of $\sqrt{\Delta^2}$ representing the degree of disturbance of the earth's crust, where

$$\sqrt{\Delta^2}=\sqrt{\left[\frac{W_{n+1}-W_n}{\tau}\right]^2},$$

and W_n is the vertical displacements of the n-th bench-mark during the period τ, and discusses its variation with respect to time.

The results of the present study are summarised as follows:

(i) In regions where the earth's crust has once been greatly disturbed by destructive earthquakes, the values of $\sqrt{\Delta^2}$ vary, i.e., decreases exponentially.

(ii) In regions where the earth's crust has not been greatly disturbed by earthquakes, the values of $\sqrt{\Delta^2}$ remain approximately constant.

(iii) This decrease in values of $\sqrt{\Delta^2}$ after an earthquake or volcanic eruption may be due to variations in the mobility of the earth's crust or crustal blocks.

(iv) The foregoing discussion is based on the assumption that the degree of disturbance along a line of levels represents that of the region under consideration; that is, if in said region its horizontal dimensions were properly limited, the crustal disturbance would be uniform, and the translational and tilting movements of crustal blocks in that region will be at random.

The study is being continued, the results of which will be reported in due course.

35. 地殼變動の程度に就て

地震研究所 宮部直巳

地震に伴つて生ずる地盤の隆起，沈降は，比較的急速に行はれ，裂罅等を現出するこさが屢々である．然るに，この地盤の運動は地震後には，漸次鎭まつてゆく傾向にあるやうである．

本文に於いては，この地盤運動の時さ共に變遷する有様を何かの形式で圖示しやうさ試みた．

ある地域を選び，その地域に在る水準線路に沿うての，水準點の變動量の Gradient の rate をさり，次の如き量を以て，その地域のある時期（2回の測量期の間の期間）の變動の程度を示すことにする．即ち $\sqrt{\Delta^2}$ を以てそれを表はすさ

$$\sqrt{\Delta^2}=\sqrt{\frac{1}{N}\sum_{m=1}^{N-1}\left[\frac{W_{m+1}-W_m}{\tau}\right]^2}.$$

玆で N は水準點の數，W_{m+1}，W_m は期間 τ の間に生じた $m+1$ 及び m 番目の水準點の垂直變動量である.

斯樣な量は，單なる觀測誤差の分布から必然的に豫期されるものと考へるより，實際の地殼の運動，或は地塊の無秩序な運動によると考へる方が妥當ではないかと考へられる.

$\sqrt{\Delta^2}$ なる量が時と共に如何に變るかを調べてみると，

(i) 激震によつて甚だしく騷亂を蒙つた地域では，激震後，次第に地殼の動き方が不活潑となつてくる有樣が，大約對數曲線的に示される.

(ii) 測量の施行された期間内に於いて，激震に襲はれた事のない地域では，$\sqrt{\Delta^2}$ の値は概して小さい，のみならず，常に殆ど定數であつて，些少の變化あるのみである.

一面からみると，この $\sqrt{\Delta^2}$ なる量は，地殼內部から加へられる力と，その力によつて動かされる地殼それ自體の動き易さとのある目安となるわけであつて，激震によつて騷き亂された地域は，其故に地震後非常に動き易い狀態にあるのであるけれども，時を經るに從つて，次第に「動き易さ」が減少してくることを示すと共に，激震に襲はれたことのない地域では，さういふ力の變化も，從つて，地殼の動き易さの變化もなかつた，といふ樣な考へ方もこの問題に對する一つの解であらう.

36. *A Discussion on the Results of a Statistical Investigation of Earthquake Phenomena.*

By Seiti YAMAGUTI,

Earthquake Research Institute.

(Read June 16, 1936.—Received June 20, 1936.)

Introduction.

Before giving a summary or entering into the discussion on the results of my statistical investigations of earthquakes, I shall set down a short note on the development of statistical problems in seismology, most of which may be seen in books on seismology.[1]

Statistical investigations on the frequency and periodicity of earthquakes have been made since the early days of seismology by many seismologists in Japan and elsewhere, such as J. Milne, C. G. Knott, A. Schuster, C. Davison, and others abroad, and F. Ômori, K. Honda, T. Terada, A. Imamura, K. Shiratori, Saem. Nakamura, S. Ono, and others in Japan. The same problems have recently been attacked by M. Ishimoto, T. Matuzawa, Ch. Tsuboi, N. Miyabe, and others.

In 1897, Professor Schuster communicated a paper to the Royal Society of London on lunar and solar periodicities of earthquakes, which was to a large extent a critical examination of the results given in Knott's earlier paper on the same subject. It is important to refer to Schuster's critique, which is a criterion of the reality of an apparent periodicity in statistics of the kind we are now dealing with.

The question is purely one of probabilities, and Schuster, by developing a result given by Rayleigh[2] in 1880, arrived at a conclusion which may be stated in the following terms: Suppose that we have n disconnected events occurring at random within a given interval of time, and that we consider the probability of the frequency of these events being expressed harmonically by a Fourier Series in which the periods are submultiples of the interval of time; then it is shown that the probability of any amplitude lying between the limits r and $r+dr$

1) "A Historical Sketch of the Development of Seismology in Japan", by T. Terada and T. Matuzawa, C. G. Knott's "The Physics of Earthquake Phemomena", and C. Davison's "A Manual of Seismology".

2) Lord RAYLEIGH, "On the resultant of a large number of vibrations of the same pitch and of arbitrary phase", *Phil. Mag.*, [v], **10** (1880).

is

$$\frac{1}{2} nrdre^{-\frac{nr^2}{4}};$$

that the expectancy for the value of the amplitude is $\sqrt{(\pi/n)}$; and that the probability, W_p, of the amplitude exceeding any given value p is

$$W_p = e^{-\frac{\pi p^2}{4}}.$$

It is important that the catalogues which are being subjected to analyses should be as complete as possible and should cover a long series of years. Should the total number of earthquakes included be small, analysis of the figures may produce a period that does not really exist. Schuster has shown that, if earthquakes occur at random, harmonic analysis may give an apparent seismic period of amplitude $\sqrt{(\pi/n)}$, where n is the number of earthquakes. But earthquakes occur not at random, but in groups. Thus, in any isolated record, unless the amplitude exceeds this amount or expectancy, the period indicated by the analysis cannot be regarded as established. Should, however, the maximum epochs of a particular period approximately agree for neighbouring regions or for the same region at different intervals of time, existence of the period may be regarded as probable even if the calculated amplitude were to fall below expectancy.

For example, in Fig. 1 are shown curves representing the annual period in three neighbouring countries for the years 1865~1884. The continuous curve is that for Austria, the amplitude being 0·37, the number of earthquakes 461, and the expectancy 0·08. The broken line represents the annual period for Hungary, Croatia, and Transylvania, the amplitude being 0·31, the number of earthquakes 384, and expectancy 0·09. The dotted line shows the same period for Switzerland and the Tyrol, the amplitude being 0·56, the number of earthquakes 524 and the expectancy 0·08. Even had the amplitude in each case fallen below expectancy, the fact that the maximum epochs occur at the end of *January, December, and Jauary* would support the reality of the period.

C. G. Knott summarised his arguments on the cause of earthquakes as follows: "The cause of earthquakes is probably to be referred to the earth's heterogeneity of structure or to the inequality of stress due to irregularities of its surface. Rupturing or yielding is not determined by the amount of stress only; it depends in great measure upon how the stress is applied. For rupture to take place the stress must be different directions; and the difference between the greatest and

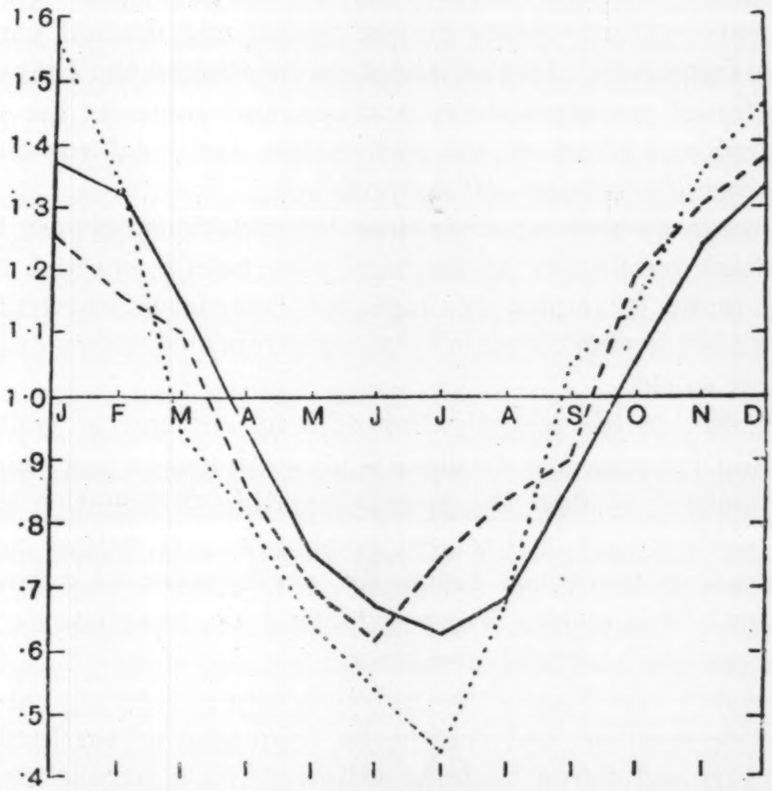

Fig. 1. Annual periodicity of earthquakes in (i) Austria, (ii) Hungary, Croatia and Transylvania, and (iii) Switzerland and the Tyrol.

least stresses is an important datum in estimating the tendency to break. So far as can be judged, the only periodic stresses that of period long enough to tell upon the earth's substance are the fortnightly, monthly, semi-annual, and annual tides, the annual variation of snowfall, and the steady annual and perhaps semi-annual oscillation of barometric pressure over the earth's surface. Inasmuch as the earthquake frequency reaches its maximum in winter wherever there is a marked winter season, we must pass from the annual tidal stress due to the sun as of little account. We seem, however, to find in the accumulations of winter snow, and in the long period oscillations of the atmospheric pressure, two possible determining factors in earthquake frequency".

The views advanced by Dr. Davison differ from this in only one respect. He attaches more importance to the annual changes in pressure over the seismic district itself.

The annual and seasonal variation in the frequency of earthquakes

was for long extensively studied by F. Ômori[3], who discussed the effects of barometric pressure on the annual and diurnal variations in earthquake frequency. In the meantime he studied the changes in sea-level at different mareographical stations and came to the conclusion that the combined effect of the barometric and tidal pressures is an important secondary cause of earthquakes.

Certain sympathetic or contagious interrelations between the activities of distant earthquake zones have also been suspected by Ômori, who cited many examples of Japanese destructive earthquakes that occurred within a short time of the occurrence of severe ones in other parts of the world.

K. Honda[4], in his investigation of level changes in wells, noticed some relation between the frequency of earthquakes and tidal phases.

A. Imamura[5] studied the synodic-monthly distribution of the frequency of earthquakes. The results obtained are rather complicated. Four maxima or two were found for earthquakes of submarine and inland origins, the results being explained by interference of effects due to barometric and tidal pressures.

T. Terada[6] investigated the relation between the annual variations in barometric gradient and that in the frequency of earthqukes in different regions and found that the latter shows a parallelism with the component of the gradient in a certain direction proper to each region. He[7] also drew attention to the fact that an apparent or "phantom" periodicity may be brought about by a quite arbitrary sequence of events.

Saem. Nakamura[8] studied the frequencies of days with 0, 1, 2∼9 earthquakes recorded instrumentally, with reference to the data observed in Tokyo during four years. On comparing the results with theoretical expectations corresponding to random distribution, it was found that the number of days with no shock was less than the theoretical value, while those with one or two shocks exceeded expectation.

Rebeur Paschwitz's horizontal pendulum for registering the tilting of the crust relative to the direction of gravity having been installed in the Kamigamo Observatory, observations were made by Shida[9] and

3) F. Ômori, *Report I. E. I. C.*, **2** (1894); **25** (1899); **30** (1900); **32** (1900); **54** (1906); **57** (1906). *Publ. I. E. I. C.*, **8** (1902). *Bull. I. E. I. C.*, **2** (1902), No. 1. *Jour. Coll. Sci., Tokyo*, **11** (1899).

4) K. Honda, *Publ. I. E. I.C.*, **18** (1904).

5) A. Imamura, *Report I. E. I. C.*, **18** (1904).

6) T. Terada, *Jour. Met. Soc.*, **28** (1909), 1.

7) T. Terada, *Proc. Tokyo Physico-Math. Soc.*, **8** (1916),492.

8) Saem. Nakamura, *Jour. Met. Soc.*, **39** (1920).

9) Prof. Shida, *Memoirs Coll. Sci., Kyôto*, **4** (1912), 1.

his assistants since Feb. 1910. In spite of the considerable distance of the station from the sea, the tilting due to the tidal load was remarkable compared with the component due to variation in the level directly derivable from the tide-generating potential, so that the difficulties that had to be overcome in analysing the different components were considerable. To give an example, he had to take account of the actual tides instead of assuming simple ideal tides, as was done in his previous work. His results thus obtained are interesting from the seismological as well as from the geophysical point of view, in that they show a reliable measure of the actual deformation of the crust due to the water load applied along the coast.

On the occasion of the recent Tazima Earthquake, K Suyehiro noticed the remarkable fact that most of the strong earthquakes in the Japan Sea coast of the San'indô occur within a few years after destructive shocks have occurred in the Pacific zone.

As a secondary cause of earthquakes, the effects of surface loading over a circular area were considered by H. Nagaoka[10]. Even a very remote centre of atmospheric depression can affect the equilibrium of the earth's crust and give rise to pulsatory motions. Later, he treated an allied problem in connection with the effect of a barometric gradient on earthquake frequency, and showed that rupture of the crust is to be expected near the maximum of the gradient. As to pulsatory motions, he discussed the stationary vibration of one end of a semi-infinite solid with two parallel edges.

A similar problem of surface loading was treated later by K. Terazawa[11], when he discussed the periodic disturbances of level due to the load of neighbouring oceanic tides.

M. Ishimoto[12] after a study of the periodicity of earthquake occurrences stated that could be explained as arbitrary events.

In presenting here a resume of my papers hitherto published, based on investigations extending over a period of years, I will refer to investigations made and theories advanced by a number of seismologists, to which I will add new opinions of my own.

Resume and Discussions.

1. Relation between Tidal Phases and Earthquakes.

In my first paper[13], the reduced frequency of after-shocks, was

10) H. Nagaoka, *Proc. Tokyo Physico-Math. Soc.*, **3** (1906), **6** (1912).
11) K. Terazawa, *Jour. Coll. Sci., Tokyo*, **37** (1916), Art. 7.
12) M. Ishimoto, A report read before the P. M. C. of Japan; not yet published.
13) S. Yamaguti, *Bull. Earthq. Res. Inst.*, **8** (1930), 393.

calculated for comparing various curves corresponding to different epochs and to different localities, but this time, the frequency alone for the total epochs of each regions was taken and plotted as ordinate against the tidal phase.

The relation between the frequency of the after-shocks of the Great Kwantô Earthquake and the tidal phases at Yokosuka, are shown in Fig. 2. For convenience, the region including the origin of the after-shocks is divided as follows:

A. Area including Sagami Bay and the Province of Sagami as the main part.

B. Bôsô peninsula and near its S. E. coast.

C. Tokyo and its environs.

The total number of after-shocks, N=479.

The frequency in occurrence of after-shocks usually shows a maximum, slightly before low water, suggesting a secondary maximum frequency also about one and a half hours before high water.

The fact that the curves for different independent epochs and for different localities usually show some characters common to the two curves as revealed in the mean curve of long duration, or in the sum curve for these localities, may be regarded as proof of the existence of a certain physical relation between the frequency in occurrence of shocks and the tidal phase.

The frequency in the after-shocks of the Tango Earthquake, N=1464, March 7, 1927~July 16, 1928, shows a conspicuous maximum near low water and also a secondary maximum about one and a half hours after high water at Wazima, as shown in Fig. 3. These relations, referred to the tides at Kôbe, are not so conspicuous as those referred to the tides at Wazima; They are also shown in the case of after-shocks of the Tazima Earthquake, N=358, May 23~June 17, 1925, referred to the tides at Wazima and at Kôbe, as shown in Fig. 5. The existence of the difference between the effects of tides at Wazima and Kôbe on the occurrence of after-shocks of the Tango and Tazima Earthquakes may be regarded as showing the real physical relations between the frequency of shocks and the tidal phase, and not an arbitrary occurrence of the relation.

The fact that the earthquake frequency and tide curves for the after-shocks of these four great earthquakes, namely, the Kwantô, Tango, Tazima, and Ômati, show unmistakable resemblance to one another, especially with regard to the maximum frequency at low tide, may be considered as pointing to a real physical relationship between the two phenomena of earthqnakes and tides.

Prof. T. Matuzawa's investigation[14] on the probability of the existence of a relation between earthquake frequency and tidal phase, has given 0·214, as its value, assuming that the relation might hold quite accidentally.

The shocks on the northern side of the Yamada Fault in Tango have their maximum of frequency about low water and the secondary maximum about high water. The shocks in the sea bed near Tango show an entirely opposite course compared with the above as shown in Fig. 4—a result that may suggest some essential differences in the mechanism of the earthquakes for the two origins, i. e., in the sea bed and on the land north of the Yamada Fault.

The fact that amplitudes of frequency curves for the after-shocks of four different regions referred to the tidal phases, are as a rule, greater than those referred to the solar time intervals, as shown in Figs. 12 and 13 in the earlier paper above cited, shows how conspicuous is the tidal effect on the occurrence of shocks compared with the other elements that are supposed to induce shocks.

The physical explanation of these results may be as follows:

About middle water, the earth's crust, acted upon by many forces, is assumed to be in equiliblium, which may be broken down at low water by decrease in the tidal load (an increase at high water), with earthquakes as the result.

The result of investigations on tiltings of the earth's crust made by Prof. Ishimoto, with his ingenius instrument at Miyatu and Kawabe[15] immediately after the Great Tango Earthquake, and that made by Prof. Ishimoto and Mr. R. Takahasi[16], at Itô in Idu, and also that made by Mr. Takahasi[17] at Aburatubo in Sagami, may support the above explanation regarding the effect of tides on the occurrence of earthquakes.

Only the amplitudes of frequency curves for the Ômati Earthquake, N=433, Nov. 11, 1918～Feb. 28, 1919, referred to the tide at Wazima and to solar time, are almost alike. This result appears perfectly reasonable if one takes into consideration the fact that Ômati is situated much farther from the sea than the other three districts, and that the effects of some other elements on the occurrence of shocks, such as daily variations in atmospheric pressure, may operate.

---

14) T. Matuzawa, *Bull. Earthq. Res. Inst.*, **14** (1936), 38.
15) M. Ishimoto, *Bull. Earthq. Res. Inst.*, **4** (1928), 203.
16) M. Ishimoto and R. Takahasi, *Bull. Earthq. Res. Inst.*, **8** (1930), 427.
17) R. Takahasi, *Bull. Earthq. Res. Inst.*, **7** (1929), 95.

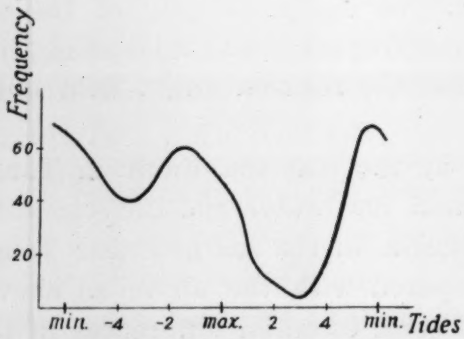

Fig. 2. Frequency curve of after-shocks of the Great Kwantô Earthquake, referred to tides at Yokosuka. Sept. 2~Oct. 1. (A+B+D)

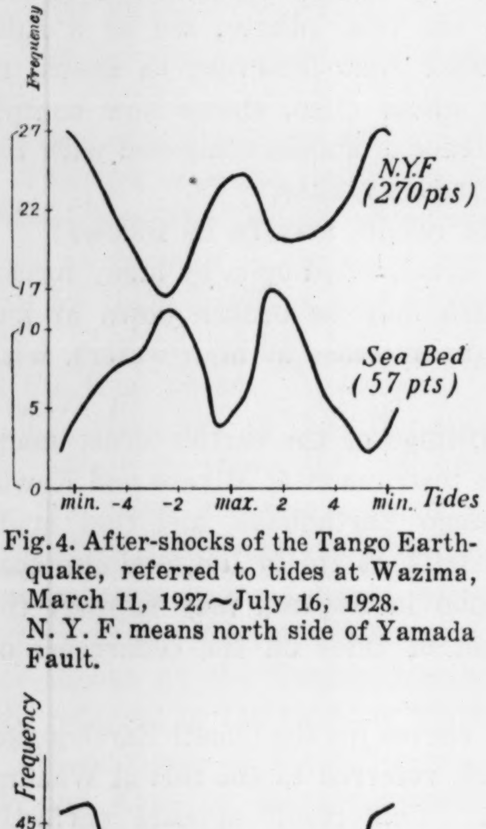

Fig. 4. After-shocks of the Tango Earthquake, referred to tides at Wazima, March 11, 1927~July 16, 1928. N. Y. F. means north side of Yamada Fault.

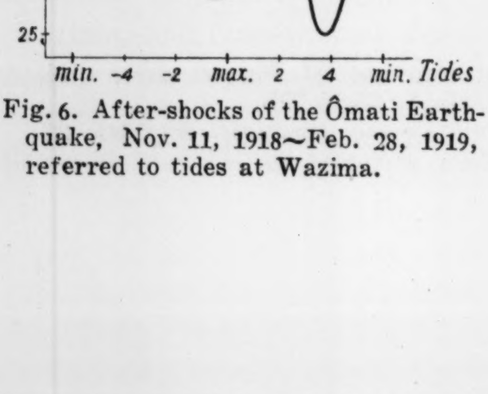

Fig. 6. After-shocks of the Ômati Earthquake, Nov. 11, 1918~Feb. 28, 1919, referred to tides at Wazima.

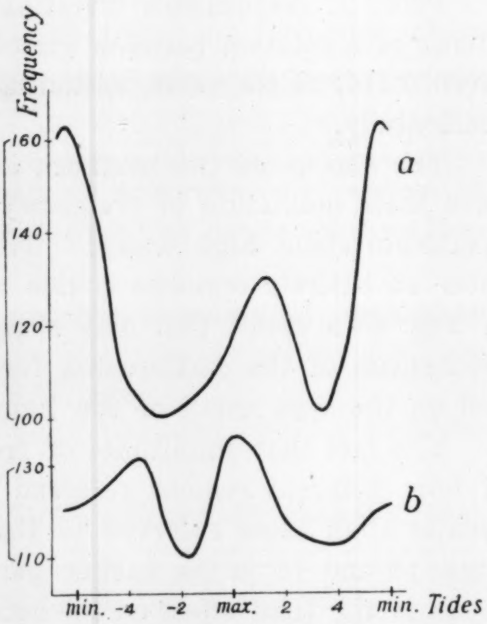

Fig. 3. After-shocks of the Tango Earthquake,
(*a*) referred to tides at Wazima,
(*b*) referred to tides at Kôbe.
March 7, 1927~July 16, 1928.

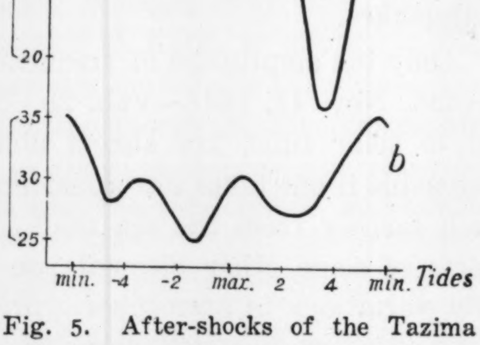

Fig. 5. After-shocks of the Tazima Earthquake, May 23~June 17, 1925,
(*a*) referred to tides at Wazima,
(*b*) referred to tides at Kôbe.

2. On Time and Space Distribution of Earthquakes.

a) Fissure line.

The epicentres of earthquakes that occurred in the Kwantô Districts were plotted on a map for each month and joined by a straight line successively in the order of time. The number, n, of the directions of these straight lines falling in the direction within each sector of an azimuth angle of 15°, which is formed by dividing all directions into 24 parts, were counted and plotted in vector diagrams against the azimuth angle, N-direction being taken as zero, as shown in Fig. 1, in my first paper[18] "On Time aud Space Distribution of Earthquakes". The vector diagram for n's were transformed into the corresponding *xy-diagram* and arranged as in Fig. 4, *a*, taking the directions of the monthly mean pressure gradients at Iwaki as the respective origins of directions, an error of $\pm 7°5$ having been allowed for. Similar *xy-diagrams* were also constructed for deviations of n from the yearly mean. The results are shown in Fig. 4, *c*, in the same paper, in which the dotted lines on the left-hand quarter are the means of the four quadrants. From this mean curve distinct maxima are seen to be somewhere near 0°, 45°, and 90°. The maximum at 45° may correspond to the direction of maximum shearing stress in the earth's crust due to the pressure gradient, while the maxima at 0° and 90° may mean that a tangential or normal stress on a preexisting fissure might induce a succession of earthquakes along that fissure line.

b) Preferential ratios.

Before inquiring into the physical meaning of sequnces of earthquakes in different regions, it is neccessary to make a calculation of the statistical probability of sequence for the case in which the earthquakes occur quite at random. The following calculation was made for this purpose:

Let N_k, N_l, ...be the number of earthquakes that occurred in region, k, l,... respectively during the epoch taken. Then the probability P_{kl} that the earthquakes will occur in region l, next to k may be expressed by $P_{kl}=\dfrac{N_k N_l}{\sum\sum N_k N_l}$, while the expected number N' to occur at l, next to k, is given by $N'=P_{kl}\sum N$. The value of the ratio r of the actual number of occurrences N_0 to the calculated number N', that is $r=N_0/N'$, were calculated.

In the paper above cited, the severe earthquakes, 420 in number,

18) S. YAMAGUTI, *Bull. Earthq. Res. Inst.*, **11** (1933), 46.

that convulsed different parts cf the world during the period of 31 years from 1900 to 1931 were taken from Rikwa-Nenpyô and geographically classified into 8 groups according to regions of occurrence, and the values of the preferential ratios r calculated as shown in Table IV, *a*, and in Fig. 8, *a*, *b*.

Such preferential ratios as have values greater than 1·43, may be regarded, at least, as suggesting that in such particular sequences of regions an earthquake is liable to be followed by another. Prof. Matuzawa's criterion for the accidental and the real occurrence of sequences of earthquakes seems to be taken as $1 \pm 0{\cdot}241$, approximately, as above explained.

In other earthquakes, the sequence of regions, Japan → South America, and South America → Japan, always give preferential ratios greater than 1·43, which result may be regarded as supporting the statement that an earthquake in Japan is liable to be followed by another in the antipodes. The same result may also be obtained by the other method of investigation described in a paper[19], "Statistical Relation between the Frequencies of Earthquakes in Japan and Other Parts of the World".

We also calculated the preferential ratios given quite at random by throwing a dice 400 times in succession. The result shows that the range of fluctuation in the values of preferential ratios lies between 0·68 and 1·43. The pairs of regions therefore that have values of preferential ratios decidedly greater than 1·5 and less than 0·6, may at least be suspected to have some particular physical relation to sequences of earthquakes.

Moreover, no pair of regions for which equally large ratios are obtained for the reversed sequences of earthquakes, such as between Japan and South America, could be found in this artificial case.

c) Periodicity of Earthquakes.

The time intervals from an occurrence of a great earthquakes to the next one in the world, $N=420$, were obtained, and the frequencies of these intervals for every 10 days were counted and plotted as ordinates, the days of the intervals being taken as abscissa. The general trend of the curve shows the random occurrence of the earthquakes. We calculated the frequency f for purely random occurrences, assuming $f=ae^{-bt}$, and obtained the deviations of the actual frequencies from this theoretical value of f, which are shown in Fig. 9 in my first paper above cited. In order to satisfy ourselves that the periodicity of the

19) *Bull. Earthq. Res. Inst.*, **10** (1932), 36.

deviation curve is not due to the apparent one proper to any accidental phenomena, we also tried to take the half intervals or else the overlapping intervals of days for comparison. The features of these curves remained essentially the same.

For the particular pairs of earthquakes corresponding to $r > 1{\cdot}25$, $N = 118$, and $r > 1{\cdot}6$, $N = 78$, which are results from the previous investigation with respect to the sequence of earthquakes, the same methods were used.

The frequency curves of time intervals of the great earthquakes of the world seem to show a period of 27·5 days. The same period is obtained whether we choose 5 days or 10 days for the division of the time axis of the curve. This period is also obtained in the case of "deep" Japanese earthquakes as shown in Fig. 7 in the paper[20], "Distribution of Earthquakes in Japan". Moreover, periods that are multiples of 27·5 days, namely periods of about 55 and 105 days, are also observed from those curves both for the worlds great earthquakes and for the "deep" Japanese earthquakes.

The period of 27·5 days seems to correspond to the 27·3 days period of rotation of the sun relative to the earth.

The reason for the existence of this period is not yet clear, but according to investigations on the sun made by the Wilson Astronomical Ovservatory as well as by the Greenwich Observatory, it seems that the great eruptions of hydrogen gas from the sun's surface occur with this period, so that it may be the cause of variations in a certain solar force or forces acting on the earth, but of which nothing is yet known to us, the result of which may be regarded as inducing the world's great earthquakes and the "deep" earthquakes of Japan.

3. Relation between Cyclones or Atmospheric Pressure Distribution and Earthquakes.

Some preliminary investigations on the relation between cyclones and earthquakes were made by the writer. First, he counted the number J representing shifts of epicentres in E→W or W→E direction in almost the same latitude in the Tôhoku region and Hokkaidô for every month during a period of 7 years, from June, 1924 to May, 1931, and compared it with the corresponding number of tracks of cyclones that traversed these regions. Taking, instead of J, the ratio r of J to the whole number, *an xy-diagram* was drawn as shown in Fig. 7, *c*, in his paper[21], "On Time and Space Distribution of Earth-

20) *Bull. Earthq. Res. Inst.*, **11** (1933), 500.
21) *loc. cit.*, 18).

quakes". In this diagram the curved line was constructed by joining the mean point of each y corresponding to each x, and an ellipse drawn from sight so as to contain all the points properly. I also calculated the correlation coefficient of r with respect to the number of tracks of cyclones, applying the ordinary formula, and obtained 0·47 as the value.

The result may suggest the possible existence of a close relation between earthquakes and cyclones.

Second, I counted the number n for three successive months, (a) for the "deep" earthquakes during 6 and a half years from Jan., 1926 to June, 1932, (b) for the "conspicuous and rather conspicuous" earthquakes that occurred in the region from Kyûsyû to the sea off Sanriku, (d) for the "felt" earthquakes that occurred in the region from Wakayama to Idu. At the same time I counted the number of tracks of cyclones that passed across the "deep" earthquake zone over a length of ± 1000 km, measured from the origin near the mouth of the Bay of Ise along a line perpendicular to the Japanese arc for 3 successive months.

Looking at these curves of n plotted against the time axis, there seem to exist certain fluctuations of long period superposed upon an annual period. Thus, I assumed that the curve for earthquakes, E consists of two parts, the one of longer period E_l and the other of annual periods E_a and $E=E_l+E_a$. Similarly, for the cyclones, I denoted the frequencies of cyclones by $C=C_l+C_a$.

In the paper[22], "Distribution of Earthquakes in Japan", the values of E_a and C_a were calculated with certain assumption and C_aE_a-*diagrams* drawn as shown in Fig. 6.

The results show that "deep" earthquakes as well as "conspicuous and rather conspicuous" earthquakes, show to some extent negative correlations with respect to cyclones, while on the contrary, "felt" earthquakes show positive correlation.

As to the physical meaning of these results, I may suggest the following:–

a) The excessive stress stored in the relatively shallow parts of the earth's crust may be released by frequent occurrences of earthquakes of the magnitude of "felt" earthquakes, which are affected directly by the cyclones that frequent the region.

b) When the excessive stress released as the result of "felt" earthquakes is comparatively small in amount, then earthquakes of the magnitudes of "conspicuous and rather conspicuous" and "deep"

22) *loc. cit.*, 19).

earthquakes will occur.

Since then I have made further investigations on the relation between cyclone and earthquake.

The distances to the epicentres of "deep" earthquakes from the nearest cyclonic centres at the time of occurrences of the earthquakes were estimated and counts made of the frequencies coming within every 200 kilometres.

To eliminate the areal effect as well as the characteristic geographical distributions of cyclonic tracks regardless of earthquakes, the frequencies of the total cyclones, 3500 in number, during a period of exactly 8 years from 1926 to 1933, falling on the same zonal areas between concentric circles with "centre of gravity" of the "deep" earthquakes near the coast of Siduoka as origin, were counted. The value of the ratios r, of the actual frequency f_a to the total frequnency f_t, that is $r_1=f_a/f_t$, were calculated and plotted as ordinates, the distances in kilometres being taken as abscissa as shown in Fig. 1 (*a*), in the paper[23]—"Relation between Cyclone and Earthquake".

From this curve it will be seen at a glance that very near the cyclonic centres, that is, within 200 kilometers from them, "deep" earthquakes very rarely occur, while a marked maximum of frequency seems to exist about 900 kilometers distant from the cyclonic centres.

This latter result seems to suggest that the region of maximum stress difference in the earth's crust due to cyclones occurs at points about 900 kilometers distant from the cyclonic centre.

To test, on the other hand, if the results have any real physical meaning or not with respect to the relation between "deep" earthquakes and cyclones, an artificial case was investigated, in which the positions of epicentres and cyclonic centres were obtained at random by drawing 270 lots. With the artificial epicentres, not corresponding to the cyclones actually, a similar frequency in distances f_b was obtained and the value of the ratio $r_2=f_a/f_b$ calculated and drawn as shown in Fig. 1, (*b*).

The latter curve for r_2 showed a character similar to that of the former r_1. These results therefore seem to suggest that there is some real physical meaning with respect to the relation between "deep" earthquakes and cyclones.

Next, a quite similar method was used for "conspicuous and rather conspicuous" earthquakes. In this case, however, the epicentres are distributed over a wide area along the Japanese Islands, compared with the former case with a limited area, the so-called "deep" earthquake zones. Consequently, the value of the ratio $r_3=f'_a/f'_t$, shows

23) S. YAMAGUTI, *Bull. Earthq. Res. Inst.*, **12** (1934), 742.

features of purely accidental occurrence as shown in Fig. 2, (*a*), the centre of gravity of the epicentres being taken at a point in the offing near Iwaki. Thus, using the function $f_x=2(n+1-x)$, already given in another paper[24], the percentage value of $r_4=f_x/\sum f_x$ was calculated and drawn as shown in Fig. 2, (*a*). The deviation of r_3 from this value of r_4, *i.e.*, $\Delta r=r_3-r_4$, was obtained and shown in Fig. 2, (*b*). On the other hand the value of the ratio $r_5=f'_a/f'_b$ was calculated and plotted as shown in Fig. 2, (*c*).

The two curves in Fig. 2, (*b*) and (*c*) show similar characters as they do in the case of "deep" earthquakes, except that a rather marked maximum of frequency occurs at a distance of about 500 kilometres in this case, instead of 900 kilometres in the preceding one.

The same results may also be seen from the maps showing the distributions of values of the ratios $r_{10}=N_a/N_t$ and $r_{11}=N'_a/N_t$ as shown in Fig. 5 and 6, in which N_a is the number of cyclones at the time of occurrence of the earthquakes during a period of 8 years from 1926 to 1933 and which fall in a mesh formed by dividing the wide area, each mesh differing from one another by 5° of latitude and 5° of longitude, N_t being its corresponding value for total cyclones at noon in latitude 135°E for every day during the same period of 8 years.

To see under what type of configuration of cyclones and anti-cyclones surrounding the epicentre, earthquakes are most liable to occur, the following procedure was adopted: All possible distributions of low and high pressure regions were classified into five types as shown in Fig. 11, and the actual number of occurrences of earthquakes M_a belonging each type was counted from weather charts for the days on which the earthquakes actually occurred. The number of arbitrary earthquakes M_b corresponding to M_a was similarly counted from weather charts for days on which no earthquakes occurred, the positions of the artificial epicentres being substituted for the actual ones by drawing a lot successively.

The ratios $r_{14}=M_a/M_b$ and $r_{15}=M'_a/M'_b$ were evaluated respectively for "deep" and "conspicuous and rather conspicuous" earthquakes as shown in the annexed table in the same paper, page 751.

From this table we may say that "deep" as well as "conspicuous and rather conspicuous" earthquakes occur most frequently in such arrangements of low and high pressures as represented by II-type, and further that they are also liable to occur in such a distribution as I-type.

The foregoing results may be regarded as free from accidental occurrences of earthquakes in connexion with the cyclones owing to the

24) S. YAMAGUTI, *Bull. Earthq. Res. Inst.*, **12** (1934), 214.

particular method of investigation as already explained.

As to the physical meaning of these results, we may say that earthquakes are liable to occur when the stress difference in the earth's crust due to cyclones or barometric pressure difference is maximum.

It might also be supposed that the equilibrium of forces acting on the earth's crust may break down with tidal load as the result of abnormal rise of sea level owing to waves probably generated in the region near the cyclonic centre, as already mentioned in another paper[25], "On the Effect of Cyclone upon Sea Level".

In conclusion, I wish to express my heartiest thanks to Prof. M. Ishimoto for his guidance in the course of these studies and his many useful suggestions.

---

36. 地震現象の統計的研究の成果に關する檢討

地震研究所 山口生知

地震回數の統計的研究に對する檢討が最近喧しく叫ばれる樣になつた．卽ち石本博士の「地震の偶發性」と題する研究や，松澤博士の「大地震前後の三陸沖の地震活動及び一般に大地震の餘震に就いて」と題する論文等が發表され，統計的研究に對する注意を喚起された．

著者は昭和5年以來爲したる統計的研究の成果に關し，再檢討を試み且つ出來るだけの註解を附け加へ度いと思ふ．

其の前に A. Schuster の地震の週期性に關する論文の結果の一部分を，紹介致すことゝする．

卽ち地震回數の最大なる時期が，數箇の場所に就いて略一致するか又は同一場所に於いても異つた樣々の期間に就いて，類似の形勢を示すならば假令曲線の振幅の計算値が豫想値よりも小であつても，週期が存在すると云ふことを證明して居る．其の一例として第1圖に示される通り1865年より1884年に至る約20年間にオーストリヤに起つた461の地震，ハンガリー，クロアシア及びトランシルバニアに起つた384の地震及びスキス，チロル地方に起つた524の地震を採つた場合の各月の頻度曲線は，よく，一月頃に於いて，3曲線共最大を示して居ることは週期の實在することを證明して居る．

1. 地震と潮汐との關係に就いて著者は，關東，丹後，但馬及び大町の4箇所の大地震の餘震を採り，横須賀又は輪島の潮汐との關係を調べて見たのであるが，4 箇所共低潮時附近に於いて地震回數の最大を與へて居ること及び樣々の期間に於いても略同樣の結果を與へて居ることは確かに物理的關係の實在を示すものと思はれる．

 松澤博士が伊豆地震の餘震に就いて研究された結果に依ると地震と潮汐との關係が，偶然起り得るものとしても 0·214 位の確率の値が出ると云ふことである．

 私の場合に於ける一時間の內の地震の平均數を1とし 1+0·214 と 1−0·214 との間の範圍を考へて見ると低潮時附近の地震の數は，前述の4地方共此の範圍より大なることを示して居る．

---

25) S. YAMAGUTI, *Bull. Earthq. Res. Inst.*, **7** (1929), 115.

又太陽時に對する地震回數の分布を見るさ大町地震を除いては，いづれも皆潮位に對するものよりも，其の振幅が小であるさ云ふこさは，卽ち地震發生に對して潮汐の影響が如何に明瞭であるかを示すものさ思はれる.

大町は他の3地方に比較して，海より遠方にある爲め大氣壓の日變化の影響らしきものが現はれ太陽時及び潮位に對する振幅が略同程度さなつて居るのは當然である.

潮汐の影響の物理的意義を考へて見るさ，地殼に或る荷重を及ぼし中等水位附近に於いて，地殼內の應力が釣合にあるものさすれば，低潮時の時は荷重を減するこさゝなるから，其の時に地殼の破壞が起り，從つて地震が發生するものさ考へられる.

之は石本博士の研究にかゝる「丹後大地震後の宮津町及び河邊村に於ける地表傾斜變化觀測」の結果より見るも，亦石本博士，高橋學士共著「伊東地震さ地表傾斜變化の觀測」並びに高橋學士の「油壺灣內の海水の副振動に因る地殼の傾斜運動」等の研究の結果に徵するも，上述の說明を支持するものさ考へられる.

2. 震源移動の問題に關して，實際に移動した數 N_0 さ理論上豫期される數 N' さの比，$r=N_0/N'$ の値を計算したのであるが，r の値が 1·45 以上及び 0·6 以下のものは眞の物理的意義を有するものさ考へるこさが出來る樣に思はれる.

地震の週期性を研究する目的を以つて世界地震の內 1900 年より 1931 年に至る 31 年間に起つた 420 ものに就いて，時間の間隔が，次々の10日每の內に這入る樣な地震の回數曲線を見るさ一般の形勢は偶發性を示して居る. 故に今之を $f=ae^{-bt}$ で表はされるものさして計算し之を實際に起る回數より差引いて其の殘りのものを畫いて見るさ，27·5 日，55 日及び 105 日さ云ふ週期が見られる. 而して全體の地震に就いても，亦此の內特別なもの，卽ち震源が引續いて起り易いもの，$N=118$, $r>1·25$ に就いても又更に，$N=78$, $r>1·6$ のものに就いても上述の週期が見られるさ云ふこさは決して偶然の出來事では無いさ信ずる.

日本に於ける深層地震に就いても之さ全く同樣の週期を有する事は誠に面白いこさゝ思ふ. 此の週期は地球に對する太陽の自轉の週期 27·3 日及び其の倍數に相當する. 米國のウエルスン天文臺及び英國のグリニッチ天文臺の調査に因るさ，この週期を以つて太陽面に水素瓦斯の大爆發が起つて居るこさが明らかにされて居る. 之に關聯して太陽より地球に及ぼす何等かの力に，かゝる週期的變化を與ふるのではなからうかさ云ふ疑問を起さしめるのである.

3. 低氣壓或は氣壓分布さ地震さの關係に就いて豫備的研究を試みた結果，之等の間には，密接な關係のあるこさが分つて居る. 而して有感地震さ低氣壓さは正の相關係數を有し，深層地震或は顯著及稍顯著地震さ低氣壓さの間には負の相關係數を有する.

其の後更に詳細なる研究を試みた結果は，深層地震に就いては，低氣壓の中心より900粁の地點に於いて又顯著及稍顯著地震に就いては500粁位の距離の場所に於いて，地震が最も起り易いこさを示して居る. 之は偶發性を考慮に入れてそれを消去して居るから眞の物理的關係を有するものさ考へられる.

以上の結果に就いては，低氣壓に因り，又一般には氣壓分布に因つて，地殼の中に生ずる應力の差異が最大になる樣な時に地震が發生し易いものさ推定される. 或は又低氣壓が現はれるさきは，低氣壓の中心附近に於いて發生する波浪に因つて近海面が異常上昇を來す爲めに地殼に餘分の荷重を與へてその結果地殼の釣合を破るやうになるのではなからうかさ想像される

37. *An Experimental Method to solve the Equation of Motion of the Seismograph**.

By Takato FUCHIDA.

(Read Mach 17, 1936.—Received June 20, 1936.)

1. Introduction.

It goes without saying that it is one of the most important problems in the earthquake research to solve the equation of motion of the seismograph,

$$\ddot{x}+2\varepsilon\dot{x}+n^2x=f''(t). \tag{1}$$

The method of numerical calculation which has been adopted for the use of solving the above equation cannot be employed in the case in which the form of $f''(t)$ is very complicated. The writer therefore tried to solve the equation experimentally. By this method, the solution of (1) can easily be obtained in the cases when the form of $f''(t)$ is complex as well as simple. By this experimental method, however, the solution can be obtained only for the initial conditions,

$$x=0,\ \dot{x}=0 \text{ at } t=0. \tag{2}$$

2. Principle.

The sensitive galvanometer of moving coil type is used for the purpose of measuring the weak direct current or the ballistic current. The transient motion in the oscillation of the suspension of the galvanometer was used in this experiment.

The equation of motion of the galvanometer is

$$K\ddot{\theta}+a\dot{\theta}+c\theta=Gi, \tag{3}$$

in which K, a, c and G are respectively the moment of inertia of the moving coil, the coefficient of damping of air, the restitutive force of a string and the torque by unit current. Therefore in case of the connection as shown in Fig. 1, the equation of motion is expressed in a form

$$K\ddot{\theta}+\left(a+\frac{G^2}{S}\right)\dot{\theta}+c\theta=GI'. \tag{4}$$

* Communicated by N. Miyabe.

Taking into account the next relation,

$$I' = I\frac{R'}{R+R'}$$

and substituting

$$2\varepsilon = \frac{\left(a+\frac{G^2}{S}\right)}{K}, \qquad n^2 = \frac{c}{K}, \qquad A = \frac{G}{K}\frac{R'}{R+R'},$$

the equation (4) becomes

$$\ddot{\theta} + 2\varepsilon\dot{\theta} + n^2\theta = AI.^{1)} \qquad (5)$$

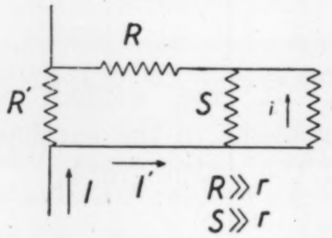

Fig. 1.

Although the last equation is of the same type as the equation (1), the right hand side in it corresponding to $f''(t)$ in (1) is proportional to the current.

Now, as (5) is the equation of motion of the galvanometer, it is possible to know θ experimentally which represents the variation in I. Hence when I is proportional to $f'(t)$, the record of θ shows the quantity proportional to x in (1). But as the moving coil of the galvanometer is at rest at the zero position till the current I begins to flow, the initial conditions must be

$$\theta = 0 \text{ and } \dot{\theta} = 0 \text{ at } t = 0$$

without regard to the form of I. The solution thus obtained cannot always stand for the solution of the equation (1) of motion of the seismograph, for the initial conditions by above mentioned solution cannot always be satisfied in the actual case of the motion of the seimograph when it is subjected to earthquake shocks.

3. Experimental Arrangement.

The experimental arrangements are shown in Fig. 2. A photoelectric cell was used to supply the current I proportional to $f''(t)$ in (1). In Fig. 2 P is a glass plate in which is printed the curve of $f''(t)$ just like a talky film of variable area system. A light source L_1 has a linear filament the image of which is adjusted to focus to P. The flux of rays passing through P is condensed by a lense and projected on the photoelectric cell P. T.. P is driven by a small series-motor the speed of which can be changed at will and a drum

1) When the self-inductance L of the circuit is an important factor, the term $\frac{LK}{R}\dddot{\theta}$ must be added, though it is neglected in the present discussion because of its smallness in comparison with the other terms.

of a camera is also rotated by the same motor therefore the driving speed of the film is proportional to that of P. In the writer's experiment, it was felt most convenient to make the speed of the film proportional to that of P without making it constant, so that the speed of P can be changed within a range, the ratio of the maximum to the minimum speed being about one hundred. Time marks were recorded on the film by means of a lamp L_3 to check the time axis of records.

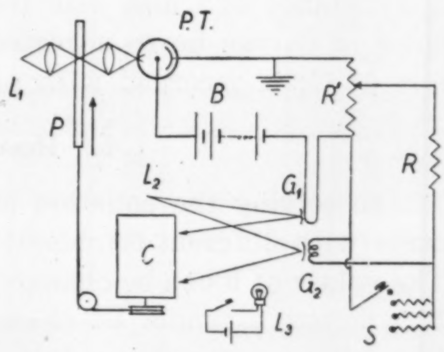

Fig. 2.

The characteristic curve of the photoelectric cell P. T. (P. T.—50—G) was made almost linear by taking care of connections, in order to avoid the effects due to sparks in the motor and other disturbances that may happen in weak current experiments.

To measure the current I, a torsion-string galvanometer G_1 was used, the instrumetal constants of which being;

Period	1/50 sec.
Resistance of string	10 Ω.
Current sensitivity	$4 \cdot 10^{-7}$ Amp.

The proper period of the torsional oscillation of this galvanometer suspension is 1/50 sec, very short compared with the variation of $f''(t)$ in the present experiment, so that its deflection is approximately proportional to $f''(t)$.

The galvanometer G_2 is of a type of moving coil which plays the most important rôle in this experiment, its constants being as follows:

Period	7 sec.
Resistance of coil	420 Ω.
Current sensitivity	$7 \cdot 10^{-10}$ Amp.
Resistance for critical damping	14000 Ω.

The shunt resistance S was placed to change the damping ratio in the galvanometer G_2.

Experiments are made for four cases with different shunt resistances: e. i.,

$S=\infty$ . . . . $b=0{\cdot}05$
$S=36000\ \Omega$ . . . . $b=0{\cdot}4$
$S=20000\ \Omega$ . . . . $b=0{\cdot}7$
$S=14000\ \Omega$ . . . . $b=1{\cdot}0$
$(b=\varepsilon/n)$

As shown in Fig. 1, the larger the resistance R compared with

that of the galvanometer G_2, the simpler the relations between I and I'. A resistance of 1 meg was therefore used for R. The current which flows in G_2 can be so adjusted by a potentiometer R' that the deflection of G_2 is recorded with proper amplitudes.

4. Results of Experiments.

In solving the equation of motion of the seismograph (1), various cases with different combinations of n, b and $f''(t)$ must be dealt with. The values of b can be changed at will by changing the shunt resistance S, whereas n cannot be changed, as it is an instrumental constant of the galvanometer G_2 used in this experiment. The same results as if n is changed, however, can be obtained by changing the driving speed of P. When P is driven at the speed N times as large, the equation of motion (1) becomes

$$\ddot{x}+2\varepsilon\dot{x}+n^2x+f''(Nt). \tag{6}$$

Putting $Nt=\tau$, (6) becomes

$$\frac{d^2x}{d\tau^2}+2b\left(\frac{n}{N}\right)\frac{dx}{d\tau}+\left(\frac{n}{N}\right)^2 x=\frac{1}{N^2}f''(\tau). \tag{7}$$

In the last equation $\frac{n}{N}$ and $\frac{1}{N^2}f''(\tau)$ correspond to n and $f''(t)$ in (1) respectively. The solution of the equation,

$$\ddot{x}+2b\left(\frac{n}{N}\right)\dot{x}+\left(\frac{n}{N}\right)^2x=f''(t),$$

can therefore be found by reading records through the N^2 times larger scale.

The constancy in dynamical magnifying power of the apparatus, corresponding to the accelerograph, can be tested by the observation of the deflection of G_2 when P is driven at different speed.

For the test of the apparatus, in the present experiment, $f''(t)$ is given in square form which is expressed analytically by

$$f''(t)=\frac{4}{\pi}\left(\sin t+\frac{1}{3}\sin 3t+\frac{1}{5}\sin 5t+\cdots\cdots\right). \tag{8}$$

Several examples of the results are shown in Fig. 3. From the results as shown in Fig. 3, it can be said that the apparatus, the period of which is about one third of that of the square wave and is critically damped, can record practically the squre form of the wave. From the results of theoretical calculation of the amplitude charactristics, it is concluded that the condition, $b\doteqdot 0{\cdot}7$, under which the apparatus is slightly oscillatory, is needed in order to extend the range of use of it

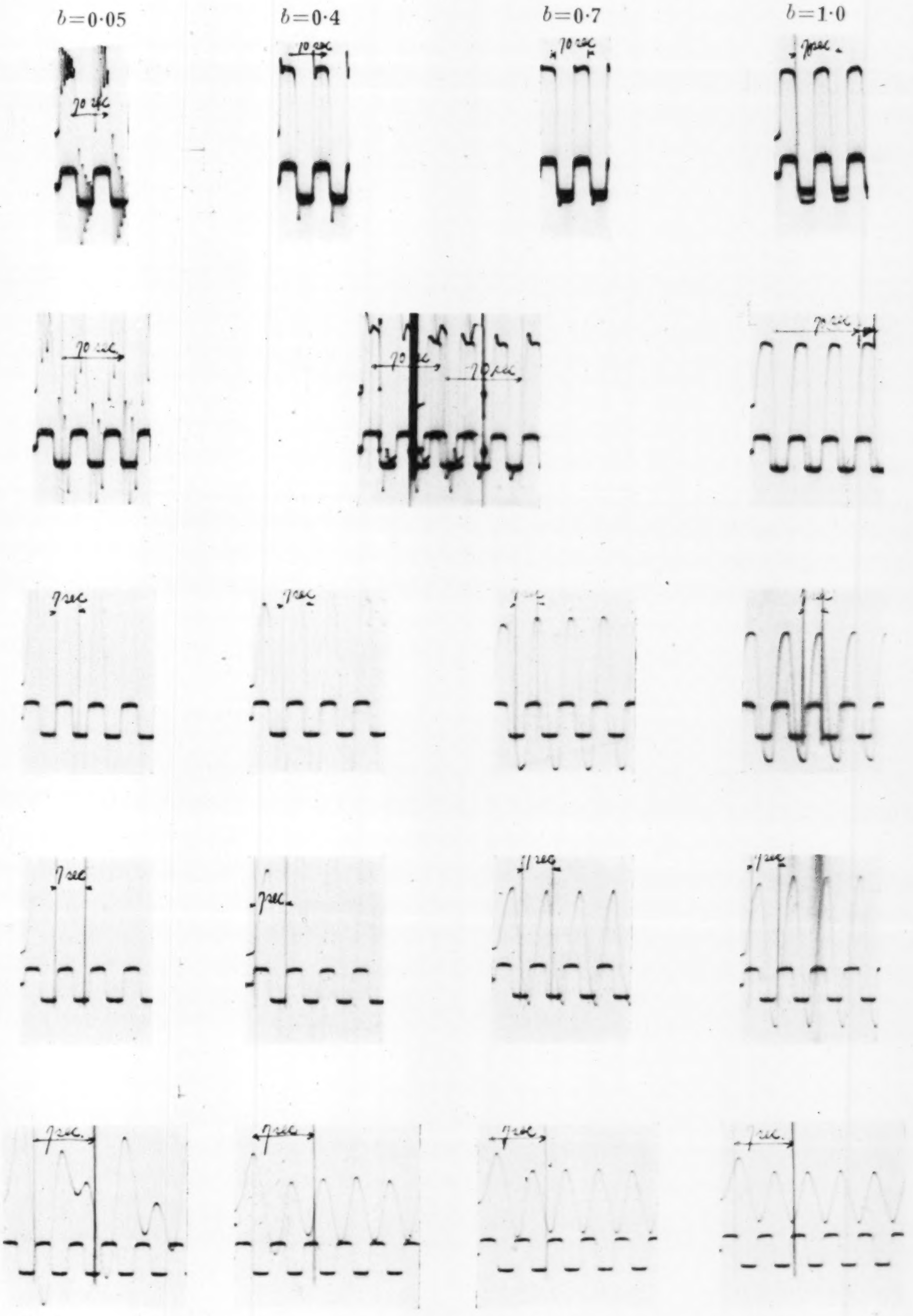

Fig. 3. Time marks of 7 sec are recorded in this experiment, which is equal to the period of G_2.

（震研彙報 第十四號 圖版 淵田）

$b=0{\cdot}05$ $b=0{\cdot}7$ $b=1{\cdot}0$

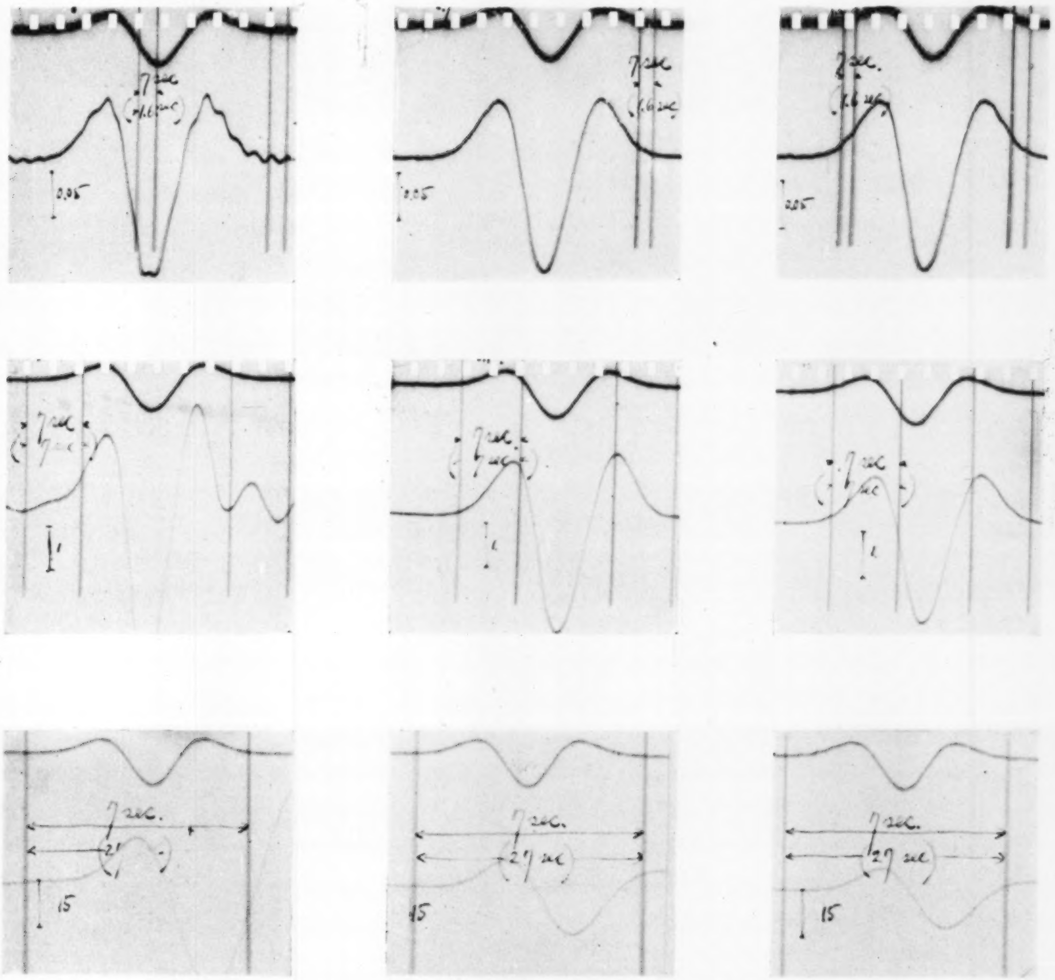

Fig. 4. Time marks in b ackets and scales at sides show periods and scales corresponding to n/N.

（震研彙報 第十四號 圖版 淵田）

$b=0{\cdot}05$ $b=1{\cdot}0$

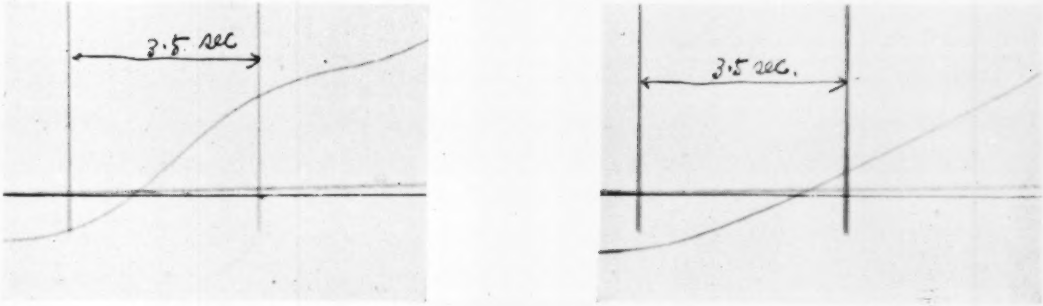

Fig. 6.

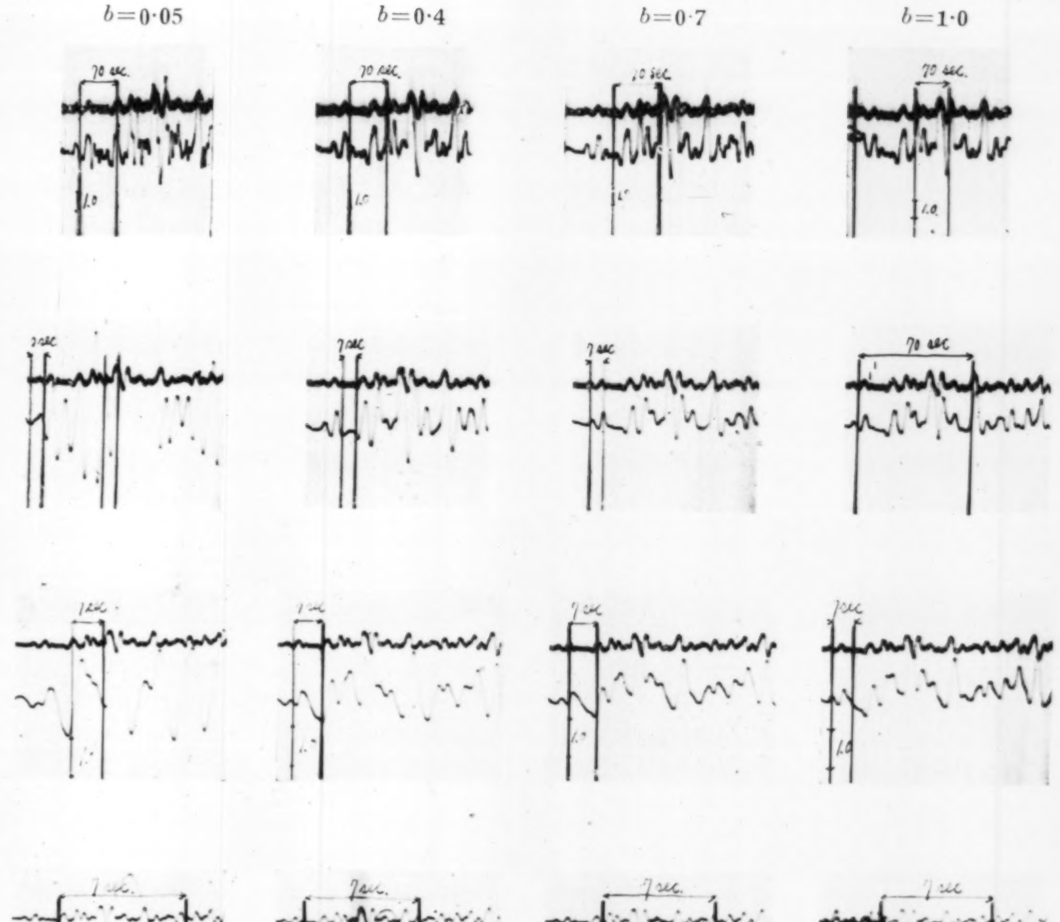

Fig. 5.

（震研彙報 第十四號 圖版 淵田）

up to the resonance. But this conclusion is of cource correct only in the case of pure sine wave and is nothing but the reference to the case of complex waves.

Fig. 4 shows results obtained when $f''(t)=2(2t^2-1)e^{-t^2}$. This example has been already numerically calculated by Mr. S. Suzuki[2] which the present writer took for the purpose of comparing the experiment with the calculation. Comparing the both results, We notice that they are very similar in forms.

In Fig. 5 several examples are shown when $f''(t)$ is given in very complicated form. The preliminary portion in a record of Ishimoto's accelerograph was taken as an example of complex waves. It is also found that the more fast P is driven, the more distinctly the deflection of the galvanometer tend to show the quantity of $\iint f''(t)\,dtdt$. If therefore $f''(t)$ shows the acceleration of the earthquake shocks, the deflection of the galvanometer when P is driven very fast, is almost proportional to the displacement of the ground. In Fig. 5, the deflection of the galvanometer seems to show the permanent displacement. The fact that the image of the mirror deflects to one side only, does not seem to have come from errors due to the nonlinear photoelectric characteristics, the slight inclination of the axis of the curve of $f''(t)$ which affects, as shown in Fig. 6, and so on. But it cannot be concluded that it is the true permanent displacement, since the adopted record of the accelerograph does not always show the true acceleration of the ground due to the earthquake shocks and the problem concerning the initial conditions and the continuity of the true displacement have not yet been discussed thouroughly.

In conclusion the writer wishes to express his best thanks to Dr. N. Miyabe for his kind advices and guidances.

---

37. 振動方程式を實驗的に解く一方法

淵 田 隆 門

$t=0$ に於いて $x=\dot{x}=0$ なる初期條件に對する $\ddot{x}+2\varepsilon\dot{x}+n^2x=f''(t)$ の解を實驗的に求むる方法である. 即ち $f''(t)$ に比例する電流を檢流計に流して其の運動を記錄せしめるのである. $f''(t)$ の簡單な場合や複雜な場合等を二三試みた. 本法は數値計算によりて出來ないやうな複雜な場合も容易に解を得る事の出來るのを利點とする.

---

2) S. Suzuki, *Bull. Earthq. Res. Inst.*, **12** (1934), 15.

38. 關東地方に於ける震原の垂直分布*

永　田　　武

1. 緒　　言

關東地方の震原の分布に就ては，1924年から1931年迄の間の地震について，既に小平氏[1] に依つて調査されてゐる．其の結果，全體としては，40～50 km の深さに最も著しく地震の發生を見る事，此の地方の震原の分布は山岳地方に少く，且地表と約45°の角をなして交る一つの凹狀面内に著しく，其の最深部は東京灣北部にあつて深さ約 70 km である事等が知られた．

然し關東大地震後の關東地方の震央の分布を見るに，特に，利根川，鬼怒川に沿ふ一帶及び東京灣北部から西方への一帶に著しく，然も房總半島に於ては殆ど不連續的に減少してゐる．且1931年以後1935年に亘る間に於ては，東京灣北部に於ても，深さ 70～80 km の地震は殆ど見當らないので，筆者は1924年から1935年迄の間の記錄について再吟味をし，1931年以後の變化をも調べて見た．

2. 震原の分布

震原の位置は總て，地震研究所觀測報告1924年より1935年6月に至る間の中，深さの決定されてゐるもの528個を用ひた．

深さを 10 km 毎の層に分けて，其の各々に於ける震原の分布を圖示したものが第1圖 (a)……(h) である．

第1圖の震原の分布を統計的に調査する爲に，緯度及經度共に10′宛の單位區域に分ち，互に相隣れる4個の單位區域の地震發生頻度をその中央の點の頻度として，各點に於ける震原分布の深さに於ける頻度も分布圖を求めると第2圖に示す如くになる．第2圖に於て，各々の曲線は黒丸で示した點に於ける震原の深さに對する頻度を表はしてゐる．圖に於て明らかなる如く，利根川，鬼怒川附近に於ける震原の鉛直分布は 50 km を最大として，誤差函數的に分布してゐるのに對して，東京灣北部に於ては頻度最大の深さが，著しく深い方へ偏り，凡そ 70 km 附近にある．

全體としては小平氏の指摘された如く[2]，上記の2地帶を中心として，四方へ擴る

---

* 高橋所員紹介．

1) T. Kodaira, *Bull. Earthq. Res. Inst.*, **11** (1933), 350.

2) 前揭，356頁．

に從つて，震原の深さの限度は漸次淺くなり．椀狀曲面を示すのであるが，特に房總半島に於ては地震の發生回數が著しく減少し，且震原の深さも淺くなつてゐるのが注目される．

3. 結果に對する二三の考察

（i） 前述の如く關東地方に於ても，特に地震發生頻度の著しいのは，利根川一鬼怒川附近，及東京灣北部の2個所である．この事を一層明らかにする爲に，上記2地域を含む様に，東經 139°50′ から 140°10′ に至る間を幅とする帶狀區域について，震央分布頻度と緯度との關係を求めれば第3圖（a）に示す様になる．

即ち，前記2地帶に最大頻度を有する二つの誤差函數的分布が相隣つてゐる事を示し，二つの地震頻發地域の存在が明らかである．

更に，之を 1924～1930 年，1931～1933 年の2期間に分けて，同様の分布圖を求めれば第3圖（b）になり，關東大地震後，1930 年頃迄は東京灣北部に於て比較的地震活動が著しかつたのであるが，其の後は漸次この地域は安定し，1931 年以後は利根川一鬼怒川附近に地震活動が著しい事を示す．

（ii） 次に東京灣北部及其の西方の震原分布は又一群を爲してゐるので，北緯 35°20′ から 35°40′ の間を幅とする帶狀地域について，南北方向へその震原の鉛直分布の投影圖を求めれば第4圖に示す如くになる．

即ち，東經 140°5′，千葉沖附近に於て，最も深く迄地震が頻發し，その限界はおよそ 80 km に達する．此の點から西方へは，地震發生深度の限界の深さは緩やかに減少するのに對して，東方房總半島方向へは急激に減少してゐるのが見られる．

小平氏も指摘されてゐるが[3] 關東地方に於ける重力のブーゲー異常の分布は第5圖より明らかなる如く，東京灣北部に極小區域が存在し，その點から西方へは Gradient が小さく，東方へは大きい．

大體に於て，かゝるブーゲー異常はその地下構造によるものと考へられ，重力異常の極小區域は，密度の大きい下層が凹狀を爲して，その上にある密度の小さい上層が厚くなつてゐると考へられる．この事と第4圖の結果を照合して震原の深度の限界は，この地域に於ては，上記の2層の境界と一致するのではないかと思はれる．關東大地震以後，東京灣北部の地震活動が活潑になつたのは，關東大地震の影響として，この上層の部分が不安定になつた爲に，地震の頻發を見るのであらう．

一つの事實として，この東京灣北部の地震頻發地域，北緯 35°20′～35°40′，東經

3） 前揭，359頁．

139°50′～140°10′ の方形區間に於て，1924～1930 年，1931～1935 年の 2 期間に於ける震原の深さの分布を求めれば第 6 圖（a）に示す樣になる．同圖から明らかなる如く，1924～1930 年の期間に於ては，深さ 70 km 附近に最も著しく，地震の發生を見たのであるが，其の後深さ 70 km 以上の地震は殆ど無くなり，50～60 km に於て最も地震の發生が著しい事を示す．卽ち凹狀の下層の上を埋める上層は，關東大震災によつて，その平衡を破られたのであるが，漸次下の方から再び安定の狀態に復しつゝあるものと考へて良いであらう．

（iii） 之に對して，利根川―鬼怒川地域に於て同樣にして 1924～1930 年，1931～1935 年の 2 期間に於ける深さの分布を求めれば（第 6 圖（b）），共に，深さ 40～50 km に最大値を有する誤差函數的分布を爲し，關東大地震直後より現在に到る迄，依然 40～50 km の深さに，最も著しく地震の發生する事を示してゐる．

此の地域は小平氏も注意せられた如く，ブーゲー異常の Gradient が著しく大きい場所であつて（第 5 圖參照），地下の構造が殆ど不連續的に變化してゐると考へられる．且，地震の頻發地域が，等ブーゲー異常線に沿ふてゐる事を考へ合せれば，地層の不連續區域に於ける上層が未だ不安定にある事に起因して地震の頻發を見るものと思はれる．

4. 結　語

以上の事を要約すれば，關東地方の震原の垂直分布に於て，關東地震後，特に目立つて著しく地震の發生を見た千葉沖附近深さ 70～80 km の所は，其の後 1931 年以降殆ど地震の發生を見なくなり，50～60 km の深さに著しくなつて來た．之に對して鬼怒川下流，筑波山附近に於てはこの間依然 40～50 km の深さに於て地震發生の頻度が最大であり時間的變化は見えない．

以上の統計に於ては地震の大さは考の中に入れてゐないし，且又個々の地震及其等の間の關係等については一切觸れない事にし，唯統計的な結果のみを論じたのであるから，實際の地震の發生，時に大きい地震の發生等に迄言及する譯には行かないと思ふ．

擱筆するに當り，御懇切な御指導を賜つた藤原先生及高橋先生に厚く御禮申上る．

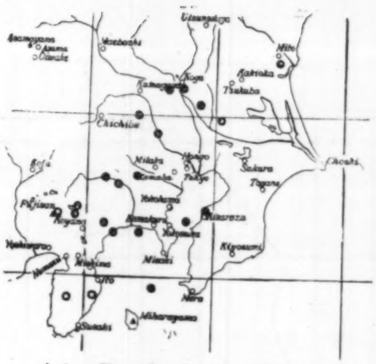

(a) Depth $d=0\sim10$ km

(b) $d=11\sim20$ km

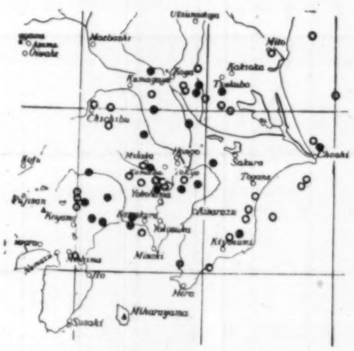

(c) $d=21\sim30$ km

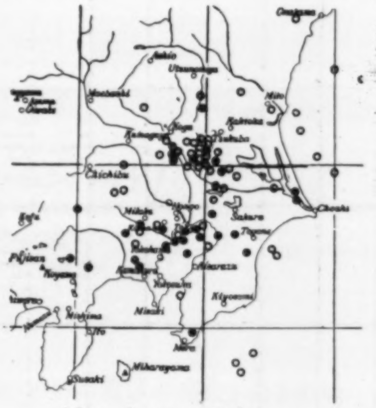

(d) $d=31\sim40$ km

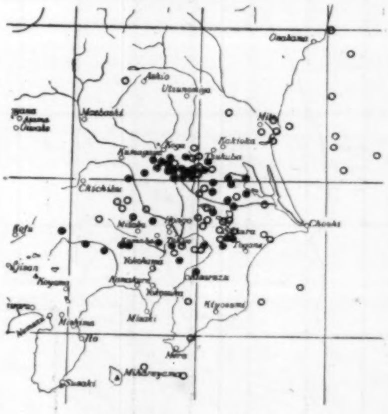

(e) $d=41\sim50$ km

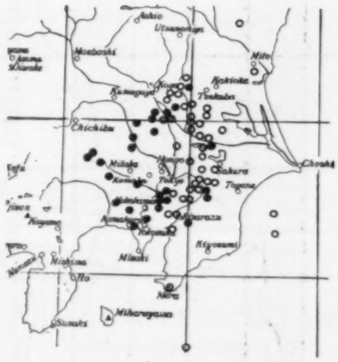

(f) $d=51\sim60$ km

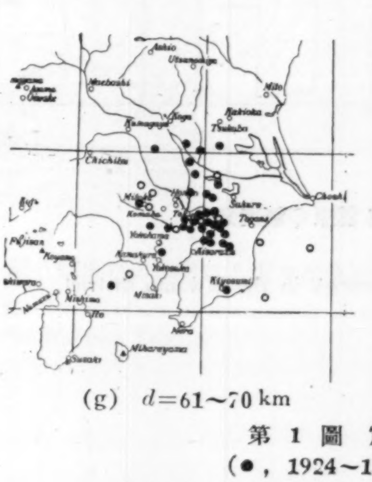

(g) $d=61\sim70$ km

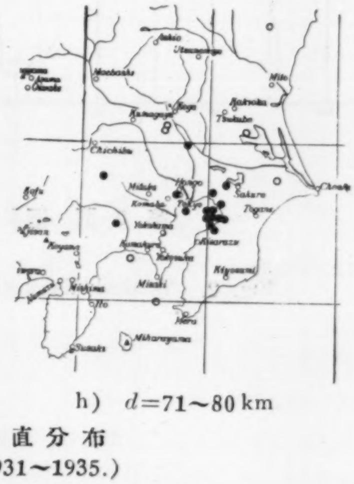

h) $d=71\sim80$ km

第 1 圖 震原の垂直分布

(●, 1924～1930. ○, 1931～1935.)

Fig. 1. Distribution of hypocentres in various depths.

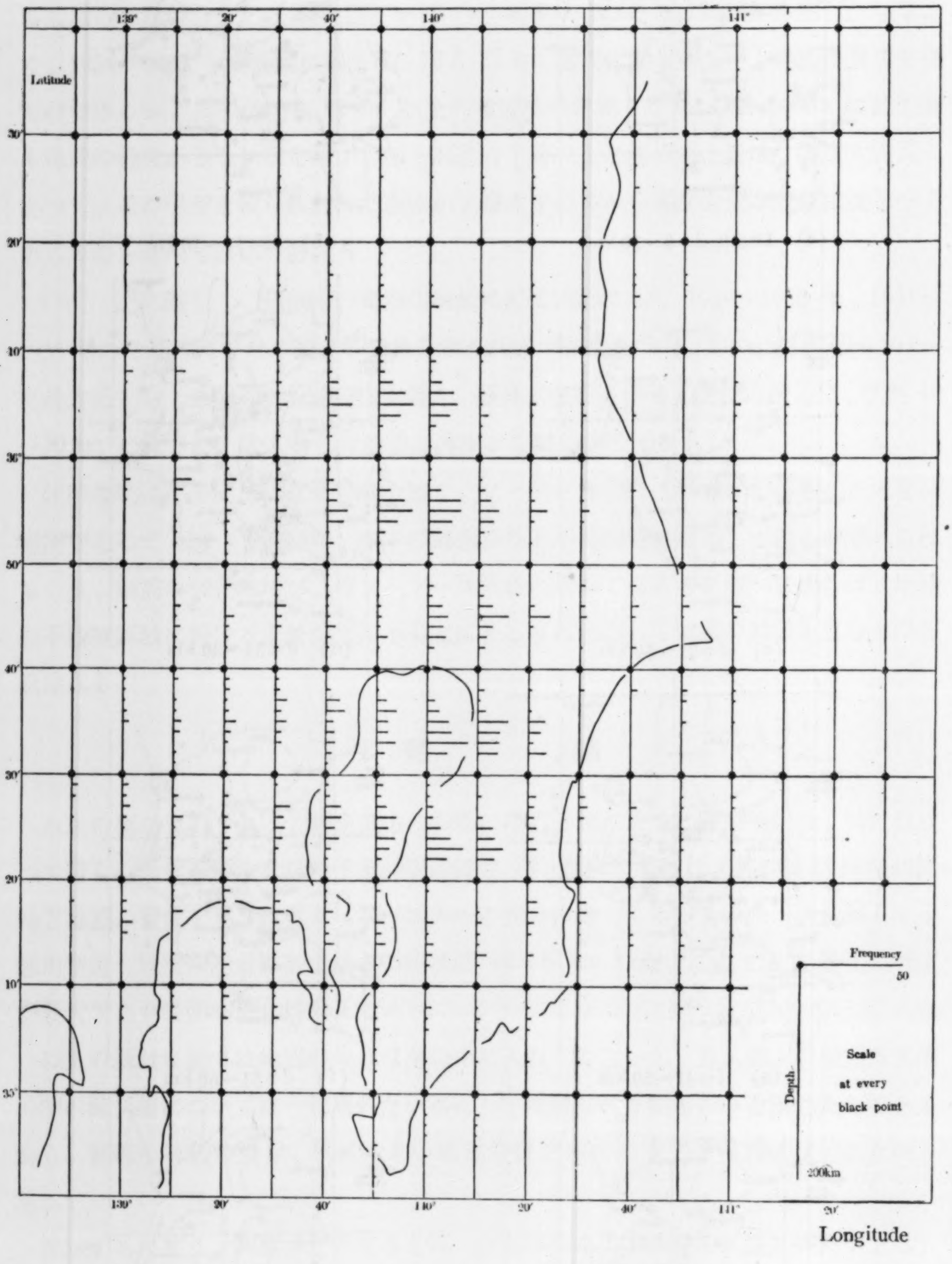

第 2 圖 關東地方に於ける震原の頻度分布

Fig. 2. Vectical distribution of hypocentres in the Kwanto district.

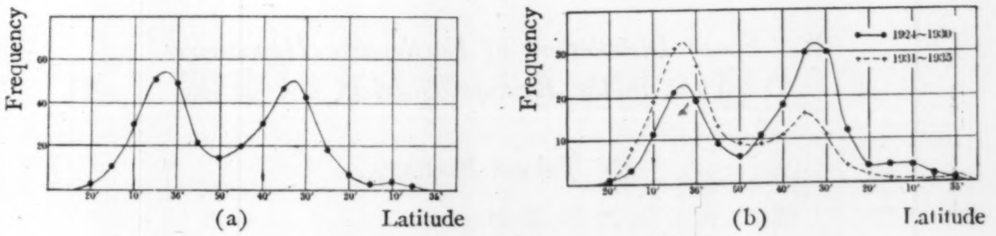

第 3 圖 震央の頻度分布

Fig. 3. Frequency of distribution of epicentres.

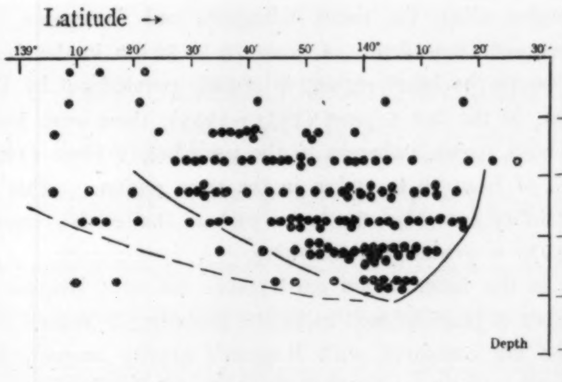

第 4 圖 東京灣北部を含む帶狀區域に於ける震原の垂直分布投影圖

Fig. 4. Vertical distribution of hypocentres in the band region, containing the northern part of Tokyo-bay.

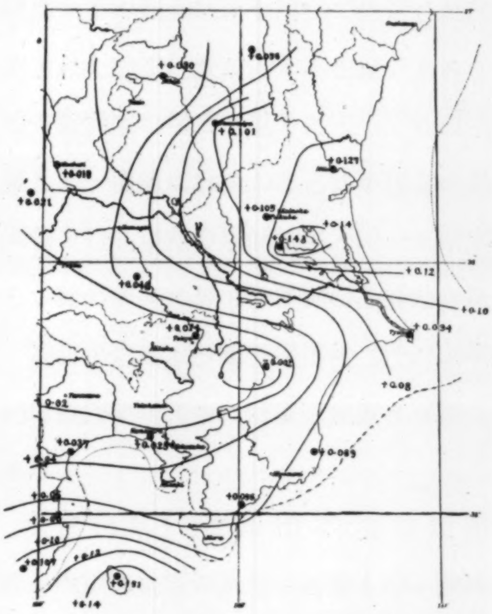

第 5 圖 關東地方に於ける重力異常分布

Fig. 5. Distribution of the gravity anomaly in the Kwanto District.

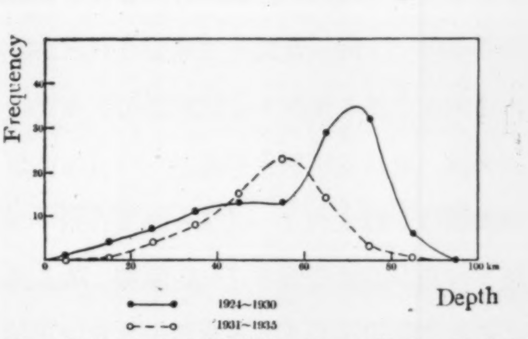

第 6 圖 (a) 東京灣北部に於ける震原の垂直分布

Fig. 6. Vertical distribution of hypocentres in the northern part of Tokyo-bay.

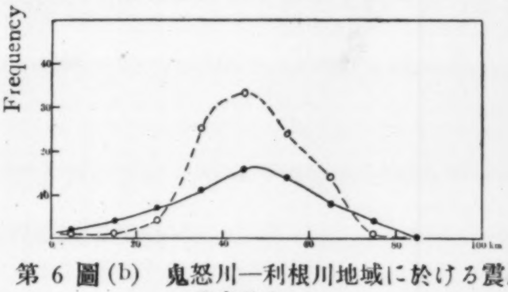

第 6 圖 (b) 鬼怒川—利根川地域に於ける震原の垂直分布

Fig. 6. Vertical distribution of hypocentres in R. Kinu-gawa and R. Tone-gawa regions.

38. *Space Distribution of Earthquake Hypocentres in the Kwanto District.*

By Takesi NAGATA.

The space distribution of the hypocentres of earthquakes that occurred in the Kwanto District within the last 12 years was statistically investigated. As is well known, the epicentres of earthquakes in this district are most closely distributed in two regions, namely, the northern part of Tokyo Bay and the region along the rivers Kinugawa and Tonegawa. Generally speaking, earthquakes are most frequent from depth of from 70 to 80 km in the former region, and from depth of from 40 to 50 km in the latter region, as already pointed out by Dr. T. Kodaira. The writer found however that, in the last 5 years (1931~1935), there were hardly any hypocentres beneath 60 km in the former region, whereas in the preceding 7 years (1924~1930) they were most frequent from depth of from 70 to 80 km in the same region. This fact may be regarded as showing that the instability caused in the lower part of the earth's crust as the result of the Kwanto Earthquake of 1923 is gradually diminishing.

On the other hand, in the latter region earthquakes are most frequent from depth of from 40 to 50 km within the last 5 years as well as in the preceding 7 years.

Finally, these results are compared with Bouguer's gravity anomaly in this district, with discussions.

39. 關東地方に於ける地震の發生（其 1）

地震研究所 那須信治
萩原尊禮
表俊一郎

（昭和11年6月6日發表——昭和11年6月20日受理）

緒言　大正 12 年の關東大地震後關東地方に發生せる地震の研究は數多なされたが地震研究所に屬する各地の觀測所の觀測結果に基き震原の分布を研究されたものには先には今村博士[1] 及び保田桂二氏によつてなされたものがあり，その後小平理學士[2] によつて震原の立體分布にまで論究されたものがある．小平理學士の研究は大正 13 年（1924）より昭和 6 年に至る期間に發生せる地震に就いてなされたものであるが今回の筆者等の研究はその後に起つた地震をも含めてある．即ち期間は大正 13 年より昭和 10 年（1935）末日までの 12 箇年である．

此の研究の資料は地震研究所の地震觀測報告である．此の報告中大正 13 年より 2～3 年間に起つた地震の震原位置は東京本郷に於ける觀測に宇都宮，銚子，熊谷等の諸測候所の觀測結果を用ひて決定されたものであるが觀測點が 3 乃至 4 であるため決定された震原位置が稍々不正確であることは否めない．地震研究所創立以來順次に地方觀測點の增設を見るに至つて震原決定に一段の正確さを加へられた現今の觀測結果と同一價値に取扱ふことは不穩當に思はれるが，前期 2～3 年間の地震に就いて再調査を行ひ現在の觀測結果と同一正確度で震原位置を決定することは不可能であるから，此の研究に於ては差別の必要なき限り同一價値に取扱つた．

震原決定は本所囑託保田桂二氏の多年の經驗努力によつてなされたものであるが前記地震觀測報告中には震原位置は東經（λ），北緯（φ）及び深さ（km）を以て示してある．

大正 13 年より昭和 10 年に至る 12 箇年間東京に於ける有感覺地震の回數及びそれ等の內震原位置の決定されたものゝ數は次表の通りである．

1）今村明恒，保田桂二　地震研究所彙報　**3**（1927），105.
2）小平孝雄　地震研究所彙報　**11**（1933），350.

年　號		東京有感地震回數	震原決定數
大正 13 年	(1924)	60	52
大正 14 年	(1925)	34	29
大正 15 年 昭和元年	(1926)	68	51
昭和 2 年	(1927)	65	54
3	(1928)	78	71
4	(1929)	50	46
5	(1930)	58	50
6	(1931)	89	86
7	(1932)	59	58
8	(1933)	63	62
9	(1934)	64	64
10	(1935)	78	78

以下述べる研究は主として地震の發生位置に關するものである．即ち震央の分布及び震原の立體分布である．震原立體分布に就いては筆者の一人が丹後地震の餘震の研究の際に行つたと同様に，或る垂直平面に震原を投影する方法を用ひた．前記小平理學士の研究にも勿論この方法が用ひられてゐる．此の垂直面は夫々場所に適する樣に選ぶのであるが小平理學士の選んだ垂直面の方向，即ち略 NE-WS, 及びこれに直角なる方向は關東地方の地震を論ずる場合には最も適當と思はれるから此の研究に於てもこの 2 方向の垂直面を選んである．尙ほ關東地方に發生する地震はこれを幾つかの地域に別けてその分布を調べて見ると地域によつて特有な性質が稍明瞭に表はされるので此の研究に於ては關東地方を數箇の地域に區劃して考へて見た．

昭和 5 年春より翌 6 年秋に至る間，伊東，伊豆の兩地震を始め道志川附近の地震，埼玉地震と順を追つて地震活動が關東平野の西部周邊に沿つて北進した事實はよく知られてゐるが，これらの震原の立體分布を詳細に研究する目的のため，西部地方は特に區域を限つてこれを取扱つた．

震原の深さが 100 km を越えるものは僅かに數箇に過ぎないがこれ等は或る一定の比較的小區域に限られてゐる樣に思はれる．此の事實については後に説明する．以下研究の結果を述べる．

震原の分布狀態を詳細に知らんが爲に，先づ地震を其の震原の深さに從つて 0～25 km のもの，26～50 km，40～60 km，51～75 km，76～100 km 及 100 km 以上のもの等に分類し各組毎に震央を別々の地圖上に記入して見ると深さが異るに應じて震央の分布も夫々特徴のある事が判明する．其等の中最も特徴ある分布を示すものは震原が 20 km より淺い地震， 100 km より深い地震及び 40～60 km の間の地震である．就

中，40～60 km の深さに起る地震の回數は非常に多く，而も其れ等が第7圖に見られる如く利根川，鬼怒川流域と東京灣北部との二つの地方に著るしく密集して居るのである．

今之等震原の立體的分布の有樣を知らんとするに當つて，全部の地震の震原を總括して一つの垂直面に投影してしまふ代りに，幾つかの適當な區域に分け，各區域毎に其の投影圖を作る方が眞相を知るに便宜と思はれる．依つて今回は關東平野を利根川鬼怒川流域地方，東京灣北部地方，關東平野西の周緣地方等の地域に分割して夫々別々に立體分布圖を作製することを試みたのである．（第1圖～第5圖）

以下簡單に其等の立體分布圖より察知せられる事項に就き說明を試みる事とする．

1） 利根川，鬼怒川流域と東京灣北部地方との間に震央の分布が非常に粗である帶狀の地域が存在する（第7圖參照）．故に利根川，鬼怒川流域地方の震原の立體的分布

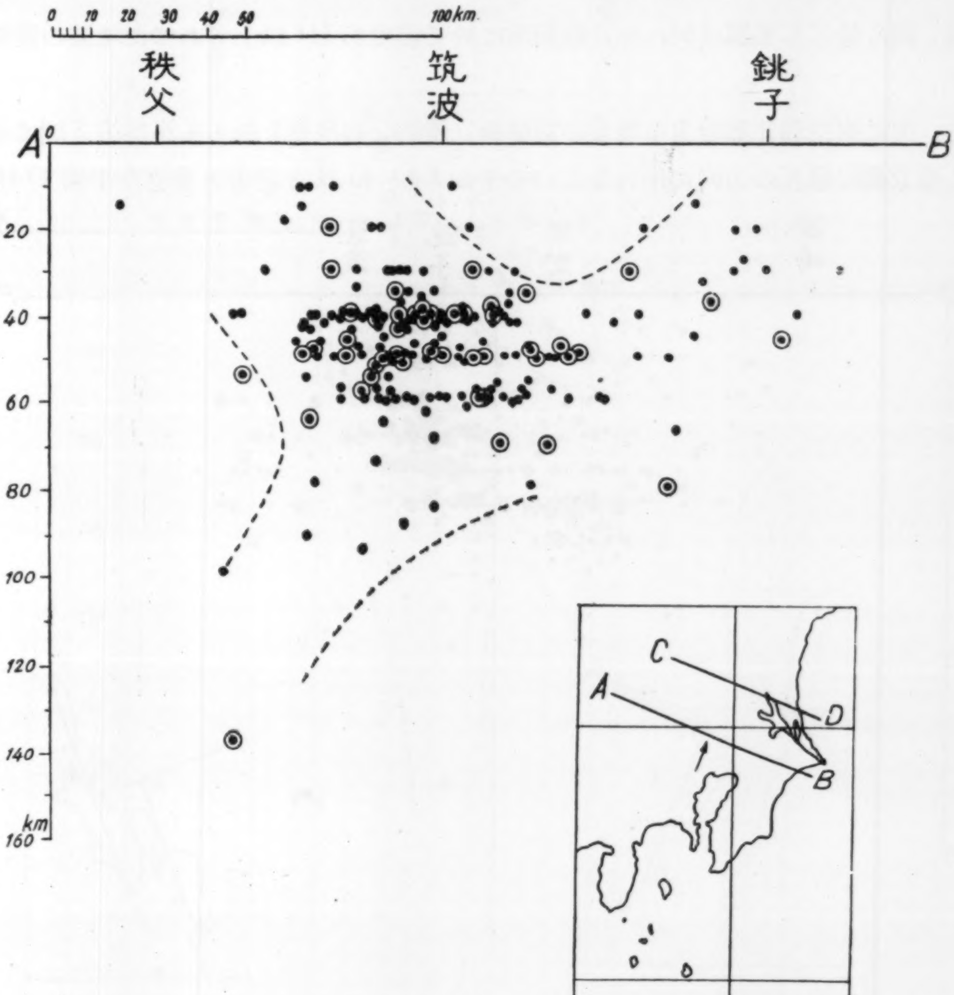

第 1 圖　二つの垂直平面 AB, CD 間に含まれたる震原の位置を矢の方向に投影す．
◉は少くも一觀測所に於て震度 III に達したる地震の震原
●はそれ以下の震度の地震の震原

を知るために，便宜上，第1圖に示す如く此の帶狀の所に A B なる面を作り之と平行に約 30 km の距離に他の平面 C D を置き，此の二つの面で區切られた地域内の震原を C D 面に矢印の方向に投影した。(第1圖參照)

此圖から次の事柄が氣付かれる。

i) 大多數の地震卽ち全體の中の殆んど7割は 40～60 km の深さに起つてゐる。

ii) 霞ケ浦から印旛沼に至る場所の下では 30km より淺い地震が殆んど起つて居ない。

iii) 小平氏は先に關東地方に發生する地震の震原は一つの楔形の部分内に分布して居ると考へられたが，第1圖を見るときは震原は謂はば地表に向つて開口して居る漏斗形に類似した部分に分布して居ると見る方が至當の樣である。

震原の最も深きものは 1927 年 12 月 31 日熊谷に於て震度 III を與へた地震であつて其の深さは 140 km である。

尙，圖に於て二重圓は何れかの觀測所に於て震度が III 以上であつた地震の震原を示す。

2) 次に東京灣北部地方の地震の震原の立體的分布狀態を知らんが爲第2圖に示す如く東京灣の縱長の方向に平行な二つの平面 E O, G H と之等と垂直な平面 O H な

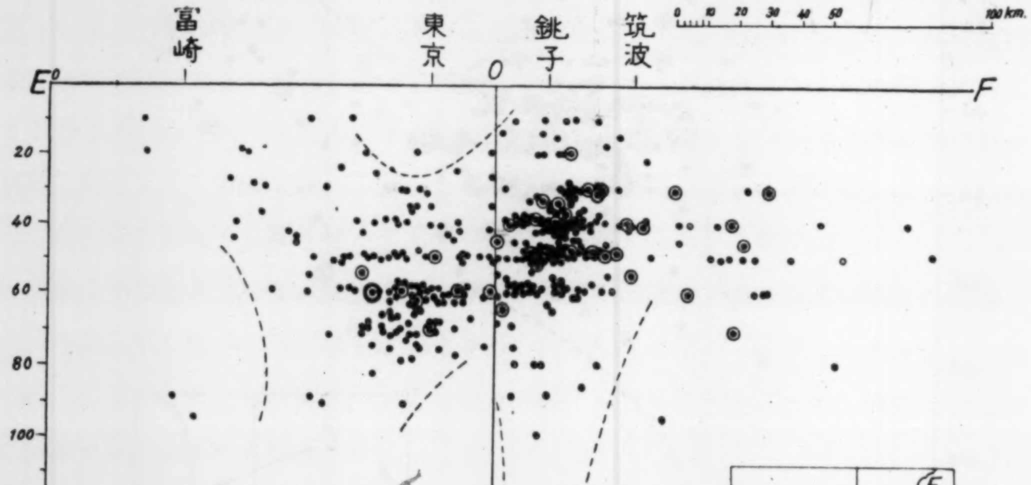

第 2 圖　GH, EO 及び AO, OF 間に含まれたる震源の位置を矢の方向に投影す，
◉は少くも一觀測所に於て震度 III 以上に達したる地震の震原
●はそれ以下の震度の地震の震原

る三平面で圍まれてゐる地域內の震原をＧＨ面に矢の方向に投影した.（第２圖の左方參照）. 之れによれば此の地方に起る地震の震原は前の場合よりも稍深く，50 km 內外から 80 km 位までのものが多い樣である. 又東京灣北部の眞下にはやはり淺い地震の起らない所が存在してゐる. 更に立入つた震原の分布狀態を考へるには第４圖を參照した方が便利であると思はれるから後に再論する事とする.

圖中１と書いた地震は 1923 年１月 27 日房總半島中央部に發生し深さ 140 km と報告されて居るものであるが，深さ及震央の位置に對し疑問があるので調査中のものである. 且又此の震原は唯一つ飛び離れて深い所にあるからこれと東京灣北部の地震との間に關係がある如く考へるのは無理の樣である.

第２圖の右半分は平面ＡＯより北の地域に存在する震原をＡＯに垂直な平面に總て矢を以て示す方向に投影したものであり，第１圖の場合を側方より見た場合に

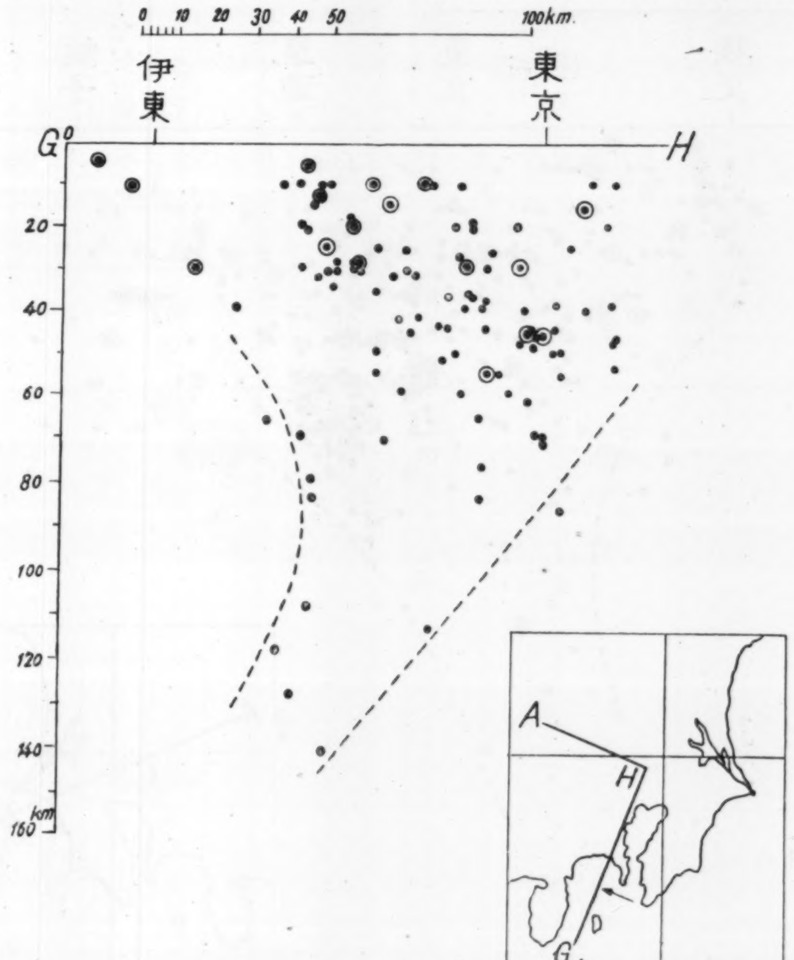

第３圖　二つの垂直面 AH, GH 間に含まれたる震原の位置を矢の方向に投影す.
◉少くも一觀測所に於て震度 III 以上に達したる地震の震原
●はそれ以下の震度の地震の震原

相當するのである．之で見ると筑波以西の淺い地震のために霞ケ浦，印旛沼附近の淺い地震の起らない地域が圖に於ては隱されてしまつて居る．併し震原が漏斗狀の內に分布されて居る有樣は明らかに見られる．鹿島灘にも淺いものが起らない事が明瞭となる．

3） 次に第2圖の東京灣の西方の部分，卽ち3圖に於て平面GH及びAHに境せられた地域內に存在する震原を矢を以て示す方向に投影したものが第3圖である．之に於て 100 km より深い地震は相模灣及其の直ぐ北の所に起つて居るのみである．圖には 10 km より淺い所に頻發した伊東地震群，15～16 km までの深さに起つた北伊豆地震及其の餘震，又主として 20 km より淺い所に起つた秩父地震及其の餘震は記入されてないがそれでも淺い地震の多い事が注目せられる．震原の分布はやはり漏斗狀

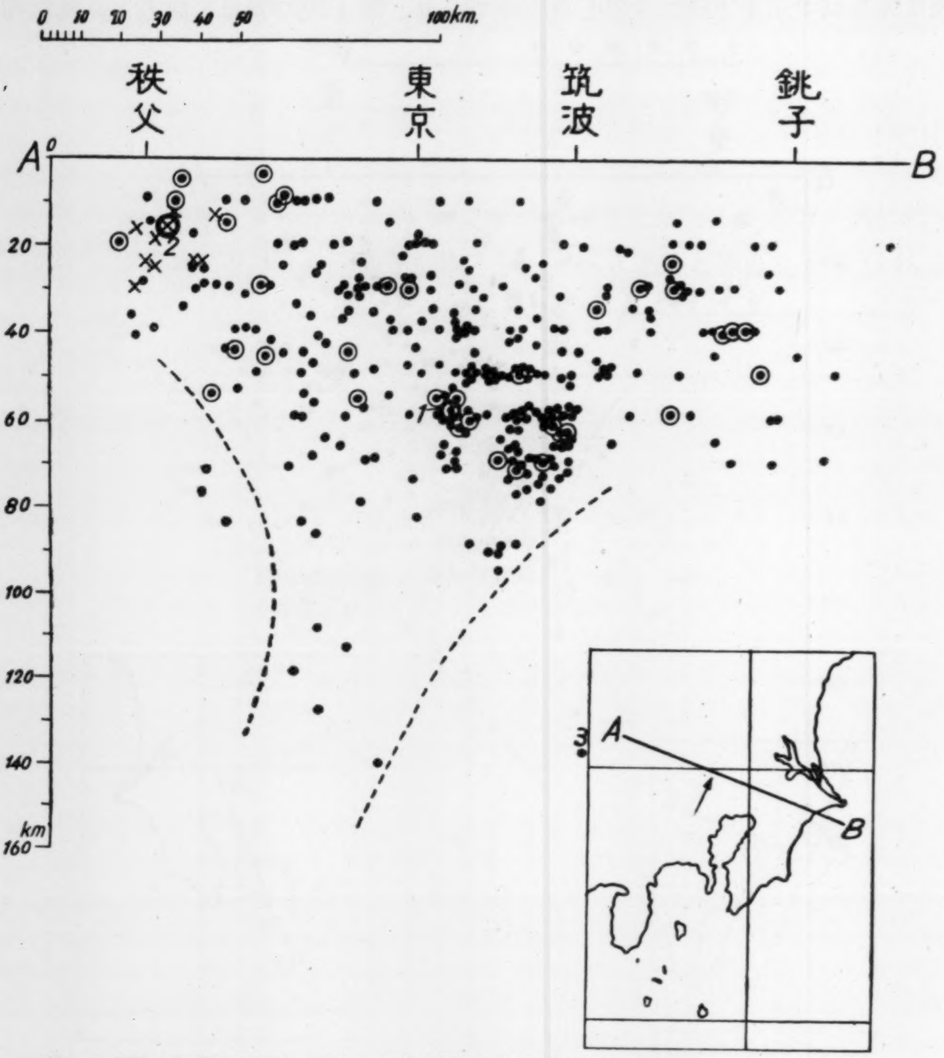

第 4 圖　垂直面 AB に對して北東側にある震原の位置を矢の方向に投影す．
◉は少くも一觀測所に於て震度 III 以上に達した地震の震原
●はそれ以下の震度の地震

をなして居ると見る事が出來る．

4）第4圖は AB より南の部分に存在する震原を總て AB 面に矢の方向に投影したものである．此の圖で注意する事は

i）東京灣に深いものが多く西方の山地に近づくに從つて淺い地震が多くなつて居る事が明らかに見られる．

ii）東京灣北部にも淺い震原がある如く見えるのは東京灣口及三崎附近の相模灣に起つた淺いものが投影されて居る爲である．

iii）圖中1と書いて大きい二重圓で示したのは 1926 年 8 月 3 日の羽田地震で東京に於ける震度 IV であつて，1924 年 1 月 15 日の關東大地震の餘震以後東京で感じた最も大きな地震であつた．

iv）×印で示したのは 1931 年の秩父地震の餘震であり，それに二重圓を附して 2と記してあるのが9月21日の本震の震原である．大體に於て此等の震原の深さは淺いものばかりであつた．

v）圖に3と示したのは第2圖の説明中に述べた房總半島の中央部に起つた深さ 140 km の地震である．

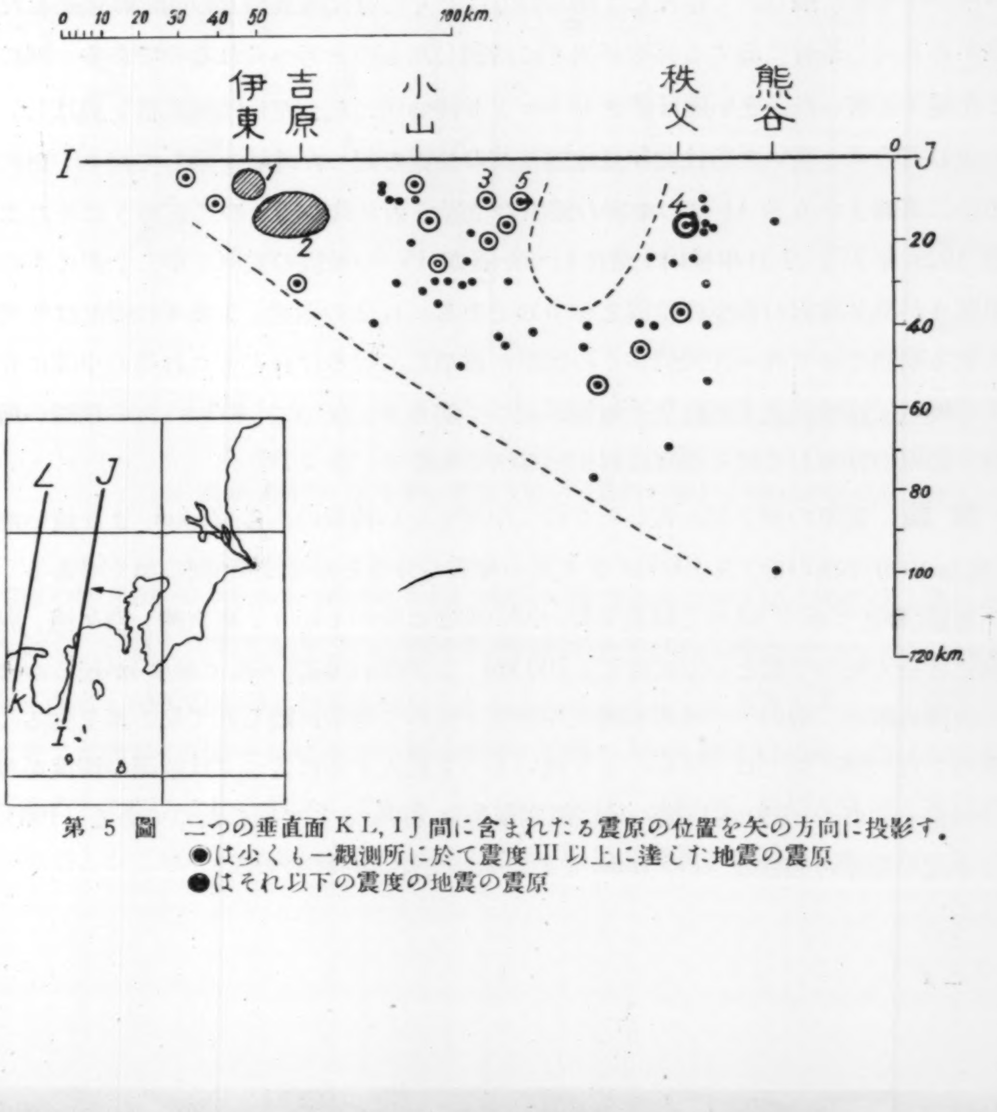

第 5 圖　二つの垂直面 KL, IJ 間に含まれたる震原の位置を矢の方向に投影す．
◉は少くも一觀測所に於て震度 III 以上に達した地震の震原
●はそれ以下の震度の地震の震原

vi) 第4圖と第2圖とを綜合して考へれば相模灣北岸附近に震央を有する深い地震と 80 km から 50 km までの間に多い東京灣の地震とは同じ系統に屬するものであつて其の分枝の一つが東京灣に延び他の分枝が西方の山地へ延びたものと考へてもよいと思はれる．

5) 第5圖は圖中 IJ，KL と書いた二つの垂直面で區切られてゐる部分內の地震の震原を KL 面に矢の方向に投影したものである．

1930年2月より同年8月まで約6ヶ月の期間伊豆半島伊東町附近に於て震原の極めて淺い地震が頻發し，次で同年11月26日其の少しく北方に於て起つた北伊豆地震は震度 V 以上にも達し其の前震及餘震が夥しかつた點に於ても注目せられたのであつたが，同年の終り頃それが大體終息すると間もなく，翌年6月1日約 50 km 距つた道志川上流地方に震度 III の地震が起り，其の後更に 50 km 程北の秩父山地に9月 21 日震度 V にも及ぶ地震が起つたのであつた．恰も震央が飛び飛びに北に移動して行つたかの如く見え其等の地震相互の間には何等の關係もない如く思へるのであるが，第5圖の如く細長き地帶に付き震原の立體的分布圖を製作して見ると震原は飛び飛びの地域に限られて存在して居るのではなくて實は地震相互の間には連絡した關係があり同じ系統に屬する其等が次々に活動したものと考へられるのである．圖に於て左端1と書いた大きい圓は深さ 10 km より淺い所に起つた伊東地震群を表はし，その少し右方2と書いた所は北伊豆地震及其の餘震の起つた地域を示して居り，更に右方の二重圓3が6月11日の地震の震原の位置であり其の隣りの二重圓5はそれより前 1929 年7月 27 日相模川上流に起つた震度 IV の地震の震原を示し，更に右の二重圓4が秩父地震の震原の位置を示すのである．1，2の附近，3及4の附近は今考へて居る期間に於て夫々比較的多くの震原が群集して居るけれどもこれ等の中間に存在する地域では地表近くには全く地震が起つて居らず，反つて 40 km 位の稍深い所に於て震原の分布して居る事は注目すべきであらう．

結 論 震原の深さ別に書いたものゝ中著るしい特徵のある 20 km より淺い地震（但し1930年後の分）及 100 km より深い地震の分布を示せば第6圖の如くである．淺い地震（●にて示す）は殆ど關東平野の西の周邊に沿つて起り，東京灣，霞ケ浦，鹿島灘には全く起つて居ないのに反し，100 km より深い地震（×にて示す）が起るのは一つは熊谷附近，他の一つは相模灣北岸附近で此の二地域に限られて居る事を知るのである．此の圖に於ては 20 km より淺いものを記入するに當つては觀測の精度が可なり增進せられた1930年以後の地震觀測報告を data として採つたのである．100 km より深い震原の深さは Underline をした數字で記入されてある．

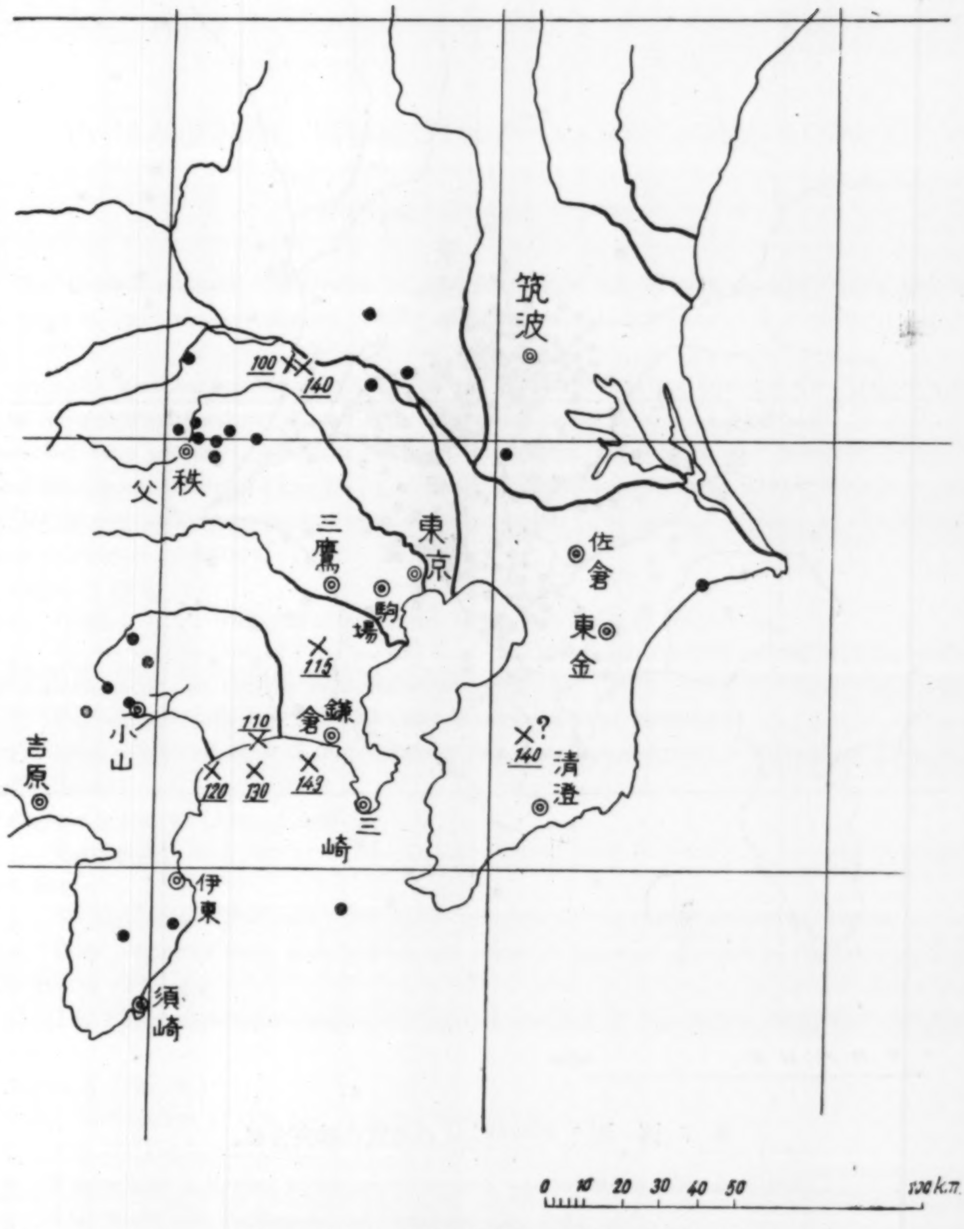

第 6 圖 ◉ 震原 20 km より淺い地震
× 震原 100 km より深い地震〔數字は震原の深さ (km) を示す〕

震原の深さが 40 km から 60 km の間の地震の震央分布を示す第 7 圖には，既に述べた如く，一見して明らかな二つの震央密集地域があらはれて居る．

6） 今若し地震の原因を岩漿運動なりと考ふるならば以上の事實を基として闘東地方に於ては熊谷の附近と相模灣との地下深所に岩漿の Neck 或は Origin と思はれるものがあるとしてもよいと思ふのである．かく考へれば，利根川，鬼怒川流域と東京灣北部地方との二地域に地震が密集して起る理由，又闘東平野の西邊に沿ひ次第に震原

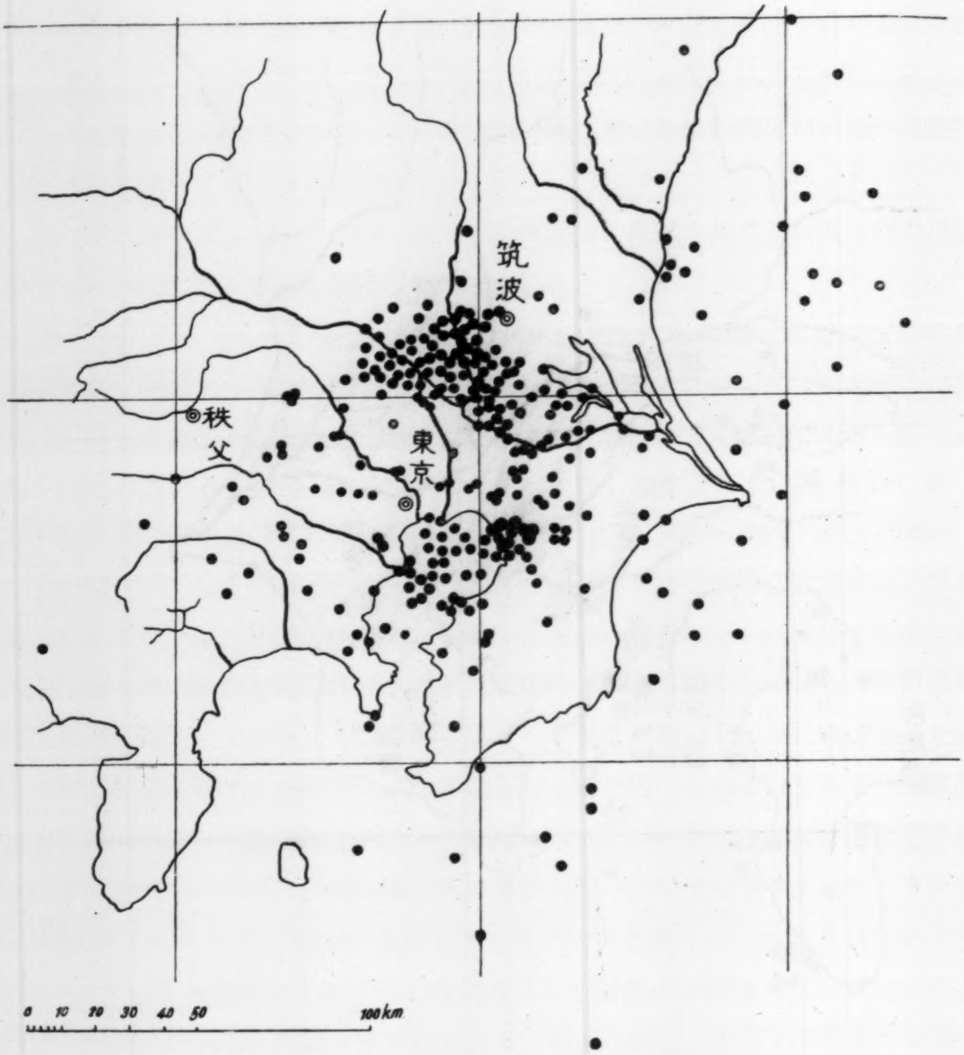

第 7 圖　深さ 40～60 km の地震の震央分布．

が淺くなる理由なども極自然に說明せられる．然し乍ら，立體的の分布に於ては上述の如き結果が得られたとしても，此等の地震相互の時間的關係，例へば時間と共に次第に震原位置が上昇する等の事實は未だ判明せられないのであるから，本文に於ては之以上立入つた議論は避け將來の研究に俟つとする．

尙觀測の誤差は深さについては ± 10 km 水平距離についても大體其れ位の範圍であらう．

39. *Studies on Earthquakes in the Kwantô District. Part I. Three-dimensional Distribution of the Seismic Foci.*

By Nobuji NASU, Takahiro HAGIWARA and Syun-itirô OMOTE,

Earthquake Research Institute.

The three-dimensional distribution of seismic foci in the Kwantô district during the period from 1924 to 1935 was investigated, basing on data from the Seismometrical Reports of our Institute.

Generally speaking, earthquakes occurred most frequently in the basin of the Kinugawa River and in the neighbourhood of Tôkyô Bay. To study these distributions in detail, the positions of seismic foci were projected on certain vertical planes. For convenience, the Kwantô district was divided into several sections (Figs. 1~5). In the Figures earthquakes of seismic intensities greater than III at any station are marked with double circles. The general manner of distribution in these sections is as follows.

Region 1 (Fig. 1).

1) Shallow seated earthquakes are found in the two ends of this section.

2) In the middle part of this region, i.e., in the neighbourhood of Mt. Tukuba and the Lake Kasumi-ga-ura, no shallow earthquakes occurred.

3) Earthquakes with depths of 40~60 km occurred most frequently.

4) Deep origins of more than 100 km are found near Kumagaya (north-western part of the Kwantô district).

Regions 2 and 3. (Figs. 2 and 3).

1) Earthquakes with depths of 60~80 km occurred most frequently in the neighbourhood of Tôkyô Bay.

2) No earthquakes shallower than 20 km occurred in the neighbourhood of Tôkyô.

3) Deep origins of more than 100 km are found in the northern part of Sagami-wan Bay.

Section 4 (Fig. 4.)

1) The Figure shows that shallow earthquakes occurred in the western margin of the Kwantô plain.

Region 5 (Fig. 5.)

Strong earthquakes in this part occurred since 1930, i.e.,

1) The Itô Earthquake-swarms in the period from February to July, 1930.

2) The seismic activities in the north-western part of Itô on October, 1930.

3) The North Idu Earthquake of November 26, 1930.

4) The strong after-shock of the North Idu Earthquake near Heta on March 7, 1931.

5) The strong earthquake on the upper course of the Dôsi-gawa River on June 11, 1931.

6) The Titibu Earthquake of September 21, 1931.

The diagram was constructed to show clearly the migration of these earthquakes.

From these investigations it may be concluded that the three dimensional distribution of seismic foci in the Kwantô district is funnel-shaped, two deep sources lying at a depth of more than 100 km beneath the region near Kumagaya and in the northern part of the Sagami-wan Bay.

40. The Takasegawa Green Tuff beds of the Yuri district, Akita pref., Japan, and Correlation of the Lower Neogene in Japan.

By Yanosuke OTUKA,

Earthquake Research Institute.

(Read May 19, 1936.—Received June 20, 1936.)

Introduction.

It was known[1] for some years past that Tertiary fossils had been collected from the Yuri and Hiraga regions in the southern part of Akita prefecture, Northeast Japan. In 1926, Dr. M. YOKOYAMA[2] studied and described some ten fossil mollusca collected from these regions by Y. CHITANI and K. MURAYAMA, geologists of the Imperial Geological Survey, Japan. In the Spring of 1936, the writer had occasion to visit these regions when he collected fossil shells there. From his field observations and from his study of these fossil shells, the writer believes that he has made some discoveries relating to the Neogene stratigraphy in Japan. The writer, in describing these discoveries here, will make up some of the results in the palaeontological study of M. YOKOYAMA, and in the stratigraphic study of K. MURAYAMA[3] who surveyed these regions for the explanatory text and the geological map of "Honjô", scale 1/75,000.

Stratigraphic succession of the Yuri and Hiraga regions.

The stratigraphic succession of Akita prefecture has already been studied by Prof. R. ÔHASHI[4], I. ÔMURA[5], and Y. CHITANI[6]. According to them, the succession of the Neogene strata in this prefecture is typically exposed in the Oga peninsula. Y. CHITANI classified the Neogene beds into four series in descending order:

Takanosu series

  Sibikawa sandstone bed

1) *Expl. text, geol. map.* "Honjô", *scale* 1/200,000, (1896).
2) M. YOKOYAMA, *Jour. Fac. Sci. Imp. Univ. Tokyo*, Sec. II, **1** (1926), 377~389.
3) K. MURAYAMA, *Expl. text* and *Geol. map* "Honjô", *scale* 1/75,000, (1934).
4) R. ÔHASHI, *Jour. Geol. Soc. Tokyo*, **37** (1930), 740~754, (in Japanese).
5) I. ÔMURA, *Jour. Geol. Soc. Tokyo*, **37** (1930), 755~765, (in Japanese).
6) Y. CHITANI, *Jour. Geol. Soc. Tokyo*, **37** (1930), 732~739, (in Japanese).

Yuri series
  Wakimoto sandy shale bed
  Kitaura alternation bed
Ogasima series
  Hunagawa shale bed
  Onnagawa siliceous shale bed
  Daisima (or Nisikurosawa) sandstone bed
Innai series
  Sugoroku volcanic and pyroclastic rock bed.

K. MURAYAMA[7] classified the Neogene formation in the Yuri and Hiraga regions into four series as done by Y. CHITANI, and subdivided them as follows:

Takanosu series
  Sibikawa (=Shibikawa) sandstone bed.

The Sibikawa sandstone bed is composed of bluish grey or yellow sandstones intercalated with layers of clay and conglomerate in the upper part. *Glycymeris* sp., *Pecten* sp. etc., are found in it. (After Murayama's descriptions.)

The Anden shell bearing sand bed on the north shore of Oga peninsula, from which M. YOKOYAMA[8] described many fossil shells, is the basal part of this series.

Yuri series
  Wakimoto sandy shale bed
  Katurane sand and shale bed
  Hosogoe shale bed.

The Yuri series consists of the three beds listed above. The Wakimoto sandy shale bed is the sandy mud intercalated with soft tuffaceous sandstone, conglomeratic sandstone, a compact white tuff bed, and a hard marly bed. (After Murayama's descriptions.)

The conglomeratic sand exposed on the cliff wall of a hill east of Manganzi village contains many fossil mollusca representing the fauna of the Wakimoto sandy shale bed. These molluscan fauna were described by M. YOKOYAMA[9] in 1926. The writer collected the species in Table I from this locality. In this table, the specific names that differ from those of YOKOYAMA are shown in parentheses.

Judging from the fauna there listed, the writer found that the fauna of the Wakimoto sandy shale bed from Manganzi is the same as the fauna of the Omma series of ONOYAMA[10] near the city of Kanazawa. Of these *Mercenaria yokoyamai* MAKIYAMA, *Pandora pulchella* YOKOYAMA, *Umbonium* (*Suchium*) *akitanum* SUZUKI, *Turritella* (*Haustator*) *saishuensis* YOKOYAMA, *Tachyrhynchus venustellus* (YOKOYAMA),

7) K. MURAYAMA, *op. cit.* (1934).
8) M. YOKOYAMA, *op. cit.* (1926).
9) M. YOKOYAMA, *op. cit.* (1926).
10) T. ONOYAMA, *Chikyû*, **19** (1933), (in Japanese).

Table I. Fossil shells from Manganzi. O=occurrence of Omma series. S=occ. of Sawane bed.

— —	*Nucula (Nucula) niponica* SMITH
— O	*Yoldia (Cnesterium) keppeliana notabilis* YOKOYAMA
S O	*Limopsis tokaiensis* YOKOYAMA
S O	*Glycymeris yessoensis* (SOWERBY)
S O	*Arca boucardi* JOUSSEAUME
— O	*Anadara satowi ommaensis* OTUKA.
S O	*Astarte borealis* (SCHUMACHER)
S O	*Astarte hakodatensis* YOKOYAMA
S O	*Venericardia ferruginea* (CLESSIN)
S O	*Cardium (Cerastoderma) ciliatum*? (FABRICIUS)
S O	*Mercenaria yokoyamai* MAKIYAMA (=*Venus stimpsoni* GOULD)
S —	*Spisula* cfr. *grayana* SCHRENCK
— —	*Tellina* sp.
— O	*Pandora (Kennerlia) pulchella* YOKOYAMA
— O	*Umbonium (Suchium) akitanum* SUZUKI (=*Umbonium suchiense* YOKOYAMA)
— O	*Turritella (Haustator) saishuensis* YOKOYAMA
— O	*Tachyrhynchus venustellus* (YOKOYAMA)
S O	*Bittium yokoyamai* OTUKA (n. n. for *Bittium binodulosum* YOKOYAMA* from Sawane bed.)
S O	*Polynices didyma* (BOLTEN)
S O	*Natica janthostoma* DESHAYES
— —	*Tritonalia (Ocinebrellus) adunca* (SOWERBY) subsp.
— —	*Cancellaria murayamai* YOKOYAMA
— O	*Antiplanes perversa contraria* (YOKOYAMA)**
S —	*Lora ogurana* (YOKOYAMA)
S —	*Lora dissoluta* (YOKOYAMA)
— O	*Glycymeris vestitus* (DUNKER)
S —	*Pseudogrammatodon dalli obliquata* (YOKOYAMA)

* M. YOKOYAMA, *Jour. Fac. Sci. Imp. Univ. Tokyo*, Sec. II, 1 (1926), 270, Pl. 32, Fig. 15.

** M. YOKOMAMA, *Jour. Fac. Sci. Imp. Univ. Tokyo*, Sec. II, 1 (1926), 383, Pl. 44, Fig. 2 a, 2 b.

and *Bittium yokoyamai* OTUKA[11] are the characteristic fossils in both formations. Some species of fossil shells from Manganzi are the same as those of the Sawane fauna in Is. Sado[12]. The molluscan fauna from the lower part of the Anden shell bed, which will be described in other paper, is slightly allied to the Manganzi fauna *Turritella (Haustator) saishuensis* YOKOYAMA, *Umbonium akitanum*

11) *Bittium yokoyamai* OTUKA=*n. n.* for *Bittium binodulosum*, YOKOYAMA 1926 (*Jour. Fac. Sci. Imp. Univ. Tokyo*, Sec. II, 1 (1926), 270, Pl. 32, f. 15.) (not of YOKOYAMA 1920.)

12) M. YOKOYAMA, *Jour. Fac. Sci. Imp. Univ. Tokyo*, Sec. II, 1 (1926), 249~312.

SUZUKI are replaced, in the Anden fauna, with *Turritella andenensis* OTUKA, *Turritella (Haustator) fortilirata* SOWERBY and *Umbonium moniliferum costatum* (KIENER). From the above written the writer is inclined to conclude that the Wakimoto sandy shale bed may be contemporaneous with the Omma series of ONOYAMA and the Sawane bed in Is. Sado.

The Katurane sandstone and shale bed, which is conformably overlain by the Wakimoto sandstone bed, is an alternation complex of sandstone and mudstone, rarely intercalated with tuffaceous beds.

The Hosogoe shale bed, which is below the Katurane bed, consists of white compact platy tuff, soft tuff, and thin marly bed.

Ogasima series
Hunagawa shale bed
Onnagawa shale bed.

The Hunagawa shale bed which principally consists of black shale or black mud, intercalating with a thin bed of tuff, tuffaceous sandstone, and marl, apparently conforms with the Hosogoe shale bed of the Yuri series.

The Onnagawa siliceous shale consists mainly of diatomaceous shale and siliceous shale intercalating with tuff, tuffaceous sandstone, and marl. (After MURAYAMA.)

The siliceous shale of the lower part of the Onnagawa bed alternates with greenish tuff. The Onnagawa shale bed contains diatoms of genus *Coscinodiscus*, tests of *Sagarites*, and fish scales.

The foregoing stratigraphic succession agrees with that of the Yuri and the Ogasima series in the type localities of Oga peninsula, the fossils contained in these two series in Oga peninsula resembling those in the Yuri and Hiraga regions. Consequently it is natural for previous authors to have correlated these series with each other. I. ÔMURA subdivided the Yuri series in the Yuri-Hiraga regions into the Sasaoka, Katurane, and Tentokuzi beds. His subdivision is largely similar to that of MURAYAMA.

In the Ogasima series of Oga peninsula, the Daisima (or Nisikurosawa) sandstone bed is overlain by siliceous shale of the Onnagawa bed with conformity, and is underlain by the Sugoroku volcanic and pyroclastic rock bed of the Innai series with unconformity. I. ÔMURA[13] believes that the Daisima (or Nisikurosawa) sandstone bed is the basal part of the Ogasima series, while the Ogasima series of the Yuri and Hiraga regions lacks the Daisima sandstone bed. The siliceous shale of the Onnagawa bed of the Ogasima series in the Yuri and Hiraga regions is underlain by the Takasegawa green tuff bed of the Innai series with a parallel stratigraphic boundary. That is to say, the formation corresponding to the Daisima (or Nisikurosawa)

13) I. ÔMURA, *op. cit.* (1930).

sandstone bed seems to be lacking in these districts, but it will now be shown that it is not lacking.

Innai series

Takasegawa green tuff bed.

This bed mainly consists of tuffaceous rocks, the upper part of which is overlain by the Onnagawa shale bed with parallel stratigraphic boundary consisting of tuffaceous mud stone, tuff, tuffaceous sandstone, conglomerate, and some thin coal seams. The lower part of this bed consists of agglomerate tuff, agglomerate, intercalating with hypersthene andesites and basalt. (After MURAYAMA's descriptions.)

The Takasegawa green tuff bed.

According to the writer's field observations from Tateai in Tômaimura to Zigenosawa along the river Takase (-gawa), the siliceous shale of the Onnagawa shale bed is exposed where it is underlain by light bluish green tuffaceous sandstone beds with conformity at Takinosawa. The siliceous shale bed of the Onnagawa shale bed here contains fossils of fish-scales and tests of *Sagarites*.

The light bluish green tuffaceous sandstone bed below the Onnagawa bed, which intercalates with a *Balanus* bearing calcareous sandstone bed and a marl bed, is underlain by a bluish grey tuffaceous muddy sandstone bed. Below this muddy sandstone bed a thick tuffaceous conglomerate bed develops and intercalates with some thin coal seams and siliceous wood stem bearing shale and agglomeratic conglomerate. This coal and siliceous wood stem bearing shale is exposed near Zigenosawa. The lower part of the Takasegawa tuff beds that are overlain by these beds consists of andesite agglomerate, hypersthene andesite, and two pyroxene andesite flows.

Fossil mollusca are contained in the *Balanus* bearing calcareous sandstone bed and in the bluish grey tuffaceous muddy sandstone below the calcareous sandstone. The fossil mollusca collected from the river floor east of a reservoir about 1 km west of Sugota village are listed below (Table II).

Table II.

Nucula sp.
Patinopecten tokyoensis kimurai YOKOYAMA
Patinopecten healeyi yamasakii YOKOYAMA
Pecten protomollitus NOMURA
Lucina acutilineata CONRAD
Venericardia ferruginea (CLESSIN)
Dosinia (Kanehara) kaneharai YOKOYAMA
Cultellus izumoensis YOKOYAMA
Panope japonica A. ADAMS
"*Panomya*" *simotomensis* OTUKA
Phalium yokoyamai NOMURA et HATAI
Fulgoraria rupestris (GMELIN)

According to K. MURAYAMA fossil remains occur from Ukibuta and Iwaizawa in Simogô-mura, where light green thick tuffaceous coarse sandstone intercalating

with thin coal seams is exposed, being underlain by hypersthene andesite flows. The shell-bearing bed is a *Balanus* bearing calcareous sandstone bed in the greyish tuffaceous muddy sandstone bed underlain by the tuffaceous coarse sandstone bed. The following fossils were collected from the calcareous sandstone exposed some 100 m east of the Ukibuta tunnel (Table III).

Takinoue pass in Yasawagi-mura is another fossil locality of the upper Takasegawa tuff bed. The locality of Kinonezaka reported by M. YOKOYAMA is identical with the writer's Takinoue pass. In Takinoue, the fossil bearing tuffaceous grey mudddy sandstone bed is overlain by a *Balanus* bearing calcareous sandstone bed and underlain by a tuffaceous conglomerate bed, both of which formations are underlain by hypersthene andesite flows. The siliceous shale of the Onnagawa shale bed overlies these tuffaceous sandstone formations at Oota east of Takinoue. MURAYAMA and the writer collected the following species from this locality (Table IV).

Table III.

Patinopecten healeyi yamasakii (YOKOYAMA)
Patinopecten tokyoensis kimurai (YOKOYAMA)
Pecten cfr. *kagamianus* YOKOYAMA
Chlamys notoensis YOKOYAMA
Chlamys akitanus YOKOYAMA
Chlamys aff. *akihoensis* MATSUMOTO
Anomia sp.
Coptothyris grayi (DAVIDSON)

Stratigraphic position of the Takasegawa green tuff bed.

As the Takasegawa green tuff formation is clearly overlain by the siliceous shale of the Onnagawa shale bed with conformity, the former bed is probably contemporaneous with the Daisima (or Nisikurosawa) bed or the Sugoroku volcanic and pyroclastic rock bed, both of which are overlain by the siliceous shale of the Onnagawa bed in Oga peninsula.

Table IV.

Anadara aff. *ninohensis* OTUKA
Ostrea gravitesta YOKOYAMA
Chlamys akitanus YOKOYAMA
Patinopecten tokyoensis kimurai (YOKOYAMA)
Patinopecten tokyoensis murayamai (YOKOYAMA)
Lima sp.
Venericardia ferruginea (CLESSIN)
Dosinia (Kaneharaia) kaneharai YOKOYAMA (fig. 3)
Dosinia (Kaneharaia) kaneharai var.
Cultellus izumoensis YOKOYAMA
Cardium nuttalli CONRAD
Cardium muticum REEVE
Dentalium sp.
Calyptrea sp.
Natica sp.

According to the writer's observations, the Daisima (or Nisikurosawa) bed is overlain by the Onnagawa bed at the shore of Nisikurosawa in Oga peninsula with conformity, while at the east end of this shore, the former bed thins out, the latter bed abutting on the

Daisima (or Nisikurosawa) bed to be directly underlain by Sugoroku andesite and a pyroclastic bed as shown in Fig. 2.

Operculina complanata DEFRANCE and *Miogypsina ozawai* HANZAWA[14] are contained in a bluish sandstone of the Nisikurosawa sandstone bed at a horizon a few meters below the Onnagawa siliceous shale bed, while a basal conglomerate-like bed is exposed offshore. If then we assume the Onnagawa siliceous shale bed in the Yuri and Hiraga districts to be contemporaneous with the Onnagawa siliceous shale bed in Oga peninsula, the fossil marine mollusca bearing upper Takasegawa green tuff bed will be found to be more closely related to the Daisima bed than to the Sugoroku beds.

There are two types of fossil molluscan fauna in the upper Takasegawa bed. The "A" type, rich in *Patinopecten tokyoensis kimurai* (YOKOYAMA). The fauna from Sugota and Takinoue pass are of "A" type. The "B" type is associated with *Balanus* bearing calcareous sand. The locality east of Ukibuta tunnel is of "B" type.

In studying both types of the fauna we are reminded of the writer's Kadonosawa[15], except *Patinopecten healeyi yamasakii* (YOKOYAMA) and *Pecten* aff. *kagamianus* Yokoyama.

NOMURA and HATAI[16] reported *Phalium yabei* NOMURA et HATAI from the writer's Kadonosawa series. The specific character of *Phalium yabei* NOMURA et HATAI is however observable in the spiral sculpture of the holotype of *Phalium yokoyamai* NOMURA et HATAI (=*Galeodea japonica* YOKOYAMA)[17] from the Kimati bed in Simane prefecture. *Phalium yabei* NOMURA et HATAI cannot be distinguished from *Phalium yokoyamai* NOMURA et HATAI not at any rate in its spiral ornamentations. The *Phalium* collected from the Takasegawa tuff bed resembles *Phalium yabei* NOMURA et HATAI in its spiral ornamentations, but in the width of the spiral ribs it resembles *Phalium yokoyamai* NOMURA et HATAI. The writer has treated these two species as one without distinction. At all events, his specimen (fig. 4) closely agrees with the type species of YOKOYAMA from the Neogene of Simane prefecture.

The geologic formations exposed in the Nisitugaru district in Aomori prefecture were palaeontologically studied by S. NOMURA[18]. YAGI's Oirase series (=the upper part of the Oodose series of IIZUKA[19])

14) S. HANZAWA, *Sci. Rep. Tohoku Imp. Univ.*, Ser. II (Geology).
15) Y. OTUKA, *Bull. Earthq. Res. Inst.*, **12** (1934), 566~638.
16) S. NOMURA and K. HATAI, *Jap. Jour. Geol. Geogr.*, **11** (1933), 1~2.
17) M. YOKOYAMA, *Jap. Jour. Geol. Geogr.*, **2** (1923), 3, Pl. 3, Fig. 4.
18) S. NOMURA, *Saitō Ho-on Kai Museum, Research Bull.*, **6** (1935).
19) Y. IIZUKA, *Jour. Geol. Soc. Tokyo*, **37** (1930), 727~731.

of these formations contains many fossil mollusca. The upper Takasegawa fauna written above is closely allied to that of the Oirase series. The fossil species common to the Oirase series and the Takasegawa tuff formation are listed below:

Ostrea gravitesta YOKOYAMA, *Pecten protomollitus* NOMURA, *Patinopecten tokyoensis kimurai* (YOKOYAMA), *Patinopecten healeyi yamasakii* (YOKOYAMA), *Venericardia ferruginea* (CLESSIN), *Lucina acutilineata* CONRAD, *Cultellus izumoensis* YOKOYAMA, *Panope japonica* (A. ADAMS), and "*Panomya*" *simotomensis* OTUKA.

Besides the foregoing, there occurs *Pecten s-hataii* NOMURA which is closely related to *Pecten kagamianus* YOKOYAMA.

This Oirase series contains *Operculina complanata* DEFRANCE, *Miogypsina ozawai* HANZAWA, which are characteristic foraminifera of the lower part of the Japanese Neogene. The Daisima sandstone in Oga peninsula may be of contemporaneous horizon with the Oirase series in the foraminifera community. Consequently the upper part of the Takasegawa tuff formation may be almost contemporaneous with the Daisima sandstone bed as inferred from the stratigraphic succession already referred to.

The Neogene of the Yuri and Hiraga districts therefore correlates with that of Oga peninsula as follows:

Oga peninsula		Yuri and Hiraga
Yuri series	Wakimoto bed Kitaura bed	Wakimoto bed Katurane bed Hosogoe bed
Ogasima series	Hunagawa bed Onnagawa bed Daisima bed	Hunagawa bed Onnagawa bed Upper Takasegawa bed
Innai series	Sugorokn bed	Lower Takasegawa bed

MURAYAMA's Takasegawa bed contains the Daisima (or Nisikurosawa) bed and the Sugoroku andesite and pyroclastic rock bed, whence the writer calls the fossil bearing bed of the upper part of the Takasegawa green tuff bed, the Sugota tuffaceous muddy sandstone bed.

Older Neogene beds in Japan.

As just said, the Sugota bed (upper part of Takasegawa green tuff bed) contains a molluscan fauna similar to that of the Oirase series (upper part of IIZUKA's Oodose series), and the Kadonosawa series in Iwate prefecture. These three formations usually are asso-

ciated with volcanic rocks and pyroclastic rock beds that may be successive, or of a geologic age not so different from the overlying formation.

Judging from the fossil mollusca, the Sugota beds (upper part of Takasegawa tuff bed), the Kadonosawa series, and the *Operculina complanata* DEFRANCE, *Miogypsina ozawai* HANZAWA bearing Oirase series are not so different in their faunal characters, but are rather contemporaneous or almost contemporaneous with one another. From palaeontological evidences the *Operculina complanata* DEFRANCE and the *Miogypsina ozawai* HANZAWA bearing Nisikurosawa sandstone (or Daisima sandstone) bed, which is clearly contemporaneous with the Sugota bed from the stratigraphic view point, may be regarded as contemporaneous with the Sugota bed.

The lower half of the Kadonosawa series and the same series at Yuda, the latter of which was formerly regarded[20] as a lower horizon under the Kadonosawa series, contains *Desmostylus japonicus* TOKUNAGA* et IWASAKI. While the Daisima (or Nisikurosawa) bed and the Oirase series, which are regarded as contemporaneous with the Kadonosawa series, contains *Operculina complanata* DEFRANCE and *Miogypsina ozawai* HANZAWA, so that the *Desmostylus japonicus* TOKUNAGA and *Operculina complanata* DEFRANCE bearing formation are probably contemporaneous with one another.

H. YABE[21] believed that the "*Desmostylus*" of Ozawa from Is. Sado associated with *Miogypsina ozawai* HANZAWA and *Operculina complanata* Defrance, belongs to the other genus, and that *Desmostylus japonicus* of MATSUMOTO from the Kadonosawa bed at Sikonai may be another species. The formation in which these fossils are contained may not differ so much in geologic age from one another, although the generic or specific name of these so-colled "*Desmostylus*" fossils differs.

Operculina complanata DEFRANCE ranges from Miocene to Recent. According to GALLOWAY[22] Genus *Miogypsina* ranges from Pliocene to Miocene, in which case then *Operculina complanata* DEFRANCE and *Miogypsina ozawai* HANZAWA bearing bed is not necessarily limited

20) H. YABE "Recent Stratigraphical and Palaeontological Studies of the Japanese Tertiary", *Spec. Publ. Bernice P. Bishop. Mus.*, **7** (1921), 780~781.

* TOKUNAGA (formerly YOSHIWARA). The writer errorneously reported the name of authors in his previous paper. The specific name of *Desmostylus japonicus* was established 12 years after the first report of its occurrence. (TOKUNAGA and IWASAKI, *Jour. Geol. Soc. Tokyo*, **21** (1914)).

21) H. YABE, *Sci. Rep. in Japanse, Tohoku Imp. Univ. Sendai*, **12** (1935).

22) GALLOWAY, Man. Foraminifera. (1933).

to the lower Miocene as hitherto supposed. It is said[23] that the *Operculina complanata* DEFRANCE and the *Miogypsina* bearing bed is underlain by a lower Miocene *Amphilepidina* and *Miogypsina* bearing bed in the Misaka mountainland of Central Japan, consequently the *Miogypsina* and *Operculina* bearing formation is not necessarily Lower Miocene, but is probably contemporaneous with the *Desmostylus* bearing bed.

If we assume that the *Desmostylus japonicus* IWASAKI et TOKUNAGA bearing bed is contemporaneous with the formation containing *Operculina complanata* DEFRANCE and *Miogypsina ozawai* HANZAWA, we may expect some resemblance to the marine molluscan fauna in these formations containing these fossils. The writer finds the *Phalium yokoyamai* NOMURA et HATAI, *Cultellus izumoensis* YOKOYAMA, *Pecten s-hatai* NOMURA, *Pecten* cfr. *kagamianus* YOKOYAMA, *Tellina optiva* YOKOYAMA between the *Desmostylus japonicus* TOKUNAGA et IWASAKI bearing Huzina-Kimati bed in Simane prefecture[24] and the Sugota (=upper Takasegawa) bed, Oirase series, Kadonosawa series, in Northeast Japan. And the formations containing *Soletellina minoensis* YOKOYAMA, "*Proclava*" aff. *ishiiana* (YOKOYAMA) are common with the Kadonosawa and Tukiyosi-Togari formation, the latter formation containing *Desmostylus japonicus* IWASAKI et TOKUNAGA,

In the stratigraphic table for the west part of Hokkaido studied by T. NAGAO and Y. SASA[25], the Neogene strata is divided into the following successions in descending order:

Setana, Kuromatunai, Yakumo, Kunnui, and Hukuyama series.

The Kuunui series is overlain by the Yakumo series which is contemporaneous with the Onnagawa and Hunagawa beds of Oga peninsula, it being underlain by the Hukuyama volcanic and pyroclastic rock series which may be the Sugoroku bed in Oga peninsula.

Stratigraphically, the Kunnui series is the Nisikurosawa (or Daisima) bed in Oga peninsula. According to the preceding two authors[26], *Desmostylus japonicus* YOSHIWARA et IWASAKI and *Miogypsina ozawai* HANZAWA and *Operculina complanata* DEFRANCE occur in the Kunnui series.

Recently H. YABE reported *Miogypsina* from the Neogene of Mino from which many notable mammals were reported by H. MATSUMO-

---

23) H. YABE, *op. cit.*, (1935).

24) TSUBOTA, *Graduate thesis of Kyôto Imp. Univ.* (*Partly sited in Chikyû*, **19**, (1933)).

25) T. NAGAO and Y. SASA, *Jour. Geol. Soc. Japan*, **40~41** (1933~1934).

26) T. NAGANO and Y. SASA, *op. cit.* (1933~1934).

TO[27]. The Neogene of Mino has been divided by SAGA[28] into following order:

Togari／Tukiyosi bed
Hiramaki bed
Nakamura bed

Dr. J. MAKIYAMA[29] recently wrote that the Togori bed is a contemporaneous deposit with the Tukiyosi, although in appearance the two rocks slightly differs from each other. *Miogypsina* was found from the lower part of the Tukiyosi bed. A holotype of *Desmostylus japonicus* IWASAKI et TOKUNAGA was collected from the Togari bed. J. MAKIYAMA found a *Mastodon* (=*Trilophodon*) *palaeindicus* (LYDEKKER) from the Togari bed.

As just said, the association of *Operculina complanata* DEFRANCE and *Miogypsina* or *Miogypsina ozawai* HANZAWA with *Desmostylus japonicus* TOKUNAGA et IWASAKI suggests that the geologic range of the former fossils must be younger than hitherto believed. Whatever may be the standard geologic age, it seems that these three fossils are contained in one formation in which no remarkable stratigraphic breaks are seen. But in every locality *Desmostylus* seems to always occur in a horizon above that bearing *Operculina-Miogypsina*.

As to the stratigraphic succession of the Japanese Neogene, especially in Oil bearing Tertiary, what the palaeontologists advocate differ from that of the oil field geologists, but if these fossils just mentioned occur in one and the same formation, the difference between the palaeontologists and the oil geologists may be said to have disappeared.

If the writer were to boldly correlate the Japanese lower Neogene bed with one another according to the remarks just made, the result would be shown in Table V.

In the circumstances, the geologic age of *Desmostylus japonicus* IWASAKI et TOKUNAGA may be Middle Miocene (Vindobonian), judging from studies of the Tukiyosi and Togari beds of Mino in which *Mastodon* (*Trilophodon*) *palaeindicus* (LYDEKKER) occurs.

Brief notes on Table V.

The stratigraphic succession of west Hokkaido (loc. 1 in Fig. 1) as referred to in the studies of T. NAGAO and Y. SASA was explained above. The Kunnui series contains *Desmostylus japonicus* TOKUNAGA

27) H. MATSUMOTO, *Sci. Rep. Tôhoku Imp. Univ.*, Ser. II, **5** (1921), No. 3.
28) Y. SAGA, cited in H. Yabe's paper. (*op. cit.* 1921).
29) J. MAKIYAMA, *op. cit.*

et IWASAKI and *Operculina complanata* DEFRANCE and *Miogypsina ozawai* HANZAWA. The Setana series, which contains many fossil mollusca, is contemporaneous with the Takanosu series in Oga peninsula as judged by its molluscan fauna.

The stratigraphy near Oodose (loc. 2 in Fig. 1) was studied by T. IIZUKA, T. YAGI, and S. NOMURA, by whom the following stratigraphic succession was established:

Kanita series
Wakayama series
Azigasawa series
Oirase series
Oodose series.

Of these series, the Oirase, which is underlain by the Oodose volcanic and pyroclastic series, contains many mollusca and *Miogypsina ozawai* HANZAWA and *Operculina complanata* DEFRANCE.

The writer's Kadonosawa series (loc. 3 in Fig. 1) in Iwate prefecture has been referred to already here. According to J. MAKIYAMA[30], the molluscan fauna from the lower part of the Kadonosawa series may be slightly younger than the fauna of J. MAKIYAMA's Heiroku sandstone in North Tyôsen (Korea). (loc. 23 in Fig. 1).

S. NOMURA[31] who studied the fossil mollusca from the Siogama formation (loc. 6 in Fig. 1) near Sendai, concluded that the Siogama formation may be contemporaneous with the writer's Kadonosawa series, so that in Table V, the Siogama bed stands in the same column as the Daisima sandstone.

The fossil molluscan fauna of Moniwa[32] (loc. 8 in Fig. 1) in the lower part of the Saoyama group is closely related to that of the Nanao series in Isikawa prefecture and the Huzina and Kimati beds in Simane prefecture. *Pecten kagamianus* YOKOYAMA, *Pecten notoens s* YOKOYAMA, are the noteworthy fossils in this fossil locality of Moniwa.

The Yanagawa series[33] (loc. 10 in Fig. 4) in the Hukusima basin contain molluscan fauna similar to that of the Saoyama and Oirase series. The Ryôzen volcanic complex is overlain by this series. In its faunal characteristics, the Yanagawa series may be contemporaneous with the Saoyama and Oirase series.

H. Fujimoto and I. ÔMURA reported the occurrence of *Miogypsina*

30) J. MAKIYAMA, *Mem. Coll. Sci. Kyoto Imp. Univ.*, [B], **11** (1936), No. 4.
31) S. NOMURA, *Saitô Hô-on Kai Museum Research Bull.*, **6** (1935).
32) H. MATSUMOTO, *Sci. Rep. Tôhoku Imp. Univ.*, Ser. II, **13** (1930), No. 3.
33) S. NOMURA and N. ZIMBO, *Saitô Ho-on Kai Mus. Res. Bull.*, **6** (1935).

ozawai HANZAWA from the lower part of his Kubiki series (loc. 7 and 11 in fig. 1) in Niigata prefecture.

In Is. Sado (loc. 9 in fig. 1), the late Y. OZAWA[34] reported teeth of "*Desmostylus*" and *Operculina complanata* DEFRANCE and *Miogypsina ozawai* HANZAWA from the lower part of the Nakayama series, which last is overlain by a Diatomaceous bed and underlain by the Aikawa volcanic complex. This stratigraphic succession closely agrees with that of Oga peninsula.

S. Imamura[35] collected *Operculina complanata* DEFRANCE and *Miogypsina ozawai* HANZAWA with *Vicarya yokoyamai* TAKEYAMA from the Miocene of Yatuo (loc. 14 in fig. 1) in Toyama prefecture. From its foraminifera, the Miocene of Yatuo, which is called the Yatuo series by Imamura, may be contemporaneous with the Daisima (or Nisikurosawa) sandstone bed in Oga peninsula. The lower part of the Yatuo series, which consists of andesite and pyroclastic rock series, contains some plant fossils.

From its molluscan fauna, the Sirado series[36] of the Zyoban coal field (loc. 12 in fig. 1) has been correlated by H. YABE with the Huzina and Kimati bed, but the upper part of the Sirado series or the lowest part of the overlying Taga series contains *Stegolophodon latidens* (CLIFT) which is a later Miocene mammal of Asia. The marine beds of Yunagaya series may be contemporaneous with the lower Kadonosawa series, from its stratigraphic position.

The molluscan fauna of the Nanao bed[37] in the Nanao series (loc. 13 in fig. 1) in Isikawa prefecture is closely allied to that of the Kimati bed in Simane prefecture, the Moniwa shell bed of the Saoyama group, and the Yanagawa series in Hukusima prefecture. The Domi series, which is overlain by the Nanao bed is a volcanic and pyroclastic rock bed containing some Miocene plant leaves.

The Wakura bed above the Nanao bed may be contemporaneous with the upper part of the Ogasima series in Oga peninsula. The Nanao series is overlain by the Omma series with unconformity, the formation of which, from its faunal characteristics, is contemporaneous with the Yuri series in Oga peninsula.

The lower part of the Saoyama group contains *Lepidocyclina*[38].

It is well known that the Miocene of Mino (loc. 18 in fig. 1) contains many fossil mammals. According to a recent study of J.

34) Y. OZAWA, *Jour. Geol. Soc. Tokyo*, **31** (1924), 317.
35) S. IMAMURA, *Jour. Geol. Soc. Tokyo*, **38** (1931).
36) K. WATANABE, *Expl. Geol. Map*, "Jôban Coal Field", (1934).
37) Y. OTUKA, *Bull. Earthq. Res. Inst.*, **13** (1935).
38) S. HANZAWA, *Jour. Geol. Soc. Japan*, **42** (1935), 533.

MAKIYAMA, the Togari bed and the Tukiyosi bed, which are deposits contemporaneous with each other, contain *Desmostylus japonicus* TOKUNAGA et IWASAKI and *Miogypsina ozawai* HANZAWA, and *Mastodon (Trilophodon) palaeindicus* (LYDEKKER).

Judging from the above fossils, the Togari and Tukiyosi beds may be contemporaneous with the Kunnui series and the Nisikurosawa bed.

The Kimati and Huzina beds in Simane prefecture (loc. 17 in Fig. 1) contain *Desmostylus japonicus* I. et T.[39] *Pecten kagamianus* YOKOYAMA, *Cultellus izumoensis* YOKOYAMA, and *Phalium yokoyamai* NOMURA et Hatai.

The Miocene in the Tuyama basin (loc. 20 in Fig. 4) is divided into the Uetuki and Tuyama beds, both of which contain *Operculina complanata* DEFRANCE. Recently YABE and MABUTI[40] found a *Miogypsina* bearing limestone in the Miocene in Okayama pref. The molluscan fauna of the Uetuki series is closely allied to that of the Heiroku sandstone in North Tyôsen.

The Heiroku sandstone bed is overlain by the Banko and Kantin beds, containing *Mastodon (Trilophodon) angustidens* (CUVIER), whence it follows that the Heiroku bed is older than the age represented by *Mastodon (Trilophodon) angustidens* (CUVIER).

The Molluscan fauna of the Enniti series of south Tyôsen (Corea) was studied by K. KANEHARA[41], who concluded that the series may be contemporaneous with the Huzina and Kimati bed, and the writer's Kadonosawa series, as judged from its faunal characters.

The so-called Misaka formation is a thick volcanic and pyroclastic rock series developed around Mt. Huzi. This formation contains *Lepidocyclina* and *Miogypsina* foraminifera. According to K. YAMAMOTO *Lepidocyclina* bearing limestone occupies the lower horizon of the Misaka series, while *Operculina* and *Miogypsina* occupy a horizon above the *Lepidocyclina* zone in the Misaka region.

From the stratigraphy given above, the writer concludes that the Japanese Lower Neogene has a *Lepidocyclina* bearing bed at the lowest and *Miogypsina* and *Operculina* bearing beds above that; and that the *Desmostylus japonicus* IWASAKI and TOKUNAGA beds occurs in a slightly higher horizon. Also that these three horizons, the upper two horizons at least, may occupy one series of formations. He also concludes from its mammalian fauna that the upper of these horizons,

39) E. SAKAI, *Jour. Geol. Soc. Japan*, **42** (1935), 161.
40) YABE and MABUCHI, *Jour. Geol. Soc. Japan*, **41** (1934), 161~2.
41) K. KANEHARA, *Jour. Geol. Soc. Japan*, **43** (1936), 73~103.

at least, may be Middle Miocene (=Vindobonian).

In this connection it is notable that the most of these fossil bearing series in Japan are either preceded by volcanic rock formations at their bases or are underlain by volcanic and pyroclastic rocks that sometimes gradually transit into these upper series with but little difference in geologic age between them. This stratigraphic relation may indicate the existence of a close relationship between the epeirogenetical crustal movement and regional volcanic activities. The writer has referred to the marine transgression of the early Miocene in Japan in his previous paper. His early Miocene transgression, namely his early Kadonosawa transgression, agrees with the transgression of the *Lepidocyclina-Miogypsina-Operculina* and *Desmostylus* bearing series that were preceded by the regional volcanic activities just referred to.

---

40. 秋田縣由利郡地方の高瀬川綠色凝灰岩及び日本の下部新第三系の對比

地震研究所 大 塚 彌 之 助

緒論に於いてこの地方の層位學的，古生物學的研究の概略を記した.

次にこの地方に發達する地層の層序を記し，最後に古生物學上より高瀬川凝灰岩層の地質時代を論じ，高瀬川凝灰岩層の上半は男鹿半島の臺島砂岩，青森縣の追良瀨統，岩手縣の門ノ澤統と對比できるやうに見えると結んでゐる.

日本の下部新第三系の對比は上記の對比論に基き第 V 表の如き對比を行ひ，之の對比表に關する簡單な說明が附してある.

附記として火山活動と造陸運動的地殼運動との密接な關係が注意してある.

Loc. in Fig. 1	Locality
1.	West Hokkaidô
2.	Aomori pref.
3.	Iwate pref.
4.	Oga penin.
5.	South. Akita pr.
8. 6.	Sendai
7. 11,	Niigata pref.
9.	Is. Sado
10.	Hukusima b.
14.	Toyama pref.
12.	Zyoban coal.
13.	Noto penin.
18.	Gihu pref. (Mino)
17.	Simane pref.
20.	Tuyama
24.	South Tyosen
23.	North Tyosen

Table V. Correlation of old Neogene in Japan. [1936, OTUKA.]

Loc. in Fig. 1	Locality	Basal complex	Palaeogene	Miocene Lower	Miocene Middle	Miocene Upper	Lower Pliocene.
1.	West Hokkaidô	Palaeozoic & granite etc.		Hukuyama series	Kunnui series	Yakumo series	Kuromatunai series
2.	Aomori pref.			Oodose series	Oirase series	Azigasawa series	Wakayama series
3.	Iwate pref.	Palaeozoic etc.		Yotuyaku series	Kadonosawa series		Suenomatuyama serie
4.	Oga penin.			Innai ser.	Ogasima series		Yuri series
				Sugoroku bed	Daisima s.s.	Onnagawa-	Kitaura-Wakimoto be
5.	South. Akita pr.			Lower Takasegawa	Upper Takasegawa	Hunagawa bed	Hosogoe-Katurane -Wakimote bed.
8. 6.	Sendai				Saoyama group Siogama bed		
7. 11,	Niigata pref.	Granite and Palaeozoic etc.			Kubiki series		Tyuetu series
9.	Is. Sado	Palaeozoic etc.		Aikawa ser.	Nakayama series		Sawane series
10.	Hukusima b.	Palaeozoic etc.		Ryozen volc. compl.	Yanagawa series		
14.	Toyama pref.	Palaeozoic. Jurassic etc.		Basal volc. Yatus ser	Yatuo series		
12.	Zyoban coal.	Palaeozoic etc.	Siramidu series	Yunagaya series		Sirado series	Taga series
13.	Noto penin.	Gneiss and granite.		Dômi series	Nanao series: Nanao bed	Wakura bed	Omma series
18.	Gihu pref. (Mino)	Palaeozoic etc.	Nakamura beds.	Hiramaki group. ?	Tukiyosi bed Togari bed		
17.	Simane pref.			Volc. rock	Kimati and Huzina beds		
20.	Tuyama	Palaeozoic etc.			Uetuki and Tuyama bed		
24.	South Tyosen	Palaeozoic etc.	Tyôki bed		Enniti series		
23.	North Tyosen	Palaeozoic etc.	Ryûdo bed		Meisen group. Heiroku-Kantin-Banko beds		

Desmostylus.
Operculina and Miogypsina
Amphilepidina

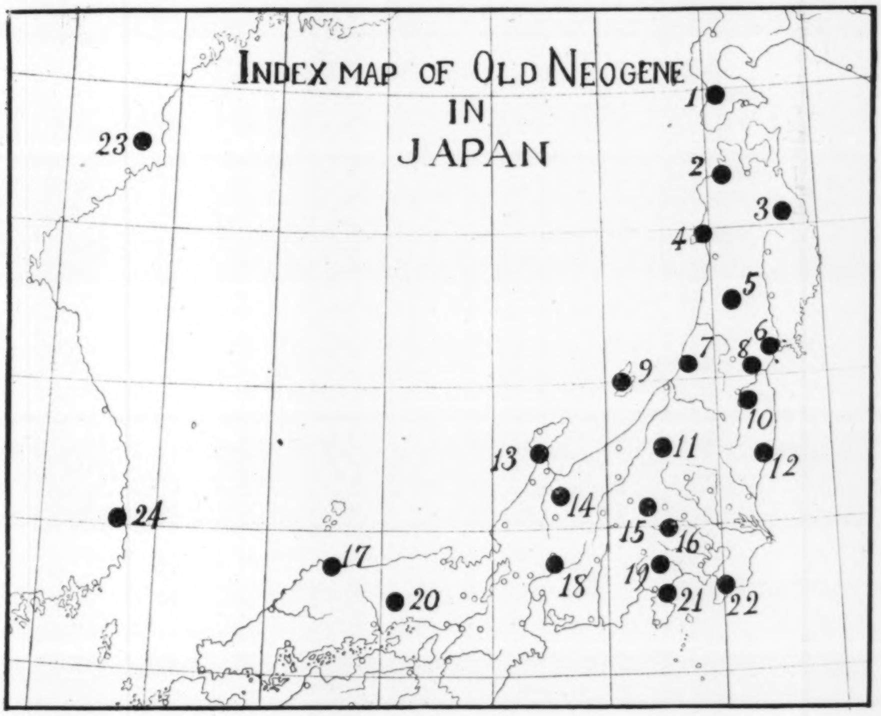

Fig. 1. Index map of the old Neogene in Japan.

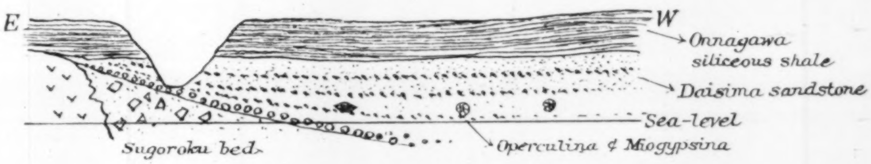

Fig. 2. Schematic sketch of the coastal cliff near Nisikurosawa.

Fig. 3.

Fig. 4.

Fig. 3. *Dosinia (Kaneharaia) kaneharai* YOKOYAMA. (Height 51·0 mm.)
Fig. 4. *Phalium yokoyamai* NOMURA et HATAI. (Largest diameter 27·0 mm.)

(震研彙報 第十四號 圖版 大塚)

41. *Geology and Petrography of Io-sima (Sulphur Island), Volcano Islands Group.*

By Hiromichi TSUYA,

Earthquake Research Institute.

(Read March 16, 1936.—Received June 20, 1936.)

Introduction.

Io-sima, situated 24°47′N. and 141°18′E., or Naka Io-sima, as it is frequently called to distinguish it from Kita Io-sima (San Alessandro I.) and Minami Io-sima (San Augustino I.), is a volcanic island entirely composed of andesitic rocks showing a distinct alkalic tendency. Although his opportunity in 1935 of studying this island was restricted to only four day's of field-work, the writer succeeded in obtaining some critical data concerning the geologic structure and rocks of this island, which will now be described in some detail.

Morphology.

In outline, Io-sima, which is the largest of the Volcano Islands group, is quite unlike the circular or elliptical form of the lesser ones (Kita Io-sima and Minami Io-sima) of the group. It has the form of a gourd with its neck at the S. W. end, with a SW.-NE. length of about 8 km and widths of from 1000 m to 4 km. As viewed from the sea it has the appearance usual to flat-topped islands of raised coral reefs, although its SW. end rises as a conical hill above the adjoining flat ground. The submarine topography roundabout suggests that the island represents the supermarine part of a large and flat dome-shaped swell that rests, in common with the lesser islands of the group, on a submarine ridge which, lying about 1000 m below the sea, separates the deep trough on the east of the island from the deep on the west.

Morphologically, the island may be divided into three parts: Motoyama, Suribatiyama, and Tidorigahara.

1. *Motoyama.* Occupying the NE. half of the island, Motoyama is a flat-topped, dome-shaped hill rising at its central part to a height 116 m above the sea. It is surrounded by vertical sea-cliffs on all sides, except at its SW. side where it is connected by a flat (Tidori-

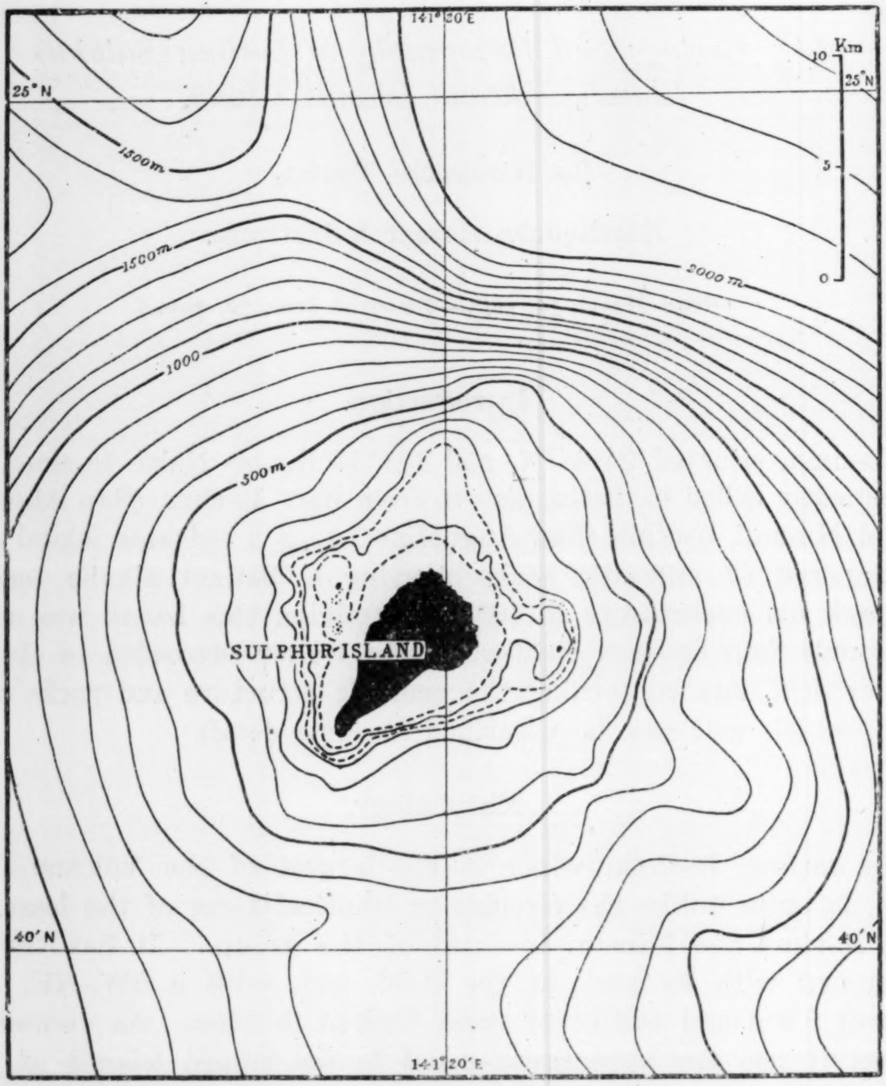

Fig. 1. Position of Sulphur Island in relation to the submarine areas about it. (Based on the chart, No. 50, of the Hydrographic Office, Imperial Japanese Navy).

gahara) with Suribatiyama. The sea-cliffs around Motoyama enclose flat coastal terraces that rise 5∼10 m above the sea and generally terminate abruptly inland in cliffs. These inland cllifs again enclose a series of higher inland terraces that are completely separated from the present sea. The inland terraces are displayed most magnificently on the N. and NE. sides of Motoyama, where they rise one above another up to the summit, being bounded respectively by vertical cliffs, 5∼20 m in height, each of which runs nearly parallel to the present coast. Thus the N. and NE. sides of Motoyama display as

a whole a stepped topography. The S. side, where such inland terraces are generally absent, shows a gentle, uniformly curved slope. The SW. side descends gradually to the flat of Tidorigahara.

The terraces, with which Motoyama is surrounded, are undoubtedly uplifted wave-cut platforms, for not only are they planed across gently dipping strata of the tuff of which Motoyama is built, but they leave many traces of marine erosion. They are besides covered locally with thin beds of old beach-gravels and -sand; curiously curved rock-pinnacles are left on the terraces; while the inland cliffs, which represent old marine cliffs, are here and there deeply caved. The summit of Motoyama, wherein may be traced many marks of the marine erosion, is rough and rocky and traversed by fissure-like caves and depressions. Many reef-forming corals, which, according to T. Wakimizu[1], are of Recent and even of forms now living, are found preserved there in excellent condition.

From the foregoing facts it is evident that the terraces were formed during intermittent halts in a succession of uplifts to which Motoyama would have been subjected. Since the terraces grew outward through progressive uplifts, the highest one in the central part must be the oldest, the lower terraces having been formed successively later. It is thus quite likely that Motoyama was at first below sea level, and that its emergence occurred in recent geologic times, seeing that the reef-forming corals are preserved on the erosion relics above the oldest terrace. The first emergence of Motoyama and its succeeding stepwise uplifts can however be explained as the result of neither eustatic lowering of the sea nor regional crustal uplift. If the terraces were cut by successive lowering of the sea due to either of these causes, then equivalent terraces should probably be found on the adjacent shores. But seeing that none are found on the lesser islands of the Volcano group nor on the Bonin Islands, it seems necessary to invoke a more local cause than general crustal movement, and it is suggested that Motoyama emerged as the result of local upwarping of the sea-floor due to injection of magma that occurred as a cripto-volcanic phase in the course of the volcanic history of the island. Such an interpretation of the emergence of Motoyama is entitled to serious consideration, particularly as there are several additional factors in its favor, as will be mentioned presently.

2. Suribatiyama (Mt. Pipe). Suribatiyama is a truncated conical volcano with a base diameter of about 1km. At its summit is a funnel-shaped crater, roughly circular in outline and about 500 m in

1) T. WAKIMIZU, *Report Imp. Earthq. Inv. Comm.*, **56** (1906).

diameter. Nearly three parts of the crater-rim has an elevation of over 130 m, the highest point lying NE., where the rim reaches a height of 165 m above the sea. The crater-walls are very steep,

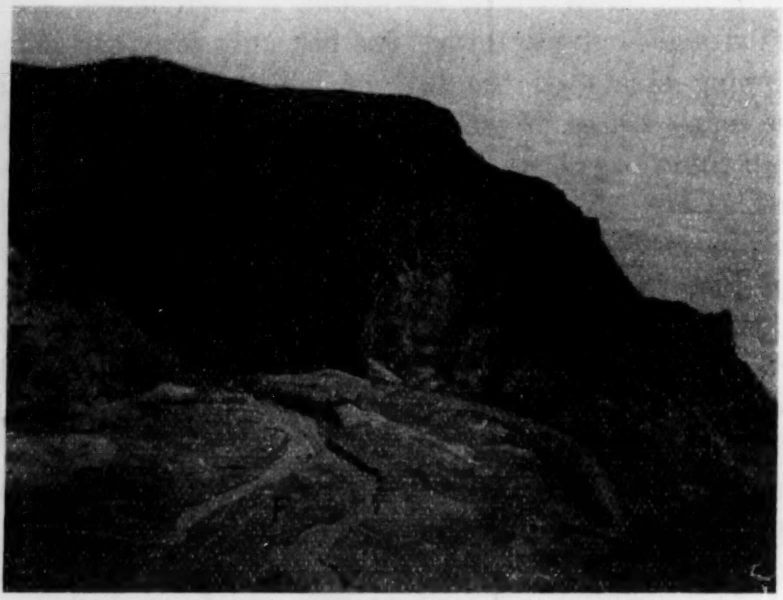

Fig. 2. The inside of the Suribatiyama crater, looking down from the NE. rim of the crater.
S: Solfataric pit, F: Crater-floor, G: Gap in the NW. crater-wall.

nearly vertical locally, although the W. wall is breached by a steep-walled gulch. The crater-bottom, which is circular in outline with a diameter of about 300 m, has a depth of about 100 m as measured at the highest point of the crater-rim. It is a flat ground covered with detritus from the surrounding walls, although it is marked by numerous branched stream-channels which converge to an axial channel that drains to the breach of the W. wall.

The outer flanks of the cone slopes at an angle of about 30° for only a little distance down the crater-rim, showing a natural slope of loose material ejected from the summit-crater, whence downward they form an almost vertical cliff with heights varying from over 100 m on the SW. side to 20 m on the NE. On the NE. side fronting the flat of Tidorigahara, the cliff is fringed along its base by an uplifted terrace, about 20 m high above the sea, while on the SW. side the much higher vertical cliff faces directly the present gravel beach without being fringed at its base by the uplifted terrace corresponding to that on the NE. side.

The vertical cliffs clearly represent old sea cliffs that have been cut away from the lower flanks of the cone by marine erosion at the

time the sea stood 20 m or more above its present level, and when the cone was surrounded by that sea as an isolated insular volcano. Although the old sea cliff on the NE. side has undergone but little alteration since its position became out of reach of the waves, while that on the SW. side has suffered severely from the prevailing wind and the consequent high waves from the southwest. The cliff on the SW. side has thus been excavated by the elements, showing many scars and slips, it being now higher than it was originally, its upper edge reaching a little below the crater-rim. The absence of the uplifted terrace on that side probably indicates that quarrying is more active than benching.

3. *Tidorigahara.* Tidorigahara, by means of which the preceding two parts of the island are connected with each other, is an elevated plateau land elongated in a NE.-SW. direction for a distance of about 2 km with breadths varying from 1000 m near Suribatiyama to 2 km at the opposit side. The SW. part of this area is about 40 m above the sea, and from this point the surface rises gradually to the northeast until it virtually reaches the summit of Motoyama. The NW. and SE. sides of the land, which for the most part show a gentle outward slope without any terraces or inland cliffs, are bounded respectively by extensive sand beaches extending in fairly straight lines for nearly 2·5 km between the cliffbound coasts of Suribatiyama and Motoyama.

A large part of Tidorigahara is veneered with drifting dune sand. Although some of the dunes are barchans of a more or less regular form, most are irregular heaps of sand, rather stable in position owing to the growth of grass and bushes. Between these heaps of sand are numerous conical depressions or holes varying up to a few meters in diameter, and arranged in lines running NE.-SW. Although some of them are decidedly solfataric, several traces of which remain thereabouts, most are of unknown origin. The system of holes and fissures indicates however possible lines of rupture along the longer axis of the island due to the upwarping to which the island has been subjected.

Geology.

Sulphur Island is formed entirely of volcanic rocks and their detritus, which the present study has shown to be separable from older to younger into the following seven formations.

1. Motoyama bluff tuff and Suribatiyama bluff tuff.
2. Motoyoma intrusive rock and Suribatiyama lava.

3. Suribatiyama cone ejecta.
4. Tidorigahara sand bed.
5. Terrace deposit.
6. Dune sand.
7. Beach deposit.

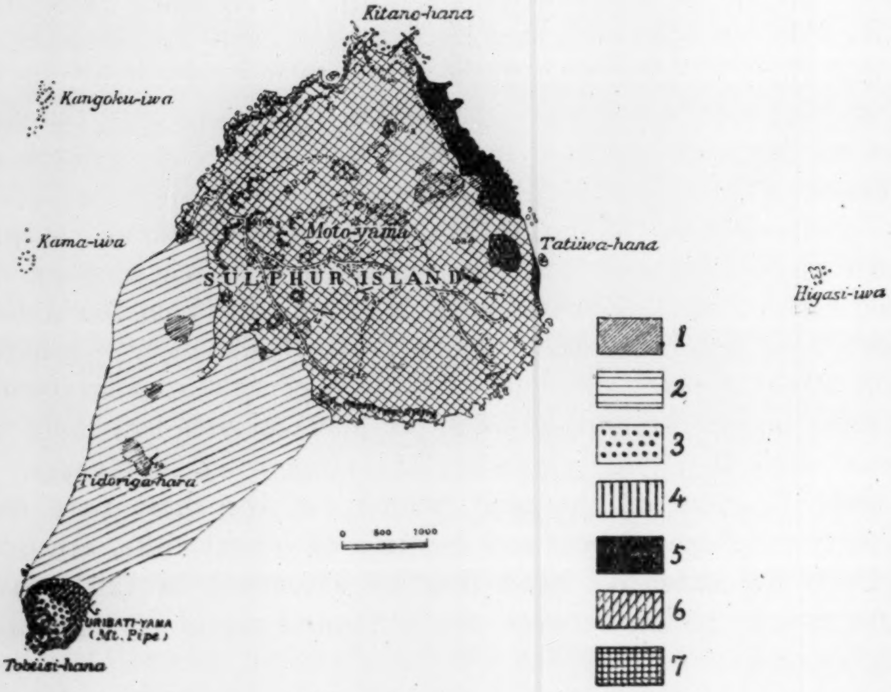

Fig. 3. Geological map of Sulphur Island; beach- and terrace-gravels, and dune-sand omitted.

1. Solfatara.
2. Tidorigahara sand bed.
3. Suribatiyama cone ejecta.
4. Suribatiyama.
5. Motoyama intrusive.
6. Suribatiyama tuff.
7. Motoyama tuff.

1. Motoyama Bluff Tuff. The oldest formation in the island, which the writer calls Motoyama bluff tuff, because its outcrops are characteristically bounded by bluffs (sea- and inland-cliffs), forms the greater part of Motoyama. Stratification is evident, though usually of a rude kind, showing gentle dips, mostly up to 15°, which radiate in all direction from the northeast-side part of Motoyama as the centre.

The tuff is divisible roughly into two horizons, according to the size of material of which it is composed. The upper horizon is represented by a yellowish-gray, fine, pumiceous tuff, occasionally interstratified with sandy tuff or tuff-breccia. Being covered locally with terrace deposit and blown sand, it is distributed widely and continuously not only in the central part, but on both the northern

and southern sides of Motoyama. On the southern side, where the uplifted coastal terraces are generally absent, strata of fine pumiceous tuff occur continuously from central Motoyama downward and sink on the southern shore below the sea. They show a gentle southward dip coinciding with the surface slope of that side. On the northern side, however, the northwardly dipping strata are cut into vertical cliffs at the edges of the step-like uplifted terraces that are planed across the strata.

The lower horizon of the bluff tuff is represented by a pyroclastic accumulation, the greater part of which may fairly be termed obsidian agglomerate. It forms the lower parts of the inland- and sea-cliffs on the northeast side of Motoyama, and is intruded by the Motoyama intrusive to be described later. It contains abundant lava pieces, mostly of obsidian form, varying up to about 1 m in diameter. Bedding is more or less evident in the finer part of the accumulation; and even in the coarser, stratification of a kind is apparent in the distribution of the enclosed blocks.

The Motoyama bluff tuff is wholly volcanic, consisting exclusively of trachytic materials. Neither detrital material from an adjoining shore nor fossil has beed observed in it. But it is quite likely that the tuff is a product of submarine eruptions. T. Wakimizu[2], who visited the island in 1905 on his way to explore the ephemeral volcanic island that formed in 1904 near Minami Io-sima, suggested that Motoyama itself is a dome-shaped tuff-volcano that emerged in very recent geologic time. Although there seems to be little doubt that the tuff is of recent geologic age, his suggestion that Motoyama itself represents a tuff volcano is unacceptable to the writer, for if such were the case, then it should have its crater. No topographic feature of the summit of Motoyama gives any proof of the former existence of a central crater from which the materials composing the tuff would have been ejected, nor is there any such regular disposition of materials in the tuff as to suggest that the materials had been ejected radially from the summit of Motoyama as the centre. T. Tsujimura's opinion[3] with respect to the morphological aspect of the island is that Motoyama may be a dome that resulted from upwarping of the tuff. This is the conclusion the writer arrived at independently and which he sets forth in this paper, namely, that after being deposited nearly horizontally on the sea-floor at the time of its ejection from a submarine volcano, the tuff had been upwarped and placed in the

2) T. Wakimizu, *loc. cit.*
3) T. Tsujimura, *Jour. Geol. Soc., Tokyo*, **24** (1917).

present position. The occurrence of a trachytic intrusive into the tuff at Motoyama may be taken as indicating the probability of a genetic connection between its intrusion and the upwarping of the tuff.

Suribatiyama Bluff Tuff. Along the NE. coast of Suribatiyama for a distance of about 200 m southward from the SE. corner of Tidorigahara, occurs a series of rudely stratified agglomerate and sandy tuff, which the writer calls the Suribatiyama bluff tuff. In the whole northern half of the coast it forms a raised wave-cut terrace, about 20 m high, veneered with a terrace deposit; while in the south, where the terrace has entirely been eroded away by the quarrying action of the waves, it is exposed near the base of the precipitous cliff, being overlain by the Suribatiyama lava to be described later. The tuff thus represents the oldest formation visible of Suribatiyama. Its strata as a whole show a gentle southeastward dip. The sandy part of the strata is composed of small fragments of pumice and obsidian, together with isolated feldspar crystals, while the agglomeratic part contains angular blocks, up to 1 m in diameter, of obsidian, pumice, and compact lava of trachytic nature.

The direct stratigraphical relation between the tuff and the Motoyama bluff tuff is veiled by the Tidorigahara sand bed which separates the exposure of the one from that of the other. Y. Kikuchi[4], who visited the island in 1887 first as geologist, regarded the tuff under discussion as representing an outlier of the Motoyama tuff. The writer also believes that the Suribatiyama bluff tuff as a whole may probably be correlated with the lower horizon of the Motoyama bluff tuff formation. The close resemblance, structural as well as petrographical, between them suggests that they are the products of submarine eruptions from one or more than one source during the same age, although there is no definite evidence of this age, and that they join each other at the base of the Tidorigahara sand bed.

2. Motoyama Intrusive Rock. This mass, which is exposed patchwise at and near the NE. shore of Motoyama, extends along the shore southeastward for a distance of about 3 km from the northern promontory (Kitano-hana). Although this body has been neglected by many geological visitors to the island, its occurrence was noted by F. Homma[5], who, in an account of his tour to the Bonin Islands, wrote on the geology of the island with brief petrographic descriptions. He regards the mass as a lava-flow associated with th Moto-

4) Y. KIKUCHI, *Toyo Gakugei Zassi*, **5** (1888).
5) F. HOMMA, *Tikyu* (*the Globe*), **4** (1925).

yama tuff, and in his geologic map, indicates only about a half of its actual distribution. The writer however finds that the mass occurs as an intrusive into the Motoyama tuff instead of as a lava-flow. At the middle part of the north-eastern shore, where a rocky coastal terrace rises about 15 m above the sea, there is a good outcrop on the face of the sea-cliff that shows the actual mode of occurrence of the intrusive mass, as diagrammatically illustrated in Fig. 4.

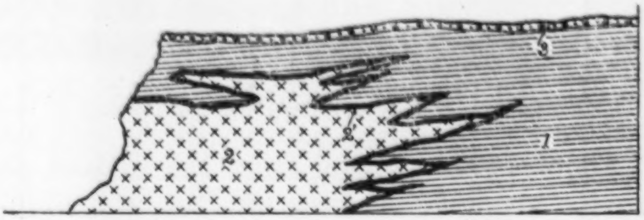

Fig. 4. Diagrammatic sketch showing the exposure in a sea-cliff on the NE. coast (Fig. 5.). 1: Motoyama tuff, 2: Motoyama intrusive, 2′: Quenched marginal facies (obsidian) of the Motoyama intrusive, 3: Terrace deposit (gravel and sand).

The sea-cliff, which represents a natural profile of the coastal terrace, consists of a rudely stratified sandy tuff or tuff-breccia and a massive trachytic rock, both of which are covered unconformably with a thin bed of terrace gravels. The main mass of the trachytic rock has cut the tuff bed vertically, and several wedge-shaped offshoots of the former, 0·5∼1 m in thickness, have intruded laterally into the latter to about 5 m. The offshoots have well-defined walls exhibiting a pitch-black quenched border against the tuff into which they have intruded. It is possible that the intrusive had some effect on the structure of the adjoining tuff, seeing that the latter near its contact with the former displays an irregularly bent stratification.

Fig. 5. Motoyama intrusive exposed in a sea-cliff on the NE. coast. (Fig. 4.)

A similar intrusive relation between the trachytic rock and the Motoyama tuff may be seen at a number of points in the inland-cliffs about 500 m south of the last-mentioned outcrop. The strata of tuff show an inclination entirely independent of the intrusive rock exposed,

the former being traversed by the latter with highly inclined or quasi-vertical walls, although the very contacts between them have generally become indistinct as the result of decomposition due to the solfataric gases that frequently have their outlets on or near the contacts.

About 1000 m inland from the eastern shore is an exposure of the intrusive about 70 m above the sea, the highest exposure of the mass so far observed. This mass forms a sheet, less than 1 m in thickness, with a southward dip of about 35°. Its floor is an agglomeratic tuff representing the lower horizon of the Motayama tuff. Although the roof-rock is not exposed in contact with the sheet, it may be that it is represented by the fine pumiceous tuff that is exposed about 300 m seaward from the latter, the dip and strike of which are 35° S. and E.-W. respectively. The steep dip of the roof-rock, which is never found elsewhere, may be explained as a local effect caused by intrusion of the sheet rock.

Besides the exposures above described, the intrusive rock is exposed at several places on the uplifted terraces along the northeastern shore as erosion-relics projected above the flat surface of the latter, although its intrusion structures are veneered with the terrace deposit.

Petrographical characters of the intrusive mass are fairly uniform throughout all the exposures, suggesting that the exposed parts of the intrusive may be the apophysal border facies of a more extensive and continuous mass underlying a large area of Motoyama where it does not reach the present surface. It is inferred from the dome-shaped structure of the Motoyama tuff that, at a moderate depth beneath Motoyama, the continuous intrusive mass oocurs in the nature of a laccolith, and that the intrusion of this buried laccolith caused the dome-like upwarping of Motoyama. If that is the case, the exposed intrusive body seems to be offshoots insinuated through ruptures in the roof (the upper horizon of the Motoyama tuff) of this supposed laccolith at the time of its intrusion.

Suribatiyama Lava. This mass is exposed in the old sea-cliffs around Suribatiyama, forming a lava-flow about 20 m thick. It does not show a quaquaversal dip from the summit crater of Suribatiyama as the centre, but slopes gradually southwestward from the northeastern side of the volcano, where it rises about 40 m above the sea up to the upper edge of the old sea-cliff, to the rear where it descends to near the base of the cliff, beyond which the lava is buried beneath the beach gravels. Although S. Kozu and M. Watanabe[6] mention that

6) S. Kozu and M. Watanabe, *Proc. 3rd. Pan-Pacific Sci. Congr. Tokyo*, **1** (1926).

Fig. 6. Diagrammatic section of Suribatiyama from SW. to NE.
1. Suribatiyama tuff. 2. Suribatiyama lava.
3. Suribatiyama cone ejecta. 4. Tidorigahara sand bed.
5. Terrace gravel. 6. Dune sand.
7. Beach gravel. S'. Solfatara.

"the cone is formed of the different layers of lava-flows", no lava-flows, except the present one, are actually observed.

The lava overlies disconformably the Suribatiyama bluff tuff. Near the contact with the latter the lava develops as a glassy, more or less vesicular form, while its inner part is uniformly and highly

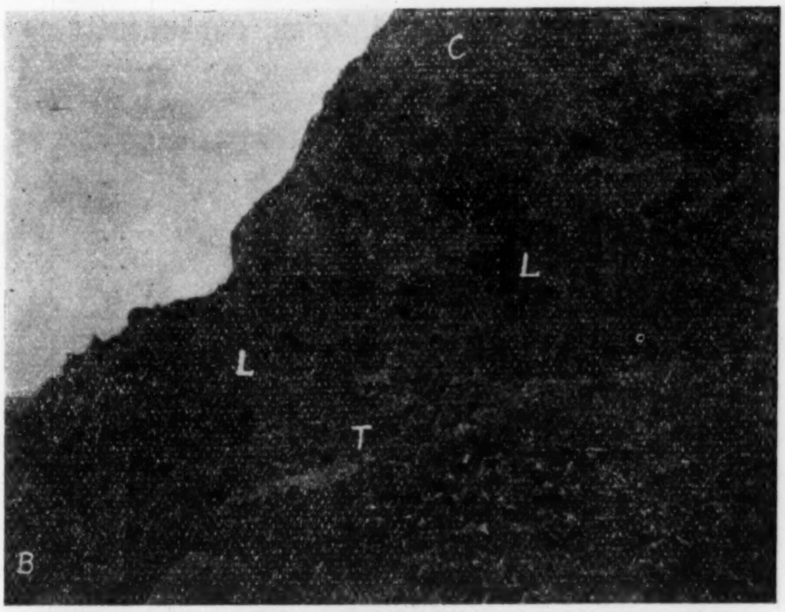

Fig. 7. The lower part of the E. slope of Suribatiyama.
B: Beach gravel. C: Suribatiyama cone ejecta.
L: Suribatiyama lava. T: Terrace gravel.

crystalline with no sign of flow structure, but displaying gross columner jointing. The roof-rock of the lava is not uniform throughout; on the southwest side it is represented by an accumulation of angular lava blocks or a breccia, and on the northeast, by a fine whitish tuff.

The extrusion of the lava may be nearly contemporaneous with the intrusion of the Motoyama intrusive. Although there is no structural evidence that the extrusion took place at the present summit-crater of Suribatiyama, there is no reason to suppose that the lava has come from Motoyama as the centre. Therefore, even though the

lava is not the product of the present Suribatiyama crater, it would have extruded through a conduit not far from the latter, whence it is possible to regard the Motoyama intrusive as having been injected satellitically from this conduit at a moderate depth. Whether the postulated conduit lies beneath Suribatiyama or not, the Suribatiyama lava for the most part would primarily be below the sea, seeing that the overlying whitish tuff seems to be a submarine deposit.

3. *Suribatiyama Cone Ejecta.* The Suribatiyama cone ejecta have accumulated as well-defined strata forming the conical part of the whole upper half of Suribatiyama. These strata for the most part, except the lowest one, fall outward with dips varying up to 35° from the summit-crater of the cone as the centre. The lowest bed, so far as observed on the northeast flank of the cone, is the whitish tuff which, as noted above, seems to be a submarine deposit, while on the southwest flank it is represented by an agglomerate consisting of

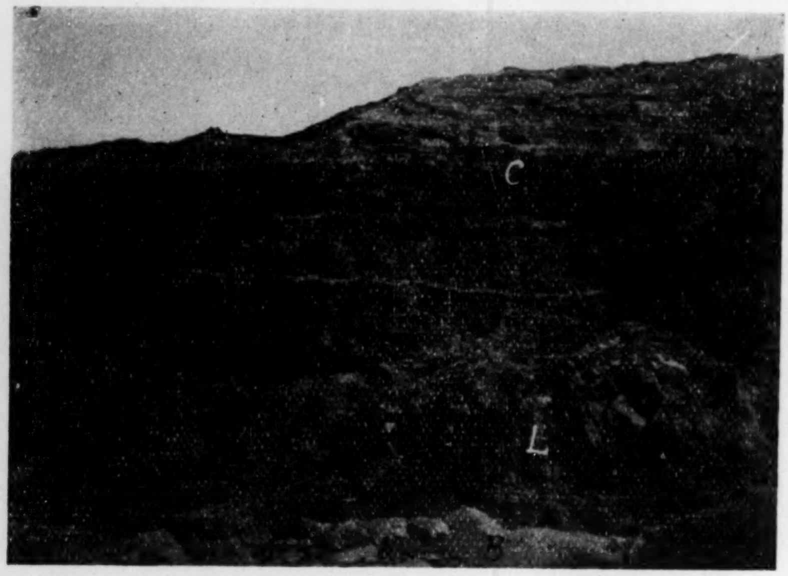

Fig. 8. The SE. slope of Suribatiyama, looking up from the SE. coast.
B: Beach gravel C: Suribatiyama cone ejecta
L: Suribatiyama lava.

angular lava blocks and ash material. Then follow alternating beds of finer and coarser grayish tuff which are exposed not only half way down the lateral slopes, but as the northeast crater-rim. Next to these beds come massive or rudely stratified beds of black scoriae occupying the whole outer slope near the crater-rim. A few accessory ejecta, evidently signs of the last explosive activity of the volcano, are scattered over the black scoriae.

The steep quaquaversal dip of the strata is evidence that they were subaerially accumulated on the underlying Suribatiyama lava after the sea had dropped relatively from the old sea-cliff with which the lava is bounded. As will be discussed later, the eruptions from which the cone was formed, must have occurred shortly before or during the deposition of the Tidorigahara sand bed now to be described.

4. *Tidorigahara sand bed.* The extensive flat of Tidorigahara should not be interpreted as an abrasion platform of the Motoyama bluff tuff, but as being formed largely of a sand bed thinly veneered with dune sand, although the exposure of the sand bed is limited to a few points in Tidorigahara, where the overlying dune sand is removed by artificial cutting or by solfataric action.

The sand bed as a whole must not be confused with the bluff tuff. Neither must the former be confused with the dune sand, although the materials composing them are quite the same. Thus the sand bed is composed of sandy grains of trachytic rock (pumice, obsidian, compact lava, and isolated feldspar crystals) and tuff fragments. These materials, which are evidently water-worn, are consolidated as a more or less coherent bed displaying irregular stratification with a gentle dip to the southeast.

Although the very bottom of the sand bed has not yet been uncovered, it is highly probable that the bed rests on the bluff tuff with the Suribatiyama cone ejecta in between them, seeing that not a few blocks of these supposed bed-rocks, which may owe their origin to solfataric explosions of unknown date, lie scattered at and near the solfataras in the northeastern part of Tidorigahara. Since it is expected that the surface of the Motoyama tuff gradually descends from Motoyama to the bottom of Tidorigahara and joins a similar tuff at the base of Suribatiyama without any marked discontinuity between them, the thickness of the sand bed may be no more than 50 m.

Both structure and composition of the sand bed indicate that the materials composing it must have been derived at second hand from either Motoyama or Suribatiyama or from more than one such source in the neighbourhood. The limited distribution of the sand bed and the well-worn form of its material point to the probability that Sulphur Island, in the course of its emergence, passed an epoch when, while its northeastern and southwestern parts (Motoyama and Suribatiyama) had emerged, its central part (Tidorigahara) remained as a slightly submerged sea-floor, and that the materials derived from the emerged land parts were accumulated on the sea-floor between these lands as

the Tidorigahara sand bed. Together with the farther uplifting of the land parts subsequent to its deposition, the sand bed must have emerged to the present position with a slight tilt southeast.

5. *Terrace Deposit*. The terrace deposit, which consists of gravels and sand, lies on the floors of the terraces that cut into the bed rocks of the island. Although the deposit is not uniformly distributed on the floor of each terrace, locally it attains a thickness of more than 1 m. Thus whereas the terraces are usually covered on their inland edges, where they abut against the old marine cliffs, with gravels and sand accumulated as old beach ridges more than 1 m in height, they are swept clear in places at or near their seaward edges.

The terrace deposit at the northeastern foot of Suribatiyama, which is more than 2 m thick, consists practically of lava cobbles and lava blocks up to 2 m diameter, derived from the lava-cliff above the terrace. On the northeastern side of Motoyama, the terrace deposit on the lower terraces are composed of gravels and sand derived from the underlying Motoyama tuff and trachytic intrusive rock, while that on the higher terraces including the summit part of Motoyama, where the bed rock is exclusively the tuff, consists wholly of gravels, together with sand of this rock. The tuff gravels show generally a disk-like form, mostly less than 50 cm diameter, and 5～10 cm thick, as the result of being easily stripped off as platy blocks along the plane of stratification of the rock.

6. *Dune Sand*. The surface of Tidorigahara is covered with loose sand no more than 1 m thick, although locally they form sand-drifts, several meters higher than the general surface. They consist of small fragments of trachytic rock, such as pumice, obsidian, scoriae, solid lava pieces, and isolated feldspar crystals, besides a few pebbles (5～10 cm dia.) of the same rock. Based on the observations of O. Warburg who, although not a geologist, writes on the geology of the island, J. Petersen[7] mentions the feldspar sand as having been derived from the Motoyama tuff. Wakimizu[8], who opposes Petersen's view, stresses the fact that the sand are volcanic material ejected from Suribatiyama during its eruptions. Wakimizu's view, however, does not appeal to the writer for several reasons. If the sand were ejected from Suribatiyama, similar sand ought to have been found on its outer flanks. They bear no physical resemblance to the ejecta on Suribatiyama, although petrographically both are of the same tra-

7) J. PETERSEN, Beiträge zur Petrographie von Sulphur Island, Peel Island, Hachijo and Miyakeshima. (1890).

8) T. WAKIMIZU, *loc. cit.*

chytic character. The isolated feldspar crystals which amount to about 85% of the sand, are rounded off their face angles, occasionally showing a perfectly rounded shape. The rest of the sand, together with additional large pebbles, are likewise rounded. Thus most of the sand are evidently water-worn, although their rounded forms might be the result of wind-abrasion that gave rise to the three-facetted stones that one meets with although rarely among them. Some of the pebbles moreover are of fine pumiceous tuff similar to the Motoyama tuff. It is therefore highly probable that, while one part of the sand is blown sand drifted from the shores by the wind, the other has been derived from the loosely-coherent sand bed underlying Tidorigahara.

7. *Beach Deposit.* The beach deposit, which is the youngest formation of the island, consists of gravels and sand besides a few remains of the living marine shells piled up on the shores by winds and storms. The beach gravels are well developed along the shores of both Motoyama and Suribatiyama, where the sea-cliffs above the shores are being attacked by the waves, while the beach sand are practically confined to both shores of Tidorigahara. The gravels and sand are lithologically similar to the terrace deposit already described.

Solfataras.

Sulphur Island has more than twenty solfataras, some of which are emitting steam and sulphurous vapors, the column of steam being visible some distance out at sea. These solfataras are aligned on what may be two intersecting fissures; the Suribatiyama solfataras on the one and the Tidorigahara and Motoyama solfataras on the other.

The Suribatiyama solfataras are arranged on a fissure running in a NNW.-SSE. direction —the trend of the island-chain of the Volcano group— through a gap in the northwestern wall of the crater. The most active of them in 1935 was located at the southwestern corner of the crater-bottom, where sulphurous gases and vapor were issuing with a hissing noise from a circular opening some 10 m in diameter. Rock decomposition due to solfataric action is complete at the surface where it adjoins the solfatara. Not only does it cover the bottom ground of the crater, but it extends to the outer slopes of the crater-wall. Thus the NW. and SE. slopes of the cone, where several solfataras, active and extinct, occur, have been similarly decomposed. An extinct solfatara marked by rock decomposition is located in an isolated position half way down the northeastern slope, where the cliff of the Suribatiyama lava has been reduced to a talus by means of which the sumnit is barely accessible. This solfatara, together with

the Tidorigahara solfataras next to be described, lies on a what may be a fissure running from the summit of Suribatiyama to Motayama through Tidorigahara.

Although the Tidorigahara solfataras are for the most part extinct, in the same areas are many traces of their former activity. Thus the surface of areas containing the solfatara have not only been incrusted by salt patches, but reduced by the thermal action of the solfataras to a fine sticky mud which dries out and becomes baked into a thin crust. There are local fissures and depressions in some of these areas. It is possible that the ground material of these areas consisting of the Tidorigahara sand bed was slowly carried away by the ground water owing to disintegration under the influence of solfataric action, with

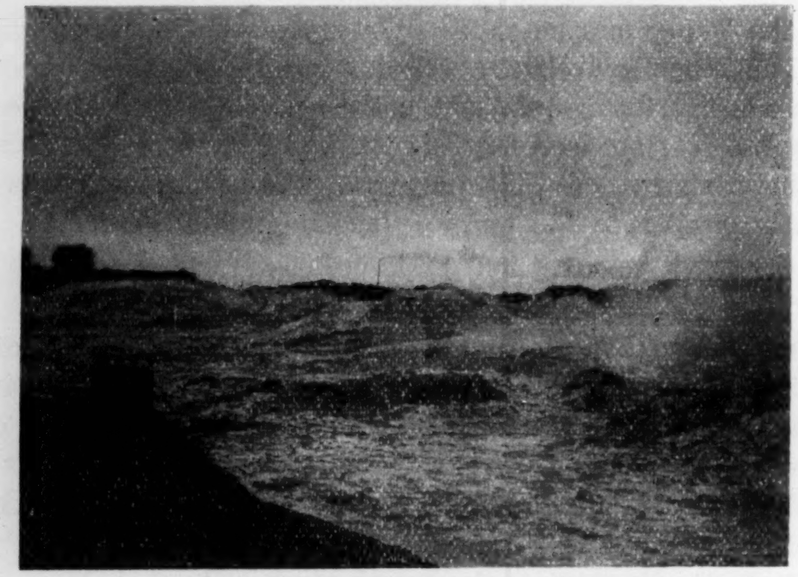

Fig. 9. Motoyama Solfatara.

the result that the ground was undermined and parts of the surface slumped in.

The Motoyama solfataras occur mostly in a zone extending northeast ward from the summit of Motoyama to the northeastern shore. The most active of them, in 1935, was situated at the summit, quantities of sulphurous vapors issuing from several orifices scattered over a large area. The ground forming the solfatara area, which is composed of Motoyama tuff, is much decomposed, the accumulation of incrusting salt being greater in this area than in any other. Thus sulphur deposits are now worked commercially, although still on a small scale. Near the northeastern shore, where, the trachytic intrusive is exposed in contact with the tuff, numerous solfataras are developed at or near

the contact between these rocks. On the SE. and NW. sides of Motoyama are almost no sign of solfataric activity, past or present, although a few solfataras, which are submerged at high water, occur close to the beach on these sides. The suggestion therefore arises that the solfataric vapors rise from the buried intrusive mass through ruptures in its roof (Motoyama tuff).

The temperatures of the solfataras are not the same, and no doubt they change from time to time. A vapor jet from a solfatara at the

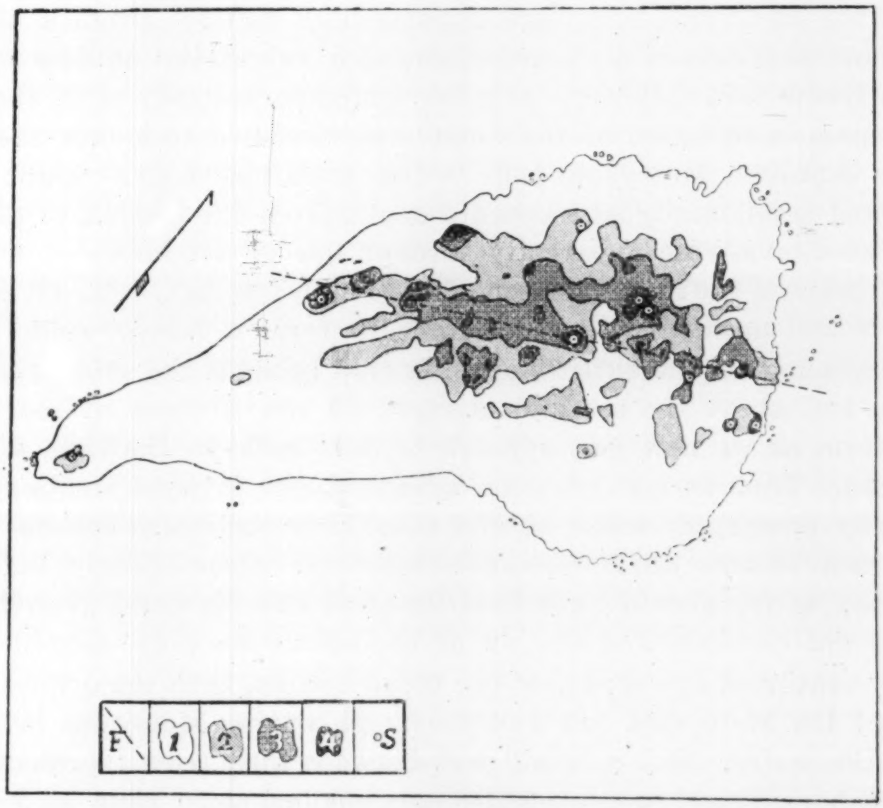

Fig. 10. Ground temperatures in Sulphur Island, May 1926. (After Toyoshima)

1: $<35°$C. 2: $\frac{>35°}{<60°}$C. 3: $\frac{>60°}{<100°}$C. 4: $>100°$C.

S: Solfataras F: Possible centre-line of solfataric activity.

summit of Motoyama showed, in 1935, a temperature of 102°C. (atm. temp. 28°), while another one on the northeastern shore had a temperature of about 80°C. The ground in the immediate vicinity of the active solfataras are, naturally, unpleasantly hot and dry, even ground some distance away from the solfataras showing temperatures higher than that of the normal ground. Thus, according to Toyoshima's systematic survey[9] conducted in May, 1926, the ground temperatures in

9) J. TOYOSHIMA, *Ringyo-siken-iho* (*Bull. Forestry Experim. St.*), **17** (1925).

the island 0·5 m below the surface were distributed as shown in Fig. 5.

Geological History.

From the foregoing descriptions, the geological history of Sulphur Island may be summarized as follows:

Whatever the history of the foundation may have been, there seems to be little doubt that the island is, geologically speaking, very recent. It first saw the light with the submarine explosive outbursts that gave rise to the Motoyama and Suribatiyama bluff tuffs. From a central vent, now represented by Suribatiyama, a submarine outflow of the Suribatiyama lava followed. Almost contemporaneously with the outflow began an injection of the Motoyama intrusive rock into the previously deposited Motoyama tuff. The intrusion, which might have originated satellitically at moderate depth from the conduit of the Suribatiyama lava, rose apparently through one or a number of fissures until it reached the lower horizon of the Motoyama tuff, where it spread laterally and upward with great force to form a laccomorphic mass. The beginning of the extensive uplift that brought the submarine Motoyama tuff above the sea and changed it into a dome of much the same form as we now see, appears to date back to the time of that intrusion. Thus as the intrusion advanced, the invaded strata of tuff gradually upwarped, while at the same time the ocean-bottom above the strata became shallower and shallower. Immediately before it emerged, its top should have been an ideal site for coral growth, forming a flat coral-covered summit of the submarine dome-shaped ridge.

By continued upwarping of the ocean-bottom, both the dome-shaped ridge of the Motoyama tuff and the neighbouring Motoyama lava rose above the water. But a small part between them, now represented by Tidorigahara, would have remained as a shallow sea. Thus, in its early stage, the present Sulphur Island consisted of a pair of smaller islands, Motoyama island and Suribatiyama island, separated by a shallow-water platform. These islands, as soon as they were formed, were attacked and reduced in size by marine erosion. The sandy material transported by the waves from the shores of these two supposed islands, were deposited on the shallow-sea platform as the Tidorigahara sand bed.

It was to the time of the deposition of the Tidorigahara sand bed that subaerial eruptions took place from a central crater, now represented by the Suribatiyama crater. The Suribatiyama cone ejecta are the products of these eruptions.

Together with the subsequent uplift of both Motoyama and Suribatiyama, Tidorigahara also emerged, the three parts having joined

together into one island as we see at present. The uplif. of the island was not continuous, but occurred intermittently for a long period with frequent halts of the sea, during which intervals marine erosion was active on weaker rock like the Motoyama tuff, giving to the island its present terraced feature. Such stepwise uplift will be naturally expected, it being likely that the intrusion of the Motoyama intrusive rock occurred recurrently through a long period of time.

Motoyama tuff being a fairly homogeneous rock, one would expect the number of terraces to be fairly uniform throughout, even when due regard is had to varying conditions, such as protection by reefs and heavier erosion on windward shores; yet it is considerably greater at the northern and northeastern sides of Motoyama than it is elsewhere. This expressive development the writer considers to be due to a slight southward tilt to which the island was subjected in the course of its uplift. The Motoyama intrusive and the lower horizon of the Motoyama tuff are exposed only near the northeastern shore, where the uplift was relatively great. A number of the shoals and reefs off the northern and northeastern shores may be detached fragments of the tuff and/or the intrusive, which at one time would be exposed continuously and extensively outward from the shores.

As stated above, Sulphur Island and its adjoining sea-floor during a recent geologic age was an area of local but great crustal instability, beginning with a period of volcanic activity and continuing with a complex sequence of stepwise uplifts that involve frequent and sometimes great sudden changes of sea-level. Minor uplifts continued after that time, and is doing so to the present day. Thus, according to Homma, there are several places, now many meters inland from the sea, from which it was once possible to fish, or launch canoes, so that the island must be rising, although little is known regarding the actual rate of such rising.

There is no volcanic material that was ejected since the Suribatiyama cone ejecta had been formed, nor is there any historic record of an eruption in the island. But volcanic activity is manifested in the island even at the present day by numerous solfataras. One of these solfataras on the northwestern side of Motoyama is said to have culminated a few years ago in ejecting a small volume of solid material. It is also said that detonations are often heard from the sea northeast of the island.

Petrography.

A number of authors, who have written on the geology of Sulphur

Island, have also touched on its petrography. Thus Kikuchi[10] wrote of the Suribatiyama lava as basalt. Petersen[11] described several rock specimens collected by Warburg from the island as augite-andesite, and classified them as vitrophyric, pumiceous, and sulphur-bearing of its kind. Wakimizu[12] also defined the Suribatiyama lava as augite-andesite. The last two writers identified the feldspar phenocrysts in all the rocks of the island as an oligoclase. Later, Homma[13] adopted trachyandesite, instead of augite-andesite, as a preferable name for the Suribatiyama lava as well as for his "lava-flow" (the writer's Motoyama intrusive) exposed at Motoyama, citing in this connection the occurrence of not a few blocks of augite-syenite in the tuffs and terrace deposits. He identified the feldspar phenocrysts in the lavas and the isolated feldspar crystals in the Tidorigahara sand as an andesine—an identification to which the writer also arrived independently. Kozu and Watanabe[14] also refered the "lavas" of Suribatiyama to trachy-andesite, and proposed a new name "Iwozimite" for these rocks, naming it afer the island.

As noted above, the rocks of the island, which could probably be determined only with difficulty from hasty cbservations, were defined in various way by different authors. So far as the writer's observations go, they may be called trachyandesite since they are close in petrographic characters, microscopical as well as chemical, to some trachytes of the Pacific islands rather than to the common Japanese pyroxene-andesites. This will be seen to be justified from the descriptions that follow.

1. Suribatiyama Lava (Crystalline olivine-augite-andesine-trachy-andesite).

This lava occurs as a massive flow, more than 20 m thick, forming the vertical cliffs that encircle Suribatiyama. Near its contact with the underlying tuff it exhibits a narrow platy parting parallel to the contact, while farther from the contact the parting gives place to hexagonal columnar jointing.

Megascopically, the rock is dense and more or less porphyritic with phenocrysts of feldspar, augite, and olivine, scattered through an aphanitic, but not glassy, groundmass. Although a more or less vesicular form is represented by an obsidian found near the contact with the underlying tuff, nowhere has a pumiceous facies been found. The

10) Y. KIKUCHI, *loc. cit.*
11) J. PETERSEN, *loc. cit.*
12) T. WAKIMIZU, *loc. cit.*
13) F. HOMMA, *loc. cit.*
14) S. KOZU and M. WATANABE, *loc. cit.*

color, except that of the pitch-black obsidian, is generally medium to dark gray with a greenish tint, while in a smaller number of specimens it is cream to light gray with pinkish tint, apparently due to incipient weathering, as seen in a specimen from the middle part of the lava-cliff on the NE. side of Suribatiyama.

Microscopically, no differences are observed in the specimen within the mass except the change in crystallinity of the groundmass from near where it has been in contact with the underlying tuff. Thus the rock, which is generally perpatic, consists of phenocrysts of plagioclase, augite, olivine, and subordinate magnetite and apatite, together with a groundmass which is either highly crystalline or more or less hyaline (Figs. 11, 12). The phenocrysts often form a glomeroporphyritic aggregate.

Phenocrysts: Plagioclase, which makes up the greater portion of the phenocrysts, is euhedral, some of them up to 5 mm in diameter, but often indented with inlets of the groundmass. It is simple or multiple-twinned in the usual way, rarely showing any twinning. Zonal structure is virtually absent save for a narrow clear border zone, although in a small number of crystals it is faintly exhibited near the border zone. Indices of refraction on (010) or (001) are $n_{1D}=1{\cdot}5493$, $n_{2D}=1{\cdot}5567$. Composition $Ab_{57}An_{43}$. The narrow clear border zone is an alkali feldspar (anorthoclase) having a lower refraction than Canada balsam and $2V=62°$, $49°$, or $46°$ $(-)$[15].

Augite is euhedral, $0{\cdot}5\sim3$ mm in diameter, and pale brownish without perceptible pleochroism. Zonal structure is faintly exhibited; the interior of each zonally-built crystal has $2V=55°(+)$, while the marginal zone $2V=48°(+)$. But some crystals, in which the zonal structure is inperceptible, have $2V=57°$, or $61°$ $(+)$. The refractive indices are larger in the intrior ($n_{1D}=1{\cdot}6974$) than in the marginal part. The approximate composition of the pyroxene is $Wo_{40}En_{37}Fs_{23}$, according to the Tomita Diagram[16].

Olivine is euhedral to rounded, up to 1 mm in diameter, and nearly colorless. It has $2V=84°(-)$ with $\beta_D=1{\cdot}7020$ corresponding to $Fo_{66}Fa_{34}$.

Magnetite, which is euhedral to anhedral and $0{\cdot}1\sim0{\cdot}3$ mm in diameter, occurs as isolated grains or in close association with augite and olivine.

---

15) The values of 2V for feldspar and mafic minerals were measured on the universal stage using hemispheres of refractive index 1·57 for feldspar and 1·649 for mafic minerals.

16) T. TOMITA, *Jour.Shanghai Sci. Inst.*, **1** (1934).

Apatite, which is prismatic, up to 0·5 mm in length, and nearly colorless, occurs either as enclosures in phenocrysts of feldspar, augite, and olivine, or is dispersed as isolated crystals throughout the rock.

The phenocrysts in the obsidian near its contact with the underlying tuff are identical with those above-mentioned except the plagioclase which, in the obsidian, is not rimmed with alkali feldspar.

Groundmass: The groundmass of the Suribatiyama lava, except that of the contact facies, is highly crystalline, consisting of feldspar, pyroxene, hornblende, and iron-ore, with a texture that is not typically trachytic because of the predominance of equant anhedral feldspar.

Feldspar includes both plagioclase and alkali feldspar. The plagioclase, which occurs as prismoids measuring 0·1 mm and less in length, is multiple twinned in the usual way. It has $2V = 82 \sim 86°(-)$ with $n_{1D} = 1{\cdot}5439$ corresponding to a calcic oligoclase $Ab_{72}An_{28}$, which is identical with the marginal part of the faintly zoned phenocrystic plagioclase. The alkali feldspar occurs either as euhedral thin laths (0·05 mm in length) or as anhedral crystals filling the interstices between other groundmass minerals. It also attaches to the margin of the plagioclase laths. The refractive indices are $\alpha_D = 1{\cdot}5253$, $\gamma_D = 1{\cdot}5325$. Zoning is observable in some of the larger crystals, in which the optic angle gradually decreases from the core toward the margin of each crystal; $2V = 71°(-)$ in the core, and $2V = 48°(-)$ in the margin. These optical characters are almost those of anorthoclase, corresponding to what attaches to the margin of the phenocrystic plagioclase.

The pyroxene, which is dispersed through the groundmass as minute grains (0·03 mm dia.) and prismoids (0·1 mm long), includes both pale brown augite and greenish alkali pyroxene. Besides occurring as isolated crystals of each pyroxene, they are combined as zoned crystals, in each of which the core is always represented by the augite and the margin by the alkali pyroxene. The boundary between the two pyroxenes is generally sharp, although there are some crystals in which the augite in the core gives way gradually outward to the alkali pyroxene of the margin. The augite has $n_{1D} = 1{\cdot}6997$, $2V = 55°(+)$, and the extinction angle $c \wedge Z' = 51{\cdot}5°$(max.). The approximate composition is $Wo_{40}En_{36}Fs_{24}$. The alkali pyroxene shows distinctly but not strong pleochroism, X = pale green, Y = green, Z = greenish brown, with absorption $X > Y > Z$. Its refractive indices are higher than 1·750. $2V = 68 \sim 73°(-)$. The optic plane is parallel to (010); the extinction angle $c \wedge X$ is very small or nearly zero. These optical characters indicate the alkali pyroxene to be an acmite[17].

17) Washington and Barth describe this mineral in a trachyte from the island of Hawaii. H. S. Washington, *Am. Jour. Sci.*, **23** (1923); T. W. Barth, *ibid.*, **31** (1931).

Hornblende, which occurs as minute laths and scraps, 0·05 mm in diameter, is deep brownish with distinct, but not strong, pleochroism, Z (or Y) = reddish brown, X = light greenish brown, and absorption Z (or Y) > X. The extinction angle $c \wedge Z'$(max.) = 21°. $n_{1D} = 1·6465$, $n_{2D} =$ 1·6552.

Chemical Composition: Chemical analyses of two specimens of the rocks from the islands were made by Petersen[18], of one by K. Yokoyama for S. Kozu[19], and of one by the Imp. Geol. Survey for D. Sato[20]. Unfortunately however, since the exact localities of the analyzed specimens are not mentioned by the respective analysts, it is uncertain which of these analyses is of the Suribatiyama lava under discussion. A new analysis was therefore made by S. Tanaka of a gray-colored highly crystalline specimen which the writer collected from the columnar lava exposed near the south coast (Tobiisi-hana) of Suribatiyama. Another new analysis was made also by Tanaka of a specimen from the Motoyama intrusive to be described later. These two new analyses are shown in Table I, in which the four old analyses are also given for comparison, together with three others — Homma's augite-syenite[21] from Sulphur Island, andesitic pumice[22] of the 1914 eruption from the submarine volcano near Minami Io-sima, and a trachyte from Hawaii.

The Suribatiyama lava is, like others from the island, decidedly high in alkalies, especially soda. Thus the normative plagioclase is an oligoclase $Ab_{84}An_{16}$. The normative pyroxene has the composition $Wo_{35}En_{39}Fs_{26}$ (Wt. %). The presence of a little quartz (excess silica) in the norm, although the rock carries silica mineral neither as phenocryst nor as a constituent of its crystalline groundmass may be ascribed to the assumption in calculating the norm. Some of the iron molecules which, in calculating the norm, are assigned to form magnetite, are believed to have primarily entered modal pyroxene and thus to have been combined with silica. As compared with the Motoyama intrusive, the only notable difference is in the ratios of the ferric and ferrous oxides, the differences between the amounts of the other constituents being quite insignificant. Assuming, therefore, that the iron oxides in the rock under consideration are 0·6% Fe_2O_3 and 4·6% FeO, which corresponds with the distribution in the analysis of the Motoyama intrusive, the norm shows 3·45% olivine instead of quartz.

---

18) J. PETERSEN, *loc. cit.*
19) H. S. WASHINGTON, *Chem. Anal. Ign. Rock*, (1917).
20) D. SATO, *Ganseki Tisitugaku*, (1925).
21) F. HOMMA, *loc. cit.*
22) T. WAKIMIZU, *Toyo-gakugei-zassi*, **37** (1919).

2. *Motoyama Intrusive* (Vitrophyric olivine-augite-andesine-trachyandesite).

This rock is exposed on the northeastern side of Motoyama as an intrusive into the Motoyama tuff. Megascopically it is various, as it exhibits every gradation between highly vitreous and more or less felsitic characters. Specimens from near its contact with the tuff are jet-black obsidian with sporadic phenocrysts of feldspar, augite, and olivine, while those from some distance away from the contact are pale to dark gray and contain phenocrysts of feldspar, augite, and olivine scattered through an aphanitic groundmass.

Microscopically, the rock carries a few phenocrysts of plagioclase (1~5 mm dia.), augite (0·5~1 mm) and olivine (0·5~1 mm), with subordinate magnetite (0·5 mm) and apatite (0·5 mm long) in a glassy groundmass (Fig. 13.). The phenocryts often form a glomeroporphyritic aggregate (Fig. 14.).

Phenocrysts: Plagioclase has almost the same optical characters as that of the above-described rock; $n_{1D}=1\cdot5499$, $2V=83°(+)$, composition $Ab_{55}An_{45}$, but it is not rimmed with alkali feldspar.

Augite, which is pale brown without discernible pleochroism, is not zonally built; $n_{1D}=1\cdot6970$, $2V=54\cdot5°(+)$, composition $Wo_{40}En_{37}Fs_{23}$ (Wt. %).

Olivine, which is euhedral to rounded, has $2V=83°(-)$.

Groundmass: The groundmass of the obsidian consists wholly of a pale to dark brown glass of refractive index varying from 1·5237 to 1·5277 for Na light. Microscopic flow-banding is exhibited by color differences between the bands, which vary from faint to quite pronounced.

The groundmass of the felsitic specimen consists of feldspar microlites, pyroxene granules, and glass base filled with black dust material of what appears to be magnetite. The feldspar microlites are for the most part an alkali feldspar of refractive indices less than Canada balsam. The pyroxene granules are greenish with distinct pleochroism suggestive of an alkali pyroxene. But these minerals are so small that no satisfactory determinations of optical properties could be made. They are crowded in microscopic bands exhibiting sinuous flow lines.

Chemical Composition: A specimen of the Motoyama intrusive at the exposure illustrated in Fig. 5 was chemically analyzed with the result given in (II) of Table I. Chemically the rock resembles the Suribatiyama lava, although microscopically the former is more hyaline than the latter; the normative plagioclase is an oligoclase $Ab_{89}An_{11}$. The only notable difference between them is in the ratios of the iron

Table I.

	I	II	III	IV	V	VI	VII	VIII	IX
SiO_2	58·91	59·60	59·30	60·32	59·87	61·28	60·55	60·82	62·02
Al_2O_3	17·71	16·81	16·61	16·09	17·23	18·16	17·29	16·63	18·71
Fe_2O_3	2·81	0·83	1·51	4·88	9·96	5·97	2·72	1·15	4·30
FeO	2·67	5·87	5·02	3·04	n.d.	1·76	3·22	3·46	0·10
MgO	0·88	1·34	1·55	1·34	0.77	0·79	1·12	1·79	0·40
CaO	3·47	3·10	3·16	3·10	2·96	3,55	3·22	3·35	0·86
Na_2O	6·01	6·11	5·63	4·93	6·21	5·51	5·37	5·62	6·90
K_2O	3·94	4·17	4·41	3·90	2·92	2·75	4·36	4·21	4·93
H_2O +	0·34	0·25	0·95	} 0·65	} 0·61	} 1·72	0·53	1·84	0·80
H_2O −	0·30	0·10					0·21	(ign. 1)	0·31
TiO_2	0·82	0·86	1·11	0·66			0·85	0·45	0·31
P_2O_5	0·49	0·50	0·44	0·56			0·28	0·22	0·24
MnO	0·16	0·26	0·21	0·25			0·19	0·39	0·15
Total	100·23*	99·80	99·90	99·83			99·91	99·93	100·13⁑
Q	1·62	——	——				4·50	1·98	1·80
Or	23·37	24·49	26·16				25·60	25·04	28·91
Ab	50·83	51·91	47·71				45·62	47·71	58·16
An	9·74	6·12	6·95				10·29	7·51	2·22
Py wo	1·97	2·32	2·44				1·51	3·02	C 1·43
Py en	2·20	1·10	3·81				2·81	4·42	1·00
Py fs	1·45	3·43	6·59				2·64	5·27	
Ol fo	——	1·55	——				——	——	——
Ol fa	——	4·48	——				——	——	——
Mt	4·17	1·16	2·08				3·94	1·52	Hm 4·30
Il	1·52	1·67	2·12				1·67	0·91	0·15
Ap	0·99	1·32	0·99				0·65	0·65	0·67
									Ru 0·24
Norm plag.	Ab_{89} An_{16}	Ab_{89} An_{11}	Ab_{87} An_{13}				Ab_{82} An_{18}	Ab_{86} An_{14}	Ab_{96} An_4

* includes S=1·71; ⁑ includes ZrO_2=0·06, SO_3=0·02, BaO=0·02.

I. Olivine-augite-andesine-trachyandesite. Suribatiyama (Mt. Pipe), Io-sima (Su'phur Island). S. Tanaka, anal.

II. Olivine-augite-andesine-trachyandesite. Motoyama, Iô-sima. S. Tanaka, anal.

III. "Oligoclase-andesite". Io-sima. K. Yokoyama, anal.

IV. "Pyroxene-andesite", Io-sima. Imp. Geol. Survey, anal.

V., VI. "Augite-andesite". Io-sima. J. Petersen, anal.

VII. Augite-syenite. Io-sima. Ushijima, anal.

VIII. Olivine-pyroxene-andesite. Pumice of 1914 eruption, "Sin Io-sima" (New Sulphur Island). Imp. Geol. Survey, anal.

IX. Albite-trachyte. Puu Anahulu near Hualalai, Hawaii. H. S. Washington, anal.

oxides. With almost the same total amount of iron (reduced to either oxide), the Motoyama intrusive contains much more ferrous and less ferric oxide, while the Suribatiyama lava has more ferric than ferrous oxide. Therefore, whereas the former has normative olivine, the latter carries normative quartz.

The old analyses (III, IV, V, and VI of Table I) of the rocks from the island are not seriously inconsistent, so far as the determinations go, with the new ones of the rocks above described. Although there are some differences in the rate of oxidation of the iron, the total amount of the iron oxide is about the same in each analysis. The close chemical resemblance betwen the two new analysis and also that between these two and the old analyses indicate the chemical definiteness of the rocks of the island. Thus these rocks differ greatly from the common pyroxene-andesites of the Huzi Volcanic Zone or the average Japanese andesite of Yamada, the differences being shown chiefly in the much higher alkalies, especially soda, with the consequent very sodic nature of the normative plagioclase, and also in the very small amount or entire absence of normative quartz of the former as contrasted with the latter.

The above-described rocks resemble, in chemical composition, the pumice (VIII of Table I) that was ejected in 1914 from the submarine volcano near Minami Iô-sima. They also resemble the trachytes from Hawaii, an analysis of which is given in IX of Table I.

3. Motoyama Tuff, Suribatiyama Ejecta, and Tidorigahara Sand.

There is no need to describe these rocks in detail here, as they arer composed of fragmentary material which, although of diverse appeaances such as pumiceous (Fig. 16.), vitreous, scoriaceous, and felsitic, are petrographically very similar to either the Suribatiyama lava or the Motoyama intrusive, as shown in the examples that follow.

Motoyama tuff: Plagioclase $Ab_{55}An_{45}-Ab_{60}An_{40}$ ($n_{1D}=1{\cdot}5512-1{\cdot}5475$).
Augite $n_{1D}=1{\cdot}6923-1{\cdot}6970$.
Olivine present.
Obsidian glass $n_D=1{\cdot}5210-1{\cdot}5260$.

Suribatiyama tuff: Plagioclase $Ab_{55}An_{45}-Ab_{58}An_{42}$ ($n_{1D}=1{\cdot}5512-1{\cdot}5489$).
Augite $n_{1D}=1{\cdot}6964-1{\cdot}6996$.
Olivine present,
Obsidian glass $n_D=1{\cdot}5201-1{\cdot}5253$. $n_D=1{\cdot}5332-1{\cdot}5370$.

Suribatiyama ejecta (scoriae): Plagioclase $Ab_{57}An_{43}$ ($n_{1D}=1{\cdot}5497$).

Tidorigahara sand: Plagioclase $Ab_{40}An_{60}-Ab_{60}An_{40}$ ($n_{1D}=1{\cdot}5596-1{\cdot}5475$).
Augite $n_{1D}=1{\cdot}6970$,
Obsidian glass $n_D=1{\cdot}5400-1{\cdot}5450$.

Homma mentions whitish holocrystalline blocks that lie scattered

in the Motoyama tuff, terrace deposit, and in the Tidorigahara sand. According to him, they are of augite-syenite, consisting of anorthoclase (α_D=1·530), pale green augite, aegirine-augite, olivine, cataphorite (?), magnetite, and apatite, with a little interstitial glass; one of them having the composition shown in VII of Table I. A similar blook collected by the writer from the Tidorigahara sand is subangular, about 5 cm in diameter, and medium-grained with pyroxene, olivine, and obsidian glass in a whitish feldspathic ground. Microscopically it is a hypidiomorphic aggregate composed of plagioclase, alkali feldspar, monoclinic pyroxene olivine, magnetite, and apatite, with a little interstitial glass. (Fig. 15.). The plagioclase, which occurs only as the core of the alkali feldspar, is zonally built, with composition varying from $Ab_{76}An_{24}$(n_{1D}=1·5402) to $Ab_{83}An_{17}$(n_{1D}=1·5366). The alkali feldspar, which also shows zonal structure, has 2V ($\rho > v$) = 62°∼55° in the core part and 2V=45°∼40°(−) in the marginal part. The refractive indices are α_D=1·5238−1·5256, γ_D=1·5316−1.5339, corresponding to an anorthoclase. The monoclinic pyroxene is greenish brown without discernible pleochroism. Zonal structure is very faintly exhibited, the core part having 2V=59∼60°(+) and the marigin 2V=55°(+). The refractive indices (n_{1D}=1·7014) indicate an augite rather rich in iron. Olivine, which is subordinate in amount, is pale yellowish green and has 2V=68°(−). Much of isometric magnetite and prismatic colorless apatite are enclosed in the feldspar and augite crystals. The interstitial glass is pale greenish brown with n_D=1·5117−1·5170.

Although the crystalline block was not chemically analyzed, it is expected from its mode that it may be chemically almost equivalent to the Suribatiyama lava and Motoyama intrusive. Homma's augite syenite is indeed chemically similar to these rocks.

The crystalline blocks cannot be regarded as having been derived from secretionary patches in either the Suribatiyama lava or the Motoyama intrusive, if patches there had been. They are probably a plutonic equivalent of either the Suribatiyama lava or the Motoyama intrusive. which, although not exposed at present, underlies the island, and which was thrown out as accessory ejecta during past volcanic eruptions of the island.

41. 火山列島硫黄島の地質及岩石に就いて

地震研究所 津屋弘逵

硫黄島（俗稱中硫黄島）は北硫黄島こ南硫黄島この略中間に位し，橄欖石・輝石・中性長石・粗面安山岩の熔岩，迸入岩，凝灰岩，砂礫等より成る火山島である．此島の大部分は最近の地質時代に活動した海底火山の隆起に依つて生じたもので，特に其北東過半部を占めてゐる元山の地質構造は嘗て海底に沈積した凝灰岩が粗面安山岩質岩漿の餅盤狀淺處迸入に因つて圓頂丘狀に押し上げられた事を示してゐる．本文では同島の地形及び地質構造を述べ，其結果から島の發育の歴史を推定し，最後に同島を構成する岩石の顯微鏡的並びに化學的性質を記載した．

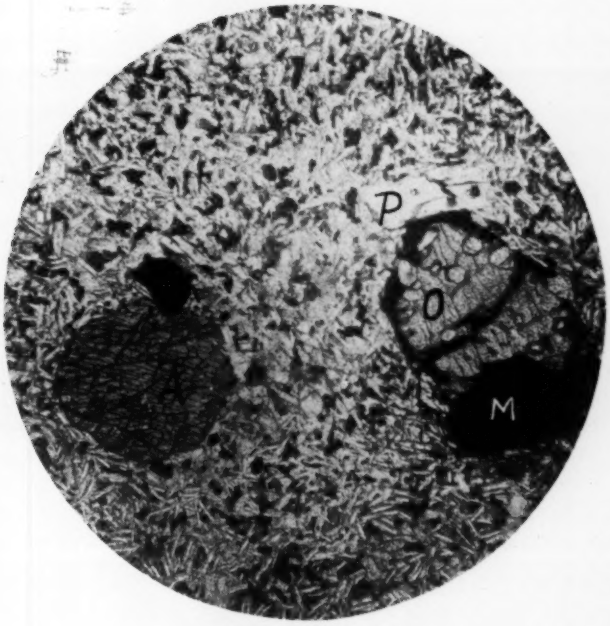

Fig. 11. Suribatiyama Lava (Crystalline olivine-augite andesine-trachyandesite). P: Andesine A: Augite O.: Olivine M: Magnetite. ×32

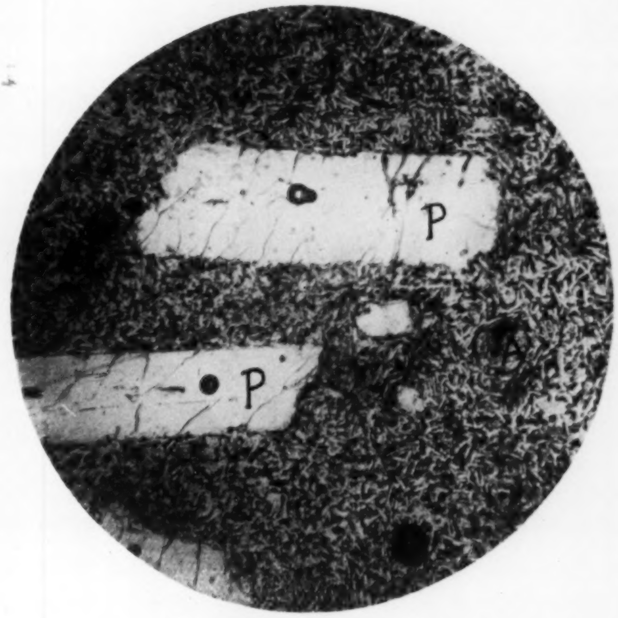

Fig. 12. Ditto. P: Andesine A: Augite ×30

Microphotographs of the Rocks of Sulphur Island.

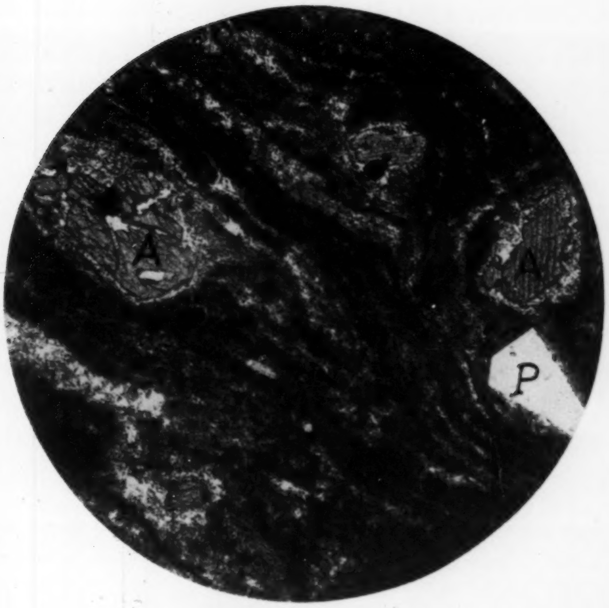

Fig. 13. Motoyama intrusive (Glassy olivine-augite-andesine-trachyandesite). P : Andesine A : Augite ×21.

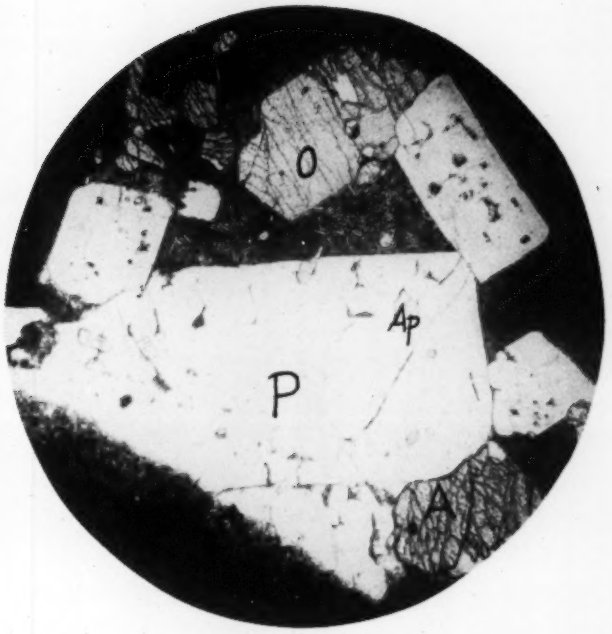

Fig. 14. Motoyama intrusive (Glomeroporphyritic aggregate of phenocrysts). P : Andesine O : Olivine A : Augite Ap : Apatite. ×30

Microphotographs of the Rocks of Sulphur Island.

(震研彙報 第十四號 圖版 津屋)

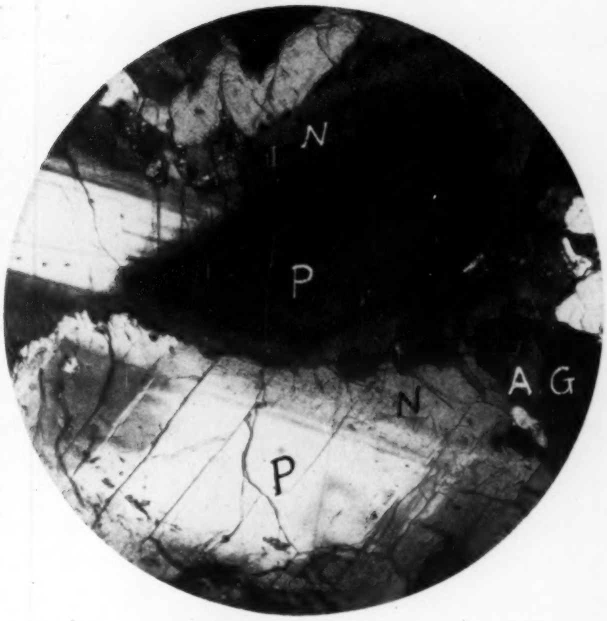

Fig. 15. Crystalline block (Crossed nicols). P: Oligoclase N: Anorthoclase A: Augite G: Interstitial glass. ×21

Fig. 16. Motoyama tuff composed of microscopic fragments of pumice. ×30

Microphotographs of the Rocks of Sulphur Island.

(震研彙報 第十四號 圖版 津屋)

42. 袋井—興津—小田原間及び興津—甲府間の一等水準檢測成果報告

昭和10年7月11日靜岡附近を中心とする地域に損害を與へたる强震の後，その復舊作業として，陸地測量部に於ては，袋井—興津—小田原，及び興津—甲府の各區間に就き，一等水準檢測を施行せり．その結果，上記の各區間にある水準點の垂直變動量として，附圖第一乃至第三の各圖に示すが如きものを得たるを以て，陸地測量部の好意により，茲に掲載して，各研究者の參考に資せんとす．

尙，測量作業並に垂直變動量の算出に關する要項は次の如し．

（1） 測量期日

袋井—興津間

前測量： 昭和6年8月～11月

新測量： 昭和10年12月～昭和11年1月

興津—小田原間

前測量； 昭和5年12月～昭和6年1月

新測量： 昭和11年2月～3月

興津—甲府間

前測量： 昭和6年6月～7月

新測量； 昭和10年12月～昭和11年1月

（2） 各水準點の垂直變動量は袋井に在る水準點 143·1 號を不動として算出せるものとす．

以　上

昭和11年7月　　　　地　震　研　究　所

---

42. *Relative Vertical Displacements of Bench-marks along the Lines of Levels from Hukuroi to Okitu, from Okitu to Odawara, and from Okitu to Kôhu.*

In connection with the strong earthquake that occurred on July 11, 1935, in the neighbourhood of Siduoka, a revision of precise levelling was carried out by the Military Land Survey along the lines from Hukuroi to Odawara via Okitu and from Okitu to Kôhu. As the result of this relevelling the vertical displacements of the bench-marks distributed on these sections of lines of levels

are measured as shown in annexed plates.

The following points should be noted regarding the results obtained as mentioned above.

(i) Dates of former and recent surveys for different sections are given in the following table.

Section of the Line	Dates of former survey	Date of recent survey
Hukuroi–Okitu	Aug.~Nov., 1931	Dec., 1935~Jan. 1936
Okitu–Odawara	Dec., 1930~Jan., 1931	Feb.~March, 1936
Okitu–Kôhu	June~July, 1931	Dec., 1935~Jan., 1936

(ii) The vertical displacements of the bench-marks measured are referred to a bench-mark situated at Hukuroi, B. M. 143·1, the height of which is assumed to have been unchanged during the period between two successive surveys mentioned above.

June., 1936.

The Earthquake Research Institute.

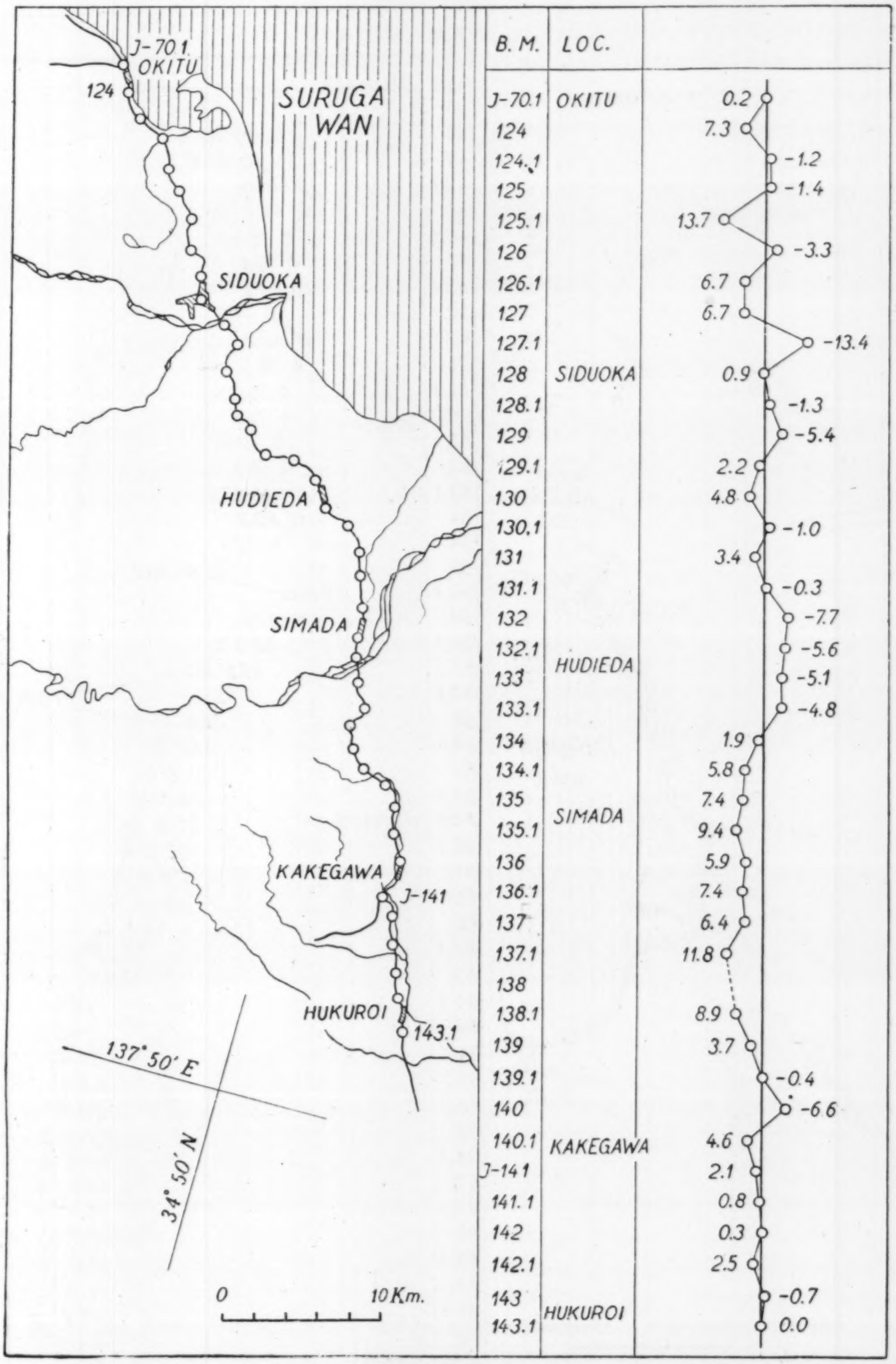

第 1 圖 袋井—興津間に於ける水準點の配置と垂直變動.（變動量の單位は mm.）

Fig. 1. Distribution of bench-marks along the line from Hukuroi to Okitu, and the vertical displacements. The unit for the displacement is mm.

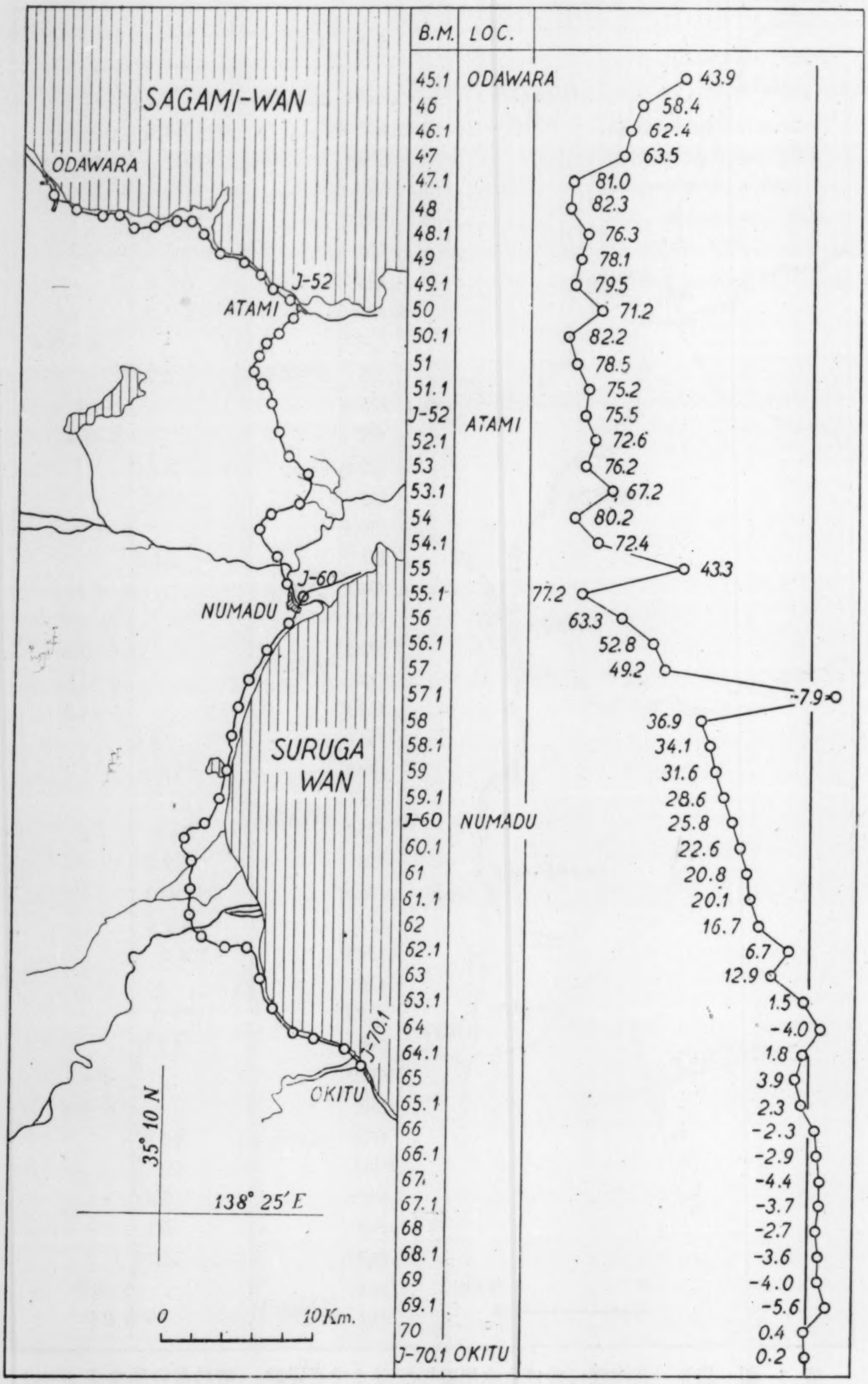

第 2 圖 興津—小田原間に於ける水準點の配置と垂直變動. (變動量の單位は mm.)

Fig. 2. Distribution of bench-marks along the line from Okitu to Odawara, and the vertical displacements. The unit for the displacement is mm.

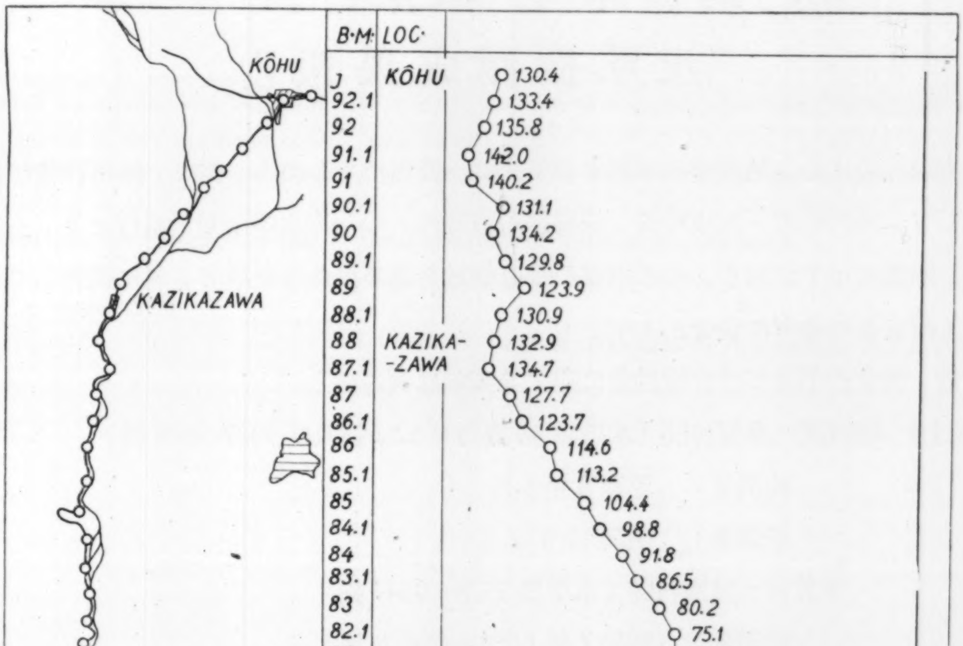

第 3 圖 興津—甲府間に於ける水準點の配置さ垂直變動.（變動量の單位は mm.）

Fig. 3. Distribution of bench-marks along the line Okitu to Kôhu, and the vertical displacements. The unit for the displacement is mm.

43. 湯河原町—城東村間の一等水準檢測成果報告

本所に於ける，地殼變形に關する研究の一資料たらしめんが爲に，陸地測量部に委托して，湯河原町—城東村間（靜岡縣田方郡內）の一等水準檢測を施行せり．その結果，附圖に示すが如き，各水準點の垂直變動を認め得たるを以て，玆に揭載して，普ねく研究者の參考に資せんとす．

尙，測量作業及び垂直變動量に關する要項は次の如し．

（1） 湯河原—多賀村間（水準點 50 號乃至 52·2 號及び 9327, 9328 號）

前測量： 昭和 8 年 3 月

新測量： 昭和 11 年 2 月

多賀村—城東村間（水準點 9328～9344 號）

前測量； 昭和 7 年 12 月～昭和 8 年 1 月

新測量： 昭和 11 年 2 月～3 月

（2） 各水準點の垂直變動量は湯河原町所在の水準點 50 號を不動として算出せられたるものなり．

以上の測量の一部は，服部報公會より本所所員坪井忠二氏に寄せられたる研究費によつて行はれたるものなり．玆に附記して深甚なる謝意を表す． 以 上

昭和 11 年 7 月

地 震 研 究 所

---

43. Relative Vertical Displacements of Bench-marks along the Line of Levels from Yugawara to Zyôtô-mura, on the East Coast of the Idu Peninsula.

The line of levels from Yugawara to Zyôtô-mura, on the east coast of the Idu peninsula, was re-levelled in Jan.～March, 1936, by the Military Land Survey, at our disposal. As the result of this re-levelling, the vertical displacemerts of the bench-marks in this region are measured as shown in the annexed plate.

The dates of field works of former and recent surveys are

(a) For the line from Yugawara to Taga-mura (B. M.'s 50~9328)
March, 1933, and Jan.~Feb., 1936;

(b) For the line from Taga-mura to Zyôtô~mura (B. M.'s 9328~9344)
Dec., 1932-Jan., 1933, and Feb.~March, 1936,

respectively. It must also be noted that the vertical displacements of the bench-marks are computed on the assumption that the height of B. M. 50, situated at Yugawara has been unchanged during the period of two successive surveys mentioned above.

The present revision of levelling was carried out by the research fund granted from the Hattori Hôkôkwai to Dr. C. Tsuboi, a member of the staff of the Institute. Best thanks of the above named and the Director are due to the Authorities of the Hattori Hôkôkwai.

June, 1936.

The Earthquake Research Institute.

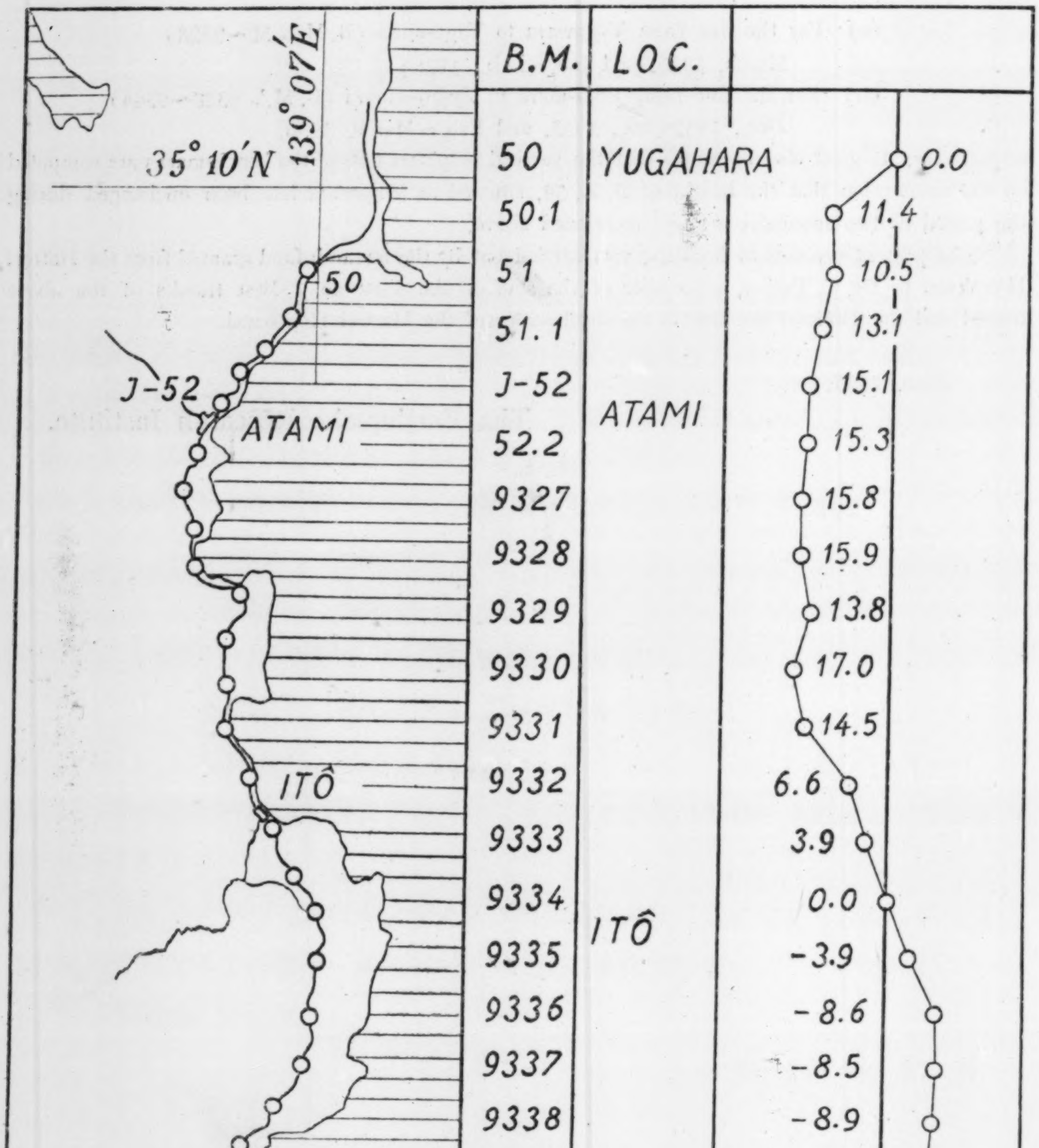

第 1 圖 湯河原—城東村間に於ける水準點の配置と垂直變動. (變動量の單位は mm.)

Fig. 1. Distribution of bench-marks along the line from Yugawara to Zyôtô-mura, on the east coast of the Idu peninsula, and the vertical displacements. The unit for the displacement is mm.

44. *Polarization of Elastic Waves generated from a Plane Source.*

By Katsutada SEZAWA and Kiyoshi KANAI,
Earthquake Research Institute.

(Read Sept. 15, 1936.—Received Sept. 21, 1936.)

1. *Introduction.*

It is an established fact that, in the case of acoustic problems, the smaller the length of transmitted waves compared with the linear dimension of the source, the more polarized is the wave transmission in the direction of movement of that source. The same phenomenon is also seen in the case of the dissipation waves that accompany seiches in a bay.[1] In the seismological field, hardly any formal investigation of the problem has been made. Recently, Inouye,[2] using our previous solution,[3] succeeded in ascertaining the manner in which the displacement distribution of harmonic type in a wave front is kept towards infinity when the length of the waves differs. While in the case of a cylindrical or spherical source, the direction of wave transmission is simply radial, the amplitude of each harmonic wave is determined fairly easily by ascertaining the particular argument of a given Bessel's function that would correspond to the boundary of the source. It is not possible however to fit such an argument to the condition of the boundary in the case of a plane source. Although the accurate mathematical solution may be to apply Mathieu's function, which we[4,5] once did use, and which Hidaka[6] greatly developed. Owing however to

1) K. SEZAWA and K. KANAI, "Dissipation Waves Accompanying Forced Seiches in a Bay", *Bull. Earthq. Res. Inst.*, **14** (1936), 360~366.

2) W. INOUYE, "On the Mechanism of a Seismic Origin", *Disin*, **8** (1936), 387~403, (in Japanese).

3) K. SEZAWA, "Dilatational and Distortional Waves generated from a Cylindrical or Spherical Origin", *Bull. Earthq. Res. Inst.*, **2** (1927), 13~20.

4) K. SEZAWA, "Propagation of Elastic Waves from an Elliptic or a Spheroidal Origin", *Bull. Earthq. Res. Inst.*, **2** (1927), 29~48.

5) K. SEZAWA, "On the Diffraction of Elastic Waves", *Bull. Earthq. Res. Inst.*, **5** (1928), 59~70.

6) K. HIDAKA, "Tables for Computing the Mathieu Functions...", *Mem. Imp. Marine Obs.*, **6** (1936), 137~157.

a certain practical difficulty, we have not used it here, the solution given here being a combination of Bessel's functions of different orders, by means of which approximately all the boundary conditions will be satisfied.

We shall first solve the case of a plane source with normal changing stress and then discuss the case of a plane source with changing shearing stress, and finally solve the case wherein a plane source generates dilatational waves of the same phase along that source.

2. ***A plane source with normal disturbance.***

Let the source be of the form of a circular disc ($\theta=\pi/2$) of radius a, and let the normal stress acting per unit area of the surface of the disc under consideration be $p_n e^{ipt}$. Were the length of the generated waves relatively long compared with the diameter of the disc, the boundary condition at the source would be approximately,

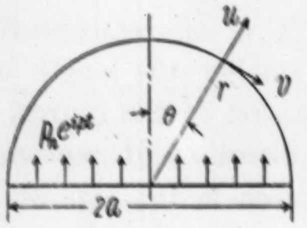

Fig. 1.

$$\left.\begin{aligned} p_n e^{ipt}\cos\theta &= \widehat{rr}\cos\theta-\widehat{r\theta}\sin\theta,\\ 0&=\widehat{rr}\sin\theta+\widehat{r\theta}\cos\theta \end{aligned}\right\} \tag{1}$$

at $r=a$, in which $\widehat{rr}$, $\widehat{r\theta}$ are the radial and tangential components of stress due to the outwardly radiated waves, namely,

$$\left.\begin{aligned} \widehat{rr}&=\lambda\Delta+2\mu\frac{\partial u}{\partial r},\\ \widehat{r\theta}&=\mu\left(\frac{\partial v}{\partial r}-\frac{v}{r}+\frac{1}{r}\frac{\partial u}{\partial\theta}\right). \end{aligned}\right\} \tag{2}$$

Assuming the displacement of the radiated waves in the vicinity of $r=a$ to be composed of an aggregate of waves,

$$\begin{aligned} \Delta&=\sum_n A_n\frac{H^{(2)}_{n+\frac{1}{2}}(hr)}{\sqrt{r}}P_n(\cos\theta)e^{ipt},\\ u_1&=-\sum_n\frac{A_n}{h^2}\frac{d}{dr}\frac{H^{(2)}_{n+\frac{1}{2}}(hr)}{\sqrt{r}}P_n(\cos\theta)e^{ipt},\\ v_1&=-\sum_n\frac{A_n}{h^2}\frac{H^{(2)}_{n+\frac{1}{2}}(hr)}{r^{3/2}}\frac{dP_n(\cos\theta)}{d\theta}e^{ipt}, \end{aligned} \tag{3}$$

$$\left.\begin{aligned} u_2 &= -\sum_n \frac{n(n+1)}{k^2} B_n \frac{H^{(2)}_{n+\frac{1}{2}}(kr)}{r^{3/2}} P_n(\cos\theta) e^{ipt}, \\ v_2 &= -\sum_n \frac{B_n}{k^2} \frac{1}{r} \frac{d}{dr}\left(\sqrt{r}\, H^{(2)}_{n+\frac{1}{2}}(kr)\right) \frac{dP_n(\cos\theta)}{d\theta} e^{ipt}, \end{aligned}\right|$$

where $u_1+u_2=u$, $v_1+v_2=v$, $h^2=\rho p^2/(\lambda+2\mu)$, $k^2=\rho p^2/\mu$. Substituting (3) in (2)

$$\left.\begin{aligned} \widehat{rr} &= \sum_n \frac{P_n(\cos\theta)e^{ipt}}{\sqrt{r}} \Bigg[A_n \Bigg\{ \left(\lambda - 2\mu \frac{n(n-1)}{h^2r^2}\right) H^{(2)}_{n+\frac{1}{2}}(hr) \\ &\quad + 2\mu\left(\frac{2n+1}{hr} H^{(2)}_{n+\frac{3}{2}}(hr) - H^{(2)}_{n+\frac{5}{2}}(hr)\right)\Bigg\} \\ &\quad + 2\mu B_n n(n+1) \left\{ -\frac{n-1}{k^2r^2} H^{(2)}_{n+\frac{1}{2}}(kr) + \frac{1}{kr} H^{(2)}_{n+\frac{3}{2}}(kr) \right\} \Bigg], \\ \widehat{r\theta} &= \sum_n \frac{\mu}{\sqrt{r}} \frac{dP_n(\cos\theta)}{d\theta} e^{ipt} \Bigg[2A_n \left\{ -\frac{(n-1)}{h^2r^2} H^{(2)}_{n+\frac{1}{2}}(hr) + \frac{1}{hr} H^{(2)}_{n+\frac{3}{2}}(hr) \right\} \\ &\quad + B_n \Bigg\{ -\frac{2(n+1)(n-1)}{k^2r^2} H^{(2)}_{n+\frac{1}{2}}(kr) \\ &\quad + \frac{2n+1}{kr} H^{(2)}_{n+\frac{3}{2}}(kr) - H^{(2)}_{n+\frac{5}{2}}(kr) \Bigg\} \Bigg]. \end{aligned}\right\} \quad (4)$$

Substituting (4) in (1), we obtain

$$\left.\begin{aligned} A_0 &= \frac{p_n\sqrt{a}}{3\mu} \left\{ \frac{\lambda}{\mu} H^{(2)}_{\frac{1}{2}}(ha) + \frac{2}{ha} H^{(2)}_{\frac{3}{2}}(ha) - 2H^{(2)}_{\frac{5}{2}}(ha) \right\}^{-1}, \\ A_2 &= \frac{2p_n\sqrt{a}}{3\mu\Phi} \Bigg[\left\{ -\frac{6}{k^2a^2} H^{(2)}_{\frac{5}{2}}(ka) + \frac{5}{ka} H^{(2)}_{\frac{7}{2}}(ka) - H^{(2)}_{\frac{9}{2}}(ka) \right\} \\ &\quad - 6\left\{ -\frac{1}{k^2a^2} H^{(2)}_{\frac{5}{2}}(ka) + \frac{1}{ka} H^{(2)}_{\frac{7}{2}}(ka) \right\} \Bigg], \\ B_2 &= \frac{p_n\sqrt{a}}{3\mu\Phi} \Bigg[\left\{ \left(\frac{\lambda}{\mu} - \frac{4}{h^2a^2}\right) H^{(2)}_{\frac{5}{2}}(ha) + \frac{10}{ha} H^{(2)}_{\frac{7}{2}}(ha) - 2H^{(2)}_{\frac{9}{2}}(ha) \right\} \end{aligned}\right|$$

$$-4\left\{-\frac{1}{h^2a^2}H^{(2)}_{\frac{5}{2}}(ha)+\frac{1}{ha}H^{(2)}_{\frac{7}{2}}(ha)\right\}\Bigg], \tag{5}$$

$$\Phi=\left\{\left(\frac{\lambda}{\mu}-\frac{4}{h^2a^2}\right)H^{(2)}_{\frac{5}{2}}(ha)+\frac{10}{ha}H^{(2)}_{\frac{7}{2}}(ha)-2H^{(2)}_{\frac{9}{2}}(ha)\right\}$$

$$\cdot\left\{-\frac{6}{k^2a^2}H^{(2)}_{\frac{5}{2}}(ka)+\frac{5}{ka}H^{(2)}_{\frac{7}{2}}(ka)-H^{(2)}_{\frac{9}{2}}(ka)\right\}$$

$$-24\left\{-\frac{1}{h^2a^2}H^{(2)}_{\frac{5}{2}}(ha)+\frac{1}{ha}H^{(2)}_{\frac{7}{2}}(ha)\right\}\left\{-\frac{1}{k^2a^2}H^{(2)}_{\frac{5}{2}}(ka)\right.$$

$$\left.+\frac{1}{ka}H^{(2)}_{\frac{7}{2}}(ka)\right\},$$

$$A_1=B_1=A_3=B_3=A_4=B_4=\;.\;.\;.\;.\;=0.$$

The general expression for radiated waves are now $u_1=u_1'+u_1''$, $v_1=v_1'$, $u_2=u_2'$, $v_2=v_2'$, and in the special case, $\lambda=\mu$, they are as follows:

$$u_1'=\frac{p_n a}{3\mu hr}\left\{\left(\frac{\sin hr}{hr}-\cos hr\right)+i\left(\sin hr+\frac{\cos hr}{hr}\right)\right\}$$

$$\cdot\left[\left\{\frac{4}{ha}\cos ha+\left(3-\frac{4}{h^2a^2}\right)\sin ha\right\}\right.$$

$$\left.+i\left\{\left(3-\frac{4}{h^2a^2}\right)\cos ha-\frac{4}{ha}\sin ha\right\}\right]^{-1}e^{ipt},$$

$$u_1''=\frac{A_2}{4h^2r^{3/2}\sqrt{\frac{1}{2}\pi hr}}\left[\left\{\left(-\frac{9}{hr}+hr\right)\cos hr+\left(\frac{9}{h^2r^2}-4\right)\sin hr\right\}\right.$$

$$\left.+i\left\{\left(\frac{9}{h^2r^2}-4\right)\cos hr-\left(-\frac{9}{hr}+hr\right)\sin hr\right\}\right](3\cos 2\theta+1)\,e^{ipt},$$

$$v_1'=\frac{3A_2}{2h^2r^{3/2}\sqrt{\frac{1}{2}\pi hr}}\left[\left\{-\frac{3}{hr}\cos hr+\left(\frac{3}{h^2r^2}-1\right)\sin hr\right\}\right. \tag{6}$$

$$\left.+i\left\{\left(\frac{3}{h^2r^2}-1\right)\cos hr+\frac{3}{hr}\sin hr\right\}\right]\sin 2\theta e^{ipt},$$

$$u_2'=\frac{3B_2}{2k^2r^{3/2}\sqrt{\frac{1}{2}\pi kr}}\left[\left\{\frac{3}{kr}\cos kr+\left(-\frac{3}{k^2r^2}+1\right)\sin kr\right\}\right.$$

$$
\left.\begin{aligned}
&\qquad +i\left\{\left(-\frac{3}{k^2r^2}+1\right)\cos kr-\frac{3}{kr}\sin kr\right\}\Bigg](3\cos 2\theta+1)\,e^{ipt},\\
&v_2'=-\frac{3B_2}{2k^2r^{3/2}\sqrt{\frac{1}{2}\pi kr}}\Bigg[\left\{\left(\frac{6}{kr}-kr\right)\cos kr+3\left(-\frac{2}{k^2r^2}+1\right)\sin kr\right\}\\
&\qquad +i\left\{3\left(-\frac{2}{k^2r^2}+1\right)\cos kr-\left(\frac{6}{kr}-kr\right)\sin kr\right\}\Bigg]\sin 2\theta\, e^{ipt}.\\
&A_2=\frac{2p_na\sqrt{\frac{1}{2}\pi h}}{3\mu\Phi}\Bigg[\left\{\frac{1}{ka}\left(\frac{120}{k^2a^2}-11\right)\cos ka+\left(-\frac{120}{k^4a^4}+\frac{51}{k^2a^2}-1\right)\sin ka\right\}\\
&\qquad +i\left\{\left(-\frac{120}{k^4a^4}+\frac{51}{k^2a^2}-1\right)\cos ka-\frac{1}{ka}\left(\frac{120}{k^2a^2}-11\right)\sin ka\right\}\Bigg],\\
&B_2=\frac{p_na\sqrt{\frac{1}{2}\pi k}}{3\mu\Phi}\Bigg[\left\{\frac{1}{ha}\left(\frac{120}{h^2a^2}-17\right)\cos ha+\left(-\frac{120}{h^4a^4}+\frac{57}{h^2a^2}-3\right)\sin ha\right\}\\
&\qquad +i\left\{\left(-\frac{120}{h^4a^4}+\frac{57}{h^2a^2}-3\right)\cos ha-\frac{1}{ha}\left(\frac{120}{h^2a^2}-17\right)\sin ha\right\}\Bigg],\\
&\Phi=\Bigg[\left\{\frac{1}{ka}\left(\frac{48}{k^2a^2}-5\right)\cos ka+\left(-\frac{48}{k^4a^4}+\frac{21}{k^2a^2}-1\right)\sin ka\right\}\\
&\qquad +i\left\{\left(-\frac{48}{k^4a^4}+\frac{21}{k^2a^2}-1\right)\cos ka-\frac{1}{ka}\left(\frac{48}{k^2a^2}-5\right)\sin ka\right\}\\
&\qquad .\Bigg[\left\{\frac{1}{ha}\left(\frac{72}{h^2a^2}-13\right)\cos ha+\left(-\frac{72}{h^4a^4}+\frac{37}{h^2a^2}-3\right)\sin ha\right\}\\
&\qquad +i\left\{\left(-\frac{72}{h^4a^4}+\frac{37}{h^2a^2}-3\right)\cos ha-\frac{1}{ha}\left(\frac{72}{h^2a^2}-13\right)\sin ha\right\}\Bigg]\\
&\qquad -\frac{24}{hka^2}\Bigg[\left\{\left(-\frac{12}{k^2a^2}+1\right)\cos ka+\frac{1}{ka}\left(\frac{12}{k^2a^2}-5\right)\sin ka\right\}\\
&\qquad +i\left\{\frac{1}{ka}\left(\frac{12}{k^2a^2}-5\right)\cos ka+\left(\frac{12}{k^2a^2}-1\right)\sin ka\right\}\Bigg]\\
&\qquad .\Bigg[\left\{\left(-\frac{12}{h^2a^2}+1\right)\cos ha+\frac{1}{ha}\left(\frac{12}{h^2a^2}-5\right)\sin ha\right\}\\
&\qquad +i\left\{\frac{1}{ha}\left(\frac{12}{h^2a^2}-5\right)\cos ha-\left(-\frac{12}{h^2a^2}+1\right)\sin ha\right\}\Bigg].
\end{aligned}\right\}\quad (7)
$$

The radial and transverse components of the displacement due to the dilatational waves are u_1 and v_1 respectively, whereas the radial and transverse components of displacement due to the distortional waves are u_2 and v_2 respectively. The cases $\sqrt{\rho/\mu}pa=1$, 2π, 10π were calculated, and the displacement distribution in every wave front for u_1, v_1, u_2, v_2 at distances of $r/a=1, 10, \infty$ plotted in Figs. 2~10. It has been already ascertained that both the transverse component of the dilatational waves and the radial component of the distortional waves should vanish at an infinite radial distance.[7] The present result confirms this fact. The result furthermore tells us that, while the polarization of dilata-

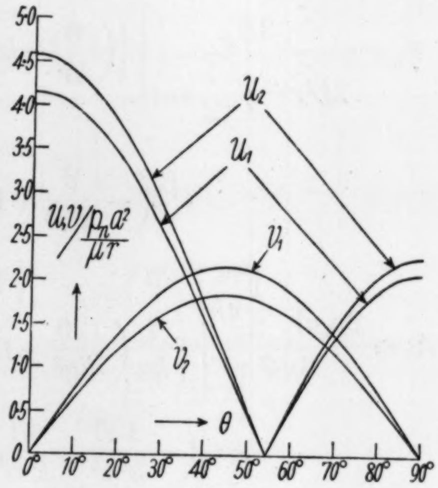

Fig. 2. $\sqrt{\rho/\mu}\,pa=1$, $r/a=1$.

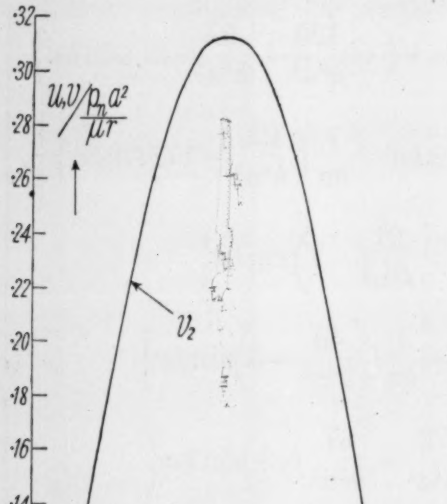

Fig. 3. $\sqrt{\rho/\mu}\,pa=1$, $r/a=10$.

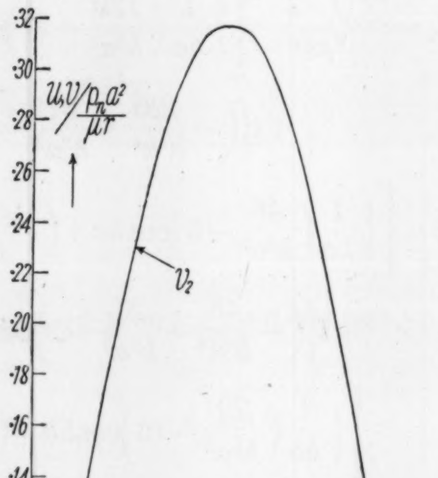

Fig. 4. $\sqrt{\rho/\mu}\,pa=1$, $r/a=\infty$.

7) K. SEZAWA and K. KANAI, "Amplitudes of P- and S-waves at Different Focal Distances", *Bull. Earthq. Res. Inst.*, **10** (1932), 299~334.

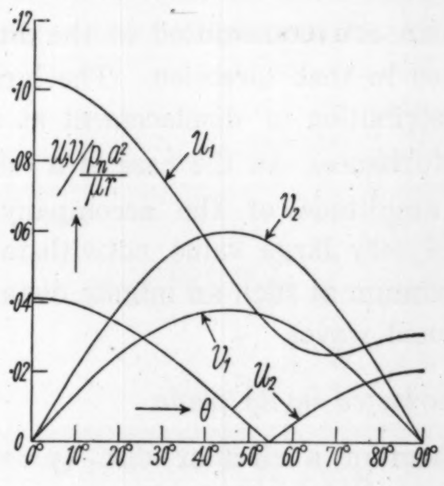

Fig. 5. $\sqrt{\rho/\mu}\, pa = 2\pi,\ r/a = 1.$

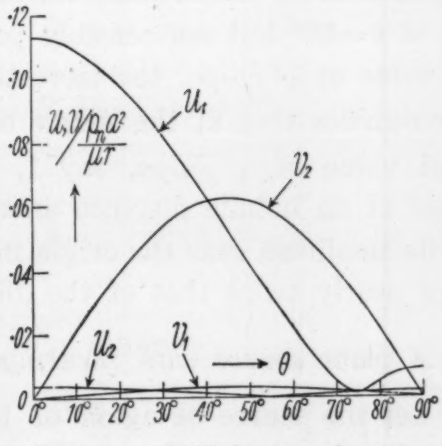

Fig. 6. $\sqrt{\rho/\mu}\, pa = 2\pi,\ r/a = 10.$

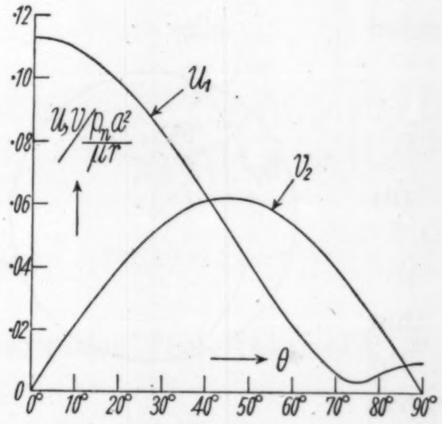

Fig. 7. $\sqrt{\rho/\mu}\, pa = 2\pi,\ r/a = \infty.$

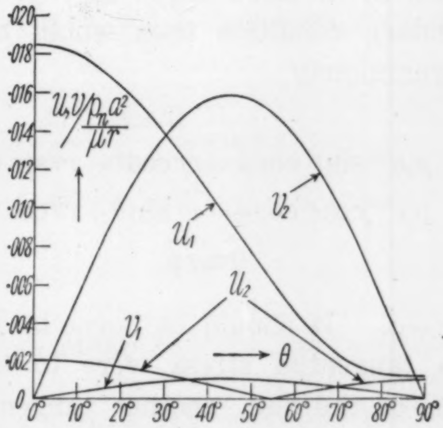

Fig. 8. $\sqrt{\rho/\mu}\, pa = 10\pi,\ r/a = 1.$

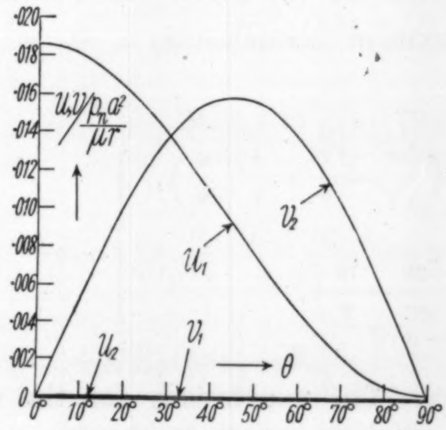

Fig. 9. $\sqrt{\rho/\mu}\, pa = 10\pi,\ r/a = 10.$

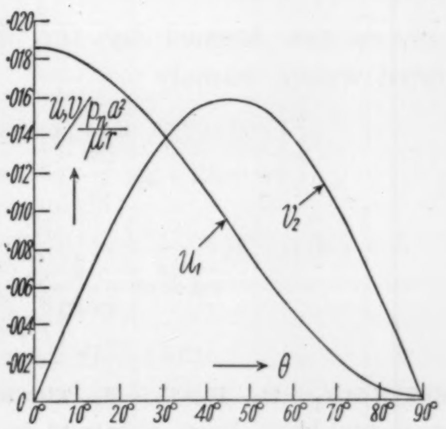

Fig. 10. $\sqrt{\rho/\mu}\, pa = 10\pi,\ r/a = \infty.$

tional waves in the direction of $\theta=0$ is rather gradual, the same waves are accompanied by distortional waves, which are transmitted in the direction of $\theta=45°$ but not sensibly polarized in that direction. The larger the value of $\sqrt{\rho/\mu}pa$, the more the distribution of displacement at $r=\infty$ resembles that at the source of disturbance. In the case of a fairly small value of $\sqrt{\rho/\mu}pa$, say 1, the amplitude of the accompanying waves at an infinite distance assumes a very large value notwithstanding its smallness near the origin its maximum at such an infinite distance being nearly twice that of the dilatational waves.

3. *A plane source with shearing disturbance in its plane.*

Let the source be again of the form of a circular disc $(\phi=\pi/2)$ of radius $r=a$, the shearing stress acting in a single direction in its plane, namely, in the vertical direction in the plane of the circular disc shown by a thick curve in Fig. 11. The boundary condition then would be written approximately

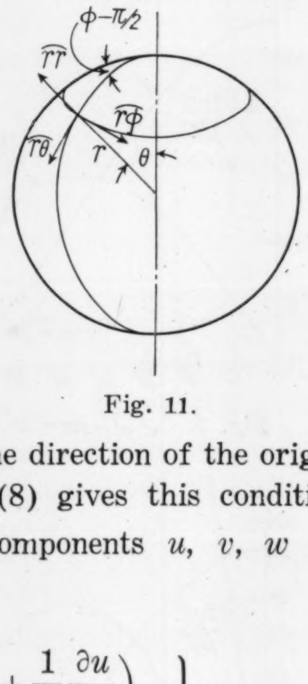

Fig. 11.

$$\left.\begin{aligned} p_s e^{ipt}\sin\theta\cos\phi &= \widehat{rr}\cos\theta-\widehat{r\theta}\sin\theta, \\ p_s e^{ipt}\cos\theta\cos\phi &= \widehat{rr}\sin\theta+\widehat{r\theta}\cos\theta, \\ 0 &\approx \widehat{r\phi} \end{aligned}\right\} \qquad (8)$$

at $r=a$. It should be borne in mind that if a tangential stress were to act in the plane of the disc, another tangential stress of the same magnitude would also act in a plane perpendicular to the disc as well as to the direction of the original tangential stress. The second equation of (8) gives this condition. $\widehat{rr}$, $\widehat{r\theta}$, $\widehat{r\phi}$ are formed by the displacement components u, v, w for radiated waves, namely

$$\left.\begin{aligned} &\widehat{rr}=\lambda\Delta+2\mu\frac{\partial u}{\partial r}, \qquad \widehat{r\theta}=\mu\left(\frac{\partial v}{\partial r}-\frac{v}{r}+\frac{1}{r}\frac{\partial u}{\partial\theta}\right), \\ &\widehat{r\phi}=\mu\left(\frac{1}{r\sin\theta}\frac{\partial u}{\partial\phi}+\frac{\partial w}{\partial r}-\frac{w}{r}\right), \end{aligned}\right\} \qquad (9)$$

where $u=u_1+u_2$, $v=v_1+v_2$, $w=w_1+w_2$. The expressions for the displacements have been obtained in the previous paper[8] in the forms

8) K. SEZAWA and K. KANAI, *loc. cit.* 7).

$$\Delta=\sum_n A_n \frac{H^{(2)}_{n+\frac{1}{2}}(hr)}{\sqrt{r}} P'_n(\cos\theta)\cos\phi\, e^{ipt}, \tag{10}$$

$$\left.\begin{aligned}
u_1&=-\sum_n \frac{A_n}{h^2}\frac{d}{dr}\frac{H^{(2)}_{n+\frac{1}{2}}(hr)}{\sqrt{r}} P'_n(\cos\theta)\cos\phi\, e^{ipt},\\
v_1&=-\sum_n \frac{A_n}{h^2}\frac{H^{(2)}_{n+\frac{1}{2}}(hr)}{r^{3/2}}\frac{dP'_n(\cos\theta)}{d\theta}\cos\phi\, e^{ipt},\\
w_1&=\sum_n \frac{A_n}{h^2}\frac{H^{(2)}_{n+\frac{1}{2}}(hr)}{r^{3/2}}\frac{P'_n(\cos\theta)}{\sin\theta}\sin\phi\, e^{ipt},
\end{aligned}\right\} \tag{11}$$

$$\left.\begin{aligned}
u_2&=-\sum_n \frac{n(n+1)B_n}{k^2}\frac{H^{(2)}_{n+\frac{1}{2}}(kr)}{r^{3/2}} P'_n(\cos\theta)\cos\phi\, e^{ipt},\\
v_2&=-\sum_n \frac{B_n}{k^2}\frac{1}{r}\frac{d}{dr}\left\{\sqrt{r}\,H^{(2)}_{n+\frac{1}{2}}(kr)\right\}\frac{dP'_n(\cos\theta)}{d\theta}\cos\phi\, e^{ipt},\\
w_2&=\sum_n \frac{B_n}{k^2}\frac{1}{r}\frac{d}{dr}\left\{\sqrt{r}\,H^{(2)}_{n+\frac{1}{2}}(kr)\right\}\frac{P'_n(\cos\theta)}{\sin\theta}\sin\phi\, e^{ipt},\\
\text{where}\quad P^m_n(z)&=(1-z^2)^{\frac{m}{2}}\frac{d^mP_n(z)}{dz^m}.
\end{aligned}\right\} \tag{12}$$

Substituting (10), (11), (12) in (9), we obtain

$$\left.\begin{aligned}
\widehat{rr}&=\sum_n \frac{\mu}{\sqrt{r}}P'_n(\cos\theta)\cos\phi\, e^{ipt}\Bigg[A_n\left\{\left(\frac{\lambda}{\mu}-\frac{2n(n-1)}{h^2r^2}\right)H^{(2)}_{n+\frac{1}{2}}(hr)\right.\\
&\quad\left.+\frac{2(2n+1)}{hr}H^{(2)}_{n+\frac{3}{2}}(hr)-2H^{(2)}_{n+\frac{5}{2}}(hr)\right\}\\
&\quad+\frac{2n(n+1)}{kr}B_n\left\{-\frac{(n-1)}{kr}H^{(2)}_{n+\frac{1}{2}}(kr)+H^{(2)}_{n+\frac{3}{2}}(kr)\right\}\Bigg],\\
\widehat{r\theta}&=-\sum_n \frac{\mu}{\sqrt{r}}\frac{dP'_n(\cos\theta)}{d\theta}\cos\phi\, e^{ipt}\Bigg[\frac{2A_n}{hr}\left\{-\frac{(n-1)}{hr}H^{(2)}_{n+\frac{1}{2}}(hr)\right.\\
&\quad\left.+H^{(2)}_{n+\frac{3}{2}}(hr)\right\}+B_n\left\{-\frac{2(n-1)(n+1)}{k^2r^2}H^{(2)}_{n+\frac{1}{2}}(kr)\right.\\
&\quad\left.+\frac{(2n+1)}{kr}H^{(2)}_{n+\frac{3}{2}}(kr)-H^{(2)}_{n+\frac{5}{2}}(kr)\right\}\Bigg].
\end{aligned}\right\} \tag{13}$$

Substituting (13) in (8), we get

$$
\left.\begin{aligned}
A_2\Phi &= \frac{2}{3}\frac{p_s\sqrt{a}}{\mu}\left[\left\{\frac{6}{k^2a^2}H^{(2)}_{\frac{5}{2}}(ka)-\frac{5}{ka}H^{(2)}_{\frac{7}{2}}(ka)+H^{(2)}_{\frac{9}{2}}(ka)\right\}\right.\\
&\qquad\left.+\frac{6}{ka}\left\{\frac{1}{ka}H^{(2)}_{\frac{5}{2}}(ka)-H^{(2)}_{\frac{7}{2}}(ka)\right\}\right],\\
B_2\Phi &= \frac{1}{3}\frac{p_s\sqrt{a}}{\mu}\left[\left\{\left(\frac{\lambda}{\mu}-\frac{4}{h^2a^2}\right)H^{(2)}_{\frac{5}{2}}(ha)+\frac{10}{ha}H^{(2)}_{\frac{7}{2}}(ha)\right.\right.\\
&\qquad\left.\left.-2H^{(2)}_{\frac{9}{2}}(ha)\right\}+\frac{4}{ha}\left\{-\frac{1}{ha}H^{(2)}_{\frac{5}{2}}(ha)+H^{(2)}_{\frac{7}{2}}(ha)\right\}\right],\\
\Phi &= \left\{\left(\frac{\lambda}{\mu}-\frac{4}{h^2a^2}\right)H^{(2)}_{\frac{5}{2}}(ha)+\frac{10}{ha}H^{(2)}_{\frac{7}{2}}(ha)\right.\\
&\quad\left.-2H^{(2)}_{\frac{9}{2}}(ha)\right\}\left\{\frac{6}{k^2a^2}H^{(2)}_{\frac{5}{2}}(ka)-\frac{5}{ka}H^{(2)}_{\frac{7}{2}}(ka)+H^{(2)}_{\frac{9}{2}}(ka)\right\}\\
&\quad+\frac{24}{hka^2}\left\{\frac{1}{ha}H^{(2)}_{\frac{5}{2}}(ha)-H^{(2)}_{\frac{7}{2}}(ha)\right\}\left\{\frac{1}{ka}H^{(2)}_{\frac{5}{2}}(ka)-H^{(2)}_{\frac{7}{2}}(ka)\right\},\\
A_0 &= A_1=B_1=A_3=B_3=\;\ldots\;=0.
\end{aligned}\right\}\quad(14)
$$

These conditions in the special case, $\lambda=\mu$, are as follows:

$$
\left.\begin{aligned}
A_2\Phi &= \frac{2}{3}\sqrt{\frac{1}{2}\pi h}\,\frac{p_sa}{\mu}\left[\left\{\frac{1}{ka}\left(\frac{24}{k^2a^2}-1\right)\cos ka\right.\right.\\
&\quad\left.+\left(-\frac{24}{k^4a^4}+\frac{9}{k^2a^2}+1\right)\sin ka\right\}\\
&\quad\left.+i\left\{\left(-\frac{24}{k^4a^4}+\frac{6}{k^2a^2}+1\right)\cos ka-\frac{1}{ka}\left(\frac{24}{k^2a^2}-1\right)\sin ka\right\}\right],\\
B_2\Phi &= \frac{1}{3}\sqrt{\frac{1}{2}\pi k}\,\frac{p_sa}{\mu}\left[\left\{\frac{1}{ha}\left(\frac{24}{h^2a^2}-9\right)\cos ha+\left(-\frac{24}{h^4a^4}\right.\right.\right.\\
&\quad\left.\left.+\frac{17}{h^2a^2}-3\right)\sin ha\right\}+i\left\{\left(-\frac{24}{h^4a^4}+\frac{17}{h^2a^2}-3\right)\cos ha\right.\\
&\qquad\left.\left.-\frac{1}{ha}\left(\frac{24}{h^2a^2}-9\right)\sin ha\right\}\right],
\end{aligned}\right\}
$$

$$
\begin{aligned}
\Phi = &\left[\left\{\frac{1}{ha}\left(\frac{72}{h^2a^2}-13\right)\cos ha+\left(-\frac{72}{h^4a^4}+\frac{37}{h^2a^2}-3\right)\sin ha\right\}\right.\\
&+i\left\{\left(-\frac{72}{h^4a^4}+\frac{37}{h^2a^2}-3\right)\cos ha-\frac{1}{ha}\left(\frac{72}{h^2a^2}-13\right)\sin ha\right\}\\
&.\left[\left\{\frac{1}{ka}\left(-\frac{48}{k^2a^2}+5\right)\cos ka+\left(\frac{48}{k^4a^4}-\frac{21}{k^2a^2}+1\right)\sin ka\right\}\right.\\
&+i\left.\left\{\left(\frac{48}{k^4a^4}-\frac{21}{k^2a^2}+1\right)\cos ka-\frac{1}{ka}\left(-\frac{48}{k^2a^2}+5\right)\sin ka\right\}\right]\\
&+\frac{24}{hka^2}\left[\left\{\left(\frac{12}{h^2a^2}-1\right)\cos ha+\frac{1}{ha}\left(-\frac{12}{h^2a^2}+5\right)\sin ha\right\}\right.\\
&+i\left.\left\{\frac{1}{ha}\left(-\frac{12}{h^2a^2}+5\right)\cos ha-\left(\frac{12}{h^2a^2}-1\right)\sin ha\right\}\right]\\
&.\left[\left\{\left(\frac{12}{k^2a^2}-1\right)\cos ka+\frac{1}{ka}\left(-\frac{12}{k^2a^2}+5\right)\sin ka\right\}\right.\\
&\qquad\qquad+i\left.\left\{\frac{1}{ka}\left(-\frac{12}{k^2a^2}+5\right)\cos ka-\left(\frac{12}{k^2a^2}-1\right)\sin ka\right\}\right].
\end{aligned}
\tag{15}
$$

in which $h^2=\rho p^2/3\mu$, $k^2=\rho p^2/\mu$.

The transverse and radial components of the distortional waves v_2, u_2 and the radial and transverse components of the dilatational waves, u_1, v_1, are calculated for the cases $\sqrt{\rho/\mu}=1$, 10π, while the displacement distribution for every kind of wave front at

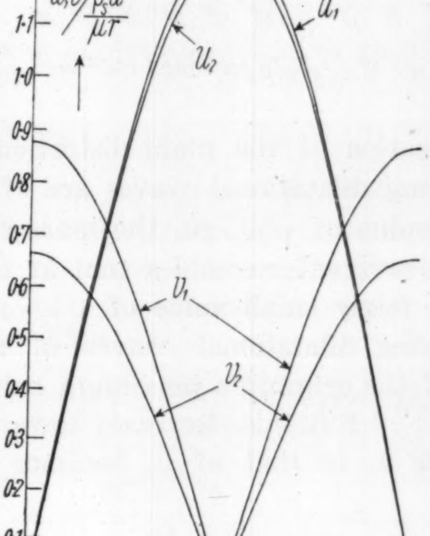

Fig. 12. $\sqrt{\rho/\mu}\,pa=1$, $r/a=1$.

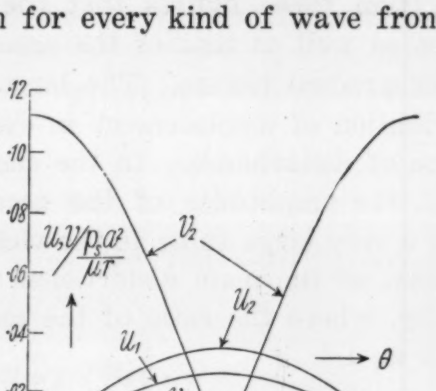

Fig. 13. $\sqrt{\rho/\mu}\,pa=1$, $r/a=10$.

distances $r/a=1,\ 10,\ \infty\ (\cos\phi=1)$ is plotted in Figs. 12~17. It will be

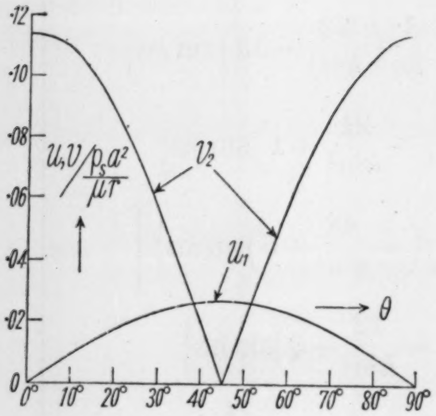

Fig. 14. $\sqrt{\rho/\mu}\,pa=1,\ r/a=\infty$.

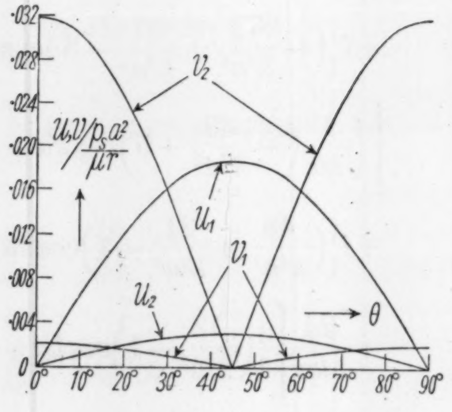

Fig. 15. $\sqrt{\rho/\mu}\,pa=10\pi,\ r/a=1$.

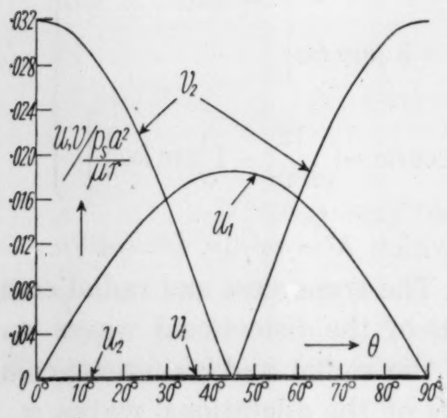

Fig. 16. $\sqrt{\rho/\mu}\,pa=10\pi,\ r/a=10$.

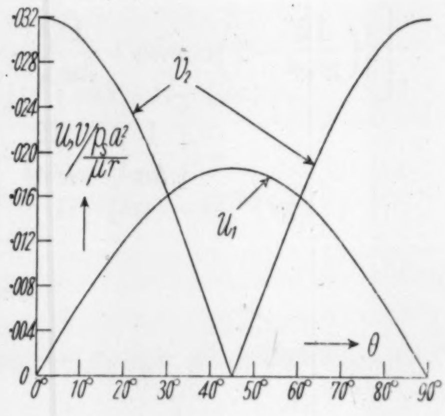

Fig. 17. $\sqrt{\rho/\mu}\,pa=10\pi,\ r/a=\infty$.

seen from these figures that the polarization of the main distortional waves as well as that of the accompanying dilatational waves are of a rather gradual nature. The larger the value of $\sqrt{\rho/\mu}\,pa$, the more the distribution of displacement in every wave front resembles that at the source of disturbance. In the case of a fairly small value of $\sqrt{\rho/\mu}\,pa$, say 1, the amplitudes of the accompanying dilatational waves u_1 assume a very large value in the vicinity of the origin, its maximum being 3/2 that of the main distortional waves v_2. But this decreases towards infinity, where the ratio of the amplitude u_1 to that of v_2 becomes as small as 1/4.

4. *A plane source with normal disturbance of the same phase within the plane of the source.*

The condition at the origin for the problem shown in Section 2

was approximate, due partly to the fact that the stress change at every point of that origin is not in the same phase, but varies somewhat along the radius of the disc at the origin. In the present section we deal with the case where the phase of the stress is everywhere the same within the disc under consideration. For that purpose we put the normal stress in the vicinity of the origin the form such that

$$p_n e^{ipt} = \mathrm{P} e^{i(pt-hx)}. \qquad (x>0) \tag{16}$$

It is possible to write

$$e^{-ihx} = \sum_{n=0}^{\infty} (2n+1)(-1)^n i^n \frac{J_{n+\frac{1}{2}}(hr)}{\sqrt{r}} P_n(\cos\theta), \tag{17}$$

when the condition of (1) is replaced by

$$\left.\begin{aligned} \widehat{rr}\cos\theta - \widehat{r\theta}\sin\theta &= p_n e^{ipt} \sum_{n=0}^{\infty} (2n+1)(-1)^n i^n \frac{J_{n+\frac{1}{2}}(hr)}{\sqrt{hr}} \cos\theta P_n(\cos\theta), \\ \widehat{rr}\sin\theta + \widehat{r\theta}\cos\theta &= 0 \end{aligned}\right\} \tag{18}$$

The general expressions of $\widehat{rr}$, $\widehat{r\theta}$, which are found from (2), (3), (4), should be put in (18), the result being such that

$$\left.\begin{aligned} &\sum_{n=0}^{\infty} \phi_n \sin\theta P_n(\cos\theta) + \sum_{n=0}^{\infty} \psi_n \cos\theta \frac{dP_n(\cos\theta)}{d\theta} = 0, \\ &\sum_{n=0}^{\infty} \phi_n \cos\theta P_n(\cos\theta) - \sum_{n=0}^{\infty} \psi_n \sin\theta \frac{dP_n(\cos\theta)}{d\theta} = \sum_{n=0}^{\infty} \frac{p_n\sqrt{a}}{\mu} \chi_n \cos\theta P_n(\cos\theta), \end{aligned}\right\} \tag{19}$$

where

$$\left.\begin{aligned} &\phi_n = \alpha_n A_n + \beta_n B_n, \quad \psi_n = \gamma_n A_n + \delta_n B_n, \\ &\chi_n = (2n+1)(-1)^n i^n \frac{J_{n+\frac{1}{2}}(ha)}{\sqrt{ha}}, \end{aligned}\right\} \tag{20}$$

in which

$$\left.\begin{aligned} \alpha_n &= \left\{1 - \frac{2n(n-1)}{h^2a^2}\right\} H^{(2)}_{n+\frac{1}{2}}(ha) + \frac{2(2n+1)}{ha} H^{(2)}_{n+\frac{3}{2}}(ha) - 2H^{(2)}_{n+\frac{5}{2}}(ha), \\ \beta_n &= \frac{2n(n+1)}{ka}\left\{-\frac{n-1}{ka} H^{(2)}_{n+\frac{1}{2}}(ka) + H^{(2)}_{n+\frac{3}{2}}(ka)\right\}, \\ \gamma_n &= \frac{2}{ha}\left\{-\frac{n-1}{ha} H^{(2)}_{n+\frac{1}{2}}(ha) + H^{(2)}_{n+\frac{3}{2}}(ha)\right\}, \end{aligned}\right\} \tag{21}$$

$$\delta_n = \frac{2(1+n)(1-n)}{k^2a^2} H^{(2)}_{n+\frac{1}{2}}(ka) + \frac{2n+1}{ka} H^{(2)}_{n+\frac{3}{2}}(ka) - H^{(2)}_{n+\frac{5}{2}}(ka) \,. \Big\}$$

Now the values of $P_0(\cos\theta)$, $P_1(\cos\theta)$, ..., $dP_1(\cos\theta)/d\theta$, $dP_2(\cos\theta)/d\theta$ are of the forms

$$P_0=1,\quad P_1=\cos\theta,\quad P_2=\frac{3}{2}\cos^2\theta-\frac{1}{2},\quad P_3=\frac{5}{2}\cos^3\theta-\frac{3}{2}\cos\theta,$$

$$P_4=\frac{35}{8}\cos^4\theta-\frac{15}{4}\cos^2\theta+\frac{3}{8},\quad P_5=\frac{63}{8}\cos^5\theta-\frac{35}{4}\cos^3\theta+\frac{15}{8}\cos\theta,$$

$$P_6=\frac{231}{16}\cos^6\theta-\frac{315}{16}\cos^4\theta+\frac{105}{16}\cos^2\theta-\frac{5}{16},$$

$$P_7=\frac{429}{16}\cos^7\theta-\frac{693}{16}\cos^5\theta+\frac{315}{16}\cos^3\theta-\frac{35}{16}\cos\theta,$$

....

$$\frac{dP_1}{d\theta}=-\sin\theta,\quad \frac{dP_2}{d\theta}=-3\sin\theta\cos\theta,\quad \frac{dP_3}{d\theta}=\sin\theta\Big(\frac{3}{2}-\frac{15}{2}\cos^2\theta\Big),$$

$$\frac{dP_4}{d\theta}=\sin\theta\Big(\frac{15}{2}\cos\theta-\frac{35}{2}\cos^3\theta\Big),$$

$$\frac{dP_5}{d\theta}=\sin\theta\Big(-\frac{15}{8}+\frac{105}{4}\cos^2\theta-\frac{315}{8}\cos^4\theta\Big),$$

$$\frac{dP_6}{d\theta}=\sin\theta\Big(-\frac{105}{8}\cos\theta+\frac{315}{4}\cos^3\theta-\frac{693}{8}\cos^5\theta\Big),$$

$$\frac{dP_7}{d\theta}=\sin\theta\Big(\frac{35}{16}-\frac{945}{16}\cos^2\theta+\frac{3465}{16}\cos^4\theta-\frac{3003}{16}\cos^6\theta\Big),$$

....

Equating each coefficient of the harmonic terms in (19) for the case $ha=1$, $ka=\sqrt{3}$, we find that

$$\phi_0=\frac{1}{240}(80\chi_0+32\chi_2-385\chi_6+\cdots)\frac{p_n\sqrt{a}}{\mu},$$

$$\phi_1=\frac{1}{560}(336\chi_1+96\chi_3-4095\chi_7+\cdots)\frac{p_n\sqrt{a}}{\mu},$$

$$\phi_2=\frac{1}{42}\left(28\chi_0+22\chi_2+8\chi_4-245\chi_6+\cdots\right)\frac{p_n\sqrt{a}}{\mu},$$

$$\phi_3=\frac{1}{990}(396\chi_1+506\chi_3+200\chi_5-10395\chi_7+\cdots)\frac{p_n\sqrt{a}}{\mu},$$

$$\phi_4=\frac{1}{385}(132\chi_2+195\chi_4-1785\chi_6+\cdots)\frac{p_n\sqrt{a}}{\mu},$$

$$\phi_5=\frac{1}{819}(260\chi_3+413\chi_5-5229\chi_7+\cdots)\frac{p_n\sqrt{a}}{\mu},$$

$$\phi_6=\frac{1}{33}(10\chi_4-45\chi_6+\cdots)\frac{p_n\sqrt{a}}{\mu},$$

$$\phi_7=\frac{1}{143}(42\chi_5-231\chi_7+\cdots)\frac{p_n\sqrt{a}}{\mu},$$

....

$$\psi_1=\frac{1}{560}(112\chi_1-48\chi_3-455\chi_7-\cdots)\frac{p_n\sqrt{a}}{\mu},$$

$$\psi_2=\frac{1}{1008}(336\chi_0+48\chi_2-64\chi_4-735\chi_6+\cdots)\frac{p_n\sqrt{a}}{\mu},$$

$$\psi_3=\frac{1}{990}(132\chi_1+22\chi_3-50\chi_5-1155\chi_7+\cdots)\frac{p_n\sqrt{a}}{\mu},$$

$$\psi_4=\frac{1}{3080}(264\chi_2+40\chi_4-1995\chi_6+\cdots)\frac{p_n\sqrt{a}}{\mu},$$

$$\psi_5=\frac{1}{819}(52\chi_3+7\chi_5-630\chi_7+\cdots)\frac{p_n\sqrt{a}}{\mu},$$

$$\psi_6=\frac{1}{198}(10\chi_4-45\chi_6+\cdots)\frac{p_n\sqrt{a}}{\mu},$$

$$\psi_7=\frac{1}{143}(6\chi_5-33\chi_7+\cdots)\frac{p_n\sqrt{a}}{\mu},$$

....

Substituting the values of ϕ_n, ψ_n thus obtained and those of α_n, β_n,

γ_n, δ_n written in (21) into the equations in (20), and solving the resulting equations, it is possible to calculate A_n, B_n, C_n, D_n from (20), the result being

$$A_0=0{\cdot}01856+i0{\cdot}055,$$
$$A_1=-0{\cdot}05375-i0{\cdot}0363,$$
$$A_2=-0{\cdot}02814-i0{\cdot}0667,$$
$$A_3=-0{\cdot}01997+i0{\cdot}00556,$$
$$A_4=0{\cdot}0^42143+i0{\cdot}0^3931,$$
$$A_5=0{\cdot}0^41841+0i,$$
$$A_6=0-i0{\cdot}0^62352,$$
....

$$[B_0=0{\cdot}221+i0{\cdot}03487],$$
$$B_1=-0{\cdot}3228-i0{\cdot}1887,$$
$$B_2=-0{\cdot}1321-i0{\cdot}3115,$$
$$B_3=-0{\cdot}1173+i0{\cdot}03258,$$
$$B_4=0{\cdot}0^31697+i0{\cdot}007377,$$
$$B_5=0{\cdot}0^32064+0i,$$
$$B_6=0-i0{\cdot}0^53872,$$
....

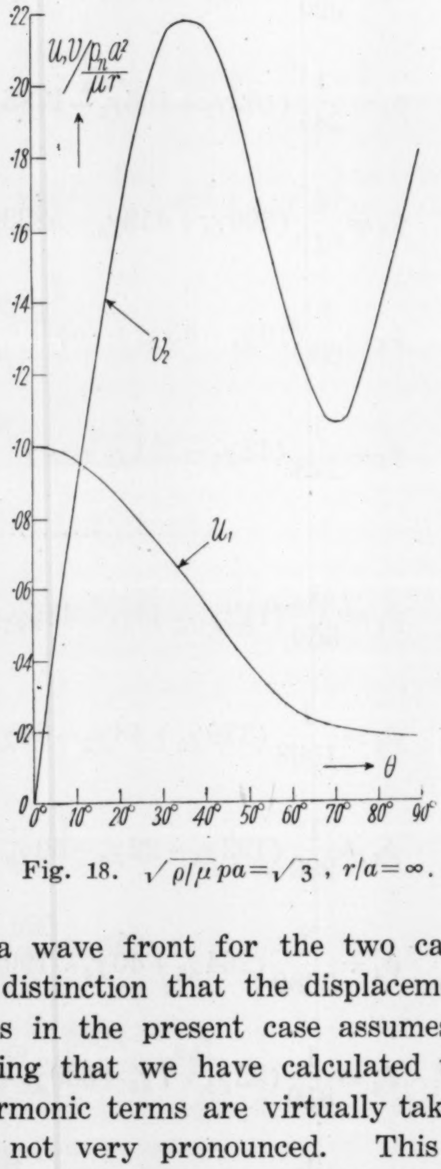

Fig. 18. $\sqrt{\rho/\mu}\,pa=\sqrt{3}$, $r/a=\infty$.

The calculation for the case $\sqrt{\rho/\mu}\,pa=\sqrt{3}$, $r=\infty$ is plotted in Fig. 18. Comparison of this figure with Fig. 4, where $\sqrt{\rho/\mu}\,pa=1$ instead of $\sqrt{\rho/\mu}\,pa=\sqrt{3}$, still shows that the displacement distribution in a wave front for the two cases are fairly similar, with however the distinction that the displacement of the accompanying distortional waves in the present case assumes a relatively large value. Notwithstanding that we have calculated the case wherein an infinite number of harmonic terms are virtually taken, polarization in a certain direction is not very pronounced. This is however easily accounted for by the fact that the expression $ha=1$ indicates the case in which the ratio of the generated dilatational waves to the radius of the source is 2π. Were we to take the case where the wave length is fairly small, say a fraction of the radius of the source, the generated dilatational waves would probably be polarized in a thin beam of waves directed normally to the plane of the disc at the source.

---

44. 平面源を有する彈性波勢力の偏り

地震研究所 {妹澤克惟
金井清

彈性波源が球形の如き場合には波動方向と球面の法線とが一致してゐるから，問題が比較的に簡單である．平面源例へば圓形板の如き波原がある場合は以前に試みた Mathieu の函數の取扱等で解決できる筈であるけれども具體的には餘り簡單ではない．それで Bessel 函數を適當に組合して問題を近似的に解くことも一つの方法であるから，それを試みた次第である．

このやうにして見ると波動原が垂直振動の場合でも横振動の場合でも，その振動波長が可なり短くなつても彈性波勢力の方向性偏りが思つた程著しくないことがわかつた．又，波動原が縦波(横波)だけ出すやうに見える場合でも相當大きな横波（縦波）が必ず伴ふこともわかつたのである．それにしても波長が短くなると波動原に近い所の振幅の方向的分布と遠方でのそれとは大體よく一致するけれども，波長が長くなるとそのやうな分布の相應性が著しく變ることがわかつた．その上縦波に伴ふ横波は遠方では益々大きくなり，横波に伴ふ縦波は遠方では少しづゝ小さくなることもわかる．尙，波動原に沿ふての振動分布が時間的に正確に同じ位相になるといふことを入れると計算が著しく複雜になる．その計算結果として例へば縦波に伴ふ横波の振幅が，位相について近似的に出した場合の横波の振幅よりも可なり大きくなることがわかるのである．この位相を正確に合す場合に波長を極く短くすれば特に強い方向性偏りが得られることはセイシの問題の場合に照して明かであるが，この論文ではそこまでの計算を出す餘裕が得られなかつた．

45. *The Effect of Differences in the Media on the Distribution of Displacements in a Seismic Wave Front.*

By Katsutada SEZAWA,

Earthquake Research Institute.

(Read Sept. 15, 1936.—Received Sept. 21, 1936.)

1. *Introduction.*

Some years ago[1] I gave formulae relating to the energy separation of elastic waves into dilatational and distortional waves when they are radiated from a spherical origin, the forces on the spherical surface being distributed in the form of zonal harmonics. As the object of that paper was merely to show the mechanism of energy separation under consideration, we gave no numerical example or any varification of the correctness of the symbolic expressions. Although another paper[2] was later written with a view to showing accurately the corrected expressions of the solution, the nature of the original problem was not studied. Inouye[3], who recently made use of our formulae in his study of initial motion of seismic waves, showed that the distribution of initial motion in a wave front is possible only in the case of short waves —a condition familiar to us in the case of acoustic waves—although no study to speak of has been made of it in the field of seismology. The results of his studies therefore seem to have thrown some light on the problem of initial motion that is being discussed frequently now in Japan.

The distribution of the initial motion, that is, the distribution of the displacements in a wave front at different radial distances is also affected by the nature of the medium through which the waves are transmitted. Unless both the density and the elasticity of the seismic region are about the same for different earthquakes, the study of the mechanism of a seismic origin from the data of the initial motion would be impossible even if the frequency of the initial motion were specified.

---

1) K. SEZAWA, "Dilatational and Distortional Waves generated from a Cylindrical or Spherical Origin", *Bull. Earthq. Res. Inst.*, **2** (1927), 13~20.

2) K. SEZAWA and K. KANAI, "Amplitudes of P- and S-waves at Different Focal Distances", *Bull. Earthq. Res. Inst.*, **10** (1932), 299~334; *Sindôgaku* (1932), 656.

3) W. INOUYE, "On the Mechanism of a Seismic Origin", *Disin*, **8** (1936), 387~403, (in Japanese).

With the aid of Kanai[4] the formulae for calculating the foregoing has recently been improved to such a degree of accuracy as to entirely exclude errors, even in the algebraic signs of the resultant displacement. The present paper is the outcome of Inouye's suggestion to publish in a form available for ready use the somewhat inconvenient formulae that I had originally obtained.

Although the generation of dilatational and distortional waves from a spherical origin may appear to be preferable from the practical point of view, the treatment of such a problem is somewhat difficult. Since in contrast to it, radiation of pure distortional waves from a spherical origin is very simple, and it still gives a general idea of the problem, whence, a full explanation of it will be made in my treatment here of radiation of pure distortional waves. The case in which both kinds of waves are generated will be dealt with mainly from the theoretical standpoint, argumented with a few numerical examples.

2. *Pure distortional waves generated from a spherical origin.*

The problem was shown in my previous paper[5], the solution being

$$w_n = A_n \frac{H^{(2)}_{n+\frac{1}{2}}(kr)}{\sqrt{kr}} \frac{dP_n(\cos\theta)}{d\theta} e^{ipt}, \tag{1}$$

where $k^2 = \rho p^2/\mu$ and w_n is the displacement directed azimuthally. If the disturbance at the surface of the spherical origin be $S_n dP_n(\cos\theta)/d\theta$, the condition at $r=a$ is

$$\mu \frac{\partial w_n}{\partial r} = S_n \frac{dP_n(\cos\theta)}{d\theta} e^{ipt}, \tag{2}$$

from which

$$A_n = \frac{S_n}{k\mu} \Big/ \left(\frac{d\phi}{d(kr)} \right)_{r=a}, \tag{3}$$

ϕ being written for $H^{(2)}_{n+\frac{1}{2}}(kr)/\sqrt{kr}$. If we write $x=ka$, the algebraic expression for ϕ for a few cases are as follows:

4) K. SEZAWA and K. KANAI, "The Polarization of Elastic Waves generated from a Plane Source, "*Bull. Earthq. Res. Inst.*, **14** (1936), 489~505.

5) K. SEZAWA, *loc. cit.* 1).

$$n=0;\quad \phi(x)=\sqrt{\frac{2}{\pi}}\frac{i}{x}e^{-ix},$$

$$n=1;\quad \phi(x)=\sqrt{\frac{2}{\pi}}\Big(\frac{i}{x^2}-\frac{1}{x}\Big)e^{-ix},$$

$$n=2;\quad \phi(x)=\sqrt{\frac{2}{\pi}}\Big\{i\Big(\frac{3}{x^3}-\frac{1}{x}\Big)-\frac{3}{x^2}\Big\}e^{-ix},$$

$$n=3;\quad \phi(x)=\sqrt{\frac{2}{\pi}}\Big\{i\Big(\frac{15}{x^4}-\frac{6}{x^2}\Big)-\Big(\frac{15}{x^3}-\frac{1}{x}\Big)\Big\}e^{-ix},$$

$$n=4;\quad \phi(x)=\sqrt{\frac{2}{\pi}}\Big\{i\Big(\frac{105}{x^5}-\frac{45}{x^3}+\frac{1}{x}\Big)-\Big(\frac{105}{x^4}-\frac{10}{x^2}\Big)\Big\}e^{-ix}.$$

The displacement at an infinite distance from the origin then becomes

$$w_n=\frac{(i)^n e^{ik(a-r)}}{k^2\mu r M_n}S_n\frac{dP_n}{d\theta}e^{-ipt},\tag{4}$$

M_n being

$$n=0;\quad M_0=\Big(\frac{1}{x}-\frac{i}{x^2}\Big)e^{-ix},$$

$$n=1;\quad M_1=\Big\{\frac{2}{x^2}-i\Big(\frac{2}{x^3}-\frac{1}{x}\Big)\Big\}e^{-ix},$$

$$n=2;\quad M_2=\Big\{\Big(\frac{9}{x^3}-\frac{1}{x}\Big)-i\Big(\frac{9}{x^4}-\frac{4}{x^2}\Big)\Big\}e^{-ix},$$

$$n=3;\quad M_3=\Big\{\Big(\frac{60}{x^4}-\frac{7}{x^2}\Big)-i\Big(\frac{60}{x^5}-\frac{27}{x^3}+\frac{1}{x}\Big)\Big\}e^{-ix},$$

$$n=4;\quad M_4=\Big\{\Big(\frac{525}{x^5}-\frac{65}{x^3}+\frac{1}{x}\Big)-i\Big(\frac{525}{x^6}-\frac{240}{x^4}+\frac{11}{x^2}\Big)\Big\}e^{-ix}.$$

If $S_n dP_n(\cos\theta)/d\theta$ be a constant for different n, the ratio of $|w_n|/|w_1|$ assumes the values shown in Table I.

Table I.

$p\sqrt{\frac{\rho}{\mu}}a$	10	2	1	0·5	0·1
$\|w_2\|/\|w_1\|$	1·0	0·734	0·184	0·152	0·0213
$\|w_3\|/\|w_1\|$	1·035	0·322	0·0276	0·00830	$0{\cdot}0^3334$
$\|w_4\|/\|w_1\|$	1·05	0·0578	0·00316	$0{\cdot}0^3471$	$0{\cdot}0^4384$

Let the period of the waves and the circumference of the spherical origin be $T=1$ sec and $2\pi a=1$ km respectively. If $|w_1|$ for the case $\sqrt{\mu/\rho}=1$ km/s is assumed to be unity, then the values of $|w_n|$ for different $\sqrt{\mu/\rho}$'s under the assumption that $S_n|dP_n/d\theta|$ as well as ρ always remain constants, are shown in Table II. Since the respective maximum values of $|dP_1/d\theta|$, $|dP_2/d\theta|$, $|dP_3/d\theta|$,……are 1, 3/2, $8/\sqrt{15}$,…, the order of each value in this table would not change even were S_n assumed to be constant in lieu of $S_n|dP_n/d\theta|$.

Table II.

$\sqrt{\mu/\rho}$ km/s	0·1	0·5	1	2	10
$\|w_1\|$	17·3	3·10	1	0·108	$0{\cdot}0^3866$
$\|w_2\|$	17·3	2·27	0·184	0·0164	$0{\cdot}0^4185$
$\|w_3\|$	17·9	1·00	0·0276	$0{\cdot}0^3896$	$0{\cdot}0^6296$
$\|w_4\|$	18·2	0·179	0·00316	$0{\cdot}0^4509$	$0{\cdot}0^7333$

It will be seen from the foregoing table that the higher the rigidity of the ground through which the waves are transmitted, the more neutralized is the distribution of the displacement in a wave front. If, on the other hand, the ground were fairly soft, the distribution under consideration would be pronounced even at a great distance from the origin. For example, if the amplitude w_1 is unity for any $\sqrt{\mu/\rho}$, the maxima of the amplitudes w_2 for the cases of $\sqrt{\mu/\rho}=0{\cdot}1$ km s, 0·5 km s, 1 km s, 2 km s, 10 km s assume the values 1, 0·734, 0·184, 0·152, 0·0213 respectively, the relation $S_2|dP_2/d\theta|=S_1|dP_1/d\theta|$ being assumed to exist in every case.

3. *Both dilatational and distortional waves radiated from a spherical origin.*

The solution for the present case will be found in the previous papers[6], the expressions being

6) K. Sezawa, *loc. cit.* 1), 4).

$$\left.\begin{aligned}
\Delta &= A_n H^{(2)}_{n+\frac{1}{2}}(hr) P_n(\cos\theta) e^{ipt}, \\
u_1 &= -\frac{A_n}{h^2}\frac{d}{dr}\frac{H^{(2)}_{n+\frac{1}{2}}(hr)}{\sqrt{r}} P_n(\cos\theta) e^{ipt}, \\
v_1 &= -\frac{A_n}{h^2}\frac{H^{(2)}_{n+\frac{1}{2}}(hr)}{r^{\frac{3}{2}}}\frac{dP_n(\cos\theta)}{d\theta} e^{ipt}, \\
u_2 &= -n(n+1)\frac{B_n H^{(2)}_{n+\frac{1}{2}}(hr)}{k^2 \; r^{\frac{3}{2}}} P_n(\cos\theta) e^{ipt}, \\
v_2 &= -\frac{B_n}{k^2}\frac{1}{r}\frac{d}{dr}\left\{\sqrt{r}\, H^{(2)}_{n+\frac{1}{2}}(kr)\right\}\frac{dP_n(\cos\theta)}{d\theta} e^{ipt},
\end{aligned}\right\} \tag{5}$$

where $h^2=\rho p^2/(\lambda+2\mu)$, $k^2=\rho p^2/\mu$, $u_1+u_2=u$, $v_1+v_2=v$. Substituting these solutions in the boundary conditions

$$\left.\begin{aligned}
\widehat{rr} &= \lambda\Delta + 2\mu\frac{\partial u}{\partial r} = p_n P_n(\cos\theta) e^{ipt}, \\
\widehat{r\theta} &= \mu\left(\frac{\partial v}{\partial r} - \frac{v}{r} + \frac{1}{r}\frac{\partial u}{\partial \theta}\right) = 0,
\end{aligned}\right\} \tag{6}$$

we obtain at $r=a$

$$\left.\begin{aligned}
&\sqrt{h}\, A_n\left[\left\{\left(\frac{y}{x}\right)^2 - 2\right\}\phi(x) - 2\frac{d^2\phi(x)}{dx^2}\right] - \sqrt{k}\, B_n 2n(n+1)\frac{d}{dy}\frac{\phi(y)}{y} = \frac{p_n}{\mu}, \\
&\frac{\sqrt{k}\, B_n}{\sqrt{h}\, A_n} = \frac{-\dfrac{d}{da}\dfrac{\phi(x)}{x} - \dfrac{\phi(x)}{x^2} - \dfrac{1}{x}\dfrac{d\phi(x)}{dx}}{\dfrac{d}{dy}\dfrac{1}{y}\dfrac{b}{dy}\left\{y\phi(y)\right\} - \dfrac{1}{y^2}\dfrac{d}{dy}\left\{y\phi(y)\right\} + n(n+1)\dfrac{\phi(y)}{y^2}},
\end{aligned}\right\} \tag{7}$$

where $x=hr$, $y=kr$. Substituting (7) in (5) we get the general solutions. In the particular cases $n=0$, 1, 2, 3, 4; the solution of u_1 at $r=\infty$ assumes the form

$$u_1(=u_{1n}) = -(i)^n \frac{p_n}{\mu h^2 r}\frac{e^{ih(a-r)}}{M_n} P_n(\cos\theta) e^{ipt}, \tag{8}$$

where M_n for a few cases are of the forms:

$$n=0; \quad M_0 = \frac{4}{x^2} - i\left(\frac{4}{x^3} - \frac{c^2}{x}\right),$$

$$n=1;\quad M_1=\left(\frac{12}{x^3}-\frac{c^2}{x}\right)-i\left(\frac{12}{x^4}-\frac{4+c^2}{x^2}\right)$$

$$-4\frac{\sqrt{k}B_1}{\sqrt{h}A_1}\left\{\frac{2}{y^3}-i\left(\frac{3}{y^4}-\frac{1}{y^2}\right)\right\},$$

$$\frac{\sqrt{k}B_1}{\sqrt{h}A_1}=\frac{\frac{6}{x^3}-i\left(\frac{6}{x^4}-\frac{2}{x^2}\right)}{\left(\frac{6}{y^3}-\frac{1}{y}\right)-i\left(\frac{6}{y^4}-\frac{3}{y^2}\right)},$$

$$n=2;\quad M_2=\left(\frac{72}{x^4}-\frac{4+3c^2}{x^2}\right)-i\left(\frac{72}{x^5}-\frac{28+3c^2}{x^3}+\frac{c^2}{x}\right)$$

$$-12\frac{\sqrt{k}B_2}{\sqrt{h}A_2}\left\{\left(\frac{12}{y^4}-\frac{1}{y^2}\right)-i\left(\frac{12}{y^5}-\frac{5}{y^2}\right)\right\},$$

$$\frac{\sqrt{k}B_2}{\sqrt{h}A_2}=\frac{\left(\frac{24}{x^4}-\frac{2}{x^2}\right)-i\left(\frac{24}{x^5}-\frac{10}{x^3}\right)}{\left(\frac{48}{y^4}-\frac{5}{y^4}\right)-i\left(\frac{48}{y^5}-\frac{21}{y^3}+\frac{1}{y}\right)},$$

$$n=3;\quad M_3=\left(\frac{600}{x^5}-\frac{52+15c^2}{x^3}+\frac{c^2}{x}\right)-i\left(\frac{600}{x^5}-\frac{252+15c^2}{x^4}+\frac{4+6c^2}{x^2}\right)$$

$$-24\frac{\sqrt{k}B_3}{\sqrt{h}A_3}\left\{\left(\frac{75}{y^5}-\frac{8}{y^3}\right)-i\left(\frac{75}{y^6}-\frac{33}{y^4}+\frac{1}{y^2}\right)\right\},$$

$$\frac{\sqrt{k}B_3}{\sqrt{h}A_3}=\frac{\left(\frac{150}{x^5}-\frac{16}{x^3}\right)-i\left(\frac{150}{x^6}-\frac{66}{x^4}+\frac{2}{x^2}\right)}{\left(\frac{450}{y^5}-\frac{51}{y^3}+\frac{1}{y}\right)-i\left(\frac{450}{y^6}-\frac{201}{y^4}+\frac{8}{y^2}\right)},$$

$$n=4;\quad M_4=\left(\frac{6300}{x^6}-\frac{660+105c^2}{x^4}+\frac{4+10c^2}{x^2}\right)-i\left(\frac{6300}{x^7}-\frac{2750+105c^2}{x^5}\right.$$

$$\left.+\frac{84+45c^2}{x^3}-\frac{c^2}{x}\right)-40\frac{\sqrt{k}B_4}{\sqrt{h}A_4}\left\{\left(\frac{630}{y^6}-\frac{95}{y^4}+\frac{1}{y^2}\right)\right.$$

$$\left.-i\left(\frac{630}{y^7}-\frac{285}{y^5}+\frac{12}{y^3}\right)\right\},$$

$$\frac{\sqrt{k}B_4}{\sqrt{h}A_4}=\frac{\left(\frac{1260}{x^6}-\frac{170}{x^4}+\frac{2}{x^2}\right)-i\left(\frac{1260}{x^7}-\frac{570}{x^5}+\frac{24}{x^4}\right)}{\left(\frac{5040}{y^6}-\frac{615}{y^4}+\frac{12}{y^2}\right)-i\left(\frac{5040}{y^7}-\frac{2295}{y^5}+\frac{105}{y^2}-\frac{1}{y}\right)},$$

where $x=ha$, $y=ka$, $c^2=k^2/h^2$.

If $p_nP_n(\cos\theta)$ be a constant for different n's, the ratio of $|u_{1n}|/|u_{10}|$ assumes the values shown in Table III. Mark (R) indicates that resonances of a certain kind are likely to exist for vibrations of type u_{1n}.

Table III.

$p\sqrt{\frac{\rho}{\lambda+2\mu}}a$	2	1	0·5	0·1
$\lvert u_{11}\rvert/\lvert u_{10}\rvert$	1·35	0·235	0·650 } (R)	4·0 (R)
$\lvert u_{12}\rvert/\lvert u_{10}\rvert$	0·74	0·0848 } (R)	0·310 } (R)	0·00061
$\lvert u_{13}\rvert/\lvert u_{10}\rvert$	——	0·0490 } (R)	0·053	——
$\lvert u_{14}\rvert/\lvert u_{10}\rvert$	——	0·0009	0·00004	——

Let the period of the waves and the circumference of the spherical origin be again $T=1$ sec and $2\pi a=1$ km respectively. Assuming that $|u_{10}|$ for $\sqrt{\mu/\rho}=1$ km/s is unity, the values of $|u_{1n}|$ for different $\sqrt{\mu/\rho}$'s under the assumption that $p_nP_n(\cos\theta)$ as well as ρ are invariably constant for any n, are shown in Table IV.

Table IV.

$\sqrt{\mu/\rho}$ km/s	0·5	1	2	10
$\lvert u_{10}\rvert$	2·91	1	0·134	0·00103
$\lvert u_{11}\rvert$	3·93	0·235	0·0870	0·00412
$\lvert u_{12}\rvert$	2·15	0·0848	0·0415	$0{\cdot}0^6629$
$\lvert u_{13}\rvert$	——	0·0490	0·0071	——
$\lvert u_{14}\rvert$	——	0·0009	$0{\cdot}0^555$	——

These tables show that in this case too, the higher the rigidity of the ground composing the seismic region, the more neutralized is the distribution of the displacements in a wave front. In the case of soft ground the distribution of the displacement under consideration is rather pronounced.

It is not clear to us as why the resonance-like conditions should be present, particularly in this case. As however we are investigating now only the problem of a vibrating sphere radiating dissipation waves, we shall probably be able to find an answer to the question when it has been investigated for its own sake.

In conclusion I wish to express my thanks to Dr. Inouye for his suggestions and to Dr. Kanai for his assistance in obtaining the mathematical formulae.

---

45. 媒體の異同が地震初動の分布に及ぼす影響

地震研究所 妹 澤 克 惟

震動原の大さに比較して波長が短い場合には原點の震動機構が地震初動の分布に割合によく現れるけれども，波長が長い場合には之が打消されて初動分布の狀態に現れ難いといふやうな事が井上氏によつて面白く發表された．この論文では同じ週期のものが原點に働いても，波動の傳播する媒體が違ふと，初動分布の狀態に著しい影響を與へるといふ事を示したのである．例へば原點が球狀をなしその球周が 1 km であり，週期 1 秒の橫波だけが出ると假定する．媒體の $\sqrt{\mu/\rho}=$ 1 km/s のときに $P_1(\cos\theta)$ 分布の波動振幅が無限大距離で 1 とする．同じ剪應力が働いて P_1, P_2, P_3, P_4 分布の波動が出る場合に，$\sqrt{\mu/\rho}=1$ km/s ではそれ等の無限大遠方に於ける振幅は 1, 0·184, 0·0276, 0·00316 となる．然るに $\sqrt{\mu/\rho}=0{\cdot}1$ km/s になると同じ振幅は 17·3, 17·3, 17·9, 18·2 となり，$\sqrt{\mu/\rho}=10$ km/s になると $0{\cdot}0^3866$, $0{\cdot}0^4185$, $0{\cdot}0^6296$, $0{\cdot}0^7333$ となる．卽ち初動分布から震原機構を推定するには震動週期が違ふと結果が勿論違ふけれども，その媒體の彈性等が異なるものであると又同樣に著しく異なる結果が出ることを示すものである．

震原から縱波と橫波とが出る場合も計算を試みた．この場合は筆者が 1926 年頃發表した數式の表し方に多少不完全な所があり，これは筆者が前から氣がつきながら明瞭な訂正をしなかつた所が（但し振動學 656 頁には具體的の表し方が記載してある）井上氏から親切に之を誰でも直ちに使用できるやうに正しく記錄して置くやうとの御注意もあり，かたがた數式に特に力を入れて論文に示して置いたのである．

---

46. *Energy Dissipation in Seismic Vibrations of an Eight-storied Structure.*

By Katsutada SEZAWA and Kiyoshi KANAI,

Earthquake Research Institute.

(Read Sept. 15, 1936.—Received Sept. 21, 1936.)

1. *Mathematical theory.*

The problem of energy dissipation in the seismic vibrations of a structure that does not exceed 7-stories having already been studied, we shall now discuss a similar problem for an 8-storied sturcture, and in doing so, shall begin with the mathematical formulae that will necessarily be involved.

It is very important to know whether or not the floors are in a flexible condition. Our investigations[1] showed that were the formulae for extremely rigid floors used, the flexibility of the floors of virtually every building in Tokyo would be equivalent to a reduction to one-half the original effective value of $\sqrt{EI/ml^3}$.

The solutions and the boundary conditions of the problem for the case in which the floors are extremely rigid are shown in (32) ~ (41) of our previous paper[2]. When $E_1=E_2=\ldots$, $I_1=I_2=\ldots$, $m_1=m_2=\ldots$, the constants that belong to expressions for deflections of columns are as follows:

$$A_1=\phi\frac{2\Gamma}{\Phi}=\Bigg[(\gamma-12)^2\Big\{(\gamma-12)(\gamma-24)-144\Big\}\Big[-36\gamma(\gamma-24)(\gamma-36)$$

$$+\Big\{(\gamma-12)(\gamma-24)-144\Big\}^2\Big]-12\gamma\Big\{(\gamma-12)^2(\gamma-36)$$

$$-144(\gamma-24)\Big\}\Big\{(\gamma-12)(\gamma-36)^2-144(\gamma-24)\Big\}\Bigg]\frac{2\Gamma}{\Phi},$$

$$l^3D_1=\psi\frac{2\Gamma}{\Phi}=-2\Bigg[\gamma(\gamma-24)\Big\{(\gamma-24)^2-288\Big\}\Big[\Big\{(\gamma-24)^2$$

1) K. SEZAWA and K. KANAI, "The Effect of Stiffness of Floors on the Horizontal Vibrations of a Framed Structure", *Bull. Earthq. Res. Inst.*, **14** (1936), 367~376.

2) K. SEZAWA and K. KANAI, "Improved Theory of Energy Dissipation in Seismic Vibrations of a Structure", *Bull. Earthq. Res. Inst.*, **14** (1936), 164~188.

$$-288\Big\}^2-2.12^4\Big]\Big]\frac{2\Gamma}{\Phi},$$

$$A_2=-12(\gamma-12)\Big\{(\gamma-12)(\gamma-24)-144\Big\}\Big[-36\gamma(\gamma-24)(\gamma-36)$$

$$+\Big\{(\gamma-12)(\gamma-24)-144\Big\}^2\Big]\frac{2\Gamma}{\Phi},$$

$$l^3D_2=2.12\gamma\Big\{(\gamma-12)^2(\gamma-36)-144(\gamma-24)\Big\}\Big\{(\gamma-12)(\gamma-36)^2$$

$$-144(\gamma-24)\Big\}\frac{2\Gamma}{\Phi},$$

$$A_3=12^2\Big[\Big\{\gamma(\gamma-24)^2-12(\gamma-12)^2\Big\}^2-12\gamma(\gamma-12)^2(\gamma-36)^2\Big]\frac{2\Gamma}{\Phi},$$

$$l^3D_3=-2.12^2\gamma(\gamma-12)(\gamma-24)(\gamma-36)\Big\{(\gamma-24)^2-432\Big\}\frac{2\Gamma}{\Phi},$$

$$A_4=-12^3\Big[(\gamma-12)\Big\{(\gamma-12)^2-12\gamma\Big\}^2-12\gamma(\gamma-24)\Big[\Big\{(\gamma-12)^2$$

$$-12\gamma\Big\}+(\gamma-12)(\gamma-36)\Big]\Big]\frac{2\Gamma}{\Phi},$$

$$l^3D_4=2.12^3\gamma\Big\{(\gamma-12)(\gamma-24)-144\Big\}\Big\{(\gamma-24)(\gamma-36)-144\Big\}\frac{2\Gamma}{\Phi},$$

$$A_5=12^4(\gamma-12)\Big\{\gamma(\gamma-36)^2-12^3\Big\}\frac{2\Gamma}{\Phi},$$

$$l^3D_5=-2.12^4\gamma(\gamma-24)\Big\{(\gamma-24)^2-288\Big\}\frac{2\Gamma}{\Phi},$$

$$A_6=-12^5\Big\{\gamma(\gamma-24)(\gamma-36)-12^3\Big\}\frac{2\Gamma}{\Phi},$$

$$l^3D_6=2.12^5\gamma(\gamma-12)(\gamma-36)\frac{2\Gamma}{\Phi},$$

$$A_7=12^6\Big\{(\gamma-12)(\gamma-24)-144\Big\}\frac{2\Gamma}{\Phi},$$

$$l^3D_7=-2.12^6\gamma(\gamma-24)\frac{2\Gamma}{\Phi},$$

$$A_8=-12^7(\gamma-12)\frac{2\Gamma}{\Phi},$$

$$l^3D_8=2.12^7\gamma\frac{2\Gamma}{\Phi},$$

$$B_s=0, \qquad C_s=\frac{3}{2}lD_s, \quad (s=1,\ 2,\ \ldots.\ 8) \tag{1}$$

where

$$\left.\begin{aligned}
\Phi&=\phi\Gamma+\frac{18Ej^2\varepsilon}{\mu l^3}\psi\Lambda,\\
\Gamma&=\Gamma_1+i\Gamma_2, \qquad \Lambda=\Lambda_1+i\Lambda_2,\\
\Gamma_1&=3\left(\frac{\lambda}{\mu}+2\right)+\nu\gamma\left(\frac{\lambda}{\mu}-3\sqrt{\frac{\lambda}{\mu}+2}\right),\\
\Gamma_2&=\sqrt{\nu\gamma}\left\{3\left(\frac{\lambda}{\mu}+2+\sqrt{\frac{\lambda}{\mu}+2}\right)+\nu\gamma\left(\sqrt{\frac{\lambda}{\mu}+2}-2\right)\right\},\\
\Lambda_1&=\left(\frac{2\lambda}{\mu}+5\right)-\nu\gamma,\\
\Lambda_2&=\sqrt{\nu\gamma}\left(2\sqrt{\frac{\lambda}{\mu}+2}+1\right),\\
\nu&=\frac{E\rho I\varepsilon^2}{\mu m l^3}.
\end{aligned}\right\} \tag{2}$$

The values of the constants thus obtained should be substituted in the expressions for the deflections, namely,

$$y_s=(A_s+B_sx_s+C_sx_s^2+D_sx_s^3)e^{ipt}. \qquad (s=1,\ 2,\ \ldots.,\ 8) \tag{3}$$

The ratio of bending moments in the columns on each floor to the product of ml due to the acceleration of the ground (on which no structure stands) is expressed by equations of the forms

$$EI\frac{d^2y_1}{dx_1^2}\bigg/2p^2ml=6(24-\gamma)\left\{(24-\gamma)^2-288\right\} \cdot\left[\left\{(24-\gamma)^2-288\right\}^2-2.12^4\right]\left(1+\frac{2x_1}{l}\right)M,$$

$$EI\frac{d^2y_2}{dx_2^2}\bigg/2p^2ml=6.12\left\{(12-\gamma)^2(36-\gamma)-144(24-\gamma)\right\}$$

$$\cdot\left\{(12-\gamma)(36-\gamma)^2-144(24-\gamma)\right\}\left(1+\frac{2x_2}{l}\right)M\,,$$

$$EI\frac{d^2y_3}{dx_3^2}\Bigg|\,2p^2ml=6.12^2(12-\gamma)(24-\gamma)(36-\gamma)$$

$$\cdot\left\{(24-\gamma)^2-432\right\}\left(1+\frac{2x_3}{l}\right)M\,,$$

$$EI\frac{d^2y_4}{dx_4^2}\Bigg|\,2p^2ml=6.12^3\left\{(12-\gamma)(24-\gamma)-144\right\}$$

$$\cdot\left\{(24-\gamma)(36-\gamma)-144\right\}\left(1+\frac{2x_4}{l}\right)M\,,$$

$$EI\frac{d^2y_5}{dx_5^2}\Bigg|\,2p^2ml=6.12^4(24-\gamma)\left\{(24-\gamma)^2-288\right\}\left(1+\frac{2x_5}{l}\right)M\,,$$

$$EI\frac{d^2y_6}{dx_6^2}\Bigg|\,2p^2ml=6.12^5(12-\gamma)(36-\gamma)\left(1+\frac{2x_6}{l}\right)M\,,$$

$$EI\frac{d^2y_7}{dx_7^2}\Bigg|\,2p^2ml=6.12^6(24-\gamma)\left(1+\frac{2x_7}{l}\right)M\,,$$

$$EI\frac{d^2y_8}{dx_8^2}\Bigg|\,2p^2ml=6.12^7\left(1+\frac{2x_8}{l}\right)M\,, \tag{4}$$

where

$$\left.\begin{aligned} M&=\sqrt{\frac{\Gamma_1^2+\Gamma_2^2}{P^2+Q^2}}\cos\left(pt+\tan^{-1}\frac{\Gamma_2}{\Gamma_1}-\tan^{-1}\frac{Q}{P}\right),\\ P&=\phi\Gamma_1+\frac{18Ej^2\varepsilon}{\rho l^3}\psi\Lambda_1\,,\qquad Q=\phi\Gamma_2+\frac{18Ej^2\varepsilon}{\rho l^3}\psi\Lambda_2\,.\end{aligned}\right\} \tag{5}$$

2. *Resonance and corresonance frequencies.*

$\phi=0$ gives the natural vibration frequencies in the usual sense, that is, the frequencies where the ground is infinitely rigid. γ satisfies the equation $\phi=0$ when

$$\gamma=0{\cdot}3521,\ 3{\cdot}6,\ 9{\cdot}2,\ 17{\cdot}435,\ 26{\cdot}2,\ 34{\cdot}7,\ 41{\cdot}76,\ 46{\cdot}38,$$

or when

$$\sqrt{\gamma}=0{\cdot}5933,\ 1{\cdot}897,\ 3{\cdot}034,\ 4{\cdot}176,\ 5{\cdot}12,\ 5{\cdot}89,\ 6{\cdot}46,\ 6{\cdot}81.$$

$\psi=0$ gives the natural vibration frequencies of the structure in the case where the ground is extremely soft. This we have called the corresonance condition. γ satisfies $\psi=0$ when

$$\gamma=1{\cdot}8269,\ 7{\cdot}0296,\ 14{\cdot}816,\ 24,\ 33{\cdot}185,\ 40{\cdot}9704,\ 46{\cdot}17,$$

or when

$$\sqrt{\gamma} = 1{\cdot}3518,\ 2{\cdot}6515,\ 3{\cdot}85,\ 4{\cdot}899,\ 5{\cdot}759,\ 6{\cdot}399,\ 6{\cdot}795.$$

3. *Application of the theory to the Marunouti Building.*

The Marunouti Building, in Marunouti, Tokyo, is an 8-storied steel-framed reinforced concrete structure with a partial basement as well as a partial penthouse roof and a machine room roof, and let for shops and business offices by the owners, the Mitsubishi Co.. Although the building was completed in February 1923, some strengthening members were added to it soon after the Great Kwanto Earthquake of the same year. In the present prediction calculation, use has been made of data covering its present structural condition. The general view of the building and the general plan of the second floor are shown in Figs. 1, 2. (Fig. 1 was photographed by Mr. T. Takayama, whereas Fig. 2 was reproduced by Mr. K. Kaminaga from a sketch in the Architectural Engineering Pocket Book).

Fig. 1. A View from NE-corner.

The general and structural arrangements of floors higher than the 2nd and up to 7th, inclusive, are similar to the plan in Fig. 2. An arcade runs through the middle of the ground floor in a NS-direction. On the 1st floor are spaces over such parts of the arcade as correspond to the inner court yards. The positions of the columns are the same for every floor excepting the parts of the arcade just mentioned. The sizes of the columns and all the other structural members naturally diminish with their proximity to the roof floor.

The section of the steel frame in every column is of plate type, forming the built-up I in a plate and four angles, while that of some

of the girders consists of two channels, so as to form box girders, the remainder being the simple I-shape, although the frame of every beam consists of a smaller I-bar.

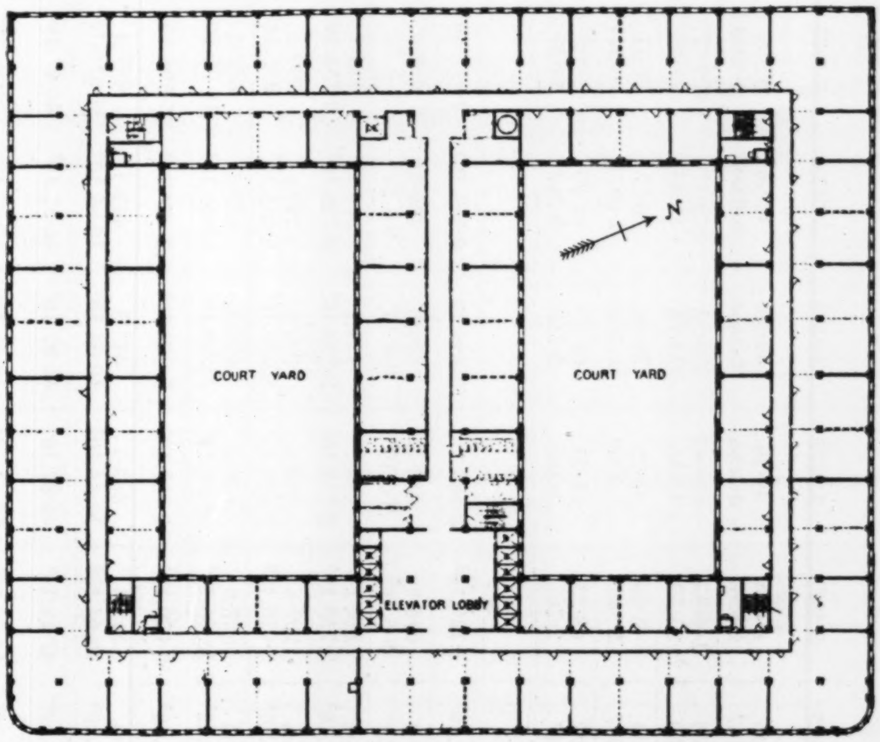

Fig. 2. General Plan of the Second Floor. Scale 1/580.

It was assumed in the numerical calculation that $E = 2{\cdot}1.10^9$ kg m^2 $= 2{\cdot}1.10^9.9{\cdot}8$ kg mass m/s^2/m^2, and that the floors are so rigid that the ends of the columns are always vertical. The calculated results of the important elements are shown in Table I, which may be used in almost any theoretical treatment of horizontal vibration of the structure under consideration. The moments of inertia of the columns in the table can be used for the case of vibration in a NS-direction.

By adjusting "the additional items" in the table, the total weight of the structure was made to be the same as that calculated by the designer. Since the weight due to the penthouse roof and the machine room roof is $73{\cdot}66.10^5$ kg, we added $73{\cdot}66.10^5$ kg/8 to the mean weight $67{\cdot}13.10^5$ kg of every floor from the lst floor to the roof. Thus $76{\cdot}33.10^5$ kg was used as the concentrated mass on every floor. The value of I was calculated as $21{\cdot}035$ m^4, but 1/2 of the value of $\sqrt{I}$ obtained here was used in the dissipation calculation to adjust the condition of slight flexibility of the floors.

To obtain the dissipation we put $\sqrt{\mu/\rho} = 50$ m/s, which may be some-

Table I.

Floor		1	2	3	4	5	6	7	Roof	Mean
Height of floor below l (m)		5·0325	3·5075	3·5075	3·5075	3·5075	3·5075	3·5075	3·5075	3·6981 +0·4194 =4·1175
Steel frames in columns	a (m^2) I (m^4)	96·77 0·946	96·77 0·946	69·40 0·5567	69·40 0·5567	49·20 0·3666	49·20 0·3666	32·90 0·2308	32·90 0·2308	62·07 0·5250
Remaining parts in columns	a (m^2) I (m^4)	169·05 25·97	158·95 21·53	143·75 13·60	140·52 13·09	139·02 12·56	133·53 11·78	129·17 11·03	129·17 11·03	142·89 15·07
Outside walls	a (m^2) I (m^4)	29·95 1·3525	37·61 1·2865	46·43 1·3897	43·48 1·3053	43·26 1·2900	39·44 1·1368	36·77 1·0572	36·77 1·0572	39·21 1·2344
Inside walls	a (m^2) I (m^4)	103·57 5·832	86·08 4·417	81·92 4·547	68·23 3·767	68·23 3·767	68·23 3·767	68·23 3·767	68·23 3·767	76·59 4·204
Totals	a (m^2) I (m^4)									320·8 21·04
Steel frames in columns	W(kg)	$2{\cdot}443.10^5$	$1{\cdot}642.10^5$	$1{\cdot}189.10^5$	$1{\cdot}189.10^5$	$0{\cdot}864.10^5$	$0{\cdot}864.10^5$	$0{\cdot}517.10^5$	$0{\cdot}517.10^5$	$1{\cdot}153.10^5$
Remaining parts in columns	v (m^3) W(kg)	650·1 $15{\cdot}61.10^5$	449·8 $10{\cdot}80.10^5$	400·0 $9{\cdot}6.10^5$	400·0 $9{\cdot}6.10^5$	400·0 $9{\cdot}6.10^5$	400·0 $9{\cdot}6{\cdot}10^5$	400·0 $9{\cdot}6.10^5$	400·0 $9{\cdot}6.10^5$	437·5 $10{\cdot}50.10^5$
Outside walls	v (m^3) W (kg)	103·1 $2{\cdot}473.10^5$	90·13 $2{\cdot}162.10^5$	114·1 $2{\cdot}738.10^5$	114·1 $2{\cdot}738.10^5$	114.1 $2{\cdot}738.10^5$	114·1 $2{\cdot}738.10^5$	114·1 $2{\cdot}738.10^5$	114·1 $2{\cdot}738.10^5$	109·7 $2{\cdot}633.10^5$
Inside walls	v (m^3) W (kg)	379·4 $9{\cdot}11.10^5$	251·4 $6{\cdot}04.10^5$	209·6 $5{\cdot}035.10^5$	209·6 $5{\cdot}035.10^5$	209·6 $5{\cdot}035.10^5$	209·6 $5{\cdot}035.10^5$	209·6 $5{\cdot}035.10^5$	209·6 $5{\cdot}035.10^5$	236·1 $5{\cdot}670.10^5$
Floors	v (m^3) W (kg)	736·0 $17{\cdot}66.10^5$	718·5 $17{\cdot}24.10^5$	627·5 $15{\cdot}06.10^5$	627·5 $15{\cdot}06.10^5$	627·5 $15{\cdot}06.10^5$	627·5 $15{\cdot}06.10^5$	627·5 $15{\cdot}06.10^5$	627·5 $15{\cdot}06.10^5$	652·4 $15{\cdot}66.10^5$
Frames in girders & beams	W (kg)	$2{\cdot}929.10^5$	$2{\cdot}929.10^5$	$2{\cdot}929.10^5$	$2{\cdot}929.10^5$	$2{\cdot}929.10^5$	$2{\cdot}929.10^5$	$2{\cdot}929.10^5$	$2{\cdot}506.10^5$	$2{\cdot}876.10^5$
Remaining parts in girders & beams	v (m^3) W (kg)	443·3 $10{\cdot}64.10^5$	443·3 $10{\cdot}64.10^5$	443·3 $10{\cdot}64.10^5$	443·3 $10{\cdot}64.10^5$	443·3 $10{\cdot}64.10^5$	443·3 $10{\cdot}64.10^5$	443·3 $10{\cdot}64.10^5$	459·0 $11{\cdot}016.10^5$	445·3 $10{\cdot}687.10^5$
Sum	W (kg)	$60{\cdot}87.10^5$	$51{\cdot}45.10^5$	$47{\cdot}19.10^5$	$47{\cdot}19.10^5$	$46{\cdot}87.10^5$	$46{\cdot}87.10^5$	$46{\cdot}52.10^5$	$46{\cdot}47.10^5$	$49{\cdot}18.10^5$
Additional items	W (kg)	$21{\cdot}92.10^5$	$21{\cdot}00.10^5$	$15{\cdot}33.10^5$	$14{\cdot}68.10^5$	$16{\cdot}45.10^5$	$16{\cdot}45.10^5$	$17{\cdot}87.10^5$	$19{\cdot}86.10^5$	$17{\cdot}95.10^5$
Total sum	W (kg)	$82{\cdot}79.10^5$	$72{\cdot}45.10^5$	$62{\cdot}52.10^5$	$61{\cdot}87.10^5$	$63{\cdot}33.10^5$	$63{\cdot}33.10^5$	$64{\cdot}39.10^5$	$66{\cdot}33.10^5$	$67{\cdot}13.10^5$

what too small, and $\rho=2$, whence

$$\frac{18Ej^2\varepsilon}{\mu l^3}=6{\cdot}68\,,$$

$$\Gamma_1\quad 9-0{\cdot}02518\gamma,\qquad \Gamma_2=1{\cdot}0994\sqrt{\gamma}-0{\cdot}0001246\gamma^{3/2},$$

$$\Lambda_1=7-0{\cdot}006\gamma,\qquad \Lambda_2=0{\cdot}3458\sqrt{\gamma}\,.$$

The calculated result is shown in Figs. 3 a, 3 b[3].

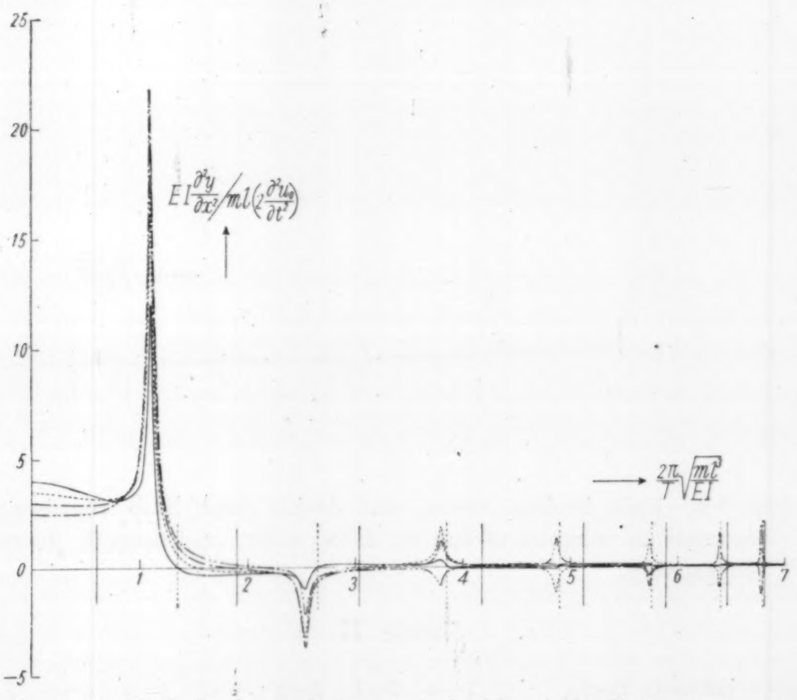

Fig. 3 a. Full, broken, chain, and double chain lines represent moments in columns of ground, first, second, and third floors respectively.

For the bending moment in every column, it is assumed that its maximum value at the frequency corresponding to $\sqrt{\gamma}=1{\cdot}10$, which is intermediate between the virtual first resonance and the first corresonance. The actual resonance period is

$$T=\frac{2\pi}{\sqrt{\gamma}}\sqrt{\frac{ml^3}{EI}}=\frac{2\pi}{1{\cdot}10}\sqrt{\frac{ml^3}{EI}}=0{\cdot}566\,\text{sec}\,.$$

The greatest value of the maximum bending moments is induced in columns between the third and fourth floors, the bending moments

3) The effect of such a deeply piled foundation as in the case of Marunouti Building is rather to greatly increase the energy dissipation owing to the fact that the area of contact surface between the piles and the ground soil is enormously increased. However, we are here discussing the problem of a hypothetical pileless structure wherein the dissipation is never very marked.

in all columns at this resonance period being of the magnitudes in Table II.

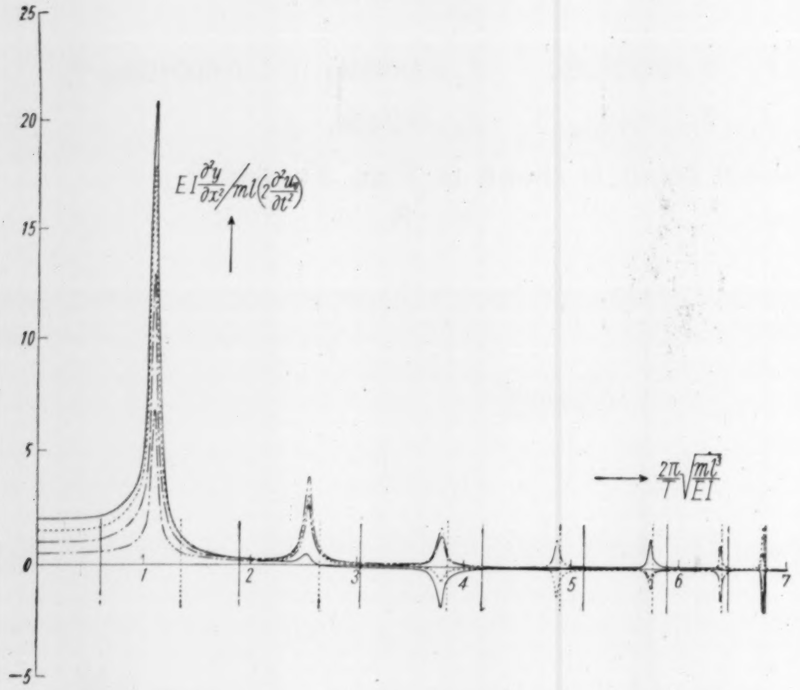

Fig. 3b. Full, broken, chain, and double chain lines represent moments in columns of fourth, fifth, sixth, and seventh floors respectively.

Table II.

Column between floors	1~0	2~1	3~2	4~3	5~4	6~5	7~6	8~7
Number of moment value at resonance	7	5	3	1	2	4	6	8
$\dfrac{EI\dfrac{d^2y}{dx^2}}{ml\left(2\dfrac{\partial^2 u}{\partial t^2}\right)}$ at resonance	12·0	17·3	20·5	21·8	20·9	17·8	13·0	6·8
The same at zero frequency	4·0	3·5	3·0	2·5	2·0	1·5	1·0	0·5

The full and broken vertical lines along the abscissa in Figs. 3a, 3b represent the virtual resonance and corresonance conditions, namely, the condition wherein the ground is very rigid and one in which it is very soft.

It was pointed out in the previous paper[4] that the vibrational frequency at which the bending moments become maximum, and the floor

4) K. SEZAWA and K. KANAI, "Energy Dissipation in Seismic Vibrations of Actual Buildings Predicted through Improved Theory", *Bull. Earthq. Res. Inst.*, **14** (1936), 377—386.

number at which the bending moments in the columns assume the greatest value at such vibrational frequency, depend on the ratio of $Ej^2\varepsilon/\mu l^3$. In the present case the first resonance condition in the sense that the bending moment becomes maximum at that condition takes place at a frequency that is not far from the one for the corresonance condition. It was furthermore ascertained that the higher the order of resonance, the more its frequency approaches that of the corresponding corresonance condition. The greatest bending moment at these higher resonance conditions are induced in different columns according as they differ in their order of resonance. But, it is easily confirmable from Figs. 3a, 3b that the greatest bending mements under consideration are fairly small for the second or any higher resonance condition.

It was also ascertained in writing this paper that in seismic vibrations, the greatest bending moment is not likely to be induced in the columns in the lower floors, such as the ground floor or the first, unless of course dissipation of the vibrational energy into the ground is neglected.

In conclusion we wish to express our thanks to the Council of the Foundation for the Promotion of Scientific and Industrial Research in Japan, by whose aid the present series of investigation was made, and also to the members of the staffs of the Mitsubishi Co., who kindly allowed us the use of the valuable data on the structure.

---

46. 8階建築に於ける震動勢力の地中逸散性

地震研究所 {妹澤克惟
金井清

これまで7階以下の建築構造について震動勢力が地中に逸散する割合を算出して置いたが，その後研究が著しく進んで8階の場合を確めることができた．計算の理論は以前の考方であるけれども，8階の場合の結果を出すには相當の困難を伴つた．丸ノ内ビルディングの場合に計算をあてはめて見て大體尤もらしい結果が出た．構造中の粘性抵抗を入れずに振動勢力が基礎から彈性波として逃げるとして試みた計算の結果がこれ程迄によくあふといふ事は以前には全く豫期しなかつたところである．

7階の場合に既に述べたことであるが，$Ej^2\varepsilon/\mu l^3$ 卽ち建物の剛度と土地の剛度の比が高くなるに從つて最も破壞し勝ちの柱のある床が少しづゝ屋根の方へ移つて行くことは依然として同樣

である．丸ビルの場合に土地の横波の速度を 50 m/s に取つて見るさ，第１共振に於ける柱の屈曲モーメントの大さの床についての順序，そのさきの屈曲モーメントの大さ，同じ加速度が働いて震動週期無限大のときの屈曲モーメントを表示するさ次の如くなる．

柱のある床	1 階	2 階	3 階	4 階	5 階	6 階	7 階	8 階
共振に於けるモーメント値の順	7	5	3	1	2	4	6	8
共振に於ける $EI\frac{d^2y}{dx^2}\Big/\left(ml2\frac{\partial^2 u}{\partial t^2}\right)$	12·0	17·3	20·5	21·8	20·9	17·8	13·0	6·8
零振動數に於ける $EI\frac{d^2y}{dx^2}\Big/\left(ml2\frac{\partial^2 u}{\partial t^2}\right)$	4·0	3·5	3·0	2·5	2·0	1·5	1·0	0·5

共振に於けるモーメント値の順は $k_1^2\varepsilon/\rho b^2$ の値によつて勿論變化する．尚，基礎の中へ深く入つてゐる杭がある爲に $k_1^2\varepsilon/\rho b^2$ の値が割合に小さくなりはしないかさいふ懸念があるかも知れぬが，實際は杭さ土地さの接觸面が著しく増加し，ρ が大きくなることよりも ε の大きくなる方が急であり，從て實際の振動逸散性は玆に計算したのよりも寧ろ甚しいのではないかさ思はれる．この論文で之等の數値を正確に合さずに大體の定量的結果を出したことに對して或は議論の餘地があるかも知れぬけれども，實はこのやうな研究は構造物に限らず殆どすべての力學的問題に未だ何國にもやつてないから，この新しい物理的問題を提出して一般の正しい了解を得るのが先決問題の積りでやつてゐるのである．

47. *On the Seismic Vibrations of a Gozyûnotô (Pagoda).*

By Katsutada SEZAWA and Kiyoshi KANAI,

Earthquake Research Institute.

(Read July 7, 1936.—Received Sept. 21, 1936.)

1. *Introduction.*

The question why a *gozyûnotô* (5-storied Japanese Pagoda), notwithstanding its slender tower-like construction, is earthquake-proof seems to have received not little attention of investigators. Omori[1] studied the vibrations of several *gozyûnotôs* in Japan, and Muto[2] later attempted to explain their earthquake-proof properties. Of the various possible explanations, either that bases on the deformation damping of the structure or on the dissipation of vibrational energy, seems most plausible, particularly owing to the relative safety of the tower under resonance conditions. Although Muto,[2] in his study of the towers, applied the idea of deformation damping, due originally to us,[3] his idea is not very well adapted to the problem because of the improbability of such damping feature's predominating in the vibration in question. Taniguti,[4] on the other hand, with our dissipation theory in mind, believed that the enormous damping in the vibration of structures generally is due to deformation damping in the foundations of such structures, but our opinion is that damping of this kind is involved in the dissipation of vibrational energy into the ground, because deformation damping is a phenomenon that takes place when the vibrational energy has already been dissipated.

Mere application of the idea of dissipation of vibrational energy does not solve the whole problem. Our close investigation into the subject showed however that the resistance of the tower in question to seismic vibration is due to the smallness of its effective height and also to the accompanying marked dissipation of vibrational energy in the

1) F. OMORI, *Bull. Earthq. Inv. Comm.*, **9** (1918～21), 110～152.

2) K. MUTO, *Proc. World Eng. Congr., Tokyo, 1929*, **3**.

3) K. SEZAWA, *Bull. Earthq. Res. Inst.*, **3** (*1929*), 50. K. SEZAWA's papers published thereafter relating to the material damping were merely applications of the idea shown in *Bull.* **3** under consideration to various similar problems.

4) T. TANIGUTI, verbally, at a meeting in which the problems of earthquake-proof construction were discussed.

form of elastic waves.

Some hold that the resistibility of the tower might be due in part to the *sinbasira*, a kind of central post within the tower, in some cases hanging from the top of the tower and serving as an oscillating damper. Investigators without full knowledge of the nature of the oscillating damper are liable to believe that the solid surface friction caused by the massive oscillator resists tearing action in any joint within the structure. Our studies however show that the oscillator under consideration, instead of participating in any reduction of the seismic vibration, acts sometimes quite contrarily.

Section 2 of the present paper discusses the case in which the tower is free from the effects of the *sinbasira*, but its vibrational energy is dissipated into the ground; Section 3 the case in which the tower vibration is affected by the pendulum action of the *sinbasira* but without energy dissipation, and Section 4 the case in which the tower vibration is under the influence of the *sinbasira* as well as of the energy dissipation.

2. *The condition under the influence of energy dissipation, but not of pendulum action.*

Careful examination of the structure of a *gozyûnotô* showed that its effective height is fairly small. An extremely rigid structural block that forms a part of each roof rests between the successive purely columned structures of relatively small rigidity. This condition corresponds to the case of a tall structure with rigid floors that was dealt with in our previous paper,[5] the formulae from which we shall use here. For example, from (13'), (19) for the case in which a structure is subjected to horizontal ground vibrations due to the vertical incident transverse waves, we get

$$u_0 = 2\cos pt, \tag{1}$$

and we have a horizontal displacement of the structure such that

$$u' = 4\sqrt{\frac{\Gamma_1^2+\Gamma_2^2}{P^2+Q^2}}\cos k'(x+l)\cos\left(pt+\tan^{-1}\frac{\Gamma_2}{\Gamma_1}-\tan^{-1}\frac{Q}{P}\right), \tag{2}$$

where

$$P = 2\Gamma_1\cos k'l + \frac{3G\varepsilon}{\mu l}\Lambda_1 k'l\sin k'l,$$

5) K. SEZAWA and K. KANAI, Section 3 of the paper "Improved Theory of Energy Dissipation in Seismic Vibrations of a Structure," *Bull. Earthq. Res. Inst.*, **14** (1936), 167.

$$
\left.
\begin{aligned}
&Q=2\,\Gamma_2\cos k'l+\frac{3G\varepsilon}{\mu l}\Lambda_2 k'l\sin k'l\,,\\
&\Gamma_1=3\left(\frac{\lambda}{\mu}+2\right)+\nu(k'l)^2\left(\frac{\lambda}{\mu}-3\sqrt{\frac{\lambda}{\mu}+2}\right),\\
&\Gamma_2=\sqrt{\nu}\,(k'l)\left\{3\left(\frac{\lambda}{\mu}+2+\sqrt{\frac{\lambda}{\mu}+2}\right)+\nu(k'l)^2\left(\sqrt{\frac{\lambda}{\mu}+2}-2\right)\right\},\\
&\Lambda_1=\left(\frac{2\lambda}{\mu}+5\right)-\nu(k'l)^2\,,\\
&\Lambda_2=\sqrt{\nu}\,(k'l)\left(2\sqrt{\frac{\lambda}{\mu}+2}+1\right),\\
&\nu=\rho G\varepsilon^2/\rho'\mu l^2\,.
\end{aligned}
\right\}\qquad(3)
$$

As the meanings of these notations have been given in the paper cited, they will not be repeated here.

It is now possible to calculate the theoretical values of the displacements of the tower in seismic vibrations, provided we have the structural dimensions as well as the physical constants of the tower, besides data regarding the nature of the ground.

We shall take the case of the Ueno gozûnotô[6] in Tokyo as an example. The important numerical constants are as follows:

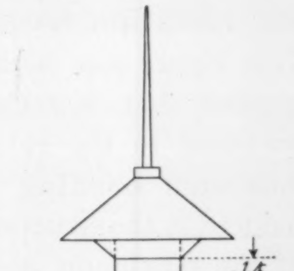

Fig. 1.

Total height of the tower body $=79{\cdot}5$ shaku $=24{\cdot}095$ m,

Effective height of the tower body (estimated) $=l=25{\cdot}0$ shaku $=7{\cdot}575$ m,

Height of each elementary elastic part of the tower body $=l/5=5$ shaku $=1{\cdot}515$ m,

ε for each column $=1{\cdot}5/2$ shaku $=0{\cdot}2273$ m,

j (roughly) $=0{\cdot}5$ shaku $=0{\cdot}1515$ m,

E (assumed) $=100.10^3$ kg/cm^2 $=10^9$ kg/m^2 $=9{\cdot}8.10^9$ kg mass/(m sec^2),

$G=12{\cdot}4\,Ej^2/l_1^2=1{\cdot}215.\ 10^9$ kg mass/(m sec^2),

$T=$ period of natural vibration without dissipation, (assumed), $=1$ sec,

$G/\rho'=(4l/T)^2=30{\cdot}3^2$ m^2/sec^2,

$N=$ number of columns excepting the central post $=16$,

---

6) F. OMORI, *loc.cit.* 1).

$a = N\pi\varepsilon^2 = 2{\cdot}596\ \mathrm{m}^2$,
$\sqrt{\mu/\rho}$ (assumed) $= 100$ m/sec,
ρ (assumed) $= 2.10^3$ kg mass/m^3,
μ (calculated) $= 2.10^7$ kg mass/(m sec^2).
From these values of the constants we obtain

$$k'l = p/4\,,$$

$$\Gamma_1 = 9 \quad 0{\cdot}0^4 2172\, p^2\,,$$

$$\Gamma_2 = 0{\cdot}03226\, p - 0{\cdot}0^8 3153\, p^3\,,$$

$$P = (18 - 0{\cdot}0^4 4344\, p^2) \cos p/4 \quad (9{\cdot}573\, p - 0{\cdot}0^5 707\, p^3) \sin p/4\,,$$

$$Q = (0{\cdot}06452\, p - 0{\cdot}0^8 6306\, p^3) \cos p/4 + 0{\cdot}01388\, p^2 \sin p/4\,. \tag{4}$$

From (2), (4) it is possible to get the resonance curve of the seismic vibrations of the tower. Fig. 2 indicates the ratio of the maximum horizontal displacement of the tower (not restricted to the part $x = -l$), u', to that of the ground, u_0, for any vibration frequency p. This figure also indicates the number that is roughly proportional to the ratio of the maximum bending moment induced in the structure to that of the maximum acceleration of free ground, that is, ground on which there is no tower standing.

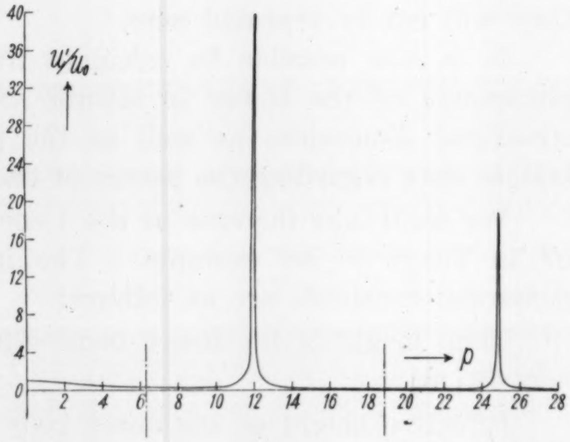

Fig. 2.

Although the natural frequency shown by the present resonance curve is somewhat too large, the character of the dissipation is not greatly affected.

This result shows that the dissipation of vibrational energy is not so marked as was expected, the maximum displacement of the tower at resonance condition being about fourty times that of one at zero frequency vibration. Since however the effective height of the tower is only 7·575 m, the tower under consideration is virtually nothing more than a sort of a low house, suggesting that the induced bending moments at any vibration frequency are exceedingly small, being sometimes smaller than that of a 2-storied house. Thus, even the sharp peak of the curve

under resonance condition is of no great importance.

3. *The condition under pendulum action, and free from energy dissipation.*

Let the vibratory motion of the tower and the central post be

$$\left.\begin{aligned} u' &= A\cos(k'x+B)\cos pt\,, \\ \xi &= \xi_0\cos pt \end{aligned}\right\} \qquad (5)$$

respectively, where $k'=p\sqrt{\rho'/G}$. Then the displacement of the tower at $x=0$ is the same as that of the ground, namely

$$u'=2\cos pt\,, \qquad (6)$$

whereas the condition at $x=-l$ is

$$Ga\frac{\partial u_1'}{\partial x}=\frac{Mg\xi_0}{L/2}, \qquad (7)$$

where $u_1'=A\cos(k'x+B)_{x=-l}$, $a=N\pi\varepsilon^2$; and M, $L/2$ are the mass and the pendulum length of the central post respectively. The dynamical relation between u' and ξ can be obtained by the equation of motion of the centre of gravity of the central post, namely,

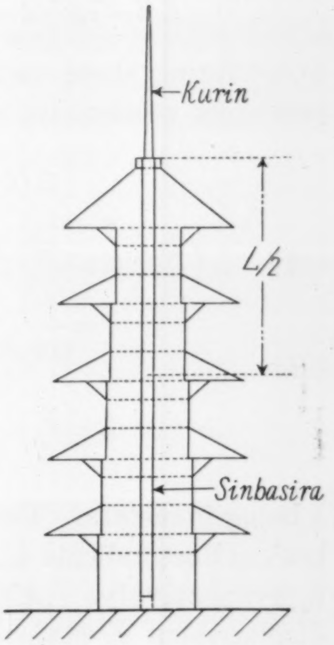

Fig. 3.

$$\frac{d^2\xi}{dt^2}+\frac{2g}{L}\xi=-\frac{d^2u'}{dt^2}. \qquad (8)$$

From (5), (8) we get

$$\xi_0=\frac{p^2u_1'}{2g/L-p^2}. \qquad (9)$$

Substituting u', ξ in (5) in conditions (6), (7), we obtain

$$u'=\frac{2(n_0{}^2-p^2)\cos(k'x+B)}{\cos B\sqrt{(n_0{}^2-p^2)^2+\left(\dfrac{2Mgp^2}{LGak'}\right)^2}}\cos pt\,, \qquad (10)$$

$$\xi=\frac{2p^2}{\cos B\sqrt{(n_0{}^2-p^2)^2+\left(\dfrac{2Mgp^2}{LGak'}\right)^2}}\cos pt\,, \qquad (11)$$

where $n_0^2 = 2\,g/L$ and

$$B = -\left[k'l + \tan^{-1}\left\{\frac{2Mgp^2}{LGak'(n_0^2 - p^2)}\right\}\right]. \tag{12}$$

In this case

$$L/2 = 79{\cdot}5/2 \text{ shaku} = 12{\cdot}05 \text{ m}, \qquad M = 5{\cdot}95.10^3 \text{ kg mass}.$$

Substituting these values as well as the numerical values shown in the preceding section, we obtain

$$\left.\begin{aligned} u' &= \frac{2\,(0{\cdot}8132 - p^2)\cos\left(\dfrac{px}{30{\cdot}29} + B\right)\cos pt}{\cos B\sqrt{(0{\cdot}8132 - p^2)^2 + (0{\cdot}0^4 4646p)^2}}, \\ \xi &= \frac{2\,p^2 \cos pt}{\cos B\sqrt{(0{\cdot}8132 - p^2)^2 + (0{\cdot}0^4 4646p)^2}}, \\ B &= \frac{p}{4} + \tan^{-1}\frac{0{\cdot}0^4 4646}{0{\cdot}8132 - p^2}, \end{aligned}\right\} \tag{13}$$

x being in meters. The result is plotted in Fig. 4, in which the full and broken lines indicate u'_{max}, and ξ_0 respectively. Although displacement u'_1 vanishes at a frequency that is equal to the natural frequency of the central post, namely $p = n_0 = \sqrt{0{\cdot}8132}$, a new resonance condition manifests itself near $p = n_0$, namely at frequency $p = \sqrt{0{\cdot}8132} - 0{\cdot}0^5 533$, although the original resonance conditions of the tower itself still exist, the corresponding frequencies changing but very slightly. It will be seen from this result that the pendulum action of the central post rather defeats the intended object of the post which is to prevent seismic vibration of the tower, excepting however increase in statical frictional force at any joint of the structure due to the weight of the post.

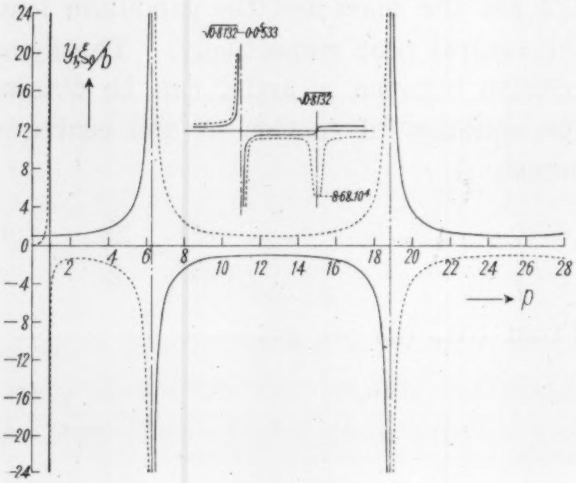

Fig. 4.

4. *The condition under the influence of both energy dissipation and pendulum action.*

While the conditions at $x=0$ are the same as those shown in the previous paper[7], the condition at $x=-l$ is that as given by (7) in the last section. The final result shows that if the ground vibration is expressed by

$$u_0=2\cos pt\,, \tag{1'}$$

the vibrations of the tower and the central post may be written in the forms

$$u'=4\sqrt{\frac{\Gamma_1^2+\Gamma_2^2}{P^2+Q^2}}\left\{(n_0^2-p^2)\cos k'(x+l)+\gamma p^2\sin k'(x+l)\right\}$$
$$.\cos\left(pt+\tan^{-1}\frac{\Gamma_2}{\Gamma_1}-\tan^{-1}\frac{Q}{P}\right), \tag{14}$$

$$\xi=4p^2\sqrt{\frac{\Gamma_1^2+\Gamma_2^2}{P^2+Q^2}}\cos\left(pt+\tan^{-1}\frac{\Gamma_2}{\Gamma_1}-\tan^{-1}\frac{Q}{P}\right), \tag{15}$$

where

$$\left.\begin{aligned}P=&\left\{2(n_0^2-p^2)\,\Gamma_1-\frac{3k'G\varepsilon\gamma p^2\Lambda_1}{\mu}\right\}\cos k'l\\&+\left\{2\gamma p^2\Gamma_1+\frac{3k'G\varepsilon(n_0^2-p^2)\Lambda_1}{\mu}\right\}\sin k'l\,,\\Q=&\left\{2(n_0^2-p^2)\,\Gamma_2-\frac{3k'G\varepsilon\gamma p^2\Lambda_2}{\mu}\right\}\cos k'l\\&+\left\{2\gamma p^2\Gamma_2+\frac{3k'G\varepsilon(n_0^2-p^2)\Lambda_2}{\mu}\right\}\sin k'l\,,\end{aligned}\right\} \tag{16}$$

and $\gamma=2Mg/Gak'L$, the meaning of Γ_1, Γ_2, Λ_1, Λ_2, n_0, k', ν being shown in the preceding two sections.

In the present case (14), (15) become

$$\left.\begin{aligned}P=&\{2(n_0^2-p^2)\,\Gamma_1-0{\cdot}0^46358\,p^2\Lambda_1\}\cos k'l\\&+\{0{\cdot}0^49292\,p\Gamma_1+1{\cdot}3675\,p\,(n_0^2-p^2)\,\Lambda_1\}\sin k'l\,,\\Q=&\{2(n_0^2-p^2)\,\Gamma_2-0{\cdot}0^46358\,p^2\Lambda_2\}\cos k'l\\&+\{0{\cdot}0^49292\,p\Gamma_2+1{\cdot}3675\,p\,(n_0^2-p^2)\,\Lambda_2\}\sin k'l\,.\end{aligned}\right\} \tag{17}$$

The result of the calculation, particularly that for u'_{max}, is plotted

7) *loc. cit.* 5).

in Fig. 5. In this case too, displacement $u'_1 = u'(x=-l)$ vanishes at $p=\sqrt{0{\cdot}8132}$. But, the additional resonance condition due to the central post appears at $p=\sqrt{0{\cdot}8132-0{\cdot}0^5525}$.

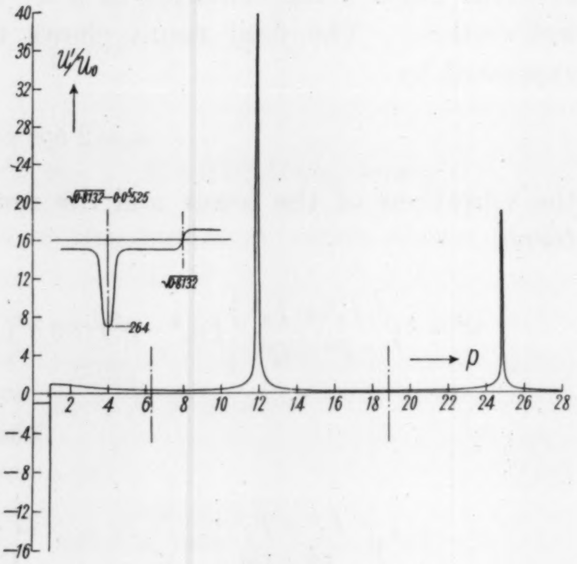

Fig. 5.

5. *Concluding remarks.*

From the present investigation it has been ascertained that the gozyûnotô is earthquake-proof solely because of the fact that the effective height of the elastic part of its structure is extremely small, the induced stress due to the ground vibration being consequently very small. The relatively large stress under resonance condition is still restricted to a certain limiting value due to the fairly large dissipation of the vibrational energy into the ground. The central post, even in the hanging state, has no effect in preventing large vibrations, although it rather gives rise to an additional resonance condition of the tower.

Nevertheless, in order to make the central post effective on the vibration damping of the tower, it is rather advisable to insert some viscous damper between the central post and the tower body, its full character being now investigated.

47. 五重塔の耐震性

地震研究所 {妹澤克惟
金井清

五重塔が見たところ細長いのに拘らず耐震性があるために以前から多くの人の注意をひいた．例へば大森博士の數多くの振動測定や武藤博士の推論などはそのあらはれであるとしてもよい．耐震性のある理由として或人は心柱が振子の作用と鉛直壓力とを與へるからであるといひ，他の人はその構造上から材料を破壞しないけれども構造や基礎の振動減衰摩擦が多いからであるとしてゐるが，何れも研究して見れば見る程これ等の特異性がわからなくなるものである．

筆者等の研究によると，五重塔は構造力學的には決して細長いものではなく，震動問題として取扱つて見ると彈性抵抗から考へても外力の剪斷力から考へても普通の二階建より低い場合にしか當つてをらぬことがわかつたのである．従て筆者等の研究にかゝる震動逸散性がなくても破壞力が極めて少いことがわかつた．又，共振に當る場合の強い筈の震動性は，構造が効果的に低いことから當然逸散性の影響を受けて，これ亦可なり少くなることが知られたのである．

心柱の振子の作用は昔からの構造のままでは共振を更に一つ増加する以外何等の利益もないことがわかつた．卽ちそのまゝの狀態では寧ろ風力に對して効果があるものである．心柱を耐震の目的に役立たせるには心柱と五重塔の間に適當な粘性摩擦を設けることである．如何なる粘性摩擦が適當であるかは目下研究中であり，近く報告できる筈である．

48. 土の粘彈性と剪斷抵抗

地震研究所 { 石本巳四雄
飯田汲事

(昭和11年9月15日發表――昭和11年9月20日受理)

I. 緒言

土は一般に可塑物質として取扱はれる一方，彈性體としても考へられて居る．即ち長時間働く力に對しては其の儘變形し，力を取り去つても復元する事はないが，地震波の如き短周期の波動は其の中を通過するのである．斯くの如く土は全く異る2性質を保有するのであつて吾々は斯樣の性質を表はすに粘彈性の名稱を採用する．而して粘彈性物質の種々の性質に就ては已にピツチ，パラフィン，砂岩等を用ひて研究し報告[1]してある．本論文は土に關して粘彈性を2方面から調べたものである．第1の部分はピツチ，パラフィン等に就て行つた研究を其のまゝ土に應用したものである．第2の部分は破壞に關する事柄を取扱つたものである．吾々は地表に於て地辷り，山崩れ等の現象を見るが，此れは土に關する破壞的現象と考へられ此等を調査研究するには土の破壞に與る剪斷抵抗の測定が必要となる．從來土の剪斷抵抗の測定に關しては種々の實驗が行はれて居るが，未だ力の働く緩急を顧慮して研究したものが殆ど無い樣である．本論文は特に此の點に注意し，力の時間的與へ方に關し抵抗が如何に變化するかを實驗したものである．本實驗は豫備的のものであり，土の種類に就ても只1種類のものを採用し，然も其の性質，組成の相當判つて居る人工の加はつた土に就て行つた．從つて自然土に關しては將來研究を進める積である事を述べて置く．

II. 粘彈性測定實驗

吾々の實驗に使用した土は純粘土であつて，特に土の特性を知る目的の爲めに粒子の小さいものを取扱つた．其の機械的分析の結果は第I表に示してある．又從來の方法によつて求められた緊硬度試驗，壓縮試驗，抗剪强度試驗の結果は土の性質を知る上に必要であるから，此れも第I表に揭げる事とした．

1) 飯田汲事　地震研究所彙報 13 (1935), 198; 443.

第I表 機械的分析表

篩分 (%)						沈泥 粒徑 (mm) 0·05～0·01 (%)	粘土 粒徑 (mm) 0·01～0 (%)
8目[2]	14目	28目	48目	100目	200目		
0	0	0·06	0·48	1·36	2·02	11·94	84·14

凝集力 (C) kg/cm²	摩擦角 (θ) in deg.	摩擦係數 tan θ	比重		間隙率 P (%)	間隙比 e	含水率 (%)	流動限界 (含水比)
			見掛	眞				
0·145	1·00	0·0175	2·06	2·551	41·93	0·72	28·09	1·467

a) **實驗裝置** 此の實驗に用ひた實驗裝置は前實驗[3]に採用したものと同様であつて第1圖に示す如き同心圓筒裝置である．但し前回と異る點は外側圓筒の內壁及び內側圓筒の外壁に，何れも厚さ3 mm程度の刄形突起物を附着し，土の捩れ變形の際，滑動の生ずるのを防止した．

土を滿せる眞鍮製圓筒（B）の中に鋼鐵針金（W）を通じて眞鍮製圓筒が吊されて居る．針金の上端はチャック(C)にて固定され，針金は螺子(D或はT)によつて一定角捩られる．此の捩力によつて內側の圓筒（A）は回轉する事となるが，その偏角は M_1, M_2 の小凹面鏡により，時計仕掛により回轉する圓筒上の感光紙上に記錄される．溫度及び濕度の影響は特に注意し，實驗中成る可く一定値を保つ爲め，4 m の深さの地中室を選び其の中にて實驗した．卽ち溫度は自記寒暖計を使用して記錄し，濕度は常に 100% に保ち且つ又土の直接空氣に接する部分には濕布を輕く當てゝ實驗を行つた．此等の觀測より見るに1回の實驗が1週間に亘る場合と雖も試驗土の含水率の變化は 0·3～0·4% の範圍であり，溫度も 0·2°～0·5°C の範圍であつた．なほ土の緻密さは殆ど最大の狀態になつて居る．

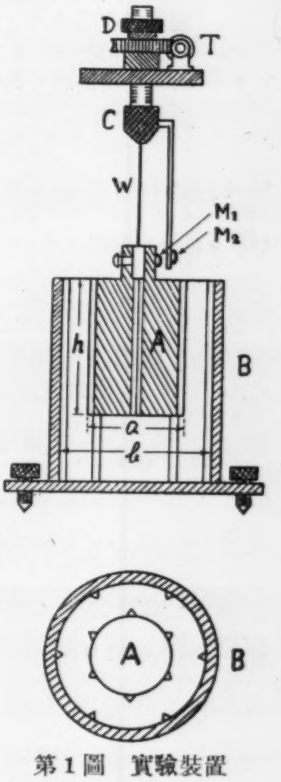

第1圖 實驗裝置

A 內側の圓筒
B 外側の圓筒 (高さ 10 cm)
C チャック
D, T 螺子
W 鋼鐵製針金（長さ 4·467 cm, 半徑 0·765 mm.)
M_1, M_2 凹面鏡
a=4 73 cm
b=7·3 cm
h=8·96 cm

b) **實驗結果** 以上の實驗裝置により得られた結果の二三の例は第2圖に示してある．何れも時の經過と共に偏角し，或る一定角値に接近するものである．今此の終局角と時の經

2) Tyler の標準篩目　3) 飯田汲事 前揭

過に從つて變化する偏角との差を對數値にて表はし，時刻を横軸に採つて圖示すれば，

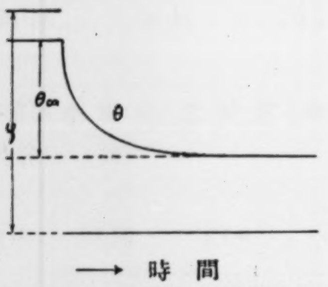

第3圖　土の捩れ變形曲線の略圖
φ:　最初針金に與へし捩角
θ∞:　土の終局の捩角
θ:　土の時の經過と共に變化する捩角

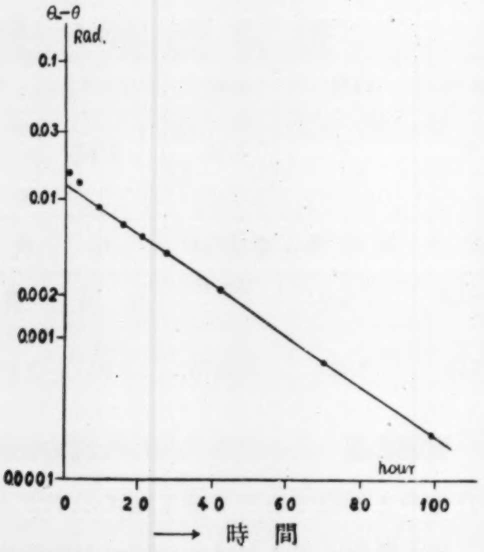

第4圖　時間と $\log(\theta_\infty-\theta)$ とは直線的關係にある事を示す．含水率 37·8%

第4圖の如く直線となる．從つて原曲線は $\theta=\theta_{t=\infty}(1-e^{-at})$ なる形を以て表はされ[4]（第3圖），結局

$$k=\frac{c(\varphi-\theta_{t=\infty})}{\theta_{t=\infty}},\qquad \varepsilon=\frac{k+c}{a}$$

として k なる彈性値及び ε なる粘性常數が誘導出來る．而して次に此等に裝置の常數 $\dfrac{1}{4\pi h}\dfrac{b^2-a^2}{a^2b^2}$ を乘ずれば，粘性及び彈性係數が求められる．次に含水率の差違によつて，此等の係數が如何に變化するかを檢べる爲めに，以上の試驗土に適當に水を加へ又は間燥せしめて同樣の實驗を繰返した．此の記錄は第2圖中に見られる如く同樣の變形曲線を示す．斯樣の曲線を上述の分析と同樣に處理して得た結果は第 II 表及び第5圖，第6圖に示すものである．此等の圖から判る如く彈性及び粘性の2係數は

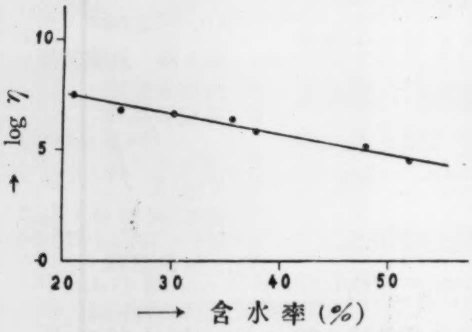

第5圖　含水率と粘性係數との關係

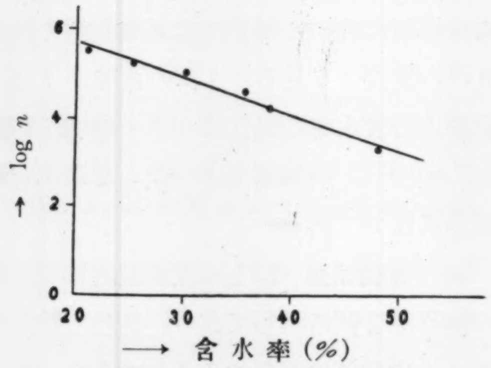

第6圖　含水率と剛性率との關係

4）飯田汲事　前揭

孰れも含水率の增加と共に對數曲線をなして變化してゐる．而も含水率 53·4％ に於ては彈性は消失し，粘性のみとなる．なほ此等の値には內側圓筒の底面の影響に對する補正が加へてある事は勿論である．

第 II 表　含水率，粘性係數，剛性率

No.	含水率 (%)	粘性係數 η (c.g.s)	剛性率 n (c.g.s.)	溫度 °C
1	21·0	$3{\cdot}335\times10^{7}$	$3{\cdot}109\times10^{5}$	17·5
2	25·3	$7{\cdot}508\times10^{6}$	$1{\cdot}593\times10^{5}$	18·0
3	30·1	$5{\cdot}026\times10^{6}$	$1{\cdot}032\times10^{5}$	18·2
4	35·6	$2{\cdot}625\times10^{6}$	$3{\cdot}950\times10^{4}$	19·0
5	37·8	$7{\cdot}545\times10^{5}$	$1{\cdot}671\times10^{4}$	18·8
6	48·0	$1{\cdot}588\times10^{5}$	$2{\cdot}175\times10^{3}$	19 8
7	53·4	$3\ 784\times10^{4}$	——	20·0

III. 剪斷抵抗測定

此の實驗には前の時使用したと同じ土を用ひた．

a) **實驗器械**　實驗に使用した器械は第7圖に示すもので，內外2箇の圓筒から成り，其の間に試驗土を詰め，外側の圓筒（C_2）を一定速度にて回轉せしめる．內側の圓筒（C_1）には振子が附してあるから，外圓筒の回轉によつて振子も偏り，此の重錘の偏りによつて生じた能率と土の剪斷抵抗とは釣合ふ事となる．從つて振子の偏角を測定すれば土の剪斷抵抗が求められる．

第7圖 a は剪斷器械であり，b は器械及び圓筒回轉裝置である．C_2 は外側の眞鍮圓筒で，臺上にて E, F なる2個の足にて支へられ，一端はウォームギア（G）を經て回轉裝置に連る．C_1 は內側の眞鍮製圓筒で C_2 同樣に K_1, K_2 なる 2個の足にて支へられて居る． K_1, K_2 には夫れ夫れ 3個の小車があり，其れ等が C_1 圓筒を輕く押へて居る．圓筒の回轉を滑らかにする爲め小車はピボットにより回轉するが，其の軸受には石が入れてある．又 C_2 の內壁，C_1 の外壁には土の滑動を防ぐ目的上，刄形の齒が附けてある．C_1 圓筒に附置した振子（P）の重錘（W）は自由に上下或は取替へる事が出來るので，偏角に對して適當な力率を與へる事が出來る．振子の偏角を記錄するために其の一部から腕を出し，其の先きに描針（N）が付けてある．此の描針の先端が時計仕掛回轉ドラム上に卷いた煤煙紙上に接觸して居るので，時の經過に從つて振子の偏角を記錄する事となる．なほ時計仕掛回轉ドラムは 1時間1回轉，1 日 1 回轉，1 週間 1 回轉等，適當のものを隨時使用した．

又 C_2 圓筒を回轉するためには同期電動機（M）（第7圖b）を使用したが，此れは1分間300回轉である．又 C_2 圓筒を種々の速度にて回轉せしめるために，一連の齒車系（H）を中間に入れてある．此れは齒車にて噛み合ふ10箇の軸が並列して居て，次々に軸數を增加する事によつて C_2 圓筒に傳達される回轉が遲くなる樣になつて居る．C_2 圓筒を1回轉せしめるに要する時間は第 III 表に示してある．

なほ實驗は先づ C_2 圓筒に土を詰め，其れと同心となる樣に C_1 圓筒を差し込み，器械を組立て C_2 をある速度で回轉せしめ，振子の偏角を時計仕掛回轉ドラム上に記錄せしめるのである．又土の直接空氣に接する部分には濕布を輕く當てゝ，一實驗中に於ては土の含水量の變化を防止するやうになした．實驗室の溫度は自記寒暖計を使用して記錄した．

第 III 表 外側の圓筒を1回轉せしめる時間

番號	時間 (時 分 秒)
1	26·6
2	2 08
3	10 40
4	25 30
5	53 20
6	2 08 00
7	4 26 40
8	10 40 00
9	22 13 20
10	53 20 00
11	111 06 40

b） 實驗結果 含水量の同じ土に就て C_2 圓筒を種々の速度にて回轉せしめ，更に含水量を變へて同樣の實驗を繰返した．卽ち剪斷速度により，或ひは含水量により抵抗に變化ある事を確め得た次第である．

記錄として得られた代表的のものは第8圖 a, b に示すものである．圖の說明より判る如く溫度は概ね 18°C～22°C の範圍に於て變化するが，これらは何れも實驗室內の溫度である．從つて土の溫度に於てはそれ程の變化があるとは思はれない．

孰れの記錄に於ても，最初は急速に捩れて行くが，最大偏角にて剪斷が行はれ，後は C_2 を回轉せしめる速度に從つて急速に或は徐々に元の狀態に戾る．今其の剪斷の行はれた最大偏角を θ とすれば剪斷抵抗 F は

$$Mga \sin\theta$$

なる形で求める事が出來る．但し M は振子の質量，a は振子の回轉軸と重心との距離，g は重力加速度である．又最大偏角に達する迄の時間 T も記錄から讀取る事が出來るが，此等の關係は第 IV 表及び第9圖～第11圖に示してある．なほ剪斷抵抗は單位面積に對するものとして計算した．

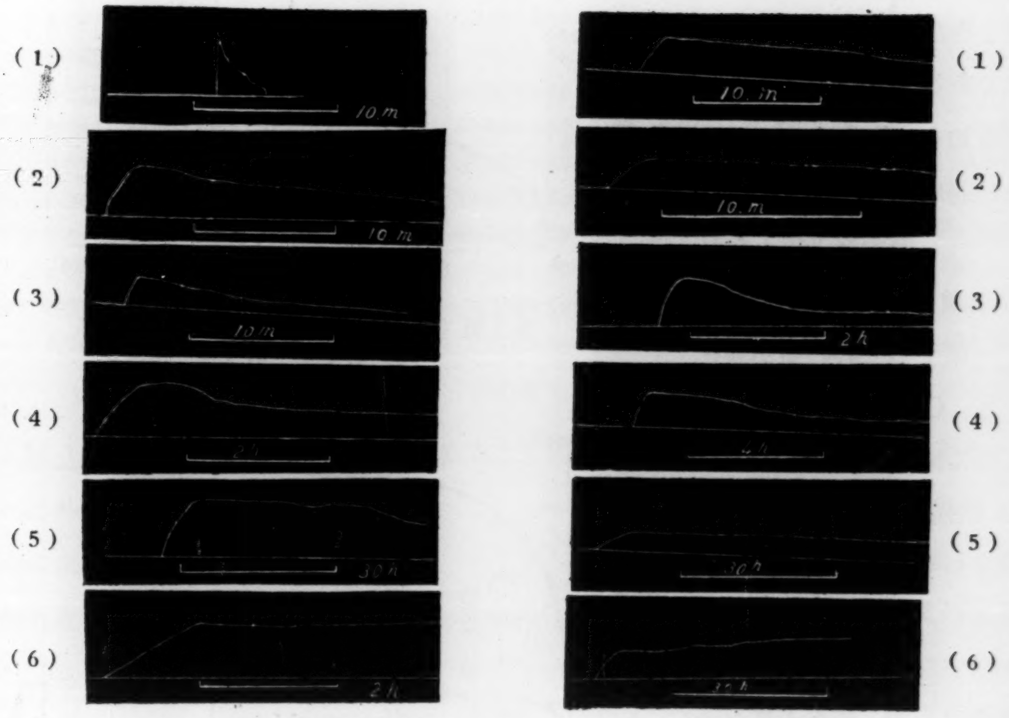

(a) 含水率 26·6%　　(b) 含水率 30·7%

第8圖　剪斷抵抗の回轉速度に對する變化を表はす曲線（原圖の $\frac{1}{3}$）

WL=能率，T=外側の圓筒を1回轉せしめるに要する時間，θ=溫度

(a)	(1)	WL=398·5 kg.cm,	T=2 m 10s,	θ=18·5°C
	(2)	WL=396·5 kg.cm,	T=128 m,	θ=19·6°C
	(3)	WL=396·5 kg.cm,	T=4 h 26 m,	θ=18·6°～19·7°C
	(4)	WL=162·9 kg.cm,	T=10 h 40 m,	θ=18·6°C～19·7°C
	(5)	WL=133·96 kg.cm,	T=53 h 20 m,	θ=17·8°C～19·9°C
	(6)	WL=141·5 kg.cm,	T=22 h 14 m,	θ=17·9°C～20·2°C
(b)	(1)	WL=130·4 kg.cm,	T=25·6 m,	θ=18°C
	(2)	WL=128·2 kg.cm,	T=4 44 h,	θ=18·2°C
	(3)	WL=106·5 kg.cm,	T=10 h 40 m,	θ=21·5°C
	(4)	WL=106·5 kg.cm,	T=22·55 h,	θ=21·5°C
	(5)	WL=123·8 kg.cm,	T=53 h 20 m,	θ=18·2°C～21·1°C
	(6)	WL=105·9 kg.cm,	T=111·11 h,	θ=19°C～22°C

第9圖は能率と速度との關係に於て含水量により其値の異る事を示し，a は回轉速度 $\left(\frac{d\theta}{dt}\right)$ の小なる場合であり，b は試驗した回轉速度を全部網羅して書いたものである．此れ等の圖から判る如く，能率は $\frac{d\theta}{dt}$ の小なる間は比較的小なるに反し，$\frac{d\theta}{dt}$ の大なる値となれば急激に增加する．即ち $\frac{d\theta}{dt}$ によつて其の値が變化する．C_2 を 4日以上もかゝつて回轉せしめた時と，10 秒程度の短時間で 1 回轉せしめた時とでは，剪斷抵抗が 3 倍以上も異なる値を示すのは特に注目すべき現象である．又含水量の增加に從つて剪斷抵抗が減少する．此の關係は第 10 圖に於て明かなる如く，長時間に C_2 を 1 回轉せしめる場合に剪斷抵抗の減ずるものと比較して考へる事が出來る．即ち剪斷抵抗の減少は含水量が增す時或ひは，長周期の力が作用する時であり，此の二つ乍らの作用が同時に働くとすれば，剪斷抵抗は極めて底下するのである．斯くの如き現象は全く粘彈性物質の特長であつて，自然の土の變形剪斷に關しても充分此の性質を考へて置かないと說明出來ない多くの現象がある樣である．

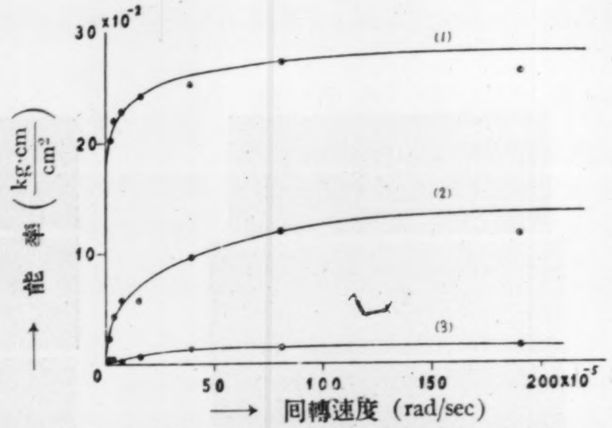

第9圖 (a) 剪斷抵抗と回轉速度との關係
(1) 含水率 26·6%
(2) 〃 30·7〃
(3) 〃 33·7〃

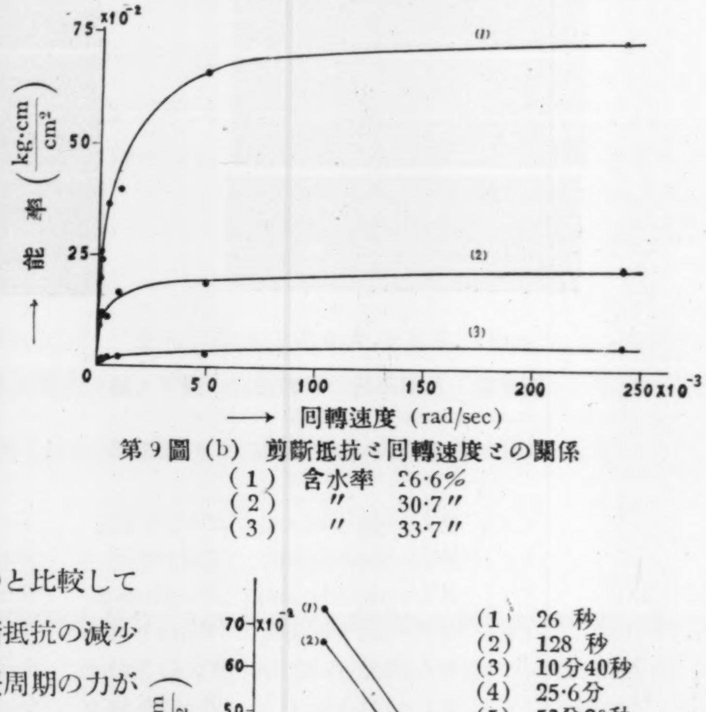

第9圖 (b) 剪斷抵抗と回轉速度との關係
(1) 含水率 26·6%
(2) 〃 30·7〃
(3) 〃 33·7〃

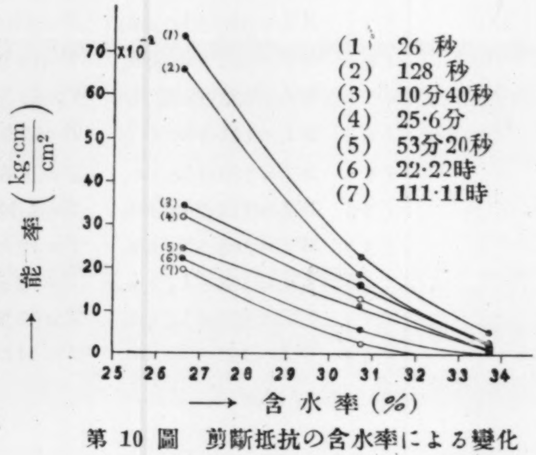

第 10 圖 剪斷抵抗の含水率による變化
(數字は C_2 を一迴轉せしめる時間)

第 IV 表　剪斷抵抗，回轉速度，剪斷に至る迄の時間

$F_1\left(\frac{kg\cdot cm}{cm^2}\right)$	$F_2\left(\frac{kg\cdot cm}{cm^2}\right)$	$F_3\left(\frac{kg\cdot cm}{cm^2}\right)$	$\frac{d\theta}{dt}$ rad/sec	T_1(min)	T_2(min)	T_3(min)
0·734	0·229	0·052	$241{\cdot}64\times10^{-3}$	0·06	0·02	0·01
0·657	0·189	0·028	$49{\cdot}087\times10^{-3}$	0·59	0·143	0·408
0·345	0·165	0·021	$9{\cdot}817\times10^{-3}$	1·99	0·820	0·612
0·316	0·113	0·021	$40{\cdot}903\times10^{-4}$	2·21	2·26	0·819
0·244	0·117	0·015	$19{\cdot}038\times10^{-4}$	6·07	2·76	1·808
0·271	0·119	0·014	$8{\cdot}181\times10^{-4}$	10·6	9·64	1·64
0·250	0·094	0·013	$39{\cdot}270\times10^{-5}$	21·5	10·09	1·53
0·240	0·057	0·006	$16{\cdot}362\times10^{-5}$	44·4	30·65	7·37
0·228	0·057	0·002	$7{\cdot}854\times10^{-5}$	81·20	80·05	73·56
0·221	0·043	0·003	$3{\cdot}272\times10^{-5}$	300·7	160·05	117·00
0·201	0·023	0·003	$1{\cdot}571\times10^{-5}$	412·5	308·5	180·00

F_1, T_1: 含水率 26·6%　　F_2, T_2: 含水率 30·7%　　F_3, T_3: 含水率 33·7%.

又第 11 圖にて見る如く $\frac{d\theta}{dt}$ が小であると剪斷に至る迄の時間は比較的大となる．其れは外力が極めて緩徐に作用する場合に土は變形して剪斷に至る事が困難となるに反し，急激に働く力に對しては土は直ちに剪斷破壞されるからである．此れも粘彈性物質の特長として，此れを破壞せんとする時には衝擊的の力を用ふる事を必要とするのはパラフィン，封臘等に於て日常吾々が經驗するものに當て嵌めて考へる事が出來るものである．

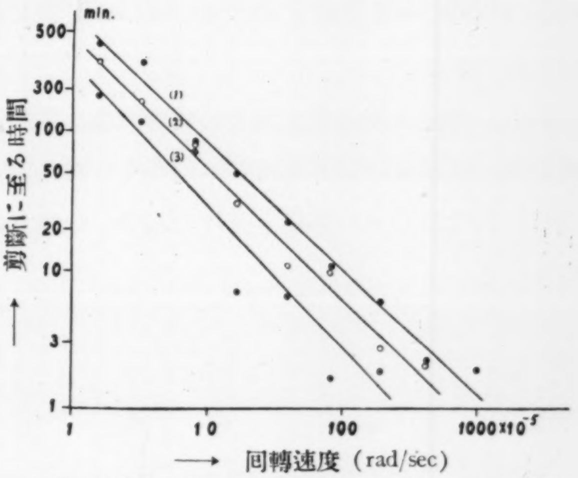

第 11 圖　剪斷に至る時間と回轉速度との關係
(1)　含水率　26·6%
(2)　〃　30·7〃
(3)　〃　33·7〃

IV. 結　　語

以上行つた實驗を要約すると次の如くなる．此等は何れも粘彈性物質の特長を示すものと見る事が出來る．

（1） 含水率により粘性及び彈性の諸係數は變化する．その變化を檢べると，含水率が增加すると何れも急激に小となる．含水率約 25·3% における兩者の値は夫れ夫れ $7{\cdot}5\times10^5$ 及び $1{\cdot}59\times10^5$ c.g.s. である．

（2） 含水率約 53%においては彈性は消失し，粘性のみとなる．

（3） 剪斷抵抗は剪斷速度によつて異り，速度が小であると抵抗が小となり，其の逆も行はれる．極端の場合には速度の變化により剪斷抵抗は3倍も異る．

（4） 剪斷抵抗は土の含水量により著しく異る．含水量が增加すると抵抗は小となる．

（5） 剪斷に到達する時間は力の働く速度に關係する．卽ち剪斷速度が大であると剪斷に達する時間が短く，小であると時間が長い．

（6） 物質の構造に就ては海綿構造と見る事が適當の如くである．

なほ以上の實驗は緻密度に就ては少しも觸れて居ないが．此れは常に一定である様に努めた．卽ち重量と體積とは常に比例する様に注意した．又實驗は濕度，溫度の一定の下に行ふべきは勿論であるが，斯様の設備が完全で無かつたのは頗る遺憾である．或る機會に於ける條件の完備した下に實驗をなほ延長する事を希望して止まない．又器械の性能に就ても多少不滿足の點はあつたが，實驗の進行上其の儘となした所もある．例へば振子を內側圓筒 C_1 に直接附加したが，次回には振子を別に作り，兩者の回轉のみを聯結する方法，或ひは記錄裝置に就ても二三改良すべき點のある事は勿論である．

以上の實驗は鐵道省土質委員會の仕事と連絡を保つて成されたものであり，實驗の遂行上，幹事渡邊貫博士に負ふ所多く，玆に厚く感謝の意を表すものであり，又同委員會の其他の方々の應援を受けた結果，短時日に以上の結論を得た事に對し厚く御禮申上げる．

---

48. *Expériences sur le sol*

par Mishio Ishimoto et Kumizi Iida,

Institut de Re herches sur les Tremblements de terre.

Nous avons executé certaines expérinces sur le sol, dont la propriété mécanique est connue, avec deux appareils construits dernièrement, et obtenu les résultats suivants:

1) La viscosité et l'élasticité du sol changent avec le contenant d'eau: les deux diminuent assez rapidement quand de l'eau augumente.

2) Quand le contenant d'eau devient plus que 53%, l'élasticité du sol disparait et il n'y reste que la propriété de viscosité.

3) La résistance cisaillante depend la vitesse de force appliquée: quand la force est rapide, la resistance est grande et vice versa. Nous constatons que la resistance devient 3 fois grande aux deux cas extrêmes.

4) La résistance cisaillante diminue avec le contenant d'eau: elle devient petite avec l'augumentation d'eau.

5) Le maximum de résistance apparait relativement tard quand on applique la force lentement et vice versa.

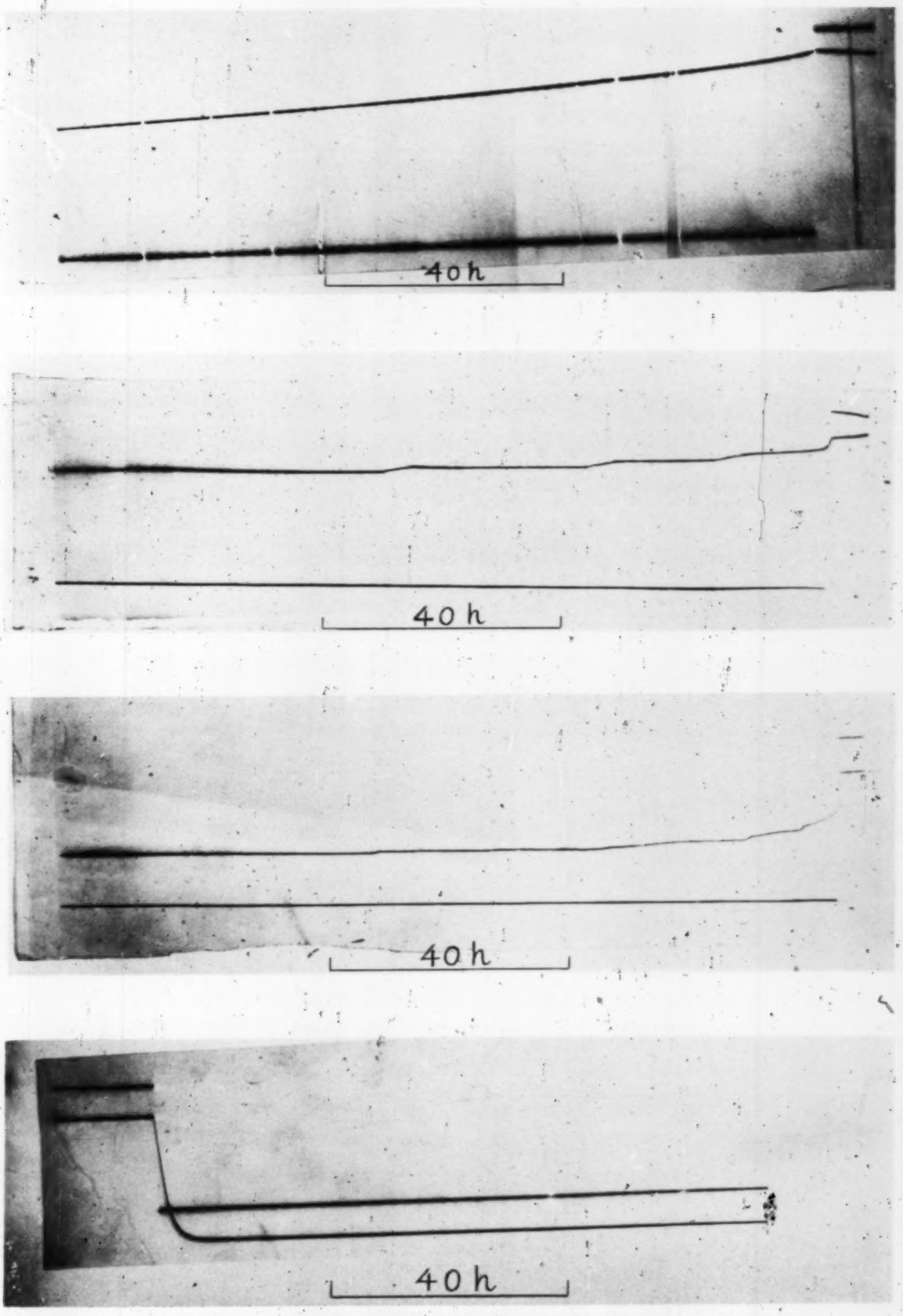

(a)

(b)

(c)

(d)

第 2 圖 粘土の捩れ變形曲線 (原圖の $\frac{1}{3}$)

(a)	含水率	30·1%	溫度	18·2°C
(b)	〃	35·6%	〃	19·0°C
(c)	〃	37·8%	〃	18·8°C
(d)	〃	53·4%	〃	20·0°C

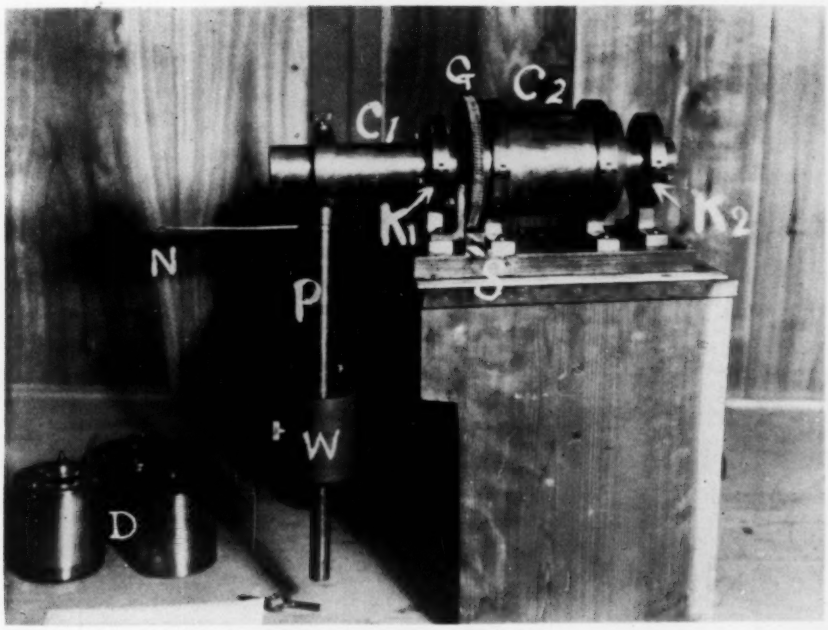

(a)

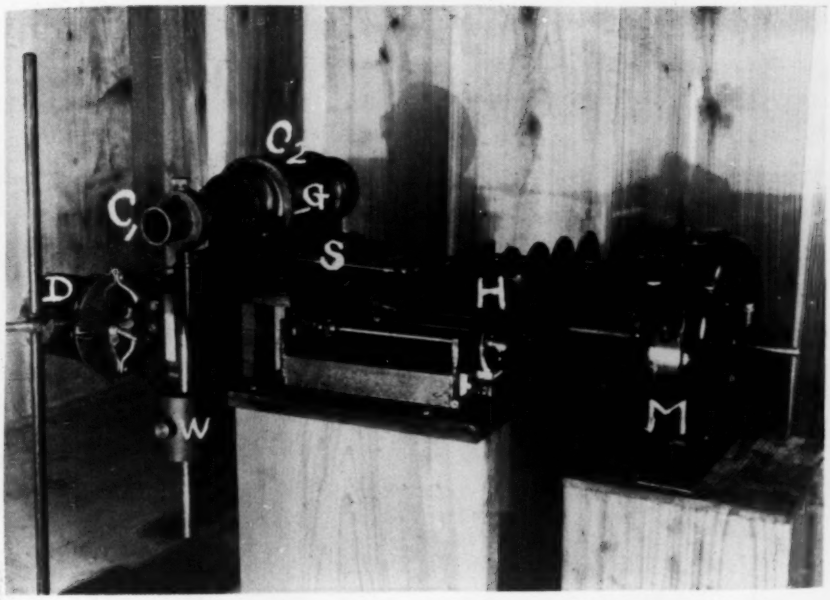

(b)

第7圖 實驗裝置 (a) 剪斷器械 (b) 實驗裝置全體

C_1	內側圓筒	N	記錄針
C_2	外側圓筒	M	同期電動機
D	記錄用時計	S	外側圓筒回轉用接續軸
G	ウオームギア	W	重錘
H	變速用齒車	K_1, K_2	內側圓筒の支へ臺

49. *Preliminary Notes on Experimental Studies on the Plastic Deformation of Soil.*

By Naomi MIYABE,

Earthquake Research Institute.

(Read April 2, 1936.—Received Sept. 21, 1936.)

1. Introduction. In investigating the conspicuous subsidences of the earth's surface in certain restricted areas, as those that occurred in the Kôtô district in the city of Tokyo[1] and in low ground in the city of Osaka[2], the necessity was felt for studying the physical properties of the soils composing the surface layers, the contraction of which seems to have been an important factor in bringing about the remarkable subsidence.

The writer describes in this paper some of these preliminary experiments that were made for studying the mechanical properties of soils. On carrying out the experiments, however, it was found that not only are the test pieces of the soils deformed elastically, but that time played a very important rôle in the progress of deformation under statical loading, even when the soil was perfectly dry. A non-linear relation between the applied load and the deformation obtained as the result of these experiments was therefore explained tentatively by assuming a visco-elastic or plastic property of the soil.

2. Soils Prepared for the Experiments. The soils used in the present experiments were taken from various depths from where a pier of the Komatugawa-basi (bridge)[3] is built.

Sieving showed the soil to be composed of particles of various sizes. Since the most important information sought by sieving is the percentage of the finer grained soil particles, which may be gel-forming material if the soil mass contains a considerable amount of water and becomes a colloidal gel, it was decided to use Stoke's method of sieving. The composition of the soil is thus separated into three components, i. e., (I) that which deposits in a very short time after the soil is mixed with an excessive quantity of water, (II) that which deposits from the re-

1) N. MIYABE, *Bull. Earthq. Res. Inst.*, **10** (1932), 844; **13** (1935), 763; etc.

2) A. IMAMURA, *Proc. Imp. Acad.*, **9** (1933), 378; **11** (1935), 186; etc.

3) Komatugawa-basi is a bridge built over the Arakawa (river), connecting Kameido and Komatugawa, in the eastern part of the city of Tokyo.

sidual suspension during the next 40 minutes, and (III) that which deposits during the next 10 hours.

The percentages of the components of the soil grains, i. e., the so-called mechanical ratios, are obtained as shown in Table I for soils from different depths.

Table I. Mechanical Ratios of Soils from Different Depths.

Sample	Depth	I deposites	II deposites	III deposites	Residuals
A	− 3·3 m	35%	39%	5%	1%
B	−19·0 m	2%	78%	12%	8%
C	−27·5 m	73%	7%	3%	17%

N. B. Height of this point about 1 m above mean sea-level.

3. Apparatus and Results of Experiments. The experimental study of the mechanical properties of soil was made by two different methods, i. e., by bending and by torsion. For the bending tests, the apparatus shown in Fig. 1 was used. To the soil test piece, which is supported at two edges A, A′, a load is applied to its middle P. The tilt of the surface of the test piece at point A″ was measured for different loads by means of scale S and the mirror M.

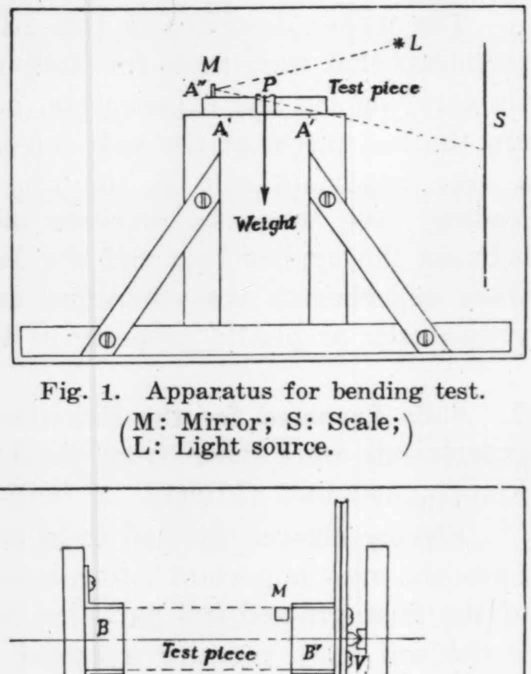

Fig. 1. Apparatus for bending test.
(M: Mirror; S: Scale; L: Light source.)

The apparatus for torsion test is shown in Fig. 2. In the case of torsion tests, the soil test piece is clamped at one end to B and the other end fixed to B′, the centre of wheel S being supported at V by a pivot. The wheel is rotated by weights as shown in Fig. 2, and the test piece consequently subjected to torsional deformation.

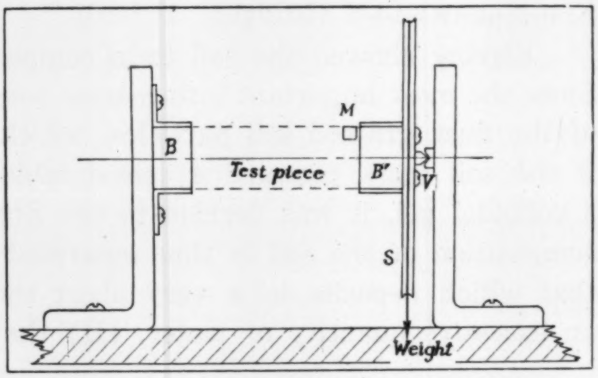

Fig. 2. Apparatus for torsion test.
(M: Mirror; V: Pivot; S: Wheel.)

The soil test pieces each from a different depth, are formed into rectangular bars of approximate dimensions, 2 × 3 × 10 cm, for use in the bending tests,

and 3 × 3 × 6 cm for use in the trosion tests. Two series of tests were made in the present experiments, the one being the series of tests for wet soils, and the other for perfectly dry soils. Perfect dryness of soil was obtained by exposing the test pieces *in situ* for several days and weighed at times, untill the dacrease in weight diminished.

The results showed that the differences in the mechnical ratios and in the methods of experiments, i. e., bending or torsion, do not greatly affect the relation between deformation and applied load. On the other hand, as shown in Figs. 3∼8, the difference in water contents, as may be expected, was the greatest factor affecting the load-deformation relation of soils.

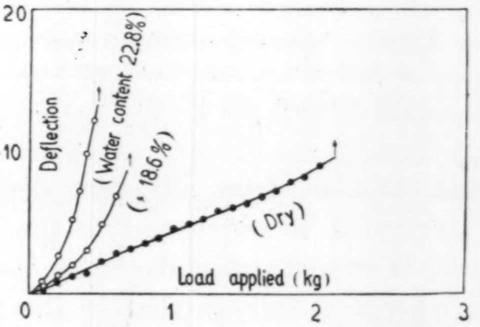

Fig. 3. Load-deformation in the case of bending of wet and dry state of soil A.

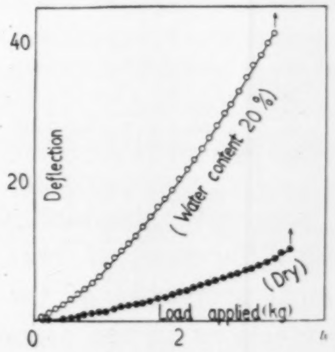

Fig. 4. Load-deformation relation in the case of bending of wet and dry state of soil B.

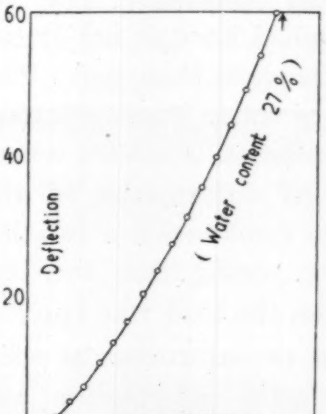

Fig. 5. Load-deformation relation in the case of bending of wet state of soil C.

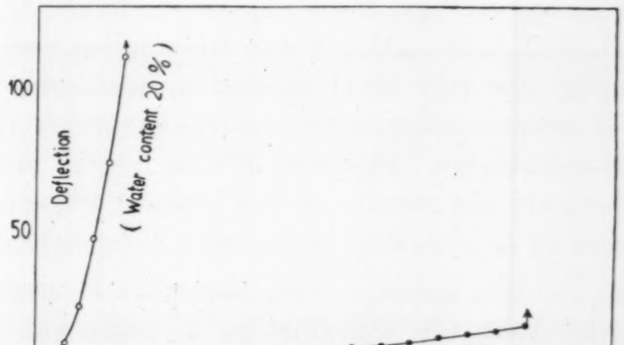

Fig. 6. Load-deformation relation in the case of torsion of wet and dry state of soil A.

It was noticed that the deformation differed in mode with the loads

applied according to whether they were bending tests or torsion tests

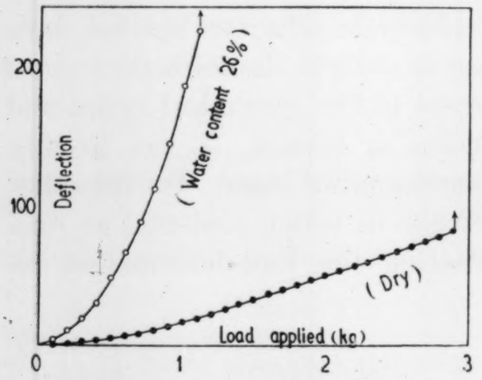

Fig. 7. Load-deformation relation in the case of torsion of wet and dry state of soil B.

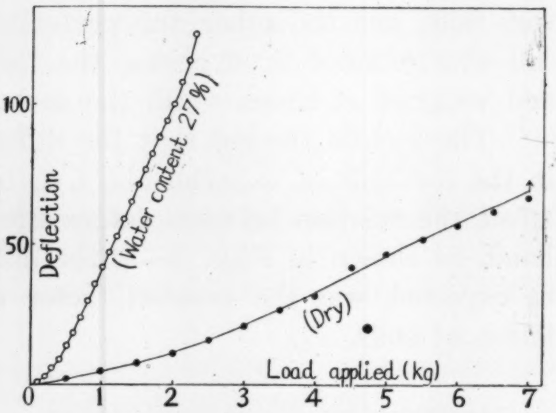

Fig. 8. Load-deformation relation in the case of torsion of wet and dry state of soil C.

and also with the kind of soil tested, that is, from different depths. These differences, if real, may be attributed to differences in the mechanical properties of the soils as well as to instrumental errors due to imperfections in the apparatus used, whence it follows that in the present results we can deal only with the effects of the water content under the applied loads.

4. Relaton between Deformation and the Loads Applied. The relation beween the deformations and the loads applied, though not linear as shown in Figs. 3∼8, can be explained in more ways than one. The fact, that deformation E and the applied load S are not in linear relation, may in one way be elucidated by assuming the relation $E=NS^n$. where n is greater than unity, as in numerous cases of deformation of the soft materials[4]. However it may not in order to invoke such a relation to explain the results of the present experiments, seeing that the test pieces of soil showed permanent deformation when the load was applied.

Soil-like material may therefore be regarded as deforming in such a way that the deformation is composed of elastic deformation and deformation due to viscous flow[5]. For such visco-elastic deformation, the relation between deformation and applied load is expressed in two different forms, the one by a formula introduced by Voigt and the other

4) BACH and BAUMANN, "Elastizität und Festigkeit", S-36.

5) R. K. SCHOFIELD and G. W. S. BLAIR, *Proc. Roy. Soc.*, A-**138** (1932), 707; **139** (1933), 557; **141** (1933), 72.

by a formula due to Maxwell.

To explain the results of the present experiments, it seems convenient to use Maxwell's formula, which is given in the form

$$\frac{de}{dt}=\frac{1}{n}\frac{dS}{dt}+\frac{1}{\eta}S,$$

where $\frac{de}{dt}$ is the rate (velocity) of deformation, S the stress, and n, η are the elastic constant and the coefficient of viscosity respectively.

It is of course a debatable question whether or not deformation of soil can rightly be regarded as being of the nature of visco-elastic deformation. It is well known that soil-like substances holding varying quantities of sandy materials differ in their resistance to shearing deformation under varying normal pressures, which makes it seem that the frictional resistance between the particles composing the soil mass is the most important factor in their resistance to external forces. Therefore, a theoretical treatment of deformation of such material is best developed rather on such lines as those taken by R. Becker in his investigations[6], in which the deformation of crystalline aggregates and the formations of slip lines are discussed statistically. In this paper however such phases of the subject are not dealt with: in being merely an attempt to explain the non-linear relation between deformation and applied loads from the stand point of visco-elasticity.

Since we are to use Maxwell's formula, it may perhaps be worth while to show a mode of deformation of soil under constant load, i. e., the time effect on deformation.

A sample of soil was subjected to deformation as described in the preceding paragraph under a constant load and the deformation plotted

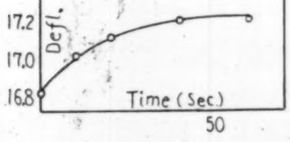

Fig. 9. Progress in torsional deformation with time (dry soil, under the statical load of 1·0 kg.).

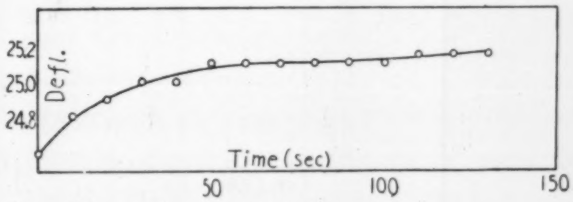

Fig. 10. Progress in torsional deformation with time (dry soil, under the statical load of 1·5 kg.).

against time, the results being shown in Figs. 9∼12. Although as

6) R. BECKER, *Phys. ZS.*, **26** (1925), 919.

shown in these figures, the deformation progresses, though very slowly, with time, it does not tend to any asymptotic value, from which we may tentatively explain the mode of deformation of soils as follows, on the basis of visco-elasticity.

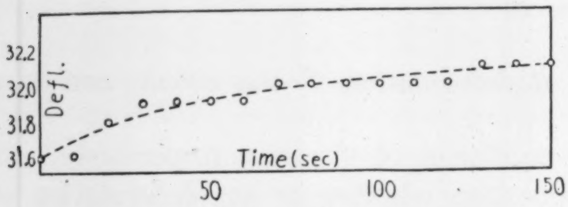

Fig. 11. Progress in torsional deformation with time (dry soil, under the station load of 2·0 kg.).

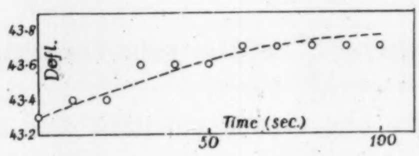

Fig. 12. Progress in torsional deformation with time (dry soil, under the statical load of 3·0 kg.).

To use Maxwell's formula in explaining the results of the present experiments, it is expressed in the form of finite differences, as

$$\Delta e = \frac{1}{n}\Delta S + \frac{1}{\eta} S\Delta t,$$

where Δe is the amount of deformation caused by application of the load ΔS and lapse of time Δt. After adding unit load m times with a constant time interval, the resultant deformation E is expressed by

$$E = \sum_m \Delta e = \frac{1}{n}\sum_m \Delta S + \frac{1}{\eta}\sum S\Delta t.$$

It is evident that $\sum_m \Delta S = S$ and $\sum_m S\Delta t$ may be calculated as follows;

$$\sum_m S\Delta t = S_0\Delta t + \{S_0 + (\Delta S)_1\}\Delta t + \{S_0 + (\Delta S)_1 + (\Delta S)_2\}\Delta t + \cdots\cdots$$
$$= mS_0\Delta t\Delta + t\{(m-1)(\Delta S)_1 + (m-2)(\Delta S)_2 + \cdots\cdots\}.$$

Assuming that $S_0 = 0$, i. e., no load was applied initially, and that ΔS, Δt are constant, we have

$$\sum_m S\Delta t = \{(m-1) + (m-2) + \cdots\cdots + 1\}\Delta S\cdot\Delta t$$
$$= \frac{m(m-1)}{2}\Delta S\cdot\Delta t = \frac{1}{2}(S\cdot m\Delta t - S\Delta t).$$

Since in plotting the result of the present experiment in an $S-E$ diagram, the addition of unit load ΔS corresponds to lapse of time Δt, we have $m\Delta t = AS$, the equation being finally obtained in the form

$$E = \left(\frac{1}{n} - \frac{\Delta t}{2\eta}\right)S + \frac{A}{2\eta}S^2,$$

which may suitably represent the experimental results obtained above.

5. Effect of Water Content on Elasticity and Viscosity. The relation between E and S deduced form Maxwell's formula is, as obtained in the preceding paragraph, written in the form

$$E = aS + bS^2,$$

where

$$a = \frac{1}{n} - \frac{\Delta t}{2\eta},$$

$$b = \frac{A}{2\eta}$$

Hence, constants a and b that were determined from actual data by the method of least squares may represent some measure of the elastic constant and the coefficient of viscosity of the visco-elastic soils.

In a case of torsion test, these constants were determined for dry and wet soils separately with the following results:

$$\begin{aligned} a &= -5{\cdot}6 \times 10^{-3} \text{ for dry soil} \\ &= -1{\cdot}4 \times 10^{-1} \text{ for wet soil}, \\ b &= 1{\cdot}3 \times 10^{-5} \text{ for dry soil} \\ &= 1{\cdot}8 \times 10^{-3} \text{ for wet soil}. \end{aligned}$$

As the scale for the deformation was quite arbitrary, the absolute values of these constants could not be obtained.

From the results obtained above, we can say that the viscosity of the soil, i. e., the value corresponding to the reciprocal of the value of b, is greater in dry than in wet soil.

Although it is also noticed that the order of magnitude of constant a varies parallel to b, it does not always indicate that the elastic constant of the soil parallel to the variation of viscosity. Since the constant a is composed of an elastic constant and the coefficient of viscosity, as in the above expression, $\frac{1}{n}$ could not contribute much to changes in the value of a even though considerable changes occurred in the value of n, in the case when $\frac{1}{n} \ll \frac{\Delta t}{2\eta}$. The negative value of a obtained in the foregoing examples suggests that these facts should be taken into consideration.

6. Hysteresis. In the case of a torsion test for dry soil, deformation due to increasing and decreasing loads were measured. As might be expected, the curve representing the relation between deformation and load in this case is a hysteresis loop as shown in Fig. 13.

It may also be noticed that in deformation due to decreasing load after it had been deformed by an increasing load, for several tens of seconds, the soil shows no sign of plastic flow, whereas it does so in the case of deformation due to increasing load, as shown in Fig. 14, in which the deformation is plotted against the time that elapsed.

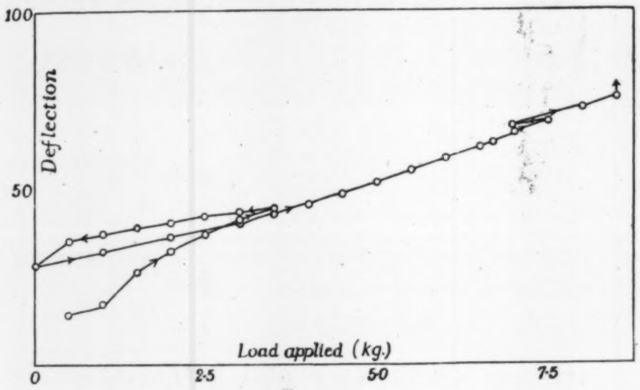

Fig. 13. Hysteresis in load-deformation relation in the case of torsion test of dry soil.

The hysteresis in deformation due to alternate applications of increasing and decreasing loads may be explained in the way as has been developed by Mr. Iida[7] in studying hysteresis in the deformation of soft materials.

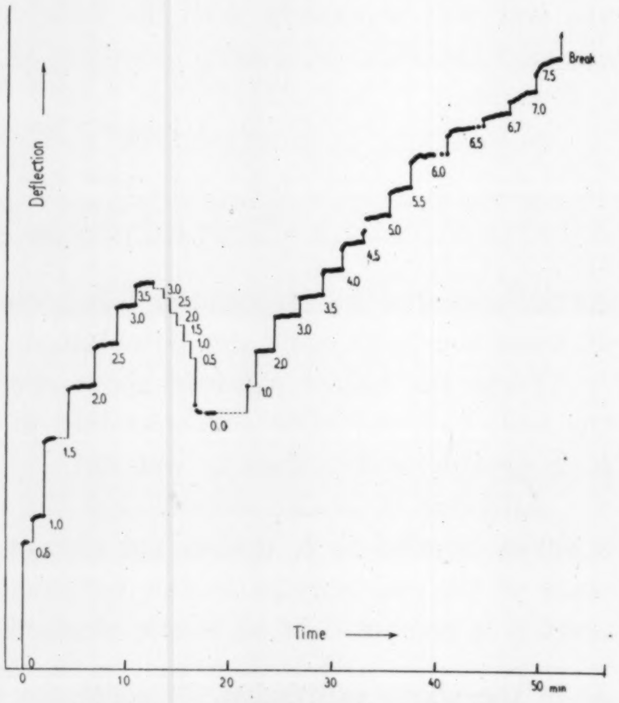

Fig. 14. Time-deformation relation under various statical loads, in the case of torsion of dry soil. (numerical figures denote the load for corresponding deformation).

7. Ultimate Strength of Soil. As shown in the results of the present experiments, deformation of the soil was visco-elastic, that is, the relation between deformation and applied load was not at all linear. The critical load for breaking of the test piece of soil however was

7) K. IIDA, *Bull. Earthq. Res. Inst.*, **13** (1935), 198.

determined rather clearly.

At the moment of breaking of the test piece of dry soil, visible cracks begin to develop and the velocity of deformation increases abruptly.

The surface of break that developed in the test piece of dry soil seems to have a regular orientation. It was however unfortunate that we could not make systematic studies in this respect. In the case of wet soil, the velocity of deformation of the test piece seems to increase in the neighbourhood of the ultimate load for break. This fact suggest that several micro-cracks, although invisible, would have developed in any case before the test piece broke down. For the breaking strengths of soils, we obtained the values as shown in Table II.

Table II. Strength of Soil.

Bending			Torsion		
Sample	Water content	Critical Load kg/cm^{-2}	Sample	Water content	Critical Load $kg/cm^{-2}/cm$
A	22·8%	0·06	A	20~17%	0·0068
A	18·6″	0·09	A	0″	0·028
A	0·0″	0·41	B	28~26″	0·021
B	20·0″	0·62	B	0″	0·080
B	0·0″	0·85	C	28~27″	0·057
C	28·0″	0·27	C	0″	0·209

The breaking strength of soil seems, as shown in Table II, to differ somewhat according to the size of the particles composing it. The above results however are not so reliable owing to scantiness of data and to the fact that the experimental apparatus was not complete in every respect.

8. Concluding Remark. In the above mentioned preliminary notes on experiments in connection with deformation of soils, the modes of deformations within the limit of their breaking strengths are explained by assuming a visco-elastic property for the soil as expressed by Maxwell's formula.

As to the points left unexplained, of which there are a number, it is hoped that it will be possible to deal with them in a future investigation, particularly as there may be some points in the physical and chemical properties of soil that could be discussed in connection with its colloidal nature. The results of such studies will be closely related to a number of problems in geophysical phenomena, for instance, oscil-

lations of surface layers, the remarkable local subsidences as referred to at the beginning of this paper, etc.

In conclusion, the writer wishes to express his sincere thanks to the council of the Hattori Hôkôkwai for aid received for studying the crustal deformation in the Kôtô region, by means of which the present experiments were carried out. The writer's best thanks are also due to Mr. Umezawa, civil engineer, for his kindness in placing samples of soils at the writer's disposal.

---

49. 土のプラスティック變形に關する實驗（序報）

地震研究所 宮 部 直 巳

東京市内小松川に於ける架橋工事場に於いて種々の深さから採取した土の試片に就き，撓曲及び振りの試験を行ひ，その結果にあらはれた土の變形に關する性質について述べた．

荷重—變形の關係が直線的でないことは從來知られてゐる所と全く同じであるが，之を解釋するのに，Maxwell の粘彈性式を用ひた．Maxwell の式から導かれる結果は

$$E = aS + bS^2$$

であつて，非直線的な荷重—變形の關係を解釋するに都合がよい．又，試片の含水量の多少によつて上式の a，b 等が變化する點についても一顧を費した．

以上の如き結果は土のコロイド的性質に關係する所が多いやうに思はれる．

---

50. *Experimental Studies on the Deformation of Sand Masses due to Vertical Loads. I.*

By Naomi MIYABE,

Earthquake Research Institute.

(Read Sept. 15, 1936.—Received Sept. 21, 1936.)

1. Introduction. Deformation of sand masses is one of the geophysical problems especially related to crustal deformations, while at the same time it may constitute an important subject in civil engineering.

This paper discusses the relation between the vertical loads applied and the resulting amounts of depression, which relation, however as been already studied by many authors, such as, Rankine[1], Coulomb, Boussinesq, Prandtl[2], Visal, Caquot[3], etc. The results obtained by these workers differ in several respects; for instance, Rankine has shown that the bearing power of the ground for a pier placed in depth h is

$$P_R = \rho h \tan^4\left(\frac{\pi}{4} + \frac{\varphi}{2}\right),$$

where φ is the angle of repose of the material composing the ground, whereas the bearing power for the same pier as recently deduced by Caquot has the form

$$P_C = \rho h \tan^2\left(\frac{\pi}{4} + \frac{\varphi}{2}\right) e^{\pi \tan \varphi}.$$

The difference in the numerical values of the calculations made from the formulae of different authors is sometimes considerable. If, for example, we assume $\varphi = 30°$, that is, nearly equal to the angle of repose of ordinary sand, P_R, the bearing power calculated from Rankine's formula, is only one-half of P_C as calculated from Caquot's formula.

This large difference may be due to scantiness of data for the study of modes of deformation of sand masses. This is a preliminary report of experimental studies on this subject.

2. Experiments. Sand contained in a box was depressed by a stamping rod over a small area on the surface by means of a lever and

1) RANKINE, *Phil. Trans. Roy. Soc. London*, (1856).
2) PRANDTL, *ZS. f angew, Math. u. Mech.* **1** (1921), 15
3) A. CAQUOT, "*Equilibre des Massifs a Frottement Interne*" Paris (1934).

weights, as shown schematically in Fig. 1.

Upon application of load W at W, the amount of depression was measured on scale S. The weights and the amounts of depression thus obtained plotted on the S–W diagram, from which the relation between S and W was studied.

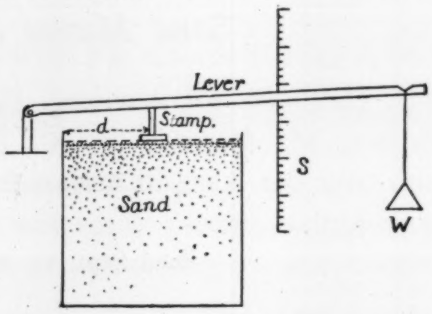

Fig 1. Experimental apparatus.

The sands used in the present experiment were as follows:

i) Sand sieved with meshes of from 1·0 mm² to 0·25 mm², are classed as coarse sand.

ii) Sand sieved with meshes of from 0·25 mm² to 0·01 ∼ 0·04 mm², are classed as fine sand.

iii) A mixture of sands i) and ii), called here mixed sand.

As mentioned already in the preceding paper[4], the sand was washed and dried to free it from any adbering colloidal particles and moisture that would undoubtedly greatly affect the mode of deformation.

As the state of packing of the sand particles is also an important factor that affects the mode of deformation, the experiments were made with both closely and loosely packed layers for each kind of sand.

3. Results. The results of the experiments are shown in Figs. 2 ∼ 7, in which the amounts of depression are plotted against the loads applied. It will be seen from these figures that the depressions and the loads have an approximately linear relation. The slope of the straight line drawn to represent this relation is less steep in the case of closely packed sand than in that of loosely packed sand. It will also be noticed that in the case of loosely packed sand, the curve representing the relation is composed of two straight lines having different slopes or that it shows a fluctuating rela-

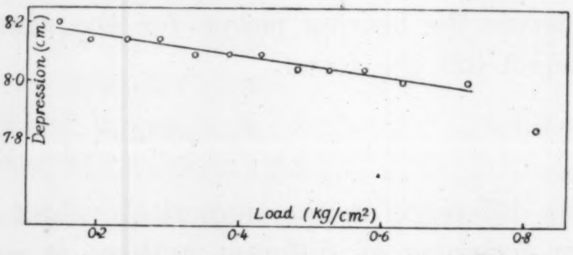

Fig. 2. Load-deformation relation. (Closely packed fine sand.)

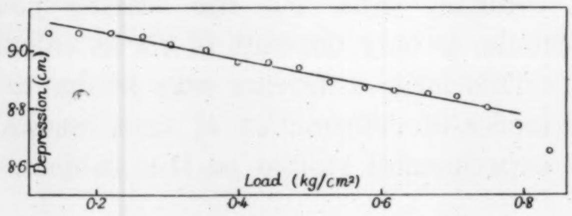

Fig. 3. Load-deformation relation. (Closely packed couse sand.)

4) T. TERADA and N. MIYABE, *Bull. Earthq. Res. Inst.*, **4** (1928), 33; **6** (1929), 109; etc.

tionship, as shown in Figs. 5~7. In the case of closely packed coarse sand, however, the relation was also fluctuating as shown in Fig. 4.

On applying a critical load, the sand mass deforms considerably, the stanping rod burying itself in the sand. The values of these critical loads are given in Table I.

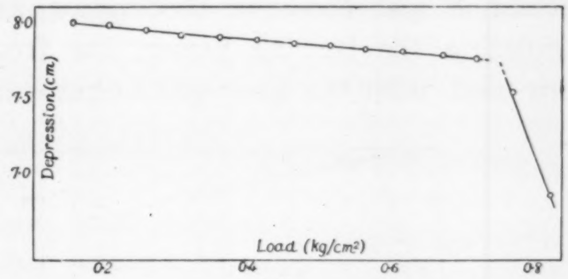

Fig 4. Load-deformation relation. (Closely packed mixed sand.)

Table I. Critical Loade Valne.

Packing \ Sand	Fine	Coarse	Mixed
Loose	421g/cm²	349g/cm²	422g/cm²
Close	815 〃	837 〃	825 〃

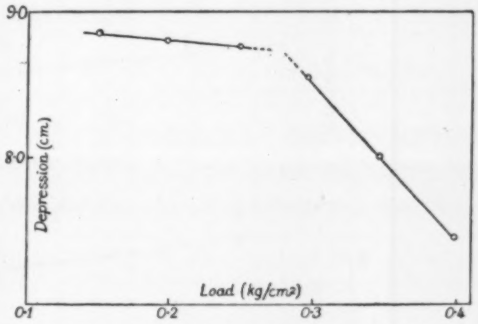

Fig. 5. Load-deformation relation (Loosely packed fine sand).

The effect of the boundary wall of the box that holds the sand should also be considered. In Figs. 8~9, the curves showing the relation between the depression and the loads applied at various distances from the centre of the surface of the sand mass are drawn for closely and loosely packed fine sands. The slopes of these curves have been measured and plotted against the distance from the wall, as shown in Fig. 10.

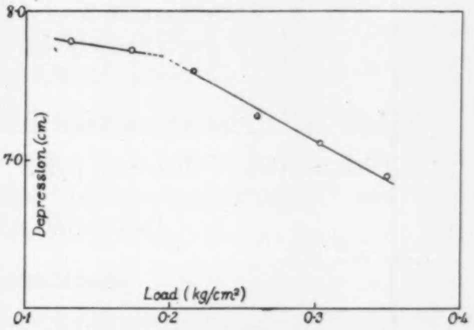

Fig. 6. Load-deformation relation. (Loosely packed course sand.)

These figures show that the effect of the boundary wall is practically negligible in experiments with central loading.

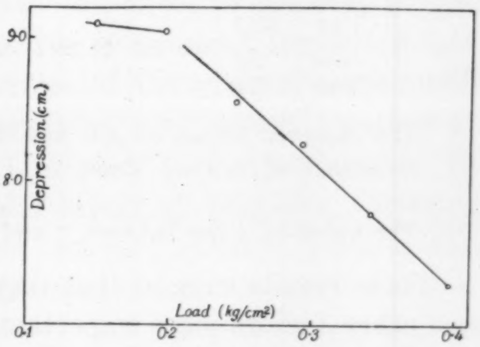

Fig. 7. Load-deformation relation. (Loosely packed mixed sand.)

4. Discussion. In explaining the results of these experiments, it is well to bear in mind the fromulae of Rankine, Prandtl, and Caquot, referred to in the beginning of this paper. The results obtained by evaluating these formulae differed more

or less from those obtained in the present experiments. The results of calculation and those of observation are compared in Table II. In calculating the bearing power, the fromulae of Rankine and Caquot, were used, with the assumption that $\varphi=30°$ and $\varphi=40°$.

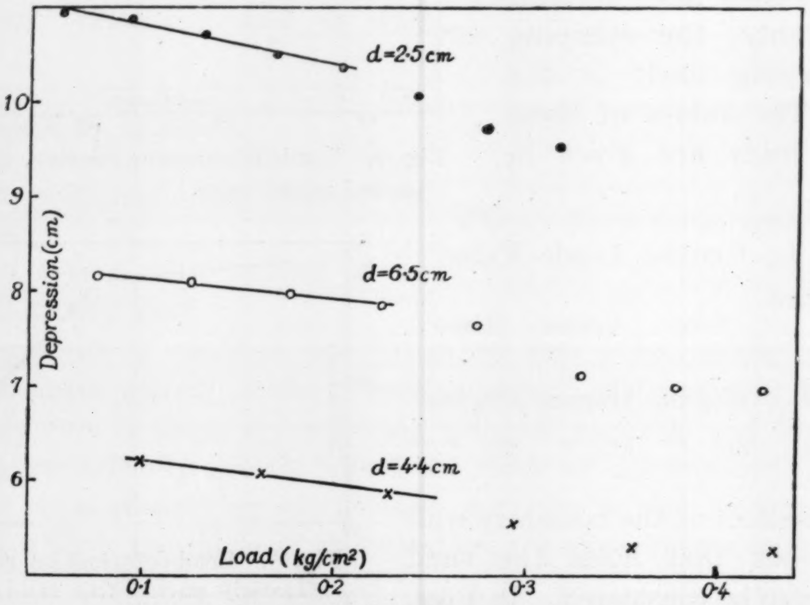

Fig. 8. Difference in load-deformation relation, and to different values of d's. (Loosely packed mixed sand).

Table II. The Observed and Calculated Values of p/h.

Observed p/h			Calculated p/h		
				Rankine	Caquot
Coarse,	Loose	237*	$\varphi=30°$	$9.0\times\rho$**	$22.0\times\rho$
	Close	1230			
Fine,	Loose	179			
	Close	1863	$\varphi=40°$	$21.2\times\rho$	$63.8\times\rho$
Mix,	Loose	137			
	Close	578			

* The observed values of p/h are those measured at critical loads, in Figs. 2~7.

** The value of ρ lies between 1 and 2.

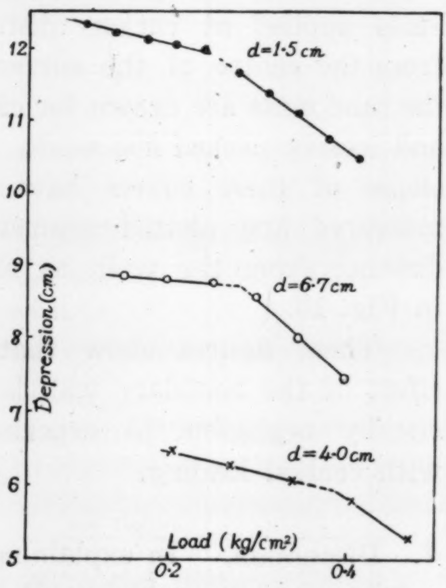

Fig. 9. Difference in load-deformation relation due to defferent valuer of d's. (Loosely packed fine sand).

These results suggest that there are some other factors more important than those that have been mentioned by Rankine, Caquot, etc., operating to cause the depression of the sand mass by surface loading.

According to Reynolds[5], dilatancy theory, sandy material, when most closely packed, increases its apparent volume owing to external disturbances.

This increase in apparent volume may occur as the result of changes in the arrangements of the sand particles, while re-arrangements of the particles in the sand mass may also bring about changes in their contact to adjacent particles. As the consequence of such a change in the sand mass, the values of $\rho \tan^2\left(\frac{\pi}{4}+\frac{\varphi}{2}\right)e^{\pi \tan\varphi}$ in Caquot's formula may also change.

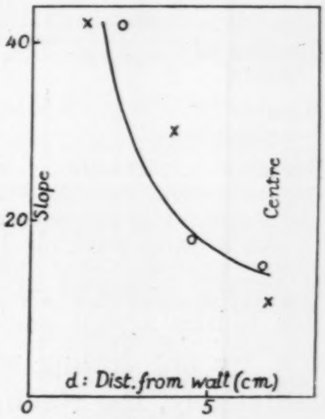

Fig. 10. Relation between the slope the curve in *S-W* diagram and *d*.

We shall suppose that the amount of depression of the surface in the loaded area upon application of load P is Δh, whence we have

$$P\Delta h=\int \mu N d\varepsilon + \rho V g \Delta h' ,$$

where μ is the coefficient of friction, N the force normal to the adjacent particle, and $d\varepsilon$ a small displacement along the contacting surface. The integration should be carried out throughout the whole of the volume that as been disturbed by the application of load P. The normal force N may be a function of the coordinates, r, h, i. e., the depth from the surface and the horizontal distance from the centre, P; the applied load, α; the direction of the normal to the adjacent particles; and n, the number of contacts. The last two factors may be a function of the mode of arrangement of the sand mass[6].

Since in cases such as those dealt with in the present paper, for resistance to vertical loads, the state of contact, or friction between particles, is much more important than the effective density, modes of arrangement of the sand mass may be one of the most important factors to be considered in explaining the results of the present experiments.

The ways in which spherical particles are packed together have been studied by L. C. Graton and H. J. Fraser[7], as reproduced in Table III, in which the spacing of horizontal layers of particles, the number of contact. and the porosity are given for each state of packing named after their cristallog raphical analogy.

5) O. Reynolds, *Sci. Papers*, **2** (1901), 203.

6) The fluctuation of the angle of repose of sand between 28~29° and 35~36° seems to be one of the reasons for the packing of the sand.

7) L. C. Graton and H. J. Fraser, *Journ. Geol.*, **43** (1935), 785.

Table III.

Packing	Cubic	Ortho-rhombic	Rhombo-hedral	Ortho-rhombic	Tetragonal-Sphenoidal	Rhombohed.
Spacing of lagers	$\sqrt{4}R$	$\sqrt{3}R$	$\sqrt{2}R$	$\sqrt{4}R$	$\sqrt{3}R$	$2\sqrt{2/3}R$
Number of contact	6	8	12	8	10	12
Porosity	47·64%	39·54%	25·95%	39·54%	30·19%	25·95%

As a sand particle has approximately the form of an uneven ellipsoid, the results obtained in the case of spherical particles seem to be inapplicable to the actual packing of the sands. Since, in the present discussion, we are dealing with local changes in the states of packing only qualitatively, the results of Graton and Fraser are very informative.

As will be seen from the foregoing table, there are several modes in packings; the number of contacts varying from 6 to 12, and the porosity from 47·64% to 25·95%. When the sand mass is deformed upon application of the load, the state of packing of the sand mass may be disturbed locally. The porosity and frictional resistance in the sand mass may be changed more or less by these local disturbances, and a slip surface also develop. Such local disturbances in the packing of a sand mass are more considerable in loosely packed or coarse sand.

The fluctuations in the S–W diagrams in the present experiments and those in forming slip surfaces when the sand mass was pressed laterally[8], may therefore be related to such local disturbances in the state of packing of the sand mass, as just mentioned.

These studies are being continued and the results will be reported in due course.

---

8) T. TERADA and N. MIYABE, *Bull. Earthq. Res. Inst.*, **7** (1929), 65.

50. 垂直荷重による砂層の變形（序報）

地震研究所 宮 部 直 巳

砂層の表面を重錘で壓した時に重錘の埋沒する深さと重錘の重量との關係を調べた．その結果，上述の關係は土壓論の公式から期待される樣な直線的のものではなく，砂層の變形してゆくに伴ひかなり變化する．

この事實は，本實驗の如き場合には，砂層内部の砂粒間の摩擦の狀況が變化してゆくことから期待され，砂の Packing の狀態如何が，重大な影響を有するものゝ如くに思はれる．

砂の息角がある範圍内で變化することや，Reyno'ds の指摘したやうな Dilatancy の性質などから，砂層が變形する場合には，Packing の狀態や摩擦の條件などが局部的に變化することが期待され，そしてそれが上述の種々な Fluctuation の原因となるのではないかと思はれるのである．

51. 土壤層中に於ける人工地震波の傳播並に土壤の彈性に關する研究（其 1）

地震研究所 {那須信治 / 萩原尊禮 / 表俊一郎}

（昭和11年9月15日發表――昭和11年9月21日受理）

緒言 地表近くの土壤層中に於ける彈性波の傳播速度の測定により土壤の彈性體としての性質を明かにし得，且つ波動の傳播經路を知る事によつて地下に於ける地層の分布狀態を知り得る事は周知の事柄である．此の測定は人爲的に發生せしめられた彈性波に就いて行ふのであるから任意の場所に於て反復施行し得る故に各種の土壤層に於てそれ等の彈性を實驗的に求めることが出來る．

從來彈性波探査法によつて各種地層中の彈性波の傳播速度を求めた例は數多ある．但しそれらの多くは岩石層中のもので土，砂或は粘土層等の所謂土壤層中の傳播速度の測定された例は案外少い．

表面土壤層の彈性はその土地固有の地盤振動に關係し，地震の際に於ける震動，引いては震害の程度に密接の關係がある．それ故に表面土壤層の彈性を知ることは震害を論ずる上に於て有效なる手段となり得ることは疑はない．

尙ほ人爲地震波の傳播狀況より地下に於ける地層の狀態を知り得る故に所謂基盤と稱せられる地下の稍硬質の地層をも探査し得る便利がある．一般に行はれてゐる彈性波探査法は主として鑛床の探査が目的であり，從つて所要の調査範圍も廣く又求める地層も深い．然しこれと同じ原理に基いて地表に極めて近い層のみを探査し得るとすれば土木工事其他建築の基礎工事等の計畫上の一助たり得る事と信ずる．そこで筆者の1人は先年來この方面の研究を續けて來た．斯の樣な場合には調査の範圍は一般の彈性波探査法の場合に比較して極めて狹く，又地層の深さも淺い．從つて火藥を用ひて彈性波を發生せしめる必要もなく簡單に重錘を地表に落下せしめるだけで十分である．斯樣にして發生せしめられた彈性波の地表下數十 m 以內に於ける反射，屈折の現象を明かにし地層の分布狀態を知るために本論文に述べる實驗が行はれたのである．こゝに列記しある實驗中，東京市內濱松町及び白河驛に於ける實驗は彈性波の傳播速度を求めるのが主たる目的ではなく，寧ろ所謂基盤と稱せられる地層の位置を求

めるのが目的であつた．然し地層の彈性そのものを論ずる場合は地層の他の物理的或は化學的性質をも知つて置く必要があるので其後に行はれた鎌倉及び駒場の實驗に於ては土壌の標本を採取して含水量，空隙比，密度及び成分等を實驗によつて求めた．

1. 彈性波觀測法の一般的說明

重錘落下裝置　濱松町及び白河驛に於ける實驗には彈性波を發生せしめるに約 150 kg の重錘を用ひた．この重錘は圓墻狀のものを用ひ 3 箇重ねてボールト締めとするときは 150 kg となり中央には心矢の通る直徑 10 cm の孔がある．この心矢は鐵材 Angle を組んだ櫓の前面に裝備され，地面に對して 90° 乃至 45° の範圍內で自由に角を變化し得る樣に設計してある．

重錘の落高及び質量を調節して所期の震動振幅を有する彈性波を發生せしめることが出來る．一般に重錘の Potential energy を Mh（M=質量，h=落高）とすれば Mh の何分の一かゞ波動の Energy となつて四方に傳播するのである．それ故に或る點での波動の振幅はこの Energy の平方根に比例すると考へてよいのであるが，勿論これは極めて概略の價を求める場合に適用し得る假定であり，濱松町に於ける實驗に徵して見ても上述の如き關係が常に存在するとは言ひ得ない．但し比較的規則正しい關係が見出された場合もあつた．

鎌倉及び駒場に於ける實驗には地動を或る程度まで幾何學的に擴大し更にそれを光學的に擴大する所謂 Mechanical-optical seismograph を用ひたので前述の如き特殊な落下裝置によつて質量の大なる重錘を落下せしめる必要もなく，僅かに數 kg の石塊或は金屬重錘を手を以て差上げ 1 m 內外の高さより落下せしめるだけで數十 m 以內の測定距離の範圍では十分であつた．

前述の落下裝置により重錘を落下せしめる場合でも亦手によつて落下せしめる場合でも重錘の地面を打つ點には特殊なる炭素棒を横たへ，此の兩端に導線を結び付け，此の導線を微動計に附屬してゐる時刻記錄裝置の電磁石の Coil に導き電流回路を作る．重錘落下の瞬間炭素棒は破碎し，電流は切斷されて電磁石に吸付けられてゐた鐵片は離れる．器械的に煤煙紙上に地動を記錄する器械に於てはこの鐵片に描針を附し，又光學的に記錄する器械に於ては小鏡を附し，何れも重錘落下の瞬間に於て線の段違ひを生じ，これを時間の起點として波動の走時を計算するのである．

2. 地　震　計

（a）濱松町及び白河驛に於ける實驗には器械的に地動を記錄する上下動地震計を用

ひた．その一つの型式のものでは振子重錘の質量約 5 kg，自己週期 0·10 秒，幾何倍率約 150 である．又他の型式のものでは振子重錘の質量約 15 kg, 自己振動週期 0·4 秒幾何倍率 250～300 である．濱松町に於ては第 1 の型式のもの 4 臺，第 2 の型式のもの 1 臺を用ひ，白河に於ては第 1 の型式のものゝみ 4 臺用ひた．何れの型式の地震計に於ても空氣減衰器を附し振子は極限減衰に近く調節してある．

(**b**) 鎌倉及び駒場に於て用ひられた地震計は重錘の質量約 6 kg，幾何倍率及び光學的倍率の相乘積は約 60,000 乃至10,000 に調節し得，振子の自己振動週期は 0·10 秒で別に 100 分の 1 秒の間隔を以て時間を記錄する裝置を有してゐる．

以下各地に於ける實驗の結果につきて述べる．

3. 濱松町に於ける實驗

(**a**) 此の實驗は鐵道省土質調査委員會の研究事項の一つとして行はれ石本博士[1] 及び筆者がこれに當り鐵道大臣官房研究所裏手の元運動場に於て I, II, III, IV の 4 方向に測定線を取り（第 1 圖及第 10 圖參照），昭和 10 年 5 月中旬より 6 月上旬に至る間隨時行つたのである．

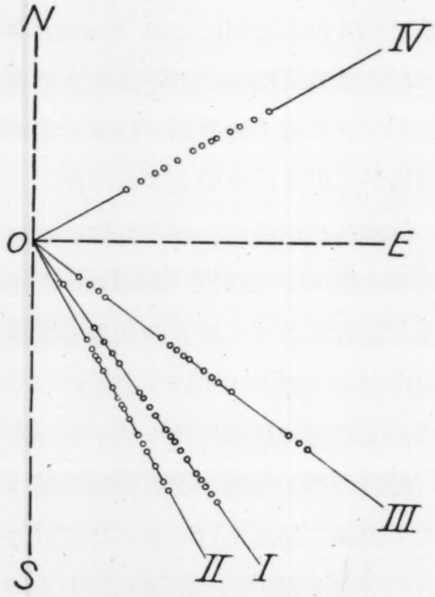

第 1 圖　濱松町地震計配置圖

O は重錘落下點
° は地震計配置位置を示す．
I, II, III, IV は夫々測定線である．
方向 { I = S 35° E,　III = S 52° E,
　　　II = S 30° E,　IV = N 60° E.

此の場所に於て前述の如き方法によつて得た震動記象は第 2 圖に示してある．此の圖を一見すると直接波が始めの部分に於ては優勢である．最初に到着したものは縱波であることは明かである．其後に振幅及び週期が急激に變化してゐる場所がある．そこで先づそれ等の場所を位相と見て I, II, III, IV, の測定線に就いて求めた記象からそれ等の走時を求めて全部一緒に一つの圖に曲線を引いた（第 3 圖）．これ等の位相中横波相の鑑定には稍困難を感じた．上下動の記錄のみで位相の判定は多少無理のやうにも思はれた．

第 2 圖中最も興味あることはどの記錄にも最初から暫く時を經て(0·8 秒乃至 1·0 秒)

1) 石本巳四雄，那須信治，"彈性波地盤調査法の研究(其 1)"，鐵道省土質調査委員會報告，第 4 輯 (1935).

振幅が再び增大してゐる事である．そこで直ちにこの部分が反射波ではないかといふ疑が起る．然し縱波の反射したものか或は橫波の反射したものかは最初から斷定することは出來ない．それ故にこの位相の走時を求め，後述の反射波の一般解法によつて橫波の反射波に相當するものであることを確めたのである．

（b）實驗結果の解析

官房硏究所裏手の廣場に於て行つた實驗によれば明瞭に反射波と認め得るものは圖中 sR と記したものである．この位相は 10 m 以上の距離に於て觀測した場合には明瞭に認め得るのである．これに反し距離の小さい場合には比較的認め難かつた．これは sR なる波動の實在することには何等相違はないのであらうが距離が小さい場合には表面に沿つて傳はる波動の方が優勢なために反射波の識別が困難となるからである．且つ距離の小さい場合は重錘の質量及び落高を小さくして最初の波動で描針が脫出しないやうにしたため反射波の振幅が小となつた．これらのために識別が困難となつたのであらう．各位相の走時曲線は第 3 圖に示してある．

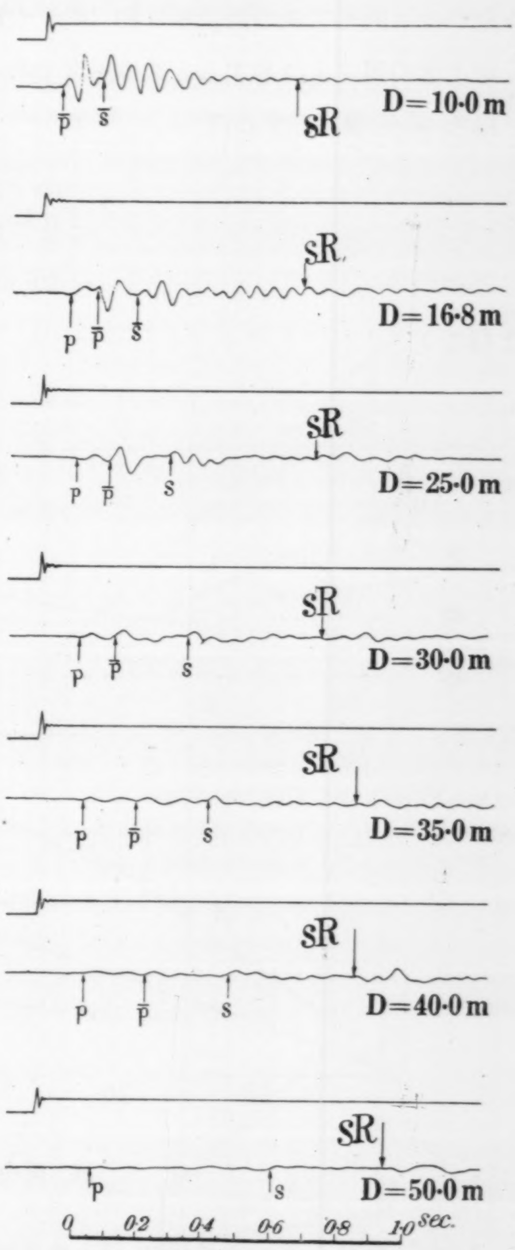

第 2 圖　濱松町に於いて得たる記象

（c）屈折波の解析　I，II，III，IV の各測定線に就て夫々走時曲線を求めた（第 4〜7 圖）．屈折縱波（P）及び直接縱波（P）は比較的容易に測定することが出來た．この兩方の波動の走時曲線（第 4〜7 圖）から最上層及その下に存在する層內に於ける縱波の平均傳播速度は夫々

$$V_1 = 117 \text{ m/sec},$$

$$V_2 = 370 \text{ m/sec},$$

となつた．而して此の兩位相は約 10 m の距離に於て同時に到着することを認めたから最上層の厚さを計算すると次の通りである．

卽ち Z を厚さとすれば[2)]

$$Z=\frac{10}{2}\sqrt{\frac{370-117}{370+117}}$$

$$=3{\cdot}6\ \mathrm{m}$$

を得る．

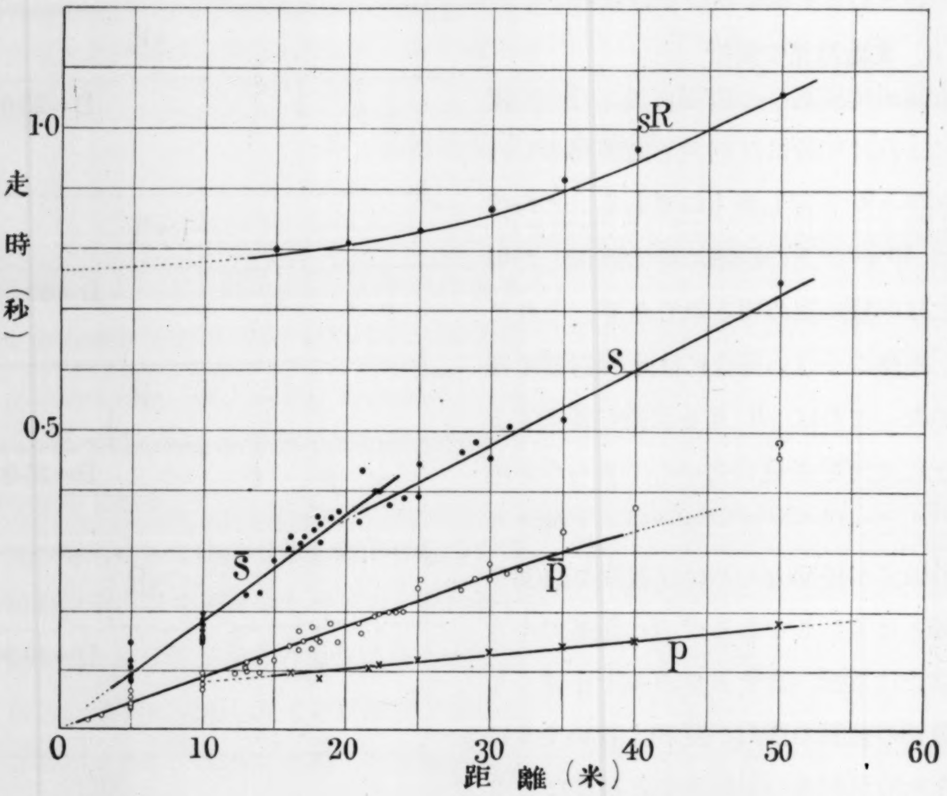

第 3 圖 濱松町に於ける走時曲線

屈折横波（S̄）及び直接横波（S）の走時曲線からも上層の厚さを求め得る筈であるけれども横波の走時は位相の判定が難しいために誤差が大きく，從つて速度の値が縱波の場合程正確とは言ひ得ない．且つ屈折，直接兩波動が同時に到着する點の位置が判然としてゐないために計算で求めた層の厚さには相當誤差が大きい．假りに走時曲

2) 屈折波と直接波とが同時に到着する點の距離を x_0，上層の厚さを Z とすれば x_0 及び Z の間には次の關係がある．

$$Z=\frac{x_0}{2}\sqrt{\frac{v_2-v_1}{v_2+v_1}}.$$

こゝに v_1 及び v_2 は上層及び下層内の彈性波の傳播速度である．

線より $x_0=20\text{ m}$, $v_2=80\text{ m}$, $v_1=53\text{ m}$ と定めて Z を求めると

$$Z=\frac{20}{2}\sqrt{\frac{80-53}{80+53}}$$
$$=4\cdot5\text{ m}$$

となる.

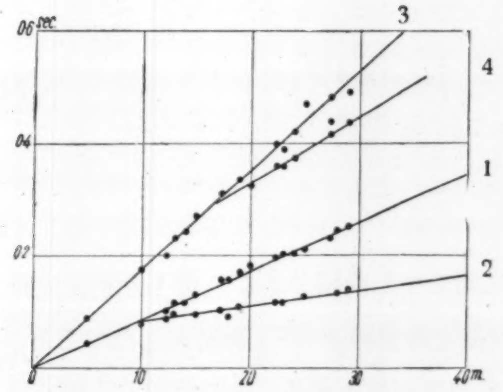

第　4　圖

濱松町に於ける I の測定線に對する走時曲線

曲線：1 最上層中の縱波 $(V_l)_1=116$ m/sec
2 中間層中の縱波 $(V_l)_2=376$ m/sec
3 最上層中の橫波 $(V_t)_1=56$ m/sec
4 中間層中の橫波 $(V_t)_2=85$ m/sec.

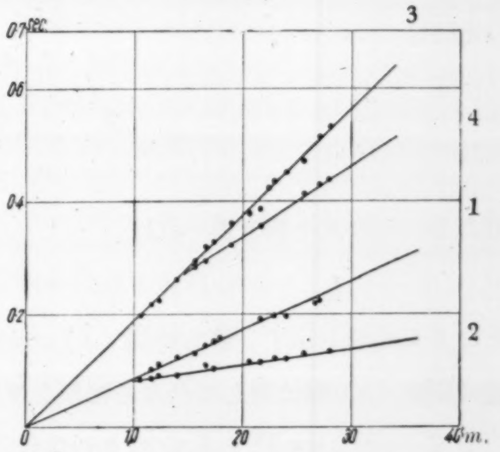

第　5　圖

濱松町に於けす II の測定線に對する走時曲線

曲線：1 最上層中の縱波 $(V_l)_1=116$ m/sec
2 中間層中の縱波 $(V_l)_2=361$ m/sec
3 最上層中の橫波 $(V_t)_1=53$ m/sec
4 中間層中の橫波 $(V_t)_2=81$ m/sec.

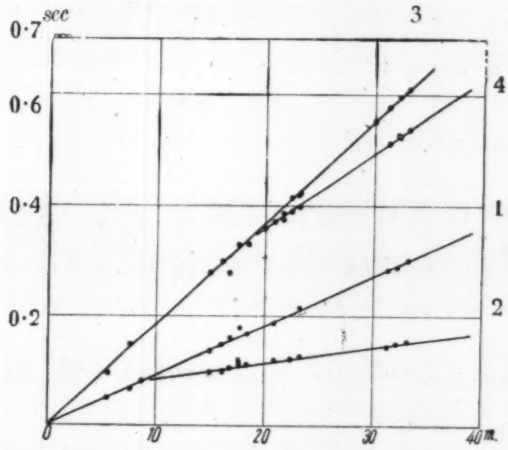

第　6　圖

濱松町に於ける III の測定線に對する走時曲線

曲線：1 最上層中の縱波 $(V_l)_1=118$ m/sec
2 中間層中の縱波 $(V_l)_2=362$ m/sec
3 最上層中の橫波 $(V_t)_1=55$ m/sec
4 中間層中の橫波 $(V_t)_2=76$ m/sec.

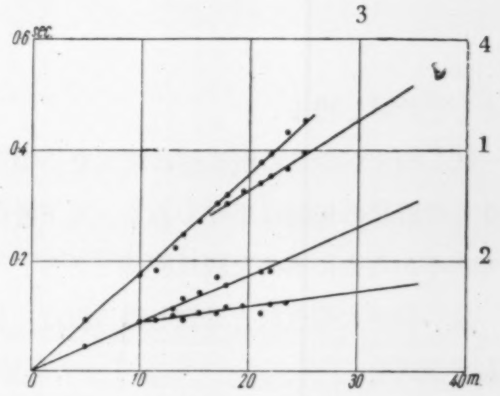

第　7　圖

濱松町に於ける IV の測定線に對する走時曲線

曲線：1 最上層中の縱波 $(V_l)_1=115$ m/sec
2 中間層中の縱波 $(V_l)_2=365$ m/sec
3 最上層中の橫波 $(V_t)_1=56$ m/sec
4 中間層中の橫波 $(V_t)_2=80$ m/sec.

縱波及び橫波の走時曲線より最上層の厚さを求めると平均 4 m となる. これは恐らく地表の盛土或は埋土層の厚さであらう.

(d) 反射波の解析

i) 一般解析法

一般には地表及び岩盤面が何れも平行な場合に於ける彈性波の傳播經路を論じてゐる．且つ事柄を簡單にするために上層の厚さ一様，又彈性も一様と考へる．上層内に於ける彈性波の速度を v_1 とし，上層の厚さを h，觀測點の距離を x とすれば反射波の走時は

$$T=\frac{2\sqrt{h^2+\left(\frac{x}{2}\right)^2}}{v_1}=\frac{\sqrt{x^2+4h^2}}{v_1} \tag{1}$$

である．この式を書き換へれば

$$x^2-v_1^2T^2=-4h^2 \tag{2}$$

となり双曲線を示す．即ち時間 (T) の軸に對して凸曲線である．即ち屈折波走時曲線は距離 (x) 軸に對して凸なるに反し反射波走時曲線は (T) 軸に對し凸である．

さて $b=x^2$，$a=T^2$ として a, b の曲線を造れば直線を得る．その直線の方程式は

$$\omega a_i-b_i=\zeta \tag{3}$$

である．こゝに $\omega=v_1^2$, $\zeta=4h^2$ である．この直線の傾斜より v_1 を求めることが出來る．

又上層の厚さは

$$h=\frac{1}{2}\sqrt{\zeta} \tag{4}$$

として計算し得る．

若し測定が餘りに廣範圍に渉らない場合には v_1 は一定であり從つて ω も一定となりこの直線の傾斜は不變である．又下層の面が地表面と平行である場合には h は一定であるから上に求めた線は直線である．

此の線が大體直線と見做し得る程度に眞直であるならば h, v_1 は何れも不變と假定して上式を

$$\omega a_i-\zeta=b_i \tag{5}$$

なる形に書き更め以下計算を行ふ．2 箇以上の觀測がある場合には ω 及び ζ を最小二乘法によつて求めることも出來るが一般には次の解法による．

さてこゝに述べる解法では平均走時及び平均距離を用ひて計算する．

今 n 箇の觀測のある場合走時及び距離の夫々の二乘の算術平均値を a_0 及び b_0 とす，即ち

$$\left.\begin{aligned} a_0 &= \frac{1}{n}\sum_{i=1}^{n} a_i , \\ b_0 &= \frac{1}{n}\sum_{i=1}^{n} b_i \end{aligned}\right\} \qquad (6)$$

である．

一般に a_i 及び b_i は次の二つの關係式で示される．

$$\left.\begin{aligned} a_i &= a_0 + \alpha_i , \\ b_i &= b_0 + \beta_i . \end{aligned}\right\} \qquad (7)$$

それ故に（5）式は

$$(a_0 + \alpha_i)\omega - \zeta = b_0 + \beta_i \qquad (8)$$

となる．

而して最小自乗解法の Normal equations は次の二式となる．

$$\left.\begin{aligned} A\omega - B\zeta &= D , \\ B\omega - C\zeta &= E , \end{aligned}\right\} \qquad (9)$$

玆に

$$\begin{aligned} A &= \Sigma(a_0 + \alpha_i)^2 = na_0^2 + 2a_0\Sigma\alpha_i + \Sigma\alpha_i^2 , \\ B &= \Sigma(a_0 + \alpha_i) = na_0 + \Sigma\alpha_i , \\ C &= n , \\ D &= \Sigma(a_0 + \alpha_i)(b_0 + \beta_i) = na_0b_0 + b_0\Sigma\alpha_i + a_0\Sigma\beta_i + \Sigma\alpha_i\beta_i , \\ E &= \Sigma(b_0 + \beta_i) = nb_0 + \Sigma\beta_i \end{aligned} \qquad (10)$$

である．

而して（6）の關係により

$$\begin{aligned} \Sigma\alpha_i &= \Sigma a_i - na_0 = 0 \\ \Sigma\beta_i &= \Sigma b_i - nb_0 = 0 \end{aligned} \qquad (11)$$

なる關係があるから

$$\begin{aligned} A &= na_0^2 + \Sigma\alpha_i^2 , \\ B &= na_0 , \\ C &= n , \\ D &= na_0b_0 + \Sigma\alpha_i\beta_i , \\ E &= nb_0 \end{aligned} \qquad (12)$$

となる．

Normal equations の解は次の通りである．

$$\left.\begin{aligned} \omega &= \frac{\Delta_\omega}{\Delta} , \\ \zeta &= \frac{\Delta_\zeta}{\Delta} , \end{aligned}\right\} \qquad (13)$$

玆に

$$\left.\begin{aligned}\varDelta_\omega&=BE-CD=-n\Sigma\alpha_i\beta_i\,,\\ \varDelta_\zeta&=AE-BD=nb_0\Sigma\alpha_i^2-na_0\Sigma\alpha_i\beta_i\,,\\ \varDelta&=B^2-AC=-n\Sigma\alpha_i^2\,.\end{aligned}\right\}\tag{14}$$

故に

$$\left.\begin{aligned}\omega&=\frac{\Sigma\alpha_i\beta_i}{\Sigma\alpha_i^2}\,,\\ \zeta&=\frac{a_0\Sigma\alpha_i\beta_i-b_0\Sigma\alpha_i^2}{\Sigma\alpha_i^2}=a_0\omega-b_0\,.\end{aligned}\right\}\tag{15}$$

平均速度 v_1 及び厚さ h は

$$\left.\begin{aligned}v_1&=\sqrt{\omega}\\ h&=\frac{1}{2}\sqrt{\zeta}\,,\end{aligned}\right\}\tag{16}$$

となる．

ii) sR の速度及び反射面の深さ

先づ近似解法の一手段として最上層の存在を無視して地表より反射面までは一様な層であると假定し，この場合に於ける反射波の平均速度及び層の厚を求める．反射波が比較的明瞭に観測された場合を選び，x を距離，t を走時として $b=x^2$ を縦軸に，$a=t^2$ を横軸としてグラフを作れば第 8 圖を得．この圖に於て直線の傾斜卽ち db/da は平均速度 ω の自乘となる．又この直線が横軸と交はる點は重錘落下點に於ける反射波の走時の自乘となり，この圖から平均速度及び層の厚さを概略知ることが出來る．

平均速度及び層の厚さを正確に求めるには前述の計算法に依るを可とす．sR 波の走時の観測値は第 I 表の通りである．

第 I 表 sR 波の走時

距離 (m)	走時 (sec)	距離 (m)	走時 (sec)
15	0·80	35	0·92
20	0·81	40	0·97
25	0·83	50	1·06
30	0·87		

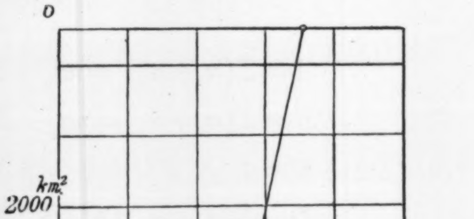

第 8 圖 濱松町に於ける反射波に對する a, b 曲線

a_0 及び b_0 の値を求むれば

$$a_0=\frac{1}{n}\sum_{i=1}^{n} a_i=0{\cdot}8075\ \mathrm{sec}^2,$$

$$b_0=\frac{1}{n}\sum_{i=1}^{n} b_i=1068\ \mathrm{m}^2$$

を得.

此等の値を用ひ ω 及び ζ を求むれば

$$\omega=4457{\cdot}51\ \mathrm{m}^2/\mathrm{sec}^2,$$

$$\zeta=2531{\cdot}44\ \mathrm{m}^2$$

となる. 故に平均速度 v_1 及び層の厚さ h は

$$v_1=\sqrt{\omega}=66{\cdot}76\ \mathrm{m/sec},$$

$$h=\frac{1}{2}\sqrt{\zeta}=25{\cdot}16\ \mathrm{m}$$

となる.

この結果より見れば反射面は地表より 25·16 m の所にあり反射波の速度は 66·76 m/sec であるから走時曲線から見ても sR なる波動は反射の前後常に横波であると考へられる.

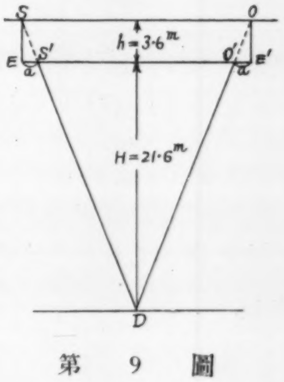

第 9 圖

第 2 回目の近似解法としては次の様な方法がある. 前に述べた屈折, 直接縱波から求めた最上層の存在することを考慮に入れ基盤の上に二つの層のある場合として解くのである. 最上層中の横波の速度は第 9 圖の走時曲線から 53 m/sec である事を知り得るから最上層内を傳はる橫波の走時を求める.

卽ち第 9 圖中 (SS′+OO′) の部分の走時を求めるのである. この場合 S′O′ 面に於て波動は實際は屈折するがこゝでは簡單な爲めに屈折しないものとして計算する. 上下の層内の傳播速度が餘り差異のない場合には多くはこの假定がなされる.

S 及び O より夫々垂線を下し, S′ O′ との交はる點を E, E′ とし $O'E'=ES'=a$ の長さを求めることが必要である. 斯くして S′ DO′ の距離及び走時を計算し再び前述の計算法に依つて速度及び層の厚さを求めるのである. この場合 $h+H=25{\cdot}16$ として前の近似解法によつて得た値を用ひる. 又最上層内の速度は走時曲線より得た値

53 m/sec を用ひ $h=3{\cdot}6$ m とする．最上層内の走時を t とし，t 及び a を示せば次の通りである（第 II 表）.

第 II 表

距離 (SO)	t	a
m 15	sec 0·144	m 1·0
20	0·147	1·3
25	0·151	1·8
30	0.159	2·0
35	0·162	2·4
40	0·170	2.7
50	0·188	3·7

下の層内に於ける走時卽ち S′ DO′ の經路に對する走時を T' とし S′ O′ の距離とを示せば次表の如し．

第 III 表

距離 (SO)	S′ O′	T
m 15	m 13·0	sec 0·656
20	17·4	0·663
25	21·4	0·679
30	26·0	0·711
35	30·2	0·732
40	34·6	0·782
50	42·6	0·872

此の表に與へられたる走時及び S′ O′ を用ひ前述の方法と同樣にして a_0 及び b_0 を求むれば

$$a_0=\frac{1}{n}\sum_{i=1}^{n} a_i=0{\cdot}5351\ \mathrm{sec}^2,$$

$$b_0=\frac{1}{n}\sum_{i=1}^{n} b_i=789{\cdot}95\ \mathrm{m}^2$$

となる．

ω 及び ζ は

$$\omega=4806{\cdot}9\ \mathrm{m^2/sec^2},$$

$$\zeta=1782{\cdot}22\ \mathrm{m}^2$$

となり速度 V 及び層の厚さ H は

$$V=69{\cdot}3\ \mathrm{m/sec},$$

$$H=21{\cdot}1\ \mathrm{m}$$

となる．

故に反射面は $h+H=3{\cdot}6+21{\cdot}1=24{\cdot}7$ m となり前の近似解法によりて得たる 25·1 m とは大差なく，差は勿論観測誤差の範圍内である．

而して $V=69{\cdot}3$ m/sec なる値は走時曲線より求めたる $V=80$ m/sec とは一致しない．この不一致の説明には種々あらう．例へば S′ O′ の面の附近だけが特に硬い物質があり $V=80$ m/sec の速度になる様な狀態であり，それより下の部分は比較的軟い物質があるため速度がこれより小であるとも考へられる．又同じ物質でも含水量により彈性波の傳播速度が大いに異るから含水量の差異を以ても此の程度の速度の差は説明し得るであらう．

尚近似解法を進めて S′ O′ 面に於て波動の屈折を考慮して反射波の速度及び層の厚さを再び近似的に求めることも出來るがこゝでは以上の 2 回の近似計算で止めておく．この近似解法を行つてもこゝに求めた速度及び層の厚さに左程大なる差異は生じない．差は勿論観測誤差の範圍内にある．

以上の如くにして求められた速度及び層の厚さが實際に有意義のものであるか否かを一應吟味しておく必要がある．

(e) 反射波の吟味

反射波の平均速度 66·76 m なる値は盛土，埋土及び冲積層等の比較的軟弱なる地盤を傳はる彈性横波の速度の値としては適當である．更に詳しく言へば地表より 3·6 m までは横波は 58 m/sec の速度を以て傳播し，これより下の層内では平均 69·3 m/sec の速度で傳播する．而して屈折横波より求めた中間層の上部の速度は約 80 m/sec であるから前にも述べた如く此の層の上部が比較的彈性に富む物質であることが想像される．此事に關しては層の吟味のところで更めて述べる．

この實驗では反射横波のみを用ひたが反射縦波の測定からも層の分布狀態を決定し得る筈であるけれども反射縦波の到着時刻が他の優勢なる波動の到着時刻と略同じであるために記錄上確かに反射縦波を判定することが困難である．

現在の實驗の如く比較的淺い所にある層を見出す爲には反射縦波を目當にするより反射横波を用ひる方が得策であらう．横波は地表近くの軟弱なる地盤に於ては速度が數十 m 毎秒程度であり縦波の速度に比較して 2 分の 1 或はそれ以下の場合もあらう．それ故に反射横波の位相は他の優勢なる位相に遙かに遲れて到着し振動記錄上に於て比較的容易に識別し得るので土壤層の調査には反射横波を利用するのが得策であらうと思はれる．

f） 反射面の吟味

此の實験によつて求められた反射面は地表下 24·7 m にある．而して此の反射面までには二つの層がある．即ち地表より 3·6 m までを最上層，それより反射面までの 21·1 m の厚さの層を中間層とし此等の層を實際の試錐の結果と比較して見よう．24·7 m の反射面は東京附近に於ける基盤と稱せられる所謂第三紀層の表面であらうといふことだけは容易に想像される．

關東大地震後復興局建築部に於てなされた東京及び横濱の地質調査の内今回の實験場所に近い所で行はれた試錐の結果により第三紀層の上に横たはる各地層の厚さを見ると次の通りである．

第 IV 表

場所	(記號)	盛土埋土 (m)	沖積層 (m)	地表より第三紀層に至る深さ (m)
芝區濱崎町埋立地	(K 37)	4·5	22·1	26·9
同上	(I 37)	3·6	22·8	26·4
芝區汐留驛舊御料車庫東側	(K 35)	3·8	19·0	22·8
芝恩賜公園	(k 37)	2·3	11·5	13·8
芝區神明小學校	(K 36)	3·6	27·3	30·9

以上は何れも上總掘機によりて知り得たる地層の厚さである．これによれば實験地附近に於ては地表より 30 m 乃至 14 m の深さに第三紀層の基盤が存在してゐることがわかる．濱離宮を中心とする地域に於ける第三紀層基盤の同深線は第10圖に示してある．同圖には平均海水面より第三紀層の表面に至る深さを m で示してある．これによつて推定すれば此の實験より求めた基盤面の深さ 24·7 m は左程桁違ひのものではないことがわかる．

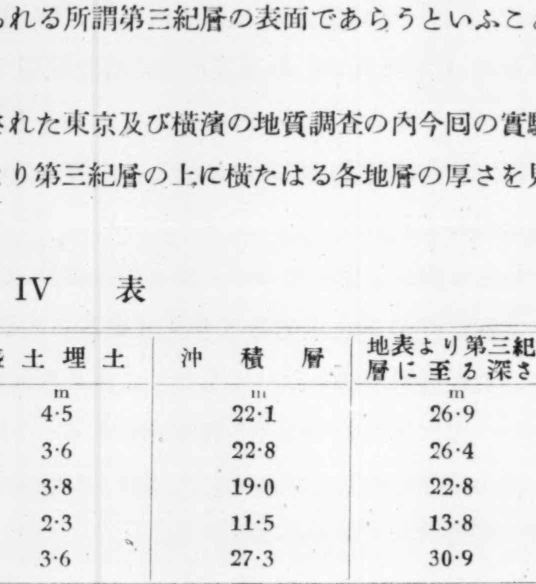

第 10 圖 ×は實験場所，同深線の數字は平均海水面より基盤までの深さ (m)

上記試錐の結果によると此等5ヶ所に於ける地層の分布は第 11 圖の通りである．これによつて見れば盛土，埋土の直下には沖積層が分布され，沖積層の上部は細粒の砂層である（但し汐留舊御料車庫及び芝恩賜公園に於てはこの砂層は認められない）．この層の下は介化

石を含む粘土層である．此の沖積層の上部の砂層は下の粘土層よりも彈性に富み從つて傳播速度も大である．

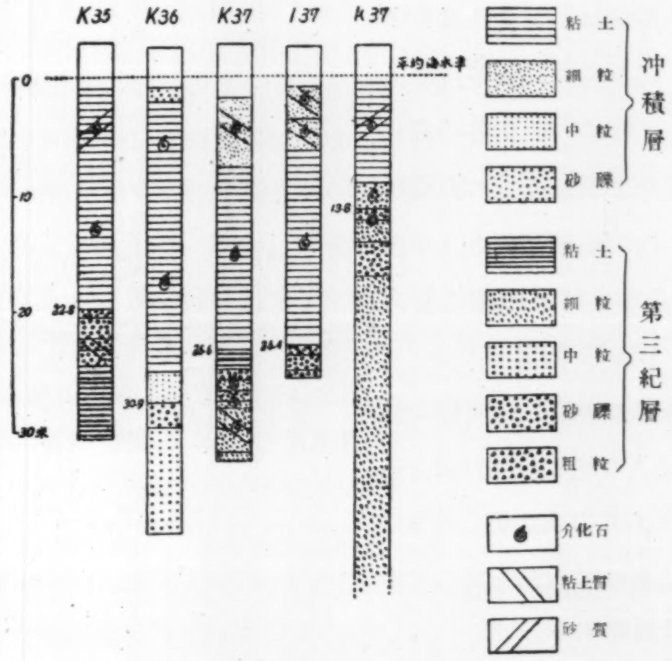

第　11　圖

第 3 圖中の P 波及び S 波の走時曲線より求めた傳播速度は恐らくこの砂層內の速度であらう．第三紀層に達すると砂礫層になる．地耐力の實驗によると一般には沖積層，洪積層．第三紀層の順序に地質年代の古いもの程鞏固であり新しいもの程軟弱である．又岩種に就いては粘土，砂礫の順に地耐力を增加し粘土を交へるに從ひ又含水量を增加するに伴つて軟弱となり砂礫を交へるに從つて鞏固となるが普通である．それ故に第 11 圖の如く粘土層と砂礫層が上下に重なつてゐる場合は上層と下層とでは强度の差異は可成りある．從つて彈性も可成り異なるであらう．それ故に彈性波の傳播に對しこの兩層の境界面は不連續面の役割をなし，この面に於て波動の反射，屈折の現象が見られるのであらう．

4. 福島縣白河町に於ける實驗

（a） 福島縣白河驛構內に於て最近鑿井工事が計畫された．而もこの井戶よりは相當多量の水量を得なければならないのでどうしても地下の岩盤層（周圍の地質から推定すれば石英粗面岩層）まで掘り下げる必要がある．この岩盤層を探査するために鐵道省土質調査委員會の依囑により昭和 11 年 6 月上旬彈性波探査法を實施することゝなつた．尙この探査法と同時に同會に於ては電氣探査法をも實施し，兩方法によつて岩盤層を求めたのである．

（b）此の實驗に於ては前述の濱松町に於て使用された第1の型式の上下動地震計4臺を用ひた．又彈性波を發生せしむるには前と同様鐵製の櫓により 150 kg の重錘を 3·0 m 内外の高さから落下せしめた．實驗を行つた場所は白河驛構内の荷物集配所附近及び西方約 300 m の地點で測定距離は最大 60 m であつた．(第12圖參照)

（c）**實驗結果の解說**　白河驛に於ける實驗の結果より地下の反射面たる岩盤の位置を求める方法は總て前述の濱松町の實驗結果の解析法と同じであるからこゝでは省略する．

反射波の測定　白河に於ける2箇所の實驗によれば2通りの反射波が認められる．これを sR_1, sR_2 として前述の a–b 圖（第8圖參照）をこれ等の反射波に就いて造ると第13圖及第14圖を得た．

sR_1 に就いて造られた a–b 圖（第13圖）は可成り綺麗な直線を得るが sR_2 の a–b 圖（第14圖）は稍不規則に點が散在してゐる．

而して sR_1 の反射面の深さ Z_1 及び sR_1 波の傳播速度 $V(sR_1)$ を前述の方法によつて I, II の測定線に就いて求めた．

(I)　$Z_1 = 24{\cdot}2$ m,

$V(sR_1) = 160$ m/sec.

又 sR_2 波に就いても同様に

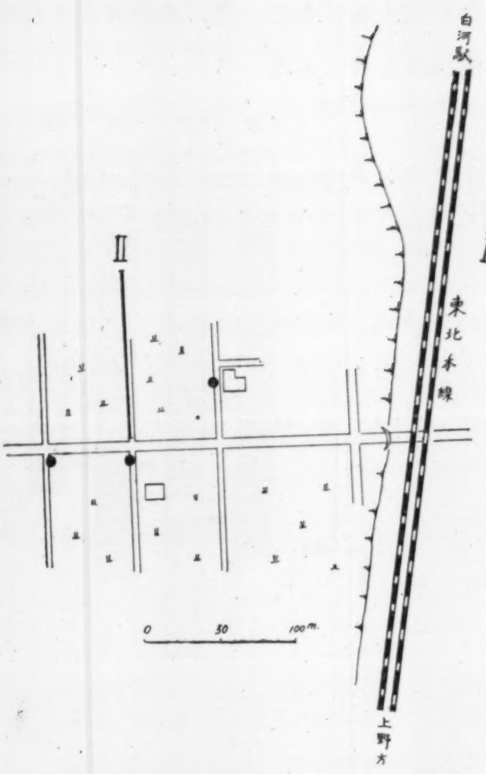

第12圖　白河驛に於ける觀測點配置圖
I, II, は彈性波による觀測線
●は電氣抵抗調査中心點

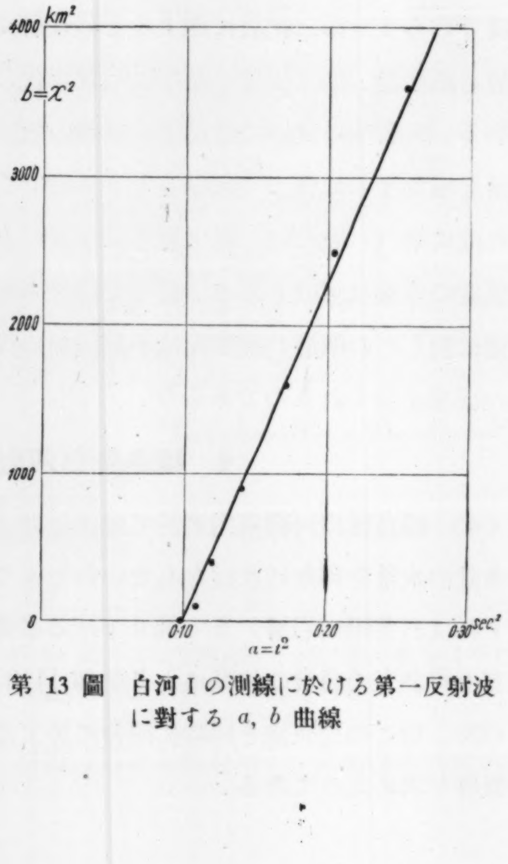

第13圖　白河Iの測線に於ける第一反射波に對する a, b 曲線

$Z_2 = 57$ m,

$V(\mathrm{sR}_2) = 162$ m/sec.

(II)　$Z_1 = 20{\cdot}0$ m,　$V(\mathrm{sR}_1) = 160$ m/sec,

$Z_2 = 51{\cdot}0$ m,　$V(\mathrm{sR}_2) = 162$ m/sec.

上記の sR_2 に就いて Z_2 及び $V(\mathrm{sR}_2)$ を求める場合は地表より sR_2 の反射面までは一様と假定し sR_1 の反射面の存在すること及びこの面に於ける屈折の現象を無視した．斯くして求めた sR_2 波の傳播速度と sR_1 波の傳播速度との差は 8 m/sec で sR_2 が僅かに大きいと言ひ得るであらう．それ故地表から基盤と想像されてゐる sR_2 の反射面までには中間に sR_1 なる反射面が存在してゐるけれども地表から基盤に至る間の物質は彈性的には左程違つてゐるとは言ひ得ない．此の實驗を行つた場所の地下には砂礫層の存在することは豫め知られてゐる．若しこの砂礫層が sR_1 の反射面に相當すると假定すればその砂礫の堆積してゐる厚さは左程厚いものではないと考へればよい．

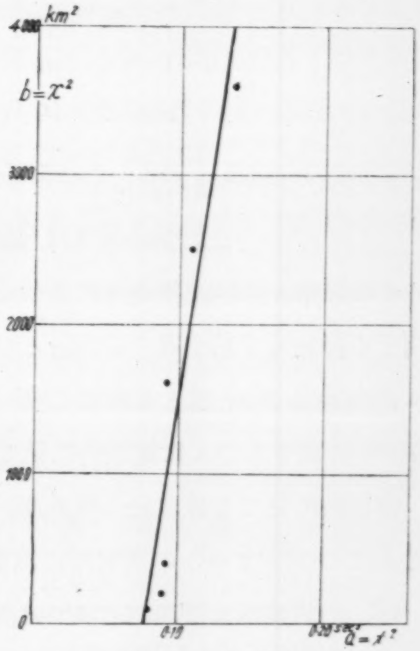

第　14　圖
白河 I の測線に於ける第二反射波に對する a, b 曲線

sR_2 は附近の地形から推定すると石英粗面岩よりなる基盤らしく思はれるがその確證を擧げるには今少し廣範圍に亘つて調査して見なければならない．

縱波及び横波の傳播速度——地表に近く傳播する所謂直接波の速度は第 15 及び 16 圖に示してある走時曲線より求めることを得．而して横波の速度は平均 160 m/sec で sR_1 及び sR_2 なる反射横波の傳播速度と大略一致し sR_1, sR_2 が横波の反射波であるといふ推定も強ち無理ではない．

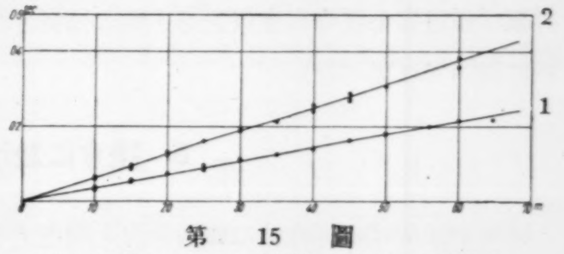

第　15　圖
白河に於ける I の測定線に對する走時曲線
曲線：1 縱波 $V_l = 282$ m/sec；2 横波 $V_t = 160$ m/sec.

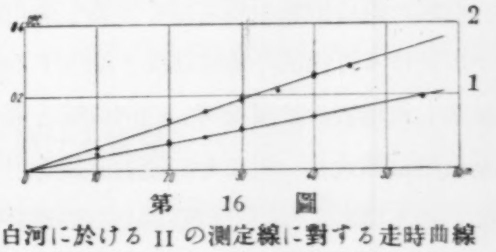

第　16　圖
白河に於ける II の測定線に對する走時曲線
曲線：1 縱波 $V_l = 279$ m/sec；2 横波 $V_t = 160$ m/sec.

(d)　**反射面の吟味**　白河に於ては前述の如く彈性波探査法と同時に電氣探査法が行はれた．その測定場所は圖中 II 線の附近である．

その結果によれば地下構造は次の通りである．

深　さ	推定地質
0～1 乃至 2 m	泥土混り砂利
1（或は 2）～10 乃至 15 m	濕潤せる砂利
10 乃至15～35 乃至 42 m	粘土混り砂利
42 m 以上	粘土
岩盤の深さは 60 m 以上	

この結果と彈性波探査法によつて得た結果とを綜合して地下の地質を推定するに濕潤せる砂利及び粘土混り砂利層との境界面は 15 m 內外（I の場所は II の場所より數 m 高いから 20 m 位とも推定し得）の深さにあり電氣抵抗も 55,000 Ω-cm より 16,000 Ω-cm に底下しこゝに電氣的に見て不連續面が存在してゐる．

彈性的に見ても或は此の境界面が不連續面であるらしく，若しこの推定が許されるならばこの面は sR_1 の反射面に該當するのである．

sR_2 の岩盤面は電氣的方法では測定範圍が局限されてゐたため深さに對して十分なる水平測定距離に達し得なかつたために確實に求めることが出來なかつたが 42 m より深い所では益々電氣抵抗を減じ 3,000 Ω-cm 以下になるらしく，或は岩盤に近づいたため含水量を增し抵抗を減ずるのではないかと思はれる．

以上の如く彈性波探査法と電氣探査法とで行つた實驗が略一致した結果に到着したことは興味あることと思ふ．又 I の測定線附近に直徑約 1 m の鑿井を行つた結果地下 51 m で岩盤に達し彈性波による推定が正しい事が證明された．尙ほ此の實驗結果の詳細は鐵道省土質委員會報告第 5 輯に揭載される筈であるからこゝではこれ以上の事柄に就いては述べない．

5. 鎌倉に於ける實驗

砂層中に於ける彈性波の傳播狀況を調査する目的を以て昭和 11 年 8 月中旬鎌倉町由比ケ濱地震觀測所庭內に於て實驗を行つた．觀測所は海岸より約 600 m の所に在り，附近一帶は砂層が相當厚く發達し所謂基盤までの深さは可なり深いと考へられ砂層中に於ける彈性波の傳播速度を測定するに好都合の場所であつた．

使用した地震計は濱松町，白河の時と異り水平動微動計であり，地動を或る程度まで器械的に擴大し，更にその運動を鏡を附した尖軸の回轉に變へ，其れを光學的に記錄せしめる事により，三萬倍以上の倍率を得るものであつた．

從つて重錘落下裝置として前記 2 箇所の實驗に於ける如き特別の裝置を必要とする事なく，表面層中に於ける速度を測定するに充分なる距離，5～60 m 以內の實驗に於ては重錘を手に持つて之を投下する位で測定に十分なる Energy を有する彈性波を發

生し得たのである．鎌倉の場合は記錄裝置の Daylight exposure が不可能であつた爲微動計を觀測所内の暗室に据ゑ，其の前方 5 m 置きに一直線上に重錘落下點を配置して實驗を行つた．記錄用圓筒に同期電動機を使用する事を廢し，別に Time の測定が 1/100 秒程度の精度を以て測定し得る如き裝置を用ひた．斯くして得られた記象が第 17 圖である．之より P 波及 S 波の走時を讀み取り走時曲線を書けば第 18 圖の如くになる．實驗記象に見られる如く平常可なりの振幅の微動が存在する故に P 波の初動を大きくする事が必要であつたためなるべく大なる衝擊を與へた．そのため 5 m, 10 m 等の近距離に於ては S 波は優勢なる P 波に隱されて其の始まりを知る事は出來なかつた．P 波の始まりについても近距離のものは平均の直線より多少偏倚し，何れも平均の速度よりも大なる速度を與へて居るが，之は微動計をコンクリート造りの暗室内に置いた爲彈性波が約 2 m 程のコンクリート中を砂層中よりも大なる速度で通過した影響が近距離の觀測結果に特に著るしかつた爲と思惟される．此の始めの二つを除き最少自乘法により決定した縱波及橫波の速度は夫々次の如くである．縱波の速度＝275 m/sec，橫波の速度＝108 m/sec．

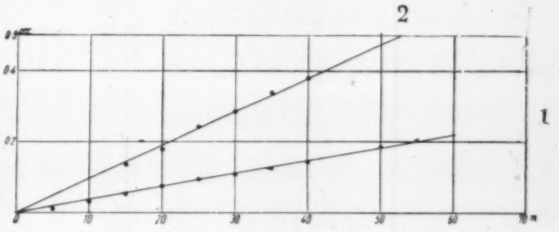

第　18　圖
鎌倉に於いて得たる走時曲線
曲線：1 砂層中の縱波 V_l=275 m/sec；
2 砂層中の橫波 V_t=108 m/sec.

然し波の速度は砂質及び砂の內部組織の如何により異なるを以て如何なる砂について以上の如き傳播速度を得たかを知る事が必要である．そこで由比ケ濱の砂を出來るだけ自然の狀態に於て採取し測定した結果は第 V 表の通りであつた．

1 m 以下は深さを增すにつれて含水量も多少增加すると思はれる．尙地下水面は地表面下大略 10 m 位の所に存在して居る．之等の砂についての成分分析及び化學分析を行ふ事も必要と思ふ．

第　V　表

比　重		1·38
空隙率		36·8 %
含水量	地　表	6·04%
	表面下 1 m	6·11%

6. 駒場に於ける實驗

所謂ローム層と呼ばれる層中に於ける彈性波の傳播狀況を調査する爲，鎌倉に於ける實驗終了後東京市駒場にある地震研究所駒場支所の裏手に於て實驗を行つた．

支所附近は表面を 1 m 程の黑色の土壤層が薄く覆つて居るが其の下は可なりの深さまで一樣にローム層が發達して居るのである．此所に於ける實驗には鎌倉の場合と

同一の微動計を使用し記錄裝置に Camera を用ひて Daylight exposure を可能ならしめた、彈性波發生の爲には簡單に重錘を手に持ちて投下する方法に依つたが 80 m の遠方に於ても十分明瞭なる記錄を取る事が出來た．重錘投下點は水平動微動計の重錘振動方向及之に直角なる二つの方向に沿ひ略一直線上に夫々 5 m，及び 10 m 毎に配置した．

斯くして得られた記象は第 19 圖，第 20 圖に示してある．之等の記象より縱波及び横波の始まりを讀取つて走時曲線を書けば第 21 圖及び第 22 圖の如くである．

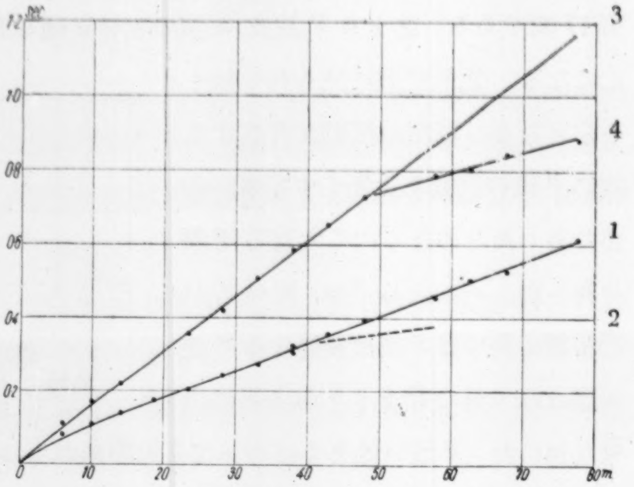

第　21　圖
駒場に於けるＩの測定線に對する走時曲線
曲線：1 ローム層中の縱波 $V_l=135$ m/sec；
3 ローム層中の横波 $V_t=69$ m/sec.

a）重錘の振動の方向に平行な測定線（I）に關して得たる走時曲線(第21圖)によれば 5 m 及 10 m 位の距離に於ては縱波，横波共に見懸けの速度が遲く現はれるのは表面に存在する黑色土壤の影響であると思はれる．

b）重錘の振動方向と直角の測定線（II）に就ては 15 m以下の近距離に重錘投下點を設置しなかつた爲正確な事は云ひ得ないが他の重錘投下點に於ける縱波及び横波の走時より推定すれば近距離に於ては I の場合と同樣の曲線になると考へられる．(第22圖參照)

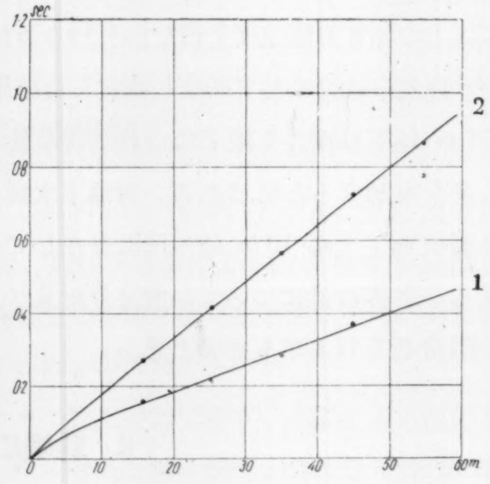

第　22　圖
駒場に於ける II の測定線に對する走時曲線
曲線：1 ローム層中の縱波 $V_l=115$ m/sec；
2 ローム層中の横波 $V_t=65$ m/sec.

駒場に於ては附近を通る電車其の他による微動の振幅が鎌倉の場合よりは遙かに大であるため記象の讀取りは多少困難であつた．例へば 50 m より遠方に於ては稍彈性に富む地下層を通過した屈折波の横波(第 21 圖中 4 の曲線參照)は明らかに現はれて居るに拘らず之に相當する屈折縱波は不斷の微動に妨げられその始りを明瞭に讀取る事は困難である．それ故に走時曲線上に大體の位置を破線を以て示

してある．又 II の方向に於て重錘投下點の位置と振子の振動方向との關係より縱波の Energy が小であるため不斷の微動に妨害せられて 55 m の距離にて縱波の始めを定める事が困難で，それより近い距離に於ても讀取りの誤差は大きく，點は散在する傾向がある．

以上の讀取り値につき最少自乘法によりローム層中の速度を決定すれば（I），（II）の方向につき夫々次のやうになる．

（I）の方向に就き： 縱波の速度＝135 m/sec． 横波の速度 68·7 m/sec.

（II）の方向に就き： 縱波の速度＝155 m/sec， 横波の速度＝65·4 m/sec.

實驗を行つた場所の表土黑色及びロームを出來るだけ自然の狀態に於て採取し比重及含水量を測定した結果は次の如くである．

第 VI 表

地 質	比 重	含 水 量
黑色表土	1·0	47·8%
ロ ー ム	1·3	50·3%

以上 4 ケ所に於ける實驗の結果夫々の表面層に對し縱波及び横波の傳播速度を求める事が出來た．之等の波の中鎌倉の砂層を傳播する波と駒場のローム層を傳播する波との波長を記象より算出すれば次の値を得る．

第 VII 表

	鎌 倉		駒 場	
	週 期	波 長	週 期	波 長
縱 波	$\frac{3.5\sim4}{100}$ sec	9·5～10 m	$\frac{3\sim3.5}{100}$ sec	4～4·5 m
横 波	$\frac{4.5\sim5}{100}$	4·7～5·3 m	$\frac{4.5\sim5}{100}$	3～3·5 m

即砂層中に於て 縱波は波長約 10 m，ローム層に於ては縱横波共 5 m 以下の波長を有す．而して斯くの如き短週期の波に對しては土地は彈性體であると考へられるから計算によりこれ等の地層の有効彈性率及ポアソン比を求め得る．

7. ポアソン比 σ 及びヤング率 E の測定

今 V_l を縱波の速度，V_t を横波の速度，D を密度，σ 及び E を夫々 Poisson 比及び Young 率とすれば

$$V_l=\sqrt{\frac{E}{D}\frac{1-\sigma}{(1+\sigma)(1-2\sigma)}}, \qquad V_t=\sqrt{\frac{E}{D}\frac{1}{2(1+\sigma)}}.$$

である．從つてポアソン比 σ は

$$\sigma=\frac{1}{2}\frac{V_l^2-2V_t^2}{V_l^2-V_t^2}$$

である．斯くして得られた σ を上の式に代入すれば E を求める事が出來る．E 及び σ を求めた結果は次の表に示してある．

第 VIII 表　ポアソン比及ヤング率

場所		V_l (m/sec)	V_t (m/sec)	D	σ	E (C. G. S. $\times 10^8$)	地質
濱松町(最上層)	I	116	56	1·5	0·35	1·3	
	II	116	53	1·5	0·37	1·2	
	III	118	55	1·5	0·37	1·2	表土
	IV	115	56	1·5	0·35	1·3	(盛土 埋土)
	平均	116·3	55	1·5	0·36	1·2	
濱松町(中間層)	I	367	85	2	0·47	4·2	
	II	361	81	2	0·47	3·8	
	III	362	76	2	0·47	3·4	粘土
	IV	365	80	2	0·48	3·8	
	平均	364	81	2	0·47	3·8	
白河	I	282	160	2	0·26	1·3	砂礫
	II	279	160	2	0·26	1·3	
鎌倉		275	108	1·38	0·41	4·5	砂
駒場	I	135	69	1·3	0·33	1 6	ローム
	II	155	65	1·3	0·39	1·6	
		30～70			0·46～0·49	4·8～5·2 $\times 10^9$	(彈性ゴム)
		10·96	2·61		0·47	2·0 $\times 10^5$	(寒天)

之によるとヤング率は全て 10^8 の Order である．彈性ゴムの E に較べれば Order が 1 だけ小さく，坪井博士の測定せられた寒天の E に較べれば遙かに大きい値である．E を算出する時に採用した密度 D の値の中，濱松町及白河の値は地質標本を得る事が出來なかつた故に適當と思はれる値を假定し，鎌倉及駒場のものに於ては能ふ限り自然に近い狀態に於て採取した標本から測定した値である．

8. 測定の精度

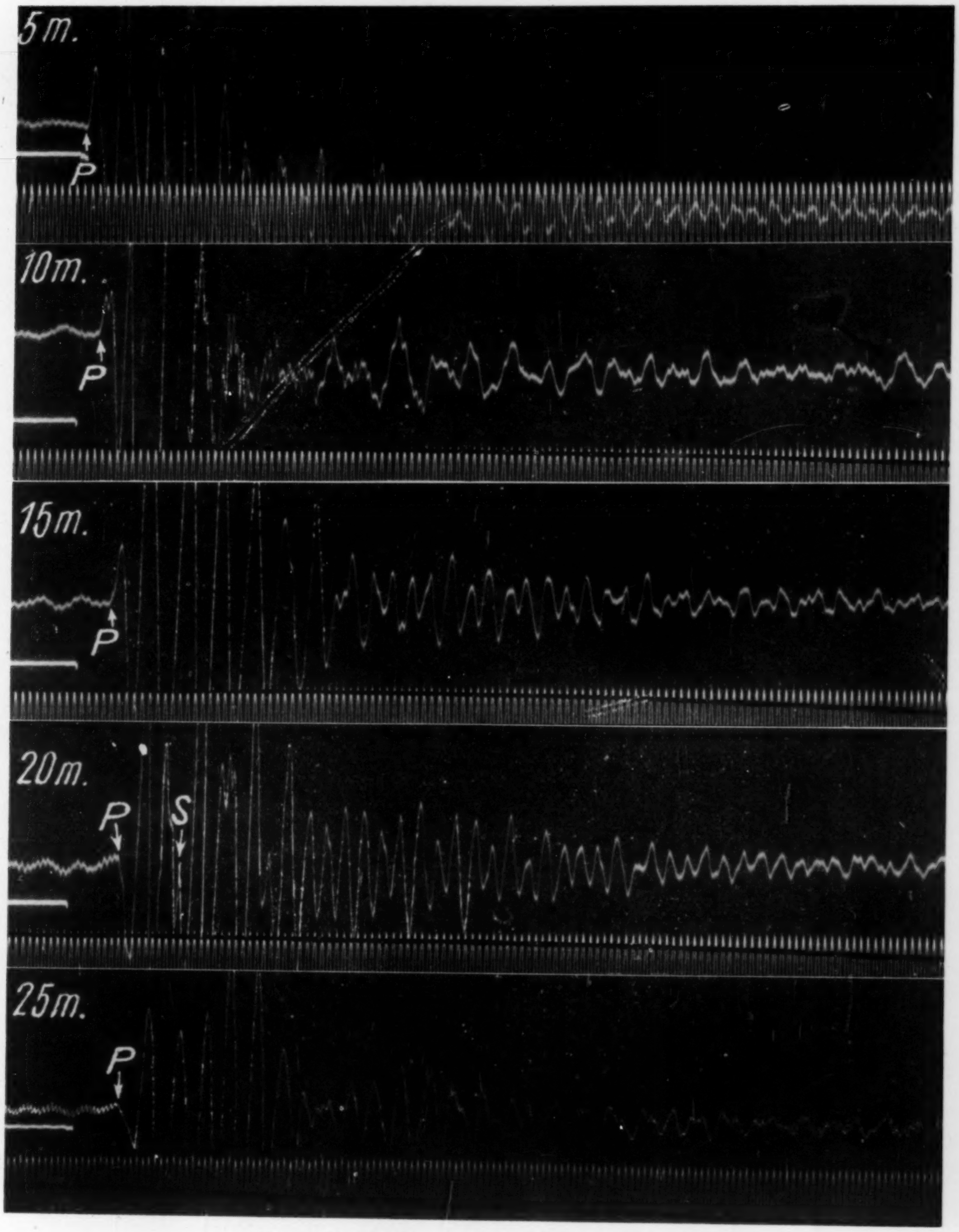

第17圖（其1） 鎌倉に於ける記象

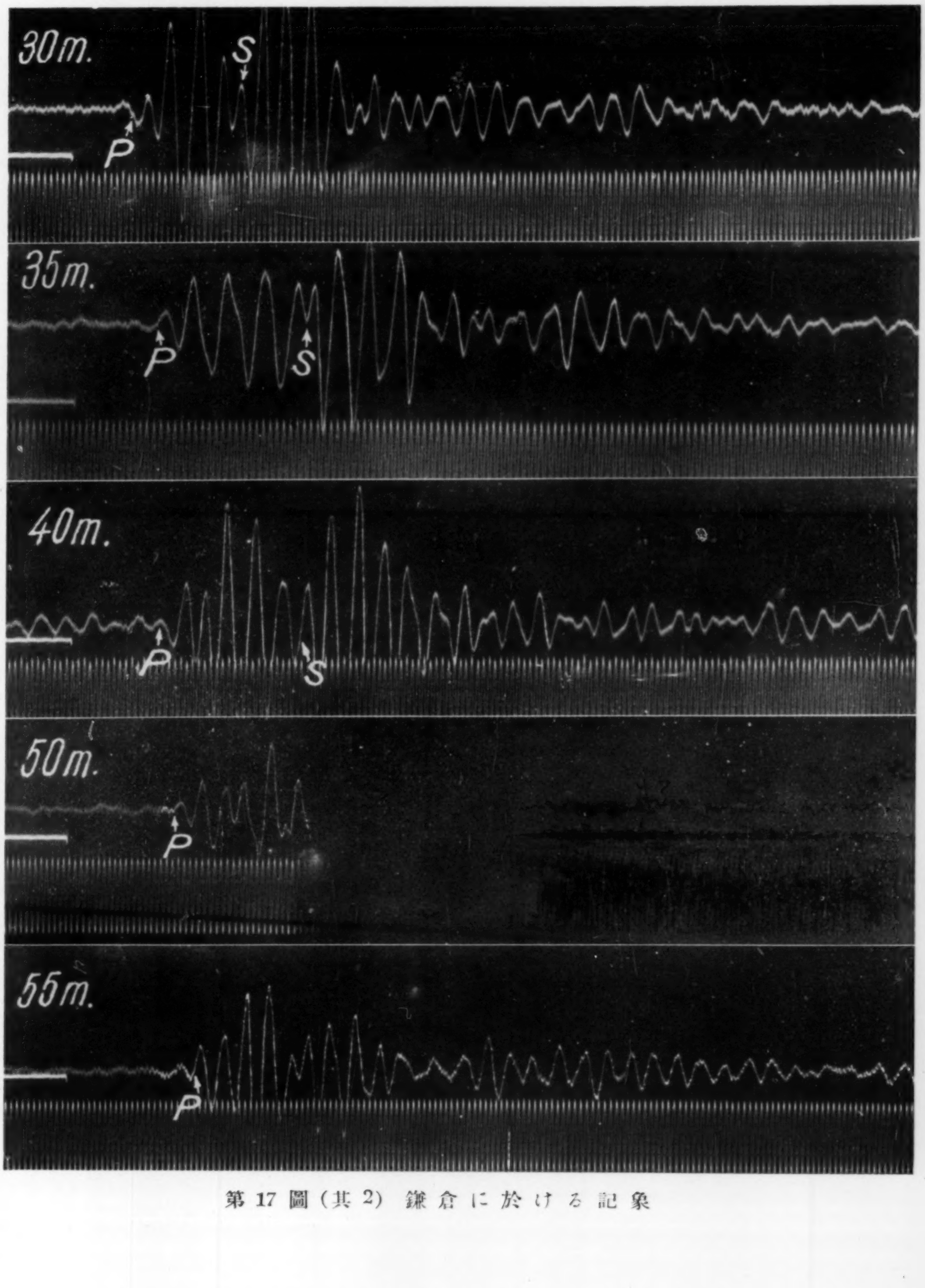

第17圖（其2）鎌倉に於ける記象

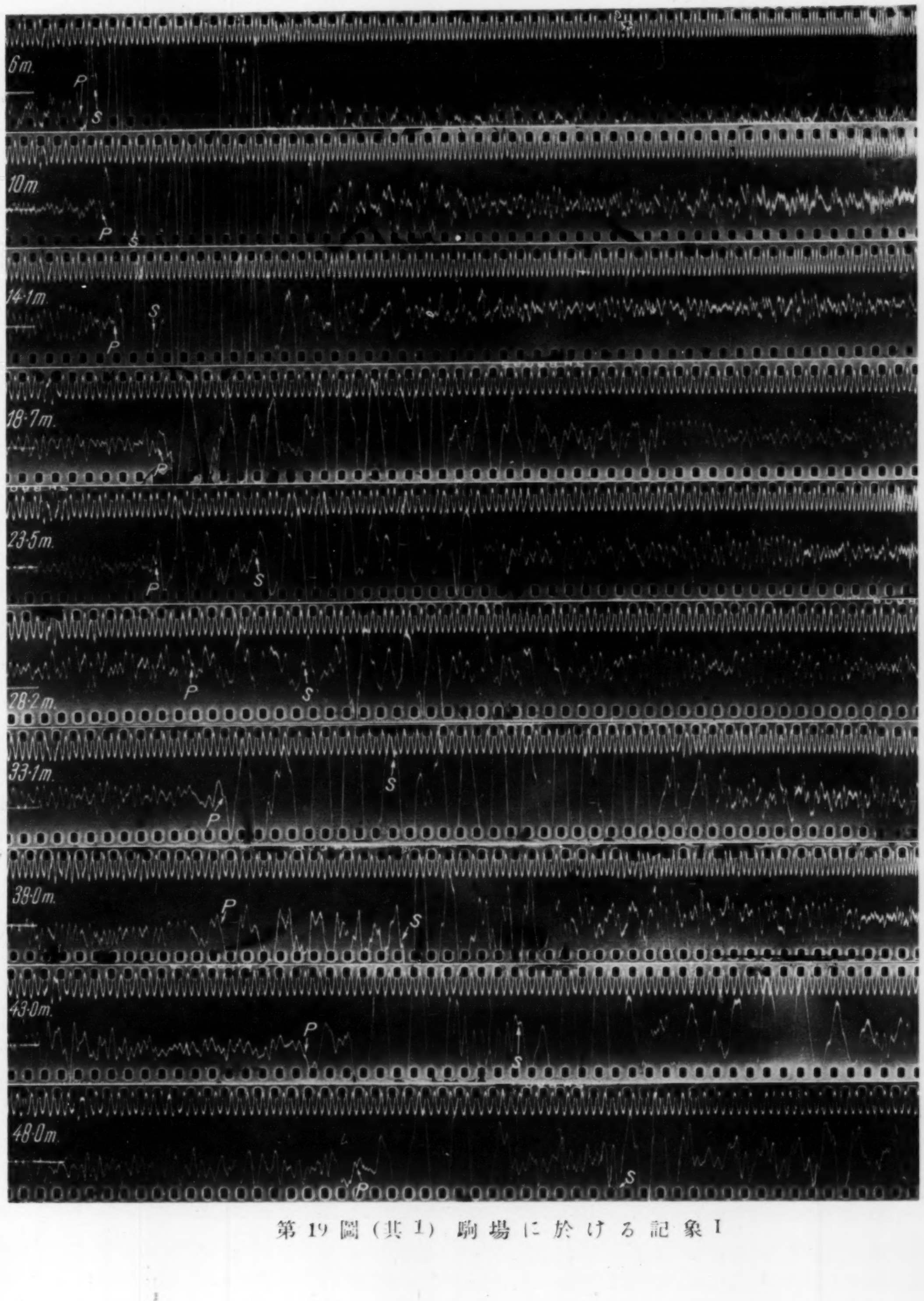

第19圖（其1）駒場に於ける記象 I

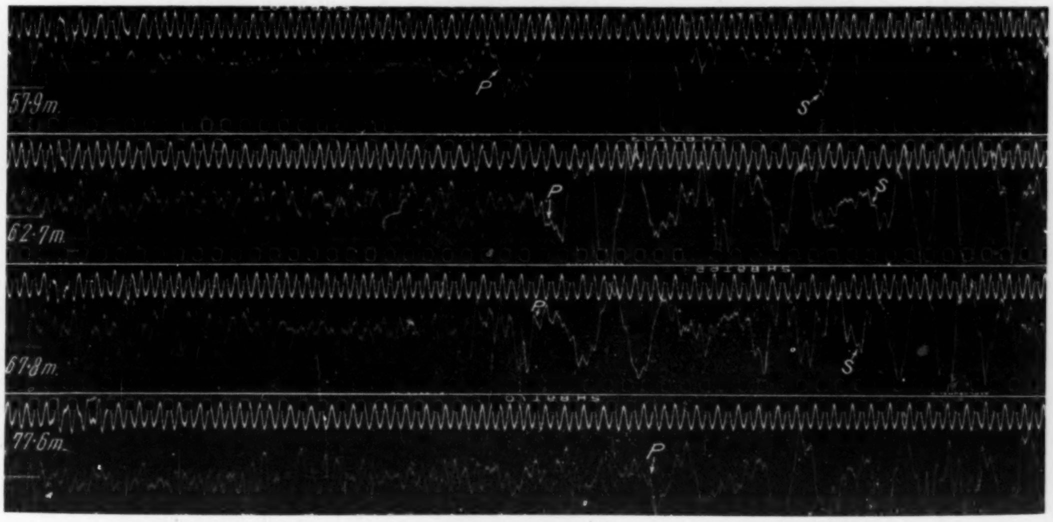

第19圖（其2） 駒場に於ける記象 I

（震研彙報 第十四號 圖版 那須・萩原・表）

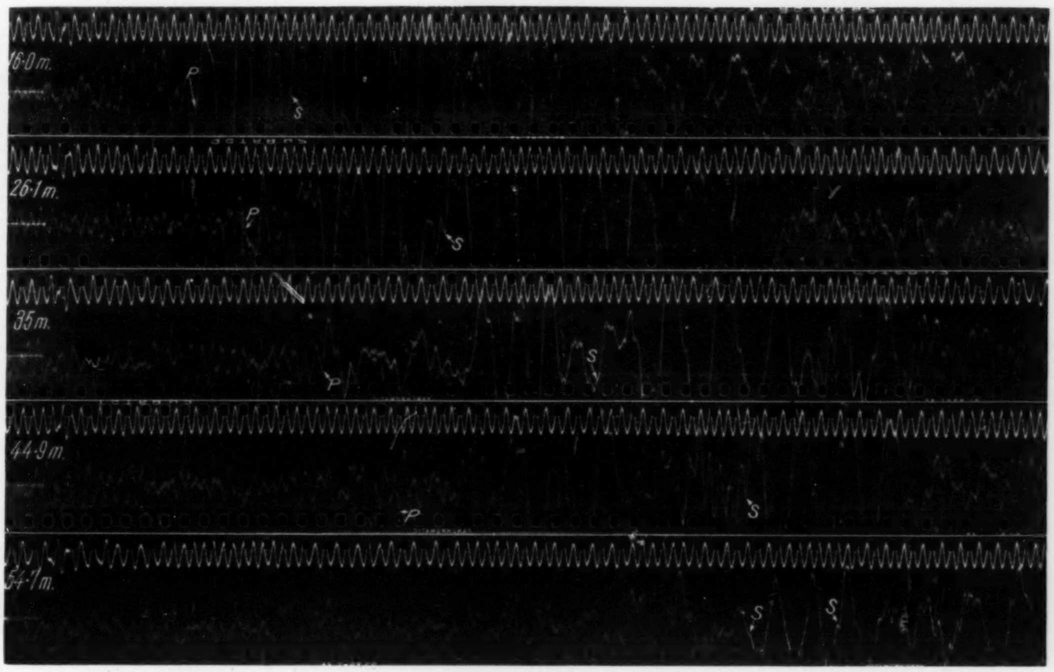

第20圖 駒場に於ける記象 II

鎌倉及び駒場に於て求められた速度に對し Most probable value を決めた際 Probable error も計算した．その値は次のやうである．

鎌倉		駒場 I	駒場 II
縦波	± 3·1 m/sec	± 2·8 m/sec	16 m/sec
横波	± 3·4 m/sec	± 3·0 m/sec	1·5 m/sec

51. *Studies on the Propagation of the Artificial Earthquake Waves through superficial Soil or sand Layers and the Elasticity of Soil and Sand.*

By Nobuji NASU, Takahiro HAGIWARA and Syn'itirô OMOTE,

Earthquake Research Institute.

Propagation of the artificial earthquake waves caused by falling heavy weights were investigated. The Measurements were made at four places, namely, Hamamatu-tyo in Tokyô, Sirakawa in Hukusima Prefecture, Kamakura, and Komaba in Tokyo.

At Hamamatu-tyô and Sirakawa four vertical-component seismographs of mechanical registration type were used. The aim of the measurements at these places consisted in prospecting the bed rocks, being the tertiary rocks at the former place and the liparite layer at the latter place. The bed rocks were determined from the travelling time of the transverse waves which underwent reflection on the surface of the bed rocks.

At Hamamatu-tyo, the depth of the bed rock was 25·1 m from the ground surface and at Sirakawa it was 51 m. At the latter place another reflection-surface was found at a depth of about 24 m from the ground surface, being probably the upper surface of the sandy clay.

At Kamakura and Komaba high magnification seismographs were employed and the velocities of the elastic waves in the sand and loam layers were determined with results as shown in Table VIII.

The Poisson's ratio σ, and the Young's modulus E, were determined and taburated in the Table VIII.

52. *Notes on the Origins of Earthquakes.*

By Win INOUYE,

Earthquake Research Institute.

(Read July 7, 1936.—Received Sept. 21, 1936.)

1. *Introduction*

It is well known that a study of the initial motions of earthquakes is of utmost importance in understanding the mechanism of the earthquake waves from the seismic origin.

Nowadays, the initial motions of the *S* waves are also invoked in obtaining knowledge regarding seismic origins, notwithstanding the difficulty of determining the phases on the seismograms. It may moreover, prove advantageous in connection with this problem to study the surface waves at the times of shallow earthquakes as also the *ScS* waves, which are the reflected waves at the margin of the central core of the globe in the case of deep-focus earthquakes.

The pull and push waves in the *P* phase were known since the time of the late Prof. F. Omori,[1] but it was the late Prof. T. Shida who first showed some excellent examples of the geographical distribution of the pull and the push waves and discussed the mechanisms of seismic origins.

In accordance with the results of later studies of shallow earthquakes, the pull and push waves were grouped separately into four quadrants divided by two lines (nodal) intersected perpendicularly at the epicenters. To explain these phenomena, the late Prof. T. Shida offered formations of fissures at the seismic origins. Against this idea, Prof. S. T. Nakamura[2] proposed the fault theory on the ground that frequently one of the nodal lines fairly coincided with faults observed in the epicentral regions. Very interesting distributions of the initial motions were found by Mr. K. Tanahasi[3] at the time of the deep-focus earthquake of June 2, 1931, in the central part of the main island of Japan.

In this case, the boundaries between the pull and the push waves were well expressed by a pair of parabolas. Later studies of Mr. K.

1) F. OMORI, *Bull. Earthq. Invest. Commit.*, **1** (1907), 145~154.

2) S. T. NAKAMURA, *Kishô-Shûsi*, **37** (1918), 390~401; **38** (1919), 395~404; [ii], **1** (1923), 1~13.

3) K. TANAHASI, *Umi to Sora*, **11** (1931), 277~288.

Sagisaka[4] and Mr. M. Takehana[5], showed that even in the case of deep-focus earthquakes there are conical types as well as quadrant types among the lines dividing the regions where pull waves or push waves were observed.

Prof. M. Ishimoto[6] after carefully examining cases in which conical types were observed, found that the push waves were always on the conical surfaces with their vertices at the hypocentre. He also expressed the distribution of the pull and the push waves projected on the spherical surface with its centre at the seismic origin by the simple zonal harmonic functions, $P_0(\cos\theta)$ and $P_2(\cos\theta)$, and further pointed out, in the case of shallow earthquakes, instances in which the nodal lines of the initial motions assumed peculiar forms. He explained these cases by refraction of the P waves at the boundary between the Mohorovicic layer and the substratum; and that otherwise the nodal lines might assume simple conical forms.

Mr. T. Minakami,[7] in his paper on the origins of shallow earthquakes, satisfactorily explained the geographical distribution of initial motions in a number of earthquakes, assuming that the pull waves were concentrated in cones with their vertices at the seismic origins and that the solid angles of these cones were all $\pi/2$. Mr. K. Fukutomi[8], after a study of the earthquakes that occurred in the Kwanto district, obtained the interesting result in the case of shallow earthquakes, the directions of the axes of the nodal cones of the initial motions were horizontal, while in the case of rather deep earthquakes their directions were indefinite.

Valuable investigations were next made by the able seismologists Dr. H. Kawasumi[9] and Dr. K. Honda[10] regarding the sense and magnitude of the P phases and the S phases of some deep earthquakes. Dr. K. Honda explained the observed P and S phases of some deep-focus earthquakes, assuming that the normal stress on the spherical surface with its centre at the origin might be expressed by a simple spherical harmonic function ($P_2^1(\cos\theta)$), taking into consideration the effects of the reflection of the waves at the earth's surface and the effects due

4) K. Sagisaka, *Geophys. Mag.*, **3** (1930), 165~176.

5) M. Takehana, *Kensin-Jihô*, **7** (1933).

6) M. Ishimoto, *Bull. Earthq. Res Inst.*, **10** (1932), 449~471; *Proc. Imp. Acad., Japan*, **8** (1932), 36.

7) T. Minakami, *Bull. Earthq. Res. Inst.*, **13** (1935), 114~129.

8) T. Fukutomi, *Bull. Earthq. Res. Inst.*, **11** (1933), 510~529.

9) H. Kawasumi, *Bull. Earthq. Res. Inst*, **11** (1933), 403~453; **12** (1934), 660~705.

10) H. Honda, *Geophys. Mag.*, **8** (1934), 153~164; **8** (1935), 327~332.

to the refraction of the waves in the earth's crust. In these investigations the observed fact that the periods of the P phases differ from those of the S phases were not taken into considerations. We may, with Mr. T. Ishikawa,[11] conclude that the wave lengths of the P waves and S waves are almost equal. But we do not yet know the mechanism by which such waves are radiated from the seismic origin.

2. We are now thinking of the distribution of the initial motions as we know them to be on the earth's surface as distributions on a spherical surface with the seismic origin as its centre.

As Prof. T. Matuzawa has already pointed out, it is possible to imagine various kinds of mechanisms for the origin of an earthquake corresponding to any one type of distribution of initial motions. We shall take for example the case in which the conical type of distribution of the initial motions is observed.

a) We can explain these observed distributions of initial motions by assuming that the internal pressure on the spherical surface with its centre at the hypocentre is expressed by $P_0(\cos\theta)$ and $P_2(\cos\theta)$. Changing the ratio in the combination of the quadruple source P_2 and the single source P_0, we can obtain an arbitrary solid angle of the cone.

b) We shall suppose that a combination of a pair of doublet forces acting along one axis and a single source. Changing the proportion of the doublet to the sink, or the negative single source, we can obtain an arbitrary solid angle of the cone.

c) Let us suppose that three pairs of these doublets are co-acting at the seismic origin, and that one of the two pairs of the doublets in the same phase lies on top of the other, each of which is acting along the axis perpendicular to each other, and that the last pair of the doublets in the opposite phase, perpendicularly to the plane, on which are the above two pairs of doublets, also lie, one pair on top of the other. If we take the intensities of the last pair of doublets to be different from those of the other two pairs, we can obtain an arbitrary solid angle of the cone.

Now what we can deduce from the observations of seismic waves is limited to variations in the stresses on a certain closed surface taken at the seismic origin. As to what occurs in that closed surface we can only imagine. For example, the stress distribution on a certain closed surface may assume more or less complicated features as the result of the co-action of a number of single sources, positive or nega-

11) T. ISHIKAWA, *Kishô-Shûsi*, [ii], **10** (1932), 260.

tive, within that surface, owing to the interference of waves from each source and the reflections of waves from that closed surface.

3. Let us suppose a sphere at the seismic origin and consider the effect of variation in internal pressure within it.

Actually, it is natural to assume that the shape of the magma pocket may be more or less flat, rather than a sphere, but for simplicity we here assume that the cavity that is filled with magma is spherical. Should the vapour pressure within that spherical cavity increase, yielding of the surrounding medium will follow, and should the pressure exceed the limit of the breaking strength at some point on the spherical surface, the magma will break out through that weakened part. The seismic waves that are generated then might be assumed to correspond to those that are generated through the action of a pair of doublets acting along an axis. The normal stresses on the spherical surface in that case may be expressed by $P_2(\cos\theta)+\frac{1}{2}P_0(\cos\theta)$ or $\cos^2\theta$.

The pressure diminution and the reduction in volume of the magma within the cavity accompanied by the eruption of magma may act as a negative single source. The total volume of the magma might remain constant during its eruption as is generally the case when plastic material change their shape. To satisfy the condition that the volume of the magma shall be constant during its deformation (outflow) we have to assume a sink $(-\frac{1}{2}P_0)$ co-acting with a pair of the doublets. At all events, we may conclude that seismic waves that are generated in this case correspond to that case in which the normal stresses may be expressed by $P_2(\cos\theta)$.

Since the normal component displacement that results from the internal pressure $P_2(\cos\theta)$ on the spherical surface, the radius of which is a, are expressed by

$$u_1+u_2=-P_2(\cos\theta)e^{ipt}\left[\frac{A}{h^2}\frac{d}{dr}\frac{H_{\frac{5}{2}}^{(2)}(hr)}{\sqrt{r}}+12\frac{B}{k^2}\frac{1}{r^{3/2}}H_{\frac{5}{2}}^{(2)}(kr)\right]_{r=a},$$

where u_1 and u_2 corresponds to the dilatational and distortional waves respectively, the azimuthal distributions are also expressed by $P_2(\cos\theta)$.

We shall next consider the proportion of the amounts of the positive displacements to those of negative displacements.

Since $$P_2(\cos\theta)=\frac{1}{2}(3\cos^2\theta-1)$$

and
$$\int_0^{\frac{\pi}{2}} P_2(\cos\theta)2\pi a^2 \sin\theta\, d\theta = 0,$$

the positive and the negative parts cancel each other, so that the volume remains constant during deformation.

As it is assumed that the pressure distributions are $P_2(\cos\theta)$, the sum of the positive and negative parts in the pressure change is zero.

The fact that the distribution of the initial motions of many earthquakes are fairly well expressed by $P_2(\cos\theta)$ may partly be due to cause just mentioned. Even in the case just considered, the proportion of the single source to the quadruple source may be influenced by a number of causes, and there will be a case in which the distributions of the initial motions may be expressed by $P_2(\cos\theta)-\frac{1}{4}P_0(\cos\theta)$ and in which the solid angle of the cone is $\frac{\pi}{2}$. And since, at any rate, the single source $P_0(\cos\theta)$ is the simplest, and may be assumed to be the one that is most likely to occur, it is plausible to assume that the single source may generally be found accompanied by complex sources, such as $P_2(\cos\theta)$ or $P_2^1(\cos\theta)$.

4. We shall next consider the case in which the normal stresses at the spherical surface are distributed in a simple manner and can be expressed by a zonal harmonic series. Bearing in mind the principle of the "conservation of momentum", the normal stresses may be expressed by harmonics of even order, namely,

$$\text{normal stress} = a_0P_0(\cos\theta) + a_2P_2(\cos\theta) + a_4P_4(\cos\theta) + \cdots.$$

We shall here study the case in which the normal stress can be expressed by the first two terms. The general solution has been already obtained by Prof. K. Sezawa.[12]

Displacements due to dilatational waves in an isotropic elastic solid body are expressed by

$$u_{1,n} = -\frac{A_n}{h^2}P_n(\cos\theta)\frac{d}{dr}\frac{H^{(2)}_{n+\frac{1}{2}}(hr)}{\sqrt{r}}e^{ipt},$$

$$v_{1,n} = -\frac{A_n}{h^2}\frac{dP_n(\cos\theta)}{d\theta}\frac{1}{r^{3/2}}H^{(2)}_{n+\frac{1}{2}}(hr)e^{ipt}.$$

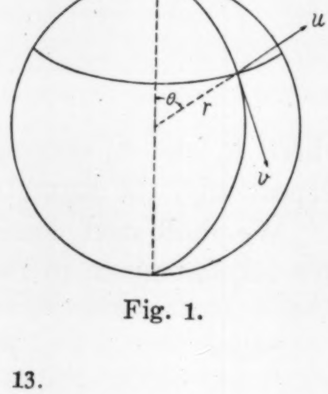

Fig. 1.

Displacements due to distortional waves are expressed by

12) K. SEZAWA, *Bull. Earthq. Res. Inst.*, **2** (1927), 13.

$$u_{2,n} = -2B_n \frac{n(n+1)}{k^2} P_n(\cos\theta) \frac{1}{r^{3/2}} H^{(2)}_{n+\frac{1}{2}}(kr) e^{ipt},$$

$$v_{2,n} = -\frac{2B_n}{k^2} \frac{dP_n(\cos\theta)}{d\theta} \frac{1}{r} \frac{d}{dr} \sqrt{r}\, H^{(2)}_{n+\frac{1}{2}}(kr) e^{ipt},$$

where $h^2 = \dfrac{\rho p^2}{\lambda+2\mu}$, $k^2 = \dfrac{\rho p^2}{\mu}$,

$\dfrac{2\pi}{p}$ = period of oscillations,

u, v = radial and transverse component of displacement respectively,

ρ = density of isotropic solid,

λ, μ = Lame's elastic constants.

The surface $r=a$ being assumed to be free from tangential traction and to be under normal pressure $p_n P_n(\cos\theta) e^{ipt}$, the equations

$$\widehat{rr} = \lambda\Delta + 2\mu \frac{\partial u}{\partial r} = p_n P_n(\cos\theta) e^{ipt},$$

$$\frac{\widehat{r\theta}}{\mu} = \frac{\partial v}{\partial r} - \frac{v}{r} + \frac{1}{r}\frac{\partial u}{\partial \theta} = 0,$$

in which Δ is the dilatation, $u = u_{1,n} + u_{2,n}$ and $v = v_{1,n} + v_{2,n}$ must hold on that surface.

Satisfying the above boundary conditions, we have

$$\frac{B_n}{A_n} = \frac{-\dfrac{k_2}{h^2}\left[\dfrac{d}{dr}\dfrac{H_{n+\frac{1}{2}}(hr)}{r^{3/2}}\right]_{r=a}}{\left[\dfrac{1}{\sqrt{r}}\dfrac{d^2}{dr^2} H_{n+\frac{1}{2}}(kr) - \dfrac{1}{r^{3/2}}\dfrac{d}{dr} H_{n+\frac{1}{2}}(kr) + \dfrac{1}{r^{5/2}}\left(n(n+1) - \dfrac{4}{5}\right) H_{n+\frac{1}{2}}(kr)\right]_{r=a}} \equiv R,$$

$$A_n\left[\lambda \frac{H^{(2)}_{n+\frac{1}{2}}(hr)}{\sqrt{r}} - \frac{2\mu}{h^2}\frac{d^2}{dr^2}\frac{H^{(2)}_{n+\frac{1}{2}}(hr)}{\sqrt{r}} - 4\mu R \frac{n(n+1)}{k^2}\frac{d}{dr}\frac{1}{r^{3/2}} \cdot H^{(2)}_{n+\frac{1}{2}}(kr)\right]_{r=a} = p_n.$$

Henceforth, we shall consider only the case $\lambda=\mu$, or the Poisson

ratio $\sigma=\frac{1}{4}$.

(1) The single source, in which the normal pressure at the origin is expressed by $P_0(\cos\theta)e^{ipt}$.

In this case we have

$$A_0=\frac{p_0}{\mu a^{-\frac{1}{2}}}\Big/\Big[(3h^2a^2-4)\,H^{(2)}_{\frac{1}{2}}(ha)+4haH^{(2)}_{-\frac{1}{2}}(ha)\Big]\equiv a_0+ib_0\,.$$

The radial component of the displacement of the dilataional wave is given by

$$u_{1,0}=-\frac{a_0+ib_0}{h^2}P_0(\cos\theta)\frac{d}{dr}\frac{H^{(2)}_{\frac{1}{2}}(hr)}{\sqrt{r}}e^{ipt}$$

$$=-\sqrt{\frac{2}{\pi}}\frac{1}{h^{3/2}}\frac{1}{r}P_0(\cos\theta)\left\{\left(a_0+\frac{b_0}{hr}\right)\cos(pt-hr)\right.$$

$$\left.+\left(\frac{a_0}{hr}-b_0\right)\sin(pt-hr)\right\},$$

and at a distant point from the origin as compared with the wave length, we have

$$hr=2\pi\frac{r}{L}\gg 1\ \text{(where } L \text{ is the wave length)},$$

$$u_{1,0}=-\sqrt{\frac{2}{\pi}}\frac{1}{h^{3/2}}\frac{1}{r}P_0(\cos\theta)\left\{a_0\cos(pt-hr)-b_0\sin(pt-hr)\right\}$$

$$=-\sqrt{\frac{2}{\pi}}\frac{1}{h^{3/2}}\frac{1}{r}P_0(\cos\theta)\sqrt{a_0^2+b_0^2}\cos\left(pt-hr+\tan^{-1}\frac{b_0}{a_0}\right).$$

The constants a_0 and b_0 are given by the equations

$$a_0=\frac{p^0}{\mu a^{-\frac{1}{2}}}\frac{a}{a^2+b^2},\quad b_0=\frac{p_0}{\mu a^{-\frac{1}{2}}}\frac{-b}{a^2+b^2},$$

where

$$a=(3h^2a^2-4)J_{\frac{1}{2}}(ha)+4haJ_{-\frac{1}{2}}(ha),$$

$$b=(3h^2a^2-4)J_{-\frac{1}{2}}(ha)-4haJ_{\frac{1}{2}}(ha),$$

and $ha=2\pi\frac{a}{L}$ is the ratio of the radius of the seismic origin to the

wave length of the seimic waves generated from the origin.

The relations between the amplitude of $u_{1,0}$ at a distant point and ha are shown graphically in Fig. 2. As will be seen from the figure, the amplitude decreases as the wave length diminishes.

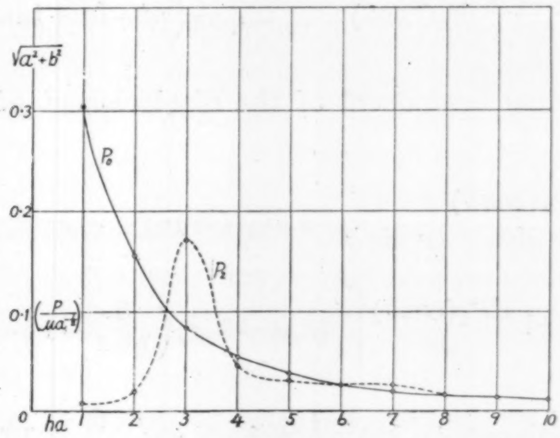

Fig. 2.

(2) The quadruple source in which the normal pressure at the origin is expressed by $P_2(\cos\theta)e^{ipt}$.

In this case we have

$$A_2 = \frac{p_2}{\mu a^{-\frac{1}{2}}} \Bigg/ \Bigg[(3h^2a^2-24)H^{(2)}_{\frac{5}{2}}(ha) + 4haH^{(2)}_{\frac{3}{2}}(ha)$$

$$-24\,U\Big\{-4H^{(2)}_{\frac{5}{2}}(ka) + ka\,H^{(2)}_{\frac{3}{2}}(ka)\Big\}\Bigg] \equiv a_2 + ib_2,$$

where

$$U = \frac{h^2}{k^2}R\,.$$

The radial component of the displacement of the dilatational wave is given by

$$u_{1,2} = -\frac{a_2+ib_2}{h^2}P_2(\cos\theta)\frac{d}{dr}\frac{H^{(2)}_{\frac{5}{2}}(hr)}{\sqrt{r}}e^{ipt}$$

$$= -\sqrt{\frac{2}{\pi}}\frac{1}{h^{3/2}}\frac{1}{r}P_2(\cos\theta)\Bigg[\Big\{a_2\Big(\frac{9}{h^2r^2}-1\Big) - \frac{b_2}{hr}\Big(-\frac{9}{h^2r^2}+4\Big)\Big\}\cos(pt-hr)$$

$$-\Big\{b_2\Big(\frac{9}{h^2r^2}-1\Big) + \frac{a_2}{hr}\Big(-\frac{9}{h^2r^2}+4\Big)\Big\}\sin(pt-hr)\Bigg],$$

and at a great focal distance as compared with the wave length, we

have

$$u_{1,2}=-\sqrt{\frac{2}{\pi}}\frac{1}{h^{3/2}}\frac{1}{r}P_2(\cos\theta)\left\{a_2\cos(pt-hr)-b_2\sin(pt-hr)\right\}$$

$$=-\sqrt{\frac{2}{\pi}}\frac{1}{h^{3/2}}\frac{1}{r}P_2(\cos\theta)\sqrt{a_2^2+b_2^2}\cos\left(pt-hr+\tan^{-1}\frac{b_2}{a_2}\right).$$

The colatitudinal component of the displacement of the dilatational wave is given by

$$v_{2,2}=-\frac{2A_2R}{k^2}\frac{dP_2(\cos\theta)}{d\theta}\frac{1}{r}\frac{d}{dr}\sqrt{r}\,H^{(2)}_{\frac{5}{2}}(kr)e^{ipt}$$

$$=-\frac{2}{h^2}\frac{1}{r}\sqrt{\frac{2}{\pi}}k^{\frac{1}{2}}\frac{dP_2(\cos\theta)}{d\theta}\left[\left\{(a_2\alpha-b_2\beta)\left(\frac{6}{k^2r^2}-1\right)-(a_2\beta+b_2\alpha)\right.\right.$$

$$\left.\cdot\left(-\frac{6}{k^3r^3}+\frac{3}{kr}\right)\right\}\cos(pt-kr)-\left\{(a_2\beta+b_2\alpha)\left(\frac{6}{k^2r^2}-1\right)\right.$$

$$\left.\left.+(a_2\alpha-b_2\beta)\left(-\frac{6}{k^3r^3}+\frac{3}{kr}\right)\right\}\sin(pt-kr)\right],$$

and at a great focal distance as compared with the wave length, we have

$$v_{2,2}=-\frac{2}{h^2}\frac{1}{r}\sqrt{\frac{2}{\pi}}k^{\frac{1}{2}}\frac{dP_2(\cos\theta)}{d\theta}\left\{(a_2\beta+b_2\alpha)\sin(pt-kr)\right.$$

$$\left.-(a_2\alpha-b_2\beta)\cos(pt-kr)\right\}$$

$$=-\frac{2}{h^2}\frac{1}{r}\sqrt{\frac{2}{\pi}}k^{\frac{1}{2}}\frac{dP_2(\cos\theta)}{d\theta}\sqrt{(a_2\beta+b_2\alpha)^2+(a^2\alpha-b_2\beta)^2}$$

$$\cdot\sin\left\{pt-kr-\tan^{-1}\frac{a_2\alpha-b_2\beta}{a_2\beta+b_2\alpha}\right\}.$$

Satisfying the boundary conditions at the seismic focus, the constants a_2, b_2, α and β are given by the following equations:

$$R=\frac{k^2}{h^2}U=\frac{k^2}{h^2}(\alpha+i\beta),$$

$$\alpha=-\frac{aa'+bb'}{a'^2+b'^2},\quad \beta=\frac{a'b+ab'}{a'^2+b'^2},$$

where

$$\begin{cases} a = -4J_{\frac{5}{2}}(ha) = haJ_{\frac{3}{2}}(ha) \\ b = J_{-\frac{5}{2}}(ha) + haJ_{-\frac{3}{2}}(ha) \\ a' = (16-k^2a^2)J_{\frac{5}{2}}(ka) - 2kaJ_{\frac{3}{2}}(ka) \\ b' = (16-k^2a^2)J_{-\frac{5}{2}}(ka) + 2kaJ_{-\frac{3}{2}}(ka), \end{cases}$$

and $$A_2 = a_2 + ib_2 = \left(\frac{p_2}{\mu a^{-\frac{1}{2}}}\frac{a''}{a''^2+b''^2}\right) + i\left(\frac{p_2}{\mu a^{-\frac{1}{2}}}\frac{b''}{a''^2+b''^2}\right),$$

where

$$a'' = (3h^2a^2-24)J_{\frac{5}{2}}(ha) + 4haJ_{\frac{3}{2}}(ha)$$
$$-24\alpha\{-4J_{\frac{5}{2}}(ka) + kaJ_{\frac{3}{2}}(ka)\} - 24\beta\{4J_{-\frac{3}{2}}(ka) + kaJ_{-\frac{3}{2}}(ka)\},$$
$$b'' = -(3h^2a^2-24)J_{-\frac{5}{2}}(ha) + 4haJ_{-\frac{3}{2}}(ha)$$
$$+24\beta\{-4J_{\frac{5}{2}}(ka) + kaJ_{\frac{3}{2}}(ka)\} - 24\alpha\{4J_{-\frac{5}{2}}(ka) + kaJ_{-\frac{3}{2}}(ka)\}.$$

The amplitudes of the radial component of the displacement of the dilatational wave are plotted against ha in Fig. 2. As will be seen from the figure, the curve has a maximum at $ha=3$, exhibiting a spectrum-like feature.

At a point distant from the origin as compared with the wave length, both dilatational and distortional waves have only the radial and the colatitudinal component of displacement, respectively.

In that case, the proportion of the displacement of the distortional to that of the dilatational wave is represented in Fig. 3, omitting the term relating to the azimuthal difference between the two waves.

It will be seen from the figure that, as the wave length diminishes compared with the size of the seismic origin, S waves appear less intensely than P waves.

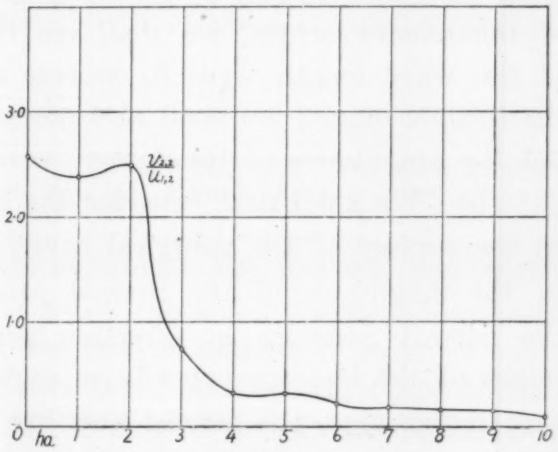

Fig. 3.

(3) The case in which the normal pressure is expressed by two zonal harmonics $P_0(\cos\theta)$ and $P_2(\cos\theta)$.

In this case, the radial component of the displacement at a distant point is given by

$$u_{1,0}+u_{1,2}=-\sqrt{\frac{2}{\pi}}\frac{1}{h^{3/2}}\frac{1}{r}\Big[\Big\{a_0P_0(\cos\theta)+a_2P_2(\cos\theta)\Big\}\cos(pt-hr)$$

$$-\Big\{b_0P_0(\cos\theta)+b_2P_2(\cos\theta)\Big\}\sin(pt-hr)\Big].$$

(a) We shall first take the case in which a pair of the doublets act along an axis. Here the normal pressure on the surface of the spherical cavity is given by

$$\Big\{-p'P_2(\cos\theta)-\frac{1}{2}p'P_0(\cos\theta)\Big\}e^{ipt}.$$

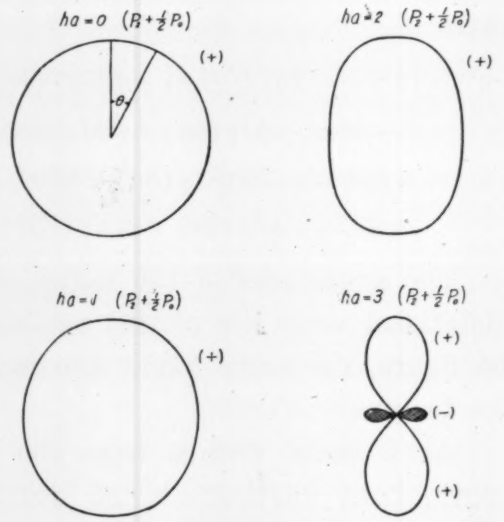

Fig. 4.

The change in the azimuthal distributions of the push and the pull waves as the value of ha varies is shown in Fig. 4. In the figure, the axis $\theta=0$ is taken upwards and the amount of the displacement is represented by the vector from the centre. The push and the pull waves are represented by $(+)$ and $(-)$ respectively. As will be seen from the figure, so long as the wave length is greater than the dimension of the seismic origin, we shall see the push waves in all directions. If the wave length were to become comparable with the diameter of the seismic origin, we shall also see pull waves as well as push waves, but the amplitudes of the former will be less than those of the latter.

(b) We shall next consider the case in which the normal pressure on the surface of the spherical cavity is expressed by $(\cos^2\theta-\frac{1}{2})$, that is, the magnitude of the normal pressure at the axis equals that of the normal pressure at direction perpendicular to the axis, but the senses of the two are opposite to each other.

In this case, the normal pressure can be expressed by

$$\Big\{-p'P_2(\cos\theta)+\frac{1}{4}p'P_0(\cos\theta)\Big\}e^{ipt}.$$

The azimuthal distributions of the push and the pull waves are shown in Fig. 5. As will be seen from the figure, so long as the wave length is greater than the dimension of the seismic origin, the displacements

due to the term $P_0(\cos\theta)$ will be far greater than those due to the

Table I.

hr	$\mu a^{-\frac{1}{2}}\alpha_0/p_0$		$\mu a^{-\frac{1}{2}}\alpha_2/p_2$	
	$ha=1$	$ha=2$	$ha=1$	$ha=2$
1	0·4312	——	0·0755	——
2	0·3409	0·1743	0·0122	0·0323
3	0·3212	0·1643	0·0080	0·0211
4	0·3142	0·1606	0·0077	0·0204
5	0·3110	0·1589	0·0097	0·0204
6			0·0078	
∞	0·3048	0·1559	0·0080	0·0211

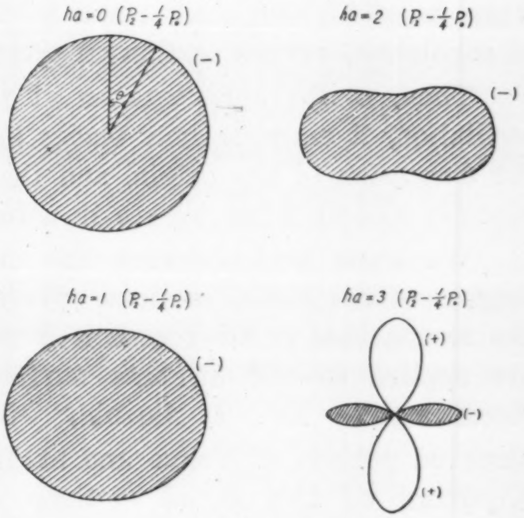

Fig. 5.

term $P_2(\cos\theta)$, so that we shall see pull waves regardless of the azimuth. Should the wave length become comparable with the dimension of the seismic origin we shall see push waves as well as pull waves.

The foregoing arguments are valid only for great focal distances. Nevertheless, as will be seen from Table I, the values

$$\alpha_0 = \sqrt{\left(\frac{a_0}{hr} - b_0\right)^2 + \left(a_0 + \frac{b_0}{hr}\right)^2}$$

in the case of P_0 and

$$\alpha_2 = \sqrt{\left\{a_2\left(\frac{9}{h^2r^2} - 1\right) - \frac{b_2}{hr}\left(-\frac{9}{h^2r^2} + 4\right)\right\}^2 + \left\{b\left(\frac{9}{h^2r^2} - 1\right) + \frac{a_2}{hr}\left(-\frac{9}{h^2r^2} + 4\right\}^2}$$

in the case of P_2 approach values at infinity the moment we recede a few wave lengths from the focus. The foregoing arguments also apply fairly well to neighbourhoods of the seismic origin.

Now, generally speaking, should there be the term $P_0(\cos\theta)$, however small, besides $P_2(\cos\theta)$, in the normal pressure, the displacements due to the single source will predominate so long as the wave length is greater than the dimension of the seismic origin, but when the wave length becomes comparable with the dimension of the origin, the displacements due to P_0 and P_2 become of the same order of magnitude (see Fig. 2), so that we shall find that the pull and the push waves are equal in magnitude.

We shall now consider the free oscillation of an isotropic elastic sphere. In the $P_0(\cos\theta)$ type oscillation, proper oscillation takes place when $ha=2{\cdot}57$, $6{\cdot}07, \ldots\ldots$ and in the $P_2(\cos\theta)$ type (spheroidal type) of oscillation, proper oscillation occurs when $ha=1{\cdot}52$.

Then, if the sphere taken at the seismic origin makes its proper oscillation, it emits seismic waves having wave lengths comparable with the dimension of the origin, and the distribution of the initial motions becomes almost what we see in actual earthquakes.

We shall next examine the orders of magnitude of the wave lengths of the initial motions. Here we exclude severe earthquakes, for the reason that in their case it is plausible to assume that the forces are applied to the earth's surface. According to Mr. T. Suzuki,[13] the observed periods at Tokyo and at Mt. Kiyosumi of the initial motions of sensible earthquakes that have occurred in the Kwanto district are mostly less than one second. The periods of the initial motions observed at Mt. Kiyosumi, situated at the south-eastern corner of the Kwanto district, are often 0·5 sec. (See Table II.)

Table II.

Period	Frequency
0·1 sec	0
0·2	0
0·3	4
0·4	8
0·5	6
0·6	5
0·7	1
0·8	4
0·9	2
1·0	1
1·1	1
1·2	1
1 3	1

If then we assume the diameter of a seismic origin to equal the wave length the magnitude of the dimension of the seismic origin works out to about 3 km, assuming that the velocity of the dilatational waves is about 6 km/sec. Further, according to studies made by Dr. N. Nasu on the observed data of the Ito earthquake swarms that occurred in 1930, the dimensions of these seismic origins might be less than 1 km. The periods of the waves were then about 0·15∼0·20 sec and the velocity of the dilatational waves was about 3·5 km/sec, whence the wave length was determined to be about 500∼700 m. By assuming that the dimension of the seismic origin and the wave length are of the same order of magnitude, what has just been said is consistent with the findings of Dr. N. Nasu.

Dr. H. Honda, in his paper already referred to, assumed that the dimension of a seismic origin was infinitesimal compared with the wave lengths of the seismic waves generated from that orgin. In the deep-

13) T. SUZUKI, *Bull. Earthq. Res. Inst.*, **10** (1932), 517; *Jisin*, **8** (1936), 72∼83.

focus earthquake of June 2, 1929, the observed directions of the initial motions of the S waves were fully in accord with his theory, but the observed magnitudes were only about a half of the calculated values. This discrepancy may be obviated by assuming that the dimensions of the seismic origin were moderate compared with the wave lengths.

At any rate, it is unnatural to assume that waves, the wave lengths of which are infinitely greater than its dimension, are radiated from a seismic origin.

5. We shall next consider the case in which a pair of the doublets act on two points separated from each other along an axis.

The radial component of displacement due to the doublet is given by

$$u_{1,1} = -\frac{A}{h^2} P_1(\cos\theta)\frac{d}{dr}\frac{H^{(2)}_{\frac{3}{2}}(hr)}{\sqrt{r}}e^{ipt}$$

$$= -\frac{1}{h^{3/2}}\frac{1}{r}\sqrt{\frac{2}{\pi}}P_1(\cos\theta)\left[\left\{\frac{2a_1}{hr} - b_1\left(1-\frac{2}{h^2r^2}\right)\right\}\cos(pt-hr)\right.$$

$$\left. - \left\{\frac{2b_1}{hr} + a_1\left(1-\frac{2}{h^2r^2}\right)\right\}\sin(pt-hr)\right],$$

and at a distant point, we have

$$u_{1,1} = -\frac{1}{h^{3/2}}\frac{1}{r}\sqrt{\frac{2}{\pi}}P_1(\cos\theta)\sqrt{a_1^2+b_1^2}\cos\left\{pt-hr+\tan^{-1}\frac{a_1}{-b_1}\right\}.$$

The constants a_1 and b_1 are determined by the boundary conditions on the spherical surface at the seismic origin.

For simplicity, we next put

$$A = -\sqrt{\frac{2}{\pi}}\frac{\sqrt{a_1^2+b_1^2}}{h^{3/2}}, \quad \varepsilon = \tan^{-1}\frac{a_1}{-b_1},$$

and we have

$$u_{1,1} = -\frac{A}{r}P_1(\cos\theta)\cos(pt-hr+\varepsilon)$$

$$= -\frac{A}{r}\cos\theta\cos(pt-hr+\varepsilon).$$

Assuming that the two doublets act on two points, s_1 and s_2, separated from each other by d along an axis, the radial component of displacement of the dilatational wave is given by

$$u_{1,1} = -\frac{A}{r}\cos\theta\cos(pt-hr+\varepsilon)$$

$$+\frac{A}{r}\cos\theta\cos(pt-hr+\varepsilon+\varphi)$$

$$= -2\frac{A}{r}\cos\theta\sin\frac{\varphi}{2}\sin\left(pt-hr+\varepsilon+\frac{\varphi}{2}\right).$$

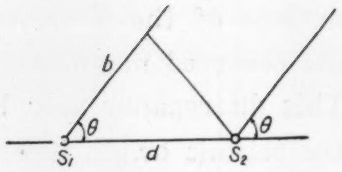

Fig. 6.

From the relation

$$\varphi = \frac{2\pi b}{L} = \frac{2\pi d}{L}\cos\theta \text{(in which } L = \text{wave length)},$$

we have

$$u_{1,1} = -2\frac{A}{r}\cos\theta\sin\left(\frac{\pi d}{L}\cos\theta\right)\sin\left(pt-hr+\varepsilon+\frac{\pi d}{L}\cos\theta\right).$$

The azimuthal distributions of the initial motions in cases in which the distances between the two points differ are shown in Fig. 7. As will be seen from the figure, so long as the distances between the two points are less than the wave lengths, we shall simply have push waves, regardless of the azimuths. Should the distance become comparable with the wave length, we shall have pull waves as well as push waves, and the features of the azimuthal distributions of these waves will become fairly complex.

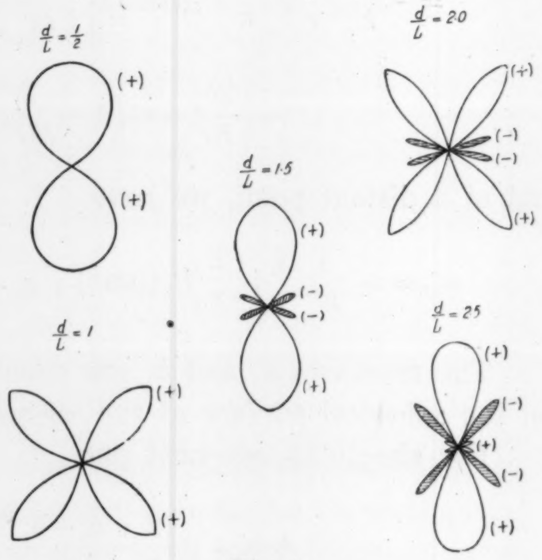

Fig. 7.

6. Model experiments on initial motions by artificial earthquakes were conducted by the writer[14] as a preliminary step to this study.

The case of a weight being allowed to fall on the earth's surface or into a pit dug in the earth corresponds to the source of the doublet. When the weight falls into the pit, we observe pull waves in the neighbourhood of the pit and push waves at a distance. This case may be applied to volcanic earthquakes generated by reactions of the erupted material and of the air waves.

14) W. INOUYE and H. KIMURA, *Bull. Earthq. Res. Inst.*, **13** (1935), 194.

When explosives are fired underground, the initial motions are all push waves. If the explosives are packed between covers (see Fig. 8.) and then fired, we also observe push waves in all azimuths, although here the displacements in direction *aa* are greater than those in direction *bb*. These facts may be explained on the assumption that the single source co-acted with the quadruple source.

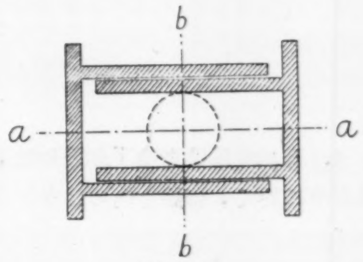

Fig. 8.

7. Summary.

1) The author has made a theoretical study of the initial motions of dilatational waves generated from a seismic origin, in which the normal pressure on the surface of the spherical cavity can be expressed by the sum of two zonal harmonics $P_0(\cos\theta)$ and $P_2(\cos\theta)$.

It is shown that so long as the wave length exceeds the dimension of the focus, we only observe the push and the pull waves according as the single source is the source or the sink, respectively. If the wave length becomes comparable with the diameter of the seimic origin, the displacements of the dilatational waves due to the single source turn out to be of the same order of magnitudes as those due to the quadruple source, so that we observe both pull and push waves.

2) It is shown that it is not unreasonable to assume that the mechanisms above stated can be applied to the origins in the case of actual earthquakes. If so, then in order to be consistent with the observed distributions of the initial motions, we shall have to assume that the dimensions of the seismic origins are comparable with the wave lengths of the seismic waves radiated from these origins.

Our next object for study should be the polarizations in the propagations of very short seismic waves that accompany earthquake sounds, and which cause anomalies in the distributions of the felt areas, owing probably to the short wave lengths compared with the dimensions of the seismic origins.

Finally, the author's cordial thanks are due to Prof. M. Ishimoto, Prof. K. Sezawa, Dr. N. Nasu, Dr. G. Nishimura, Prof. F. Kishinouye, and Prof. R. Takahasi for their kind advices.

52. 發震機構に就いて

地震研究所 井上宇胤

1. 石本所長はその「地震初動方向分布より震源に四重源の推定」なるエポツクメイキングの論文中に於て，初動方向の分布は帯球函數の $P_0(\cos\theta)$ と $P_2(\cos\theta)$ の和で現はし得る事を示されてゐる.

然し此の初動方向分布から震源の發震機構は一義的には定まらぬものである.

其の中の一つの解釋となり得る場合として球形震源を考へ，其の球面上の壓力變化の方位的分布が P_0 と P_2 の重合に依つて現はし得る場合を數理的に取扱つて見た.

2. 此の計算に依ると，波長が震源の大きさに比較して相當長い場合には單源が正の單源であるか負の單源であるかに從つて，方向に無關係に押し波或は引き波のみを觀測する事となる.

然し波長が震源の大きさと同程度に成つて來ると，單源から出る縱波の振幅と四重源から出る縱波の振幅とが同程度に成つて來て，從つて押し波引き波が同程度に現はれる事になる. 此の樣な發震機構を考へる事は餘り無理で無い事を多少論じておいたが，實際に此の樣な場合があるとすると，震源の大きさはそれから出る波の波長と同程度であると考へるのが自然である事となる.

53. 茨城縣大寶村及上大津村に於ける地震動卓越週期の觀測

地震研究所　萩原尊禮

(昭和11年9月15日發表——昭和11年9月21日受理)

加速度地震計に依り記錄せられる地震動は比較的均一の週期の振動より成つて居るが，此の卓越週期は各地に於て一定ではなく所謂地盤の良否と密接な關係があることは既に石本教授[1]等に依り屢々報告せられて居る．例へば東京本郷の如き山の手に於ては其の卓越週間は約 0·3 秒であるが，丸の內の如き下町に於ては約 0·6 秒であつて，地盤惡しと稱せられて居る土地に於ては 1 秒附近の卓越週期を示すことが屢々ある．斯樣な事實は東京市附近のみならず橫濱市に於ても實證せられてゐる．一方筑波山山腹に於て觀測せられた加速度大なる地震動の卓越週期は 0·04～0·05 秒[2]であつて，此の地方の如く軟弱な表面層を欠いて居る土地に於ては其の卓越振動週期は極めて小である．今回の報告は筑波山山麓の大寶村と霞浦湖畔の上大津村に於て地震動加速度の觀測を行ひ，强固な岩石も露出せず又軟弱な表面層も比較的厚くはないと思はれる是等の土地に於て如何なる卓越振動週間が現れるかを調査したものである．

觀測場所　茨城縣眞壁郡大寶村は筑波山の西方約 10 粁，小貝川の沿岸にある．今回地震計を設置した場所は同村字橫根，橫瀨謙次郎氏宅であつて，同氏の援助に依り昭和 10 年 4 月より昭和 11 年 5 月に至る約 1 箇年間觀測を續行することが出來た．他方の茨城縣新治郡上大津村は土浦町より約 5 粁，霞ケ浦（西浦）の北岸に在る．地震計は山口生知博士の好意に依り同村字沖宿の同氏宅へ設置し，昭和 10 年 4 月より觀測を開始し現在尙繼續しつゝある．使用せる地震計は何れも石本加速度地震計であるが，其の要素は次の如くである．

成　分	水平 2 成分
振子の重錘	15 kg
振子の週期	0·1 秒
幾何倍率	200

1) 例へば石本巳四雄　地震研究所彙報　**10** (1932), 171; **12** (1934), 234; **13** (1935), 592; **14** (1936), 240.

2) T. Hagiwara, *Bull. Earthq. Res. Inst.*, **12** (1934), 222.

感　　度	1 mm が 1·7 gal に相當す
減 衰 器	空氣減衰器（臨界減衰狀況に保つ）
起 動 機	シンクロナスモートル（50 サイクルに對し毎分 300 廻轉）
圓筒（直徑 20 cm）回轉速度	
	4 分 10 秒に 1 廻轉（大寶），5 分に 1 廻轉（上大津）

機械は毎月 1 回點檢し且感度試驗を行つた．

觀測結果　元來此の地方を震央とする地震の發生は極めて多い[3]ため，1 箇年間の觀測に依つて相當數多くの記錄を得ることが出來たが，今回は其の中，次表に示す代表的のもの 5 箇を撰んで卓越振動週期を調査した．地震記象は第 3 圖及び第 4 圖に示してある．

昭和 10 年	震　央	大寶村				上大津村		
		最大加速度 (gal)		卓越週期 (秒)		最大加速度 (gal)		卓越週期 (秒)
A. 4 月 19 日 1 時 30 分頃	鬼怒川流域	NE	24·0	0·11	0·45	NW	32·0	0·13
B. 7 月 18 日 2 時 55 分頃	鬼怒川流域	NW	53·0	0·10	0·40	SE	37·0	0·10
C. 7 月 19 日 9 時 37 分頃	鹿島灘北部	SE	36·0	0·10	0·40	NW	36·0	0·10
D. 8 月 30 日 7 時 19 分頃	大寶村附近	NE	12·0	0·10	0·40	NE	16·0	0·10
E. 9 月 11 日 23 時 06 分頃	釧路南北沖	SE	4·0	0·10	0·40	NE	8·0	0·10

卓越週期の決定法は從來の方法と同樣であつて，地震記象中に零線に相當する線を引き，之を振動の曲線が同一方向に過ぎる點を求め，相次ぐ是等の 2 點間の時間を以て其の週期と定めた．第 1～2 圖は斯の如くして求められた地震動週期の頻度圖である．是等の頻度圖は何れも主要動より約 30 秒間の振動に就て求められたものである．然し大寶村に於ける場合は，地震記象を一見すれば明白なる如く，0·13 秒程度の比較的小週期の規則正しい振動と 0·4 秒程度の比較的大きい週期の振動との 2 種類の週期の振動が卓越して居り，主要動の始めの部分に於ては後者は前者に掩蔽されて居るが，尾部に至ると明かに後者の存在が認められる．此の爲大寶に於ける場合には，便宜上週期の頻度圖を主要動より約 20 秒間のもの（第 1 圖左側），其の後の約 20 秒間のもの（第 1 圖右側）とに分割したのである．上大津に於ける場合は一般に此の樣な現象は認められない．

第 1 圖の示す如く大寶村の卓越周期は 0·1～1·15 秒と 0·4 秒程度との 2 種であつて，震央の遠近に依る差異は少い．然し C 地震は大寶村の殆ど直下約 40 粁の所に發生したものであるが，此の場合は 0·1～0·15 秒の週期のみ卓越し 0·4 秒附近のものは現

3） 地震研究所地震觀測報告參照．

れて居ない．此の2種の卓越週期の比は略々3となつてゐることから，表面層の基本振動と第3次振動と考へることが出來やう，C地震の場合の如く震央が極めて近い場合に第3次振動のみ誘發せられるのは斯樣な場合には地震波中に比較的大週期の波動を欠いて居ることに起因するものと考へられる．

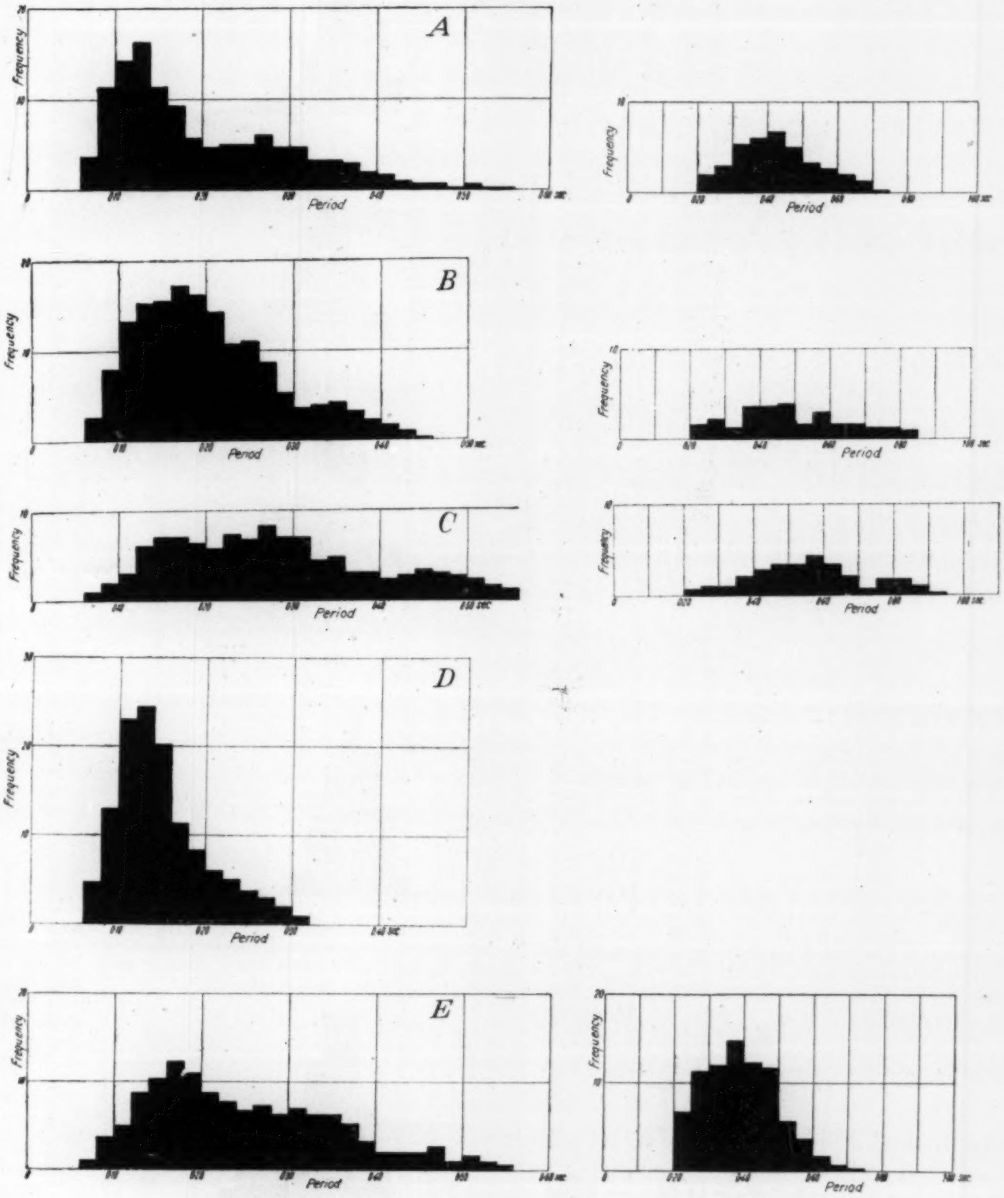

第　1　圖　　地震動週期頻度圖(大寶村)

上大津村に於ける卓越週期は第2圖に示す如く 0·1～0·15 秒であるが，比較的大週期の頻度は極めて少いことが大寶村と大いに異つてゐる．恐らく 0·1～0·15 秒が此の土地では基本振動週期であると考へられる．震央の遠近に依る頻度圖の差異は大寶村の場合と同じく極めて少い．

表面層の厚さ，基盤の性質等に關して未だ正確な材料を入手することが出來ないため，今回は之と卓越週期との關係を明確に述べることは出來ないが，附近の地形より察して此の地方は地下餘り深からざる所に極めて强固な基盤が存在することは明かである．振動週期の頻度圖が震央位置に依り殆ど影響されないこと，卽ち震央が遠い場合に於ても比較的大週期の振動が餘り現れないことは，此の地方の地層の構成が彈性學的に單純なることに歸因するものと思はれる．之に比較すると一般に東京附近に於ける地震動の週期は相當に複雜した分布を示してゐると云へやう．

尙一言すべきは，是等の地方に於ては東京附近に比較して地震動の加速度は極めて大きいことである．然し乍ら大なる加速度を與へる振動の週期は大寶村，上大津村共に 0·1～0·15 秒程度の小週期のものある關係上，假令加速度は大であつても構造物に災害を與へることは極めて少い．例へば B 地震の如きは大寶村た於ては最大加速度 53 gal，上大津村に於ては 37 gal の多きに達したが，構造物には僅かの損傷もないのである．

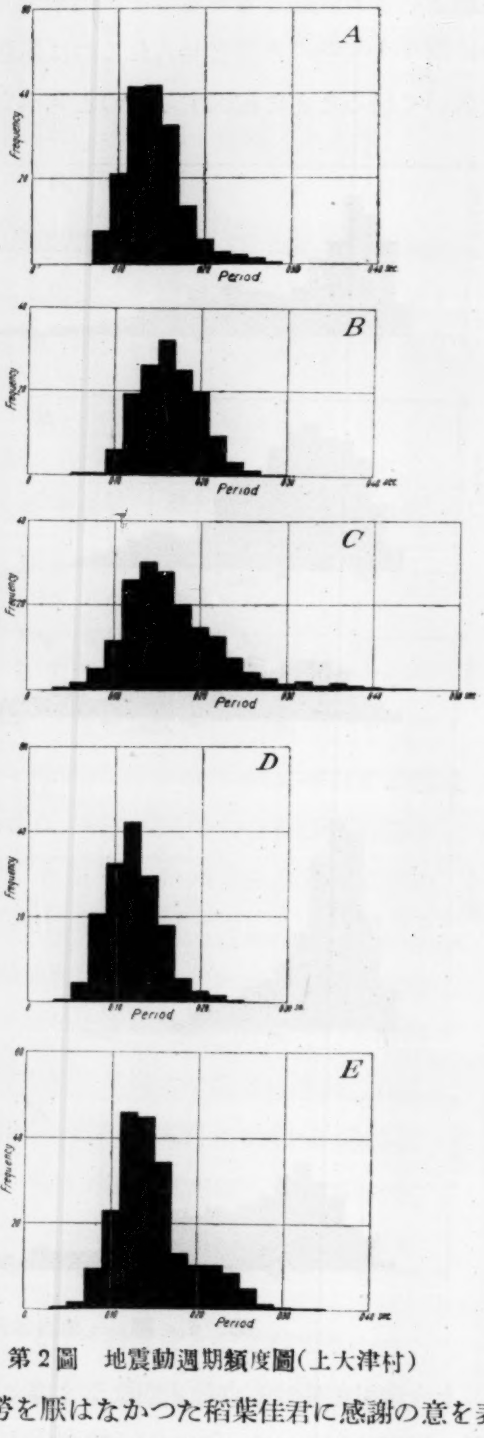

第2圖　地震動週期頻度圖(上大津村)

終りに臨み，機械の調整及び感度試驗に勞を厭はなかつた稻葉佳君に感謝の意を表する．又觀測の勞をとられた横瀨，山口兩家の方々に對し深く感謝する次第である．

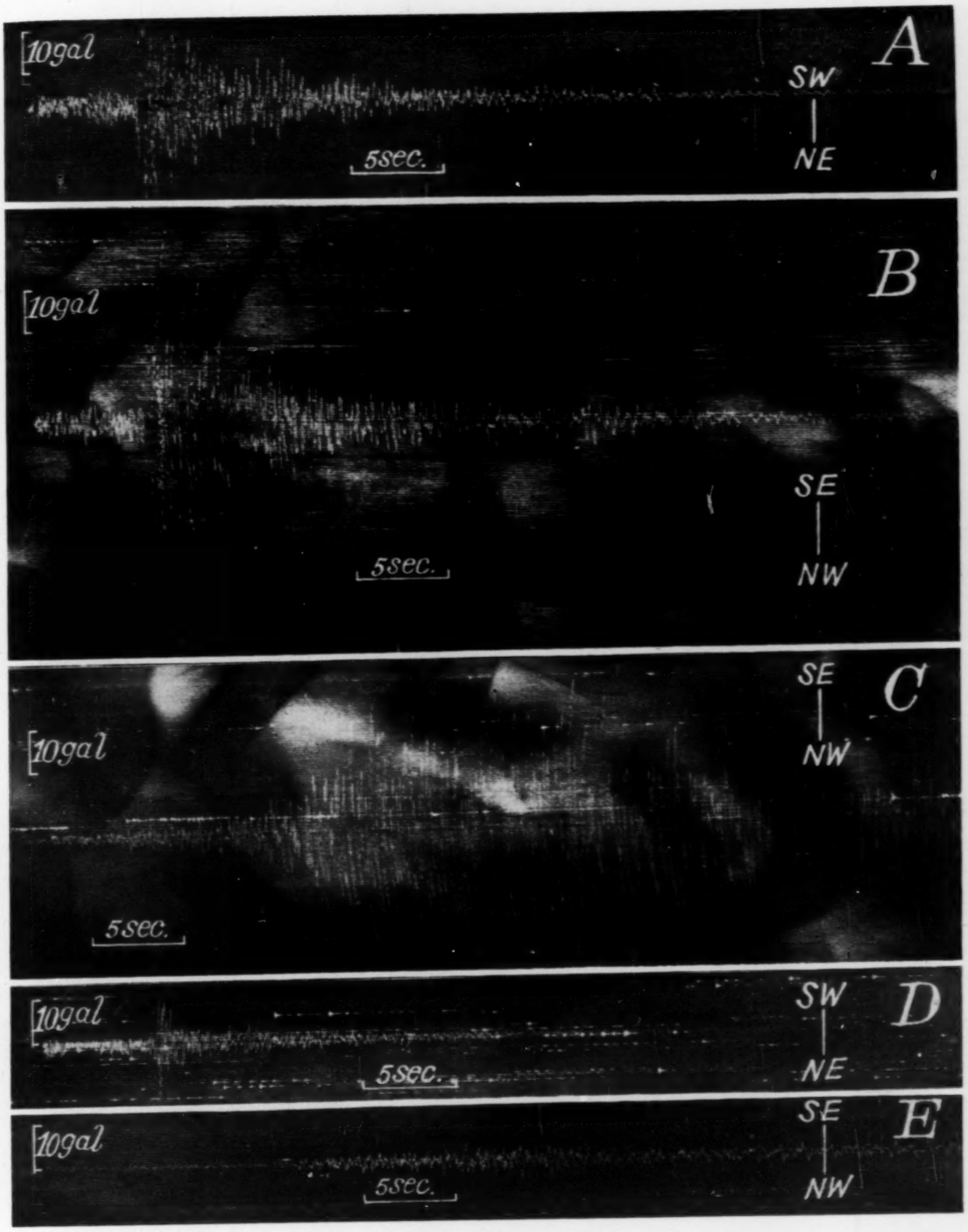

第 3 圖　加速度地震記象（大寶村）

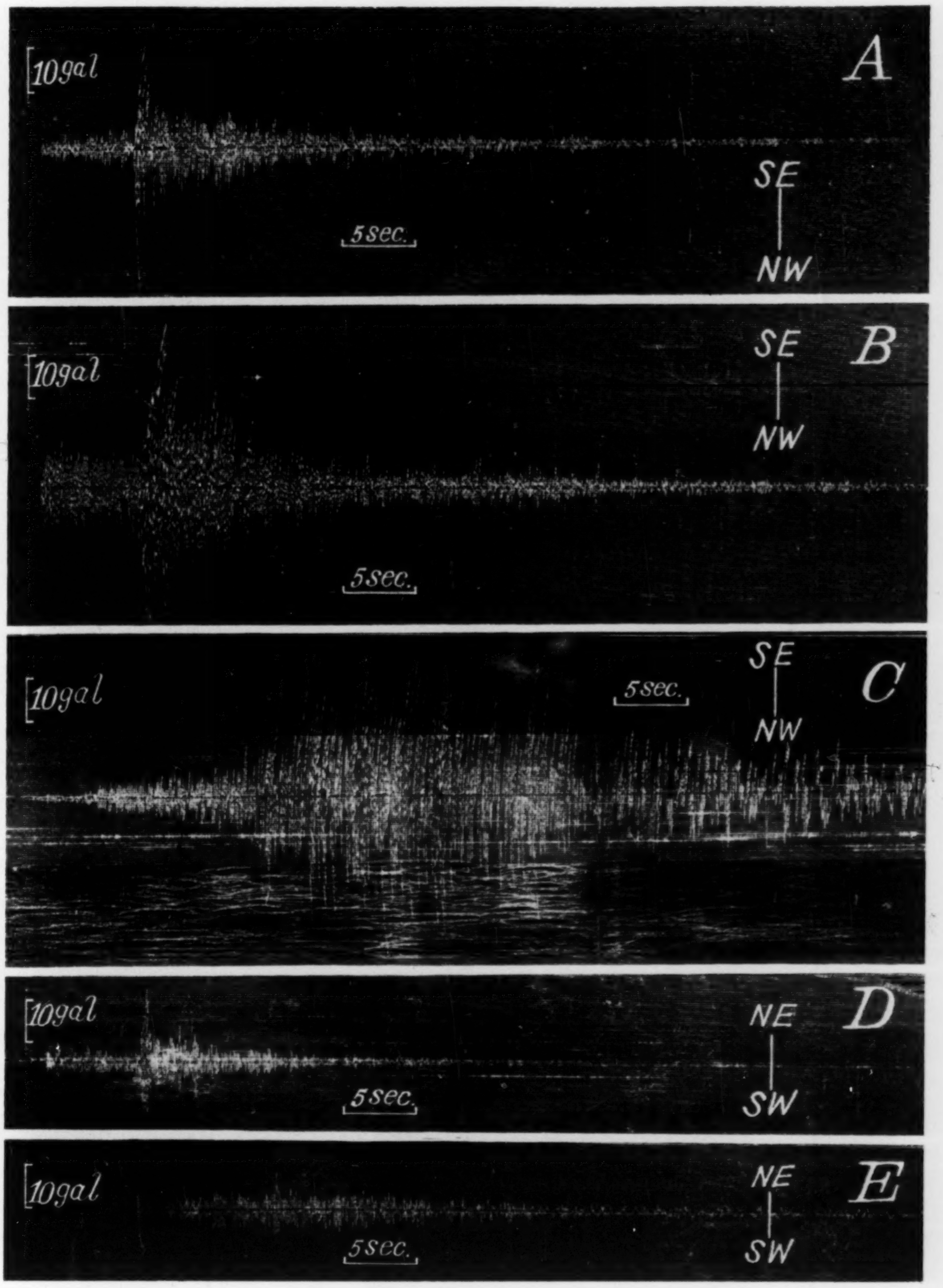

第4圖 加速度地震記象（上大津村）

53. *Observation of the Predominating Periods in the Earthquake Motions at Daihô-mura and Kamiôtu-mura, Ibaraki Prefecture.*

By Takahiro HAGIWARA,

Earthquake Research Institute.

For investigating the predominating periods in the earthquake motions, the acceleration seismographs were installed at Daihô-mura and Kamiôtu-mura, Ibaraki Prefecture.

---

54. *On the Diurnal Periodicity of Felt Earthquakes.*

By Fuyuhiko KISHINOUYE,

Seismological Institute, Faculty of Science,

Tokyo Imperial University.

(Read July 7, 1936.—Received Sept. 21, 1936.)

It has been known that felt earthquakes, as a rule, is frequent at night.[1] The writer inquired also into the time distribution of felt earthquakes at Tôkyô during twelve years since 1924, and obtained the similar result as before. Then he investigated statistically whether men are more sensitive to earthquake motions at night or in the day-time.

Diurnal Frequency Variation of Felt Earthquakes at Tôkyô.

The statistical investigation of earthquakes observed at Tôkyô has been carried out by F. Omori[2] in 1900. In his paper 2208 earthquakes were included, or on an average 92 in a year. But observation in the twelve years analysed hereafter comprises 64 earthquakes as the average number of only near earthquakes which were felt, and in addition 481 unfelt earthquakes and 81 distant earthquakes were recorded at the Seismological Institute in a year on an average. Such a great difference between old and new data might be due to the progress of seismometry during about twenty years.

The data used here are given in the Seismometrical Reports of the Earthquake Research Institute. The earthquakes in the reports were felt by several staffs of the above institute or the Seismological Institute who reside in Tôkyô, and their epicentres were within the radius of 160 km from Tôkyô. As regard to the harmonic analysis of the frequency distribution of felt earthquakes, the first harmonic of the diurnal variation has been noticed in the previous investigations. Then the writer looked upon only the first harmonic.

The results of the harmonic analysis in 1924～1935 are shown in Table I.

1) See for instance, B. GUTENBERG, *Handb. d. Geophys.* Bd. **4**, § 277.

2) F. OMORI, *Rep. Imp. Earthq. Inv. Comm.*, **32** (1900), 30～116, and *Publ. Imp. Earthq. Inv. Comm.*, **8** (1902), 1～94.

Table I.

Year	Total number	Mean no. a_0	a_1/a_0	b_1/a_0	c_1	ε	α_1
1924	60	2·50	+ ·196	+ ·122	·229	·229	2^h02^m
25	34	1·42	− ·128	+ ·069	·145	·304	10 07
26	68	2·83	+ ·157	+ ·251	·296	·215	3 52
27	65	2·71	+ ·207	+ ·227	·306	·220	3 02
28	78	3·25	+ ·244	− ·010	·244	·201	23 51
29	50	2·08	+ ·566	+ ·156	·605	·251	1 01
30	58	2·42	+ ·249	+ ·145	·288	·233	2 01
31	89	3·71	+ ·139	+ ·015	·140	·188	0 25
32	59	2·46	+ ·262	− ·134	·294	·231	22 11
33	63	2·62	+ ·285	+ ·053	·290	·224	0 42
34	64	2·66	− ·250	− .116	·275	·221	13 39
35	78	3·25	+ ·383	+ ·007	·383	·201	0 04
		(mean)	+ ·193	+ ·066			1 15

Comparing the amplitude c_1 of each year with the corresponding expectancy ε, it may be deduced from the theory of the periodogram analysis that the frequency distribution might depend on chance, for corresponding values of c and ε are nearly equal. But phase angles α_1 are mostly maximum at night. Then the theory of random walk was applied again on the above data. The theory has been used by Prof. T. Matuzawa[3] in a paper in this bulletin on the earthquake on March 2, 1933, so the explanation of it is omitted here. Applying the theory the expectancy for the average vector c was obtained as 0·09, and the amplitude of the average vector c_m as 0·217. Therefore c_m/c is equals to 2·42, and the probability that the average amplitude becomes greater than the above value is only 0·003. And the maximum of c_m is at about

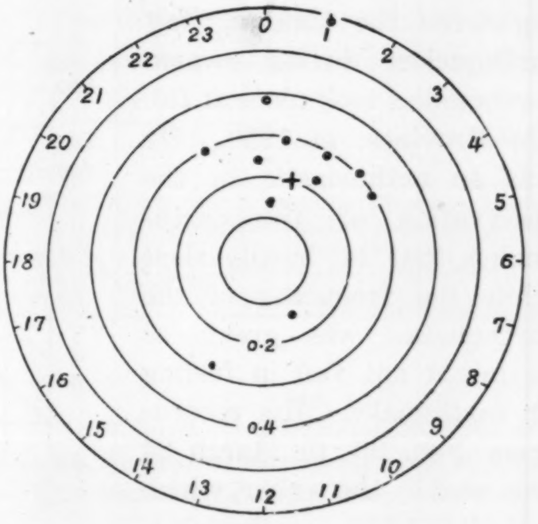

Fig. 1. Harmoinc dial.
Cross indicates the average vector.

3) T. MATUZAWA, *Bull. Earthq. Res. Inst.*, **14** (1936), 38～67.

1 h 15 m. Then it might be not accidental that the felt earthquakes occurred mostly at night at Tôkyô.

Two alternative interpretations may be put on the frequency distribution of felt earthquakes before mentioned. As F. de Montessus de Ballore[4] described, at night men are in repose and surroundings are silent, so men are sensitive to earthquake motions. Nextly if the frequency of moderate earthquakes be greater at night than in the daytime, the above mentioned Ballore's hypothesis may become wrong. But ascertaining of the latter consideration is difficult at present, for the times of occurrence of small earthquakes are hardly obtainable. Then according to the former interpretation the writer investigated the diurnal variation of the proportions of felt earthquakes to that of the total ones.

Diurnal Variation of Frequency-ratio of Felt Earthquakes to Total Ones observed with Seismographs.

Suitable data for the investigation were difficult to be obtained, and a few were available.

i) Late E. Makino who was an instructor of the Itô Primary School registered the time of felt earthquakes during swarm earthquakes took place at Itô, Idu Province, in 1930. He was so enthusiastic in the observation of the earthquakes that he hardly slept while the frequency of the earthquakes was great, as he might not fail in feeling an earthquake. His records from Feb. 20 to March 24 was used by the writer, which includes 1835 earthquakes. The frequency of the earthquakes at Itô was compared with that of the earthquakes registered at Misaki with an Omori portable seismograph ($V=120$ and $T=4$ sec). The total number of the earthquakes observed

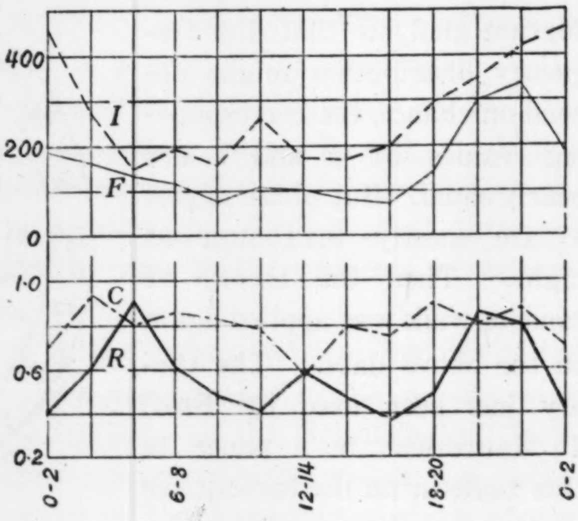

Fig. 2.

I = Number of earthquakes observed at Misaki in 2 hours,
F = Number of felt earthquakes at Itô,
R = Ratio (F/I),
C = Correlation coeffecient of I and F.

4) F. Montessus de BALLORE, *Arch. d. sciences phys. nat. Genf.*, **22** (1889).

at Misaki during the same interval was 3109. Supposing that the number of felt earthquakes is independent to that of the total earthquakes observed with seismographs, ratios of the two quantities were calculated, and the time variation of the ratios was investigated. The ratio and

Table II.

Hour	0~2	2~4	4~6	6~8	8~10	10~12	12~14	14~16	16~18	18~20	20~22	22~0	Sum
No. of earthq. felt at Itô	190	167	135	118	77	107	102	79	72	144	302	339	1832
No. of earthq. obs. at Misaki	460	275	152	193	160	263	174	170	198	294	349	421	3109
Ratio	·41	.61	·91	·61	·48	·41	·59	·47	·36	·49	·87	·80	
Correl. coeff.	·71	·95	·81	·87	·83	·79	·57	·80	·76	·91	·81	·87	

frequency of earthquakes in every two hours are shown in Table II and in Fig. 2. The number of the ratios, or number of pairs of felt and total earthquakes, obtained was as many as 278, then in addition correlation coefficients of felt and total earthquakes were calculated. The variations with respect to time of both ratios and correlation coefficients probably indicate that the felt earthquakes are more at night than in the day–time.

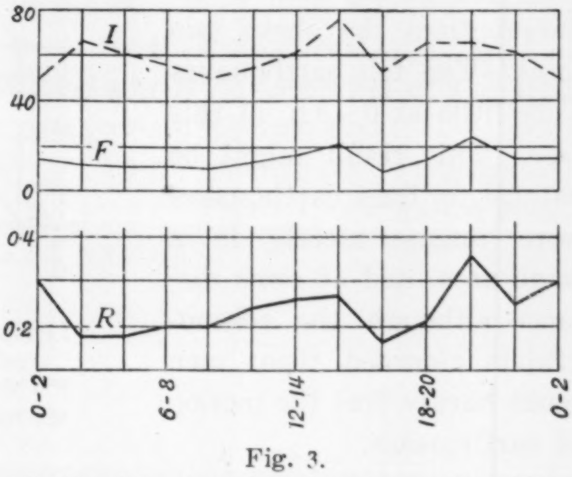

Fig. 3.
I = Number of earthquakes observed at Mito.
F = Number of earthquakes felt at Mito.
R = Ratio (F/I)

ii) Nextly the writer looked for other seismometrical reports which include considerably many felt earthquakes, for if the data include a little felt earthquakes time variation of sensitibity of men to the earthquake motions will not be found but frequency variation of moderate earthquakes will be shown. For the present purpose, the seismometrical reports of the Mito Meteorological Station in 1929 and Jan.~July, 1931 were used. The distribution of the frequency–ratios is shown in Table III and Fig. 3. The epoch of maximum sensitivity was obtained as at about 1h 20 m.

Table III.

Hour	0~2	2~4	4~6	6~8	8~10	10~12	12~14	14~16	16~18	18~20	20~22	22~0	Sum
No. of felt earthq.	15	12	11	11	10	13	16	21	9	14	24	15	170
No. of total earthq.	50	67	61	56	50	54	61	77	53	66	65	61	722
Ratio	·30	·18	·18	·20	·20	·24	·26	·27	·17	·21	·36	·25	

iii) The hourly numbers of fore-shocks and after-shocks of the Idu earthquake on Nov. 26, 1930 are given in the *Kensin-Zihô* **5** (1931), 136 ~ 137 by S. Sagisaka. The frequency ratios of earthquakes were obtained as before and are shown in Table IV and Fig. 4. Though the values of the ratios are small and the variation is not distinct, the distribution is different from the above two cases. The felt earthquakes were little at 0 ~ 3 h in this case. This result might be natural, for these earthquakes were intense merely in a small area, and at some distance although the seismographs recorded them men could hardly feel the motion of earthquakes.

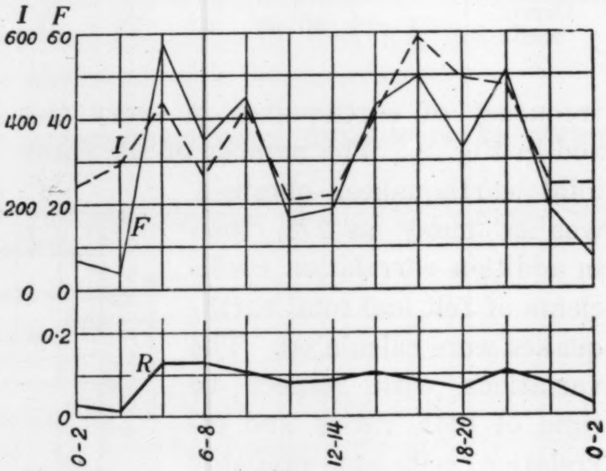

Fig. 4.
I = Number of earthquake observed with seismographs.
F = Number of felt earthquake.
R = Ratio (*F*/*I*).

Table IV.

Hour	0~2	2~4	4~6	6~8	8~10	10~12	12~14	14~16	16~18	18~20	20~22	22~0	Sum
No. of felt earthq.	7	4	58	35	45	17	19	43	50	33	51	19	381
No. of total earthq.	246	295	440	266	424	210	220	414	590	495	477	245	4322
Ratio	·03	·01	·13	·13	·11	·08	·09	·10	·09	·07	·11	·08	

Conclusion.

From the above investigations, the writer arrived at a conclusion that men are more sensitive to feel earthquake motions at night than in the day time. The result may be interpreted as Ballore wrote, or in another way as follows: moderate earthquakes are frequent at night, consequently men feel more earthquakes at night. But the latter consideration is not proved now, so in statistics of earthquake frequeuency the influence of the intensity of the earthquakes may be worthy of caution.

---

54. 有感地震の1日中の分布に就いて

地震學教室 岸上冬彦

地震研究所の地震觀測報告を用ひて大正 14 年から昭和 10 年まで 12 年間の東京に於ける有感地震の1日中の分布を統計理論によつて調べた. 其の結果有感地震は午前1時頃に最も多かつたことが判つた. 次に此の事は人が夜に地震動を感じ易い爲であるか否かを調べて見た. 卽ち昭和5年の伊東地震, 水戸測候所觀測の地震, 昭和5年の伊豆地震の前震餘震等について, 有感地震と地震計觀測による地震總數との比をとつて, その比の1日中の變化を見ると夜間地震を感じ易い樣に見えるが, 又地震の强さが感覺に影響することもある樣である. 其故地震計觀測結果について統計するには各地震の强さを考慮に入れる必要があらう.

---

55. 明治9年以降東京觀測各月地震回數統計

地震研究所　石本巳四雄

（昭和11年9月15日發表—昭和11年9月21日受理）

東京における地震觀測は明治9年から行はれて居る．同年から明治15年迄の6ヶ年は赤坂葵町測量課に於てパルミエリー（Palmieri）地震計により觀測された．明治16年より18年に至る間は同じくパルミエリー地震計なれども觀測地點は麴町區代官町本丸内におけるものであつた．從つて報告された地震は凡て此の地震計によつて得たものであり有感覺，無感覺の區別は無い．

明治19年より大正9年頃迄はミルン普通地震計により觀測され，其の後は所謂微動計の觀測が初つたが，有感覺地震を對象とする限りに於ては地震の發生が證明立てられゝばよいのであつて，地震計の種別は問題とならぬ．卽ち明治31年以降は地震計に賴る事なく有感覺地震のみを目標として報告される事になつたのである．而して有感覺の判定は全く人體感覺による爲め，晝夜の區別，擔當者の變更，注意者數，市内における判定者の居住地等に於て多少の齟齬あるは免れ得ない事である．例へば大正12年關東地震に於ては人々の注意が特別に高潮されたのは勿論，地震研究に携る人數も激增した關係上，有感覺地震の判定も增加した傾向にあるのは否み難き事實の樣に思はれる．

第I表は明治9年より昭和10年に至る60年間の各月地震回數である．明治30年

第I表　東京觀測地震數

年＼月	I	II	III	IV	V	VI	VII	VIII	IX	X	XI	XII	計
明治 9 (1876)	3	4	6	11	5	3	3	5	3	3	4	6	56
10 (1877)	4	5	6	5	8	9	6	4	1	8	6	9	71
11 (1878)	3	8	7	2	5	4	4	1	2	4	6	4	50
12 (1879)	6	7	14	0	9	4	3	4	1	7	6	9	70
13 (1880)	9	9	6	6	2	9	8	4	1	3	10	10	77
14 (1881)	13	8	8	8	4	3	3	3	2	3	3	8	66
15 (1882)	4	7	15	6	3	2	2	1	1	4	1	0	46
16 (1883)	6	0	3	3	6	2	3	1	0	1	3	4	32
17 (1884)	5	2	8	2	9	4	1	4	2	8	8	15	68
18 (1885)	7	9	8	4	3	6	0	3	8	10	3	7	68
19 (1886)	3	3	3	2	8	4	2	8	7	4	2	8	54
20 (1887)	10	4	3	8	14	5	6	2	9	0	5	14	80

（次頁へ續く）

年 ＼ 月	I	II	III	IV	V	VI	VII	VIII	IX	X	XI	XII	計	
21 (1888)	4	15	7	7	11	9	9	7	11	4	13	4	101	
22 (1889)	5	16	11	18	13	7	5	8	7	8	9	6	113	
23 (1890)	5	5	6	15	14	5	12	7	4	8	10	2	93	
24 (1891)	1	4	6	7	10	7	8	4	4	45	12	15	123	
25 (1892)	9	11	3	7	7	9	14	2	7	11	4	8	92	
26 (1893)	5	4	5	7	10	10	4	3	6	3	3	1	61	
27 (1894)	7	8	23	11	9	9	6	3	8	4	8	5	101	
28 (1895)	20	9	8	17	11	12	11	5	10	17	6	3	129	
29 (1896)	42	18	15	21	10	52	22	18	7	5	7	10	227	
30 (1897)	11	18	11	8	17	6	11	32	5	8	15	22	164	有感覺(53)
31 (1898)	2	4	4	6	3	7	9	7	5	1	4	2	54	以下有感覺
32 (1899)	3	5	10	9	5	2	5	10	2	3	3	2	55	
33 (1900)	4	5	8	2	4	5	1	5	1	3	10	3	51	
34 (1901)	4	1	1	5	4	3	4	8	9	4	9	3	55	
35 (1902)	5	5	5	3	4	6	4	4	2	2	2	8	50	
36 (1903)	5	9	4	4	3	3	5	2	1	3	6	1	46	
37 (1904)	6	3	4	6	6	3	11	6	2	7	3	3	60	
38 (1905)	0	2	3	4	4	5	3	2	3	5	2	3	36	
39 (1906)	5	7	2	10	14	0	2	8	3	6	3	0	60	
40 (1907)	2	3	4	4	3	3	4	1	2	8	4	3	41	
41 (1908)	6	1	1	1	4	2	4	3	2	2	1	4	31	
42 (1909)	2	4	11	3	5	2	9	6	3	4	6	6	61	
43 (1910)	2	1	0	3	11	4	4	3	10	7	7	5	57	
44 (1911)	4	3	5	3	2	3	1	4	6	5	12	7	55	
(大正1)45 (1912)	10	2	5	3	10	7	4	6	3	4	5	7	63	
大正 2 (1913)	1	6	5	3	6	5	5	4	4	4	3	2	48	
3 (1914)	5	6	4	1	4	4	4	2	2	5	1	3	41	
4 (1915)	0	1	5	9	10	5	3	3	1	7	18	2	64	
5 (1916)	1	4	3	3	2	2	4	10	2	5	5	2	43	
6 (1917)	8	7	4	3	2	4	4	4	3	5	9	3	56	
7 (1918)	3	3	5	10	5	1	6	2	2	4	4	4	49	
8 (1919)	2	3	3	5	7	5	4	4	0	2	3	1	39	
9 (1920)	2	3	1	2	3	2	6	2	1	2	1	7	32	
10 (1921)	2	1	3	2	1	0	1	0	1	1	3	11	26	
11 (1922)	4	4	5	11	5	5	3	1	2	2	5	2	49	
12 (1923)	7	6	6	0	7	17	5	3	471	33	34	26	615	
13 (1924)	31	1	2	4	3	4	2	3	5	2	0	3	60	
14 (1925)	7	5	1	1	2	4	2	1	1	2	5	3	34	
(昭和1)15 (1926)	10	10	5	4	7	5	7	6	2	3	7	2	68	
昭和 2 (1927)	4	3	6	3	5	2	4	9	9	8	9	3	65	
3 (1928)	6	5	7	8	16	4	8	6	2	8	3	5	78	
4 (1929)	5	4	5	4	3	6	6	2	5	3	4	3	50	
5 (1930)	4	4	4	5	13	3	1	7	5	5	3	4	58	
6 (1931)	3	6	12	3	5	11	12	4	14	6	5	8	89	
7 (1932)	0	8	11	5	2	4	5	4	6	8	3	3	59	
8 (1933)	2	7	5	7	3	4	6	3	5	9	7	5	63	
9 (1934)	4	10	3	7	6	8	5	5	3	0	10	3	64	
10 (1935)	10	6	8	8	3	11	10	3	9	4	2	4	78	

備　考　明治 9 年 (1876) より明治 43 年 (1910) 迄は中央氣象臺年報第2編地震の部による.

明治 44 年 (1911) より大正 12 年 (1923) 迄は中央氣象臺官報記事及び地震學教室觀測による.

大正 13 年 (1924) 以降は地震研究所地震觀測報告による.

以前は著しく地震回數が多い事になつて居るが，此れは上述の如く有感覺，無感覺の區別なく器械にて觀測し得たものを擧げた結果であつて，時の經過と共に地震動計器の改良發達のために次第に地震數の增加が行はれたと見られる．即ち斯樣にして報告された地震回數は今日實際に行つて居る有感覺地震の制限とは異る關係上，直接統計にのぼせる事の出來ないのは頗る遺憾である．從つて此所に統計を行つた期間は結局明治 31 年以降となつた次第である．

統計を行ふに就て先づ各月地震回數の頻度表を作つて見た．此れは第 II 表に示すものである．

第 II 表 東京有感覺地震頻度

期間 / 1ヶ月地震回數	明治 31 年～明治 42 年	明治 43 年～大正 12 年 8 月	大正12年9月～昭和 10 年	**明治 31 年～昭和 10 年**
0	3	6	3	**12**
1	12	19	6	**37**
2	23	26	14	**63**
3	29	28	25	**82**
4	26	26	21	**73**
5	17	24	23	**64**
6	12	9	12	**33**
7	4	11	10	**25**
8	5	1	10	**16**
9	6	2	5	**13**
10	4	6	6	**16**
11	2	3	3	**8**
12	0	1	2	**3**
13	0	0	1	**1**
14	1	0	1	**2**
15	0	0	0	**0**
16	0	0	1	**1**
17	0	1	0	**1**
18	0	1	0	**1**
19	0	0	0	**0**
20	0	0	0	**0**

なほ統計期間を三つに分けたのは此の各期間に變化する狀況を見やうと思つたからである．先づ初めに明治 31 年より昭和 10 年に至る 37 年間のものを對象として，以上の數値を圖に表したのが第 1 圖である．

此の表から見ると，最大頻度を示すのは 1 ケ月 3 回の地震が發生する場合であり，

又 10 回の所にも最大が現はれて居る．今此の曲線を二つの頻度曲線から成立すると考へ，一つは3回附近に，他は10回附近に最大値があるとなし，曲線を破線で分けて見た．而して3回附近に最大値を持つ曲線のみに着目して，此れに就いて數學的に頻度曲線を決定する事を試みた．卽ち第1圖から次の如き數値を撰び出した．

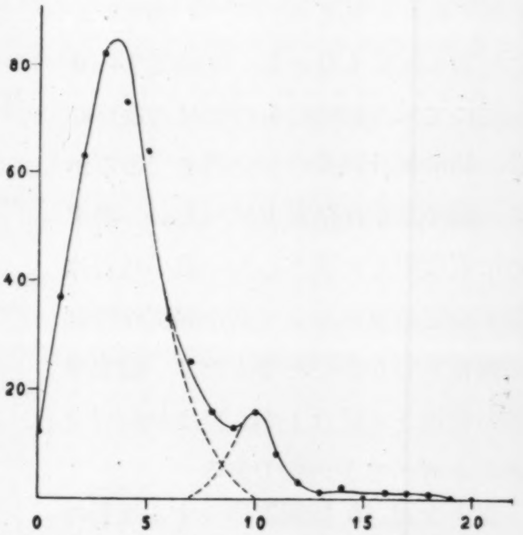

第1圖 東京有感覺地震1ヶ月回數頻度曲線
縱軸：頻度， 横軸：1ヶ月地震回數

第 III 表

1ヶ月地震回數 (X_k)	頻度 (f_k)	地震數 ($f_k X_k$)	1ヶ月地震回數 (X_k)	頻度 (f_k)	地震數 ($f_k X_k$)
0	12	0	6	33	198
1	37	37	7	21	147
2	63	126	8	11	88
3	82	246	9	4	36
4	73	292	10	0	0
5	64	320	月數 (N)	400	地震總數1490

平均地震數 $M=3{\cdot}73$
標準偏差 $\sigma=1{\cdot}929$
$\sigma^2=3{\cdot}721$

結局頻度曲線としては

$$f=207{\cdot}36\left\{\frac{1}{\sqrt{2\pi}}e^{-\frac{1}{2}\left(\frac{\xi}{\sigma}\right)^2}\right\}.$$

此れを圖に示したものは第2圖である．

又大正 12 年關東地震の前後に於て地震回數の消長を見るために以上の期間を第 II 表の如く 3 分し，各期間に就て頻度曲線を作つたものは第3圖で

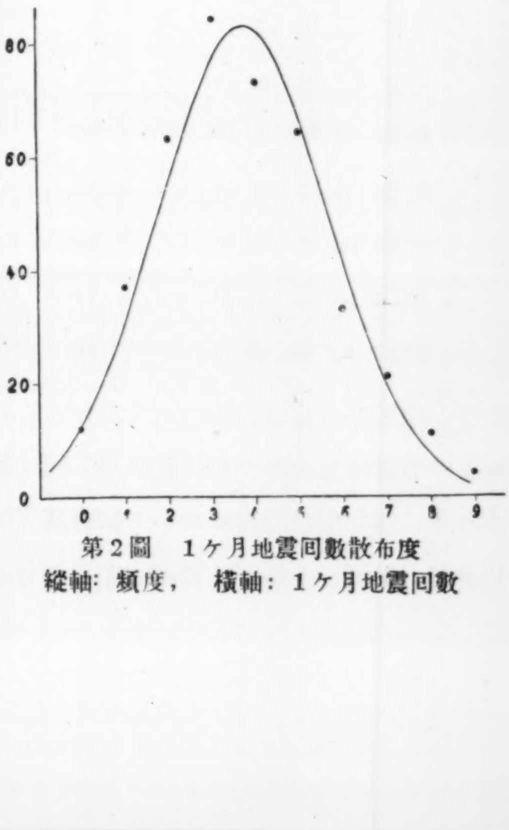

第2圖 1ヶ月地震回數散布度
縱軸：頻度， 横軸：1ヶ月地震回數

ある．此れを見ると，A，B 期間においては殆ど同じく，C 期間に於て頻度が多少減じて居る様にも見える．又頻度5～10附近にては共通的のものが見えないのは，結局統計回數の少い爲めであるから，論ずる事は穩當と思へない．要するに東京附近に發生した一般小地震は關東地震前後において其の頻度は特別の變化をしなかつた事となり，關東地震の發現とは統計上から見て無關係であると考へてよい樣である．

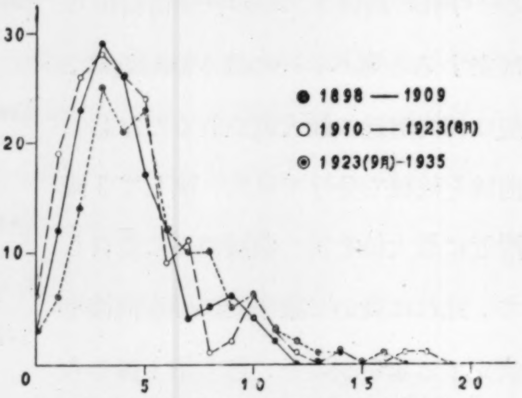

第3圖　期間別1ケ月地震回數頻度
縱軸：頻度，橫軸：1ケ月地震回數

又1ケ月 10 回程度發生する地震の多くは群生地震型であつて震央は殆ど一定の所から起るものが多い．勿論大正 12 年 9 月以後及び昭和6年9月の如き餘震群もあるが左樣でない場合にても群生地震と認められるものが多いのである．其例は

年　月	地震回數	震　央
明治 42 年 3 月	11	銚子沖より房總海中
明治 42 年 7 月	9	東京灣
明治 43 年 5 月	11	磐城沖
大正 4 年 5 月	10	房州西海岸
大正 4 年 11 月	18	三陸沖及び上總沖
大正 6 年 11 月	9	淸澄山東北側
大正 10 年 12 月	11	霞浦小貝川中間
大正 12 年 6 月	17	鹿島沖，銚子沖及び九十九里濱
昭和 3 年 5 月	16	千葉附近
昭和 6 年 6 月	11	三鷹北方
昭和 10 年 1 月	10	江戸川河口，多摩川
昭和 10 年 6 月	11	小貝川流域，房州沖
昭和 10 年 7 月	10	同　上

此等の地震群は頻度曲線の示すが如く，其の發生數は多い事はなく，37 年間に 10 回以上の有感地震のあつた月數は 33 回（餘震は除く）であり，約1ケ年に1回の割合となる．即ち東京附近においては有感覺地震は1ケ月 3～4 回を普通とし，1ケ年に1ケ月 10 回のものが1回發生する割合となつて居る．

又明治 31 年以來年每の回數の消長を見たのであるが，此れによると大正 12 年關東地震前は稍少きに對し，地震後は多少多い樣である．此れは以上述べた理由により地震後は特別の注意が地震に向けられた結果として必ずしも實相を傳へて居るものとは思へない．

なほ以上の表の製作は專ら保田囑託の努力に俟つものであり，玆に感謝の意を表するものである．

---

55. *Etudes statistiques sur les séismes observés à Tôkyô depuis 1876*

par

Mishio ISHIMOTO,

Institut de Recherches sur les Tremblements de terre.

Nous avons étudié surtout la fréquence des séismes ressentis à Tôkyô pendant la période 1898～1935. Nous constatons qu'il y a deux maxima dans la courbe de fréquence correspondant à 3 séismes et à 10 séismes par mois. Nous distingons très bien le premier et ses épicentres partagent dans la région de Kantô, tandis que deuxième apparu, ordinairement une fois par an, comme le groupe ayant ses épicentres dans la région limité.

---

56. *On the Slow Migratory Motion of the Volcanic Activity in Japan.*

By Torahiko TERADA,†

Earthquake Research Institute.

(Read Jan. 21, 1930.—Received Sept. 21. 1936.)

The regular sequence of activity from one volcano to another has often been pointed out by Omori and others and some real physical significance has been suggested to be attributed to this phenomenon. The problem has, however, not yet been subjected to any systematical investigation free from the danger of picking up an arbitrary sequence from an entirely irregular chaos of materials, an error which is often committed in similar cases. As a trial for the systematic investigation, the following procedure was taken.

The materials for the investigation were taken from the chronological list of the conspicuous eruptions of Japanese volcanoes given in the Rikwa Nenpyô, 1929. Taking the time (year) as the abscissa and the latitudes of the volcanoes as the ordinates, the conspicuous eruptions were plotted on the diagram as shown in Fig. 1. In the case when a volcano is recorded to have been active for an interval of several years, the interval is shown by the line.

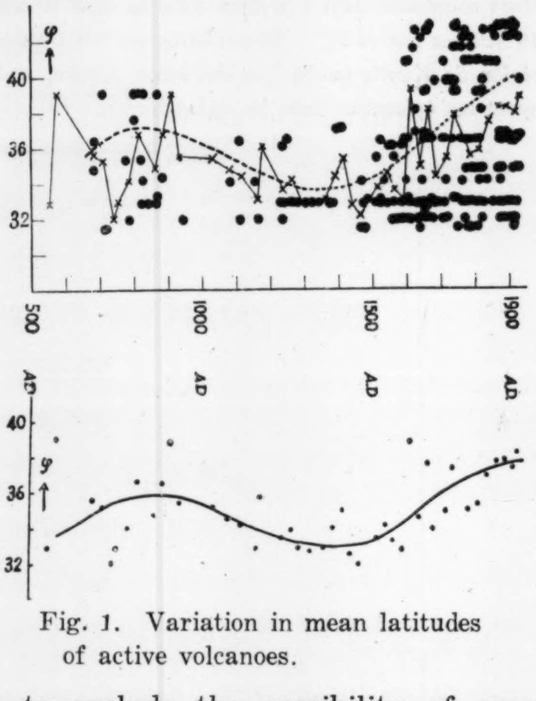

Fig. 1. Variation in mean latitudes of active volcanoes.

A glance on the diagram will show that the latitudinal migratory motion of activity, even if such may exist, is by no means simple one and that it will be entirely irrelevant to speak of any regularity from a few number of examples.

It seems, however, premature to exclude the possibility of some

† Professer Torahiko TERADA died on Dec. 31, 1935. This paper was written by him but has been left unpublished up to the present.

kind of regularity in the time-space distribution of volcanic activity and it will be worth while to attempt to seek after any possible clue which may be suggested.

In the previous paper by the present author and N. Miyabe it was shown that there seems to exist a long period fluctuation of the mean latitude of the seismically active zone of the world. It may, therefore, be suggested that some similar slow variation may also be found in the latitudinal migration of the volcanic activity. The dotted wavy lines are drawn tentatively to trace a possible fluctuation of the kind suggested. On the other hand, the mean latitude of the points in the diagram falling within each successive 25-years interval was calculated, excluding those volcanoes with their latitudes greater than 43° and less than 32°[1]. These mean latitudes are connected by a continuous curve at the foot of the diagram. In the interval 1600～1800 the general trend of the continuous curve seems to be nearly parallel to dotted wavy curves.

If the suggested dotted curves may be of any real significance, it will mean that the centres of activity are scattered on different latitudes and each centre is subjected to a periodic migratory motion in the *N-S* direction. In such case, the time variation of the mean value taken within a limited interval of latitude cannot always be parallel to the variation of the latitudes of the discrete centres. This consideration may explain the discrepancy between the dotted and continuous curves in the epoch later than 1800.

The comparison of the dotted curves with the curve showing the latitude variation of seismic activity[2] given in the previous paper cited is not much relevant, except that the supposed periods of variation are of the same order of magnitude.

On the other hand, the variation such as implied by the dotted waves be established as anything real, it will afford an invaluable clue for the nature of secular change going on in the earth crust. The alternation of the direction of motion of the activity may be connected with the change of relative motion of the surface crust and the inner core. Such a conjecture is in these days something more than an idle speculation, as the recent results of investigations of a number of astronomers and the secular change of the length of day makes such a relative motion highly probable.

---

1) The choice was made since the data of the volcanoes excluded date from a near past may be utterly defective.

2) T. TERADA and N. MIYABE, *Bull. Earthq. Res. Inst.*, **6** (1929), 333.

56. 本邦に於ける火山活動の移動に就て

地震研究所　寺　田　寅　彦

（本篇は故寺田寅彦先生の在世中書かれたものであるが，未だ發表されてゐないもので，先生の沒後筐底より發見された原稿である．原文には邦文の抄錄は附してない．）

理科年表所載の本邦に於ける火山活動の記錄を資料として，各年代に於いて活動した火山の平均緯度が年とともに如何なる變化を示すかを調べたのが本文の趣旨である．

結果として著しい事實が認められたわけではないけれども，長期に亘る緩徐な移動と，且つ左樣な火山活動の移動を生じ得べき一二の理由とについて述べてある．（宮部記）

57. *On the Displacement of the Tanna Fault since the Pleistocene.*[*,1)]

By Hisashi KUNO,

Geological Institute, Imperial University of Tokyo.

(Read Nov. 19th, 1935.—Received Sept. 21, 1936.)

Introduction.

The Tanna fault runs meridionally through the western slopes of the volcanoes that are arranged along the eastern coast of north Idu. Owing to its fresh fault-scarp topography, this fault has received considerable attention from geologists.[2)] At the time of the north Idu earthquake of November 26th, 1930, an earthquake fault appeared along the foot of the fault-scarp, accompanied by ground disturbances. It should interest geologists and seismologists to trace the geologic history of this fault and to compare its history with what occurred at the time of the earthquake.

The purpose of the present paper is to discuss the nature and the amount of displacement of the Tanna fault during geological times as deduced from geological and geomorphological observations made in the region. The conclusion reached is that, since the Pleistocene, the block on the western side of the fault has been displaced horizontally about 1 km southward and elevated about 100 meters in its southern part, relatively to the block on its east. The nature of this displacement is similar to that which occurred at the time of the earthquake of 1930.

This fault traverses the centre of the Tanna basin, which is a circular depression about 2 km across. The underground structure of this basin was fully investigated along the wall of the Tanna railway tunnel, which was excavated underneath the basin, details of which have been already given in an earlier paper.[3)] The main topic discussed in this paper is the relation between the geomorphological development of the basin and the Tanna fault displacement.

---

* Communicated by S. TSUBOI.

1) Already published in Japanese: H. KUNO, *Geogr. Rev. Japan*, **12** (1936), 18.

2) N. YAMASAKI, *Jour. Geol. Soc. Tokyo*, **26** (1919), 165.
T. WATANABE, "On the Geology of the Tanna Basin." (Published by the Railway Department in 1925).

3) H. KUNO, *Bull. Earthq. Res. Inst.*, **14** (1936), 92.

Acknowledgement.

My geological survey of the northern part of Idu Peninsula, a part of the results of which forms the topic of this paper, was carried out under the auspices of the Earthquake Research Institute, Tokyo Imperial University. To the Director and members of the staff of the said Institute I wish to take this opportunity of offering my heartiest thanks for many courtesies received, particularly to Professor Dr. Seitarô TSUBOI who was so kind as to go over my manuscript.

Outline of the Geology and Geomorphology of the District.

The district concerned in this paper, which occupies the eastern half of north Idu, is a mountainous land situated between the Kanô-gawa plain and Sagami Bay. Its general topography is shown in the map Fig. 1.

The figure shows only the contour lines for every 100 meters as reproduced from the 1/50,000 topographic maps "Atami" and "Numadu", published by the Land Survey Department. For further details, the reader is referred either to the original maps or to the 1/25,000 maps "Atami", "Aziro", "Misima", and "Nirayama", published by the same Department.

In this district, three partly demolished volcanic cones of lower Pleistocene age are built upon a foundation of thick accumulations of Tertiary volcanic rocks. These volcanoes, enumerated from the south, are Taga, Yugawara, and Hakone. They were erupted in the order named.

The semi-circular ridge that runs from a point south of Aziro, through Yamabusi-tôge, to a point north of Kuro-dake (Fig. 1), corresponds to that part forming the southern to the western margin of the caldera of the Taga volcano. A gentle periclinal slope of the volcano is still preserved outside of this caldera margin. The semi-circular ridge that runs from a point northeast of Atami-mati, through Iwato-san and Zyukkoku-tôge, to Kurakake-yama of the Hakone district (situated beyond the northern limit of the map Fig. 1), corresponds to that part forming the southern to the western margin of the caldera of the Yugawara volcano. Outside of this caldera margin, mostly in the western part, a gentle periclinal slope of the volcano is still preserved. Thus the western slopes of these two adjacent volcanoes form one continuous slope on the western side of the main ridge, or divide, that runs meridionally through the middle of the map Fig. 1. In the northern extension of this slope the contour lines change their directions to

NW–SE. This area corresponds to the southwestern slope of the Hakone volcano. In the map Fig. 1, the boundaries between these three volcanoes are marked with broken lines.

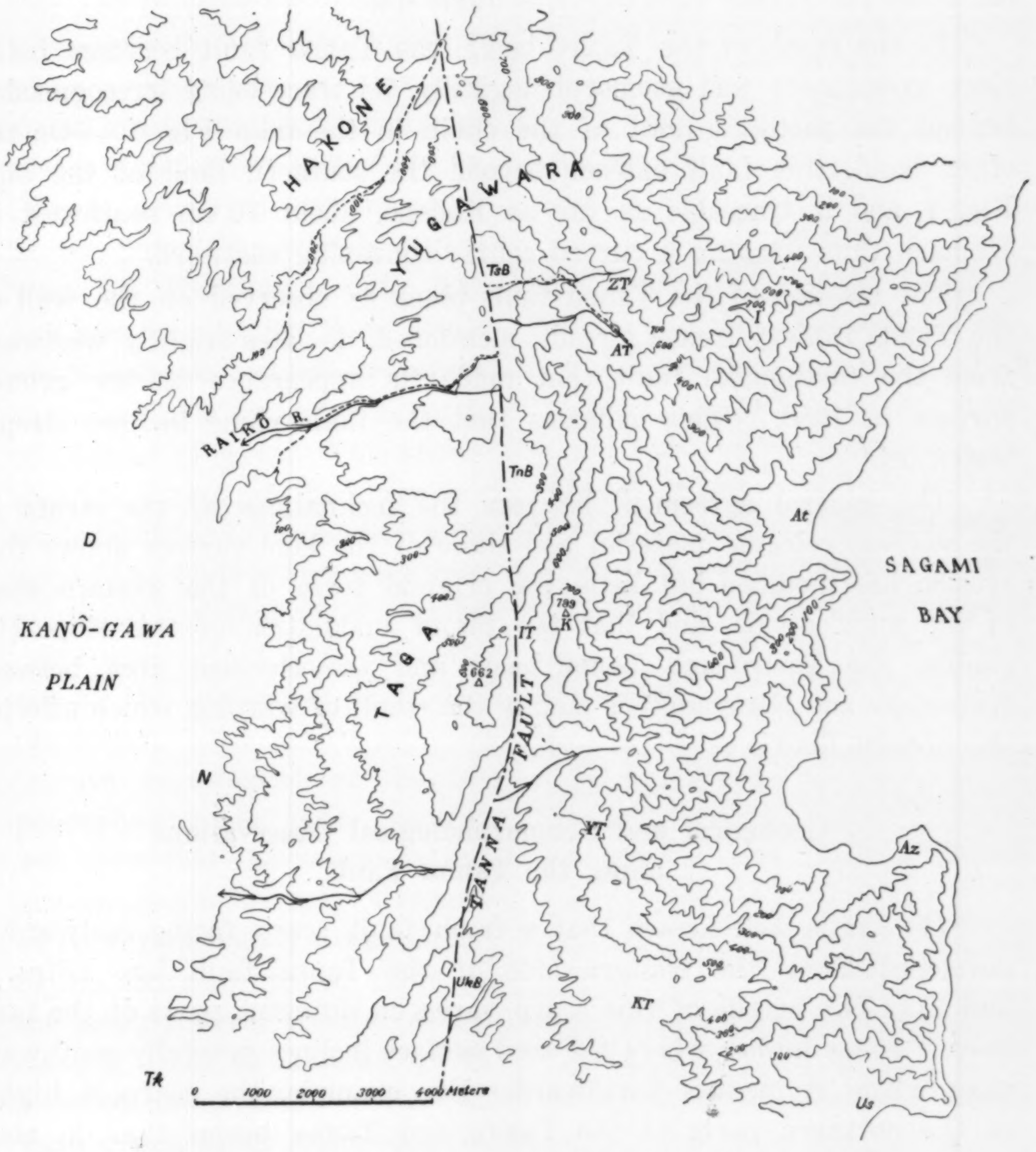

Fig. 1. Topographical map of the north Idu district. The figure shows only the contour lines for every 100 meters. Full lines—river courses. Broken lines—boundaries between the volcanoes. Chain—Tanna fault line.
At—Atami-mati, Az—Aziro, Us—Usami,
ZT—Zyukkoku-tôge, AT—Atami-tôge, K—Kuro-dake,
YT—Yamabusi-tôge, KT—Kameisi-tôge,
TsB—Tasiro basin, TnB—Tanna basin,
IT—Ikenoyama-tôge, UkB—Ukihasi basin,
D—Daiba, N—Nirayama, Tk—Takyô.

The Tanna fault, with which this paper is concerned, traverses meridionally the central part of the slope on the western side of the main divide just mentioned (shown with a chain in Fig. 1). Three circular or elliptical depressions, Tasiro, Tanna, and Ukihasi (enumerated from the north) lie along this fault line.

To the north of the Tasiro basin, the Tanna fault becomes indistinct, geologically and geomorphologically, its trace being irrecognizable beyond the northern limit of the chain in the map Fig. 1. On the other hand, this fault extends beyond the southern limit of the map Fig. 1, and is traceable as far as Kadono, about 10 km southwest of Ukihasi, thus forming a curved course convexing eastward.

The position of the Tanna fault plane as observed on the wall of the Tanna railway tunnel already mentioned, deviates slightly westward from the earthquake fault that made its appearance on the ground surface in 1930. This indicates that the fault plane inclines steeply westward.[4]

The general agreement between the inclinations of the strata of the various volcanic material and those of the land surface shows that erosion has modified but little the original form of the western slope of the main divide, and that the major undulation of this slope (including the Tasiro and Tanna basin and the elevated area between Kuro-dake and Nirayama) is mainly the result of warping which affected the present district.

Geological and Geomorphological Observations along the Tanna Fault.

(1) It is well known that a fresh fault scarp facing eastward is developed along the western side of the Tanna fault line (Figs. 1 and 2). The height of this scarp varies in different parts of the fault line, it being higher where the land surface inclines generally southward than where it inclines northward. For example, the scarp is higher in the northern parts of the Tasiro and Tanna basins than in their southern parts (cf. Fig. 2). Moreover, the scarp is almost irrecognizable on the northern side of Ikenoyama–tôge, while it attains to a considerable height on the southern side, namely, between Ikenoyama–tôge and Ukihasi.

It is worthy of note that the scarp at the northwestern corner of the Tasiro basin disappears a short distance northward, thus assuming the form of a depressed triangle (cf. Fig. 2).

4) H. KUNO, *Bull. Earthq. Res. Inst.*, **14** (1936), 101.

(2) The gentle slope that spreads out on the western side of the Tanna fault is dissected by numerous valleys directed westward. A few of these valleys extend their channels up to the Tanna fault line and traverse the fault scarp, giving rise to windgap topographies. Examples of this are found in two southern tributaries of the Raikô river, east of Daiba (Fig. 1), which traverse the scarp at two points immediately southwest of Karuisawa (Fig. 2), and also in a valley 2 km south of Nirayama, which traverses the scarp at a point 2 km north of Ukihasi (Fig. 1). This shows that these channels had been extended further to the eastern area before the fault scarp came into existence, and that their eastern parts were cut off from the western by the subsequent fault displacement.

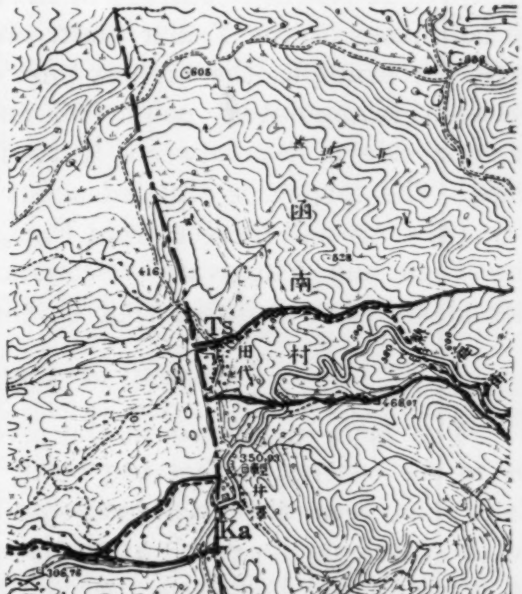

Fig. 2. Topographical map (1/50,000) of the neighbourhood of the Tanna and Tasiro basins. The heights are expressed in meters. Ts—Tasiro, Ka—Karuisawa, Tp—Tanna primary school, Ta—Tanna, Ni—Niiyama, Ik—Ikenoyama-t ge, Ku—Kuro-dake.

An examination of the topographical maps Figs. 1 and 2 will show that the valleys in the eastern area, which may be regarded as corresponding respectively to the above-mentioned three in the western area, are the valley running from Zyukkoku-tôge to a point immediately north of Tasiro, that from Atami-tôge to a point immediately south of Tasiro, and that from a point north of Yamabusi-tôge to a point 3 km south of Ikenoyama-tôge. In Figs. 1 and 2, these valley courses on both sides of the fault are marked by full lines. It is important to note that every valley course marked in these figures on

the western side of the fault is invariably situated about 1 km south of the corresponding one on the eastern side.

(3) A marked contrast in the distribution of land reliefs is noticed on both sides of the Tanna fault. In the neighbourhood of Ikenoyama-tôge, for example, the highest part of the land on the western side lies between triangulation point 662 meters and Nirayama, while on the eastern side it lies between Kuro–dake (799 meters) and Ikenoyama-tôge. The former is situated about 1 km south of the latter.

(4) As will be seen from Figs. 1 and 2, the boundary line between the Taga and Yugawara volcanoes on the western side of the fault lies about 1 km south of that on the eastern side.

Amount of Fault Displacement.

The facts mentioned in the preceding paragraphs (2) .... (4) lead us to the conclusion that the block on the western side of the Tanna fault has been displaced horizontally about 1 km southward relatively to the block on its east[5] after the present district had been subjected to warping and had been dissected by consequent valleys. This alone, however, is insufficient to explain the unequal height of the fault scarp mentioned in (1) of the preceding chapter.

In order to eliminate the effect of the above–mentioned horizontal displacement from the present topography and the distribution of the rocks, the map Fig. 1 was modified in the following way. The map was cut into two parts along the Tanna fault line, and the western part displaced northward along the fault line for a distance corresponding to 1 km, after which the two parts were again joined to each other. Each contour line in one part of the map was again joined to the corresponding one in the other across the fault line. The complete map thus obtained is shown in Fig. 3. The valley courses, the boundaries between the volcanoes, and the Tanna fault line, are marked as in Figs. 1 and 2.

In this map, the three valleys in question are seen to run along quite simple courses across the fault line, and the southern boundary of the Yugawara volcano is represented by a smooth line. Moreover, the highest parts of the neighbourhood of Ikenoyama–tôge are disposed symmetrically on both sides of the fault line.

On the other hand, the map Fig. 3 shows a fault scarp topography

5) From the distribution of valley courses in the neighbourhood of the Tasiro basin, Y. OTUKA also inferred the southward displacement of the block on the western side of the Tanna fault (Y. OTUKA, *Bull. Earthq. Res. Inst.*, **11** (1933), 555). He gives the amount of this displacement as 4 km, which however is a misprint for 1 km.

developed symmetrically on both the northern and southern sides of Ikenoyama–tôge. Along this scarp, a marked discontinuity is seen in the slope of the Taga volcano. Thus, if the surface of the slope on the western side of the scarp were produced eastward, this imaginary

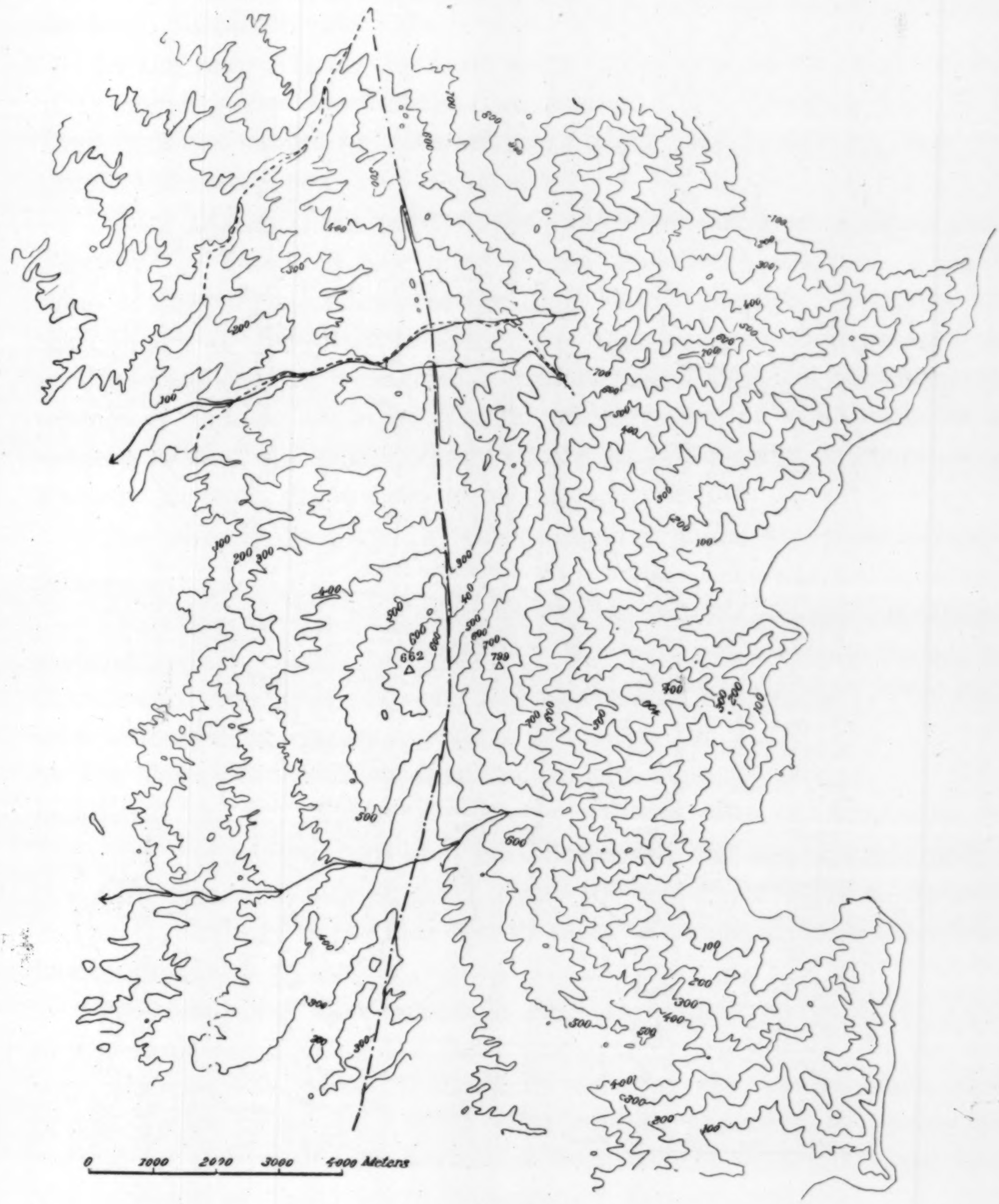

Fig. 3.

plane would pass above the actual surface of the slope on the eastern side. Therefore, it may be inferred that the western block here has been elevated relatively to the eastern block, the amount of which

elevation is estimated to be about 100 meters or more.

In order to eliminate the effect of the above-mentioned vertical displacement, the map Fig. 3 was modified so as to represent a topography in which the block on the western side of the fault has sunk

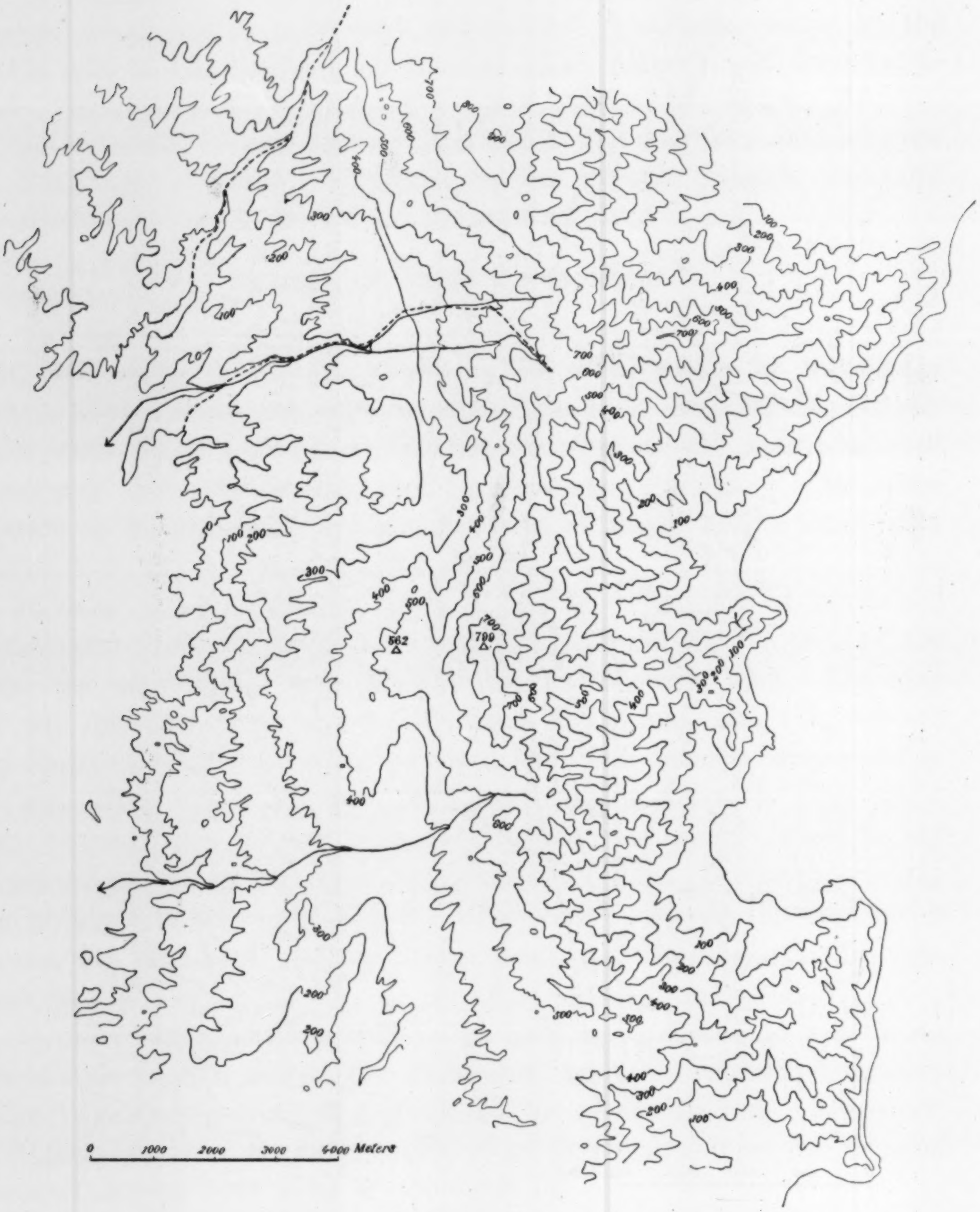

Fig. 4.

100 meters uniformly throughout the whole length of the fault from the position shown in Fig 3. Each contour line of the western block of Fig. 3 was reduced 100 meters in altitude, and again joined to the

corresponding lines of the eastern block. The map thus obtained is shown in Fig. 4, in which the valley courses and the boundaries between the volcanoes are marked as in the preceding figures. This map may be regarded as approximately representing the topography in which the effects of both horizontal and vertical (uniform vertical displacement assumed) displacements have been eliminated.[6)]

In the map Fig. 4, the fault scarp topography in the neighbourhood of Ikenoyama–tôge has mostly disappeared. The western slope of the Taga volcano shows no discontinuity, being represented by that of a simple volcanic cone.

Along the northern part of the fault line, however, a scarp facing westward is found on the slope of the Yugawara volcano. Here the slope of the volcano shown in the map Fig. 3 is more continuous than that shown in the map Fig. 4. This fact suggests that scarcely any vertical displacement occurred in the northern part of the fault line, whence it follows that the amount of elevation of the block on the western side of the fault, which attains to 100 meters or more in the southern district, diminishes as one goes northward.

The discussions given in the foregoing pages are summarized as follows:

The slopes of the Taga and Yugawara volcanoes were subjected to warping, which caused subsidence of the Tanna and Tasiro basins and elevation of the area between Kuro–dake and Nirayama. The slopes were dissected by consequent valleys. Later, the district was disturbed by the Tanna fault which occurred in the central part of the above-mentioned slopes. The block on the western side of this fault was displaced horizontally about 1 km southward for the greater part of the fault line, and was elevated about 100 meters or more in its southern part, relatively to the block on its east. This elevation of the western block diminishes in amount toward the northern part of the fault line.

The foregoing view makes it easy to explain the unequal height of the fault scarp along the fault line (cf. (1), p. 622). In the same way, the peculiar shape of the fault scarp at the northwestern corner of the Tasiro basin (cf. (1), p. 622) may be explained as having been formed by the southward horizontal displacement of the western block. The absence of fault scarp topography farther north of the Tasiro basin may be partly due to the smallness of the vertical displacement.

It is interesting to note that the fault displacement that occurred

6) Although the effects of the displacements have been eliminated, that of the erosion which acted intensely along the fault line may be remained.

at the time of the earthquake of 1930, is very similar in character to the above–mentioned displacement that occurred in geological times. Thus, according to C. TSUBOI[7] and Y. OTUKA,[8] the block on the western side of the Tanna earthquake fault was displaced horizontally 2 or 3 meters southward, and was slightly depressed in the northern district (north of the Tanna basin) and elevated in the southern (south of the Ukihasi basin), relatively to the block on its east. It will be seen that the fault displacement that occurred at the time of the recent earthquake is a repetition of the fault activity that has taken place in geological times.

Although in the foregoing pages, the fault displacement has, for convenience, been discussed as if it had occurred in two distinct directions, horizontal and vertical, it is scarcely nescessary to add that, actually, the displacement must have occurred in a direction generally with both horizontal and vertical components.

History of the Tanna Fault.

In the northwest of the Ukihasi basin, the surface of the fault scarp is covered by gravel beds that show, although indistinctly, horizontal stratification planes. The pebbles are slightly water-worn and subangular in form. The manner in which these pebbles are arranged shows that these gravel beds were deposited by a river that ran from north to south. This river was probably formed along the Tanna fault line which had then made its appearance. The presence of the gravel beds almost up to the top of the scarp indicates that the former was already deposited during the earliest stage of the fault activity and was later uplifted. The probability is therefore strong that the fault displacement was accomplished, not in a short time, but intermittently through a long period of time.

As the eruption of the Taga volcano dates to lower Pleistocene, it follows that the fault displacement is post–lower Pleistocene in age. As to whether or not the fault existed prior to the eruption of the Taga volcano, scarcely anything is known.

Geomorphological Development of the Tanna Basin.

The origin of the Tanna basin has been the subject of much debate by previous writers. Most of these writers seem to have overstressed the importance of the Tanna fault displacement as a factor in the

7) C. TSUBOI, *Bull. Earthq. Res. Inst.*, **9** (1931), 271.
8) Y. OTUKA, *Bull. Earthq. Res. Inst.*, **11** (1933), 530.

geomorphological development of the basin. However, as already mentioned, it is highly probable that the basin had subsided prior to the fault displacement. Besides, it should not be overlooked that the fault in question passes through the centre of the basin. This fact, taken together with the nature of the fault displacement, suggests that the geomorphology of the basin can hardly be explained by the fault displacement alone.

The observations on the Tanna district and along the wall of the Tanna tunnel have yielded ample data on the geologic structure of the basin, a detailed account of which has been already given in an earlier paper,[9] so that only the results of the observations are given here in brief.

The strata of volcanic material, that make up the Taga volcano and the Hata beds lying underneath the former, incline gently toward the centre of the basin, roughly agreeing with the surface topography. They probably form a syncline or a basin structure. The Tanna fault in question traverses the centre of this basin structure. The relative vertical displacement of the strata caused by the fault is apparently slight. Along the eastern margin of the basin, we find a set of meridional faults closely spaced to each other, the blocks on the western side of which are down-faulted stepwise toward the basin (see Fig. 1, paper just cited).

From these facts, it may be inferred that the Tanna basin is a structural basin formed chiefly through down-warping of the slope of the Taga volcano. Probably, the basin thus formed was rather simple in topography. The subsidence of the basin may have been augmented by dislocation caused by the step-faults along its eastern margin.

Later, the basin was traversed by the Tanna fault through its centre. As a result of this fault displacement, which occurred mostly in a horizontal direction, the basin was changed somewhat with complexity added to its topography. Thus, the hill which now lies back of the Tanna primary school (see Fig. 2), and which once formed a part of the more northerly lying mountain, was projected southward into the basin. The gently sloping area that now forms the background of Niiyama, southwest of the basin, was at one time situated in the central part of the basin. It was displaced southward and elevated slightly by the fault displacement. This view is supported by the occurrence in this area of a lacustrine deposit, consisting of stratified clays, up to a point about 100 meters above the present surface of the

9) H. KUNO, *Bull. Earthq. Res. Inst.*, **14** (1936), 101.

basin.

Although it is emphasized in the foregoing discussion that the fault displacement itself played only a subordinate role in the development of the Tanna basin, it is not to be overlooked here that all the three basins, Tasiro, Tanna, and Ukihasi, are arranged on the fault line. This fact suggests that the genesis of these basins has something to do with the Tanna fault.

Summary.

Warping of the slopes of the Taga and Yugawara volcanoes (lower Pleistocene) caused subsidence of the Tanna and Tasiro basins and at the same time elevation of the area between Kuro–dake and Nirayama. Later, this district was affected by the Tanna fault. The block on the western side of the fault was displaced about 1 km horizontally southward for the greater part of the fault line, and was elevated about 100 meters or more in its southern part, relatively to the block on its east.

The fault displacement that occurred at the time of the earthquake of 1930 is similar in character to the above–mentioned displacement that occurred in geological times.

The fault displacement itself is not the sole cause of the origin of the Tanna basin. This basin was formed chiefly through down–warping of the volcanic slope. As a result of the fault displacement, the topography of the basin became somewhat more complex than it had been before.

Addendum.

It is interesting to note that the horizontal component of the Tanna fault displacement attains to nearly 10 times that of the vertical. Displacement with dominant horizontal component along an almost vertical fault plane is often caused by differential movements of the front of an overthrusting block. But the Tanna fault is quite independent of any thrust faults.[10]

The importance of the horizontal component in an ordinary fault displacement seems generally to be overlooked. For example, when a series of monoclinal strata is displaced by a dip-fault, and an older stratum on one side of the fault comes into contact with a younger on another side, the block on the side of the older stratum is inferred as

10) S. AWADI recognized horizontal displacements in several NW-SE faults on the slope of the Yugawara volcano east of the Tasiro basin (T. TSUJIMURA and S. AWADI, *Geogr. Rev. Japan*, **10** (1934), 1122). It is probable that fault displacements with dominant horizontal components are common in north Idu and adjacent district.

having been elevated relatively to the block on the other side. But this inference is not necessarily correct if the horizontal component in the fault displacement is taken into consideration. The same result should obtain when the block on the side of the older stratum is displaced horizontally toward the direction of the dip of the strata. It follows therefore that the true direction of a fault displacement cannot be inferred merely from the contact relation of rocks of different ages at one point alone, or from the manner of displacement of a series of monoclinal strata.

---

57. 更新世以後に於ける丹那斷層の運動に就いて

東京帝國大學
地質學教室　久　野　久

丹那斷層に沿ふた地域に於ける地質學的並に地形學的觀察の結果を基にして，更新世以後に於ける本斷層の運動を推定した．其の結果，斷層の西側の地塊は，東側の地塊に對して，南方に向つて約1km 水平に移動し，且つ本斷層線の南部（浮橋—池ノ山峠間）に於いて約100 m 若くばそれ以上隆起して居る事が判明した．

此の地質時代に行はれた斷層運動は昭和5年（1930 年）11 月の北伊豆地震の際の丹那斷層の運動と其の性質が極めて類似して居る．

丹那斷層の運動そのものは，丹那盆地成因の根本的要素ではない．同盆地は多賀火山の斜面に働いた撓曲によつて沈降したものである．丹那斷層の運動の結果は本盆地の地形を以前より複雜にしたに過ぎない．

---

58. *Determination of Elastic Constants of Soils by means of Vibration Methods.*

Part I. Young's Modulus.

By Mishio ISHIMOTO and Kumizi IIDA,

Earthquake Research Institute.

(Read Sept. 15, 1936.—Received Sept. 21, 1936.)

1. Introduction.

Since the research of Prof. F. Omori[1] it has been noticed that earthquake motions show different properties according to the geologic or topographic conditions of the regions in which the seismic disturbances are experienced. Recently the same subject was also studied by means of the acceleration seismograph, and the proper period of the ground was determined.[2]

When an earthquake takes place and the seismic waves produced at the hypocenter arrive at the surface of the earth's crust, it is considered that they cause an excitement of the frequent vibration due to the proper elastic properties of the surface layer of each place. This kind of vibration is frequent mostly in the earthquake motion. We wish to explain the reason why each region has its proper period of vibration. It is believed that the vibration of the surface layer, in which the moduli of elasticity are comparatively small, resolves into the proper vibration of each place. It will thus be seen that most of the vibrations of the surface layer are included in the earthquake motion. In order to know the properties of the earthquake motion, a study of the properties of soils in the surface layer of the earth's crust seems to be one of the most important matters of investigation. Therefore we intend to investigate the properties of soils, the present experiments being the first step in the direction above pointed out.

It is difficult to ascertain distinctly the properties of soils in the surface layer owing to such various causes as heterogeneity, moisture

1) F. OMORI, *Pub. Earthq. Inv. Com.*, **10** and **11** (1902).

2) M. ISHIMOTO, *Bull. Earthq. Res. Inst.*, **10** (1932), 171; **12** (1934), 234; **13** (1935), 592; **14** (1936), 240.

T. SAITA and M. SUZUKI, *ditto*, **12** (1934), 517.

N. NASU and T. HAGIWARA, *ditto*, **14** (1936), 290.

content, pressure, etc. In order to discover the complicated properties of surface layers, homogeneous soils were selected as being readily accessible. For the purpose of investigation of the distinct properties of soils the present experiments were carried out in the laboratory by using the boring-matters taken out in the natural state from the sub-surface soil of some regions.

Studies of the elastic properties of soils have in the past been made in our country,[3] but most of them have been carried out by the static method. Studies of soils by means of the dynamic method do not seem to have been made. Since soils are known as visco-elastic substances,[4] the results obtained by each method, that is, static or dynamic method, are considered to be different from each other. In the present experiments we investigated the elastic properties of soils by means of the dynamic method, and determined the velocity of the longitudinal wave in the soils. From the velocity thus obtained, Young's modulus of soils was calculated. According to the results of these experiments it was found that the moduli of elasticity of soils obtained by the present experiments are in good agreement with those obtained by the field measurements of the velocity of elastic waves generated by falling bodies.[5]

2. Mechanical Analysis of Soils.

By means of the method of mechanical analysis adopted by the

Table I. Mechanical Analysis of Soils.

Source of soil	Mesh number (Tyler's standard sieves)						Silt grain size 0·05～0·01 mm %	Clay grain size 0·01～0 mm %	Porosity %	Density app.	Density real	Mois. Cont. %
	8	14	28	48	100	200						
	%	%	%	%	%	%						
Maru-no-uti	0·58	0·40	0·60	1·18	1·50	2·34	24·92	68·48	73·15	1·46	2·660	50·0
Hongô	2·10	3·76	7·14	8·38	11·24	1·76	21·84	34·78	73·85	1·44	2·632	52·3
No. 1	0	0·02	0·14	0·32	2·04	17·60	46·20	33·60	51·50	1·838	2·717	24·15
No. 2	0	0	0·06	0·48	1·36	2·02	11·94	84·14	41·93	2·06	2·551	28·09

3) See *Bull. Geotechnical Committee, Government Railways*, **1** (1931); **2** (1932); **3** (1934); **4** (1936); (in Japanese).

A. TAKATA, *Publ. Res. Office of Public Works, Department of Home Affairs*, **20** (1931), 1, (in Japanese).

4) M. ISHIMOTO and K. IIDA, *Bull. Earthq. Res. Inst.*, **14** (1936), 534, (in Japanese).

5) N. NASU, T. HAGIWARA, and S. OMOTE, *ditto* **14** (1936), 560, (in Japanese).

Geotechnical Committee of the Government Railways of Japan, the mechanical analysis of the sedimentary soils to be tested was carried out. The results are shown in Table I. The sedimentary soils to be tested were of 5 kinds, that is, the soils taken from underground in Hongô, Imperial University, Maru-no-uti,[6] Komatugawa,[7] and two other kinds No. 1 and No. 2.[8] The two last-named soils have been used for the other experiments. On the basis of the results of mechanical analysis, the soils were divided into 4 classes, that is, clay, silt, silty-clay and loam. The soils taken from Maru-no-uti and Komatugawa belong to the class of silty-clay and silt respectively and that taken from Hongô belongs to the class of loam. The other two soils belong to the class of clay and loam.

3. Theoretical Treatment.

Take the x- and y-axis horizontally and the z axis vertically upwards, the origin being at the bottom of a prismatic bar (Fig. 1). The equation of motion for the longitudinal wave in the bar, is expressed by

$$\rho\frac{\partial^2\zeta}{\partial t^2}=E\frac{\partial^2\zeta}{\partial z^2}+\gamma\frac{\partial^3\zeta}{\partial z^2\partial t},\text{[9]} \qquad (1)$$

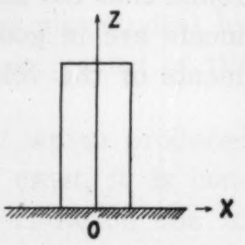

Fig. 1.

in which ζ is the displacement in the direction of z, t the time, ρ the density, and E, γ Young's modulus, the coefficient of solid viscosity (or internal friction) respectively.

Put

$$\zeta=Ae^{ifz-\omega t}, \qquad (2)$$

then substitute this in (1), under the following boundary conditions of free vibration of clamped- and free-end bar, the height of which is h,

$$\left.\begin{array}{ll} z=0; & \zeta=0, \\ z=h; & \dfrac{\partial\zeta}{\partial z}=0, \end{array}\right\} \qquad (3)$$

we have $\omega=\dfrac{\gamma f^2}{2\rho}\pm i\sqrt{\dfrac{Ef^2}{\rho}-\left(\dfrac{\gamma f^2}{2\rho}\right)^2}$, and

6) See T. SAITA and M. SUZUKI, *Bull. Earthq. Res. Inst.*, **12** (1934), 517.
7) See N. MIYABE, *Bull. Earthq. Res. Inst.*, **14** (1936), 543.
8) See M. ISHIMOTO and K. IIDA, *Bull. Earthq. Res. Inst.*, **14** (1936), 534.
9) The similar equation has already been quoted by T. Fukutomi, *Bull. Earthq. Res. Inst.*, **12** (1934), 498.

$$\zeta = Ae^{-\frac{\gamma f^2}{2\rho}t}\cos\left\{\sqrt{\frac{Ef^2}{\rho}-\left(\frac{\gamma f^2}{2\rho}\right)^2}\,t-\alpha\right\}\sin fz, \tag{4}$$

$$f=\frac{2r-1}{2h}, \qquad r=1,\ 2, \ldots .$$

where $\frac{2\pi}{f}$ is the wave length and A is the constant.

Next we consider the forced vibration of this system. We assume the motion of the floor, on which the prismatic bar is placed, as

$$\zeta = Ce^{ipt}, \tag{5}$$

then the particular solution of (1) may be written

$$\zeta = C\,D(z)\,e^{ipt}, \tag{6}$$

where D is a normal function. Substituting this in (1), we get

$$\left.\begin{aligned}\frac{\partial^2 D}{\partial z^2} &= -f'^2 D,\\ f'^2 &= \frac{p^2}{\dfrac{E}{\rho}+ip\dfrac{\gamma}{\rho}}.\end{aligned}\right\} \tag{7}$$

Put

$$\varepsilon = \frac{1}{2}\frac{\gamma}{\rho}f^2, \quad n^2=\frac{E}{\rho}f^2, \tag{8}$$

then we obtain

$$f' = \frac{fp}{(n^4+4p^2\varepsilon^2)^{\frac{1}{4}}}\left\{\sqrt{\frac{1}{2}\left(1+\frac{n^2}{\sqrt{n^4+4p^2\varepsilon^2}}\right)}-i\sqrt{\frac{1}{2}\left(1-\frac{n^2}{\sqrt{n^4+4p^2\varepsilon^2}}\right)}\right\}.$$

For the sake of simplicity we write this equation in the form of $f_1 - if_2$. (9)

As the boundary conditions are such that

$$\left.\begin{aligned} z=0;\quad & D=1,\\ z=h;\quad & \frac{\partial D}{\partial z}=0,\end{aligned}\right\} \tag{10}$$

we substitute these conditions in (7), and get

$$D=\cos f'z+\tan f'h\sin f'z, \tag{11}$$

or

$$D=\cos f_1 z \cosh f_2 z + \frac{1}{\vartheta}(\sin f_1 h \cos f_1 h \sin f_1 z \cosh f_2 z$$

$$-\cos f_1 z \sinh f_2 z \sinh f_2 h \cosh f_2 h) + i\Big\{\sin f_1 z \sinh f_2 z$$

$$-\frac{1}{\vartheta}(\sin f_1 h \cos f_1 h \cos f_1 z \sinh f_2 z + \sin f_1 z \cosh f_2 z \sinh f_2 h \cosh f_2 h)\Big\}, \quad (12)$$

where, $\vartheta = \cos^2 f_1 h \cosh^2 f_2 h + \sin^2 f_1 h \sinh^2 f_2 h.$

Substituting (12) in (6), we obtain

$$\left.\begin{aligned} &\zeta = C(\zeta_1 + i\zeta_2)e^{ipt}, \\ &\zeta_1 = \cos f_1 z \cosh f_2 z + \frac{1}{\vartheta}(\sin f_1 h \cos f_1 h \sin f_1 z \cosh f_2 z \\ &\qquad -\cos f_1 z \sinh f_2 z \sinh f_2 h \cosh f_2 h), \\ &\zeta_2 = \sin f_1 z \sinh f_2 z - \frac{1}{\vartheta}(\sin f_1 h \cos f_1 h \cos f_1 z \sinh f_2 z \\ &\qquad + \sin f_1 z \cosh f_2 z \sinh f_2 h \cosh f_2 h). \end{aligned}\right\} \quad (13)$$

The displacement of forced vibration in the bar is given by this equation. The ratio of its amplitude to that of motion of floor is also given by

$$R = \sqrt{\zeta_1^2 + \zeta_2^2}. \quad (14)$$

The relation between R and $u = \frac{n}{p} = \frac{T_p}{T}$ in the case $z=h$ is shown in Fig. 2, in which T_p, T being the period of forced vibration and of the bar respectively and k the damping ratio of the bar deduced from the equation

$$\log_e k = \frac{\pi}{\sqrt{n^2/\varepsilon^2 - 1}}. \quad (15)$$

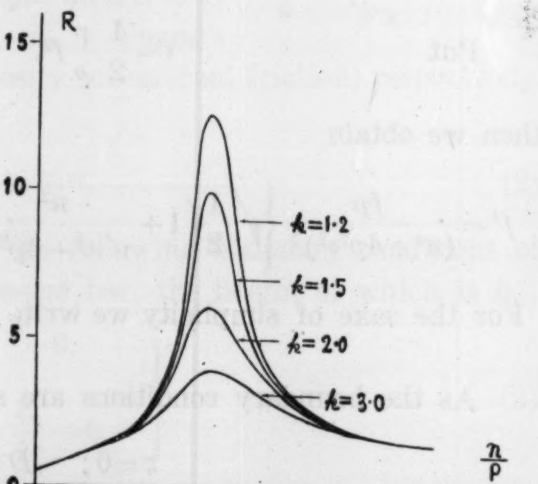

Fig. 2. Relation between R and $\frac{n}{p}$ in damped longitudinal vibration of the bar at $z=h$.

As will be seen from Fig. 2, R takes the maximum value when n/p becomes 1. It is believed that the state in which R becomes great is the phenomenon of resonance. Consequently, in resonance, the amplitude of vibration of

the bar becomes the greatest and the period of forced vibration coincides with that of free vibration of the bar. Therefore the period of free vibration of the bar can be determined in the case of forced vibration. The period of free vibration of the bar, that is, the period of resonance vibration, T, is given by

$$T = \frac{4h}{(2r-1)\sqrt{\dfrac{E}{\rho} - \dfrac{(2r-1)^2\pi^2\gamma^2}{16\rho^2h^2}}}. \qquad (16)$$

An example of the relation between the fundamental period T and the height h is shown in Fig. 3, in which we take T as ordinate and h as abscissa. The larger the value of the solid viscosity coefficient, the more the line in question curves and deviates from the ideal condition. When the soild viscosity coefficient attains a certain value, the

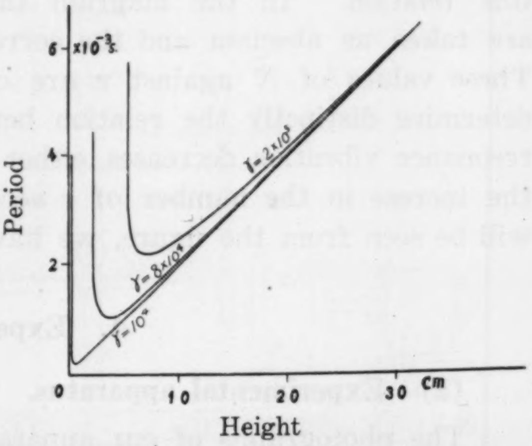

Fig. 3. Relation between the fundamental period of resonance vibration, T, and the height of the bar, h. In this case $\rho=1{\cdot}5$, $\sqrt{\dfrac{E}{\rho}}=200$ m/sec.

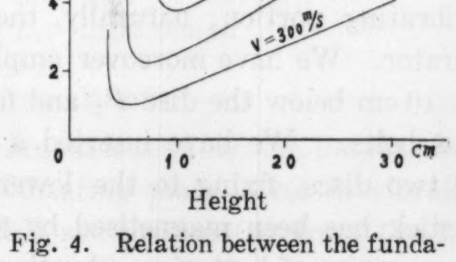

Fig. 4. Relation between the fundamental resonance period T and the height h. In this case $\rho=1{\cdot}5$, $\gamma=2\times10^5$.

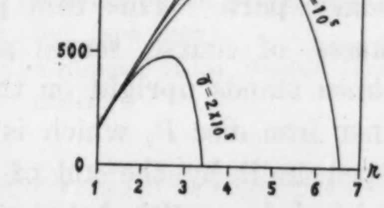

Fig. 5. Relation between the resonance frequency of the bar and the order r of its partials. In this case $\rho=1{\cdot}5$, $v=200$m/sec, $h=30$cm.

proper period T becomes infinitely great. In Fig. 4, however, we take

the velocity $v=\sqrt{\frac{E}{\rho}}$ as a parameter, and the solid viscosity coefficient γ is kept constant.

Further, we consider the relation between the frequency of the vibration, N, and the order of partials. Fig. 5 is the diagram showing this relation. In the diagram the values of r ($r=1, 2, 3, \ldots\ldots$) are taken as abscissa and the corresponding values of N as ordinate. These values of N against r are combined with a curve in order to determine distinctly the relation between them. The frequency of the resonance vibration decreases either slowly or somewhat rapidly, with the increse in the number of r according to the magnitude of γ. As will be seen from the figure, we have only 3 partials when $\gamma=2\times10^5$.

4. Experiments.

(a) Experimental apparatus.

The photographs of our apparatus used in the present experiments are shown in Figs. 6 and 7, and also a schematic diagram of the arrangement of the apparatus is shown in Fig. 8. As will be seen from these figures, the principal parts of this apparatus consist of a vibrating iron plate, on which the soil specimen S stands upright, and a connection circuit of a motor-generator M–D_1, that produces variable frequencies of electric current to provoke the vibration of the iron plate. The idea[10] of our experiment is to give the various frequency of vibration at the foot of the soil specimen, and to find the fundamental resonance frequency and then the elastic constant of the soils computed therefrom. The particular characteristics of our apparatus are described in the following:

Vibrating plate. We have adopted a circular steel disc P_1 of 23·7 cm in diameter; the middle concentric part of which is thinner than its boundary part. This thin part, 11·0 cm in diameter and 0·5 cm in thickness, of course, serves as a vibrating portion; naturally, the soil specimen stands upright on this vibrator. We have moreover employed another iron disc P_2 which is about 10 cm below the disc P_1 and firmly clamped to it by the aid of 4 brass bolts. We have inserted a solid cylindrical iron stick between these two discs, fixing to the lower and not touching the upper. This iron stick has been magnetised by a coil $M.C$ carrying a direct current from a series of batteries. Another coil

10) John. M. IDE, has been experimented on the rock specimens by means of the same idea as adopted by us. *Rev. Sic. Instruments*, **6** (1935), 296. *Proc. Nat. Acad. Sci.*, **22** (1936), 81.

C, which is also fixed to the same iron stick, is intended to carry an alternating current produced in the generator D_1. The vibrating plate is set in forced vertical vibration of the same frequency as the alternating electric current.

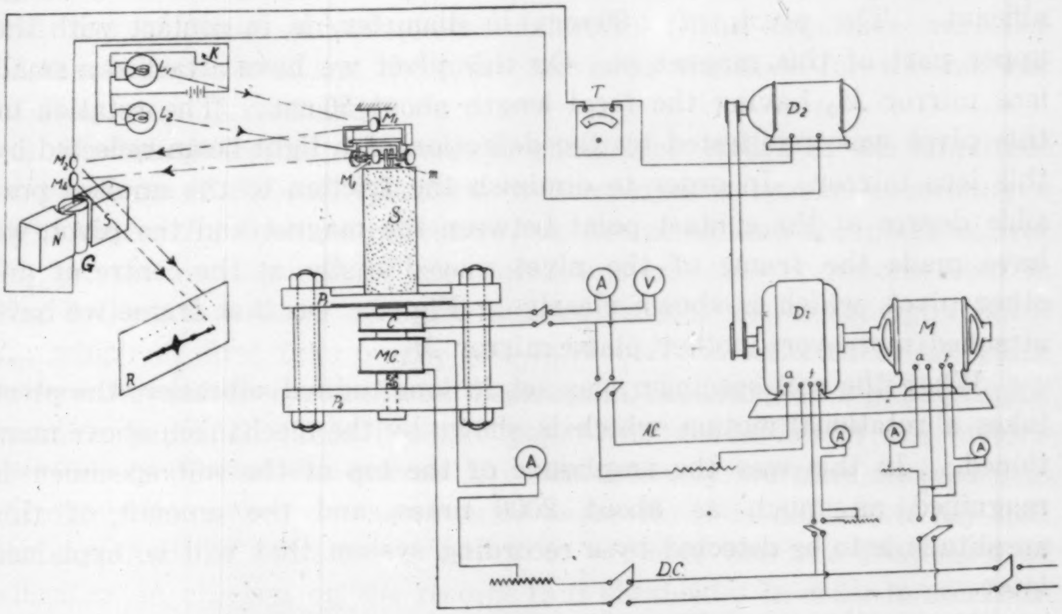

Fig. 8. Sckematic diagram of arrangement of the experimental apparatus for producing longitudinal vibrations of soils by vibration method.

- *a*: Armature terminal.
- *A*: Ampere-meter.
- *A.C*: Alternating current circuit.
- *C*: *A.C.* coil.
- *D.C*: Direct current circuit.
- D_1: Alternating generator.
- D_2: Dynamo of the Weston tachometer.
- *f*: Field terminal.
- *G*: Galvanometer.
- *K*: Key.
- L_1: Light source.
- L_2: 〃 〃
- *m*: Magnet.
- *M*: *D.C.* motor.
- M_1: Lens mirror.
- M_3: 〃
- M_2: Plane mirror.
- M_4: 〃
- *M.C*: *D.C.* coil.
- P_1: Circular iron disc for vibration.
- P_2: Circular iron disc with electromagnet.
- *R*: Bromide paper for record.
- *S*: Soil (specimen).
- *T*: Voltmeter of the Weston tachometer.

Magnification of the amplitude of the top of soil specimen. When the vibrating plate is set in vibration, the longitudinal waves produced by this are propagated from the bottom of the soil specimen *S*. When the frequency of this vibrating plate reaches a condition suitable to provoke a stationary wave in the soil specimen, the amplitude of its top attains to the maximum. The vibration of its top should be perceived even by the tip of a finger, but we must magnify by some device to

record continuously the variation of its vibration amplitude. We have, therefore, adopted a pair of pivot and small magnet m to get a sufficient magnification of it. A part of this small magnet m, then, was inserted into the top of the soil specimen. This small magnet will not disturbe the vibration of the soil specimen as its weight is very insignificant. The pivot, of 1·99 mm in diameter, is in contact with the upper part of this magnet m. On this pivot we have attached a small lens mirror M_3 having the focal length about 50 cm. The rotation of this pivot was manifested by the deflection of a light beam reflected by this lens mirror. In order to diminish the friction to the smallest possible degree at the contact point between the magnet and the pivot, we have made the frame of the pivot moved easily at the centre of another pivot, which is shown clearly in Fig. 8. On that frame we have attached moreover another plane mirror M_1.

When the soil specimen was set in longitudinal vibration, the pivot takes a rotational motion, which is shown by the mechanism above mentioned. In this way the amplidude of the top of the soil specimen is magnified as much as about 2000 times, and the amount of this amplitude is to be detected by a recording system that will be explained later.

Motor-generator. We have employed a motor-generator driven by a direct current fed by secondary cells. The number of rotation of the generator D_1 of 20 pole pieces can be changed continuously with the increase of resistances in the speed regulation circuit. We have, therefore, the output of the alternating current, having a preferred frequency within the limit of 700 per second.

Tachometer. In order to determine the number of revolutions of the generator D_1, an electric Weston tachometer was employed. This tachometer consisted of two elements, that is, a small dynamo D_2 and a voltmeter T. This dynamo is connected with the generater D_1 by means of a cloth belt. We have, however, employed two pulleys of different diameters, one diameter being twice the other, so as to reduce the number of revolutions to half. The number of revolutions of this small dynamo is, of course, read off from the index of the voltmeter which corresponds to the frequency of the vibrating plate, which frequency we wish to know.

Galvanometer. In order to get a continuous reading of the variable frequency of the vibrating plate, we employed a galvanometer G; and to obtain a suitable sensibility of this galvanometer, we have regulated the amount of direct current which passes through the field of exciting coils. The moving coil of this galvanometer was inserted in the tacho-

meter circuit. The amount of deflection of this moving coil is, therefore, proportional to the deflection of the voltmeter T. Consequently we can determine the frequency of the vibrating plate from the amount of this deflection.

We have attached two plane mirrors M_2 and M_4 on this moving coil, one of these serves as the detector of the amplitude variation of the soil specimen, and the other serves as the scale for the number of frequency of resonance.

Recording device. In order to obtain the record of the amplitude of vibration of the soil specimen, we employed a system containing a light source L_2, the lens mirror M_3 on the pivot, and the plane mirror M_4 on the moving coil of the galvanometer. As is demonstrated in Fig. 8, there is a beam of light radiated from a slit of the light source L_2, which at first falls on the lens mirror M_3 is reflected to the plane mirror M_4 and then re-reflected back again, focussing on a photographic bromide paper R. This bromide paper was set at about one meter's distance from the lens mirror M_3 In this way we have succeeded in obtaining the record on the bromide paper R; it is needless to say that the amplitude of vibration is given in ordinate and the frequency of vibration in abscissa on the records thus obtained. In order to ascertain the accurate frequency at the resonance position, we have further employed another system which contains a light sourece L_1, the lens mirror M_1 on the frame of the pivot, and the plane mirror M_2 on the moving coil of the galvanometer. A beam of light radiated from a slit of the light source L_1, formerly reflected by the fixed lens mirror M_1, is now reflected by the plane mirror M_2. The formation of the slit image of this light source L_1 is also made on the same bromide paper R near the image representing the amplitude of vibration of the soil specimen.

When we close the circuit of light L_1 by a key K, corresponding to any frequency read off from the voltmeter T, we can get a point on the same bromide paper R. At any rate, we have closed the circuit every 200 revolutions per minute of the generator D_1, so that a series of points was obtained in the record such as is shown in Fig. 8.

In this way we can determine precisely the frequency of the resonance position.

(b) Testing of the apparatus.

Proper period of the vibrating plate. It seems to us that it is one of the most important matters of investigation to ascertain whether or not the effects of the proper period of the vibrating plate predominate in

the photographic record, where we hope there is no vibrational effect, but that of the soil specimen itself. To diminish the effect of the proper period of the vibrating plate in our experiment, we employed three degrees of plate thickness one by one and reached, at last, the thickness of 0·5 cm. With the last-obtained thickness, we proved by passing the alternating current in the coil *C*, that the proper period of this vibrating plate was beyond our use. Naturally, in this case we have no soil specimen on the vibrating plate.

We have found, anyhow, that the fundamental frequency of the vibrating plate was about 400 per second. In order to find whether or not this period should be varied by a dead weight of metal loaded on the vibrating plate, we repeated the same experiment with several weights up to the limits of 2 kg. From the results of these experiments, we have ascertained that the proper period is scarecely affected by these loaded weights. We may, therefore, conclude in our results that there are no effects to be taken into consideration, but the characteristics of the soil specimens.

Calibration of the tachometer. To obtain the real reading of the Weston tachometer, we have executed a calibration on this tachometer in comparing it to another standard tachometer and then an experiment with the stroboscopic method. We compared, at any rate, the readings of the voltmeter with the number of revolutions of the generator measured by these above two methods. The relation between them thus obtained is shown in Fig. 9. From this relation, we can find the correction to the readings of the Weston tachometer.

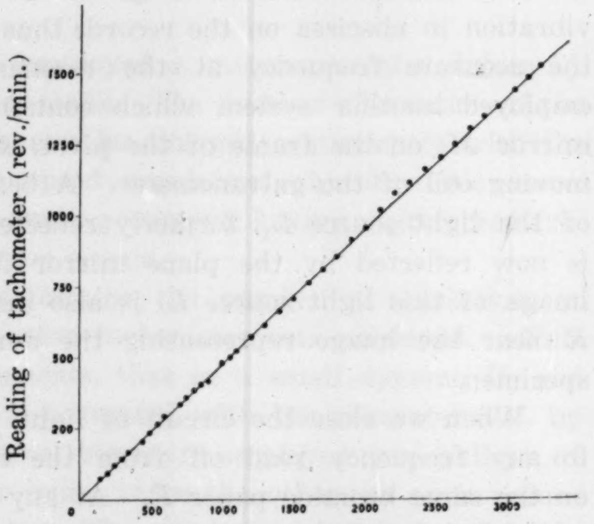

Reading of the standard tachometer (rev./min.).

Fig. 9. Relation between the reading of the Weston tachometer and that of standard one.

(c) Methods of the experiments.

The methods of the experiments are the following:

1) Setting the soil specimen on the vibrating plate, we gave it the vibration up to the limit. Naturally, during this process its amplitude was continuously recorded by the photographic method. We repeated

the same manipulation on the identical material with variable heights so as to get a reducing curve, from which we could calculate the constant of its elasticity.

2) We have experimented with the soils in the natural state and sometimes in the recomposed state. At any rate, the specimens were taken from several places in Tôkyô by means of the boring process. The soils of Maru-no-uti, Hongô, and Komatugawa are taken out from depths of 8 m, 2 m, and 20 m repectively beneath the ground surface.

3) The soils of Maru-no-uti and Hongô were tested in both the natural and recomposed states, and other soils in the recomposed state only. The specimens in the natural state were made into the form of a rectangular prism, about 4 cm × 5 cm in cross section, and the ranges of 20 cm∼40 cm in initial height, which was dinimished by and by with a cutting knife. The specimens in the recomposed state were also made into the form of the rectangular prism, the dimensions of which were about the same as those used in the natural state. To make the form of these specimens we have put the soil into a mould made of a wooden box. Consequently it seems to us that the degree of packing is in the state of the maximum.

By the way, we took substances, such as agar-agar and a kind of commercial rubber, for the purpose of comparing their elastic constants with those of soils. We have made a solution of agar-agar, the weight of which is 125 gr in 5·5 *l* of water, and poured into a hollow rectangular box of zinc. This solution was thereafter solidified. We have cut this block of agar-agar in the form of a rectangular prism to make a testing specimen. We have also experimented on the rubber specimen in the form of a cylinder, the diameter of which was 4·83 cm, and the height of which was changed in the range of 2 cm∼20 cm.

4) We determined the apparent density of the soil specimen from the measuring of its mass and the volume of the specimen just after every experiment.

5) In order to know the properties of the specimen in relation to moisture content, we have executed the same manipulation on the same material with the variable moisture content. We have made the change in moisture content by drying the specimen from the initial wet state leaving it in the ordinary room conditions. The moisture content of the specimen was calculated from the ratio of the weight of water in the specimen to that of its original wet state.

When the soil specimen becomes hard like a solid body by the diminishing of its moisture content, it is rather removable owing to its jumping on the vibrating plate during its vibration; however, we have succeeded

in carrying out the experiments by fixing the lower part of the soil specimen to the vibrating plate by means of oil clay.

5. Results of the Experiments.

(a) Records.

Some examples of actual photographs[11] thus obtained are shown in

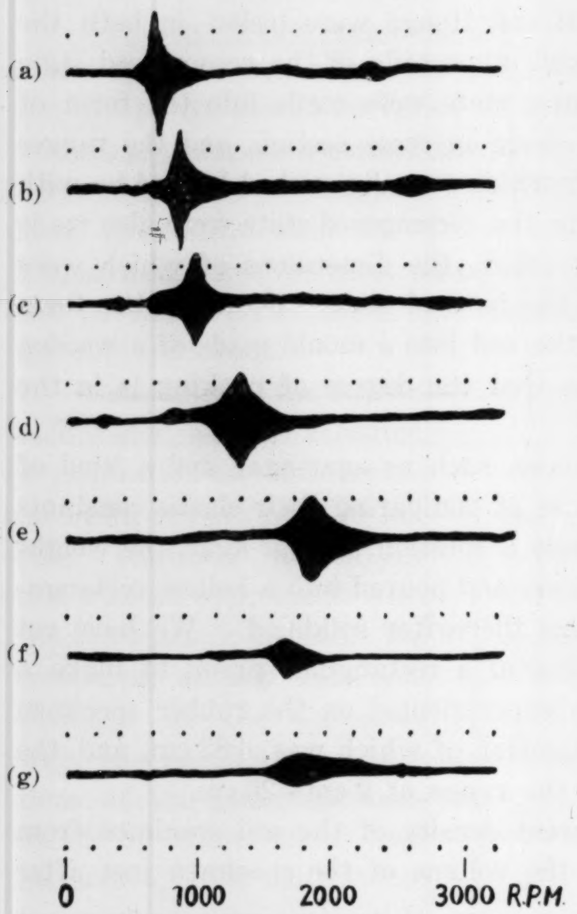

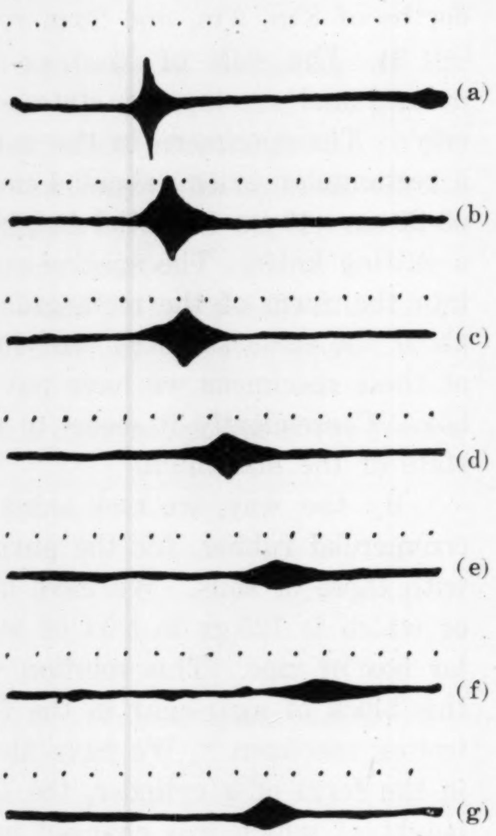

Fig. 11. Resonance curves of soil taken from Maru-no-uti. Moisture content 48·6%.

(a) $h=24{\cdot}3$ cm, $N=110$ sec^{-1}.
(b) $h=19{\cdot}7$, $N=134$.
(c) $h=14{\cdot}9$, $N=151$.
(d) $h=10{\cdot}0$, $N=201$.
(e) $h=5{\cdot}9$, $N=297$.
(f) $h=3{\cdot}1$, $N=255$.
(g) $h=1{\cdot}6$, $N=300$.

Fig. 12. Resonance curves of soil taken from Maru-no-uti. Moisture content 42·3%.

(a) $h=24{\cdot}8$ cm, $N=161$ sec^{-1}.
(b) $h=20{\cdot}2$, $N=177$.
(c) $h=16{\cdot}0$, $N=208$.
(d) $h=11{\cdot}1$, $N=250$.
(e) $h=6{\cdot}5$, $N=318$.
(f) $h=3{\cdot}5$, $N=365$.
(g) $h=2{\cdot}0$, $N=310$.

11) Some of the curves are deviated from horizontal. The reason for this departure from horizontal is due to a shrinkage of the soil specimen during its vibration.

Figs. 10, 13 and 15, and some of hand reproductions from actual photographs are shown in Figs. 11, 12, 14, and 16~19. These show the difference according to the kinds, the heights, and the moisture contents of the soil specimens.

As will be seen in these figures, the characteristics of resonance are almost alike; but we observe the fact that the resonance curves tend to flatten when their heights or their moisture contents are diminished. As we have already stated in the theoretical part in Section 3 that the sharpness of the curves shows the degree of the solid viscosity in the specimen, we can, therefore, determine its value from the flatness of these curves. It will be confirmed from these curves that the apparent effect of solid viscosity becomes great in the following two cases;

1) When the height of the specimen is lowered.

2) When the moisture content of the specimen is diminished.

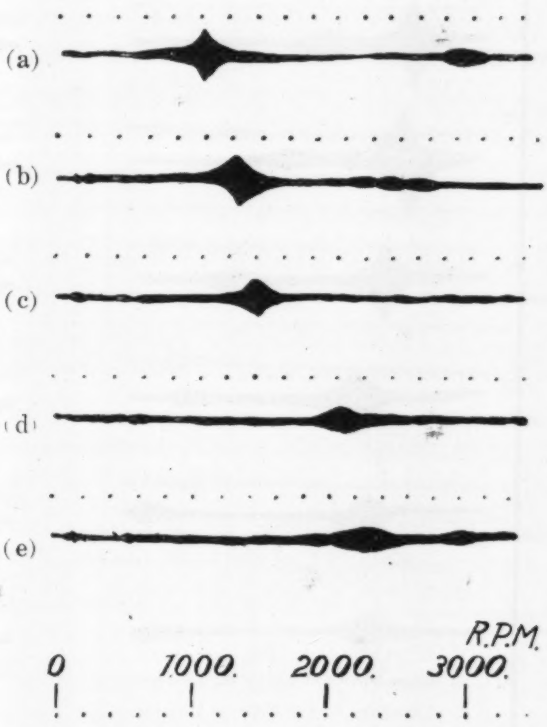

Fig. 14. Resonance curves of soil taken from Hongô. Moisture content 52·3%.

(a) $h=27{\cdot}5$ cm, $N=173$ sec^{-1}.
(b) $h=20{\cdot}5$,, $N=212$,,
(c) $h=14{\cdot}4$,, $N=242$,,
(d) $h=9{\cdot}5$,, $N=347$,,
(e) $h=6{\cdot}0$,, $N=392$,,

However, in this effect, any other disturbances caused by the friction between the pivot and the magnet, etc., seem to be included; therefore this flatness of the curve may not be suitable for determining the coefficient of solid viscosity of the soil specimens. For determining its value we have, therefore, noticed the curved portions near the origin in the reducing curves. We have succeeded in obtaining its values.

(b) Determination of velocity of the elastic waves and the solid viscosity coefficient of soil specimen.

As is already known from the theoretical treatments of the longitudinal vibration in a prismatic bar of various heights, which are shown graphically in the figures 3 and 4, we can determine the velocity and the

solid viscosity coefficient. The theoretical relation between the resonance period T and the hight h of the specimen is given in equation (16).

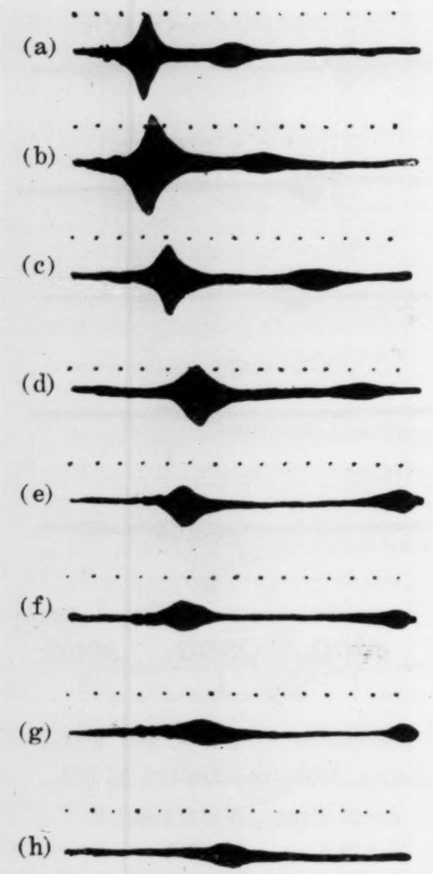

Fig. 16. Resonance curves of loam.

(a)~(d): moisture content 17·3%, $\rho=2{\cdot}02$.

(e)~(f): " " 22·1%, $\rho=2{\cdot}15$.

(a) $h=14{\cdot}1$ cm, $N=99$ sec^{-1}.
(b) $h=11{\cdot}0$, $N=110$.
(c) $h=8{\cdot}0$, $N=130$.
(d) $h=5{\cdot}0$, $N=161$.
(e) $h=13{\cdot}5$, $N=139$.
(f) $h=11{\cdot}0$, $N=162$.
(g) $h=8{\cdot}0$, $N=183$.
(h) $h=5{\cdot}0$, $N=231$.

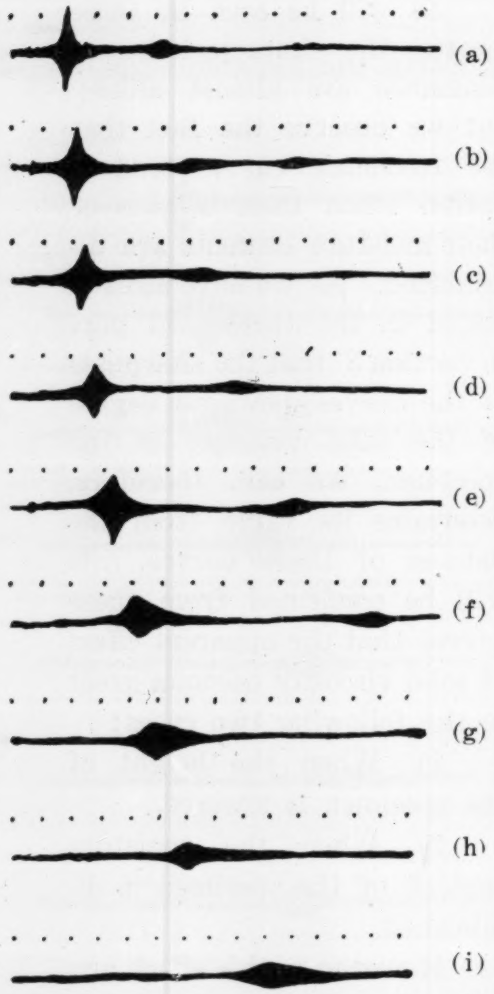

Fig. 17. Resonance curves of clay Moisture content 30·7%, $\rho=1{\cdot}98$.

(a) $h=45{\cdot}5$ cm, $N=68$ sec^{-1}.
(b) $h=40{\cdot}0$, $N=78$.
(c) $h=34{\cdot}8$, $N=91$.
(d) $h=30{\cdot}0$, $N=99$.
(e) $h=24{\cdot}9$, $N=113$.
(f) $h=20{\cdot}2$, $N=142$.
(g) $h=14{\cdot}9$, $N=175$.
(h) $h=10{\cdot}0$, $N=216$.
(i) $h=5{\cdot}1$, $N=328$.

We have anyhow employed this equation to determine these two quantities.

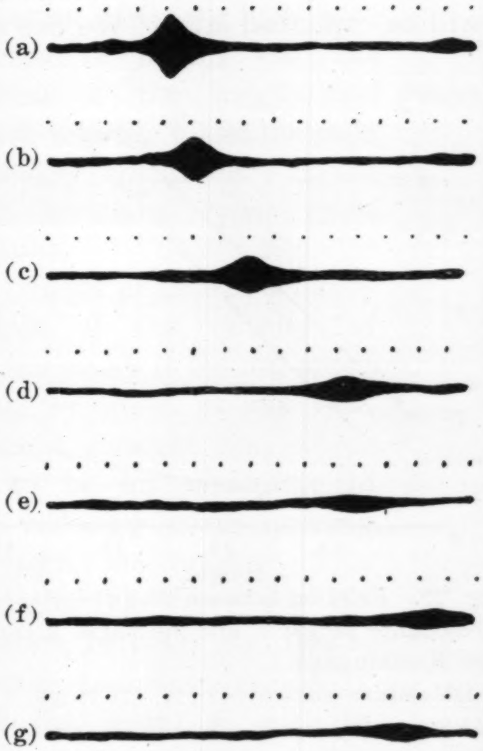

Fig. 18. Resonance curves of rubber.

(a) $h=20\cdot0$ cm, $N=142$ sec^{-1}.
(b) $h=14\cdot6$,, $N=170$,,
(c) $h=10\cdot0$,, $N=242$,,
(d) $h=5\cdot0$,, $N=367$,,
(e) $h=2\cdot8$,, $N=342$,,
(f) $h=2\cdot05$,, $N=488$,,
(g) $h=1\cdot15$,, $N=407$,,

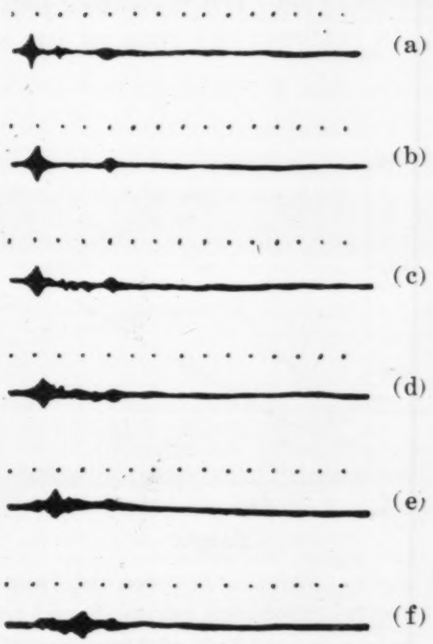

Fig. 19. Resonance curves of agar-agar.

(a) $h=12\cdot8$ cm, $N=28$ sec^{-1}.
(b) $h=10\cdot0$,, $N=33$,,
(c) $h=8\cdot0$,, $N=39$,,
(d) $h=6.0$,, $N=50$,,
(e) $h=4\cdot3$,, $N=59$,,
(f) $h=2\cdot0$,, $N=97$,,

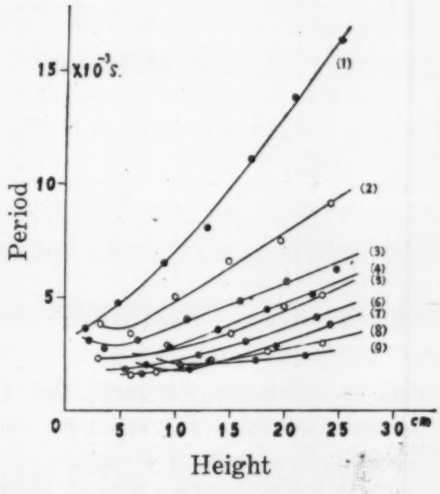

Fig. 20. Relation between the fundamental resonance period T and the height h. (Soil of Maru-no-uti in the natural state.)
(1) Moisture content 50%. (2) 48·6%. (3) 42·3%. (4) 36·7%. (5) 43·6%. (6) 40·8%. (7) 36·7%. (8) 30·5%. (9) 32·7%.

(*I*) *Velocity of longitudinal wave in soils.* By means of the fundamental resonance period T and the corresponding height h of the soil specimen, we have traced a diagram, in which the period T is taken as ordinate and the height h as abscissa. Figs. 20∼26 are the diagrams showing these relations, the values of which are tabulated in Tables II∼VII. It is believed that the mode of vibration of the soil specimen corresponds to that of the

clamped- and free-end bar, the loop of which is at its top and the node is at its bottom; the reasons for which will be explained later. We can see

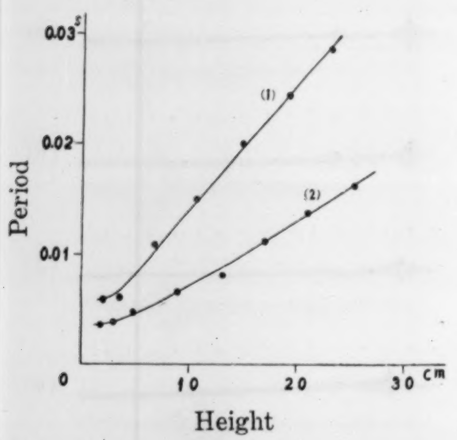

Fig. 21. Relation between the fundamental resonance period T and the height h. (Soil of Maru-no-uti.) Moisture content 50%.
(1) Recomposed state.
(2) Natural state.

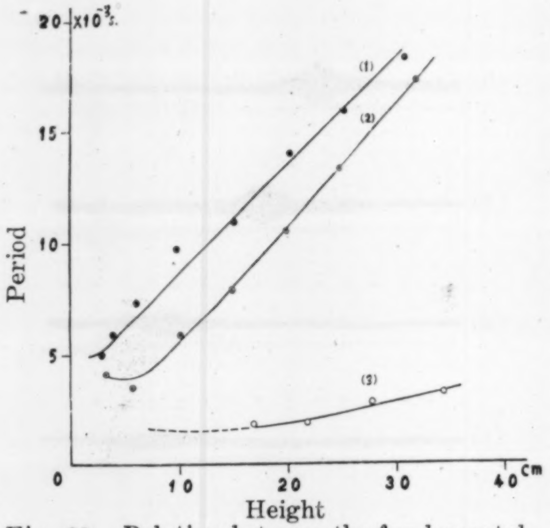

Fig. 22. Relation between the fundamental resonance period T and the height h. (Silt of Komatugawa.)
(1) Moisture content 49·5%. (2) 29·3%. (3) 15·9%.

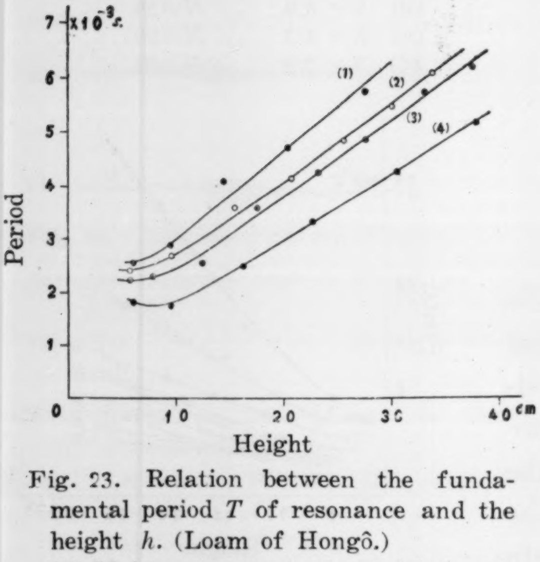

Fig. 23. Relation between the fundamental period T of resonance and the height h. (Loam of Hongô.)
(1) Moisture content 52·3%. (2) 49·7%. (3) 46·8%. (4) 41·5%.

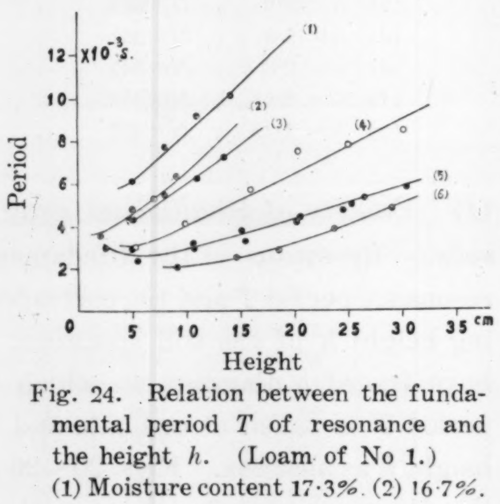

Fig. 24. Relation between the fundamental period T of resonance and the height h. (Loam of No 1.)
(1) Moisture content 17·3%. (2) 16·7%. (3) 22·1%. (4) 19%. (5) 21%. (6) 15·5%.

that the characteristics of these curves are similar to those obtained by the theoretical treatment shown in the figures 3 and 4. It is almost impossible to find the height corresponding to the period that be-

comes infinitely great. According to the relation represented by the equation (16), we have succeeded in finding out the values of the longitudinal wave velocity v and the solid viscosity coefficient γ of the soil specimen from these graphs.

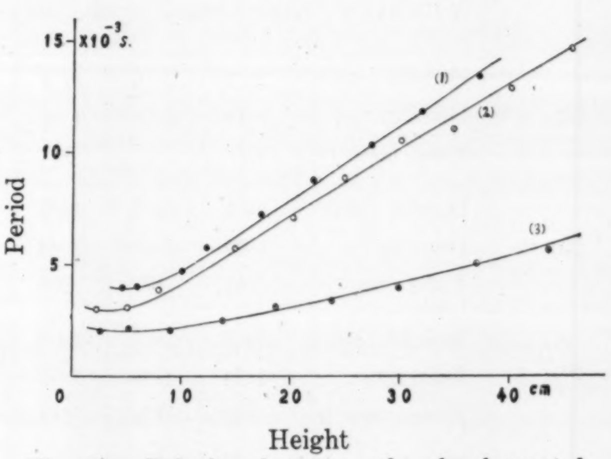

Fig. 25. Relation between the fundamental resonance period T and the height h. (Clay of No. 2.)
(1) Moisture content 30·7%. (2) 26·6%. (3) 22·6%.

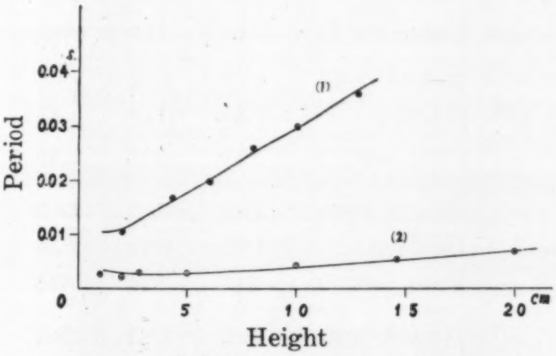

Fig. 26. Relation between the fundamental period T of resonance and the height h.
(1) Agar-agar. (2) Rubber.

In the process of determination of the velocity of elastic waves in the soil specimen, we must, at any rate, trace a straight line, which is to be an asymptote to the reducing curve passing through the origin. This straight line represents the relation between the fundamental resonance period T and the height h, such as $T=4h\sqrt{\dfrac{E}{\rho}}$.

(2) *Solid viscosity coefficient.* In order to determine the solid viscosity coefficient γ, we have compared a series of the theoretical curves of different value of γ, which is represented by equation $T=4h\sqrt{\dfrac{E}{\rho}-\dfrac{\pi^2\gamma^2}{16\rho^2h^2}}$, and picked up one of these which coincides with the reducing curve obtained experimentally. We can thus decided the value of γ. These values of v and γ thus obtained are shown in Table VIII. Young's moduli E of these soil specimens were then computed from the relation $E=v^2\rho$, in which ρ is the density and v is the velocity. These values are also shown in Table VIII.

All of Young's moduli and the solid viscosity coefficients of the soil specimen in the natural state have larger value compared with those in the recomposed state. This phenomenon can be seen, for example, in the soils taken from Maru-no-uti shown in Fig. 10 or in the reducing curves in Fig. 22.

Table II. Height, Fundamental Frequency of Resonance Vibration, and Density of Silty-clay of Maru-no-uti.

No. 1	Height (cm)	25·2	21·0	17·0	13·1	8·9	4·8	2·9	1·7
	Density	1·44	1·44	1·45	1·46	1·47	1·48	1·47	1·49
	Freq. (sec⁻¹)	61	73	90	124	153	210	256	277
No. 2	Height (cm)	24·8	20·2	16·0	11·1	6·5	3·5	2·0	
	Density	1·49	1·45	1·44	1·44	1·44	1·49	1·50	
	Freq. (sec⁻¹)	161	177	208	250	318	365	310	
No. 3	Height (cm)	24·3	19·7	14·9	10·0	5·9	3·1	1·6	
	Density	1·34	1·36	1·37	1·35	1·40	1·38	1·38	
	Freq. (sec⁻¹)	110	134	151	201	297	255	300	
No. 4	Height (cm)	23·5	20·0	15·1	9·2	5·5	3·0		
	Density	1·61	1·61	1·61	1·70	1·75	1·78		
	Freq. (sec⁻¹)	197	217	319	318	558	419		
No. 5	Height (cm)	22·0	17·3	14·2	10·5	6·9	3·8		
	Density	1·50	1·66	1·62	1·70	1·84	1·72		
	Freq. (sec⁻¹)	417	451	465	487				
No. 6	Height (cm)	22·6	18·4	13·9	9·5	5·1			
	Density	1·62	1·64	1·66	1·60	1·59			
	Freq. (sec⁻¹)	195	223	280	457				
No. 7	Height (cm)	23·0	16·5	11·2	7·0				
	Density	1·58	1·59	1·56	1·50				
	Freq. (sec⁻¹)	247	328	416	624				
No. 8	Height (cm)	24·2	19·3	13·2	11·3	7·4	4·6		
	Density	1·64	1·63	1·64	1·64	1·60	1·58		
	Freq. (sec⁻¹)	263	355	470	554	490			
No. 9	Heignt (cm)	23·5	18·5	13·3	8·3	6·0			
	Density	1·45	1·46	1·48	1·49	1·50			
	Freq. (sec⁻¹)	332	341	451	590	658			
No. 10 recomp.	Height (cm)	23·0	19·1	14·9	10·6	6·8	3·8	2·1	
	Density	1·44	1·44	1·43	1·49	1·48	1·49	1·49	
	Freq. (sec⁻¹)	35	41	49	67	87	168	173	

Table III. Height, Frequency, and Density of Silt of Komatugawa.

No. 1	Height (cm)	31·0	25·4	20·3	15·2	9·9	6·1	4·0	3·0
	Density	1·69	1·69	1·72	1·72	1·81	1·98	1·92	1·70
	Freq. (sec⁻¹)	55	63	71	97	103	137	198	170

(*to be continued.*)

Table III. (*continued.*)

No. 2	Height (cm)	32·0	24·9	20·0	15·0	10·1	5·80	3·3	2·1
	Density	1·80	1·88	1·95	2·01	2·13	2·14	2·03	2·00
	Freq. (sec^{-1})	57	75	96	129	172	288	247	207
No. 3	Height (cm)	34·4	27·9	21·9	16·9	11·1	6·0		
	Density	1·70	1·75	1·76	1·76	1·78	1·86		
	Freq. (sec^{-1})	196	365	532	583				

Table IV. Height, Frequency, and Density of Loam of Hongô.

No. 1	Height (cm)	27·5	20·5	14·4	9·5	6·0			
	Density	1·43	1·46	1·42	1·43	1·48			
	Freq. (sec^{-1})	173	212	242	347	392			
No. 2	Height (cm)	33·8	30·0	25·6	20·6	15·4	9·7	5·8	
	Density	1·28	1·28	1·28	1·29	1·29	1·29	1·29	
	Freq. (sec^{-1})	163	182	207	239	277	384	417	
No. 3	Height (cm)	37·4	33·0	27·5	23·2	17·5	12·4	7·8	5·8
	Density	1·21	1·24	1·23	1·23	1·19	1·18	1·22	1·26
	Freq. (sec^{-1})	160	173	205	235	277	392	435	450

Table V. Height, Frequency, and Density of Loam (No. 1).

No. 1	Height (cm)	9·0	7·0	5·0	4·7	3·0	2·0	
	Density	2·41	2·43	2·40	2·30	2·41	2·27	
	Freq. (sec^{-1})	158	190	208	231	260	284	
No. 2	Height (cm)	14·1	11·0	8·0	5·0			
	Density	2·03	2·15	2·25	2·26			
	Freq. (sec^{-1})	99	110	130	161			
No. 3	Height (cm)	13·5	11·C	8·0	5·0			
	Density	1·90	1·96	1·90	1·92			
	Freq. (sec^{-1})	139	162	183	231			
No. 4	Heigot (cm)	30·5	25·4	20·6	15·5	10·7	5·5	3·1
	Density	2·05	2·09	2·10	2·15	2·20	2·26	2·26
	Freq. (sec^{-1})	173	202	228	305	338	430	263
No. 5	Height (cm)	26·5	24·5	20·3	15·1	10·6	5·0	2·5
	Density	2·06	2·10	2·10	2·13	2·12	2·25	2·21
	Freq. (sec^{-1})	190	212	245	260	309	343	333

(*to be continued.*)

Table V. (*continued.*)

No. 6	Height (cm)	30·2	25·0	20·3	16·0	9·9	5·3	3·0
	Density	2·08	2·09	2·09	2·15	2·14	2·16	2·23
	Freq. (sec^{-1})	119	130	133	177	238	333	470
No. 7	Height (cm)	29·1	23·6	18·6	14·6	9·0	4·7	
	Density	2·11	2·12	2·12	2·14	2·15	2·29	
	Freq. (sec^{-1})	212	257	353	400	485		

Table VI. Height, Frequency, and Density of Clay (No. 2).

No. 1	Height (cm)	45·5	40·0	34·8	30·0	24·9	20·2	14·9	10·0	5·1	2·2
	Density	1·86	1·87	1·83	1·87	1·86	1·88	1·90	1·95	2·02	2·03
	Freq. (sec^{-1})	68	78	91	99	113	142	175	216	328	333
No. 2	Height (cm)	37·1	31·9	27·3	22·0	17·3	12·3	7·9	3·0		
	Density	1·73	1·77	1·78	1·78	1·83	1·89	1·79	1·97		
	Freq. (sec^{-1})	75	85	97	115	139	173	260	254		
No. 3	Height (cm)	43·5	36·9	29·9	23·8	18·7	13·8	9·0	5·2	2·6	
	Density	1·92	1·92	1·95	1·99	1·99	1·99	2·04	2·01	2·08	
	Freq. (sec^{-1})	177	197	257	295	321	399	490	462	454	

Table VII. Height, Frequency, and Density of Agar-agar and Rubber.

Agar-agar	Height (cm)	12·8	10·0	8·0	6·0	4·3	2·0	
	Density	1·02	0·99	1·01	1·03	1·06	1·05	
	Freq. (sec^{-1})	28	33	39	50	59	97	
Rubber	Height (cm)	20·0	14·6	10·0	5·0	2·8	2·05	1·15
	Density	1·76	1·73	1·79	1·79	1·73	1·78	1·73
	Freq. (sec^{-1})	142	170	242	367	342	488	407

(c) Effect of moisture content on the constants of elasticity and solid viscosity.

In order to observe the effect of moisture content on the physical properties of soils, we have arranged the computed values from the experiments (Table VIII) in several diagrams. Always the moisture content is considered abscissa; and the velocity v, Young's modulus E, and the solid viscosity coefficient γ as ordinate in each case. These curves are shown in Figs. 27∼29.

Table VIII. Young's Modulus, Velocity, Coefficient of Solid Viscosity, and Moisture Content of Soils.

Kinds of Soils	No.	Density ρ	Moisture content %	Velocity m/sec	Young's modulus E (c.g.s.)	Coef. of solid viscosity γ (c.g.s.)
Silty-clay (Maru-no-uti) (No. 1~9: natural state. No. 10: recomposed state.)	1	1·46	50·0	62	5.61×10^{7}	4.05×10^{4}
	2	1·46	42·3	166	4.05×10^{8}	2.32×10^{5}
	3	1·40	48·6	110·7	1.72×10^{8}	1·27 〃
	4	1·68	43·6	189	6.00×10^{8}	2·51 〃
	5	1·67	32·7	437	3.19×10^{9}	1.11×10^{6}
	6	1·63	42·9	181	5.34×10^{8}	2.48×10^{5}
	7	1·56	40·8	240	8.99×10^{8}	3·77 〃
	8	1·62	36·7	267	1.16×10^{9}	2·95 〃
	9	1·47	30·5	344	1.74×10^{9}	6·30 〃
	10	1·48	50·0	31	1.42×10^{7}	2.26×10^{4}
Silt (Komatugawa) (Recomposed state)	1	1·78	49·5	69	8.47×10^{7}	1.28×10^{5}
	2	1·99	29·3	75	1.12×10^{8}	6.18×10^{4}
	3	1·77	15·9	426	3.21×10^{9}	7.61×10^{5}
Loam (Hongô) (Natural state)	1	1·44	52·3	200	5.76×10^{8}	2.86×10^{5}
	2	1·29	49·7	221	6·30 〃	2·52 〃
	3	1·22	46·8	245	7·32 〃	2·50 〃
	4	1·15	41·5	300	1.04×10^{9}	2·84 〃
Loam (No. 1) (Recomposed state)	1	2·37	16·7	76	1.37×10^{8}	1.40×10^{5}
	2	2·11	17·3	64	0·86 〃	1·17 〃
	3	1·92	22·1	94	1·70 〃	1·74 〃
	4	2·16	19·0	219	1.04×10^{9}	4·86 〃
	5	2·14	21·0	150	4.82×10^{8}	3·63 〃
	6	2·13	15·5	250	1.51×10^{9}	4·97 〃
Clay (No. 2) (Recomposed state)	1	1·91	30·7	112	2.40×10^{8}	1.81×10^{5}
	2	1·82	26·6	126	2.89×10^{8}	1·85 〃
	3	1·99	22·5	309	1.90×10^{9}	6·28 〃
Rubber		1·77		114·5	2.35×10^{8}	1.41×10^{5}
Agar-agar		1·03		14·8	2.25×10^{6}	6.53×10^{3}

We can conclude that the velocity or Young's modulus of soils decreases somewhat rapidly with the increase of the moisture content, though the manner of decreasing differs according to each soil specimen. The solid viscosity coefficient of the soils at Maru-no-uti decreases with the increase of the moisture content, while in the case of the loam at

Hongô, this coefficient is somewhat constant, even with the increase of the moisture content to a certain limit.

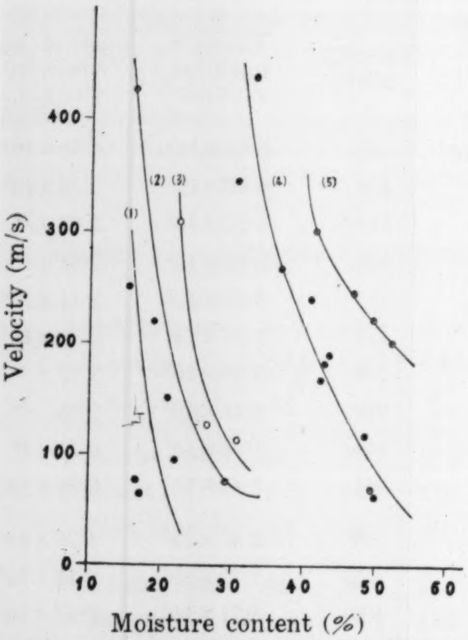

Fig. 27. Relation between the velocity and the moisture content.
(1) Loam of No. 1. (2) Silt of Komatugawa. (3) Clay of No. 2. (4) Silty-clay of Maru-no-uti. (5) Loam of Hongô.

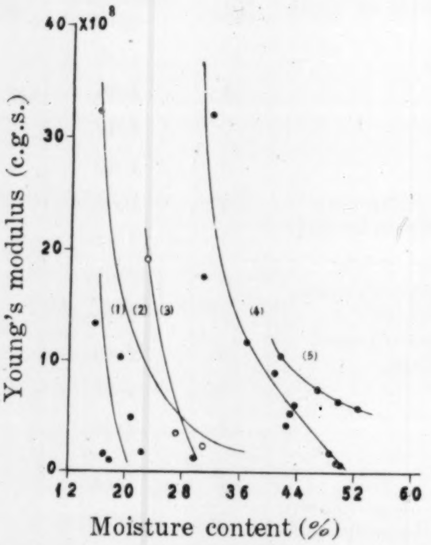

Fig. 28. Relation between Young's modulus and the moisture content.
(1) Loam of No. 1. (2) Silt of Komatugawa. (3) Clay of No. 2. (4) Silty-clay of Maru-no-uti. (5) Loam of Hongô.

(d) Partials.

As the determination of the mode of vibration of soil specimen is very important in our experiments, we have studied especially the resonance frequencies of the partials in every case. Three examples of the relation between the frequency of resonance and the order of partials are shown in Fig. 30. In this figure we take the frequency as ordinate and the order of successive maximum amplitude in the record as abscissa. We find that these points are not in a straight line which corresponds to the result obtained from the theoretical treatment in Section 3. We believe that this is due to the effect of solid

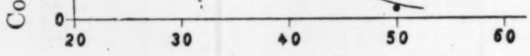

Fig. 29. Relation between the coefficient of solid viscosity and the moisture content.
(1) Silty-clay of Maru-no-uti.
(2) Loam of Hongô.

viscosity in the soil specimen. As will be seen in this figure, the frequency of the partial of the second maximum amplitude attiains about three times that of the first. In general, the frequency of the partials is about odd number of times that of the first maximum amplitude which represented in the figures 10 and 11.

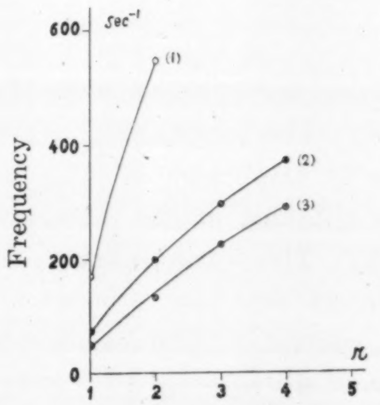

Fig. 30. Relation between the resonance frequency and the order of partials, r, of soils.
(1) Loam of Hongô, h=27·5 cm. (2) Silty-clay of Maru-no-uti, h=25·2cm. (3) Silt of Komatugawa, h=31·0 cm.

We ascertain, therefore, that the observed vibration of the soil specimen can be explained as the longitudinal vibration in a clamped-and free-end bar.

From the curvature of these curves represented in Fig. 30, we were able to determine the solid viscosity coefficient by comparing these with the theoretical values shown in Fig. 5. However, in this case we have not adopted this method for determining the solid viscosity coefficient γ.

6. Summary and Conclusion.

We may now briefly summarize the results of the present study.

1) We studied the elastic properties of sub-surface soils of several regions in Tôkyô. The soils were taken out in the natural state from underground in Hongô, Maru-no-uti, and Komatugawa by means of the boring process. All of soil specimens were made into the form of a rectangular prism, and tested in both the natural and recomposed states.

2) We obtained the longitudinal wave velocity v in these soil specimens by means of the vibration method, and then computed their Young's moduli E from the relation $E=\rho v^2$.

3) The apparent effect of solid viscosity becomes great according to the variable height and variable moisture content of the soil specimen. The smaller the height and the degree of moisture content of the specimen, the more the resonance curves tend to flatten.

4) We determined the solid viscosity coefficient γ by comparing the reducing curves obtained experimentally, with the theoretical curves which are represented by the equation

$$T=\frac{4h}{\sqrt{\frac{E}{\rho}-\frac{\pi^2\gamma^2}{16\rho^2h^2}}},$$

in which the symbols have the same meaning as before.

5) The longitudinal wave velocity, Young's modulus, and the solid viscosity coefficient of the soils in the natural state are greater than those obtained in the recomposed state.

6) The wave velocity, Young's modulus, and the solid viscosity coefficient decrease somewhat rapidly with the increase of the moisture content. The coefficient of solid viscosity of these soils is of the order of $10^4 \sim 10^6$ and the velocity varies from about 60 m sec ~ 400 m sec at moisture content ranges of about 50% ~ 20%.

7) The frequency of the partials of the second maximum amplitude attains about three times that of the first. The observed vibration of the soil specimen can be, therefore, explained as the longitudinal vibration in a clamped- and free-end bar.

In conclusion, our sincerest thanks are due to Dr. T. Watanabe, the member of Geotechnical Committee, Government Railways of Japan, who kindly gave us the soils and the results of their mechanical analysis, which we used in these experiments.

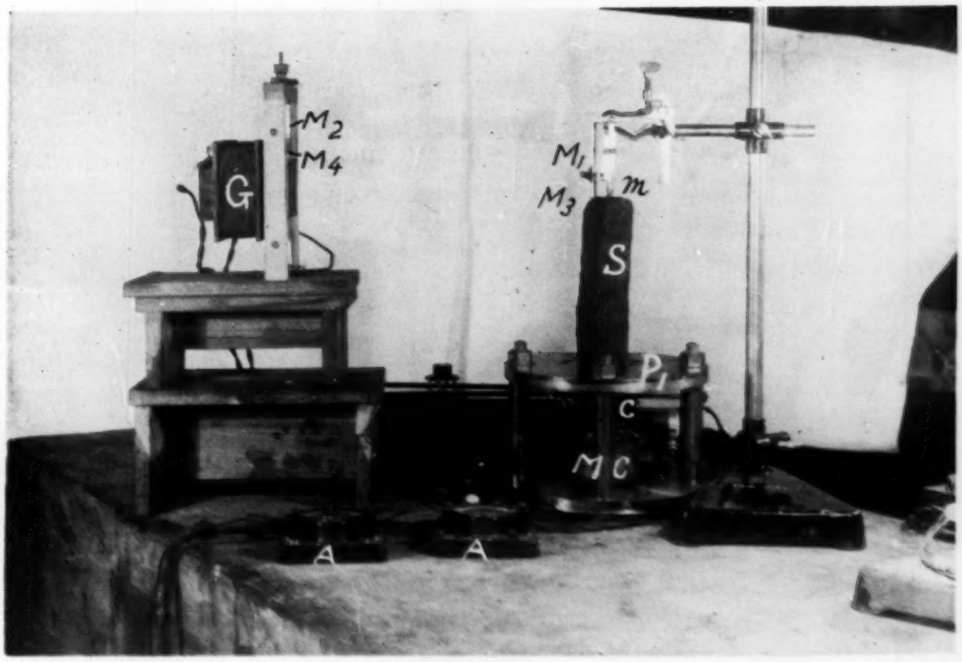

Fig. 6. Experimental Apparatus (1).
(The symbols in this figure have the same meaning as in Fig. 8.)

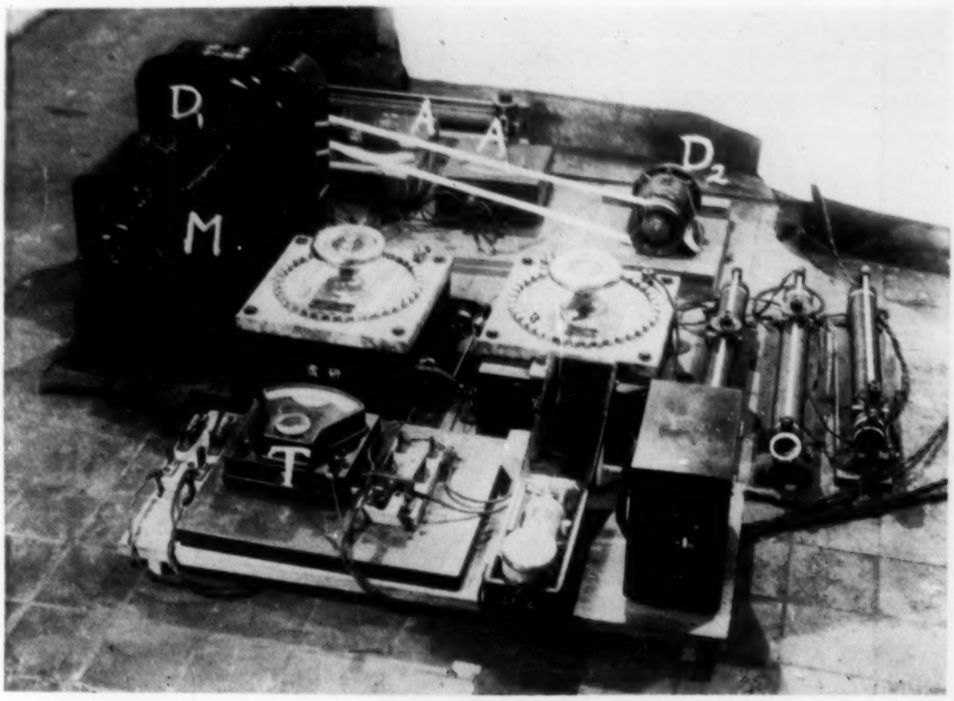

Fig. 7. Experimental Apparatus (2).
(The symbols in this figure have the same meaning as in Fig. 8.)

(震研彙報 第十四號 圖版 石本・飯田)

（震研彙報 第十四號 圖版 石本・飯田）

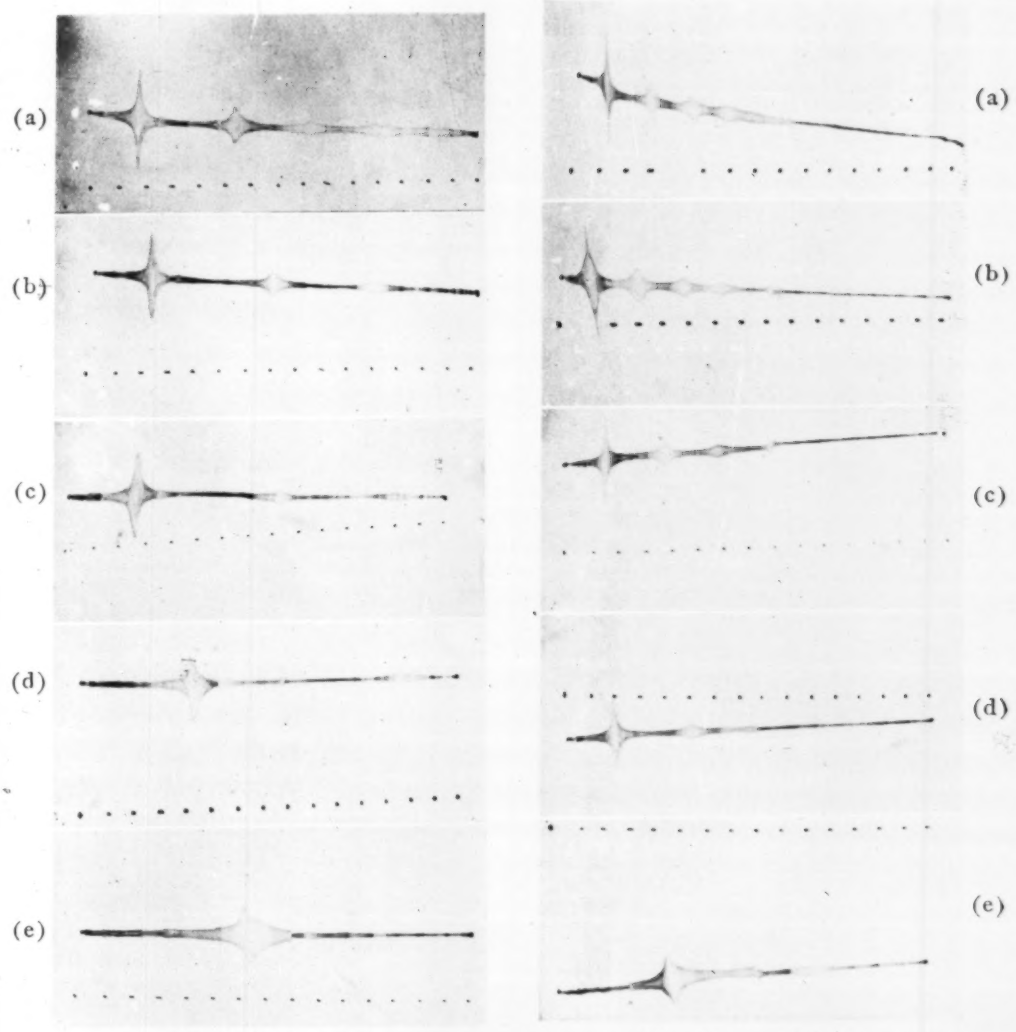

(i) Natural state. (ii) Recomposed state.

Fig. 10. Resonance curves of soils taken from Maru-no-uti. Moisture content 50%, $\rho=1\cdot46$, h=height, N=frequeney.

		h	N
(i)	(a)	$h=25\cdot2$ cm,	$N=$ 61 sec^{-1}.
	(b)	$h=21\cdot0$,	$N=$ 73 .
	(c)	$h=17\cdot0$,	$N=$ 90 .
	(d)	$h=$ 8·9 ,	$N=$153 .
	(e)	$h=$ 4·8 ,	$N=$210 .
(ii)	(a)	$h=23\cdot0$ cm,	$N=$ 35 sec^{-1}.
	(b)	$h=19\cdot1$,	$N=$ 41 .
	(c)	$h=14\cdot9$,	$N=$ 49 .
	(d)	$h=10\cdot6$,	$N=$ 67 .
	(e)	$h=$ 3·8 ,	$N=$168 .

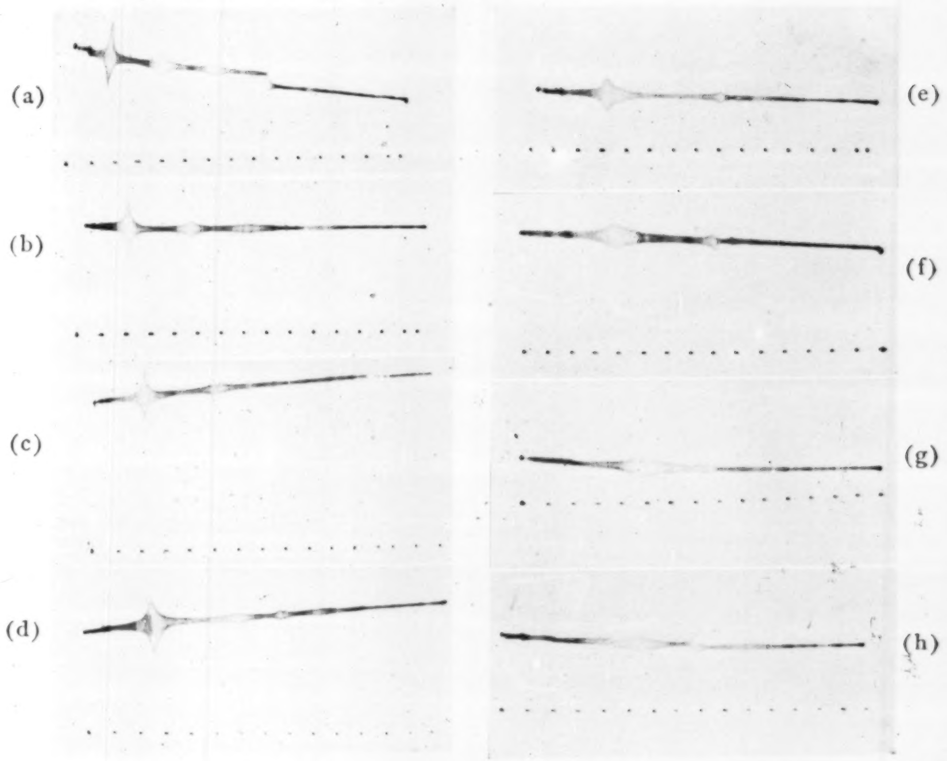

Fig. 13. Resonance curves of soils taken from Komatugawa.
Moisture content 49·5%, $\rho=1{\cdot}78$.

(a)	$h=31{\cdot}0$ cm,	$N=55\ \mathrm{sec}^{-1}$.	(b)	$h=25{\cdot}4$ cm,	$N=63\ \mathrm{sec}^{-1}$.
(c)	$h=20{\cdot}3$,,	$N=71$,,	(d)	$h=15{\cdot}2$,,	$N=97$,,
(e)	$h=9{\cdot}9$,,	$N=103$,,	(f)	$h=6{\cdot}1$,,	$N=137$,,
(g)	$h=4{\cdot}0$,,	$N=198$,,	(h)	$h=3{\cdot}0$,,	$N=170$,,

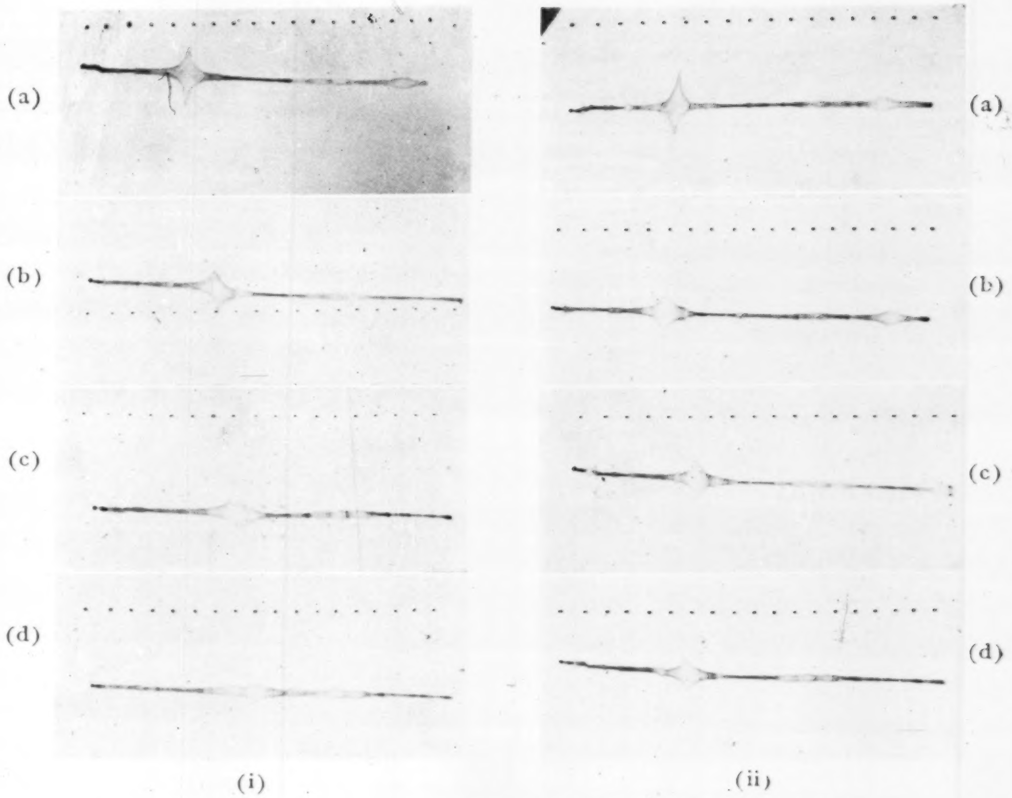

Fig. 15. Resonance curves of soils taken from Hongô, Imperial University.

(i) Moisture content 49·7%, $\rho=1\cdot29$. (ii) Moisture content 46·8%, $\rho=1\cdot22$.

(i)
- (a) $h=33\cdot8$ cm, $N=163$ sec^{-1}.
- (b) $h=25\cdot6$,, $N=207$,,
- (c) $h=20\cdot6$,, $N=239$,,
- (d) $h=15\cdot4$,, $N=277$,,

(ii)
- (a) $h=37\cdot4$ cm, $N=160$ sec^{-1}.
- (b) $h=33\cdot0$,, $N=173$,,
- (c) $h=27\cdot5$,, $N=205$,,
- (d) $h=23\cdot2$,, $N=235$,,

58. 振動方法による土の彈性測定

第1報 ヤング率の測定

地震研究所 石本巳四雄
飯田汲事

地震動の性質の各地に於て異る事は大森博士等の注目した事であるが，最近加速度地震計等の觀測により各地に卓越振動の存在する事が明かにされ，地震動の解釋に就て一段の發展を示した如く思はれる.

地震の發生により地震波が震源より放射され，地殼内を傳播して地表に到達すれば各土地に存する固有振動の二次的に誘發され，共れが地震動中，特に加速度の大なる卓越振動として觀測される．各土地に斯樣の卓越振動の存する所以は，地表に比較的彈性の小なる所謂表面土層の存在する結果であり，此の層の固有振動が卓越振動を生ぜしめるさ考へられるに至つた．從つて地震動の性質を闡明するに當つては，先づ表面層を形成する物質の彈性の研究が重要であるさ信じられる.

此の論文は要するに表面土の彈性を研究したものであり，一般の自然土に於ては多くの因子に左右されて其の本性を取り出す事が比較的困難であるために，各地に於ける自然の堆積狀態の土を成る可く害さぬ樣にして實驗室に持ち來し，其れを適當の形狀を具へた土柱さなし，其の彈性を測定する事さした．土の彈性に就ては從來靜力學的の研究はあるが，元來土は粘彈性物質であつて以上の方法を以てしては粘性，彈性の兩性質を分けて測定する事が殆ど不可能である．從つて今同の實驗には每秒 0～700 の範圍に連續的に振動數の變化し得る振動盤を採用し，其の上に土柱を乘せ其の共鳴する振動數を求めて結局土中に於ける縦波の速度 v を測定し，次いで

$v=\sqrt{\frac{E}{\rho}}$ の式より其の物質のヤング率を求めたのである.

試驗土の種類は沈泥，赤土，粘土等であるが，この外に此れらさ比較するために寒天及び彈性ゴムをも取扱つた．自然の堆積狀態に於て試驗した土は丸の內の第一生命保險相互株式會社建築敷地の地表面下約 8 m の表面層中より採取せる沈泥及び本郷帝國大學構內第二食堂わきの地表下 2 m の表面層より採取せる赤土（ローム層土）である．此の丸の內の土に於ては 50% の含水率で 62 m/sec の速度及び $5{\cdot}61\times10^{7}$ c.g.s.（比重 1·46）のヤング率を得，本郷の土に於ては 52·3% の含水率に於て 200 m/sec の速度及び $5{\cdot}76\times10^{8}$ c.g.s.（比重 1·44）のヤング率を測定した．上述の速度及びヤング率は含水量さ共に變化する，卽ち含水量の減少に伴ひ增加し，含水量の增加さ共に減少する事が判明した．丸の內の土では速度に於て 60 m/sec より 400 m/sec の程度に迄變化し，ヤング率に於て 10^{7} より 10^{9} (c.g.s.) の程度に迄變化する．但し含水率の變化の範圍は 50% より 30% 迄の程度である．本郷の赤土では 50% より 40% 迄の含水率の變化に對し，速度及びヤング率の變化は夫々 200 m/sec より 300 m/sec 迄及び 10^{8} より 10^{9} (c.g.s.) 迄の程度である．又固體粘度は大略 10^{5} の程度であるが，含水量さ共に變化する．例へば丸の內の土に於て含水量の 50% より 30% 迄の範圍の變化に對し，固體粘度の變化は 10^{4} より 10^{5} (c.g.s.) の程度の範圍である.

自然の堆積狀態の土さその組織を破碎してねり直した狀態の土さではその速度及び彈性率は著しく異り，ねり直しの狀態のものは小さな値を示す事が判明した.

Professor Torahiko TERADA

Professor Torahiko TERADA, whose death occurred on December 31, 1935, at his home in Hongo, Tokyo, at the age of 57, is best known and universally remembered for his contributions to pure and applied physics, especially geophysics.

Professor TERADA was born in Tokyo in November 28, 1878, the eldest son of General Tosimasa TERADA. During his high school days at Kumamoto, he was fortunate enough to come under the guidance of the late Professor Takuro TAMARU in physics and of the late Professor Kinnosuke (Soseki) NATUME in literature, both very distinguished savants in their respective lines.

In 1903, he graduated from the Department of Physics, College of Science, Tokyo Imperial University, after which he was engaged in directing the physical experiments at his *Alma meter* as a Lecturer, and in 1909 was conferred the Doctorate of Science. The following year he was appointed Assistant Professor and despatched to Europe to extend his studies in cosmic physics. After several years since his return to Japan, he was appointed Professer of Physics in 1916, and in 1918, upon the founding of the Aeronautical Research Institute became one of its principal members. In 1926, he became a member also of the Earthquake Research Institute. These two posts he held to the time of his death. He was also one of the chief staff members of the Institute of Physical and Chemical Research, in which most of his recent creative investigations in the field of physics were made. He was also honoured with memberships of numerous learned societies and institutions, among which may be mentioned the Imperial Academy of Japan.

His scientific contributions, as shown by more than two hundred papers, are known as creative in all sections of pure and applied physics, especially in geophysics. In 1917, he received from the Imperial Academy the Imperial Prize for his work "On the transmission of X-rays through crystals". His recent investigations on the deformations of the earth's crust and on the stability of the continental crust drew the attention of geophysics. It may be said that most of the younger geophysicists in Japan have been influenced by his ideas as revealed in these investigations.

He was tall but spare in build, and somewhat stoop-shouldered, probably the result of his old complaint, gastric ulcer, from which he

had been suffering for the last twenty odd years. It is indeed a marvel that despite his physical disability, he so faithfully discharged his duties to the numerous societies and institutions with which he was affiliated and at the same time wrote such an enormous quantity of scientific papers. This energy was probably the outcome of his deep sympathy with nature and of his strong sense of responsibility.

In directing the researches of his pupils and the younger physicists, he always encouraged them by pointing out their merits; never being given to fault-finding. He was indeed the object of veneration of young investigators.

Under the pseudonym of YOSIMURA-Huyuhiko, he was also known as a man of letters.

Even though his scientific and literary work may be carried on by his pupils, there is his beautiful and noble character, the like of which we shall probably never see again. His is a name that will long be remembered in Japanese scientific and literary circles.

東京帝國大學地震研究所々員
寺田寅彦教授小傳

昭和10年12月31日，本所々員寺田寅彦教授は，59歳の正月をひかへて遂に薨去された．物理學殊に地球物理學界に特に秀でたる先達として，又，後進の最もよき指導者として，期待される所が大であつただけ，その喪失は全く文字通り惜しみても猶足らざるものがある．

先生は，明治11年11月28日，陸軍主計監寺田利正氏の長男として，東京に於いて誕生せられた．その熊本で過された五高生活に於いて，先生の後年に輝き出でた天賦の才能に最初の磨きをかけられたといふことである．それは，物理學に於いて，故田丸卓郎先生の指導を受け，文學に於いて，故夏目漱石先生の指導を受けられたことを意味するものである．明治36年，東京帝國大學理科大學實驗物理學科を卒業せられてからは，同じ教室に講師として，物理實驗の指導を受け持たれること數年，明治42年に理學博士の學位を得られた．翌明治43年には，助教授に任ぜられ，同時に歐米へ留學を命ぜられた．主として，獨逸に於いて，地球物理學に關する研讃を積まれたやうである．歸京後幾ばくもなくして，教授に任ぜられ，更に，大正7年には，航空研究所の創立に參劃されて，その創立と共に同所員となり．大正14年，地震研究所の創立に際しても同様に所員となられて最後までその職にあられた．又，理化學研究所にも寺田研究室を持たれて，近年に於ける先生の物理學上の仕事の大部分をこゝに於いてなされたものである．其他，帝國學士院にも會員の席を持ち，學術研究會議其他の學術上の諸機關にも關係せられた．

先生の物理學界に寄與された所は，その二百有餘の論文の內容に盛られてゐるわけであるが，就中，“On the transmission of X-rays through crystals” と題する研究に對しては學士院より恩賜賞を以て報ひられ，更に，最近の，地殼變動に關する多くの研究は，地球物理學上注目に價する研究であると稱へられてゐる．先生の研究の獨創的なる點は，全く他の追隨を許さぬのである．而して，先生の思想や研究の方法は，今日の我國に於ける多數の新進地球物理學者に多かれ少なかれ影響を與へてゐるやうである．

先生は，日本人としては脊の高い方であつたが，痩形で，やゝ猫脊であつた．この先生の體格は，20年來惱んでゐられた宿痾の胃潰瘍の影響が大いにあらはれてゐたのではないかと思ふ．先生がこの肉體の苦惱を冒して，研究にいそしみ，後進の指導に

力を注ぎ，而して，關係せられた幾多の學會や研究機關の爲の事務上の義務を果し，その餘力を驅つて，音樂，繪畫，文學等の藝術の方面にも少なからざる寄與をのこされた努力は，眞に尊敬に値すべく，先生の日常が，如何に有意義に而も充實せるものであつたかが忍ばれるのである．この努力の源泉は，到底，先生の纖弱な體格から求め得べしとは思はれないが，恐らくは，自然と人間に對する限りなき愛情と，負ふた役目に對する强い責任の念に基くものであらうと想像されるのである．

先生は，後進や弟子の研究を指導される際に，決して「あらさがし」をされなかつた．そして，其等の研究の長所を見出して，之を發展させる樣に指導されたものである．後進の研究者達の尊敬が先生の一身に蒐められたのも亦決して偶然ではないと言はねばならない．

吉村冬彦の名で文壇にも知られてゐることは人も知る所である．

先生の研究は，多くの弟子達によつて，繼承され，夫々の方面に發展し得る可能性はあるとしても，先生の溫い情愛と，崇高なる人格とは再び接し得べくもない．「寺田寅彦」といふ名こそは，日本の科學界，文學界に永久に銘記せらるべき名である．

——所　報——

○談話會記事

第109回談話會（昭和10年11月19日）

1. 丹那斷層に就て　久野久
1. 箱根火山西部の地質　久野久
1. 箱根火山の構造と發育史　久野久
1. 南伊豆下田附近に於ける過去地震津浪の高さに就て　福富孝治
1. 昭和8年3月3日の大地震（IV）
   大地震前後の三陸沖の地震回數及他の大地震の場合の餘震に就て　松澤武雄
1. 海峽に於けるセイシの持續性　{妹澤克惟・金井清}
1. 不連續面が彈性波の傳播に及ぼす影響（其の11）　{西村源六郎・高山威雄}
1. 楕圓體座標による彈性體釣合式の一般解と其の應用　西村源六郎

第110回談話會（昭和10年12月17日）

1. 地震回數の統計的研究補遺　松澤武雄
1. 埼玉縣賀須町の試錐　大塚彌之助
1. 地震斷層の諸特徴　大塚彌之助
1. 自由振子の持續性と共振の振幅との關係．海峽のセイシの場合
1. 6階建築に於ける震動勢力の逸散性　} 妹澤克惟・金井清
1. 宮古—青森間地殼の垂直變動　{寺田寅彦・宮部直巳}
1. 地震動による木造家屋の振動觀測（第2報）　齊田時太郎
1. 地震計針先の太さに就て　石本巳四雄
1. 本年8月以降に於ける臺灣餘震觀測報告　那須信治
1. 本年9月以降に於ける臺灣地電流觀測報告　萩原尊禮
1. 本年4月21日の臺灣地震の走時曲線と地殼構造上の一問題　{河角廣・本間正作}
1. リフトヴアレー其他の斷層線に就き　{長岡半太郎・白井俊明}

第111回談話會（昭和11年1月21日）

1. 港灣の深さに及ぼす主風の影響　中野猿人
1. 淺間火山の高さの變化に就いて
1. テンプ逡り地震計起動機を等速回轉に直す裝置　} 水上武
1. 筑波山に於ける地電流變化の觀測　萩原尊禮
1. 地震の初動と震源機構との關係に就て　妹澤克惟
1. 7階建築に於ける震動勢力の逸散性．餘共振の性質　{妹澤克惟・金井清}

1. 臺灣地震餘震の分布に就いて	那須信治
1. 深層地震帶と火山帶及び海溝との關係	長岡半太郎 白井俊明

第112回談話會（昭和11年2月18日）

1. 地震と雨雪量との關係（續報）	山口生知
1. 南伊豆，下賀茂・蓮臺寺・下河津3溫泉の物理化學的性質に就て（第1報）	福富孝治
1. 鎌倉町の地質構造 附 地殼の一性質を暗示する斷層構造の一例	大塚彌之助
1. 仙臺大年寺山の山崩	田山利三郎
1. 地震動による木造家屋の震動觀測（第3報）	齊田時太郎 鈴木正治
1. 地震の初動と震源機構との關係に就て	妹澤克惟
1. 3階建築に於ける震動勢力の逸散性．餘共振の性質	妹澤克惟 金井清
1. 370倍器械的記錄微動計の製作	石本巳四雄
1. 地震による鐵道軌條の波狀屈曲について	高橋龍太郎
1. 苗栗に於ける井水位の變化	宮部直巳 川島正治
1. 土壌の强度	宮部直巳 猪俣眞三郎

第113回談話會（昭和11年3月17日）

1. 彈性波の生成及び傳播に關する實驗	木下潤一
1. 檢流計を使用して振動方程式を解く實驗	淵田隆門
1. 硫黃島（火山列島）に就いて	津屋弘逵
1. 地震發生に關係のある斷層の性質	妹澤克惟
1. 不連續の層を通過する橫波の性質	妹澤克惟 金井清
1. 構造物震動に於ける逸散理論の吟味	妹澤克惟 金井清
1. 清澄山に於ける地電流の觀測（第1報）	高橋龍太郎
1. 昭和11年2月21日河內大和强震調查報告 1. 大阪市內に於ける地盤固有振動測定	那須信治 萩原尊禮
1. 2月21日河內大和地震に關する調查報告	宮部直巳
1. 河內大和强震被害情況	齊田時太郎
1. 靜岡地方に於ける震災地復舊測量に就て	梅本豊吉
1. 地軸變動と大地震	長岡半太郎

――所　報――

○ 談話會記事

第114回談話會（昭和11年4月21日）

1.	中部駿河の地質構造と靜岡地震との關係	吉井政敏
1.	出羽村及び濱松町に於ける地震動觀測	石本巳四雄
1.	地震回數の統計的研究	井上宇胤
1.	本邦最初の震災記錄に就て	齊田時太郎
1.	地震計用小型無線時報受信器	岸上冬彦 波江野清藏
1.	三鷹天文臺構内深さ10米の時計庫内に於ける傾斜觀測報告（第1）	河角廣 佐藤柳造
1.	天文臺構内の1淺井に於ける水位變化（豫報）	河角廣 佐藤柳造
1.	昭和10年8月28日颱風による近畿四國及び九州地方の風津浪	西村源六郎 高山威雄
1.	固體破壞面の表面仕事に就て	妹澤克惟
1.	實在建物の震動問題に應用せる勢力逸散の改良理論	妹澤克惟 金井清
1.	地球の核心とこれを通過する地震波	長岡半太郎

第115回談話會（昭和11年5月19日）

1.	臺灣地震の餘震調査補遺	那須信治
1.	南伊豆谷津溫泉の溫度湧出量，鹽分含有量と潮汐との關係（豫報）	福富孝治
1.	南伊豆須崎に於ける地電流の觀測（第1報）	福富孝治
1.	地殼の變動度に就いて	宮部直巳
1.	地質時代に於ける火山活動と地殼運動との一關係	大塚彌之助
1.	地震初動の理論的實驗的研究（共1）	
1	衝擊性地動による地震計記象及び地震記象より初動を求むる簡便法に就いて	河角廣 佐藤柳造
2	各種地震計の檢定及び振動臺による初動の研究	河角廣 木下潤一
1.	變位，速度及び加速度地震記象に於ける卓越周期	萩原尊禮
1.	斜のディスターバンスによつて生じた地表層固有振動の減衰	妹澤克惟 金井清
1.	地震波の發生する機構に就いて	妹澤克惟
1.	床の剛度が構造物の振動に及ぼす影響	妹澤克惟 金井清

1. 風に因つて生ずる湖水の運動（其の2）　西村源六郎

第116回談話會（昭和11年6月16日）

1. 地震の偶發性と持續性と週期性と　渡邊慧
1. 地震に關する統計の結果に就いて　山口生知
1. 昭和5年11月26日北伊豆地震に伴へる蘆ノ湖靜振誘發の原因　鈴木武夫
1. 銚子港附近の砂丘の移動に就て　松尾春雄
1. 火山岩の石基の研究に就いて　坪井誠太郎
1. 伊豆箱根地方火山岩の化學成分に就いて　久野久
1. 灣のセイシに伴ふ逸散波　妹澤克惟、金井清
1. 昭和8年三陸津浪の記象の周期解析　高橋龍太郎
1. 關東地方に於ける震源の垂直分布　永田武
1. 關東地方に於ける地震の發生（其1）　那須信治、萩原尊禮、小平孝雄
1. 毎日の記錄より見たる地震と緯度變化　長岡半太郎

第117回談話會（昭和10年7月7日）

1. 東京に於ける有感地震の1日中の分布　岸上冬彦
1. 岩漿から輝石の晶出する作用に就て　坪井誠太郎、久野久
1. 地震初動方向の分布に就て　井上宇胤
1. 五重塔の耐震性に就て　妹澤克惟、金井清
1. 6月19日日食時の各支所に於ける地電流の觀測結果　高橋龍太郎、萩原尊禮、井上宇胤、水上武
1. 地電流測定に關する二三の試み　永田武
1. 房總半島の地質構造（其1）　大塚彌之助

第118回談話會（昭和11年9月15日）

1. 表面土壤層中に於ける人工地震波の傳播速度　表俊一郎
1. 明治9年以降東京觀測各月地震回數統計　石本巳四雄
1. 伊豆熱海溫泉に就て　福富孝治
1. 茨城縣大寶村及び上大津村に於ける地震動加速度の觀測　萩原尊禮
1. 垂直荷重による砂層の變形（序報）　宮部直巳
1. 平面源を有する彈性波勢力の偏り　妹澤克惟、金井清

1. 媒體の異同が地震初動の分布に及ぼす影響　妹澤克惟
1. 8階建築に於ける震動勢力の地中逸散　妹澤克惟・金井清
1. 淺間山麓千ケ瀧溫泉及び地下水に就て　水上武
1. 時計の遲速に就て　白井俊明
1. 土の粘彈性と剪斷抵抗　石本巳四雄・飯田汲事
1. 振動方法による土の彈性測定（第1報 ヤング率の測定）　石本巳四雄・飯田汲事

第119回談話會（昭和11年10月20日）

1. 世界に於ける深層地震に就て　山口生知
1. 箱根火山北麓，小田原，山北，御殿場間の地質　久野久
1. 富士火山帶火山岩の化學成分に就て　津屋弘逵
1. 關東地方の地震に關する二三の報告　小平孝雄
1. 明治 42 年の江濃地震による被害と地盤との關係　齊田時太郎
1. 安政元年の伊賀上野地震による被害と地盤との關係　齊田時太郎
1. 球形震源から出る波に就て　井上宇胤
1. 東京市内に於ける最近の水準測量の結果　宮部直巳
1. 半無限體の振動に於ける共振現象及び逸散波　妹澤克惟
1. 伊豆大島に於ける地磁氣測定結果概報　高橋龍太郎・永田武
1. 中國地方の中新統とその構造に關する二三の特徴　大塚彌之助
1. 不連續面が彈性波の傳播に及ぼす影響（其の12）　西村源六郎・高山威雄

第120回談話會（昭和11年11月17日）

1. 淺間火山近傍に於ける重力偏差の觀測　水上武
1. 餘震に就て　石本巳四雄
1. 西南日本生代の海侵と地殼變動の概察　小林貞一
1. 房總，三浦西半島地層擾亂と地下構造の一推論　大塚彌之助
1. 中生代末以來の海岸線の變化に關する現在の知識　大塚彌之助
1. 球高の振動に於ける共振現象及び逸散波　妹澤克惟・金井清
1. 地磁氣伏角變化計の製作　永田武
1. 1931 年より4年間の地軸變動と大地震　長岡半太郎

第 14 號索引

頁
淵田隆門 (37) 振動方程式を實驗的に解く一方法 (英文)……………………… 415
福富孝治 (6) 伊豆下田に於ける過去地震津浪の高さ (邦文) ……………………… 68
福富孝治 (23) 南伊豆，下賀茂・蓮臺寺・下河津 3 溫泉の物理，化學的性質に就て (第 1 報) (英文)……………………… 259
荻原尊禮 (53) 茨城縣大實村及上大津村に於ける地震動卓越週期の觀測 (邦文)……………………… 599
荻原尊禮・那須信治；那須信治・荻原尊禮 参照
荻原尊禮・表俊一郎・那須信治；那須信治・荻原尊禮・表俊一郎 参照
本間正作；河角廣・本間正作 参照
飯田汲事；石本巳四雄・飯田汲事 参照
今村學郎・矢嶋仁吉 (8) 武蔵野臺地の地質構造に就いて (佛文)……………………… 83
井上宇胤 (52) 發震機構に就いて (英文)……………………… 582
石本巳四雄 (21) 出羽村及び濱松町における地震動卓越周期の觀測 (邦文)…… 240
石本巳四雄 (22) 器械的記錄を行ふ微動計の製作 (佛文)……………………… 248
石本巳四雄 (55) 明治 9 年以降東京觀測各月地震回數統計 (邦文)……………………… 610
石本巳四雄・飯田汲事 (48) 土の粘彈性と剪斷抵抗 (邦文) ……………………… 534
石本巳四雄・飯田汲事 (58) 振動方法による土の彈性測定 (英文) ……………………… 632
金井清；妹澤克惟・金井清 参照
河角廣 (29) 地震計初動の理論的及實驗的研究並びに地震初動の定量的研究 (其 1) (英文) ……………………… 319
河角廣・木下潤一 (30) 地震計初動の理論的及實驗的研究並びに地震初動の定量的研究 (其 2) (英文)……………………… 339
河角廣・本間正作 (18) 昭和 10 年 4 月 21 日臺灣地震の走時曲線と地殼構造上の一問題 (英文) ……………………… 201
木下潤一；河角廣・木下潤一 参照
岸上冬彦 (54) 有感地震の 1 日中の分布に就いて (英文)……………………… 604
久野久 (9) 丹那隧道の地質斷面圖 (英文)……………………… 92
久野久 (57) 更新世以後に於ける丹那斷層の運動に就いて (英文)……………………… 619

松澤武雄 (5) 昭和8年3月3日の大地震 (III). 大地震前後の三陸沖の地震活動及一般に大地震の餘震に就て (獨文) ………… 38
水上武 (19) 最近の活動に伴へる淺間火山の高さの變化 (英文) ………… 222
宮部直巳 (27) 昭和11年2月21日河内大和强震に關する調査報告 (邦文) …… 297
宮部直巳 (35) 地殼變動の程度に就て (英文) ………… 387
宮部直巳 (49) 土のプラスティック變形に關する實驗 (序報) (英文) ………… 543
宮部直巳 (50) 垂直荷重による砂層の變形 (序報) (英文) ………… 553
永田武 (38) 關東地方に於ける震原の垂直分布 (邦文) ………… 420
那須信治・萩原尊禮 (25) 昭和11年2月21日河内大和强震調査報告 (邦文) …… 285
那須信治・萩原尊禮 (26) 大阪市内に於ける土地の固有振動の測定 (邦文) …… 290
那須信治・萩原尊禮・表俊一郎 (39) 關東地方に於ける地震の發生 (共1) (邦文) 427
那須信治・萩原尊禮・表俊一郎 (51) 土壤層中に於ける人工地震波の傳播並に土壤の彈性に關する研究 (共1) (邦文) ………… 560
表俊一郎; 那須信治・萩原尊禮・表俊一郎 参照
大塚彌之助 (7) 中部關東平野の海成洪積層 (關東造盆地運動の一資料) (英文) 75
大塚彌之助 (40) 秋田縣由利郡地方の高瀬川綠色凝灰岩及び日本の下部新第三系の對比 (英文) ………… 438
齊田時太郎 (28) 昭和11年2月21日河内,大和强震被害の地質及地形的考察 (邦文) 307
齊田時太郎・鈴木正治 (10) 高層建築の地震動による振動 (邦文) ………… 104
妹澤克惟 (14) 震源と震波との關係に就て (英文) ………… 149
妹澤克惟 (45) 媒體の異同が地震初動の分布に及ぼす影響 (英文) ………… 506
妹澤克惟・金井清 (1) 自由振動の持續性と共振の振幅との關係一海峽に於けるセイシの問題 (英文) ………… 1
妹澤克惟・金井清 (32) 灣のセイシに伴ふ逸散波 (英文) ………… 360
妹澤克惟・金井清 (2) 局所的內力を種々の速さで變化する場合に生ずる彈性波 (英文) ………… 10
妹澤克惟・金井清 (11) 三菱仲7號館別館, 仲8號館別館, 仲13號館の種々の狀態に於ける震動勢力の逸散性 (英文) ………… 119
妹澤克惟・金井清 (16) 構造物に於ける震動逸散理論の吟味 (英文) ………… 164
妹澤克惟・金井清 (12) 6階建築に於ける震動勢力の逸散性. 共振と餘共振とが一致する問題 (英文) ………… 134

妹澤克惟·金井淸 (17) 7 階建築に於ける震動勢力の逸散性 (英文) …………… 189
妹澤克惟·金井淸 (46) 8 階建築に於ける震動勢力の地下逸散性 (英文) ……… 514
妹澤克惟·金井淸 (34) 改良せる理論から見た實在建物の震動勢力逸散性 (英文) …………………………………………………………………… 377
妹澤克惟·金井淸 (15) 不連續層を通過する横波の性質 (英文) ………………… 157
妹澤克惟·金井淸 (31) 斜のディスターバンスによつて生じた地表層の固有振動の減衰 (英文) …………………………………………………………… 354
妹澤克惟·金井淸 (33) 床の剛度が架構の水平振動に及ぼす影響 (英文) ……… 367
妹澤克惟·金井淸 (44) 平面源を有する彈性波勢力の偏り (英文) ……………… 489
妹澤克惟·金井淸 (47) 五重塔の耐震性 (英文) ………………………………… 525
鈴木正治; 齊田時太郎·鈴木正治 參照
高橋龍太郎 (3) 淺間火山の精密水準測量結果 (邦文) ………………………… 18
高橋龍太郎 (4) 小淺間及棒鎚三角點に於ける緯度の測定 (邦文) …………… 26
田山利三郎 (24) 仙臺大年寺山の山崩 (邦文) ………………………………… 271
寺田寅彥 (56) 本邦に於ける火山活動の移動に就て (英文) ………………… 616
津屋弘逵 (41) 火山列島硫黄島の地質及岩石に就いて (英文) ……………… 453
山口生知 (20) 地震と雨雪量, 氣壓, 及氣溫との關係 (補遺) (英文) …………… 235
山口生知 (36) 地震現象の統計的研究の成果に關する檢討 (英文) ………… 399
矢嶋仁吉; 今村學郎·矢嶋仁吉 參照
(13) 宮古－青森間水準檢測成果 (邦文) ………………………………………… 146
(42) 袋井－興津－小田原間及び興津－甲府間の一等水準檢測成果報告 (邦文)… 481
(43) 湯河原町—城東村間の一等水準檢測成果報告 (邦文) ……………………… 486

Index to Vol. XIV.

Pege

FUCHIDA, T. (37) An Experimental Method to solve the Equation of Motion of the Seismograph. (in English) 415

FUKUTOMI, T. (6) Heights of Tunamis at Simoda in Southern Idu Peninsula. (in Japanese) 68

FUKUTOMI, T. (23) Physical and Chemical Properties of the Simogamo, Rendaizi and Simokawazu Thermal Springs in Southern Idu Peninsula. I. (in English) 259

HAGIWARA, T. (53) Observation of the Predominating Periods in the Earthquake Motions at Daihô-mura and Kamiotu-mura, Ibaraki Prefecture. (in Japanese) 599

HAGIWARA, T. and NASU, N., *See* NASU, N. and HAGIWARA, T.

HAGIWARA, T., OMOTE, S. and NASU, N., *See* NASU, N., HAGIWARA, T. and OMOTE, S.

HONMA, S., *See* KAWASUMI, H. and HONMA, S.

IIDA, K., *See* ISHIMOTO, M. and IIDA, K.

IMAMURA, G. et YAZIMA, N. (8) Contribution à l'Etude Géologique du Plateau de Musasino, près de Tokyo. (en français) 83

INOUYE, W. (52) Notes on the Origins of Earthquakes. (in English) 582

ISHIMOTO, M. (21) Observation des périodes prédominantes dans les secousses séismiques à Dewa-mura et à Hamamatu-tyô. (en japonais) 240

ISHIMOTO, M. (22) Construction d'un microséismographe mécanique. (en français) 248

ISHIMOTO, M. (55) Etudes statistiques sur les séismes observés à Tôkyô depuis 1876. (en japonais) 610

ISHIMOTO, M. et IIDA, K. (48) Experiences sur le sol. (en japonais). 534

ISHIMOTO, M. and IIDA, K. (58) Determination of Elastic Constants of Soils by means of Vibration Methods. Part I. Young's Modulus. (in English) 632

KANAI, K., *See* SEZAWA, K. and KANAI, K.

KAWASUMI, H. (29) Theoretical and Experimental Study of Initial Motion of Seismographs and the Quantitative Study of First Impulsion of Earthquake. Part I. (in English) 319

KAWASUMI, H. and KINOSITA, Z. (30) Theoretical and Experimental Study of Initial Motion of Seismographs and the Quantitative Study of First Impulsion of Earthquake. Part II. (in English). 339

KAWASUMI, H. and HONMA, S. (18) On a Problem Concerning the Internal Structure of the Earth as Discussed from the Time-distance Curve of the Formosa Earthquake of April 20, 1935. (in English) 201

KINOSITA, Z., *See* KAWASUMI, H. and KINOSITA, Z.

KISHINOUYE, F. (54) On the Diurnal Periodicity of Felt Earthquakes. (in English) 604

KUNO, H. (9) The Geologic Section along the Tanna Tunnel. (in English).. 92

KUNO, H. (57) On the Displacement of the Tanna Fault since the Pleistocene. (in English) 619

MATUZAWA, T. (5) Seismometrische Untersuchungen des Erdbebens vom 2. März 1933. III. Erdbebentätigkeit vor und nach dem Grossbeben. Allgemeines über Nachbeben. (in deutsch).............. 38

MINAKAMI, T. (19) Changes in the Heights of Volcano Asama caused by Eruptions in 1935. (in English) 222

MIYABE, N. (27) Some Phenomena associated with the Kawati-Yamato Earthquake of Feb. 21, 1936. (in Japanese) 297

MIYABE, N. (35) On the Degree of Disturbance of the Earth's Crust. (in English)... 387

MIYABE, N. (49) Preliminary Notes on Experimental Studies on the Plastic Deformation of Soil. (in English).......................... 543

MIYABE, N. (50) Experimental Studies on the Deformation of Sand Masses due to Vertical Loads. I. (in English) 553

NAGATA, T. (38) Space Distribution of Earthquake Hypocentres in the Kwantô District. (in Japanese) 420

NASU, N. and HAGIWARA, T. (25) The Kawati-Yamato Earthquake of February 21st, 1936. (in Japanese) 285

NASU, N. and HAGIWARA, T. (26) Determination of the Proper Periods of the Ground in Osaka. (in Japanese) 290

NASU, N., HAGIWARA, T. and OMOTE, S. (39) Studies on Earthquakes in the Kwantô District. Part I. Three-dimensional Distribution of the Seismic Foci. (in Japanese) 427

NASU, N., HAGIWARA, T. and OMOTE, S. (51) Studies on the Propagation of the Artificial Earthquake Waves through Superficial Soil or Sand Layers and the Elasticity of Soil and Sand. (in Japanese) 560

OMOTE, S., *See* NASU, N., HAGIWARA, T. and OMOTE, S.

OTUKA, Y. (7) Marine Lower Pleistocene of the Central Kwanto Plain. (An evidence of basin forming force of the Kwanto plain). (in English) 75

OTUKA, Y. (40) The Takasegawa Green Tuff beds of the Yuri district, Akita pref., Japan, and Correlation of the Lower Neogene in Japan. (in English) 438

SAITA, T. (28) Geological and Topographical Investigation of the Earthquake Damages on the Boundary between Osaka and Nara Prefecture on the 21st of February, 1936. (in Japanese) 307

SAITA, T. and SUZUKI, M. (10) Vibration of a Tall Building Caused by Earthquake Shocks. (in Japanese) 104

SEZAWA, K. (14) On the Relation between Seismic Origins and Radiated Waves. (in English) 149

SEZAWA, K. (45) The Effect of Differences in the Media on the Distribution of Displacements in a Seismic Wave Front. (in English) 506

SEZAWA, K. and KANAI, K. (1) Damped Free Oscillation and Amplitudes in Resonance, with Special Reference to Decay of Seiches in Straits. (in English) 1

SEZAWA, K. and KANAI, K. (32) Dissipation Waves Accompanying Forced Seiches in a Bay. (in English) 360

SEZAWA, K. and KANAI, K. (2) Elastic Waves Formed by Local Stress Changes of Different Rapidities. (in English) 10

SEZAWA, K. and KANAI, K. (11) Energy Dissipation in Seismic Vibrations of Actual Buildings of Unlike Structure. (in English). 119

SEZAWA, K. and KANAI, K. (16) Improved Theory of Energy Dissipation in Seismic Vibrations of a Structure. (in English) ... 164

SEZAWA, K. and KANAI, K. (12) Energy Dissipation in Seismic Vibrations of a Six-storied Structure. Coincidence of Resonance and Corresonance. (in English) 134

SEZAWA, K. and KANAI, K., (17) Energy Dissipation in Seismic Vibrations of a Seven-storied Structure. Nature of Corresonance. (in English) 189

SEZAWA, K. and KANAI, K., (46) Energy Dissipation in Seismic Vibrations of an Eight-storied Structure. (in English) 514

SEZAWA, K. and KANAI, K., (34) Energy Dissipation in Seismic Vibrations of Actual Buildings Predicted by means of an Improved Theory. (in English) 377

SEZAW, K. and KANAI, K., (15) The Nature of Transverse Waves transmitted through a Discontinuity Layer. (in English)........... 157

SEZAWA, K. and KANAI, K., (31) Damping in Seismic Vibrations of a Surface Layer due to an Obliquely Incident Disturbance. (in English)... 354

SEZAWA, K. and KANAI, K. (33) The Effect of Stiffness of Floors on the Horizontal Vibrations of a Framed Structure. (in English). 367

SEZAWA, K. and KANAI, K. (44) Polarization of Elastic Waves generated from a Plane Source. (in English).......................... 489

SEZAWA, K. and KANAI, K. (47) On the Seismic Vibrations of a Gozyûnotô (Pagoda). (in English)...................................... 525

SUZUKI, M., *See* SAITA, T. and SUZUKI, M.

TAKAHASI, R. (3) Precise Levelling at the Asama Volcano. (in Japanese) 18

TAKAHASI, R. (4) Latitude Determination at the Koasama and the Boroku Triangulation Points. (in Japanese)............................ 26

TAYAMA, R. (24) Landslide in Dainenzi Hill, Sendai. (in Japanese). 271

TERADA, T. (56) On the Slow Migratory Motion of the Volcanic Activity in Japan. (in English) 616

TSUYA, H. (41) Geology and Petrography of Io-sima (Sulphur Island), Volcano Islands Group. (in English) 453

YAMAGUTI, S. (20) Relation between Earthquakes and Precipitation, Barometric Pressure, and Temperature. A Supplementary Note. (in English) 235

YAMAGUTI, S. (36) A Discussion on the Results of a Statistical Investigation of Earthquake Phenomena. (in English) 399

YAZIMA, N., *See* IMAMURA, G. and YAZIMA, N.

(13) Precise Levelling along the Line from Miyako to Aomori. (in Japanese) 146

(42) Relative Vertical Displacements of Bench-marks along the Lines of Levels from Hukuroi to Okitu, from Okitu to Odawara, and from Okitu to Kôhu. (in Japanese) 481

(43) Relative Vertical Displacements of Bench-marks along the Line of Levels from Yugawara to Zyôtô-mura, on the East Coast of the Idu Peninsula. (in Japanese) 486